NASA Conference Publication 2400

Rotorcraft Dynamics 1984

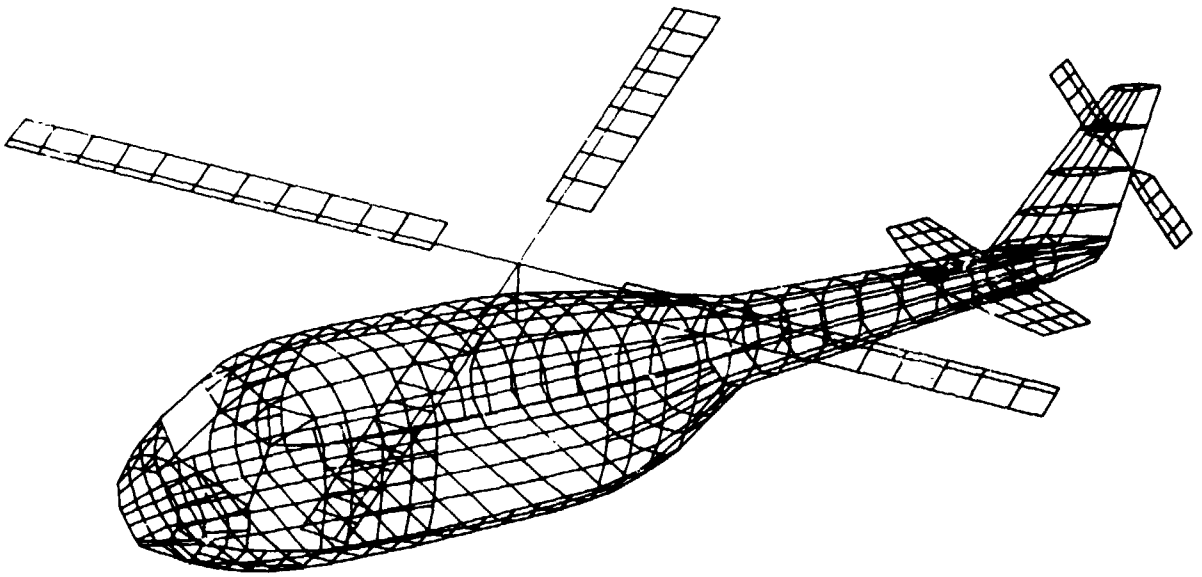

November 1985

Proceedings of the 2nd Decennial
Specialists' Meeting on Rotorcraft Dynamics
sponsored by
NASA Ames Research Center and
the American Helicopter Society
and held at
NASA Ames Research Center
Moffett Field, California
November 7-9, 1984

National Aeronautics and
Space Administration

NASA Conference Publication 2400

Rotorcraft Dynamics 1984

November 1985

National Aeronautics and
Space Administration

Ames Research Center
Moffett Field, California 94035

Proceedings of the 2nd Decennial
Specialists' Meeting on Rotorcraft Dynamics
sponsored by
NASA Ames Research Center and
the American Helicopter Society
and held at
NASA Ames Research Center
Moffett Field, California
November 7-9, 1984

PREFACE

These are the proceedings and the papers presented at the 2nd Decennial Specialists' Meeting on Rotorcraft Dynamics held at Ames Research Center on November 7-9, 1984. This conference was jointly sponsored by NASA Ames Research Center and the American Helicopter Society. The meeting was recorded on audio tape and a transcription was made of the Welcome, Opening Remarks, the discussion of the papers, and the panel presentations. The transcribed material is included in these proceedings in its chronological order. Except for the panel presentations or as otherwise noted, the transcription has not been reviewed by the participants. I have tried to correct the normal grammatical errors that occurred in spontaneous discussion without affecting the style or content of what was said. To the extent that information has been lost in this process, I apologize.

William G. Bousman
Technical Chairman

ORGANIZING COMMITTEE

General Chairman
C. Thomas Snyder, Director of Aerospace Systems
NASA Ames Research Center

Assistant General Chairman
H. Kipling Edenborough, NASA Ames Research Center

Technical Chairman
William G. Bousman, US Army Aeromechanics Laboratory

Technical Co-chairman
Raymond A. Piziali, US Army Aeromechanics Laboratory

Administrative Chairman
Stephen L. Haff, NASA Ames Research Center

Administrative Co-chairman
Laurel G. Schroers, US Army Aeromechanics Laboratory

Publicity Chairman
Peter D. Talbot, NASA Ames Research Center

Finance Chairman
John F. Madden, III, NASA Ames Research Center

San Francisco Bay Area Chapter Representative
Martin D. Maisel, US Army Aeromechanics Laboratory

AHS Dynamics Committee Representative
Donald L. Kunz, US Army Aeromechanics Laboratory

Session and Panel Chairmen

Session One
Inderjit Chopra, University of Maryland

Session Two
Robert H. Blackwell, Sikorsky Aircraft

Session Three
Wayne Johnson, NASA Ames Research Center

Session Four
Robert B. Taylor, Boeing Vertol Company

Panel One
Richard Gabel, Boeing Vertol Company

Panel Two
W. E. Hooper, Boeing Vertol Company

WELCOME

William F. Ballhaus, Jr.
Director
NASA Ames Research Center

Good morning, and welcome to Ames. It is a great pleasure to welcome you here, on behalf of Ames and the American Helicopter Society, to the 2nd Decennial Specialists' Meeting on Rotorcraft Dynamics. I spent a good part of this morning trying to figure out how to pronounce decennial--it is a word that wasn't in my vocabulary. I guess it means you hold this meeting every 10 years. The last one was held at Ames 10 years ago and we are very pleased to host it again. Ames is one of the three NASA Research Centers involved in aeronautical research, and we were designated the lead center for helicopter technology development. In addition, here at Ames we have the Army Aeromechanics Laboratory so the combined efforts of the two make this a very interesting meeting for us. We do a great deal of work with the Army; a lot of this work is conducted jointly and you will see some of this today. In fact it is very gratifying, when you look over the program, to see that there is a very broad representation at this meeting. We have all of the major helicopter manufacturers represented, eight universities, three Army laboratories, one Navy laboratory, and two NASA Centers. I hope you will find the papers and the panel discussions interesting. It should be an informative and entertaining meeting. I also hope you enjoy your stay in the Bay Area. I very much look forward to welcoming all of you to the 3rd Decennial Meeting in 1994. Better get your hotel reservations early. Thank you very much.

OPENING REMARKS

C. Thomas Snyder
Meeting General Chairman

Director, Aerospace Systems
NASA Ames Research Center

I guess we really hadn't been thinking to 1994 yet; we've been working toward this meeting so hard. Good morning again. I would like to add my personal welcome to each of you and also my thanks to all of those who helped to bring this 2nd Decennial Specialists' Meeting on Rotorcraft Dynamics to fruition. The field of rotorcraft dynamics has to be one of the most complex and difficult facing the engineering community today. To be effective as a specialist in this field--and I can say this because I don't consider myself a dynamics specialist--one must be well-based in several disciplines: one must be well-based in structural dynamics, in aerodynamics both steady and unsteady, in modern controls, and must have a strong theoretical background and good physical insight. And he probably should be a good computer jock, as my kids would say. Such a combination of capabilities really makes a dynamicist a rare breed and if you have tried to hire one lately you will know that. I'm reminded of one definition of an expert--and some of you may have heard this definition--an expert has been defined as someone who is more than 50 miles from his home base. Now, I'm confident that those are not the kind of experts we have here today, but I think you will find that we have a very excellent set of papers and discussions.

Because of the complex nature of rotorcraft dynamics and the fact that they are influenced by so many aspects of rotorcraft technology the subject and challenge will probably be around as long as rotorcraft are. That, together with your unique capabilities, really relates to good job security. Ten years have passed since the last specialists' meeting in rotorcraft dynamics at Ames. During those years, much of the promise shown back at that meeting has been realized and many of the ideas and approaches have paid off. The ability to accurately predict rotor systems' behavior and stability characteristics has improved significantly. Difficult problems of rotor loads and vibration are being addressed through improvements in modeling of the rotor aerodynamic environment, through upgrading of prediction codes, and through application of advanced control concepts. Major advances in computer power in terms of both speed and capability are making it possible to analytically approach solutions to problems that could not be attempted previously. For example, the Cray 2 to be delivered here next year is anticipated to have a speed capability of 250 megaflops sustained in a main memory of 256 million words. Now in comparison with 10 years ago, probably one of the most capable computers was a CDC 7600; it was pretty much a workhorse at that time and that had a speed of about 3 to 5 megaflops and a memory of under 1 million words. So in the space of 10 years we have seen about a 50-fold increase in speed and about a 250-fold increase in memory. We have also seen major advances in the algorithms and that has also added significantly to computational capabilities. The advent of Fast Fourier Transform methods and other on-line analysis techniques as well as array processing has made the process of understanding the dynamic complex systems quicker and more complete.

The second generation comprehensive analyses are making it possible to better understand how the dynamics and the other technology areas play together and how they interact. Unique test facilities, like the Rotor Systems Research Aircraft, the RSRA, offer a chance to study dynamics from the point of load application down through the mast, and to the body vibrations. You can measure the loads in terms of blade pressures and loads, you can measure at the load cells what is happening there, and then you can measure the body vibrations through accelerometers and look at all aspects of the dynamics. The calibration of the instrumentation system, the dynamic calibration, remains a technical challenge and you will hear a paper on that in this meeting. We also look forward to the restoration of the 40 by 80 foot wind tunnel to operation in about January 1986 and to the new capabilities offered by the new 80 by 120 foot test section. With its increased speed capabilities, the 40 by 80 promises to be an important tool in the current effort to push helicopter rotors to higher speeds. This current thrust is of course putting increased pressure on you dynamicists as rotors are pushed to the limits of their envelopes.

Since the last specialists' meeting, a clear trend toward the simplified rotor systems has emerged. Offering significant advantages in many respects these simpler structural designs such as bearingless rotors or soft inplane hingeless rotors seem to make the dynamicist's job harder. Prediction techniques have to be modified to handle these types of rotors and it is important to be right in the prediction of their stability the first time. Dynamics considerations are certainly prominent and are receiving increased attention in the rotorcraft programs I see here at Ames. In addition to the fundamental rotor dynamics research, dynamics considerations are of major importance in our rotorcraft project activities. For example in the XV-15 Tilt Rotor Research Aircraft the rotor pylon stability problem was perhaps the most important objective of that program. In the current RSRA X-Wing project the very stiff circulation control rotor depends upon hub moment feedback and higher harmonic control to maintain acceptable rotor loads and vibration levels. In the new Heavy Lift Research Vehicle Program, or as some of you know it the reborn heavy lift helicopter, the low frequency range of the rotor system raises the possibility of resonance for the internal body organs of the pilot and crew. So there are a number of dynamics questions of considerable interest in that program. In summary, a great deal has been achieved in the last 10 years, important new capabilities and challenging new problems promise that the next 10 years will be even more exciting.

CONTENTS

SESSION TWO--ROTOR LOADS

SESSION THREE--ROTORCRAFT STABILITY II

SESSION FOUR--VIBRATION

PANEL ONE--PRACTICAL DYNAMICS PROBLEM SOLVING EXPERIENCES

PANEL TWO--DATA BASES--THE USER'S VIEWPOINT

THE USE OF ACTIVE CONTROLS TO AUGMENT ROTOR/FUSELAGE STABILITY

Friedrich K. Straub
Dynamics Engineer
Hughes Helicopters, Inc.
Culver City, California
and
William Warmbrodt
Aerospace Engineer
NASA Ames Research Center
Moffett Field, California

Abstract

The use of active blade pitch control to increase helicopter rotor/body damping is studied. Control is introduced through a conventional nonrotating swashplate. State variable feedback of rotor and body states is used. Feedback parameters include cyclic rotor flap and lead-lag states and body pitch and roll rotations. The use of position, rate, and acceleration feedback is studied for the various state variables. In particular, the influence of the closed loop feedback gain and phase on system stability is investigated. For the rotor/body configuration analyzed, rotor cyclic inplane motion (ζ_S,$\dot{\zeta}_C$,$\dot{\zeta}_S$) and body roll-rate and roll-acceleration feedback can considerably augment system damping levels and eliminate ground resonance instabilities. Scheduling of the feedback state, phase and gain with rotor rotation speed can be used to maximize the damping augmentation. This increase in lead-lag damping can even be accomplished without altering any of the system modal frequencies. Investigating various rotor design parameters (effective hinge offset, blade precone, blade flap stiffness) indicates that active control for augmenting rotor/body damping will be particularly powerful for hingeless and bearingless rotor hubs.

Notation

e	blade root hinge offset
h	offset of rotor hub from fuselage c.g.
k	blade index, k=1 .. N
K	feedback gain constant
NR	nominal rotor speed
q	vector of generalized coordinates
R_x,R_y	fuselage longitudinal, lateral motion
$\underline{u}$	vector of control inputs
$\underline{x}$	vector of state space variables
β,ζ	blade flap, lag motion
β_C,β_S	rotor cosine, sine cyclic flap degrees of freedom
β_p	precone
ε	order of magnitude
ζ_C,ζ_S	rotor cosine, sine cyclic lead-lag degrees of freedom
η	modal damping coefficient, % critical
η_ζ	blade lead-lag damping, % critical
θ_0	rotor collective pitch angle
θ_A	active control blade feathering angle
θ_{AC},θ_{AS}	active control feathering inputs to nonrotating swashplate
θ_{Amax}	maximum active control blade feathering angle per degree of lead-lag motion
θ_G	blade aerodynamic pitch angle
θ_S	orientation of blade root springs at flat pitch
θ_x,θ_y	fuselage roll, pitch motion
σ	real part of eigenvalue, i.e., modal damping, rad/sec
ϕ	feedback phase
ψ	nondimensional time parameter, rotor azimuth
ω	imaginary part of eigenvalue, i.e., modal frequency, rad/sec
Ω	rotor speed
$\bar{(\ )}$	nondimensional quantity
$(\ )_0$	steady-state equilibrium value
$(\ )'$	$d(\ )/d\psi$

Introduction

Aeromechanical rotor/fuselage instabilities can occur for articulated, hingeless, and bearingless rotors. Due to the wide range of helicopter operating conditions, payload configurations, and flight regimes, it can be very difficult for the helicopter designer to tailor all rotor and fuselage body frequencies to avoid modal frequency coalescences or resonances for all conditions. Consequently the rotor designer often has to resort to including mechanical or elastomeric blade dampers to improve system aeromechanical stability. This results in increased cost, complexity, maintenance, weight, and hub drag for the rotor system. In addition, soft inplane hingeless rotor configurations without damping augmentation have inherently low rotor blade structural damping. These systems have not been used extensively in the helicopter industry, in part, because of poor aeroelastic stability characteristics. Consequently a means to increase aeromechanical stability in a reliable manner could significantly improve the operational characteristics of this rotor hub design.

The use of active blade pitch control has been successfully demonstrated for vibration reduction (Ref. 1). A significant amount of analytical and experimental research has been performed to develop this technology for both N per rev and gust-induced vibration control. The technology is now available for advanced applications. Showing analytically the feasibility of using active control to augment rotor damping would represent a further step towards an advanced, fully integrated, multimode helicopter rotor control system.

Presented at the American Helicopter Society and NASA Ames Research Center 2nd Decennial Specialists' Meeting on Rotorcraft Dynamics, November 7-9, 1984

Only a limited number of studies have been performed investigating active blade pitch feathering to affect helicopter rotor/fuselage stability (Refs. 2-4). References 3 and 4 use active control implementation approaches which do not utilize a conventional swashplate and consequently have limited application to current rotorcraft control systems. In Reference 2, Young, Bailey and Hirschbein investigated the aeromechanical stability of a hingeless helicopter rotor and the application of feedback control to augment system damping through conventional swashplate control. The use of active control was studied by implementing fuselage roll position and roll rate feedback into a set of swashplate actuators in order to generate longitudinal and lateral cyclic blade pitch commands. Feedback of fuselage pitching motion was not pursued since the unstable mode of the system being studied had only a relatively small pitch component. Their results showed that feedback of roll position and roll rate could stabilize the unstable roll mode both on the ground and in hover. This study extends these results by also investigating the influence of body acceleration feedback, various rotor state feedback systems, and the influence of control feedback gain and phasing.

The purpose of the present study is to evaluate the potential use of active blade pitch control to increase rotor/body system damping. This is accomplished by using state variable feedback with the appropriate gain and phase. Such an application could possibly eliminate the need for mechanical lead-lag dampers. In addition, a marginally stable rotorcraft configuration could be further stabilized by increasing the rotor damping levels and thereby expanding the rotorcraft's operating envelope. The detailed objectives of the present study are:

1) Investigate the influence of state variable feedback on system damping, including body acceleration and rotor state feedback systems which have not been previously considered.

2) Use of a systematic approach to study the effects of the feedback gain and the weighting between the time-dependent cyclic blade pitch controls on system stability levels.

3) Investigate the use of control scheduling with rotor speed to ensure stability at all rotation rates.

4) Assess the influence of rotor design parameters (hinge offset, blade precone, and blade flapping stiffness) on the performance of feedback control.

To carry out this investigation a new mathematical model was developed to analyze coupled rotor/fuselage dynamics. This model, which was used for the numerical simulations of active feedback control, is discussed in the next section. The manner in which active blade pitch feathering is introduced is also described. To validate the governing equations of motion, frequency and damping predictions without active controls are correlated with experimental data (Ref. 5). Numerical results are then presented based on state variable feedback control. These active control simulations are intended to show the effect of various feedback variables on system stability and response and provide a systematic approach in choosing the feedback parameters. Key rotor design parameters are also investigated as to their influence on rotor behavior with feedback control.

Analytical Model

The details of the mathematical model used in this study are presented in this section. The approach used in modelling state variable feedback through a conventional swashplate is discussed and the method of solution for the governing equations of motion is reviewed. More details on the mathematical model, the control laws, or the solution method may be found in Ref. 6.

Rotor/Fuselage Model

A brief description of the mathematical model developed for this study follows. The math model is similar to the models used in Refs. 7 and 8. The helicopter body is represented as a rigid fuselage having pitch and roll rotations (θ_y,θ_x) about the center of mass and longitudinal and lateral translations (R_x,R_y) of the center of mass, see Fig. 1. The fuselage physical properties required for modelling are its mass, pitch and roll inertias, and effective landing gear stiffnesses and damping in rotation and translation. The rotor hub, having three or more blades, is located a distance h directly above the fuselage mass center. The blades are assumed to be rigid and rotate against spring and damper restraints about coincident flap and lead-lag hinges offset from the axis of rotation, see Fig. 2. The orientation of the hinges can be different from the aerodynamic pitch angle, thus allowing modelling of variable structural flap-lag coupling with blade feathering inboard or outboard of the hinges. Blade precone is included. This parameter is particularly important in this study since it directly contributes to the inplane Coriolis forces which augment blade lag damping. In deriving the governing equations, rotor rotation speed is assumed constant. The aerodynamic forces are based on two-dimensional quasi-steady theory. Apparent mass, compressibility and stall are neglected. No low frequency unsteady aerodynamic model (dynamic inflow) is used. The pitch control input is composed of two parts: the time-independent

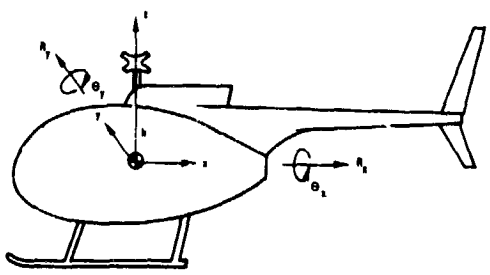

Fig. 1 Fuselage model.

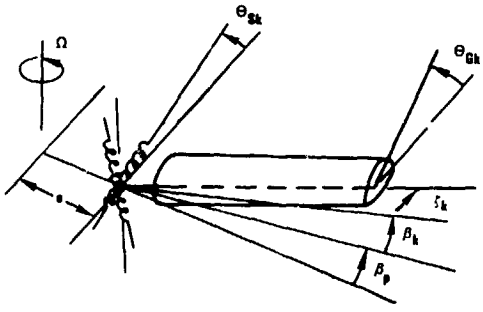

Fig. 2 Rotor blade model

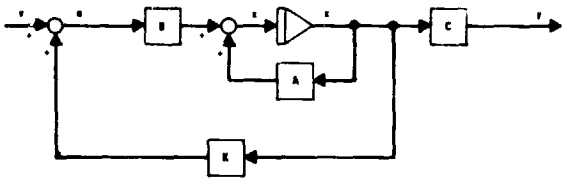

Fig. 3 State variable feedback control system.

collective pitch, identical for all blades; and the time-varying "active" pitch. The active control pitch input appears as aerodynamic forcing expressions in the equations of motion.

In deriving the equations of motion for this model a large number of small terms appear. Many of these were neglected systematically by use of an appropriate ordering scheme based on the magnitude of blade slopes (typically $0.1 < \varepsilon < 0.2$). The various parameters in the equations were assigned orders of magnitude. Fuselage motions are assumed to be of order $O(\varepsilon^{1.5})$. The active control portion of the blade pitch angle is assumed to be of order $O(\varepsilon^{1.5})$, based on experience with the higher harmonic control inputs of Ref. 1. In applying the ordering scheme it is assumed that terms of order $O(\varepsilon^2)$ are negligible in comparison with unity. In addition, all terms that contain products of the fuselage degrees of freedom are neglected.

Control Law Development

In implementing the active control, it is assumed that feedback is applied through a conventional swashplate, i.e., control motions are generated by actuators in the fixed system. The active pitch input to the k'th blade can then be expressed as

$$\theta_{Ak} = \theta_{AC(\psi)} \cos\psi_k + \theta_{AS(\psi)} \sin\psi_k \qquad (1)$$

where the control inputs θ_{AC} and θ_{AS} are to be determined functions of the nondimensional time parameter ψ. A block diagram for the state variable feedback system used in the current study is shown in Fig. 3. The system equations are

$$\dot{\underline{x}} = [A]\underline{x} + [B]\underline{u} \qquad (2)$$

$$\underline{y} = [C]\underline{x}$$

where

$$\underline{u}^T = [K\cos\phi, K\sin\phi]d^n q_j/d\psi^n \quad n=0,1,2 \qquad (3)$$

The vector $\underline{x}$ denotes the state space variables, $\underline{y}$ is the vector of output measurements, and $\underline{u}$ is the vector of control inputs. K is the control gain. The angle ϕ, herein termed feedback phase, defines the relative weighting between the time dependent cyclic controls. In other words, ϕ defines the swashplate azimuthal position where the gain that individual blades experience has its maximum value. This point is 90 degrees from the axis of no feathering about which the swashplate oscillates; see Fig. 4. The quantity q_j is one of the system degrees of freedom. In this analysis state feedback is directly introduced into the second order equations, thus $\underline{u}$ is proportional to q_j rather than $\dot{x}_j$. State feedback can then be thought of as an additional contribution to the system stiffness, damping, and/or mass matrix, for n=0,1,2 respectively.

Solution Method

The nonlinear periodic equations of motion can be solved directly in the time domain. However, for parametric stability studies an eigenvalue analysis is much more convenient. The equations are therefore linearized. The steady-state, nonlinear equilibrium position is obtained assuming

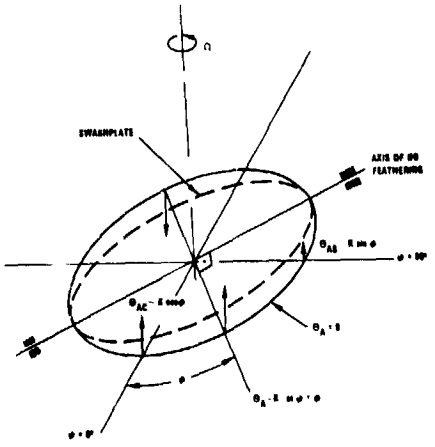

Fig. 4 Control implementation through swashplate.

that the fuselage degrees of freedom and the active blade pitch are zero. In the case of hover, the blade equilibrium position is independent of time and is obtained iteratively using the Newton-Raphson technique.

The linearized periodic coefficient perturbation equations are converted into a constant coefficient system using a multiblade or Fourier coordinate transformation. This is possible under the assumptions that all blades are identical and that the active pitch input is generated through a conventional swashplate with three "active" actuators in the fixed system. With the rotor being in a hover condition, only the first cyclic blade motions in flap and lead-lag couple with the fuselage motions. The collective and reactionless blade equations are not needed. The final set of equations is

$$[M(q_o)]\ddot{\underline{q}} + [C(q_o)]\dot{\underline{q}} + [K(q_o)]\underline{q} + [F(q_o)]\underline{u} = 0$$

$$\underline{q}^T = [\zeta_c, \beta_c, \zeta_s, \beta_s, \theta_x, \theta_y, R_x, R_y], \qquad (4)$$

$$\underline{u}^T = [\theta_{AC}, \theta_{AS}]$$

Stability of the ground resonance problem in the fixed system is then evaluated by transforming the equations into first order form and performing an eigenvalue analysis. This form of the governing equations is also used to compute the time history response and frequency response of the system

$$\dot{\underline{x}} = \begin{bmatrix} 0 & I \\ -[M]^{-1}[K] & -[M]^{-1}[C] \end{bmatrix} \underline{x} + \begin{bmatrix} 0 \\ -[M]^{-1}[F] \end{bmatrix} \underline{u} \qquad (5)$$

$$\underline{x}^T = [\underline{q}^T, \dot{\underline{q}}^T]$$

Discussion of Governing Equations

Development of control laws and their evaluation for this study were made with the objective to increase rotor/body system damping while observing constraints on state and control variables in order to avoid adversely affecting overall system performance.

The basic mechanism for influencing lead-lag dynamics is provided through aerodynamic, Coriolis, and kinematic coupling with blade flapping and feathering inputs. For elastic blades, elastic flap-lag coupling would also play a major role Fuselage dynamics are coupled with blade flapping through aerodynamic and gyroscopic forces. Looking closely at the governing equations of motion used in this study, the active control pitch input appears as aerodynamic forcing expressions in all equations. The values in the blade lag and fuselage translation equations are one order of magnitude smaller than in the flap equations and in the fuselage pitch and roll equations. From these equations it therefore seems that two primary mechanisms exist to stabilize ground resonance. First, the fuselage pitch and roll motion can be controlled through the pitch and roll moments arising from flapping. The magnitude of each is directly related to the blade root hinge offset and flap spring stiffness. The second mechanism is lead-lag damping augmentation through Coriolis coupling with blade flap motion. This requires presence of either steady blade coning deflection or built-in precone.

From the above it is clear that the aeromechanical stability of a helicopter is a multi-input/multi-output control problem. In this study, it is assumed that all the states are known. However, only one state at a time is used for feedback. Combined feedback of two or more state variables was not considered. Likewise no attempt was made at this stage to use multivariable optimal control techniques to maximize the damping augmentation since gaining a basic understanding of the problem was thought to be more important. Also, in the development of this simulation model it is recognized that unsteady aerodynamic effects (dynamic inflow) can at times have a considerable effect on the blade flap motion (Ref. 9). Since flapping plays an important role in stabilizing ground resonance perhaps the conclusions of the present study would be changed to some degree. In particular for high flap stiffness rotors unsteady aerodynamics should be included in a more refined model.

Validation of Analytical Model

Prior to presenting closed loop active control results, the fidelity of the math model to adequately predict aeroelastic stability characteristics is studied using experimental data from Ref. 5 (configuration 1). Rotor and body properties are listed in Table 1. No active controls are utilized for these results. The corresponding predictions from Ref. 10 using the E-927 analysis are also shown.

Table 1. Rotor/body properties

Number of blades	3
Radius, cm	81.1
Chord, cm	4.19
Nominal rotor speed, rpm	720
Hinge Offset, cm	8.51
Precone, deg	0
Blade airfoil	NACA 23012
Lift curve slope	2π
Profile drag coefficient	0.0079
Lock number	7.73
Solidity ratio	0.0494
Blade mass, Kg	0.209
Blade first mass moment, Kg cm	3.887
Blade second mass moment, Kg cm^2	173
Nonrotating flap frequency, Hz	3.13
Nonrotating lead-lag frequency, Hz	6.70
Damping in lead-lag, % critical	0.52
Height of rotor hub above gimbal, cm	24.1
Fuselage mass in pitch, Kg	22.60
Fuselage mass in roll, Kg	19.06
Fuselage inertia in pitch, Kg cm^2	6330
Fuselage inertia in roll, Kg cm^2	1830

Table 1. Rotor/body properties (cont).

Pitch frequency, Hz	1.59; 2*
Roll frequency, Hz	3.9; 4*
Damping in pitch, % critical	3.20
Damping in roll, % critical	0.929

*Body Frequencies used in study of active control.

Comparison between modal frequencies as a function of rotor speed at flat pitch show very good agreement in Fig. 5. In particular, regressing inplane mode resonances with the body pitch mode (550 rpm) and the body roll mode (765 rpm) are accurately predicted. In Fig. 6, the corresponding damping levels for the lead-lag regressing mode, body pitch mode, and body roll mode are presented. Lead-lag damping (Fig. 6a) shows relative good agreement. The corresponding pitch (Fig. 6b) and roll (Fig. 6c) damping levels are generally higher than the experimental data but in the same range as E-927 predictions.

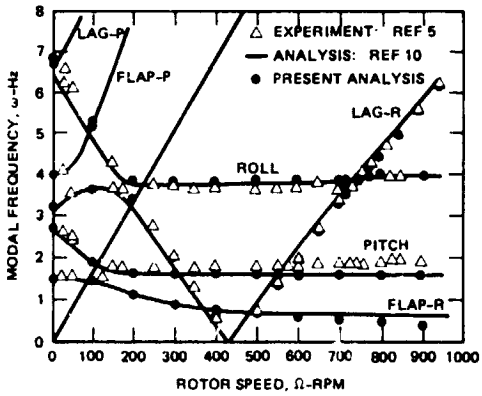

Fig. 5 Modal frequencies versus rotor speed at flat pitch.

Lead-lag damping for nine degrees of collective pitch as a function of rotor speed is shown in Fig. 7. Agreement of the present analysis (solid symbols) with experimental damping values is very good up to 650 rpm. This includes the crossover of the regressing lag mode with the body pitch mode. For higher rotor speeds (including crossover with the body roll mode), only general trends in damping are captured. This is certainly a shortcoming but it is felt that a better knowledge and/or adjustment of the body roll frequency and damping would improve these predicted results considerably. Furthermore, Fig. 8 shows that the current analysis predicts damping trends as a function of collective pitch angle quite well for the regressing lag mode (Fig. 8a) and body pitch motion (Fig. 8b) at 650 rpm. Only the trend with collective pitch is captured for the body roll mode (Fig. 8c).

From the correlation presented, it is clear that in certain cases considerable differences exist between analytical predictions and experimental results. However, the simple analytical model used for the present investigation can be expected to predict the frequency crossovers and

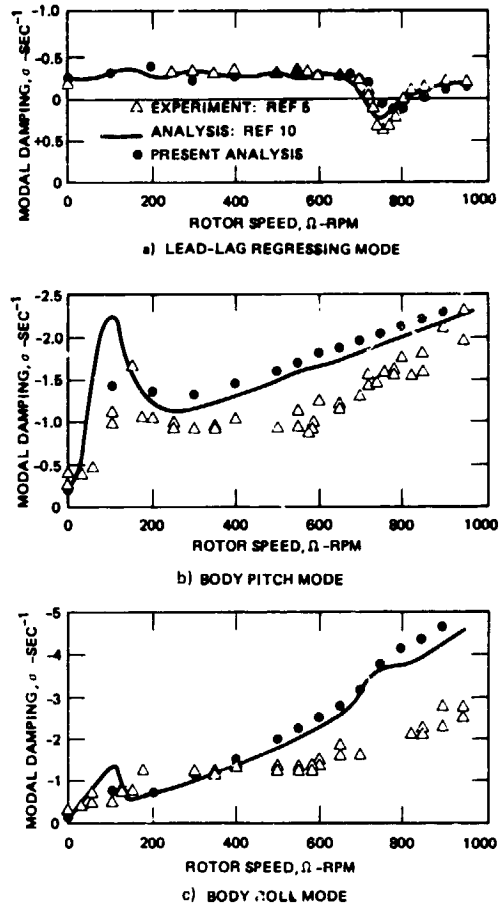

Fig. 6 Damping versus rotor speed at flat pitch.

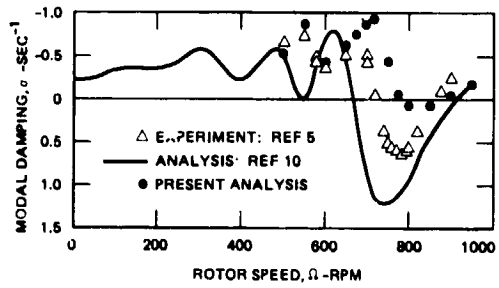

Fig. 7 Lead-lag regressing mode damping versus rotor speed, θ_0 = 9 deg.

damping trends adequately for the rotor/body systems studied here. It is concluded that the present model is adequate to investigate the effects of active controls on rotor/body aeromechanical stability.

Active Control Results

All the active control simulations in this study were performed for the same rotor/body configuration used in the previous section (configuration 1 of Ref. 5). This is a soft inplane hingeless

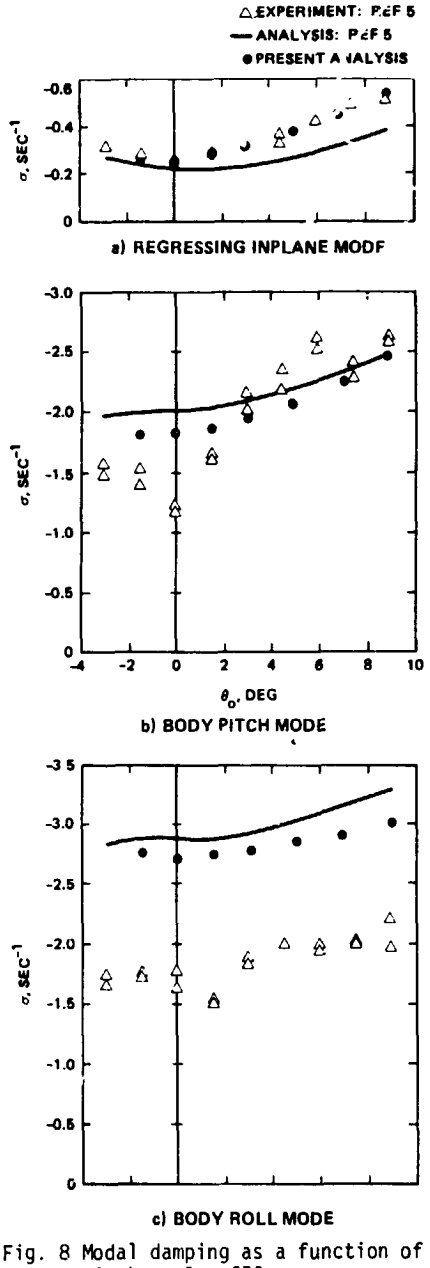

Fig. 8 Modal damping as a function of blade pitch angle, 650 rpm.

rotor supported on a gimbal with pitch and roll degrees of freedom. The baseline system parameters are listed in Table 1. Nominal rotor speed for this configuration is 720 rpm. All cases are for flat pitch operation. However, this rotor has a cambered airfoil which gives a small positive thrust at zero collective. The modal frequencies and damping for the baseline case without feedback are shown in Figs. 5 and 6. For this configuration, the regressing lag mode experiences an instability at the frequency crossover with the body roll mode at 765 rpm.

First, the effect of individual feedback state variables on system stability is explored by varying feedback gain and phase systematically. These studies are performed at the point of minimum stability, i.e., at the coalescence rotor speed of 765 rpm. Plots of system damping and frequency versus feedback phase are used to select candidate feedback states and define feedback phase angles for maximum damping augmentation. Next, these candidate feedback states are investigated in more depth by considering a range of rotor speeds to simulate rotor run up. Results show the sensitivity of the system dynamic behavior with respect to changes in feedback gain and phase. Following this, the effect of rotor configuration on active control damping augmentation is studied. To this end the blade root hinge offset, blade precone, and flap spring stiffness, which are key parameters in terms of control effectiveness, are varied to cover a range of values typical for articulated, hingeless, and bearingless rotors. Lastly, the rotor/body response behavior is considered. This provides a quantitative measure of the active blade feathering amplitudes required to achieve adequate stability margins. It also gives a better understanding of the participation of the individual degrees of freedom in the unstable or lightly damped rotor/body mode.

State Feedback Studies

Figures 9 through 13 show the effect of feedback on system damping (the real part of the eigenvalue) and frequencies (the imaginary part of the eigenvalue). Gain values of K=1, 2, and 3 and a complete range of feedback phase angles, $0<\phi<360$, are considered. Also shown are the damping and frequency of the baseline system without active controls, i.e., K=0. The rotor speed is 765 rpm which corresponds to coalescence of the body roll mode and regressing lead-lag mode frequencies, Figure 5.

Figure 9 shows the influence of cosine cyclic lead-lag position feedback (ζ_c) on system dynamics. The baseline (K=0) lead-lag regressing mode is unstable for this operating condition. Depending on the feedback phase, variations in feedback gain

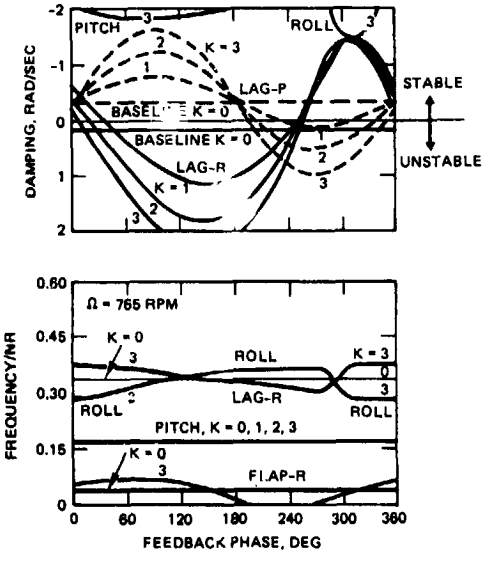

Fig. 9 Modal damping and frequencies versus feedback phase with cosine cyclic lag feedback, ζ_c.

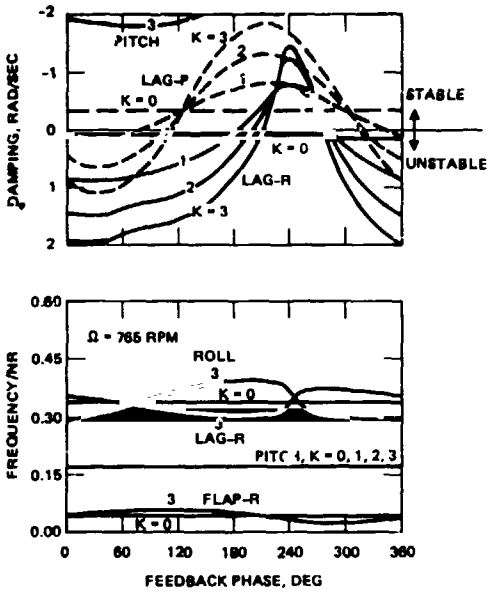

Fig. 10 Modal damping and frequencies versus feedback phase with sine cyclic lag feedback, ζ_s.

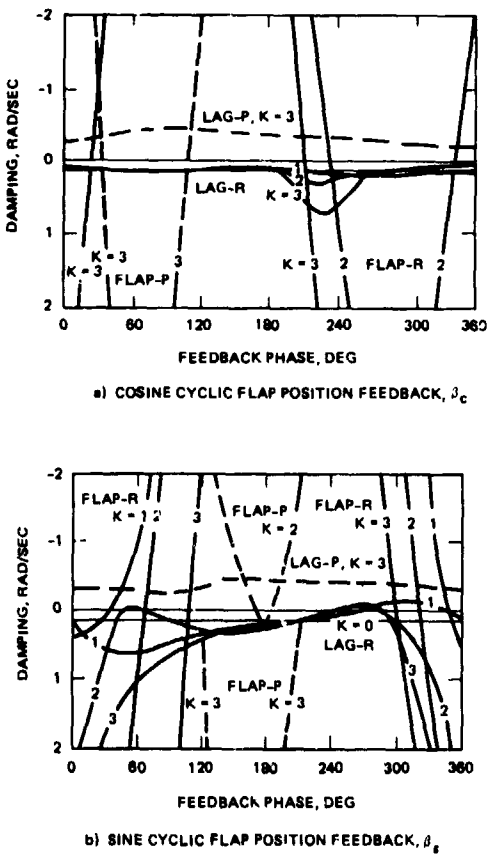

Fig. 11 Modal damping versus feedback phase with cyclic flap position feedback (Ω = 765 rpm).

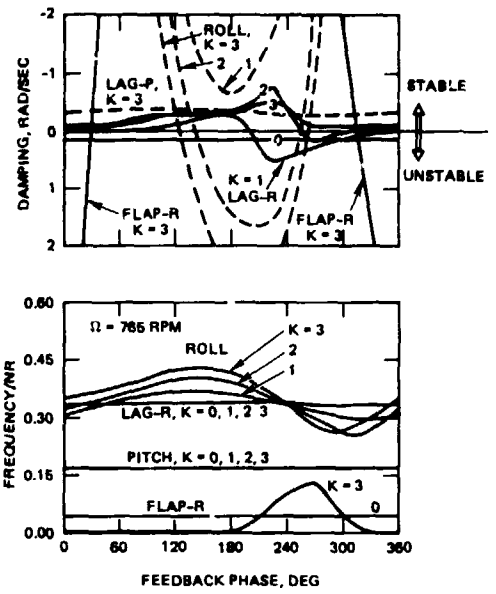

Fig. 12 Modal damping and frequencies versus feedback phase with roll feedback, θ_x.

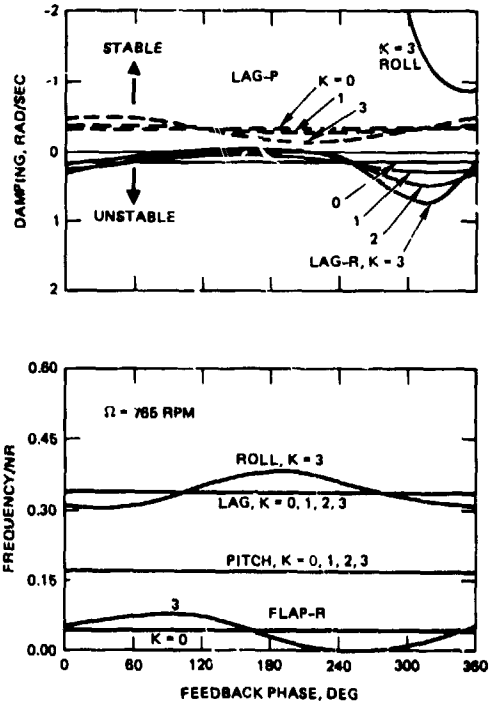

Fig. 13 Modal damping and frequencies versus feedback phase with roll rate feedback, $\dot{\theta}_x$.

can increase damping and stabilize this mode ($250<\phi<30$ deg) or decrease damping and further destabilize it ($30<\phi<250$ deg). The opposite behavior is observed for the progressing lead-lag mode which is stable for K=0. It's damping is decreased for feedback phase between 180 and 360 degrees and increased for feedback phase between 0 and 180 degrees. This makes the progressing lead-lag mode

the least damped mode for feedback phase between 250 and 360 degrees and, depending on the gain value, can result in system instability. Therefore there exists only a small range of feedback phase angles, around ϕ=0, where the rotor/body system could be stabilized through active control. Feedback of ζ_C is therefore not considered to be a suitable choice. Similar findings were made for $\dot{\zeta}_C$ and $\dot{\zeta}_S$ feedback.

Figure 10 shows the influence of sine cyclic lead-lag feedback (ζ_S) on system dynamics. Again, depending on the feedback phase, the damping of the regressing and progressing lead-lag modes can be increased or decreased from the baseline values. This time, however, damping for both modes is increased over approximately the same range of feedback phase values. As a result the system can be stabilized for feedback phase between 220 and 270 degrees. The maximum increase in damping occurs at approximately 240 degrees feedback phase and is directly proportional to the feedback gain. It is seen that ζ_S feedback control changes the roll and regressing lag mode frequencies only to a limited extent. For clarity only the frequencies for the baseline system (K=0) and for K=3, which exhibits the largest frequency changes, are shown. Furthermore, at feedback phase angles of approximately 70 and 240 degrees these modal frequencies remain unchanged for all values of feedback gain. This clearly shows that the improved system stability at ϕ=240 degrees is a direct result of increasing the inherent regressing lag mode damping and not due to a change in coalescence rotor speed. Inspection of the roll mode and its modal damping indicates that the source of the increased lag damping is a reduction in roll mode damping. However, the roll mode is well damped in the baseline system and this exchange of damping is therefore beneficial for overall system stability. Feedback of ζ_S is thus considered to be a suitable candidate for stability augmentation. Similar findings were made for feedback of $\dot{\zeta}_C$ at ϕ=60 degrees and feedback of $\ddot{\zeta}_S$ at ϕ=60 degrees.

The influence of flap feedback states on system damping is shown in Fig. 11 for β_C and β_S feedback. While leading to large changes in damping of the regressing and progressing flap modes, the damping of the regressing lag mode is not improved. This same result was found for all other flap feedback states ($\dot{\beta}_C, \ddot{\beta}_C, \dot{\beta}_S, \ddot{\beta}_S$). Consequently the flap state variables are not further considered for rotor/body damping augmentation.

The effect of roll attitude and rate feedback is shown in Figs. 12 and 13. Again, damping of the regressing and progressing lead-lag mode is increased or decreased depending on the feedback phase. In addition, roll attitude feedback (Fig. 12) can lead to considerable instability of the roll mode and regressing flap mode at certain values of feedback phase. Roll attitude feedback could be used to stabilize the system for feedback phase between 45 and 120 degrees. However, the frequency plot shows that in this range the roll mode frequency is raised considerably. Any gains in system damping at 765 rpm would thus largely be due to a shift of the coalescence rotor speed rather than an increase in inherent regressing lag mode damping. Feedback of roll attitude is therefore not further considered. Feedback of roll rate (Fig. 13) at a feedback phase between 90 and 120 degrees adds damping to the regressing lag mode while keeping the regressing lag and roll mode frequencies almost unchanged. However, the feedback gain would have to be increased to provide adequate system stability margins. On the other hand, too large a gain can result in the same roll and regressing flap mode instabilities found with roll attitude feedback. Similarly, it was found that roll acceleration feedback at a feedback phase between 240 and 270 degrees can stabilize the regressing inplane mode. Thus, both roll rate and acceleration seem to be suitable feedback states and will be studied in more depth.

Feedback of pitch attitude was found to have very little effect on damping of the regressing lead-lag mode. At the same time, damping of the pitch mode and regressing flap mode can be lowered to a point of considerable instability. Results from pitch rate and acceleration feedback also show no change in regressing lag mode damping and, for larger gains, can be expected to exhibit similar pitch mode instabilities as for feedback of pitch attitude. Pitch feedback is therefore not considered a suitable choice for eliminating the regressing lag/roll mode instability considered here.

Summarizing these results for the unstable resonant operating condition of 765 rpm, there exist rotor and fuselage states which can be used in a state feedback control approach to stabilize the entire system. The states most suitable for stability augmentation are $\dot{\zeta}_C, \zeta_S, \ddot{\zeta}_S, \dot{\theta}_X$ and $\ddot{\theta}_X$.

Based on the above results, feedback of ζ_S and $\dot{\theta}_X$ are further evaluated in Figs. 14 and 15 by considering rotor rpm sweeps and varying the gain K while keeping the feedback phase ϕ constant. The value of ϕ was chosen as the phase yielding the greatest stability augmentation at 765 rpm. The feedback results for ζ_S and $\dot{\theta}_X$ are representative of the damping augmentation results that can be obtained with $\dot{\zeta}_C$ and $\ddot{\zeta}_S$ and with $\ddot{\theta}_X$, respectively. In selecting the gains K, an attempt was made to obtain approximately the same range of regressing lag mode damping values for both feedback states. In both cases the system can be stabilized at all previously critical rotor speeds, although to a lesser degree with roll rate feedback. For clarity only the regressing lag mode damping, which governs system stability, is shown in Figs. 14 and 15. Feedback of the lead-lag state ζ_S, Fig. 14, adds considerable damping to the regressing lag mode above 700 rpm and stabilizes the system. System frequencies have been changed, particularly at the coalescence rotor speed. However much smaller feedback gains (K<.5), which would adequately stabilize the system, were found to have little effect on the system frequencies. At the crossover of the regressing lag mode with the body pitch mode (600 rpm) this feedback control can destabilize the system, depending on the value of feedback gain. Feedback of roll rate, Fig. 15, also augments the damping of the regressing lag mode above 700 rpm and could be used to stabilize the system. Roll rate feedback has no effect on the regressing lag mode damping at coalescence with the pitch mode. This is consistent with the previous observation that pitch feedback is not suitable to eliminate the coupled regressing lag/roll mode instability. It is further interesting to note that feedback of the body roll rate (and roll acceleration also) leads to considerable shifts in the frequency of the roll mode and therefore changes the coalescence

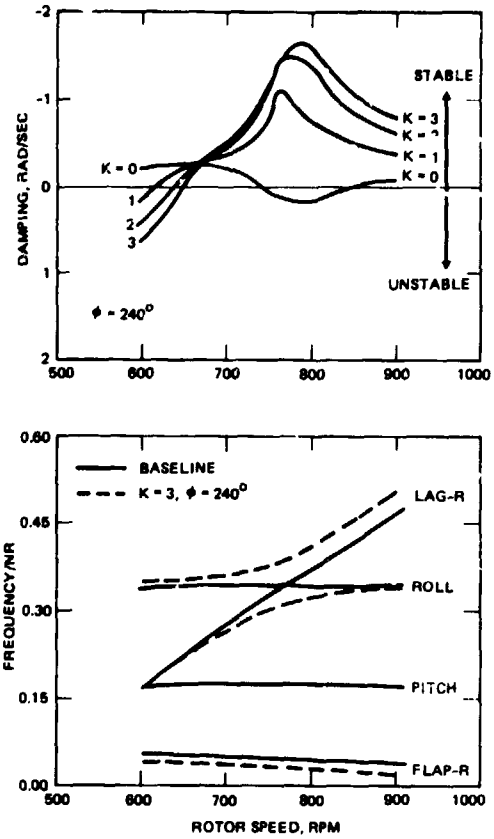

Fig. 14 Effect of sine cyclic lag (ζ_S) feedback gain on modal frequencies and regressing lag mode damping versus rotor speed.

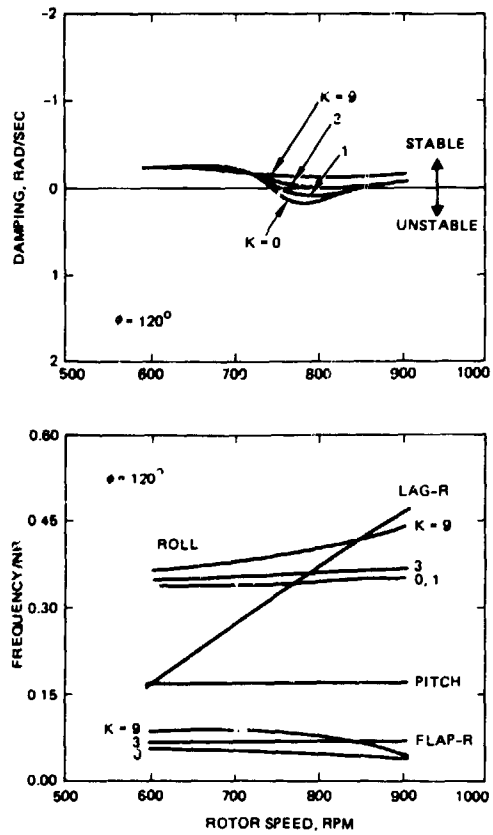

Fig. 15 Effect of roll rate ($\dot{\theta}_x$) feedback gain on modal frequencies and regressing lag mode damping versus rotor speed.

rotor speed. The stability gains seen in Fig. 15 are thus attributable to a combination of increased inherent damping and frequency shifts.

The sensitivity of the system dynamic behavior with respect to the feedback phase is explored in Figs. 16 and 17 for feedback of ζ_S and $\dot{\theta}_x$, respectively. In each case, three phase angles near the previously observed optimum value were chosen while the gain was kept at a particular value representing approximately similar control effort in terms of active blade pitch angle amplitudes. These values were determined from response studies to be K=0.3 and 9.0, for ζ_S and $\dot{\theta}_x$ feedback, respectively. For clarity only damping curves for the regressing lag mode are shown. Again, feedback of ζ_S for the gain K=0.3 keeps the system frequencies unchanged. Damping results show that feedback phase can be used to maximize the regressing lag mode damping at each rotor speed. This indicates that a phase schedule with rpm could be used. Feedback of the roll rate, Fig. 17, leads to roll mode frequency changes. However, the system is stable at the new coalescence rotor speed which means that innerent damping has been added to the regressing lag mode. Furthermore, while the feedback phase has little effect on system damping it is seen to be a powerful parameter for changing the roll mode frequency.

In summary, these results show that the feedback gain K can be varied to obtain a specified level of regressing lag mode damping at the coalescence rotor speed. The feedback phase ϕ can then be used to maximize the regressing lag mode damping augmentation at other rotor speeds or change the roll mode frequency which indirectly changes the regressing lag mode damping. Results also show that a different choice of feedback state variables and control parameters (K,ϕ) would be needed to eliminate an inplane/pitch instability. Quantitative results are given in Table 2. For ζ_c,ζ_s,ζ_s, and θ_x feedback about 1 percent of critical damping is introduced for the regressing lag mode at a maximum active blade pitch angle, θ_{Amax}, of approximately one third degree for a cyclic lead-lag amplitude of one degree. For $\ddot{\theta}x$ about 1.5 percent of critical damping is introduced with the same control angle. The control angles shown in Table 2 are quite small in particular when considering the low frequency of the control motion. These results are very promising. They indicate that several ways exist to augment rotor/body stability. The important aspect of control mechanization can thus be approached with considerable flexibility.

Effects of Rotor Configuration

Very important rotor parameters in terms of control effectiveness are the blade root hinge

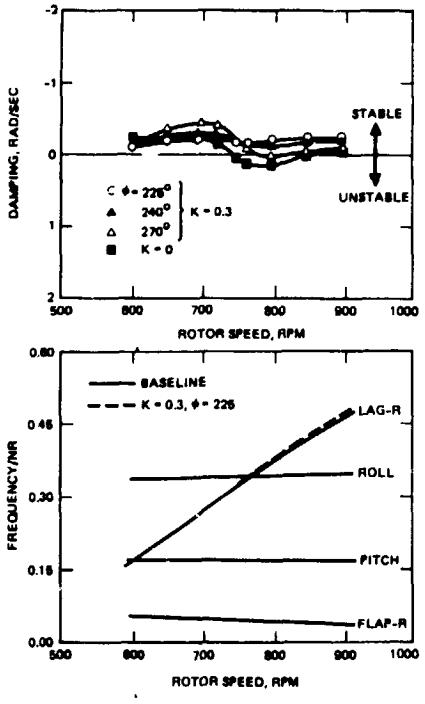

Fig. 16 Effect of sine cyclic lag (ζ_s) feedback phase on modal frequencies and regressing lag mode damping versus rotor speed.

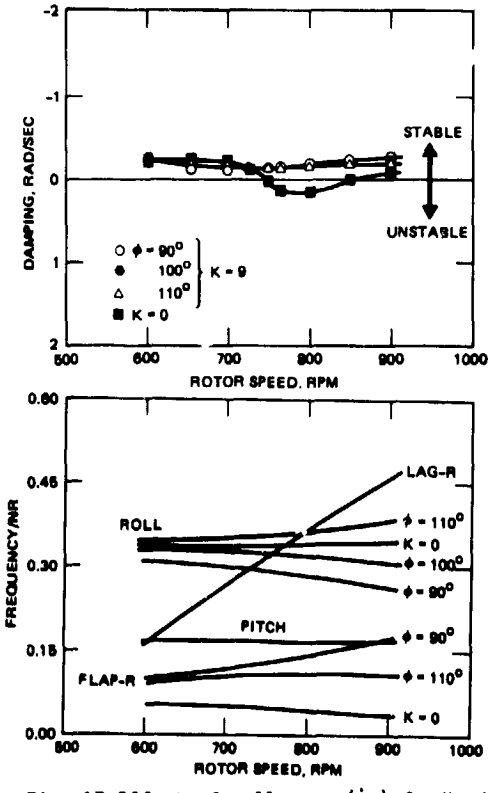

Fig. 17 Effect of roll rate ($\dot{\theta}_x$) feedback phase on modal frequencies and regressing lag mode damping versus rotor speed.

Table 2. Summary of state feedback results (Ω = 765 rpm)

Feedback State	K	ϕ deg	σ rad/sec	η % critical	θ_{Amax} deg
Baseline	0	-	0.145	-0.58	-
$\dot{\zeta}_c$	1	60	-0.164	0.65	0.32
ζ_s	.3	240	-0.137	0.54	0.29
$\dot{\zeta}_s$	3	60	-0.178	0.71	0.34
$\dot{\theta}_x$	9	90	-0.149	0.59	0.33
$\ddot{\theta}_x$	27	270	-0.284	1.13	0.39

offset, precone, and flap spring stiffness. These parameters were varied from their baseline values (Table 1) to cover a range of values representative of articulated, hingeless, and bearingless rotors. At the same time the blade root spring stiffnesses, lead-lag damping and body roll stiffness were changed so that the modified rotor/body systems would closely approximate the baseline system dynamics, i.e. have the same coalescence rotor speed, roll frequency, and regressing lag mode frequency and damping. Thus, without application of active control (K=0), all the rotor configurations studied in this section exhibit the same instability at 765 rpm with η = -.58% critical as the baseline system (Table 2).

Investigation of active control with different rotor design parameters is limited to feedback of the sine cyclic lead-lag position (ζ_s) and roll acceleration ($\ddot{\theta}x$) state variables. For these two feedback states, the baseline configuration optimal feedback phase angles and feedback gain levels were used. Tables 3, 4, and 5 list the resulting system damping values for the three rotor parameter variations. Results for the various root hinge offsets (Table 3) and precone angles (Table 4) are obtained by keeping the active blade feathering angles constant (θ_{Amax} = 0.29 degrees for ζ_s feedback, approximately 0.4 degrees $\ddot{\theta}x$ feedback). It is seen that the system is stabilized for all the different rotor hub configurations. Increases in hinge offset increase the damping levels even though the flapping frequency is reduced. Similarly, increases in precone angle increase the damping levels. When reducing the flap spring stiffness to zero (Table 5), larger active blade feathering angles (~2 degrees) are required to obtain stability margins of approximately 0.5 percent critical damping. It should be pointed out, however, that typical articulated rotors have hinge offsets larger than the configurations in Table 5.

These results, while being of a limited nature, show that the root hinge offset, precone, and flap spring stiffness, have considerable influence on the active feedback control effectiveness. This was anticipated due to the action of hub moments and Coriolis coupling. It can be concluded that active control for rotor/body damping augmentation will be particularly powerful for hingeless and bearingless rotors which typically have a large virtual hinge offset and flap spring stiffness and in many cases also precone. Controlling the aeromechanical stability of typical articulated rotors will be a more difficult task. For these rotors it may be helpful to use collective blade pitch to introduce additional steady blade coning deflection.

Table 3. Effect of hinge offset on feedback results, equivalent dynamic systems (Ω = 765 rpm)

$\bar{e}$	σ rad/sec	η* % critical	θ_{Amax} deg	Feedback State	K	φ deg
0.10	-0.137	0.54	0.29	ζ_s	0.3	240
0.05	-0.097	0.38	0.29	ζ_s	0.3	240
0.02	-0.077	0.31	0.29	ζ_s	0.3	240
0.10	-0.284	1.13	0.39	$\ddot{\theta}_x$	27	270
0.05	-0.158	0.63	0.45	$\ddot{\theta}_x$	27	270
0.02	-0.119	0.47	0.37	$\ddot{\theta}_x$	27	270

Table 4. Effect of precone on feedback results, equivalent dynamic systems (Ω = 765 rpm, $\bar{e}$ = 0.02)

β_p deg	σ rad/sec	η* % critical	θ_{Amax} deg	Feedback State	K	φ deg
0	-0.077	0.31	0.29	ζ_s	0.3	240
2	-0.116	0.46	0.29	ζ_s	0.3	240
4	-0.157	0.62	0.29	ζ_s	0.3	240
0	-0.119	0.47	0.37	$\ddot{\theta}_x$	27	270
2	-0.288	1.14	0.43	$\ddot{\theta}_x$	27	270
4	-0.507	2.01	0.50	$\ddot{\theta}_x$	27	270

Table 5. Effect of flap stiffness on feedback results, equivalent dynamic systems (Ω = 765 rpm, $\bar{e}$ = 0.02)

Flap Stiffness N-m	σ rad/sec	η* % critical	θ_{Amax} deg	Feedback State	K	φ deg
38.8	-0.077	0.31	0.29	ζ_s	0.3	240
19.4	-0.181	0.71	1.00	ζ_s	1.0	240
0	-0.132	0.52	1.83	ζ_s	2.0	225
38.8	-0.119	0.47	0.37	$\ddot{\theta}_x$	27	270
19.4	-0.232	0.91	1.17	$\ddot{\theta}_x$	27	270
0	-0.334	0.36	2.41	$\ddot{\theta}_x$	27	225

*Without active control (K=0) system damping is η = -0.58% critical for all rotor configurations.

This should have similar beneficial effects on control effectiveness as would introducing blade precone angle.

Rotor Response

Response results are intended to be of a qualitative nature, to give a better understanding of the rotor/body motion and give an indication of the required control input magnitudes.

Free response from a set of prescribed initial conditions and frequency response results are presented. The free response results, Fig. 18, are computed using the regressing lead-lag eigenvector from the stability analysis, normalized to a maximum lead-lag amplitude of one degree, as an initial condition. Figure 18a shows the response of the system with no feedback controls applied. The regressing lag mode is slightly unstable, with critical damping of η = -0.58%. Its modal components consist largely of the cyclic lead-lag motions (ζ_c,ζ_s), the body roll degree of freedom (θ_x), and lateral cyclic flapping (β_s). There is very little pitch and longitudinal flap motion. The inherent stability of the rotor/body system with sine cyclic lead-lag feedback control at K=1 and φ = 240 degrees is illustrated in Fig. 18b. The time history response of the regressing lag mode shows that with feedback this previously unstable mode is stabilized and both cyclic lead-lag degrees of freedom, ζ_c and ζ_s, reduce significantly in amplitude in only ten rotor revolutions. It is also seen that feedback control increases the participation of the flap and body pitch and roll motions in the regressing lag mode. This could be one source of the increased damping of this mode. The amplitude of the active blade feathering in Fig. 18b is 0.9 degrees initially and reduces to less than 0.5 degrees over ten rotor revolutions.

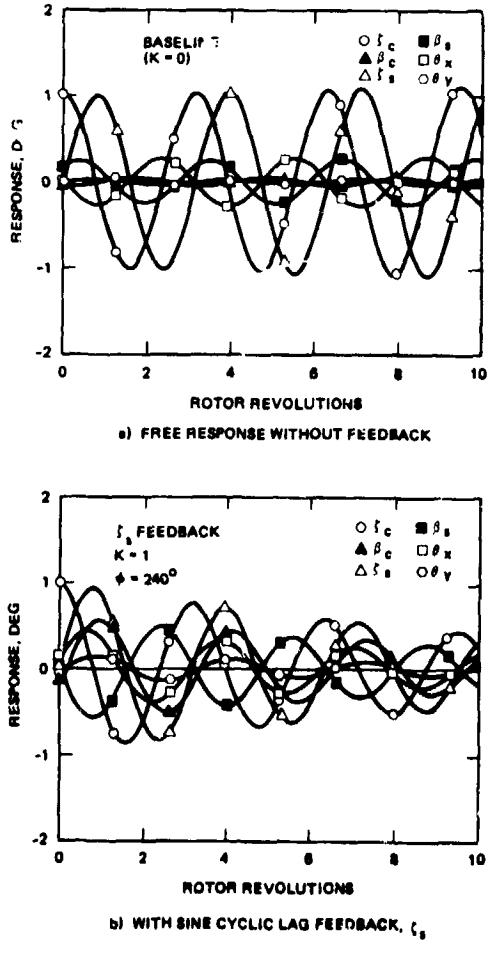

Fig. 18 System response using regressing lead-lag eigenvector from stability analysis as initial condition.

Frequency response analysis is used to compare the effect of increased blade lead-lag damping with the application of feedback control. Frequency response was computed by simulating a one degree blade pitch stick stir in the regressing direction. For frequency response the nondimensional excitation frequency is varied from 0.1 to 0.7. Rotor rotation rate is 765 rpm. Fig. 19 shows the influence of increasing the lead-lag damping from η_ζ = 0.52 percent to 2 percent and 8 percent critical. No feedback controls are applied. Fig. 20 shows, in the same manner, the influence of ζ_s feedback with increasing gain values, K = 0.3; 1.0, 3.0, and ϕ = 240 degrees. Here the damping is held at its nominal value of η_ζ = 0.52 percent. In both Fig. 19 and Fig. 20 only the frequency response of the cosine cyclic lead-lag motion is shown. Comparing both magnitude and phase plots qualitatively, it is seen that feedback control and additional blade damping have very similar effects in terms of system dynamics. This is an additional indication that active control can be used to augment rotor/body damping and reduce or possibly even eliminate the need for lead-lag dampers for articulated rotor systems.

Conclusions

This study shows that active control blade feathering through a conventional swashplate is a viable means to increase rotor/body damping levels and to eliminate ground resonance instabilities. Stability and response results have been presented using state variable feedback control for a model hingeless rotor. From these results, the following conclusions can be drawn.

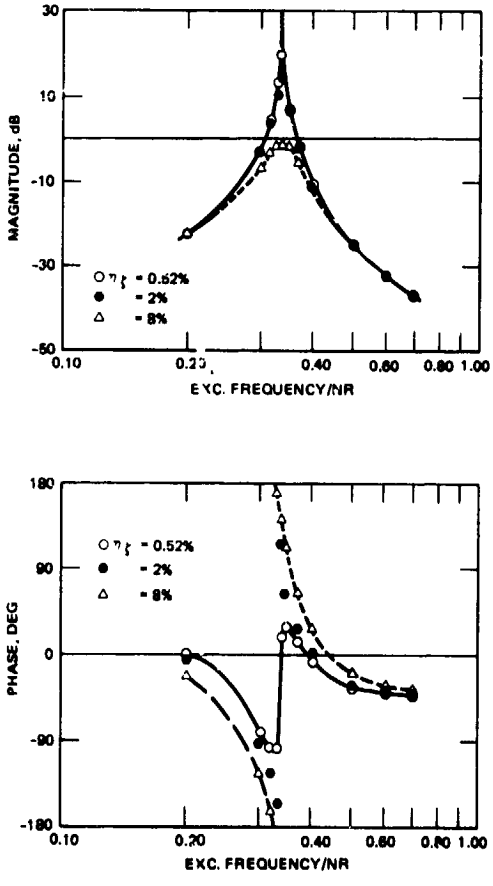

Fig. 19 Effect of blade lead-lag damping on frequency response of cosine cyclic lag motion, no feedback applied, (K=0).

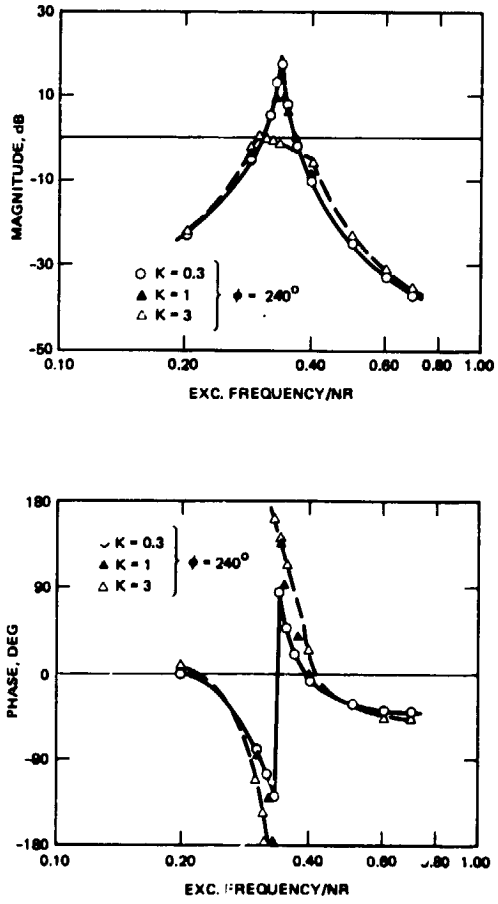

Fig. 20 Effect of sine cyclic lag (ζ_s) feedback gain on frequency response of cosine cyclic lag motion; (η_ζ = 0.52%).

1) Either rotor or fuselage states can be used to eliminate ground resonance instabilities by specifying appropriate closed-loop feedback phase and gain.

2) With the proper choice of feedback phase, damping of the regressing lag mode can be maximized without adversely affecting the damping of other system modes. The feedback gain K can then be adjusted to obtain a specified level of regressing lag mode damping at the coalescence rotor speed.

3) Approximately a one percent augmentation in critical damping in the regressing lead-lag mode can be obtained with an active blade feathering amplitude of 0.3 degree per degree of blade cyclic lead-lag motion.

4) Increased lead-lag damping with active control is due to several factors: (1) a reduction in damping of other, more highly damped system modes, and (2) an increased participation by other

system modes in the motion characterizing the regressing inplane mode.

5) System stability improvements can be a direct result of increased regressing lead-lag mode damping since system frequencies, and in particular the coalescence rotor speed, remain unchanged.

6) Rotor rpm sweeps show that with the feedback controls selected at the coalescence rotor speed, the system is stabilized throughout the range of previously unstable operating conditions. Furthermore, scheduling the feedback phase with rotor speed can be used to maximize the damping augmentation.

7) For roll feedback ($\dot{\theta}x$,$\ddot{\theta}x$) the feedback phase has a considerable effect on the roll mode frequency. Besides increasing the regressing lag mode damping, roll acceleration feedback in particular can be designed to shift the coalescence rotor speed. This would indirectly improve system stability through active control of frequency placement.

8) A different choice of feedback state variables and control parameters would be necessary to eliminate an inplane/pitch instability. For the present configuration the active controls should be applied only at rotor speeds above the crossover of the regressing lag mode with the body pitch mode.

9) Increasing the root hinge offset, flap spring stiffness, and blade precone improves the control effectiveness considerably. Active control for rotor/body damping augmentation will be particularly powerful for hingeless and bearingless rotors. Controlling the aeromechanical stability of articulated rotors will be a more difficult task.

References

1. Wood, E.R.; Powers, R.W.; Cline, J.H. and Hammond, C.E., "On Developing and Flight Testing a Higher Harmonic Control System," Proc. 39th AHS Forum, St. Louis, Missouri, May 1983, pp. 592-612.

2. Young, M.I.; Bailey, D.J., and Hirschbein, M.S., "Open and Closed Loop Stability of Hingeless Rotor Helicopter Air and Ground Resonance," Paper No. 20, NASA SP-352, 1974, pp. 205-218.

3. Ham, N.D.; Behal, B.L., and McKillip, R.M., "A Simple System for Helicopter Individual-Blade-Control and its Application to Lag Damping Augmentation," Paper No. 10.2, 8th European Rotorcraft Forum, France, 1982.

4. Peebles, J.H., "Optimal Control of a Helicopter Rotor in Hover," M.S. Thesis, George Washington University, Washington, D.C., November 1977.

5. Bousman, W.G., "An Experimental Investigation of the Effects of Aeroelastic Couplings on Aeromechanical Stability of a Hingeless Rotor Helicopter," Proceedings of the 36th Annual American Helicopter Society Forum, Paper No. 80-25, Washington, D.C., May 1980.

6. Straub, F.K., "Study to Eliminate Ground Resonance Using Active Controls," NASA CR to be published 1984.

7. Ormiston, R.A., "Aeromechanical Stability of Soft Inplane Hingeless Rotor Helicopters," Paper No. 25, Proceedings of the 3rd European Rotorcraft Forum, Aix-en-Provence, France, September 1977.

8. Friedmann, P.P., and Venkatesan, C., "Comparison of Experimental Coupled Helicopter Rotor/Body Stability Results With a Simple Analytical Model," Journal of Aircraft, Vol. 21, No. 11, November 1984.

9. Johnson, W., "Influence of Unsteady Aerodynamics on Hingeless Rotor Ground Resonance," Journal of Aircraft, Vol. 19, No. 8, August 1982, pp. 668-673.

10. Banerjee, D.B. and Johnston, J.A., "Integrated Technology Rotor Methodology Assessment," Hughes Helicopters, Inc., Report, November 1981.

THE USE OF ACTIVE CONTROLS TO ENHANCE ROTOR/FUSELAGE STABILITY
Friedrich Straub

William Warmbrodt

Evan Hooper, Boeing Vertol: I would like to congraculate you on an outstanding contribution. In the practical ground resonance case, of course, you are concerned not just with sitting simply on the ground, but with frequencies that cover a wide range of situations from blown tires to incorrectly inflated oleos to [where you become] airborne and all your natural frequencies will go from ground [values] approaching zero. So you have to prepare for a wide range of situations. Have you looked at the applications of this system to practical takeoff situations?

Straub: No, I haven't looked at takeoff situations at all so far. Lately, I have considered some cases where the fuselage mass was varied widely to simulate different payload configurations. Actually what I saw was that even with one set of controls you can handle that kind of situation. I have not looked at what happens when you increase the collective pitch angle and simulate takeoff. That would certainly be something to look into.

Bob Blackwell, Sikorsky Aircraft: I also enjoyed your paper and look forward to reading it. I have two questions. First, would you comment on the kind of design philosophy that would allow this approach in lieu of frequency placement and conventional damping--is it more weight effective, or perhaps a means of controlling ground resonance? Second, have you given thought to the instrumentation to measure the lead-lag motion of all the blades or is that not necessary and so what kind of redundancy requirements would be required of a potential system?

Straub: Well, first, the idea is to eventually replace maybe the lead-lag dampers on some of our articulated rotors and that seems to be a feasible alternative. As far as the implementation is concerned the results I presented here were mostly for the feedback of the lead-lag motion; I think that the first choice of the designer is to use a fixed system feedback--either the roll or pitch degrees of freedom. I think it would be possible to do that rather than use the inplane motion. What I did here was to consider feedback of all degrees of freedom and their time derivatives just to see how good different feedback states would be. So the argument of how the control parameters were chosen was most easily illustrated here for the inplane model feedback, but roll would be just as good.

Dave Peters, Washington University: You know when there is no initial lift on the rotor and then you plot the lift versus angle of attack it's not linear. It starts off flat and builds up. There is no mass flow to build your lift up. And this means you make small changes in pitch angle you don't get much effectiveness in terms of force. How do you think that would affect your idea when you try to stabilize ground resonance at zero lift conditions?

Straub: That is a very good question. I am not sure I have an answer to it at this moment. Certainly as you point out it is a very valid concern and also the aerodynamic model that I have used is very simple. That probably could use some improvement too. For instance, what effects do unsteady aerodynamics have on this kind of phenomena because you are oscillating the blade at half per rev or something like that. Even though it is a much lower frequency than vibration control at 4 per rev, still the aerodynamics would definitely be something to look into further.

Dick Gabel, Boeing Vertol: In these days when we deal with ground resonance qualification we have to meet failure conditions of everything--the oleos, tires, lag dampers, everything. Can you foresee with such a system if you have to accommodate failures, what the approach would be if the system was off and you were in ground resonance? That could be a disaster.

Straub: That is certainly true, but I think that in any kind of fly-by-light or fly-by-wire control system for the primary controls you deal with these same kinds of issues. Your actuators have to be redundant; you have to be able to deal with failures. So certainly that would also apply if you use active controls to replace some lead-lag dampers. You would have to have multiple sensors and you would have to have a fail-safe operating mode.

Walter Gerstenberger, Consultant: Blackwell's question and Gabel's question were well taken so I'll ask the follow-on question. We always try to couple lag motion with flapping motion or something; with inclined hinges. How would you design the mechanical system to accomplish the [feedback] that does these wonderful things that you say. Have you thought about that? In other words doing it mechanically by coupling; measuring lag motion and feeding it into your cyclic pitch with a phase shift?

Straub: Well, you can add some roll accelerometers.

Gerstenberger: No, not electronically--mechanically.

Straub: How to do it mechanically?

Gerstenberger: Whiffle trees, mixing bars . . .

Straub: I think maybe a better way of doing that would be something that you just mentioned--inclined pitch links and other kinds of kinematic couplings that are designed into the blade root end. Maybe I should add one thought we had when we did this [paper]. Obviously, when you design a helicopter you make use of all the available methods to make it as stable as you can to begin with. But then if you talk about a situation where you have a fly-by-wire control system, you already have dynamic actuators on there for the vibration reduction, then it could be very nice just to put an additional sensor on the helicopter--if required at all--and to put an additional board into your controller and have a way of augmenting the rotor fuselage damping.

Gerstenberger: Well, let me rephrase the question. I don't like you to sell me electronic control, but that's not the point. Is your feedback--I don't understand the feedback completely--is the feedback simple enough so that it is possible to design some pure mechanical feedback to give you stability which nobody has been able to do in the past with a mechanical tilting of a hinge or something like that?

Straub: Well, I haven't really thought about it too much. I would suppose you could probably do it if you look at some of the early work that Bell had done on active control for the 2P control. They had a mechanical control system on there and I think the amount of linkages they had there was probably somewhat forbidding. I don't know.

GROUND RESONANCE ANALYSIS USING A SUBSTRUCTURE MODELING APPROACH

Shyi-Yaung Chen
Senior Research Engineer
Kaman Aerospace Corporation
Bloomfield, Connecticut

Edward E. Austin
Aerospace Engineer
Applied Technology Laboratory
Ft. Eustis, Virginia

Alex Berman
Assistant Director for Research
Kaman Aerospace Corporation
Bloomfield, Connecticut

Abstract

A convenient and versatile procedure for modeling and analyzing ground resonance phenomena is described and illustrated. A computer program is used which dynamically couples differential equations with nonlinear and time dependent coefficients. Each set of differential equations may represent a component such as a rotor, fuselage, landing gear, or a failed damper. Arbitrary combinations of such components may be formulated into a model of a system. When the coupled equations are formed, a procedure is executed which uses a Floquet analysis to determine the stability of the system. Illustrations of the use of the procedures along with the numerical examples are presented.

Introduction

The mechanical instability due to the interaction of helicopter rotor and fuselage, commonly known as ground resonance, is a very important consideration in the design of rotorcraft. The classical analysis of this phenomenon by Coleman and Feingold[1] still forms the basis for many of the analyses performed at the present time. The evaluation of the mechanical stability characteristics of nonisotropic rotors, as may be due to a component malfunction or combat damage, cannot readily be determined by these techniques.

The Floquet transition matrix analysis was applied to lifting rotor stability by Peters and Hohenemser[2] and was shown to be a powerful tool for determining the stability of periodic systems. In 1974, Hammond[3] applied this technique to analyze the effect of an inoperative blade damper on ground resonance. In this analysis each rigid hinged blade is a separate dynamic entity and thus may have completely independent parameters. There are no limitations on isotropy of either the rotor or fuselage. The results of this study were quite revealing and demonstrated that certain other approaches to this problem were not completely satisfactory. Lengthy time integration procedures were shown to be difficult to interpret and a common approximation which averages the damping loss over the blades may be very nonconservative.

The Floquet theory has the general capability to determine the stability of any helicopter configuration, regardless of the number of blades, type of retention, blade positioning, number of rotors, fuselage flexibility, landing gear characteristics, ground characteristics (e.g., ice), damage to blades (mass, damping, stiffness) or landing gear, and the physical arrangement of rotors and other components. Given the periodic equations of motion, the stability may be determined.

A difficulty in this process is the determination of the equations of motion of a complex configuration. One possibility is to derive the equations for a specific physical system and write a program to evaluate the numerical coefficients. Another scheme would be to derive the equations for a complex system which includes options to allow the modeling of a broad range of configurations. Either of these tasks would be extensive and the future analysis of a configuration not previously provided for would involve a great deal of effort.

The purpose of this paper is to describe a procedure which provides a convenient means of assembling the equations of motion for a large variety of rotorcraft configurations prior to invoking a Floquet analysis. Illustrations of several applications are presented.

The Model Concept

The complete dynamic system to be analyzed is called a "model." A model is described as a coupled set of "components." Each component is considered to

Presented at the Rotorcraft Dynamics Specialists' Meeting, Moffett Field, CA, November 7-9, 1984

be represented by a set of second order differential equations of the form

$$M\ddot{X} + C\dot{X} + KX = F \tag{1}$$

where M, C, K, F are mass, damping, stiffness matrices, and a force vector. X is a vector of the displacements of the degrees of freedom. In the implementation to be described all matrix coefficients may be functions of time and the state vector. The degrees of freedom may be of any generalized form as long as the coupling to other components may be described as linear relationships between the degrees of freedom of the components.

The equations of the model formed from a set of components are of precisely of the same form as Eq. (1) where

$$\begin{aligned} M &= \sum T_I^T M_I T_I \\ C &= \sum T_I^T C_I T_I \\ K &= \sum T_I^T K_I T_I \\ F &= \sum T_I^T F_I \end{aligned} \tag{2}$$

and where the subscript I refers to the I^{th} component. The transformation matrix T_I is time invariant and relates the degrees of freedom of component I to the degrees of freedom of the model:

$$X_I = T_I X \tag{3}$$

This transformation is identical to that of Hurty[4], but is used to couple any generalized coordinates and it is recognized that the coefficients in Eq. (2) need not be constant.

Computer Implementation

A convenient implementation of this concept is described in References 5 and 6. This program (DYSCO) has three main features: 1) a "technology library" which includes various component representations ("technology modules"); 2) a "data library" which contains specific sets of data to be used by the technology modules to compute the equation coefficients; and 3) the capability to automatically form the transformation matrices and to compute the equations of motion of any assembly of components (a "model").

The main advantage to the user is that he may obtain (and solve) the numerical equations of any combination of components with no mathematical deviation. Another advantage is that he may select the most appropriate mathematical representation for each component.

The remainder of this section is a brief description of the features of the program relevant to ground resonance analysis.

The Technology Library

Included in the technology library are various representations of component equations. These modules are given a four character name, each starting with the letter "C." Those relevant to this study are briefly summarized.

CRR2 - Rigid rotor. Up to nine rigid hinged blades with optional flap, lag, pitch degrees of freedom (rotating system). Up to six degrees of freedom of the hub (fixed system). Data required includes: specification of degree of freedom options; radius, offset, spring and damper rates; and all necessary mass parameters. Up to four rotors may be included in any model.

CFM2 - Fuselage, modal. Up to six rigid body and six coupled elastic modes. Automatic coupling to rotor hub(s) and degrees of freedom of other components. Data required includes: degree of freedom options; locations of c.g., rotor(s), attachments to other components, mode shapes, all necessary mass and inertia parameters and modal frequency and damping. Up to four of these components may be included in any model.

CSF1 - Structure, finite element. Constant M, C, K, F model. Up to 40 degrees of freedom. Data required includes: degree of freedom names and the coefficient matrices. This module may represent a fairly complex structure or a single spring. Any number of these components may be used in a model (maximum number of components in a model is 20).

CLC1 - Linear constraint. Allows the user to specify any linear relationships between degrees of freedom.

In addition to the component technology modules, the library contains solution algorithms which may be invoked after the equations are formed. The solution modules names start with "S." Several of interest are:

SSF3 - Stability, Floquet. This solution module uses periodic shooting to find the initial conditions which may lead to periodic equilibrium condition for a linear or nonlinear model equation under specified control conditions. It then perturbs about the equilibrium state to form the Floquet transition matrix and

performs eigenanalysis to determine stability of the system. Data required includes: period of integration, initial integration increment, parameters for accuracy test of integration.

STH3 - Time History. Performs a time history integration on the model equations. Data required includes: length of solution, integration increment, initial conditions.

SEA4 - Eigenanalysis. Performs an eigenanalysis on the constant M, K matrices of the model.

The Data Library

The data library contains data to be used in the formation of the model equations. When the data is input, it is automatically assigned a "data member" name (DM) which is the name of the technology module with which it is to be used. Also, an arbitrary "data set" name (DS) is supplied by the user. A data unit is uniquely identified by its DS/DM name.

A particular physical component is represented by the name of the component technology module and the DS name of the data, e.g.,

CRR2 ROT1

where the user had previously identified a set of input for CRR2 as "ROT1."

The data library contains other data member types. One is the DM = MODEL which contains a definition of a model including component names and associated data set names. The data set name is a "model name" supplied by the user. The model definition is described below.

Model Definition

The user may formulate a model by specifying the component module names and the appropriate data set names which have been included in the libraries. For some components a rotor or structure number is required. A sample model may appear as shown in Fig. 1.

MODEL TEST I

INDEX	COMP	NO.	DATA SET
1	CFM2	1	FUSELAGE
2	CSF1		PAYLOAD
3	CRR2	1	MAINROT
4	CSF1		MAINGEAR
5	CSF1		TAILGEAR
6	CRR2	2	TAILROT
7	CSF1		VIBABS

Fig. 1. Example of a model definition.

Models may be conveniently edited to delete, replace, insert, and add components.

RUN Command

The program is command driven (See Reference 6 for details). The command "RUN" causes the program to perform the following sequence of operations.

1) User is requested for the name of the model.

2) Model definition is retrieved from data library.

3) Each component module and data set is accessed to define degrees of freedom.

4) Transformation matrices are formed.

5) Each component module is accessed to form equation coefficients.

6) Coefficient matrices are transformed to system equations.

During this process, data is validated for existence and uniqueness and access is provided for computation of nonconstant coefficients.

After step 6, the user has options to print certain model details, such as degrees of freedom and constant system matrices. At the completion of the RUN command the user is requested to name a solution module to be executed.

Coupling

The coupling is carried out by an automatic procedure in which the names of the degrees of freedom are recognized and processed by the program. The degree of freedom names consist of two FORTRAN words, formatted A4, I4. Certain names are automatically formed, as for example

ZETA2300

which is interpreted as: lag angle, rotor 2, blade 3.

When the program recognizes the same name in more than one component, these degrees of freedom are automatically joined. Linear relationships between degrees of freedom are also automatically processed into the transformation matrices (See Reference 5).

As a simple illustration of an application of this coupling procedure to model a failed lag damper, consider a model which includes a rotor with lag dampers

whose damping rates have been input as the numeric quantity, c. In order to represent a failed damper, the model is edited to add the following component.

CSF1 FAILDAMP

where the data set FAILDAMP contains the following information.

number of degrees of freedom = 1

name of degree of freedom = ZETA1100

M, K, F = null

C = -c

The addition of this component represents the addition of a negative damper on blade 1 of rotor 1 which cancels the original damping rate. No further action is required of the user except to execute the command RUN.

Examples and Discussions

In order to demonstrate the concepts described, several analyses have been performed which include: 1) comparison with the results of Hammond[3]; 2) Validation of a reduced model; 3) Coaxial rotor configuration; 4) Tandem rotor configuration. Throughout this study, the same rotor parameters are used which are based on the data of Reference 3. The parameters may not be realistic, but are used to illustrate the procedures described.

Table 1. Rotor parameters.

Number of blades	4	
Blade mass	6.5	slugs
Blade mass moment	65	slug-ft
Blade mass moment of inertia	800	slug-ft^2
Lag hinge offset	1	ft
Lag spring	0.0	ft-lb/rad
Lag damper	3000	ft-lb-sec/rad

It is noted that in the rotor component the blade degrees of freedom are in rotating system and hub degrees of freedom are in the nonrotating system. In the fuselage module components, all the degrees of freedom are in nonrotating system. Note also that the damaged blade is always referred to as blade 1.

The components used in this study, their associated data set names, and their characteristics are described as follows. They are used in various combinations in the examples below.

1) CRR2, ROTOR1 - 4 blades, inplane degrees of freedom (ZETA1100, ZETA1200, ZETA1300, ZETA1400), 2 hub translational degrees of freedom (XHUB1000, YHUB1000), counterclockwise rotation, various rotational speeds, 6 degrees of freedom (DOF).

2) CRR2, ROTOR2 - Same as 1) but clockwise rotation and DOF names are ZETA2100, ZETA2200, ZETA2300, ZETA2400, XHUB2000, YHUB2000.

3) CFM2, FUSELAGE - 5 rigid body modes (XCG 1000, YCG 1000, ROLL1000, PTCH1000, YAW 1000), automatically couples to rotor 1 and rotor 2, mass = 10000 lb., roll and pitch moments of inertia = 10000, 15000 slug-ft^2.

4) CLC1, REDUCE1 - Couples blades 2, 4 (ZETA1200 = -ZETA1400) and blade 1, 3 (ZETA1100 = -ZETA1300) of rotor 1.

5) CLC1, REDUCE2 - Couples blade 2, 4 (ZETA2200 = -ZETA2400) and blade 1, 3 (ZETA2100 = -ZETA1200) of rotor 2.

6) CLC1, RED124 - Couples blade 2, 4 (ZETA1200 = -ZETA1400) of rotor 1.

7) CLC1, RED224 - Couples blade 2, 4 (ZETA2200 = -ZETA2400) of rotor 2.

8) CLC1, COAX - Couples hub degrees of freedom of rotor 1 and rotor 2 to form coaxial rotor (XHUB1000 = XHUB2000, YHUB1000 = YHUB2000).

9) CSF1, LDGEAR - Equivalent damper and spring rate at fuselage CG of landing gear system, 5 DOF (XCG 1000, YCG 1000, ROLL1000, PTCH1000, YAW 1000), null mass matrix, diagonal damping matrix = [3500, 1750 lb-sec/ft, 8333, 16666, 16666 ft-lb-sec/rad], diagonal stiffness matrix = [168000, 168000 ft/lb, 250000, 666666, 666666 ft-lb/rad].

10) CSF1, DAMPFAL1 - Failed damper of blade 1 of rotor 1, 1 DOF (ZETA1100), null mass, stiffness matrices, damping matrix = [-3000 ft-lb-sec/rad].

11) CSF1, DAMPFAL2 - Same as CSF1, DAMPFAL1 but DOF = ZETA2100.

12) CSF1, HUBNON - Nonisotropic hub, 2 DOF (XHUB1000, YHUB1000), diagonal mass matrix = [552.8, 225 slug], diagonal damping matrix = [3500, 1750 lb-sec/ft], diagonal stiffness matrix = [8500, 8500 lb-ft].

13) CSF1, HUBISO - Isotropic hub, 2 DOF (XHUB1000, YHUB1000), diagonal mass matrix = [552.8, 552.8 slug], diagonal damping matrix = [3500, 3500 lb-sec/ft], diagonal stiffness matrix = [85000, 85000 lb/ft].

Comparison and Validation

Four cases have been used to compare results of this study and those of Reference 3. The first case is described as an isotropic rotor on an isotropic hub in Reference 3.

The corresponding DYSCO model is shown in Fig. 2.

MODEL II

INDEX	COMP	NO.	DATA SET
1	CRR2	1	ROTOR1
2	CSF1		HUBISO

Fig. 2. Model definition for an isotropic rotor on an isotropic hub.

The details of each component can be seen in the previous sections, 1) and 13). Note that the matched degree of freedom names in these two components is all that is needed to dynamically couple them.

The second case is a nonisotropic rotor on an isotropic hub and the corresponding model is shown in Fig. 3.

MODEL NI

INDEX	COMP	NO.	DATA SET
1	CRR2	1	ROTOR1
2	CSF1		HUBISO
3	CSF1		DAMPFAL1

Fig. 3. Model definition for a nonisotropic rotor on an isotropic hub.

Model NI is constructed by simply adding the component, CSF1, DAMPFAL1, which contains the negative damping rate of the rotor blade lag damper and makes the damping rate of the first blade equal to zero.

If component CSF1, HUBISO is replaced by CSF1, HUBNON, in Model II and NI, then Model IN and NN are obtained which correspond to an isotropic rotor on a nonisotropic hub and a nonisotropic rotor on a nonisotropic hub, respectively.

Each of the above models was formed and the Floquet stability analysis, SSF3, was executed. The results are shown in Figs. 4-7. In these figures, the circles represent the results from Reference 3 and the crosses are the results of the present study. As can be seen, the agreement is generally excellent and the validity of the techniques described is verified.

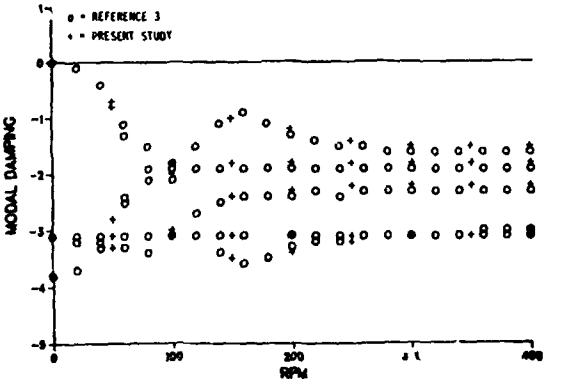

Fig. 4. Modal damping of an isotropic rotor on an isotropic hub.

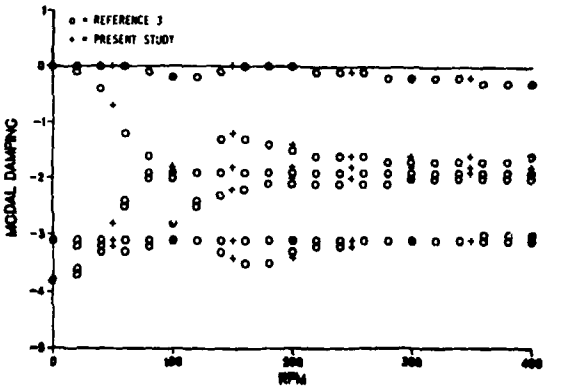

Fig. 5. Modal damping of a nonisotropic rotor on an isotropic hub.

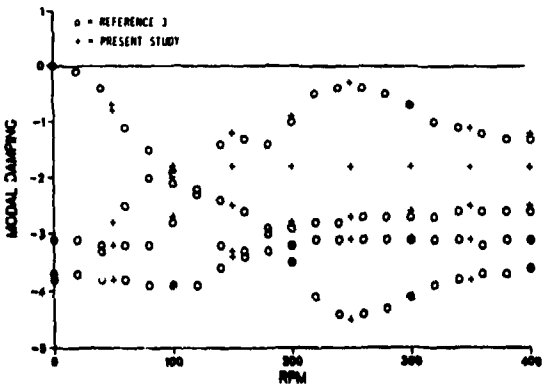

Fig. 6. Modal damping of an isotropic rotor on a nonisotropic hub.

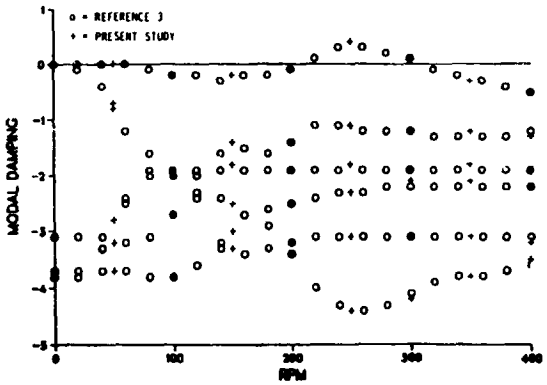

Fig. 7. Modal damping of a nonisotropic rotor on a nonisotropic hub.

Reduced Model

Eigenanalyses are often quite sensitive to multiple or close roots. Higher precision and greater computational time may be required and sometimes a failure to converge condition may arise for a highly isotropic configuration. In order to make the problem less complicated, numerically more stable, computationally more efficient and easier to interpret, it would be desirable to remove any unnecessary degrees of freedom. Consider the method of multiblade coordinates. The motion of the mass center of an isotropic rotor is proportional to the first order cyclic motion of the multiblade coordinates.[7] For the ground resonance phenomena, it is the motion of the mass center of the blades coupling with hub translational degrees of freedom that produces the instability. For this reason only two degrees of freedom have to be considered for an isotropic N-bladed rotor. For a damage analysis, however, the above-mentioned technique fails. For an N-bladed anisotropic rotor even when one transforms the blade degrees of freedom to a multiblade coordinate system, it is necessary to retain all the degrees of freedom.

In the present study, the blade degrees of freedom are in the rotating system. For a four-bladed isotropic rotor two degrees of freedom can be removed by satisfying two constraints: ZETA1300 = -ZETA1100, ZETA1400 = - ZETA1200. If blade one is damaged, there is still one degree of freedom that can be removed by setting ZETA1400 = -ZETA1200. The reasoning is as follows. For an even number of identical equally spaced blades, one may describe the motion by modes representing the sum and differences of the motions of opposite blades. The mode representing the sum of the motions does not contribute to the hub shear force. Therefore, for pairs of opposite identical blades, only equal and opposite motions need be considered. However, if these two blades are not identical then both modes contribute to the hub shear force.

Although the above-mentioned modes have no contribution to hub shear forces, when the hinge offset is not zero these modes can produce a yaw moment acting on the shaft. This, in turn, may affect the hub displacement through the coupling among fuselage degrees of freedom. In general, however, this effect should be very small.

Two cases used in the last section (Models NI, NN) were used to validate the reduced model. The action required was to add one more component, CLC1, RED124 to the original models. The function of this component is to constrain the motion of blades 2 and 4 to reduce the total system degrees of freedom. The reduced models are shown in Figs. 8 and 9.

MODEL REDUNI

INDEX	COMP	NO.	DATA SET
1	CRR2	1	ROTOR1
2	CSF1		DAMPFAL1
3	CSF1		HUBISO
4	CLC1		RED124

Fig. 8. Reduced model of nonisotropic rotor on isotropic hub.

MODEL REDUNN

INDEX	COMP	NO.	DATA SET
1	CRR2	1	ROTOR1
2	CSF1		DAMPFAL1
3	CSF1		HUBNON
4	CLC1		RED124

Fig. 9. Reduced model of nonisotropic rotor on nonisotropic hub.

The results of the Floquet stability analyses are shown in Tables 2 and 3. They illustrate that the reduced model is a good representation of the original model and that the reduced degree of freedom may be decoupled from the system. Note that the missing modes in these tables must always be stable, based on the previous discussion. In addition to the results shown in Tables 2 and 3, other tests have also been conducted for more complicated models, some of them will be shown below, which further confirm the validity of the reduced model.

Table 2. Eigenvalues of a nonisotropic rotor on an isotropic hub and its reduced model.

RPM = 175			
MODEL NI		MODEL REDUNI	
FREQUENCY	DAMPING	FREQUENCY	DAMPING
±5.36324	0.04882	±5.36309	0.04881
±5.03417	-1.30844	±5.03401	-1.30847
±4.82731	-1.78823	XXXXXXX	XXXXXXX
±5.86593	-2.04050	±5.86574	-2.04051
±6.55204	-3.05332	±6.55204	-3.05332
±6.79967	-3.46174	±6.79963	-3.46170

Table 3. Eigenvalues of a nonisotropic rotor on a nonisotropic hub and its reduced model.

RPM = 225			
MODEL NN		MODEL REDUNN	
FREQUENCY	DAMPING	FREQUENCY	DAMPING
±6.68678	0.20268	±6.68678	0.20268
±6.39124	-1.06817	±6.39124	-1.06817
±6.37237	-1.78824	XXXXXXX	XXXXXXX
±8.88663	-2.30105	±8.88663	-2.30105
±11.77885	-3.12293	±11.77885	-3.12293
±6.69736	-4.10262	±6.69736	-4.10262

Coaxial Model

A reasonable coaxial model can be easily obtained based on rotor and hub data used in the previous section. The definition of such a model is shown in Figure 10.

MODEL COAXIAL1

INDEX	COMP	NO.	DATA SET
1	CRR2	1	ROTOR1
2	CRR2	2	ROTOR2
3	CSF1		HUBNON
4	CSF1		HUBNON
5	CLC1		COAXIAL

Fig. 10. Model definition for coaxial, nonisotropic hub configuration.

As can be seen in Fig. 10 two counter rotating rotor components are used. Component CLC1, COAXIAL is used to couple the hub degrees of freedom of these two rotors. Component CSF1, HUBNON is used twice to double the mass, damping rate, and spring rate of the nonisotropic hub used in the single rotor model.

To consider the case with one damper inoperative, one simply adds component CSF1, DAMPFAL1, as shown in Fig. 11.

MODEL COAXIAL2

INDEX	COMP	NO.	DATA SET
1	CRR2	1	ROTOR1
2	CRR2	2	ROTOR2
3	CSF1		HUBNON
4	CSF1		HUBNON
5	CLC1		COAXIAL
6	CSF1		DAMPFAL1

Fig. 11. Model definition for coaxial configuration with failed damper.

The unimportant degrees of freedom may be removed as described earlier by adding two components as shown in Fig. 12.

MODEL COAXIAL3

INDEX	COMP	NO.	DATA SET
1	CRR2	1	ROTOR1
2	CRR2	2	ROTOR2
3	CSF1		HUBNON
4	CSF1		HUBNON
5	CLC1		COAX
6	CSF1		DAMPFAL1
7	CLC1		RED124
8	CLC1		REDUCE2

Fig. 12. Reduced model for coaxial configuration with failed damper.

To model failed dampers in both rotors, model COAXIAL4 may be formed as in Fig. 13.

MODEL COAXIAL4

INDEX	COMP	NO.	DATA SET
1	CRR2	1	ROTOR1
2	CRR2	2	ROTOR2
3	CSF1		HUBNON
4	CSF1		HUBNON
5	CLC1		COAXIAL
6	CSF1		DAMPFAL1
7	CLC1		RED124
8	CLC1		RED224
9	CSF1		DAMPFAL2

Fig. 13. Model for coaxial configuration with two failed dampers.

Fig. 14 shows the modal damping of the least stable mode of model COAXIAL2 and its reduced model COAXIAL3. It is seen that these two models show exactly the same damping ratio. As compared with the result with those of the corresponding single rotor model (model NN), in the unstable region, the instability is less severe for model COAXIAL3, as is to be

expected. The case with two dampers damaged can be seen in Fig. 15. It is interesting to see that there are two unstable modes in this case. The eigenvector of the mode indicated by 1 in the figure shows that this mode is primarily due to the coupling among hub translational degrees of freedom and the two damaged blades. That is why the damping ratio remains nearly constant as rotating speed is changed. The second mode, however, is the ordinary coupled hub-inplane unstable mode.

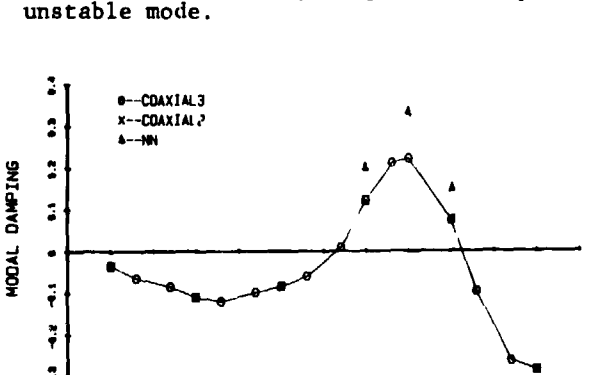

Fig. 14. Damping of the least stable mode of model COAXIAL2 and its reduced model COAXIAL3.

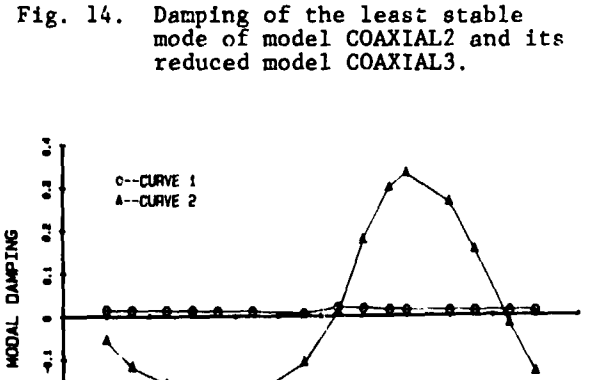

Fig. 15. Damping of two least stable modes of model COAXIAL4.

Tandem Model

Fig. 16 illustrates a model of a tandem helicopter.

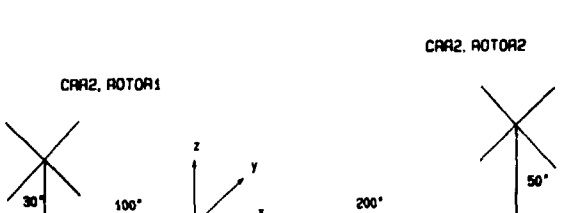

Fig. 16. Geometric configuration of tandem helicopter.

The data used in this simulation may not be realistic but the main purpose is to illustrate the modeling procedures and the convenience of the substructure modeling approach. The rotor hub and landing gear degrees of freedom are coupled with the fuselage rigid body degrees of freedom automatically by the naming convertion. The model definition is shown in Fig. 17.

MODEL TANDEM

INDEX	COMP	NO.	DATA SET
1	CRR2	1	ROTOR1
2	CRR2	2	ROTOR2
3	CFM2	1	FUSELAGE
4	CSF1		LDGEAR
5	CLC1		REDUCE1
6	CLC1		REDUCE2

Fig. 17. Model definition for TANDEM.

The model with one damper failed is TANDFAIL and depicted in Fig. 18.

MODEL TANDFAIL

INDEX	COMP	NO.	DATA SET
1	CRR2	1	ROTOR1
2	CRR2	2	ROTOR2
3	CFM2	1	FUSELAGE
4	CSF1		LDGEAR
5	CLC1		RED124
6	CLC1		REDUCE2
7	CSF1		DAMPFAL1

Fig. 18. Model definition for TANDFAIL.

The two unstable modes of this vehicle are shown in Fig. 19. The eigenvector of mode 1 reveals that it is primarily a coupled yaw, pitch, and lag mode. Mode 2, on the other hand, is due primarily to the coupling of fuselage translational degrees of freedom and in plane motion of the blade. It is also demonstrated in Fig. 19 that the instability is more severe when one blade damper is inoperative.

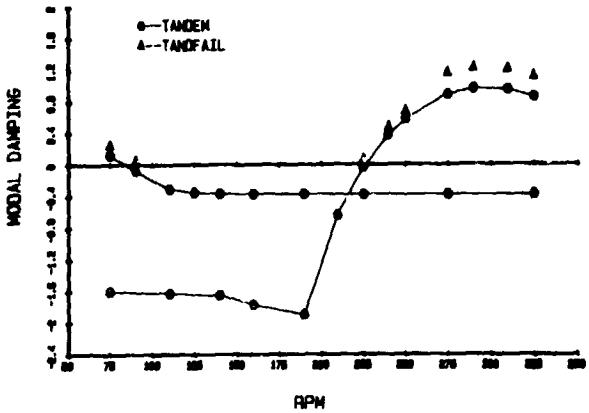

Fig. 19. Damping of the two unstable modes of tandem model.

Conclusion

The purpose of the paper was to illustrate the convenience and versatility of a procedure for ground resonance analysis through a general substructure synthesis procedure.

The ease of modeling failed dampers on conventional, coaxial, and tandem helicopters has been demonstrated.

The accuracy of the procedure has been illustrated by comparing the results with a previous analysis.

The ability to conveniently evaluate a theoretical concept (which reduces the blade degrees of freedom) has also been demonstrated.

References

1. Coleman, R.P. and Feingold, A.M., "Theory of Self-Excited Mechanical Oscillations of Helicopter Rotors with Hinged Blades," NASA Report 1351, 1958.

2. Peters, D.A. and Hohenemser, K.H., "Applications of the Floquet Transition Matrix to Problems of Lifting Rotor Stability," J. AHS, 16, (2), April 1971.

3. Hammond, C.E., "An Application of Floquet Theory to Prediction of Mechanical Instability," J. AHS, 19, (4), October 1974.

4. Hurty, W.C., "Dynamic Analysis of Structural Systems by Component Mode Synthesis," Technical Report 32-530, Jet Propulsion Laboratory, Pasadena, California, January 1964.

5. Berman, A., "A Generalized Coupling Technique for the Dynamic Analysis of Structural Systems," J. AHS, 25, (3), July 1980.

6. Hurst, P.W. and Berman, A., "DYSCO: An Executive Control System for Dynamic Analysis of Synthesized Structures," AIAA/ASME/ASCE/AHS 24th SDM Conference, Lake Tahoe, Nevada, AIAA-83-0944-CP, May 1983.

7. Ormiston, R.A., "Aeromechanical Stability of Soft Inplane Hingeless Rotor Helicopters," Third European Rotorcraft and Powered Lift Aircraft Forum, France, September 7-9, 1977.

DISCUSSION*
Paper No. 2

GROUND RESONANCE ANALYSIS USING A SUBSTRUCTURE MODELING APPROACH
Shyi-Yaung Chen
Edward E. Austin
and
Alex Berman

Peretz Friedmann, University of California, Los Angeles: I have a couple of questions so let's start with the first one. The test with which you are currently correlating DYSCO results with Hammond's analysis is a very good way to go. However, I was wondering why you didn't try to correlate the ability of this code to predict ground resonance with experimental data which Bill Bousman obtained and which Friedrich Straub showed in one of his slides at the beginning. That's a better test for the problem and a lot of ITR comparisons have been done with that particular case. If the DYSCO program could reproduce these results, it would be a good verification of the code.

Austin: Yes, I would like to do that. Actually this paper was prepared entirely extracurricularly. Not a part of any given job description. We took the expedient approach of going with Hammond's results. We felt that it was a pretty good verification of our implementation, not of the physical model, of which components we had, because we were correlating with actually three different methods of calculation. We would like to do some correlation with actual test data also.

Friedmann: The second question I have is more along the lines of a comment. When you started describing DYSCO on the right hand side of the equations you will remember you had left all the nonlinear terms in the constraints for F_C. The problem I have with these equations is that I am not convinced that it has the capability of dealing with the nonlinear effects which might be important. The correlation you have run is for a ground resonance problem where everything is always linear. I would suggest that one of the future endeavors is to look at the problem where nonlinear effects [could be important].

Austin: No question.

Jing Yen, Bell Helicopter: I have a very general question for you or for all of you. For thirty years we've been working very hard to prevent the ground/air resonance problem. The technical community has been working very hard to improve our prediction capabilities. From your point of view, right now, how much confidence level do we have in the prediction techniques? How much confidence level do we have now? In other words in the next ten years, when we have our Third Decennial Meeting here will we still be talking about the same thing again? How much confidence do we have right now versus the way we were ten years ago? This is an open question.

Austin: Well, personally, my confidence has not been real high because so often the data we have been getting from you folks has been in terms of equivalent hub impedance. We would get a scrambling of numbers--one is for a landing gear failed, another one is for ice. I've never really been able to find out from you where those numbers came from. Also, of course, these numbers are very directly related to the rotor rpm and it has never been especially clear in the material I have received in evaluations that you have actually gotten experimental data at the right rpm for those impedances. So my confidence has been pretty low. I think if we can move to a point where we have more descriptive models and then can verify their correlation with some flight test data that we ought to be able to put this thing to rest.

Jerry Miao, Sikorsky Aircraft: I heartily agree with your [comment] about getting those spring rates. [They are hard to come by--stiffness values for ground contact, concrete, turf, ice, landing gear and so forth.] They are difficult to get. But I draw a different conclusion. My conclusion is that our analysis capability is pretty good. We can predict ground resonance if we know how to put those numbers into it. Therefore, in the aircraft shake test normally we do a ground resonance test to determine where the ground roll mode is or pitch mode is. [We can find those numbers, but] finally, what is the tire stiffness, the oleo stiffness, or the ground surface contact stiffness.

Austin: I think the Army will probably continue to use analysis to try to identify the most critical cases. I don't think the industry is ever going to get away from the requirement of

*The transcript of this discussion is incomplete because of recording problems. Areas of ambiguous or missing text have been discussed with the person asking or answering the question and the text is indicated with brackets.

actually demonstrating those critical cases, even though it may mean bringing in blocks of ice on a hot summer day or whatever.

Bob Sopher, Sikorsky Aircraft: The type of blade that you used here, was it a non-elastic blade?

Austin: Yes, it was. That was a matter of choice. We're working on a representation of more complex blade elasticity models. It will then be just a matter of basically selecting one or the other and putting in some modal data for the blades.

Sopher: So that the elastic blade is not yet available?

Austin: No, but it will be very shortly according to the last schedule submitted to the Army. It may actually in fact be a little longer than that.

Sopher: Well, that may explain why you haven't tried to correlate with the Bousman data base on hingeless rotors.

Austin: Right. You would have to use equivalent springs if you were going to do it right now.

Benson Tongue, Georgia Institute of Technology: My question is substructure modeling [decreased the cost] of the technique and so I was curious about that. What is the relative content of your cost [for calculations using Floquet analysis, modal analysis, and so forth?]

Austin: The cost of the cases we ran for our machine was inconsequential. I'm not sure, it may have been ten times zero or twenty. That isn't a factor at all for us in the Army. It's your tax dollars at work. No, really the solution does not take much time so I don't think it would be a major obstacle for most folks. Alex, do you want to address that?

Alex Berman, Kaman Aerospace: Yes. Actually there is no [particular special cost in running DYSCO.] What you should have to do is compare the computational costs against the cost of developing specific models [for a new configuration and modifying the appropriate code.]

Euan Hooper, Boeing Vertol: I was going to ask is DYSCO in the public domain? I see that it was published last year at [the 24th SDM, Lake] Tahoe, but is the FORTRAN coding available in the public domain?

Austin: That's a tricky question. Our contract that Alex is working on now calls for the program itself to be in the public domain. The source code for the Executive will, however, be delivered in a binary form rather than a FORTRAN source. So you can't make changes to the Executive, but all the technical modules will be supplied and you can add technical modules without reference to that Executive.

Hooper: And when will this system be available?

Austin: Make a new guess, Alex.

Berman: A few months or so.

Austin: Personally, I would like to encourage everybody to write me a letter and ask for it. I'm hoping that we will be able to do ground resonance analysis using it in future acquisitions of interest.

Hooper: If I could just add. We've got some experience with using government programs. I would like to emphasize that you don't shortcut the documentation process. Anything you can do to not only document it well but annotate the coding. Please, do what you can, but don't short-cut the process.

Austin: We try to encourage our contractors to do that. Some of you do it better than others. But I think the documentation will be good for DYSCO.

PARAMETRIC STUDY OF THE AEROELASTIC STABILITY OF A BEARINGLESS ROTOR

W. EUAN HOOPER
Director, Vehicle Technology
Boeing Vertol Company
Philadelphia, Pa.

ABSTRACT

A trade study has been conducted to illustrate the sensitivity of the aeroelastic stability of a bearingless main rotor to the rotor hub coupling parameters that are available for the designer. The results are presented over the complete range of rotor speed and collective pitch available and the effects on air resonance of the 6 beam installation angles are compared together with the results of offsetting the cuff snubber attachment. The major part of the study was conducted using the FLAIR analysis which incorporates a uniform representation of the flexbeam. Results are also shown for a modified version of FLAIR in which the uniform beam is replaced by a member having the geometric tailoring resulting from structural optimization.

1. INTRODUCTION

The control of the stability of bearingless rotors by introducing coupling between blade flap, lag, and pitch freedoms has been frequently addressed in the literature in recent years. One of the most powerful stabilizing parameters has been identified as negative pitch-lag coupling, a powerful version of which was successfully demonstrated in full scale ground and flight experience on the YUH-61A.

In support of the Boeing Vertol/Army/NASA ITR Preliminary Design Program, a study was initiated to quantify in a consistent manner the sensitivity of the beam installation angles. This then served as a base to evaluate an alternate concept of adding stability by introducing a vertical offset to the cuff snubber. This offset causes favorable mechanical lag-pitch coupling while avoiding inducing unfavorable bending moments in the flexbeam. Further, since the coupling between blade freedoms is all important in determining stability, a comparison of the effect of rigorously representing the beam nonuniformity, versus the assumption of a uniform beam, was also undertaken.

The FLAIR program (written by Dewey Hodges of the U.S. Army Aeromechanics Lab) was chosen for the study because of the simplicity of representation of the major elements while employing an accurately modelled, but uniform, flexbeam. The program was well documented (Ref. 4) and thus amenable to the modifications considered necessary for the study.

Presented at the 2nd Decennial Specialists Meeting on Rotorcraft Dynamics.
Ames Research Center, Moffett Field, CA
Nov 7-9, 1984.

2. THE FLAIR ANALYTICAL MODEL

The FLAIR program models the fuselage and blades as rigid bodies separated by the flexbeam elements. The fuselage has 4 degrees of freedom (longitudinal, lateral, roll and pitch). Each blade is rigid and is attached to a uniform flexbeam extending from the hub offset to the blade attachment point. The 6 freedoms at the end of each flexbeam are:

u	axial
v	chordwise
w	flapwise
ζ	lag angle
β	flap angle
θ	pitch angle

expressed relative to the axis system at the root of the beam. In an air resonance case the beams are the only springs in the system as the fuselage freedoms are unrestrained to ground. In a ground resonance case, additional springs are inserted between fuselage and ground to represent the landing gear. The flex beams are axially loaded by the centrifugal forces and thus an iterative solution technique is required for the resulting nonlinear equations.

The beam and control system equations are rigorously modelled making no small angle assumptions and so the program was considered well suited to the intended trade study. The major modifications made to the program to facilitate the study included:

1. The input and output were made dimensional since the study was conducted in dimensional terms.

2. An additional control configuration (config. 5) was added to the 4 described in Ref. 4, Figs. 4-6, to allow the cuff snubber to be moved to points other than centered on the flex beam.

3. Additional outputs were added to illustrate the steady and vibratory deflected shapes of all freedoms.

4. A nonuniform beam was modelled to assess the validity of the uniform beam assumption.

The physical model used for the study was the wind tunnel model fabricated for the ITR program. In general arrangement the model was similar to the model described in Ref. 5 in that it is a 6 ft. dia. 4 bladed bearingless rotor driven by 2 electric

motors on a fuselage which is gimballed in pitch and roll about the fuselage CG. The model is Froude scaled (1/8) from the Hughes AH-64 helicopter for which the Boeing Vertol ITR is designed. Unlike the Ref. 5 model the blades are attached by 6 inch long structurally tailored flexbeams rather than localized flexures. In all stability respects except the flexbeam design the fuselage and blades are conventional and the trade study concentrates on the design parameters for the flexbeam and cuff. Throughout the study blade structural damping is assumed to be 0.5% critical and fuselage damping for ground resonance is assumed to be zero.

3. THE MODES OF AIR AND GROUND RESONANCE

To illustrate the modes which affect the stability of a bearingless rotor the natural frequencies versus RPM are shown in Fig. 1 for 3 configurations.

a. Fixed Hub - no coupling into the fuselage and each blade is uncoupled from all other blades. Since each beam has 6 degrees of freedom the generalized coordinate transformation from rotating to fixed system axes, (Ref.2) omitting the collective and differential modes, results in 12 degrees of freedom for FLAIR. The eigenvalue analysis then gives 24 roots which occur in 12 complex pairs and the 4 most significant roots are labelled in Fig. 1 a.

b. Air Resonance - to simulate air resonance with a model, without being completely free flying, the fuselage is gimballed in pitch and roll about the fuselage CG. This adds 2 more degrees of freedom to the equations (now 14 total) and is a justifiable approximation for modelling of both air and ground resonance. Even in the latter case, when pitch and roll springs to ground are introduced, the nodes of the roll and pitch modes have to lie between the fuselage CG and a point k^2/h above the CG, where k is the radius of gyration and h is the height of the CG above the ground, Ref. (1).

With 14 degrees of freedom the eigenvalue analysis now gives 28 roots of which:

- 24 occur in 12 complex pairs and are directly related to the 12 pairs of the fixed hub case.
- 2 have zero frequencies, in the nominal RPM range, resulting from the roll and pitch freedoms having no springs to ground
- and 2 more occur in an additional complex pair having a very low frequency. This root results from

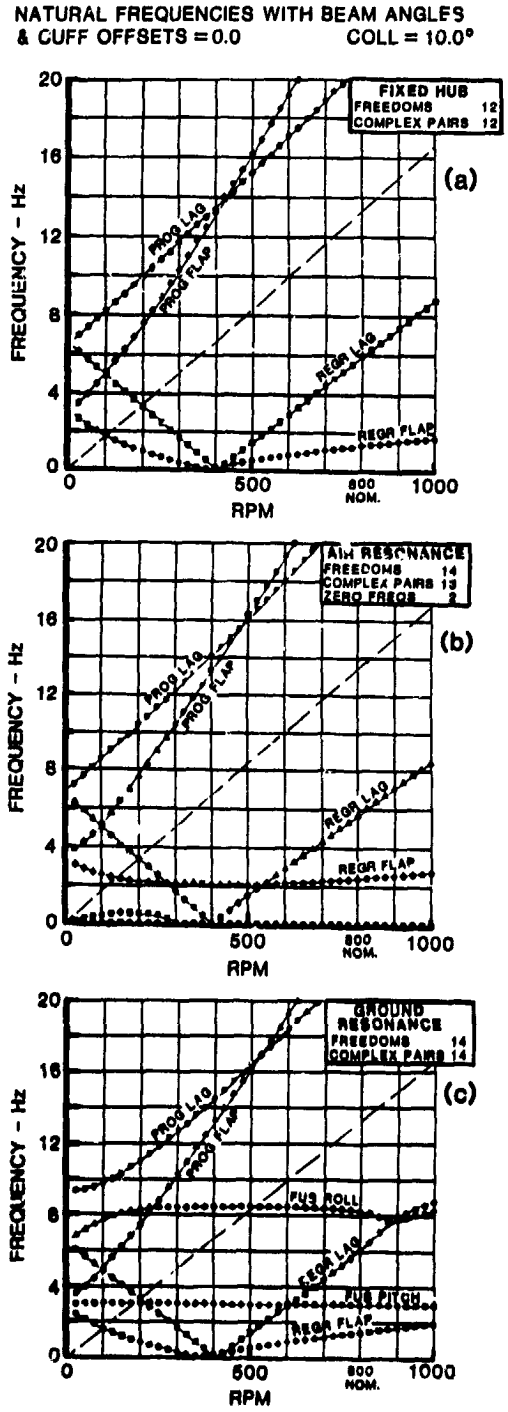

Fig. 1 Natural frequencies for fixed hub, air and ground resonance

having 2 freedoms with dampers (aero) but no springs to ground. Since the rotor strongly couples the 2 freedoms, the two 1st order lag equations then result in one 2nd order root with a very low frequency. (For a further discussion of these roots see the Appendix).

References have been made in earlier papers to 'the roll mode' and 'the pitch mode' of the fuselage in air resonance analyses as modes additional to the regressing flap mode (which couples with fuselage pitch and roll) identified in Fig. 1 b. But this paper takes issue with that characterization and invites further discussion.

c. Ground Resonance. By adding pitch and roll springs to ground, the 2 zero frequencies are removed and the 14 degrees of freedom now result in 14 complex pairs of roots all of which can be characterized as shown in Fig. 1 c.

The values of the springs added to the hover stability model approximated a heavyweight operating condition of the AH-64 and ensure that the pitch and roll mode crossings with the lag regressing mode were within the RPM range of study for the purposes of test/theory correlation.

Quantifying the stability of these equations presents a communication problem because while many engineers can readily identify with '% critical' as a measure of damping, this concept falls down when the associated frequency goes to zero. The lag regressing frequency of a bearingless rotor blade is necessarily equal to 1/rev in the rotating system (zero in the fixed system) at an RPM typically below operating RPM. Thus '% critical' goes to infinity at this RPM. This not only makes it difficult to plot but also gives a false sense of security.

An alternative measure of damping is the dimensional (1/sec) 'decrement' given by the real part of the complex root. This allows a smooth continuum of data to be plotted throughout the RPM range. To give a number which is independent of scale the real part can be normalized by the nominal rotor angular velocity. This approach was selected for this paper and the ratio of (- real part)/(nominal rotor rad/sec) is called DECREMENT RATIO.

In Fig. 2 both measures of damping are portrayed for the 3 cases of Fig. 1. The mode of most interest, regressing lag, is seen to go to infinite '% critical' at 400 RPM in each case, and this is avoided when plotting decrement ratio. Note that the decrement ratio of both regressing and progressing lag are equivalent for the fixed hub case. As will be seen later the regressing flap mode is heavily damped and off scale.

The air resonance case (Fig. 2b) shows the typical trend of a bearingless rotor, with no pitch/lag couplings, to go unstable with increasing RPM at high collective pitch.

The ground resonance case (Fig. 2c) shows the regressing lag mode briefly coupling with fuselage pitch to give an instability at 600 RPM and giving a major instability at 900 RPM when coupling with the roll mode.

To understand the factors that affect the stability of the equations the eigenvectors from the FLAIR analysis were transformed back into the rotating system to illustrate the actual motion of the blade, relative to the hub plane, at every eigenvalue. Using the relationships defined in Ref. (2), the motion of the No. 1 blade tip is calculated from the 8 fixed system eigenvector cosine and sine components.

beam chordwise defl	v_c, v_s
beam chordwise slope	ζ_c ζ_s
beam flapwise defl	w_c, w_s
beam flapwise slope	β_c, β_s

The motion of No. 1 tip can then be portrayed as a Lissajous pattern as viewed along the blade looking inboard towards the hub. Movement of the blade is to the right as shown by the horizontal arrows and the arrowhead on the ellipse shows the direction of rotation of the locus. Also shown is the location on the locus and the magnitude of the maximum nose up pitch angle (θ) occurring. In Fig. 3 these blade tip loci are shown for the reference case of beam angles and cuff offsets = 0 and for collective = -2.5 deg. The data are normalized for 10° of the tip motion (flap or lag) expressed as an angle subtended about the hub center. In the lower LH corner of each tip locus box is shown the rotating system frequencies.

Below each blade tip locus is shown a superposition of:

a. The inplane CG locus. This is the fixed system locus of the rotor blade CG resulting from inplane depatterning of the blades caused by the regressing and progressing lag motions. (To simplify the plotting scales, which are all ± 10°, these loci are normalized to the magnitude of the blade tip lag motion above).

b. The hub locus. This expresses the motion of the fuselage which in the lag modes results largely from the inplane CG coupling.

The fixed system '% critical' damping is given in the CG and hub boxes together with the fixed system frequencies.

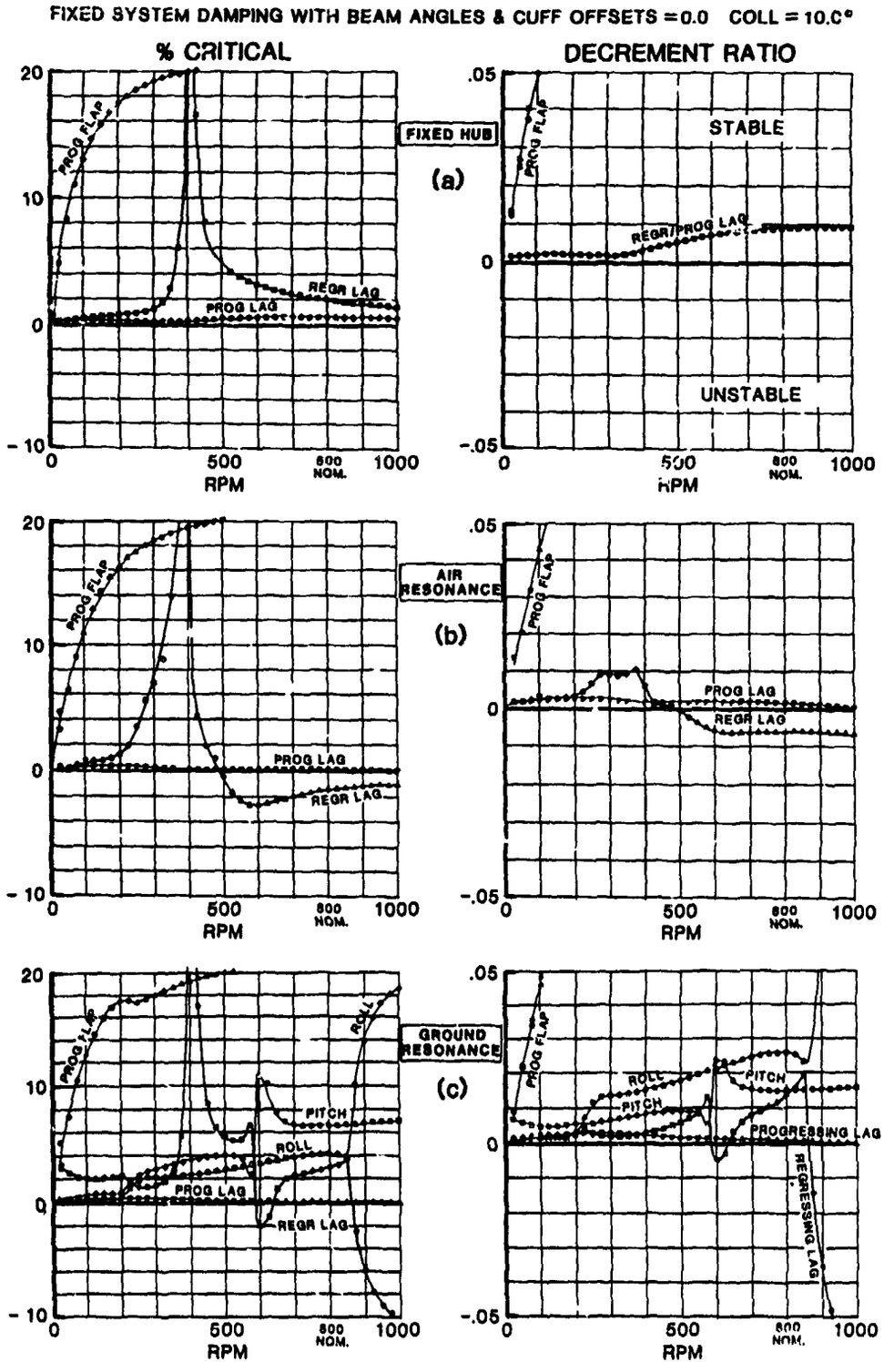

Fig. 2 Damping for fixed hub, air and ground resonance

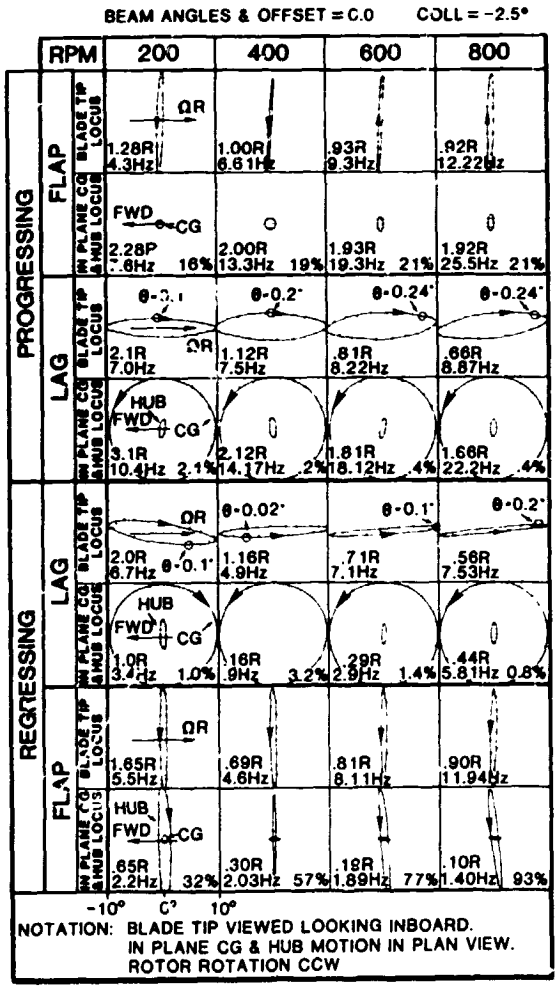

Fig. 3 Effect of RPM sweep on blade modes, collective = -2.5 deg.

Generally the blade motions do not undergo major changes of mode shape and points to note are -

- the largest hub motions are associated with the regressing flap mode.
- blade pitch motions are small (<1° for 10° of tip motions) and inconsistently phased to flap and lag.
- the largest inplane CG excitations result from the 2 lag modes.
- the predominant fuselage response is in roll for all modes.
- the loci of the flap modes are tilted forwards as might be expected from -2.5° collective.

Fig. 4 shows the same format for 10° collective, in which the lag regressing mode now goes unstable above 600 RPM but no significant change occurs in the mode shapes. Note -

- the general tilt aft of all the blade tip loci due to the high collective pitch.
- still low (<1°) pitch motion inconsistently phased to lag and flap.

Later this same format will be shown for a case that has been stabilized.

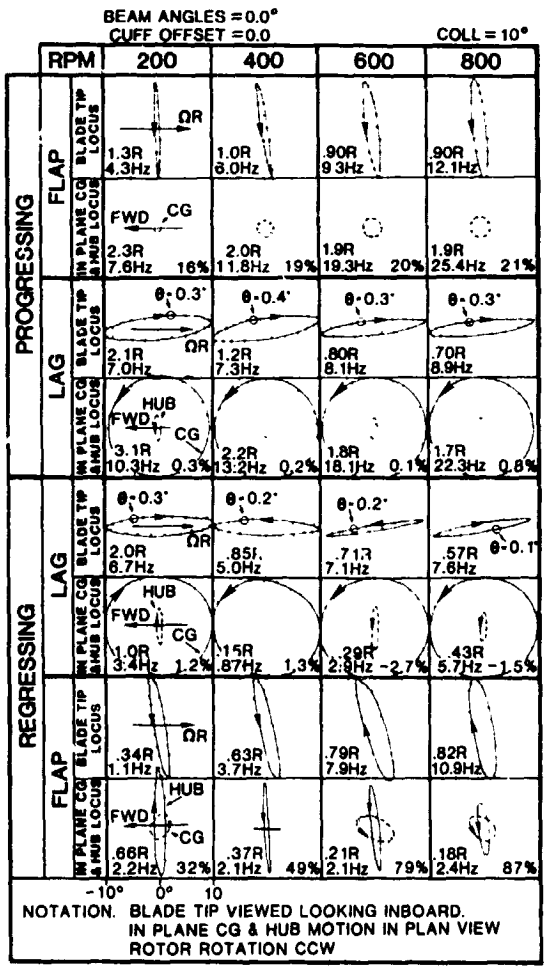

Fig. 4 Effect of RPM sweep on blade modes, collective = +10 deg.

4. THE EFFECT OF BEAM ANGLES ON STABILITY

Much previous literature and testing has established that the coupling introduced by the hub-to-beam and beam-to-blade mounting angles can strongly influence the coupling between blade lag, flap, and pitch freedoms and affect stability. In order to have a consistent display of the effects of all 6 angles to use as a base for selecting the

ITR design a systematic study was made and the results are presented below.

Since a knowledge of the stability was desired over the complete available RPM range (0 to 1000) and collective pitch range (-2.5° to 10°) a surface plot was established portraying RPM and collective on the x-y axes and the damping 'decrement ratio' on the Z axis. Fig. 5 shows the baseline case in

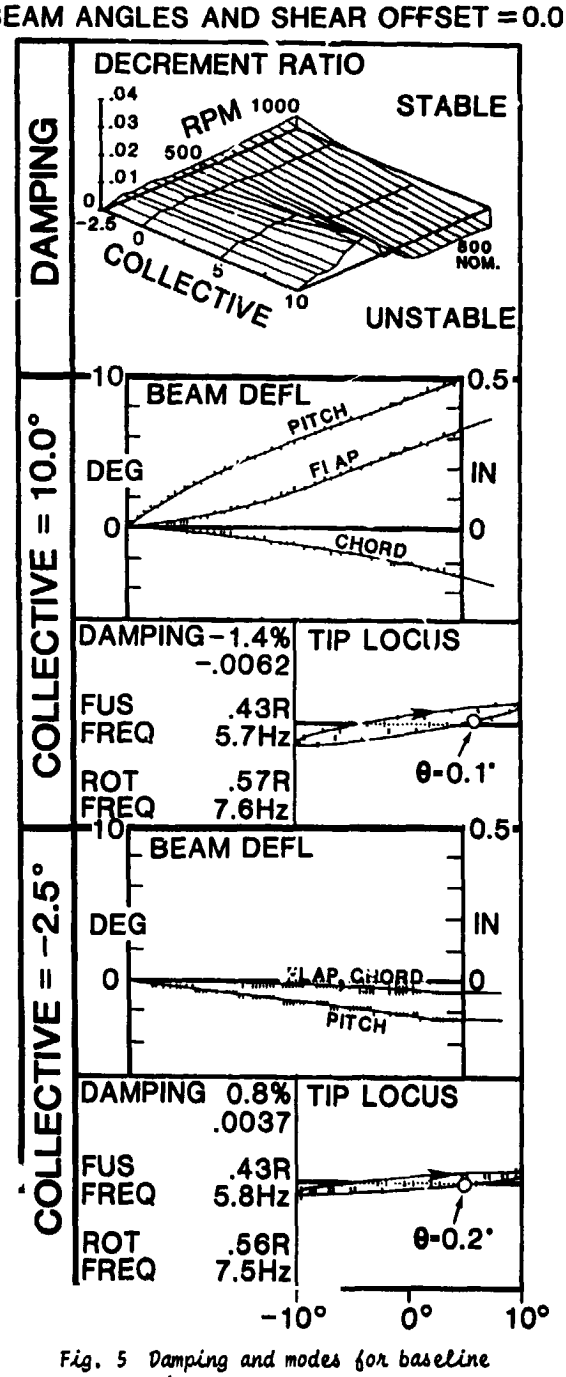

Fig. 5 Damping and modes for baseline air resonance case

which all 6 beam angles are zero and the cuff offset is zero (i.e. on the center line of the beam). At -2.5° collective the mode is stable (pos.) throughout but with increasing collective the decrement ratio is seen to go unstable (neg.) above 450 RPM in typical fashion as previously seen in the literature (Ref. (3). Below the damping plot in Fig. 5 are shown the beam deflections and the blade tip loci at the nominal 800 RPM for the extreme values of collective pitch. Note that because of the uniform beam modelled by the FLAIR analysis the pitch deflection of the beam is almost a straight line with unrealistically high slopes at either end, while the flapping deflection shows more realistic curvatures.

Fig. 6 shows the effect of individually introducing 5 degree clevises into the hub/beam attachment. Examination of the beam deflection plots shows major changes in the resultant coupling between blade freedoms and yet none of the cases show any significant change in stability, in the problem region of high collective pitch.

Fig. 7 shows results of similar 5 degree clevises introduced at the beam/blade attachments and now it is seen that outboard coning (OUTCON) has a powerful stabilizing effect. Note that the blade pitch motion now exceeds 4° and that maximum nose up pitch occurs at maximum lag.

Considering the nonlinear nature of the stability equations the beam angles were next changed in conjugate pairs to see if other effects were introduced. In Fig. 8 it is seen that both beam deflections and blade tip loci are essentially superpositions of the previous 2 figures, taking signs into account.

5. THE EFFECT OF OTHER PARAMETERS ON STABILITY

In contemporary designs the inboard shear restraint of the cuff has been typically located on the flexure axis (UH-60 tail rotor, Model 680 main rotor). But offsetting this point vertically provides a means of introducing the desirable lag pitch coupling observed from the use of outboard coning in Fig. 7. Fig. 9 shows the result of moving the cuff below and above the flexure by 0.5 inch or 8.3% of the beam length. It is seen to have a powerful effect on the stability at high collective pitch. Again note that with positive offset the maximum blade pitch angle occurs at maximum lag as with outboard coning.

Knowing the importance of the crossover of the lag and flap regressing frequencies on stability, the effect of varying the lag frequency around the nominal value was assessed. By arbitrarily varying the chordwise stiffness (EICHD) up and down the coupled lag frequencies were changed from 0.57 down to 0.51/rev and up to 0.66/rev

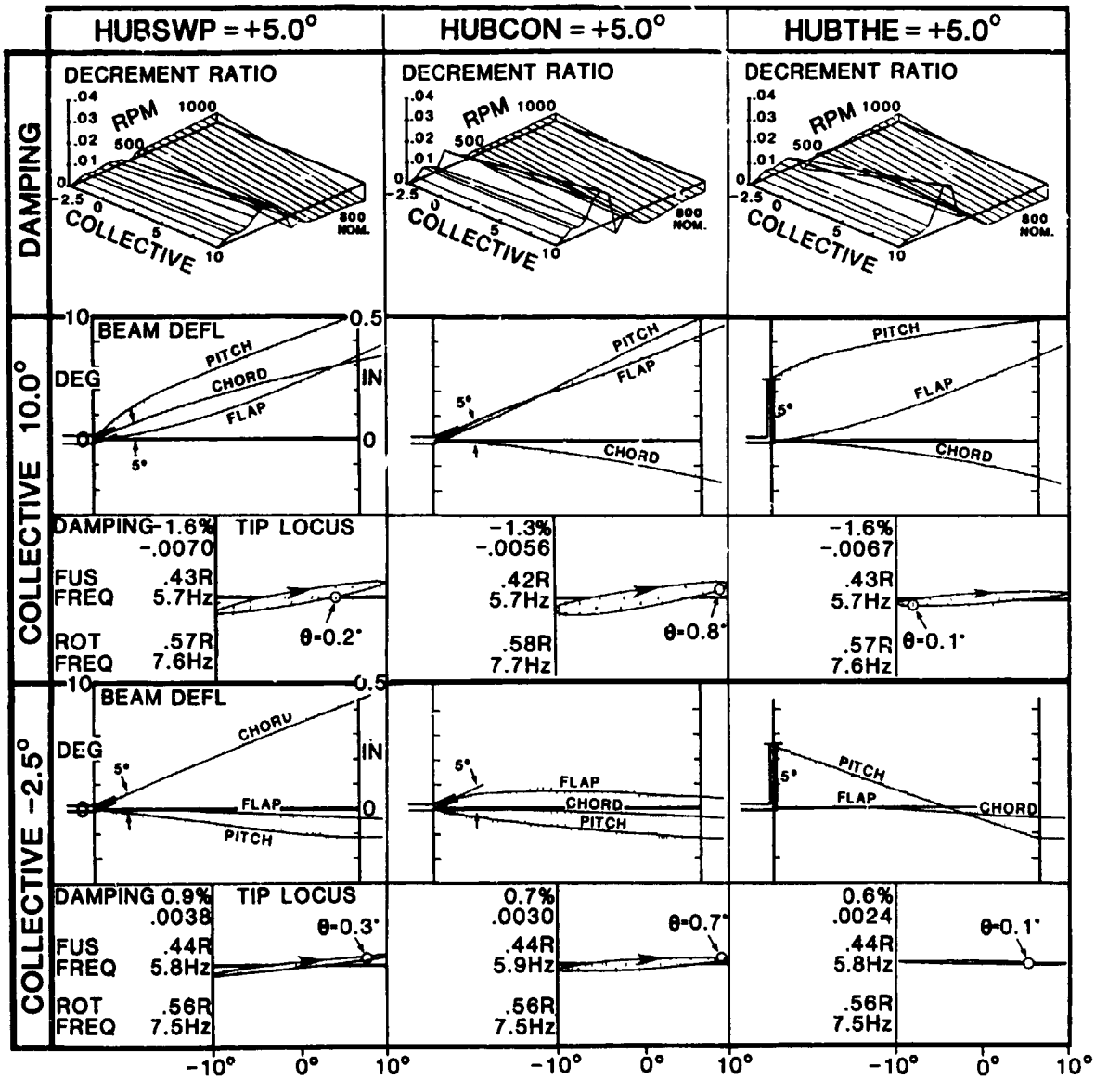

Fig. 6 Effect of hub-beam angles on damping and modes

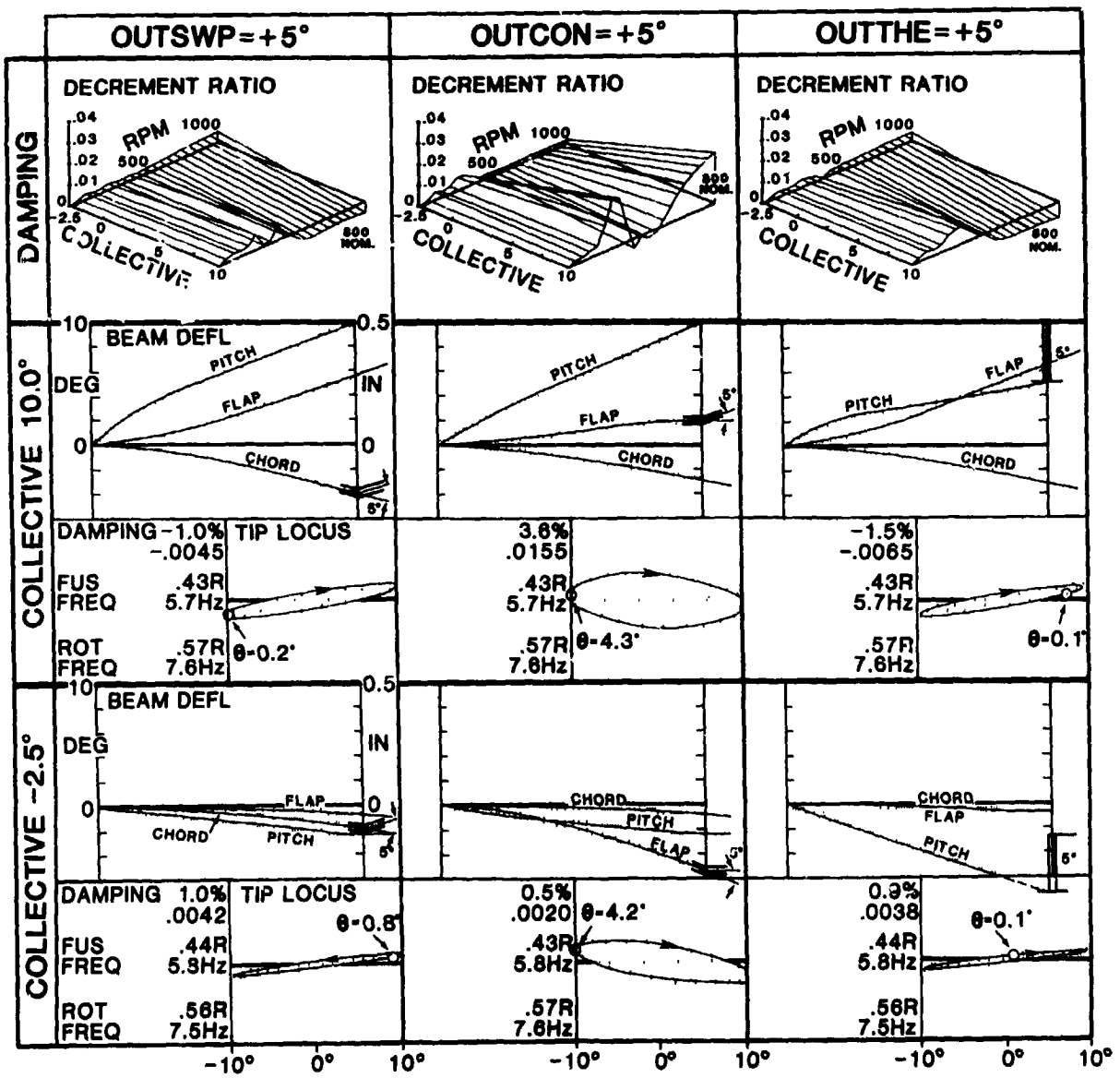

Fig. 7 Effect of beam-blade angles on damping and modes

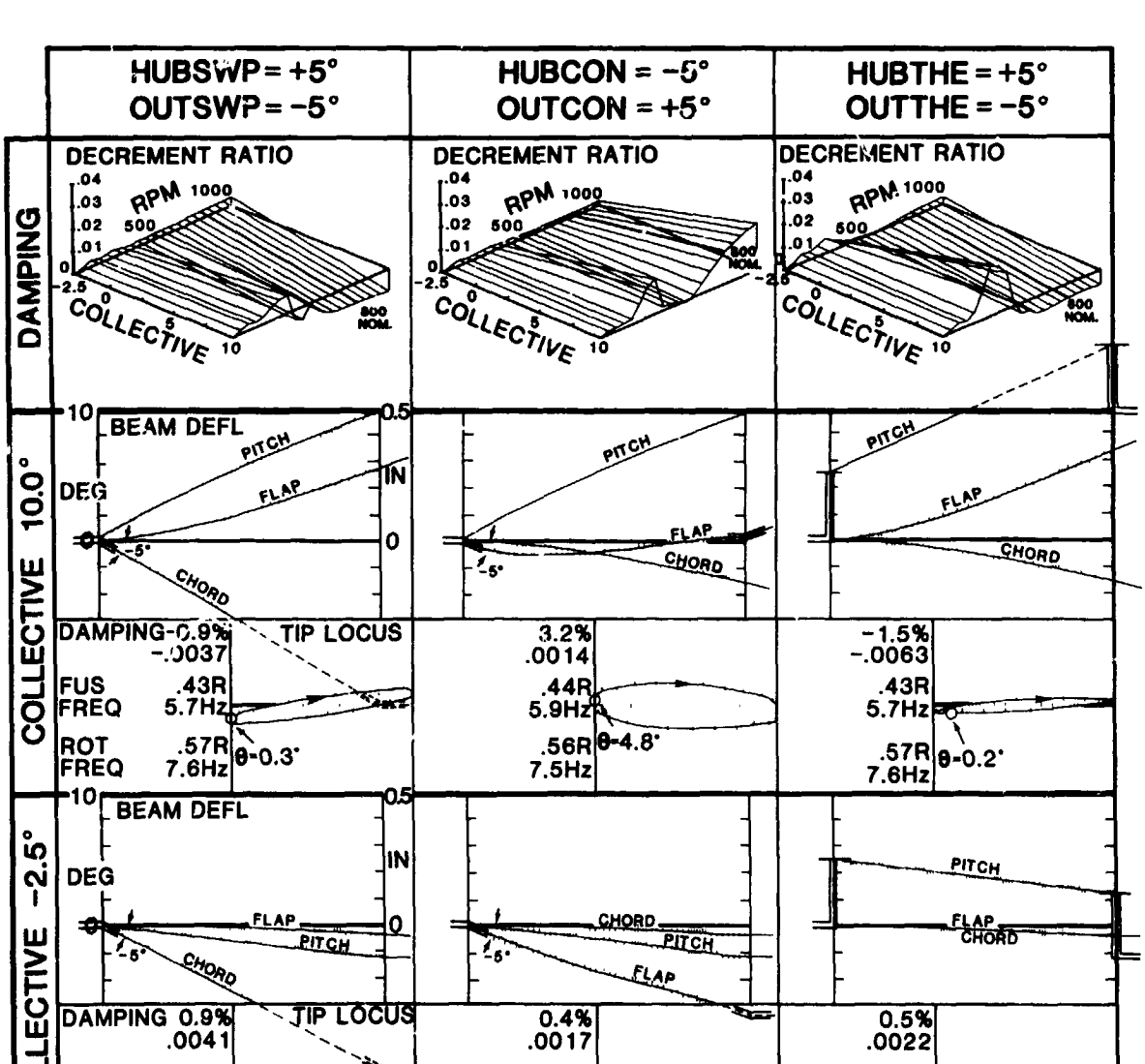

Fig. 8 Effect of changing beam angles in pairs on damping and modes

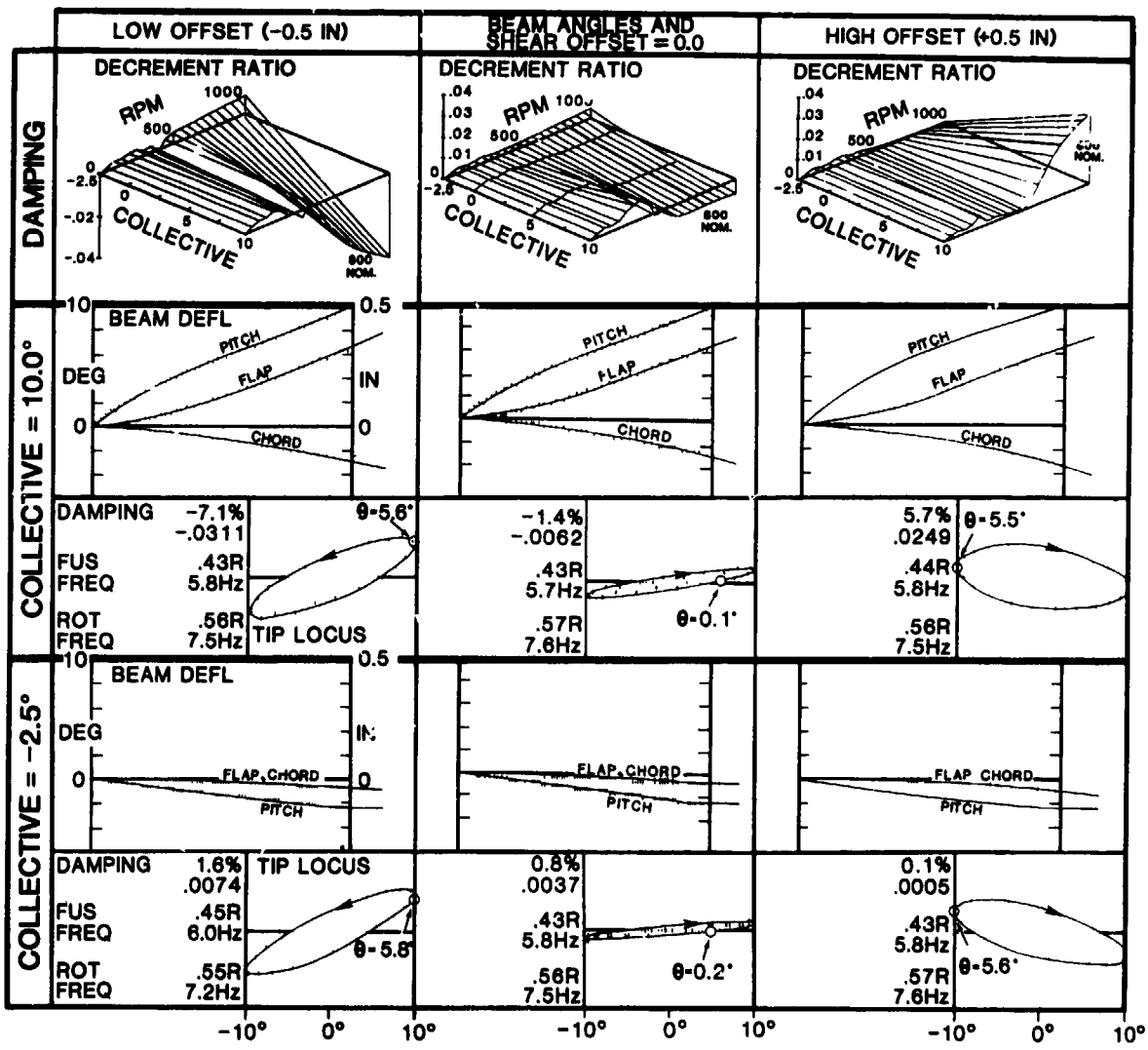

Fig. 9 Effect of cuff shear vertical offset on damping and modes

and as shown in Fig. 10 the effect on the damping decrement ratio was negligible although it does have the effect of moving the rotor speeds for instability up and down.

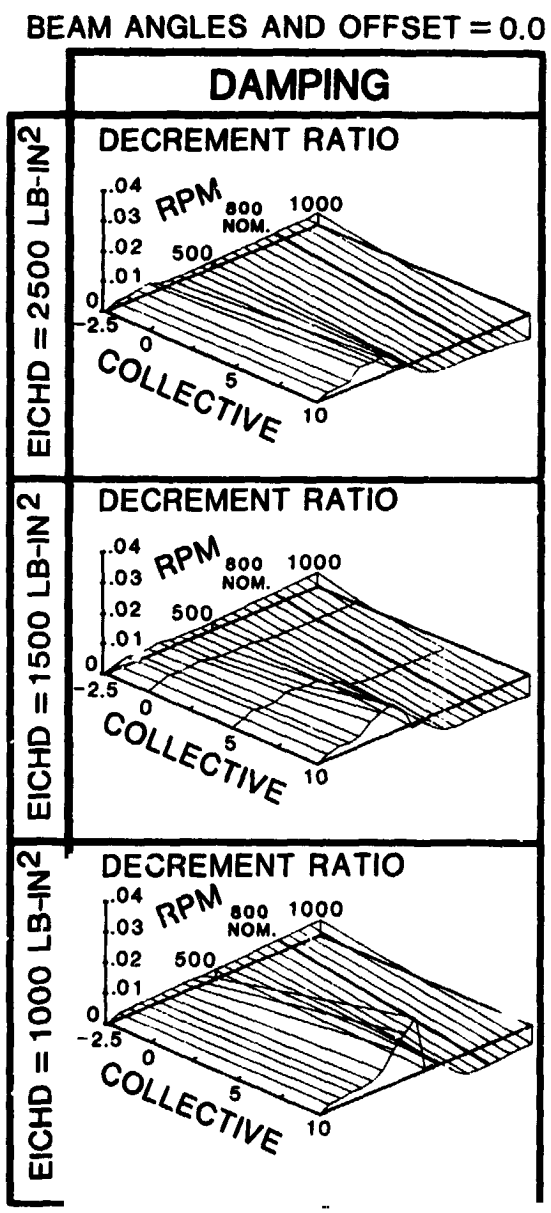

Fig. 10 Effect of chordwise EI rigidity on air resonance damping

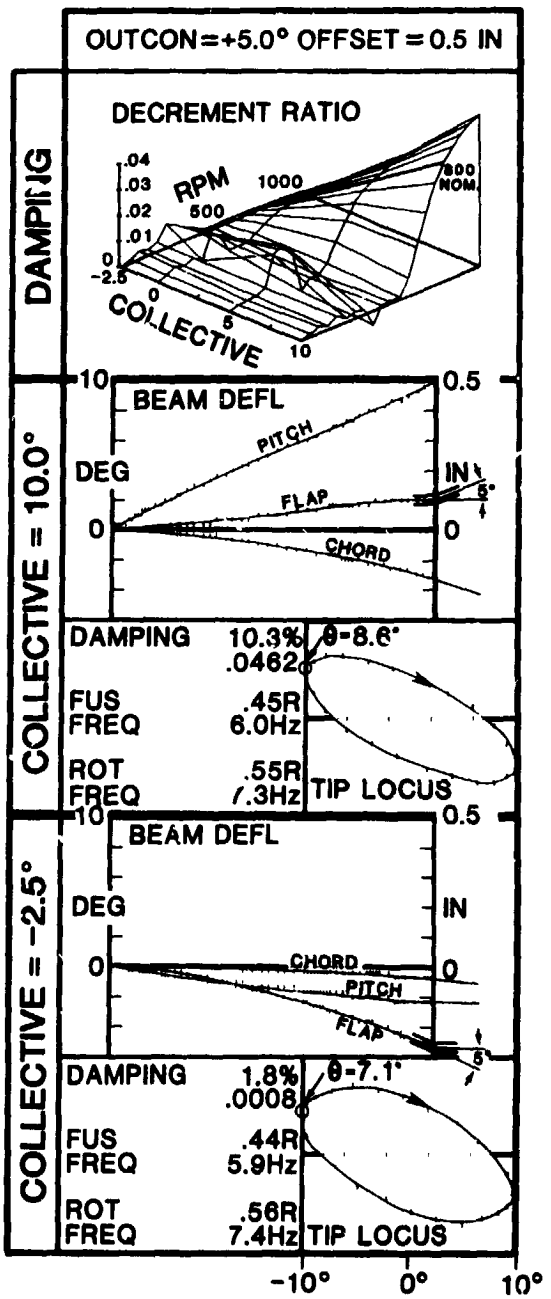

Fig. 11 Damping and modes for combined stabilizing couplings

Concern for the nonlinear nature of the equations prompted evaluating the simultaneous application of the 2 most powerful stabilizing parameters, outboard coning and positive beam offset. Fig. 11 shows the combined results and the resultant damping is 10.3% at high collective compared to the individual contribution of 3.2% from OUTCON and 5.7% from OFFSET from a base of -1.4%. Thus the combined effect is worth more than the sum of the parts. Fig. 12 shows the mode shape behavior in detail and the powerful pitch-lag coupling (8.6° pitch for 10° of inplane tip motion) causes about 7° of flap motion and a major increase in stability.

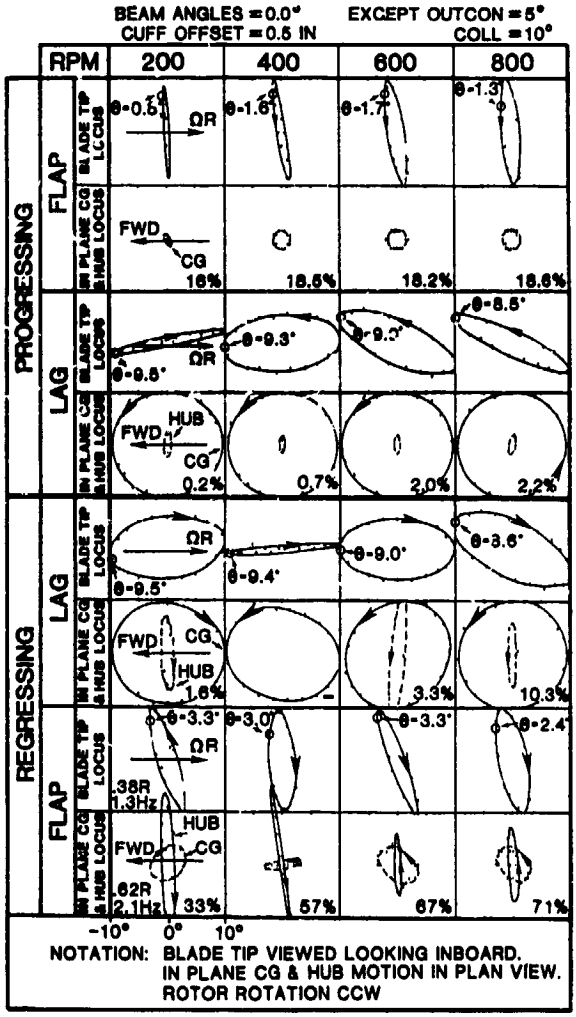

Fig. 12 Effect of RPM sweep on blade modes with combined coupling

obtained for the beam properties shown in Fig. 13 in which it is seen that the EIFLAP varies 6:1 from maximum to minimum and similar substantial changes occur in the other properties. Although there are major variations in beam rigidities, complete matching of the actual ITR beam was not possible because of convergence problems. The beam modelled in this paper represents a 1/2 way stage to the ITR properties but is still sufficiently nonlinear to be useful for assessing the effects of nonlinearity on stability.

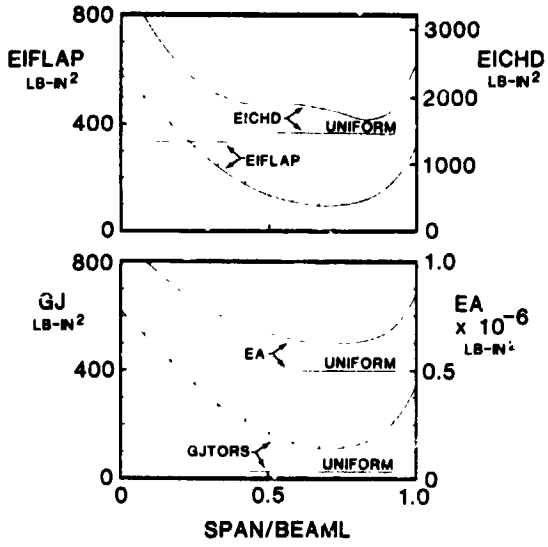

Fig. 13 Rigidities of the non-uniform beam

Finally a major objective of this study was to assess the degree that the results of the FLAIR analysis might be affected by the use of a uniform model for the flex beam. In reality the flex beam is far from uniform as its geometry results from careful optimization to achieve maximum flapping with minimum strain. Accordingly, FLAIR was modified to replace the beam by a 24 element section, defined in thickness and width, from which the correct local EI's, GJ and EA are calculated (in contrast to the original analysis which assures constant EI's, GJ and EA along the beam). The modification to FLAIR was substantial and the increased degree of nonlinearity severely taxed the convergence and integration routines used, making the analysis very sensitive to initial conditions. However, successful results were

In Fig. 14 results for the nonlinear beam of Fig. 13 are shown for the base case of zero beam angles and offset = 0, the case of OUTCON = +5°, and for the case of combining OUTCON = +5° and OFFSET = + 0.5 in. The effect of the nonlinearity is immediately apparent in the 'S' shaped distribution of pitch deflection along the beam which has hitherto been linear. Also the flap deflection of the beam is more nonlinear. But despite these substantial changes in the distribution of pitch along the beam, and the resultant accumulation into lag/flap/pitch coupling into the blade, the blade tip loci and the damping plots are relatively little affected. The most significant change occurs in the natural frequency locations and resulting rotor speeds at which the instabilities occur.

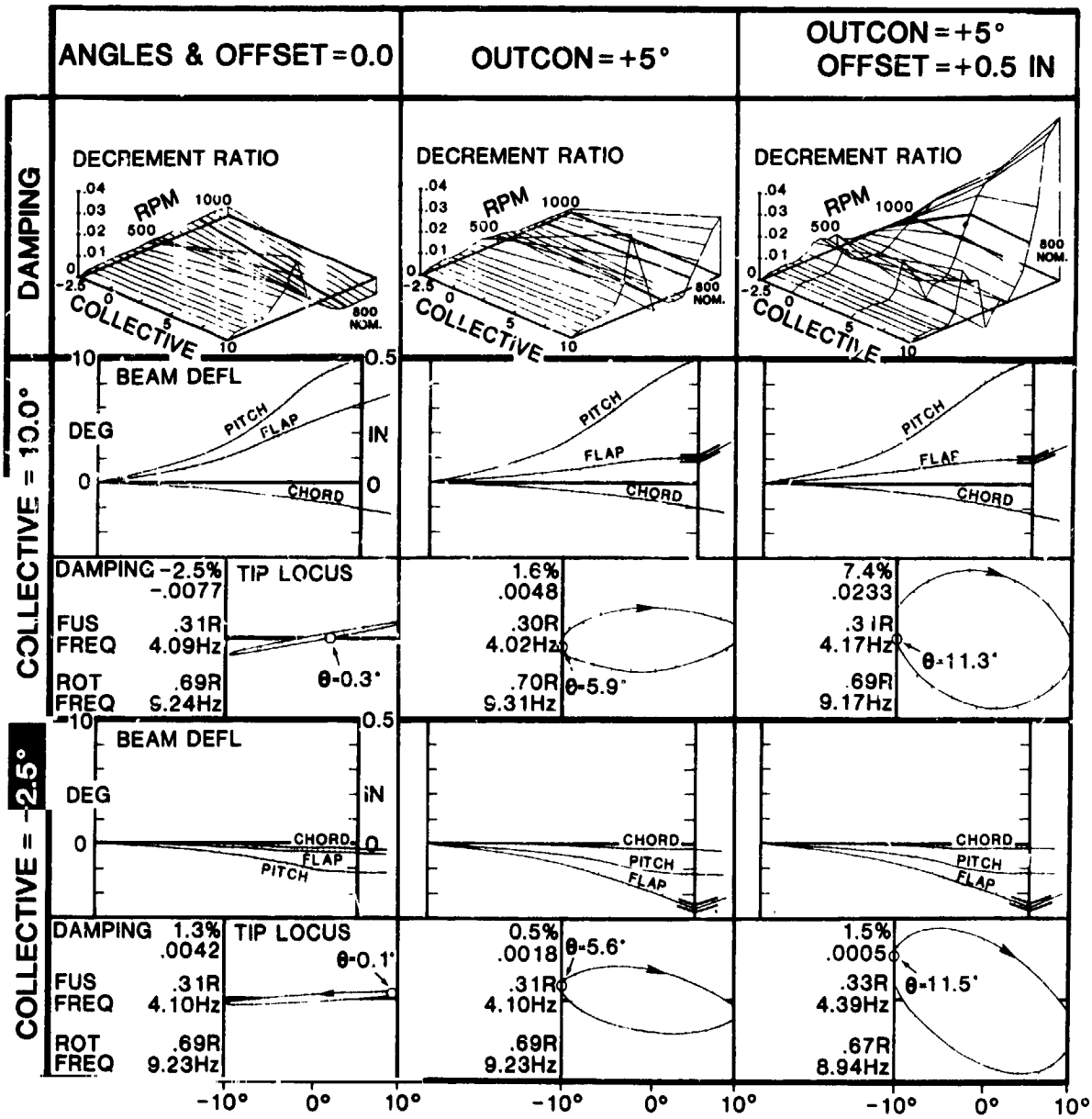

Fig. 14 Damping and modes for a non-uniform beam

6. THE EFFECT OF BLADE COUPLINGS ON GROUND RESONANCE

In Fig. 15 the effect of those couplings found to be favorable for air resonance are evaluated for ground resonance (due to the changed nature of the data the axes have been interchanged relative to the previous figures and the vertical scale changed by a factor of 3). The baseline case Fig. 15a clearly shown the small pitch instability at 600 RPM and the major roll instability at 900 RPM and a moderate stabilizing effect of collective pitch (opposite to air resonance). Adding OUTCON = +5, Fig. 15b has the effect of both increasing the stability of the stable region and increasing the instability of the unstable region. Going one stage further and adding OFFSET = +0.5 in, Fig. 15c continues the trend and now there is also a notable degradation of stability at negative collective pitch.

The pitch mode does appear to be favorably stabilized by pitch-lag coupling. But the roll mode appears to be quite immune and remains to be either avoided completely (as was the case with the YUH-61A) or suppressed by using large amounts of damping as has been the practice for articulated helicopters.

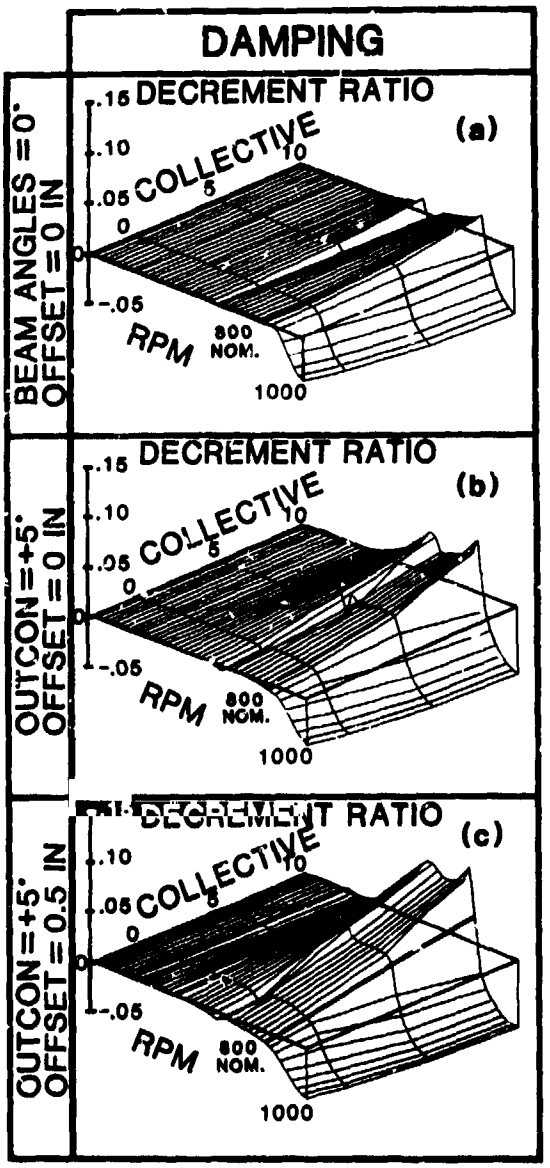

Fig. 15 Effect of pitch-lag couplings on ground resonance

7. CONCLUSION

A trade study has been completed using a modified version of the FLAIR analysis for the aeroelastic stability of bearingless rotors. The following conclusions have been drawn:

1. A baseline soft-in-plane bearingless rotor (i.e. with no flap-lag-pitch couplings introduced by beam angles or any other means) in air resonance is stable at all RPM's at low collective, but goes unstable at operating RPM at high collective. In ground resonance the typical instabilities encountered at the pitch and roll crossings with the regressing lag mode are only slightly affected by collective pitch.

2. Of the 6 available flexbeam installation angles only outboard coning (giving negative lag-pitch coupling) is powerfully effective in stabilizing air resonance at high collective pitch.

3. Vertical offset of the cuff shear pivot is shown to be equally effective in stabilizing air resonance, and the benefit is cumulative with outboard coning.

4. The effect of lag-pitch coupling on ground resonance is small at low collective, but at high collective the effect is both to increase the stability in the stable regions and to further increase the instability in the unstable regions.

5. The modification to the FLAIR program to replace the uniform flexbeam by a geometrically correct tailored flexbeam, with improved representation of coupling terms, did not affect the conclusions arrived at above for the uniform beam.

APPENDIX

BEHAVIOR OF LOW FREQUENCY ROOTS

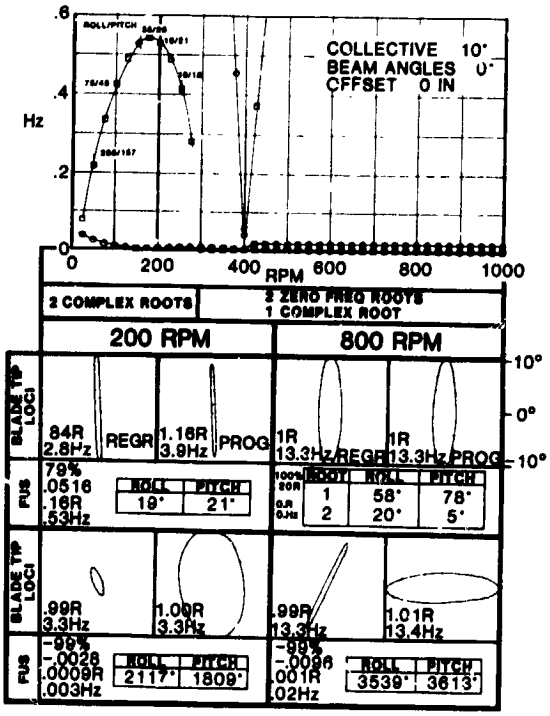

In the 300 to 1000 RPM region, there are typically two zero roots and one very low frequency complex root. The eigenvectors are dominated by fuselage pitch and roll. Below 300 RPM the two zero roots combined to give another complex root still having a low frequency compared to the regressing flap mode and, whose eigenvector varies from mainly roll to mainly pitch.

ACKNOWLEDGEMENT

My special thanks are due to Ken Bartie and Dot Kane for their patience and diligence in preparing this paper.

REFERENCES

1. Hooper, W.E., "Effect of Fuselage Dynamics on Helicopter Ground Resonance," Aircraft Engineering, August 1962.

2. Hohenemser, K. H., & Yin, S.K., "Some Application of the Method of Multiblade Coordinates," Journal of the AHS, Vol. 17, No. 3, July 1972.

3. Ormiston, R.A., "Aeromechanical Stability of Soft Inplane Hingeless Rotor Helicopters," 3rd European Rotorcraft Powered Lift Aircraft Forum, Paper No. 25, Aix-en-Provence, September 1977.

4. Hodges, D.H. "Aeromechanical Stability of Helicopters with a Bearingless Main Rotor:
   Part I: Equations of Motion
   Part II: Computer Program
   NASA TM 78459 & TM78460, February 1978.

5. Bousman, W. G. "An Experimental Investigation of the Effects of Aeroelastic Couplings on Aeromechanical Stability of a Hingeless Rotor Helicopter", Journal of the AHS Vol. 26 No. 1, January 1981.

DISCUSSION*
Paper No. 3

PARAMETRIC STUDY OF THE AEROELASTIC STABILITY OF A BEARINGLESS ROTOR
W. Euan Hooper

Bill Weller, United Technologies Research Center: Historically, I guess I've seen this before to the degree that flap-lag stability and pitch stability by virtue of blade coning or flexure inclination angle or whatever. I've seen it in some analyses and some test programs. But the [Bell] Model 680 or [Boeing Vertol] BMR [didn't show that benefit] as far as the final stability. I think this has to do somewhat with the physical characteristics of the model being used to do these types of things as opposed to the full-scale article. Would you care to comment on the applicability of this type of phenomenon to the BMR-type rotor systems?

Hooper: Well, I wouldn't agree with you that they did not show up on the BMR. The BMR had 2 1/2 degrees of outboard coning and I think that was the main feature that stabilized it. The BMR was a good stable rotor in every flight regime except one and that was [partial power descents at low forward speed. In hover and at high forward speeds] it was very stable, just a replica of the BO 105.

Weller: The point more is the degree of the effect not that the outboard blade coning is detrimental. It's generally agreed that it is beneficial to some degree, but your effect there is proving somewhat significant. The model test that I have been associated with, the 680 system, doesn't show anywhere near the benefit as far as the degree that your analytical studies would imply.

Hooper: Well that's interesting and we have yet to complete the correlation of our [own data] with our test program. So far we have not been disappointed in the tests; we'll find out in full scale.

Bill Warmbrodt, NASA Ames Research Center: [Was there a reason for choosing the 5 degree angles] used in your ITR study?

Hooper: Just arbitrary, to give the sensitivity.

Jerry Miao, Sikorsky Aircraft: Euan, I believe all the data you show [from using] FLAIR. I believe when Fort Eustis sponsored the BMR program [there was a] lot of BMR test [data obtained]. There was [shown in that test a] favorable, stabilizing parameter [and that was pre-pitch or an orienting of the] flexbeam in the pitch sense. I believe there is test data from the BMR model test that [shows that effect clearly.] I believe that if you look at modal damping vs rpm with this inboard flexbeam pitch angle the stability of the air resonance [mode] improved more than twice. Have you ever tried to use FLAIR to [compare with these data?]

Hooper: No, I haven't and you raise a very interesting point. I mentioned that [we] did not get the degree of stability from the hub pitch setting that we expected. However, there is a very significant difference with this rotor in that it is much more flexible in [flap] than the BMR or our previous YUH-61A. That may be the key to it. But it certainly surprised us [and so we] also tried it with the nonuniform beam analysis [and also found no effect of hub/beam pitch. We're going to have to go] back through those cases with the FLAIR analysis [and evaluate hub/beam pitch in combination with other parameters.] Even with the nonuniform beam that [accurately represents] the distribution of [flap and chord bending and] pitch quite differently [there was] no sensitivity [to hub/beam] pitch angle. So [the different sensitivity to hub/beam pitch angle] may be due to the lack of flap stiffness.

Jing Yen, Bell Helicopter: I'd like to [back] up what Bill [Weller] said. The aeroelastic coupling will be very powerful for a hingeless type of rotor. [The hingeless rotor clearly defines the location of the pitch axis. When we go to a bearingless rotor, especially with a soft hub, the location of the pitch axis and the coupling around the pitch axis is strongly affected by flexbeam bending.] The floating of the pitch axis will in general reduce the influence of aeroelastic coupling.

Hooper: Well, the location of the pitch axis is obviously the key and we have the experience on the YUH-61A which had zero precone, zero HUBCON in this context. That aircraft was extremely stable. In that case the pitch axis was forced physically to be [in the disk plane.] The coning [occurred] outboard of the pitch axis [and resulted in strong beneficial pitch-lag coupling.]

*The transcript of this discussion is incomplete because of recording problems. Areas of ambiguous or missing text have been discussed with the person asking or answering the question and the text is indicated with brackets.

Inderjit Chopra, University of Maryland: [Inaudible]

Hooper: The basic FLAIR is a uniform beam.

Chopra: [Inaudible]

Hooper: A single load path beam, that's right. It's been subjected to a lot of scrutiny from our point of view. Even Mychalowycz and Pete Dixon have been very suspicious that it's not an adequate representation of a beam. I have to say it has stood up to every examination. That is why we were looking at the very detailed distribution of the flexibility along the beam to see that it behaves as it should. I've been satisfied that [FLAIR uses] a rigorous representation of the beam. There are no small angle assumptions of the beam. That's one of the attractive [points]. The beam representation and the control system all use large angles.

Harry Runyan, College of William and Mary: I think your pitch deflection is correct. I don't see why you are worried about it. It's a second derivative in θ. You only have two conditions you can put on it. One would be a zero deflection at the root, [and the other zero torque at the tip]. You have no more conditions you can put in. That's it. That's what you get. Whereas in bending you have a fourth order equation. So I think it looks correct within the limits of linear theory.

Chopra: [Inaudible]

Hooper: We'll be in a better position when we [do that] test.

NONLINEAR DYNAMICS OF A HELICOPTER MODEL IN GROUND RESONANCE

D.M.Tang* and E.H.Dowell**
Department of Mechanical Engineering
and Material Science
Duke University, Durham, NC 27706

Abstract

An approximate theoretical method is presented which determines the limit cycle behavior of a helicopter model which has one or two nonlinear dampers. The relationship during unstable ground resonance oscillations between lagging motion of the blades and fuselage motion is discussed. An experiment has been carried out on using a helicopter scale model. The experimental results agree with those of the theoretical analysis.

Notation

H	geometrical length of the mode, see Fig.1
I	mass moment of inertia of blade relative to drag hinge
J_{fx}, J_{fz}	mass moment of inertia of fuselage about X and Z axis through A
J_{sx}, J_{sz}	mass moment of inertia of shaft about X and Z axis through A
K_{sf}	coupling spring coefficient between fuselage and shaft
$L_{v.h}$	distance from the axis of rotation center to drag hinge center
M_h	hydraulic damping moment coefficient
m_{hx}, m_{hz}	nondimensional hydraulic damping coefficients
M_d	dry friction moment coefficient
m_{dx}, m_{dz}	nondimensional dry friction damping coefficients
m	mass of the blade
n	number of blades
n_b	damping coefficient of blade
R	radius of the rotor blade
S	static mass moment relative to drag hinge
t	time
(A-model)	
n_0	fuselage damping coefficient
P_0	natural frequency of fuselage
ϵ_a	hinged mass ratio $nS^2H^2/2I(J_{sz}+J_{fz}+nm_bH^2)$
(B-model)	
n_2--n_8	damping coefficients
P_2--P_8	natural frequencies
ϵ_b	hinged mass ratio $nS^2H^2/2I(J_{sz}+nm_bH^2)$
(C-model)	
n_x, n_z	fuselage damping coefficients
P_x, P_z	natural frequencies of fuselage
ϵ_c	hinged mass ratio $nS^2H^2/2I(J_0+nm_bH^2)$
θ_{fx}, θ_{fz}	angular motion coordinate of fuselage about X and Z axis
θ_{sx}, θ_{sz}	angular motion coordinate of shaft about X and Z axis
$\theta_{fx0}, \theta_{fz0}$	angular amplitude of fuselage about X and Z axis
$\theta_{sx0}, \theta_{sz0}$	angular amplitude of shaft about X and Z axis
ψ_k	angular orientation of different rotor blades
ξ_k	angular deflection of k-th blade
ω_s	natural frequency of rotating blade relative to drag hinge
ρ_c	distance of center of gravity of the blade from drag hinge
η, ζ	coordinate of the center of gravity of the blade system in fixed reference frame
ν_0	nondimensional blade parameter $\sqrt{L_{v.h}S/I}$
Ω	rotor speed

Introduction

Helicopter ground resonance is a self-excited vibration phenomenon rather than a forced vibration. The safety standards for helicopter strength require that a helicopter with an articulated rotor must have enough stable margin when it is in contact with the ground, especially, in case of rough landing. Such standards are based on linear theory, but in fact the most common design of the landing gear has nonlinear damping characteristics. How much of an effect on ground resonance will be induced? Does the nonlinear damping characteristic tend to increase stability or not? These questions are waiting for investigators to solve. The present authors [1,2] and Tongue [3] have engaged in such research. The purpose of this paper is to further study such problems.

The nonlinear damping in the landing gear of a helicopter brings into action both roll and pitch motion of the fuselage. In a series of publications [3-13] about helicopter ground resonance instability, this aspect was not taken into account by many authors. Also in the past, many investigators have used Coleman' classical multi-blade coordinate theory to simplify

---

* Visiting Scholar, Nanjing Aeronautical Institute, China.
** Dean, School of Engineering, Duke University, Durham, NC.

the study of the rotor blade dynamics. Most previous authors have considered linear dynamic models.

In the present paper, an approximate method has been used to calaulate the limit cycle behavior of a given helicopter model which has a nonlinearity in the landing gear such as a hydraulic resistance which is approximately proportional to the square of velocity or dry friction resistance. An experimental investigation has been carried out as well. The test apparatus is an improved version of Bielawa's rotor model [4]. The experimental results are in good agreement with those of the theoretical analysis.

In the present paper, we study the effect of combined roll and pitch fuselage motions, and consider the relationship between the lagging motion of the blades and the fuselage motion. Also discussed are the differences in the unstable boundary between the linear and the nonlinear model. We believe that these results will be helpful in further understanding the physical essence of helicopter ground resonance instability, and in protecting against such an instability.

Approximate method of nonlinear analysis

The analysis is based on a helicopter model with an articulated rotor. A sketch of this model is shown in Fig.1. We will assume that the blades in the plane of rotation are rigid but articulated; the spring and damping coefficients of the fuselage and the shaft are isotropic, but their mass moments of inertia are anisotropic. Nonlinear damping includes hydraulic resistance which is proportional to velocity squared and also dry friction resistance; these can be represented by $M_h|\dot\theta|\dot\theta$ and $M_d\,\mathrm{sign}\dot\theta$, respectively. The equations of motion for the model are six nonlinear differential equations with unknown functions η, ζ, θ_{fx}, θ_{fz}, θ_{sx} and θ_{sz}. These are as follows (see Ref.[1]):

$$
\begin{aligned}
&\ddot\eta+2n_b\dot\eta+\omega_s^2\eta-2\Omega(\dot\zeta+n_b\zeta)=nSH\ddot\theta_{sz}/2I\\
&\ddot\zeta+2n_b\dot\zeta+\omega_s^2\zeta+2\Omega(\dot\eta+n_b\eta)=-nSH\ddot\theta_{sx}/2I\\
&\ddot\theta_{sz}+2n_2\dot\theta_{sz}+(P_2^2+P_4^2)\theta_{sz}-2n_4\dot\theta_{fz}\\
&-P_4^2\theta_{fz}=SH\ddot\eta/J_{sz}\\
&\ddot\theta_{sx}+2n_1\dot\theta_{sx}+(P_1^2+P_3^2)\theta_{sx}-2n_3\dot\theta_{fx}\\
&-P_3^2\theta_{fx}=-SH\ddot\zeta/J_{sx}\\
&\ddot\theta_{fx}+2n_5\dot\theta_{fx}+(P_5^2+P_7^2)\theta_{fx}-2n_7\dot\theta_{sx}-P_7^2\theta_{sx}\\
&+m_{hx}\dot\theta_{fx}|\dot\theta_{fx}|+m_{dx}\mathrm{sign}\dot\theta_{fx}=0\\
&\ddot\theta_{fz}+2n_6\dot\theta_{fz}+(P_6^2+P_8^2)\theta_{fz}-2n_8\dot\theta_{sz}-P_8^2\theta_{sz}\\
&+m_{hz}\dot\theta_{fz}|\dot\theta_{fz}|+m_{dz}\mathrm{sign}\dot\theta_{fz}=0
\end{aligned}
\qquad (1)
$$

In order to simplify the problem, we will discuss two special cases:

1. A model with a single nonlinear damper.

We suppose that the motion in the X direction is constrained, i.e, $\theta_{sx}=\theta_{fx}=0$, and the subscript z in θ_{sz} and θ_{fz} is thus eliminated, and define that:

$$\tilde\theta_s=m_{hz}\theta_s\ ,\quad \tilde\theta_f=m_{hz}\theta_f$$

$$\tilde\eta=\eta m_{hz}SH/J_{sz},\quad \tilde\zeta=\zeta m_{hz}SH/J_{xz}$$

Thus (1) becomes:

$$
\begin{aligned}
&\ddot{\tilde\eta}+2n_b\dot{\tilde\eta}+\omega_s^2\tilde\eta-2\Omega(\dot{\tilde\zeta}+n_b\tilde\zeta)=\xi_b\ddot{\tilde\theta}_s\\
&\ddot{\tilde\zeta}+2n_b\dot{\tilde\zeta}+\omega_s^2\tilde\zeta+2\Omega(\dot{\tilde\eta}+n_b\tilde\eta)=0\\
&\ddot{\tilde\theta}_s+2n_2\dot{\tilde\theta}_s+(P_2^2+P_4^2)\tilde\theta_s-2n_4\dot{\tilde\theta}_f-P_4^2\tilde\theta_f=\ddot{\tilde\eta}\\
&\ddot{\tilde\theta}_f+2n_6\dot{\tilde\theta}_f+(P_6^2+P_8^2)\tilde\theta_f+\dot{\tilde\theta}_f|\dot{\tilde\theta}_f|+\alpha\,\mathrm{sign}\dot{\tilde\theta}_f\\
&-2n_8\dot{\tilde\theta}-P_8^2\tilde\theta_s=0
\end{aligned}
\qquad (2)
$$

where $\alpha=m_{hz}m_{dz}$

For the nonlinear terms $\dot\theta_f|\dot\theta_f|$ and $\mathrm{sign}\dot\theta_f$, we apply an approximate procedure which is called quasi-linearization.

Let: $\theta_f=|\theta_f|\cos\lambda t$

Representing the above nonlinear terms by a Fourier series and retaining the first harmonic produces(see Ref.[3],[14])

$$\dot{\tilde\theta}_f|\dot{\tilde\theta}_f|=-\,8/3\pi^*\lambda^2|\theta_{f0}|^2\sin\lambda t$$

$$\mathrm{sign}\dot{\tilde\theta}_f=-4/\pi^*\sin\lambda t$$

Let:

$$\tilde\eta=\tilde\eta_0e^{i\lambda t}$$

$$\tilde\zeta=\tilde\zeta_0e^{i\lambda t}$$

$$\tilde\theta_s=\tilde\theta_{s0}e^{i\lambda t}$$

Once again let:

$$\tilde\theta_f=\tilde\theta_{f0}e^{i\lambda t}$$

Substitute these expressions into Eqs.(2), and require the determinant of coefficients to be zero for nontrivial solutions. The final characteristic equations are:

real part:

$$
\begin{aligned}
&a\tilde\theta_{f0}^2\lambda^8-b\tilde\theta_{f0}^2\lambda^7-c\tilde\theta_{f0}^2\lambda^6+(d\tilde\theta_{f0}^2+\beta b)\lambda^5+e\tilde\theta_{f0}^2\lambda^4\\
&-(f\tilde\theta_{f0}^2+\beta d)\lambda^3-g\tilde\theta_{f0}^2\lambda^2+\beta f\lambda+h\tilde\theta_{f0}^2=0
\end{aligned}
\qquad (3)
$$

imaginary part:

$$
\begin{aligned}
&a_1\tilde\theta_{f0}^2\lambda^8+b_1\tilde\theta_{f0}^2\lambda^7-(c_1\tilde\theta_{f0}^2+b_0a)\lambda^6-d_1\tilde\theta_{f0}^2\lambda^5\\
&(e_1\tilde\theta_{f0}^2+\beta c_1)\lambda^4+f_1\tilde\theta_{f0}^2\lambda^3-(g_1\tilde\theta_{f0}^2+\beta e_1)\lambda^2\\
&-h_1\tilde\theta_{f0}^2\lambda-g_1=0
\end{aligned}
\qquad (4)
$$

The coefficients a,b,c...etc. of the above Eqs. are given in Appendix B of Ref.[1].

For the case of $K_{sf}=\infty$, $\tilde{\theta}_s=\tilde{\theta}_f=\tilde{\theta}$, i.e the shaft is connected together with fuselage, the differential equations become a simpler nonlinear mathematical model for analysing helicopter ground resonance.

$$\begin{aligned}
&\ddot{\tilde{\eta}}+2n_b\dot{\tilde{\eta}}+\omega_s^2\tilde{\eta}-2\Omega(\dot{\tilde{\zeta}}+n_b\tilde{\zeta})=\varepsilon_a\ddot{\tilde{\theta}}\\
&\ddot{\tilde{\zeta}}+2n_b\dot{\tilde{\zeta}}+\omega_s^2\tilde{\zeta}+2\Omega(\dot{\tilde{\eta}}+n_b\tilde{\eta})=0\\
&\ddot{\tilde{\theta}}+2\tilde{n}_0\dot{\tilde{\theta}}+\dot{\tilde{\theta}}|\dot{\tilde{\theta}}|+\tilde{\theta}=\ddot{\tilde{\eta}}
\end{aligned}\qquad (5)$$

where:

$\tilde{n}_b=n_b/P_0$, $\tilde{\omega}_s=\omega_s/P_0$, $\tilde{n}_0=n_0/P_0$, $\tilde{\Omega}=\Omega/P_0$

For this case, the final characteristic equation is the same as in Ref[3].

Eq.(3) or (4) is eighth order in λ. Also, the $\tilde{\theta}_{f0}$ angular amplitude now appears explicitly. This means that the limit cycle amplitude of the nonlinear system is directly related to λ, the frequency of oscillation, and both must be solved for simultaneously.

The Broyden method [15] was used to solve the above simultaneous equations. Let functions $f_1(\tilde{\theta}_{f0},\lambda)$ and $f_2(\tilde{\theta}_{f0},\lambda)$ be equal to the left hand sides of Eq.(3) and Eq.(4), respectively.

$$f_1(\tilde{\theta}_{f0},\lambda)=0$$

$$f_2(\tilde{\theta}_{f0},\lambda)=0$$

2. A model with two nonlinear dampers.

We suppose:

$K_{sf}=\infty$, $\theta_{sx}=\theta_{fx}=\theta_x$, $\theta_{sz}=\theta_{fz}=\theta_z$

and define:

$J_0=(J_x+J_z)/2$, $\tilde{\theta}_x=\theta_x$, $\tilde{\theta}_z=\theta_z$, $\tilde{\eta}=\eta SH/J_0$,

$\tilde{\zeta}=\zeta SH/J_0$, $J_x=J_{fx}+J_{sx}$, $J_z=J_{fz}+J_{sz}$,

$\varepsilon_2=J_0/J_x$, $\varepsilon_3=J_0/J_z$

The general equations of motion for the model are given by Eqs.(6).

$$\begin{aligned}
&\ddot{\tilde{\eta}}+2n_b\dot{\tilde{\eta}}+\omega_s^2\tilde{\eta}-2\Omega(\dot{\tilde{\zeta}}+n_b\tilde{\zeta})=\varepsilon_c\ddot{\tilde{\theta}}_z\\
&\ddot{\tilde{\zeta}}+2n_b\dot{\tilde{\zeta}}+\omega_s^2\tilde{\zeta}+2\Omega(\dot{\tilde{\eta}}+n_b\tilde{\eta})=-\varepsilon_c\ddot{\tilde{\theta}}_x\\
&\ddot{\tilde{\theta}}_x+2n_x\dot{\tilde{\theta}}_x+P_x^2\tilde{\theta}_x+m_{hx}|\dot{\tilde{\theta}}_x|\dot{\tilde{\theta}}_x+m_{dx}\,\mathrm{sign}\dot{\tilde{\theta}}_x=-\varepsilon_2\ddot{\tilde{\zeta}}\\
&\ddot{\tilde{\theta}}_z+2n_z\dot{\tilde{\theta}}_z+P_z^2\tilde{\theta}_z+m_{hz}|\dot{\tilde{\theta}}_z|\dot{\tilde{\theta}}_z+m_{dz}\,\mathrm{sign}\dot{\tilde{\theta}}_z=\varepsilon_3\ddot{\tilde{\eta}}
\end{aligned}\qquad (6)$$

Eqs.(6) is a set of nonlinear differetial equations for determining four unknown functions η, ζ, $\tilde{\theta}_x$ and θ_z.

Using the method of harmonic balance and retaining only the fundamental harmonic, we take

$$\begin{aligned}
&\tilde{\theta}_x=\tilde{\theta}_{x0}\cos\lambda t\\
&\tilde{\theta}_z=\tilde{\theta}_{zc}\cos\lambda t+\tilde{\theta}_{zs}\sin\lambda t=\tilde{\theta}_{z0}\cos(\lambda t-\varphi_z)\\
&\tilde{\eta}=\tilde{\eta}_c\cos\lambda t+\tilde{\eta}_s\sin\lambda t=\tilde{\eta}_0\cos(\lambda t-\varphi_\eta)\\
&\tilde{\zeta}=\tilde{\zeta}_c\cos\lambda t+\tilde{\zeta}_s\sin\lambda t=\tilde{\zeta}_0\cos(\lambda t-\varphi_\zeta)
\end{aligned}\qquad (7)$$

Here φ_z, φ_η , φ_ζ are respectively the phase difference of $\tilde{\theta}_z$, $\tilde{\eta}$ and $\tilde{\zeta}$ with respect to $\tilde{\theta}_x$

Now we consider the term $\mathrm{sign}\dot{\tilde{\theta}}_z$ and $\dot{\tilde{\theta}}_z|\dot{\tilde{\theta}}_z|$. As was mentioned previously [2], we can obtain the following approximate result:

For λ, $\tilde{\theta}_{z0}>0$

$$\mathrm{sign}\dot{\tilde{\theta}}_z\cong\frac{4}{\pi\tilde{\theta}_{z0}}(\tilde{\theta}_{zs}\cos\lambda t-\tilde{\theta}_{zc}\sin\lambda t)$$

$$|\dot{\tilde{\theta}}_z|\dot{\tilde{\theta}}_z=\frac{-8\lambda^2}{3\pi}\tilde{\theta}_{z0}(\tilde{\theta}_{zc}\sin\lambda t-\tilde{\theta}_{zs}\cos\lambda t)$$

Inserting Eq.(7) into Eq.(6) we obtain a system of eight simultaneous nonlinear algebraic equations for determining the quantities, $\tilde{\eta}_c,\tilde{\eta}_s,\tilde{\zeta}_c,\tilde{\zeta}_s,\tilde{\theta}_{x0},\tilde{\theta}_{zc},\tilde{\theta}_{zs}$ and λ.

By elimination of the first four unknowns, the equations can be rewritten more compactly as a matrix equation with four unknowns, $\tilde{\theta}_{x0},\tilde{\theta}_{zc},\tilde{\theta}_{zs}$, λ.

Let:

$$\{F\}\equiv\{U\}+[V]^{-1}\{\tilde{\theta}\}=\{0\}\qquad (8)$$

where

$$[V]=\begin{bmatrix}-a & -b & c & d\\ b & -a & -d & c\\ c & d & a & b\\ -d & c & -b & a\end{bmatrix}\qquad \{\tilde{\theta}\}=\begin{Bmatrix}\tilde{\theta}_{zc}\\ \tilde{\theta}_{zs}\\ \tilde{\theta}_{x0}\\ 0\end{Bmatrix}$$

$$\{U\}=\begin{Bmatrix}(P_z^2/\lambda^2-1)\tilde{\theta}_{zc}/\varepsilon_3+2n_z\tilde{\theta}_{zs}/\lambda\varepsilon_3+\\ 8m_{hz}\tilde{\theta}_{z0}\tilde{\theta}_{zs}/3\pi\varepsilon_3+4m_{dz}\tilde{\theta}_{zs}/\pi\lambda^2\tilde{\theta}_{z0}\varepsilon_3\\ (P_z^2/\lambda^2-1)\tilde{\theta}_{zs}/\varepsilon_3-2n_z\tilde{\theta}_{zc}/\lambda\varepsilon_3-\\ 8m_{hz}\tilde{\theta}_{z0}\tilde{\theta}_{zc}/3\pi\varepsilon_3-4m_{dz}\tilde{\theta}_{zc}/\pi\lambda^2\tilde{\theta}_{z0}\varepsilon_3\\ (1-P_x^2/\lambda^2)\tilde{\theta}_{x0}/\varepsilon_2\\ 2n_x\tilde{\theta}_{x0}/\lambda\varepsilon_2+4m_{dx}/\pi\varepsilon_2\lambda^2+8m_{hx}\tilde{\theta}_{x0}^2/3\pi\varepsilon_2\end{Bmatrix}$$

$$a=(\omega_s^2/\lambda^2-1)/\varepsilon_1 \qquad \{F\}=\begin{Bmatrix} f_1 \\ f_2 \\ f_3 \\ f_4 \end{Bmatrix}$$

$$b=2n_b/\varepsilon_1\lambda$$

$$c=2\Omega n_b/\varepsilon_1\lambda^2$$

$$d=2\Omega/\varepsilon_1\lambda$$

In order to solve Eq.(8), the elements of {F} must be zero. Here we also apply Broyden's method to solve the above equation.

Experimental Investigation

1. Experimental equipment

An overall view of the test model and recording equipment used in this study is shown in Figs.2 and 3. The details of the various components of the model appear in Ref.[1] and [2]. The A-model has only one degree of freedom for fuselage motion. The B-model has two degrees of freedom for shaft and fuselage motion. The C-model has two degrees of freedom for the roll and the pitch motion of the fuselage. The characteristic curves of the hydraulic and dry friction damping are shown in Fig.4(a) and (b). The method of determining these parameters is described in Ref.[1].

2. Measurement system

The X and Z angular displacements and velocities of the fuselage and the shaft are obtained by RVDT, R30D, velocity transducers located near the dry friction dampers, and a LVDT located near the gimbal support assembly. The output voltage of the transformers and velocity transducers is proportional to angular displacement and velocity of the roll and the pitch of the fuselage and the shaft. The output from the transformers are amplified and recorded on a multiple channel tape recorder, HP3968A.

In order to obtain a one per revolution signal and the lagging motion of the individual blades during rotation of the blades, we mount a 13-ch brush and slip ring assembly on the shaft between the electric motor and hub, see Fig.5. One of these slip rings is not a closed ring. It gives an impulsive signal once per revolution, so a very accurate measurement of rotor speed can be provided. Three angular transducers, R30A, are mounted on the drag hinges. The signals for lagging motion of each blade were amplified and recorded through brush and slip ring assemblies. The 8 channel signals were recorded simultaneously on a tape recorder, and further analysed by a Frequency Spectral Analyzer, HP3582A. Finally, the phase plane plots and frequency spectral plots were plotted by a X-Y recorder.

The stability test needs an initial disturbance, so two electro-magnets were mounted on the test equipment. Those are used to generate a disturbance in the direction of roll or pitch of the fuselage.

The device for angular amplitude calibration is shown in Fig.6. An electric motor with stepless variable speed provides a vibration source, and drives a cam which can generate a sine wave, such that the relationship between output voltage from the transducers and the actual angle can be determined.

3. Frequency response test

The purpose of the frequency response test is to determine the natural frequencies of the system, and to provide an independent check on the system parameters. Before the test, the drag hinges are fixed, and a known block mass (3 oz) is put on a drag hinge. A centrifugal force caused by the bias mass will excite the system, and the frequency response versus rotor speed can be found.

4. Stability test

Testing the model for self-excited instability regions was accomplished by slowly varying the rotor speed until instability was observed in response to an initial disturbance.

Results and Discussion

Fig.7 shows the limit cycle behavior when only the hydraulic nonlinearity is present in the A-model. The figure shows that the maximum limit cycle amplitude occurs near the critical rotor speed of the linear system, and that the dominant response occurs in the region, $(1.7\text{-}2.0)*\Omega$. Furthermore, there is an abrupt change in response from $(1.9\text{-}1.95)*\Omega$ in Fig.7. This means that the amplitude response is very sensitive to small changes in rotor speed in this range of rotor speed.

Fig.8 shows the limit cycle behavior with both hydraulic and dry friction nonlinearities. The curve has a shape similar to that of Fig.7, but the response amplitude is smaller than that in Fig.7. Physically the action of dry friction is to increase the equivalent viscous damping in the landing gear. The instability region becomes narrower, and the response amplitude reduces.

Fig.9 shows the limit cycle behavior of the B-model. There are two instability regions in the figure. The first one is dominated by the shaft motion. Because the effect of nonlinear damping of the fuselage on the shaft is weak, the shaft has a large limit cycle amplitude (for

some range of Ω beyond the measurable angle). In contrast with the first region, in the second instability region there is not a large limit cycle amplitude because of the direct effects of nonlinear damping of the fuselage on the fuselage motion.

As far as the C-model is concerned, Fig.10 shows the results of frequency spectral analysis of the fuselage motion at a rotor speed of 1.2(HZ). The mode shape of the unstable motion is dominated by roll of the fuselage, and the oscillation frequency is equal to the roll natural frequency of the fuselage. Simultaneously, there is a small limit cycle amplitude in the pitch motion; its oscillation frequency is not equal to the pitch natural frequency, but is equal to the roll natural frequency. The phase angle between roll and pitch is equal to 51°, corresponding to a frequency of 0.84(HZ). The phase curve in the vicinity of 0.84(HZ) is almost parallel to the frequency axis, and the phase angle is quite insensitive to frequency.

Fig.11-12 show theoretical and experimental results of the limit cycle amplitude and phase angle behavior. A reasonable experimental verification of the theory is achieved. Because of the experimental complexity and calculation approximation, the quantitative accuracy of the verification is not very high. However, the general features of the experimental results are well predicted by the theory. For reference, in Fig.13 the stability boundary results from linear theory are shown and compared to experimental data obtained with the nonlinear dampers removed. The agreement between theory and experiment in this case is good.

Fig.14 shows a phase plane plot which is directly plotted by a X-Y recorder. The measurement point of displacement and velocity is located at the same position. Their phase difference approximates to 90°, the pattern displays an ellipse approximately, and the higher order harmonic components are included in the ellipse curve. From this pattern, we also can see the transient process leading to the steady state limit cycle amplitude. Different disturbances have different unstable processes. In this case the roll oscillation of the fuselage tends to a limit after about 7 pseudo cycles, and the transient process includes more higher order harmonic components.

Fig.15 shows the results of a frequency spectral analysis of the lagging motion of the individual blades at a rotor speed of 2.04(HZ). It is found that in the instability region the individual blades have an identical oscillation frequency, p, which is equal to the difference between the rotor speed and the oscillation frequency, λ, of the fuselage. This result is in agreement with conclusion which is derived by classical linear theory. However, the individual blades have different amplitudes and phase angles due to the actual small different blade damping characteristics.

The equation of motion of the k-th blade can be written as follows:

$$\ddot{\xi}_k+2n_b\dot{\xi}_k+\omega_s^2\xi_k=\frac{\nu_\beta^2}{\nu_{v.h}}(\ddot{X}\sin\psi_k-\ddot{Z}\cos\psi_k)$$

The periodic term in the above equation can be removed by using the Coleman co-ordinates.

$$\eta=\sum_{k=1}^{n}\xi_k\sin\psi_k$$
$$\zeta=\sum_{k=1}^{n}\xi_k\cos\psi_k$$

If it is expected that η and ζ are well represented by a fundamental harmonic with oscillation frequency, λ, then ξ_k may be defined as:

$$\xi_k=\xi_0\cos(Pt+2\pi k/n)$$

i.e the following conditions must be satisfied:

* $p=\Omega-\lambda$
* the amplitudes of the individual blades are identical.
* the phase angle of the k-th blade is equal to $2k\pi/n$.

In the present experiment, only the first condition is satisfied. The modest violations of the latter two conditions are the main reasons for the error between theoretical and experimental results.

In order to provide a better physical understanding of the unstable motion, we discuss the relationship between motion of the hub center and the center of gravity (C.G) of the blades. In the fixed coordinate system X0Z, the motion of the common center of gravity of the blade system is expressed by

$$X_c=X-\frac{\rho_c}{n}\sum_{k=1}^{n}\xi_k\sin\psi_k$$
$$Z_c=Z+\frac{\rho_c}{n}\sum_{k=1}^{n}\xi_k\cos\psi_k$$
$$X=H\sum_{i=1}^{m}\theta_{x0i}\cos\lambda_i t$$
$$Z=H\sum_{i=1}^{m}\theta_{z0i}\cos(\lambda_i t-\varphi_{zi})$$

Fig.16 shows the time history of η and ζ. The test curves include components with frequency $(2\Omega-\lambda)$, and λ, in addition, a $\cos\lambda t$ component. This also can be clearly found from Fig.17. The motion locus of the C.G of the blades is not exactly an ellipse, but a somewhat more complicated curve. The starting point at t=0 does not

coincide with the end point at t=2(sec.), however over a much longer time interval, the motion does appear periodic. The phase angle between hub center and C.G of blades is equal to 46° from calculation, and 15° from test. The phase angle depends upon the dampings of the fuselage and blades, as well as rotor speed.

Fig.18 shows the theoretical and experimental results for a rotor speed of 1.2(HZ). The test curves are approximately cosine waves. The motion locus of the C.G of the blades approximates to an ellipse, and excellent agreement of calculation with test is achieved for the motion locus of the hub center. As compared with Fig.17 and 18, we find that the difference between theory and experiment for the hub center motion mainly comes from the variation of blade motion from one blade to the next.

Fig.19 shows the test results for a rotor speed of 1.96(HZ). All higher order harmonic components are included in the motion of the fuselage and blades. Their motion loci have guite complex shapes, but they always tend to a limit amplitude.

Conclusions

A number of conclusions may be reached.

1. Unstable motion of a helicopter in ground resonance can occur only when the rotor speed is within a certain region, and at the same time a initial disturbance acts on it. This conclusion is suitable for both linear and nonlinear systems.

2. During unstable motion the oscillation frequency is equal to the natural frequency of the linear system, or approximately the natural frequency for a nonlinear system.

3. The nonlinear dynamic rotor system with multiple nonlinear dampers has more complex motions than the system with a single nonlinear damper. The coupled motion of roll and pitch of the fuselage is due to blade lagging motion. This coupling motion is important in understanding ground resonance of an actual helicopter.

4. The agreement of theory with the experimental results verifies that the analytical method which is described in this paper is useful and reliable.

5. The different characteristics of individual lag blade dampers will lead to different limit cycle behavior.

6. The results show that a landing gear with hydraulic nonlinear damping characteristics and dry friction damping may be advantageous for protecting against ground resonance instability. It is unlikely, perhaps, that a helicopter resigner would rely on a nonlinear damper for primary protection against ground resonance. However, such a damper may be useful as a failsafe device to ensure a benign failure mode should a primary linear damper become inoperable or prove inadequate under some operating conditions.

7. It is expected that the design and operation of blade dampers will also be very important for avoiding ground resonance. This is a logical topic for future study.

Acknowledgement

We would like to acknowledge to Mr.William Clayton of the Duke Mechanical Engineering Lab. and the staff of the Structural Engineering Lab. for their contributions to the experimental work. The experimental rotor system used in the present study is a substantially modified version of that originally designed by professor Richard Bielawa of RPI for his work on ground resonance (Ref.4). It was made available to the authors through the generous assistance of professor H.C.Curtiss,Jr., of Princeton University.

This work was supported by the National Science Foundation under Grant No. MEA-8315193. Dr. Elbert Marsh is the technical monitor.

References

1. Tang D.M and Dowell E.H, "Nonlinear Dynamics of a Helicopter Model in Ground Resonance. Part 1: Analysis and Experiment on a Helicopter Model with Single Nonlinear Damper and Fuselage Motion", Duke University, Engineering School Report, March 1984.

2. Tang D.M and Dowell E.H, "Nonlinear Dynamics of a Helicopter Model in Ground Resonance. Part 2: Analysis and Experiment on a Helicopter Model with Multiple Nonlinear Dampers and Roll and Pitch Fuselage Motion", Duke University, Engineering School Report, May 19[illegible].

3. Tongue,Benson H.,"Limit Cycle Oscillations of a Nonlinear Rotorcraft Model", AIAA Journal, to be published.

4. Bielawa,Richard L.,"An Experimental and Analytical Study of the Mechanical Instability of Rotor on Multiple-Degree-of Freedom Supports", Princeton University, M.S.E. Thesis, June 1962.

5. Coleman, R.P. and Feingold, A.M., "Theory of Self Excited Mechanical Oscillations of Helicopter Rotors with Hinged Blades", NACA Report 1351, Feb.1957.

6. Brook,G.W.,"The Mechanical Instability and Forced Response of Rotors on Multiple Degree of Freedom Supports", Ph.D Thesis, Princeton University, Department of Aeronautical Engineering, Oct.1961.

7. Hohenemser,K.H. and Yin,S.K.,"Some Applications of the Method of Multi-Blade Coordinates", Journal of the American Helicopter Society, Vol.7,No.3 July 1972.

8. Price,H.L.,"The Avoidance of Ground Resonance", Aircraft Engineering, Vol.17, No.376, June 1960.

9. Done,G.T.S."A Simplified Approach to Helicopter Ground Resonance", ARC 33254, 1971.

10. Dowell,Earl H.,et al., A Modern Course in Aeroelasticity, Sijithoff and Noordhoff, 1980.

11. Mil,M.L. et al.,"Helicopter-- Calculation and Design, Vol. II, Vibration and Dynamic Stability", NASA TT F-519,May 1968.

12. Howarth,R.M., and Jones,C.H.,"Ground Resonance of Helicopter", The Journal of Helicopter Association of G.B, Vol.7, No.4, April 1954.

13. Johnson,W., Helicopter Theory, Princeton University Press,Princeton,N.J., 1980.

14. Dowell, Earl H.,"The Behavior of A Linear Damped Modal System with A Nonlinear Spring-Mass-Dry Friction Damper Attached", Journal of Sound and Vibration, 89(1),1983.

15. Broyden, C.G.,"A New Method of Solving Nonlinear Simultaneous Equations", Computer Journal, Vol.12, No 1, 1969.

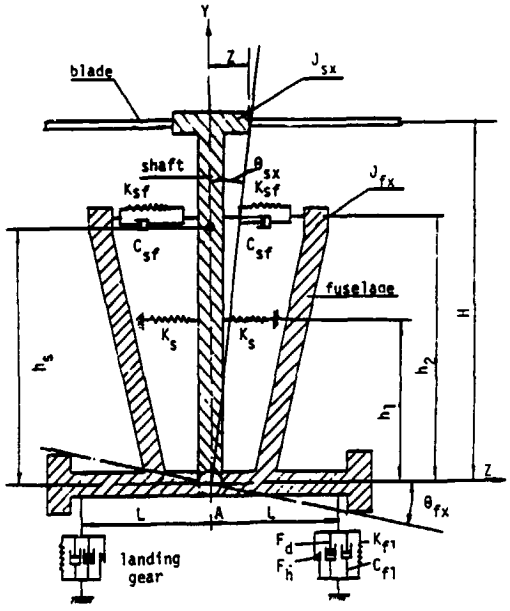

Fig.1

Fig.2. test model

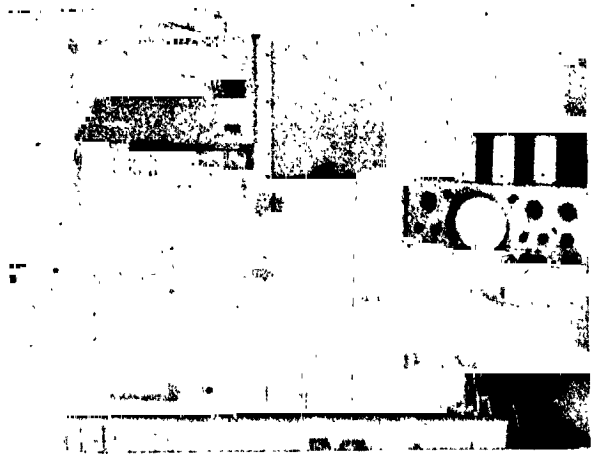

Fig.3. test equipment

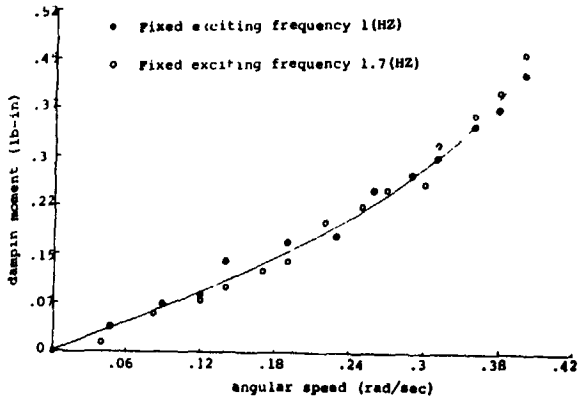

Fig.4(a). characteristic curve of damper

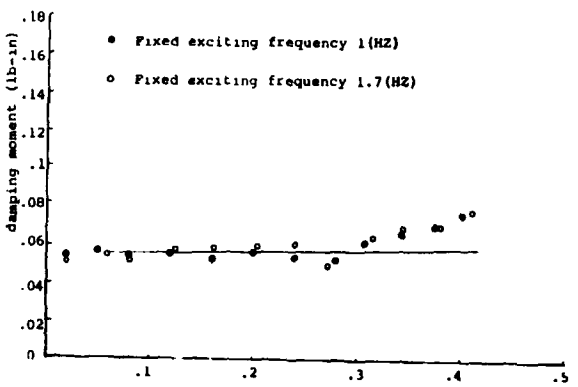

Fig.4(b). characteristic curve of damper

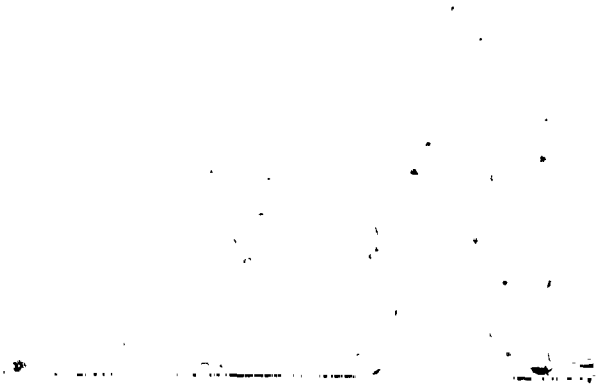

Fig.5. measurement system of rotor blade

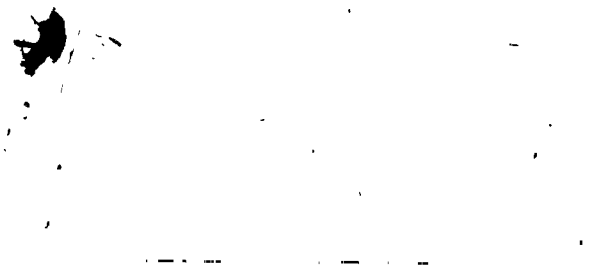

Fig.6. calibration device of angular amplitude

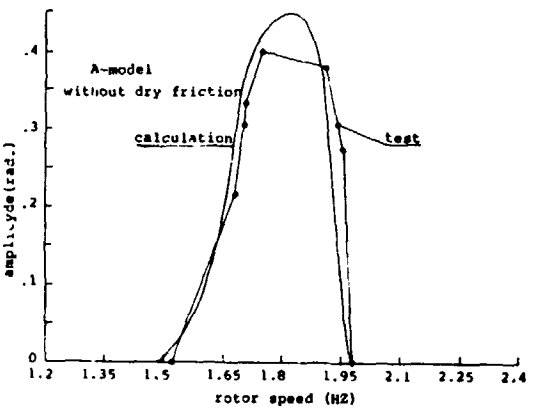

Fig.7. limit cycle behavior

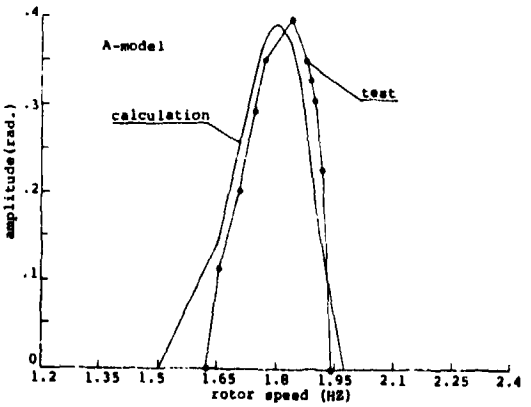

Fig.8. limit cycle behavior

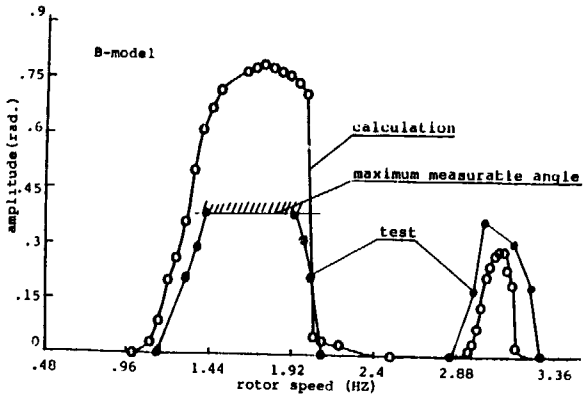

Fig.9. limit cycle behavior

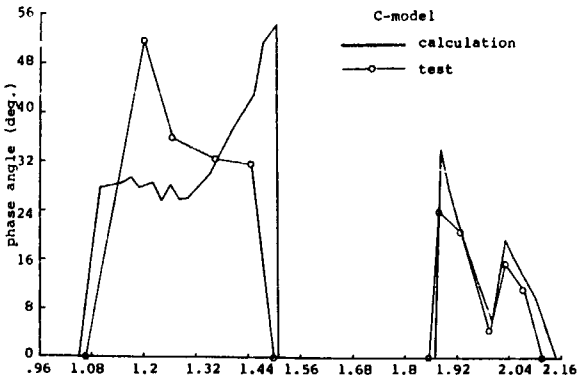

Fig.12. limit cycle behavior

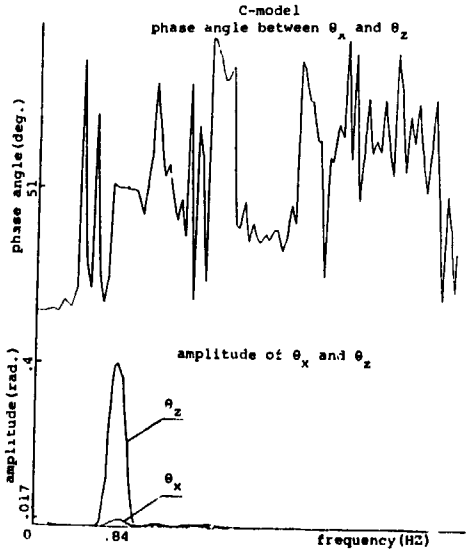

Fig.10. frequency spectral analysis

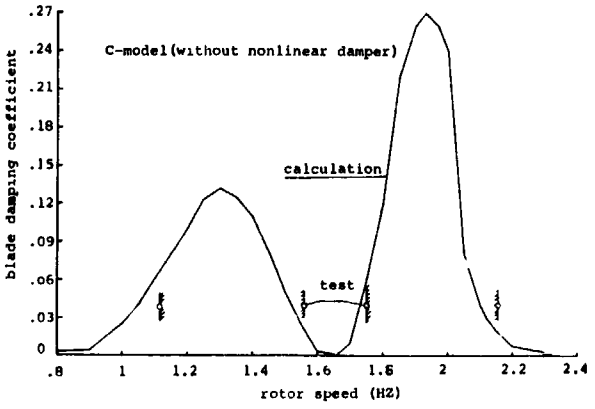

Fig.13. instability region

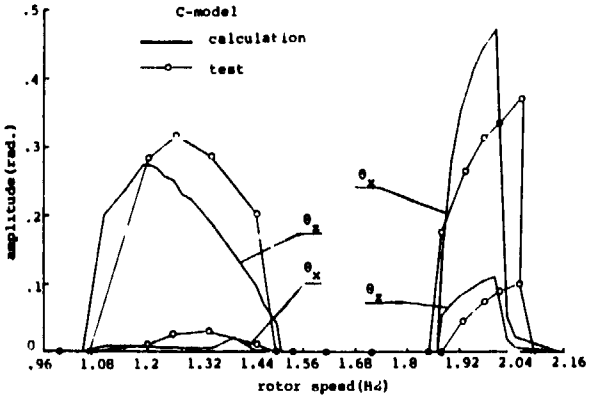

Fig.11. limit cycle behavior

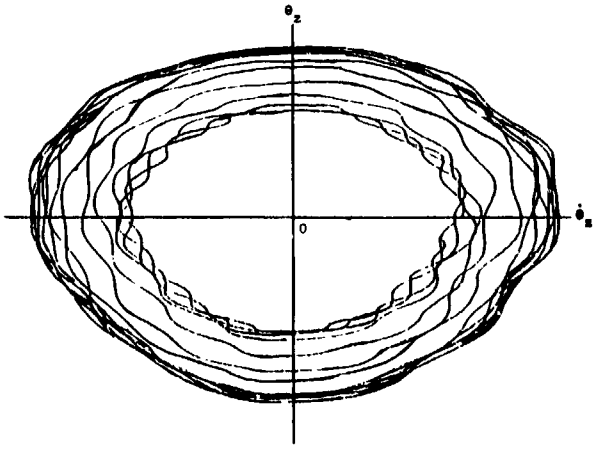

Fig.14. phase plane plot

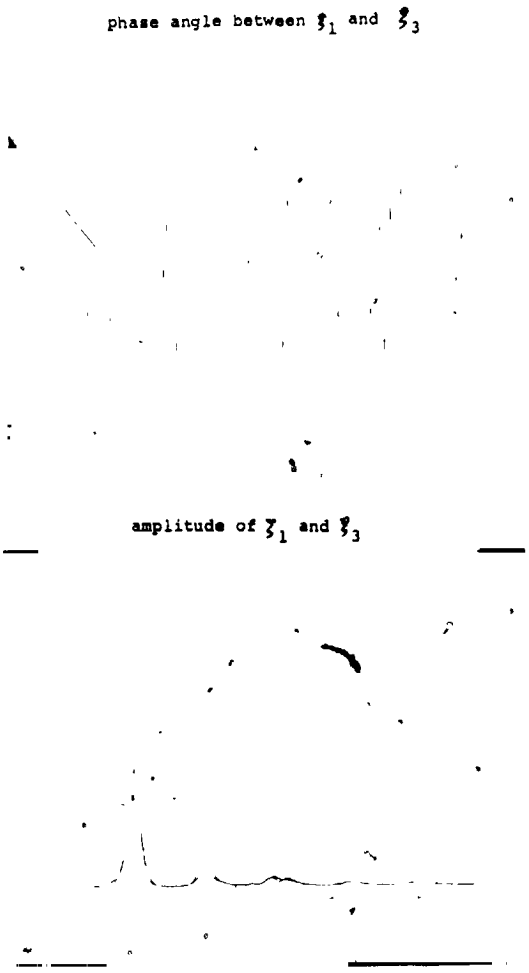

Fig.15. frequency spectral analysis

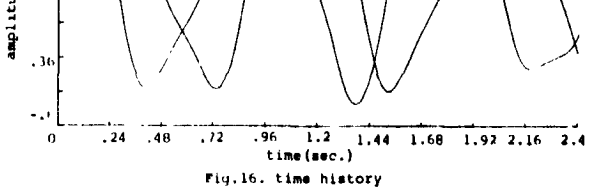

Fig.16. time history

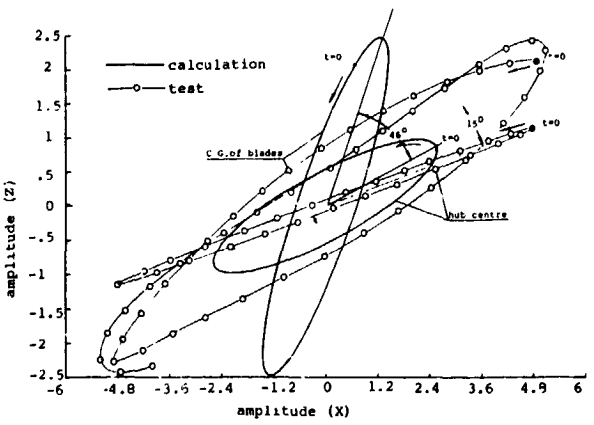

Fig.17. motion locus

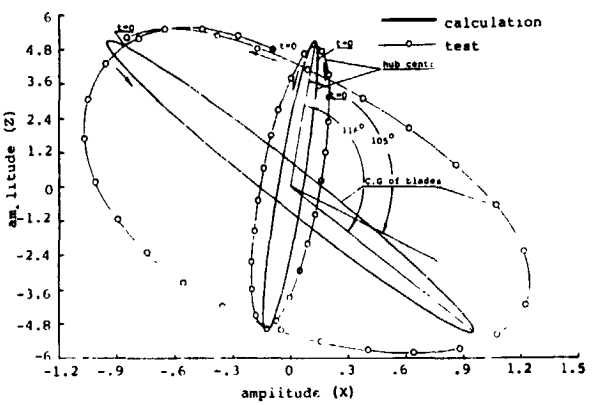

Fig.18. motion locus

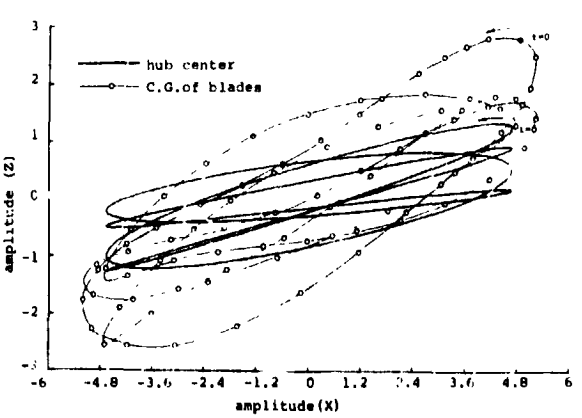

Fig.19. motion locus

DISCUSSION
Paper No. 4

NONLINEAR DYNAMICS OF A HELICOPTER MODEL IN GROUND RESONANCE
D. M. Tang
and
E. H. Dowell

Jerry Miao, Sikorsky Aircraft: I would like to make a comment. Earlier Jing Yen said that we may not be able to analyze ground resonance, but apparently from this paper we can see with a nonlinear damper we can even calculate the amplitude of the oscillation. Therefore, if you only know what numbers to put into the analysis you will be able to calculate it. Thank you.

TEST RESULTS FROM A DYNAMIC MODEL DYNAFLEX ROTOR

Charles F. Niebanck
Senior Dynamics Engineer
and
Robert K. Goodman
Dynamic Engineer
Sikorsky Aircraft
Stratford, Connecticut

Abstract

A one-fifth scale dynamic model of the Sikorsky Dynaflex rotor has been tested in hover and in forward flight conditions in the United Technologies Research Center Wind Tunnel. The Dynaflex rotor features an advanced composite structure which flexes to provide a constant speed universal joint action. Testing concentrated on confirming that the stability and dynamic response of the rotor were satisfactory. Lift conditions of up to .11 Ct/sigma and advance ratios as high as .46 were reached. Vibratory loads were comparable to those of articulated rotors. The Dynaflex rotor concept appears to be a practical concept from the standpoint of dynamic response and stability.

Introduction

Motivated by the desire to decrease complexity, weight, maintenance, and drag of the main rotor head, Sikorsky has undertaken the development of the Dynaflex rotor, a new concept for helicopter main rotor systems. The Dynaflex rotor is characterized by a bearingless rotor connected to the rotor shaft by a unique gimbal joint consisting of a spherical elastomeric bearing with comparitively flexible elastic restraint. The design has several advantages over articulated and pure bearingless rotor designs. Utilizing advances in composite material development, it offers lower weight and smaller parts count than conventional articulated rotors, while at the same time providing the option of a wide range of hub stiffness unavailable in inherently stiff pure bearingless designs. The spherical elastomeric bearing provides a constant-speed universal joint, greatly reducing Coriolis effects resulting from tip path plane tilt in articulated rotor systems. The Dynaflex rotor design is very clean aerodynamically, providing low drag, and a negative angle of zero lift so that hub downloads can be avoided at normal nose-down cruise attitudes.

Development of the Dynaflex rotor is described extensively in Reference 1. Two model rotor configurations based on a one fifth scale S-76 were fabricated and tested to demonstrate the feasibility of the concept and to evaluate the aeroelastic stability of the rotor. The first was a stiff-inplane configuration in which the first edgewise blade frequency was higher than the rotor speed. The second configuration was soft-inplane, in which the first edgewise blade frequency was lower than the rotor speed. The stiff in-plane model was tested in hover at reduced tip speed with nominal 100 percent rotor speed of 500 RPM. Rotor speeds ranged up to 650 RPM and collective pitch to 13.5 degrees. The rotor was stable over the entire test range (Fig. 1).

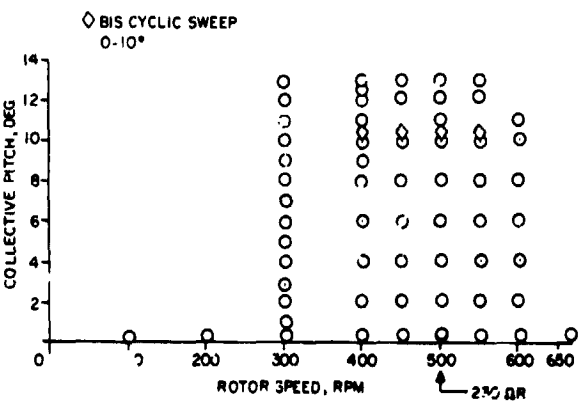

Fig. 1 Scope of Dynaflex reduced speed hover test.

Presented at the American Helicopter Society Specialists Meeting on Rotorcraft Dynamics, Moffett Field, California, November 7, 1984.

The soft-inplane Mach scale model was tested in hover at the Sikorsky hover stand and in forward flight in the UTRC wind tunnel. Hover test conditions included rotor speeds in excess of 1500 RPM (tip speed greater than 700 fps), and collective pitch up to 14 degrees. Forward flight testing covered a range of level flight conditions, with advance ratios up to 0.47 and Ct/sigma values up to 0.11 successfully achieved. Partial power descents and autorotation conditions up to 150 knots were also tested. The testing of the soft-inplane model is described in this paper.

Description of the Model

A drawing of the Dynaflex model rotor is shown in Fig. 2. The rotor incorporates composite twin C-flexbeams which accomodate flatwise, edgewise, and pitch change motions of the blades with respect to the hub. Blade pitch change is applied through a graphite/epoxy, torsionally stiff, torque shaft positioned between the twin flexbeams. The torque shaft is built into the blade/flexbeam juncture at its outboard end and restrained by ball-joint with radial slip at its inboard end. The flexbeams are rigidly fixed to the rotor hub, which in turn is connected to the rotor shaft through a spherical gimbal bearing. Hub stiffness is provided by the graphite epoxy gimbal spring, which is attached to the rotor shaft and blades. Fairings over the hub and flexbeams minimize the aerodynamic drag (Fig. 3).

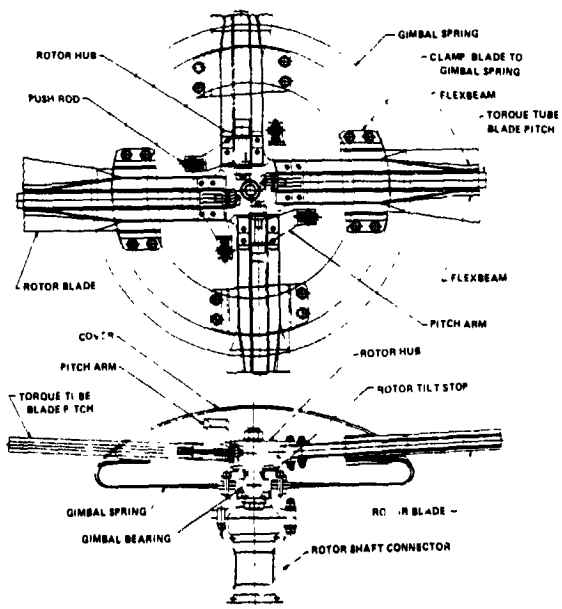

Fig. 2 Dynaflex rotor model.

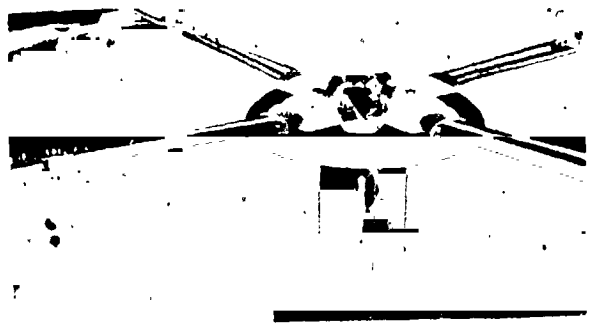

Dynaflex rotor model without fairings installed

Dynaflex rotor model with fairings installed

Fig. 3 Dynaflex rotor model with and without hub fairings.

The model was designed to be a one-fifth scale S-76 main rotor, with gimbal spring to provide approximately the same hub moment constant achieved with the S-76 articulated main rotor with its four percent flapping hinge offset. Existing S-76 articulated rotor model blades were modified for use on the model rotor. The modifications consisted of cutting off the inboard end of the blade and locally reinforcing the inner end of the remaining blade for a blade-to-flexbeam attachment clevis. The Dynaflex model attributes are shown in Table 1.

ATTRIBUTE	REDUCED SPEED TEST (STIFF IN-PLANE)	MACH SCALE TEST (SOFT IN-PLANE)
TIP SPEED, ΩR, FT/SEC	230	675
1st FLATWISE COLLECTIVE FREQ., ω_{F1}/Ω	1.10	1.082
1st EDGEWISE FREQ., ω_{E1}/Ω	1.44	69
1st TORSION FREQ., ω_{T1}/Ω	16.3	5.13
2nd FLATWISE COLLECTIVE FREQ., ω_{F2}/Ω	3.22	2.48
GIMBAL STIFFNESS, IN.-LB/DEG	16	90
GIMBAL FREQUENCY, $\nu_G^2 = \sqrt{1 + \frac{K_G}{I_B \Omega^2}}$	1.032	1.021
PRECONE AT HUB, DEG	2.8	2.5

Table 1. Dynaflex rotor attributes.

Description of Rotor Tests

Full scale speed testing of the Dynaflex model rotor took place in two phases. The first phase, hover testing, was undertaken with the objective of verifying aeroelastic and aeromechanical stability of the rotor concept for a wide range of rotor speeds, collective and cyclic pitches.

Hover testing took place at the Sikorsky Aircraft Model Rotor Test Stand. The test rig incorporates a gimbal support for a rotor strain gage balance, with adjustable springs and dampers across the gimbal pivots to provide detuning of support modes from unfavorable coupling with rotor modes. An electric motor drives the rotor through a universal joint coincident with the gimbal axes. The rig is mounted on a hydraulic ram to permit performance testing at various heights above the ground. Instrumentation was provided to measure flexbeam assembly flatwise and edgewise bending moments, forward and aft flexbeam tension, blade flatwise and edgewise bending moments, pushrod load, gimbal spring tilt, and gimbal spring strain. The rotor strain gage balance measured the six rotor force and moment components. Rig vibration was measured by six accelerometers.

Rotor hover testing was preceded by a shake test to determine rig natural mode properties. The G400 coupled rotor-fuselage aeroelastic analysis program was used with these properties to assess rotor and rig mechanical stability. Rig dynamic properties were improved by adding mass to the rotor hub.

Test conditions consisted of a rotor speed sweep at 4 degrees collective pitch, followed by collective pitch sweeps at various rotor speeds, and cyclic pitch sweeps at constant rotor speed and collective pitch settings. The scope of the hover test conditions is presented in Fig. 4. Rotor stability was probed for each test condition. The general procedure followed after proceeding to a new operating condition was to drive the support system with an electrodynamic shaker, using a slow sine sweep between 2 and 50 Hz. Support system mode frequency and damping could be evaluated from the shaker drive transfer function, as supplied on-line by an HP 5423 Dynamic Analysis System. Damping of progressing and regressing edgewise modes was evaluated by tuning the shaker to the fixed system frequency corresponding to the mode of interest. Tuning was accomplished by maximizing the response of the edgewise flexbeam gage as the shaker frequency was varied in the neighborhood of the fixed system frequency. After tuning the shaker to the proper frequency, the force level was abruptly terminated and the transient response of the edgewise gage was passed through a non-harmonic detector and recorded on an oscillograph. Damping was analyzed manually with the log decrement method.

After successful completion of the first phase of testing, forward flight testing began in the 18 foot diameter United Technologies Research Center Wind Tunnel. The primary purpose of this phase of testing was to confirm that dynamic response and stability were satisfactory over a range of simulated flight conditions. In addition, the test provided an opportunity to assess the behavior of blade, flexbeam, and gimbal spring load and stress as a function of gimbal tilt at various flight conditions. The test also provided data with which aeroelastic analyses could be correlated.

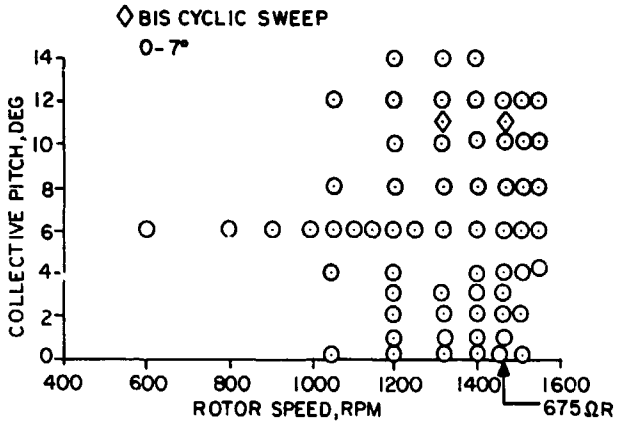

Fig. 4 Scope of Dynaflex Mach scale hover test.

The test plan called for a shake test of the wind tunnel test rig, followed by hover testing, and finally a series of simulated flight conditions, including level flight, partial powered descents, and autorotation at a variety of lifts and forward speeds. Pitch moment variation, simulating fore and aft center of gravity, was also included in the test envelope. The model configuration and instrumentation were essentially the same as for the hover testing described above. Modal properties of the rotor rig as installed in the wind tunnel are listed in Table 2.

FREQUENCY (Hz)	MASS (LB-SEC**2/IN.)	DAMPING	X (AFT)	Y (STBD)	Z (VERT)	ROLL (LEFT)	PITCH (UP)
3.15	0758	.042	0 0	1 0	0 0	0 0	0 0
5 47	334	020	0.0	1 0	0 0	-.0606	0 C
6 75	261	049	1.0	0.0	0 0	0 0	0606
36 5	127	021	1 0	0 0	0 0	0 0	0 0
56 2	.149	.136	0 0	0 0	1 0	0 0	0 0

Table 2. Wind tunnel rig modal properties.

Fig. 5 shows the Dynaflex rotor as installed in the UTRC wind tunnel. Simulated flight conditions were achieved by setting the model rotor speed at the desired value with zero collective pitch, raising the tunnel velocity to that of the simulated flight condition, and then iterating on shaft angle, collective pitch, and cyclic pitch until desired levels of rotor lift, propulsive force, gimbal tilt, and hub moment were reached. Probing of edgewise mode stability was carried out as it was in the hover testing described above.

Fig. 5 Dynaflex rotor installation at UTRC wind tunnel.

The test envelope achieved for simulated level flight conditions is presented in Fig. 6. Fig. 7 shows the test conditions at which variations in rotor pitch moment were investigated. Figs. 8 and 9 present the conditions for partial power descent and autorotation. The variations in rotor speed were not applied as originally planned, but were the result of blade limitations at the higher forward speed conditions. The limitations were manifest as a blade instability which showed characteristics of those occurring for blades with aft chordwise center of gravity. The same blade instability was encountered with the blades mounted on a fully-articulated hub in a configuration that had previously been tested and found to be fully stable. Subsequent measurement of the model blades confirmed that rearward migration of the center of gravity had occurred in the course of their modification, use, and repair over a period of several years. Despite the restrictions imposed by blade limitations a valuable body of data was acquired.

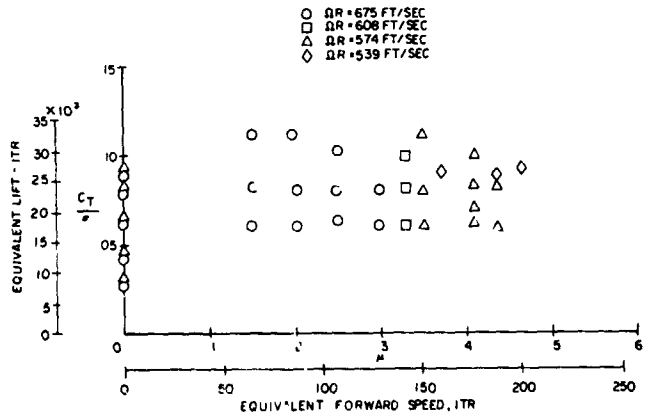

Fig. 6 Dynaflex model test conditions - level flight trim.

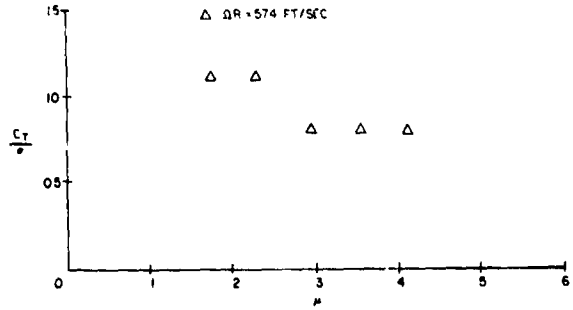

Fig. 7 Dynaflex model test conditions - level flight pitching moment variation.

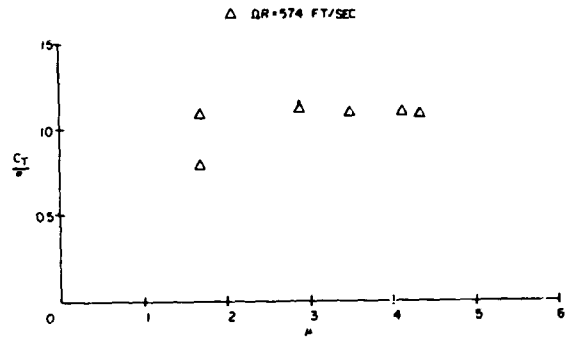

Fig. 8 Dynaflex model test condition - partial power descent.

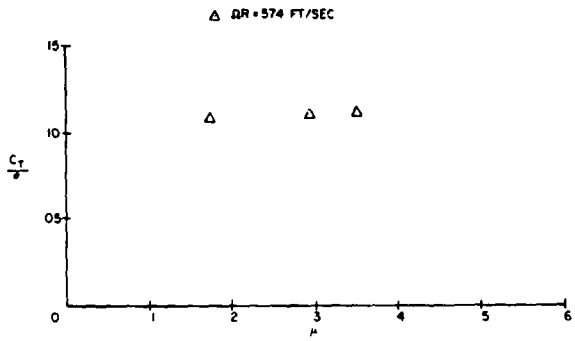

Fig. 9 Dynaflex model test conditions - autorotation.

Results

The Dynaflex model rotor was stable over the entire hover test envelope. Damping levels for the regressing edgewise mode were low, but positive. No control difficulties were encountered when the tip path plane was tilted by cyclic pitch inputs of up to degrees. Figs. 10 and 11 show the variation in regressing edgewise mode damping ratio with rotor speed for hover testing at the Sikorsky test stand and at the UTRC wind tunnels respectively. Damping of the regressing edgewise mode tended to increase slightly with increased collective pitch. Progressing edgewise mode damping was higher than that of the regressing mode. Fig. 12 shows the variation in progressing edgewise mode damping with collective pitch. Comparison of results from the G400 aeroelastic analysis and test data reveals similar trends in damping with collective pitch for hover. Attempts to correlate G400 with forward flight data from the model wind tunnel test were not successful. Resolution of mathematical difficulties encountered during the execution of the G400 computer program is currently being pursued.

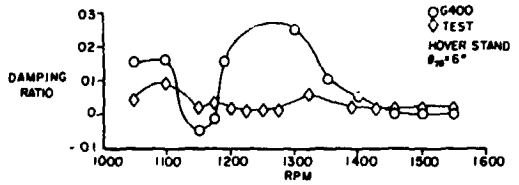

Fig.10 Regressing edgewise mode damping - hover conditions Sikorsky hover stand.

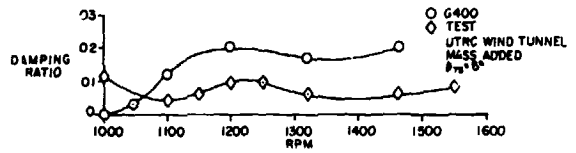

Fig.11 Regressing edgewise mode damping - hover conditions UTRC wind tunnel.

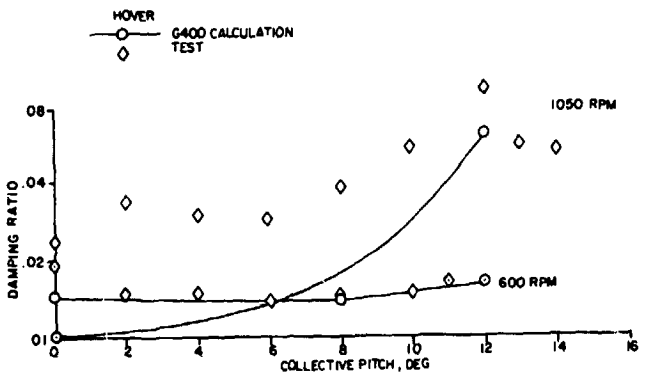

Fig.12 Progressing edgewise mode damping - hover conditions UTRC wind tunnel.

In forward flight testing, the regressing edgewise mode was the only rotor system mode that could be excited with reasonable consistency by the fixed system shaker. Damping ratio for this mode is plotted against advance ratio for various operating conditions in Figs. 13, 14, and 15. The damping variation with level flight lift, forward speed or rotational speed condition displays no clear trending, although application of positive pitching moment, partial power descent, or autorotation appear to cause damping to be generally lower.

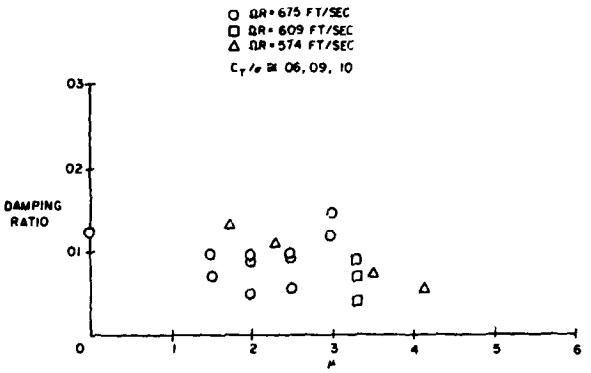

Fig.13 Dynaflex rotor edgewise mode damping - level flight trim conditions.

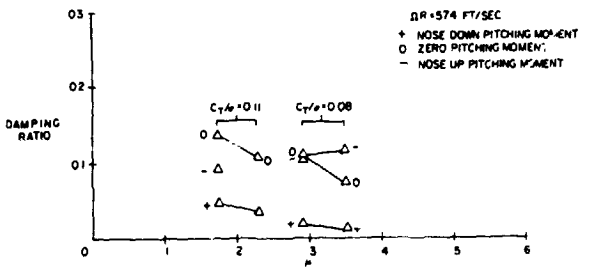

Fig.14 Dynaflex rotor edgewise damping - level flight pitching moment variation.

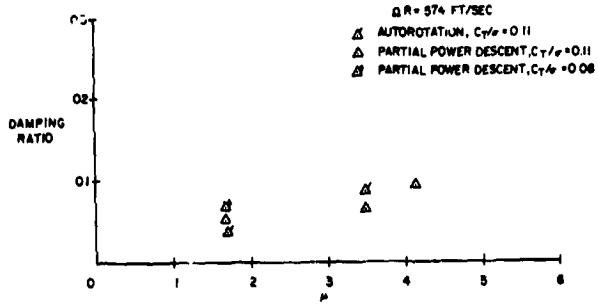

Fig.15 Dynaflex rotor edgewise damping - partial power descent and autorotation conditions.

Steady-state records of each of the simulated flight conditions were acquired to permit the assessment of blade and gimbal loads and strains, model rig vibrations, and the appropriate rotor forces and moments. Rotor forces and moments were non-dimensional and converted to coefficients, facilitating comparison with full scale and model data from other rotor configurations. The operation of the rotor at reduced tip speed to avoid blade instabilities altered the dynamic scaling parameters. At the 539 ft/sec tip speed, for example, the first edgewise blade frequency was .8 cycles per revolution, rather than the .68 cycles per revolution at the 675 ft/sec tip speed. The principal effect of operation at the reduced tip speed is to simulate a rotor with higher elastic stiffness.

Data from simulated level flight conditions with gimbal tilt essentially zero are exhibited in Figs. 15 - 19. Nondimensional one-half peak-to-peak pushrod load, flexbeam edgewise bending moment, and blade flatwise bending moment are plotted against advance ratio in these figures. The factors used for nondimensionalization are the conventional ones used in forming rotor blade loading parameters such as CT/sigma and CPM/sigma. Data from equivalent forward flight conditions taken during the S-76 dynamically scaled model test conducted in 1976 are also presented in the figures. These data show similarity in flatwise bending moments and pushrod loads for the Dynaflex and articulated rotor. This similarity suggests that the Dynaflex rotor blade flatwise and torsion loading outboard are similar to those on an articulated rotor, and provides evidence that the Dynaflex rotor's outboard blade requires no special design considerations beyond those for an articulated rotor.

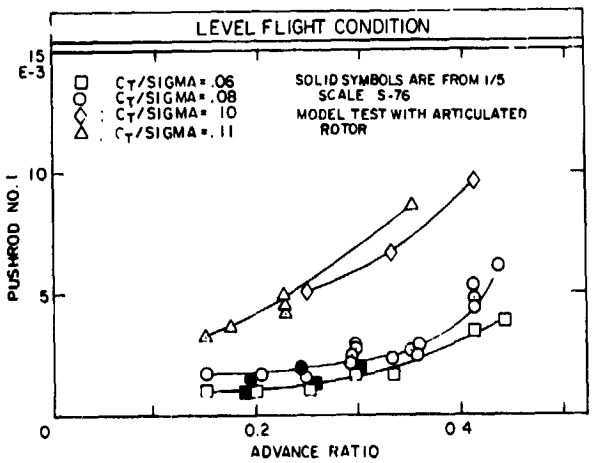

Fig.16 Half peak to peak pushrod coefficient/solidity, level flight trim conditions.

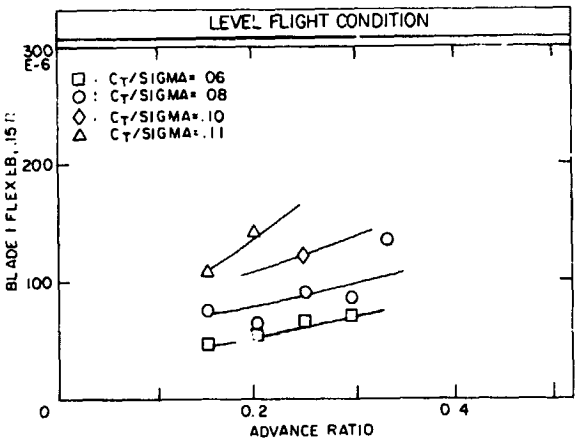

Fig.17 Half peak to peak flexbeam edgewise bending moment coefficient/solidity, level flight trim conditions.

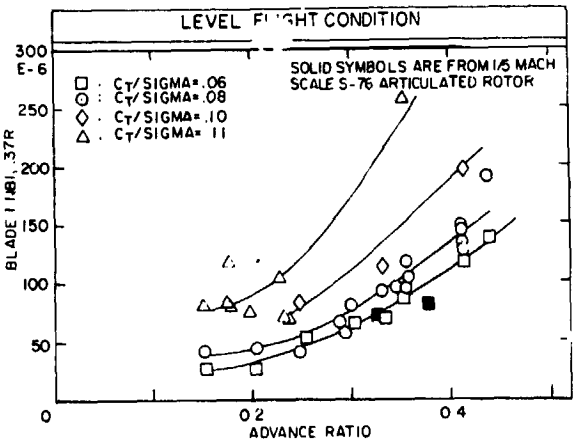

Fig.18 Half peak to peak blade flatwise bending moment coefficient/solidity at 0.37R, level flight trim conditions.

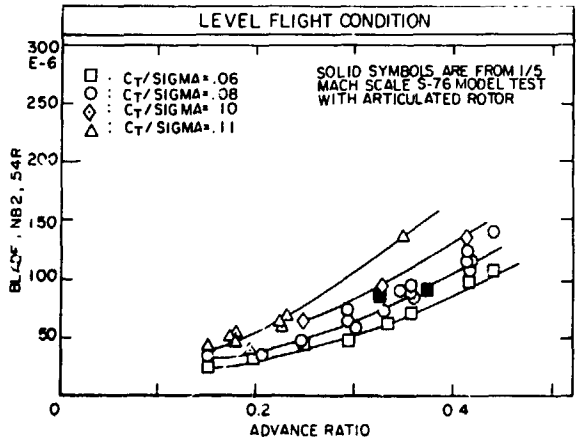

Fig.19 Half peak to peak blade flatwise bending moment coefficient/ solidity at 0.54R, level flight trim conditions.

Test data from simulated partial power descent and autorotation conditions, as well as comparative data from level flight conditions are presented in Figs. 20 - 23. Comparison reveals no unusual response due to partial power descent nor due to autorotation.

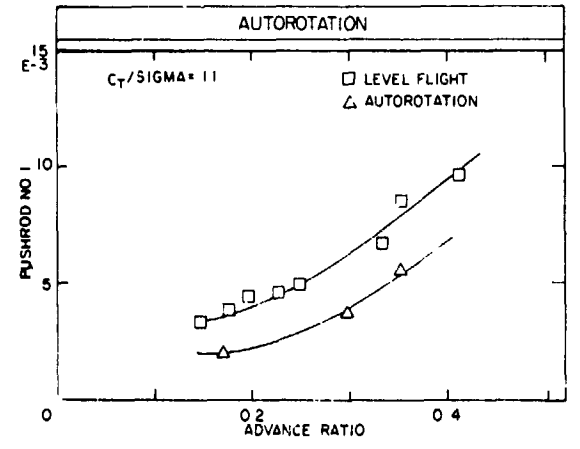

Fig.20 Half peak to peak pushrod coefficient/solidity, partial power descent conditions.

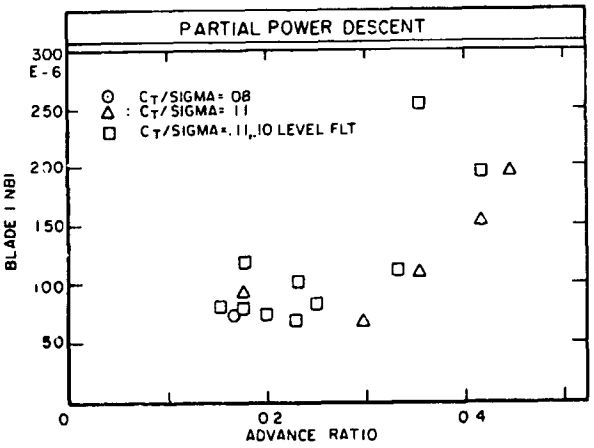

Fig.21 Half peak to peak blade flatwise bending moment coefficient/ solidity at 0.37R, partial power descent conditions.

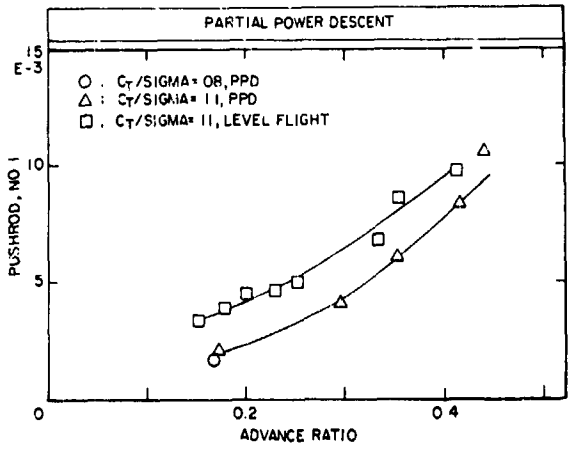

Fig.22 Half peak to peak pushrod coefficient/solidity, autorotation conditions.

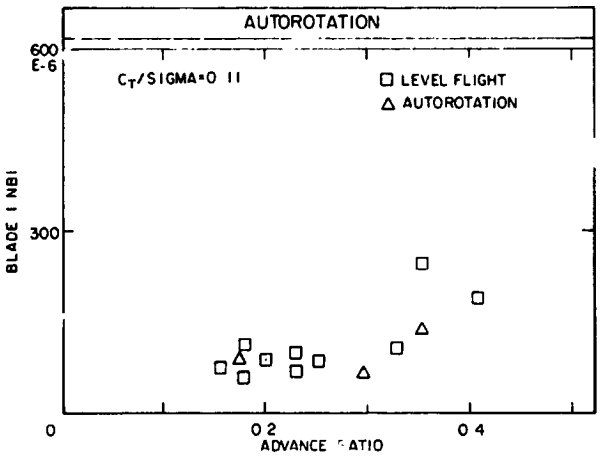

Fig.23 Half peak to peak blade flatwise bending moment coefficient/ solidity at 0.37R, autorotation conditions.

Results from pitching moment variation are presented in Figs. 24 - 27. Fig. 24 shows the gimballed hub one-per-rev tilt angle amplitudes reached during the pitch moment variation test conditions, along with the corresponding rotor shaft angle relative to zero pitching moment shaft angle. The gimbal tilt is roughly two-thirds of the shaft angle increment, i.e. tip path plane tilt consists of roughly two thirds gimbal tilt and one third first harmonic blade bending. Fig. 25 shows one-half peak-to-peak inner gimbal strain amplitude as a function of advance ratio. Gimbal strain is not affected by forward speed or lift, rather it appears to be a function of gimbal tilt.

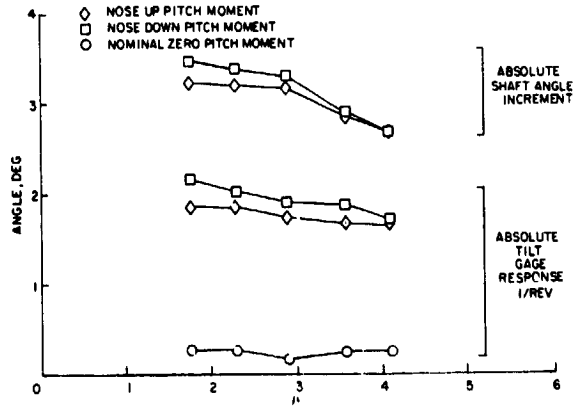

Fig.24 Gimbal and thrust vector tilt, pitching moment variation conditions.

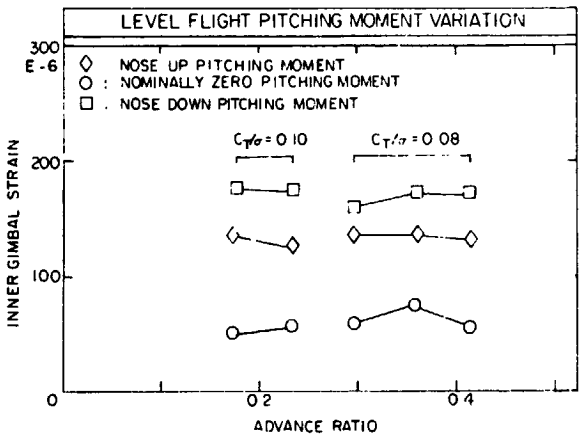

Fig.25 Inner gimbal strain, pitching moment variation.

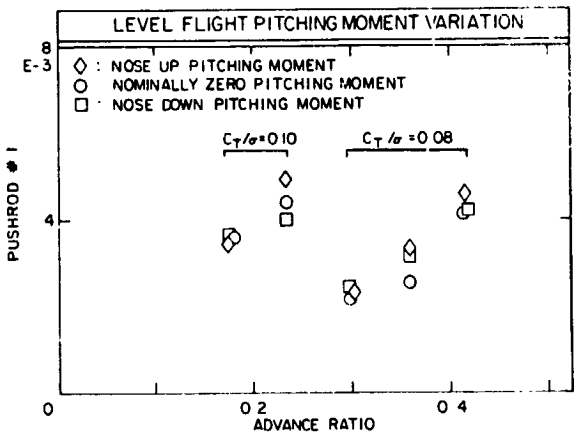

Fig.26 Half peak to peak pushrod coefficient/solidity, pitching moment variation.

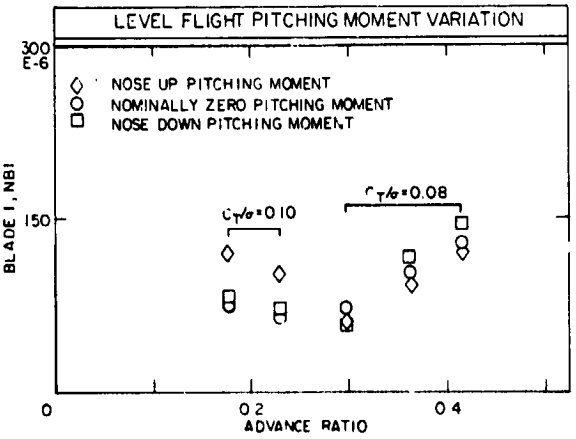

Fig.27 Half peak to peak blade flatwise bending moment coefficient/ solidity at 0.37R, pitching moment variation.

Concluding Remarks

Wind tunnel testing of the Dynaflex model rotor confirmed that the present rotor concept is feasible, offering considerable promise for advancing the state of the art for helicopter main rotor systems. Within the flight conditions boundary imposed by blade limitations, the rotor showed itself to be stable and relatively insensitive to forward flight condition. The rotor offers simplicity and lower drag than articulated rotors without sacrificing low blade loads and good flying qualities. Edgewise mode damping is quite low as no auxiliary damping device nor advantageous flap lag coupling provisions have been made. Continuing development will address this issue.

References

1. Fradenburgh, E.A., and Carlson, R.G., "The Sikorsky Dynaflex Rotor - an Advanced Main Rotor System for the 1990's," Paper No. A-84-40-17-8000, American Helicopter Society 40th Annual Forum, Arlington, VA, May 1984.

DISCUSSION
Paper No. 5

TEST RESULTS FROM A DYNAMIC MODEL DYNAFLEX ROTOR
Charles F. Niebanck
and
Robert K. Goodman

Jing Yen, Bell Helicopter: One thing is not quite clear to me, that is, what is the advantage of using a gimballed hub versus a conventional articulated hub?

Goodman: There are a couple of advantages. The first is the simplicity of the design--there are fewer parts involved and some of the other design objectives were to reduce weight. There are many composite materials which are incorporated in this design which haven't been [used] in conventional articulated rotors. In the design which we showed here, the hub fairing is an integral part of the rotor head and this decreases the download on the rotor in forward flight where there is a forward pitch angle. These are primarily the motivations for it.

Bob Taylor, Boeing Vertol: Did you obtain any test data to show the beneficial effect of constant rotor velocity on inplane rotor loads?

Goodman: Well, we did have edgewise damping or edgewise strain gauges on the model. We had quite a bit of problems with those. We lost them fairly early, rather, we lost several of them throughout the test primarily because the strain levels in the blades were higher than the gauges could handle. We do have some vibratory information from the edgewise gauges and basically it is comparable to articulated rotors. They did not bear out substantial reduction in force levels because of the Coriolis effects. They did not support that at this point.

Peretz Friedmann, University of California, Los Angeles: I'm not sure I understand. That's probably because I can't figure out your drawing precisely. What is the difference between the Dynaflex rotor, a conventional hingeless rotor, a bearingless rotor--could you please try and explain? If there are any differences then which of these is best in your opinion?

Goodman: Do you have a copy of the proceedings? There is a fundamental difference--the most unique feature I suppose is the gimballed joint. It enables you to have stiff flexbeams so that you don't have problems with blade droop and yet it allows you to have the hub moment of an articulated rotor and then as I already discussed previously the advantages over an articulated rotor are lower parts count and aerodynamic considerations for the hub. I guess if that doesn't answer your question, maybe we can talk about it afterwards.

Henry Velkoff, Ohio State University: Did you have any measurements of the torsional frequencies of the hub itself? You are basically using a pseudo-Hooks joint which is taken out elastically and with that tilt you should be getting a second harmonic variation which is analogous to the Coriolis flapping trim. Did you see anything like that? There is always the argument whether the shaft takes it out or the blades take it out. Did you happen to see what the second harmonic torsion looked like?

Goodman: Let's see. I'm not sure I understand your question. I'm kind of new to this game. Are you talking about a yawing vibration?

Velkoff: A torsional one. In any Hooks joint it's not a constant angular velocity. You're going to get a first harmonic and a second harmonic. The second harmonic in a Hooks [joint] is ideally the same as the second harmonic Coriolis term of flapping. So the argument, to quote my friends at Bell, [is] "you never see that," but I'm just curious to see whether you actually find it in this case.

Goodman: I personally did not see it, but I would not have known I was looking for it. Perhaps Jerry can bail me out.

Jerry Miao, Sikorsky Aircraft: Maybe I can help Bob out a little bit. Yes, we put in shear gauges in the drive torque shell, but unfortunately they all ran out very quickly. So I cannot answer that question, but I'm sure what you said is true, Hank. I'm sure the two/rev probably will come through, but it probably is a smaller order of magnitude [that] we cannot help. Another thing to answer Peretz's question a little bit. In this paper Bob has [given] he refers to an earlier paper presented at the 1984 AHS Forum written by Fradenburgh and Carlson and they discuss this gimballed rotor quite a bit. Essentially the major feature is you have a gimbal in the center of the hub so you figure the rotor is going to have vibratory forces and moments coming through that joint. The moments are eliminated just like for an articulated hinge; you eliminate all the moment transfer across the hinge.

Bob Ormiston, U.S. Army Aeromechanics Laboratory: I was interested in the question about Coriolis loads and I'm surprised you didn't see a reduction. I noticed in the paper you did

have some measured inplane loads. Do you know how those compare to, say, an articulated or other type rotor? Could you make an estimate of the comparison? Are they about the same?

Goodman: I can't answer that off the top of my head. I'm trying to recall now whether or not we did include any of the edgewise force level data in there.

Charles Niebanck: I think those gauges went out before we could really get very much.

Goodman: I guess the question would arise where do we get our edgewise damping calculations from and we had a variety of edgewise gauges on the blade. For instance we had tension gauges on each of the twin flexbeams so, for instance, when we would get edgewise motion going we would see this interaction of tensile strain on these two flexbeam gauges. So at times we would be using log decrement of edgewise [oscillation] on those gauges to establish damping levels and yet the calibration was not accurate enough to be able to really establish what the edgewise vibration amplitude truly was. We were looking at relative amplitudes.

Ormiston: I just want to close and jump into this controversy here. I think the rotor is different from a Hooks joint situation, so I don't think you should get the kind of loads in there that Hank was saying we should. We've talked about this before. I think it should be a constant speed and you should show up with a reduction in the inplane loads, but I would be very curious to find out what actually happened if you ever run the test again.

Goodmann: Yes. Well we are planning on it.

William Warmbrodt, NASA Ames Research Center: Two questions. You showed that you acquired quite a bit of data at low collective pitch settings and yet the paper doesn't present any stability results below a C_T of 0.05 and I was wondering what was the trend at low thrust on the rotor. Also are you pleased with the damping levels that you saw, on the order of 0.01 or less critical damping ratio, throughout the operational envelope?

Goodman: I'll answer the second part first. We are not completely satisfied with that and currently we are working on a Dynaflex rotor, I guess as an ITR candidate, and the design of that is introducing means by which edgewise damping can be increased. The first part of your question--why we didn't present stability results for lower lift conditions? It wasn't a part of our test plan. We wanted to establish a flight condition which was comparable to S-76 level flight conditions. That was the basis for the flight condition we chose.

Bob Hansford, Westland Helicopters: I noticed from the diagram at the end of your report that you had a supercritical lag frequency of 1.44.

Goodman: That was for Froude-scale testing I believe.

Hansford: But did you look at any variations of your lag frequency with blade pitch and couplings between flap and lag motions?

Goodman: We didn't see a considerable amount. I don't have the exact placement of the frequencies with pitch variation present, but there wasn't a large variation. We didn't look that closely at it.

EXPERIMENTALLY DETERMINED FLUTTER FROM TWO- AND THREE-BLADED MODEL BEARINGLESS ROTORS IN HOVER

William G. Bousman and Seth Dawson
Research Scientists
U.S. Army Aeromechanics Laboratory – AVSCOM
Moffett Field, California 94035-1099

Abstract

A series of experiments was performed on a 1.8-m-diam model rotor in hover for the principal purpose of investigating the lead-lag stability of isolated bearingless rotors. Incidental to those tests, at least three types of pitch-flap flutter were encountered; those flutter types constitute the subject matter of this paper. Type 1 flutter occurred approximately at the second flap-mode frequency on both two- and three-bladed rotors for both small and large pitch angles and appeared to be a classic pitch-flap flutter. Type 2 flutter showed mostly torsional motion and was seen on both two- and three-bladed rotors. The flutter mode appeared to be the rotor first-torsional mode and the flutter occurred just above 3/rev for low pitch angles. This behavior is similar to wake-excited flutter, but the flutter mode was in the wrong sense for a flutter dependent on lining up of the shed wakes. Type 3 flutter was a regressing flap flutter that occurred for only the three-bladed rotor configurations and appears to be a wake-excited flutter. Although flutter occurred on a number of different configurations, no rotor parameters were identified that were clearly stabilizing or destabilizing.

Introduction

In the context in which it is used in this paper, flutter refers to instabilities that primarily involve pitching or flapping motions of a rotor blade and that are essentially unaffected by lead-lag motion. The analytical efforts of Loewy and of Miller and Ellis[2] have provided a good understanding of pitch-flap flutter of articulated rotors, and the general features have been confirmed by experiment.[3] Flutter can be prevented in general if the blades are quarter-chord balanced (which is important for control loads as well) and if the control system and blade torsional mode are made relatively stiff. Stability is degraded with a rearward shift of the center of gravity (c.g.) of the blade with respect to the aerodynamic center or if the rotor torsional stiffness is reduced. For the most part, flutter has not caused major developmental problems with recent rotor designs, although the exceptions[4,5] have been remarkable in their complexity and belie the simple definition of flutter used here.

In the design of bearingless rotors in general and of bearingless tail rotors in particular, a number of flutter problems have been encountered that appear to be caused partly by the low torsional stiffness of those designs and partly by structural coupling. Development of the YUH-61A bearingless tail rotor revealed both flap-lag and flutter-type instabilities[6] that although eliminated during testing were never understood. Model tests of a similar configuration at Bell Helicopter exhibited a number of instabilities that showed flutter behavior.[7] It is not clear at the present time whether these recent problems are fundamentally more complex because of the structural coupling that is inherent in bearingless-rotor designs or that designers are simply working closer to flutter boundaries that have been there all along.

A recent series of experiments has been performed at the U.S. Army Aeromechanics Laboratory for the purpose of better understanding design parameters that will affect the lead-lag damping of an isolated bearingless rotor in hover. A number of different types of flutter were encountered in these tests, some of the results of which were presented in Ref. 8. Because the flutter encounters were incidental to the purpose of the tests, only limited data were acquired to characterize these cases. However, it is believed that sufficient data were obtained to provide a preliminary assessment of the flutter types that were encountered, and it is the purpose of this paper to provide that assessment. The series of experiments that has been run will be briefly described and the experimental procedures used when flutter was encountered will be described. The types of flutter that were encountered will be described and quantified, and some discussion will be provided on the sources of the flutter types and the effect of configuration.

Presented at the 2nd Decennial Specialists' Meeting on Rotorcraft Dynamics, Ames Research Center, Moffett Field, California, November 7-9, 1984.

Description of Experiments

A 1.8-m-diam bearingless rotor was tested in hover in both two-bladed and three-bladed configurations in a series of experiments. An overall view of the two-bladed model is shown in Fig. 1; the three-bladed model is shown in Fig. 2. Because identical blades and root hardware were used in all the experiments, the only difference between the two- and three-bladed configurations is the rotor solidity. Model properties are tabulated in the Appendix.

An exploded view of the flexbeam and root hardware for a single blade is shown in Fig. 3. The flexbeam has a uniform rectangular cross section along its length and is made of Kevlar fibers in an epoxy matrix. The flexbeam is fastened to the hub with a root socket that allows the flexbeam to be inclined at any pitch angle θ_f and a precone adapter that gives the flexbeam a precone angle β_f. The flexbeam is connected to the blade through the blade root fittings, the torque tube, and a plug socket that fits inside the torque tube. The blade can be pitched with respect to the flexbeam at the blade root fittings; the angle between the flexbeam and the blade is θ_b. The blade can be drooped either up or down (by an angle β_b) using an angled shim, and it can be swept (angle ζ_b) using a different shim. Two pitch links may be used as shown in the figure or a single pitch link may be installed on either the leading or trailing edges. The radial location of the pitch links may be changed to a number or intermediate positions between the flexbeam root and the flexbeam tip; this change in the location of the pitch links affects the pitch-flap coupling. The ends of the pitch links are small flexures that represent a frictionless rod end bearing that is very stiff axially, but very soft laterally. The blade pitch angle θ was set by raising or lowering the pitch links by hand, with the blade supported such that there was no flap deflection.

Initial testing of the three-bladed rotor configuration indicated that the determination of lead-lag damping was very sensitive to dissimilarities in the mass and stiffness of the blades. As a result, a major effort was made to make the blades and flexbeams as uniform as possible. To this end, 20 flexbeams were built and individually tested for stiffness by attaching a 0.63-kg weight to the plug socket and measuring the lead-lag frequencies. The flexbeams that showed the closest match were then modified by removing 0.001-0.002 in. of material, and a final set of matched flexbeams was obtained whose lead-lag frequencies were within 0.1% of each other. No attempt was made to match the flap frequencies. In a similar way, the blade inertias were tuned by adding tantalum weights to the blade tip at the quarter-chord location. The frequencies of the three-bladed test flexbeam/blade combinations following instrumentation and installation on the model matched within 0.3% for lead-lag and 0.4% for flap.

Each flexbeam was instrumented with strain-gage bridges to measure flap, lead-lag, and torsion bending moments. The signals were transferred from the rotating system, using a 40-channel slip ring for the two-bladed tests and a 65-channel slip ring for the three-bladed test. Fixed system instrumentation included a 1/rev pip, an accelerometer to measure the upper stand motion, and a clamp signal to indicate locking of the upper stand. The resulting data were digitized for on-line analysis and stored on disk; in most cases they were recorded on analog tape as well.

The same stand, drive system, and excitation system were used for the two- and three-bladed tests. The blades and hub were mounted to an upper stand that was free to pivot on flexures when unclamped and that was locked solidly with air clamps before data were taken. The normal procedure for obtaining lead-lag frequency and damping was to free the upper stand, oscillate the hub and stand at $\omega_\zeta + \Omega$ or at $\omega_\zeta - \Omega$ (where ω_ζ was the lead-lag frequency and Ω the rotor speed) with a shaker and, once sufficient lead-lag motion was obtained, to turn off the shaker and clamp the stand. The frequency and damping were obtained from the resulting transient decay using the moving-block analysis.

The design of the experiment did not consider the possibility that flutter might be encountered during testing, and therefore neither the experimental setup nor the on-line data analysis procedures were well-suited for an investigation of the various types of flutter that were encountered. The general procedure that was used when a flutter was encountered was to approach the flutter boundary in small increments of rotor speed, taking both digital records and analog tape records. Test points at which the rotor was unstable were recorded, unless the loads increased too quickly in which case the rotor speed was reduced to a stable condition. Considerable time was spent during the first flutter encounters in attempting to understand the character of the flutter. When it was thought that the flutter was caused by coupling of the second flap and first torsion modes, the upper stand was oscillated at the appropriate frequencies to excite those modes. This was a fairly successful technique for exciting the second flap mode, but it was ineffective in exciting the first torsion mode. This is not surprising, considering that the blades were quarter-chord balanced and could not be inertially excited with

hub shaking. A recording oscillograph was used for examining particular flutter occurrences and to infer the mode shape of the flutter and understand its behavior.

Unfortunately, these procedures were time consuming and detracted from the original objectives of the experiments. As additional flutter incidents were encountered, less effort was expended on documenting the flutter; this was particularly so if the flutter appeared to be similar to that observed in a previous encounter. At the start of the three-bladed tests, a systematic effort was made to avoid configurations that had produced flutter in the two-bladed tests. This approach was effective in maximizing the use of available test time, but did not develop the data that would allow a better understanding of the flutter incidents that had been examined in the two-bladed tests.

Data Analysis Procedures

The run logs from various experiments with the bearingless-rotor models were examined, and test points were selected at which a flutter was encountered. In addition, supplemental test points were chosen for stable conditions that were proximate in rotor speed or pitch angle to the flutter conditions. Approximately 170 cases for 13 different configurations were selected for detailed analysis.

The data recorded on analog tape were sampled at 800 Hz to provide an ample bandwidth for analysis and time-histories with good resolution. The flexbeam strain-gage bending-moment data were converted to angular deflections at the flexbeam tip to provide a basis of comparison for the flap, lead-lag, and torsion motions. The conversion used static calibration factors and, therefore, introduced some error in that the effect of the centrifugal force on the bending-mode shape was ignored. However, those errors are not considered important to obtaining a better understanding of the model rotor flutter characteristics. For each case, approximately 5 sec of data were obtained and the time-histories were examined for unstable behavior. The frequency spectrum of an appropriate coordinate was examined to determine what modes were involved, and damping was estimated using the moving-block analysis. Vector plots were obtained at the appropriate modal frequencies to determine the amplitude and phase of the modal behavior in the physical coordinates.

Description of Types of Flutter

Twenty-eight different combinations of rotor configuration, blade number, and pitch-link radial location were tested during this series of experiments; they are described in Table 1. Of the 28 combinations there were 3 in which pitch links were installed on both the leading and trailing edges [designated (1a), (6a), and (6c)]. This simulates a vertical shear restraint at the root of the blade and substantially increases the torsional stiffness of the rotor to above 10/rev. No indication of flutter was ever noted for these torsionally stiff, two-pitch-link cases. Of the remainder of the combinations tabulated, the run logs indicated that flutter was encountered on 15 of the 28. However, following the analysis of all potential flutter cases some form of flutter was seen and documented for 12 of the cases in Table 1. (Of the three undocumented cases, two appear to have been a flutter, and the other a 3/rev response.) The flutters encountered appear to fall into three general categories, as shown in Fig. 4. Type 1 flutter occurred at rotor frequencies between 2/rev and 3/rev and was seen for both two- and three-bladed rotor configurations. It appears that it occurred at all pitch angles, although most of the records are for a pitch angle of 0°. Substantial flap and torsion motions of the blade were involved in all cases, and the unstable modal frequency was near the expected second flap mode frequency. In this sense, the Type 1 flutter appears much like a classic pitch-flap flutter.

Type 2 flutter was also encountered on both the two- and three-bladed configurations, but at frequencies above 3/rev. In all cases, the flutter appeared to occur at the first torsion-mode frequency, and the modal content was almost purely torsion. This flutter could only be found at pitch angles of 0° and 2°, which suggests that coupling with the wake is important. Neutral stability or limit-cycle behavior was observed over a range of rotor speeds rather than at a specific stability boundary.

Type 3 flutter was a regressing flap-torsion flutter that occurred just above 1/rev. It was found only for the three-bladed configurations and only at a pitch angle of 0°. It occurred over a broad range of rotor speeds and, as with the Type 2 flutter, it appears to be related to the wake.

Type 1 Flutter

Flutter that was classified as Type 1 occurred on four configurations [(2a), (2b), (2c) (two blades); and (17a) (three blades)]. [Hereinafter, the rotor configurations will be referred to by their number and letter designators - e.g., (3a), (14c).] An

example of a Type 1 flutter for (2c) is shown in Fig. 5 which shows a segment of the flutter time-history and a vector phase plot. From this figure it can be seen that the flutter mode shows approximately the same flap and torsion deflections and that for each blade the flap and torsion motion is out of phase. Looking at the time-history, the motion between blades appears to be approximately in-phase and, hence, a collective motion; this is quantified on the vector plot which shows that blade 1 leads blade 2 by about 40°.

An example of a flutter point for each of these configurations [(2a), (2b), (2c), and 17a)] is given in Table 2 which shows the parameters that characterize the configuration; the pitch angle θ and the rotor speed Ω of the flutter point; and the modal frequency ω, damping σ, and mode shape. Note that the first line of the mode shape refers to the modal amplitude for blade 1, the second line for blade 2 and so forth. For (2c), unstable or neutrally stable conditions existed over rotor speeds from 700 to 762 rpm at a blade pitch angle of 0°; this is indicated in Table 2 by showing both the low and high ends of the rotor speed range. Also note that there is no lead-lag motion for any of the flutter points. All the Type 1 flutters encountered with two blades and at 0° showed an approximate in-phase behavior, with blade 1 leading blade 2 by 5°±5° for (2a) (mean±standard deviation, sample of 7); by 13°±9° for (2b) (sample of 10)/ and by 39°±4° for (2c) (sample of 7). However, different phase behavior was seen for (2c) at a pitch angle of 8° and for (17a), as is discussed below.

Configurations (2a), (2b), and (2c) were identical except for the radial location of the pitch link on the leading edge. The major effect of this change in pitch-link location is a change in the pitch-flap coupling. At the inboard location, the pitch-flap coupling is positive with more amplitude in flap than pitch for the first flap mode under nonrotating conditions. For (2b), with the pitch link located radially at about the midspan of the flexbeam, the pitch-flap coupling is zero. In the outboard location [configuration (2c)] the pitch-flap coupling is negative. The effects of these differences on the predicted modal frequencies is shown in Fig. 6 which is taken from Ref. 8. These predictions were made using the FLAIR analysis.[9] The flutter-mode frequencies have been added to this figure; they indicate the approximate location of the second flap mode which is not predicted by the FLAIR analysis. As the predicted frequencies show, the major effect of the differences in pitch-flap coupling is on the location of the first-flap-mode frequency; little effect is seen on the torsion frequency. As is shown in Table 2, the effect of pitch-flap coupling is to shift the initial flutter point to higher rotor speeds; that is, the flutter point is 700 rpm for negative pitch-flap coupling, 980 rpm for no pitch-flap coupling, and 1100 rpm for positive pitch-flap coupling. Despite this shift in the flutter point, the basic character of the flutter is unchanged; that is, the flap and torsion motions are out-of-phase regardless of the pitch-flap coupling.

A closer examination of the (2c) flutter encounters raises some additional questions about the cause of this flutter and suggests that the situation may be more complex than it first appears. Figure 7 characterizes the flutter behavior for pitch angles of 0° and 8°. At 0°, the modal damping is essentially neutral from 700 to 750 rpm. It is not until the 762-rpm point is reached that the flutter shows substantial unstable behavior. However, at each higher rotor speed the modal amplitude increases. This suggests that over the initial rotor-speed range the flutter is showing limit-cycle behavior, and it is not until 762 rpm that the destabilizing effects are sufficient to cause a normal exponential instability. It is also possible that even the 762-rpm point would have eventually shown limit-cycle behavior if it had not been necessary to shut down the rotor because of excessive loads. At 8°, a different flutter behavior is seen in that the damping changes rapidly from negative to positive values in a classic stability boundary fashion, and there is no sign of limit-cycle behavior. More interesting, still, the behavior of the flutter changes from an apparent collective second-flap mode to a differential second-flap mode (see Table 2).

The data analysis program is able to examine the flutter condition in either conventional blade coordinates (as in Fig. 5) or in multiblade coordinates. For the two-bladed rotor, the flapping multiblade coordinates are simply collective and differential coordinates, and they allow collective and differential behavior to be more easily observed. For the 8° case, two frequencies were evident and they appeared primarily in either the collective or differential coordinates. Where a lightly damped or unstable condition was observed it was always the differential mode. The collective mode appeared to be stable for these conditions, but because of its proximity to the differential mode, no acceptable estimate of its damping could be made. In the 0° case, only a collective-mode behavior was observed with no sign of a differential mode. In interpreting these differences, however, it is necessary to recognize that the blade second-flap-mode frequencies are not known to be identical and that a two-bladed rotor with dissimilar properties can

show apparent collective- and differential-mode behavior that may not be representative of rotors with identical properties. In addition, even though the collective mode is uncoupled from the stand, the differential mode will appear in the fixed system at about 50 Hz and may couple with the first stand mode, which has a frequency of 77 Hz. Further investigation is required to understand the different behavior of the collective and differential modes.

Flutter boundaries were noted at other pitch angles for (2c) in the run logs, both in the two- and three-bladed tests, but no other unstable conditions were recorded on analog tape. For (2a) and (2b), flutter was not encountered at pitch angles away from 0° within the rotor speed limits of the model.

A flutter or near-flutter case was documented for a three-bladed configuration [(17a)] that was classified as a Type 1 flutter on the basis of the modal frequency. However, in other respects this flutter case appears different from those that have been discussed so far. A segment of the time-history and the vector plot are shown in Fig. 8. Unfortunately, two of the three flapping bridges have failed (this was the last configuration tested), and the behavior must be deduced from the remaining flapping bridge and the three torsion bridges. The torsion amplitude is greater than the flap amplitude in this case and, where the previous zero pitch angle cases showed that instability was essentially a collective mode (both blades in phase), the apparent mode here is a progressing or forward whirling mode. These differences suggest a different type of flutter behavior or mechanism, but the lack of additional flutter data makes this unclear.

Type 2 Flutter

Flutter that was classified as Type 2 occurred on four combinations [(3a) (three blades); and (3a), (4a), and (5a) (two blades)]. A sample time-history and its associated vector phase plot for (3a) are shown in Fig. 9. Unlike the Type 1 flutter, which was characterized by significant amounts of flap and torsion motion, this case shows essentially all torsion motion. The flutter frequency occurs at the first-torsion-mode frequency which is slightly above 3/rev. The time-history and phase plot show that the blade motions are essentially in phase, with blade 1 leading blade 2 by 38°, hence a collective torsion flutter.

Sample flutter points are given in Table 3 for each of these configurations. As before, when flutter was observed over a range of rotor speeds, both the low and high rotor speed are shown. For (3a), blade 2 lags blade 1 by 39°±3° (sample of 11). For (4a) and (5a), amplitude and phase information are not shown because of signal calibration problems, but the phase angles, which were unaffected by the calibration problems, showed blade 2 lagged blade 1 with phase angles from -1° to 33°. As with Type 1 flutter, no lead-lag motion is observed at the flutter frequency. Unlike the Type 1 flutter cases, however, Type 2 flutter was only seen for the inboard, trailing-edge pitch-link position, which results in negative pitch-flap coupling. The difference between the three configurations in this case was the presence or absence of flexbeam or blade precone, and this seems to have had only a minor effect on the occurrence of Type 2 flutter.

Flutter was encountered on (3a) over a wide range of rotor speeds and for both the two- and three-bladed cases. Figure 10 shows the frequencies calculated with FLAIR for this configuration.[8] The flutter frequencies have been added to this figure, and it can be seen that they agree very well with the predicted first-torsion frequency. The flutter encountered with (3a) is further described in Fig. 11, which shows the modal amplitudes, damping, and frequencies for both the two- and three-bladed tests. For the range of rotor speeds over which the flutter was examined, the rotor showed neutral stability or limit-cycle behavior. However, as rotor speed increased, the modal amplitude increased as well. That this is related to the flutter and not just a response to 3/rev excitation is shown by the plot of the 3/rev response in torsion, which does not change noticeably over the range of rotor speeds investigated. As shown in Table 3, the two-bladed Type 2 flutter is mostly torsion amplitude, with the two blades nearly in phase. For the three-bladed case, this behavior is changed, as shown in Fig. 12 in which the vector phase plots are compared. Although blades 1 and 3 are not far apart in phase, blade 2 is of opposite phase. There is significantly more blade flapping now than was seen in the two-bladed case. (Note that if a response in a degree of freedom is less than 10% of the largest component, it is not shown in these vector phase plots.) Unlike the two-bladed case in which the phase relation was invariant with rotor speed, substantial differences were seen for the three-bladed rotor for different rotor speeds as indicated in Table 3.

Configurations (4a) and (5a) were tested at a pitch angle of 2° (the normal increment in pitch angle was 4°); they too showed the Type 2 flutter. However, no incidence of flutter was documented for any configuration at larger pitch angles. This absence of flutter at higher pitch angles

suggests that the flutter is related to the wake and is perhaps wake-excited.

Type 3 Flutter

Type 3 flutter was encountered on four three-bladed configurations [(7c), (14c), (15a), and (16a)]. An example is provided in Fig. 13 for (15a). The sample time-history shows a low-frequency flutter that is only slightly above 1/rev. For each blade, the flap and torsion motions are in phase, with flapping roughly twice the magnitude of torsion. Blade 3 lags the motion of blade 2, which in turn lags blade 1; this represents a regressing or backward whirl mode if viewed in the fixed system. Figure 13 gives the appearance of a coupled flap-torsion flutter; however, the flapping mode at this frequency appears in both flap and pitch coordinates, and because of the positive pitch-flap coupling the motion appears in phase. Thus, it appears that the Type 3 flutter is a single-degree-of-freedom flutter, as was seen for Type 2.

Sample flutter points are provided in Table 4 for the various Type 3 flutter cases. Except for (16a), the flutter was encountered over a range of rotor speeds and it gave the appearance of neutrally stable or limit-cycle behavior. For all configurations tested, the mode shape was the same with the blade flap and torsion in phase and a 120° phase difference between the blades. Note that as in the other flutter cases, there is no motion in the lead-lag coordinate.

More detailed information on the Type 3 flutter is provided in Fig. 14 for (7c) and (14c). These configurations differ only in the addition of a boundary-layer trip to the outer 5 in. of each blade on the upper surface at the 25% chord location. The trip used a 1/16-diam twine that was glued on. The trip was added to see if boundary-layer disturbances could significantly affect the observed flutter behavior, as has occurred in previous model investigations.[10] Configurations (7c) and (14c) show essentially identical behavior, and, although the rotor-speed range for neutral or limit-cycle behavior is shifted to higher rotor speeds for (14c), the use of the trip does not eliminate the flutter. Both configurations show a relatively wide range of limit-cycle or unstable behavior, with the amplitude increasing as rotor speed increases. No flutter was encountered for these configurations for pitch angles of ±4°, which suggests that the flutter is wake-coupled - behavior similar to that seen in the Type 2 flutter cases.

Discussion

Wake-Excited Flutter

At low blade-pitch angles and induced velocities in hover, the spacing between the shed wakes can become quite small, and, if the frequency of an oscillation is such that the shed wakes reinforce each other, a flutter can occur that is termed wake-excited flutter. It often appears as a single-degree-of-freedom flutter. Wake-excited flutter may occur for a single blade or for a rotor with any number of blades. In the latter case, the actual frequency will depend on the particular mode of the rotor that is involved. Anderson and Watts[4] provide a good discussion of how the wakes will line up for the various modes of a four-bladed rotor. The same principles can be applied for the two- and three-blade rotors that were tested in the experiments reported here. Depending on the blade mode involved, a particular frequency ratio ω/Ω will result in the shed wakes, reinforcing and causing a wake-excited flutter. The frequency ratios for potential wake-excited flutter for two- and three-bladed rotors are shown in Table 5. If, for an example, a blade torsion mode or flap mode is near a 4/rev resonance with rotor speed, then there is a potential for a wake-excited flutter in the collective mode for a two-bladed rotor or for the cyclic regressing mode for a three-bladed rotor. With the use of this table it is possible to examine the experimentally determined flutters that occurred near per-rev crossings and determine if they can be categorized as wake-excited flutter.

The Type 2 flutter was essentially a pure torsion flutter, and it occurred on both two- and three-bladed rotor configurations near the 3/rev crossing of the first torsion mode; it was not observed at pitch angles greater than 2°. In this sense, the flutter acts like a classic wake-excited flutter. From Table 5 it can be seen that a wake-excited flutter at 3/rev should occur in the differential mode for a two-bladed rotor and in the collective mode for a three-bladed rotor. However, the experimentally determined flutter mode is close to a collective mode for all the two-bladed encounters whereas for the three-bladed case no fixed system mode could be defined. This suggests that the Type 2 flutter is not wake-excited in the classic sense of a flutter induced from reinforcement of previous wakes.

The Type 3 flutter appeared close to a 1/rev crossing near the first-flapping-mode frequency and was not observed away from a pitch angle of 0°. It occurred only for the three-bladed rotor configurations. From Table 5, a 1/rev wake-excited flutter should occur only for the regressing

mode of a three-bladed rotor, and this is what was seen in the experimental measurements for all four configurations in which this type of flutter was encountered. In this case, then, it seems clear that the Type 3 flutter is wake-excited and occurs because the first flap mode is crossing the 1/rev because of positive pitch-flap coupling.

In some cases, the Type 1 flutter encounters showed behavior that appeared as though they might be related to wake reinforcement, although in no cases were the flutter frequencies as close to a per-rev crossing as in the Type 2 and Type 3 encounters. However, it may be useful to look upon Table 5 as a means by which the Type 1 flutter encounters might be better understood. For (2c), the Type 1 flutter showed limit-cycle behavior over a range from 700 to 750 rpm. The flutter mode frequency in this case ranged from 2.8/rev to 2.7/rev. This would suggest an excitation of the second flap mode by the coalescence of wakes at 3/rev; however, from Table 5 this should occur only in a differential mode, whereas experimentally the observed mode was a collective one. For (17a), the observed mode was largely a torsion response at 2.4/rev, and from Table 5 for a three-bladed rotor this suggests excitation of the second flap mode by 2/rev wake reinforcement, which should occur in a progressing mode. Interestingly enough, this is what was seen in the measurements, although the lack of additional experimental cases for (17a) makes any conclusions impossible.

Effect of Configuration

As shown in Table 1, 28 different configurations, blade numbers, and pitch-link radial locations were tested and only 12 showed a documented case of flutter. In looking at those cases that had flutter and those that were flutter-free, it may be asked if there are any definite conclusions that can be made about the effect of configuration. Clearly the configurations with two pitch links were without flutter, but this is not surprising, considering that the torsional stiffness was above 10/rev. The Type 1 flutter configurations seemed to show the largest variation in parameters, with no particular parameter obviously dominant. This flutter occurred for pitch-flap coupling of approximately -0.5, 0, and +0.5, with the pitch link on the leading edge, but in none of the cases with the pitch link on the trailing edge. The least stable configuration was (2c), with the pitch link on the leading edge and negative pitch-flap coupling. Because this configuration was purposely avoided in subsequent tests, it is difficult to determine if these results were in any sense typical.

The Type 2 flutter cases all had negative pitch-flap coupling, and the only other two-bladed configuration with negative pitch-flap coupling that did not show Type 2 behavior was (2c), which went unstable at a lower rotor speed with Type 1 flutter. Of the three-bladed configurations with negative pitch-flap coupling that were tested, one showed Type 2 flutter, but the other two did not.

Type 3 flutter occurred only for three-bladed rotor configurations with positive pitch-flap coupling. However, these cases included configurations with droop, precone, sweep, and the pitch link on either edge. Similar configurations with positive pitch-flap coupling showed no instability. The absence of an obvious dependency of a specific flutter type on configuration suggests that future design must continue to be guided by detailed analysis and model test.

Conclusions

A number of different flutter types were encountered in a series of experiments undertaken to determine the lead-lag stability in hover of a bearingless rotor mounted on a rigid hub. These flutter cases have been analyzed and the following conclusions made.

1) Three distinct types of flutter were encountered that may be separated on the basis of the flutter mode frequency. a) A flutter mode that occurs at a frequency between 2/rev and 3/rev which corresponds to the model rotor's second flap mode (Type 1); this flutter was seen on both two- and three-bladed rotors and showed significant flap and torsion motions. b) A flutter mode that occurs at a frequency above 3/rev and corresponds to the model rotor's first torsion mode (Type 2); this flutter mode was seen on both two- and three-bladed rotors, and the motion was mostly torsion with very little flapping. And c) a flutter mode that occurs at a frequency close to 1/rev and is a regressing mode when seen in the fixed system (Type 3); this occurred only for three-bladed rotors.

2) Type 1 flutter was observed at pitch angles greater than 0° for the best documented configuration and in this sense represents a classic flap-torsion flutter that is not directly dependent on unsteady wake effects.

3) Type 2 flutter was observed on four configurations at pitch angles at 0° and 2°, but not at higher pitch angles. Its occurrence near the 3/rev crossing at low pitch angles suggests the flutter is wake-excited; however, it occurs in a collective mode rather than a differential mode for th

two-bladed tests, and it does not appear in any clearly defined rotor mode in the three-bladed tests.

4) Type 3 flutter was observed on four configurations at a pitch angle of zero degrees, but not at higher pitch angles. It appeared only for three-bladed configurations in a regressing mode near the 1/rev crossing which corresponds to the expected mode of instability for a wake-excited flutter.

5) The effects of rotor configuration on the various forms of flutter were examined, but there were no configuration parameters that were clearly stabilizing or destabilizing for torsion-mode frequencies below 10/rev.

Appendix: Model Properties

The model rotor geometric properties are shown in Table 6. Rotor mass properties are given in Table 7. The blade mass is concentrated in the torque tube and root hardware, which are not representative of that of a full-scale rotor. The center of gravity of the blades alone was determined from measurements on four blades; it was located at 26.2% chord with a range of values from 25.6% to 26.6%. If the chordwise c.g. of the combined blade and root hardware is considered, the c.g. is shifted to 25.1% chord because of the mass of the root hardware. This does not adequately represent the cross-product term of c.g. offset with radius, which is important for flutter calculations; however, no estimate was made of an equivalent c.g. based on the correct cross-product term. Measurements were made of nonrotating frequencies of the blades both with and without pitch links; these are provided in Table 8. The measurements with the pitch link installed are for (3a), that is, the pitch link is located on the trailing edge at the inboard location. The nonrotating frequencies for other configurations do not differ significantly from the tabulated values in Table 8. Nonrotating measurements were made of the pitch-flap coupling for a few configurations and the values ranged from +0.41 to +0.49 for four configurations, with the pitch link at the inboard position on the trailing edge. (Comparable values of negative pitch-flap coupling have not been obtained.) The blade airfoil section of the model is a NACA 23012.

Acknowledgments

The authors acknowledge Mr. Jack Ollila for his fine hand on the rotor controls through numerous flutter encounters without damaging the rotor. Mr. Jan Drees, Bell Helicopter Textron, Inc., is acknowledged for pointing out the early Dutch experience with single-degree-of-freedom flutter encounters.

References

1. Loewy, Robert G., "A Two-Dimensional Approximation to the Unsteady Aerodynamics of Rotary Wings," Journal of the Aeronautical Sciences, Vol. 24, Feb. 1957, pp. 81-92, 144.

2. Miller, R.H. and Ellis, C.W., "Helicopter Blade Vibration and Flutter," Journal of the American Helicopter Society, Vol. 1, No. 4, July 1956, pp. 19-38.

3. Daughaday, Hamilton, DuWaldt, Frank, and Gates, Charles, "Investigation of Helicopter Blade Flutter and Load Amplification Problems," Journal of the American Helicopter Society, Vol. 2, No. 3, July 1957, pp. 27-45.

4. Anderson, William D. and Watts, George A., "Rotor Blade Wake Flutter – A Comparison of Theory and Experiment," Journal of the American Helicopter Society, Vol. 21, No. 2, Apr. 1976, pp. 32-43.

5. Neff, James R., "Pitch-Flap-Lag Instability of Elastic Modes of an Articulated Rotor Blade," Proceedings of the 40th Annual National Forum, May 1984, pp. 573-579.

6. Shaw, John and Edwards, W. Thomas, "The YUH-61A Tail Rotor: Development of a Stiff Inplane Bearingless Flexstrap Design," Journal of the American Helicopter Society, Vol. 23, No. 2, Apr. 1978, pp. 9-18.

7. Harvey, K.W., "Aeroelastic Analysis of a Bearingless Rotor," American Helicopter Society Symposium on Rotor Technology, Aug. 1976.

8. Dawson, Seth, "An Experimental Investigation of a Bearingless Model Rotor in Hover," Journal of the American Helicopter Society, Vol. 28, No. 4, Oct. 1983, pp. 29-34.

9. Hodges, Dewey H., "An Aeromechanical Stability Analysis for Bearingless Rotor Helicopters," Journal of the American Helicopter Society, Vol. 24, No. 1, Jan. 1979, pp. 2-9.

10. Tinman, R. and van de Vooren, A. I., "Flutter of a Helicopter Rotor Rotating in Its Own Wake," Journal of the Aeronautical Sciences, Vol. 24, July 1957, pp. 694-702.

Table 1. Bearingless model rotor configurations

Configuration	Number of blades	Pitch-link position	Radial location[a]	θ_β[b]	θ_f, deg	θ_b, deg	β_f, deg	β_b, deg	ζ_b, deg	Flutter type
1a	2	LE/TE	10	0	0	0	0	0	0	None
2a	2	LE	10	+	0	0	0	0	0	1
2a	3	LE	10	+	0	0	0	0	0	None
2b	2	LE	50	0	0	0	0	0	0	1
2c	2	LE	90	-	0	0	0	0	0	1
2c	3	LE	90	-	0	0	0	0	0	(c)
3a	2	TE	10	-	0	0	0	0	0	2
3a	3	TE	10	-	0	0	0	0	0	2
3b	2	TE	50	0	0	0	0	0	0	None
3c	2	TE	90	+	0	0	0	0	0	None
3c	3	TE	90	+	0	0	0	0	0	None
4a	2	TE	10	-	0	0	2.5	0	0	2
5a	2	TE	10	-	0	0	0	2.5	0	2
6a	3	LE/TE	10	0	0	0	0	0	-2.5	None
6c	3	LE/TE	90	0	0	0	0	0	-2.5	None
7a	3	TE	10	-	0	0	0	0	-2.5	None
7c	3	TE	90	+	0	0	0	0	-2.5	3
8a	3	LE	10	+	0	0	0	0	-2.5	None
8c	3	LE	90	-	0	0	0	0	-2.5	(c)
9a	3	LE	10	+	0	0	0	2.5	-2.5	None
10c	3	TE	90	+	0	0	0	2.5	-2.5	None
11a	3	LE	10	+	0	0	2.5	0	-2.5	None
12a	3	LE	10	+	0	8	0	0	0	None
13a	3	LE	10	+	-8	8	0	0	0	None
14c[d]	3	TE	90	+	0	0	0	0	-2.5	3
15a	3	LE	10	+	0	0	2.5	0	0	3
16a	3	LE	10	+	0	0	0	2.5	0	3
17a	3	LE	10	+	0	8	0	0	-2.5	1

NOTE: Symbols are defined in text. Abbreviations in pitch-link-position column refer to leading and trailing edges.

[a]Percent of flexbeam length from flexbeam root.

[b]Pitch-flap coupling, positive pitch-flap coupling is flap up, nose up.

[c]Type 1 instability noted in run logs, but no documented record.

[d]Same configuration as (7c) except with boundary-layer trip on top surface.

Table 2. Type 1 flutter cases[a]

Configuration	Pitch-link position	Number of blades	θ_f, deg	β_b, deg	θ, deg	Ω, rpm	ω, Hz	σ, 1/sec	Mode Shape[b] Flap Amplitude deg	Flap Phase deg	Chord Amplitude deg	Chord Phase deg	Torsion Amplitude deg	Torsion Phase deg
2a	LE, inboard	2	0	0	0	1100	43.77	+0.30	0.22	0	0.01	-8	0.18	174
									0.16	5	0.00	-53	0.13	-178
2b	LE, center	2	0	0	0	980	40.17	-0.05	0.72	0	0.03	-12	0.69	178
									0.46	18	0.01	-131	(c)	(c)
2b	LE, center	2	0	0	0	1011	40.72	+0.64	0.87	0	0.04	-11	0.84	178
									0.55	17	0.01	-135	(c)	(c)
2c	LE, outboard	2	0	0	0	700	32.85	-0.00	0.84	0	0.02	-34	0.92	179
									0.42	42	0.02	-124	1.44	-137
2c	LE, outboard	2	0	0	0	762	33.44	+0.35	1.68	0	0.05	-36	1.96	-179
									1.30	35	0.06	-120	1.41	-145
2c	LE, outboard	2	0	0	8	889	33.97	+0.87	1.06	0	0.04	-137	1.45	-178
									2.56	-160	0.26	10	3.34	18
7a	LE, inboard	3	8	-2.5	0	999	39.96	-0.41	(c)	(c)	0.01	155	0.12	0
									(c)	(c)	0.01	62	0.23	-118
									0.08	136	0.02	-78	0.30	109

[a]All configurations have zero flexbeam and blade precone.

[b]Values in first horizontal line for each configuration are for blade 1; those in second line are for blade 2; those in third line are for blade 3.

[c]Failed strain gage.

Table 3. Type 2 flutter cases[a]

Configuration	Number of blades	β_f, deg	β_b, deg	θ, deg	Ω, rpm	ω, Hz	σ, 1/sec	Mode Shape[b] Flap Amplitude deg	Flap Phase deg	Chord Amplitude deg	Chord Phase deg	Torsion Amplitude deg	Torsion Phase deg
3a	2	0	0	0	851	47.57	+0.02	0.04	-8	0.01	170	0.51	0
								(c)	(c)	0.03	44	1.06	36
3a	2	0	0	0	936	48.82	+0.27	0.02	-91	0.03	172	2.33	0
								(c)	(c)	0.05	54	2.08	38
3a	3	0	0	0	804	46.71	+0.02	0.06	-159	0.01	12	0.46	0
								0	102	0.00	100	0.19	-79
								0.12	-12	0.00	125	0.69	166
3a	3	0	0	0	900	47.33	+0.33	0.03	-155	0.01	3	0.35	0
								0.13	-11	0.01	11	0.26	-178
								0.06	-166	0.01	16	0.27	-42
4a	2	2.5	0	0	878	47.31	+0.98	-	-	-	-	-	-
								-	-	-	-	-	-
4a	2	2.5	0	2	940	47.95	+0.5	-	-	-	-	-	-
								-	-		-	-	-
5a	2	0	2.5	0	883	47.67	0.00	-	-	-	-	-	-
								-	-	-	-	-	-
5a	2	0	2.5	2	891	48.14	+0.10	-	-	-	-	-	-

[a]All configurations have the pitch link at the inboard location on the trailing edge and are without flexbeam pitch or blade sweep.

[b]Values in first horizontal line for each configuration are for blade 1; those in second line are for blade 2; those in third line are for blade 3.

[c]Failed strain gage.

Table 4. Type 3 flutter cases[a]

Configuration	Pitch-link position	β_f, deg	β_b, deg	ζ_b, deg	θ, deg	Ω, rpm	ω, Hz	σ, 1/sec	Mode Shape[b] Flap Amplitude deg	Flap Phase deg	Chord Amplitude deg	Chord Phase deg	Torsion Amplitude deg	Torsion Phase deg
7c	TE outboard	0	0	-2.5	0	302	5.70	+0.08	0.51	0	0.01	166	0.29	0
									0.56	122	0.01	-71	0.29	122
									0.56	-121	0.00	-5	0.34	-116
7c	TE outboard	0	0	-2.5	0	407	7.30	+0.50	0.73	0	0.01	132	0.43	1
									0.68	127	0.01	-8	0.35	126
									0.91	-118	0.01	68	0.58	-120
14c[c]	TE, outboard	0	0	-2.5	0	401	7.20	-0.16	0.55	[illegible]	0.01	156	0.33	1
									0.50	12	0.01	-49	0.11	126
									0.58	-11[illegible]	0.01	68	0.36	-115
14c[c]	TE, outboard	0	0	-2.5	0	603	10.41	-0.02	0.93	0	[illegible]	148	0.60	1
									0.85	123	0.06	-98	0.20	123
									0.73	-118	0.01	157	0.49	-118
15a	LE, inboard	0	2.5	0	0	402	7.25	+0.02	0.30	0	0.01	-134	0.13	-9
									0.32	129	0.01	64	0.14	129
									0.54	-122	0.01	-29	0.26	-122
15a	LE, inboard	0	2.5	0	0	451	7.94	+0.09	1.20	0	0.02	-158	0.54	-8
									1.27	124	0.02	-30	0.55	125
									1.52	-121	0.01	-104	0.73	-120
16a	LE,	2.5	0	0	0	402	7.12	+0.05	0.13	0	0.00	-79	0.06	8
									0.13	122	0.01	2	0.06	123
									0.12	-121	0.00	-21	0.06	-120

[a]All configurations have three blades, no flexbeam pitch, and the pitch link locations result in positive pitch flap coupling.

[b]Values in first horizontal line for each configuration are for blade 1; those in second line are for blade 2; those in third line are for blade 3.

[c]Trip strip added to outer portion of blades.

Table 5. Frequency ratios for wake-excited flutter

ω/Ω	2-Bladed collective	2-Bladed differential	3-Bladed collective	3-Bladed regressing	3-Bladed progressing
1	---	X	---	X	---
2	X	---	---	---	X
3	---	X	X	---	---
4	X	---	---	X	---
5	---	X	---	---	X
6	X	---	X	---	---

Table 6. Rotor geometric properties

Property	Value
Radius, m	0.902
Blade chord, m	0.0419
Solidity per blade	0.0148
Flexbeam length, m	0.1016
Flexbeam width, m	0.00813
Flexbeam thickness, m	0.00361
Flexbeam tip distance from center, m	0.1782

Table 7. Rotor mass properties

Property	Blade/torque-tube	Blade
Blade mass, kg	0.460	0.102
Blade spanwise c.g., % radius	27.6	56.7
Blade chordwise c.g., % chord from leading edge	25.1	26.2
Blade flapping inertia about flexbeam center, $kg \cdot m^2$	0.02358	-
Blade pitch inertia, $kg \cdot m^2$	1.59×10^{-4}	-
Lock number	8.26	-

Table 8. Blade nonrotating frequencies[a]

Blade mode	Modal frequency (pitch link installed), Hz	Modal frequency (no pitch link installed), Hz
First flap	4.88	4.69
Second flap	24.81	24.81
First lead-lag	11.13	10.94
First torsion	38.28	19.73

[a]Measurements made on isolated blade of (3a).

Figure 1. Two-bladed bearingless-rotor model.

Figure 2. Three-bladed bearingless-rotor model.

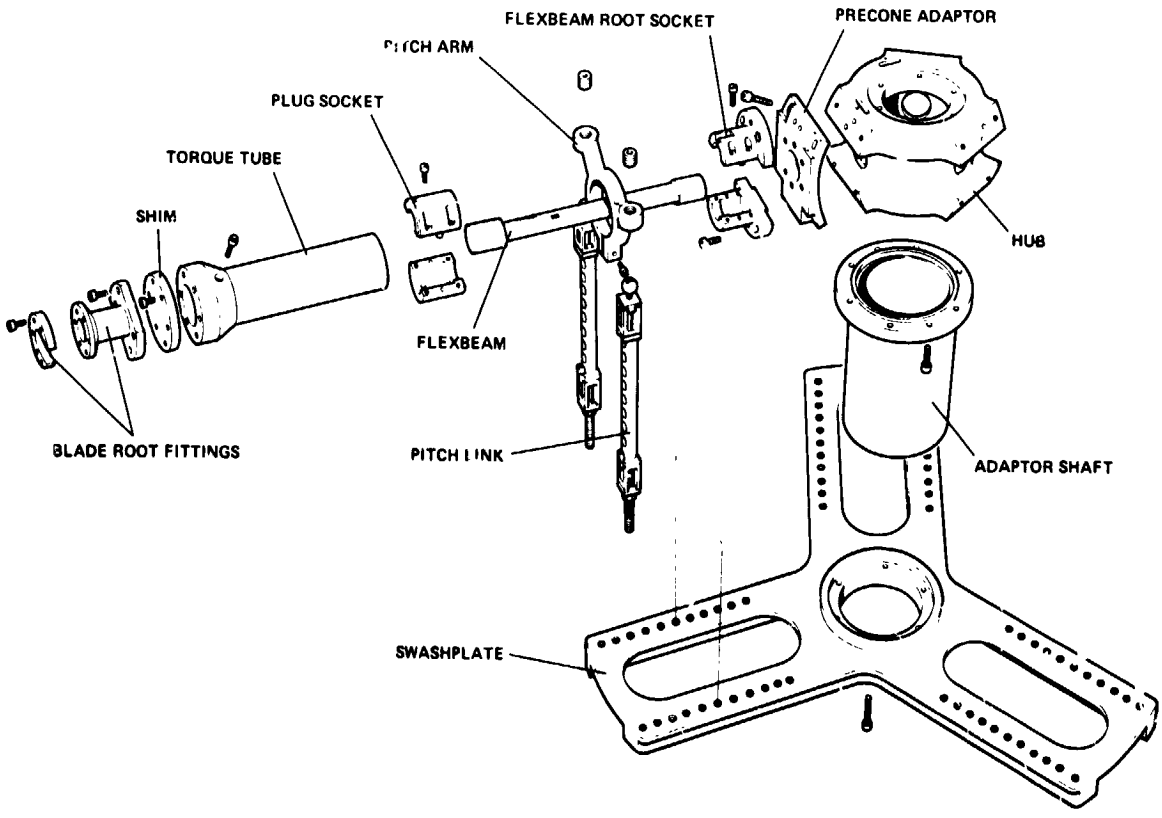

Figure 3. Exploded view of flexbeam and blade-root hardware.

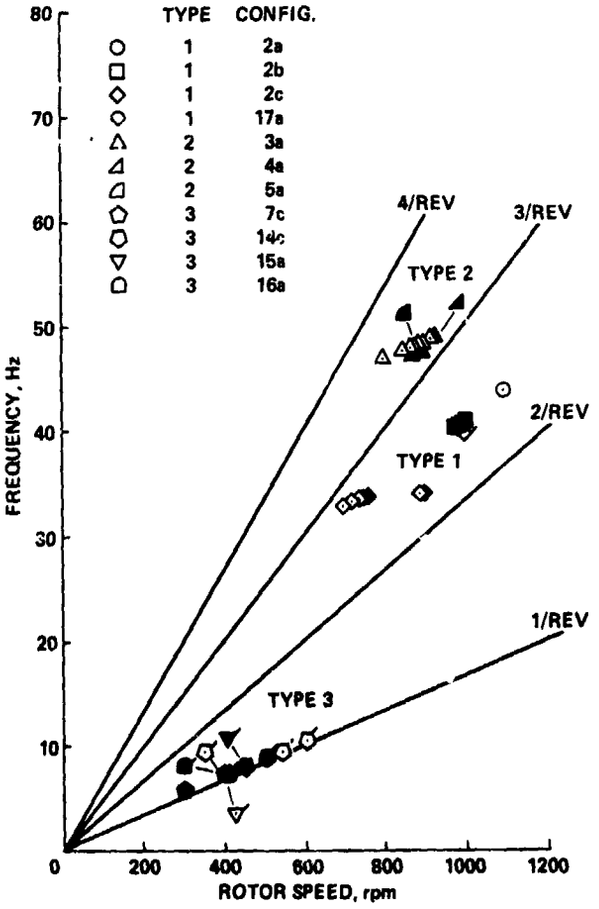

Figure 4. Frequency diagram showing types of flutter encountered. Open symbols are neutral stability points; closed symbols are unstable points; flagged symbols are for three-bladed rotor.

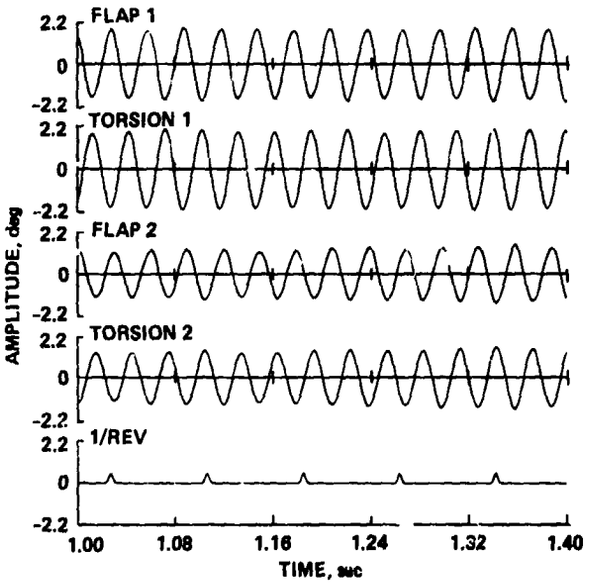

(a) Time-history.

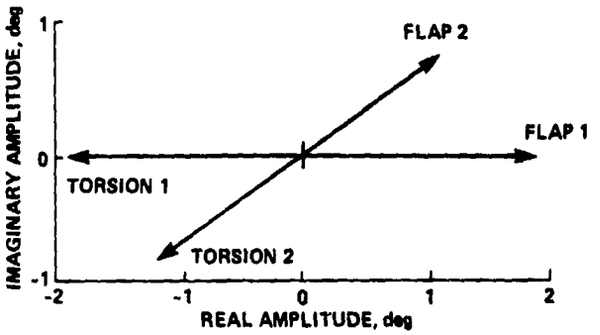

(b) Vector phase plot, ω = 33.55 Hz.

Figure 5. Time-history and vector phase plot for Type 1 flutter [(2c)]; two blades, θ = 0°, Ω = 762 rpm.

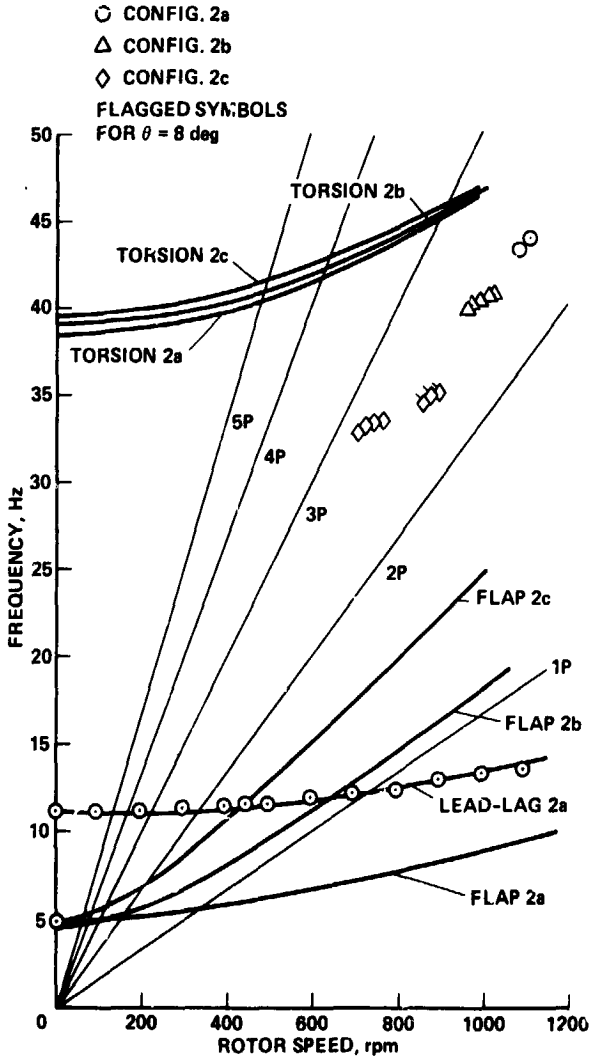

Figure 6. Frequency diagram for Type 1 flutter [(2a), (2b), and (2c)]. (Flagged symbols are for θ = 8°).

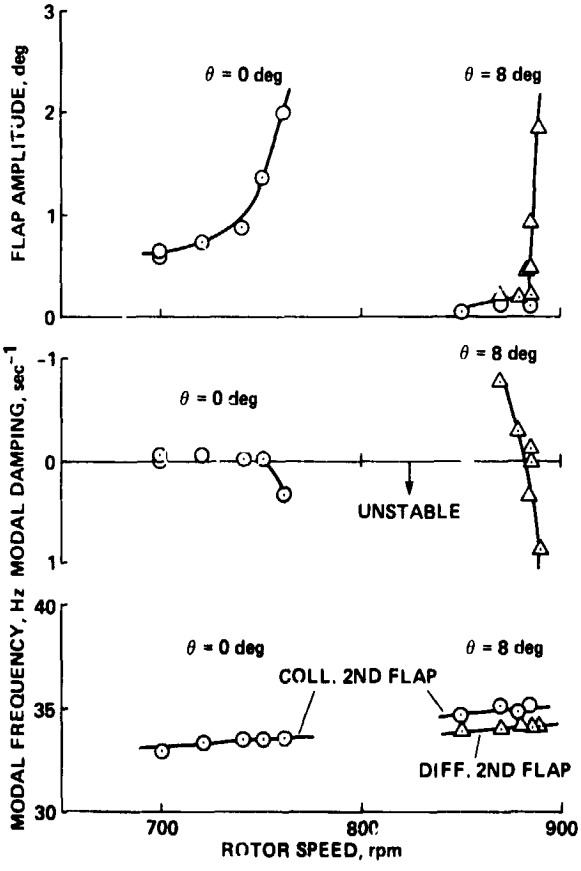

Figure 7. Type 1 flutter behavior for (2c).

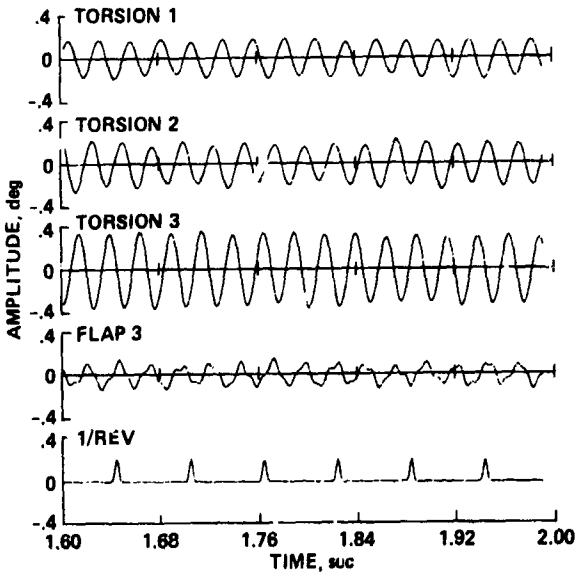

(a) Time-history.

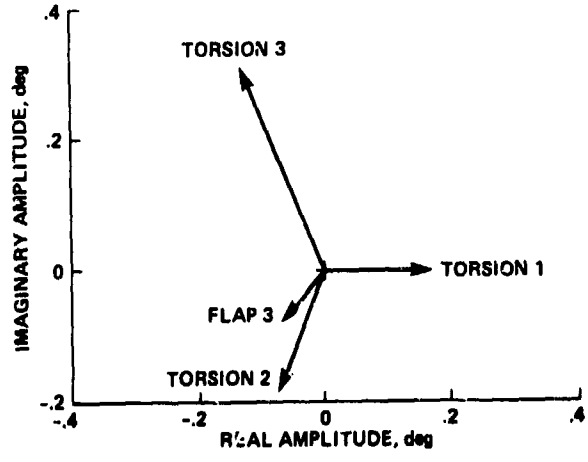

(b) Vector phase plot, ω = 39.92 rpm.

Figure 8. Time-history and vector phase plot for Type 1 flutter [(17a)]; three blades, θ = 0°, Ω = 999 rpm.

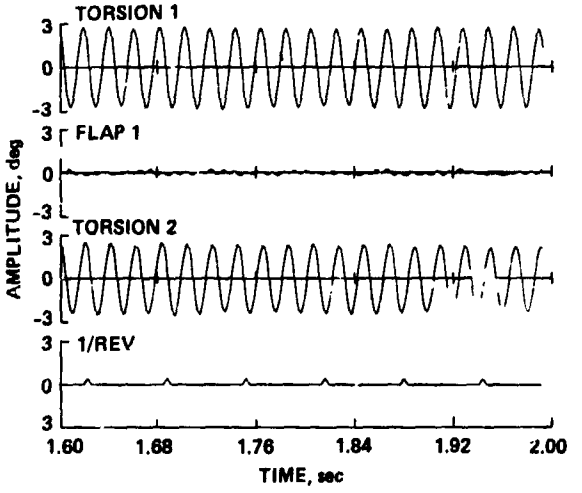

(a) Time-history.

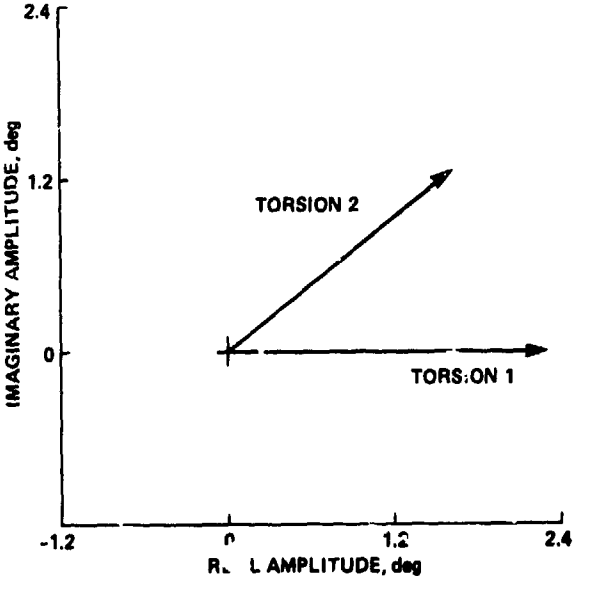

(b) Vector phase plot, ω = 48.82 Hz.

Figure 9. Time-history and vector phase plot for Type ? flutter [(3a)]; two blades, θ = 0°, Ω = 936 rpm.

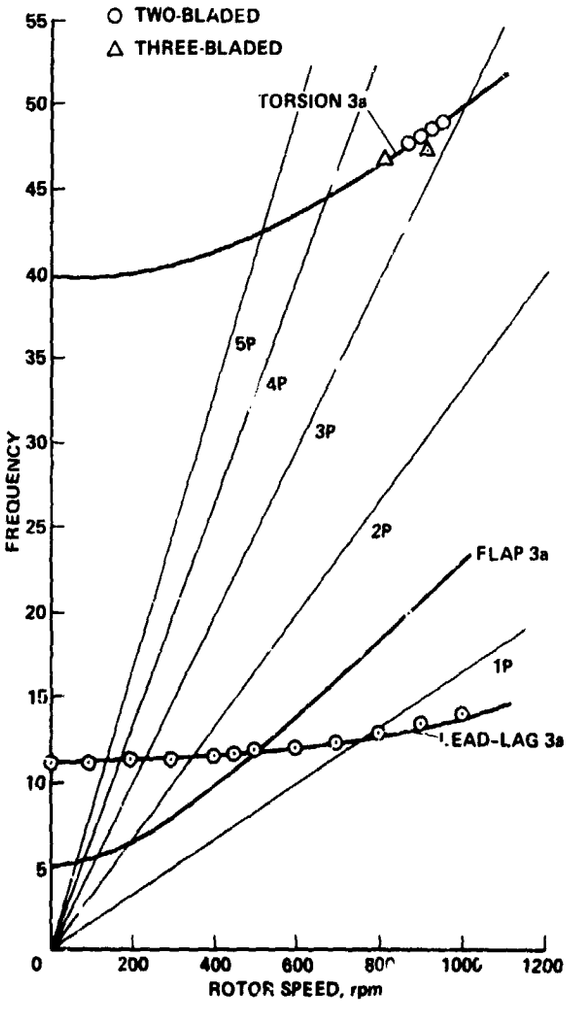

Figure 10. Frequency diagram for Type 2 flutter [(3a)].

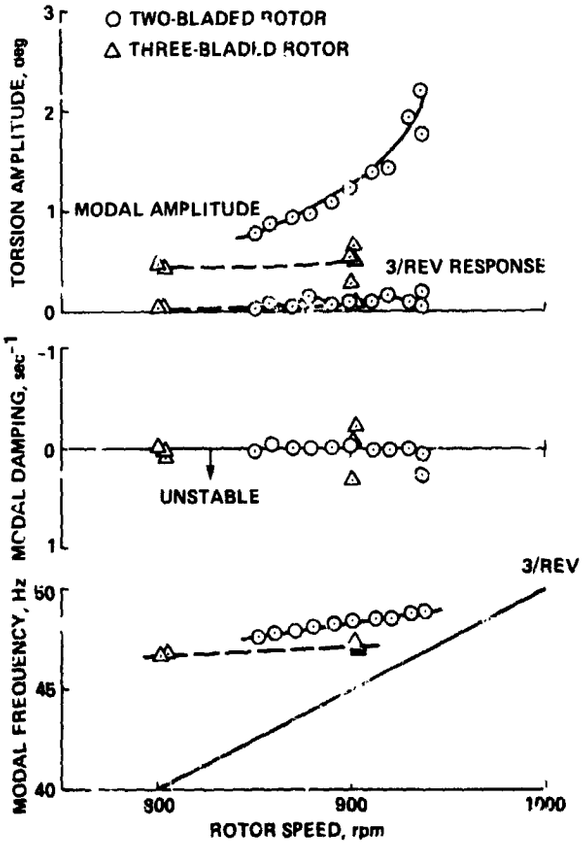

Figure 11. Type 2 flutter behavior for (3a).

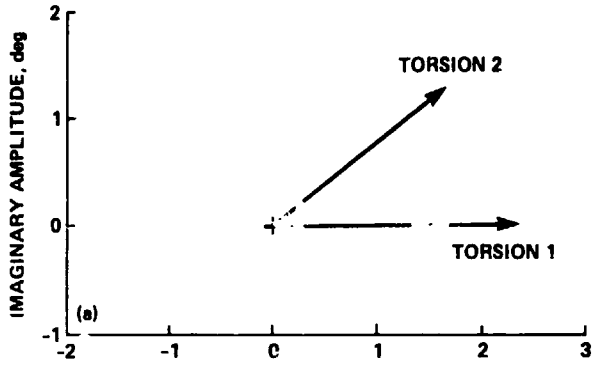

(a) Two-bladed rotor, Ω = 936 rpm, ω = 48.82 Hz.

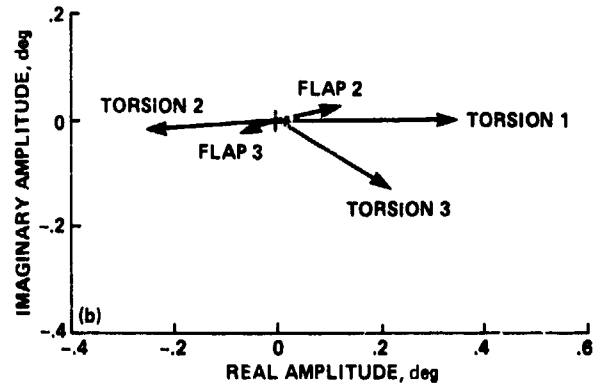

(b) Three-bladed rotor, Ω = 900 rpm, ω = 47.33 Hz.

Figure 12. Comparison of vector phase plots for two- and three-bladed rotors for (3a); θ = 0°.

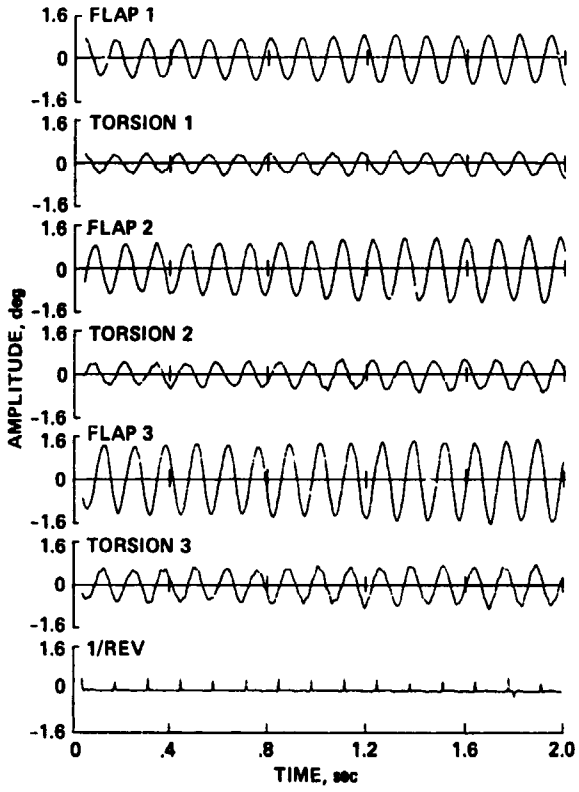

(a) Time-history.

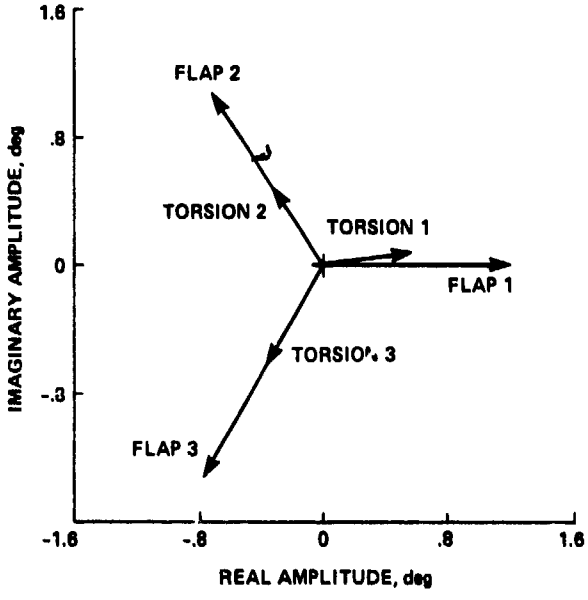

(b) Vector phase plot, ω = 7.94 Hz.

Figure 13. Time-history and vector phase plot for Type 3 flutter [(15a)]; three blades, θ = 0°, Ω = 451 rpm.

C-2

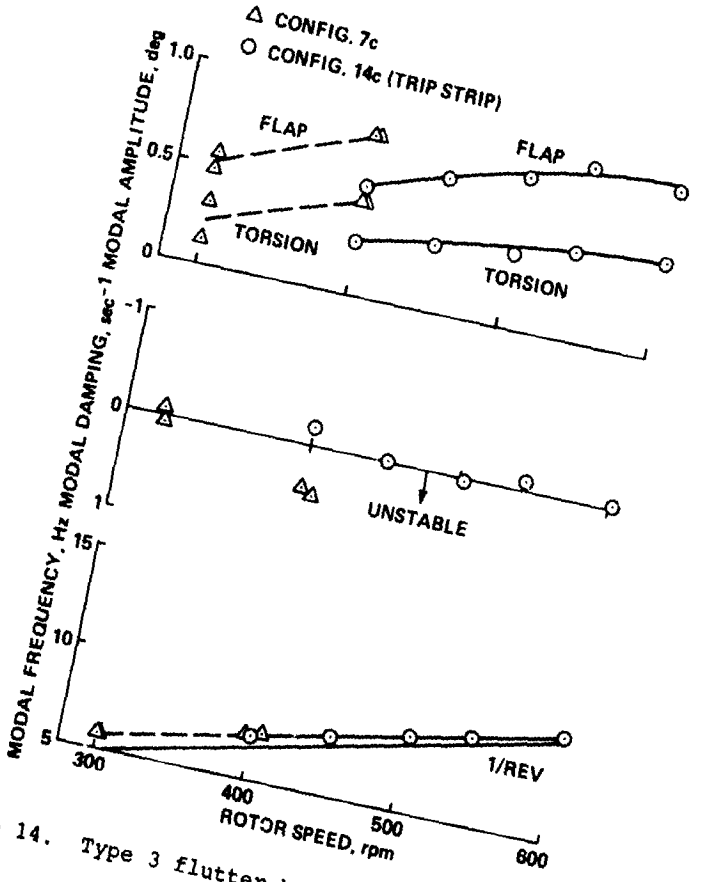

Figure 14. Type 3 flutter behavior for (7c and 14c).

DISCUSSION
Paper No. 6

EXPERIMENTALLY DETERMINED FLUTTER FROM TWO- AND THREE-BLADED MODEL BEARINGLESS ROTORS IN HOVER
William G. Bousman
and
Seth Dawson

Jing Yen, Bell Helicopter: Is there any way we can look at these mode shapes. For the Type 1 you have is the mode a predominantly beamwise mode and is Type 2 predominantly a torsion mode?

Bousman: Type 1 for almost all cases had roughly comparable motions in flapping and torsion. I would say it was a mixture of second flap and first torsion mode behavior. It's fairly near that crossing.

Yen: It looks like the frequency is a strong function of rpm.

Bousman: Yes. That frequency is occurring, as best we can tell, at the second flap mode, although we don't have any calculations, because FLAIR doesn't do calculations of higher modes.

Yen: My second question, Bill, do you still have the model parts around the lab? Can you put them back together again, run up and blow some wind?

Bousman: Blow some wind?

Yen: Yes. In other words could this be a wake flutter?

Bousman: Oh, you mean particularly for the one that we think is a wake flutter. Could we blow some wind and just see if it goes away. Yes, that's a good idea.

LIFTING SURFACE THEORY FOR A HELICOPTER ROTOR IN FORWARD FLIGHT

H. Tai
NASA Langley Research Center
Hampton, Virginia 23665

Harry L. Runyan
College of William and Mary
NASA Langley Research Center
Hampton, Virginia 23665

ABSTRACT

A lifting surface theory has been developed for a helicopter rotor in forward flight for compressible and incompressible flow. The method utilizes the concept of the linearized acceleration potential and makes use of the vortex lattice procedure. Calculations demonstrating the application of the method are given in terms of the lift distribution on a single rotor, a two-bladed rotor, and a rotor with swept-forward and swept-back tips. In addition, the lift on a rotor which is vibrating in a pitching mode at 4/rev is given. Compressibility effects and interference effects for a two-bladed rotor are discussed.

INTRODUCTION

Rotating lifting surfaces are an integral part of the propulsive unit of every aeronautical and nautical vehicle, from the compressor and turbine blades of jet engines, the pumps for rocket engines, to propeller and helicopter rotors. The aerodynamics of these rotating elements has been under extensive study since the advent of the airplane and with a combination of experimental and analytical approaches, succcessful designs have been achieved. In many cases, two-dimensional theory has been used, usually modified by an assumed spanwise distribution, and inflow velocities. This paper presents a compressible, lifting surface method for a helicopter rotor in forward flight within the limits of linearized theory.

The method is based on the concept of the acceleration potential, originally introduced by Kussner (1941). The method was first applied to an oscillating wing in uniform translatory motion including effects of compressible flow by Runyan and Woolston (1957). The acceleration potential approach has now become standard for the determination of the unsteady aerodynamic forces for flutter studies of lifting surfaces in rectilinear motion.

The first use of the acceleration potential approach for a rotating system was made in a paper by Hanaoka (1962) for the loading on a marine propeller in incompressible flow. The acceleration potential has been used in the past in studying the propeller noise problem, but in all of these noise propagation cases the problem was specialized early in the analytical development to the so-called far-field case usually with a stationary observer, whereas the lifting surface theory is essentially concerned with the details of the near-field case for a co-moving observer as well as the satisfaction of certain of certain boundary conditions. Runyan (1973) utilized the acceleration potential approach to obtain a solution to the oscillating propeller in compressible flow. Dat, (1973), has derived a general expression for an acceleration doublet for any motion. Pierce and Vaidyanathan (1983) have treated the helicopter rotor in forward flight using the method of matched asymptotic expansion for the incompressible case. The procedure developed here involves the precise numerical integration over the surface of the rotor in a time frame. The method sets forth a formulation of a fundamental three dimensional, compressible, unsteady aerodynamic theory for propellers and helicopter rotors.

The next section contains a brief derivation of the fundamental equations, including a discussion of some implications of the equations. The third section contains a description of the method of solution. Finally, the results of some calculations for the several specific examples are given.

SYMBOLS

A'	rotor blade area
A_{nm}	aerodynamic influence coefficients
A_n, B_n	Fourier coefficients
c	speed of sound
C	chord of rotor
C_T	thrust coefficient per blade $(\text{thrust}/\pi\rho\Omega^2 R_t^4)$
$\vec{D}$	vector distance from doublet to downwash point
D	absolute value of $\vec{D}$
$\hat{D} = \vec{D}/D$	unit vector of $\vec{D}$
I	value of singular integral
K	kernel function
$\vec{n}$	unit vector at downwash point, normal to velocity vector
$\vec{n}_o$	unit vector at doublet point, normal to velocity vector
ℓ, m, n	direction cosines of $\vec{n}$
ℓ_o, m_o, n_o	direction cosines of $\vec{n}_o$
p	pressure
$\vec{X}_o$	position vector of doublet from inertial frame origin
$\vec{X}$	position vector of downwash point from inertial frame origin

q	source or doublet strength
R_t	rotor tip radius
R_s	rotor root radius
r	distance of downwash point along the span
r_o	distance of doublet along the span
r_u	upper limit of spanwise panel
r_ℓ	lower limit of spanwise panel
$\hat{r}_o$	distance of doublet along span at singular point time
t	field time
U	velocity of rotor system, parallel to x-axis, positive in negative x-direction
$\vec{V}$	velocity at downwash points
V_n	velocity component of $\vec{V}$ at the downwash point normal to the rotor leading edge
$\vec{V}_o$	velocity of doublet
W	velocity of rotor system, parallel to z axis
w_n	downwash velocity
x_α	distance from pitch axis to downwash point
x,y,z	Cartesian coordinates of downwash point
x_o,y_o,z_o	Cartesian coordinates of doublet position
α	twist angle at downwash point
α_o	twist angle at doublet position
α_r	angle of axis of rotation relative to z-axis
β	$\vec{V}_o/c$
$\dot{\vec{\beta}}$	$\dot{\vec{V}}_o/c = \frac{1}{c}\frac{\partial \vec{V}_o}{\partial \tau}$
θ	angular position of blade at time t
θ_o	angular position of blade at time τ
θ_w	blade angle of attack
θ_R	blade angle relative to plane of rotation
μ	advance ratio
ρ	air density
τ,τ_o	time
$\hat{\tau}$	time at which integrand in Eq. (24) becomes singular
ϕ	velocity potential
Ψ_s	source acceleration potential
Ψ_D	doublet acceleration potential
ψ	azimuth angle
Ω	rotation speed of rotor
ω	vibration frequency of rotor

BASIC FORMULATION

The formulation of the aerodynamic equations is based on the linearized acceleration potential approach. The fluid is considered perfect, with no separation and the formulation is based upon the assumption of small perturbations. The wake created by the lifting rotor is assumed to lie in the skewed helical path taken by the rotor blade. One reason for adopting the acceleration potential approach is that the pressure discontinuity occurs only on the surface of the blade and thus the boundary conditions need only be applied on the blade surface and not throughout the wake. The blade is treated as a very thin surface of discontinuity across which a pressure jump occurs. Th effect of compressibiity is taken into account by utilizing the complete linearized potential for a lifting doublet, along with the effects of retarded time.

As shown in Fig. 1, an inertial coordinate system has been used in which the origin of coordinates is fixed to a point on the ground. The helicopter rotor is moving in the negative x-direction with velocity U, in the positive z-direction with velocity W and is rotating counter clockwise with a constant angular velocity Ω. A point of interest on the rotor blade is designated by the radius vector $\vec{X}_o(\tau)$ from the origin of the ground based coordinate system.

Let Ψ be the acceleration potential of a source (or doublet), the perturbation pressure is then given by

$$p = -\rho\Psi \qquad (1)$$

This expression represents the pressure p at point $\vec{X}$ due to a single source (or doublet) located at $\vec{X}_o$. The potential Ψ contains a constant "q" which represents the strength of the source and thus the magnitude of the pressure. In this form, there is no boundary condition available to determine the value of "q" and the resulting pressure. Recourse can be made to the velocity potential, since the spatial derivative of a velocity potential represents a velocity. The relationship between the pressure and velocity potential for an inertial coordinate system is

$$p = -\rho\frac{d\phi}{dt} \qquad (2)$$

where $\frac{d\phi}{dt}$ is the substantial derivative. Dropping out the second order terms and integrating with respect to field time results in

$$\phi(t) = \int_{-\infty}^{t} \Psi(t')\,dt' \qquad (3)$$

The acceleration potential Ψ_s satisfies the wave equation

$$\nabla^2\Psi_s - \frac{1}{c^2}\frac{\partial^2\Psi_s}{\partial t^2} = -4\pi f(\vec{X},t) \qquad (4)$$

where $f(\vec{X},t)$ is a source distribution. Furthermore, if the path of an isolated source is a function of time variable, $\vec{X}_o(t)$, then $f(\vec{X},t) = \delta(\vec{X} - \vec{X}_o)$ where δ is the delta function.

Using the Green's function formulation the acceleration potential expression for a moving source, Ψ_s can be written as (Morse and Feshbach, 1978, p. 841)

$$\Psi_s(\vec{X},t) = \frac{q(\vec{X}_o,\tau)}{4\pi\left|\vec{X}_o - \vec{X}(\tau)\right|\left|1 - \frac{\vec{V}_o(\tau)\cdot[\vec{X} - \vec{X}_o(\tau)]}{c\left|\vec{X} - \vec{X}_o(\tau)\right|}\right|} \tag{5}$$

where $\vec{X}_o(\tau)$ designates the position of the source at time τ, $\vec{X}$ is the position of the field point at the time t, $\vec{V}_o(\tau)$ is the velocity of the source point at time τ, c is the speed of sound and q is the strength of the source. An auxiliary equation which relates the time interval $(t - \tau)$ to the distance between the two points is

$$t - \tau = \frac{\left|\vec{X} - \vec{X}_o(\tau)\right|}{c} \tag{6}$$

which is usually referred to as the causality condition. Eq. (5) expresses the potential as an explicit function of τ, and only through Eq. (6) as an implicit function of t ans $\vec{X}$. From Eq. (3), the velocity potential due to a moving source is

$$\phi_s(t) = \int_{-\infty}^{t} \Psi_s(t')\,dt' = \int_{-\infty}^{t} \frac{q(\tau')}{4\pi\lfloor D - \vec{D}\cdot\vec{\beta}\rfloor_{t'}}\,dt' \tag{7}$$

$$= \int_{-\infty}^{\tau} \frac{q(\tau')}{D(\tau')}\,d\tau',$$

where $\vec{D} = \vec{X} - \vec{X}_o$, $D = \left|\vec{D}\right|$

and $dt' = \left[1 - \frac{\vec{D}\cdot\vec{\beta}}{D}\right] d\tau'$

The quantities τ', t' and t, τ satisfy Eq. (6).

By definition, the doublet velocity potential ϕ_D of a doublet aligned along $\vec{n}_o$ can be written as

$$\phi_D(t) = \frac{\partial}{\partial n_o}\phi_s(t) = \vec{n}_o \cdot \nabla_{\vec{X}_o}\phi_s = -\vec{n}_o \cdot \nabla_{\vec{X}}\phi_s \tag{8}$$

$$= \left\lfloor \frac{\vec{n}_o \cdot \vec{D}}{4\pi c(D - \vec{\beta}\cdot\vec{D})} \frac{q}{D} \right\rfloor_\tau + \int_{-\infty}^{\tau} q\,\frac{\vec{n}_o \cdot \vec{D}}{4\pi D^3}\,d\tau'$$

Note that for incompressible flow, $c \to \infty$, the first term $\to 0$ and the integral remains unchanged except for the upper limit where $\tau = t$.

To obtain the final equation for downwash Δw_n, a second directional derivative is required. This derivative is taken normal to the flight path at the location of the downwash point, as follows

$$\Delta w_n = \frac{\partial \phi_D}{\partial n} = \vec{n} \cdot \nabla_{\vec{X}}\phi_D$$

to obtain

$$\Delta w_n = \frac{q}{4\pi c D^2[1 - \hat{D}\cdot\vec{\beta}]}\{\vec{n}\cdot\vec{n}_o + \vec{n}_o\cdot\hat{D}\,\vec{n}\cdot\hat{D}$$

$$+(\vec{n}_o\cdot\vec{\beta}\,\vec{n}\cdot\hat{D} - \frac{\vec{D}}{c}\cdot\vec{n}_o\,\vec{n}\cdot\hat{D}$$

$$-\vec{n}_o\cdot\hat{D}\,\vec{n}\cdot\hat{D} + \vec{n}_o\cdot\hat{D}\,\vec{n}\cdot\vec{\beta})/(1 - \hat{D}\cdot\vec{\beta}) \tag{9}$$

$$-(\vec{n}_o\cdot\hat{D}\,\vec{n}\cdot\hat{D}[1 - \beta^2 + \frac{\vec{D}}{c}\cdot\vec{\beta} + \frac{\dot{q}}{qc^2D}])/(1 - \hat{D}\cdot\vec{\beta})\}_{\tau_o}$$

$$+ \frac{1}{4\pi}\int_{-\infty}^{\tau_o(r_o)} q\left[\frac{\vec{n}\cdot\vec{n}_o - 3\vec{n}_o\cdot\hat{D}\vec{n}\cdot\hat{D}}{D^3}\right] d\tau$$

Eq. (9) gives the downwash at a field point (x, y, z, t) due to a doublet placed at a point (x_o, y_o, z_o, τ) having a strength q. In order to represent a lifting surface such as a rotor, it is necessary to distribute the doublets over the lifting surface and integrate over the surface to obtain the downwash at a field point. If the downwash is known, the quantity "q" can be determined. Letting K be the expression on the RHS of Eq. (9), the final equation is

$$w_n = \iint_{A'} K\,dA' \tag{10}$$

where A' is the area of the rotor surface. The LHS, w_n, represents the known boundary condition and is the velocity normal to the velocity vector at the downwash point. By using the no flow condition for the velocity perpendicular to the blade surface, the velocity component in the $\vec{n}$ direction is $V_n \tan\theta_w$ or

$$w_n(r,t) = V_n\tan\theta_w = \iint_{A'} K\,dA' \tag{11}$$

where V_n is the velocity component of $\vec{V}$ at the downwash point and is normal to the rotor leading edge and θ_w is the angle of attack. Thus the problem requires setting up a method of solution of Eq. (11) from which a value of q, the unknown doublet strength, can be determined which satisfy the known velocity boundary conditions w_n.

This represents a rather formidable computing task and the history of lifting surface theory even for non-rotating wings has centered on devising approximate methods to accomplish the integration in an economical manner. One method, termed the vortex lattice method, has been very successfully applied to aircraft wings, and is probably the more economical procedure of the many variants. This method was first demonstrated for the unsteady case by Runyan and Woolston (1957) and was later expanded by Albano and Rodden (1969). This is the method adopted in this paper and the application will be discussed later.

Specification of Coordinate System

The blade has the cord C and length $R_t - R_s$, R_s being distance to the the root of the blade, R_t is the distance to the tip of the blade. Let the blade momentarily coincide with the coordinate system along the positive x-axis at t = 0 and execute a counterclockwise rotation with angular velocity Ω while moving with velocity U along the negative x direction and velocity W along the positive z direction. Since the vortex lattice method has been adopted, the doublet point lies C/4 ahead and the downwash point lies C/4 aft of the section midchord. The position of the doublet point as well as the downwash point can be established as follows. The Cartesian components of the doublet position are

$$\begin{aligned} x_0 &= -U\tau + r_0 \cos(\Omega\tau) - (C/4)\sin(\Omega\tau)\cos\alpha_0 \\ y_0 &= r_0 \sin(\Omega\tau) + (C/4)\cos(\Omega\tau)\cos\alpha_0 \\ z_0 &= W\tau + (C/4)\sin\alpha_0 \end{aligned} \tag{12}$$

where r_0 is the radial distance of the doublet along the span. With the substitution of $C \to -C$, $r_0 \to r$, $\tau \to t$ the position of the downwash point is given by

$$\begin{aligned} x &= -Ut + r\cos(\Omega t) + (C/4)\sin(\Omega t)\cos\alpha \\ y &= r\sin(\Omega t) - (C/4)\cos(\Omega t)\cos\alpha \\ z &= Wt - C/4\sin\alpha \end{aligned} \tag{13}$$

In Eqs. (12) and (13), the angles α, α_0 are the twist angles of the velocity vectors $\vec{V}$ and $\vec{V}_0$, respectively, defined by

$$\begin{aligned} \tan\alpha &= \frac{W}{U\sin(\Omega t) + r\Omega} \\ \tan\alpha_0 &= \frac{W}{U\sin(\Omega\tau) + r_0\Omega} \end{aligned} \tag{14}$$

The reference plane defined by the doublets and downwash points is a twisted surface. From Eq. (12) the doublet velocity can be computed, namely the time derivative of the position vectors.

$$\vec{V}_0 = \dot{x}_0\vec{i} + \dot{y}_0\vec{j} + \dot{z}_0\vec{k}$$

The unit vector $\vec{n}_0$ is chosen to be perpendicular to the twisted surface created by the velocity vector $\vec{V}_0$ which is a function of r_0, through Eq. (14).

Express $\vec{n}_0$ as

$$\vec{n}_0 = \ell_0\vec{i} + m_0\vec{j} + n_0\vec{k} \tag{15}$$

where ℓ_0, m_0, n_0 are the directional cosines of the unit vector $\vec{n}_0$. It can be shown that

$$\ell_0 = \frac{W(U + r_0\Omega\sin(\Omega\tau) + (C/4)\Omega\cos(\Omega\tau)\cos\alpha_0)}{V_0'\sqrt{W^2 + V_0'^2}}$$

$$m_0 = -\frac{W(r_0\Omega\cos(\Omega\tau) - (C/4)\Omega\sin(\Omega\tau)\cos\alpha_0)}{V_0'\sqrt{W^2 + V_0'^2}} \tag{16}$$

$$n_0 = \frac{V_0'}{\sqrt{W^2 + V_0'^2}}$$

where

$$V_0'^2 = (U + r_0\Omega\sin(\Omega\tau) + (C/4)\Omega\cos(\Omega\tau)\cos\alpha_0)^2 + (r_0\Omega\cos(\Omega\tau) - (C/4)\Omega\sin(\Omega\tau)\cos\alpha_0)^2 \tag{17}$$

By the same procedure, $\vec{n} = \ell\vec{i} + m\vec{j} + n\vec{k}$, where

$$\ell = \frac{W(U + r\Omega\sin(\Omega t) - (C/4)\Omega\cos(\Omega t)\cos\alpha)}{V'\sqrt{W^2 + V'^2}}$$

$$m = \frac{-W(r\Omega\cos(\Omega t) + (C/4)\Omega\sin(\Omega t)\cos\alpha)}{V'\sqrt{W^2 + V'^2}} \tag{18}$$

$$n = \frac{V'}{\sqrt{W^2 + V'^2}}$$

and

$$V'^2 = (U + r\Omega\sin(\Omega t) - (C/4)\Omega\cos(\Omega t)\cos\alpha)^2 + (r\Omega\cos(\Omega t) + (C/4)\Omega\sin(\Omega t)\cos\alpha)^2 \tag{19}$$

the vector $\vec{D} = \vec{X} - \vec{X}_0$ defined in Eq. (7) can be expressed as

$$\begin{aligned} D = \{&[U(t-\tau) + r\cos(\Omega t) - r_0\cos(\Omega\tau) \\ &+ (C/4)(\sin(\Omega t)\cos\alpha + \sin(\Omega\tau)\cos\alpha_0)]^2 \\ &+ [r\sin(\Omega t) - r_0\sin(\Omega\tau) \\ &-(C/4)(\cos(\Omega t)\cos\alpha + \cos(\Omega\tau)\cos\alpha_0)]^2 \\ &+ [W(t-\tau) - (C/4)(\sin\alpha_0 + \sin\alpha)]^2\}^{1/2} \end{aligned} \tag{20}$$

With the substitution of the quantities, the integral Eq. (11) was solved for the unknown $q(r_0,\tau)$ by using a collocation process based

on the vortex lattice assumption. The kernel is singular when D = 0, and this was handled by use of the finite part technique.

SOLUTION OF INTEGRAL EQUATION

In following the vortex lattice technique the rotor is divided into a number of predetermined panels, both spanwise and chordwise. In each chordwise panel, a line of doublets of unknown strength q_j is located at the 25% chordwise location of the particular panel, and the downwash is evaluated at the point located at 75% chordwise location of the panel. Therefore, a collocation procedure is used to obtain a set of equations in terms of the unknown loadings q_j. It is also assumed that the spanwise loading q_j is constant along each of the panels. A set of equations is thus obtained as shown below.

$$w_n = \sum_m A_{nm} q_m \qquad (21)$$

where $A_{nm} = \int_{r_\ell}^{r_u} K_{nm}\, dr_o$ and where n refers to the downwash point and m refers to the vortex lattice. The kernel K is a complicated function which involves an integration over τ.

The term $q(r_o,\tau)$ represents the strength of the doublet located at r_o and at time τ, and is proportional to the unknown loading. In order to account for unsteadiness, a solution was formulated to take into account the time variation of the strength of the wake. This was done by assuming a Fourier series of the form

$$q(r_o,\tau) = A_o + \sum_1^m (A_n \cos(n\Omega\tau) + B_n \sin(n\Omega\tau)) \qquad (22)$$

If $q(r_o,\tau)$ is assumed to be a function of r_o alone, which means that the wake strength does not vary with time, the Fourier series reduces to $q(r_o) = A_o$. A solution obtained with this approximation is termed the quasi-steady solution.

This series was inserted in the basic equation and integrated with respect to τ. However, there were more unknowns than simultaneous equations to solve for the unknowns. The additional required equations were obtained by evaluating Eq. (11) at a number of azimuth locations. For instance if m = 1, then

$$q(r_o,\tau) = A_o + A_1 \cos\Omega\tau + B_1 \sin\Omega\tau. \qquad (23)$$

The azimuth was divided into equal segments of 120° and the proper boundary conditions applied at ψ = 0°, 120°, and 240° thus providing the necessary additional equations.

Numerical Integration of Kernel

The integration was performed by numerical integration, except for the area surrounding the singularity. The integration domain was divided into areas as shown in Fig. 2. Areas 1-4 (hatched) were computed numerically using a two-dimensional Romberg integration (Davis and Rabinowitz, 1967) and the contribution of the singular region (unhatched) was obtained in closed form by consideration of the finite part as shown in the next section.

Treatment of Singular Term in Integral - The integral in the downwash equation, Eq. (11), is singular when D→0 and produces a complication which must be treated properly. It should be remembered that the integration path along "τ" is the path the doublet has taken in arriving at the final doublet point at (c/4, r_o) measured in the local blade coordinates and can be considered as the wake. The integration takes place along the path from $-\infty$ to the final doublet position at τ_o. The distance D is the distance from the integration point at time τ to the downwash point at $\vec{R}$.

There is a particular set of values of r_o and τ for which the denominator D approaches zero, thus resulting in an infinite integrand. The singular part of the Eq. (11) is

$$I = \int_{r_\ell}^{r_u} \int_{\tau_1}^{\tau_2} \frac{\vec{n}\cdot\vec{n}_o - 3(\hat{D}\cdot\vec{n})(\hat{D}\cdot\vec{n}_o)}{D^3}\, d\tau\, dr_o \qquad (24)$$

As $\vec{D}\to 0$ at the downwash point, $\hat{D}$ becomes perpendicular to $\vec{n}$, therefore, at the singular point, the second term is zero and will be neglected in the treatment of the singularity. However, this second term is retained in all of the numerical integrations involving Areas 1-4 since it represents an important contribution particularly when the blade is passing over a trailing wake.

The time and distance at which the integral I becomes singular are designated by $\hat{\tau}$ and $\hat{r}_o$. The domain of the integration in Eq. (24) consists of a rectangle in which the duration $\tau_2-\tau_1$ is kept extremely small. In other words, the integration is performed along a slit in r_o, over which the 2nd term in Eq. (24) is negligible. Therefore the integral I can be approximated by

$$I = \int_{r_\ell}^{r_u} \int_{\tau_1}^{\tau_2} \frac{\vec{n}\cdot\vec{n}_o}{D^3}\, d\tau\, dr_o \qquad (25)$$

Furthermore, noticing that D^2 is quadratic in r_o, if α_o is independent of r_o, then the integration on r_o can be performed analytically. This can be achieved by recognizing that in the vortex lattice method, the rotor is divided into spanwise panels from r_ℓ to r_u. If these spanwise panels are small then the variation in α_o is small.

$$\frac{d\alpha_o}{dr_o} \approx -\frac{W\Omega}{(U\sin\theta_o + r_o\Omega)^2 + W^2} \qquad (26)$$

If the value of α_o is approximated by its mid panel value, it is possible to integrate Eq. (24), in closed form in the r_o direction. This is quite acceptable in the helicopter mode,

because $d\alpha_0/dr_0$ is in the order of magnitude 10^{-3} or smaller. The value $\hat{n}_0$ is also a function of r_0, but in the region of the singularity it has a very small variation and is evaluated at the singular position, $(\hat{\tau},\hat{r}_0)$. Performing the r_0 integration results in the form

$$I = \int_{\tau_1}^{\tau_2} \frac{g(\tau)}{f(\tau)}\, d\tau \qquad (27)$$

where $g(\tau)$ is a function containing all the non-singular part after performing the r_0 integration and $f(\tau) = 0$, at $\tau=\hat{\tau}$ $(\tau_1 < \hat{\tau} < \tau_2)$. It can be argued physically that since the quantity $D(\tau,r_0;t,r)$ as well as its modified form $f(\tau)$ (after integration over r_0) represents the distance between two points in space it must be positive and real for all its arguments, and never become negative. Denote the value of r_0 and τ at which D becomes zero as $\hat{r}_0$ and $\hat{\tau}_0$. Thus, in the neighborhood of $\hat{\tau}$ the function $f(\tau)$ behaves like a parabolic function and has a second order zero.

Expanding $f(\tau)$ in a Taylor series about the singular point $\hat{\tau}$ results in

$$f(\tau) = f(\hat{\tau}) + f'(\hat{\tau})(\tau-\hat{\tau}) + f'(\hat{\tau})\,(\tau - \hat{\tau})^2/2 + \ldots \qquad (28)$$

Since $\hat{\tau}$ is a second order zero

$$\text{and} \qquad f(\hat{\tau}) = f'(\hat{\tau}) = 0 \qquad (29)$$

Eq. (29) has been verified numerically. If only the square term is kept in Eq. (28), Eq. (27) can be written as

$$I = \int_{\tau_1}^{\tau_2} \frac{2}{f''(\hat{\tau})} \left[\frac{g(\hat{\tau})}{(\tau-\hat{\tau})^2} + \frac{g'(\hat{\tau})}{(\tau-\hat{\tau})} + \frac{g''(\hat{\tau})}{2}\right] d\tau \qquad (30)$$

In Eq. (30), if τ_2 and τ_1 are chosen symmetrically about $\hat{\tau}$, then the odd derivative terms integrate to zero. Futhermore, the third term can be neglected since $g''(\hat{\tau})$ is small. The major contribution comes from the first term. Then using the standard integration technique (Mangler, 1952) the final result for the integral is

$$I = -\frac{g(\hat{\tau})}{f''(\hat{\tau})}\,\frac{4}{\Delta\tau} \qquad (31)$$

where $2\Delta\tau = \tau_2 - \tau_1$ and $\tau_1 < \hat{\tau} < \tau_2$.

A numerical problem arises because the finite part integration results in a negative number which is close to the total of the surrounding numerical integration areas which are positive. Thus, it is necessary to take the difference between large numbers, and the final integration accuracy is dependent on the accuracy of the two integrations. On the one hand, the numerical integration is more accurate as $\Delta\tau$ is kept large because the very large values of the integrand near the singularity are avoided. On the other hand, regarding the finite part integration, the denominator was expanded in a Taylor series about the singular point, $\hat{\tau}$. Therefore, it is desirable to maintain $\Delta\tau$ as small as possible to keep within the limits of the applicability of the series expansion. Numerous calculations were made, varying $\Delta\tau$ until a reasonable convergence was found. This value was found to be $.01(t-\hat{\tau})$, i.e. 1% of the time difference. Actually, there is very little difference between 1% or 10% of the time difference and the computing time and cost is considerably reduced by using 10%. For trend studies 10% is recommended principally to reduce computer costs, However, for final design type analysis, a smaller value of time difference $\Delta\tau$ is more appropriate.

For the spanwise direction, Δr_0 is also an integration limit variable. The finite part integral was obtained by approximating the angle of twist of the velocity vector across a segment by assuming it constant across the segment, having a value as determined at the center of segment. Numerical experimentation indicates that for a helicopter, $\Delta r_0 = 0$ is satisfactory.

APPLICATION TO SPECIFIC EXAMPLES

The foregoing analysis has been applied to several specific examples which are given in Figs. (3) and (4). The following section presents results for several paneling configurations; e.g. 5 spanwise and 1 chordwise panels (designated (5-1)) and 7 spanwise and 3 chordwise (designated (7-3)). The rotor blade was maintained at a constant pitch setting of $\theta_R = .1$ radians for all the calculations.

Single Blade

In order to investigate the convergence of the method when using the vortex lattice procedure, the program was run for several chordwise and spanwise elements for the incompressible case. The thrust coefficient C_T vs. the azimuth angle is shown in fig. (5). (In all of the following plots for thrust coefficient vs. azimuth angle, the thrust was calculated for 16 uniformly spaced azimuth angles and each curve was faired using a cubic spline). The rotor was first divided into 5 spanwise and one chordwise (5-1) panel and the results are shown by the solid line. The chordwise division was increased to (5-2) and the results are shown by the long dashed line. It can be seen that very little change has taken place. The spanwise divisions were increased to (7-1) and the largest change occurred at $\psi = 0^o$ where the difference in C_T is about 11%. Increasing the chordwise divisions to 3 (7-3) shows convergence of the (7-1) case to be very good.

An interesting phenomena occurs in the region of small azimuth angles. For ψ=0 to

37°, the lift increases to a local maximum at ψ=37° then the lift abruptly falls to a local minimum for ψ=60° and then rapidly increased to a maximum at ψ=100°. A similar phenomenon is shown analytically by Eglof and Landgrebe (1983) in Fig. 60 of that report where a local minimum and a local maximum occur in the same range of azimuth angles, even though the geometry of the two blades and the flight conditions are different. Also, in Fig. 93 of the same report some test data shows a similar variation of loading in the same azimuth range.

The chordwise pressure distributions for the (7-3) case are presented in figure 6. It should be remembered that in using the vortex lattice method, the loading is concentrated at the location of the vortex which for the (7-3) case is located at .0833C, .416C, and .75C. The pressure was faired using a cubic spline through the three vortex locations and the known value of zero at the trailing edge. The distributions are given for 7 spanwise positions. In general, the curves exhibit the expected shape, having the largest values as the leading edge is approached. For the span distribution the values at r/R_T = .85 are slightly larger than the values at r/RT = .95,, indicating a falling off in the tip region.

From these concentrated forces, the section pitching moment can be calculated. Figure 7 presents these results for ψ = 90 degrees. The section moment was taken about the 1/4 C and a nose down moment is taken as positive. The pitching moment shows some rather dramatic changes along the span. The moment is nose up near the tip (r/R_T = .95), changes to a small nose down value, then becomes nose up for most of the inboard region. Integration of the moment would result in a total pitch moment up at ψ = 90°.

Swept Tip

The segments used for the vortex lattice for the swept tip studies were(5-1), where two equal segments were used in the tip region and three equal segments were used in the unswept inboard section. In Fig. 8 the lift is shown plotted against azimuth for the two sweep conditions and for zero sweep. In general, the three results show little difference. The sweptback configuration has a larger lift from ψ = 300° to 40°. For ψ = 100° to 240°, the swept forward configuration has a slightly larger lift. It appears that the total lift for one rotation for the swept-back case and the sweptforward case would give about the same lift as produced by the unswept rotor. In Fig. 9 the lift distribution along the rotor span is given for ψ = 0°. The major effect of sweep is concentrated at the tip, where the swept-back tip load is greater than both the unswept and sweptback cases . In fig. 10, ψ = 180°. Comparing to fig. 9, the swept-back tip load is larger than both the unswept and the swept-forward tips.

Blade Oscillating in Pitch

An example of unsteady loads on a rotor blade with (5-1) paneling which is oscillating in a pitching mode about the mid-chord at a frequency of 4 per revolution (120 cycles/sec) is given on fig. 11. For this case a 17 term Fourier series (m=8) was used to simulate the oscillating load, which was comprised of one constant term, 8 cosine terms, and 8 sine terms. The steady and unsteady rotor blade loading is given for one revolution. The blade was oscillated through an angle of .1 rad. about a mean angle of .1 rad. The effect of the oscillation is readily apparent as compared to the steady case. With the harmonic representation of the loading, the magnitude and phase of the several harmonic loads are easily determined. The magnitudes are plotted in Fig. 12. The only harmonic loads that were significantly changed from the steady case were the 3rd, 4th and 5th. Both the 3rd and 5th harmonics were increased and the 4th harmonic was dramatically increased. Another calculation was made for the non-oscillatory unsteady case and compared to the quasi-steady case. Virtually no difference was observed, indicating that, at least for this case, the rate of change of loading in a revolution of the blade is small enough so that the effect of a variable wake is negligible.

Compressible Effects (5-1)

For a one-bladed rotor, the effect of compressibility is illustrated in Fig. 13, in which the C_T is plotted against azimuth angle. The incompressible result is included for comparison. As expected, the compressible load is larger than the incompressible throughout one revolution. The effect is greatest in the region of the advancing blade and smallest in the retreating region as would be expected.

Two-Bladed Rotor in Compressible Flow (5-1 per blade)

The method has been extended to the two-bladed rotor for the compressible case and the results are shown in Fig. 14. The thrust coefficient C_T per blade is given vs. azimuth angle for a single bladed rotor and for a two-bladed rotor. For azimuth angles from ψ = 20° to 120° the single blade rotor has a larger C_T. For ψ = 120° to 260°, the C_T on the one and two-bladed rotors are approximately the same. However, for ψ = 260° to 340° a dramatic reduction in lift occurs for the two-bladed rotor as compared to the one bladed results. The lowest lift occurs at ψ = 292° which places the other blade of the two-bladed rotor at ψ = 112°, the point of maximum lift on the other blade. Apparently the high lift on the blade at ψ = 112° creates a very unfavorable induced velocity on the second blade at ψ = 292° which requires the loading to go to zero in order to satisfy the boundary conditions at ψ = 292°.

CONCLUDING REMARKS

A linearized lifting surface theory including the effects of compressibility has been developed for a helicopter rotor in forward flight. The method utilizes the concept of the acceleration potential, and makes use of the vortex-lattice procedure for performing the required integrations. In addition, the method has been extended to include the effects of unsteady flow.

Sample calculations have been done for several cases. These include the effect of swept-back and swept-forward tip. The effect of these two tip configurations was minimal on the total loading for one revolution. However, the loading distribution changed considerably for several azimuth positions. A comparison of the thrust coefficient, C_T, of a one bladed rotor and a two bladed rotor was made. In the azimuthal range between 20^0 and 120^0, the one bladed rotor showed higher lift. However between $\psi = 260^0$ to 340^0 the two bladed rotor indicated a lower C_T. Compressibility was investigated for one configuration. As expected, the effect was greatest in the advancing blade region ($\psi = 90^0$) and was minimal in the retreating blade region. The effect on C_T of a blade oscillating in pitch at 4/rev is given. The effect on the total blade lift is shown and the effect of the oscillation is readily apparent. The harmonic content was calculated and the greatest difference between the oscillatory and non-oscillatory cases was found in the 4th harmonic.

REFERENCES

Albano, E.; Rodden, W. P. 1969: A Doublet Lattice Method for Calculating Lift Distribution on Oscillating Surfaces in Subsonic Flows. AIAA Journal, Vol. 7, No. 2, pp. 279-285.

Dat, Roland 1973: The Lifting Surface Theory Applied to Fixed Wings and Propellers ONRA TP No. 1298.

Davis, P. J. and Rabinowitiz, P., 1967: Numerical Integration, Blaisdell Publishing Company.

Egolf, T. A. and Landgrebe, A. J. 1983: Helicopter Rotor Wake Geometry and its Influence in Forward Flight, Vol. 1, NASA CR 3726.

Hanaoka, T. 1962: Hydrodynamics of an Oscillating Screw Propeller. ONR, ACR (92) (1962).

Kussner, Hans G. 1941: General Airfoil Theory. NACA TM 979.

Morse, P. M. and Feshback, H. 1978: Methods of Theoretical Physics, McGraw-Hill, Inc.

Mangler, K. W. 1952: Improper Integrals in Theoretical Aerodynamics.

Pierce, G. A.; and Vaidyanathan, A. R. 1983: Helicopter Rotor Loads Using Discretized Matched Asymptotic Expansions, NASA CR 166092.

Runyan, H. L., and Woolston, D. S. 1957: Method for Calculating the Aerodynamic Loading on an Oscillating Finite Wing in Subsonic and Sonic Flow. NACA TR 1322.

Runyan, H. L. 1973: Unsteady Lifting Surface Theory Applied to a Propeller and Helicopter Rotor, Ph.D. Thesis, Loughborough, University of Technology.

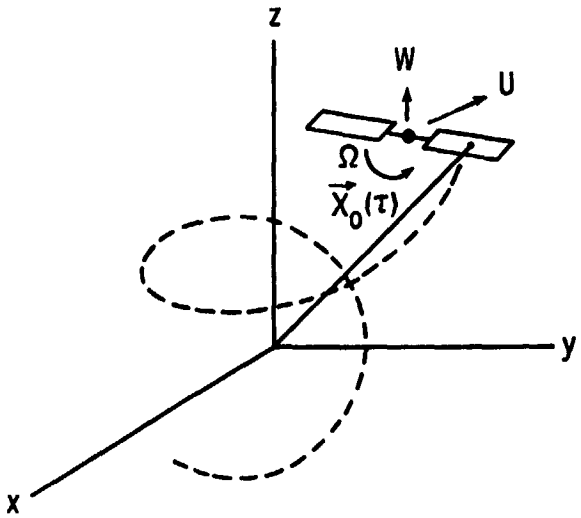

Fig. 1 Inertial Coordinate System

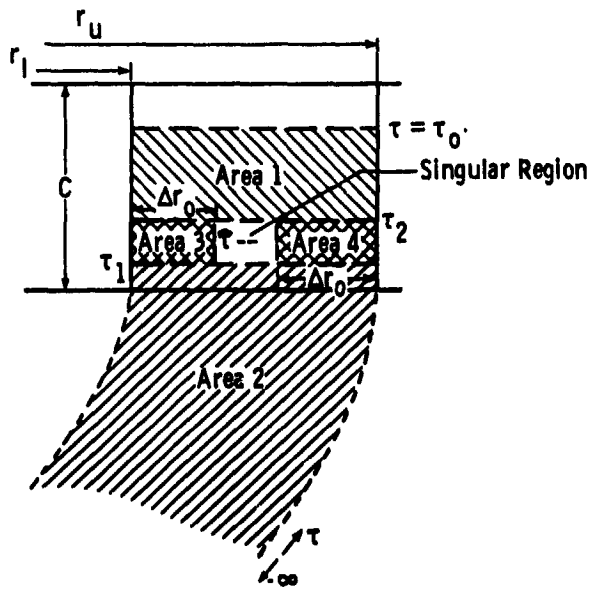

Fig. 2 Integration Areas

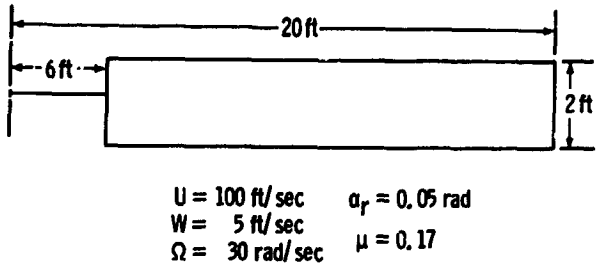

Fig. 3 Unswept Configuration and Input Parameters

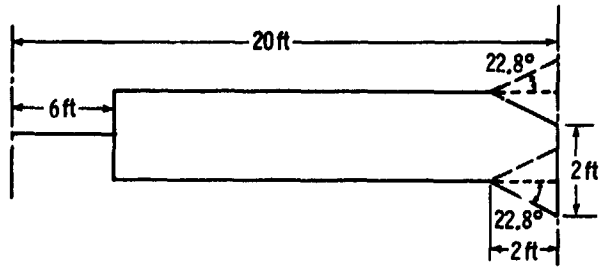

Fig. 4 Swept Tip Configurations

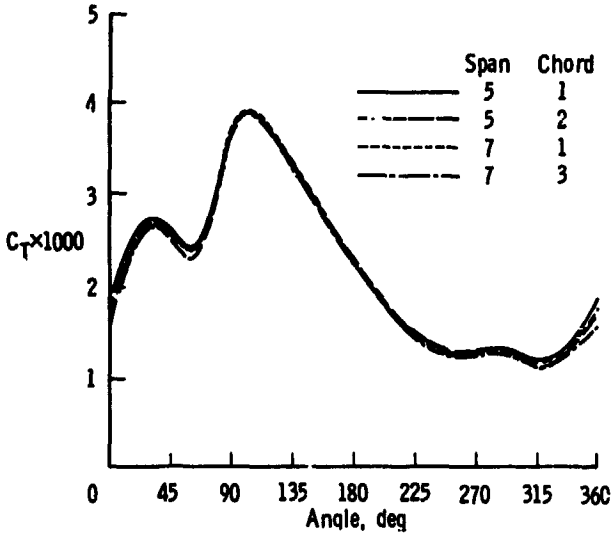

Fig. 5 Thrust Coefficient vs. Azimuth Angle for Four Panel Configurations for a Single Rotor Blade, Incompressible, (μ = 0.17, θ_β = 0.1 rad, α_r = .05 rad, Ω = 30 rad/sec)

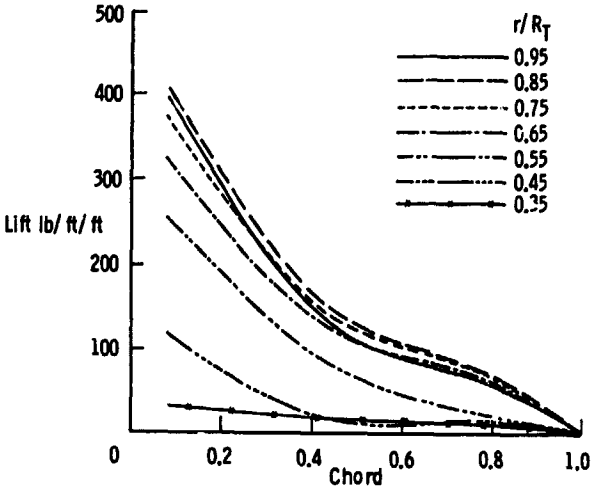

Fig. 6 Chordwise Pressure Distribution for Several Spanwise Locations, ψ = 90°, incompressible, (μ = .17, θ_β = 0.1 rad, α_r = .05 rad, Ω = 30 rad/sec)

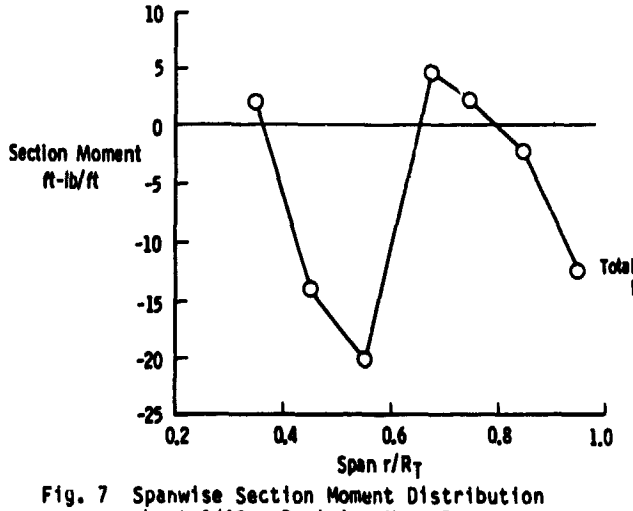

Fig. 7 Spanwise Section Moment Distribution about 1/4C - Positive Nose Down, ψ = 90°, incompressible, (μ = 0.17, θ_β = 0.1 rad, α_r = .05 rad, Ω = 30 rad/sec)

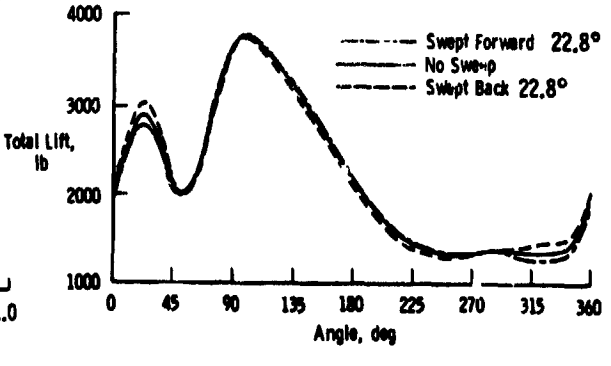

Fig. 8 Comparison of Lift on a Swept-Back Zero Sweep and Swept-Forward Blade, incompressible, (μ = 0.17, θ_β = 0.1 rad, α_r = .05 rad, Ω = 30 rad/sec)

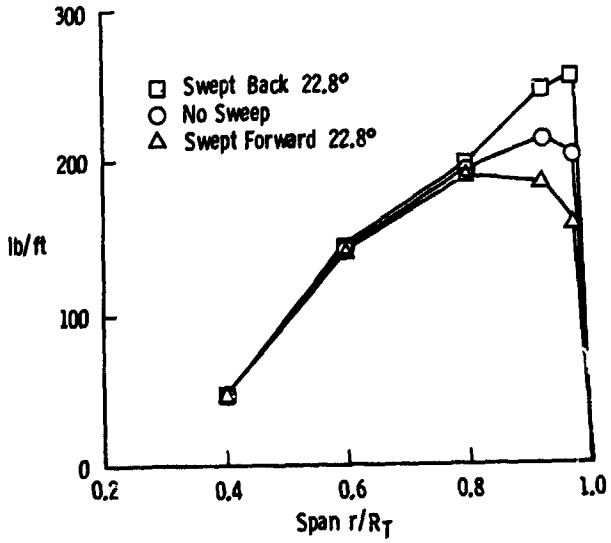

Fig. 9 Spanwise Section Lift Distribution for Swept-Tip Configurations, $\psi = 0^{o}$, incompressible, ($\mu = 0.17$, $\theta_{\beta} = 0.1$ rad, $\alpha_{r} = .05$ rad, $\Omega = 30$ rad/sec)

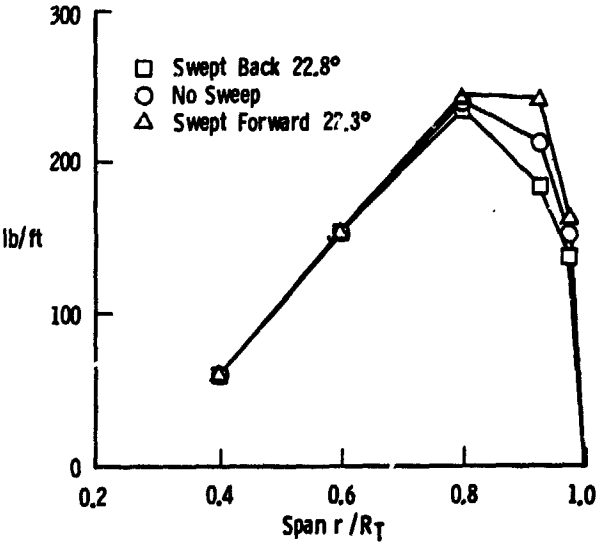

Fig. 10 Spanwise Section Lift Distribution for Swept-Tip Configurations, $\psi = 180^{o}$, incompressible, ($\mu = 0.17$, $\theta_{\beta} = 0.1$ rad, $\alpha_{r} = .05$ rad, $\Omega = 30$ rad/sec)

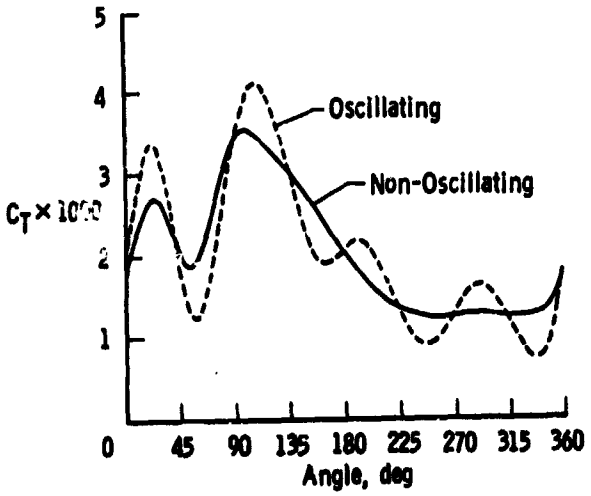

Fig. 11 Comparison of Lift on a Rotor Blade Oscillating in Pitch at 4/Rev. to the Lift on a Non-Oscillatory Blade, incompressible ($\mu = 0.17$, $\theta_{\beta} = 0.1$ rad, $\alpha_{r} = .05$ rad, $\Omega = 30$ rad/sec)

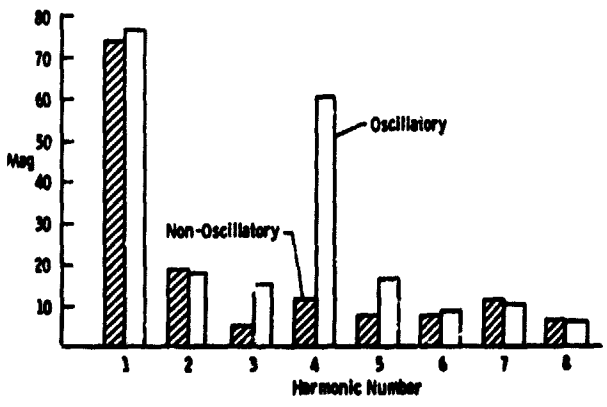

Fig. 12 Harmonic Content for Non-Oscillatory and Oscillatory Cases - $r/R = .95$, incompressible, ($\mu = 0.17$, $\theta_{\beta} = 0.1$ rad, $\alpha_{r} = .05$ rad, $\Omega = 30$ rad, sec)

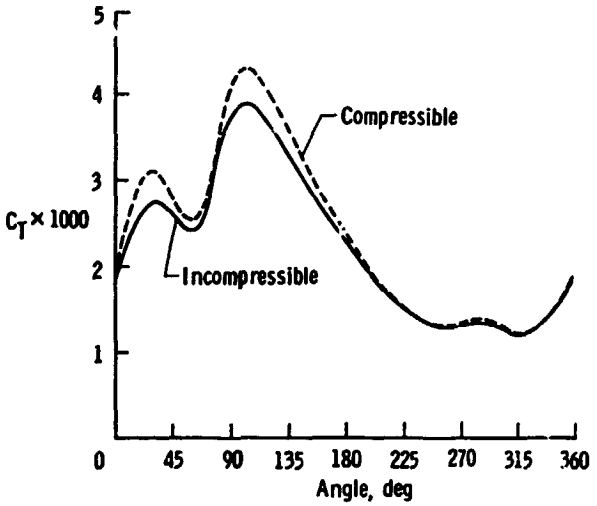

Fig. 13 Incompressible and Compressible Lift for One-Bladed Rotor, (μ = 0.17, θ_β = 0.1 rad, α_r = .05 rad, M_{TIP} = 0.54)

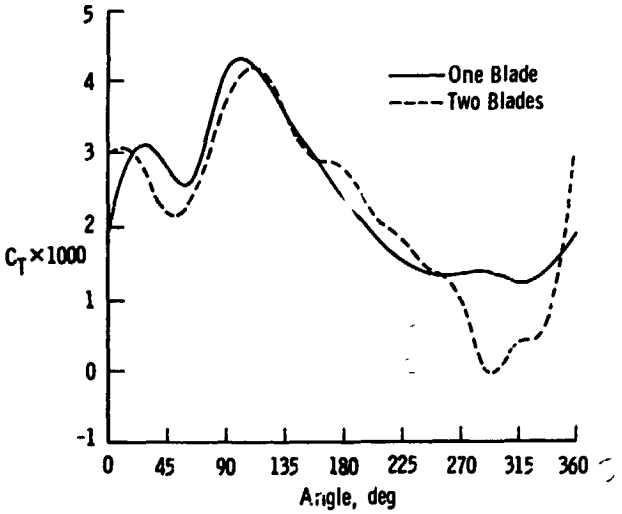

Fig. 14 Lift on Two-Bladed and One-Bladed Rotor vs. Azimuth Angle, compressible, (μ = 0.17, θ_β = 0.1 rad, α_r = .05 rad, M_{TIP} = 0.54)

DISCUSSION
Paper No. 7

LIFTING SURFACE THEORY FOR A HELICOPTER ROTOR IN FORWARD FLIGHT
H. Tai
and
Harry L. Runyan

Bob Sopher, Sikorsky Aircraft: Just a couple of questions. One, you had a rigid rotor in this analysis?

Tai: Yes.

Sopher: There is no aeroelasticity and you went up to a μ of .17?

Tai: That's correct.

Sopher: First of all, I think that as soon as you put aeroelasticity in you are going to see different trends when you put sweep on in comparison without sweep.

Tai: Oh, sure.

Sopher: The second thing is at μ equal to .17 I think that the skewed helical wake will not be a very good approximation to the actual wake, which will be substantially distorted--more like a wake that you would get under hover conditions. So I question the utility of assuming a skewed helical wake.

Tai: As I pointed out this is a first cut. Of course later you can modify this by iteration processes. You can go back and calculate the wake and put it back again. Hopefully, that procedure would give you a better result.

Sopher: The third question is what advance ratios do you expect to apply the analysis up to?

Tai: The answer is I don't know. However, I would think that the higher forward speed would probably have a better answer. Because you don't depend on the wake that much.

Sopher: I question that because as you go up to higher speeds you are going to find that you run into situations where you get transonic flow on the advancing blade and I do not believe that the linear analysis will apply accurately under those conditions.

Tai: Perhaps you are right.

Sopher: As a matter of fact this research center has developed transonic flow analyses which apply to three dimensional lifting blades so I would say that the primary utility that I would see in this analysis is for hover applications where the linear analysis is valid, but you would have to use a distorted wake.

Tai: For hover cases you would really expect the wakes to stack up and then you end up with a very difficult mathematical problem. However, I guess from my past experience you probably can get the loading by some numerical procedure. For example, you can do extrapolation. Assuming a certain W and then you extrapolate for $W = 0$. I don't know. We don't have a clear understanding. I admit that.

Jim McCroskey, U.S. Army Aeromechanics Laboratory: You have made some nice progress on this approach since you talked with us a year or so ago. It's interesting; it's nice to see some results being generated for some realistic cases. I wanted to ask a couple of minor questions. I presume this blade is untwisted, is that right?

Tai: Yes.

McCroskey: How did you treat the reverse flow region?

Tai: The twist can be added on very easily because [we only have to] add on the boundary condition. To avoid a reverse phenomenon we deliberately use very large cutoff. You can see [that it is] six feet. We try to avoid that region.

McCroskey: In fact the sketch in the book is a little misleading because the cutout is more like 30% instead of the 10 or 15% [that appears in the figure]. So you just avoided it by having a root cut out.

Tai: Yes.

McCroskey: The final thing is on the influence of compressibility. Do you have some idea of what you predict in Figure 13; is that a larger effect than you would predict if you just used some kind of Prandtl-Glauert scaling on the incompressible solution?

Tai: Well, I guess we should be blamed for not making the abstract very clear. We used a very, very honest way of doing that. We didn't use any approximation at all. In other words, as I pointed out, you find the τ as function of r_o. In other words, you give it the radius of the doublet [and] you go there and find the τ which serves as your upper limit--which is not a trivial matter. To answer your question we say that we use true, honest compressibility effect.

McCroskey: But the question is how good would the Prandtl-Glauert type approximation be to what you actually calculated?

Tai: Well, to honestly answer that question--we don't know. We didn't check [it], but I think it is not very easy to check it out.

Bob Ormiston, U.S. Army Aeromechanics Laboratory: I want to commend your results. It looks like you have made some pretty good progress in the last year or so. The methods we are using now for routine rotor loads analysis are usually based on some fairly primitive assumptions like strip theory and 2-D airfoil coefficients and so forth and what we ultimately have to get to is very, very sophisticated, maybe, 3-D CFD kinds of analyses. It looks like what you've got is an intermediate type of analysis which may be very practical. My question is do you think there is a practical way to generalize the results you have gotten, say, to come up with generalized forcing functions for specific loading distributions, a family of loading distributions that you might be able to calculate and then not have to repeat the integration problem for each particular configuration that you are analyzing? Is there a practical way to do that?

Tai: Well to answer your question, the answer is yes. I did not mention that when we break the blade into different segments. Apparently the matrix is highly diagonal. In other words off diagonal matrix you can use less accurate methods to generate. Beyond that, to answer your question, I think in a practical sense we can generate those matrix elements and store them and only change the boundary conditions to do all the types of calculations. In other words, the answer is indeed it can be very practical.

DEVELOPMENT OF AN UNSTEADY AERODYNAMICS MODEL TO IMPROVE CORRELATION OF COMPUTED BLADE STRESSES WITH TEST DATA

Santu T. Gangwani
Senior Engineer
Hughes Helicopters, Inc.
Culver City, California

Abstract

A reliable rotor aeroelastic analysis operational at Hughes Helicopters, Inc. that correctly predicts the vibration levels for a helicopter is utilized for the present study to test various unsteady aerodynamics models with the objective of improving the correlation between test and theory. This analysis called Rotor Aeroelastic Vibration (RAVIB) computer program is based on a frequency domain forced response analysis which utilizes the transfer matrix techniques to model helicopter/rotor dynamic systems of varying degrees of complexity. The analysis is a non-modal analysis and it includes effects of periodic coefficients for the forward flight conditions. The first new aerodynamics model incorporated in the analysis was based on the current state-of-art of unsteady aerodynamics. The results based on this aerodynamics model for the AH-1G helicopter rotor were compared with the flight test data during high speed operation and they indicated a reasonably good correlation for the beamwise and chordwise blade bending moments, but for torsional moments the correlation was poor. As a result, a new aerodynamics model based on unstalled synthesized data derived from the large amplitude oscillating airfoil experiments was developed and tested with RAVIB analysis. The results indicate a significant improvement in the correlation for the torsional moments.

Introduction

The rotor aeroelastic stability and response analyses (e.g., Reference 1) invariably involve computation of airloads through use of unsteady strip theories. To a significant extent, accuracy of analytically predicted parameters, such as aerodynamic damping, blade oscillatory bending and torsional moments and hub vibratory loads, depends on the correctness of the unsteady aerodynamics model utilized in the analysis. Recently there has been significant effort (References 2-5) to develop new unsteady aerodynamics models for the rotary-wing applications with a correct emphasis on incorporation of precise nature of wind and rotor blade motions. But it has not been fully demonstrated (through correlation with test data) the kind of improvements we can expect by utilizing these more sophisticated unsteady aerodynamic models. The present study was undertaken to test various unsteady aerodynamics models with the primary objective of improving the correlation between the flight test data and theory.

Background

Most of the unsteady aerodynamics models involve extension of Theoderson's flat plate theory (Reference 6) to account for the airfoil pitch-plunge motion and also to represent the effects of time-varying free stream velocity. The airfoil shape and thickness effects are normally accounted through replacement of the flat plate lift curve slope (2π) by an appropriate airfoil static lift curve slope. Blade section unsteady lift and pitching moment coefficients normally involve a lift deficiency function $C'(k)$; where k is the reduced frequency. For rotary wing applications, where blade section experiences arbitrary motions, use of reduced frequency is highly inappropriate. Therefore, in rotor aeroelastic analyses, it is practical to model unsteady aerodynamics of airfoil arbitrary motions preferably in both Laplace and time domains. This is simply achieved by converting the generalized lift deficiency function into Pade' form (e.g., Reference 7) where it is directly available in Laplace domain. For the time-domain applications, Pade' form can be easily converted into highly practical indicial formulations, such as indicial form of Wagner function for the oscillating flat plate.

Despite availability of the above-mentioned methodology for unsteady strip theory, most of the rotary-wing dynamicists find it convenient to just replace the lift deficiency function by a constant number. Conventionally a value of 0.8 to 1.0 for $C'(k)$ is used. To date, an uncertainty exists regarding the benefits of these more sophisticated unsteady aerodynamics theories. However, the present study clearly indicates that conventional aerodynamics models are highly inaccurate in predicting certain blade section airloads, such as unsteady pitching moment. More specifically, a new but conventional unsteady aerodynamics model (including aerodynamic spring-damper matrices) based on current state-of-art of the rotary-wing aerodynamics (Reference 8) was developed and it was incorporated into a reliable rotor aeroelastic analysis operational at Hughes Helicopters, Inc. (Reference 1). The computed results (airloads and oscillatory blade bending and torsional moments) for AH-1G rotor blade were compared with the available flight test data corresponding to high speed flight conditions. The correlations obtained for the beamwise and chordwise bending moments were good but for torsional moments, the correlation was poor. As a result, a new unsteady aerodynamics model based on unstalled oscillating airfoil test data was developed and incorporated in the analysis. The results indicate a significant improvement in the correlation of computed oscillatory torsional moments with test data.

Description of Aeroelastic Analysis

The aeroelastic analysis utilized for the present study is called RAVIB (Rotor Aeroelastic Vibration) computer program and it is a modified and improved version of a computer program (References 1 and 9) originally developed by Rochester Applied Science Associates. Briefly,

Presented at the 2nd Decennial Specialists' Meeting on Rotorcraft Dynamics, Ames Research Center, California, November 1984.

the RAVIB computer program is based on a frequency domain forced response analysis which utilizes the transfer matrix techniques to model helicopter/rotor dynamic systems of varying degrees of complexity. The analysis is a non-model analysis and it involves application of a standard matrix process in which the transfer matrices associated with successive characteristics of the modeled blade are combined to form the transfer or associate matrix relating the shears, moments, slopes, and deflections at a position on the blade to those occurring at the tip of the blade. The blade mass and structure characteristics are represented in a lumped parameter form. The analysis includes aerodynamic interharmonic blade coupling (periodic coefficients) and interharmonic coupling due to fuselage motion. Only a few features of the analysis will be breifly discussed here. More details are given in Reference 1. Briefly, rotor/helicopter model consists of a rotor system with flexible blades which may be articulated, gimballed, teetering or hingeless type. The rotor may be connected to fuselage through a fixed system rotor support consisting of gearbox with roll and pitch flexibility and a flexible drive shaft. Fuselage may be modeled as a flexible beam (similar to blade model but nonrotating) or fuselage effects may be represented by a hub impedance matrices. The program has capability to model a detailed swashplate-type control system. The basic rotor blade structure is represented by a lumped parameter model in which the blade is subdivided into a finite number of blade sections. Each blade section may have (see Fig. 1) arbitrary orientation and chordwise location of shear center, arbitrary spanwise distribution of mass and inertias, twist, chord, mass C.G. location, bending and torsional stiffnesses, chordwise aerodynamic center location. The aerodynamic effects include aerodynamic inertia, damping and spring rates which vary azimuthally (periodic coefficients) in forward flight. Radial and azimuthal variations of wake induced velocities may be included Also, deformed free-wake effects on helicopter rotor system dynamic response may be included in the analysis in an iterative procedure which couples RASA free-wake analysis (Reference 10) to the blade motions.

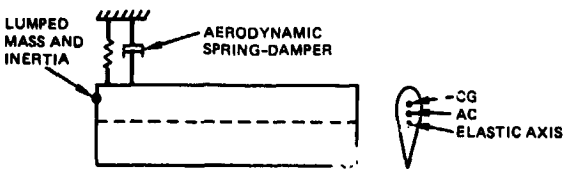

Fig. 1 General blade section model

Recent Improvements

As mentioned earlier, the RAVIB analysis has been developed by modifying an existing analysis developed by Rochester Applied Science Associates (Reference 1). A number of these modifications or improvements were absolutely necessary for obtaining a good correlation between predicted results and test data. A few other modifications were carried out to enhance its capabilities. Most significant of these modifications are listed below:

1) An iterative procedure was incorporated in the analysis to obtain the compatible steady state elastic deflections of the blade. A number of sources of blade vibratory excitations (for example, blade aerodynamic pitching moment) vary in a highly nonlinear fashion with the steady state elastic deflection of the blade. Inclusion of this procedure successfully minimizes the error due to these nonlinearities.

2) The RAVIB analysis was modified to couple the blade root motions with fuselage through a hub impedance matrix and thus to account for the fuselage motion effects. It is assumed the impedance matrix can be conveniently obtained by exercising NASTRAN.

3) Unsteady aerodynamic effects of higher harmonic control (HHC) inputs were incorporated in the analysis.

4) A new unsteady aerodynamic model based on the current state-of-art aerodynamics was developed and it was successfully incorporated in the analysis. Further discussions of this unsteady aerodynamics model is provided next.

Description of Unsteady Aerodynamics Model

The aerodynamic forces acting on a blade section in time-domain, as it goes around azimuth, can be represented in matrix form by the following relationships:

$$\{F_A\} = \{F_{Ao}\} + [M_A]\{\overset{*}{q}\} + [C_A]\{\dot{q}\} + [k_A]\{q\} \quad (1)$$

where $\{F_{Ao}\}$ is a six-component vector of aerodynamic forces and moments in an appropriate coordinate system due to all known motions of blade and wind. The matrices $[M_A]$, $[C_A]$ and $[k_A]$ represent mass, damping and spring rates respectively due to aerodynamic forces. The vector $\{q\}$ is a six-component state vector of unknown deflections and rotations. In general, for steady state helicopter flight conditions, the matrices $[M_A]$, $[C_A]$ and $[k_A]$ vary periodically around the azimuth. Furthermore, if Theoderson-type unsteady aerodynamics are utilized, these matrices contain lift deficiency function C'(k) in one form or another. Because it is not possible to precisely describe the reduced frequency k for the blade section, some approximations are required to evaluate C'(k) during the computations. The most common approximation involves assuming a constant value of 0.75 to 1.0 for C'(k). The other common procedure involves transforming C'(k) into indicial form (Reference 7) and computing the airloads in time-domain. This procedure is highly practical for computing $[F_{Ao}]$, where time-history of aerodynamic angle of attack is completely known. The most commonly used indicial form for C(k) is the Wagner functions (Reference 11) derived from the flat plate theory.

Frequency Domain Formulation for Airloads

The present study requires development of aerodynamic transfer matrices in Laplace form that can be used in the frequency-domain analysis of Reference 1. Except for a small magnitude terms involving the function [1-C'(k)], each of these periodically varying matrices $[M_A]$, $[C_A]$ and $[k_A]$ can be expanded in a Fourier series form. For example,

$$[C_A] = \sum_{n=-\infty}^{\infty} [C_n]\, e^{in\Omega t} \qquad (2)$$

Similarly, the periodic motion of the blade around the azimuth can be represented as follows:

$$\{q\} = \sum_{k=-\infty}^{\infty} [q_k]\, e^{ik\Omega t} \qquad (3)$$

Thus the aerodynamic forces generated by elastic deflections $\{F_{Aq}\}$ involve multiplication of two infinite series resulting in interharmonic coupling as follows:

$$\{F_{Aq}\} = \left(\sum_{n=-\infty}^{\infty} [M_n]\, e^{in\Omega t}\right)\left(\frac{d^2}{dt} \sum_{k=-\infty}^{\infty} \{q_k\} e^{ik\Omega t}\right)$$

$$+\left(\sum_{n=-\infty}^{\infty} [C_n]\, e^{in\Omega t}\right)\left(\frac{d}{dt} \sum_{k=-\infty}^{\infty} \{q_k\}\, e^{ik\Omega t}\right)$$

$$+\left(\sum_{n=-\infty}^{\infty} [k_n]\, e^{in\Omega t}\right)\left(\sum_{k=-\infty}^{\infty} \{q_k\}\, e^{ik\Omega t}\right) \qquad (4)$$

Thus, due to periodic coefficients, for example during high speed forward flight, a significant amount of interharmonic coupling occurs.

The Laplace transform is used to transform the differential equations into a set of algebraic equations as follows:

$$\left|F_{Aq}\right|_k = \sum_{n=-\infty}^{\infty} \left[(-ik\Omega - in\Omega)^2\, [M_n] + (-ik\Omega - in\Omega)\, [C_n]\right.$$

$$\left. + [k_n]\right] \left|\bar{q}_{k+n}\right| \qquad (5)$$

$$\text{for } k = -\infty, \ldots, 1, 2, 3, 4 \ldots \infty$$

Here vector $\{\bar{q}_k\}$ represents Laplace transform of k^{th} component of the deflection vector $\{q\}$. In principle, Equations 5 can be used to solve any number of harmonics simultaneously. But in practice, it is sufficient to truncate the summation ($n = -1, 0, +1$) for each value of k. For example, if aerodynamic transfer matrix corresponding to 4 per rev (k=4) response is desired, the blade harmonic motions at 3, 4 and 5 per rev ($\bar{q}_3\ \bar{q}_4\ \bar{q}_5$) have to be simultaneously computed under this procedure. The error involved is presumed to be small due to the exclusion of higher order interharmonic coupling (n>2). Moreover, if desired, once all the desired harmonics (N_p) have been computed (q_k, $k = 1, 2, \ldots N_p$) by above procedure, more accurate airloads can be computed during a final "pass" using Equations 5 for full N_p values of n. Thus, an iterative procedure will reduce the error due to the truncation to a minimum. There are a number of additional factors which may make it necessary to follow the iterative procedure in order to obtain more accurate results. These are discussed next.

Possible Reasons for Iterative Procedure

1) As mentioned in the previous section, the periodic coefficient matrices involve terms proportional to [1-C'(k)], which cannot be conveniently accounted for under the present procedure; unless, of course, C'(k) is given a constant value. Even though these terms are small, they can be appropriately included if an iterative procedure is followed. During each iteration, vector {q} corresponding to previous iteration can be used and [1-C'(k)] can be replaced by an indicial form equivalent (for example indicial form of Wagner function, Reference 5, Page 15). Thus, the resulting time-domain forces corresponding to [1-C'(k)] can be computed and these can be included in the vector $\{F_{Ao}\}$ of the Equations 1.

2) If the elastic deflections of the blade are significantly large, such as large torsional deflections during dynamic stall, the matrices in Equation 1 may be in error due to presence of significant nonlinearities. But, if an iterative procedure is followed, the aerodynamic forces corresponding to large blade elastic deflections (estimated from previous iteration) can be directly included into forcing vector $\{F_{Ao}\}$ of Equation 1. This procedure will minimize the errors due to the nonlinearities.

3) For correct blade dynamic response, it is necessary to use nonuniform induced velocity distribution over the rotor disk. This nonuniform induced velocity distribution is normally computed by using a free-wake analysis (Reference 10, for present analysis), wherein strength of wake vortices depend on blade dynamic response. Thus, deformed free-wake effects on rotor dynamic response can be correctly accounted only by following a solution method which involves iterative procedure that couples the free-wake circulations to the blade motions.

Application of New Conventional Unsteady Aerodynamics Model

The existing unsteady aerodynamics model in Reference 1 analysis was found to be highly inaccurate and limited in scope. For example, it assumed the aerodynamic mass matrix $[M_A]$ in Equation 1 to be equal to zero. A new unsteady aerodynamics model based on current state-of-art was developed and incorporated in the RAVIB analysis (Reference 1). The basic equations utilized were similar to the ones given in Reference 6 (Section 11-8 on Page 596). The effects of radial flow, lift deficiency function, dynamic inflow (optional) were appropriately incorporated in the model. The development essentially involved accurate formulation and programming of the aerodynamic forcing function $\{F_{Ao}\}$ and the matrices $[M_A]$, $[C_A]$ and $[k_A]$ (see Equation 1) in the RAVIB analysis. The resulting analysis was utilized to carry out a correlation of computed blade aeroelastic airloads, bending and torsional moments with flight test data with an

objective of establishing the airloads model. During an earlier study (Reference 12), the frequencies and mode shapes obtained from the Reference 1 analysis were compared with those from other independent analyses and the two results compared very well. Thus, the analysis to be utilized for the present study is a validated computer program that is believed to represent dynamics of helicopter blade quite accurately.

Application of Analysis

The RAVIB analysis has been used to compute blade airloads, blade bending and torsional moments for the AH1-G helicopter flying in steady state flight conditions. For the AH1-G helicopter, flight test data are readily available (Reference 13) through DATAMAP (Reference 14). Therefore, it was found convenient to use the Reference 13 flight test data for the present correlation study.

The AH1-G blade structural, geometric and aerodynamic characteristics were obtained from References 13 and 15. These blade characteristics may not correspond exactly to the AH1-G helicopter blade used in the flight tests. Because the main objective of the present study was to demonstrate relative improvements in the correlation between test and theory through the use of better unsteady aerodynamics model, an approximate but representative model of the AH-1G blade was considered to be adequate. The blade was modeled by approximately twenty nonuniform elastic segments. The effects of parameters such as control system stiffness, undersling and drive shaft torsional flexibility were appropriately included in the model. The effects of hub impedance and drive system damping were neglected in the present computations.

Results with Conventional Unsteady Aerodynamics

The conventional strip theory was used for computation of airloads. The blade was represented by nine nonuniform strips. At the center of each strip (aerodynamic load application point), the nonuniform azimuthal distribution of induced velocities was computed by utilizing a rotor wake analysis (modified version of Reference 10). The computations for the AH-1G helicopter rotor were carried out at two level flight conditions (114 knots and 142 knots) for which the flight test data were available (flight numbers 610 and 614 in Reference 13). The gross weight for both the flight conditions was 8,300 pounds with $C_T/\sigma = 0.006$.

A correlation between computed and measured performance parameters is shown in Fig. 2. As the results indicate, the predicted values of shaft horsepower and collective are within five HP and within half a degree respectively of the test values (Fig. 2). For a radial station corresponding to $r/R = 0.75$, correlation between calculated and test airloads is shown in Fig. 3a for a representative flight condition (114 knots). Even though there are significant differences between test and theory when the blade is in certain segments (e.g., near $\psi = 270$) of rotor disk, overall correlation between the two is reasonably good. The similar results for the 142 knots flight condition are shown in Fig. 3b.

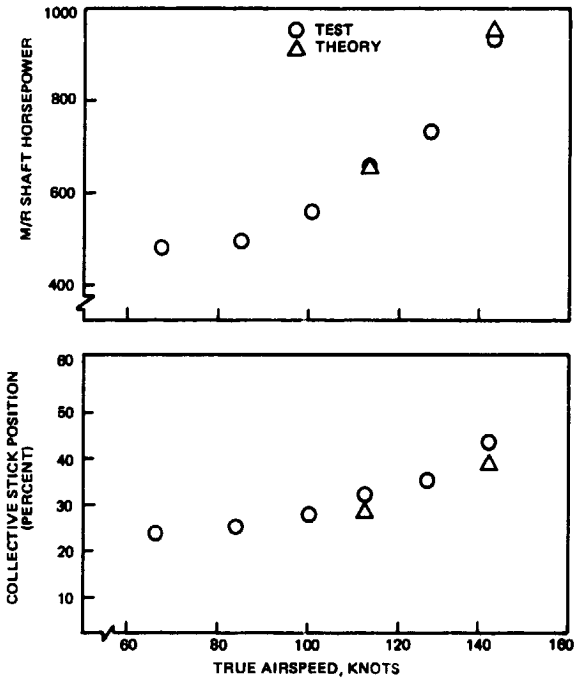

Fig. 2 Comparison of measured and computed level flight performance parameters, AH-1G helicopter, 8300 pounds, GW

Figs. 4a and 4b show the blade oscillatory beamwise bending moment correlation between the test and theory based on the conventional aerodynamics model. For 114 knots flight condition (Fig. 4a) the theory predicts peak to peak value quite accurately, but for 142 knots case (Fig. 4b), the theory underpredicts peak to peak value by 30 percent. Time histories of measured and computed chordwise bending moments for the same flight conditions are compared in Figs. 5a and 5b. From the results shown in these figures, it is seen that very good agreement between test and theory has been obtained over complete range of azimuth.

The correlations of the test blade torsional moments with the predicted results are shown in Figs. 6a and 6b. The peak to peak variation in torsional moment is highly underpredicted by the theory based on conventional aerodynamics model. A thorough analysis of these results indicated that a new aerodynamics model was needed to improve the correlation between computed and test torsional moments.

Description of New Unsteady Aerodynamics Model

An analysis of results from two-dimensional experiments (e.g., Reference 16) involving large amplitude oscillations of airfoils (under unstalled conditions) indicates that conventional aerodynamics (based on Theoderson's theory) is unable to predict the unsteady aerodynamic characteristics of the airfoil. This is partly due to the fact that Theoderson's flat plate theory is based on small amplitude oscillations. During high speed forward flight, helicopter blade sections are

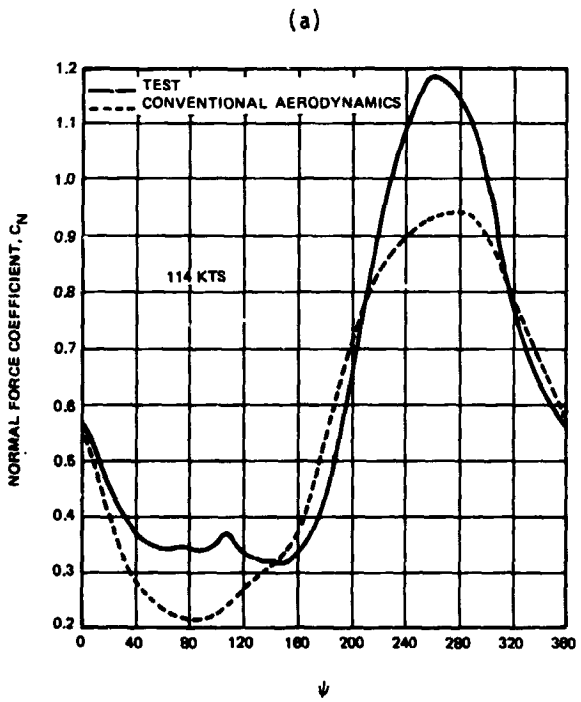

Fig. 3 Correlation between calculated and test airloads, AH-1G Blade, r/R = 0.75

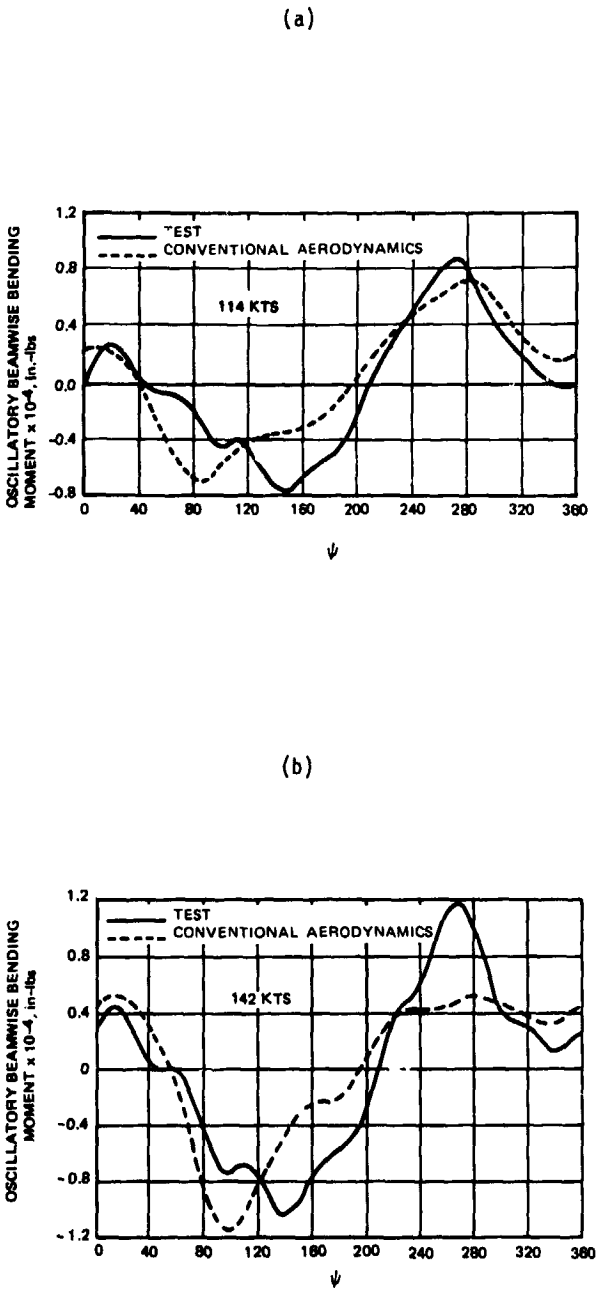

Fig. 4 Comparison between measured and computed oscillator beamwise bending moment, r/R = 0.39, AH-1G blade

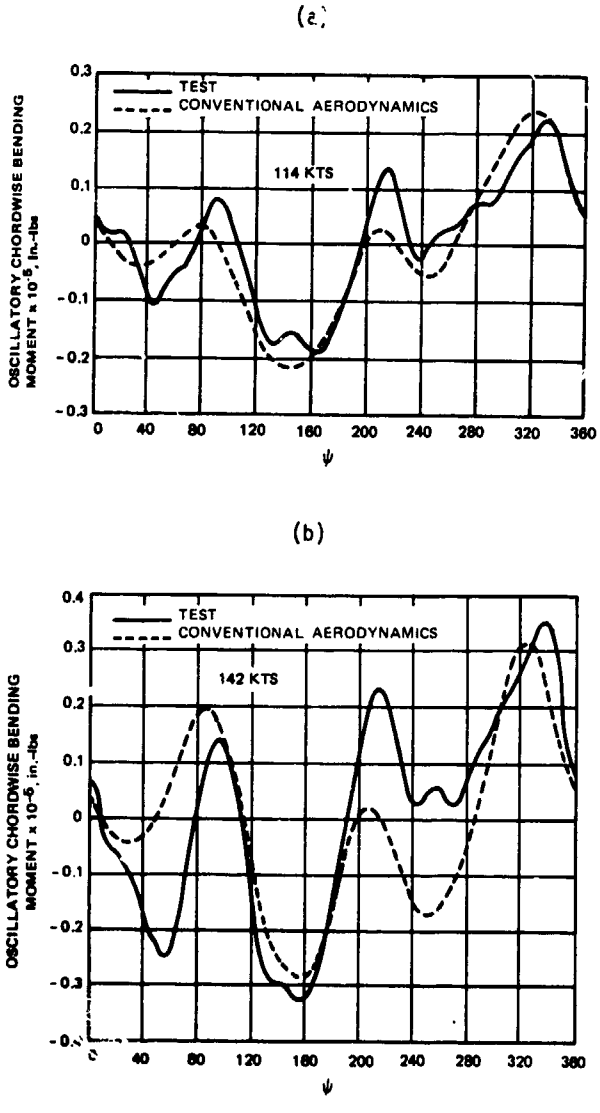

Fig. 5 Comparison between measured and computed oscillatory chordwise bending moment, r/R = 0.39, AH-1G blade

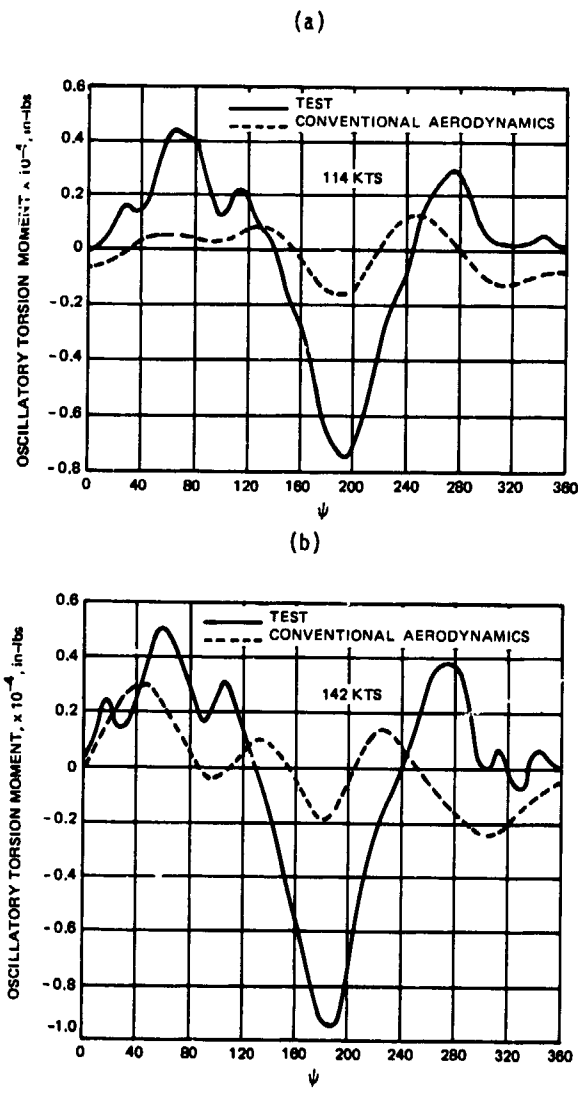

Fig. 6 Comparison between measured and computed oscillatory torsion moment, r/R = 0.30, AH-1G blade

expected to go through significantly large amplitude oscillatory changes in angle of attack. Thus, it was found necessary to include the effects of finite amplitude oscillations in the new unsteady aerodynamics model. More specifically, the new unsteady aerodynamics model utilizes empirical or synthesized data. The synthesized data are derived from the test data; by curve-fitting the appropriate analytical expressions to the measured unsteady airfoil characteristics, obtained from the oscillating airfoil experiments. The present method used the analytical expressions established in Reference 5. For example, as described in Reference 5, the unsteady lift coefficient, under unstalled conditions, is represented by

$$C_{Lu} = C_{Ls}(\alpha) + Q_1 A + Q_2 \alpha_w + Q_3 \alpha + Q_4 \alpha^2 \qquad (6)$$

Here C_{Ls} is the static lift coefficient; (A, α_w, α) are the instantaneous values of dynamic parameters (see Appendix for details) and Q_1, Q_2, Q_3 and Q_4 are the empirical parameters or the synthesized data. Because the empirical parameters Q_1 through Q_4 are based on real airfoils executing large amplitude oscillations, the Equation 6 correctly simulates general unsteady lift characteristics of a helicopter blade section. Furthermore, it should be noted that lift deficiency function effects are represented in Equation 6 through the decay parameter α_w, which is derived from a modified Wagner function (Reference 5). In fact, in future, the parameters such as Q_1 through Q_4 can be obtained from some reliable analyses.

Finally, in unsteady aerodynamics the question of what constitutes a large amplitude motion, depends to some extent on the magnitude of the Mach number. An amplitude of one degree in transonic flow is considered high amplitude; whereas at low subsonic Mach numbers, a three degree oscillation may be considered a small amplitude motion. Studies are continuing to establish these criteria.

Next, the results based on this synthesized unsteady aerodynamics model are discussed.

Results with Synthesized Unsteady Aerodynamics

Equation 6 describes the unsteady lift coefficient, C_{Lu}, of an airfoil in the time domain. Similar equation for unsteady pitching moment coefficient is given in Reference 5. These two equations were incorporated in the RAVIB analysis. The modified analysis was utilized to recompute the earlier results obtained from the conventional unsteady aerodynamics theory. Thus, the various improvements in the correlation between flight test data and the analytical computations can be systematically demonstrated.

First, the variations in the predicted airloads with aerodynamics model are shown in Figs. 7 through 10. Fig. 7 has been repeated from Fig. 3, but with the addition of computed normal force coefficient based on synthesized data. The differences between the two analytical results are small and these differences are mainly confined to the retreating blade region of the rotor disk. To further illustrate the closeness of the computed C_L from the two aerodynamic models, Figs. 8a and 8b show similar results obtained at one more radial station corresponding to $r/R = 0.86$. A close analysis of the results, however, indicates a small but significant improvement due to the use of synthesized data, but only for 142 knots flight condition (Figs. 7b and 8b). Thus, improvements in the correlation of beamwise bending moments, if any, can be expected only for 142 knots flight condition. For completeness, Figs. 9 and 10 show the corresponding correlation of chordwise force coefficients for the two radial stations (0.75 and 0.86). Because the results for the chordwise force coefficient from the two aerodynamic models differ only slightly, no significant variations in correlation for the chordwise bending moments is expected with change in the aerodynamics model.

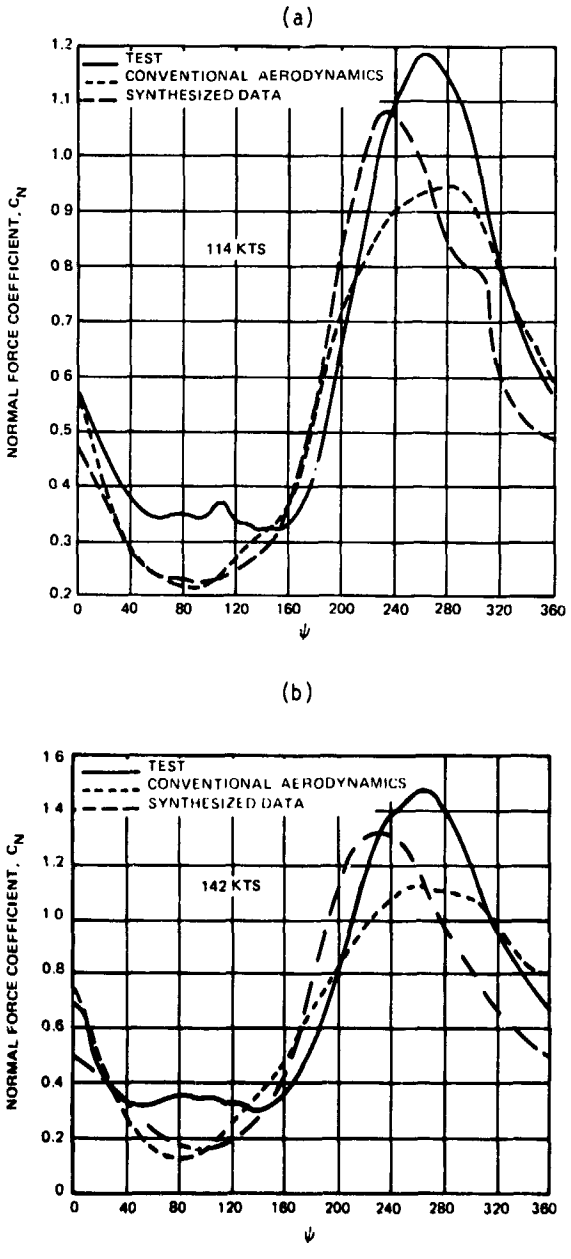

Fig. 7 Correlation between calculated and test airloads, AH-1G blade, r/R = 0.75

(a)

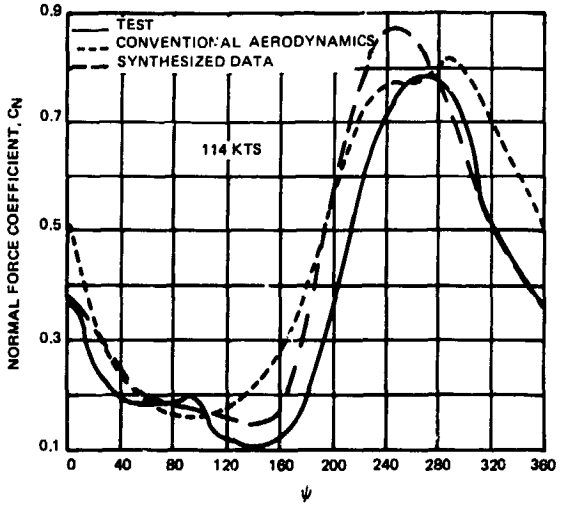

(b)

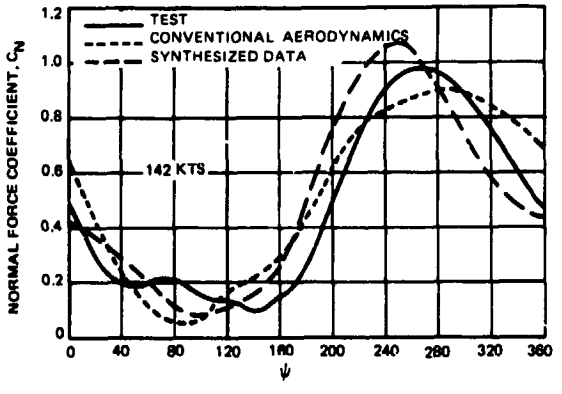

Fig. 8 Correlation between calculated and test airloads, AH-1G blade, r/R = 0.864

(a)

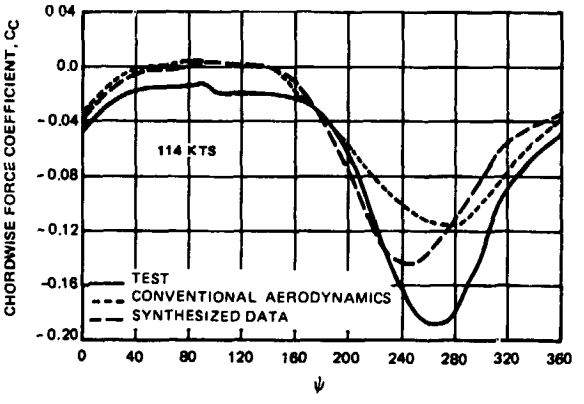

(b)

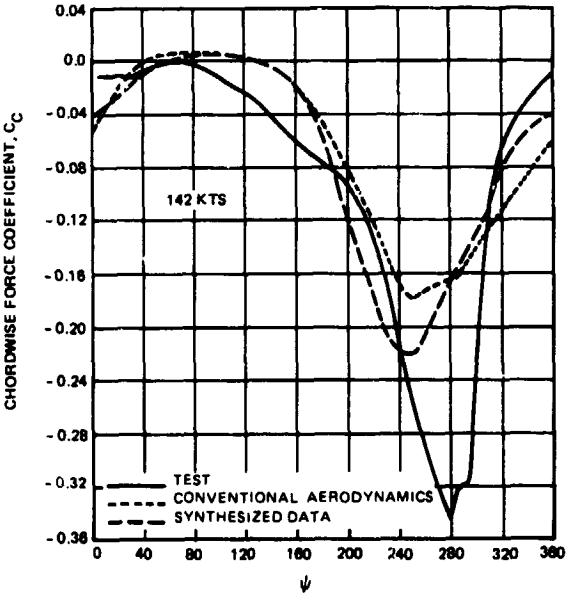

Fig. 9 Correlation between calculated and test airloads, AH-1G blade, r/R = 0.75

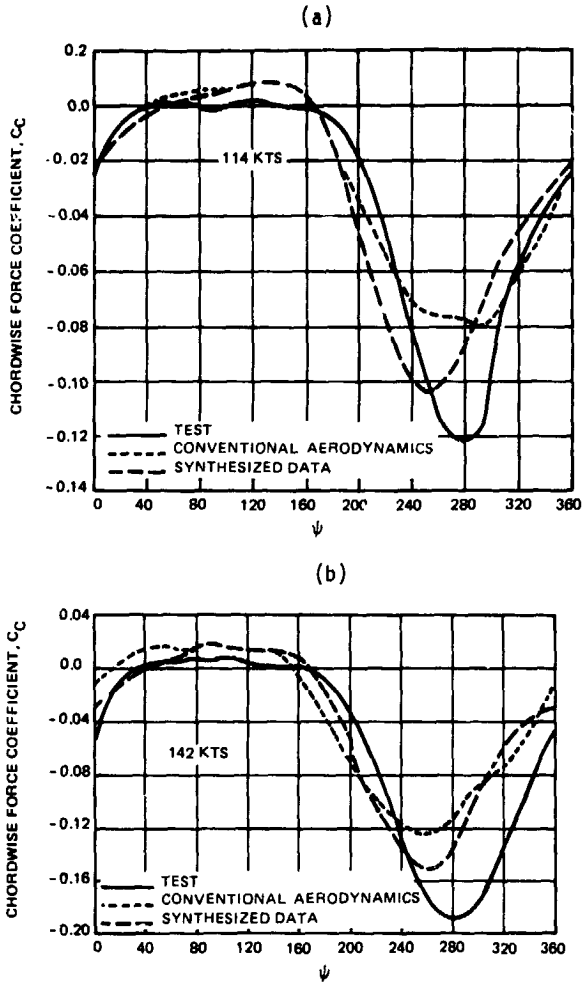

Fig. 10 Correlation between calculated and test airloads, AH-1G blade, $r/R = 0.864$

Bending Moment Correlations

Figs. 11 and 12 show the comparison between the test and the predicted beamwise bending moment values described for two different radial stations, $r/R = 0.39$ and $r/R = 0.80$ respectively. An analysis of these figures indicates the two aerodynamics models predict similar results at 114 knots flight condition (Figs. 11a and 12a). However, at 142 knots flight conditions, the predicted results based on synthesized data (Figs. 11b and 12b) seem to compare better with the test data than those based on conventional aerodynamics.

The similar variation of oscillatory chordwise bending moments for various aerodynamics models are shown in Figs. 13 and 14, corresponding to two radial stations $r/R = 0.39$ and $r/R = 0.8$ respectively. Unlike beamwise bending moments, the computed time histories of the chordwise bending moments do not show significant variation with the unsteady aerodynamic model. It should be remembered, however, that the main purpose for developing the present synthesized data model was to improve the correlation between predicted torsional moments and the test data.

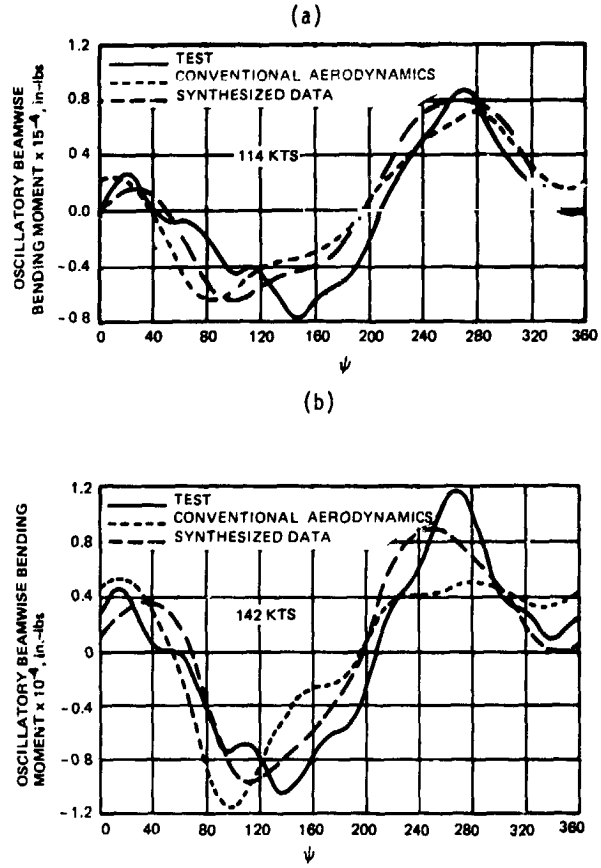

Fig. 11 Comparison between measured and computed oscillatory beamwise bending moment, $r/R = 0.39$, AH-1G blade

Torsional Moment Correlation

Measured and computed torsional moments for 114 knots flight condition are compared in Figs. 15a and 16a for two different radial stations, $r/R = 0.3$ and $r/R = 0.5$ respectively. From these figures, it is seen that very good agreement between test and new theory based on synthesized data has been obtained over the complete range of azimuth. The computed torsional moments based on conventional aerodynamics do not correlate well with the test data. The similar correlations are obtained at 142 flight conditions as indicated by the results shown in Figs. 15b and 16b. Thus, the results shown in Figs. 15 and 16 imply that for correct computations of pitch link loads, the unsteady aerodynamics model has to be based on large amplitude incidence oscillations inherently encountered by a helicopter blade section.

Finally, it should be mentioned that use of synthesized data will make it easy to extend the airloads computations in the stall region. As established in Reference 5, the unsteady aerodynamics characteristics of blade section during dynamic stall are easily obtained by adding more terms to the right-hand side of Equation 6.

Concluding Remarks

Rotor Aeroelast[illegible]ration (RAVIB) computer program is a c[illegible]nsive, elegant and efficient analysis which seems to predict blade oscillatory loads reasonably well. The conventional unsteady aerodynamics model based on small amplitude airfoil oscillations seem to highly underpredict helicopter blade pitching moments.

Use of a new aerodynamics model based on unstalled synthesized data, derived from the large amplitude oscillating airfoils tests, significaintly improves the correlation of the computed blade torsional moments with the test data. Furthermore, this new aerodynamics model is such that it can be easily extended to compute the critical pitch-link loads of rotors operating under dynamic stall conditions.

(a)

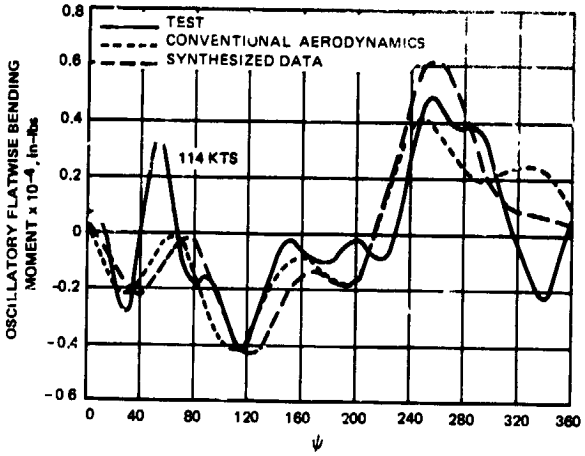

(b)

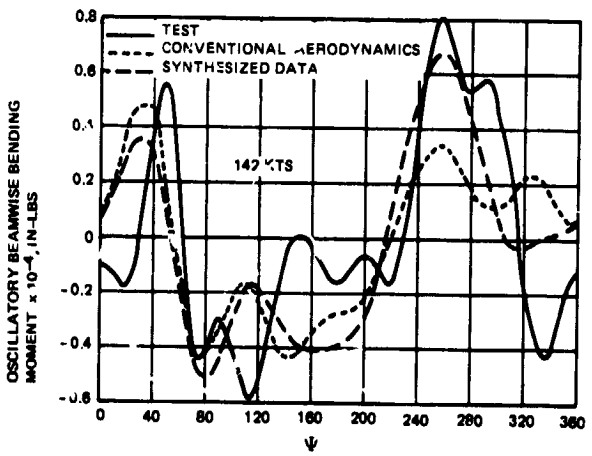

Fig. 12 Comparison between measured and computed oscillatory beamwise bending moment, $r/R = 0.80$, AH-1G blade

(a)

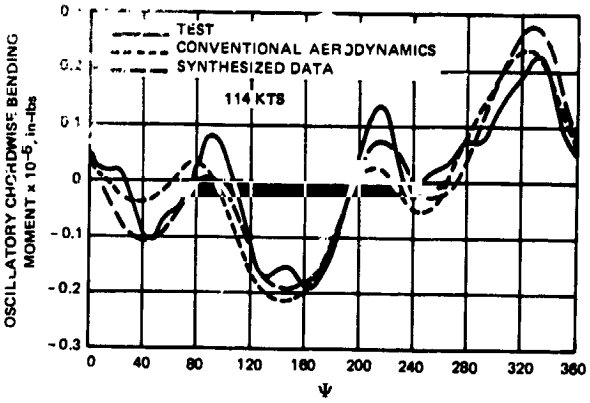

(b)

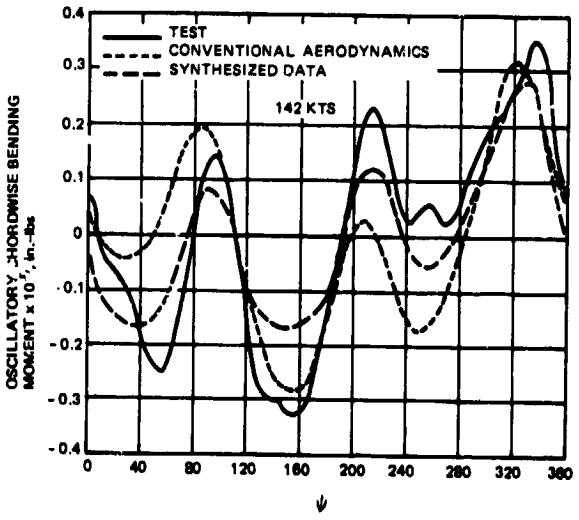

Fig. 13 Comparison between measured and computed oscillatory chordwise bending moment, $r/R = 0.39$, AH-1G blade

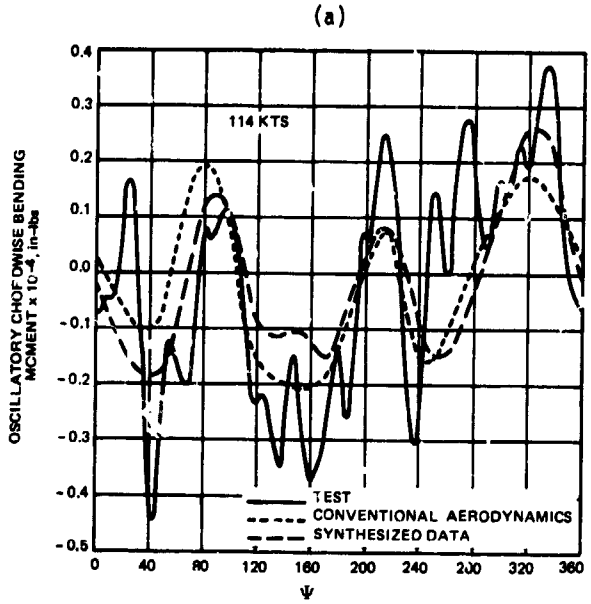

Fig. 14 Comparison between measured and computed oscillatory chordwise bending moment, r/R = 0.80, AH-1G blade

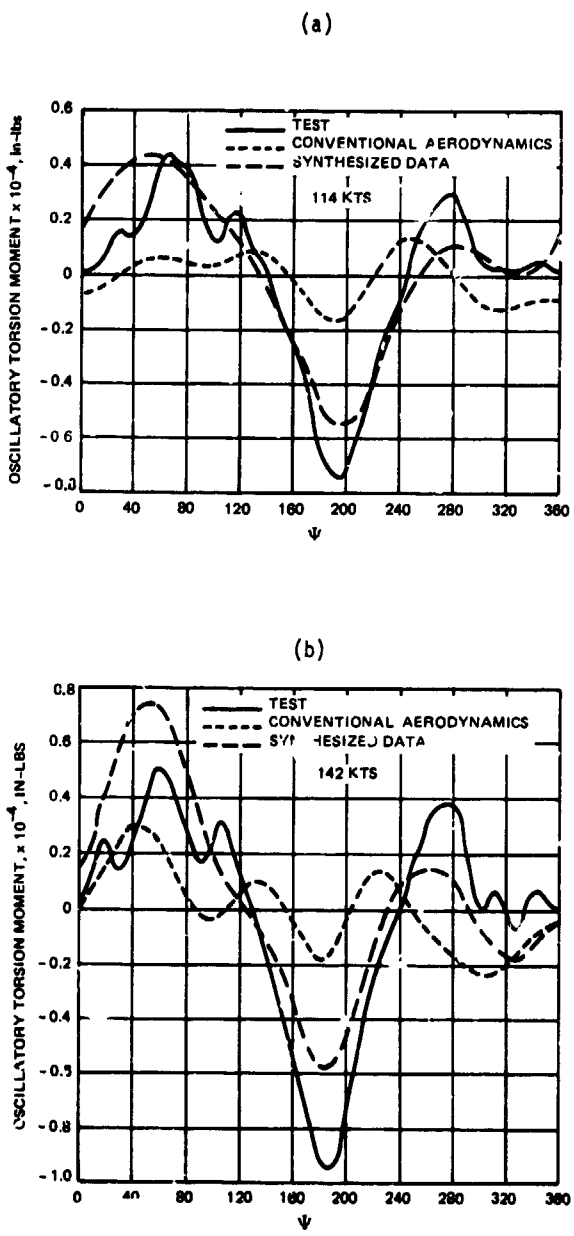

Fig. 15 Comparison between measured and computed oscillatory torsion moment, r/R = 0.30, AH-1G blade

(a)

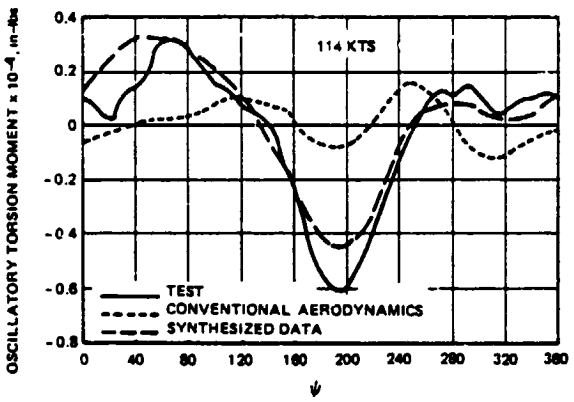

(b)

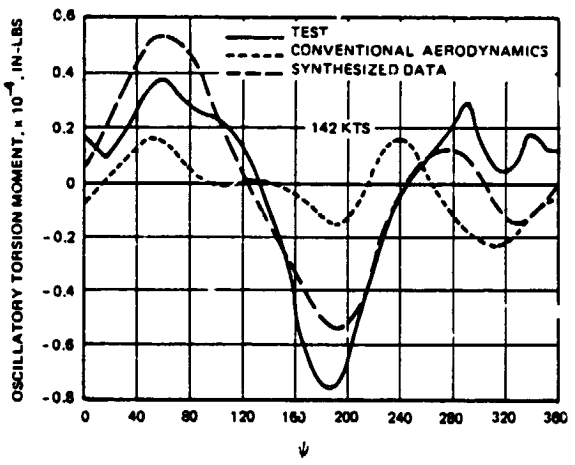

Fig 16 Comparison between measured and computed oscillatory torsion moment, $r/R = 0.50$, AH-1G blade

APPENDIX

The dynamic parameters utilized in the synthesized data aerodynamics model are: 1) the instantaneous angle of attack, α; 2) the nondimensional pitch rate A; and 3) the decay parameter α_w, which accounts for the time history effects of the change in α, and is based upon the Wagner function.

Because the motion of a helicopter blade is not known a priori, the blade section dynamic parameters are evaluated numerically in a stepwise manner by utilizing the following recursive relationships at step n.

$$\alpha_n = \theta_n + \phi_n \tag{A-1}$$

$$A_n = (\Delta\theta)_n/(\Delta s)_n + (1.5\phi_n - 2.0\phi_{n-1} + 0.5\phi_{n-2})/(\Delta s)_n \tag{A-2}$$

$$(\alpha_w)_n = X_n + Y_n \tag{A-3}$$

where

$$X_n = X_{n-1}\, e^{-0.0455(1-M^2)\,(\Delta s)_n} + 0.165\,(\alpha_n - \alpha_{n-1}) \tag{A-4}$$

$$Y_n = Y_{n-1}\, e^{-0.30(1-M^2)\,(\Delta s)_n} + 0.335\,(\alpha_n - \alpha_{n-1}) \tag{A-5}$$

$$(\Delta s) = \frac{2U_n}{\Omega c}(\Delta\psi) \tag{A-6}$$

Here $\Delta\psi$ is azimuthal stepsize, Ω is rotor speed, c is chord length, and U_n is tangential velocity component.

The instantaenous angle of attack, α_n, is described in the tip-path-plane system, θ_n and ϕ_n being the pitch angle and inflow angle, respectively. It should be noted that the time derivative of pitch angle in Eq. (A-2), $(\Delta\theta/\Delta s)$, may be computed analytically from the known cyclic or harmonic inputs, while the time derivative of ϕ has to be computed by the backward difference scheme. The derivation of Eqs. (A-1 thru A-6) for α_w is described in Reference 5.

References

1. Sutton, L.R., and Gangwani S.T., "The Development and Application of an Analysis for the Determination of Coupled Tail Rotor/Helicopter Air Resonance Behavior", USAAMRDL TR-75-35, Ft. Eustis, VA, August 1975.

2. Dinyavari, M.A.H., and Friedmann P. "Unsteady Aerodynamics in the Time and Frequency Domain for Finite Time Arbitrary Motion of Rotary Wings in Hover and Forward Flight, 25th Structures, Structural Dynamics and Materials Conference, Palm Springs, CA, May 14-16, 1984.

3. Dat, R., and Tran C.T., "Investigation of the Stall Flutter of an Airfoil with a Semi-Empirical Model of 2-D Flow", Vertica, Vol. 7, No. 2, pp. 73-96, 1983.

4. Kaza, K.R., and Kvaternik, R.G., "Nonlinear Aeroelastic Equations for Combined Flapwise Bending, Chordwise Bending, Torsion, and Extension of Twisted Nonuniform Rotor Blades in Forward Flight", NASA TM 74059, August 1977.

5. Gangwani, S.T., "Synthesized Airfoil Data Method for Prediction of Dynamic Stall and Unsteady Airloads", NASA CR-3672, February 1983.

6. Theodersen, T., "General Theory of Aerodynamic Instability and Mechanism of Flutter", NACA Report 496, 1935.

7. Dowell, E.H., "A Simple Method for Converting Frequency-Domain Aerodynamics to the Time Domain", NASA TM 81844, 1980.

8. Johnson, Wayne, "Helicopter Theory", Princeton University Press, 1980.

9. Sutton, L.R., R.P. White, Jr., and R.L. Marker, "Wind Tunnel Evaluation of Aeroelastically Conformable Rotor", USAAVRADCOM TR-81-D-43, March 1982.

10. Sadler, S.G., "Main Rotor Free Wake Geometry Effects on Blade Air Loads and Response for Helicopters in Steady Maneuvers", NASA CR-2110, September 1972.

11. Bisplinghoff, R.L., Ashley, H., and Halfman, R.L., "Aeroelasticity", Addison-Wesley Publishing Company, Inc., Reading, Mass., 1957.

12. Gangwani, S.T., "Evaluation of Helicopter Aeroelastic Stability Analysis", United Technologies Research Center Report Number UTRC82-48, East Hartford, CT, August 1982.

13. Shockey, G.A. and Williamson, J.W., "AH-1G Helicopter Aerodynamic and Structural Loads Survey", USAAMRDL TR-76-39, Ft., Eustis, VA, February 1977.

14. Philbrick, R.G., "The Data for Aeromechanics Test and Analytics - Management and Analysis Package (DATAMAP)", Volume I, USAAVRADCOM - TR-80-D-30A, Ft. Eustis, VA, December 1980.

15. Van Gaasbeck, J.R., "An Investigation of High-G Maneuvers of the AH-1G Helicopter", USAAMRDL-TR-75-18, Ft. Eustis, VA, April 1975.

16. St. Hilaire, A.O., F.O. Carta, M.R. Fink and W.D. Jepson, "The Influence of Sweep on the Aerodynamic Loading on an Oscillating NACA 0012 Airfoil", Volume 1 - Technical Report, NASA CR-3092, 1979.

DISCUSSION
Paper No. 8

DEVELOPMENT OF AN UNSTEADY AERODYNAMICS MODEL TO IMPROVE CORRELATION OF COMPUTED BLADE STRESSES WITH TEST DATA
Santu T. Gangwani

Jing Yen, Bell Helicopter: I have two questions. Number one: Does your unsteady aerodynamics model include lift, drag, and moment--everything?

Gangwani: The conventional model, you know, it includes only lift coefficient and pitching coefficient, and drag is computed mainly from the lift. In this model you still use the static data and most of the unsteady drag comes from the unsteady lift or from the static drag.

Yen: I know from my experience that the conventional or well-known unsteady aerodynamics model can give you close to good correlation--the moments and everything else, but is very poor in power, and the drag. Your unsteady aerodynamics model here includes everything, including the drag?

Gangwani: I showed you the correlation on horsepower.

Yen: Yes, it was very good.

Gangwani: Edgewise stress correlation is also very good so I don't see any problem in computing the edgewise pulses really.

Yen: My next question is where did your synthesized data come from?

Gangwani: The synthesized data I obtained as I told you from the oscillating airfoil test. Now your question is how did I get [the data] for a particular airfoil?

Yen: That's right.

Gangwani: Well, I sort of took it from other airfoils since your airfoil was a symmetric airfoil. So most of the data corresponds to a [NACA] 0012. It's not an absolute correlation, it's just qualitative to demonstrate that we do need some different aerodynamics models to compute the aerodynamic pitching moments.

Bob Blackwell, Sikorsky Aircraft: I want to ask one question. I wasn't completely clear about whether this model truly handles stall conditions or could it be extended so that it would? The second part of that is were the conditions shown at 142 knots and so forth, at that C_T/σ, did they represent conditions that really would design the control system? In other words were those loads the high loads for the system?

Gangwani: The highest data available are at 142 knots and there was no stall. The stall results that I showed were just computational results at C_T/σ of 0.1. There was no test data at that point. They were just computational data. Most of the test data are at C_T/σ much lower than that.

AEROELASTIC CONSIDERATIONS FOR TORSIONALLY SOFT ROTORS

Wayne R. Mantay & William T. Yeager, Jr.
NASA/Langley Research Center
Army Structures Laboratory
Hampton, Virginia

Abstract

A research study was initiated to systematically determine the impact of selected blade tip geometric parameters on conformable rotor performance and loads characteristics. The model articulated rotors included baseline and torsionally soft blades with interchangeable tips. Seven blade tip designs were evaluated on the baseline rotor and six tip designs were tested on the torsionally soft blades. The designs incorporated a systemmatic variation in geometric parameters including sweep, taper, and anhedral. The rotors were evaluated in the NASA Langley Transonic Dynamics Tunnel at several advance ratios, lift and propulsive force values, and tip Mach numbers. A track sensitivity study was also conducted at several advance ratios for both rotors. Based on the test results, tip parameter variations generated significant rotor performance and loads differences for both baseline and torsionally soft blades. Azimuthal variation of elastic twist generated by variations in the tip parameters strongly correlated with rotor performance and loads, but the magnitude of advancing blade elastic twist did not. In addition, fixed system vibratory loads and rotor track for potential conformable rotor candidates appears very sensitive to parametric rotor changes.

Introduction

Reducing helicopter vibratory loads while improving performance through passive control has been the goal of the Aeroelastically Conformable Rotor (ACR) concept. Initial ACR studies (ref. 1) examined the potential of a conformable rotor to alter the unfavorable blade spanwise and azimuthal load distributions which lead to increased vibratory bending loads and power requirements. Those test results on a model hingeless rotor indicated that elastic twist measurably changed blade loads on a torsionally soft blade. The incorporation of time varying elastic twist, as a promising method of achieving a passive control concept, has been identified analytically (ref. 2). Blade design features producing that desired elastic control were suggested in reference 2 for an articulated rotor.

The effect of blade tip shape on rotor performance and loads has received much attention for application to multi-bladed helicopters (refs. 3-5). Experimental data have also been obtained (ref. 6) which initiated identification of blade tip shape as a promising passive control concept. The reference 6 test utilized a model rotor blade with conventional torsional stiffness, and while the resulting loads and performance of the configurations were tip-shape-dependent, the identification of which parameter caused each load or performance change was elusive. This was due, in part, to multiple parameter variations occurring with each tip change. Nevertheless, the concept of passive control to achieve better rotor performance while reducing loads was encouraged by these results and several conformable designs were pursued. The resulting studies (refs. 7-8) considered variations in blade torsional stiffness, airfoil section, mass distribution, and trailing edge tab deflection, as well as tip geometry, in the design. The wind-tunnel tests of these ACR concepts produced encouraging loads and performance data, but the aeroelastic mechanism for design success or failure was not obvious.

Expanded testing and analysis of the configurations of reference 6 resulted in identification of several key issues for future ACR application and development (ref. 9). For the baseline torsionally stiff rotor used in that test, the parametric variations of tip sweep, taper and anhedral did measurably change the elastic twist and integrated performance, but there did not appear to be a strong connection between elastic twist and performance. Additional tests on the blades of reference 8 which incorporated large tip spans and trailing edge tab deflections (refs. 10-11) showed performance and loads variations which were not easily explainable by individual parameter effects.

The parameters most effective in improving conformable rotor performance and loads characteristics have thus not been systematically determined. Although it has been shown that changes in adjustable trailing edge tabs have significant effects on conformable rotor behavior (ref. 11), the rotor blade tip operates in a very influential portion of the rotor disk and thus provides significant research impetus. This is especially true if ACR success is dependent on elastic twist control. Consequently, the research study described herein was initiated to systematically determine the effect of selected blade tip geometric parameters on ACR performance and loads characteristics. This data is presented for advance ratios of .35 and .40 at one rotational tip Mach number.

In addition, the utilization of a conformable rotor concept should be evaluated not only for the measure of success with which it achieves its performance and loads goals, but also how well it can be "fielded." That is how much change, if any, in current installation and rotor tuning is necessary for the new rotor concept to be employed. Rotor control sensitivity is an example of such a concern (ref. 11). Another aspect of this

transition for the conformable rotor is rotor tracking characteristics and the implications for rotor and fuselage loads. Initial results from the present study (ref. 12) provided some insight into the mechanisms involved in conformable rotor behavior. The results of the completed test program are included here.

Notation

a speed of sound, ft/sec

b number of blades

C_D rotor drag coefficient, $\frac{D}{\rho\pi R^2(\Omega R)^2}$

C_L rotor lift coefficient, $\frac{l}{\rho\pi R^2(\Omega R)^2}$

$\bar{C}_L$ rotor mean lift coefficient

C_Q rotor torque coefficient, $\frac{Q}{\rho\pi R^3(\Omega R)^2}$

c blade chord, in.

c.g. measured section center of gravity location, in.

a.c. computed section aerodynamic center location, in.

D rotor drag, lb.

H rotor force perpendicular to control axis, lb.

$I_{1/4_c}$ blade tip torsional mass inertia about 1/4 chord (ft-lb-sec^2)

I_e blade section torsional mass inertia per foot about pitch axis (lb-sec^2)

L rotor lift, lb.

M_T rotor blade tip Mach number, $\frac{\Omega R}{a}$

Q rotor torque, ft-lb.

r blade radial station, ft.

R rotor radius, ft.

V free-stream velocity, ft/sec

α_s angle of attack of rotor shaft, positive tilt aft, deg.

$\Delta\theta_1$ elastic twist angle, positive nose-up, deg.

μ rotor advance ratio, $\frac{V}{\Omega R}$

ρ mass density of test medium, slug/ft3

σ nominal rotor solidity ratio, $bc/\pi R$ = .082

ψ azimuth angle of rotor blade, deg

Ω rotor rotational speed, rad/sec

ω natural frequency of rotating blade, rad/sec

Abbreviations

R rectangular
S sweep
T tapered
A anhedral

Apparatus

Wind Tunnel

The experimental program was conducted in the Langley Transonic Dynamics Tunnel (TDT) shown in figure 1. The TDT is a continuous flow tunnel with a slotted test section and is capable of operation up to Mach 1.2 at stagnation pressures up to 1 atm. The tunnel test section is 16 ft square with cropped corners and has a cross-sectional area of 248 ft^2. Either air or Freon-12[1] may be used as a test medium in the TDT. Because of its high density and low speed of sound, the use of Freon-12 aids the matching of full-scale Reynolds number and Mach number to model-scale values. Also, some restrictions on model structural design are eased, while dynamic similarity is still maintained. The heavier test medium permits a simplified structural design to obtain the required stiffness characteristics and thus eases the design and/or fabrication requirements of the model (refs. 13, 14). For this investigation, Freon-12 at a nominal density of .006 slug/ft^3 was used as the test medium.

Model Description

The experimental blades described herein were tested on the aeroelastic rotor experimental system (ARES) shown in Figures 2 and 3. The ARES has a generalized helicopter fuselage shape enclosing the rotor controls and drive system. It is powered by a variable frequency synchronous motor rated at 47 hp output at 12,000 rpm. The motor is connected to the rotor shaft through a belt-driven two-stage speed reduction system. The ARES rotor control system and pitch attitude (α_s) are remotely controlled from within the wind-tunnel control room. The ARES pitch attitude is varied by an electrically controlled hydraulic actuator. Blade collective pitch and lateral and longitudinal cyclic pitch are input to the rotor through the swashplate. The swashplate is moved by three hydraulic actuators.

[1]Freon-12: Registered trademark of E.I. du Pont de Nemours & Co., Inc.

Description of Rotor Blades

The rotor models used in this investigation were 0.175-scale, four-blade articulated rotors with coincident lead-lag and flapping hinges. The blade geometry was the same for both rotors tested (Figure 4). The blades were designed so that the tip configuration could be changed at the 89 percent radius. The rotor planform was a 0.175-scale representation of a current full-scale utility-class rotor system. An SC1095 airfoil was used on all blades from the root cutout to 49 percent radius and from 91 percent radius to the tip. Between 50 and 90 percent radius, a cambered SC1095-R8 airfoil was used. Adjustable trailing edge tabs of 6.5 percent chord were provided on both sets of baseline and ACR blades from 50 to 89 percent radius.

The baseline blades were aeroelastically representative, but blade structural and inertial characteristics did not precisely match any specific full-scale rotor. The ACR blades differed significantly from the baseline blades in torsional stiffness over the outer 55 percent of the blade span. The blade physical properties and the natural frequencies are presented in Table I.

Instrumentation

Instrumentation on the ARES allows continuous displays of model control settings, rotor forces and moments, blade loads, and pitch link loads. ARES pitch attitude is measured by an accelerometer, and rotor control positions are measured by linear potentiometers connected to the swashplate. Rotor blade flapping and lagging are measured by rotary potentiometers mounted on the rotor hub and geared to the blade cuff. Rotor shaft speed is determined by a magnetic sensor. One blade of each blade set, baseline and ACR, was instrumented with four-arm strain-gage bridges to measure loads and deflections at several blade radial stations. Flapwise (out-of-plane) moments and chordwise (in-plane) moments were measured at 26, 39, 53 and 81 percent radius, while torsional moments were measured at 29, 37, 52, and 78 percent radius. The rotating blade data are transferred through a 30-channel slip-ring assembly. Rotor forces and moments are measured by a six-component strain-gage balance mounted below the pylon and drive system. The balance is fixed with respect to the rotor shaft and pitches with the fuselage. Fuselage forces and moments are not measured by the balance.

Description of Parametric Tips

Seven blade tip designs were evaluated on the baseline rotor and six of the tip designs were tested on the torsionally soft (ACR) blades. The tip designs incorporated a systemmatic variation in geometric parameters including sweep, taper, and anhedral. These parameters were varied while tip inertial properties, airfoil contour, and twist were target constants. The magnitude of parameter variations chosen for ACR application were representative of current design values for modern helicopter rotors. Figure 5 presents the geometry of the tip designs, while Table II lists the measured tip characteristics and compares them to the design goals or controlled constants.

Test Methodology

Procedure for Performance and Loads Data Acquisition

Each rotor configuration was first tracked and balanced in hover to remove first harmonic fixed system loads. At each forward flight test point, the rotor rotational speed and tunnel conditions were adjusted to give the desired tip Mach number and advance ratio at a given shaft angle of attack. Blade collective pitch was changed to obtain the target rotor lift and propulsive force; and at each collective pitch setting, the cyclic pitch was used to remove rotor first-harmonic flapping with respect to the rotor shaft. Data were then recorded for each rotor task. The maximum value of collective pitch attained at each shaft angle of attack was generally determined by either blade load limits or ARES drive system limits.

Model deadweight tares were determined throughout the shaft angle of attack range with the blades on and with them removed. Aerodynamic rotor hub tares were determined with the blades removed throughout the ranges of shaft angle of attack and advance ratio investigated. Both deadweight and hub aerodynamic tares have been removed from the data presented herein.

Procedure for Rotor Track Sensitivity Data Acquisition

For the configurations tested for tracking characteristics, the procedure for tracked rotor data was similar to that above. During out-of-track conditions the instrumented blade was driven out of track with trailing edge tab deflections, and allowed to fly out of trim with the shaft. Flapping for the remaining three blades had first-harmonic content removed through cyclic pitch.

Accuracies

Based on controlled data points, the repeatability of the data for constant shaft angle of attack, control angles and advance ratio has been estimated to be within the following limits:

$$\frac{C_L}{\sigma} \pm 0.0025$$

$$\frac{C_D}{\sigma} \pm .0005$$

$$\frac{C_Q}{\sigma} \pm .00025$$

The accuracy for angle measurements is estimated to be within $\pm 0.25°$.

The value of solidity (σ) used throughout this report for normalizing performance coefficients is 0.082, based on a blade nominal chord of 3.625 inches and a radius of 56.224 inches.

Test Conditions

Data Obtained

All the tip configurations shown in Figure 5 were tested for the target conditions shown in Table III. The magnitudes of lift and propulsive force parameters and advance ratio were chosen as representative of a modern utility helicopter. The tip Mach number variation represents that possible due to full scale ambient environment changes and also represents an attempt to evaluate the effect of changes in advancing tip Mach number on the tip airfoil and planform behavior.

The ACR and baseline rotors with swept tips were subjected to a rotor track sensitivity study which included the target test points shown in Table IV.

Data for Analysis

Within the scope of this paper, the performance and loads data presented for analysis emphasizes the target lift and propulsive force parameters of Table III, but is limited to one rotational tip Mach number (0.65), and two advance ratios (0.35 and 0.40). The exception to this is the rotor track sensitivity data analysis which includes advance ratios of 0.20, 0.30, and 0.40.

Results

Rotor Performance

Fixed system forces and torque were obtained using the procedures and limits described earlier for all tip configurations for the test conditions listed in Table III. Parametric performance results for selected conditions are presented in Figure 6. The advance ratios and lift parameter, $C_{L/\sigma}$, conditions were selected for presentation because they showed the most significant difference in rotor performance between configurations. Below an advance ratio of .30, rotor performance differences were smaller for a given task.

The parametric effect of tip shape on rotor performance for the complete set of tips is shown in Figure 7. These diagrams present the percent reduction or increase in torque coefficient for a given rotor task for each tip shape. This method of presentation of rotor performance allows the separation of parametric geometry effects to be easily quantified. As an example, for the baseline blades tested and the conditions shown, the rotor's performance was enhanced by the addition of anhedral to a rectangular planform and the addition of sweep to the tapered planform. Tip taper improved rotor performance at μ = .35 conditions but not at higher speeds (μ = .40). Figure 6 shows that although tip configuration changes had measurable performance effects on torsionally soft and stiff blades, higher torque requirements were shown for the conformable rotor applications.

Rotor Loads

Blade oscillatory loads are important not only from vibratory fatigue considerations but also because they provide insight into the blade loading environment and elastic deformation trends. Torsional loads and flapwise oscillatory loads are associated with local blade loading and twist (ref. 8). Figure 8 presents 1/2 peak-to-peak flapwise loads at 4 spanwise stations for the configurations tested. These oscillatory loads are data points taken at the μ, M_T, $C_{L/\sigma}$ and α_s values listed for each tip configuration. The configurations are also ranked in Figure 8 according to their performance at the $C_{D/\sigma}$ values shown. Examination of Figure 8 shows a configuration variance in flapwise loads at each test condition as well as a significant relationship between performance and oscillatory flapwise loads. Specifically, the configurations which exhibited the lowest flapwise loads had the best performance characteristics while the poor performance configurations had the highest flapwise loads.

Elastic Twist

Spanwise distributions of blade torsional moment time histories were converted to elastic twist distributions through measured blade torsional stiffness properties. The deflections are shown in Figure 9 for all configurations tested at the μ, M_T, $C_{L/\sigma}$ and α_s values listed. Some interpolation of the inboard torsional loads occasionally was necessary. The elastic twist is configuration dependent for each rotor task and condition and, as might be expected, varies with rotor environment. The elastic twist waveforms are comprised of several harmonics, but are dominated by the one per rev torsional component.

The amount of azimuthal activity in the elastic twist plots is of interest, especially when it is compared with the integrated rotor performance for each configuration. The figure 9 waveforms have, in fact, been arranged in order according to each configuration's torque coefficient for the rotor tasks shown with the lowest torque configuration appearing first, and the highest torque configuration last in each case. A correlation between rotor performance and elastic twist is evident in the data shown. Specifically, the configurations which exhibited small azimuthal activity in elastic twist were the best performers.

Analysis of Results

General

The performance and loads data for the baseline and ACR configurations were examined to provide insight into the mechanism by which the tip planform and torsional stiffness parameters affected the aeroelastic behavior of the rotor blades. The designed differences between configurations were evaluated for the

fundamental changes they caused in the rotor's performance and response in light of past and current conformable design concepts, for example, elastic twist. Rigid blade analyses have been employed on this data (ref. 12). Although tip solidity effects on rotor performance were predicted fairly well using a non-uniform inflow analysis, the effects of certain tip parameters, such as anhedral, were inadequately predicted with regard to performance trends.

Blade Elastic Twist Magnitude

Past conformable rotor design concepts have considered the magnitude of advancing blade elastic twist as a solution to a potentially unfavorable angle of attack environment (ref. 2, for example). Depending on the tip airfoil section and advancing blade Mach number, a nose-up elastic twist was thought to be desirable to achieve lower rotor torque and blade loads. Figure 10 presents elastic twist magnitudes on the advancing side (ψ = 90°) for each configuration and rotor task shown. Figure 10 also contains the total geometric pitch angle for the above conditions, which is comprised of elastic twist, built-in twist, collective and cyclic pitch angles at ψ = 90°. Both types of blade angle data are also ranked according to their configuration's performance.

As is evident from Figure 10, there is no strong correlation between the magnitude of each configuration's advancing blade elastic or total pitch angle and the performance of the rotor. It is recognized that configuration performance and loads depend on local angle of attack which is affected by inflow distribution as well as pitch angle and that non-uniform inflow velocity can be very sensitive to planform configuration. Nevertheless, the design of a conformable rotor has received attention for achieving specific azimuthal placement of elastic twist magnitudes. The present studies do not support this as an ACR design goal.

Conformable Rotor Control

Conformable rotors which experience significant blade torsional response may generate rotor control characteristics which should be evaluated for their contributions to rotor stability and control (ref.8). Throughout the test program described herein, all configurations were easily controlled through the model actuator-swashplate system for all test conditions. The amount of control needed to achieve each rotor task was configuration dependent however, especially when comparing the torsionally soft rotor tip configurations with their corresponding baseline counterparts. Figure 11 shows, for a representative rotor task, the longitudinal cyclic pitch required to remove first harmonic flapping with respect to the rotor shaft for several configurations which differ in blade torsional stiffness.

The differences in longitudinal cyclic pitch for these configurations is significant not so much for control travel considerations, but for what these angles reveal about the rotor behavior for these tip shapes and torsional stiffnesses. Specifically, the differences in elastic twist measured for several configurations, shown in Figure 11a-c are offset by control input differences of nearly the same magnitude in order to remove the first harmonic flapping with respect to the rotor shaft. There were exceptions to this trend, notably for the swept tip (Figure 11d).

Another interesting connection was observed in both the pitch control required to trim the rotor and the rotor task achieved, in particular, the rotor propulsive force. For a given advance ratio, tip Mach number, force normal to the trimmed tip path plane, and shaft angle of attack, the torsionally soft rotor configurations consistently exhibit more positive rotor drag. This can be seen in the performance data of Figure 6. Examination of the rotor balance forces reveals that this increase in rotor drag occurs for two primary reasons. First, the control axis for the torsionally soft rotor has tilted aft due to the changes in longitudinal pitch mentioned above. Secondly, the rotor longitudinal force perpendicular to the control axis (H-force) is greater for the torsionally soft blade. The control axis aft-tilt is due to the test methodology used and the nose-down elastic twist magnitude observed. The H-force increase for the ACR configurations is probably due to integrated drag loading increases around the azimuth. This would also manifest itself in decreased rotor efficiency, a fact which was shown earlier in this paper for these configurations (Figure 6).

Blade Loading

It is well known that the radial and azimuthal distribution of rotor blade loading can affect both performance and loads. The potential of the conformable rotor concept to tailor these airloads has, in fact, been viewed as a key to the optimization of rotor performance (ref. 2). Specifically, a redistribution of airloads which avoids sharp radial and azimuthal gradients in loading and generates airload symmetry has been investigated for rotor performance improvement (ref. 15).

As previously shown, the rotor configurations described in this paper which exhibited good performance and low vibratory loads generated the least activity in elastic twist around the azimuth. Because several configurations provided significant aerodynamic center-elastic axis offsets, the elastic twist variations observed may be primarily due to oscillatory tip lift. Although section pitching moment variations may add to elastic twist perturbations around the azimuth, these would also be lift dependent.

It is therefore possible that the success of those configurations which exhibited low vibratory loads and increased performance is based on a redistribution of lift either radially or azimuthally, or both. This is reinforced by the previously mentioned rigid

blade analytical results (ref. 12) which correctly predicted no marked performance variations due to the small solidity differences between configurations. The cause of the apparent airload redistribution may be found in the parameter combinations which complement each other. For example, as has been shown previously in Figure 7, anhedral seems to aeroelastically help a baseline blade rectangular tip planform more that it does a swept-tapered planform. Furthermore, the addition of sweep for the baseline blade seems to enhance the aerodynamic environment of a tapered planform more than it does a rectangular tip for the configurations tested. The use of an aeroelastic analysis would be necessary to quantify this observation, but the test results included herein encourage this loading hypothesis.

Conformable Rotor Track Characteristics

General

The utilization of a conformable rotor concept should be evaluated not only for the measure of success with which it achieves its performance and loads goals, but also how well it can be "fielded." That is, how much change (if any) in current installation, maintenance, and rotor tuning is necessary for the new rotor concept to be employed. One aspect of this transition is rotor tracking sensitivity and its implications for rotor and fuselage loads.

Because the results of this study and others have indicated that the response of torsionally soft rotors to parametric changes can be significant, a track sensitivity study was initiated in which baseline and ACR blades with representative swept tips were subjected to a test matrix (Table IV) designed to perturb the track of one blade in the rotor. The perturbation was accomplished by use of trailing edge tab deflection. Specifically, the outermost two tabs (85-89 percent radius) were deflected 4 degrees down on the instrumented blade.

The use of trailing edge tabs for conformable rotor use has been described in ref. 8 for performance and ref. 16 for vibration. The use of trailing edge tabs in this study was for tracking sensitivity. Initially the tabs were undeflected and the rotor tracked in hover. One-per-rev longitudinal and lateral fixed-system loads were minimized through standard balance techniques. The rotors were then subjected to the forward flight conditions of Table IV. The forward flight process was then repeated for the deflected tabs and data acquired until either the test matrix was completed or loads became prohibitive.

Blade Torsion Due to Tab Deflection

The torsional blade loads are shown in Figure 12 for the tracking conditions. The data was chosen at a blade station just inboard of the deflected tab locations. The 0° tab cases show ACR mean nose-down moments greater than the baseline. The differences in loads would be expected to result in mean elastic twist differences similar to the trends observed earlier in this paper. The addition of tab deflection produces more nose down torsional moment for the ACR.

The oscillatory torsional moment of the ACR is comparable to the baseline rotor for 0° tab deflection, but is more sensitive to tab deflection than the baseline rotor's torsional load (Figure 12 c,d). The elastic twist resulting from these load perturbations would be expected to change the track and vibration characteristics of these rotors.

Blade Flapping Due to Tab Deflection

The flapping response of the instrumented blade to tab deflection is shown in Figure 13 for both rotors. As mentioned previously, the other three blades of each rotor were trimmed to the rotor shaft for all conditions, so that the flapping of the instrumented blade, above the mean coning, is a measure of out-of-track sensitivity.

The ACR coning for both 0° tab and 4° tab shows the effect of large mean elastic twist for this rotor as well as the increased sensitivity to tab deflection. The baseline rotor exhibits, as expected, less mean elastic twist, and hence, less effect on coning. The one-per-rev flapping (Figure 13 c,d) for the ACR blade shows a large (3.5 degrees) out-of-track sensitivity due to tab deflection, compared to that of the baseline. This phenomenon may also be due to the large ACR oscillatory elastic twist produced by tab deflection.

Flapwise Blade Loads Due to Tab Deflection

The effect of elastic twist changes to inboard blade loading is of interest for blade life and fixed system vibratory loads implications. Figure 14 shows the effect of blade configuration and tab deflection on the inboard flap loading. As might be expected from the steady elastic twist and coning data shown previously, the ACR loading shifts inboard with tab deflection and the mean inboard flapwise moment sharply drops.

In like manner Figure 14 c,d shows the effect of oscillatory elastic twist, caused by tab deflection, on the oscillatory flapwise loads for both rotors. The ACR flapwise moment appears more sensitive to tab deflection than that of the baseline rotor. These loads should manifest themselves in fixed-system vibrations as discussed in the next section.

Fixed System Vibrations Due to Tab Deflection

The blade torsional response to a parameter change such as tab deflection has thus been shown to affect blade track and blade loads. Both blade track and loads are transferred to the fixed system, an obvious practical consideration to the vibration of the helicopter during tracking procedures. Figure 15 shows that the one-per-rev vertical load in the fixed system is much more sensitive to the 4 degree tab deflection for the

torsionally soft rotor than for the baseline. This was also observed (but not shown herein) for the fixed system in-plane loads. It is also interesting that the undeflected tab configuration for the ACR produced more fixed system one-per-rev vertical loading than the baseline. This occurred even though the ACR inboard oscillatory flapwise load for 0° tab was only slightly greater than the baseline's.

Although the reduced torsional stiffness of the ACR affords greater torsional deflection for a given tab input, the implied increase in tracking capability should be weighed against the above results. These results indicate a potential coupling of blade torsional deflection, blade oscillatory loads, and fixed system vibration which results from a high sensitivity of the conformable rotor to practical tracking procedures.

Conclusions

Based on the data obtained for the test conditions and model configurations investigated, the following conclusions have been reached:

1. Significant performance and loads differences were generated by tip geometry variations.

2. Torsionally soft rotor (ACR) applications for the tip shapes tested resulted in substantially different performance and loads than for the baseline configuration.

3. Elastic torsional deflection varied with tip shape and operating conditions for both the baseline blade and the torsionally soft blade.

4. There exists a strong correlation between azimuthal variation of elastic twist and rotor performance and loads.

5. There does not exist a strong correlation of advancing blade elastic twist magnitude with rotor performance or loads.

6. Fixed system vibratory loads and rotor track for potential ACR candidates appear very sensitive to parametric rotor changes.

References

1. Doman, Glidden S.; Tarzanin, Frank J.; and Shaw, John, Jr.: Investigation of Aeroelastically Adaptive Rotor Systems. Proceedings of a Symposium on Rotor Technology, American Helicopter Society, August 1976.

2. Blackwell, R. H.; and Merkley, D. J.: The Aeroelastically Conformable Rotor Concept. Preprint No. 78-59. American Helicopter Society, May 1978.

3. Berry, John D.; and Mineck, Raymond E.: Wind-Tunnel Test of an Articulated Helicopter Rotor Model With Several Tip Shapes. NASA TM 80080, 1980.

4. Stroub, Robert H.; Rabbott, John P., Jr.; and Niebanck, Charles F.: Rotor Blade Tip Shape Effects on Performance and Loads From Full-Scale Wind-Tunnel Testing. Journal of the American Helicopter Society, Volume 24, No. 5, October 1979, pp. 28-35.

5. Philippe, J. J.; and Vuillet, A.: Aerodynamic Design of Advanced Rotors with New Tip Shapes. 39th Annual Forum Proceedings, American Helicopter Society, May 1983.

6. Weller, William H.: Experimental Investigation of Effects of Blade Tip Geometry on Loads and Performance for an Articulated Rotor System. NASA TP 1303, 1979.

7. Sutton, Lawrence R.; White, Richard P., Jr.; and Marker, Robert L.: Wind-Tunnel Evaluation of an Aeroelastically Conformable Rotor. USAAVRADCOM-TR-81-D-43, 1982.

8. Blackwell, R. H.; Murrill, R. J.; Yeager, W. T., Jr.; and Mirick, P. H.: Wind-Tunnel Evaluation of Aeroelastically Conformable Rotors. Preprint No. 80-23, 36th Annual Forum Proceedings, American Helicopter Society, May 1980.

9. Yeager, William T., Jr.; and Mantay, Wayne R.: Wind-Tunnel Investigation of the Effects of Blade Tip Geometry on the Interaction of Torsional Loads and Performance for an Articulated Helicopter Rotor. NASA TP 1926, 1981.

10. Yeager, William T., Jr.; and Mantay, Wayne R.: Loads and Performance Data From a Wind-Tunnel Test of Model Articulated Helicopter Rotors with Two Different Blade Torsional Stiffnesses. NASA TM 84573, 1983.

11. Blackwell, R. H.; and Frederickson, K. C.: Wind-Tunnel Evaluation of Aeroelastically Conformable Rotors. USAAVRADCOM-TR-80-D-32, 1981.

12. Mantay, Wayne R.; and Yeager, William T., Jr.: Parametric Tip Effects for Conformable Rotor Applications. NASA TM 85682, 1983.

13. Lee, Charles: Weight Considerations in Dynamically Similar Model Rotor Design. SAWE Paper No. 659, May 1968.

14. Hunt, G. K.: Similarity Requirements for Aeroelastic Models of Helicopter Rotors. C. P. 1245, Royal Aircraft Establishment, 1973.

15. Moffitt, Robert C.; and Bissell, John R.: Theory and Application of Optimum Airloads to Rotors in Hover and Forward Flight. 39th Annual Forum Proceedings, American Helicopter Society, May 1982.

16. Kottapalli, S. B. R.: Hub Loads Reduction by Modification of Blade Torsional Response. 39th Annual Forum Proceedings, American Helicopter Society, May 1983.

TABLE IA. Model Blade Properties

Baseline Blade

INBOARD SECTION r/R	SECTION LENGTH (ft)	SECTION MASS (slugs)	STIFFNESS (lb-ft^2) FLAP	CHORD	TORSION	I_θ (lb-sec^2) X10^{-3}
.0534	.322	.051	101,944.	104,166.7	6,763.9	.57
.1222	.166	.011	9,326.4	69,444.4	1,269.6	.143
.1577	.333	.0062	9,326.4	2,777.8	432.1	.05
.2288	.333	.0062	74.3	2,777.8	236.1	.05
.2999	.333	.0062	74.3	2,777.8	88.9	.05
.371	.333	.0062	74.3	2,777.8	88.9	.08
.4421	.333	.0062	81.3	2,777.8	91.6	.08
.5132	.333	.0062	75.7	2,777.8	93.1	.08
.5843	.333	.0062	81.3	2,777.8	94.4	.08
.6554	.333	.0062	81.3	2,777.8	94.4	.08
.7265	.333	.0062	81.3	2,777.8	94.4	.08
.7976	.333	.0062	86.8	2,777.8	92.4	.08
.8687	.207	.0054	33.3	694.4	95.4	.117
.9128	.073	.0024	33.3	694.4	27.1	.117
.9283	.336	.0045	21.5	347.2	22.0	.117

Rotating Natural Frequencies at Ω = 68.07 rad/sec

MODE	ω/Ω
Flap	2.68
Flap	4.98
Chord	5.08
Torsion	6.14
Flap	8.17

TABLE IB. Model Blade Properties

ACR Blade

INBOARD SECTION r/R	SECTION LENGTH (ft)	SECTION MASS (slugs)	STIFFNESS (lb-ft^2) FLAP	CHORD	TORSION	I_θ (lb-sec^2) X10^{-3}
.0534	.322	.05111	102,083.3	104,166.7	6,763.9	.57
.1222	.166	.0111	9,326.4	69,444.4	1,269.6	.143
.1577	.333	.00618	9,326.4	2,777.8	432.1	.05
.2288	.333	.00616	75.7	2,777.8	230.7	.05
.2999	.333	.00616	75.7	2,777.8	85.4	.05
.371	.333	.00612	75.7	2,569.4	85.4	.08
.4421	.333	.0061	78.5	2,569.4	68.6	.08
.5132	.333	.0061	75.0	2,569.4	33.5	.08
.5843	.333	.0061	71.5	2,569.4	24.1	.08
.6554	.333	.0061	71.5	2,569.4	22.9	.08
.7265	.333	.0061	71.5	2,569.4	22.9	.08
.7976	.333	.0061	88.9	2,569.4	26.2	.08
.8687	.207	.0054	59.7	694.4	27.8	.117
.9128	.073	.0024	59.7	694.4	33.3	.117
.9283	.336	.0045	20.8	347.2	22.3	.117

Rotating Natural Frequencies at Ω = 68.07 rad/sec

MODE	ω/Ω
Flap	2.65
Torsion	4.48
Flap	4.93
Chord	4.98
Flap	8.17

Table II. Model Rotor Blade Tip Characteristics

Parameter	Tip c.g. location (in.)		Tip weight (grms)	Tip twist (deg)	c.g.-a.c. / c (pos. c.g. forward)			$I_{1/4c}$ ($ft\text{-}lb\text{-}sec^2$)
Design Target	Chordwise 1.236	Spanwise 2.774	71	1.35	.96R	.98R	1.0R	x 10^{-5} .955R to R
Tip Configuration								
Rectangular	1.30	2.75	73.1	1.27	.028	-.05	.02	.448
Tapered	1.24	2.82	73.4	1.27	-.014	-.056	.007	.197
Swept	1.50	2.85	73.6	1.27	.096	-.04	.019	.56
Swept Tapered	1.31	2.94	71.4	1.27	.096	.017	.008	.371
Rectangular Anhedral	1.31	2.75	71.1	1.14	.028	-.05	.02	.448
Swept Anhedral	1.48	2.96	70.4	.93	.096	-.04	.019	.56
Swept Tapered Anhedral	1.25	3.00	71.8	1.27	.096	-.017	.008	.371

Rotor Solidity

	Tapered Configurations	Non-tapered Configurations
Area solidity	.08127	.08252
Thrust-weighted solidity	.07905	.08263
Torque weighted solidity	.07793	.08259

Table III. Target Test Conditions

μ	M_T	α_s	$\frac{C_L}{\sigma}$	α_s	$\frac{C_L}{\sigma}$	α_s	$\frac{C_L}{\sigma}$
.30	.65 .68 .70	-6.0°,-7.8°	.06	-4.5°,-5.9°	.08	-3.6°,-4.7°	.10
.35	.65 .67	-8.2°,-10.5°	.06	-6.1°,-7.9°	.08	-4.9°,-6.3°	.10
.40	.63 .65	-10.6°,-13.6°	.06	-8.0°,-10.3°	.08	-6.4°,-8.3°	.10

Table IV. Track Sensitivity Test Conditions

μ	α_s	$\frac{C_L}{\sigma}$	Tab Deflection	M_T
.05 .20 .30 .40	0° 0° -5° -10°	.075	0°, 4° down	.65

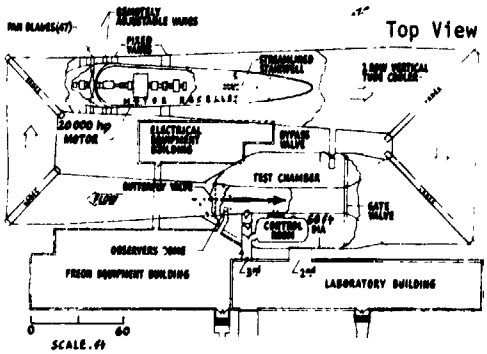

Fig. 1 Langley Transonic Dynamics Tunnel.

Fig. 2 Aeroelastic rotor experimental system (ARES) model in Langley Transonic Dynamics Tunnel.

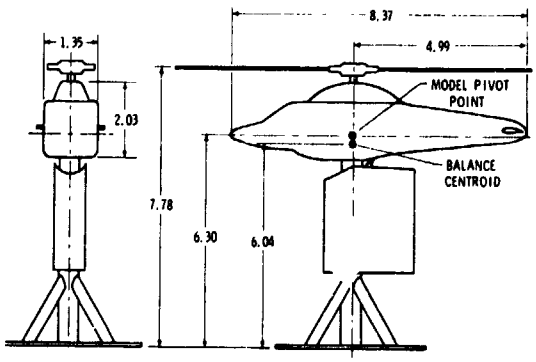

Fig. 3 Schematic diagram of aeroelastic rotor experimental system. All dimensions are in feet.

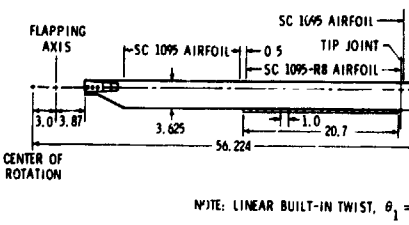

Fig. 4 Rotor blade geometry. Blade dimensions are in inches.

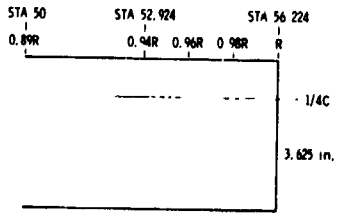

(a) Rectangular

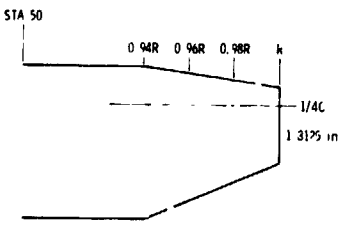

(b) Tapered

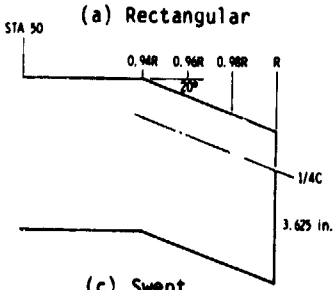

(c) Swept

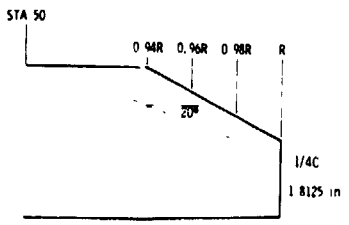

(d) Swept Tapered

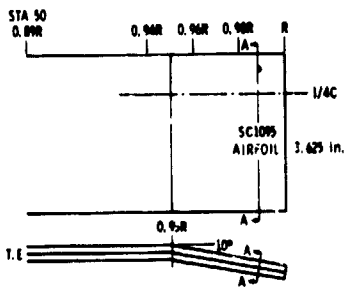

(e) Rectangular Anhedral

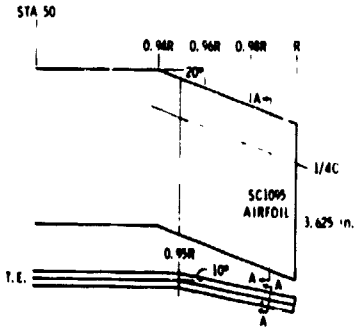

(f) Swept Anhedral

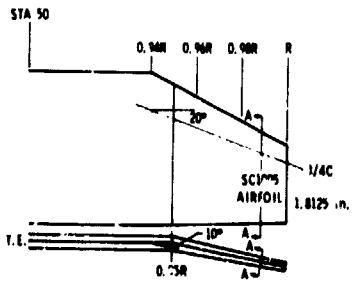

(g) Swept Tapered Anhedral

Fig. 5 Geometry of tips tested. Dimensions are in inches unless otherwise indicated.

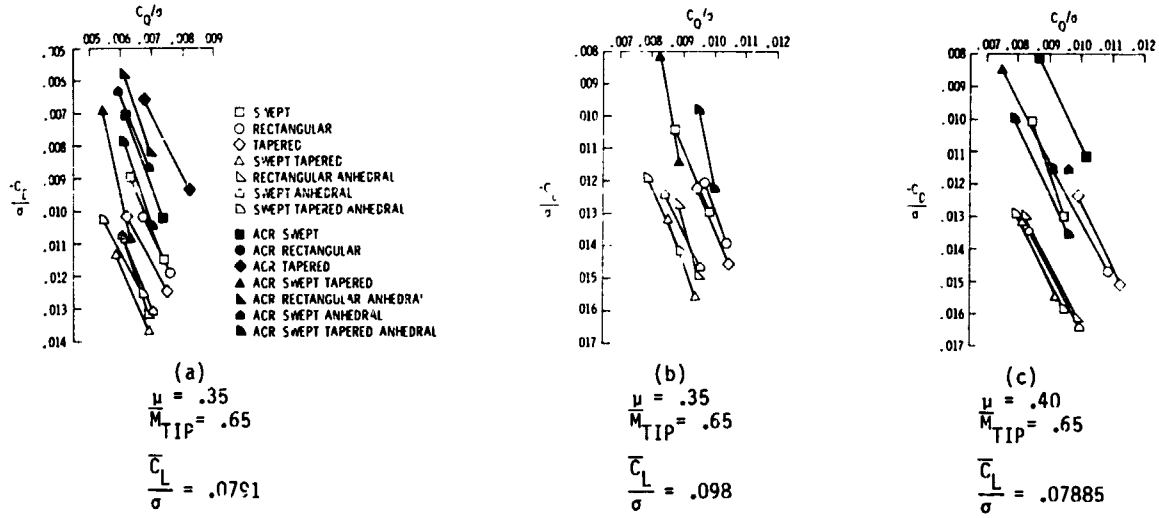

(a)
μ = .35
M_{TIP} = .65
$\frac{\overline{C}_L}{\sigma}$ = .0791

(b)
μ = .35
M_{TIP} = .65
$\frac{\overline{C}_L}{\sigma}$ = .098

(c)
μ = .40
M_{TIP} = .65
$\frac{\overline{C}_L}{\sigma}$ = .07885

Fig. 6 Experimental rotor performance.

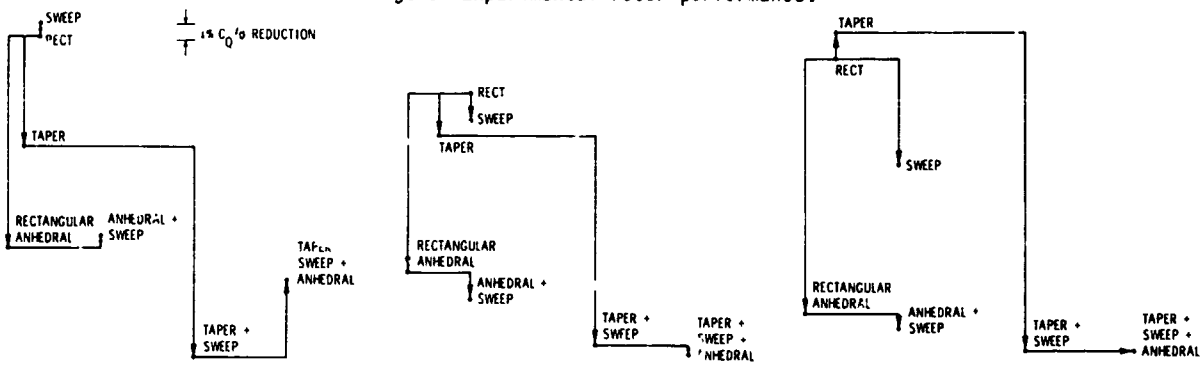

(a)
μ = .35
M_T = .65
$\frac{\overline{C}_L}{\sigma}$ = .07872
$\frac{C_D}{\sigma}$ = -.0110

(b)
μ = .35
M_T = .65
$\frac{\overline{C}_L}{\sigma}$ = .098
$\frac{C_D}{\sigma}$ = -.01325

(c)
μ = .40
M_T = .65
$\frac{\overline{C}_L}{\sigma}$ = .07885
$\frac{C_D}{\sigma}$ = -.0145

Fig. 7 Parametric tip shape effect on experimental baseline rotor performance.

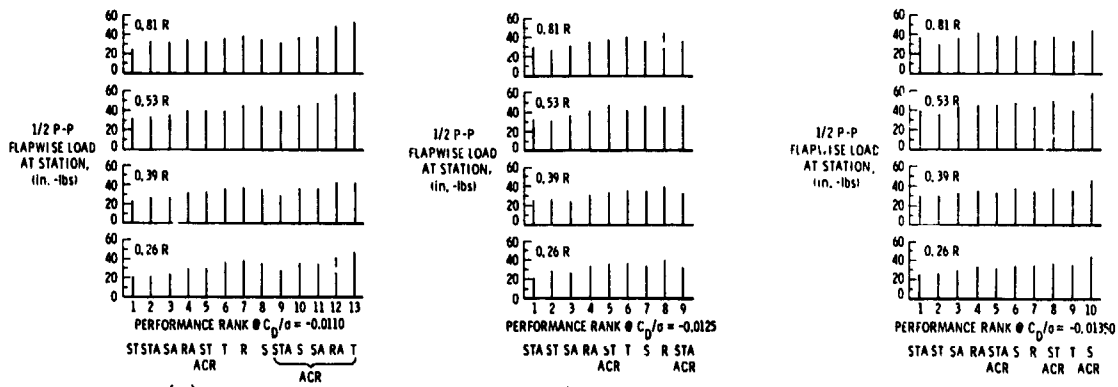

(a)
μ = .35
M_T = .65
$\frac{\overline{C}_L}{\sigma}$ = .0791
α_s = -6.1°

(b)
μ = .35
M_T = .65
$\frac{\overline{C}_L}{\sigma}$ = .098
α_s = -4.9°

(c)
μ = .40
M_T = .65
$\frac{\overline{C}_L}{\sigma}$ = .07885
α_s = -8.0°

Fig. 8 Flapwise oscillatory blade loads versus rotor performance.

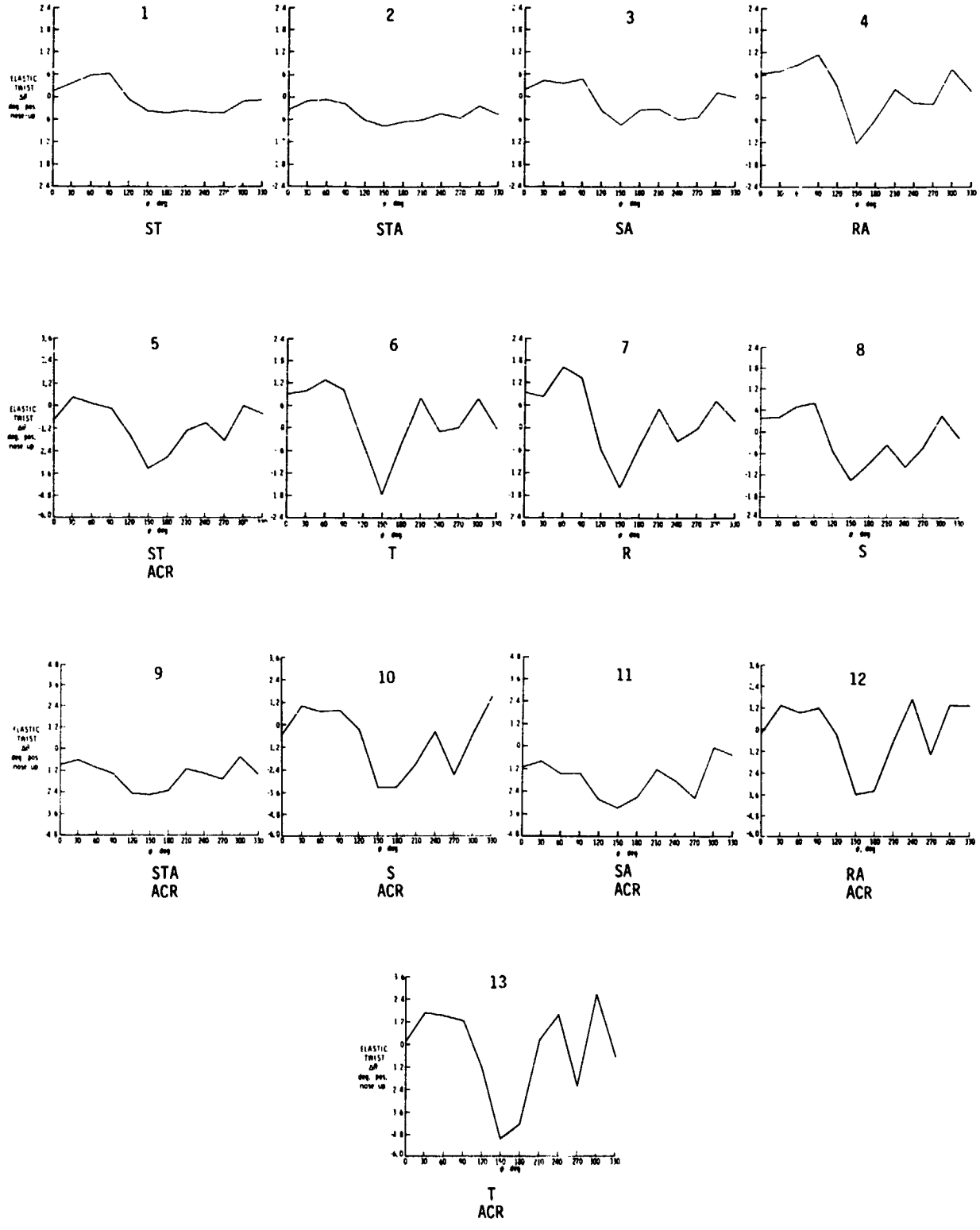

(a) $\mu = .35$, $M_T = .65$, $\frac{\bar{C}_L}{\sigma} = .0791$, $\alpha_s = -6.1°$. Performance rank at $C_D/\sigma = -.0110$

Fig. 9 Radial distribution of elastic twist versus azimuth at .78R.

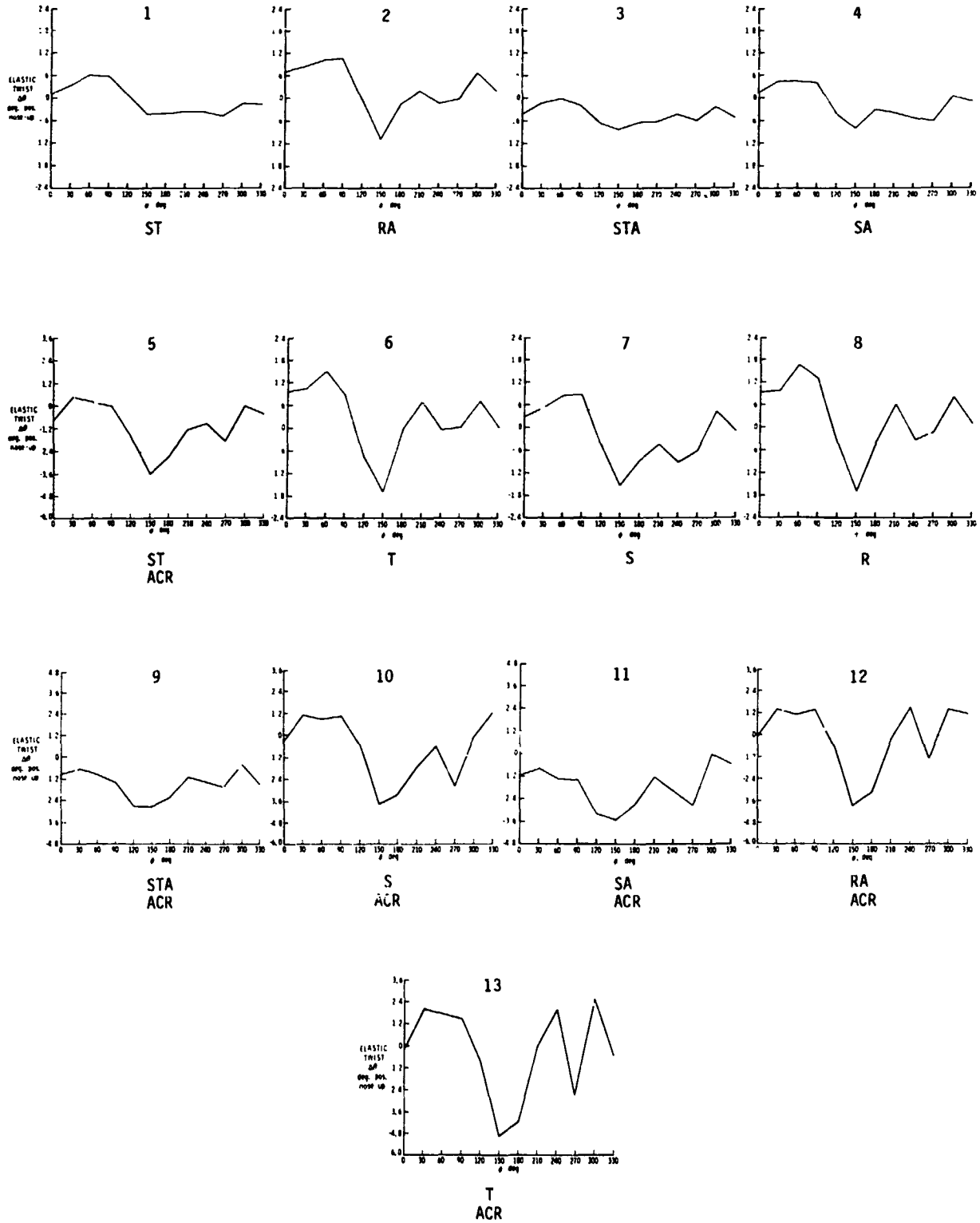

(b) $\mu = .35$, $M_T = .65$, $\frac{C_L}{\sigma} = .0791$, $\alpha_s = -7.9°$. Performance rank at $C_D/\sigma = -.01250$

Fig. 9 Continued.

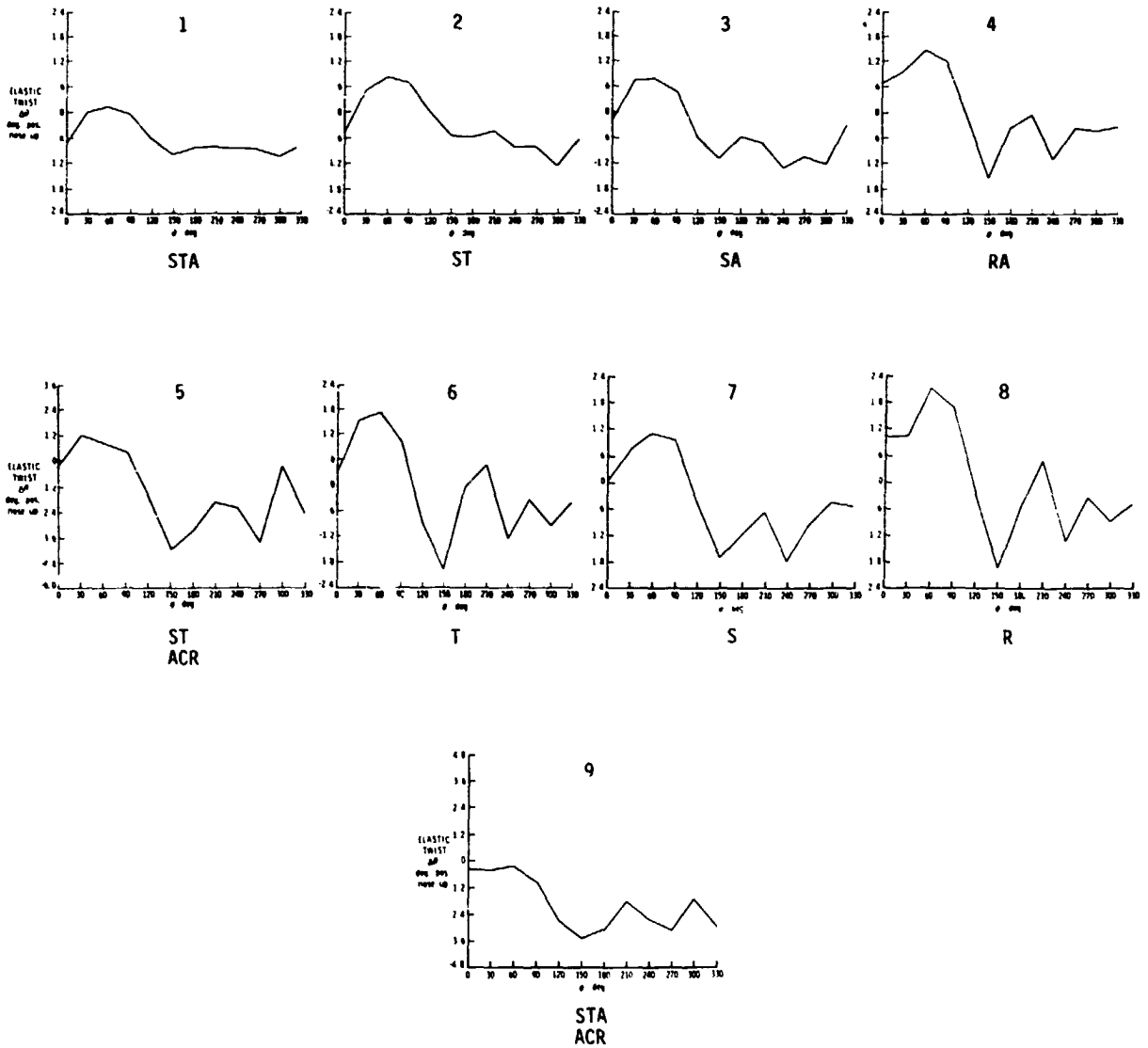

(c) $\mu = .35$, $M_T = .65$, $\frac{\tau_L}{\sigma} = .098$, $\alpha_s = -4.9°$. Performance rank at $C_D/\sigma = -.0125$

Fig. 9 Continued.

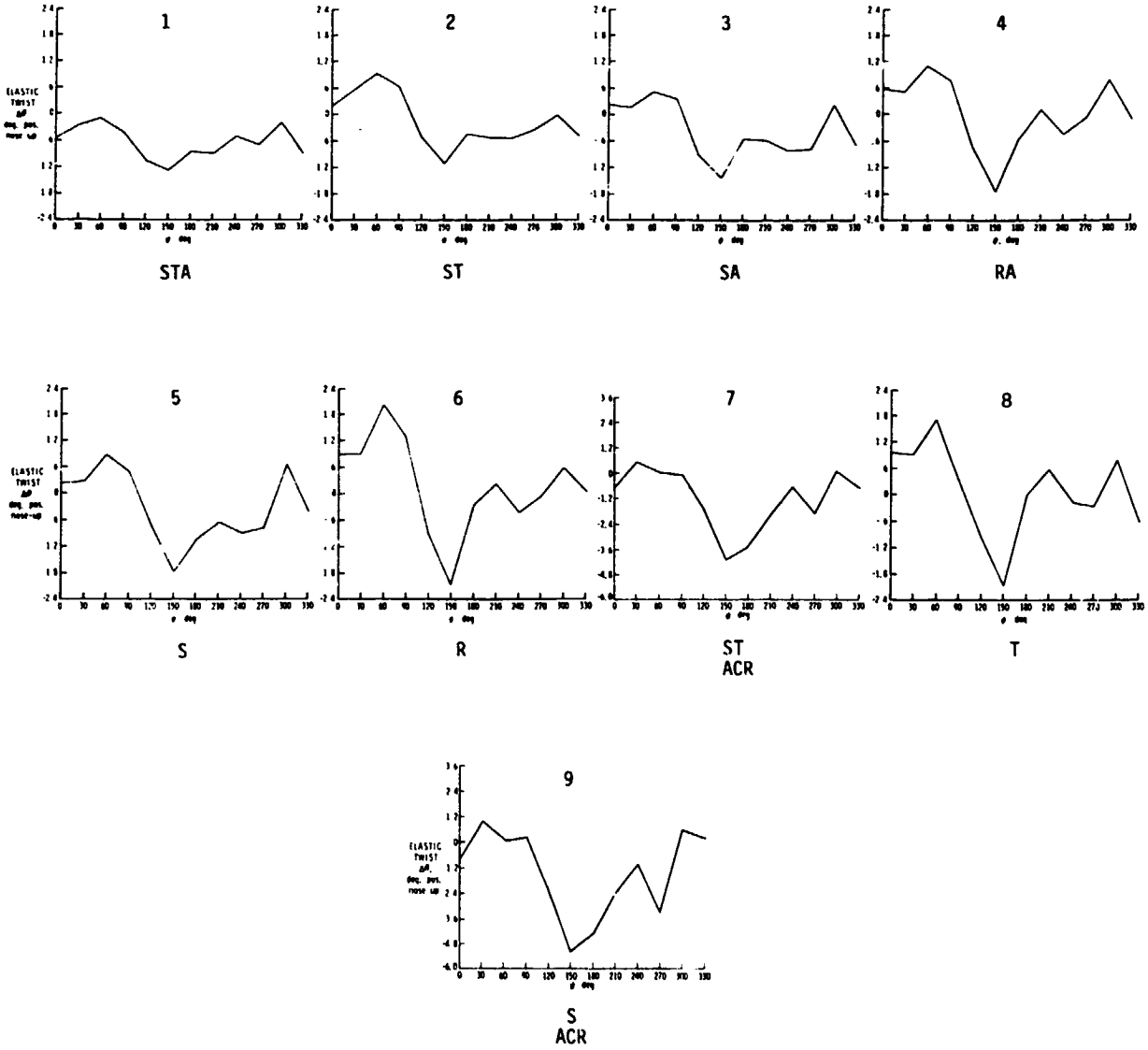

(d) $\mu = .40$, $M_T = .65$, $\frac{\bar{C}_L}{\sigma} = .07885$, $\alpha_s = -8.0°$. Performance rank at $C_D/\sigma = -.01350$

Fig. 9 Concluded.

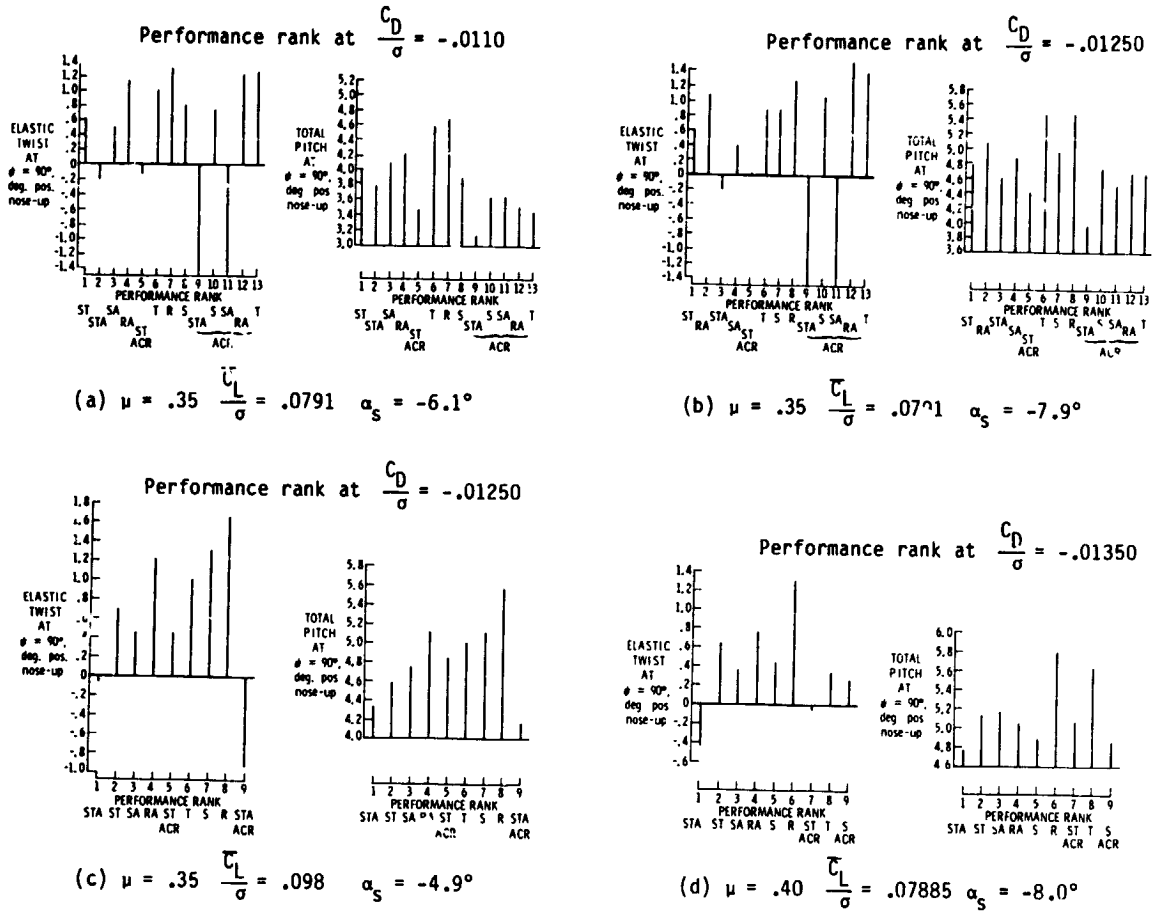

Fig. 10 Advancing side tip elastic twist and total pitch versus configuration performance (r/R = .78 M_T = .65).

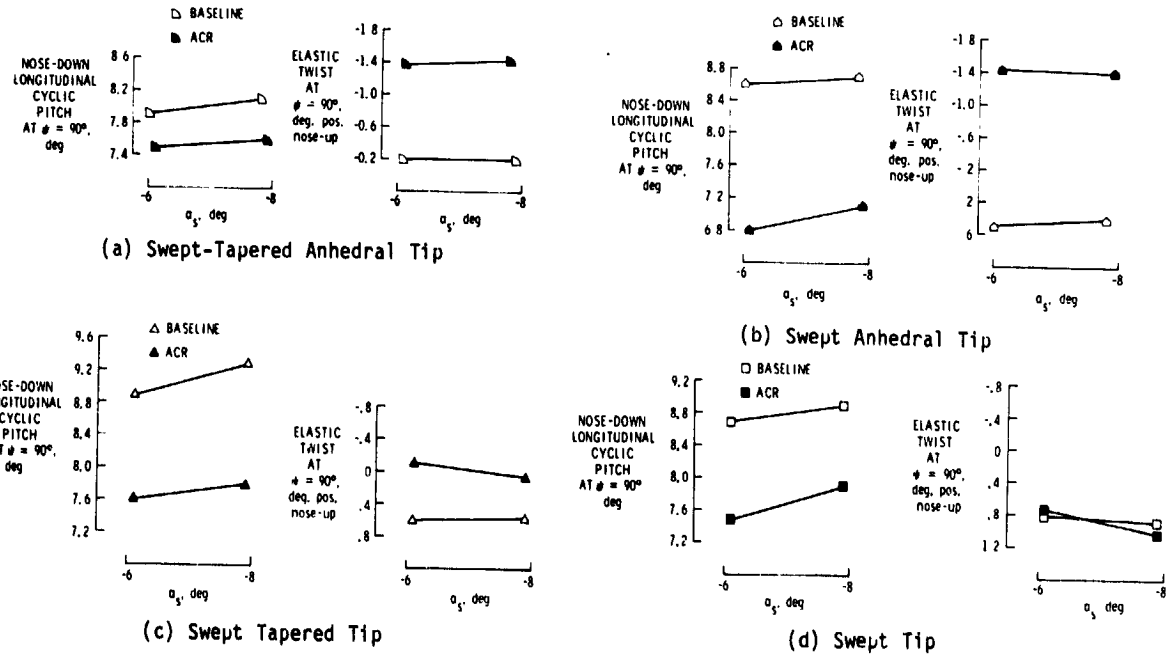

Fig. 11 Advancing blade control angle and elastic twist versus α_S (μ = .35, M_T = .65, $\bar{C}_L/\sigma$ = .08).

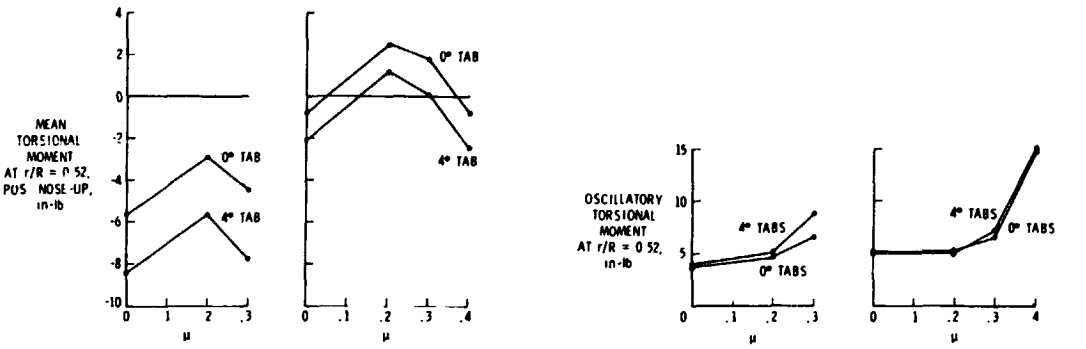

(a) ACR/Swept Tip (b) Baseline/Swept Tip (c) ACR/Swept Tip (d) Baseline/Swept Tip

Fig. 12 Effects of tab deflection on mean and oscillatory outboard torsional moments (M_T = .65, $\frac{\bar{C}_L}{\sigma}$ = 0.075).

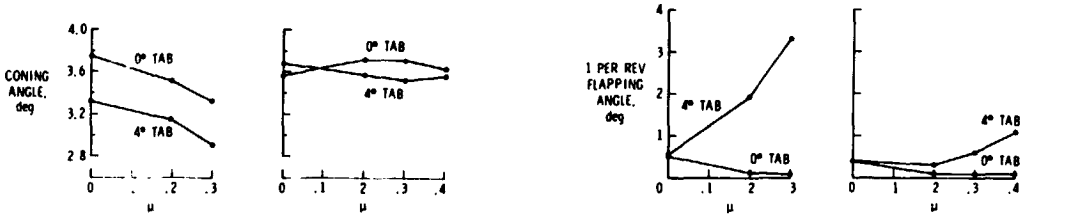

(a) ACR/Swept Tip (b) Baseline/Swept Tip (c) ACR/Swept Tip (d) Baseline/Swept Tip

Fig. 13 Effect of Tab Deflection on Blade Coning and First-Harmonic Flapping Angles (M_T = .65, $\frac{\bar{C}_L}{\sigma}$ = 0.075).

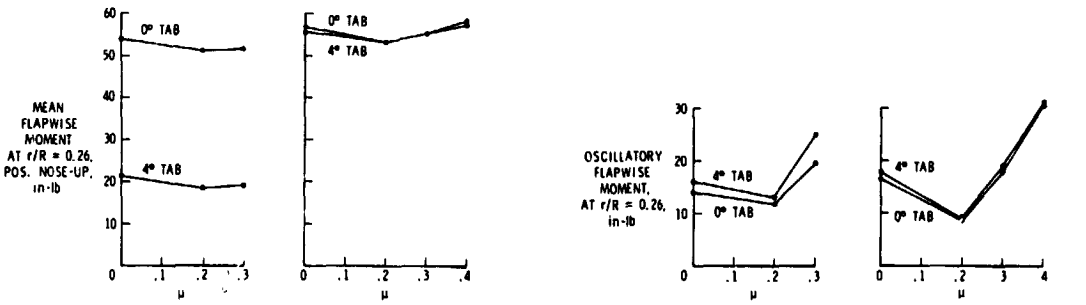

(a) ACR/Swept Tip (b) Baseline/Swept Tip (c) ACR/Swept Tip (d) Baseline/Swept Tip

Fig. 14 Effect of Tab Deflection on Mean and Oscillatory Inboard Flapwise Loads (M_T = .65, $\frac{\bar{C}_L}{\sigma}$ = 0.075).

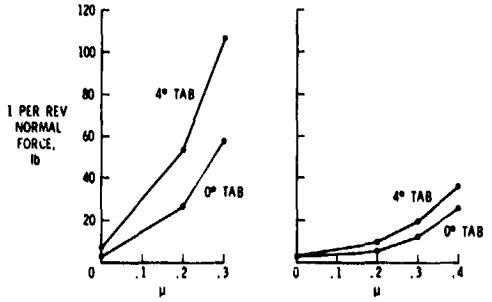

(a) ACR/Swept Tip (b) Baseline/Swept Tip

Fig. 15 Effect of Tab Deflection on Fixed System Normal Loads (M_T = .65, $\frac{\bar{C}_L}{\sigma}$ = 0.075).

DISCUSSION
Paper No. 9

AEROELASTIC CONSIDERATIONS FOR TORSIONALLY SOFT ROTORS
Wayne R. Mantay
and
William T. Yeager, Jr.

Bill Weller, United Technologies Research Center: In going from good to bad on your scales, the decreased elastic twist activity seemed to be at 2 per rev and above in harmonic order. But on the best performing rotor system you still had a 1 per rev activity, elastic twist activity that was nose up on the advancing side?

Mantay: That's correct.

Weller: Did you decompose your data to find out that perhaps higher harmonic elastic twist activity is bad, but that the 1 per rev activity might be beneficial, particularly the sin ψ type activity?

Mantay: We have tried to look at that in every way that we can. Let me tell you what we did do. We decomposed the waveforms, the energy in those gauges, before we integrated. We decomposed them into the first eight harmonics. Everything that you see there has all of those eight harmonics in it. In other words, if it was there, Bill, it would have bitten us. We didn't see it in most of our good performers. That's not to say they wouldn't be there and wouldn't be great contributors in other configurations, but for ours we didn't see it. There was mainly a 1 per rev.

Weller: That's what I'm saying. Is there some kind of correlation that 1 per rev activity might be particularly beneficial where higher harmonic activity is detrimental?

Mantay: We don't know that to be sure, but in the paper you will see if you look at some of the figures that have these waveforms there does seem to be a trigger level. The first two or three configurations that did well seem to be predominantly 1 per rev. On the performance groupings, they were close together. The greatest gradient in separation from good performance seemed to come when that harmonic trigger was triggered. Of course, all we saw in addition to the 1 per rev was the 2, but that may be the culprit, I don't know. And yet looking back historically at 10, 15 or more years ago to some of the start of this ACR, cos 2ψ, that was being advocated as a way to. I'm not sure I'm getting this right, but I think that was for propulsive force enhancement and that didn't show up with us. We stumbled over a lot of anomalies I guess.

Charlie Frederickson, Sikorsky Aircraft: I see did some work on the blade tab bending for one blade only and not surprisingly got a tremendous increase in your 1P vertical forces. Did you do any work at all in tabbing all four blades and see what effect that had on the 4P vibratory forces?

Mantay: We did not. I might mention that some of the tests that preceded ours by a year or two did deflect all tabs on all four blades for torsional twist-tailoring. There have been some fixed system 4 per rev data published by Bob [Blackwell], Bill Yeager and others which have shown some trends there. But to answer your question directly, no we did not bend just the two tabs on all four blades and look at the 4P in this study.

Jim Biggers, Naval Ship R&D Center: [You have] a really good set of correlations there [and] detective work on your part; you are to be commended for that. I want to ask you to dig a little deeper and see if there isn't also a correlation, particularly in the loads area with coupling of other blade modes like coupling of the torsion with a second flap bending and things of that nature.

Mantay: We have not looked at that.

Biggers: Let me encourage you to look for that.

Mantay: Okay.

Peretz Friedmann, University of California, Los Angeles: I think your endeavor is a very commendable one. This data base as you call it is probably very useful. To somebody who might want to try to compare an analysis which has a swept tip capability with the data which you have generated, I have a very basic question. Is the test which you have conducted, one, where if you took four isolated blade analyses and combined them would give you a good analytical tool, or due to the nature of the model which you have used [does] one have to use a coupled rotor fuselage-type model?

Mantay: Peretz, let me tell you what we intend to do analytically. I'll answer your question directly, but I would like to expand on it a tiny bit. I don't think we need a coupled rotor

fuselage analysis for it. We are trying to pick apart some of the causes and effects. Some we are doing on our own and some we have contractual arrangements to do. We are looking at, for instance, VSAERO to try to look at the aerodynamics. We have used a rigid blade analysis which was more of something to check off what we did. It was fairly useless. The solidity changes between the tips were well predicted, but in terms of the response in the integrated performance for some of the more exotic tips, that analysis which was a rigid blade, was abysmal. It was pretty useless. So we recognize that we need to pick apart some of the causes and effects analytically. When we do combine them, and we may within this next calendar year, we in all likelihood will not incorporate a coupled rotor fuselage analysis to do it. Certainly not as a first step; maybe not even as a second.

Bob Jones, Kaman: Naturally, we have worked with soft rotors for many, many years and, yes, it is a very sensitive rotor. Therefore, as Bob pointed out, you have many design parameters that you can use to achieve your total performance of the rotor. One thing I do want to point out is don't be discouraged from the standpoint that maybe the performance and even vibration went to pot because if you change your modal content of torsion you can get entirely different results. So you can still have a soft rotor, but you should fool around maybe with your GJ distributions and things like this and you can optimize from that standpoint. Ballasting of the blades can affect these results tremendously because of this type of coupling. So just let's not throw out soft rotors because you have got poor results is really what it comes down to. It takes a lot of analysis and a lot of flight testing to optimize a system like this. Tracking is going to be a very major problem. We've run into that at Kaman and you will too in soft rotors.

Mantay: I guess my comment to that, Bob, is that I wouldn't disagree with you and certainly we are not giving up on soft rotors. I hope my last comment reflected that. But I would say, which may add to what you said, I hope, that we saw the need to well-control some of the parameters we looked at to make sure we knew what was there. It was just for the configurations we looked at and on that same rotor from the tip inboard, Bob [Blackwell] was involved, in fact, in some tests at Langley that indicated that up tab deflections of 8 degrees or so actually did fairly well in terms of loads and performance.

Bob Blackwell, Sikorsky Aircraft: I want to comment about that the [statement] that says that the torsional softening of the blade would do . . . the statement [was] never really intended that softening of the blade by itself would do anything. Anhedral, or swept tip, or taper on a soft blade presumably would allow it to do just more of what it wanted to do which was to twist nose down on the advancing side; none of those things particularly tried to arrest that. So Wayne's efforts to try to correlate the twist on the advancing blade or the pitch on the advancing blade, whatever--I have been through the same fruitless exercise in trying to understand exactly what causes what. The point was that these blades were soft and as such they twisted more nose down. Despite the fact that I agree there weren't clear trends, if you step back far enough from the data you can say that softer blades sort of twisted down on the advancing side and throughout the second quadrant; maybe 90 degrees is the place to quote but maybe 150 if I looked at some of your plots. That might be a better indicator. But the blade basically had more drag on the advancing side, hence the H-force, hence the increased torque and that's entirely in keeping with what we said. If we could arrange a way through some parameter--and camber [and] airfoil pitching moment was an effective one--to in fact prevent that from happening then that's what we set out to talk about before. We have proven that if the blades twist down more [then] they will do worse than they would if they hadn't. That's clear.

Bob Hansford, Westland Helicopters: In moving to softer torsional blades, how important do you now think it is that we should be able to predict the shear center of the blade properly to get an accurate prediction? This can cause us some problems when applying it to production blades.

Mantay: I don't know. I wouldn't want to venture on a guess on a design guide, but I would say I think it would depend on how exotic the tip aerodynamics was. In other words, how much aerodynamic center-elastic axis offset you had. We were concerned about that and that's why we didn't get more ambitious than we did in terms of tip shape. We wanted to keep the shear center that was on the inboard section constant. I guess what Bob Jones was suggesting GJ and other tailoring inboard of that if it's done well--terrific, that adds to the data base. If it's done poorly as I imply from your comment, then we could just have another parameter in there muddying waters.

Bob Hansford: That's right. This could be an extra parameter, now, that you could consider just as important as c.g. and a.c. offset.

OPTIMAL DESIGN APPLICATION ON THE ADVANCED AEROELASTIC ROTOR BLADE

Fu-Shang Wei
Senior Aeromechanics Engineer
and
Robert Jones
Assistant Director of Aeromechanics
Kaman Aerospace Corporation
Bloomfield, Connecticut 06002-0002

Abstract

The vibration and performance optimization procedure using regression analysis has been successfully applied to an advanced aeroelastic blade design study. The major advantage of this regression technique is that multiple optimizations can be performed to evaluate the effects of various objective functions and constraint functions. In this application, the data bases obtained from the rotorcraft flight simulation program C81 and Myklestad mode shape program are analytically determined as a function of each design variable. Those predicted results from regression equations, such as performance, vibration, and modal parameters, when compared with C81 and Myklestad outputs, correlate exceptionally well. The regression equations also predicted the minimum of 4/rev total vertical hub shear based on the coefficients of each equation. This approach has been verified for various blade radial ballast weight locations and blade planforms. This method can also be utilized to ascertain the effect of a particular cost function which is composed of several objective functions with different weighting factors for various mission requirements without any additional effort. Utilization of this technique can significantly reduce the engineering efforts and computer time to optimally design a high performance and low vibration blade.

Introduction

It is highly desirable for most helicopter engineers to design a vehicle having high performance and low vibrations (References 1 - 13). With a best dynamic blade as an input to the airloads program, the blade having minimum vibration and maximum performance under certain constraints could be determined by using an existing optimization code; or vice versa, from an optimized airloads distribution to find a desired blade planform. Blade dynamic and aerodynamic effects are coupled within the design range of interest. Separation of these effects during the design procedure may not be possible to obtain the best result that one expects. Therefore, the approach which can be utilized to optimize dynamic and aerodynamic effects is strongly recommended.

Vibration and performance data generated from C81 and the coefficients of modal participation factor (CMPF) of hub shear and hub moment generated from Myklestad can be analytically expressed as a function of each design variable using regression analysis (References 14 - 20). Regression equations not only directly provide the sensitivity of each blade design variable, but also combine both dynamic and aerodynamic effects within the overall design procedure. Furthermore, regression technique need not be performed in a continuous run; it may be carried out individually or in groups, as convenient. This technique can also treat numerous design variables, objective functions, constraint functions, and various combinations of several objective functions in a convenient manner. After the data base is obtained from the technique program, the optimization criteria can be varied, based on various mission requirements. Therefore, a significant savings on computer time and engineering efforts have been achieved.

The optimization procedure of the regression analysis was first used at Kaman in its analytical studies of the Controllable Twist Rotor in developing secondary control requirements to minimize vibration, with constraints on horse-power, angle of attack, and blade bending moments. This control optimization was done for both steady and one-per-rev controls, as well as for higher harmonic controls (Reference 20). Blade controls on the full scale Multicyclic Controllable Twist Rotor with higher harmonics were optimized experimentally by using wind tunnel results for the data base (Reference 17).

The optimization procedure was also used to investigate the effects of several blade design parameters as independent

Presented at the 2nd Decennial Specialist Meeting on Rotorcraft Dynamics, Moffett Field, CA, November 7 - 9, 1984

variables in a study of an advanced flight research rotor (Reference 18). All previous results are obtained either from Kaman's program, 6F, or from the wind tunnel test, on the hinged blade. The input mode shapes for the 6F are uncoupled modes with pitch horn control and servo flap control degrees of fr >dom.

The main rotor in this study is a hingeless, 4-bladed General Purpose Research Rotor (GPRR) (References 18, 19) which weighs 287.5 lbs per blade and has 27 ft radius, 25.5 in. thrust weighted chord, 256 rpm angular speed, and 723.8-ft/sec tip speed. Bingham RC airfoil tables are used to determine blade aerodynamic coefficients. The fuselage has 18,400 lbs total gross weight and 23 square ft flat plate drag area. C81 was modified to incorporate variable sweep stations along the blade radial direction.

Thirty-six C81 quasi-static (QS) trim cases as a function of blade built-in twist, sweep angle, percent tip taper, and taper ratio have been generated to find the regression equations for performance analysis at five different airspeeds from hover to 160 knots. The predictions of the horsepower from regression equations, which are not included in those 36 QS trim cases, compared with C81 are within 1.5% of the total range of interest.

The regression equations of the modal parameters also have been generated using 84 Myklestad cases by adding blade ballast running weights along the blade radial stations. The predicted results from regression equations, compared with the Myklestad, are in excellent agreement up to the first six modes.

Thirty-five C81 QS Trim, followed by Time-Varying Trim (TVT), cases as a function of blade built-in twist, percent tip taper, and taper ratio are used for vibration analysis. The multiple correlation factors for horsepower, 4/rev vertical hub shear, oscillatory beamwise and chordwise bending moments, and torsional moments are correlated at least 95.4%. The excellent predictions from regression equations for the vibration data are also presented.

With the exceptionally well-fitted regression equations from C81 and Myklestad, the blade can be dynamically controlled by controlling each individual CMPF, or its product with MPF, to achieve the design goal under certain constraints.

Performance Analysis

In order to determine blade characteristics for the performance analysis, blade physical parameters from Reference 18 are used for the baseline blade. Blade torsional control spring is pre-determined as an input to Myklestad coupled mode shapes program such that the blade clamped torsional frequency is 25.6 Hz. Only the first out-of-plane mode shape is used as an input in C81 for the performance study. Bingham RC 8%, 10%, and 12% airfoil tables are used to look up blade local aerodynamic lift, drag, and pitching moment coefficients. Blade built-in twist, sweep angle, percent tip taper, and taper ratio are treated as independent variables input to C81 to vary blade airloads distribution. QS trim in C81 uses the first flapping mode; therefore, blade sweep angle gives no dynamic coupling effects and only has aerodynamic effects on Mach No. reduction; and aerodynamic effects on pitching moment variation due to aerodynamic center shift. The blade sweep station starts at that point at which the Mach No. is the same as the Mach No. on the blade tip. There are four independent variables in the analysis, and the range of interest of these variables is listed in Table 1.

Table 1. Independent variables for performance analysis.

Independent Variables	Levels
Built-in Twist*	-8°, -12°, -14°, -16°
Sweep Angle**	20°, 0°, -20°, -30°
Percent Tip Taper	15%, 25%, 50%
Taper Ratio	1.1:1, 2:1, 3:1

*Built-in Twist: + Nose Up
**Sweep Angle: + Forward Sweep

The quadratic regression equation of the independent variables is written as follows:

$$Y = A_o + \sum_{i=1}^{N} A_i \delta_i + \sum_{i=1}^{N} A_{ii} \delta_i^2 + \sum_{i=1}^{N-1} \sum_{j=i+1}^{N} A_{ij} \delta_i \delta_j$$

Where Y is the dependent variable; δ is the independent; and A is the coefficient of regression equation.

There are 144 different combinations for these variables. Only 36 combinations are randomly selected as inputs for C81 QS trim at each flight speed. The regression equations having linear and quadratic terms which are generated from these data are shown in Table 2 for 5 different speeds. These equations give multiple correlation coefficients of 97.5% or better at each different speed from hover to 160 knots. With the existing data

Table 2. Regression equations for performance analysis at 5 different flight speeds.

Coefficient	Variable	Hover	40 Knots	80 Knots	120 Knots	160 Knots
A_0		1975.08	1324.90	1038.82	1316.16	2054.82
A_1	δ_1	- - -	0.85 (9)	- - -	-0.45 (7)	-1.31 (7)
A_2	δ_2	12.13 (5)*	17.96 (4)	18.89 (7)	32.23 (3)	44.88 (3)
A_3	δ_3	-77.59 (7)	-47.36 (8)	-27.60 (8)	-28.33 (10)	-27.88 (4)
A_4	δ_4	- - -	- - -	-11.31 (3)	20.65 (5)	- - -
A_{11}	$\delta_1*\delta_1$	-0.067 (2)	-0.04 (2)	-0.04 (1)	-0.05 (1)	-0.08 (1)
A_{22}	$\delta_2*\delta_2$	- - -	0.52 (6)	0.74 (6)	1.46 (2)	2.078 (2)
A_{33}	$\delta_3*\delta_3$	19.43 (6)	10.91 (7)	5.45 (9)	2.84 (11)	- - -
A_{44}	$\delta_4*\delta_4$	- - -	130.55 (11)	63.80 (10)	106.75 (12)	140.25 (9)
A_{12}	$\delta_1*\delta_2$	- - -	0.04 (10)	-0.01 (4)	-0.05 (6)	-0.10 (6)
A_{13}	$\delta_1*\delta_3$	- - -	-0.11 (12)	- - -	-0.08 (13)	- - -
A_{14}	$\delta_1*\delta_4$	- - -	- - -	- - -	0.43 (14)	0.61 (10)
A_{23}	$\delta_2*\delta_3$	1.26 (1)	0.10 (1)	-0.29 (5)	-1.39 (9)	-1.84 (5)
A_{24}	$\delta_2*\delta_4$	-7.0 (3)	0.75 (5)	- - -	6.68 (8)	9.12 (8)
A_{34}	$\delta_3*\delta_4$	-106.88 (4)	-77.88 (3)	-38.14 (2)	-22.17 (4)	- - -
M.C.C.**		0.987	0.991	0.982	0.975	0.978
S.E.E.***		11.7	5.8	4.7	7.2	9.1

δ_1 Sweep δ_2 Built-in Twist δ_3 Taper Ratio δ_4 % Tip Taper
* Sensitivity ** Multiple Correlation Coefficient *** Standard Error of the Estimate

Table 3. Regression equation for performance analysis with airspeed as an independent variable.

Coefficient	Variable	Horsepower	Coefficient	Variable	Horsepower
A_0		2063.68			
A_1	δ_1	- - -	A_{12}	$\delta_1*\delta_2$	- - -
A_2	δ_2	36.55 (8)*	A_{13}	$\delta_1*\delta_3$	- - -
A_3	δ_3	-21.58 (4)	A_{14}	$\delta_1*\delta_4$	- - -
A_4	δ_4	- - -	A_{15}	$\delta_1*\delta_5$	- - -
A_5	δ_5	-22.76 (2)	A_{23}	$\delta_2*\delta_3$	- - -
A_{11}	$\delta_1*\delta_1$	-0.06 (3)	A_{24}	$\delta_2*\delta_4$	2.01 (6)
A_{22}	$\delta_2*\delta_2$	1.06 (11)	A_{25}	$\delta_2*\delta_5$	-0.12 (7)
A_{33}	$\delta_3*\delta_3$	- - -	A_{34}	$\delta_3*\delta_4$	-57.54 (10)
A_{44}	$\delta_4*\delta_4$	- - -	A_{35}	$\delta_3*\delta_5$	0.23 (5)
A_{55}	$\delta_5*\delta_5$	0.13 (1)	A_{45}	$\delta_4*\delta_5$	1.03 (9)

Multiple Correlation Coefficient: 0.999
Standard Error of the Estimate: 18.4

δ_1 Sweep δ_3 Taper Ratio δ_5 Airspeed
δ_2 Built-in Twist δ_4 % Tip Taper * Sensitivity

base, the regression equation for performance as a function of airspeed has also been analyzed. The multiple correlation coefficient from the equation with airspeed as an independent variable is correlated at 99.9%, shown in Table 3.

The sensitivity results from regression equations show that each design variable has a clear performance trend at each airspeed and for the airspeed sweep. The independent variables in these regression equations have not been normalized. Therefore, the physical parameters are treated as the input to these regression equations. From Table 2, blade sweep angle squared, built-in twist squared, and built-in twist are the three most important terms at 160 knots from the performance regression equation sensitivity result. Also, the product of taper ratio and built-in twist, sweep angle squared, the product of built-in twist and percent tip taper, and the product of percent tip taper and taper ratio are the four most important terms in hover. Blade sweep angle squared, the product of taper ratio and percent tip taper, percent tip taper and the product of sweep angle and built-in twist are the four most important terms in the regression equation at 80 knots. From Table 3, the regression equation shows that airspeed squared, airspeed, blade sweep angle squared, and taper ratio are the four most important terms in the whole airspeed sweep region. Also from Table 2, the regression equation shows that the constant term has the minimum value at 80 knots. All the design variables have either an increased or a decreased contribution to the constant term at each flight speed, depending on the combination of each individual design variable.

In order to gain a better understanding of the effects each independent variable contribution to performance, the plots of horsepower vs each independent variable at different speeds (Fig. 1 to 4) are described as follows:

1. For a blade having -10° built-in twist and 25% tip taper, results show that a 3:1 taper ratio blade saves 20 HP over a 1.1:1 taper ratio blade at 160 knots; saves 25 HP at 80 knots; and saves 80 HP in hover.

2. Results also show that a 30° aft sweep blade saves 75 HP and 35 HP at 160 knots, 60 HP and 35 HP in hover, and 35 HP and 25 HP at 80 knots over a non-swept blade and a 20° forward sweep blade, respectively.

3. The 3:1 taper ratio blade has better performance than the 2:1 and 1.1:1 taper ratio blades at all flight speeds of interest, except at 160 knots.

4. For the blade having -16° built-in twist and 50% tip taper, the 3:1 taper ratio blade uses slightly more HP than a 1.1:1 taper ratio blade at 160 knots, and saves 150 HP in hover and 40 HP at 80 knots.

5. For a high negative built-in twist blade, -16°, the best performance is at hover, with very little effect on performance at 160 knots. The best performance at 160 knots is with the blade which has approximately -10° built-in twist.

The prediction of the horsepower from regression equations compared with C81 trim results is exceptionally good. The difference between the two results is within 1.5% of the total range of interest. The comparison is shown on Tables 4 and 5.

The regression equations for horsepower at 160 knots, 80 knots, and hover are used for the performance optimization study. Power limits from C81 QS trim are treated as constraints at 160 knots and 80 knots. Those constraints for maximum power available are assumed to be 1740 HP at 160 knots and 840 HP at 80 knots. The minimum horsepower from 36 QS trim cases used as the starting point for optimization is the blade having a plan. rm 30° aft sweep, -16° built-in twist, 3:1 taper ratio, and 50% tip taper. The optimization code KAOPT (Reference 21) is used for performance optimization. There are two minimum points detected using the KAOPT volume search technique. The first point is the blade having 30° aft sweep, -15.8° built-in twist, 50% tip taper, and 3:1 taper ratio. The second point is 20° forward sweep, -10.4° built-in twist, 44% tip taper, and 3:1 taper ratio. The performance results are 1740 HP, 822 HP, 1500 HP for point 1; and 1740 HP, 841 HP, and 1616 HP for point 2 at 160 knots, 80 knots, and hover, respectively (also shown in Table 4). The contour plots of power at hover, with and without constraints, are shown in Fig. 5. For 1740 HP available constraint applied to 1 g thrust, 160 knots and 1.5 g thrust, 120 knots, level flight conditions, the minimum power at hover within constraints is 1516 HP, and the blade has 30° aft sweep -14.54° built-in twist, 3:1 taper ratio, and 50% tip taper.

Modal Analysis

The elastic rotor uses seven independent modes representation in the C81 airloads analysis. The time history of rotor

Table 4. Performance predictions for regression equation vs C81 at three different speeds.

δ_1	δ_2	δ_3	δ_4	V = 160 KNOTS		V = 80 KNOTS		V = 0 KNOTS	
SWEEP	BUILT IN TWIST	TAPER RATIO	% TIP TAPER	REGRESSION (HP)	C81 (HP)	REGRESSION (HP)	C81 (HP)	REGRESSION (HP)	C81 (HP)
- 20°	- 13°	2.5:1	30%	1753.65	1776.25	849.69	[illegible]	1624.21	1618.44
- 30°	- 9°	2.5:1	30%	1712.66	1715.82	838.76	839.81	1643.57	1629.31
- 11°	- 9.4°	3:1	46%	1766.20	1764.91	851.47	847.61	1624.22	1627.86
- 30°	- 11.8°	3:1	46%	1698.0	1709.82	816.0	814.16	1559.0	1540.03
- 30°	- 13°	2.5:1	30%	1711.29	1714.56	830.20	829.73	1590.81	1581.85
- 20°	- 9°	2.5:1	30%	1750.94	1752.02	857.88	861.98	1676.96	1678.20
20°	- 13°	2.5:1	30%	1761.53	1768.76	854.52	852.32	1624.21	1618.01
20°	- 9°	2.5:1	30%	1742.53	1748.47	861.22	862.08	1676.96	1677.67
- 30°	- 15.8°	3:1	50%	1740.0	1743.76	822.0	820.66	1500.0	1508.61
- 30°	- 13°	1.5:1	30%	1715.24	1715.92	843.64	839.34	1639.15	1616.54
- 30°	- 9°	1.5:1	30%	1723.97	1724.64	853.37	848.83	1686.86	1662.44
- 20°	- 13°	1.5:1	30%	1757.60	1770.04	863.13	865.69	1672.55	1662.93
- 20°	- 9°	1.5:1	30%	1762.26	1760.44	872.50	875.68	1720.26	1720.64
20°	- 10.4°	3:1	44%	1740.0	1749.87	841.0	839.35	1616.0	1604.04
20°	- 9°	1.5:1	30%	1753.85	1755.93	875.84	875.93	1720.26	1719.92
20°	- 13°	1.5:1	30%	1765.49	1767.46	867.96	865.14	1672.55	1662.34

Table 5. Performance predictions for regression equation vs C81 with airspeed as an independent variable.

δ_1	δ_2	δ_3	δ_4	δ_5	HORSEPOWER	
SWEEP	BUILT IN TWIST	TAPER RATIO	% TIP TAPER	AIRSPEED (KNOTS)	REGRESSION (HP)	C81 (HP)
- 30°	- 9.0°	1.5:1	30%	160.0	1716.38	1724.64
- 20°	- 13.0°	2.5:1	30%	160.0	1765.17	1776.25
- 16°	- 13.6°	3:1	44%	147.0	1507.30	1518.51
12°	- 14.4°	3:1	46%	80.0	845.81	850.02
- 11°	- 9.4°	3:1	46%	114.0	1034.92	1023.69
20°	- 10.4°	3:1	44%	0.0	1624.73	1604.04
- 20°	- 9.0°	1.5:1	30%	0.0	1733.29	1720.64
- 30°	- 15.8°	3:1	50%	160.0	1761.64	1743.76
12°	- 14.4°	3:1	46%	57.0	887.20	880.20
- 20°	- 13.0°	1.5:1	30%	0.0	1677.99	1662.93
- 16°	- 13.6°	3:1	44%	111.0	1001.60	1013.50
20°	- 9.0°	2.5:1	30%	80.0	875.04	862.08
- 16°	- 13.6°	3:1	44%	63.0	859.24	853.93
20°	- 13.0°	1.5:1	30%	160.0	1766.93	1767.46
12°	- 14.4°	3:1	46%	137.0	1344.81	1357.36
- 30°	- 11.8°	3:1	46%	160.0	1719.79	1709.82
- 11°	- 9.4°	3:1	46%	97.0	909.68	900.60

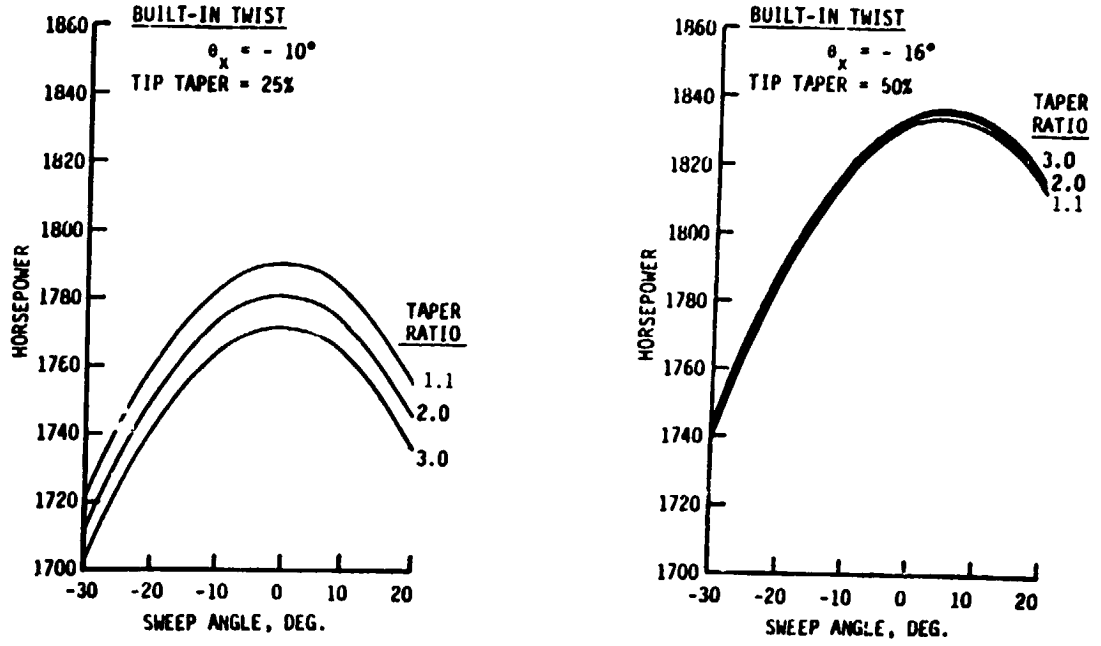

Fig. 1. Regression equation - performance vs sweep angle at 160 knots.

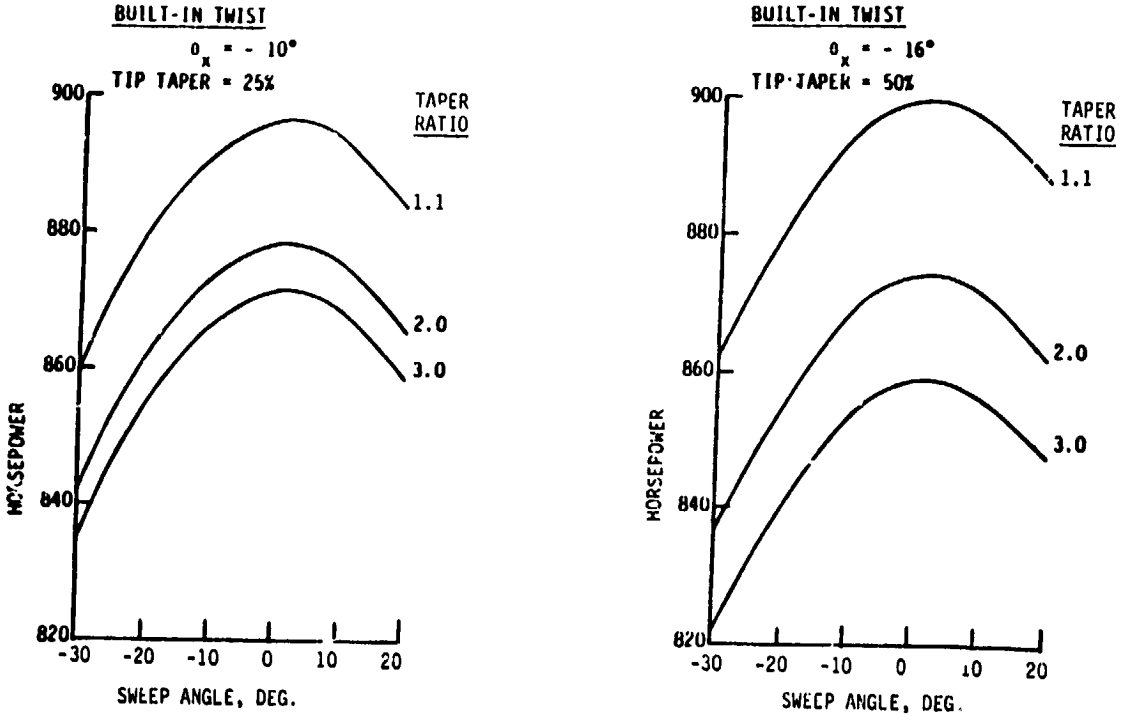

Fig. 2. Regression equation - performance vs sweep angle at 80 knots.

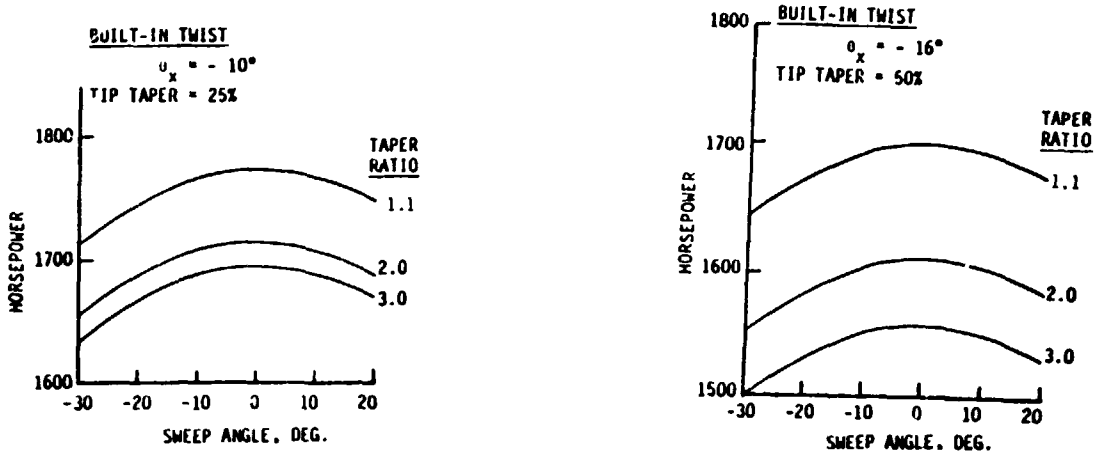

Fig. 3. Regression equation - performance vs sweep angle at hover.

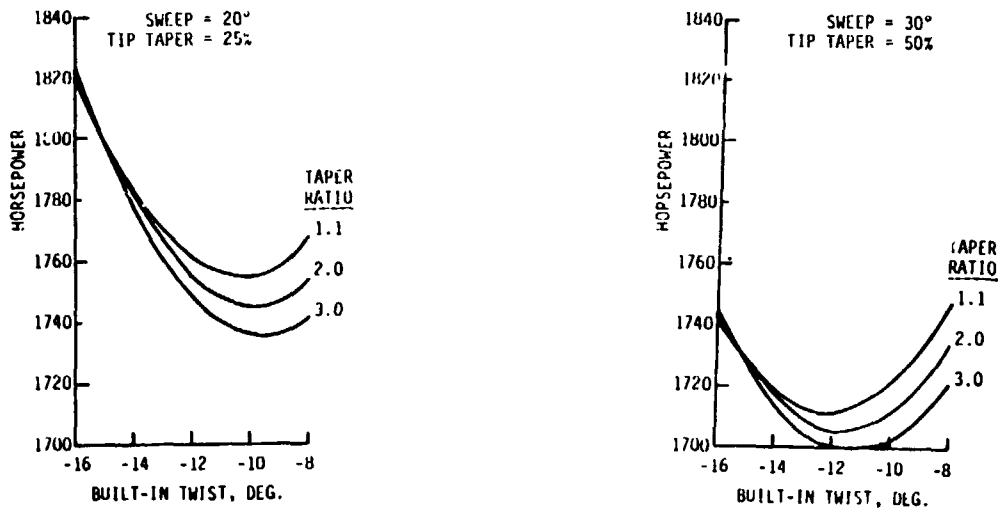

Fig. 4. Regression equation - performance vs built-in twist at 160 knots.

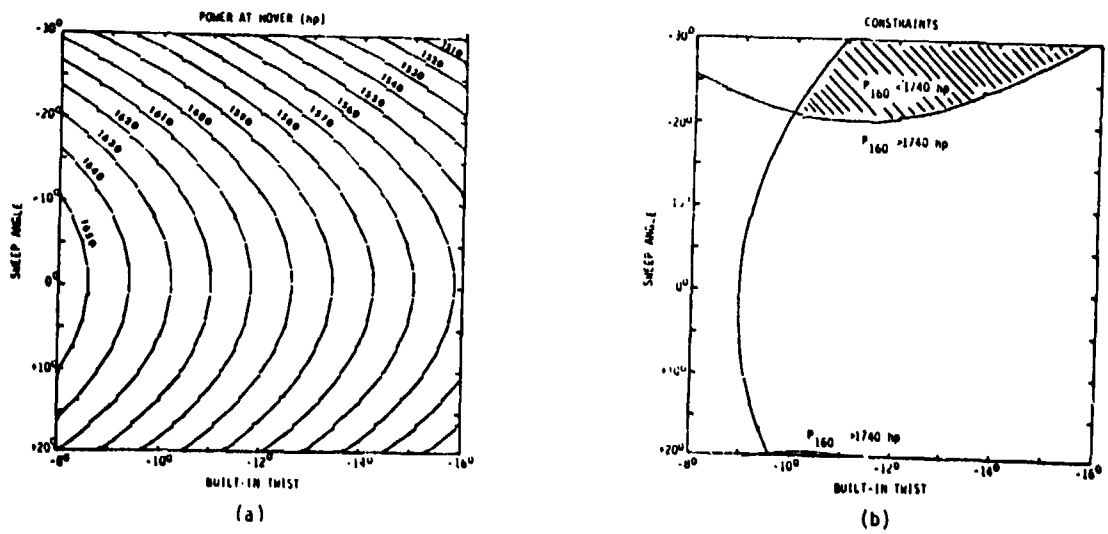

Fig. 5. Contours of power at hover; (a) without constraints (b) with constraints.

hub shear and hub moment at any given station can be computed from the modal participation factors (MPF) for the last rotor revolution in C81. Multiply the MPF for each given mode by the hub shear or the hub moment coefficient of that mode at any station and sum over all modes to get the value at that time point. Those coefficients of MPF can be obtained from the Myklestad coupled mode shape program. Regression analysis can be used to tune the coefficient of the modal participation factor (CMPF) or its product with MPF for aeroelastic blade design technique.

The baseline blade is divided into nineteen 13-inch-long equal segments, with each segment treated as an independent variable in the regression modal analysis. The regression equations of the first three out-of-plane (OP) frequencies, second and third OP deflections, static moment, flapping inertia, Lock number, and the CMPF of hub shears and moments of the first seven independent modes have been generated by adding blade ballast running weights of 1, 2, or 3 lb/in., with a total constant ballast weight of 39 lbs on each baseline blade.

There are 6,859 possible combinations for putting ballast weight in a blade with 19 independent variables and 3 levels for each. 84 cases are randomly selected to provide enough data for linear regression analysis. The linear regression equation with 19 independent variables is written as follows:

$$Y = A_o + \sum_{i=1}^{19} A_i \delta_i$$

The out-of-plane components of the CMPF of hub shear and moment have been curve fitted up to 7 independent modes based on a 1-inch tip deflection, or 10° tip torsion. Since CMPF of hub shear of the first in-plane mode is either 0 or 1, from Myklestad, no regression analysis is needed for that mode. At least 250 more cases are required if quadratic regression equations are considered in the modal analysis.

The regression equations for the modal analysis are shown in Table 6. The multiple correlation coefficients (MCC) from the regression equations are extremely well-fitted and correlated from 94.5% to 99.9% for Myklestad modal data. For the first three OP frequencies, MCC correlates those frequencies from Myklestad output at least 98.7%. For static moment, flapping inertia, and Lock no., the MCC correlates no less than 99.7%. The mode shape deflections of second and third modes correlate better than 98.5%. For CMPF of hub shear and moment of the first four OP modes, the MCC correlates at least 96.1%, and correlates torsion mode at least 95.1%.

The regression equation sensitivity results are also concluded as follows:

1. Blade outboard stations 16, 17, 18, and 19 are very sensitive to the first three OP frequencies. The intercepts of these OP frequencies are 1.0896 P, 2.5074 P, and 4.5889 P, respectively.

2. Adding ballast weight in these four stations (16, 17, 18, 19) will decrease the first OP frequency and increase the second and third OP frequencies. However, adding weight at the first blade station will increase the first three OP frequencies; and adding weight at station 8 will decrease first and second OP frequencies and increase the third OP frequency.

3. The values of static moment and flapping inertia are increased by adding ballast weight in blade outboard stations 18 and 19. However, by adding weight at inboard blade stations 1, 2, and 3, these values are decreased. Reverse trend is obtained for Lock number by adding the same ballast weight at the same stations.

4. For the second and third OP mode shape deflections, putting ballast weight at stations 18 and 19 will make minimum deflections of these modes more negative and maximum deflection of the third OP mode more positive. However, adding ballast weight at stations 11, 12, 13, and 14 gives the reverse trend of the second and third OP modes minimum deflections and the same trend of the third OP mode maximum deflection.

5. The CMPF of hub shear and moment of the first OP mode are decreased by adding blade ballast weight. Adding ballast weight at stations 17, 18, and 19 gives the second and fourth OP mode CMPF of hub shear and moment more negative and the 1st torsion mode less negative. Also, adding ballast weight at stations 18 and 19 increases the CMPF of hub shear and moment of the third OP mode.

The predicted results from the regression equations, compared with the Myklestad, are extremely well as shown on Table 7. The first three out-of-plane frequencies, static moment, flapping inertia, and Lock no. are within 1%. The predicted second and third OP deflections are within 2.5%. The predicted coefficients of hub shear and moment for the first 6 independent modes are in excellent

Table 6. Regression equation for modal analysis.

Coef-ficient	1st OP Freq.[1]	2nd OP Freq.	3rd OP Freq.	1st OP B.S.[2]	1st IP B.S.	2nd OP B.S.	1st TOR B.S.	3rd OP B.S.	2nd IP B.S.	4th OP B.S.	1st OP B.M.[3]	1st IP B.M.	2nd OP B.M.	1st TOR B.M.	3rd OP B.M.	2nd IP B.M.	4th OP B.M.	2nd OP Min Def[4]	3rd OP Max Def	3rd OP Min Def	I_x (Slug-ft)	I_y (Slug-ft^2)	Y
A_1	1.0896	2.5076	4.9089	241.8	- - -	-458.2	-1775.0	1042.0	517.4	-1594.6	7302.1	-362.9	-16187.	-19676.	29598	12288.	-42654.	-0.5513	0.5044	-0.6350	101.5	1644.6	7.808
A_2	[illegible]	[illegible]	[illegible]	-70.29	- - -	-31.06	-50.15	- - -	22.34	-70.28	-354.4	-3.99	-276.3	-1310.2	1305.9	731.1	- - -	- - -	0.0190	- - -	-6.73	-40.49	1.203
A_3	- - -	0.0523	- - -	-15.12	- - -	-35.56	-29.48	-61.17	18.12	89.41	-329.2	-3.52	-447.2	-786.4	- - -	672.8	3314.5	- - -	- - -	- - -	-6.54	-34.78	1.114
A_4	- - -	0.0332	- - -	-17.78	- - -	-22.60	-22.56	-99.48	- - -	109.0	-312.3	-2.75	- - -	-588.9	-1740.3	286.2	3872.6	- - -	- - -	- - -	-5.90	-28.02	1.101
A_5	- - -	- - -	0.0593	-15.47	- - -	- - -	-4.01	-165.3	-16.90	-312.9	-266.2	-1.62	636.9	- - -	-4058.2	-130.8	-5392.7	0.0100	-0.0405	- - -	-5.02	-12.57	0.987
A_6	-0.0006	- - -	0.1169	-14.20	- - -	7.73	- - -	-167.7	-24.55	-655.6	-239.1	-1.23	903.7	154.4	-4351.5	-337.0	-13456.	0.0130	-0.0671	- - -	-4.61	- - -	0.902
A_7	-0.0008	- - -	0.1916	-12.91	- - -	26.67	- - -	-119.7	-52.04	-648.5	-213 8	-1.19	1417.0	158.4	-3199.2	-1083.9	-13843.	0.0218	0.0304	- - -	-4.20	- - -	0.860
A_8	-0.0013	-0.0133	0.2351	-11.79	- - -	40.20	-4.11	-56.44	-55.37	-687.6	-194.1	-0.71	1898.7	- - -	-1475.5	-1143.1	-10371.	0.0277	- - -	- - -	-3.62	18.37	0.741
A_9	-0.0017	- - -	0.3027	-10.52	- - -	50.01	-13.36	46 15	-76.08	-248.1	-169.0	-0.57	2238.6	-151.9	1111.1	-1756.4	-6527.6	0.0434	0.0500	- - -	-3.33	31.37	0.699
A_{10}	-0.0021	0.0239	0.2509	-9.34	- - -	50.83	-12.03	135.3	-37.26	61.14	-145.8	- - -	2316.7	-120.7	3910.6	-767.3	2747.3	0.0497	0.1083	- - -	-2.79	45.14	0.577
A_{11}	-0.0026	0.0439	0.2649	-7.99	- - -	59.86	-21.47	214.1	-43.87	- - -	-122.6	- - -	2585.3	-300.1	5983.7	-974.6	7126.3	0.0583	0.1356	0.0069	-2.44	58.18	0.533
A_{12}	-0.0032	0.0866	0.1629	-6.81	- - -	64.47	-32.09	167.6	-13.61	-185.6	-99.42	- - -	2818.5	-603.7	5118.2	-235.4	-2000.2	0.0683	0.1517	0.0225	-1.97	72.91	0.438
A_{13}	-0 0036	0.1233	0.1705	-5.63	- - -	52.36	-30 34	99.78	- - -	-506.3	-80 71	- - -	2665 8	-476.5	3010.5	- - -	-8868.2	0.0621	0.1153	0.0442	-1.59	88.91	0.390
A_{14}	-0.0045	0.1696	0.1306	-4.68	- - -	32.63	-28 86	- -.-	23.60	-756.9	-63.05	0.23	1942.7	-422.9	- - -	625.2	-14886.	0.0503	0.0557	0.0695	-1.07	106.7	0.254
A_{15}	-0.0052	0.2122	0.1716	-3.95	- - -	- - -	-15.75	-75.05	44.41	-623.0	-41.50	- - -	1085.7	- - -	-2075.5	1132.9	-12143.	0.0270	- - -	0.0898	-0.65	124.0	0.136
A_{16}	-0.0061	0.2307	0.2927	-2.39	- - -	-40.27	- - -	-99.76	52.01	-196.8	-24.86	- - -	- - -	435.1	-3227.1	1351.4	-1749.3	-0.0132	-0 0366	0.0987	- - -	143.9	- - -
A_{17}	-0.0067	0.2477	0.4216	-1.40	- - -	-84.64	5.02	- - -	64.95	-104 3	- - -	- - -	-1269.1	657.8	-818.8	1137.5	- - -	-0.0529	- - -	0.0571	- - -	163.0	- - -
A_{18}	-0.0077	0.2106	0.4883	- - -	- - -	-110.2	5.68	218.3	- - -	-706.8	- - -	- - -	-2101.0	649.5	4863.3	- - -	-1669.1	-0.0960	0.0970	-0.0406	0.78	184.1	-0.154
A_{19}	-0.0085	0.1869	0.4090	- - -	- - -	-137.6	- - -	370.5	15.53	-891.0	- - -	- - -	2807.3	523.8	9311.6	515.1	-16557.0	-0.1293	0.1935	-0.1266	1.17	205.7	-0.261
M.C.C.*	0.997	0.998	0.987	0.999	- - -	0.990	0.951	0.981	0.957	0.961	0.999	0.990	0.990	0.962	0.982	0.964	0.962	0.993	0.986	0.985	0.999	0.999	0.997
S.E.E.**	0.001	0.013	0.055	0.36	- - -	14.75	11.85	69.98	22.71	188.5	11.54	0.46	430.9	335.1	1781.5	611.5	4183.4	0.01	0.03	0.016	0.249	6.63	0.084

(1) per rev (2) lb (3) in - lb (4) in * Multiple Correlation Coefficient ** Standard Error of Estimate

agreement, except for the fourth OP hub shear and moment. Higher order terms in the regression equation are required in order to have better prediction for the modal parameters higher than the seventh mode. However, the seventh mode, or higher than seventh modes, normally gives very little effect on blade performance and vibration analysis; therefore, the linear regression analysis is an appropriate approach for future blade design study.

Vibration Analysis

Thirty-five C81 QS Trim followed by Time-Varying Trim (TVT) cases, each having two ballasting configurations, as a function of blade built-in twist, percent tip taper, and taper ratio are used for vibration analysis at 160 knots.

During the TVT, only flapping angles of the time-variant rotor are allowed to vary; the fuselage and control positions are held fixed at the values determined by the QS trim. The hub shear, hub moment, horsepower, and modal participation factor are obtained after the rotor reaches steady state within 8 rotor revolutions. Linear and quadratic terms are adapted to determine regression equations for horsepower, 4/rev vertical hub shear, blade root oscillatory beamwise and chordwise bending moments, and torsional moments.

The coefficients of the regression equations and the multiple correlation coefficients are shown on Table 8. The multiple correlation coefficients for horsepower, 4/rev vertical hub shear, blade root oscillatory beamwise and chordwise bending moments, and torsional moments are correlated at least 95.4%.

The predictions between regression equations and C81 TVT results are shown in Table 9. The prediction of performance, bending moment and 4/rev vertical hub shear are correlated very well with C81 TVT and the regression equation results.

The best performance blade obtained from the regression equation prediction is a 3:1 taper ratio, -10° built-in twist, and 50% tip taper blade. The 1.1:1 taper ratio blade has lower 4/rev total vertical hub shear than those blades which have 2:1 or 3:1 taper ratio at 160 knots, from the regression analysis.

Also, three different planforms combined with various ballasting configurations along the blade span have been investigated. There are twelve different ballast weight locations chosen from the

Table 7. Regression equation prediction vs Myklestad for modal results.

	BASELINE + .8 lb/in. @ Sta 103, 142 + 1.4 lb/in. @ Sta 285		BASELINE + .5 lb/in. @ Sta 116, 220, 246 + 1.5 lb/in. @ Sta 272		BASELINE + .7 lb/in. @ Sta 142, 220 246 + 0.9 lb/in. @ Sta 285		BASELINE + .8 lb/in. @ Sta 103, 129 + 1.4 lb/in. @ Sta 272		BASELINE + .5 lb/in. @ Sta 116, 207, 233 + 1.5 lb/in. @ Sta 259		BASELINE + .4 lb/in. @ Sta 103, 142, 220 + 1.8 lb/in. @ Sta 233	
	MYKLESTAD	REGRESSION EQUATION	MYKLESTAD	REGRESSION EQUATION	MYKLESTAD	REGRESSION EQUATION	MYKLESTAD	REGRESSION EQUATION	MYKLESTAD	REGRESSION EQUATION	MYKLESTAD	REGRESSION EQUATION
1st OP Freq.[1]	1.0791	1.080	1.0767	1.077	1.0776	1.078	1.0805	1.081	1.0784	1.079	1.0811	1.082
2nd OP Freq.	2.8544	2.831	3.0018	2.989	2.893	2.910	2.8593	2.857	2.9202	2.915	2.7849	2.777
3rd OP Freq.	5.2696	5.273	5.1519	5.175	5.1992	5.255	5.0185	5.046	5.0794	5.064	4.8965	5.008
1st OP H. S.[2]	214	214.109	224	224.183	223	222.565	212	211.705	221	221.385	216	216.085
1st IP H. S.	0	---	0	---	0	---	0	---	0	---	1	---
2nd OP H. S.	-605	-588.461	-477	-479.024	-458	-461.022	-559	-532.534	-411	-411.061	-358	-344.066
1st Tor H. S.	-1774	-1786.013	-1810	-1810.984	-1807	-1813.136	-1785	-1796.245	-1829	-1829.988	-1855	-1851.268
3rd OP H. S.	839	828.265	902	898.196	964	1041.823	705	690.476	950	1008.5	1105	1181.704
2nd IP H. S.	559	560.664	590	597.694	543	547.634	578	576.658	556	559.369	509	502.102
4th OP H. S.	-1971	-2184.809	-2212	-2361.017	-2520	-2811.589	-2018	-2033.212	-2465	-2782.17	-2944	-2798.805
1st OP H. M.[3]	6860	6860.998	7041	7040.226	7014	7021.024	6818	6804.477	6995	6995.117	6899	6897.413
1st IP H. M.	-367	-366.102	-364	-363.947	-364	-363.62	-367	-366.414	-364	-364.064	-364	-364.514
2nd OP H. M.	-17883	-17241.222	-13810	-13806.906	-13387	-13364.227	-16596	-15679.62	-12020	-12043.57	-10617	-10296.459
1st Tor H. M.	-18666	-18900.591	-19441	-19454.057	-19422	-19492.453	-19038	-19335.908	-20058	-19981.741	-20959	-20746.979
3rd OP H. M.	23873	23578.438	25843	25576.833	27544	29398.054	20726	20441.421	27744	29242.885	33142	34627.764
2nd IP H. M.	13819	13840.247	14336	14330.965	13296	13349.15	14315	14304.599	13543	13580.914	12437	12173.862
4th OP H. M.	-45679	-50321.515	-50900	-54496.604	-57117	-63894.336	-47303	-47719.696	-57038	-63516.643	-66730	-63250.904
2nd OP Min Def[4]	-0.6313	-0.615	-0.5055	-0.512	-0.5111	-0.507	-0.5749	-0.562	-0.4525	-0.451	-0.412	-0.407
3rd OP Max Def	0.4574	0.467	0.5454	0.539	0.5844	0.617	0.4198	0.421	0.6028	0.625	0.7329	0.754
3rd OP Min Def	-0.5597	-0.555	-0.4469	-0.441	-0.5207	-0.519	-0.4929	-0.497	-0.461	-0.475	-0.5428	-0.546
S_b (slug-ft)	93.383	93.058	96.882	97.214	96.313	96.108	92.42	92.728	95.788	95.742	93.733	93.601
I_β (slug-ft^2)	1667.83	1670.272	1758.884	1759.854	1735.098	1736.989	1632.549	1633.57	1714.527	1713.713	1642.375	1642.611
Y	9.226	9.41	8.749	8.663	8.869	8.925	9.426	9.48	8.975	9.019	9.369	9.5

(1) per rev (2) lb (3) in-lb (4) in.

Table 8. Regression equation for C81 vibration results.

Coefficient	Variable	Horsepower	Chordwise Bending Moment (in-lb)	Beamwise Bending Moment (in-lb)	Torsional Moment (in-lb)	4/REV. Hub Shear (lb)
A_0		2709.16	100148	-3109	3866	-1543
A_1	δ_1	795.00 (8)*	- - -	236752 (6)	24108 (5)	16042 (4)
A_2	δ_2	113.56 (9)	16775 (7)	99279 (5)	6232 (1)	4121 (2)
A_3	δ_3	121.88 (6)	-1157 (4)	-9539 (7)	- - -	- - -
A_{11}	$\delta_1*\delta_1$	-1499.25 (2)	40948 (2)	-514400 (3)	-45008 (4)	-22194 (1)
A_{22}	$\delta_2*\delta_2$	-65.48 (5)	-4845 (6)	-5238 (8)	-626 (6)	-805 (3)
A_{33}	$\delta_3*\delta_3$	4.35 (1)	-144 (3)	187 (9)	- - -	-11 (6)
A_{12}	$\delta_1*\delta_2$	-409.90 (3)	-46025 (1)	75817 (1)	2911 (3)	-3457 (5)
A_{13}	$\delta_1*\delta_3$	-58.48 (7)	-2241 (8)	-6583 (7)	-307 (7)	-161 (8)
A_{23}	$\delta_2*\delta_3$	-21.79 (4)	-612 (5)	6121 (4)	171 (2)	-79 (7)
Multiple Correlation Coefficient		0.965	0.966	0.972	0.959	0.954
Standard Error of Estimate		45.64	2673	8362	615	334

δ_1 % Tip Taper δ_2 Taper Ratio δ_3 Built-in Twist * Sensitivity

Table 9. Regression equation prediction vs C81 TVT results.

	δ_1 = 50%, δ_2 = 3:1, δ_3 = - 10°		δ_1 = 15%, δ_2 = 2.5:1, δ_3 = - 14°		δ_1 = 50%, δ_2 = 2.5:1, δ_3 = - 14°		δ_1 = 25%, δ_2 = 2.5:1, δ_3 = - 12°		δ_1 = 25%, δ_2 = 1.5:1, δ_3 = - 10°	
	C81	REGRESSION EQUATION	C81	REGRESSION EQUATION	C81	REGRESSION EQUATION	C81	REGRESSION EQUATION	C81	REGRESSION EQUATION
HORSEPOWER	2094	2030.2	2526.8	2546.4	2400.3	2411.4	2445.7	2425	2342	2372.3
4/REV[1] VERTICAL HUB SHEAR	2959.7	2971.8	4890.2	5349.3	3299.4	3678.8	5547.4	5507.5	4693.9	4673.3
OSCILLATORY[2] BEAMWISE BENDING MOMENT	261804	286507	200099.7	206572	270584	271004	259239	236343	198050	200266
OSCILLATORY[2] CHORDWISE BENDING MOMENT	72751.5	74817	107091.9	109607	89002	89630	101425	103857	111012	111684
OSCILLATORY[2] TORSIONAL MOMENT	17054.8	18489	13463.5	13874	15413	16124	17791	16349	13621	14308

(1) lb
(2) in.-lb

no ballast blade by putting the ballasting at maximum and minimum deflections and nodal points of the OP modes.

The regression equations obtained from the combination of CMPF from Myklestad and MPF from C81 provides the sensitivity of each design variable, and also predicts two local minimum points of 4/rev total vertical hub shears from the coefficients of each equation, shown in Fig. 6 and 7. From these figures, the inboard minimum 4/rev vertical hub shear ballasting location is between station 129 and 155, and the outboard minimum hub shear ballasting location is between station 246 and 272.

Because the GPRR blade has a large third OP modal component contribution to the 4/rev total vertical hub shear from the modal analysis, the inboard ballasting location does not have strong coupling between modal forces and mode shapes. Therefore, the results show that the best vibration and performance blades for each of the three inboard ballasting configurations have converged to the same blade planforms, respectively, for each ballasting location. For the inboard converged point, the untapered blade predicts a higher power requirement and less vibration, compared with tapered blades. However, this trend is reversed for the 50% tip taper, 3:1 taper ratio, and -10° built-in twist blade.

For the outboard minimum, the data shows that there is a strong modal force and mode shape coupling which significantly reduce the third OP modal components. For the outboard minimum point, the best performance blade has a similar vibration level compared with the untapered blade, but the performance is 15% better than the untapered blade. Further study is required to investigate other possible local minimum vibration locations.

With the exceptionally well-fitted regression equations from C81 and Myklestad, the blade can be dynamically controlled by controlling each individual CMPF, or its product with MPF, to achieve the design goal under certain constraints. The best performance blade, obtained from the best ballasting configuration in this study, has at least 2.5 times the reduction of vibration level compared with the original ballasting configuration with various planform and the power requirement is at least 15% better than the untapered blade.

Conclusions

From the performance, modal, and vibration analysis of the advanced aeroelastic blade design study, the following conclusions can be obtained from the results:

1. With the exceptionally well-fitted regression equations from C81 and Myklestad, regression technique can be used for vibration analysis, modal analysis, and performance analysis for designing future advanced aeroelastic rotor blades.

2. Multiple optimizations can be performed to evaluate the effects of various objective functions and constraint functions, or to evaluate the combinations of several objective functions with different weighting factors for various mission requirements.

3. Regression technique can directly determine the sensitivity of each blade design variable and analyze the dynamic and aerodynamic effects during the entire design process.

4. The predicted results from regression equations for performance analysis, modal analysis, and vibration analysis are exceptionally good when compared with C81 and Myklestad outputs.

5. For the GPRR blade, the combination of CMPF from Myklestad and MPF from C81 predicts the same converging points for different blade planforms and different ballast weight configurations along the blade.

6. The best performance blade obtained from the best ballasting configuration has at least 2.5 times the reduction of vibration level when compared with original configurations and the power requirement is at least 15% better than the untapered blade.

References

1. Blackwell, R. H., Jr., "Blade Design for Reduced Helicopter Vibration," American Helicopter Society National Specialists' Meeting on Helicopter Vibration, November 1981.

2. Taylor, R. B., "Helicopter Vibration Reduction by Rotor Blade Modal Shaping," 38th Annual Forum of the American Helicopter Society, May 1982.

3. Yen, J. G., and Weller, W. H., "Analysis and Application of Compliant Rotor Technology," Sixth European Rotorcraft and Powered Lift Aircraft Forum, September 1980.

4. Banerjee, D., Johnson, R. A., and Messinger, R. H., "Wind Tunnel Test

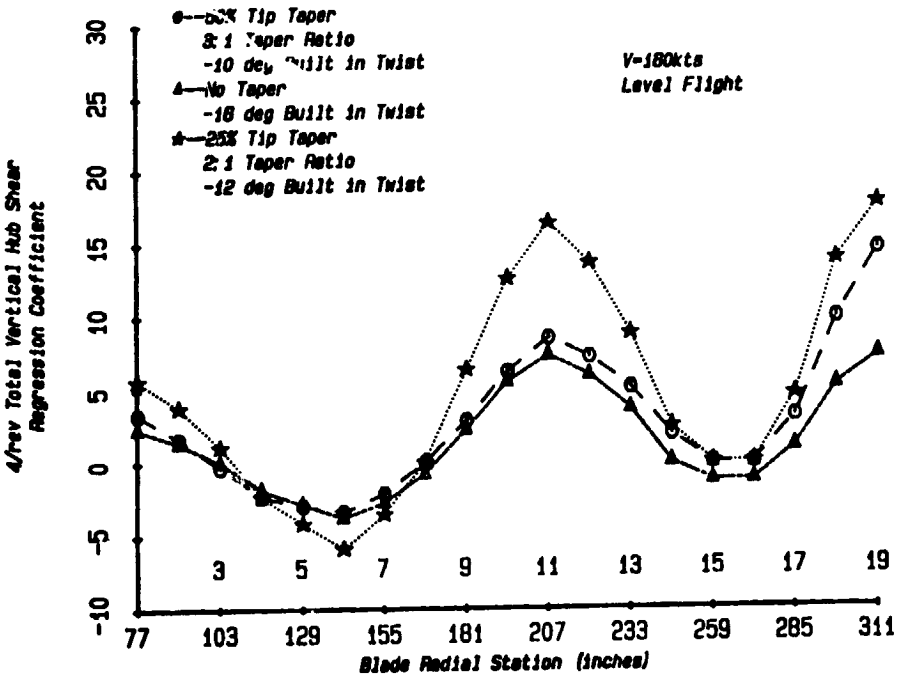

Fig. 6. 4/rev total vertical hub shear regression coefficients for ballast weight at 168.

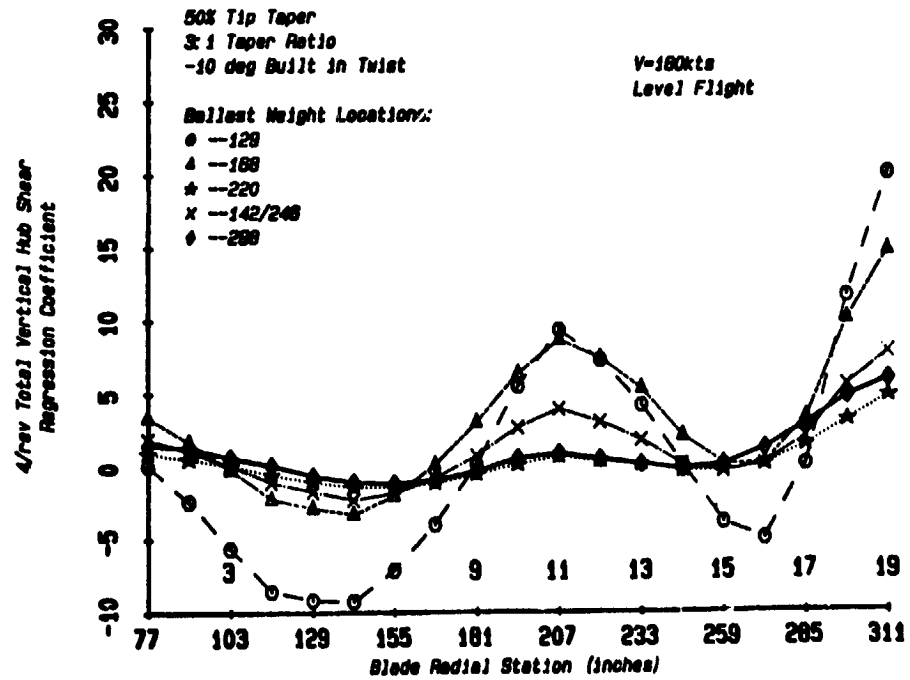

Fig. 7. Radial distribution of 4/rev total vertical hub shear regression coefficients.

of a Soft/Stiff In-plane Bearingless Rotor," 39th Annual Forum of the American Helicopter Society, May 1983.

5. Friedmann, P. P., and Shanthakumaran, P., "Optimum Design of Rotor Blades for Vibration Reduction in Forward Flight," 39th Annual Forum of the American Helicopter Society, May 1983.

6. Peters, D. A., Ko, T., Korn, A., and Rossow, M., "Design of Helicopter Rotor Blades for Desired Placement of Natural Frequencies," 39th Annual Forum of the American Helicopter Society, May 1983.

7. Viswanathan, S. P., and Myers, A. W., "Reduction of Helicopter Vibration Through Control of Hub-Impedance," Journal of American Helicopter Society, October 1980.

8. Blackwell, R. H., Campbell, T. G., and Taylor, R. B., "Predesign Study for an Advanced Flight Research Rotor," 38th Annual Forum of the American Helicopter Society, May 1982.

9. Weller, W. H., and Peterson, R. L., "Measured and Calculated In-plane Stability Characteristics for an Advanced Bearingless Main Rotor," 39th Annual Forum of the American Helicopter Society, May 1983.

10. Viswanathan, S. P., and McClure, R. D., "Analytical and Experimental Investigation of a Bearingless Hub-Absorber," 38th Annual Forum of the American Helicopter Society, May 1982.

11. Bingham, G. J., "The Aerodynamic Influences of Rotor Blade Airfoils, Twist, Taper, and Solidity on Hover and Forward Flight Performance," 37th Annual Forum of the American Helicopter Society, May 1981.

12. Philippe, J. J., and Vuillet, A., "Aerodynamic Design of Advanced Rotors With New Tip Shapes," 39th Annual Forum of the American Helicopter Society, May 1983.

13. Wilby, P. G., and Philippe, J. J., "An Investigation of the Aerodynamics of an RAE Swept Tip Using a Model Rotor," 39th Annual Forum of the American Helicopter Society, May 1983.

14. McLarty, T. T., Van Gassbeek, J. R., and Hsieh, P. Y., "Rotorcraft Flight Simulation With Coupled Rotor Aeroelastic Stability Analysis," USAAVRADCOM TR-80-D-38A, October 1981.

15. Van Gaasbeek, J. R., McLarty, T. T., Hsieh, P. Y., and Sadler, S. G., "Rotorcraft Flight Simulation, Computer Program C81, Engineers' Manual," Volume I, USAAMRDL TR-77-54A, 1979.

16. IBM Scientific Subroutine Package, Program REGR, 1966.

17. Wei, F. S., and Weisbrich, A.L., "Multicyclic Controllable Twist Rotor Data Analysis," NASA CR-152251, January 1979.

18. Jones, R., Howes, H., and Tomashofski, C., "Study of Advanced Flight Research Rotors," NASA CR 166288, November 1981.

19. Wei, F. S., "Regression Analysis for Advanced Aeroelastic Blade Vibration and Performance Study," Kaman Aerospace Corporati Research Note, No. RN-83-5, June 1983.

20. Robinson, D. W., Jr., and Dunn, F. K., "Trimming Dual Control Rotors for Optimum Performance," American Helicopter Society on Helicopter Aerodynamic Efficiency, March 1975.

21. Perley, R., "A Program for Design Optimization," Kaman Aerospace Corporation, Research Note RN-83-3, 30 June 1983.

DISCUSSION
Paper No. 10

OPTIMAL DESIGN APPLICATION ON THE ADVANCED AEROELASTIC ROTOR BLADE
Fu-Shang Wei
and
Robert Jones

Dave Peters, Washington University: Do you have some feel for a comparison like this: How many times would I have to run, say, C81 or Myklestad to get the regression analysis as opposed to how many times I would have to run it if I just hooked it up to an optimization program and just reran it every time? Do you understand the question?

Wei: I'll tell you. It depends upon how many design variables you are using. Right now we are using four independent variables. Normally we are using the quadratic regression analysis and here we have 36 cases. I personally believe that if we have less design variables and directly hook onto the analyzer combined with the optimizer, we are going to save time. If you have a tremendous [number of] design variables the regression analysis could be beneficial. I think the tradeoff here in independent variables is around seven; [this] would be a nice number.

Bob Blackwell, Sikorsky Aircraft: I might ask if you could comment on whether the blade model and the inflow model and so forth that are used for your study are really sufficient for prediction of vibratory shears and prediction of blade response. Is it your [opinion] that a model as simple as this and able to be run for 36 times is sufficient or does the model have to get so detailed it just becomes cumbersome even with that?

Wei: I personally feel that the present model still has to be improved so that we can use it for future design. Right now we only deal with four different independent variables and more independent variables are required in the future if we are going to do more in a real study. However, one thing that I can mention is that the people at Kaman [are] using the optimization technique to design for the SH-2 and they are using it now. How good are the results going to be? I don't have any answer at this moment. But we are going to see.

Bob Taylor, Boeing Vertol: Just a quick question. Do you have any plans to do any testing to back up your theory?

Wei: That's what I am saying. We are going to do the SH-2 composite rotor to hook on the SH-2 helicopter.

Taylor: That's how you are going to prove your theory? Build a full-scale blade?

Wei: No, I can't give you an answer for that.

Bob Goodman, Sikorsky Aircraft: It seems that the only way that you can really check this kind of thing is to run a variety of cases--isn't that true? I mean, really you need a baseline.

Wei: We need a data base to generate equations. I think, Bob, you can give more details.

Bob Jones, Kaman: The regression equations are never going to be any better than the data base. If you have no faith in C81 then this is lousy. If you have no faith in something else then it is lousy. What you are doing is fitting statistical [variables to the] data base. If you have a good fit then it's a good equation, but it's no better than your data base, however. And you can do this with testing. I can get a data base with testing, fit a curve, [and do some interpolating]. This [fit] is really what it's based on. So there is no proof of theory if you want to look at it from that standpoint. We are working on methods where we have our regression equations based upon analysis and change them as we get testing results.

Jing Yen, Bell Helicopter: John, I am just curious to ask you what kind of inflow model you used here.

Wei: We just used the simple one that you see in the C81.

Yen: You did not use the Dr. Gene Sadler's free wake [analysis]?

Wei: No.

DEVELOPMENT AND APPLICATION OF A TIME-HISTORY ANALYSIS FOR ROTORCRAFT DYNAMICS BASED ON A COMPONENT APPROACH

Robert Sopher
Supervisor, Dynamics Methods

Daniel W. Hallock
Dynamics Engineer

Sikorsky Aircraft Division
United Technologies Corporation, Stratford, CT

Abstract

This paper describes a time-history analysis for rotorcraft dynamics based on dynamical substructures, and non-structural mathematical and aerodynamic components. The analysis is applied to predict helicopter ground resonance and response to rotor damage. Other applications illustrate the stability and steady vibratory responses of stopped and gimballed rotors, representative of new technology. Desirable attributes expected from modern codes are realized, although the analysis does not employ a complete set of techniques identified for advanced software. The analysis is able to handle a comprehensive set of steady state and stability problems with a small library of components. It has responded to new technologies with timely solutions by limiting the effort required to implement new capabilities through its component structure. Opportunities were taken to reduce development costs by addressing more than one type of problem with a single component, such as using a minimum variance controller for trim and vibration reduction.

Notation

B	= matrix, Eq. (20), N x N
C	= independent coordinate system damping matrix, N x N
C_D	= dependent coordinate system damping matrix, N_D x N_D
C_t	= rotor thrust coefficient
D	= matrix, Eq. (15), N x N
$[c]^{(i)}$	= damping matrix for i-th substructure
$\{f\}^{(i)}$	= vector of external forces for i-th sub-structure, representing forces and moments.
f_{x1} f_{y1} f_{z1}	= components of force applied to a substructure connection node, Fig. 2, 1b
h	= time interval in Newmark-Beta method, Eq. (10), sec.
F	= independent coordinate system force vector, N x 1
F_D	= dependent coordinate system force vector, N_D x 1
F'	= matrix, Eq. (21), N x N
I	= unit matrix, N x N
K	= independent coordinate system stiffness matrix, N x N
K_D	= dependent coordinate system stiffness matrix, N_D x N_D
$[k]^{(i)}$	= stiffness matrix for i-th substructure
M	= independent coordinate system mass matrix, N x N
M_D	= dependent coordinate system mass matrix, N_D x N_D
$[m]^{(i)}$	= mass matrix for the i-the substructure

Paper presented at "Second Decennial Specialists' Meeting on Rotorcraft Dynamics", American Helicopter Society, NASA Ames Research Center, Moffett Field, California, November 7-9, 1984.

m_{x1} m_{y1} m_{z1} = components of moment applied to a substructure connection node, Fig. 2, lb-ft

n = integer step number in time-history solution, Eq. (10)

N = total number of independent coordinates in the assembled system.

N_D = total number of coordinates in the dependent coordinate vector (obtained by summing the coordinates for all substructures)

P = matrix, Eq. (16), N x N

Q = matrix, Eq. (17), N x N

$\{r\}^{(i)}$ = vector of reaction loads applied to the i-th substructure

r_{x1} r_{y1} r_{z1} = components of reaction force applied to a substructure connection node, Fig. 2, lb

r_{mx1} r_{my1} r_{mz1} = components of reaction moment applied to a substructure connection node, Fig. 2, lb-ft

R = matrix Eq. (19), N x N

R_D = dependent coordinate system reaction load vector, N_D x 1

t = time, sec

u v w = displacements at a connection node, ft

$\{x\}^{(i)}$ = vector of coordinates for i-th substructure

x_1 y_1 z_1 = rectangular coordinates, Fig. 2

X_D = vector of dependent coordinates for the system, N_D x 1, Eq. (3)

X_I = vector of independent coordinates for the system, N x 1

β = transformation matrix relating dependent coordinates to independent coordinates Eq. (4), N_D x N

β^* = Newmark-Beta factor

$\beta_0, \beta_1, \beta_2$ = transformation matrices from which β is constructed, Eq. (9)

θ_1 θ_2 θ_3 = angular displacements at a connection node, Fig. 2, rad.

σ = rotor solidity

μ = rotor advance ratio, nondimensional

ψ = rotor azimuth angle, rad

Ω = rotor speed, rad/s

[0] = matrix of zeroes

Subscripts

n = time index

D = dependent coordinate system variable

Superscripts

i = i-th substructure

T = transpose

$\dot{}$ = first derivative with respect to time

$\ddot{}$ = second derivative with respect to time

Introduction

In the 1970's dissatisfaction with first generation computer programs for predicting helicopter performance and dynamic behavior motivated the development of the Second Generation Comprehensive Helicopter Analysis System (2GCHAS). The project is funded by the U.S. Government and is managed by the 2GCHAS Project Office at the NASA/Ames Research Center, and involves the participation of industry. The 2GCHAS system aims to provide results for several helicopter related engineering disciplines, as well as helicopter dynamics.

Several approaches were identified as being of potential value for overcoming first generation deficiencies. These approaches consisted of the use of a unifying mathematical basis, executive-based software, and software design and management methodology.

One promising mathematical approach is to separate the dynamical structure into several components, or substructures, and subsequently to combine these into a system of second order differential equations. Coupled with automated assembly of the components, substructuring is expected to enable many problems to be modeled, overcoming the lack of versatility characteristic of first generation systems. Substructuring should reduce the difficulties of verifying the code by dividing the system into easily verifiable parts. Activity can be focused on areas of new code during the process of adding new components, making the system more responsive to changes.

In parallel with this, a software executive would be used to enhance system versatility and usage for components which could not be handled as dynamical substructures, such as post-processing modules and certain types of aerodynamic components.

Application of the techniques of structured design, developed in the software industry (Ref. 1), would help to improve architecture, and coding standards would make code legible. As a result, a second generation system would become more productive by being able to lead a longer useful life and would become more credible because it could be more easily verified. Finally, software management methodology, including automated software tools, would be used for configuration control of versions of the system by protecting versions from untested and undocumented changes.

The cost of applying all the approaches mentioned above to create a system with the scope of 2GCHAS appears to be beyond the resources of any single helicopter manufacturer. On the other hand, recognizing that benefits might result from application of a part of these approaches, the U.S. industry developed experimental codes utilizing some of the new concepts and limited to solution of dynamic problems (Refs. 2 to 4). Sikorsky has developed two component-based codes consisting of the Simplified Vibration Analysis (SIMVIB) of Ref. 2, and the Rotorcraft System Dynamics Analysis (RDYNE) described in this paper. Both methods utilize the same code for substructure assembly, but component libraries are different, providing solutions which differ in technique and scope. In contrast to SIMVIB which emphasizes harmonic balance solutions, RDYNE is a time-history analysis. It is the purpose of the paper to describe RDYNE, particularly with a view to its second generation attributes.

Basis of Analysis

The helicopter dynamical system is assumed to be made up of dynamical substructures and these are automatically assembled into a coupled system represented by a second order differential matrix equation. Figure 1 shows a typical substructure breakdown of a helicopter. The method is able to assemble components into many combinations and orientations. Coupled system response is obtained by integrating the differential equation with respect to time.

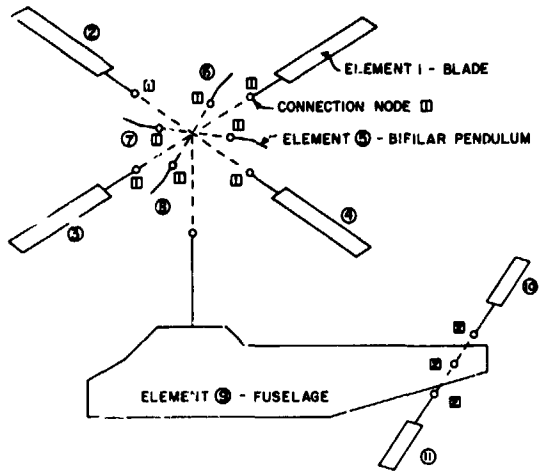

Fig. 1 Sample Substructures Used in the RDYNE Rotorcraft Dynamics Analysis

Substructure Assembly Method

The substructure method employed is the Hurty method of Ref. 5. The coordinates or degrees of freedom of a substructure (also called physical component) are physical and generalized displacements, such as modal amplitudes. The matrix equation of motion for each substructure is expressed in mass, damping, and stiffness matrix, and force vector form. Properties of the i-th sub-structure are $[m]^{(i)}$, $[c]^{(i)}$, $[k]^{(i)}$, $\{f\}^{(i)}$, and $\{r\}^{(i)}$. These are respectively mass, damping, and stiffness matrices, and external force and reaction force vectors. The submatrices for the substructures are collected into a partitioned diagonal matrix equation which represents the system. This partitioned diagonal matrix equation is

$$M_D\ddot{X}_D + C_D\dot{X}_D + K_DX_D = F_D - R_D \qquad (1)$$

The matrix M_D illustrates the typical form of the diagonal matrices as:

$$M_D = \begin{bmatrix} [m]^{(1)} & & \\ & [m]^{(2)} & \\ & & \ddots \\ & & & [m]^{(i)} \end{bmatrix} \quad (2)$$

The vector of coordinates X_D illustrates the form of the vectors F_D and R_D in Eq. (1), and is

$$X_D = \begin{Bmatrix} \{x\}^{(1)} \\ \{x\}^{(2)} \\ \vdots \\ \{x\}^{(i)} \end{Bmatrix} \quad (3)$$

The coordinate vector X_D contains unconnected (or internal) coordinates and connection node coordinates. When components are to be connected to each other, redundant coordinates occur in X_D. Fig. 2 shows the translational and rotational displacements, and forces and moments on a connection node.

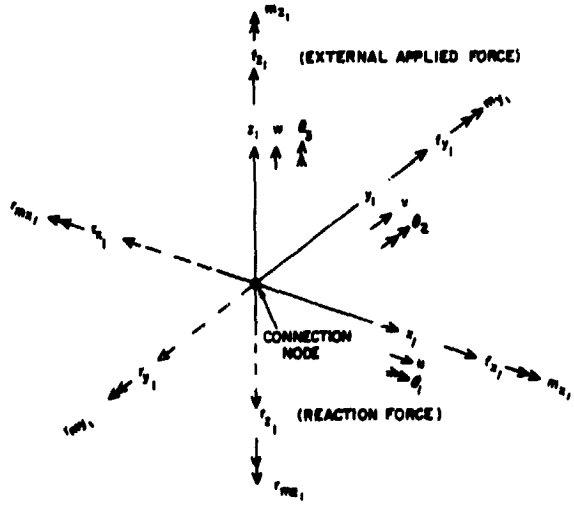

Fig. 2 Displacements and Forces Acting on a Connection Node of a Substructure

The synthesis of the equations of motion for the coupled system is accomplished by a mapping relating the dependent coordinates, X_D, to a reduced (or independent) coordinate set, X_I. Redundant coordinates are eliminated by requiring component displacements to be equal at connections. The transformation matrix relating X_D and X_I is denoted by β, and the mapping of coordinates is

$$X_D = \beta X_I \quad (4)$$

Substitution of the transformation Eq. (4) in Eq. (1) and premultiplication of equation (1) by β^T yields the final equation of motion for the coupled system. This is

$$M\ddot{X}_I + C\dot{X}_I + KX_I = F \quad (5)$$

The matrices in Eq. (5) are typified by

$$M = \beta^T M_D \beta \quad (6)$$

and the load vector is

$$F = \beta^T F_D \quad (7)$$

The component displacements X_D may be recovered from the solution to Eq. (5), X_I, by mapping Eq. (4), and component velocities and accelerations are derived similarly. With X_D and its derivatives known, connection node or interface reactions (e.g., rotor hub shears) may be determined from Eq. (1).

$$R_D = F_D - (M_D\ddot{X}_D + C_D\dot{X}_D + K_DX_D) \quad (8)$$

The transformation matrix β is the product of three transformations (Ref. 2) which assemble coupled systems from components whose properties are defined in component local axes and allow for the use of modal coordinates. The transformation β is

$$\beta = \beta_o \beta_1 \beta_2 \quad (9)$$

The transformation from dependent coordinates resolved to local axes with arbitrary angular orientations to dependent coordinates resolved to a global reference axis is β_o. The transformation from dependent coordinates, referred to a global reference axis, to coordinates from which redundant coordinates at connection nodes have been removed is β_1. The transformation from physical domain independent coordinates to coordinates which include modal coordinates, X_I, is β_2.

Time History Solution

The solution algorithm yielding the time history response is the Newmark-Beta method described in Ref. 6. Displacement responses are obtained from displacements known at prior times, and from data defining the magnitudes of known external forces acting on the system.

The vector of coordinates satisfying Eq. (5) at time step n is denoted $(X_I)_n$. The corresponding time is:

$$t_n = t_{n-1} + h \quad (10)$$

In Eq. (10) h is the step size. The integer step number n ranges from one to the number of steps in the calculation. Time t_o is the initial time. Corresponding initial conditions are $(X_I)_o$ and $(\dot{X}_I)_o$.

When $(X_I)_o$ and $(\dot{X}_I)_o$ are specified the displacement response at t_1 is found from:

$$(X_I)_1 = D^{-1} [P(X_I)_o + Q(\dot{X}_I)_o + \beta^* h^2 F_1 + RF_o] \quad (11)$$

Matrices D, P, Q and R are functions of M, C, and K in Eq. (5), time step h, and factor β^* (see equations (15) through (21)). They have dimensions NXN where N is the size of X_I in Eq. (5). The factor β^* is the Newmark-Beta Factor. Values of β^* ranging from 0 to 0.25 can be input to the program. The factor β^* is used to control the variation of acceleration assumed in the time interval (see remarks in Ref. 6). A numerical solution with $\beta^* = 0.25$ is unconditionally stable. Force vectors F_1 and F_o are known external forcing functions at t_o and t_1.

After the solution $(X_I)_1$ is known, successive solutions are obtained from the recursion formula:

$$(X_I)_{n+1} = D^{-1} [B(X_I)_n - F'(X_I)_{n-1} + \beta^* h^2 (F_{n+1} + (1/\beta^* - 2)F_n + F_{n-1})] \quad (12)$$

The NxN Matrices B and F' are known functions of M, C, and K, step size h, and factor β^* (see Eqs. (20) and (21)). Equation (12) may be used to restart solutions from solutions calculated up to the time of restart.

The additional assumption is made in the program code that the force F_{n+1} linearly extrapolates the forces F_n and F_{n-1}. For equal intervals of time h this assumption reduces to:

$$F_{n+1} = 2F_n - F_{n-1} \quad (13)$$

and Eq. (12) becomes:

$$(X_I)_{n+1} = D^{-1} [B(X_I)_n - F'(X_I)_{n-1} + h^2 F_n] \quad (14)$$

Eq. (13) allows for the insertion of aerodynamic forces which are functions of X_I and $\dot{X}_I$, by assuming F to be a function of X_I and its derivatives at a prior time.

Matrices in Eqs. (11), (12), and (14) are:

$$D = M + (h/2)C + \beta^* h^2 K \quad (15)$$

$$P = M + (h/2)C - (1/2 - \beta^*) h^2 K - (1/4 - \beta^*) h^3 C M^{-1} K \quad (16)$$

$$Q = [M - (1/4 - \beta^*) h^2 C M^{-1} C] \; h \quad (17)$$

$$R = [(1/2 - \beta^*) I + (1/4 - \beta^*) hCM^{-1}] \; h^2 \quad (18)$$

$$I = \text{unit matrix} \quad (19)$$

$$B = 2M - (1 - 2\beta^*) h^2 K \quad (20)$$

$$F' = M - (h/2)C + \beta^* h^2 K \quad (21)$$

The dimensions of matrices in Eqs. (15) through (21) are NXN where N is the dimension of the vector of independent coordinates X_I.

Main Features of Computer Program

The top-level structure of the computer program reflects the component basis of the analysis. Dynamical components are substructures which obey second order differential equations which can be assembled into coupled dynamical systems. Non-dynamical components include several types of section aerodynamic and inflow models, and a component for trim and vibration reduction.

Top-Level Structure of Program

The top level structure of the RDYNE computer program is shown in Fig. 3 and reflects the component basis of the program, showing a separation into component-dedicated and component-independent areas. This organization is responsible for several desirable attributes.

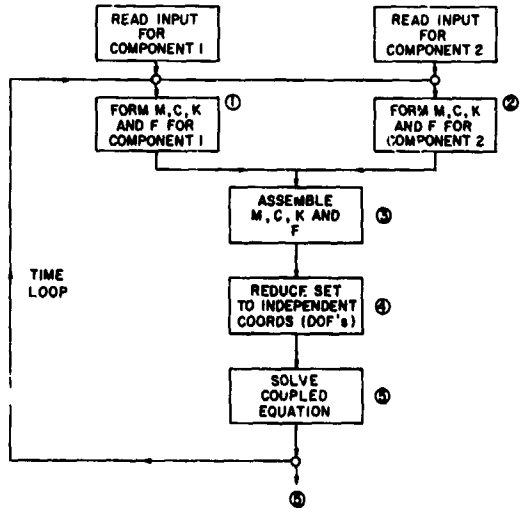

Fig. 3 RDYNE Main-line Program Flow Chart

Component routines are required for each dynamical component listed in Table 1 and a typical organization is shown in Fig. 3. Component input and processing blocks form mass, damping, and stiffness matrices and aerodynamic and gravitational loads at the component level. Component-independent code performs assembly of substructures into a coupled system, reduction to independent coordinates, and solution of the equations. An interpretive routine (not shown in Fig. 3) reads names of selected components and corresponding input, and is followed by processing which utilizes component element numbers and connection node numbers (Fig. 1) and component orientations to assemble components into a coupled system.

Non-dynamical components include several types of section aerodynamic and rotor inflow models, and a component for trim and vibration reduction. The components resemble dynamical components by having dedicated input and processing routines but otherwise do not behave like dynamical substructures because they cannot be assembled into dynamical systems by the assembly method described previously.

Usage and understanding of the program are facilitated by ability of the program to limit input data to components selected by the user for his particular problem. This contrasts with first generation systems which required an understanding of the input for the most comprehensive problem even when preparation of only a part of this input was required. Processing and storage requirements are limited to the components selected, allowing resources to be tailored to each problem and to be less than the resources for the most comprehensive problem. Verification, modification, and addition of components is confined to component routines, making the system more responsive to change requirements. User and programmer experiences and data on execution speed have confirmed the above attributes.

Dynamical Substructures

All dynamical substructures, except modal structures (see text below) employ coordinates which are unconnected (or internal) coordinates, and connection coordinates which enable the substructure to be assembled with other substructures through the equating of displacements at the connection. With the exception of modal structures, it is necessary for each substructure to include six equations of equilibrium corresponding to the six displacements at the connection node shown in Fig. 2, to enable it to be coupled to any other substructure.

A noteworthy difference between dynamical substructures (Table 1) is that the blade models contain matrices which are explicit functions of time while the fuselage and matrix structure in Table 1 have constant matrices. Explicit time dependence occurs from a resolution of blade hub loads to a non-rotating axis system (Fig. 2) to derive the connection node equilibrium equations. This allows the transformation

Table 1 - Dynamical Components in the RDYNE Analysis

Component	Description
Elastic Blade	Normal modes elastic blade with flatwise, edgewise, and torsion elastic modes (Ref. 8), augmented to include six hub displacements, and expressed in M, C, K, and F forms.
Articulated Blade	Simplified model containing a subset of the coordinates applicable to the elastic blade.
Modal Structure	Structure expressed in terms of normal mode coordinates.
Matrix Structure	Generalized structure with fully populated M,C, and K matrices.
Prescribed Force	Substructure providing for the application to any component of a harmonically varying force of specified amplitude and phase.
Fixed Absorber	Vibration absorber which may be attached to any other substructure in the non-rotating system.

matrix β in Eq. (4) to be independent of time, and can be shown to justify the transformation of the dependent coordinate Eq. (1) to the independent coordinate Eq. (5).

The theory of Ref. 8, available in older codes at Sikorsky, was used as the basis of the elastic blade model (Fig. 4) to minimize the labor required to code and check the model, and because this model has been substantiated through extensive comparisons with test data. Although the blade model is available in older codes, completely new coding was written to conform to the component basis and legibility requirements of RDYNE. The equations for the internal coordinates were augmented with six hub equilibrium equations corresponding to hub connection node coordinates. The equations also were reduced to M, C, K, and F forms.

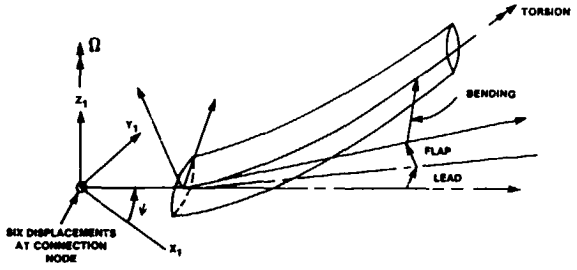

Fig. 4 Schematic of Elastic Blade Substructure

Table 2 - Mathematical and Aerodynamic Components

Component	Description
Time History Integration Method	Component used to integrate the equations of motion with respect to time which employs the Newmark-Beta finite difference method of Ref. 6.
Trim Controller	Minimum variance controller used for rotor trim and coupled system vibration reduction (Ref. 10).
Environment Input	Component defining the properties of the atmosphere.
Aerodynamic Model Type 1	Simplified formula-based section aerodynamic model for conventional airfoils.
Aerodynamic Model Type 2	Table look-up section aerodynamic model for conventional airfoils.
Aerodynamic Model Type 3	Simplified formula-based section aerodynamic model for circulation control airfoils (Ref. 7).
Aerodyramic Model Type 4	Table look-up section aerodynamic model for circulation control airfoils.
Rotor Inflow Type 1	Momentum-based uniform rotor inflow component.
Rotor Inflow Type 2	Variable rotor induced inflow component, using a matrix of wake influence coefficients, calculated by the method described in Ref. 9 and transmitted to RDYNE.
Rotor Inflow Type 3	Momentum-based annulus inflow for hover applications.
Rotor Inflow Type 4	Glauert inflow consisting of steady and first harmonic azimuthal and linear radial variations of inflow.

The modal structure is an exception to the coordinate classification for other substructures. This substructure employs the normal modes of a substructure as coordinates and has constant mass damping, and stiffness matrices, and can be used to represent fuselages, and other systems, described in the applications. Each such structure is allowed to have up to five connection nodes, at which elements of the modal matrix for each normal mode are defined, comprising three translations and three rotations, with the directions shown in Fig. 2. The substructure is coupled to others by expressing physical displacements at a connection as a summation of modes, to define β_2, in Eq. (9).

The aerodynamic generalized forces in the blade components are obtained from application of blade element theory and by invoking the section aerodynamic and inflow components listed in Table 2 to define aerodynamic properties.

Aerodynamic Components

Four section aerodynamic and four inflow models are available, and are listed in Table 2. The section aerodynamic models include formula-based and table look-up methods. Input to the formula-based section Aerodynamic Model Type 1 consists of lift curve slope, maximum lift coefficient, and coefficients required in expressions for drag and moment curves. This simple model is used when data on section characteristics are not accurately known, such as in blade damage simulations. Aerodynamic Model Type 2 is used to provide bivariant tables of characteristics expressed as functions of angle-of-attack and Mach number, obtained from wind tunnel tests.

To link an aerodynamic component to a blade component, the user specifies in the input to the blade component the element number of the aerodynamic component, which is followed by corresponding input data or file names defining the location of data. The linkage procedure provides considerable latitude for using different aerodynamic components on different blades and blade sections, and has been well received by users.

Rotor induced variable inflow is embodied in geometric influence coefficients transmitted to a file from an existing program external to RDYNE (Ref. 9). The wake form is a skewed helix and its geometry is assumed to depend on advance ratio. RDYNE determines by an iterative method wake circulations which are consistent with the inflow influencing blade section aerodynamic loads. A strong coupling is achieved of variable inflow to rotor response in RDYNE without having to rely on a procedure involving iterative coupling of large programs, such as that used for SIMVIB in Ref. 2.

Trim and Vibration Reduction

A departure was made with older derivative-based trim determination methodology by treating the trim problem as an optimization problem, and the opportunity was taken to solve both the trim problem and the vibration reduction problem. The code for the controller was derived from the vibration reduction program described in Ref. 10.

A minimum variance controller was implemented which utilized an unconstrained minimization formulation to reduce differences between a target trim state, corresponding to specified steady hub loads, and components of steady hub loads for the actual rotor state. The transfer matrix relating hub loads to control inputs is initially calculated by a difference method from the results of perturbations to the control vector and subsequently is identified by a Kalman filter procedure, which is able to speedily identify the transfer matrix. A scalar performance index embodies the objectives to be minimized and differentiation of the performance index with respect to the control variables yields an optimal control state vector. Controls are updated according to the optimal formula at user-specified intervals.

Figures 5 and 6 show the effects of application of the method to a four-bladed conventional rotor on a rigid support. The simulation employs a single elastic blade and multiplies the steady loa[illegible]y a factor of four to define the rotor [illegible]ds. Figures 5 and 6 show that severe [illegible]im objectives may be specified and s[illegible]ltaneously achieved.

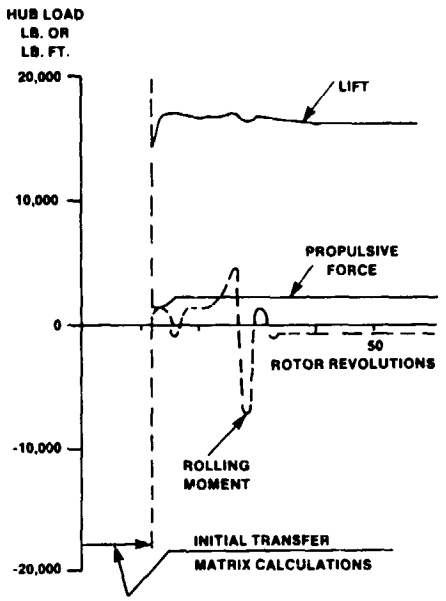

Fig. 5 Effects of Minimum Variance Controller on Steady Hub Loads For A Conventional Rotor

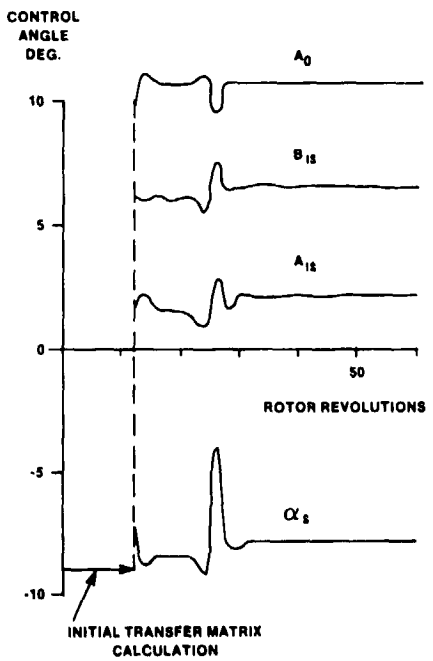

Fig. 6 Effects of Minimum Variance Controller on Trim Control Variables For A Conventional Rotor

The same approach lends itself to vibration reduction, with the vector of controlled variables containing coefficients of vibratory loads or accelerations at the blade passage frequency or at multiples of this frequency. Figures 7 and 8 show the effects of blowing controls on vibratory hub loads for a circulation control rotor, and the corresponding control state for selected blowing harmonics. A single blade analysis was used for this application although RDYNE is not limited to a single blade and can be used to reduce elastic airframe vibrations for a multiblade rotor system.

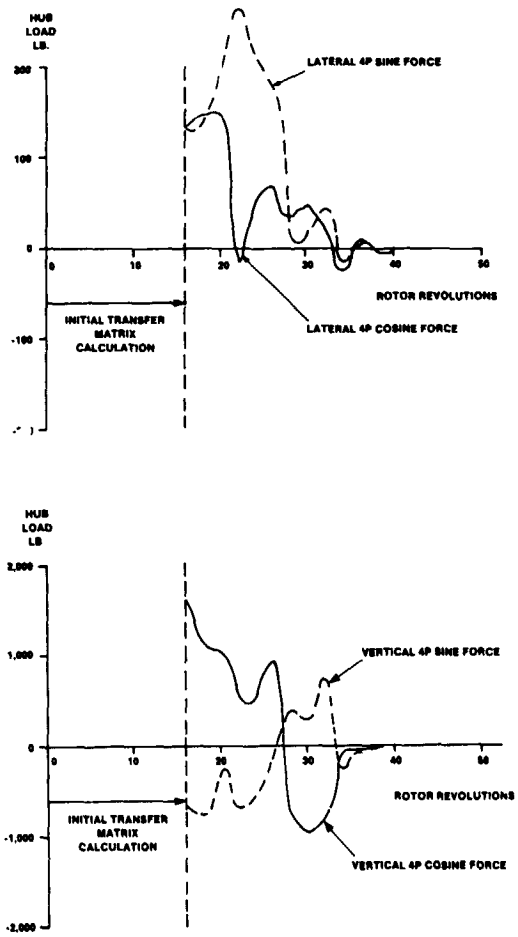

Fig. 7 Effects of Minimum Variance Controller on 4 Per Rev Hub Loads For Circulation Control Rotor

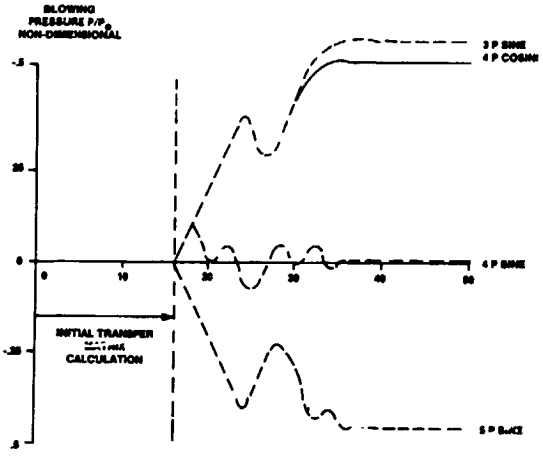

Fig. 8 Effects of Minimum Variance Controller on Control Variables For Circulation Control Rotor

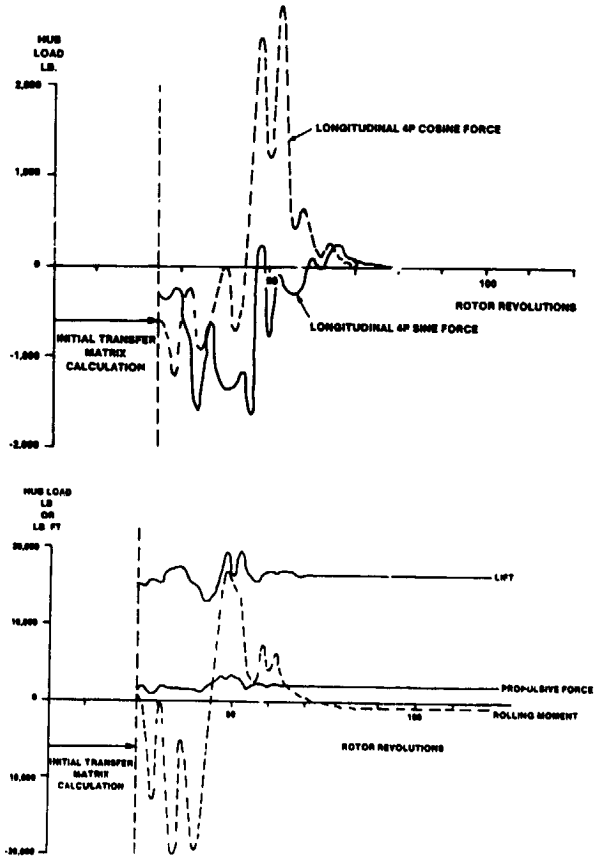

Fig. 9 Simultaneous Trim and Vibration Reduction on a Conventional Rotor

The analysis is configured to permit selection of rotor load or vibration objectives, singly on in different combinations, and Figs. 9 and 10 show the combined effects of application of mechanical controls to achieve trim and vibratory hub load reduction.

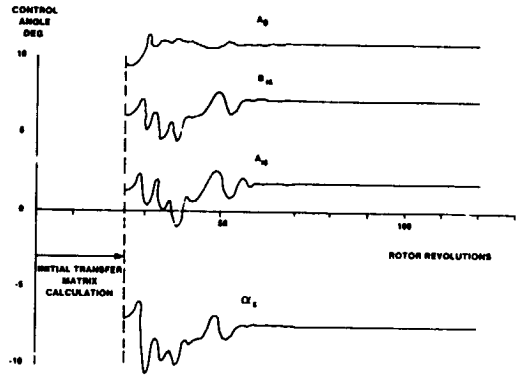

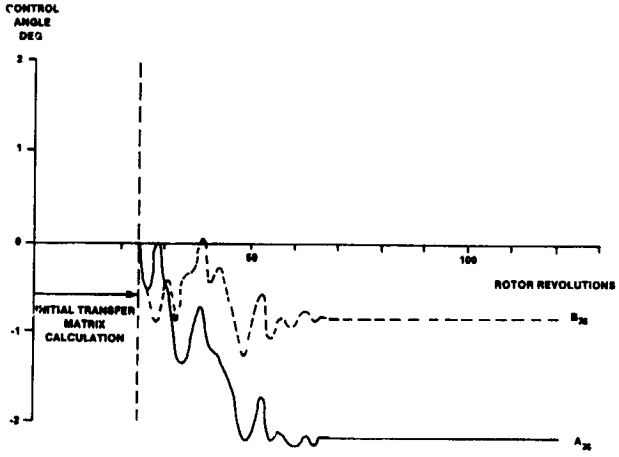

Fig. 10 Control Input History for Simultaneous Trim and Vibration Reduction on a Conventional Rotor

It is seen that a comprehensive solution such as the use of a single minimum variance controller for trim and vibration reduction can be used to reduce development costs by addressing more than one type of problem.

Applications

Applications are described which show the comprehensive ability of RDYNE to handle stability and steady state vibratory load problems using a small number of elements and a time-history basis. Applications to new technologies are described.

Ground Resonance Stability

In early 1979 RDYNE was evaluated for its ability to predict ground resonance stability involving the coupling of several articulated blades of the type shown in Table 1 to an elastic airframe. The elastic airframe was represented by a modal component (Table 1). The values of damping of the coupled systems were calculated from the decay in the responses of modal displacements in the airframe. FFT processing was not used. Figure 11 compares the percentage damping predicted by RDYNE with results from a linear stability analysis (Ref. 11) and shows very satisfactory agreement. Figure 12 compares stability boundaries from RDYNE with a Floquet solution (Ref. 12) for a rotor with a failed lag damper and again shows good agreement. The analysis is now used in a routine manner at Sikorsky to determine the stability of systems with failed lag dampers. It is seen that the time-history method can comprehensively treat problems which were solved by eigensolution and Floquet methods.

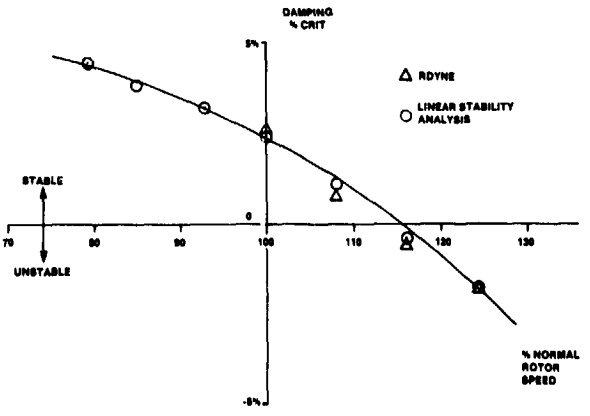

Fig. 11 Ground Resonance Stability Comparison Between RDYNE and Linear Stability Analysis

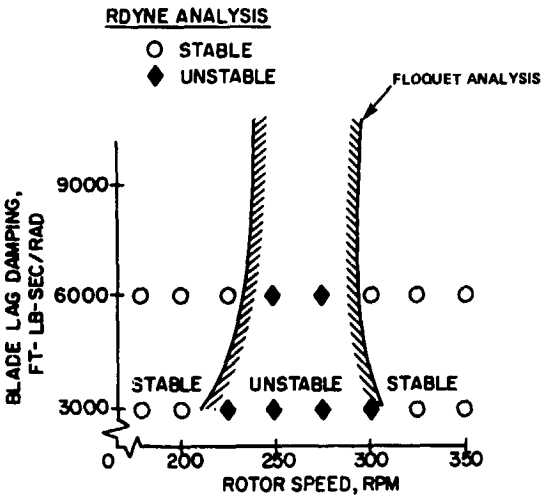

Fig. 12 Stability Boundaries Predicted by RDYNE And A Floquet Analysis For A Rotor With A Failed Lag Damper

Non-symmetric Rotor and Damage Simulation

The advent of RDYNE created new opportunities for studying non-symmetric rotor and failure/damage simulations.

The program was applied to a BLACK HAWK rotor to simulate the response of a rotor/drive train system to lightning induced damage to one of the blades. The effects of lightning were determined by passing electric currents through a portion of blade in ground tests. The aerodynamic characteristics of the blade after damage were estimated from its appearance and were loaded in as input to the simplified section aerodynamic model listed in Table 2. The normal modes of the drive train were inserted in the input to the modal component to represent the seven component drive train. Results from the program without blade damage were used as initial conditions for a restart solution with the damaged blade. Figures 13 and 14 show blade and drive train responses before and after the damage. A drive train schematic is also shown in Figure 14. The transition from four-per-rev to once-per-rev responses is evident.

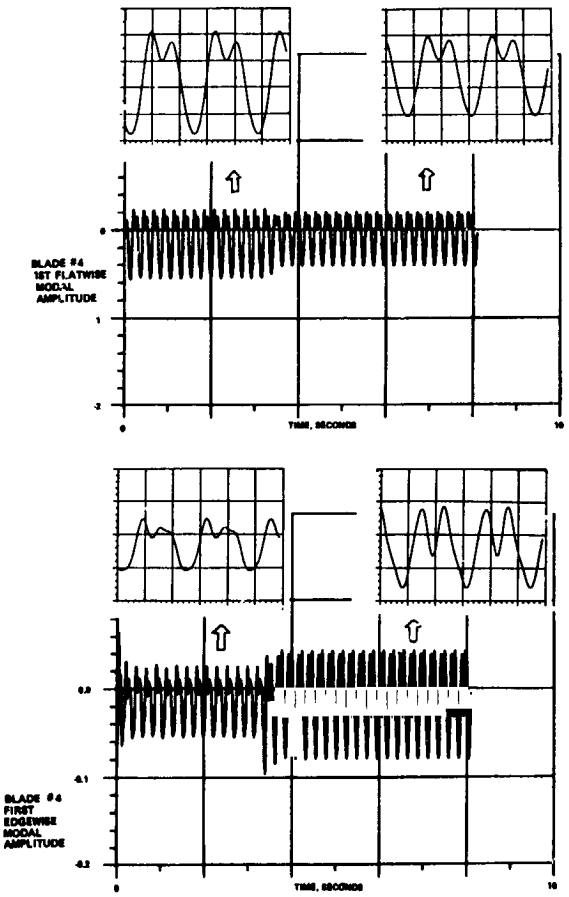

Fig. 13 Effects of Blade Damage on Time Histories of Blade Responses For A Coupled Rotor/Drive Train System

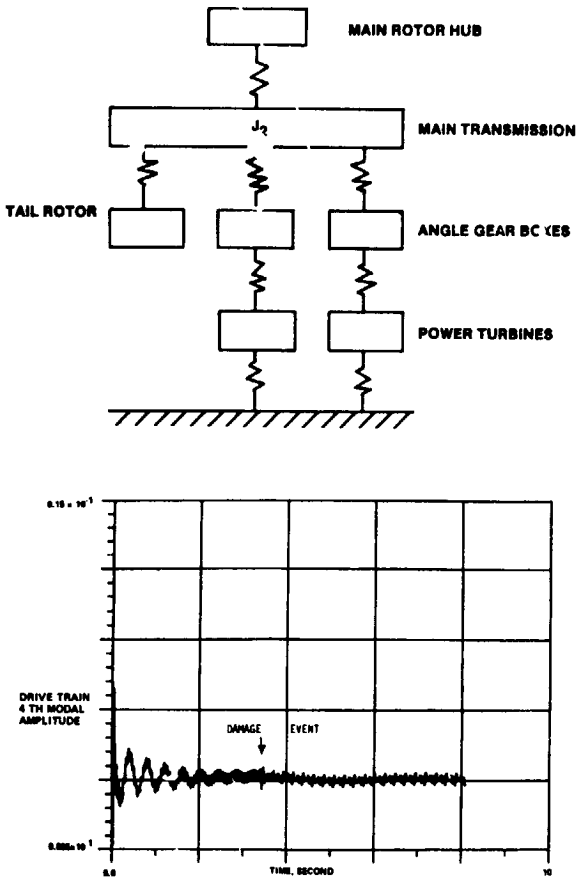

Fig. 14 Drive Train Responses to Rotor Damage For A Coupled Rotor/Drive Train System

The use of the modal component for the drive train in this problem and its use as an airframe in the ground resonance problems shows that versatility and reduced development cost can be achieved through using a single type of component for different types of problems.

Stopped and Gimballed Rotors

Stopped and gimballed rotors are new technologies to which RDYNE has been applied and for which it has provided timely solutions.

Rotors which are stopped have no centrifugal stiffening and have to be checked for bending divergence when in the swept-forward position. Figure 15 shows the increase with forward speed in damping of the first elastic flatwise mode of a hingeless rotor blade stopped at 135 degrees azimuth. At the divergence speed the frequency of the mode is zero and the modal damping becomes infinite. The divergence speed agreed well with results predicted by the doublet lattice theory in the NASTRAN analysis. The ability of RDYNE to successfully model fixed lifting surfaces by means of an elastic blade component, originally derived for rotary wing applications, is the result of designing this blade component for multiple applications. In contrast to the original derivation in Ref. 8, which non-dimensionalized variables by rotor speed, the new equations were left in dimensional form, allowing the non-rotating case to be treated without difficulty.

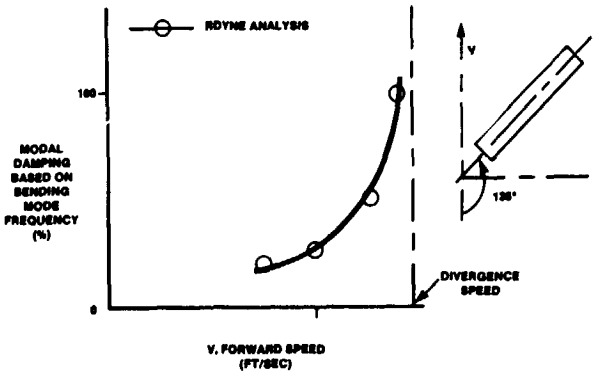

Fig. 15 Divergence of a 45 Degree Forward-Swept Stopped Rotor Blade

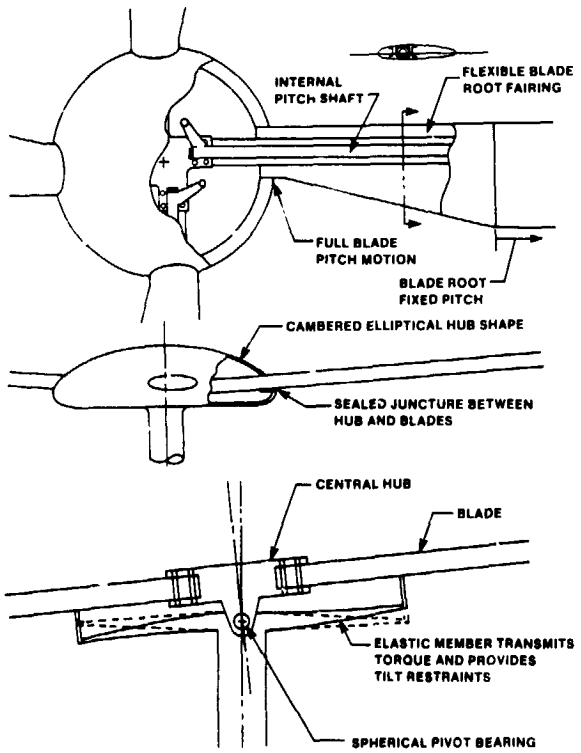

Fig. 16 General Arrangement of Dynaflex Rotor Hub and Schematic of Elastic Gimbal

The Dynaflex gimballed rotor is a new concept under development at Sikorsky which incorporates unique features (Ref. 13). Utilizing composite materials, the central hub is gimbal-mounted relative to the shaft achieving a universal joint action with a spring restraint to the tilting motion (Fig. 16). The arrangement is less cumbersome than a mechanical universal joint, and greatly reduces Coriolis forces. Lower blade loads and reduced vibrations should result. The hub design is an exceptionally clean aerodynamic form.

Tests have been conducted with a 4.4 ft radius model. Comparisons shown below are for a stiff inplane rotor tested in a hover rig from 350 to 650 rpm, and for a soft inplane rotor tested at advance ratios between .15 and .45, and C_t/σ between .06 and .11.

RDYNE was applied to this rotor to evaluate its stability and vibratory load behavior. The analysis was modified in a period of two weeks to include the matrix substructure listed in Table 1 to simulate the gimbal. The short development was evidence of the responsiveness of a component-by method to new technology.

The rotor/support system used in model tests was represented by means of four elastic blades, a matrix substructure with two connection nodes representing the gimbal, and a normal mode structure representing the support (Fig. 17). The upper connection node of the matrix substructure was attached to the elastic blades, and the lower connection at the pivot bearing was attached to the normal mode support. The properties input to the matrix substructure were established by deriving gimbal mass, damping, and stiffness elements by the Lagrangian method. Stability results were obtained by means of a moving block method, and a single blade simulation was used to calculate the trim state of the gimbal rotor in level flight.

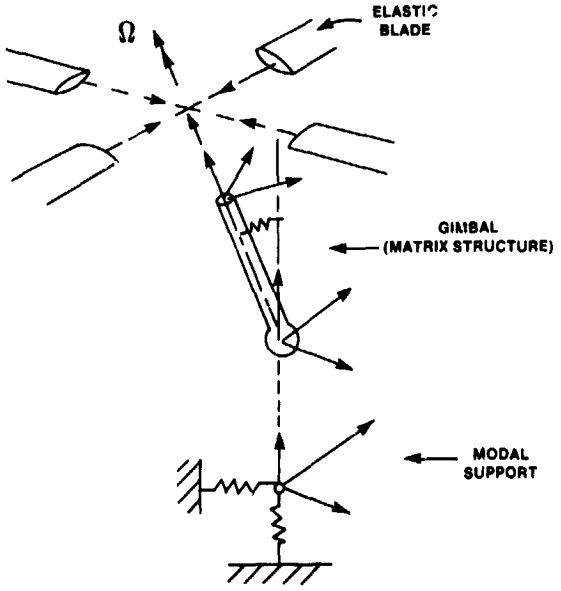

Fig. 17 Substructures Used to Represent the Dynaflex Rotor

Figure 18 compares test and analysis predictions of gimbal system frequencies and dampings in hover. Figure 19 compares test and analysis results for bending moments in level flight. Edgewise mode dampings established from a gauge on the moving blade are compared in Fig. 20. The hover stability comparisons are quite good as are flatwise bending moment variations with forward speed. The edgewise bending moments and stability in forward flight are overpredicted.

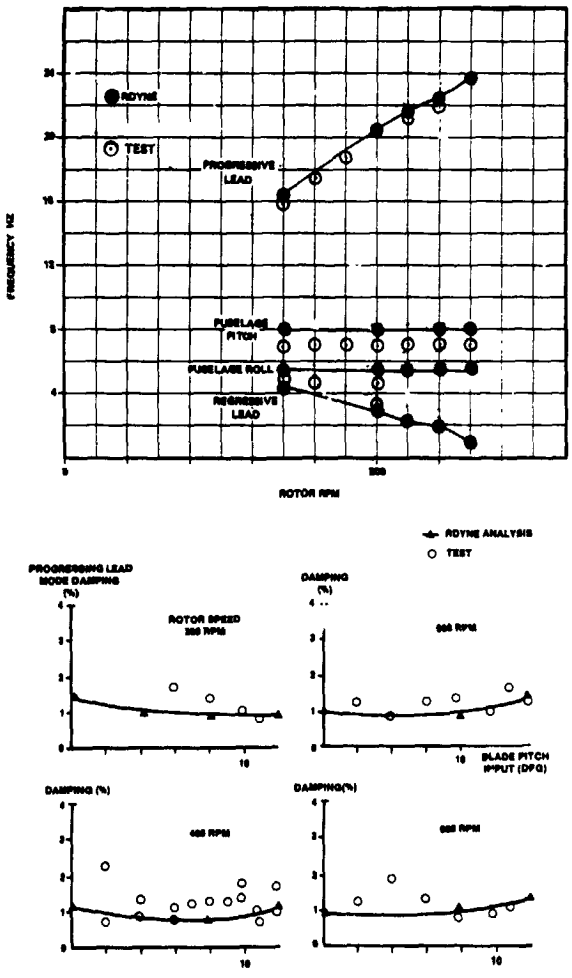

Fig. 18 Comparison of Predicted Frequencies and Dampings with Test Data For a Dynaflex Model Rotor in Hover.

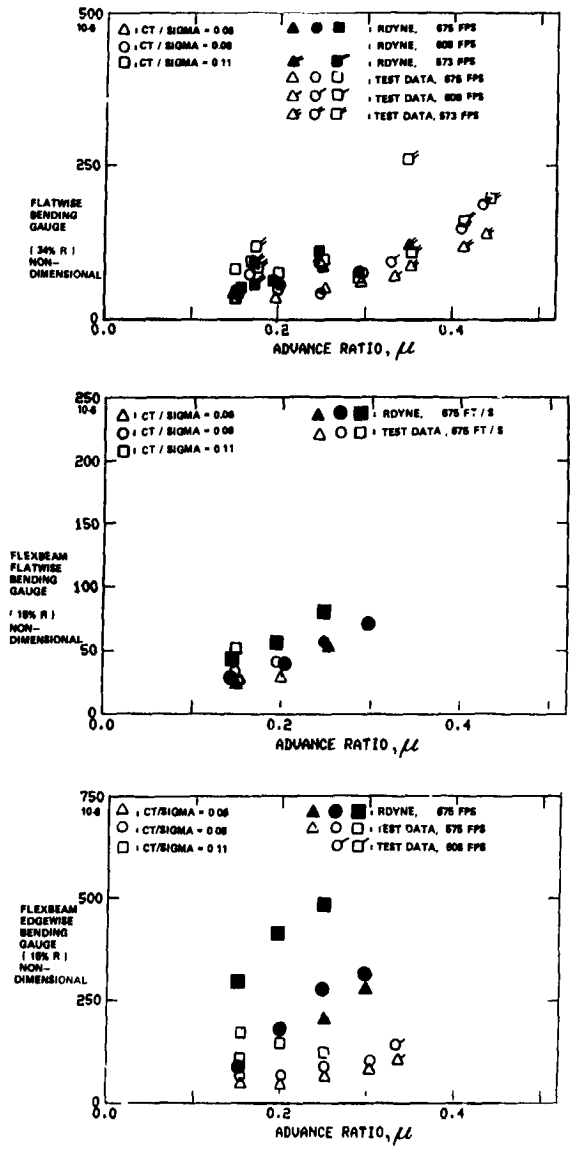

Fig. 19 Comparison of Vibratory Bending Moments for a Dynaflex Model Rotor in Level Flight.

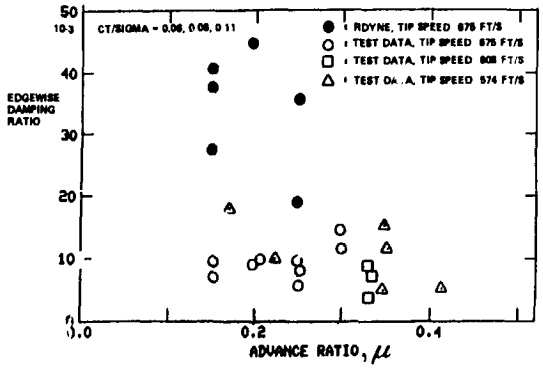

Fig. 20 Comparison of Blade Edgewise Stability for a Dynaflex Model Rotor in Level Flight.

Concluding Remarks

An analysis utilizing dynamical substructures and non-structural components has confirmed several desirable attributes expected from modern codes. These attributes include the ability to handle a comprehensive set of problems with a small library of components, supported by the ability to treat steady state vibratory and stability problems within a time-history framework. The analysis has responded to new technologies with timely solutions for advanced rotor concepts, by limiting the effort required to implement capabilities through its component structure. Comprehensive solutions, such as the use of a single minimum variance controller for trim and vibration reduction, have reduced development costs by addressing more than one type of problem.

References

1. Stevens, W.P., Myers, G.J., and Constantine, L.L., "Structured Design," IBM Systems Journal, Vol. 13, No. 2, 1974, pp. 115-139.

2. Sopher, R., Studwell, R.E., Cassarino, S., and Kottapalli, S.B.R., "Substructure Program for Analysis of Helicopter Vibrations," Journal of the American Helicopter Society, Vol. 28, No. 4, 1983, pp. 14-21.

3. Yen, J.G. and McLarty, T.T., "Analysis of Rotor - Fuselage Coupling and Its Effect on Rotorcraft Stability and Response," Vertica, Vol. 3, 1979, pp. 205-219.

4. Berman, A., "A Generalized Coupling Technique for the Dynamic Analysis of Structural Systems," Journal of the American Helicopter Society, Vol. 25, No. 3, July 1980, pp. 22-28.

5. Hurty, W.C., "Dynamic Analysis of Structural Systems Using Component Modes," AIAA Journal, Vol. 3, No. 4, 1965, pp. 678-685.

6. Chan, S.P., Cox, H.J., and Benfield, W.A., "Transient Analysis of Forced Vibrations or Complex Structural - Mechanical Systems," Journal of the Royal Aeronautical Society, Vol. 66, July 1962, pp. 457-460.

7. Chopra, I. and Johnson, W., "Flap-Lag-Torsion Stability of Circulation - Controlled Rotors in Hover," American Helicopter Society 34th Annual National Forum, May 1978.

8. Arcidiacono, P.J., "Prediction of Rotor Instability at High Forward Speeds - Volume 1 - Steady Differential Equations of Motion for a Flexible Helicopter Blade with Chordwise Mass Unbalance," USAAVLABS TR 68-18A, February 1969.

9. Landgrebe, A.J., and Egolf, T.A., "Rotorcraft Wake Analysis for Prediction of Induced Velocities," USAAMRDL TR 75-45, 1976.

10. Davis, M.W., "Development and Evaluation of a Generic Active Helicopter Vibration Controller," American Helicopter Society 40th Annual National Forum, Arlington, Virginia, May 1984.

11. Johnston, R.A. and Cassarino, S., "Helicopter Rotor Stability Analysis," USAAMRDL-TR-75-40, 1976.

12. Hammond, E.C., "An Application of Floquet Theory to Prediction of Mechanical Instability," Proceedings of the AHS/NASA Ames Specialists' Meeting on Rotorcraft Dynamics, NASA SP-352, Feb. 1974.

13. Fradenburgh, E.A. and Carlson, R.G., "The Sikorsky Dynaflex Rotor - An Advanced Main Rotor System for the 1990's," American Helicopter Society 40th Annual National Forum, Arlington, Virginia, May 1984.

DISCUSSION
Paper No. 11

DEVELOPMENT AND APPLICATION OF A TIME-HISTORY ANALYSIS FOR ROTORCRAFT DYNAMICS BASED ON A COMPONENT APPROACH
Robert Sopher
and
Daniel W. Hallock

Marty Schroeder, Solar Energy Institute: You have talked about the modularity of your code and the flexibility of it--can you give some indication of the size of the code--RAM and ROM?

Sopher: It's actually 4 megabytes now. We are upgrading the IBM System to 8 megabytes so we are not that concerned about the size. We are not interested in overlay. At some point in time we may be interested in an executive which brings in only the routines that a user is interested in applying which would compile and link-edit the routines in object time to create a module which he was interested in using. So that's something we are interested in.

Ed Austin, U.S. Army Applied Technology Laboratory: I have just reams of questions I would like to ask. I'll try to cut it down to just a few. First, with regard to the aerodynamics. Have you given any consideration to the way your executive might handle aerodynamics that are not just a function of the current state but are dependent on previous events, maybe values of the state vector or other dependent parameters?

Sopher: We have given some consideration to that. For example, if you take the case of a general response in two-dimensional linear flow to an arbitrary impulse angle of attack change the response is provided by the Wagner function. In order to calculate the resulting lift you need to retain a history of what has happened to the motion and then you apply the kernel function to that. It's a very simple thing, actually. So as far as I can see in that particular application all you have to do is store the history of the motion somewhere in the program. In regard to other types of application I haven't really thought about anything other than that. Are you concerned about, say, a time-history representation of variable inflow?

Austin: Something like that, yes.

Sopher: [I have] not really thought about that very much.

Austin: Another question regarding your algorithms for your controller. You showed all your variables as nice continuous functions of time. Do you actually treat them that way or do you only look at them once per revolution?

Sopher: No. They go like this. They are discontinuous so really what I should have drawn was a set of . . . it would look something like a bar chart, but I just drew a smooth curve through that.

Austin: But what kind of algorithm is it that actually performs your convergence?

Sopher: Well, the objective function is a weighted square of the things you want to minimize. For example, say, you want to achieve a certain level of lift. It is the square of the difference between the target value of the lift and the actual lift as harmonically analyzed in the program, say, a steady value of lift. Now that is weighted by a weighting function. In addition to that we have weights that are applied to the control vector as well and the purpose of that is to try to limit the magnitude of the excursions of the controls because this is an unconstrained minimum optimization approach. We haven't tried to use a constraint optimization approach because if you go to any of those programs like COPES/CONMIN or ADS it's an incredibly large code and itself would equal the size of this program. So this was the simple approach [that was] adopted. The relationship between the change in the state of the variables which are being used to control the system and the controlled state is obtained through what we call the T-matrix. That's identified subsequently by a Kaman filter method. As a matter of fact, I should make some acknowledgements here. Originally the controller was developed by John Molusis; Bob Taylor, who is with Boeing Vertol, went into further developments on it; and then our research labs carried out further developments. We had to reconfigure it considerably before it could be usefully used in RDYNE.

Austin: How often is that controller updated?

Sopher: Well, as often as you like. The user has the ability to define how often he wants to do it, but I believe in applications that we have typically it's after each revolution or after 2 revs or something like that. There are people who use the program who are more experienced in answering that question. It's undergoing fairly intensive use now.

Austin: You show some Floquet results. Do you use the one-pass or the N-pass approach?

Sopher: No, those results were obtained by means of a time-history response. But I compared with Gene Hammond's Floquet solution. We just use log decrement on that. In order to get the stability of the Dynaflex System we used a moving block method. As a matter of fact we haven't built the moving block into the program. Bob Goodman developed his own little post-processor. I think what would happen is you can eliminate some of the concerns about responsiveness in terms of time for providing stability results by building a post-processor into the program. That would address some of the concerns people have about the comparative efficiencies of aeroelastic stability methods versus time-history methods.

Austin: One final question. Do you have your aerodynamics and dynamics integrated into one program or they separate programs coupled by JCL?

Sopher: They are integrated into one program.

RESTRUCTURING THE ROTOR ANALYSIS PROGRAM C-60

P.G. Phelan and F.J. Tarzanin, Jr.

Boeing Vertol Company

Philadelphia, Pennsylvania

Abstract

The continuing evolution of the rotary wing industry demands increasing analytical capabilities. To keep up with this demand, software must be structured to accommodate change. The approach discussed in this paper for meeting this demand is to "restructure" an existing analysis. The motivational factors, basic principles, application techniques, and practical lessons from experience with this restructuring effort are reviewed.

Introduction

As the rotary wing industry matures it is getting increasingly difficult to extract the next significant technological advance. Improved understanding of the physical phenomena of rotary wing aircraft requires more complete analytical representations. Advances in computer technology are allowing larger more sophisticated analyses than were previously practical. As a result, the demand for complex analysis capability is growing rapidly, with increasing emphasis [illegible] plinary analysis. The changing and growing demands of rotary wing analysis necessitate that software be structured to quickly and efficiently accommodate change if it is to take advantage of continuing developments in this dynamic environment.

Software may be designed with structure emphasizing maintainability and modifiability. Software structured toward this goal provides reduced modification and maintenance costs, reduced time delay for adding new capabilities and improved reliability through a reduction in the number of undetected errors. This may be accomplished through judicious partitioning of software into functional modules, provision of well-defined paths of data flow, and adherence to a control hierarchy.

The proposed approach to obtaining a well structured rotor loads program is to "restructure" an existing analysis. Restructuring can be a time-saving and cost-saving alternative to developing new structured software. It consists essentially of reorganizing the code of an existing analysis to fit a structured design, while maintaining the theoretical basis for the analysis.

Presented at the Second Decennial Specialist's Meeting on Rotorcraft Dynamics, AHS/NASA Ames, Moffett Field, CA, November 7, 1984.

A Boeing Vertol rotor analysis program (C-60) is currently being restructured. Large complex blocks of multi-functional code are being broken down and reorganized into succinct functional modules. Related pieces of code, previously scattered throughout the program, are being gathered to form functional modules. Standardized formats for variable definitions, input data, output data, and documentation are being implemented. Even though the restructuring process is not yet complete, code performing a given task is now easier to find, understand, isolate, and modify. Variables, input data, and output data are also now easier to identify, understand, and modify as needed. The overall result is that new capabilities may be implemented in less time, at lower cost, and with improved reliability.

Background

- Motivation for More Capable Analyses

Physical understanding is expanding rapidly in areas related to analytical modeling of nonuniform downwash, rotor/fuselage coupling, vibration, noise prediction, rotor airloading, and composite material behavior, among others. There is a corresponding demand for improved analytical capability to reflect these advances More sophisticated designs, such as JVX and LHX, and expanded flight envelopes push many analyses beyond their present bounds of application, into regions where simplifying assumptions such as small angles, linearity, and low coupling breakdown.

Compounding these demands for expanded analytical capabilities is the pressing need for more accurate analytical predictions to facilitate finely tuned multi-variable design benefit trade-off studies. Many of the straight-forward one or two dimensional design problems have been solved. The largest potential rotorcraft improvements require complex trade-offs involving different technologies having a consistent level of complexity. As incremental isolated technology design benefits become smaller, the need for more complete, complex inter-disciplinary models increases. This view is supported by Kerr, Potthast, and Anderson[1]. Eventually, the requirements of more demanding interdisciplinary trade-offs will increase to the point where specialized analyses in isolated disciplines will become inadequate and possibly even misleading.

Advances in computer technology and software development add fuel to the movement for more capable analyses. These advances provide expanded resources and/or reduced cost in terms of CPU time, memory usage, and I/O (input/output) capacity and sophistication. Approaches which were previously beyond practical resource limitations are now viable current or near-future options. Current computer systems now allow program structure to be independent of memory constraints, in contrast to the memory overlay structure restrictions of the past. Increasing sophistication of computer tools (such as shown in Table I) also motivate more capable analyses.

- Practical Limitations of Current Programs

The development of more capable analyses is easier said than done. There is a history of difficulties with the development and upgrading of complex, multi-disciplinary analyses, and the prospect of developing even more sophisticated programs with the requirement for continuous updating, projects an image of long development time, high costs and questionable results.

The primary factor contributing to the difficulty of analysis development today is the tendency of large multi-user multi-analyst programs to evolve and grow in complexity beyond the comprehension of any single user/developer. It is as if such analyses follow a specialized law of entropy, tending toward ever increasing disorder until reaching "saturation of comprehensibility". Program maintenance and modification become increasingly difficult as clarity and understanding are gradually replaced by obscurity and misunderstanding. Bergland[2] presents two observations which summarize this behavior of large programs as "The Law of Continuing Change" and "The Law of Unstructuredness" as shown in Figure 1.

Eventually, at least one too many irreversible or untraceable revisions is made. Correlation and reliability falter suddenly. Previous analytical predictions can no longer be reproduced. Things that "worked" now mysteriously fail and the analysis "dies" suddenly. If a reliable backup version exists the analysis may enjoy a temporary reprieve but eventually it is likely to follow the path to extinction. Therefore, the program with chronic "saturation of comprehensibility" will eventually reach the point at which no further cost-effective growth is possible because revisions can no longer be fully understood or debugged.

The tendency toward disorder causes serious problems long before the analysis actually reaches complete "saturation of comprehensibility", that is, the point at which revisions can no longer be made. Complexity grows with each expansion of capability, as change is added to change without an overall plan or global structure. The analysis evolves gradually via the work of a variety of programmers, analysts, and engineers, with a corresponding variety of individual styles and preferences, (see Table 2). Complexity and apparent disorder result as the natural subtle accumulation of the effects of melding individual styles. These trends are compounded by a lack of adequate, accurate, current documentation and the growing innate complexity of the analysis due to expanding requirements. Excessive complexity reveals itself in highly unpredictable and often excessive person-hour costs for program maintenance and modification, and time delays for new capabilities.

As analytical capability is expanded, additions are made to program input and output. Additions for expansions of capability are often made quickly and without thorough coordination. Additions to input and output are often made more expediently than analytical revisions, and are sometimes left in "temporary version" form. The result is input and output which are not clearly defined, are possibly redundant, are not well organized, and are prone to error. This situation results in the expense of extra user-hours for preparation of program input and interpretation (sometimes deciphering) of program output, and an increased probability of undetected input error and/or output misinterpretation.

Other symptoms of saturation of comprehensibility are less obvious, but have the same root cause. For example, poor correlation may be an indication of undetected errors within the analysis, undetected misuse (such as input error), or undetected misinterpretation of analysis output. Compromised reliability is another warning sign of excessive complexity. An analysis which behaves very well sometimes and very badly other times is providing a warning. Growth of analytical complexity is often accompanied by increased dependence upon the specialized experience of experts associated with specific analyses (described by Kerr, Potthast, and Anderson[1] as "Sam's Program Syndrome"). This development implies poor or nonexistent documentation and very complex code, so that others are unable to understand the analysis.

- A Solution: Structured Program Design

The solution to this problem is the development of analysis programs which will start out and remain clear and understandable throughout a long lifecycle of maintenance and modification. This may be achieved by using "Structured Program Design" techniques to design software for maximum maintainability and modifiability.

Structured program design is a formal methodology for software design which was developed in an attempt to deal with the rapid expansion of software associated costs which began in the 1970's. Bergland[2] provides some historical perspective in "A Guided Tour of Program Design Methodologies" in which the author outlines general trends in software development from "Cottage Industry Programming" of the 1950's through "Heavy Industry Programming" of the 1960's to the birth of "Structured Programming" in the 1970's. At one point, over one percent of the GNP (gross national product) was being spent on software[2]. This stimulated early attempts at formulation of design criteria and programming techniques.

Today, a great deal of effort is being expended in attempts to formalize and standardize software design procedures to yield more maintainable, modifiable, and user-friendly programs. Structured program design is being applied in the rotorcraft field, including a government development program named 2GCHAS (Second Generation Comprehensive Helicopter Analysis System). Documentation has become a large part of most program development efforts. Efforts are being made to standardize, streamline a / nearly automate the generation of both code and documentation. Some examples of this are specification of FORTRAN coding standards[3], development of a "generic" architecture[4], development of programs which generate diagrams directly from code[5], and the proposal of formal program design procedures such as data flow design or programming calculus[2].

An Approach to Structured Program Design

- Development Strategy

Structured program design is a general term referring to an application-dependent design procedure. It may be defined as "design for the best solution". The key to this approach is a well chosen definition of "best"; one that is well matched to the specific application. The procedure begins with the selection of a general goal, followed by a trade-off of benefits to prioritize different design criteria. A variety of terms have been defined to serve as design criteria. Terminology varies, as illustrated by the list of terms provided as tables 3 and 4, but similar concepts are defines in references 1, 2, 4, and 6. Design criteria used in the present study are efficiency, generality, maintainability, modifiability, reliability, & utility as defined in table 5.

The general goal (or measure of goodness) chosen for the software design discussed here is minimum total lifecycle cost. This lifecycle includes development, checkout, release, operation/ maintenance/modification, and maturity, as shown in Figure 2. Yourdon and Constantine[6] describe the ideal program as "cheap to develop, cheap to operate, cheap to maintain, and cheap to modify". The relative cost and importance of the different phases of a program's lifecycle vary from application to application. The resulting prioritization of design criteria should vary accordingly. For example, the strategy for development of a payroll program might differ dramatically from that for a technical analysis in a volatile field because of different prioritizations for different aspects of the program lifecycle (i.e., efficiency for operating costs versus modifiability for modification costs). As another example, execution time and reliability might be most important for a real-time simulation. In each case, the goal of minimization of total lifecycle cost is reflected in the application-specific prioritization of criteria.

For our design, maintainability and modifiability were chosen as the most important design criteria. This prioritization results from heavy weighting applied to person-hour requirements for expansion of analytical capability and very-long-term accumulation of maintenance costs. In addition, coincident improvements in utility (i.e.: user-friendliness) and computational efficiency are anticipated from restructuring of input and output functions and elimination of redundant and repetitious calculations. However, improvements in these attributes are to be achieved only at no expense to maintainability and modifiability.

Two options exist for development of well structured analyses. These are (1) build a new analysis from "scratch", or (2) restructure an existing production analysis. Restructuring is reorganization of an already debugged, validated, correlated, "mature" analysis. It is the imposition of structure on an existing analysis. This approach utilizes current analysis theory, including derivation of equations, and solution method, and keeps current correlation intact. It utilizes information from current documentation in the new documentation. Checkout or validation consists of comparing results of the current poorly structured analysis with the new restructured analysis and implicitly takes advantage of all prior validation and correlation efforts. While restructuring does not, in general, include provision of any new capability it may be coincident with provision of new capability. An additional benefit is that the program remains operational and useful throughout the restructuring process, thereby providing immediate gains. In contrast, development of a new structured analysis from scratch begins with approach development and derivation of equations and thus may include new capability. However, starting from scratch does not utilize results of prior correlation, documentation, etc., and the program does not become useful until the long validation/ correlation effort is complete.

Restructuring is the preferred approach if a "mature" analysis is available which is minimally organized and has been validated and correlated. The most difficult, costly, and time-consuming tasks to perform before a large program becomes useful are validation and correlation. Validation is assuring that the analysis program computes what it is supposed to compute (as defined by the equations and method of solution). Correlation is comparison of the analysis results with the "real-world". Validation and correlation require substantial effort for a large sophistocated analysis to exercise multiple-option combinations for multiple configurations. Utilization of prior effort is possible by direct comparison of restructured modular input and output with the same quantities from the poorly structured analysis. The trade-off is the effort required to identify these intermediate values in the poorly structured analysis versus the effort saved in validation and correlation. This potential savings is one of the most significant benefits of the restructuring approach.

Utilization of information in existing documentation provides another potential reduction of effort for the restructuring approach. Since restructuring utilizes the approach and derivation of the current analysis, the documentation pertaining to theoretical

development is still valid and may be utilized in generation of new documentation. In addition, use of an existing method allows the development team to concentrate on the program structure. Thus, restructuring is favored if the current analysis approach is relatively well documented.

Another major benefit of restructuring is potential implementation of improvements in the near-term. Incorporation of at least partially restructured modules into the original program prior to completion of restructuring is possible. Small changes are simpler once a restructured module goes into production. Errors in the existing analysis may be uncovered and corrected, and new capabilities may be implemented in the restructured modules prior to completion of restructuring the whole program. Any benefits which may be incorporated into the new module are thus potential near-term benefits as well.

Determination of the suitability of a currently available analysis for restructuring requires an examination of its structure. (All programs have structure, though some have very bad structure in terms of maintainability and modifiability). The current analysis structure must be compared to a desired analysis structure, which of course, requires at least a first-cut design of a "good" structure. The goal of the comparison is a mapping of functions, and the connections between functions, from the poor structure to a good structure. The mapping is not likely to provide a one-to-one correspondence, but will provide an indication of the effort needed and trade-offs required for restructuring to be successful.

A functional mapping exercise indicates that C-60 is a good "target" analysis for restructuring. A first-cut design of "good" structure and a first-cut mapping of components from poorly structured C-60 to "well" structured modules has been performed. The first-cut design of "good" structure with clearly defined functions is shown in Figure 3. The mapping of corresponding functions in the current C-60 is illustrated by Figure 4 as a structure chart with functions distributed throughout the analysis. While the structure of current C-60 is clearly in need of reorganization, the mapping exercise indicated that validation, correlation, and near-term improvement benefits of restructuring should exceed the cost of efforts to identify, isolate, remove, replace, and reconnect pieces of analysis. In addition, the existence of relatively complete and well-written documentation makes program C-60 a good candidate for restructuring.

- The Restructuring Process

The first task in the restructuring process is development of a plan. A general outline of the plan for restructuring program C-60 is provided as Table 6. The initial tasks define desired attributes for overall program structure, data structure, and control structure, and provide coding guidelines and documentation standards. These tasks lay the groundwork which is essential to the restructuring design process, and thus merit long and serious consideration. However, flexibility to allow and in fact plan for review and revision of initial structural attributes, coding guidelines, and documentation standards is advisable to provide a better final result. Initial testing (by example or trial) of guidelines, particularly documentation and coding guidelines, may provide answers to critical questions such as 'Are the restrictions realistic?, Will they be complied with over a long program life-cycle by a variety of programmers/analysts/users?, Will the documentation be maintained? Is it too cumbersome, or incomplete?, Will this structure still work if we add more coupling considerations?' Though not explicit in the plan outline, flexibility for refinement of guidelines is assumed.

A first-cut "Strawman" design of the overall program structure begins the actual design process. (This step was actually performed, as was required, in the mapping exercise which illustrated suitability of C-60 for restructuring. See Figure 3). A first-cut design of the Main Control Executive is obtained by viewing the analysis as consisting of only its top level "global" functions (e.g.: Velocity, Airloads, Trim, Response). The main design loop may then be executed on a function by function basis until all global functional modules have been designed, built, tested, and documented. The restructuring process is completed by final refinement of the Main Control Executive design, system integration testing, and completion of system documentation. Major stages of the restructuring process as outlined above are described in more detail in the paragraphs which follow.

Design principles were selected to place the desired emphasis on high priority criteria. To improve maintainability and modifiability, design principles are selected which minimize the human effort required to identify and correct program errors, and to define and implement changes to program requirements. Yourdon and Constantine[6] define desirable characteristics of the parts of a system for maintainability and modifiability:

> "....the cost of maintenance is minimized when parts of the system are:
> - easily related to the application
> - manageably small
> - correctable separately."
>
> "....the cost of modification of a system will be minimized when its parts are:
> - easily related to the problem
> - modifiably separately."

The design procedure should provide partitioning or organization of the analysis into pieces which are manageably small (for human comprehension), clearly defined, well documented, and which reflect the "real-world" partitioning of the problem. Similarly, these pieces should be connected to one another in ways which are clearly defined, well documented, and which reflect only "real-world" relationships without extraneous links. Design principles utilized in the present effort to build such a program structure are functional decomposition, hierachal control structure, and data trace-

ability. These principles, which are described individually in the following paragraphs, are used to promote simplicity and clarity in the way the program models the solution it represents.

Functional decomposition is a top-down approach composed of repeated subdivisions from "big picture" functions to code level functions. It is the judicious partitioning of a problem into cohesive decoupled units or modules. (Detailed discussions of intermodular cohesion and intramodular coupling are presented in References 2 and 6). The trickiest aspect of this concept is determining 'functional decomposition with respect to what?'. "The choice of what to decompose with respect to has a major effect on the goodness of the resulting program and is therefore the subject of much controversy."[2] If the definition of functions is derived from a data flow diagram the result is data flow design. If the design is built on the basis of data structure it is data structure design. Bergland[2] describes data flow design (pseudonyms: transform centered design or composite design), in its simplist form as "nothing more than functional decomposition with respect to data flow. Each block is obtained by successive application of the engineering definition of a black box that transforms an input data stream into an output data stream". Another analogy is an engineering system block diagram with transfer function relationships between input and output for each block. The art or magic of functional decomposition is in definition of a model of the real world as functions.

It is in regard to this task, of judiciously breaking an analysis into functions that model the "real-world", that the role of engineer/analyst and the role of programmer/analyst have a critical interface. Careful partitioning may reflect not only the "state-of-the-art", but also the areas of anticipated expansion of capability. Careful functional partitioning should take care to explicitly represent all functions, including simple approximations of functions. This is necessary if the program structure is to accurately represent the structure of the "real-world" problem, and be easily identified and modified to improve the analytical model. The importance of good functional decomposition makes the engineer/analyst a critical, though often unused link in the software development/maintance/modification chain.

Hierachal control structure attempts to define clear traceable lines of decision-making power. This is accomplished by requiring that decisions be made only once, and by placing decisions immediately above the highest level module effected by the decision, thereby limiting authority of all lower level functions. The result may be likened to a human organization, in which "decision-making" power is graduated from top-level executives to mid-level managers to bottom level "number crunchers", as shown in Figure 5. A similar concept is defined by the term "decision-hiding"[4], in which decision information is accessible on a "need-to-know" basis. Hierarchal control structure tends to minimize extraneous control or decision connections, eliminate control redundancy, and guarantee consistency of all option selections. Involvement of engineering personnel in definition of the Control Hierarchy will provide additional insight into anticipated future analytical options and/or vehicle configuration.

Data traceability is the characteristic of having clearly defined single-source paths of data flow. This characteristic is desirable for maintainability and modifiability because it eliminates redundant and/or inconsistent variable definitions. This characteristic also tends to minimize extraneous connections by eliminating unnecessary and/or misplaced calculation of variables. The debate over transfer of information by argument list versus transfer by common "global" data is an example of an issue of data traceability. Argument list transfers can become cumbersome and may consume extra program execution time, but generally provide better data traceability. This issue is addressed specifically in definition of coding guidelines.

The third step in the restructuring process (outlined in Table 6) is the definition of a data structure. This refers to the organization of data flow from input parameters to output data. It consists of the division of program input data, variable parameters, and output data into categories and subcategories which reflect "real-world" definitions. Data structure is reflected in the organization of documentation, particularly "data dictionaries" which provide symbolic nomenclature, physical definition, units, sign convention, and FORTRAN name. The categories used for restructuring C-60 input data are trim, structural properties, aerodynamics, geometry, downwash parameters, and controls. (Program control parameters are treated with a parallel structure (e.g.: trim controls, input controls, etc.) under the topic of Control Structure). Parameters which are computed as functions of only input data, and which could, in fact, be treated as input data in that they remain fixed throughout the analysis are grouped with input data to form "extended data". Examples of additional parameters included in "extended data" are lumped physical properties derived from distributed physical property curves.

Organization of variable parameters (i.e.: parameters which change in value during the analysis) is based on functional decomposition. Variables are first defined either as "global" results of a specified function (e.g.: the results of the "response module" are deflections, slopes, loads, etc.) or as local internal values appearing only in subordinates of the specified function (e.g.: transfer matrix elements, unsteady stall time delay, etc). The resulting categories of variables thus reflect the top-level global functions. Refinement to repeatedly lower level functions provides similar organization of local variables to parallel data flow through the analysis.

Output data structure duplicates the structure of variable parameters, illustrating the concept that any resulting variable quantity may be considered an output. Highest level function output, or global output is collected for summary information.

The "output" function is otherwise distributed throughout the analysis by activation or "calling" of output utility routines or subfunctions. This treatment provides standardization of formats, simplified revision of standard formats, and simplified identification, tracing, addition or deletion of output parameters.

Definition of control structure refers to the organization of "decision-making" parameters or program controls. The organization of control parameters reflects the levels of decision-making defined by the control hierarchy as well as the functional breakup defined by functional decomposition. Controls are "decomposed" first by global function classifications: Input, Velocity, Airloads, Trim, Response, and Output. Successive subdivision from high-level decision-making to low-level decision-making is performed on a "need-to-know" basis to minimize coupling of program controls.

Coding guidelines are defined as the next step in the restructuring process to provide standardization, to improve clarity, to enforce data traceability requirements, and to maintain data and control structures. Standardization is needed to provide consistency across a variety of programmers/analysts/engineers with a corresponding variety of programming styles, nomenclature preferences, etc. The attributes of this standard will have a significant impact on future maintenance and modification costs. The most tempting trade-off in coding practices is short-term expediency at the expense of long-term clarity. The provisions made in coding guidelines may deter such practices. Standards of particular interest from the perspective of maintainability and modifiability are those which influence data traceability. These standards are any rules or guidelines which promote the identification and understanding of a source of information. Some examples of standards which promote data traceability are prohibition or restricted use of "EQUIVALENCE" statements, FORTRAN variable naming conventions which reflect the meaning and source of the data and restricted use of FORTRAN COMMON blocks for variable data storage.

Usage of common block data storage is a particularly controversial issue because the trade-off of benefits is significant. Two main drawbacks of COMMON block usage are the difficulty in tracing the origin of values, and the danger of inadvertent and undetected redefinition or "over-writing" of data. A major benefit of COMMON block usage is the ease and simplicity of multi-point access to information. Common blocks of information may best be utilized as single-source, multi-destination vehicles of information transfer and storage to achieve major benefits and avoid main drawbacks of usage, as illustrated by Figure 6.

Definition of documentation standards is one of the most difficult and time-consuming tasks of the restructuring process. Repeated review/revision iterations involving personnel with different perspectives are essential to definition of useful documentation. Insights from perspectives of programming, analytical development, and production usage are essential. Documentation must provide enough information to provide needed understanding without providing so much information that needed information is obscured. In addition, the information must be structured so as to be easily modified and quickly retrieved and to prevent conflicting or redundant information.

First-cut designs of overall structure and the Main Control Executive reflect the interaction of global functions. Refinement of the design is achieved by iterative functional decomposition based primarily on data flow. The top-level second-cut design is shown in Figure 7. An essential element of the design iteration is that it involves individuals representing computer technology, the engineering developer, and the user community. The main design loop is then activated to design, build, test and document functions on a module by module basis. A second-cut detail design of the Input function is shown in Figure 8.

For each module, requirements must be defined in the form of a first-cut module specification or "module spec" including a first cut detail "strawman" design. Discussion of a design is much more fruitful when based on a strawman. It helps to point out the more subtle and obscure requirements and restrictions. It is also useful in establishing, illustrating, and clarifying special nomenclature. However, too large an effort should not be expended in putting together the "strawman" spec, or natural reluctance to "waste" effort may compromise the design effort by discouraging changes to the strawman. The iterative design-change/review process, starting with the strawman design is performed until a satisfactory detail design results.

Steps of module-building, validation, and documentation may begin upon completion of the module design. A mapping of the module function to the current analysis code is required to identify code connections for validation. There generally will not be a one-to-one mapping of new module code and original analysis code. The original analysis will contain duplicate code (possibly inconsistent near-duplicate sections), have some functions unrecoverably distributed (in practical terms), and have some functions which do not exist as functions at all. Coding guidelines define standards for the module-building process, including specification of the format for in-line documentation which should be included as comment statements in the code of the new module. The module is then tested by comparison with the current analysis intermediate and final calculation output. This can be achieved by adding namelist or write statements as temporary modifications to the original program. (The required variables from the original analysis were identified in the mapping step above). Documentation of the global module, including global function executive and all subordinate functions is then finalized.

The Main Control Executive design is finalized after completion of design of all global functions. This is necessary because design revisions of even global level functions may occur during the itera-

tive design loop process. Testing of the main control executive is performed by exercising all combinations of global level control options with "dummy" global functions. Replacement of "dummy" functions with completed functional modules constitutes system integration, which is followed by integration testing, completion of system documentation, and finally, incremental release of the restructured program for production use.

Current Status

We are in the process of executing this restructuring plan for program C-60, and are presently in the global function design loop. Restructured functions which have been implemented in the production program are Downwash (subordinate of Velocity), Coupled Flap-Pitch Response (subordinate of Response), Aerodynamic Coefficient Determination (bottom level subordinate of Airloads), and various standard utilities of Input and Output. Some general observations we have made during this activity are (1) that no design is ever final and therefore flexibility must be built in, (2) review with other interested parties improves the resulting design, (3) definition of documentation standards is at least as difficult as the actual design process, and (4) the potential near-term benefits from implementation of restructured modules into production are extraordinary. A discussion of these points is given below.

The program design structure, even at the top global-function level, evolves during the design process, and beyond. Top-level functions of the current design, as shown in Figure 7, contrast the original design which was shown in Figure 3. Additional functions, such as nonlinear forcing, summary report, graphics, and rotor-airframe coupling, were added as a result of multi-person review, anticipation of future needs and insights from ongoing design refinement. Further revision is anticipated.

Documentation standards evolve in the design process, similar to the actual program structure evolution. Initial elements listed in Table 7 were revised to a scheme employing three documents with items listed in Table 8. The division, though still in work, is similar to that suggested by Kerr, Potthast, and Anderson[1]: model formulation, user's manual, and programming manual. This resulted from trial generation and revision of documentation, which proved to be too cumbersome in its original form. Again, multi-person review provided major insights. Documentation completed thus far, including the input data dictionary and input structure definition, has been very useful in reducing user errors in input preparation.

Restructuring can improve efficiency as a side-effect. Restructuring of the Aerodynamic Coefficient Determination function, a bottom level subordinate of Airloads, revealed inefficient loop structure resulting in unnecessary recalculation of values. Restructuring of the function to improve clarity, maintainability and modifiability also provided more efficient operation. The end result of implementing the restructured function in the production program was reduction of total CPU execution time by 17 percent for a typical case.

Previously undetected program errors may be uncovered in the process of validating restructured modules. During the validation process, differences in answers provided by the restructured module and the original program were found. Usually, this was the result of a coding error in the new module, which illustrates the primary purpose of the validation effort. However, sometimes it was found that the original program was incorrect. Most of the time these corrections were not significant, but in at least one instance, the error correction significantly improved correlation. In the past, the vibratory hub load calculations sometimes depended upon the accuracy of the initial trim guess. After an error was uncovered in the wake update routine, the dependence of the hub loads on initial trim was dramatically reduced. In addition, the correlation with measured pressure data was substantially improved, as shown in Figure 9.

Another restructuring benefit is that it has been significantly easier to incorporate new analytical capability. A number of improvements have been added, including the addition of a nonlinear multi-load path flex-beam capability, even though the Response function was only partially structured. Having a data map, control flow and partial restructuring really reduced the effort required. A number of similar improvements were attempted in the late 70's, but they had to be abandoned since the change could not be checked out with a reasonable effort. Restructuring of the Response function made a similar contribution to revisions to add nonlinear pendulum flap absorbers and consolidate calculations for load and frequency prediction capabilities.

Output capabilities have been expanded and made more user-friendly. Restructuring has facilitated development of flexible, centralized output modules from which the user can select any of 152 output record names representing different output arrays (each array is converted into one of three standard formats). Each of these arrays can be either not output or output to paper, microfiche, on-line printer plots and/or tape. The tape can then be automatically transformed into the required form for a number of display devices (both video and hard copy plots). In addition, all output is completely labeled with a description, units and sign convention.

Reorganization of input data and input processing has reduced input errors and the time required for user preparation of input data. This was accomplished by development of centralized input modules with options for using standard data files established for each aircraft and the ability to input either distributed or lumped physical properties. Scaling factors are provided for each of the physical property characteristics. Finally, the input data is printed out in both standard loader format and logically grouped, annotated and formatted arrays, with description, units and sign

convention to allow the user to easily check the input.

Restructuring aids development of interdisciplinary analysis by simplifying the incorporation of analysis components from other technical areas. This capability was demonstrated while performing the restructuring of the Downwash function in the C-60 program. The restructuring of C-60's non-uniform downwash function resulted in the definition of the functional data connections so that any 'generic' downwash function (that used airloads and geometry as inputs and provided velocity distribution as output) could be used. Next, a non-uniform downwash analysis from the L-02 program was restructured and then transplanted into C-60. Currently a third downwash analysis (from the B-65 performance program) is in the process of restructuring for inclusion in C-60 by year's end. It should be noted that this technology interchange works both ways. Since the C-60, B-65 and L-02 wake functions were restructured to the same criteria, these interface boundaries are defined identically. Therefore, it is possible for both B-65 and L-02 to use the C-60 downwash function and each others' as well. The value of this exercise is to show that it is reasonable to transfer technology from discipline to discipline and to demonstrate the value of good (and consistent) program structure in aiding the transfer. Other technologies planned for near-term cross fertilization include unsteady aerodynamics, free flight aircraft trim, and dynamic flight controls.

Another benefit of this technology interchange is that the three restructured Downwash functions in C-60 will allow the ability to evaluate different analytical formulations for the same function. Different analytical models of such concepts as shed wake, vortex sheet, roll up, lift/wake compatibility and wake convergence, etc. can be investigated with identical external formulations, (a physical impossibility when these routines were located in different programs). Using similar strategy, functional structuring also allows multiple levels of complexity for a single function. For example, C-60 currently has three levels of complexity for blade pendulum absorbers: an idealized absorber (useable for preliminary design), a linear absorber (with couplings and offsets), and a full non-linear absorber (with large angles).

As discussed above, our experience to date shows that restructuring works, and provides extensive near-term benefits with production implementation. It has been possible to develop a hybrid program, partially structured and partially unstructured, that can be utilized as a production analysis in parallel with its restructuring. Of course, after each significant restructuring effort, a new production module is developed, which has the same or improved capability of the previous version. (A modification index is kept in the front of the output to summarize each change, as shown in Figure 10). When substantial differences in the calculated results between versions occur, correlation is performed to show that the new version is at least as good as the original version. If this level of correlation cannot be reached, the old version is not replaced.

Conclusion

Experience in the effort to restructure C-60 indicates that restructuring a "mature" analysis is a viable and worthwhile remedy for the maintenance and modification problems of a current poorly structured rotorcraft analysis. The success and productivity of the restructuring effort in terms of capability-gained for effort-expended depends to a large degree on the organization and documentation of the current poorly structured analysis. Many near-term benefits are possible from incorporation of restructured functional modules into the production program. Near-term benefits achieved thus far for program C-60 are listed below.

- Reduction of program errors
- Reduction of user errors (input and output)
- Reduced run-time
- Simplified incorporation of new capabilities
- Enhanced technology transfer
- Improved correlation

In addition, some important lessons were learned concerning the procedure or process of restructuring, and are outlined below.

- No design is ever final, and therefore flexibility must be built in.
- Reviews of design and documentation standards by representatives of programming, computer technology, analytical development, and user communities provide surprising insights and better "final" results.
- The definition of standards for documentation is at least as difficult and as important as the actual design process.

References

1. A.W. Kerr, A.J. Potthast, and W.D. Anderson, "An Interdisciplinary Approach to integrated Rotor/Body Mathematical Model", AHS Symposium on the Status of Testing and Modeling for V/STOL Aircraft, October 1972.
2. G.D. Bergland, "A Guided Tour of Program Design Methodologies", IEEE, October 1981.
3. FORTRAN Programming Standard for BCS Scientific Systems (VSD), Boeing Computer Services, Inc., February 1983.
4. C. Berggren, "Development of a Generic Architecture", AHS 40th Annual Forum Proceedings, pp. 429-437, May 1984.
5. H.H. Hyndman, Jr., "TOTAL FLOW" Computer Program, Boeing Computer Services, Inc., July 31, 1981.
6. E. Yourdon, and L.L. Constantine, Structured Design, Yourdon Press, New York, 1975.

Table 1.

SOPHISTICATED COMPUTER TOOLS

- GRAPHICAL DISPLAY PACKAGES
- OPERATING SYSTEMS
- COMPILERS
- DEBUGGING AIDS
- DATABASE MANAGEMENT SYSTEMS
- FLOW DIAGRAM UTILITIES
- CHART GENERATION PACKAGES
- WORD PROCESSORS

Table 2.

INDIVIDUAL PREFERENCES IN PROGRAM DEVELOPMENT

- NOMENCLATURE
- FORMAT
- VARIABLE NAMES
- UNITS/NONDIMENSIONALITY
- SIGN CONVENTIONS
- IN-CODE COMMENTS
- ARGUMENT OR COMMON TRANSFERS
- IMPLIED OR EXPLICIT LOOPS
- EXPLICIT OR VARIABLE DIMENSIONS
- INTEGER OR REAL PROGRAM CONTROLS
- VARIABLE PRECISION

Table 3.

SOFTWARE ATTRIBUTES AS DESIGN CRITERIA

- CLARITY
- COHESION
- COMPLEXITY
- CONNECTIVITY
- CONSISTENCY
- CONTINUITY
- CORRECTNESS
- CORRESPONDENCE
- COUPLING
- EFFICIENCY
- EXTENDIBILITY
- FLEXIBILITY
- GENERALITY
- INDEPENDENCE
- MAINTAINABILITY
- MODIFIABILITY
- MODULARITY
- PORTABILITY
- RELIABILITY
- REUSEABILITY
- ROLE ADAPTABILITY
- TESTABILITY
- TRANSPARENCY
- UTILITY

Table 4.

SOFTWARE DESIGN PRINCIPLES AND TECHNIQUES

- ABSTRACTION
- BOTTOM-UP DESIGN
- COMPOSITE DESIGN
- DATA ENCAPSULATION
- DATA FLOW DESIGN
- DATA STRUCTURE DESIGN
- DATA TRACEABILITY
- DECISION HIDING
- FUNCTIONAL DECOMPOSITION
- HIERARCHY
- HIERARCHAL CONTROL
- HYBRID (TOP-DOWN/BOTTOM-UP) DESIGN
- INFORMATION HIDING
- PARTITIONING BY OBJECTIVE
- PROGRAMMING CALCULUS
- STEPWISE REFINEMENT
- TOP-DOWN DESIGN
- TRANSFORM-CENTERED DESIGN

Table 5.

DESIGN CRITERIA DEFINITIONS

EFFICIENCY	—	OVERALL COMPUTATIONAL EFFICIENCY
GENERALITY	—	BROADNESS, SCOPE, OR ABSTRACTNESS OF TASK DEFINITION
MAINTAINABILITY	—	EASE OF DETECTION AND CORRECTION OF PROGRAM ERRORS
MODIFIABILITY	—	EASE OF ACCOMMODATING NEW REQUIREMENTS
RELIABILITY	—	CONSISTENCY AND REPEATABILITY OF CORRECT PERFORMANCE
UTILITY	—	EASE OF USE OR USER-FRIENDLINESS

Table 6.

PLAN FOR RESTRUCTURING C-60

1. PRIORITIZE DESIGN CRITERIA
   - MAINTAINABILITY
   - MODIFIABILITY
2. DEFINE DESIGN PRINCIPLES
   - FUNCTIONAL DECOMPOSITION
   - HIERARCHAL CONTROL
   - DATA TRACEABILITY
3. DEFINE DATA STRUCTURE
4. DEFINE CONTROL STRUCTURE
5. DEFINE CODING GUIDELINES
6. DEFINE DOCUMENTATION STANDARDS
7. DESIGN 1st-CUT OVERALL STRUCTURE ("STRAWMAN")
8. DESIGN 1st-CUT MAIN CONTROL EXECUTIVE
9. GLOBAL FUNCTION DESIGN LOOP
   - DESIGN/REVIEW ITERATION
   - BUILD MODULE
   - TEST MODULE
   - COMPLETE MODULE DOCUMENTATION
   - (NEXT GLOBAL FUNCTION)
10. COMPLETE MAIN CONTROL EXECUTIVE
11. SYSTEM INTEGRATION TESTING
12. COMPLETE SYSTEM DOCUMENTATION

Table 7.

ORIGINAL DOCUMENTATION REQUIREMENTS

MODULE SPEC (FOR EACH SUBROUTINE)

I. SUMMARY SHEET
   (FUNCTION NAME AND DESCRIPTION, SUBORDINATES AND SUPERORDINATES, INPUT AND OUTPUT PARAMETERS)

II. LOCAL MODULE MAP (DIAGRAM)
   (SHOWS SUBORDINATES, SUPERORDINATES, ARGUMENT LIST I/O, COMMON I/O)

III. MODULE STRUCTURE DIAGRAM
   (SHOWS INTERNAL STRUCTURE SUBFUNCTIONS)

IV. SEQUENCE FLOW DIAGRAM
   (CLASSICAL FLOW CHART)

V. CONTROL DECISIONS
   (PRESENTS OPTIONS AND TESTS MADE ON CONTROL PARAMETERS)

VI. EQUATIONS

VII. DERIVATION OF EQUATIONS

VIII. FORTRAN VARIABLES
   (FORTRAN NAMES, SYMBOLIC REFERENCES, AND DEFINITIONS)

IX. CODE (WITH COMMENTS)
   (LISTING OF ACTUAL FORTRAN CODE WITH IN-LINE COMMENTS)

X. ADDITIONAL NOTES
   (ANY ADDITIONAL COMMENTS, A SUCH AS NOTING EXCEPTIONS TO CODING GUIDELINES, ASSUMPTIONS OR ANTICIPATION OF FUTURE REVISIONS)

DATA DICTIONARIES - INPUT, VARIABLES, OUTPUT

- ALPHABETIZED AND CROSS-REFERENCED
- PROVIDE SYMBOLIC NOMENCLATURE, PHYSICAL DEFINITION, UNITS, SIGN CONVENTION, FORTRAN NAME, AND DERIVATION REFERENCE

Table 8.

REVISED (2nd CUT) DOCUMENTATION REQUIREMENTS

DERIVATION DOCUMENT

- CONTINUOUS/SEMI-CONTINUOUS DERIVATION (NOT BROKEN INTO SUBROUTINES)
- CROSS-REFERENCED TO SUBROUTINES, INPUT DATA, OUTPUT DATA, AND FORTRAN VARIABLES

PROGRAMMING MANUAL

- MODULE SPEC*
  - I. SUMMARY SHEET
  - II. LOCAL MODULE MAP
  - III. MODULE STRUCTURE DIAGRAM
  - IV. SEQUENCE FLOW DIAGRAM
  - V. CONTROL DECISIONS
  - VI. FORTRAN VARIABLES (WAS VIII)
  - VII. CODE WITH COMMENTS (WAS IX)
  - VIII. ADDITIONAL NOTES (WAS X)
    - REGARDING CODE
- DATA DICTIONARY - VARIABLES

USER'S MANUAL

- MODULE SPEC*
  - I. SUMMARY SHEET
  - II. EQUATIONS (WAS VI)
  - III. ADDITIONAL NOTES (WAS X)
    - REGARDING EQUATIONS
- DATA DICTIONARIES-INPUT AND OUTPUT

*ASSEMBLED FROM PIECES OF ORIGINAL MODULE SPEC STANDARD

Figure 1.

LAW OF CONTINUING CHANGE:

A SYSTEM THAT IS USED UNDERGOES CONTINUING CHANGE UNTIL IT IS JUDGED MORE COST-EFFECTIVE TO FREEZE AND RECREATE IT.

LAW OF INCREASING UNSTRUCTUREDNESS:

THE ENTROPY (DISORDER) OF A SYSTEM INCREASES WITH TIME UNLESS SPECIFIC WORK IS EXECUTED TO MAINTAIN OR REDUCE IT.

Figure 2.

COMPUTER PROGRAM LIFE CYCLE

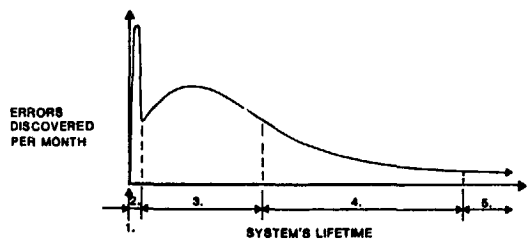

1. UNDER DEVELOPMENT
2. CHECKOUT
3. INITIAL RELEASE
4. OPERATION/MAINTENANCE/MODIFICATION
5. MATURE PROGRAM

Figure 3.

FIRST CUT FUNCTIONAL DECOMPOSITION

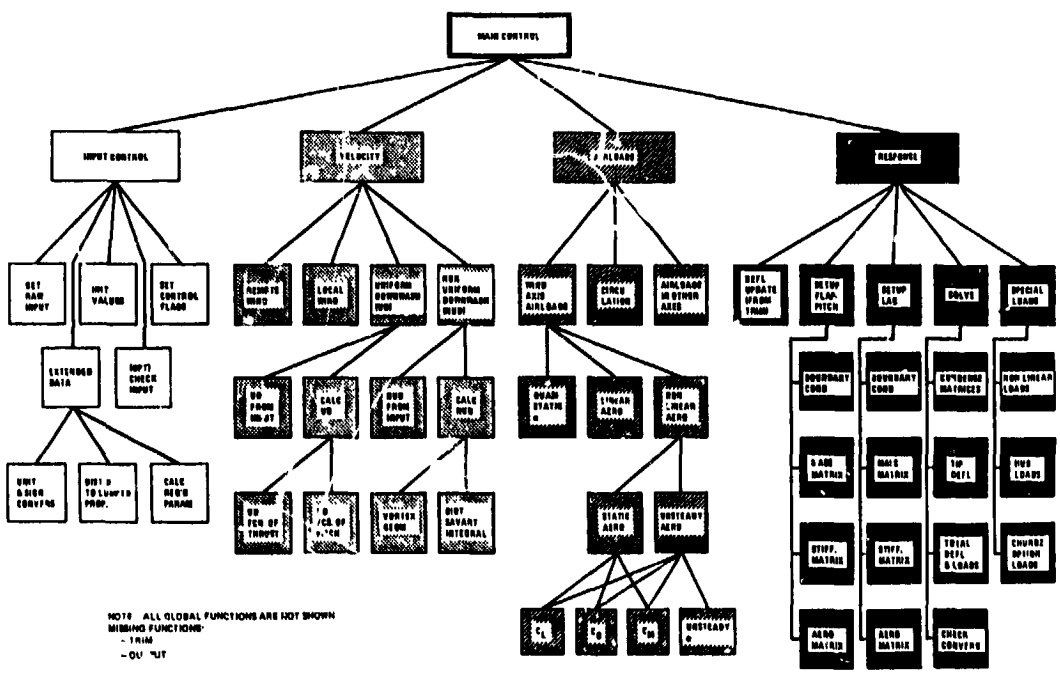

Figure 4.

FUNCTIONAL MAPPING FOR CURRENT C-60 PROGRAM

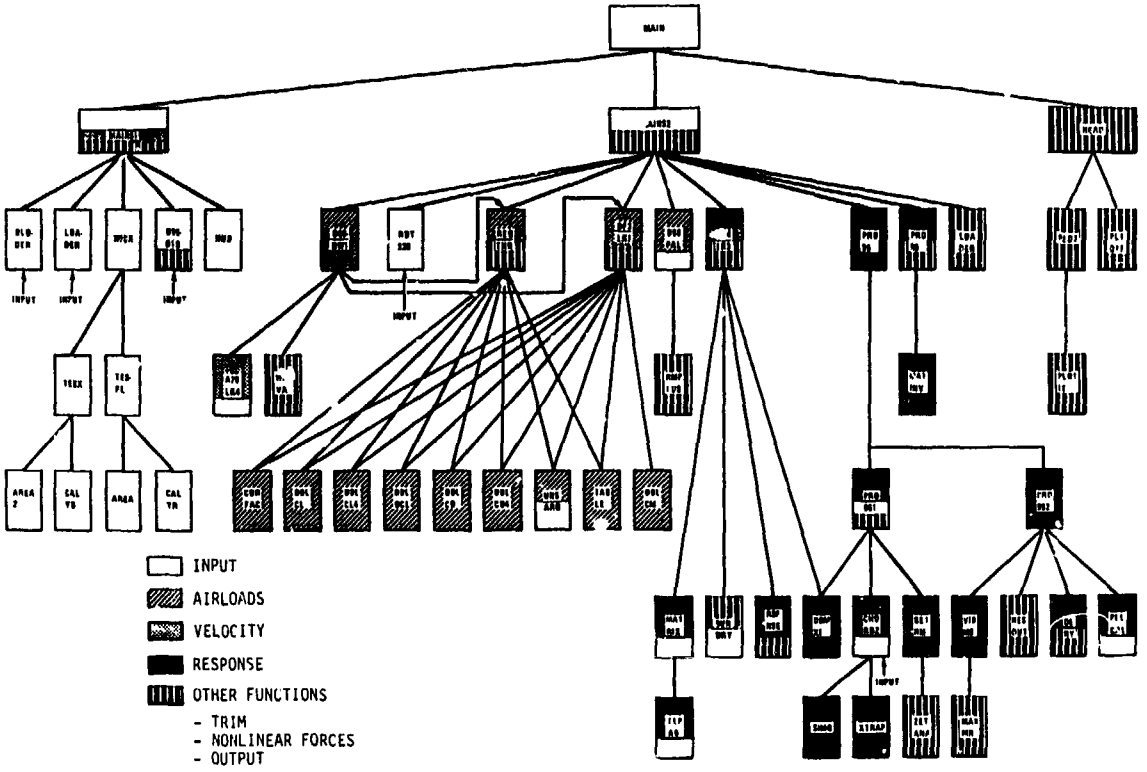

Figure 5.

HIERARCHAL CONTRC

GRADUATION OF DECISION-MAKING

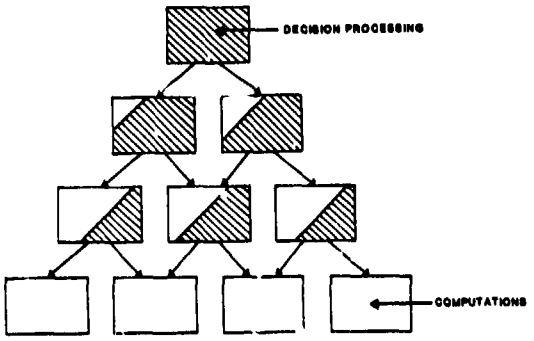

Figure 6.

GOOD AND BAD DATA TRACEABILITY
FROM COMMON BLOCK USAGE

- GOOD DATA TRACEABILITY

SINGLE-SOURCE COMMON

- BAD DATA TRACEABILITY

MULTIPLE-SOURCE COMMON

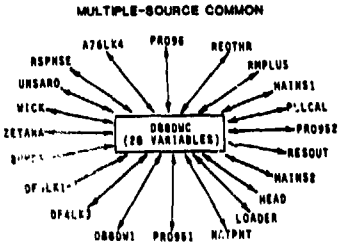

Figure 7.

TOP LEVEL OF SECOND CUT DESIGN

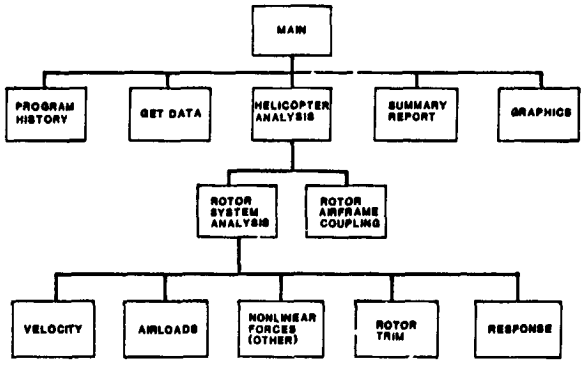

Figure 8.

INPUT FUNCTION - SECOND CUT DESIGN

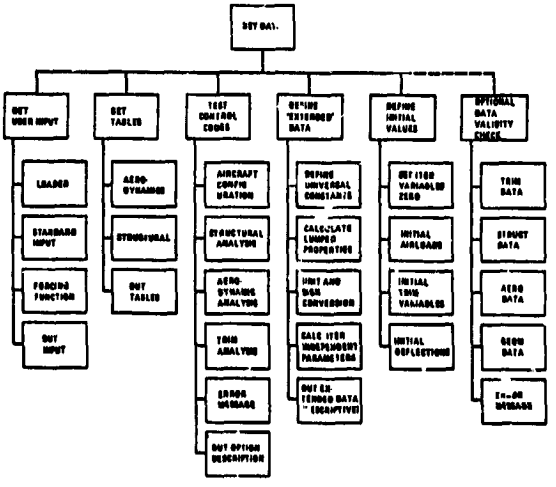

Figure 9.

IMPROVED VIBRATORY AIRLOAD CORRELATION
USING RESTRUCTURED C-60 DOWNWASH MODEL

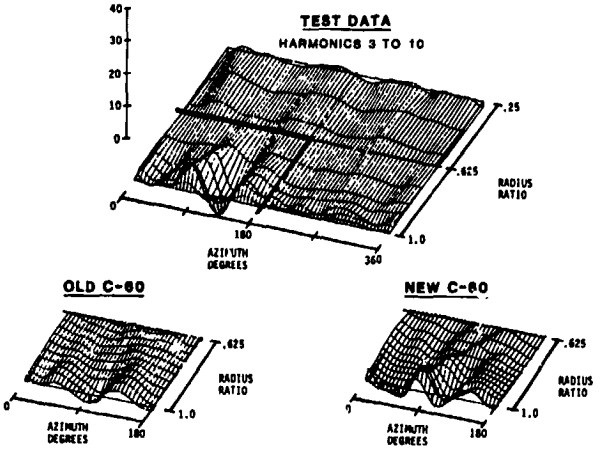

Figure 10.

C-60 AUTO-HISTORY

LOAD MODULE	CWA NO.	REV NO.	TITLE	DATE INSTALLED
C607801	881202	1	TOTAL SOURCE MODIFICATIONS	01/14/78
C607802	881024	2	ELASTIC MATRIX CHANGE	02/16/78
C607803	881202	3	SIGMA 9 CONVERSION	03/16/78
C607804	881202	4	SHEAR BMR CHANGES	03/23/78
C607805	881202	5	MODIFIED SHORT PRINTOUT	05/[illegible]/78
C607806	881202	6	CD AND CM AEROFOIL TABLE FACTORS	06/16/78
C607807	881040	7	TIP RELIEF MOD TO CD & CL CALCS	11/03/78
C607808	881202	8	SLOPE CHECK CORRECTION	11/03/78
C607809	881806	9	ALPHA .2 AND ZERO THRUST CORRECTION	02/12/79
C607810	891202	10	DISTRIBUTED BLADE PROPERTIES	04/20/79
C607811	891806	11	REVISED UNIFORM DOWNWASH FOR TRIM	05/30/79
C607812	891806	12	NON LINEAR CYCLIC TRIM CONTROL	07/13/79
C607813	891806	13	CORRECTED TIP RELIEF FOR ALPHA=0.	07/13/79
C607814	891810	14	RADIS INFLOW VELOCITIES	01/10/79
C607815	891812	15	FLIME PLOT FILE GENERATION	01/09/80
C6000	DC1053	41	NATURAL FREQ. UNIT FORCED RESPONSE, VERT	
C6500	831806	42	HUB SPRING AT FLP ARMST, & ABSORBER MOD. MISC CORRECTIONS FOR ABSORBER AND/OR	12/17/82
C6000	831806	43	HATP AND UNIT FORCING	01/21/83
C6000	831806	43	TEST HUB SPRING SINGLE HARMONIC	02/16/83
C6000	831831	44	CORRECT & EXTEND PERFORMANCE PARAMETERS.	03/10/83
C6000	831805	45	RESTRUCTURE RESPONSE ROUTINES.	03/21/83
C6000	831836	46	NONLINEAR FLAP ABSORBER ANALYSIS	03/24/83
C6000	831832	47	TWO BLADE HUB CONTROL FORCES	04/05/83
C6000	831832	48	ADD FLAP ABSORB OUTPUT TO SUP/SCP TAP	04/15/83
C6000	832444	49	CORRECT SWEEP ON [illegible] BLADE INERTIAS	05/09/83
C6000	830643	50	MULTIPLE HARMONIC ARTICAL HUB SPRINGS	07/08/83
C6000	831806	51	ONLINE PLOT OF TIMETA, MBETA, & MEETA	08/04/83
C6000	831869	52	PITCH BOUNDARY CONDITION	10/07/83
C6000	831806	53	MULTIPLE HATP/UPD CARDS WITH WICK	10/[illegible]/83
C6000	831839	54	NEW DOWNWASH ROUTINE (2 REQ. [illegible]. LOD)	04/[illegible]/84
C6000	841806	55	TRAILING WAKE DEPIF VEL. PAC'ed	04/[illegible]/84
C6000	841844	56	DESCRIPTIVE PRINT OUT FOR DOWNWASH	05 4/84
C6000	841841	57	FLAP HINGE OFF-SET IN DOWNWASH CAL.	05/[illegible]/84
C6000	841841	58	IMPROVE CAL OF VORTEX CORE EFFECT	07/[illegible]/84
C6000	841825	59	PSEUDO COUPLING & CL-ALPHA VSC. TECH. YNA	07/13/84

DISCUSSION
Paper No. 12

RESTRUCTURING THE ROTOR ANALYSIS PROGRAM C-60
P. G. Phelan
and
F. J. Tarzanin, Jr.

Wayne Mantay, U.S. Army Structures Laboratory: I have two questions that I think are related, I hope you do too. When you restructured you said you uncovered at least one major problem. Was it in fact that error in the downwash, was that the one?

Phelan: That showed one of them, yes. Part of the improved correlation was that. That wasn't the total improvement in correlation; we also had improved capability.

Mantay: No, I understand about the correlation, but the error that you uncovered in C-60, was that the major error you alluded [to]?

Phelan: Yes.

Mantay: That was in the downwash?

Phelan: Yes, that was in the downwash.

Mantay: I didn't pick it up on your slide for that correlation, but was that the high speed case from Euan Hooper's data base that he had trouble with; was that the problem child that you set straight?

Phelan: Yes.

Marty Schroeder, Solar Energy Institute: Your presentation was [very good] and I think the work in structured programming is sorely needed. I'm not familiar with C-60 though. What language is it written in?

Phelan: FORTRAN.

Shroeder: Have you considered looking at other languages like PASCAL or C for a structured program?

Phelan: We are working on restructuring an existing analysis for a lot of reasons that I didn't really get into, but are in the paper. We haven't looked at also changing languages, but you could do that. We haven't looked at doing that.

Wendell Stephens, U.S. Army Aeromechanics Laboratory: I wanted to thank you for your paper, also. I have noticed that your paper, the one previous to it by Bob Sopher, a related paper [on] DYSCO involving Kaman, [and] perhaps, even the paper by Gangwani at Hughes when he spoke about a new program all have tended to go this direction which I applaud. My specific question to you is when you begin restructuring this program have you come across any executive-type utilities that you have had to build in FORTRAN that have helped your ability to transfer data from module to module. It sort of relates to the previous question back here of perhaps going to a different language for certain structures for your executive functions. I was wondering if you found that you had to develop any utilities for data transfers?

Phelan: We haven't yet, but I think part of that is maybe that our final main control executive design is . . . the first cut comes at the beginning of the process--the last final design comes at the end after you have decided and really finalized what your global top level functions are. So we've discussed different ways to implement a main control executive quite a bit, but we have not implemented it as of yet. So, we will see.

Ed Austin, U.S. Army Applied Technology Laboratory: I think it's very interesting the approach you have taken to conceive of restructuring an entire program and then to work from kind of the bottom up. Do you have any speculations about what will happen on that day when suddenly the master program is the only thing left to change and you have all these pieces and you haven't designed apparently the final master program? It doesn't sound to me like you have anyway.

Phelan: You mean the main control as far as the . . .

Austin: I saw this incredible diagram of the program the way it was before you started and wires go every which way. I saw your final version which is a very simple wiring diagram. I guess I don't see how you plan to go from this complicated set down to just a few wires. It's kind of like the time my wife decided to rewire our car and she took all the wires off the distributor at the same time.

Phelan: I don't see it as a big problem because the reason why the design is . . . we have done a lot of work on laying out a first cut executive, but the problem is you cannot implement the executive in a piecemeal way because that defines . . . one of the very last things is how you are going to make these common blocks all well structured. Well, when you start out with one that is connected everywhere, you can't do that first; you have to wait until you have consolidated things. I can't take the connections from airloads that go everywhere and eliminate the connections until I've brought all the pieces together and once they are in one piece then you have identified your single source. Do you see what I mean? Do you have a better explanation?

Frank Tarzanin: We have done some partial module restructuring and then we have done, actually completing the downwash module restructuring and once you connect those wires you can isolate the downwash as a kind of structured subprogram. We're going to slowly build structured subprograms then build the total program on top. In fact we are learning and what we started to do was take one thing in airloads, in fact that routine that saved a lot of time was an experiment. Can we grab a routine out of the middle of this mess and restructure it and put it back in and have it work. And it did. You've got to find the connections, and define the interface.

Phelan: I think that another thing that is important too is when you do that the connections are reduced Because what started out as a ball with a whole bunch of strings attached--you can eliminate the strings. You have identified a single source that can go everywhere as you consolidate all through; they kind of connect.

Tarzanin: Each step makes it simpler.

A REVIEW OF DYNAMIC INFLOW AND ITS EFFECT ON EXPERIMENTAL CORRELATIONS

Gopal H. Gaonkar
Professor
Department of Aeronautical Engineering
Indian Institute of Science
Bangalore, INDIA 56-0012

and

David A. Peters
Professor and Chairman
Department of Mechanical Engineering
Washington University
St. Louis, Missouri 63130

Abstract

A review is given of the relationship between experimental data and the development of modern dynamic-inflow theory. Some of the most interesting data, first presented 10 years ago at the Dynamic Specialists' Meeting, is now reviewed in light of the newer theories. These pure blade-flapping data correlate very well with analyses that include the new dynamic inflow theory, thus verifying the theory. Experimental data are also presented for damping with coupled inplane and body motions. Although inclusion of dynamic inflow is often required to correlate this coupled data, the data cannot be used to verify any particular dynamic inflow theory due to the uncertainties in modeling the inplane degree of freedom. For verification, pure flapping is required. However, the coupled data do show that inflow is often important in such computations.

Notation

a	slope of lift curve, rad^{-1}
B	tip loss factor
C_L	roll moment coefficient
C_M	pitch moment coefficient
C_T	thrust coefficient
e_{pc}	root cut-out divided by R
k	reduced frequency based on free-stream velocity, ω/v
K_m	normalized apparent mass
K_I	normalized rotary inertia
L	gain of Hohenemser inflow law
$[L]$	matrix of inflow gains
$[\bar{L}]$	[L] normalized on V
$[L(k)]$	complex [L] matrix
$[M]$	apparent mass matrix
p	flapping frequency, per revolution
r	distance from rotor center, m
R	blade tip radius, m
t	time, sec
$[T]$	transform for tip loss
λ	inflow mass-flow parameter, $\dfrac{(\lambda+\bar{\nu}_o)(\lambda+2\bar{\nu}_o)+\mu^2}{\sqrt{(\lambda+\bar{\nu}_o)^2+\mu^2}}$
V_T	total velocity at rotor, $\sqrt{(\lambda+\bar{\nu}_o)^2+\mu^2}$
α	disk angle at rotor, $\tan^{-1}\left(\dfrac{\lambda+\bar{\nu}_o}{\mu}\right)$
α_s, α_c	hub angles, advancing blade down, nose up, rad
β	flapping angle, rad
γ	Lock number
$\theta_o, \theta_s, \theta_c$	collective and cyclic pitch, rad
λ	normalized free-stream velocity perpendicular to rotor disk
μ	normalized free-stream velocity in the plane of rotor disk
ν	induced flow perturbation, $\nu = \nu_o + \nu_s \sin\psi + \nu_c \cos\psi$
$\bar{\nu}_o$	steady part of induced flow
ν_o, ν_s, ν_c	induced flow perturbation harmonics
σ	blade solidity
τ	time constant, Hohenemser inflow law
$[\tau]$	matrix of time constants

C-3

ψ	blade azimuth angle, rad
ω	frequency of oscillations, per revolution
Ω	rotor speed, rad/sec (RPM in Ref. 20)
$(\dot{})$	d( )/dt
$(^*)$	d( )/dψ

Introduction

From its inception over 30 years ago to its full development today, the theory of dynamic inflow has been driven constantly by the impetus of experimental data. In 1950, Ken Amer noticed that the theoretical pitch-roll damping of helicopters did not agree with flight measurements, Reference 1.

Although most of the differences could be attributed to the angle between thrust and tip-path plane, there remained a discrepancy that Amer attributed to a variation in inflow over the rotor disk. Sissingh provided a mathematical model to explain this phenomenon, Reference 2, and his model initiated the study of dynamic (or variable) inflow. In short, Sissingh showed that the side-to-side thrust perturbation (created by a roll rate) could create perturbations in the induced flow field that substantially affected roll damping. It was essentially this inflow model that was later simplified and extended by Curtiss and Shupe and applied extensively to problems of flight dynamics via an "equivalent Lock number" to account for induced flow perturbations, References 3 and 4.

In 1971-1972, Lockheed performed some wind tunnel tests that would change the course of the theory of dynamic inflow. These tests, on a 7.5 ft. diameter rotor in NASA's 7×10 ft. wind tunnel, measured 15 static rotor derivatives (C_T, C_L, C_M, with respect to θ_o, θ_s, θ_c, α_s, α_c) as functions of advance ratio from μ = 0 to 1.4, Reference 5. The results revealed major qualitative differences between conventional rotor theory and the experimental data. Most importantly, these differences could not be explained by classical excuses (reversed flow, blade elasticity, dynamic stall, etc.). As a result of this comparison, a variable-inflow theory was included in the equations, based on momentum developments similar to those in References 2-4. The results were very interesting. In hover, the momentum-theory model of dynamic inflow provided beautiful correlation with the data. In forward flight, however, the model was of little use in aiding the correlation. As a result, the authors of Reference 5 formulated other theories in forward flight based on simple vortex considerations. Finally, they formulated an empirical inflow model based on the best fit of the static data.

The above narrative describes the development of the static theory of variable inflow. In 1953, Carpenter and Fridovitch noticed that there was a time delay in the development of induced flow following rapid changes in blade collective pitch, Reference 6. They formulated a time constant for induced flow that was based on the apparent mass of an impermeable disk, and they showed that this time constant accounted for the measured transients in induced flow. In 1972, new experimental data (Reference 7) spurred the incorporation of these time delays into the variable inflow theories, Reference 8. Reference 8 compares theory and experiment for the oscillatory response (magnitude and phase) of roll and pitch moments due to oscillations of θ_o, θ_s, θ_c, α_s, and α_c. These results show that the variable inflow theories of Reference 5, while giving good static correlation, give poor correlation as ω is increased. Furthermore, the data show that the cause of the poor correlation is that the effect of variable inflow decreases with increasing ω. In other words, the induced flow does not have time to respond to rapid changes in loads, which points back to the need for time delays such as those in Reference 6. As a result of this new information, the apparent mass terms were incorporated into both the empirical and momentum-theory variable inflow models; and thus was created dynamic inflow theory, Reference 8.

Background

Before going on to the further developments in dynamic inflow, it might be good first to review the form of the dynamic inflow theories. First, dynamic inflow assumes a limited number of induced flow distributions of unspecified magnitude. The relative amounts of each distribution (that might be present at a particular instant in time) become degrees of freedom in the dynamic analysis. Although several alternatives have been tried through the years, it is now believed that the most useful is

$$v(r,\psi) = v_o + v_s \frac{r}{R} \sin\psi + v_c \frac{r}{R} \cos\psi \qquad (1)$$

Some investigators have used only the v_s and v_c terms, References 9-10; and some have added second-harmonic terms, References 11-12. However, in forward flight for rotors with 3 or more blades, the model in Eq. (1) has proved to be the most useful.

In dynamic inflow theory, the air mass degrees of freedom (v_o, v_s, v_c) are described by differential equations as follows.

$$[\tau]\begin{Bmatrix}\dot{\nu}_o\\ \nu_s\\ \nu_c\end{Bmatrix} + \begin{Bmatrix}\nu_o\\ \nu_s\\ \nu_c\end{Bmatrix} = [L]\begin{Bmatrix}C_T\\ C_L\\ C_M\end{Bmatrix}_{aero} \qquad (2a)$$

or

$$[M]\begin{Bmatrix}\dot{\nu}_o\\ \nu_s\\ \nu_c\end{Bmatrix} + [L]^{-1}\begin{Bmatrix}\nu_o\\ \nu_s\\ \nu_c\end{Bmatrix} = \begin{Bmatrix}C_T\\ C_L\\ C_M\end{Bmatrix}_{aero} \qquad (2b)$$

Several explanations are in order for Eq. (2). First, the quantities in Eq. (2) are perturbation values (ν_o, ν_s, ν_c, C_T, C_L, C_M). Thus, the theory is formulated for a linearized analysis. Second, the thrust, roll, and pitch coefficients refer to the aerodynamic components only. Thus, they may be obtained from integrated air loads; or they may be obtained by correction of total hub loads for inertial effects. The matrix [L] is the static coupling matrix between induced flow and aerodynamic loads. The matrix [M] represents the apparent inertia of the air mass, and $[\tau] = [L][M]$ is a matrix of time constants.

Several different definitions of [L] have been used throughout the years. For example, some have used $< C_T\ -C_L\ -C_M >$ on the right-hand side since this avoids negative apparent mass elements. Also, some have factored out of [L] the mass flow parameter, V,

$$[L] = \frac{1}{V}\,[\mathscr{L}] \qquad (3)$$

in order to make $[\mathscr{L}]$ a function of disk angle only and not of free-stream velocity. In addition Reference 13 outlines a nonlinear version of Eq. (2) in which ν_o, ν_s, ν_c, C_T, C_L, C_M are total quantities rather than perturbation quantities. This is accomplished with the replacement of V by V_T in the C_T terms,

$$[L] = [\mathscr{L}]\begin{bmatrix}V_T & 0 & 0\\ 0 & V & 0\\ 0 & 0 & V\end{bmatrix}^{-1} \qquad (4)$$

where V_T is the normalized flow at the rotor and V is a weighted downstream velocity.

$$V_T = \sqrt{\mu^2 + (\lambda+\bar{\nu}_o)^2}, \quad V = \frac{d}{d\bar{\nu}_o}\,(\bar{\nu}_o V_T) \qquad (5a,b)$$

The detailed formulation of the elements $[\mathscr{L}]$ and [M] is the essence of the theory of dynamic inflow. All investigators, however, have chosen [M] to be a diagonal matrix of the form

$$[M] = \begin{bmatrix}K_m & 0 & 0\\ 0 & -K_I & 0\\ 0 & 0 & -K_I\end{bmatrix} \qquad (6)$$

where K_m and K_I are the nondimensional mass and moment of inertia of the participating air mass. Thus far, no one has considered the explicit effect of tip loss on the $[\mathscr{L}]$ and [M] matrices. A theoretical case can be made for replacing K_m by B^3K_m, K_I by B^5K_I, and for transforming $[\mathscr{L}]$ by $T^T\mathscr{L}T$ where

$$[T] = \begin{bmatrix}B & 0 & 0\\ 0 & B^2 & 0\\ 0 & 0 & B^2\end{bmatrix} \qquad (7)$$

The transformation in Eq. (7) assumes that only the radius BR is effective in dynamic inflow, but this has not been verified experimentally. Thus, we continue to use [M] and [L] uncorrected for tip loss.

Correlation with Flapping Data

With the form of dynamic inflow theory now set forth, we can proceed to outline the development of the [L] and [M] matrices and of the V parameter. In Reference 8, presented at this same conference 10 years ago, the experimental data from Reference 7 are compared with results calculated from new dynamic inflow theory (including both $[\mathscr{L}]$ and [M]). In hover, $[\mathscr{L}]$ and [M] are taken from momentum theory and are diagonal matrices.

$$\mathscr{L}_{11} = \frac{1}{2},\ \mathscr{L}_{22} = \mathscr{L}_{33} = -2.\ V = 2\bar{\nu}_o$$

$$M_{11} = \frac{8}{3\pi},\ M_{22} = M_{33} = \frac{-16}{45\pi} \qquad (8a\text{-}e)$$

The results are extremely interesting. Fig. 1 gives the magnitude and phase of both roll and pitch moments in hover due to oscillations in θ_s. The frequency is given per revolution. The theory without dynamic inflow is not even qualitatively accurate. When quasi-steady inflow is included (no apparent mass) the data are precisely captured for $\omega < .2$. For larger ω, the quasi-steady theory is inaccurate; but the unsteady theory (with apparent mass) captures the effect. Fig. 2 presents a similar plot from Reference 8 but for oscillations of shaft angle. Because of the theoretical symmetry in roll and pitch oscillations, data for both excitations are presented together. Above $\omega = .3$, the two sets of data diverge due to stand resonances. For $\omega < .3$ both agree. Once again, we find that the theory with no dynamic inflow is qualitatively in error but that momentum theory completely captures the response for $\omega < .3$. It is hard to look at Figs. 1 and 2 and not be impressed that dynamic

inflow is not only a true physical occurrence but that it is also well-modeled in hover by momentum theory with apparent-mass time delays.

At the same time as Army scientists were discovering that dynamic inflow was necessary to correlate the Lockheed data, an Army contractor at Washington University made the identical discovery in an entirely different test, Reference 14. Fig. 3 presents the data of Hohenemser and Crews for pitch stirring excitation. Rather than momentum theory, they used parameter identification to determine a gain L and a time constant τ for an inflow theory. Amazingly, the values of L and τ they obtained turned out to be within a few percent of the similar values from momentum theory; and the correlation with data was excellent. This is further verification of the validity and universality of dynamic inflow. It should be noted that the researchers in Reference 14 (along with D. Banerjee) also attempted to identify a full [L] matrix from transient blade dynamics. However, because their rotor could not be excited in collective pitch, they were unable to develop an adequate response to identify [L].

The good news from the experiments in References 7 and 14 was that momentum theory is nearly perfect in hover. The bad news was that it is nearly useless in forward flight. To be more specific, experimental data in forward flight also showed large deviations from conventional theory, but momentum theory could not make up the difference. There was one bright spot, however. The empirical model, which had been identified based on static (ω=0) derivatives, gave very good agreement with dynamic data for all ω provided that the apparent mass terms were added. This implies that the same apparent mass terms are valid at all advance ratios and that the empirical model is not far from accurate. There are, however, several major problems with the empirical model. First, it is inconveniently formulated in terms of tabulated coefficients. Second, it has no fundamental basis in aerodynamics. Third, the [L] matrix shows singularities at μ = .32 and μ = .80. Fourth, and the most serious, the empirical model is formulated only for edgewise flow. Therefore, there is no accounting for the transition from hover to forward flight.

In summary, the aforementioned experimental data clearly show that, although momentum theory is adequate in hover, a different theory is required for forward flight. Other experimental data and theories were also developed during this time, e.g. Reference 15, but none provided an adequate theory for forward flight.

Pitt Model

The first serious attempt to develop a forward-flight dynamic inflow theory is found in Reference 16. Here, Ormiston began to sort out the various induced-flow components of an actuator disk. The effort fell short due to the complexities of blade motion that are coupled into the lift-flow problem. It became clear that one would have to isolate the induced flow from the blade dynamics in order to solve the problem. This was soon done; and, in 1981, Pitt and Peters introduced a new formulation of dynamic inflow, based on fundamental principles and a rigorous actuator-disk theory, Reference 11.

This theory provides a smooth transition from hover to edgewise flow and has no singularities. In hover, it is identical to classical momentum theory (both for [M] and [L]); and, in forward flight, it develops similar characteristics to those of the empirical model. In the absence of direct experimental inflow measurements, the model has been compared to numerical wake computations, Reference 17. For the static case, comparisons are made with the Landgrebe prescribed wake model applied to a 4-bladed lifting rotor, Reference 18. Figs. 4-6 show this comparison for the nine inflow derivatives, L_{ij}, as functions of disk angle of attack (0° = edgewise flow, 90° = hover). Results from Landgrebe's computer program are labelled "WAKE" on the figures. Clearly, the Pitt model gives reasonable results at all disk angles.

For the dynamic case, the Pitt model has been compared with a Theodorsen-type actuator-disk theory for frequency-response calculations, Fig. 7. In the results of the Pitt model, labelled "superposition of pressures", the formulation assumes that the harmonic induced velocities are all in phase. Consequently, these velocities create pressures that add as in Eq. (2b): 1) in-phase loads due to L, and 2) out-of-phase loads due to M. In the other results, labelled "superposition of velocities", the formulation assumes that the oscillatory loads are all in phase. The resultant induced velocities are then calculated by an involved, Theodorsen-type integration over the entire wake, Reference 17. One must assume that true rotor behavior would be some mixture of the two results. Therefore, the agreement between the two results is confirmation that the simple formulation of Eq. (2b) is adequate. Thus, Figs. 4-7 attest to the reasonableness of the actuator-disk model even for modeling a 4-bladed rotor with flapping dynamics and wake contraction.

The exact formulation of the Pitt model is given below.

$$[L] = \frac{1}{V}\begin{bmatrix} \frac{1}{2} & 0 & \frac{15\pi}{64}\sqrt{\frac{1-\sin\alpha}{1+\sin\alpha}} \\ 0 & \frac{-4}{1+\sin\alpha} & 0 \\ \frac{15\pi}{64}\sqrt{\frac{1-\sin\alpha}{1+\sin\alpha}} & 0 & \frac{-4\sin\alpha}{1+\sin\alpha} \end{bmatrix} \quad (9a)$$

$$[M] = \begin{bmatrix} \frac{128}{75\pi} & 0 & 0 \\ 0 & \frac{-16}{45\pi} & 0 \\ 0 & 0 & \frac{-16}{45\pi} \end{bmatrix} \quad (9b)$$

Several comments are in order. First, α is the wake angle at the rotor

$$\alpha = \tan^{-1}\left(\frac{\lambda+\bar{v}_o}{\mu}\right) \quad (10a)$$

Therefore, $\alpha = 0°$ corresponds to edgewise flow and $\alpha = 90°$ to hover or axial flight. Second, the V parameter from Eq. (5b) is taken from momentum theory.

$$V = \frac{(\lambda+\bar{v}_o)(\lambda+2\bar{v}_o)+\mu^2}{\sqrt{(\lambda+\bar{v}_o)^2+\mu^2}} \quad (10b)$$

Thus, in edgewise flow $V = \mu$ and in axial flow $V = \lambda + 2\bar{v}_o$. Because of this, the [L] matrix in Eq. (8a) exactly reduces to momentum theory at $\alpha = 90°$. The elements for $\alpha = 90°$ are consequently identical to virtually all of the previous work in dynamic inflow, References 2, 3, 4, 5, 8, and 9. [It should be noted, however, that Eq. (9a) for $\alpha = 90°$ differs significantly from the corresponding matrix in References 19 and 20. In particular, there is a difference of the factor of 2 on the L_{22} and L_{33} terms. A detailed discussion of this difference is given in Reference 13.] It follows that the Pitt model provides the identical good correlation in hover as does momentum theory.

Another interesting aspect of Eq. (9a) is the (3,1) element. This element provides for a fore-to-aft gradient in induced flow due to thrust and is identical to the Coleman equation for the classical Glauert constant, Reference 21. This L_{31} term is also one of the more important terms found from the empirical model. The other elements of L behave similarly to the empirical model. Of special importance is the fact that $L_{33} = 0$ (at $\alpha=0$) for both models.

With respect to the [M] matrix, the elements in Eq. (6) are also derived from the unsteady, actuator-disk theory. When a uniform lift distribution is used for C_T, the elements are identical to those of momentum theory. When the lift is forced to be zero at the rotor center, however, then M_{11} becomes $\frac{128}{75\pi}$ (= .54) rather than $\frac{8}{3\pi}$ (= .85); while M_{22} and M_{33} remain identical to the values from momentum theory (i.e., from an impermeable disk).

Thus, the Pitt model provides all of the important ingredients for a good dynamic inflow model:

1) Simplicity of closed-form expressions
2) Recovery of momentum theory in axial flow
3) Reasonable behavior for edgewise flow
4) Correlation with wake calculations.

The only missing ingredient from the Pitt model is a direct comparison with experimental flapping data, and that will be given in this paper.

Experimental Data for Rotor-Body Motion

In the previous sections, we have described the role of experimental data in the development of dynamic inflow. All of this data has been associated with purely flapping degrees of freedom and with loads normal to the blade disk (β, C_T, C_L, C_M) which relate directly to the normal flow of induced velocities. However, early on in the development of dynamic inflow, investigators realized that dynamic inflow could have an indirect effect on rotor body and inplane motions, thereby influencing lead-lag damping and helicopter pitch-roll dynamics, Reference 22. Here, again, the experimental data played a key role.

Reference 23 describes detailed frequency and damping measurements for a model rotor with inplane and body degrees of freedom. This data did not agree with theory and motivated the work in Reference 24 which shows that dynamic inflow can explain many of the phenomena found in Reference 23. It was Wayne Johnson, however, Reference 20, who provided the first direct correlation with this more sophisticated data. Reference 20 includes 12 figures, and almost every one of them shows a strong effect of dynamic inflow. For the sake of completeness, we would like to reproduce two of those results here. First, Fig. 8 gives a comparison of measured and calculated frequencies as a function of Ω. In particular, we note a theoretical frequency branch in Fig. 8a labeled λ, which implies that it is dominated by dynamic inflow, although it is certainly coupled with regressing

flapping (β_R) and body pitch (θ). The experimental data agree very well with this branch for Ω > 400 RPM. In comparison, the theory with no dynamic inflow, Fig. 8b, does not have such a branch; and it cannot, therefore, even begin to match the data.

The second result from Reference 20 is given in Fig. 9 and is a comparison of experimental roll damping with results of the Ames analysis (both with and without dynamic inflow). The results show that dynamic inflow gives a substantial improvement in correlation. Also shown in the figure is a similar analysis by Bell Helicopter (with and without dynamic inflow) which was presented at the ITR workshop, Reference 25. One can see that both the Ames and Bell results show the same improved correlation due to dynamic inflow. In general, the ITR results (which included many such comparisons) show that dynamic inflow often has a large effect on rotor-body and inplane damping and that modeling it generally improves correlation. On the other hand, the ITR results also show that, for some modes and frequencies, dynamic inflow has very little effect. Furthermore, there remain discrepancies between theory and experiment that cannot be accounted for by dynamic inflow. Therefore, the major conclusions from such comparisons are: 1) Dynamic inflow can have a pronounced effect on lead-lag and rotor-body damping, and 2) Rotor-body data cannot be used to validate or invalidate a particular dynamic inflow model. The justification for the second conclusion is straightforward. Our predictive capabilities in rotor-body dynamics are not sufficiently refined to isolate the effect of one single phenomenon. On the other hand, our predictive capabilities in flapping response are much better. Therefore, once we identify dynamic inflow as a true physical phenomenon based on flapping response, we have no choice but to: 1) believe that it has an effect on inplane and body dynamics, as shown in Reference 25, and 2) to include it in such analyses.

Comparison of Pitt Model with Static Data

The previous sections of this paper have dealt with the history of dynamic inflow. In particular, we have:

1) Reviewed the development of dynamic inflow theory and its close ties to experimental data;
2) Described the most promising inflow model, the Pitt model;
3) Shown that, although dynamic inflow is often important for inplane dynamics and rotor-body problems, only pure blade flapping response provides an appropriate data base to verify a particular inflow model.

With this as background, we are ready to introduce some new results in this paper. In these results, we compare the Pitt model to the Lockheed-Ames data of Reference 7. The first comparison concentrates on the nine static derivatives analyzed in Reference 5. The derivatives are for $p = 1.17$ and are given as functions of advance ratio for $0 < \mu < .5$. Comparison is made of the theory without dynamic inflow, momentum theory, the Pitt model, and the experimental data. All coefficients are normalized on σa.

We begin with the C_T derivatives, Figs. 10a-c. For C_T/θ_0, momentum theory and the Pitt model give equally good data correlation. For C_T/θ_s, the data show an initial sign reversal followed by a return to a more conventional response. The Pitt model also gives this sign reversal, which is not predicted by momentum theory. For $\mu \geq .2$, however, momentum theory is a little better. For C_T/θ_c, only the Pitt model gives any derivative, but no data is available for comparison. We now turn to the C_L derivatives, Figs. 10d-f. For C_L/θ_0, momentum theory is little different from the no-inflow theory; and neither gives even a qualitative correlation. The Pitt model, however, is nearly perfect here. For C_L/θ_s, momentum theory is again completely inadequate while the Pitt model is very good. In C_L/θ_c, both inflow models do fairly well for $\mu < .4$. The theory without dynamic inflow is not satisfactory. Next, we consider the C_M derivatives, Figs. 10g-i. For C_M/θ_0, only the Pitt model predicts the large increase in the derivative for $\mu < .2$; but momentum theory does better at higher μ. For C_M/θ_s, momentum theory is slightly better than the Pitt model; and, for C_M/θ_c, the Pitt model correctly predicts the increase in derivative for $\mu > .1$. For $\mu \geq .1$, however, momentum theory seems better.

The above static comparisons have a mixture of judgements with momentum theory sometimes better and with the Pitt model sometimes better. To obtain a quantitative measure of the relative merits of the models we define the following scoring system for correlation of experiments with theoretical results.

0 - no better than "no dynamic inflow"
1 - moves theory in correct qualitative direction
2 - substantially improves data correlation
3 - excellent correlation with data

The first two columns of Table 1 give a comparison of methods under this scoring system. Numbers given are average scores over the above 8 static derivatives. The empirical model, not shown in Figs. 10a-i, is included based on the results in Reference 5.

Table 1. Comparison of methods.

Model Data	Static Data p = 1.17	Dynamic Data p = 1.15
Momentum Theory	1.6	0.8
Pitt Model	2.5	2.1
Empirical Model	2.7	2.2

The Pitt model is an overall winner over momentum theory, the former averaging between "substantial improvement" and "excellent correlation" while the latter averages a whole category less. Surprisingly, the Pitt model is almost as good as the Empirical model which was identified solely on the basis of best fit of this static data. In the following section, we will be able to compare at a different value of flapping frequency, p = 1.15.

Comparison with Dynamic Data

We are now ready to compare the Pitt model with the dynamic measurements of Reference 7. It is interesting that the original attempt at correlation of this data was presented at the First Decennial Dynamics Specialists' Meeting, ten years ago. This data, for p = 1.15, is nearly the same configuration as that of the static data. Thus, the $\omega = 0$ results closely resemble the static data of Fig. 10. The original dynamic data in Reference 8 was presented only for $\mu = .51$. Here, we expand the data base to include three advance ratios: $\mu = .27$, .36, .51. Thus, we present entirely new data correlations and provide a broader and fairer comparison. Only roll and pitch moments are given because no dynamic thrust measurements were made. Consequently, the following figures are for the 6 dynamic roll and pitch moment derivatives (magnitude and phase). For the sake of brevity, phase angles are not presented for all derivatives. However, the phase angles that are given are entirely representative of those omitted.

Figs. 11-13 give $C_L/\sigma a$ due to θ_o at three advance ratios. The points near $\omega = 0$ correspond to the static data in Fig. 10. We give the magnitude of the response as a function of ω. Phase is given only for $\mu = .36$ (our reference advance ratio) but is typical of the other advance ratios. Several items are noteworthy. First, the static results at p = 1.15 (inferred from $\omega = 0$) show the same deviations as do the derivatives in Fig. 10d. In particular, the derivative from the Pitt model is smaller than the data, and the null point is shifted. Despite this, however, the theory does a good job of data correlation as ω is increased. For example, at all 3 values of μ, the no-inflow and momentum theories show a nearly null point at $\omega = .4$ accompanied by a near discontinuity in phase from 90° to 270°. The data and the Pitt model, however, do not follow this pattern and show a level amplitude and smooth phase change through the region. (Recall that $\theta = 0°$ and $\theta = 360°$ are identical.) Another note here is that momentum theory provides virtually no improvement in theory, whereas the Pitt model provides a positive influence.

In Figs. 14-16, we examine $\partial C_L/\partial\theta_s$ at the same three advance ratios. The phase at $\mu = .36$ is representative. Unlike $\partial C_L/\partial\theta_o$, this derivative is nonzero in hover (Fig. 1) so that we truly have four advance ratios to compare. In hover, momentum theory and the Pitt model are identically good. As advance ratio increases, however, the data begin to change dramatically while the no-inflow and momentum theories barely budge. The Pitt model on the other hand changes with the data and provides nearly identical static correlation ($\omega = 0$). Similarly, as ω increases, the Pitt model causes the theory to follow the data well up to $\omega = .6$. Beyond that, the data seem to fall below all three theories. In terms of phase, the Pitt model does well except for the rapid change in phase at $\omega = .4$ associated with the antiresonance. Thus, the Pitt model does well at all advance ratios from 0 to .51. For the remainder of the derivatives, we will present only the $\mu = .36$ correlations since these are fairly representative.

Fig. 17 gives $\partial C_L/\partial\theta_c$. For comparison purposes we can again refer to Fig. 1 since, in hover, C_L/θ_c is analogous to $\partial C_M/\partial\theta_s$. At $\mu = 0$, the momentum theory and Pitt model are equally good (being identical); and they show the large drop in static derivative followed by a peak and return to no-inflow values. At $\mu = .36$, both theories still show the proper reduction in static value, but the Pitt model does better at reproducing the return to no-inflow theory. Both theories do well on phase angle (not shown).

We now turn to pitch-moment data. Fig. 18 provides $C_M/\sigma a$ with θ_o. This derivative is zero in hover but is quite large at $\mu = .36$. In this case, momentum theory shows too much reduction in the static value while the Pitt model is nearly perfect. (Recall that the momentum theory was better at p = 1.17.) One notices two ripples in the data (at $\omega = .4$ and $\omega = .7$). These are stand resonances and introduce some contamination of the data. It is possible that these resonances account for some deviations in roll-moment data, especially the null point in $\partial C_L/\partial\theta_s$. The phase angle for $\partial C_M/\partial\theta_c$ (not shown) is insensitive to inflow model, and all models show equally good correlation.

In Fig. 19, we have $\partial C_M/\partial\theta_s$ at $\mu = .36$, which can be compared with the hover value in Fig. 1. The stand resonance is clearly seen at $\omega = .4$ as an anamolous data point. Both the Pitt model and the momentum theory do well at $\mu = .36$ with the slight edge going to momentum theory. C_M with θ_s is the only derivative for which momentum theory is consistently better than the empirical and the Pitt models. Once again, all models give good phase correlation.

The final figure to be presented is $C_M/\sigma a$ with θ_c, Fig. 20. Both magnitude and phase are shown, and the corresponding hover results are $\partial C_L/\partial\theta_s$, Fig. 1. The Pitt model predicts the increased static derivative ($\omega = 0$), and the model does well for $\omega < .5$. For larger values of ω, it is hard to distinguish the best theory. On phase angle, the Pitt model gives the correct trend at all ω's but does not capture the complete phase shift near $\omega = .4$. Once again, the stand resonance could be a factor.

We can again use the scoring method mentioned earlier in the paper to compare the various models. All advance ratios and derivatives are included in the scoring, and we also rank the empirical model of Reference 8 (although empirical results are not plotted here). The scoring is given in the last column of Table 1. The usefulness of momentum theory diminishes greatly as compared with the static case. It produces a score of less than unity. (Most of the time it does not even move the theory in the right direction.) The Pitt model, on the other hand, scores close to the empirical model; and both give, on the average, more than a substantial improvement in correlation. The overall impression of Table 1 places the Pitt model as the best model in forward flight.

Conclusions

Over the past thirty years, the theory of dynamic inflow has developed due to the desire to correlate with experimental data. The preponderance of data correlations over that time (as well as the new comparisons presented here) lead to the following conclusions:

1) The effect of dynamic inflow has been demonstrated to be a valid physical phenomenon that can change the qualitative nature of rotor response in hover and forward flight.

2) In hover, dynamic inflow is represented nearly exactly by momentum theory coupled with apparent mass terms (three first-order equations).

3) In forward flight, momentum theory does very poorly and cannot capture the major effects of dynamic inflow.

4) The Pitt model, developed from an analytical base, provides excellent data correlation in forward flight and is identical to momentum theory in hover. Thus, it stands as the premier model for rotor analysis.

5) Although dynamic inflow is often important for problems of inplane and rotor-body dynamics (and often improves correlation), such studies are not reliable for the validation of inflow models. Dynamic inflow theories must be verified on the basis of flapping response and inflow measurements.

Acknowledgement

This work was sponsored by the U.S. Army Research Office, Grant No. DAAG-29-80-C-0092. The view, opinions, and/or findings contained in this report are those of the author(s) and should not be construed as an official Department of the Army position, policy, or decision, unless so designated by other documentation.

References

1. Amer, K. B., "Theory of Helicopter Damping in Pitch or Roll and a Comparison with Flight Measurements," NACA TN-2136, October 1950, p. 11.

2. Sissingh, G. J., "The Effect of Induced Velocity Variation on Helicopter Rotor Damping in Pitch or Roll," Aeronautical Research Council Paper No. 101, Technical Note No. Aero 2132, November 1952.

3. Shupe, N. K., A Study of the Dynamic Motions of Hingeless Rotored Helicopters, Ph.D. Thesis, Princeton, September 1970.

4. Curtiss, H. C., Jr. and Shupe, N. K., "A Stability and Control Theory for Hingeless Rotors," Proceedings of the 27th Annual National Forum of the American Helicopter Society, May 1971, Paper No. 541.

5. Ormiston, Robert A. and Peters, David A., "Hingeless Rotor Response with Nonuniform Inflow and Elastic Blade Bending," Journal of Aircraft, Vol. 9, No. 10, October 1972, pp. 730-736.

6. Carpenter, P. J. and Fridovitch, B., "Effect of Rapid Blade Pitch Increase on the Thrust and Induced Velocity Response of a Full Scale Helicopter Rotor," NACA TN-3044, November 1953.

7. Kuczynski, W. A. and Sissingh, G. J., "Characteristics of Hingeless Rotors with Hub Moment Feedback Controls Including Experimental Rotor Frequency Response," NASA CR 114427, January 1972.

8. Peters, David A., "Hingeless Rotor Frequency Response with Unsteady Inflow," Rotorcraft Dynamics, NASA SP-352, February 1974, pp. 1-13.

9. Ormiston, Robert A., "Application of Simplified Inflow Models to Rotorcraft Dynamic Analysis," Journal of the American Helicopter Society, Vol. 21, No. 3, July 1976, pp. 34-39.

10. Gaonkar, Mitra, and Reddy, "Feasibility of a Rotor Flight Dynamics Model with First-Order Cyclic Inflow and Multi-Blade Modes," Proceedings of the AIAA Dynamics Specialists' Meeting, Atlanta, Georgia, April 9-10, 1981, p. 15.

11. Pitt, Dale M. and Peters, David A., "Theoretical Predictions of Dynamic Inflow Derivatives," Vertica, Vol. 5, No. 1, March 1981.

12. Gaonkar, et al., "The Use of Actuator-Disc Dynamic Inflow for Helicopter Flap-Lag Stability," Journal of the American Helicopter Society, Vol. 28, No. 3, July 1983, pp. 79-88.

13. Peters, David A., "The Importance of Steady and Dynamic Inflow on the Stability of Rotor-Body Systems," Proceedings of the ITR Methodology Workshop, NASA-Ames Research Center, June 21-22, 1983.

14. Crews, S. T., Honenemser, K. H., and Ormiston, R. A., "An Unsteady Wake Model for a Hingeless Rotor," Journal of Aircraft, Vol. 10, No. 12, December 1973, pp. 758-760.

15. Azuma, Akira and Nakamura, Yoshiya, "Pitch Damping of Helicopter Rotor with Nonuniform Inflow," Journal of Aircraft, Vol. 11, No. 10, October 1974, pp. 639-646.

16. Ormiston, Robert A., "An Actuator Disk Theory for Rotor Wake Induced Velocities," AGARD Specialists Meeting on the Aerodynamics of Rotary Wings, Marseille, France, September 13-15, 1972.

17. Pitt, Dale M. and Peters, David A., "Rotor Dynamic-Inflow Derivatives and Time Constants from Various Inflow Models," 9th European Rotorcraft Conference, Stresa, Italy, September 13-15, 1983, Paper No. 55.

18. Landgrebe, A. J., "An Analytical Method for Predicting Rotor Wake Geometry," Journal of the American Helicopter Society, Vol. 14, No. 4, October 1969.

19. Johnson, Wayne, Helicopter Theory, Princeton University Press, 1980, pp. 520-526.

20. Johnson, Wayne, "Influence of Unsteady Aerodynamics on Hingeless Rotor Ground Resonance," Journal of Aircraft, Vol. 19, No. 8, August 1982, pp. 668-673.

21. Coleman, Feingold, and Stempin, "Evaluation of the Induced Velocity Field of an Idealized Helicopter Rotor," NACA WRL-126, June 1945.

22. Peters, David A. and Gaonkar, Gopal H., "Theoretical Flap-Lag Damping with Various Dynamic Inflow Models," Journal of the American Helicopter Society, Vol. 25, No. 3, July 1980, pp. 29-36.

23. Bousman, W. G., "An Investigation of the Effects of Aeroelastic Couplings on Aeromechanical Stability of a Hingeless Helicopter Rotor," Journal of the American Helicopter Society, Vol. 26, No. 1, January 1981, pp. 46-54.

24. Gaonkar, G. H., Mitra, A. K., Reddy, T.S.R., and Peters, D. A., "Sensitivity of Helicopter Aeromechanical Stability to Dynamic Inflow," Vertica, Vol. 6, No. 1, January 1982, pp. 59-75.

25. Bousman, W. G., "Rotorcraft Stability Methodology Assessment," Proceedings of the ITR Methodology Workshop, NASA-Ames Research Center, June 21-22, 1983.

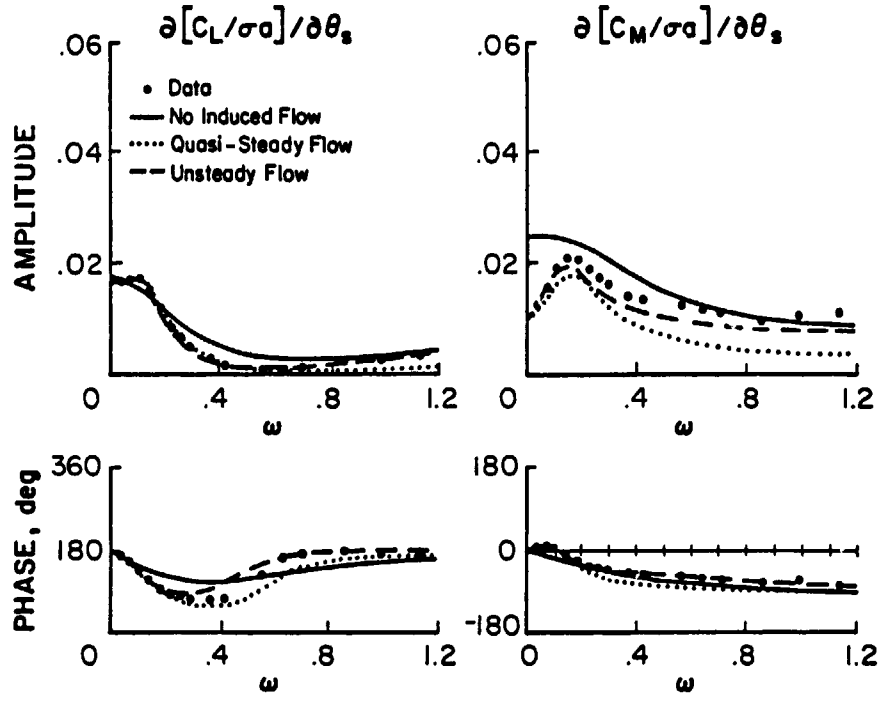

Figure 1. Rotor Response to Cyclic Pitch in Hover, p=1.15, γ =4.25, B=.97, e_{pc}=.25, μ =0, σa=.7294, $\bar{v}_o$ =.03, θ_o =4°, λ =0 momentum theory, single rotating mode.

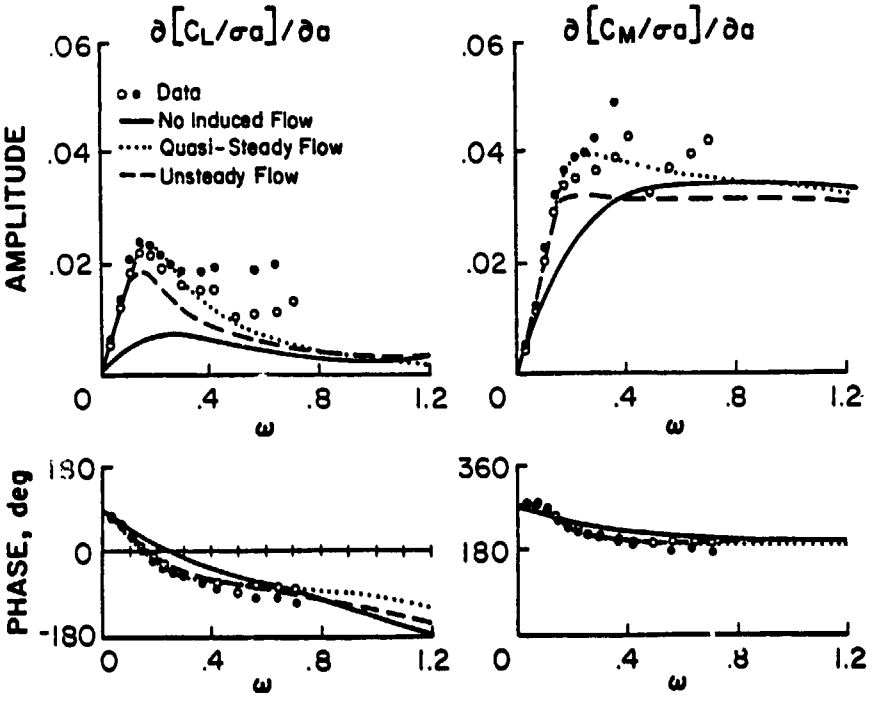

Figure 2. Rotor response to Hub Motions in Hover, p=1.15, γ =4.25, B=0.97, e_{pc}=0.25, μ =0, σa=.7294, λ=0, $\bar{v}_o$ =.03, momentum theory, single rotating mode.

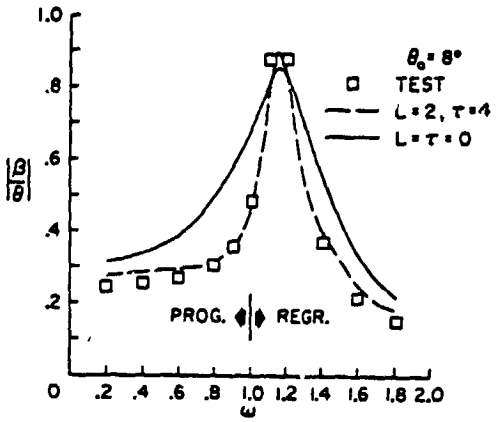

Figure 3. Rotor Response to Pitch Stirring, $p = 1.21$, $\gamma = 4.0$, $\mu = 0$, $\beta = 0.97$.

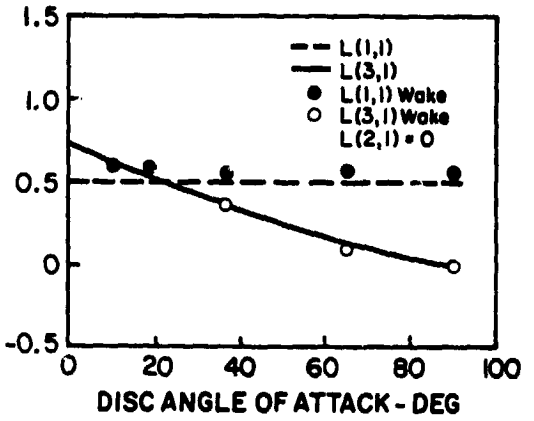

Figure 4. Verification of First Column of L.

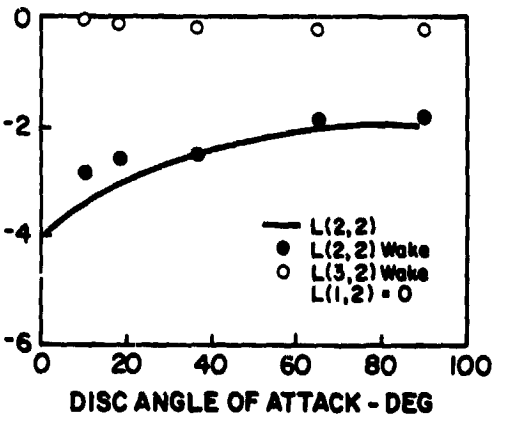

Figure 5. Verification of Second Column of L.

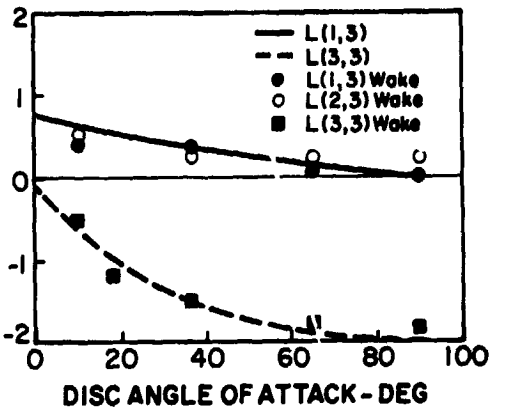

Figure 6. Verification of Third Column of L.

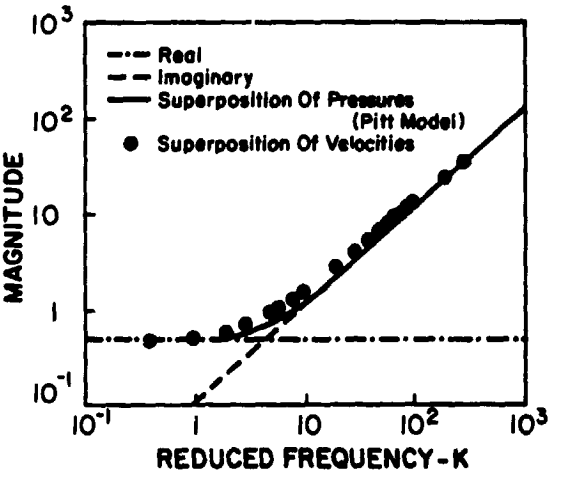

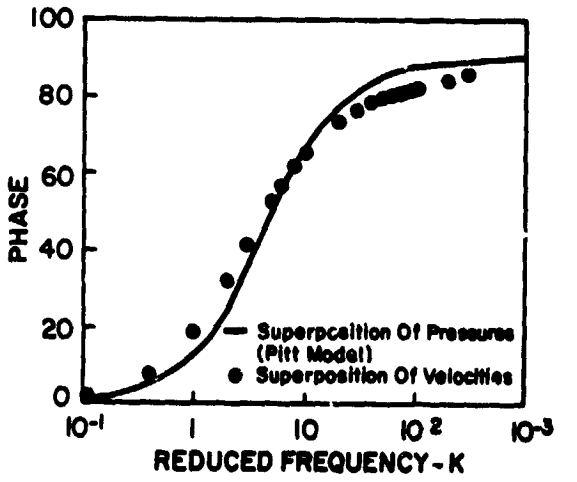

Figure 7. Comparison of Harmonic Pressure Distributions as Calculated by the Pitt Model (Superposition of Apparent-Mass Pressure) with those of an Unsteady Wake Calculation (Superposition of Velocities).

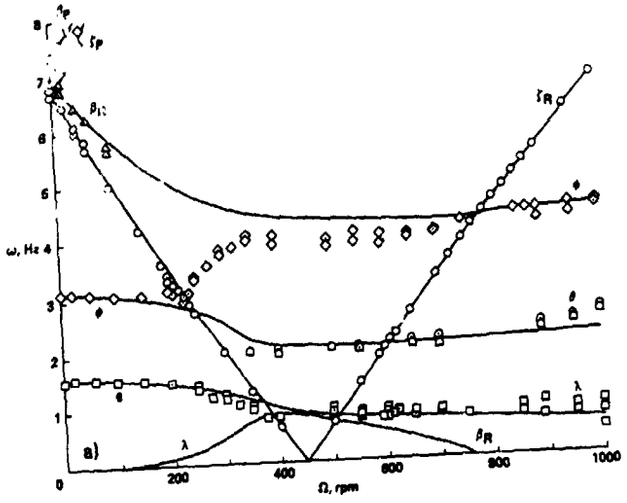

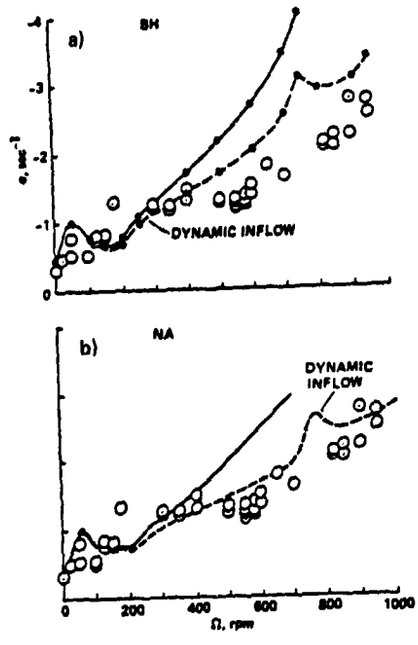

Figure 9. Comparison of roll mode damping. a) Bell Helicopter model, b) NASA Ames model.

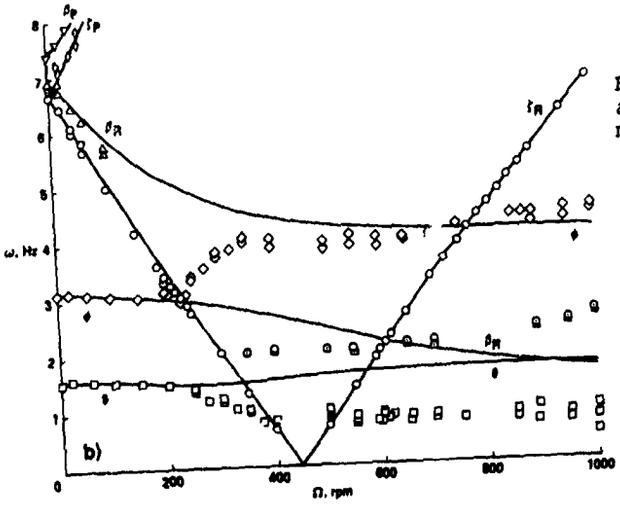

Figure 8. Modal frequencies as a function of rotor speed for configuration 4 (Reference 20). Comparison of measurements (open symbols) and calculation (lines). a) With inflow dynamics; b) without inflow dynamics.

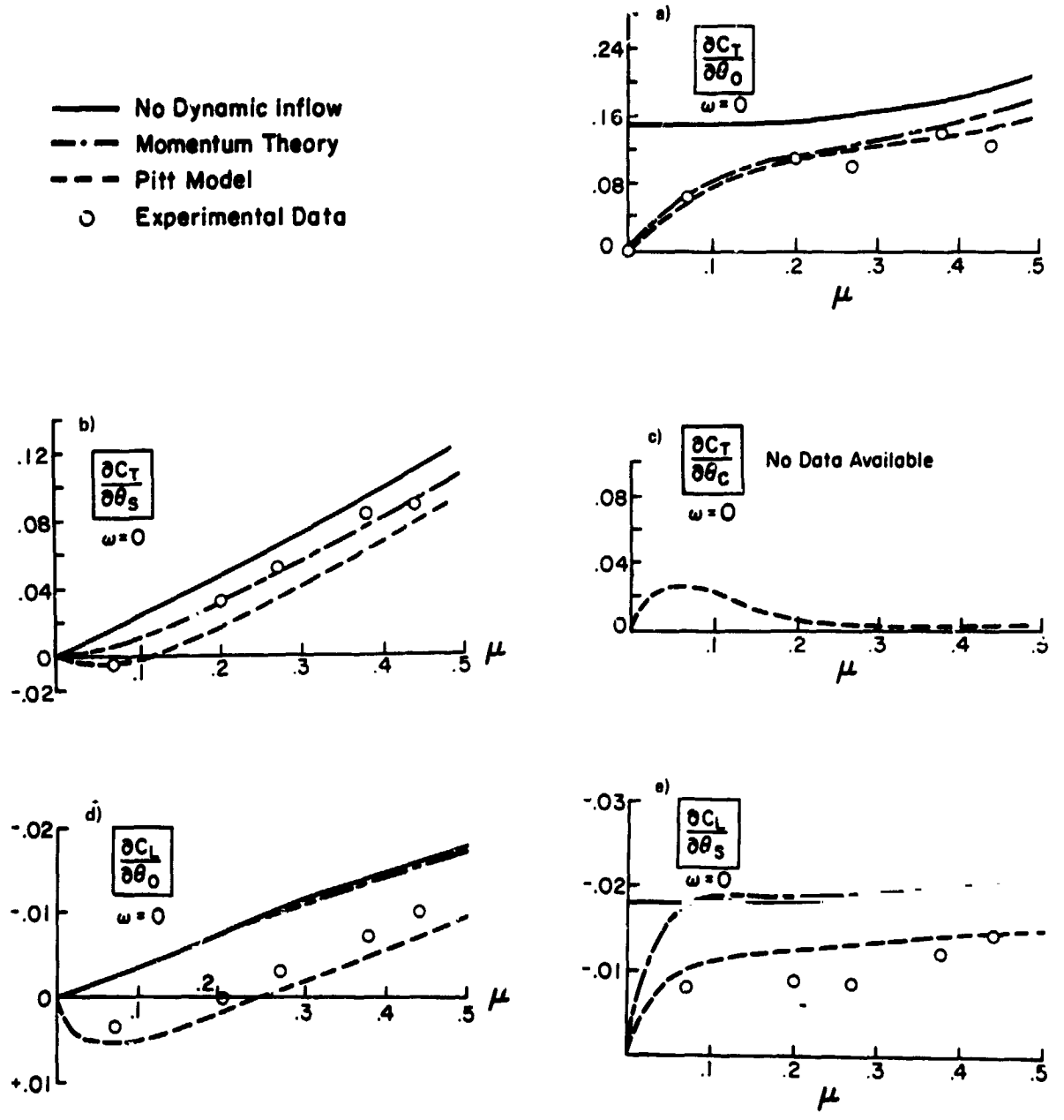

Figure 10. Rotor response for $\omega = 0$, $p = 1.17$, $\gamma = 4.2$, $B = 0.97$, $e_{pc} = 0.25$, $\sigma a = 0.73$, $\bar{v}_0 = \lambda = 0$, all coefficients normalized on σa.

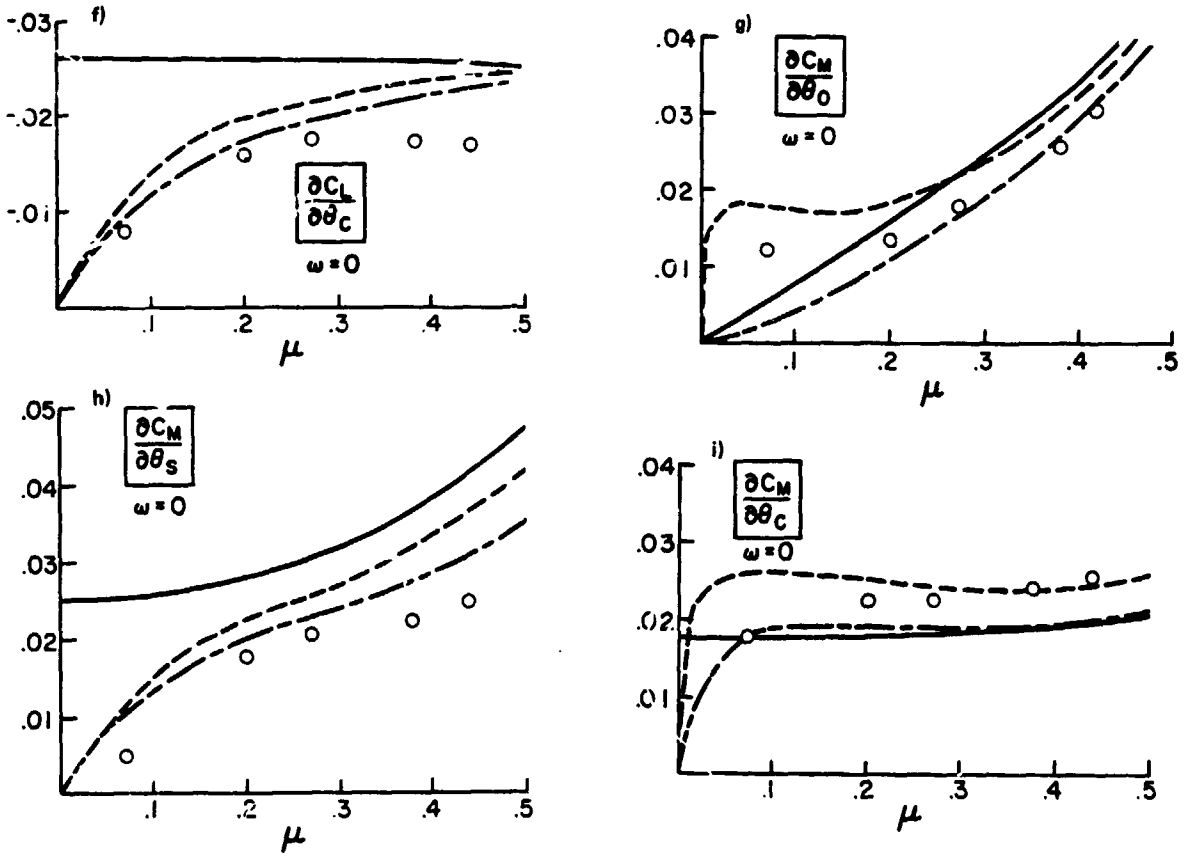

Figure 10. Concluded.

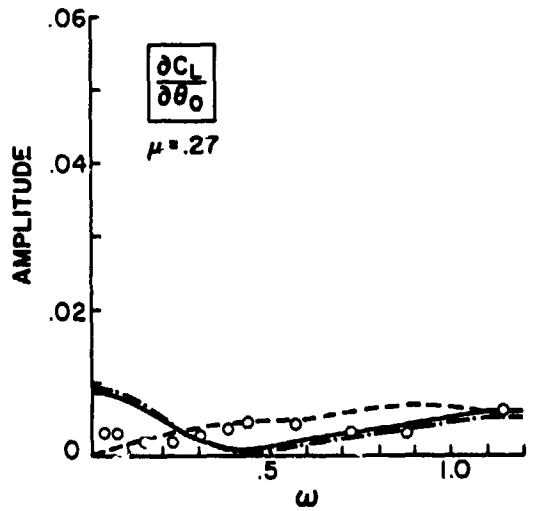

igure 11. Rotor response in forward flight, $C_L/\sigma a$ due to θ_o for $\mu = 0.27$, $\rho = 1.15$, $\gamma = 4.25$, $B = 0.97$, $e_{pc} = 0.25$, $\sigma a = 0.73$, $\bar{v}_o = \lambda = 0$. (See Fig. 10 for legend.)

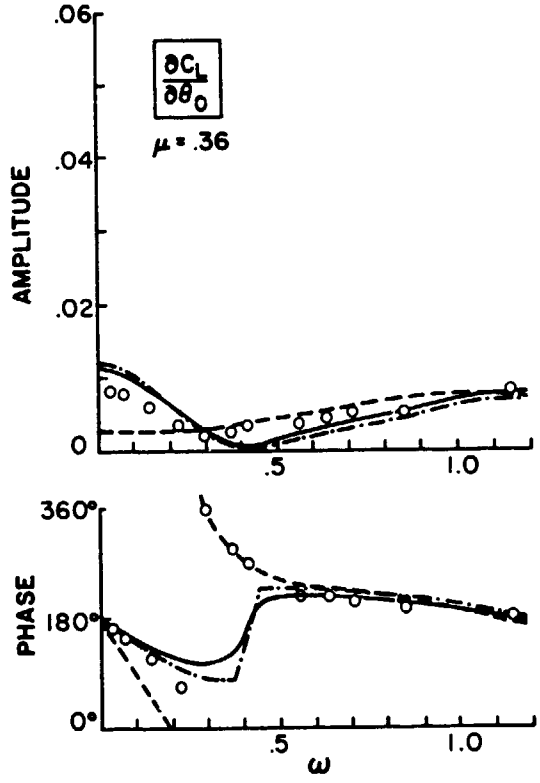

Figure 12. Rotor response in forward flight, $C_L/\sigma a$ due to θ_o for $\mu = 0.36$, $p = 1.15$, $\gamma = 4.25$, $B = 0.97$, $e_{pc} = 0.25$, $\sigma a = 0.73$, $\bar{v}_o = \lambda = 0$. (See Fig. 10 for legend.)

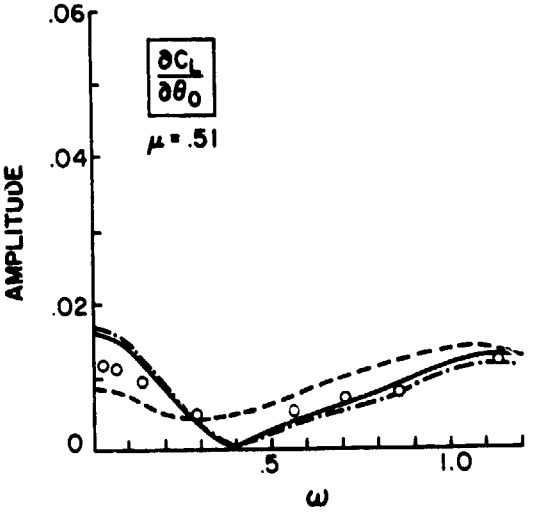

Figure 13. Rotor response in forward flight, $C_L/\sigma a$ due to θ_o for $\mu = 0.51$, $p = 1.15$, $\gamma = 4.25$, $B = 0.97$, $e_{pc} = 0.25$, $\sigma a = 0.73$, $\bar{v}_o = \lambda = 0$. (See Fig. 10 for legend.)

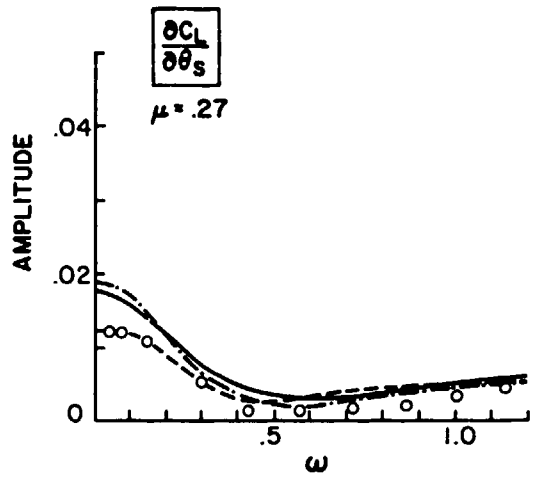

Figure 14. Rotor response in forward flight, $C_L/\sigma a$ due to θ_s for $\mu = 0.27$, $p = 1.15$, $\gamma = 4.25$, $B = 0.97$, $e_{pc} = 0.25$, $\sigma a = 0.73$, $\bar{v}_o = \lambda = 0$. (See Fig. 10 for legend.)

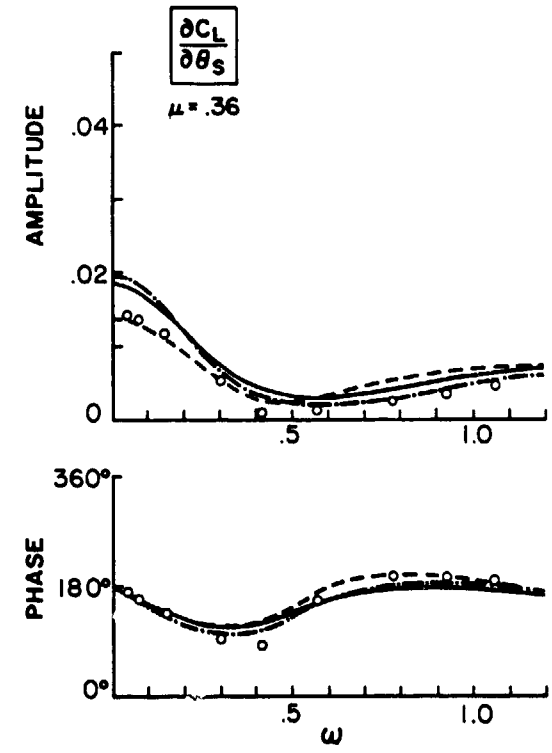

Figure 15. Rotor response in forward flight, $C_L/\sigma a$ due to θ_s for $\mu = 0.36$, $p = 1.15$, $\gamma = 4.25$, $B = 0.97$, $e_{pc} = 0.25$, $\sigma a = 0.73$, $\bar{v}_o = \lambda = 0$. (See Fig. 10 for legend.)

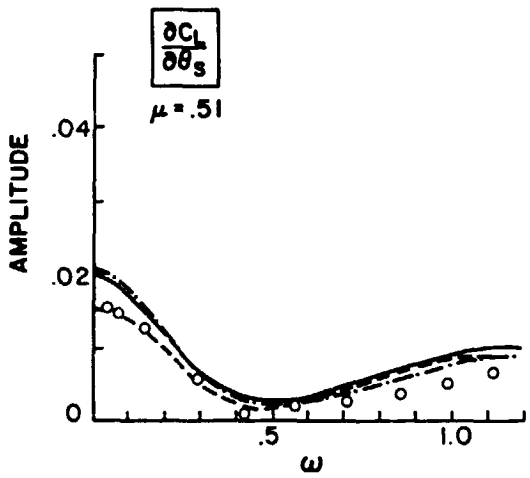

Figure 16. Rotor response in forward flight, $C_L/\sigma a$ due to θ_s for $\mu = 0.51$, $p = 1.15$, $\gamma = 4.25$, $B = 0.97$, $e_{pc} = 0.25$, $\sigma a = 0.73$, $\bar{v}_o = \lambda = 0$. (See Fig. 10 for legend.)

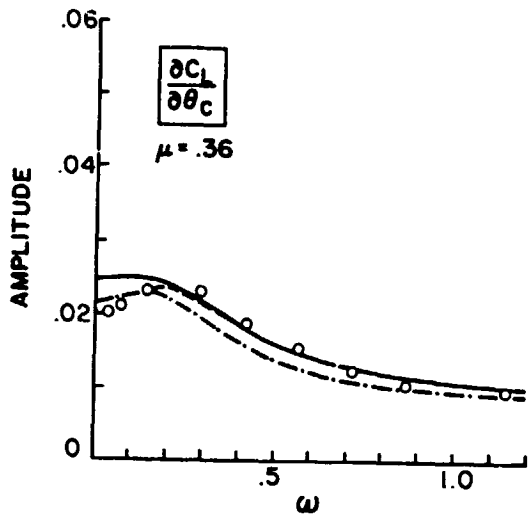

Figure 17. Rotor response in forward flight, $C_L/\sigma a$ due to θ_c for $\mu = 0.36$, $p = 1.15$, $\gamma = 4.25$, $B = 0.97$, $e_{pc} = 0.25$, $\sigma a = 0.73$, $\bar{v}_o = \lambda = 0$. (See Fig. 10 for legend.)

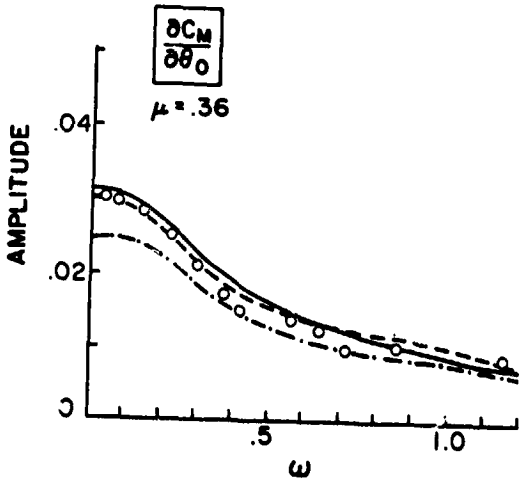

Figure 18. Rotor response in forward flight, $C_M/\sigma a$ due to θ_o for $\mu = 0.36$, $p = 1.15$, $\gamma = 4.25$, $B = 0.97$, $e_{pc} = 0.25$, $\sigma a = 0.73$, $\bar{v}_o = \lambda = 0$. (See Fig. 10 for legend.)

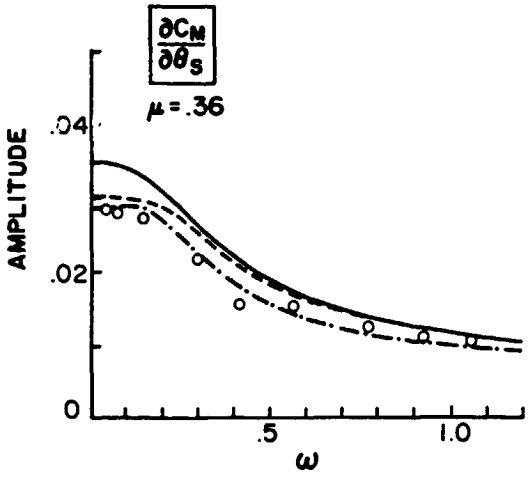

Figure 19. Rotor response in forward flight, $C_M/\sigma a$ due to θ_s for $\mu = 0.36$, $p = 1.15$, $\gamma = 4.25$, $B = 0.97$, $e_{pc} = 0.25$, $\sigma a = 0.73$, $\bar{v}_o = \lambda = 0$. (See Fig. 10 for legend.)

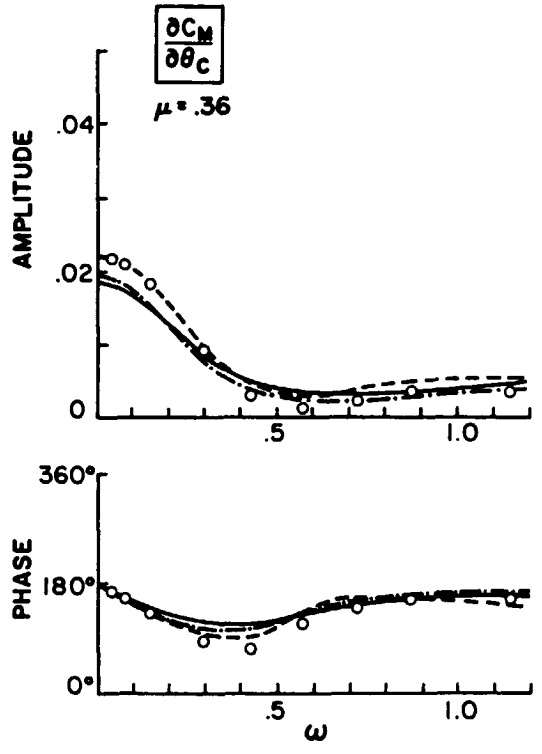

Figure 20. Rotor response in forward flight, $C_M/\sigma a$ due to θ_c for $\mu = 0.36$, $p = 1.15$, $\gamma = 4.25$, $B = 0.97$, $e_{pc} = 0.25$, $\sigma a = 0.73$, $\bar{v}_o = \lambda = 0$. (See Fig. 10 for legend.)

DISCUSSION
Paper No. 13

A REVIEW OF DYNAMIC INFLOW AND ITS EFFECT ON EXPERIMENTAL CORRELATIONS
Gopal H. Gaonkar
and
David A. Peters

Wayne Johnson, NASA Ames Research Center: In your conclusions you discussed the qualitative ratings you gave for momentum theory and for the Pitt model, but you neglected to mention that the empirical model you rated best of all. Perhaps you would like to comment on that.

Peters: It would be surprising if the momentum theory did better than the empirical model because the empirical model was identified to give the best possible fit of that data that you could with nine elements in an L matrix. All right, so if I got better I think, well, I must have identified wrong. So what it says is [that] that wasn't good enough because it had these singularities in it and it had the other disadvantages. Now the question is with the Pitt model, which comes from basic principles, how close can I get to the old optimum and it's pretty close. I do just about as good as the empirical model so I'm almost to the optimum that I can get. That is, if you try another tweak to the Pitt model and try to make it better you don't have that much more better that you can get because we already have got about as close as we can.

Dev Banerjee, Hughes: I was curious in your comparison between the empirical model and Pitt's model did you identify the singularities that you saw in the empirical results through Dale Pitt's model?

Peters: The Pitt model does not have these singularities. There were basically two in the empirical model. One was at an advance ratio of 0.8 and we sort of think that that was just the dynamic inflow model trying to explain other things. In other words since you are trying to match the data exactly, the L matrix has to do everything, so we sort of feel that somewhere at 0.8 the reverse flow region is getting so large that maybe we're just not doing that well. The other singularity--I don't know why the empirical model has a singularity at μ of 0.32. That is, at the one place L exists, but L inverse doesn't. At 0.32 it is the opposite. L inverse exists but L doesn't. I have no idea why the Pitt model does not show that. It just shows smooth transitions, the determinant is always positive, it never goes through zero, and I don't know if that's just a numerical coincidence or why the empirical model has that singularity in it. I take it back, there may be one possibility. There was a stand resonance that shows up in some of the data that you can see--you couldn't see it in this too well, but some of the others right around a certain frequency range. You wouldn't think that that would be just at one advance ratio where that would show up as a singularity. I don't know.

Bob Ormiston, U.S. Army Aeromechanics Laboratory: An interesting paper Dave and Gopal. My comment just has to do with one of the conclusions about the use of experimental testing to validate the models. I would think in my opinion that the rotor-body flapping dynamic experiments would be excellent for correlating with dynamic inflow. I tend to agree with you when you say that maybe the inplane measurements aren't the best for correlating this type of aerodynamic analysis, but I don't think you need just pure flapping data say, as opposed to coupled flapping and body motion data. The latter is a lot easier to get in an experiment sometimes as we have found out. Maybe I misinterpreted what you said, but I think that two degrees of freedom are okay.

Peters: I partially agree with you. I think that as we get better that will happen. But here is an example: in the next paper you are going to see that if you put a factor of 2 in some of the terms of the L matrix you can get maybe a 15 to 20 percent change in the damping of roll and pitch and maybe get a slightly better correlation. All right? But if you put a factor of 2 into this flapping data you are going to throw that beautiful correlation completely off. So that makes you scratch your head and say, now wait, if I have to do that much to get this much sensitivity in roll and pitch maybe the other is wrong. But someday we should be able to verify it on any data if we are good enough at predicting.

Euan Hooper, Boeing Vertol: I'd like to ask the chairman if he has any plans to incorporate this Pitt model in CAMRAD? Wouldn't it be useful for tilt rotor stability?

Johnson: Not for tilt rotors. Tilt rotors, the ones that people are looking at now--not the Boeing design of 15 years ago--but the ones they are doing now, are really low equivalent flap hinge offset, low flap frequency. So they do not generate much in the way of hub moments which is where we really see the large dynamic inflow effects. Most of the stuff that Dave was showing [had] flap frequencies of 1.15 and the like. Really for tilt rotors you only have to worry about the thrust component and it's in axial flight and we've got that one as good as we probably need it. Now probably somebody will design a tilt rotor someday that isn't true about, but right now I don't think that is quite the most important area.

Hooper: But it's in the frequency range isn't it, Dave? Do you agree with Wayne's comment?

Peters: Yes, I guess I have two comments. One in Wayne's defense--if you look at who has come into the dynamic inflow fold through the years--he was one of the first. He has dynamic inflow in CAMRAD and like you say it wouldn't be hard to change that. But remember when you look at the right hand side of the equations it's the aerodynamic component of roll and pitch moment. Even though you've got zero hub moment in roll you've got inertia and aerodynamics that are canceling, right? The inertial moments are pushing on Newton's law, but the aerodynamics parts are pushing on the wake. And that is why Sissingh could find out there was an effect on roll damping even for an articulated blade. Because it's the aerodynamic parts that go on the side. Although somehow for hingeless rotors I think it is bigger than for articulated. But it's still an effect.

Johnson: I think what we are talking about are two different things. The Pitt model is really for forward flight [in the] helicopter mode and in the tilt rotors you will have as much an effect there as you would on any other helicopter. But in axial flight for the tilt rotor you are really back down to momentum theory which does pretty good. There the thrust one is dominant. In support of that I will simply say that I have looked at it. Even the thrust perturbations in dynamic inflow don't seem to matter much in tilt rotor dynamics. I think it's just largely because the other aerodynamics in tilt rotors just overpower things like that.

Jack Landgrebe, United Technologies Research Center: Dave, just so there is no misunderstanding in the audience here, you are talking about dynamic inflow and there is also what we consider variable inflow. You are working with the perturbation inflows required for the stability problem. There is also of course the major area of the actual inflow required to compute the airloads and so forth. In some ways they are connected and in some ways they are two distinct problems. Is there anything that you can glean from the Pitt model that would be helpful in what we call the variable inflow airload prediction sense or do you feel it's strictly applicable to the stability problem?

Peters: I think the latter. I think it's not applicable to loads or things like that. It is a very gross, crude approximation to the induced flow field. In fact, if you look at how it developed, when Dale Pitt first came as my student I said, "Let's take Landgrebe's prescribed wake program and develop the dynamic inflow equations by averaging and getting those gradients." But he did a literature search and anybody that did variable inflow he thought was a candidate--he has about 150 references in his thesis. And one pulled up this old stuff that he used which was the Kinner distribution. So really we come from you. We've gleaned from those the gems that we needed for dynamic inflow.

Landgrebe: That is what I thought. I had heard from you earlier and I just wanted to make sure there was not a misconception in the audience that the variable inflow problem has been solved through this.

Peters: That is a common misconception, too. A lot of people say, "Wait a minute. People did all those inflow distributions before." They really did and we are thankful they did. We just picked from that the things we needed.

INFLUENCE OF VARIOUS UNSTEADY AERODYNAMIC MODELS ON THE AEROMECHANICAL STABILITY OF A HELICOPTER IN GROUND RESONANCE*

P.P. Friedmann
Professor of Engineering and Applied Science

and

C. Venkatesan
Assistant Research Engineer
Mechanical, Aerospace and Nuclear Engineering Department
University of California, Los Angeles, California 90024

Abstract

The aeromechanical stability of a helicopter in ground resonance was analyzed, by incorporating five different aerodynamic models in the coupled rotor/fuselage analysis. The sensitivity of the results to changes in aerodynamic modelling was carefully examined. The theoretical results were compared with experimental data and useful conclusions are drawn regarding the role of aerodynamic modeling on this aeromechanical stability problem. The aerodynamic model which provided the best all around correlation with the experimental data was identified.

Nomenclature

a	- lift curve slope
C	- lift deficiency factor
C_1	- coefficient in inflow equations, C_1 = 0.5 or 1.0
C_T	- Thrust coefficient
C_{Mx}, C_{My}	- moment coefficients in roll and pitch
$[L]$	- induced flow matrix
$\dot{m}$	- mass flow rate
M	- rotor aerodynamic moment
M_1	- apparent inertia
r	- radial location of a typical blade section
R	- rotor radius
s	- eigenvalue
dT	- differential thrust
β_{1c}, β_{1s}	- cyclic flap coordinates
β_P, β_R	- progressing and regressing flap modes respectively
γ	- Lock number
γ^*	- equivalent, reduced or effective Lock number
λ_0	- steady or mean inflow
λ	- total inflow, $\lambda = \lambda_0 + \delta\lambda$; also inflow mode, in figures only
$\lambda_1, \lambda_{1c}, \lambda_{1s}$	- inflow variables
$\delta\lambda$	- unsteady wake induced perturbational inflow
ω	- modal frequency, imaginary part of s
Ω	- rotor R.P.M.
ϕ	- body roll mode
ψ	- azimuthal angle or nondimensional time $\psi = \Omega t$
ρ	- density of air
σ	- modal damping, real part of s
$\bar{\sigma}$	- solidity ratio
θ	- body pitch mode
θ_c	- collective pitch setting of the blade
ζ_{1c}, ζ_{1s}	- cyclic lag coordinates
ζ_P, ζ_R	- progressing and regressing lag modes respectively

1. Introduction

Unsteady aerodynamics have a significant influence on the aeroelastic and the aeromechanical stability characteristics of helicopters. The mathematical sophistication of refined unsteady aerodynamic models is sometimes prohibitive to incorporate in the aeroelastic analyses and therefore it is quite frequent that rotary-wing aeroelastic analyses are based upon quasisteady aerodynamic theory. Fortunately, there are some relatively simple unsteady aerodynamic models, known as inflow models, which can be conveniently incorporated in the aeroelastic and aeromechanical studies of helicopters. These simple models are based upon the definition of certain inflow parameters which represent essentially the unsteady wake-induced flow through the rotor disk. A number of such inflow models are available in the literature; however the applicability of a particular model to a given rotor dynamic problem and the sensitivity of the stability boundaries to the choice of the inflow model and comparisons with experimental data have not been considered in detail in the literature. Bousman[1] has carried out an experimental study of the aeromechanical stability of a hingeless rotor supported on a special gimbal which simulated the pitch and roll degrees of freedom. The availability of this high quality experimental data provides an

*This research was supported by NASA Grant NAG 2-209, funded by Ames Research Center, Moffett Field, California

opportunity; (a) to test the validity of mathematical models representing the coupled rotor/fuselage dynamics and (b) to determine the influence of various aerodynamic models on this aeromechanical problem. Bousman attributed some of the discrepancies, found between the theoretical results presented in his paper and the experimental results, to dynamic inflow. This conclusion was examined by Johnson[2], in a recent study, where the unsteady aerodynamic effects on the rotor were represented by a dynamic inflow model[3]. Johnson's[2] results with the dynamic inflow model[3,4] indicated better agreement with the experimental data than the results obtained using the quasi-steady aerodynamic model. Using the coupled rotor/body model[5,6] with simple quasi-steady aerodynamics, the authors[7] also obtained good agreement with the experimental results generated by Bousman[1]. Based on the agreement with the experimental data, they concluded that the coupled rotor/fuselage model developed, was reliable.

The purpose of this study is to extend Ref. 7 and study the sensitivity of the results obtained to changes in the aerodynamic assumptions used. To accomplish this objective, five different aerodynamic models were incorporated in the mathematical model representing the coupled rotor/fuselage dynamics and the sensitivity of the stability boundaries to changes in aerodynamic modelling was determined. The theoretical results were compared with the experimental data and based on this comparison, conclusions are drawn regarding the selection of the parameters used in defining these aerodynamic models.

2. Aerodynamic Models Used in the Analysis

The aerodynamic models, incorporated in this aeromechanical stability study representing a coupled rotor/fuselage system, were: (a) quasi-steady aerodynamics, (b) two different perturbation inflow models and (c) two different dynamic inflow models. A brief description of these aerodynamic models is provided below.

Quasi-steady Aerodynamic Model

The quasi-steady aerodynamic model, employed in the analysis, is based on Greenberg's[8] formulation of unsteady aerodynamic loads on an oscillatory airfoil in a pulsating flow. Greenberg's theory is a modified form of Theodorsen's unsteady aerodynamic theory. The quasi-steady model is obtained by assuming $C(k) = 1$ and neglecting the apparent mass terms (noncirculatory terms). In this model, the assumption of $C(k) = 1$ implies that the unsteady wake effects are totally neglected.

Inflow Models

The inflow models represent the unsteady wake effects in a simple form. In these models, the unsteady wake-induced flow through the rotor disk is defined by a set of inflow variables and these variables essentially provide a correction to the inflow assumed in the quasi-steady aerodynamic theory. When inflow models are used in the analysis of rotor dynamic problems the blade loads have to be calculated from the quasi-steady aerodynamic expressions. An important fact to be noted is that the quasi-steady aerodynamic model is a two dimensional local model and hence it is applied at a typical cross section located at a spanwise station along the rotor blade, in the blade fixed, rotating coordinate system. On the other hand, the inflow models represent the global effects of the unsteady wake and therefore they are applicable to the complete rotor. The various inflow models are described below.

Perturbation Inflow Model

Prior to describing the perturbation inflow model, it is useful to clarify certain aspects of the terminology used in the literature which deals with this subject. In some cases, the perturbation inflow model is referred to as quasi-static inflow model[2] and in other cases as quasi-steady inflow model[9].

The induced flow-field acting on a helicopter rotor affects both rotor equilibrium (trim loadings) and rotor response (transient loading). Therefore, it is reasonable to assume that the induced flow will also be affected by the oscillations of the rotor. This assumption is the basis of both the perturbation inflow models and dynamic inflow models. A detailed derivation of these inflow models can be found in Refs. 3 and 9.

In these models the total induced velocity on the rotor disk due to the wake is assumed to consist of two parts: (1) a steady inflow, λ_0, (for trim loadings) and (2) a perturbation inflow, $\delta\lambda$, (for transient loadings). Therefore, the total induced velocity normal to the rotor disk is expressed as

$$\lambda = \lambda_0 + \delta\lambda \tag{1}$$

Assuming that the perturbation inflow, $\delta\lambda$, varies azimuthally as well as linearly along the radius, the total inflow can be written as

$$\lambda = \lambda_0 + \lambda_1 + \lambda_{1c}\frac{r}{R}\cos\psi + \lambda_{1s}\frac{r}{R}\sin\psi \tag{2}$$

where the inflow variables λ_1, λ_{1c}, λ_{1s} are functions of time. These inflow variables are related to the perturbational thrust, roll and pitch moment coefficients through the following relation.

$$[L]^{-1}\begin{Bmatrix}\lambda_1\\ \lambda_{1c}\\ \lambda_{1s}\end{Bmatrix} = \begin{Bmatrix}C_T\\ -C_{My}\\ C_{Mx}\end{Bmatrix}_{P.A} \tag{3}$$

where P.A stands for perturbational aerodynamics. The elements of [L] can be obtained either theoretically, by using momentum theory[3,9] or experimentally[10].

In ground resonance type of aeromechanical problems, the inflow variable λ_1 does not couple with the body and cyclic blade degrees of freedom and hence it does not have to be considered in the analysis. Thus only the equations for the inflow variables λ_{1c} and λ_{1s} are relevant to this specific problem and these can be written as

$$[L]^{-1}\begin{Bmatrix}\lambda_{1c}\\ \lambda_{1s}\end{Bmatrix} = \begin{Bmatrix}-C_{My}\\ C_{Mx}\end{Bmatrix}_{P.A} \tag{4}$$

For axial flow through the rotor, which corresponds to the present case, the elements of [L] can be obtained by applying momentum theory[9]. The differential thrust on an elemental area dA (= rdrdψ) of the disk is related to the inflow by the equation

$$dT = \dot{m}\, 2\lambda\Omega R \tag{5}$$

It should be mentioned that by relating the total differential thrust (steady and perturbation) to the total induced velocity (steady and perturbation) in the form, given in Eq. (5), it is assumed that the thrust-inflow relation is the same for steady as well as perturbational conditions. This basic assumption implies that the variation of the forces on the rotor is sufficiently slow so that the classical actuator disk theory is valid for both steady and perturbational inflow velocities. Therefore, this inflow theory is also recognized to be a low frequency approximation to the unsteady aerodynamics of the rotor.

Following Johnson[2], the mass flow rate in Eq. (5) can be written as

$$\dot{m} = \rho\lambda_0\Omega R dA \tag{6}$$

It is important to note that the mass flow rate is defined with respect to the steady or mean value of the inflow λ_0.

The aerodynamic pitch and roll moments on the rotor disk, acting at the hub, can be obtained by taking moments of the elemental thrust about the hub center and integrating over the complete rotor disk. The pitch and roll moments are

$$M_{pitch} = \int_0^R \int_0^{2\pi} -r\cos\psi dT \tag{7}$$

$$M_{roll} = \int_0^R \int_0^{2\pi} r\sin\psi dT \tag{8}$$

Substituting Eqs. (2), (5) and (6) in Eqs. (7) and (8) and integrating, the pitch and roll moments become

$$-M_{pitch} = \frac{\pi}{2}\rho R^3\lambda_0\lambda_{1c}(\Omega R)^2 \tag{9}$$

$$M_{roll} = \frac{\pi}{2}\rho R^3\lambda_0\lambda_{1s}(\Omega R)^2 \tag{10}$$

After nondimensionalization, the relation between inflow variables and the perturbational aerodynamic moment coefficients becomes

$$\begin{bmatrix} \frac{\lambda_0}{2} & 0 \\ 0 & \frac{\lambda_0}{2} \end{bmatrix} \begin{Bmatrix} \lambda_{1c} \\ \lambda_{1s} \end{Bmatrix} = \begin{Bmatrix} -C_{My} \\ C_{Mx} \end{Bmatrix}_{P.A} \tag{11}$$

On the other hand, if the mass flow rate $\dot{m}$, is defined as (following Peters and Gaonkar[9])

$$\dot{m} = \rho\lambda\Omega R dA \tag{12}$$

where the mass flow is defined with respect to the total induced velocity λ, the inflow equations for λ_{1c} and λ_{1s} become

$$\begin{bmatrix} \lambda_0 & 0 \\ 0 & \lambda_0 \end{bmatrix} \begin{Bmatrix} \lambda_{1c} \\ \lambda_{1s} \end{Bmatrix} = \begin{Bmatrix} -C_{My} \\ C_{Mx} \end{Bmatrix}_{P.A} \tag{13}$$

Comparing Eqs. (11) and (13), it is evident that depending on the definition of mass flow rate, i.e. Eq. (6) or (12), the coefficients of the elements of $[L]^{-1}$ matrix differ by a factor of two.

Equations (11) or (13) are complete only after identifying the right hand side. This is done by obtaining expressions for the moment coefficients using blade element theory. Once these have been obtained, a relation is established between the inflow variables and rotor blade motion. It was shown in Refs. 3, 9 and 11 that incorporation of a perturbational inflow model, as represented by Eq. (11) or (13), in rotor dynamic problems yields a modification of the aerodynamic loads acting on the blade which can be represented by a reduced or effective Lock number

$$\gamma^* = C\gamma \tag{14}$$

If Eq. (11) is used in the rotor dynamic problem, the lift deficiency factor C becomes

$$C = \frac{1}{1 + \frac{\bar{\sigma}a}{8\lambda_0}} \tag{15}$$

This factor is found to be equal to the low frequency approximation of Loewy's lift deficiency function for harmonic loadings[3]. On the other hand, Eq. (13) produces a lift deficiency factor

$$C = \frac{1}{1 + \frac{\bar{\sigma}a}{16\lambda_0}} \tag{16}$$

which is higher than that given in Eq. (15).

The two perturbation inflow models, used in the present analysis, can be written in a general form as

$$\begin{bmatrix} C_1\lambda_0 & 0 \\ 0 & C_1\lambda_0 \end{bmatrix} \begin{Bmatrix} \lambda_{1c} \\ \lambda_{1s} \end{Bmatrix} = \begin{Bmatrix} -C_{My} \\ C_{Mx} \end{Bmatrix}_{P.A} \tag{17}$$

when $C_1 = 0.5$. Eq. (17) corresponds to Eq. (11) and when $C_1 = 1.0$ it corresponds to Eq. (13).

The concept of equivalent Lock number in the coupled rotor/fuselage type problems appears to involve a certain inconsistency. The fuselage equations of motion in pitch and roll contain terms due to both aerodynamic hub moments and aerodynamic hub forces. When using the perturbation inflow, one can make the observation that only the Lock number associated with the aerodynamic moment terms is modified, however the Lock number associated

with the aerodynamic force terms remains unchanged. Of course, the reason for this inconsistency lies in the formulation of the equations for the inflow variables which are related only to the hub moments, as given in Eq. (4).

Dynamic Inflow Models

The perturbation inflow model does not account for the time lag between the aerodynamic load and the time variation in inflow. The dynamic inflow models represent an extension of the perturbation inflow model by taking into account the time lag between the aerodynamic loading and the response. When using the dynamic inflow model the equations for λ_{1c} and λ_{1s} can be written as

$$\begin{bmatrix} M_1 & 0 \\ 0 & M_1 \end{bmatrix} \begin{Bmatrix} \dot{\lambda}_{1c} \\ \dot{\lambda}_{1s} \end{Bmatrix} + \begin{bmatrix} C_1\lambda_0 & 0 \\ 0 & C_1\lambda_0 \end{bmatrix} \begin{Bmatrix} \lambda_{1c} \\ \lambda_{1s} \end{Bmatrix} = \begin{Bmatrix} -C_{My} \\ C_{Mx} \end{Bmatrix} P.A \tag{18}$$

where M_1 represents the nondimensional apparent inertia associated with the inflow and the quantity C_1 is either 0.5 or 1.0, depending on the definition of mass flow rate. The value of M_1 can be obtained either theoretically or experimentally. Tuckerman[12] evaluated the apparent inertia associated with an impermeable disk subject to an angular acceleration. The nondimensional value of the apparent inertia was found[12] to be $M_1 = 0.1132$. This theoretical value is also supported by parameter identification studies[10]. In Ref. 13, it was noted that M_1 can also be influenced by the pressure distribution on the rotor and hence M_1 could be also assumed to be a function of rotor loading distribution. In Ref. 14, the identified value of M_1 is found to vary between 0.05 to 0.2. In the present analysis, the value of M_1 is assumed to be the theoretically evaluated value i.e., $M_1 = 0.1132$. The implication of using Eq. (18) in rotor dynamic problems[15], under harmonic loadings, can be shown to be equivalent to a modification of the Lock number, which can be written as

$$\gamma^* = \gamma \left[1 - \frac{1}{1 + \frac{16C_1\lambda_0}{\bar{\sigma}a} + \frac{16M_1(i\omega)}{\bar{\sigma}a}} \right] \tag{19}$$

$$= \gamma C$$

Equation (19) indicates that addition of an apparent inertia term to the perturbation inflow model introduces a phase lag between the aerodynamic loads and the response. Furthermore the value of C is now different from the previous values given in Eq. (15) and (16).

The five aerodynamic models, described briefly above, were selected for incorporation in this study. Using these theories, the sensitivity of the aeromechanical stability problem to changes in the aerodynamic assumptions was investigated. For convenience, these five aerodynamic models are concisely summarized below:

Case (a): quasi-steady aerodynamics

Case (b): perturbation inflow model with $C_1=0.5$

Case (c): dynamic inflow model with $C_1=0.5$ and $M_1=0.1132$ which corresponds to Johnson's model[2]

Case (d): perturbation inflow model with $C_1=1.0$

Case (e): dynamic inflow model with $C_1=1.0$ and $M_1=0.1132$

These aerodynamic models can also be viewed as a special case of a general dynamic inflow model. When $M_1=0$, the general inflow model becomes a perturbation inflow model and when $M_1 \to \infty$, the effects of inflow perturbations are totally eliminated and the resulting model is a quasi-steady aerodynamic model.

3. A Brief Summary of the Experiment

A clear description of the experimental set up, used for simulating the fundamental aspects of the aeromechanical stability of a hingeless rotor helicopter, was presented in Ref. 1. The rotor consisted of three blades and five different configurations were tested. The different configurations represent different blade parameters characterized by the nonrotating natural frequencies of the blade in flap and lag, pitch-lag coupling and flap-lag coupling. The rotor was designed such that most of the blade flexibility is concentrated at the root by building in root flexures. The rotor assembly was supported on a gimbal which had pitch and roll degrees of freedom. In this paper the analytical results obtained are compared with the experimental results, presented by Bousman, for rotor configurations 1 and 4, where the designation of these configurations is consistent with those in Bousman's paper[1]. A brief description of these configurations is presented for the sake of completeness, additional information can be found in Refs. 1, 2 and 7. Configuration 1 had different stiffnesses in flap and lag respectively; the corresponding nonrotating flap frequency was 3.13 Hz and that for lead-lag was 6.70 Hz. Configuration 4 was a matched stiffness case where the nonrotating flap frequency was 6.63 Hz and that for lead-lag was 6.73 Hz. The pitch-flap and pitch-lag coupling for these two configurations was zero. For cases where the pitch angle was nonzero, the experimental rotor was designed such that pitch changes were introduced outboard of the flexures and therefore the structural flap-lag coupling for these cases was zero. The blade was also designed to be very stiff in torsion.

4. Method of Solution

The degrees of freedom considered in this aeromechanical stability analysis are: the fundamental flap and lag modes of the blade and the pitch and roll degrees of freedom of the body. In this class of problems, it has been established that the collective flap and lag modes do not couple with the body motion and thus, these modes are not considered. Since the inflow variable λ_1 also has the role of a collective mode, it need not be considered. Therefore, the total number of degrees of freedom governing the aeromechanical problem are six. They are: cyclic flap (β_{1c},β_{1s}), cyclic lead-lag (ζ_{1c},ζ_{1s}), body pitch (θ) and body roll (ϕ). For the cases when the dynamic inflow models are used, two additional degrees of freedom, namely λ_{1c} and λ_{1s}, are also present in the problem.

The solution of the coupled rotor/fuselage problem follows essentially the procedure outlined in Refs. 6 and 7. The procedure for obtaining the stability boundaries of the system consists of the following steps.

1. Evaluation of the equilibrium position of the blade.
2. Linearization of the nonlinear equations of motion about the equilibrium position.
3. Transformation of the linearized equations with periodic coefficients to equations with constant coefficients by using a multiblade coordinate transformation.
4. Evaluation of the eigenvalues of the linearized system with constant coefficients to obtain the stability boundaries.

The eigenvalues appear in complex conjugate pairs, $s = \sigma \pm i\omega$. The real part of the eigenvalue represents the modal damping and the imaginary part modal frequency, respectively. The mode is stable if σ is negative and it is unstable if σ is positive.

In the present problem, the number of complex eigenvalue pairs depends on the type of aerodynamic model used in the analysis. When quasi-steady aerodynamics or the perturbation inflow models are used, there are only six pairs of complex eigenvalues, each one representing one of the six degrees of freedom, namely, β_{1c}, β_{1s}, ζ_{1c}, ζ_{1s}, θ and ϕ. The modes corresponding to the rotor degrees of freedom (β_{1c}, β_{1s}, ζ_{1c}, ζ_{1s}) are referred to either progressing or regressing mode depending on the numerical value of the rotating natural frequency. A more detailed description of this terminology can be found in Refs. 3 and 7. When the dynamic inflow model is used, the six eigenvalue pairs are augumented by one additional pair of eigenvalues corresponding to the inflow variables. Since the equations for the inflow variables λ_{1c} and λ_{1s} are given in first order state variable form, Eq. (18) the stability analysis will yield only one pair of eigenvalue corresponding to these two inflow variables. The mode corresponding to this eigenvalue pair is designated as the "inflow mode", (λ), following Johnson's[2] terminology.

5. Results and Discussion

In the present study, aimed at predicting the aeromechanical stability of a model helicopter, the behavior of the model is studied at various values of rotor speed Ω. Two rotor configurations are analyzed. Configuration 1, in which the nonrotating flap frequency is lower than the nonrotating lag frequency, and configuration 4, in which these two frequencies are almost equal, which corresponds to a matched stiffness configuration. These different configurations have an influence on the dynamic behavior of the coupled rotor/fuselage system. In a matched stiffness configuration the structural flap-lag coupling is eliminated. Furthermore the root torsional moment due to the combined flap-lag motion, which is somewhat similar to an effective flap-pitch and lag-pitch coupling, is also eliminated. It should be mentioned however that these effective flap-pitch and lag-pitch couplings are not structural couplings. It was mentioned in the previous section that the experimental model was designed so as to eliminate structural flap-lag coupling, for these configurations. Therefore, the difference between these two configurations consists of the root torsional moment due to combined flap-lag motion which is present in configuration 1 and absent in configuration 4. This root moment acts as an exciting moment for the body pitch and roll motions.

The numerical data used in the analysis is presented in the Appendix. It should be mentioned that the roll inertia used in the present calculations is slightly higher than the value (183 gm$\cdot$m^2) provided in Ref. 1. The value for roll inertia used in our calculation is 194 gm$\cdot$m^2 which is 6% higher than 183 gm$\cdot$m^2. This value of roll inertia was obtained by using the body spring stiffness in roll, provided by Bousman[16], such that the calculated nonrotating coupled roll frequency matches the measured frequency.

5.1 Results for Configuration 1

The results for Configuration 1 are presented in Figs. 1-8. The variation of various modal frequencies with Ω are shown in Figs. 1-2, together with the experimental data, taken from Ref. 1. It can be seen from Fig. 1 that the analysis with quasi-steady aerodynamics predicts the modal frequencies which are in excellent agreement with the experimental results. Figure 2 presents the calculated modal frequencies for Case (b), perturbation inflow with C_1=0.5, and Case (c) dynamic inflow model with C_1=0.5 and M_1=0.1132. With the perturbation inflow model, the predicted frequencies for roll (ϕ) and pitch (θ) are over estimated in the range Ω > 300 R.P.M.. On the otherhand, by incorporating a time delay in the inflow model, Case (c), the calculated pitch and roll frequencies are in good agreement with the measured values. However, the predicted pitch frequency is still slightly higher in the range Ω > 300 R.P.M. A similar trend was also observed in the results for Case (d), perturbation inflow model, with C_1=1.0, and Case (e) dynamic inflow model with C_1=1.0 and M_1=0.1132.

It was mentioned earlier that the analysis with dynamic inflow model produces an additional eigenvalue corresponding to the inflow mode (λ). For Case (c), there are two eigenvalues with frequencies below 0.6 Hz in the range Ω > 200 R.P.M. as evident from Fig. 2. The frequency corresponding to one mode remains almost constant ($\simeq$0.5 Hz), while the other decreases to zero and then increases. It is difficult to identify which one of these two corresponds to the flap regressing mode (β_R) and which one should be associated with the inflow mode (λ). The mode with the constant frequency, in Fig. 2, is identified as inflow mode (λ) and the other mode is identified as flap regressing mode (β_R). Johnson[2] also identified the mode with a constant frequency as inflow mode (λ) and the second mode as flap regressing mode (β_R). Some additional comments on this identification procedure will be made later.

Figure 3 presents the variation of damping in flap regressing mode (β_R) and inflow mode (λ) with Ω. It is evident from Fig. 3 that the damping in the flap regressing mode increases rapidly with Ω for the analysis with quasi-steady aerodynamics. The introduction of the perturbation inflow model with C_1=0.5, Case (b), drastically reduces the damping in β_R mode. This reduction in damping is caused by reduced aerodynamic damping with perturbation inflow. For this case the relevant quantities are: solidity ratio $\bar{\sigma}$ = 0.0494; lift curve slope a = 5.73 and steady inflow λ_0=0.014.

Therefore the deficiency function C, based on Eq. (15), is C=C.284. Hence, the effective Lock number $\gamma^*=0.284\gamma$. This shows that perturbation inflow reduces the magnitude of aerodynamic forces by approximately 72%. In the case of dynamic inflow with $C_1=0.5$ and $M_1=0.1132$, Case (c), the damping in the mode which is identified as the inflow mode (λ) remains relatively low, but the damping in flap regressing mode (β_R) increases with Ω. These results indicate that the damping in flap regressing mode reverts to the value obtained in the analysis with quasi-steady aerodynamics, as a consequence of the time delay present in dynamic inflow model. This seems to contradict the earlier results published in Refs. 9, 10 and 17. It was mentioned in Ref. 17 that flap regressing mode damping is substantially decreased by dynamic inflow for small values of collective pitch setting of the blade. Furthermore, it was found in Ref. 10 that dynamic inflow reduces the damping in flap regressing mode. This raises a question whether the inflow mode identified in Fig. 2, and also identified as such by Johnson[2], is a flap regressing mode and the mode identified as the flap regressing mode is really an inflow mode. To ascertain the reliability of this identification procedure, the eigenvectors corresponding to these modes were also analyzed. Table I shows the eigenvectors corresponding to the mode identified as the flap regressing (β_R) and the inflow mode (λ) at Ω = 900 R.P.M. It can be seen that in the flap regressing mode, the flap motion has a higher participation factor than the inflow variables. In the inflow mode, the flap and inflow variables have almost equal participation factor. Also in this (λ) mode, the pitch and roll motions have substantial participation factors. However, from these results, one can conclude that the flap regressing mode and inflow mode are highly coupled modes.

Figures 4 and 5 illustrate the variations of damping in pitch as a function of Ω. Using quasi-steady aerodynamics, a higher damping, in the range $200 < \Omega < 800$ R.P.M. is predicted as evident from Fig. 4. However when dynamic inflow, Case (c), with $C_1=0.5$ and $M_1=0.1132$ is used the damping is predicted very well in the range $200 < \Omega < 800$ R.P.M., however the damping is somewhat under predicted beyond Ω = 800 R.P.M. Figure 5 shows that using the dynamic inflow model, Case (e) with $C_1=1.0$ and $M_1=0.1132$, the damping predictions are in very good agreement with the experimental results over the complete range of Ω. When the value of C_1 is increased from 0.5 to 1.0, in the dynamic inflow models, one finds that the corresponding damping in pitch increases by 10% ~ 25% for $\Omega > 400$ R.P.M. It is also evident from Figs. 4-5 that perturbation inflow models do not seem to predict the correct damping levels.

The variation of damping in roll mode is shown in Figs. 6-7. When using quasi-steady aerodynamics, the damping, in the range of $\Omega > 500$ R.P.M., is over predicted as evident from Fig. 6. Using the perturbation inflow model, with $C_1=0.5$, Case (b), the damping in the range of $\Omega < 600$ R.P.M. is under estimated, beyond this range of Ω, the predictions are good. The damping levels predicted using the dynamic inflow model, with $C_1=0.5$ and $M_1=0.1132$, Case (c), are in good agreement with experimental data over the whole range of Ω, as shown in Fig. 6. It can be seen from Fig. 7 that calculations with the perturbation inflow model, with $C_1=1.0$, Case (d), yield damping levels which are too low in the range $\Omega < 500$ R.P.M. and too high for the range $\Omega > 600$ R.P.M. Calculations with the dynamic inflow model, with $C_1=1.0$ and $M_1=0.1132$, Case (e), also overpredict the damping in the range $\Omega > 700$ R.P.M. It should be mentioned, that in the range $\Omega > 700$ R.P.M., when using dynamic inflow models, the percentage increase in roll damping as a result of increasing C_1 from 0.5 to 1.0 is 5% to 12%.

Based on the results obtained for the damping in the pitch and roll modes, it appears that the theoretical results are quite sensitive to the value selected for C_1. It is also evident that introduction of a time delay in the inflow model seems to be an important factor. Based on the overall agreement with the experimental data, it appears that the dynamic inflow model with $C_1=0.5$ and $M_1=0.1132$, Case (c), seems to be somewhat superior to the dynamic inflow model with $C_1=1.0$ and $M_1=0.1132$, Case (e).

Figure 8 presents the variation of regressing lag mode damping with Ω. The predicted damping levels are in good agreement with the experimental results in the range $\Omega < 700$ R.P.M. and $\Omega > 900$ R.P.M. for all the aerodynamic models used. For the cases analyzed with perturbation inflow models, Case (b) with $C_1=0.5$ and Case (d) with $C_1=1.0$, the value of Ω at which the resonant peak occurs is shifted from 760 R.P.M. to 800 R.P.M. This shift is associated with the fact that when using both models the roll frequency predicted is higher than the experimental result and as a consequence, the resonance is also shifted to a higher value of Ω. Calculations with quasi-steady aerodynamics predict correctly the value of Ω at which resonance occurs, however the stability of this mode is overpredicted. In the analyzes with dynamic inflow models, the predicted damping levels are in excellent agreement with the experimental results, including the damping at resonance. The level of agreement with experimental data found in this case is somewhat better than those shown in Refs. 1 and 2. This result seems to support the statement made in Ref. 7, that the coupled rotor/fuselage model derived in Ref. 5 is a reasonably accurate model for the configuration tested in Ref. 1.

5.2 Results for Configuration 4

The results for Configuration 4 are presented in Figs. 9-16. Figures 9 and 10 show the variation of modal frequencies as a function of Ω. It can be seen from Fig. 9 that all the frequencies except the one corresponding to 0.7 Hz are predicted well by the quasi-steady aerodynamic model. In the range $250 < \Omega < 350$ R.P.M., the pitch, roll and flap regressing modes undergo a change in their characteristics. The flap regressing mode (β_R) becomes a roll mode (ϕ) and roll mode (ϕ) becomes a pitch mode (θ) and the pitch mode (θ) becomes a flap regressing mode (β_R). In this range of Ω, the predicted roll frequencies are higher than the measured values. Quasi-steady aerodynamics is incapable of predicting a frequency close to 0.7 Hz in the range $300 < \Omega < 1000$ R.P.M. Figure 10 illustrates the results for the cases where the perturbation inflow model, Case (b) with $C_1=0.5$ and dynamic inflow model, Case (c), with $C_1=0.5$ and $M_1=0.1132$, were used. Although calculations based on the perturbation inflow model are capable of predicting a frequency close to the experimentally measured frequency of 0.7 Hz, the pitch and roll modes frequencies are overpredicted. With dynamic inflow

model, all the frequencies are predicted well. However, in the range $250 < \Omega < 350$ R.P.M., the roll mode frequency is still overpredicted. In this range of Ω, none of the aerodynamic models used in the present study, is capable of correctly predicting the roll frequency. Johnson[18] attributed this discrepancy to either the deficiency of the aerodynamic model or the presence of some higher mode of the rotor or body. In any case, this problem remains unresolved. In the range $\Omega > 400$ R.P.M., the mode with a frequency close to 0.7 Hz is identified as inflow mode (λ) and the other mode with a frequency which is lower than 0.7 Hz is identified as flap regressing mode (β_R). This identification is based on the analysis of the eigenvectors corresponding to these two modes. Table II shows the eigenvectors of the identified inflow mode and flap regressing mode, for $\Omega = 900$ R.P.M. In this case, as in Configuration 1, these two modes are highly coupled. However, in the β_R mode, the flap motion has a higher participation factor than the participation of the inflow variables. In the λ mode, the body pitch has the highest participation factor, with the flap, body roll and inflow having almost equal participation factors. As a result of this identification procedure one finds that using the dynamic inflow model the damping for the flap regressing mode is predicted to have a value comparable to that obtained when using quasi-steady aerodynamics. This seems to contradict some results which have been published earlier in Refs. 9, 10 and 17 where it was found that using dynamic inflow yields a substantial reduction in regressing flap mode damping.

The variation of roll damping as a function of Ω is illustrated in Figs. 11-12. Calculations based on quasi-steady aerodynamics overpredict the damping in the range $\Omega > 300$ R.PM., as evident in Fig. 11. Calculations based on the perturbation inflow model, with $C_1=0.5$, under predicts the damping in the range $\Omega < 800$ R.P.M. The damping levels predicted by using the dynamic inflow model, with $C_1=0.5$ and $M_1=0.1132$, are in reasonable agreement with the experimental values. From Fig. 12, it is evident that using the perturbation inflow model with $C_1=1.0$, yields a damping prediction which is too high for $\Omega > 700$ R.P.M. Using the dynamic inflow model, with $C_1=1.0$ and $M_1=0.1132$, yields damping level predictions which are in reasonable agreement with the experimental results.

The variation of damping for the pitch mode (θ) and the mode which has been identified as the inflow mode (λ) are presented in Figs. 13 and 14. It is evident from Fig. 13 that predictions based on quasi-steady aerodynamics yield higher values of damping than the measured values. Calculations based on dynamic inflow, with $C_1=0.5$ and $M_1=0.1132$, predict the pitch damping well, but the damping associated with the inflow mode (λ) is lower than the experimental values. Figure 14 shows that using the dynamic inflow model, with $C_1=1.0$ and $M_1=0.1132$, yields a higher value of pitch damping than measured in the test. The damping in inflow mode is also higher than the experimental values. From the results shown in Figs. 13 and 14, it is evident that an increase in the value of C_1 from 0.5 to 1.0 increases the pitch mode damping by about 25%. Therefore, it can be concluded that for Configuration 4, as well as Configuration 1, the predicted damping levels in pitch and roll modes are quite sensitive to the dynamic inflow model used in the analysis. By using a different combination of the values of C_1 and M_1, better correlation with the experimental results could have been achieved. However, among the aerodynamic models employed in the present study, the dynamic inflow with $C_1=0.5$ and $M_1=0.1132$, Case (c), yields better agreement with the experimental results than the other aerodynamic models.

The variation of lag regressing mode damping with Ω is shown in Fig. 15. The resonant frequency obtained with the perturbation inflow models exhibits a shift to a higher value of Ω than the one observed in the experiment. Calculations based quasi-steady aerodynamics predict the damping levels and the resonant frequency very well, the mode is more stable at resonance, than the stability indicated in the test. Calculations with the dynamic inflow models yield results which are in excellent agreement with the experimental data.

Figure 16 shows the variation of regressing lag mode damping as a function of collective pitch setting of the blade, at $\Omega = 1000$ R.P.M. Calculations with the dynamic inflow model, using $C_1=0.5$ and $M_1=0.1132$, yields damping values which are in very good agreement with the measured values.

6. Conclusions

The aeromechanical stability of a helicopter in ground resonance is analyzed, using five different aerodynamic models and the analytical results are compared with the experimental results. Based on the comparison, the following conclusions can be drawn:

(1) For the aeromechanical stability problem studied here, the perturbation inflow models do not predict correctly the modal frequencies and damping.

(2) Quasi-steady aerodynamics predicts the modal frequencies very well for Configuration 1, but is incapable of predicting a frequency of 0.7 Hz measured in the experiment, for Configuration 4. The damping in body roll and pitch modes are over predicted. The regressing lag mode damping is predicted well.

(3) The dynamic inflow models predict the modal frequencies and damping values which are in very good agreement with the experimental results. This implies that for the present problem the time lag is an important ingredient in the dynamic inflow model.

(4) The predicted damping levels for the lag regressing mode, using dynamic inflow models, are in excellent agreement with the experimental results including the value at resonance. This indicates that the mathematical model for the coupled rotor/fuselage system is accurate.

(5) From the cases studied with dynamic inflow models, it is evident that the predicted damping levels for the body modes, increase when C_1 is increased from 0.5, Case (c), to 1.0, Case (e). For both rotor configurations, the pitch damping increases by 10% to 25% and the roll damping increases by 5% to 12%.

(6) Based on the comparison of results obtained with various aerodynamic models, it seems that the

dynamic inflow model with C_1=0.5 and M_1=0.1132 is the most suitable aerodynamic model, for the specific aeromechanical problem studied in this paper.

(7) Identification of the flap regressing mode and the inflow mode proved itself to be quite complicated. These modes were identified by using the frequency information together with a careful examination of the eigenvectors. The results based on this identification procedure seem to indicate that when using the dynamic inflow model the predicted values of damping for the regressing flap mode are comparable to those obtained with quasi-steady aerodynamics.

References

1. Bousman, W.G., "An Experimental Investigation of the Effects of Aeroelastic Couplings on Aeromechanical Stability of a Hingeless Rotor Helicopter", Journal of the American Helicopter Society, Vol. 26, No. 1, Jan. 1981, pp. 46-54.

2. Johnson, W., "Influence of Unsteady Aerodynamics on Hingeless Rotor Ground Resonance", Journal of Aircraft, Vol. 19, No. 8, Aug. 1982, pp. 668-673.

3. Johnson, W., Helicopter Theory, Princeton University Press, Princeton, New Jersey, 1980.

4. Johnson, W., "A Comprehensive Analytical Model of Rotorcraft Aerodynamics and Dynamics", NASA TM 81182, June 1980.

5. Venkatesan, C. and Friedmann, P.P., "Aeroelastic Effects in Multirotor Vehicles with Application to a Hybrid Heavy Lift System, Part I: Formulation of Equations of Motion", NASA CR 3288, August 1984.

6. Venkatesan, C. and Friedmann, P.P., "Aeroelastic Effects in Multirotor Vehicles, Part II: Method of Solution and Results Illustrating Coupled Rotor/Body Aeromechanical Stability", NASA CR Report, Submitted for publication.

7. Friedmann, P.P., and Venkatesan, C., "Comparison of Experimental Coupled Helicopter Rotor/Body Stability Results with a Simple Analytical Model", Paper Presented at the Integrated Technology Rotor (ITR) Methodology Workshop, NASA Ames Research Center, Moffett Field, California, June 20-21, 1983, to be published in the Journal of Aircraft, November 1984.

8. Greenberg, J.M., "Airfoil in Sinusoidal Motion in a Pulsating Flow", NACA TN 1326, 1947.

9. Peters, D.A. and Gaonkar, G.H., "Theoretical Flap-Lag Damping with Various Dynamic Inflow Models", Journal of the American Helicopter Society, Vol. 25, No. 3, July 1980, pp. 29-36.

10. Banerjee, D., Crews, S.T., Hohenemser, K.H., and Yin, S.K., "Identification of State Variables and Dynamic Inflow from Rotor Model Dynamic Tests", Journal of the American Helicopter Society, Vol. 22, No. 2, April 1977, pp. 28-36.

11. Curtiss, H.C., Jr. and Shupe, N.K., "A Stability and Control Theory for Hingeless Rotors", Annual National Forum of the American Helicopter Society, Washington, D.C., May 1971.

12. Tuckerman, L.B., "Inertia Factor of Ellipsoids for Use in Airship Design", NACA Report No. 210, 1925.

13. Pitt, D.M. and Peters, D.A., "Theoretical Prediction of Dynamic Inflow Derivatives", Vertica, Vol. 5, No. 1, 1981, pp. 21-34.

14. Banerjee, D., Crews, S.T. and Hohenemser, K.H., "Parameter Identification Applied to Analytic Hingeless Rotor Modelling", Journal of the American Helicopter Society, Vol. 24, No. 1, Jan. 1979, pp. 26-32.

15. Peters, D.A., "Hingeless Rotor Frequency Response with Dynamic Inflow", NASA SP-352, Vol. 1, 1974.

16. Bousman, W., Private Communication, Oct. 1983.

17. Ormiston, R.A., "Application of Simplified Inflow Models to Rotorcraft Dynamic Analysis", Journal of the American Helicopter Society, Vol. 21, No. 2, July 1976, pp. 34-37.

18. Johnson, W., "The Influence of Unsteady Aerodynamics on Hingeless Rotor Ground Resonance", NASA TM 81302, July 1981.

Appendix

Rotor Geometry

Number of blades	3
Radius, cm	81.1
Chord, cm	4.19
Hinge offset, cm	8.51
Blade Airfoil	NACA 23012
Profile drag coefficient	0.0079
Lock number	7.37
Solidity ratio	0.0494
Lift curve slope	5.73
Height of rotor hub above gimbal, cm	24.1

Blade Mass Properties

Blade mass (to flap flexures), gm	209
Blade mass centroid (Ref. flexure centerline), cm	18.6
Blade flap inertia (Ref. flexure centerline), $gm \cdot m^2$	17.3

Blade Frequency and Damping

	Conf. 1	Conf. 4
Nonrotating Flap frequency, Hz	3.13	6.63
Nonrotating Lag frequency, Hz	6.70	6.73
Damping in lead-lag (% critical)	0.52%	0.53%

Body Mass Properties

Rotary inertia in pitch, $gm \cdot m^2$	633
Rotary inertia in roll, $gm \cdot m^2$	194

Body Stiffness and Damping

Pitch stiffness, $gm \cdot cm^2/sec^2 \cdot rad$	0.8687×10^9
Roll stiffness, $gm \cdot cm^2/sec^2 \cdot rad$	0.1113×10^{10}
Damping in roll (% critical)	0.929%
Damping in pitch (% critical)	3.20%
Pitch frequency, Hz	1.86
Roll frequency, Hz	3.81

Table I. Eigenvectors of Flap Regressing (β_R) and Inflow (λ) modes at Ω = 900 R.P.M. for Configuration 1

Degree of freedom	Flap Regressing mode β_R	Inflow mode λ
β_{1C}	1.000	.989
β_{1S}	.593	1.000
ζ_{1C}	.012	.020
ζ_{1S}	.030	.020
ϕ	.072	.563
θ	.034	.718
λ_{1C}	.475	.779
λ_{1S}	.377	.765

Table II. Eigenvectors of Flap Regressing (β_R) and Inflow (λ) modes at Ω = 900 R.P.M for Configuration 4

Degree of freedom	Flap Regressing mode β_R	Inflow mode λ
β_{1C}	.584	.763
β_{1S}	1.000	.785
ζ_{1C}	.033	.013
ζ_{1S}	.023	.013
ϕ	.166	.745
θ	.050	1.000
λ_{1C}	.426	.619
λ_{1S}	.545	.592

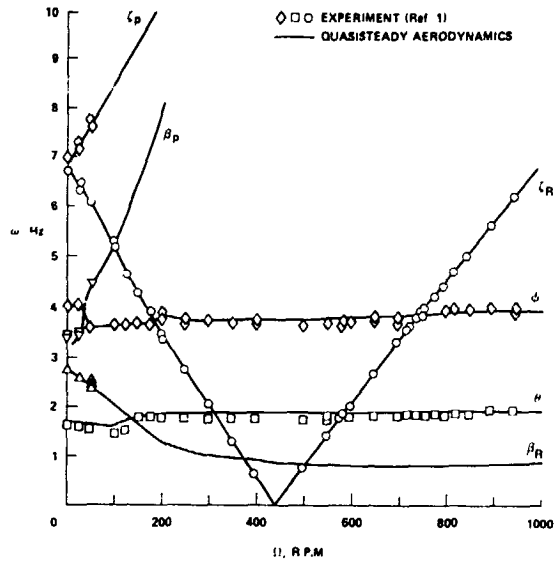

Fig. 1 Modal Frequencies as a Function of Ω; θ_c=0; Configuration 1

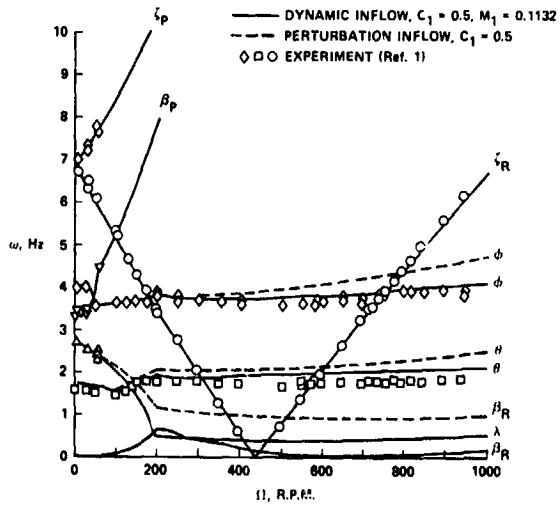

Fig. 2 Modal Frequencies as a Function of Ω; θ_c=0; Configuration 1

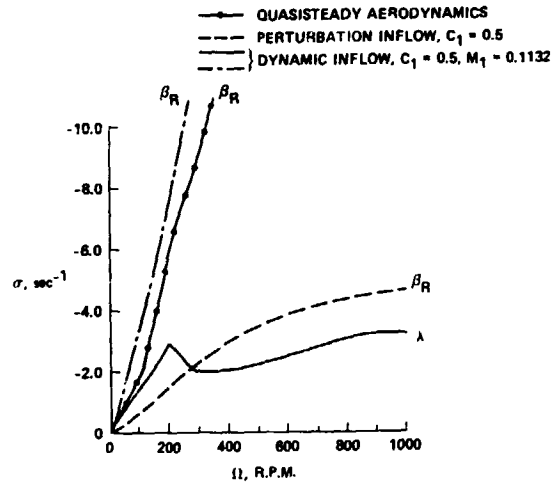

Fig. 3 Variation of Damping in Regressing Flap Mode and Inflow Mode with Ω; θ_c=0; Configuration 1

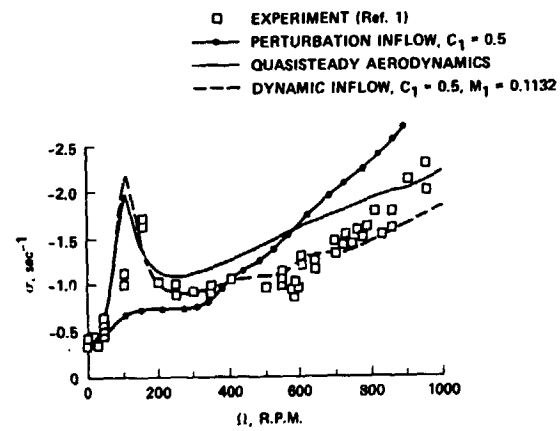

Fig. 4 Body Pitch Mode Damping as a Function of Ω; θ_c=0; Configuration 1

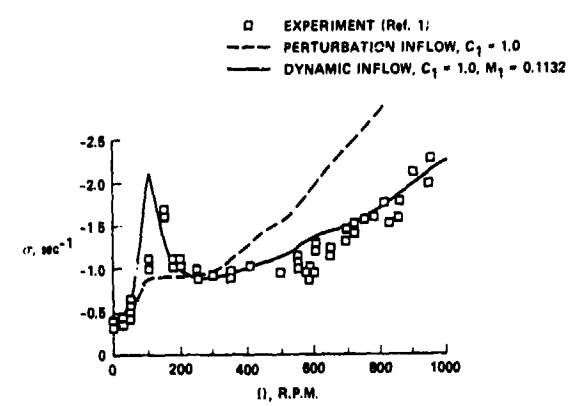

Fig. 5 Body Pitch Mode Damping as a Function of Ω; θ_c=0; Configuration 1

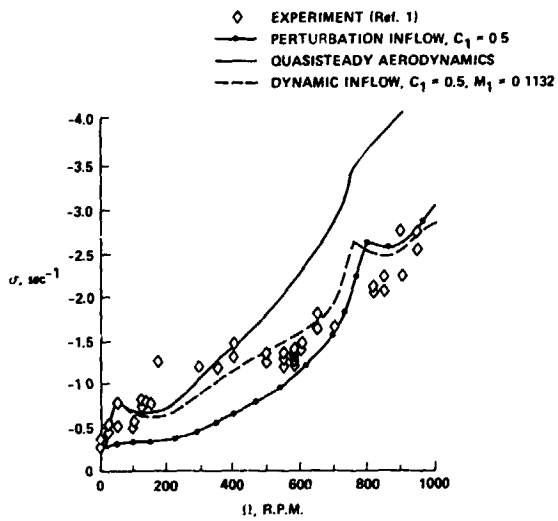

Fig. 6 Body Roll Mode Damping as a Function of Ω; θ_c=0; Configuration 1

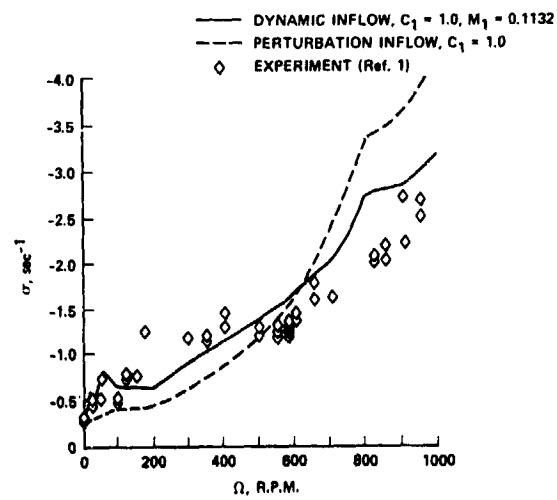

Fig. 7 Body Roll Mode Damping as a Function of Ω; θ_c=0; Configuration 1

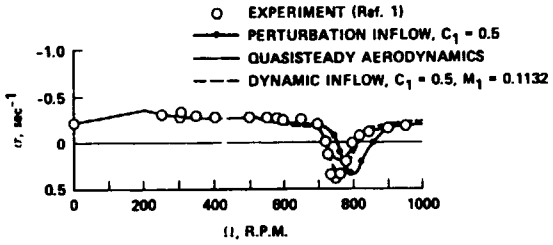

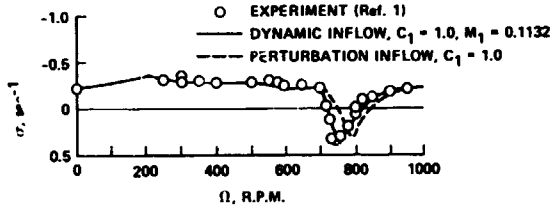

Fig. 8 Regressing Lag Mode Damping as a Function of Ω; θ_c=0; Configuration 1

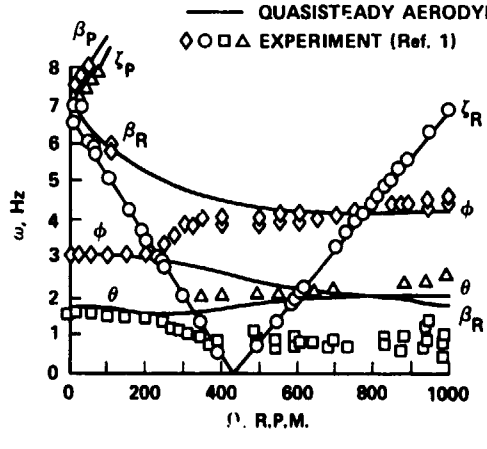

Fig. 9 Variation of Modal Frequencies with Ω; θ_c=0; Configuration 4

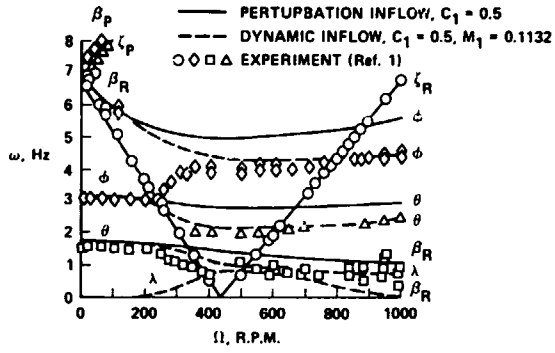

Fig. 10 Variation of Modal Frequencies with Ω; θ_c=0; Configuration 4

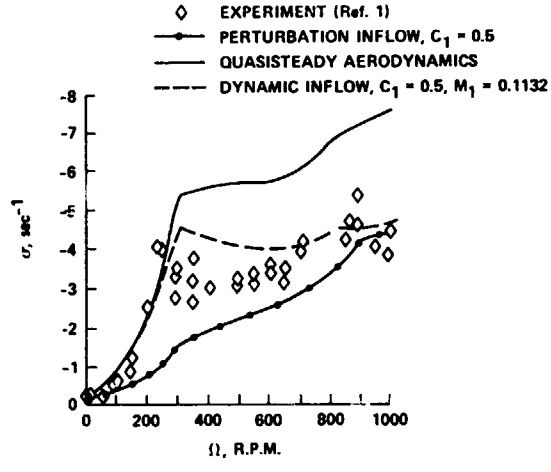

Fig. 11 Variation of Roll Mode Damping with Ω; θ_c=0; Configuration 4

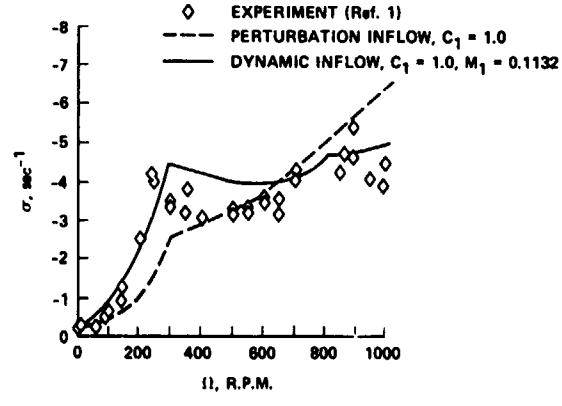

Fig. 12 Variation of Roll Mode Damping with Ω; θ_c=0; Configuration 4

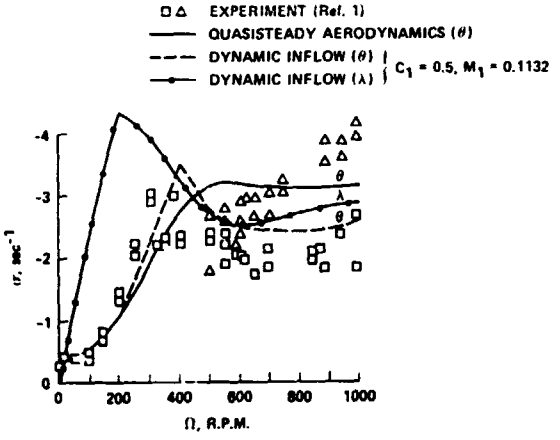

Fig. 13 Variation of Pitch (θ) and Inflow (λ) Modes Damping with Ω; θ_c=0; Configuration 4

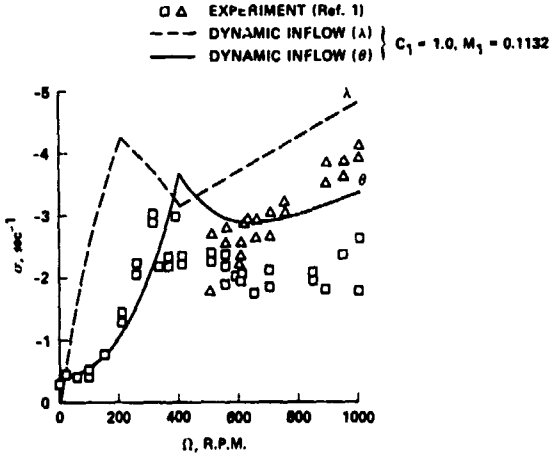

Fig. 14 Variation of Pitch (θ) and Inflow (λ) Modes Damping with Ω; θ_c=0; Configuration 4

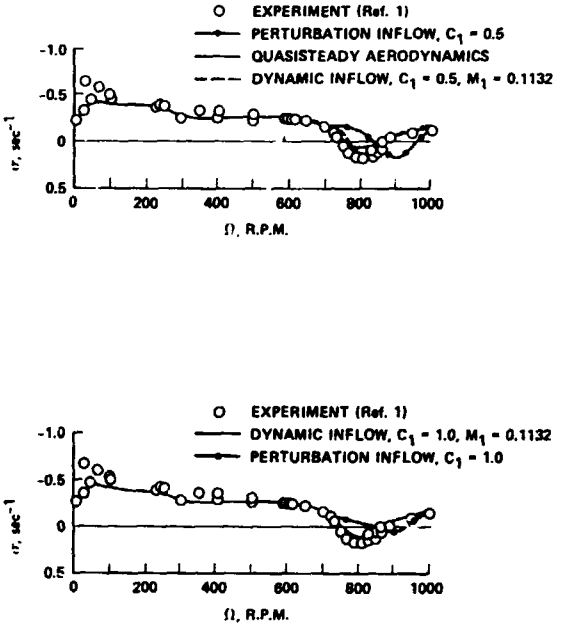

Fig. 15 Regressing Lag Mode Damping as a Function of Ω; θ_c=0; Configuration 4

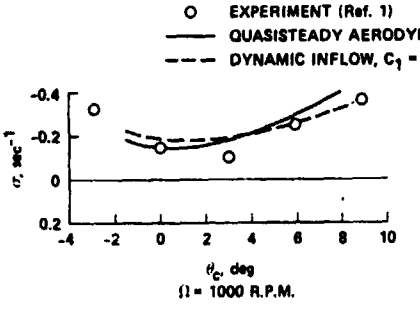

Fig. 16 Regressing Lag Mode Damping as a Function of θ_c; Configuration 4

DISCUSSION
Paper No. 14

INFLUENCE OF VARIOUS UNSTEADY AERODYNAMIC MODELS ON THE AEROMECHANICAL STABILITY OF A HELICOPTER IN GROUND RESONANCE
P. P. Friedmann
and
C. Venkatesan

Bill Bousman, U.S. Army Aeromechanics Laboratory: Jack Landgrebe put a perspective on dynamic inflow as not really contributing to the loads problem and I think that the conclusions from the first two papers show that although it has a strong effect on the flapping degree of freedom, from the designer's point of view, it is not really important for the lag degree of freedom. I guess my question is to all three of these guys. Are there applications for dynamic inflow in something like the handling qualities area where simulation needs the speed of the model and has any work been done in here or are there paths that we should be going?

Friedmann: I'll tell you I was expecting this question so I have a slide. "Can I have the slide, please?" The last slide [Fig. 3] is something which in your experiment you might have data, but it wasn't in your paper so I don't know whether you have data or not. It shows the flap regressing mode damping with various kinds of aerodynamics. What it really shows you is that the damping with quasisteady aerodynamics is here. If you put in the perturbation inflow it knocks down this damping in the flap mode very significantly. And when you put in the dynamic inflow with C_1 of 0.5 it brings it up again to almost where the damping was with the quasisteady aerodynamics. You can also see how the damping of inflow mode changes as a function of Ω. So in relation to the first question which you have asked I think that the better test for how much global truth is in dynamic inflow should really be based on the behavior of the flapping mode as has been indicated by both Dave Peters and [Gopal] Gaonkar. Maybe in the future some calculations associated with that type of examination could be revealing.

Dave Peters, Washington University: On the question about handling qualities, I think it definitely has an effect. There was one figure in the paper we didn't show which shows the pitch and roll moment on the rotor due to a roll oscillation or a pitch oscillation. As you go to an ω of zero the slope of that curve then is the roll rate or pitch rate moment as a function of θ_s or θ_c, like a control derivative. There's more than a factor of two difference with or without dynamic inflow; almost a factor of three in one case. I think if you are going to do handling qualities, anything in the less than once per frequency range then the dynamic inflow is going to have importance. That's a great paper, Peretz. I think we should have an altar call and everyone who wants to put dynamic inflow in their analysis should come forward or something after a paper like that because it's really good. One question I had--on a model like yours, how much extra complexity does it take to put the dynamic inflow in? Is it 2% or 10%? Maybe you can give us a feeling for that.

Friedmann: It may be 10% additional work. It's not really very difficult to do. Particularly if you have somebody as good as Venkatesan who does it.

Bob Loewy, Rensselaer Polytechnic Institute: My question pertains to the off-diagonal terms in the L matrix and really takes up a little bit on Euan Hooper's earlier question on the earlier paper. And that is it seems to me that swirl would make those kind of terms nonzero and that particularly in tilt rotors and high speed forward flight you would expect more swirl than we are used to. I wonder if you have thought about these things?

Friedmann: I have to phrase this very carefully. I am essentially somebody who uses dynamic inflow. I am not a person who has ambitions of improving dynamic inflow. I am a believer in unsteady aerodynamics and as a consequence you might be aware a year ago one of my students completed an arbitrary motion type of unsteady airfoil theory in which you can essentially do the same things you do with dynamic inflow, but for hover and forward flight. It is based on essentially an assumed wake. [It has] all the mathematical complexities and maybe mathematical fundamentals which an unsteady aerodynamics theory provides you and you don't have to use the assumptions which are embedded in dynamic inflow and cannot be removed. We have used this particular arbitrary motion theory to essentially extend the so-called Loewy lift deficiency function, which you might be familiar with, to arbitrary motions. In that AIAA paper which was given last year we have not been very successful. But since then Dr. Venkatesan has managed to do an arbitrary motion approximation to the theory and that theory can probably be used to capture the same behavior which is predicted by the dynamic inflow model and you might be able to see whether based on such a theory you do get off-diagonal terms or not.

THE INFLUENCE OF DYNAMIC INFLOW AND TORSIONAL FLEXIBILITY ON ROTOR DAMPING IN FORWARD FLIGHT FROM SYMBOLICALLY GENERATED EQUATIONS

T. S. R. Reddy
National Research Council Research Associate

and

William Warmbrodt
Aerospace Engineer

NASA Ames Research Center
Moffett Field, California

Abstract

The combined effects of blade torsion and dynamic inflow on the aeroelastic stability of an elastic rotor blade in forward flight are studied. The governing sets of equations of motion (fully nonlinear, linearized, and multiblade equations) used in this study are derived symbolically using a program written in FORTRAN. Stability results are presented for different structural models with and without dynamic inflow. The study shows that symbolic and numerical programs written in FORTRAN can be conveniently used in a complicated helicopter-rotor aeroelastic modeling and analytical process. It is observed that for a large number of degrees of freedom and for fully nonlinear models, the amount of data needed for the symbolic program increases exponentially, making it inconvenient to consider the multiblade equations explicitly. However, a combination of symbolic and numerical programs at the proper stage in the derivation process makes the obtainment of final stability results an efficient and straightforward procedure. The symbolically generated equations are subsequently used to investigate the influence of elastic torsion modes and dynamic inflow on isolated rotor inplane stability in forward flight. Results are presented for both single-rotor-blade models and multiblade rotor systems. For both soft inplane and stiff inplane hingeless rotors, the elastic torsion mode significantly affects the predicted inplane damping. Dynamic inflow does change the magnitude of the predicted damping, but the influence on damping trends is generally small with varying advance ratio or elastic coupling parameter.

Notation

a = lift-curve slope, 2π/rad

b = number of blades

c = chord, m

C_{d_o} = profile drag coefficient

C_{mx}, C_{my} = rotor steady pitch and roll moments, Eq. (11)

$\bar{C}_T, C_H, C_W$ = rotor steady thrust, drag force, and weight coefficient, Eq. (11)

C_T, C_M, C_L = harmonic perturbation coefficients of thrust, pitching moment, and rolling moment, Eq. (3)

D = partial derivative matrix, Eq. (14)

$\bar{f}$ = flat-plate area

F = forcing function, Eq. (6)

J = number of points used in harmonic analysis, Eq. (5)

K_A = blade cross-section polar radius of gyration, m

K_m = blade cross-section mass radius of gyration, m

K_{m_1}, K_{m_2} = principal mass radii of gyration, m

L = number of harmonics used in the harmonic analysis, Eq. (10)

$[m], [\ell]$ = dynamic inflow matrices

$[M], [C], [K]$ = constant mass, damping, and stiffness matrices, Eq. (6)

n = number of the harmonics in harmonic analysis, Eq. (9)

N = total number of blade modes used

q = perturbation degrees of freedom, Eq. (15)

q_o, q_c, q_s = vectors of collective and cyclic modes, respectively

R = rotor radius, m

Presented at the Second Decennial Specialists' Meeting on Rotorcraft Dynamics, Ames Research Center, Moffett Field, California, November 7-9, 1984.

u = dynamic inflow quantities, Eq. (19)

U_T, U_P = tangential and perpendicular velocity components, m/sec

v_i = induced velocity

w, v, ϕ = flap, lag, and torsion deflections

$\bar{w}, \bar{v}, \bar{\phi}$ = steady flap, lag, and torsion deflections, Eq. (2)

x = blade coordinate along the radius

z = first-order variable degrees of freedom, Eq. (15)

α = rotor-shaft plane angle of attack, Eq. (11)

α_R = wake skew angle, Eq. (4)

β_{pc} = precone angle, rad

γ = Lock number

$\Delta w, \Delta v, \Delta\phi$ = perturbation flap, lag, and torsion deflections, Eq. (2)

ζ_K, ω_K = real and imaginary parts of the characteristic exponent

$\eta_i, \zeta_i, \theta_i$ = mode shapes for flap, lag, and torsion

θ = pitch angle, rad

λ_K = characteristic exponent

$\bar{\lambda}$ = steady inflow (free stream plus induced flow)

μ = advance ratio

ν = inflow parameter, Eq. (5)

ν_o, ν_c, ν_s = uniform, longitudinal, and lateral inflow components

σ = solidity ratio = $bc/\pi R$

ψ = azimuth angle, nondimensional time

$\omega_w, \omega_v, \omega_\phi$ = nondimensional rotating flap, lag, and torsional frequencies

Ω = blade rotational speed, rad/sec

$(\bar{\ })$ = nondimensionalized quantity, equilibrium deflection

$(\dot{\ })$ = time derivative

Introduction

Hingeless rotor blades are less complex mechanically and provide more rotor control power and damping than articulated rotor blades. However, the complex aeroelastic behavior of hingeless rotors requires a rigorous analysis for an effective design procedure. The modeling requirements of hingeless-rotor-blade aeroelasticity have been studied for many years and are briefly reviewed here.

Initial analyses focused on the investigation of flap-lag stability of torsionally rigid blades with spring-restrained hinges at the hub to simulate bending flexibility. The stability of this type of model was analyzed for both hover[1] and forward flight.[2] Flap-lag stability of elastic blades with uniform properties was studied by Ormiston and Hodges,[1] based on a derivation of nonlinear partial differential equations suitable for elastic hingeless blades. Similar equations were studied by Friedmann and Tong.[3] Efforts were also made to investigate the complete blade problem by including blade torsional deflections. Friedmann and Tong[3] approximated the torsional deflection by rigid-body pitching motion (root torsion); they found that torsion motion was important and that the stability characteristics were sensitive to the number and type of assumed bending-mode shapes used. Flap-lag structural coupling was not included. Hodges and Ormiston[4] presented extensive numerical results for the stability characteristics of elastic hingeless blades with flap-lag-torsion motion in hover. They found that torsional deflections of hingeless rotor blades are strongly influenced by the nonlinear structural moments caused by flap and lead-lag bending. This bending-torsion structural coupling is proportional to the product of the flap and lead-lag bending curvatures and to the difference between the two bending flexibilities. This study also showed the effect of precone, structural coupling, and torsional rigidity on the isolated blade stability boundaries.

Friedmann and Kottapalli[5] analyzed the coupled flap-lag-torsional dynamics of hingeless rotor blades in forward flight. They noted that nonlinearities are important in an aeroelastic stability analysis and that forward flight is strongly coupled with the trim state. However, only flapping motion was used in calculating the rotor trim condition. It was observed that forward flight (increasing advance ratio) is stabilizing for soft inplane rotors and destabilizing for stiff inplane rotors. In all these studies, the aerodynamic forces were obtained from strip

theory based on a quasi-static approximation of two-dimensional, unsteady airfoil theory.

Simultaneous efforts have been made to improve the aerodynamic model used in these analyses by including unsteady airflow effects. One approach is to model the induced velocity as a time-dependent, three-degree-of-freedom system. This dynamic inflow theory has been applied to rigid-blade flap-lag analyses, both in hover and forward flight,[6-8] and to the coupled rotor-fuselage problem in hover.[9,10] It was observed that the dynamic inflow increased the lag regressing-mode damping and reduced the body pitch and roll damping for the parameters considered. These analytical results correlated well with experimental results.[10] However, the conclusions presented in Refs. 6-10 were based on several restrictive assumptions; for example, zero elastic coupling, fixed solidity ratio, and rigid flap-lag rotor-blade models with no torsional flexibility. The effects of dynamic inflow and torsion flexibility on the aeroelastic stability of an elastic rotor blade in hover to a number of parameters was recently presented.[11] It was shown that for torsionally flexible blades, the dynamic inflow effects depend on the elastic coupling parameter. For certain values of elastic coupling, the dynamic inflow effect may in fact be negligible.

In summary, general nonlinear differential equations for the elastic rotor blades (used in the above analyses) have been developed by several researchers.[12-14] These models have elastic flap, lead-lag, and torsion degrees of freedom, with nonlinearities owing to moderate elastic deflections. In those studies, it was observed that for a given ordering scheme, the final equations differed by a number of small nonlinear terms. These differences depend in part on the stage at which, in the process of derivation, the ordering scheme is applied. The application of the ordering scheme at a later stage in the derivation process requires much time in deriving and independently checking the final equations. This has led to attempts to share the algebra with computers through symbolic processors. Both general and special purpose programs have been developed and are available.[15] The program Helicopter Equations for Stability and Loads (HESL), appropriate to rotary-wing aeroelasticity investigations written in FORTRAN IV, was presented in Ref. 16. The approach used in developing this program and its use in analyzing the aeroelastic stability of an elastic rotor blade in hover was presented in Ref. 11.

In the present paper, the HESL program has been extended to derive the governing equations of motion for an elastic rotor blade in forward flight. A Lagrangian formulation is used to obtain the equations in generalized coordinates. The program generates the steady-state and linearized perturbation equations in symbolic form and then codes them into FORTRAN subroutines. Subsequently the coefficients for each equation and for each mode are identified through a numerical program. The harmonic balance equations, if required in the calculation of the deflected equilibrium position of the blade, can also be obtained from the symbolic program. The governing multiblade equations are derived explicitly using HESL. This is the first time that multiblade equations are derived explicitly using this symbolic formulation approach to study the stability of an elastic rotor blade in forward flight. The multiblade equations are capable of accommodating any number of elastic blade modes. Because the complete analytical process, from derivation to numerical calculation, is automated, it is an efficient and accurate means for analyzing helicopter rotor aeroelasticity.

The present study differs from previous ones in the following respects: 1) symbolic manipulation with FORTRAN is used to derive the governing equations in forward flight for an elastic rotor blade; 2) complete elastic flap-lag-torsion blade degrees of freedom are used for the trim calculation; 3) explicit multiblade equations are derived symbolically for stability calculation to compare with the single-blade solution; 4) dynamic inflow is included in the aeroelastic stability solution of an elastic blade in forward flight; and 5) damping data in forward flight are presented for varying elastic structural coupling.

To demonstrate the usefulness of this analytical capability, stability results are presented for several hingeless-rotor-blade structural models. The influence of dynamic inflow in forward flight with an elastic hingeless rotor is also investigated. The hingeless-rotor stability results presented in this paper using the symbolic program reflect the combined effect of an improved structural model (by including torsion) and an improved aerodynamic model (by including dynamic inflow). Results are presented for elastic blade flap-lag-torsion analysis and for flap-lag analysis with and without dynamic inflow.

Formulation

Figure 1 shows an elastic blade with the coordinate system used in this study. The blade has uniform mass and stiffness,

no twist, and no chordwise offsets of the elastic axis, tension axis, or center of mass. The elastic axis is coincident with the x-axis of the x,y,z coordinate system rotating with a constant angular velocity (Ω) about a fixed point at the origin. The y-axis lies in the plane of rotation, and the x-axis is rotated through a small angle (β_{pc}) from the plane of rotation. The deflections of the beam are u (axial deflection), v (lagwise bending), and w (flapwise bending) of the elastic axis parallel to the x,y,z coordinates, respectively. A second coordinate system, x', y', and z', is fixed to the blade, with y' and z' axes parallel to the principal axes of the deformed blade cross section. This coordinate system moves with the blade cross section as it undergoes bending, torsional displacements, and pitch angle (θ) rotation. Before deformation, the principal axes of the blade cross section are rotated with respect to the undeformed coordinates by the pitch angle. After deformation, the elastic axis is displaced by u,v,w, and the blade is twisted through the angle ϕ. The aerodynamic inflow dynamics couple with the blade dynamics as a feedback loop (Fig. 2). The total inflow (v_i) is assumed to consist of a steady value ($\bar{\lambda}$) and dynamic inflow components (ν_o, ν_c, and ν_s) that vary with time.

In this study, the entire problem formulation is performed by the computer; there is minimum user interface other than specifying blade geometry and the desired blade model representation. In general, the formulation of the rotary-wing aeroelastic problem consists of the following: writing the transformation matrices between the coordinate systems before and after deformation; calculating the position vector of a mass point of the deformed blade section; forming strain displacement relations; and calculating stresses and air velocity components in the flap, lag, and torsion directions (see Refs. 12-14 for more details). These expressions include geometrical nonlinearities owing to the assumption of small strains and moderate deflections which give rise to numerous higher-order nonlinear terms. So an ordering scheme, based on assigning orders of magnitude to the various physical parameters, is used to reduce the number of terms. The governing equations of motion are then obtained using Hamilton's principle. These equations are nonlinear, partial differential equations in u,v,w, and ϕ deflections. These are converted to ordinary differential equations using Galerkin's method by expressing the bending and torsion deflections in terms of generalized coordinates and mode-shape functions,

$$w = \sum_{i=1}^{N_F} Rw_i(\psi)\eta_i(\bar{x})$$

$$v = \sum_{i=1}^{N_L} Rv_i(\psi)\zeta_i(\bar{x}) \qquad (1a)$$

$$\phi = \sum_{i=1}^{N_T} \phi_i(\psi)\theta_i(\bar{x})$$

and by expressing the induced velocity as

$$v_i = \bar{\lambda} + \nu_o + \nu_c\bar{x}\cos\psi + \nu_s\bar{x}\sin\psi \qquad (1b)$$

where $\psi = \Omega t$, $\bar{x} = x/r$, and η_i,ζ_i,θ_i are mode shapes; R is the blade radius; and N_F, N_L, and N_T are the numbers of flap, lag, and torsion modes, respectively, used in the analysis. In this study uncoupled rotating modes evaluated at zero pitch are used. This yields N nonlinear, nonhomogeneous ordinary differential equations in terms of modal generalized coordinates w_i, v_i, and ϕ_i, where N is the total number of flap, lag, and torsion modes used in the analysis. The equations have periodic coefficients in the mass, damping, and stiffness matrices. These equations are then linearized for small perturbation motions about the deformed blade time-dependent equilibrium position by expressing the generalized coordinates in terms of the equilibrium quantities and small perturbation quantities:

$$w_i = \bar{w}_i(\psi) + \Delta w_i(\psi)$$

$$v_i = \bar{v}_i(\psi) + \Delta v_i(\psi) \qquad (2)$$

$$\phi_i = \bar{\phi}_i(\psi) + \Delta\phi_i(\psi)$$

Two sets of equations are obtained from this operation: a set of N nonlinear equations in $\bar{w}_i$, $\bar{v}_i$, and $\bar{\phi}_i$, which define the deflected equilibrium position of the blade, and a set of N equations obtained by subtracting the equilibrium equations and discarding all nonlinear products of the perturbation quantities, Δw_i, Δv_i, and $\Delta\phi_i$. Three more equations are obtained for the dynamic inflow components from rotor perturbations in aerodynamic thrust (C_T) and in pitch (C_M) and roll (C_L) moments (see Dynamic Inflow, below). The coefficients of these equations are also functions of the equilibrium solution.

Dynamic Inflow

The dynamic inflow equations are related to the blade degrees of freedom through the variations in thrust, pitching, and rolling moments:

$$[m]\begin{Bmatrix}\dot{\nu}_o\\ \dot{\nu}_c\\ \dot{\nu}_s\end{Bmatrix} + [\ell]^{-1}\begin{Bmatrix}\nu_o\\ \nu_c\\ \nu_s\end{Bmatrix} = \begin{Bmatrix}C_T\\ C_M\\ C_L\end{Bmatrix} \qquad (3)$$

The elements of [m] and [ℓ] define the various dynamic inflow models that can be included in an analysis. Reference 8 presents a hierarchy of models having different elements for [m] and [ℓ] from actuator disk theory in forward flight. The elements of [ℓ] depend on the wake skew angle at the rotor:

$$\alpha_R = \tan^{-1}\left[\frac{\bar{\lambda}}{\mu}\right] \qquad (4)$$

where $\bar{\lambda}$ is the steady inflow.

Of the 13 models presented in Ref. 8, the partially constrained model gave good results. In the present paper, this partially constrained theory is used to obtain the dynamic inflow results. The elements of [m] and [ℓ] are given by

$$m_{11} = \frac{128}{75\pi}, \quad m_{22} = m_{33} = \frac{-16}{45\pi},$$

$$m_{ij} = 0, \quad i \neq j$$

$$\ell_{11} = \frac{1}{2}, \quad \ell_{13} = \frac{15\pi}{64}\left(\frac{1 - \sin\alpha_R}{1 + \sin\alpha_R}\right)^{1/2},$$

$$\ell_{22} = \frac{-4}{1 + \sin\alpha_R}$$

$$\ell_{31} = \ell_{13}, \quad \ell_{33} = \frac{-4\sin\alpha_R}{1 + \sin\alpha_R},$$

$$\ell_{12} = \ell_{21} = \ell_{23} = \ell_{32} = 0$$

$$\ell_{ij} = \frac{1}{\nu}\ell_{ij}, \quad \nu = \frac{\mu^2 + \bar{\lambda}(2\bar{\lambda} - \mu\tan\alpha)}{(\mu^2 + \bar{\lambda}^2)^{1/2}} \qquad (5)$$

Equations from HESL

The governing equations of motion of the rotor blade are derived using HESL with two modes for each blade degree of freedom. The principles involved in the development of the symbolic program HESL are described in detail in Refs. 11, 16, and 17. Basically, the program assigns numbers to the variables forming the required expressions and then manipulates those numbers to obtain the required algebraic quantities. The integration, differentiation, perturbation, and multiblade coordinate transformation are performed by substituting known relations required for these operations. The symbolic program can handle both individual expressions and matrices. The program generates the steady and perturbed equations in a single operation and outputs them individually. This is convenient in the case of forward flight because of the large number of terms present in each equation; it is also convenient for the different analytical processes required for the steady and perturbed sets of equations.

The inputs to the program are the relations, in alphanumeric format, for the position vector, for the strain expressions, for the air-velocity components, and for the transformation matrices as given by Kaza and Kvaternik.[13] The integration relations (if known), differentiation relations, the order of the variables, the ordering scheme to be used, and the variables for which coefficients are to be collected are also given as data. In the present paper, the order of the variables and the ordering scheme used are the same as those followed in Ref. 4. All the $0(\varepsilon)^2$ terms, compared to $0(1)$, except those that contribute to lead-lag and torsion damping, are neglected. Nonlinear rate products ($\dot{v}\dot{w}$, $\dot{v}^2$, etc.) are retained since they contribute to the linearized stability analysis. Although any general ordering scheme could have been used to obtain the final equations of motion, this ordering scheme is considered representative and adequate for demonstrating the capability of the symbolic analysis process. The program calculates the strain energy, kinetic energy, and generalized forces for a given ordering scheme in generalized coordinates using Eq. (1). The perturbation relations as given in Eq. (2) are substituted to obtain the steady and perturbed terms. The program generates both the steady-state (nonlinear) and linearized perturbation equations and the loading terms necessary for an aeroelastic stability and response analysis. The rotor-thrust, pitch-moment, and roll-moment equations required in the dynamic inflow equations are also obtained using the perturbed aerodynamic forces. The equations are written into FORTRAN subroutines for subsequent numerical calculations. A numerical program subsequently identifies the mass, damping, stiffness, and forcing coefficients for each generalized degree of freedom. For the results presented here, it took about 300 sec to symbolically derive both the structural

and aerodynamic equations on a VAX 11/780 computer.

A brief description of the program input and output follows. Figure 3 is a flow diagram of the aeroelastic analysis using the symbolic and numerical programs. Table 1 shows the FORTRAN symbol definitions used for the original variables. Table 2 shows the input required to calculate tangential and perpendicular blade cross-section velocities U_T and U_P, using the transformation matrix LAFP(READ MATRIX) and the air-velocity vector VEL(READ MATRIX). By multiplying the two matrices (FORM MATRIX) with ordering scheme *E2D1, the vector AVEL is obtained, which gives the components of the velocities in radial, tangential, and perpendicular directions. The vector components are redefined as expressions by command MATRIX EXPRESSION. The actual velocity components are the negative of the original expression, and are therefore negated by calling the NEGATE command, thus giving the actual velocity expressions. This procedure is slightly different from the one presented in Ref. 11, where manipulations were performed at the expression level. Here the manipulations are extended to include matrix operations. It should be noted that for a hingeless rotor, the axial displacement can be solved for a priori as a function of flap and lag bending. In the present paper, expressions for axial displacement and axial velocity are taken from Ref. 4 and supplied as data to the program.

Trim and Periodic Equilibrium Solution

The nonlinear periodic coefficient equations obtained earlier can be solved for the periodic response in the time domain using a Floquet method or in the frequency domain using a harmonic balance method. Either will yield the time-dependent equilibrium position about which the nonlinear equations can be linearized for an eigensolution. In forward flight, this equilibrium position is coupled with the entire trim state of the helicopter. The trim state is the steady-state condition achieved by the system as time increases without bound, with the controls fixed and no external output. Calculation of trim position requires establishing the control settings for a given flight condition. The control settings are collective pitch, longitudinal and lateral cyclic pitch, and the rotor-shaft angle of attack. The induced velocity, which depends on the generated thrust and advance ratio, is also calculated.

In this paper, the harmonic analysis method, coupled with an iteration on the trim state, is used to calculate the equilibrium position and the trim settings. This procedure[18] consists of the following. An iterative inner loop in which the solution for the periodic motion is obtained with fixed values of the trim variables is nested within an outer loop in which the solution for the trim variables is obtained. The rotorcraft motion is solved for the periodic motion by the harmonic analysis method, which directly calculates the harmonics of a Fourier series representation of the motion. The procedure advances the rotor around the azimuth, calculating the forcing functions in the time domain and then updating the harmonics of the response. The forces and moments acting on the rotor are calculated from this response and the controls are adjusted until the equilibrium of forces and moments required for the specified operating state is achieved.

For the harmonic analysis method, the governing equations of motion are written, with all the time-dependent and nonlinear terms as a forcing function, as

$$[M]\{\ddot{X}\} + [C]\{\dot{X}\} + [K]\{X\} = F(\dot{X},X,\psi) \quad (6)$$

where matrices M, C, and K are the constant mass, damping, and stiffness matrices and X is the vector of degrees of freedom. The function F is evaluated at J points around the rotor azimuth

$$F_j = F(\psi_j) \quad (7)$$

and the harmonics of a complex Fourier series representation of F are given by

$$F_n = \frac{1}{J}\sum_{j=1}^{J} F_j\, e^{-in\psi_j} \quad (8)$$

Then the nth harmonic of the motion is given by

$$X_n = H_n^{-1}F_n \quad (9)$$

where

$$H = K - n^2M + iCn$$

The iterative solution proceeds as follows. At a given azimuth ψ_j, the blade motion is calculated using the current estimates of the harmonics:

$$X = \sum_{n=-L}^{L} X_n\, e^{in\psi_j}$$
$$\dot{X} = \sum_{n=-L}^{L} X_n in\, e^{in\psi_j} \quad (10)$$

where L is the number of terms used in the complex expansion of X. The forcing

function is evaluated with this motion. Then the change in the harmonics owing to the change in the forcing function is calculated and added to the harmonics calculated in the last revolution. After every revolution, the old and new harmonics are checked until convergence.

After obtaining the harmonics of the blade motion, the equilibrium of the forces and moments is checked. If equilibrium is not satisfied, the trim settings are increased and the procedure is repeated until equilibrium is met. The following assumptions are made in arriving at the equilibrium of the forces and moments. The helicopter is in straight and level steady flight; the rotor-hub moments are trimmed to zero; and tail, fuselage moments, and side-force components are neglected. Then the equilibrium forces and moments are given by

$$\begin{aligned} \bar{C}_T \cos\alpha + C_H \sin\alpha &= C_w \\ -\bar{C}_T \sin\alpha + C_H \cos\alpha &= -C_x \\ C_{mx} = C_{my} &= 0.0 \end{aligned} \tag{11}$$

where $C_x = (1/2)\bar{f}\mu^2$ and α is the angle of attack of the shaft.

In calculating thrust, horizontal force, and the hub moments, the steady inflow appears as a parameter that in turn depends on the rotor thrust and shaft angle of attack. In this paper, the steady inflow is taken as an equation of constraint and solved along with the four equations above:

$$\bar{\lambda} - \mu\tan\alpha - \bar{C}_T/[2(\bar{\lambda}^2 + \mu^2)^{1/2}] = 0.0 \tag{12}$$

The increments in the trim settings are calculated using a modified Newton-Raphson method.[18] If v is the control variable and M is the target to be achieved, then a first-order approximation of $M(v)$ is

$$M(\text{target}) = M_{n+1} = M_n + \frac{\partial M}{\partial v}(v_{n+1} - v_n) \tag{13}$$

or

$$v_{n+1} = v_n + D^{-1}[M(\text{target}) - M_n]F$$

where v_n and v_{n+1} indicate the current and new estimates of v, respectively, and $F < 1$ is included to avoid overshoot oscillations in the trim iteration by reducing the step size. The partial derivative matrix D is

$$D = \frac{\partial M}{\partial v} = \left[\cdots \quad \frac{\partial M}{\partial v_i} \quad \cdots\right]$$

$$= \left[\cdots \quad \frac{M(v_i) - M(v_i - \Delta v_i)}{\Delta v_i} \quad \cdots\right] \tag{14}$$

where v_i is the ith control variable and Δv_i is its increment. The convergence is checked when the tolerance level, as specified by the parameter ε, is met. For more details on this procedure see Ref. 18. In the present paper, all the degrees of freedom—blade flap, lead-lag, and torsion degrees of freedom—are used in calculating the trim state and periodic response.

The periodic response can also be obtained using Floquet methods.[3] A review of the use of these methods to obtain the initial conditions, forced response, and stability data is given in Ref. 19.

Aeroelastic Stability Solution: Single Blade

Once the time-dependent equilibrium position is determined, the nonlinear equations are perturbed about this equilibrium position, as given by Eq. (2). As mentioned earlier, the symbolic program generates the perturbed equations and writes them into subroutines. It should be noted that squares of the perturbation quantities are neglected by the symbolic program by employing the ordering scheme. The final system of equations for stability is

$$[P]\{\Delta\ddot{q}\} + [Q]\{\Delta\dot{q}\} + [R]\{\Delta q\} = 0 \tag{15}$$

or

$$\{\dot{z}\} = [A_s]\{z\}$$

The stability of this linearized system is determined from Floquet theory by evaluating the characteristic exponents of $[A_s]$,

$$\lambda_K = \zeta_K + i\omega_K \tag{16}$$

The mass, damping, and stiffness terms are identified by a numerical program for each time-step. The linearized system is stable when $\zeta_K < 0$.

Multiblade Coordinate Transformation

To provide a better understanding and to include dynamic inflow effects, which are referenced to the fixed system, it is necessary to convert the equations into a fixed coordinate system. In the case of

hovering flight, this transformation can be easily performed by rearranging the coefficients of the equations, since the coefficients are constant. For forward flight, the degrees of freedom, as well as the coefficients, are periodic. Hence, the multiblade coordinate transformation (MCT) is more complicated. The MCT or Fourier coordinate transformation is a linear transformation of the degrees of freedom from the rotating to nonrotating frame. Let X be a degree of freedom (dimensionless) in the rotating frame for the ith blade. Then, for a three-bladed rotor, the relations

$$X_i = X_o + X_c \cos \psi_i + X_s \sin \psi_i$$

$$\dot{X}_i = \dot{X}_o + (\dot{X}_c + X_s)\cos \psi_i + (\dot{X}_s - X_c)\sin \psi_i$$

$$\ddot{X}_i = \ddot{X}_o + (\ddot{X}_c + 2\dot{X}_s - X_c)\cos \psi_i + (\ddot{X}_s - 2\dot{X}_c - X_c)\sin \psi_i \qquad (17)$$

give the ith blade degree of freedom, using multiblade coordinates in the nonrotating frame. The variables X_o, X_c, and X_s are the rotor degrees of freedom, and describe the motion of the rotor as a whole in the nonrotating frame.

The MCT involves the following steps[20]: 1) expansion of each degree of freedom into multiblade coordinates; 2) multiplying the resulting expression with multiblade functions like 1, cos ψ, sin ψ, cos 2ψ, sin 2ψ, etc., depending on the number of blades; 3) replacing products of sines and cosines as sums of sines and cosines, using trigonometric relations; and 4) deleting terms that are not multiples of the number of blades (summation rules). Using the symbolic program, this is achieved as follows. The multiblade expansions of each degree of freedom and their time derivatives are given as a table of relations (Eq. (17)). The multiblade functions like 1, cos ψ, sin ψ, cos 2ψ, sin 2ψ, etc., required in transforming the equations, are read as data (or can be generated within the program). The trigonometric relations giving the product of sines and cosines as sums of sines and cosines are given as a table of relations. These require that the equation derivation be several runs until all the required relations are included in the table of relations. Then the command PERFORM MULTIBLADE TRANSFORMATION multiplies the equation with each of the multiblade functions, substitutes the multiblade expansion for each degree of freedom, substitutes the trigonometric relations (from the given tables of relations), and checks for the multiples of the blade harmonics. Only terms containing multiples of the number of blades are retained. The interface routines separate the terms into constant and periodic parts, with the coefficient of each harmonic separated, and writes them into subroutines. In this manner, the constant-coefficient approximation is easily done. In the present paper, the perturbed governing equations of motion and perturbations in thrust and moment equations are converted into multiblade coordinates. The multiblade solution was checked for accuracy with a single-blade solution without dynamic inflow. It should be noted that the trim-value harmonics entering as nonlinear contributions should be defined as symbolic data. The input data increase as more nonlinear terms are taken into account in addition to the data given for the multiblade expansion of the degrees of freedom. However, the output may be smaller since only terms that are multiples of the number of blades are retained. Since this is a feasibility study undertaken to obtain explicit multiblade equations using a symbolic program in FORTRAN, the nonlinear quantities are assumed to provide only first harmonic forcing contributions. For the results presented here, the program was run on a VAX 11/780 computer. It took about 250 sec to derive the multiblade equations for each blade degree of freedom, and about 120 sec to write these into subroutines for numerical analysis.

It should be noted that by giving the expansion of each degree of freedom into its harmonics and by giving the trigonometric relations as data to the symbolic program, explicit harmonic balance equations can also be derived. However, because of the amount of input required to perform a symbolic formulation of the harmonic balance and multiblade equations, the program HESL is convenient for explicitly considering the symbolically derived equations only if the number of degrees of freedom is small. As pointed out in Ref. 20, numerical schemes are better suited to general models for efficiently obtaining the harmonic balance equations and multiblade equations after the steady and perturbed equations are obtained from the symbolic program.

The symbolic program separates the terms containing the periodic variable cos Nt and sin Nt and writes the equation as

$$A(t) = A_o + A_N \cos Nt + B_N \sin Nt \qquad (18)$$

In subroutine form they are referred to as A(1), A(2), and A(3). This allows for direct elimination of the matrices A(2) and A(3) for a simple constant-coefficient approximation analysis.

Stability Solution: Multiblade and Dynamic Inflow

The final governing equations of motion can be written as

$$[P]\{\ddot{q}\} + [Q]\{\dot{q}\} + [R]\{q\} + [T]\{u\} = 0 \tag{19a}$$

for the blade equations, and as

$$[A]\{\ddot{q}\} + [B]\{\dot{q}\} + [C]\{q\} + [G]\{u\} = [m]\{\dot{u}\} + [\ell]^{-1}\{u\} \tag{19b}$$

for the dynamic inflow equations, where

$\{q\}$ is $\{q_c, q_c, q_s\}$

$\{q_o\}$ is vector of all collective modes

$\{q_c\}$ is vector of all lateral cyclic modes

$\{q_s\}$ is vector of all longitudinal cyclic modes

$\{u\}$ is $\{\nu_o, \nu_c, \nu_s\}$

Defining $\dot{\Lambda} = \{u\}$, Eqs. (19a) and (19b) can be combined as

$$\begin{bmatrix} P & 0 \\ A & -m \end{bmatrix}\{\ddot{X}\} + \begin{bmatrix} Q & T \\ B & (G - \ell^{-1}) \end{bmatrix}\{\dot{X}\} + \begin{bmatrix} R & 0 \\ C & 0 \end{bmatrix}\{X\} = 0 \tag{20}$$

where $\{X\}$ is

$$\begin{Bmatrix} q \\ \Lambda \end{Bmatrix}$$

The final stability equations in state vector form are

$$\{\dot{Y}\} = [A_s]\{Y\} \tag{21}$$

where

$$\{Y\} = \begin{Bmatrix} X \\ \dot{X} \end{Bmatrix}$$

The stability results are obtained by calculating the eigenvalues of $[A_s]$, in a manner similar to that used in the single-blade case.

The size of the state matrix depends on the number of modes and blades. For the flap-lag-torsion model with two modes each, the size of the state matrix is 36 × 36 without dynamic inflow and 39 × 39 with dynamic inflow. The corresponding values for a flap-lag model are 24 × 24 and 27 × 27, respectively.

Results and Discussion

Results are presented for a uniform blade with zero built-in twist, zero precone angle and zero blade offsets. Reversed-flow effects are neglected. A three-bladed rotor is considered. Two rotating modes for each flap, lag, and torsion degrees of freedom are used in the calculation. These modes are calculated at zero pitch and are obtained from five nonrotating modes. Results for both a single-blade solution and a multiblade solution are presented for different blade structural models. All results are for a propulsive trim condition, specified for a weight coefficient of $C_W/\sigma = 0.07$ and an equivalent drag area $D/q = f = 0.0\,(\pi R^2)$, where D is the drag force, and q is the dynamic pressure.

In the derivation of the equations, the order of magnitude assigned for each parameter is the same as that followed in Ref. 4. The other parameters used for the numerical study are

$$\omega_\nu = 0.7,\ 1.4;\ \omega_w = 1.15;\ \omega_\phi = 3.0;$$
$$c/R = 0.07854;\ \gamma = 5.0;\ \sigma = 0.1;$$
$$a = 2\pi;\ C_{d_o} = 0.01;\ \beta_{pc} = 0.0;$$
$$K_{m_1}/K_{m_2} = 0.0;\ K_m/R = 0.025;$$
$$(K_A/K_m)^2 = 1.5$$

Lead-lag damping values (real part of the characteristic exponent) are presented for a soft inplane and a stiff inplane rotor with and without dynamic inflow. The results are presented for investigating 1) the effect of degrees of freedom used in the trim analysis on the lead-lag damping, 2) the effect of using only one torsion mode, 3) the inclusion of a dynamic inflow model, and 4) the difference between periodic and a constant-coefficient approximation.

Single-Blade Results

The effect of the number of degrees of freedom used in the trim analysis on the lead-lag damping is shown in Figs. 4 and 5. Figure 4 shows the lead-lag damping plotted versus advance ratio for a soft inplane rotor ($\omega_\nu = 0.7$). It can be seen that a flap-lag-torsion stability analysis from a flap-trim analysis underpredicts the lead-lag damping. The second mode shows the same trend with the difference in predicted damping increasing with advance ratio. Figure 5 shows the lead-lag damping plotted for a stiff inplane

rotor (ω_y = 1.4) as a function of advance ratio. The results also show an increase in damping when a flap-lag-torsion trim analysis is used. It is also noted that for an advance ratio of $0.37 < \mu < 0.41$, the first-mode roots separate and one root becomes less stable and the other becomes more stable. The damping does reduce as the advance ratio is increased. The second mode remains stable at all advance ratios considered.

The increase in damping observed above for both soft inplane and stiff inplane rotors is perhaps a result of the different time-dependent equilibrium positions used. A full flap-lag-torsion trim analysis is consistent in that the blade model has the same degree of complexity in both the trim and the stability analysis. It should be noted that qualitatively the same type of trend was reported in Ref. 5, for both soft inplane and stiff inplane rotors. This verifies the symbolic and numerical programs for the single-blade results and forms the basis for checking the symbolically derived multiblade equations (and numerical results) subsequently.

Figures 6 and 7 present the lead-lag damping plotted versus advance ratio from a flap-lag model, flap-lag-torsion model (two modes for each degree of freedom), and flap-lag-torsion model with only one torsion mode, for a soft inplane rotor (ω_y = 0.7). Figure 6 presents the damping results for full elastic coupling (R = 1.0). It can be seen that the flap-lag model underpredicts the lead-lag damping. The model with only one torsion mode increases the damping above that of the model with two modes each. Figure 7 shows the lead-lag damping value plotted for zero elastic coupling (R = 0.0). The damping levels are very much reduced compared with those in the full elastic coupling case. However, the flap-lag model is again the least damped.

Lead-lag damping is plotted for a stiff inplane rotor (ω_y = 1.4) with varying advance ratio in Figs. 8 and 9. Figure 8 presents the damping results for full elastic coupling. The same trend that was observed for the case of soft inplane (Fig. 6) exists. Here, it is to be noted that root splitting for high advance ratios occurs even when only one torsion mode is used. Figure 9 presents the lead-lag damping for increasing advance ratio for a stiff inplane rotor for zero elastic coupling parameter. Although a flap-lag model predicts a stable system, the rotor is unstable. This demonstrates the importance of elastic blade torsion in a forward-flight stability analysis.

Figure 10 shows the lead-lag damping plotted for an advance ratio of μ = 0.25 while varying the elastic coupling parameter for a stiff inplane rotor. Here a flap-lag model predicts positive damping for all values of R, whereas for a flap-lag-torsion model the damping varies with the elastic coupling value, increasing with the elastic coupling parameter.

Multiblade-Equation Results

The following figures present the lead-lag regressing mode damping results obtained from multiblade equations. The multiblade equations were explicitly derived using the symbolic program. This required explicit definition of all nonlinear contributions and degrees of freedom in terms of their harmonics. The result was a significant increase in the amount of data required by the symbolic program. Since this is a feasibility study on the use of symbolic programs in FORTRAN, only first harmonics were considered in the nonlinear contributions. Consequently, damping data determined from the multiblade equations may differ from the single-blade solution. Additionally, the multiblade results are obtained by retaining only one torsion mode, although the nonlinear contribution from both torsion modes is used. This significantly reduces the time required for the Floquet stability analysis.

The damping values were first checked with those obtained from a single-blade solution obtained previously to validate the multiblade equation derivation process. It was found that the approximation $\cos\theta = 1.0$, used in deriving the explicit multiblade equations, will predict slightly higher (but less than 2%) damping for stiff inplane rotors with full elastic coupling parameter; this is because the approximation has its greatest effect on the coupling elements. For all other values of the elastic coupling parameter, this approximation does not affect the resultant damping values. Where required for comparisons, the single-blade damping values are recalculated using this approximation; this is done to avoid the rederivation of the multiblade equations.

Figures 11 and 12 show the lead-lag regressing mode damping plotted for a varying advance ratio with and without dynamic inflow from a flap-lag-torsion and flap-lag model for a soft inplane rotor. Figure 11 shows the damping for full elastic coupling (R = 1.0). For the flap-lag-torsion model, the dynamic inflow reduces the damping at practically all advance ratios. Its effect is negligible at advance ratios of 0.15 to 0.25. For the flap-lag model, the dynamic inflow increased the damping up to an advance ratio of 0.33; at higher advance ratios it reduced the damping. Figure 12 presents

the damping results for the zero elastic coupling (R = 0.0). It is seen that for the flap-lag-torsion model, the dynamic inflow again reduced the damping in hover. Yet at intermediate advance ratios, dynamic inflow increased the damping, and at higher advance ratios, it once again reduced the damping. For the flap-lag model, the dynamic inflow increased lead-lag damping for all advance ratios. This is consistent with the flap-lag model results of previous studies (e.g., Ref. 7).

The lead-lag regressing mode damping is plotted for a stiff inplane rotor for a varying advance ratio in Figs. 13 and 14. Figure 13 is for a rotor with full elastic coupling. For a flap-lag-torsion model, the dynamic inflow reduced the damping up to an advance ratio μ of 0.41. For $\mu > 0.41$, this model slowed a slightly increased damping value. The flap-lag model with dynamic inflow shows a small increase in damping. This damping increment gets smaller with higher advance ratios. Figure 14 is for a rotor with zero elastic coupling. For this configuration, the dynamic inflow increases damping for all advance ratios. Consequently both the flap-lag-torsion and flap-lag model show the same trend.

Figure 15 shows the lead-lag regressing mode damping plotted for a stiff inplane rotor at an advance ratio of 0.25, for varying elastic coupling. For the flap-lag-torsion model, dynamic inflow reduces the damping for $R > 0.3$, but it increases the available damping for $R < 0.3$. However, this increase is not sufficient to stabilize the inplane mode. With the flap-lag model, dynamic inflow shows an increase in damping for all values of elastic coupling. This is the same trend as was observed in Ref. 11 for the case of hover with both flap-lag and flap-lag-torsion blade models.

Constant-Coefficient Approximation Results

The effect of a constant-coefficient approximation (CCA) is presented in Fig. 16, where the real part of the exponent is plotted for a stiff inplane rotor with full elastic coupling that did show a splitting of roots with a full periodic coefficient analysis (Fig. 13). The CCA does not show this splitting, since the frequencies are very much away from the real axis. For this analysis, the regressing and collective modes did predict the same damping trend with advance ratio as shown by the full Floquet analysis. However, the progressing mode showed poor agreement between a CCA analysis and a Floquet-theory analysis. This is because the constant-coefficient approximation will only be good for low-frequency modes.

Conclusions

A symbolic manipulation program written in FORTRAN was used to derive the aeroelastic analysis equations of an elastic blade with flap-lag-torsion degrees of freedom in forward flight. The feasibility of using the program to obtain explicit equations in a harmonic balance method and multiblade equations was studied. Numerical results were presented, with and without dynamic inflow for a propulsive trimmed rotor. Both a flap-lag-torsion model and a flap-lag model were analyzed. Soft inplane and stiff inplane rotors were considered.

The following conclusions were drawn from this study of the use of a symbolic program for predicting rotor aeroelastic stability.

1) The symbolic program can be used to obtain explicit equations.

2) With the present program capability, the amount of data to the symbolic program increases greatly with the number of harmonics and degrees of freedom.

3) In deriving the explicit harmonic balance equations and multiblade equations, the following should be noted: a) to obtain the harmonic balance equations, a numerical method is suggested since an arbitrary number of harmonics can be used without increasing the input data to the symbolic program; b) to obtain the multiblade equations, the perturbed equations in their Fourier series form are derived using the symbolic program. Then the multiblade equations themselves are obtained numerically.

It is recommended that a selective (judicious) combination of symbolic and numerical programs is required for an efficient derivation and numerical-study process.

The following conclusions were drawn from the numerical study of a single-blade solution.

1) A flap-lag-torsion stability analysis from a trim procedure in which only the flap degree of freedom is used underpredicts the lead-lag damping.

2) In the case of stiff inplane rotors, high forward flight speed is destabilizing. At high advance ratios, a splitting of the roots is encountered, yielding two real-part characteristic exponents at the same frequency.

3) Using only one torsion mode usually increases the damping value from the flap-lag structural model.

4) The damping values for a stiff inplane rotor are very sensitive to elastic coupling parameter Depending on this parameter, the rotor can be either stable or unstable.

The following conclusions were drawn from the numerical study of a multiblade solution with dynamic inflow.

1) For a flap-lag model, and for both soft inplane and stiff inplane rotors with zero elastic coupling, the dynamic inflow increased damping at all advance ratios considered; with full elastic coupling, the dynamic inflow increased the damping at low advance ratios, but reduced damping at high advance ratios.

2) For a flap-lag-torsion model, dynamic inflow slightly reduced lead-lag regressing-mode damping for full elastic coupling. The same trend was observed for both soft inplane and stiff inplane rotors.

3) For a given advance ratio, the variation of damping with elastic coupling parameter for a stiff inplane rotor showed the same trend as did the hover case.

4) The constant-coefficient approximation for the stiff inplane rotor does not show the splitting of the roots, since the frequency of the lag mode is away from the real axis.

References

1. Ormiston, R. A. and Hodges, D. H., "Linear Flap-Lag Dynamics of Hingeless Rotor Blades in Hover," Journal of the American Helicopter Society, Vol. 17, No. 2, 1972, pp. 2-14.

2. Peters, D. A., "Flap-Lag Stability of Helicopter Rotor Blades in Forward Flight," Journal of the American Helicopter Society, Oct. 1975, pp. 2-13.

3. Friedmann, P. P. and Tong, P., "Nonlinear Flap-Lag Dynamics of Hingeless Helicopter Blades in Hover and Forward Flight," Journal of Sound and Vibration, Vol. 30, No. 1, 1973, pp. 9-31.

4. Hodges, D. H. and Ormiston, R. A., "Stability of Elastic Bending and Torsion of Uniform Cantilever Rotor Blades in Hover with Variable Structural Coupling," NASA TN D-8192, 1976.

5. Friedmann, P. P. and Kottapalli, S. B. R., "Coupled Flap-Lag-Torsional Dynamics of Hingeless Rotor Blades in Forward Flight," Journal of the American Helicopter Society, Vol. 27, No. 4, Oct. 1982, pp. 28-36.

6. Peters, D. A. and Gaonkar, G. H., "Theoretical Flap-Lag Damping with Various Inflow Models," Journal of the American Helicopter Society, Vol. 25, No. 3, 1980, pp. 29-36.

7. Gaonkar, G. H. and Peters, D. A., "Use of Multiblade Coordinates for Helicopter Flap-Lag Stability with Dynamic Inflow," Journal of Aircraft, Vol. 17, No. 2, 1980, pp. 112-118.

8. Gaonkar, G. H., Sastry, V. V. S. S., Reddy, T. S. R., Nagabhushanam, J., and Peters, D. A., "The Use of Actuator-Disk Dynamic Inflow for Helicopter Flap-Lag Stability," Journal of the American Helicopter Society, Vol. 28, No. 3, 1983, pp. 79-88.

9. Gaonkar, G. H., Mitra, A. K., Reddy, T. S. R., and Peters, D. A., "Sensitivity of Helicopter Aeromechanical Stability to Dynamic Inflow," Vertica, Vol. 6, No. 1, 1982, pp. 57-59.

10. Johnson, W., "Influence of Unsteady Aerodynamics on Hingeless Rotor Ground Resonance," Journal of Aircraft, Vol. 19, No. 8, Aug. 1982, pp. 668-673.

11. Reddy, T. S. R., "Flap-Lag Damping of an Elastic Rotor Blade with Torsion and Dynamic Inflow in Hover from Symbolically Generated Equations," AIAA Paper 84-0989, Palm Springs, Calif., 1984.

12. Hodges, D. H. and Dowell, E. H., "Nonlinear Equations of Motions for the Elastic Bending and Torsion of Twisted Nonuniform Rotor Blades," NASA TN D-7818, 1974.

13. Kaza, K. R. and Kvaternik, R. G., "Nonlinear Aeroelastic Equations for Combined Flapwise Bending, Chordwise Bending, Torsion, and Extension of Twisted Nonuniform Rotor Blades in Forward Flight," NASA TM-74059, 1977.

14. Rosen, A. and Friedmann, P. P., "Nonlinear Equations of Equilibrium for Elastic Helicopter or Wind Turbine Blades Undergoing Moderate Deformation," Report No. 7718, U. of California, Los Angeles, Calif., Jan. 1977.

15. "Proceedings of the 1977 MACSYMA User's Conference," NASA CP-2012, 1977.

16. Nagabhushanam, J., Gaonkar, G. H., and Reddy, T. S. R., "Automatic Generation of Equations for Rotor-Body Systems with Dynamic Inflow for A Priori Ordering Schemes," Paper No. 37, 7th European Rotorcraft Forum, Garmisch-Partenkirchen, W. Germany, 1981.

17. Reddy, T. S. R., "Symbolic Generation of Elastic Rotor Blade Equations Using a Fortran Processor and Numerical Study on Dynamic Inflow Effects on the Stability of Helicopter Rotors," NASA TM in preparation, 1985.

18. Johnson, W., "A Comprehensive Analytical Model of Rotorcraft Aerodynamics and Dynamics. Pt. I. Analysis Development," NASA TM-81182, 1980.

19. Dugundji, J. and Wendell, J. H., "Some Analysis Methods for Rotating Systems with Periodic Coefficients," AIAA Journal, Vol. 21, No. 6, June 1983, pp. 890-897.

20. Johnson, W., Helicopter Theory, Princeton University Press, Princeton, N. J., 1980.

Table 1. FORTRAN symbols

Original variable	FORTRAN symbol	Original variable	FORTRAN symbol
R	RAD	v'	VS
u	U	$\bar{v}_i$	LAMB
$\dot{u}$	UD	w	W
U_T	UT	w'	WS
U_P	UP	$\dot{w}$	WD
$\dot{U}_F$	UF	x	XCOR
$\dot{U}_F$	UFD	θ	THTA
v	V	ϕ	PHI
$\dot{v}$	VD	Ω	OMEG

Table 2. Typical input to HESL and output to calculate tangential and normal velocities (U_T and U_P)

```
READ MATRIX
#LAFP0303
03
1.0
-0.5      VS    VS
-0.5      WS    WS
01
1.0       VS
01
1.0       WS
02
-1.0      VS%EONE
-1.0      WS%ETWO
03
1.0    %ETRE
-1.0     PHI   THTA
-1.0      VS     WS THTA
02
1.0      PHI
1.0    %EFUR THTA
02
1.0       VS%ETWO
-1.0      WS%EONE
03
-1.0   %ETRE THTA
-1.0     PHI
-1.0      VS    WS
02
-1.0     PHI THTA
1.0    %EFUR
READ MATRIX
#VEL0301
04
-1.0      UD
1.0      UFD
1.0     OMEG     V
1.0       MU OMEG   RAD CSCY
03
-1.0      VD
-1.0   %XUUF OMEG
-1.0      MU OMEG   RAD SNCY
02
-1.0    OMEG   RAD%LAMD
-1.0      WD
FORM MATRIX
#LAFP VEL#AVEL*E2D1
MATRIX EXPRESSION
02#AVEL
%   UT0201%   UP0301
NEGATE EXPRESSION
%   UT
NEGATE EXPRESSION
%   UP
```

Note: %EONE, %ETWO etc. are expressions read earlier in the program.

Output of U_T

```
*********************************************
*     DETAILS OF THE EXPRESSION     UT      *
*              NUMBER OF TERMS      22      *
*********************************************

1      1.000*  VS*OMEG*    V*
2      1.000*  VS*OMEG*   MU* RAD*CSCY*
3      1.000*THTA*   WS*OMEG*   MU* RAD*CSCY*
4      1.000* PHI*   WS*OMEG*   MU* RAD*CSCY*
5      1.000*   VD*
6      1.000*XCOR*OMEG*
7      1.000*    U*OMEG*
8     -1.000*   UF*OMEG*
9      1.000*OMEG*   MU* RAD*SNCY*
10    -0.500*   VS*   VS*   VD*
11    -0.500*   VS*   VS*XCOR*OMEG*
12    -0.500*   VS*   VS*OMEG*   MU* RAD*SNCY*
13    -0.500* PHI* PHI*   VD*
14    -0.500* PHI* PHI*XCOR*OMEG*
15    -0.500* PHI* PHI*OMEG*   MU* RAD*SNCY*
16    -1.000* PHI*THTA*   VD*
17    -1.000* PHI*THTA*XCOR*OMEG*
18    -1.000* PHI*THTA*OMEG*   MU* RAD*SNCY*
19     1.000* PHI*LAMB*OMEG* RAD*
20     1.000* PHI*   WD*
21     1.000*THTA*LAMB*OMEG* RAD*
22     1.000*THTA*   WD*
```

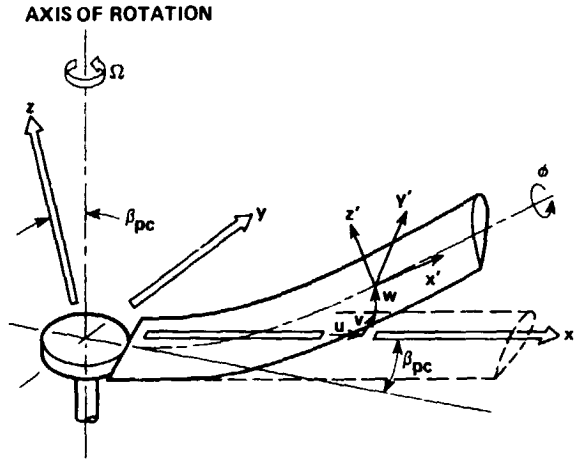

Fig. 1 Rotor-blade coordinate systems and deflections.

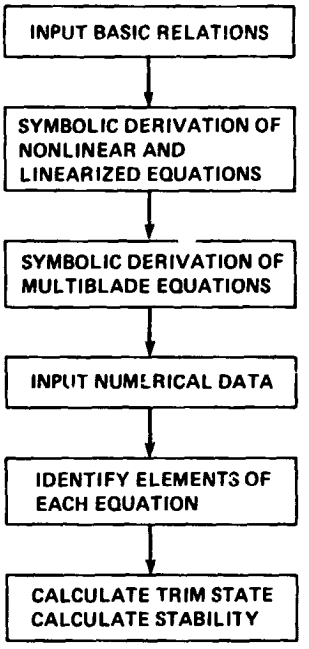

Fig. 3 Flowchart of the aeroelastic analysis.

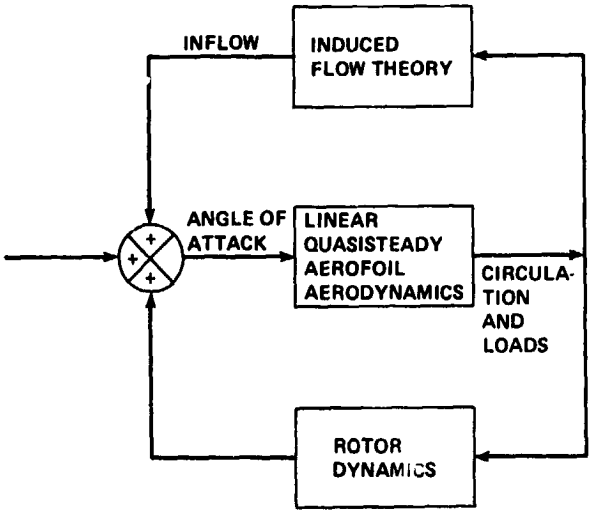

Fig. 2 Inflow dynamics.

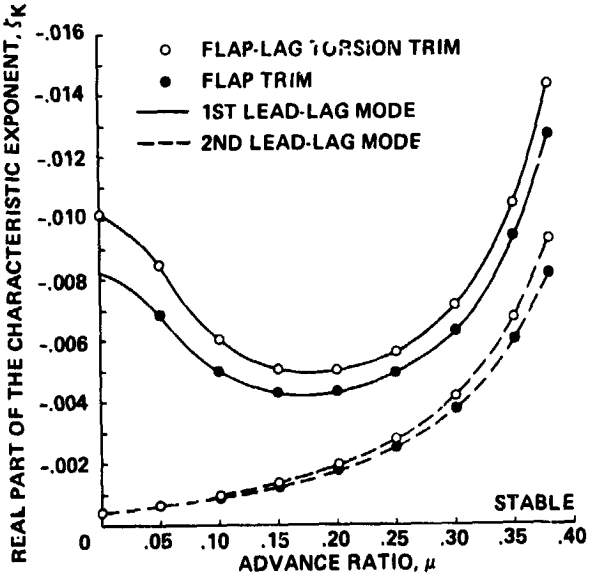

Fig. 4 The effect of the number of degrees of freedom used in trim analysis on lead-lag damping versus advance ratio: soft inplane, ω_v = 0.7, R = 1.0, propulsive trim.

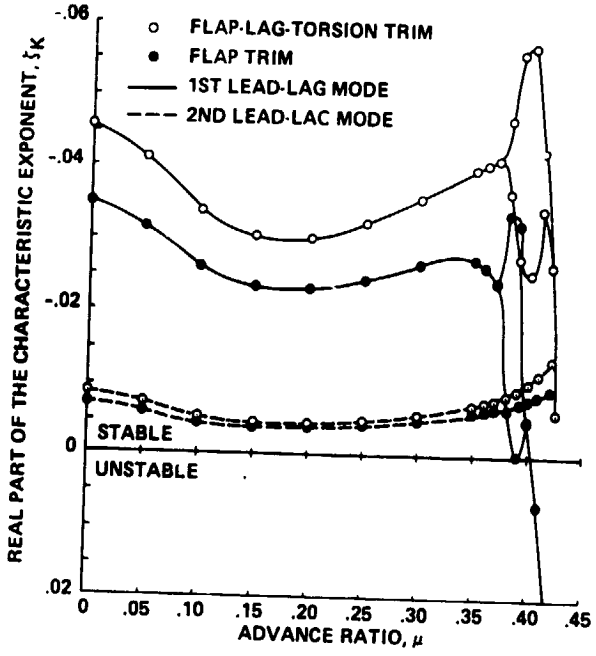

Fig. 5 The effect of number of degrees of freedom used in trim analysis on lead-lag damping versus advance ratio: stiff inplane, $\omega_V = 1.4$, R = 1.0, propulsive trim.

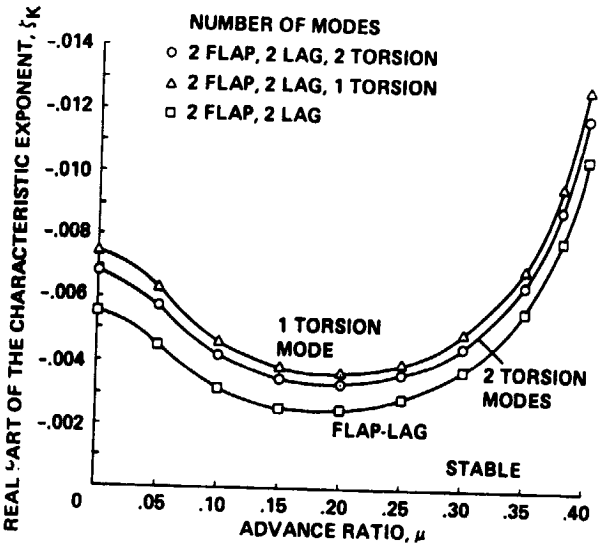

Fig. 7 Lead-lag mode damping versus advance ratio for a flap-lag-torsion model and a flap-lag model: soft inplane, $\omega_V = 0.7$, R = 0.0.

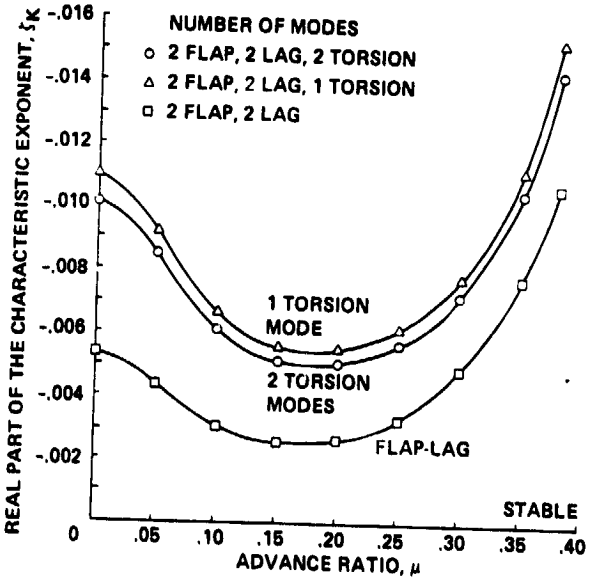

Fig. 6 Lead-lag mode damping versus advance ratio for a flap-lag-torsion model and a flap-lag model: soft inplane, $\omega_V = 0.7$, R = 1.0.

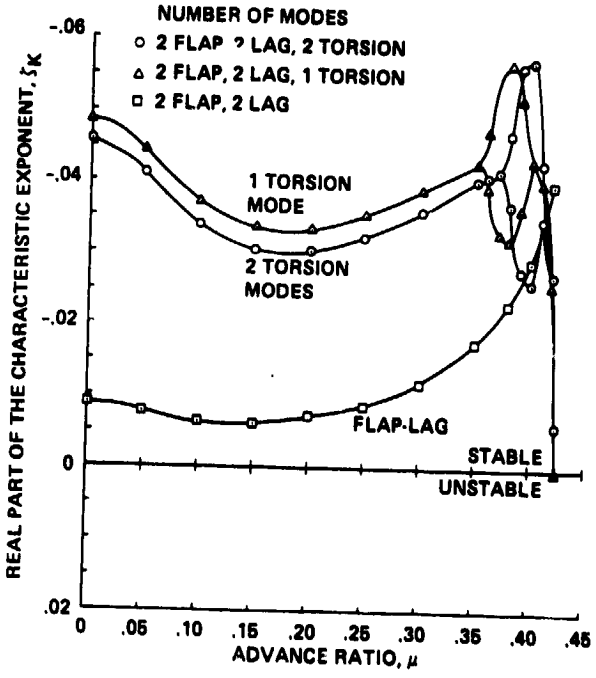

Fig. 8 Lead-lag mode damping versus advance ratio for a flap-lag-torsion model and a flap-lag model: stiff inplane, $\omega_V = 1.4$, R = 1.0.

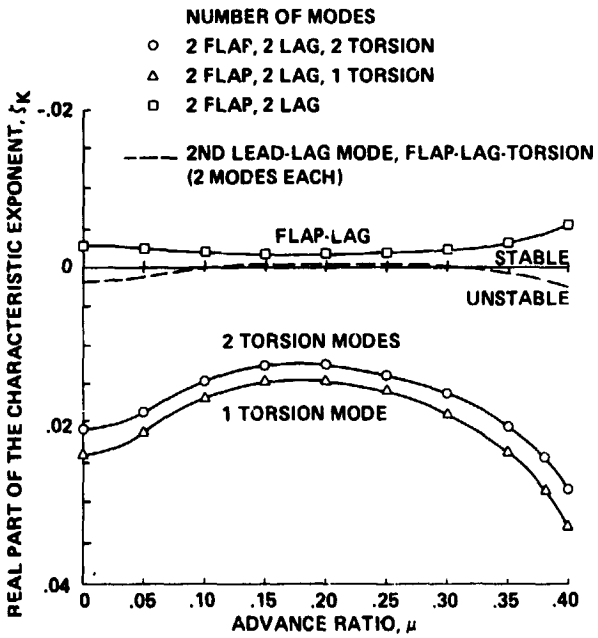

Fig. 9 Lead-lag mode damping versus advance ratio for a flap-lag-torsion model and a flap-lag model: stiff inplane, $\omega_v = 1.4$, R = 0.0.

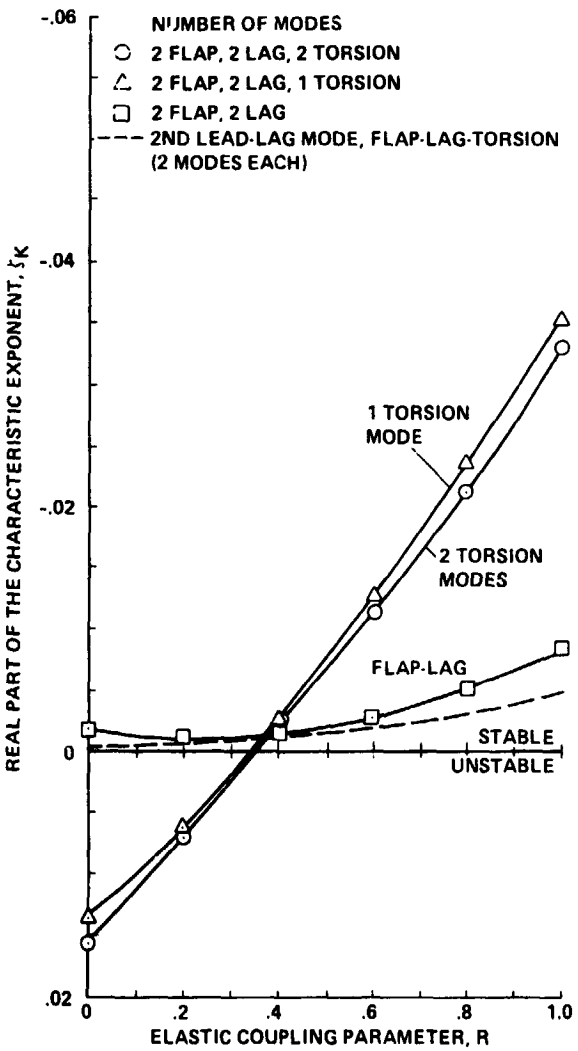

Fig. 10 Lead-lag mode damping versus elastic coupling for a flap-lag-torsion model and a flap-lag model: stiff inplane, $\omega_v = 1.4$, $\mu = 0.25$.

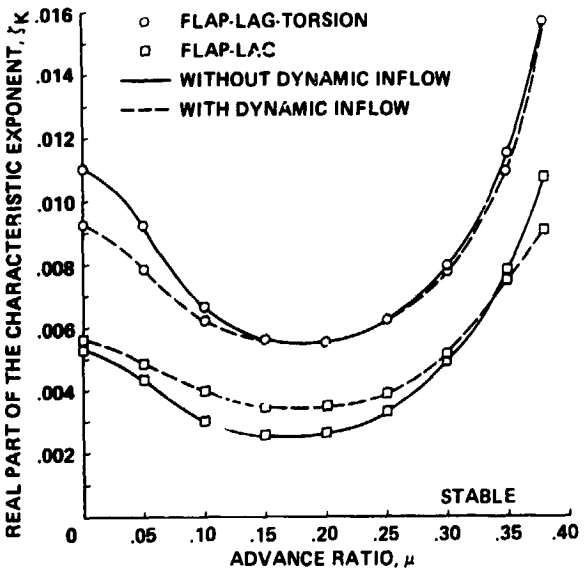

Fig. 11 The effect of torsion and dynamic inflow on lead-lag regressing mode damping versus advance ratio: soft inplane, $\omega_\zeta = 0.7$, R = 1.0 (multiblade equations).

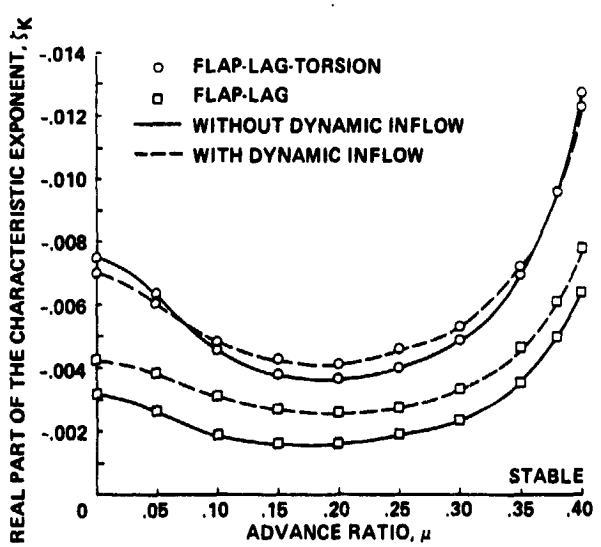

Fig. 12 The effect of torsion and dynamic inflow on lead-lag regressing mode damping versus advance ratio: soft inplane, $\omega_\zeta = 0.7$, R = 0.0 (multiblade equations).

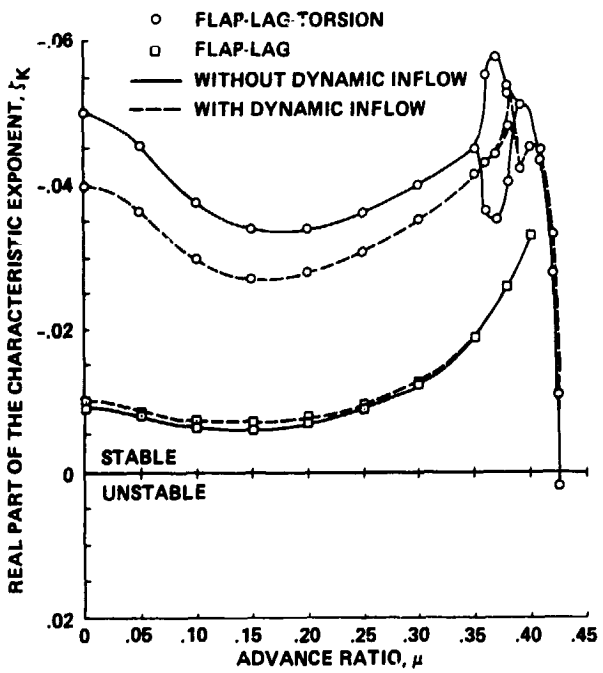

Fig. 13 The effect of torsion and dynamic inflow on lead-lag regressing mode damping versus advance ratio: stiff inplane, $\omega_\zeta = 1.4$, R = 1.0 (multiblade equations).

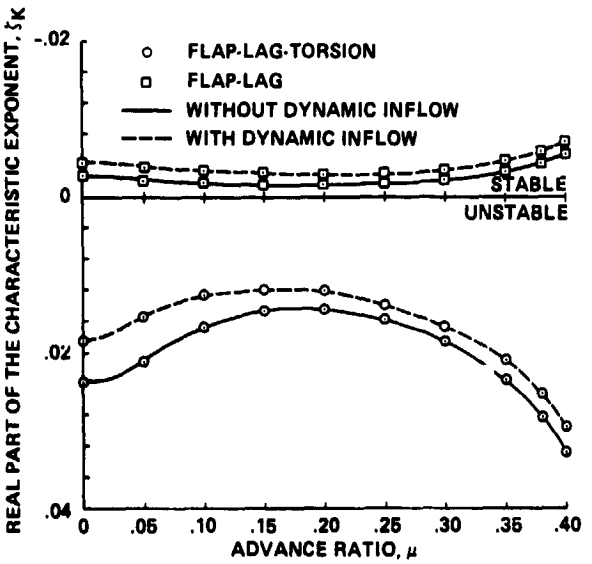

Fig. 14 The effect of torsion and dynamic inflow on lead-lag regressing mode damping versus advance ratio: stiff inplane, $\omega_\zeta = 1.4$, R = 0.0 (multiblade equations).

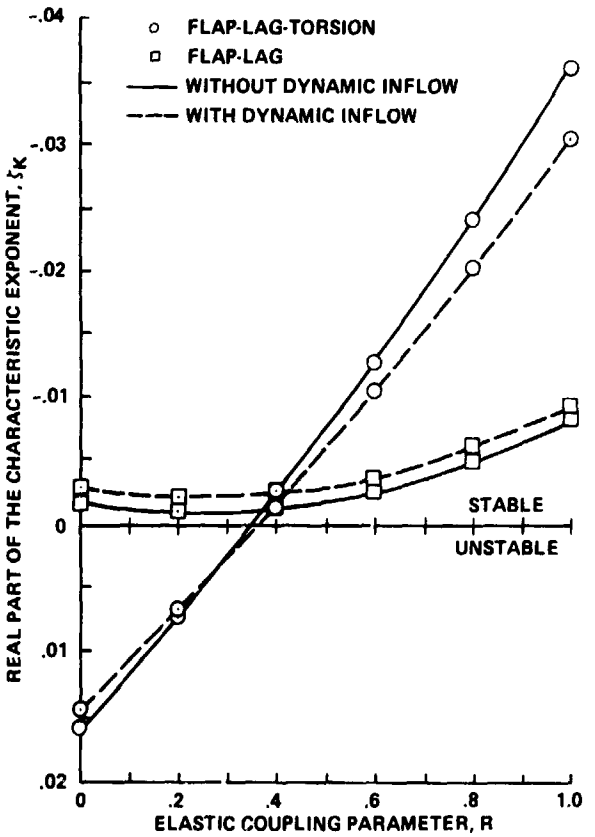

Fig. 15 The effect of torsion and dynamic inflow on lead-lag regressing mode damping versus elastic coupling, stiff inplane, $\omega_\zeta = 1.4$, $\mu = 0.25$ (multiblade equations).

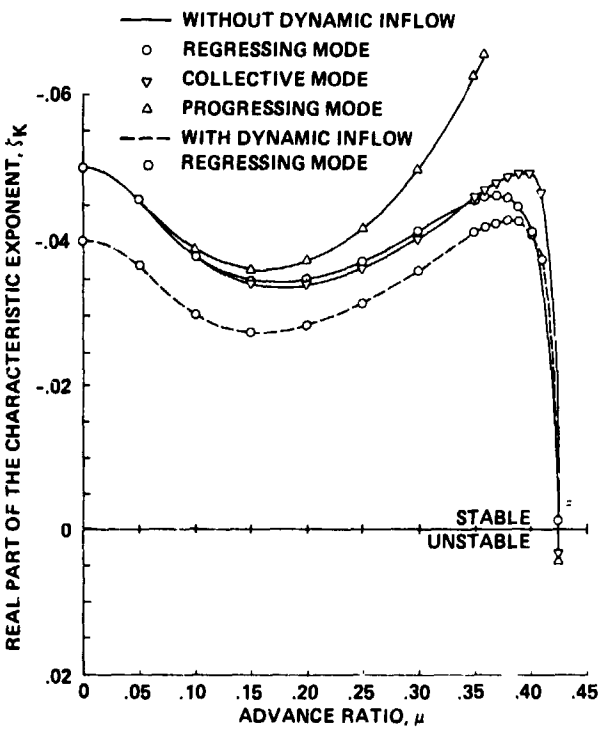

Fig. 16 Comparison of constant-coefficient approximation and Floquet analysis: stiff inplane, $\omega_\zeta = 1.4$, R = 1.0 (multiblade equations).

DISCUSSION
Paper No. 15

THE INFLUENCE OF DYNAMIC INFLOW AND TORSIONAL FLEXIBILITY ON ROTOR DAMPING IN FORWARD FLIGHT FROM SYMBOLICALLY GENERATED EQUATIONS
T. S. R. Reddy
and
William Warmbrodt

Peretz Friedmann, University of California, Los Angeles: I'd like to congratulate you on a very nice paper. Obviously I have a vested interest because for the last three years I have been waiting for somebody to redo the problem to find out whether Kottapalli and I have done it correctly. Now that you have shown these results and Neelakanthan has shown some results at the last European Forum where also the same trends were exhibited I guess I can sleep in peace. What I really wanted to emphasize are two things. One is the contribution you have made is a really significant one because as somebody who has derived equations by hand for a long time I definitely believe that the way to go is to use a computer. The second comment which I have--and it is in the form of a question--is if I correctly understand the results you have shown then it seems to be that dynamic inflow doesn't have an awful lot of influence in the case of coupled flap-lag-torsion in forward flight. I was wondering if you would agree with this statement?

Reddy: Yes, that's what our results show.

Wayne Johnson, NASA Ames Research Center: Following along these lines of what Peretz was discussing about using the computer: in dealing with this subject, if you were going to do the same work, but do it over again were there any pieces of the problem that you did with pencil and paper, [that you] did by hand that if you had to do it all over again you would automate these pieces also. In other words, was there anything left to put into the computer?

Reddy: Yes, we are now finding that the required input data has increased tremendously so we will have to change the program to minimize data inputs.

Friedrich Straub, Hughes Helicopters: How long did it take you to include the forward flight in the equations coming from the hover results?

Reddy: I attended the SDM Conference on the 14th to the 16th of May. Then we came back to this area and submitted the abstract--that was the end of May. We finished the paper by August, but most of this time was spent on developing the trim and response solution program, so it took even less time.

Bill Warmbrodt, NASA Ames Research Center: You might point out that the original derivation was done including the influence of forward flight; however, the program was first exercised to develop the hover results presented at the SDM Conference.

FLAP-LAG-TORSION STABILITY IN FORWARD FLIGHT

Brahmananda Panda
Graduate Student
and
Inderjit Chopra
Associate Professor

Center for Rotorcraft Education and Research
Department of Aerospace Engineering
University of Maryland
College Park, MD 20742

ABSTRACT

An aeroelastic stability of three-degree flap-lag-torsion blade in forward flight is examined. Quasisteady aerodynamics with a dynamic inflow model is used. The nonlinear time dependent periodic blade response is calculated using an iterative procedure based on Floquet theory. The periodic perturbation equations are solved for stability using Floquet transition matrix theory as well as constant coefficient approximation in the fixed reference frame. Results are presented for both stiff-inplane and soft-inplane blade configurations. The effects of several parameters on blade stability are examined, including structural coupling, pitch-flap and pitch-lag coupling, torsion stiffness, steady inflow distribution, dynamic inflow, blade response solution and constant coefficient approximation.

NOTATIONS

a	=	lift curve slope
$\underset{\sim}{A}$	=	matrix in first order equations in rotating system
$\underset{\sim}{A}_f$	=	matrix in first order equations in fixed system
$\underset{\sim}{B}_1, \underset{\sim}{B}_2$	=	matrices in dynamic inflow equations
c	=	blade chord
C_d	=	blade section drag coefficient
C_ℓ	=	blade section lift coefficient
C_m	=	blade section moment coefficient
$\underset{\sim}{C}_r, \underset{\sim}{C}_r^p$	=	damping matrices in response and perturbed equations respectively
C_T	=	thrust coefficient, $T/\pi\rho\Omega^2R^4$
C_w	=	weight coefficient, $W/\pi\rho\Omega^2R^4$
$C_{d_\alpha}, C_{\ell_\alpha}, C_{m_\alpha}$	=	differential aerodynamic coefficients wrt α
D	=	drag force of the helicopter
e	=	hinge offset divided by rotor radius
f	=	equivalent drag area of helicopter
$\underset{\sim}{F}_{NL}$	=	nonlinear force vector in response equation
I_b	=	moment Inertial of blade (flap)
I_f^*	=	ratio of torsional inertia to blade flap inertia
h	=	distance of hub from helicopter c.g.
H	=	rotor drag force, positive rearward
K_{p_β}, K_{p_ζ}	=	pitch-flap and pitch-lag couplings respectively
$\underset{\sim}{K}_r, \underset{\sim}{K}_r^p$	=	stiffness matrices in response and stabilty equations
K_x, K_y	=	coefficients in Drees model
$\underset{\sim}{\ell}, \underset{\sim}{m}$	=	coefficient matrices in dynamic inflow equation
$\underset{\sim}{M}_r, \underset{\sim}{M}_r^p$	=	mass matrices in response and stability equations
M_{xf}, M_{yf}	=	Aerodynamic rolling and pitching moments respectively
$M_\beta, M_\zeta, M_\theta$	=	aerodynamic flap, lag and pitch moments respectively
N_b	=	number of blades
$\underset{\sim}{N}_f$	=	matrix in fixed system defined by eqn. (29)
$\underset{\sim}{Q}$	=	transition matrix
R	=	rotor radius
R_s	=	structural coupling parameter

Presented at the Second Decennial Specialists' Meeting on Rotorcraft Dynamics at Ames Research Center, Moffett Field, CA, November 7-9, 1984.

T	=	rotor thrust force
U_p, U_t	=	blade section normal and inplane velocity
V	=	blade section resultant velocity, $\sqrt{U_t^2 + U_p^2}$
$\bar{V}$	=	forward speed
W	=	helicopter gross weight
x	=	blade radial coordinate (nondimensionalized wrt radius)
X_A	=	chordwise offset of blade aerodynamic center behind pitch axis
X_I	=	chordwise offset of blade center of gravity behind pitch axis
X_r	=	vector consisting degrees of freedom in rotating system
Y_r	=	state vector in rotating system
Y	=	rotor side force, positive towards advancing side
Y_f	=	fuselage side force
α	=	blade section angle of attack
α_k	=	real part of kth characteristic exponent
β,ζ,θ	=	angular deflections (flap, lag, torsion)
β_p	=	precone angle
γ	=	blade lock number, $\rho acR^4/I_b$
$\theta_0,\theta_{1c},\theta_{1s}$	=	collective, lateral cyclic, longitudinal cyclic pitch angles
λ	=	rotor inflow ratio
λ_k	=	kth characteristic exponent
μ	=	advance ratio, $V\cos\alpha/\Omega R$
$\nu_\beta,\nu_\zeta,\nu_\theta$	=	rotating flap, lag and torsional frequencies
ω_β, ω_ζ, ω_θ	=	nonrotating flap, lag and torsional frequencies
ρ	=	air density
σ	=	solidity ratio, $N_b c/\pi R$
ϕ	=	section induced angle, $\tan^{-1} U_p/U_t$
ϕ_s	=	lateral tilt of shaft
ψ	=	azimuth angle of the blade
ω_k	=	imaginary part of the kth exponent
Ω	=	speed of rotation
$\delta()$	=	perturbation quantity

INTRODUCTION

Several researchers have examined the aeroelastic stability of a helicopter blade in hover and forward flight (see recent reviews [1-3]). The phenomenon is complex involving nonlinear structural, inertial and aerodynamic forces. With a forward flight, the equations of blade motion get more involved because of the presence of many periodic terms. Due to the complexities of formulation and analysis of rotorary-wing dynamics problems, most of the analytical studies are of limited scope; more so, in forward flight conditions. The objective of the present paper is to examine aeroelastic stability in forward flight, including the effects of dynamic inflow on stability results. For this a simple flap-lag-torsion blade model consisting of three degrees of motion will be studied.

For design and analysis of a helicopter rotor, it is essential to analyze its aeroelastic stability. For this, a study on the dynamics of a single blade forms an important fundamental step to the complete understanding of the rotor-body dynamics. The blade stability analysis consists of three major phases; vehicle trim, blade steady response and stability of perturbation motion. The vehicle trim solution determines control settings for perscribed flight conditions and is calculated from the vehicle overall equilibrium equations. The blade response solution consists of time dependent blade position and is calculated from the blade equilibrium equations. In the calculations of blade response one needs the vehicle trim solution. For stability solution, a perturbation is given to the blade at its equilibrium position and the subsequent response amplitude is investigated for stability. For stability calculations, one needs the vehicle trim solution as well as blade response solution. These three phases of study are inherently coupled. A complete coupled solution is very involved and therefore most of the researchers uncouple these three phases and study each phase separately. It is possible however to achieve a certain degree of coupling between three phases through an iterative process.

The simplest form of a rotor blade representation is the rigid blade model with spring restrained hinges. Many researchers have examined the aeroelastic stability of this simple blade configuration. For example, Peter[4] and Kaza and Kvaternik[5] investigated the aeroelastic stability of two-degree flap-lag blade in forward flight. An improvement for this type of modelling is to introduce a third degree of motion, i.e., feather rotation. A better representation for a hingeless blade is to treat it as an elastic beam. As an example, Friedmann and Kottapalli[6] have investigated aeroelastic stability of flap bending, lag bending and torsion of an elastic hingeless blade in forward flight. In the present paper, a simple blade representation consisting of three degrees of motion, flap, lag and feather rotations, is used to study the stability phenomena in forward flight.

There are many forms of vehicle trim solutions available in literature. Johnson[7], for example, presented in a summary form many trim options. For free flight conditions, the control settings and the vehicle angles are determined from the satisfaction of three force and three moment equilibrium equations. One of the popular trim procedure is to neglect altogether yawing moment equilibrium equation and thereby neglect the influence of tail rotor on solution. This form of trim solution is used in the present paper. The next simple form of trim procedure[6] is to neglect the lateral force equilibrium equation, and thereby exclude the determination of lateral shaft tilt angle (ϕ_s) from equilibrium equations. Generally, this may cause only slight influence on trim and

stability solutions, because the shaft lateral tilt angle does not introduce any vertical flow component on the blade. Some researchers[4,5,8] have simplified the trim procedure further by assuming that the vehicle center of gravity lies at the rotor hub, and thereby neglect the equilibrium of pitching and rolling moments of the vehicle. This will cause cyclic flap angles β_{1c} and β_{1s} (with respect to hub plane) to be zero. Here, the control settings and shaft angle α_s are calculated from the vertical and longitudinal force equilibrium equations. This may again have a small influence on trim solution for free level flight conditions at low forward speeds. At high forward speeds, the cyclic flap angles are not small and therefore must not be neglected. Another form of trim procedure called moment trim is often used by many researchers[4,9,10], and for this the solution is calculated from the rolling moment and the pitching moment equilibrium equations. The force equilibrium equations are not considered. Here, the rotor cyclic controls (θ_{1c} and θ_{1s}) are calculated for a prescribed shaft angle α_s. Some people refer it as a wind tunnel trim and it can be quite different from propulsive trim[4,6].

The blade time dependent positon is calculated from blade equilibrium equations. These are coupled equations and contain nonlinear geometric terms as well as periodic terms. The objective is to calculate steady periodic response solution. In the present paper, the nonlinear equations are solved in the rotating frame in an iterative procedure based on Floquet theory[11]. A somewhat similar type of quasilinearization procedure was used by Friedmann and Kottapalli[6]. The solution contains all harmonics for flap, lag and torsion response amplitudes. Another popular method, harmonic balancing[12] (Fourier Series) is quite commonly used to calculate the blade steady response where response is assumed periodic and consists of sum of finite harmonics. This procedure gets quite involved for coupled systems with nonlinearities. Quite frequently, researchers[4] have obtained simple response solution using harmonic balance method where the flap response is assumed to undergo a single harmonic motion (β_0, β_{1c} and β_{1s}) and the lag and torsion responses are neglected. In literature[1,2], the importance of accurate determination of blade equilibrium position on blade stability has been pointed out, including nonlinear terms as well as higher blade harmonics.

For stability analysis, the perturbation equations of motion are linear about the blade equilibrium position and these equations contain many periodic terms. These linearized equations are solved using three different approaches in the present paper. The first approach[6] is to analyze the stability of the blade in the rotating reference frame using Floquet transition matrix theory. This approach is applicable if the inflow is assumed to be steady. The second and third approach analyze the stability or rotor perturbation equations in the fixed reference frame. It is assumed that the rotor is tracked and all the blades are identical. The blade equations in the rotating reference frame are transformed to the fixed reference frame as rotor equations using Fourier coordinate transformation[13]. In the present paper, these transformations are performed numerically and thus the working through the laborious algebraic expressions is avoided. In the second approach, the rotor equations in the fixed frame are solved using Floquet transition matrix theory. Through the coordinate transformation, many periodic terms present in the rotating frame get cancelled out in the fixed frame. Therefore, the rotor equations in the fixed frame contain only selected periodic terms, for example, third harmonic for three-bladed rotor and second and fourth harmonic for four-bladed rotor. In the third approach[14], a constant coefficient approximation is made by averaging out periodic terms and solving the resulting equations.

In all these three approaches an eigenanalysis is made and the nature of eigenvalues explains the stability of the blade. Another commonly used method[15] is numerical integration of complete equations. This approach is though simple in implementation, but is quite heavy from computation point of view.

For trim and response solutions, the quasi-steady approximation is used for the determination of aerodynamic loads. For the perturbation solution, the unsteady aerodynamics effects can be important and these are introduced in an approximate manner, through a dynamic inflow modelling. The effect of dynamic inflow on coupled flap-lag two degrees of motion in forward flight has been investigated earlier[9-10] and has been shown to be quite important for blade stability. In the present paper, the influence of inflow dynamics has been investigated for a coupled flap-lag-torsion motion with improved trim and response solutions. The dynamic inflow modelling is based on the actuator disk theory. This necessitates the transformation of blade aerodynamic forces to the fixed reference frame and therefore only second and third approach can be conveniently used to analyze blade stability.

In the paper, the effects of several parameters on blade stability is examined, including, structural coupling, pitch-flap coupling, pitch-lag coupling, lag stiffness, torsion stiffness, steady inflow distribution, dynamic inflow, blade response and constant coefficient approximation.

EQUATIONS OF MOTION

The blade is assumed to undergo three degrees of motion: rigid body flap, lag and feather rotations about hinges at the blade root, with hinge springs to obtain arbitrary natural frequencies. The hinge sequence is flap inboard, lag, and then feather outboard. The flap angle β is positive up the lag angle ζ is positive aft (opposite to rotation) and the feather angle θ is positive nose up. The equations of motion are derived for this configuration, and in general, terms up to second order are retained in the flap and lag equations and terms up to third order are retained in the feather equation. The equations are

Flap Equation:

$$\overset{**}{\beta} + \nu_\beta^2\beta + 2\omega_\beta\zeta_\beta\overset{*}{\beta} - 2\beta\overset{*}{\zeta} - \frac{3}{2}\frac{X_I}{R}(\overset{**}{\theta} + \theta)$$

$$+ I_f^*(\zeta\overset{**}{\theta} + \zeta\theta) + \frac{R_s}{\Delta}(\omega_\zeta^2 - \omega_\beta^2)\sin\theta\cos\theta$$

$$\zeta = \frac{M_\beta}{I_b\Omega^2} + \omega_\beta^2\beta_p \qquad (1)$$

Lag Equation:

$$\overset{**}{\zeta} + \nu_\zeta^2\zeta + 2\omega_\zeta\zeta_L\overset{*}{\zeta} + 2\beta\overset{*}{\beta} - \frac{3}{2}\frac{X_I}{R}(\theta\overset{**}{\theta} + 2\beta\overset{*}{\theta})$$

$$+ I_f^*\beta\theta + \frac{R_s}{\Delta}(\omega_\zeta^2 - \omega_\beta^2)\sin\theta\cos\theta\cdot\beta = M\zeta/I_b\Omega^2$$

Feather Equation:

$$I_f^*(\overset{**}{\theta} + \nu_\theta^2\theta + 2\omega_\theta\zeta_\theta\overset{*}{\theta} + \zeta\overset{**}{\beta} + \beta\zeta)$$

$$+ \frac{3}{2}\frac{X_I}{R}(-\theta\overset{**}{\zeta} + 2\frac{X_I}{R}\theta\overset{**}{\ } + \overset{**}{\ } + 2\beta\overset{*}{\zeta} - \beta) = \frac{M_\theta}{I_b\Omega^2}$$

$$+ I_f^*\omega_\theta^2\theta\ \text{con}$$

where I_f^* is the ratio of the feathering inertia to flapping inertia; X_I is the chordwise offset of the center of gravity from the pitch axis (positive aft), the ζ_β ζ_L and ζ_θ are the viscous damping coefficients; the ω_β, ω_ζ and ω_θ are the nonrotating natural frequencies of the blade (divided by rotational speed Ω) and β_p is the precone angle. The M_β, M_ζ, M_θ are the aerodynamic flap, lag and feather moments respectively. For a uniform blade the nondimensional rotating frequencies are given as

$$\nu_\beta^2 = 1 + \frac{3}{2}\frac{e}{1-e} + \frac{R_s}{\Delta}(\omega_\beta^2 + R_s(\omega_\zeta^2 - \omega_\beta^2)\sin^2\theta)$$

$$\nu_\zeta^2 = \frac{3}{2}\frac{e}{1-e} + \frac{R_s}{\Delta}(\omega_\zeta^2 - R_s(\omega_\zeta^2 - \omega_\beta^2)\sin^2\theta)$$

$$\nu_\theta^2 = 1 + \omega_\theta^2$$

$$\Delta = 1 + R_s(1-R_s)\frac{\omega_\beta^2 - \omega_\zeta^2}{\omega_\beta^2\ \omega_\zeta^2}\sin^2\theta$$

The e is the hinge offset (divided by radius of the blade) and R_s is the structural coupling parameter. A simple means of representing structural coupling effect in the rigid blade representation is illustrated in Fig. 1(a). It is used to characterize the hub to blade stiffness and is defined as

$$R_s = \frac{K_\zeta}{K_{\zeta_B}} = \frac{K_\beta}{K_{\beta_B}} \quad \text{where } K_\beta = \frac{K_{\beta_B}K_{\beta_H}}{K_{\beta_B}+K_{\beta_H}},\ K_\zeta = \frac{K_{\zeta_B}K_{\zeta_H}}{K_{\zeta_B}+K_{\zeta_H}}$$

K_β, K_ζ are the combined hub and blade stiffnesses in flap and lag directions. The R_s=0 represents the configuration with blade part as rigid and all the flexibility concentrated at the hub. The structural fully coupled is represented by R_s=1 and this idealizes flexible blade with rigid hub. The intermediate values of R_s represent the case where both blade as well as hub are flexible.

Quasisteady airfoil characteristics are used to obtain the aerodynamic forces. The perturbation section aerodynamic forces and pitch moment (in the shaft axis) are

$$\delta F_z = \frac{1}{2}\rho c[\delta U_t\{-\frac{U_p}{V}(U_tC_{\ell_\alpha} - U_pC_{d_\alpha}) + \frac{U_t^2}{V}C_\ell + C_\ell V$$

$$- C_d\frac{U_pU_t}{V}\} + \delta U_p\{-\frac{U_t}{V}(U_tC_{\ell_\alpha} - U_pC_{d_\alpha}) + \frac{U_pU_t}{V}C_\ell$$

$$- C_dV - U_p^2/V\,C_d\} + \delta\theta\{V(U_tC_{\ell_\alpha} - U_pC_{d_\alpha})\}]$$

$$\delta F_x = \frac{1}{2}\rho c[\delta U_t\{\frac{U_p}{V}(U_pC_{\ell_\alpha} + U_t\,C_{d_\alpha}) + \frac{U_pU_t}{V}C_\ell + C_dV$$

$$+ \frac{U_t^2}{V}C_J\} + \delta U_p\{-\frac{U_t}{V}(U_pC_{\ell_\alpha} + U_tC_{d_\alpha}) + \frac{U_p^2}{V}C_\ell$$

$$+ C_\ell V + \frac{U_pU_t}{V}C_d\} + \delta\theta\{V(U_pC_{\ell_\alpha} + U_tC_{d_\alpha})\}]$$

$$\delta M_a = \frac{1}{2}\rho c\ [\delta U_t\{2U_t(C_m - \frac{X_A}{c}C_\ell) + U_pC_{m_\alpha} - \frac{X_A}{c}U_pC_{\ell_\alpha}\}$$

$$+ \delta U_p\{2U_p(C_m - \frac{X_A}{c}C_\ell) - U_tC_{m_\alpha} + \frac{X_A}{c}U_t\,C_{\ell_\alpha}\}$$

$$+ \delta\theta\{V^2(C_{m_\alpha} - \frac{X_A}{c}C_{\ell_\alpha})\}] \qquad (2)$$

where X_A is the chordwise offset of the aerodynamic center from elastic axis (positive aft), c is the chord, V is the resultant velocity and U_p and U_t are airflow velocity components in tangential and normal directions (Fig. 1(b)). The steady and perturbation flow components for forward flight are

Steady:

$$U_t = \{x(1-e) - x(1-e)\overset{*}{\zeta} + \mu\sin\psi - \zeta\mu\cos\psi\}$$

$$U_p = \{\lambda - x(1-e)\ \beta\zeta + x(1-e)\overset{*}{\beta} + \mu\beta\cos\psi\}$$

Perturbation: (3)

$$\delta U_t = \{\delta\zeta\mu\cos\psi - x(1-e)\delta\overset{*}{\zeta}\}$$

$$\delta U_p = \{-x(1-e)\beta\delta\zeta - x(1-e)\zeta\delta\beta + x(1-e)\delta\overset{*}{\beta} +$$

$$\mu\delta\beta\cos\psi - \frac{c}{R}(\frac{1}{2} + \frac{X_A}{c})\overset{*}{\delta\theta}\}$$

The perturbation aerodynamic moments required for the stability analysis are written as

$$\delta M_\beta = \int_e^B x \cdot \delta F_z \cdot dx$$

$$\delta M_\zeta = \int_e^B x \cdot \delta F_x \, dx \qquad (4)$$

$$\delta M_\theta = \int_e^B \delta M_a \, dx + \int_e^B M_{NC} \, dx$$

where M_{NC} is the noncirculatory aerodynamic pitch moment and is expressed as

$$M_{nc} = \frac{1}{4}\pi\rho\Omega^2 c^3 R \left[\ddot{\beta}\left(\frac{1}{4}+\frac{X_A}{c}\right) - \frac{1}{4}\frac{c}{R}\left(\frac{2X_A}{c}+\frac{3}{8}\right)\right.$$
$$+ \dot{\beta}\left\{\mu\cos\psi\left(\frac{1}{4}+\frac{X_A}{c}\right) - \frac{1}{4}\frac{c}{R}\left(\frac{2X_A}{c}+\frac{3}{8}\right)\right\}$$
$$- \dot{\theta}\left\{(x+\mu\sin\psi)\left(\frac{1}{2}+\frac{X_A}{c}\right)\right\} \qquad (5)$$
$$\left. - \theta\left[\frac{x}{4} + \left(\frac{1}{2}+\frac{X_A}{c}\right)\mu\sin\psi\right]\right]$$

where x is the nondimensional distance from the hub and μ is the advance ratio ($V\cos\alpha_s/\Omega R$).

The final blade equations of motion in forward flight can be written as

$$\underset{\sim}{M}_r(\psi)\ddot{\underset{\sim}{X}}_r + \underset{\sim}{C}_r(\psi)\dot{\underset{\sim}{X}}_r + \underset{\sim}{K}_r(\psi)\underset{\sim}{X}_r = \underset{\sim}{F}_{NL}(\psi,\underset{\sim}{X}_r,\dot{\underset{\sim}{X}}_r) \qquad (6)$$

where the inertia matrix $\underset{\sim}{M}_r$, the damping matrix $\underset{\sim}{C}_r$ and stiffness matrix $\underset{\sim}{K}_r$ contain periodic terms. The vector $\underset{\sim}{X}_r$ consists of three states; flap, lag and torsion deflections in the rotating system. The (*) shown in the equations refers differentiations with respect to ψ and ψ is the azimuth angle (nondimensional time, Ωt). All the geometric nonlinearities are put into the force vector $\underset{\sim}{F}_{NL}$. The blade response is calculated from the solution of above equations.

For the stability solution, the flutter motion is assumed to be a small perturbation about the blade equilibrium position.

$$\underset{\sim}{X}_r = \underset{\sim}{X}_r + \delta\underset{\sim}{X}_r \qquad (7)$$

The final linearized perturbed equations are obtained as

$$\underset{\sim}{M}_r^p(\psi)\delta\ddot{\underset{\sim}{X}}_r + \underset{\sim}{C}_r^p(\psi,\underset{\sim}{X}_r,\dot{\underset{\sim}{X}}_r)\delta\dot{\underset{\sim}{X}}_r + \underset{\sim}{K}_r^p(\psi,\underset{\sim}{X}_r,\dot{\underset{\sim}{X}}_r)\delta\underset{\sim}{X}_r = 0 \qquad (8)$$

The perturbation inertia matrix $\underset{\sim}{M}_r^p$, damping matrix $\underset{\sim}{C}_r^p$, stiffness matrix $\underset{\sim}{K}_r^p$ also contain periodic terms. To determine blade stability one needs blade response solution. To calculate this blade response solution one needs the vehicle trim solution.

VEHICLE TRIM SOLUTION

The propulsion trim which is described here simulates the free flight condition. The trim solution in forward flight involves the calculations of pilot-control setting as well as the vehicle orientation for a prescribed flight conditions. For a specified weight coefficient C_w and a fixed forward speed (μ) the trim solution evaluates β_0, β_{1C}, β_{1s}, θ_0, θ_{1C}, θ_{1s}, α_{HP}, ϕ_s and λ. The trim solution is calculated from the vehicle equilibrium equations. Fig. 1(c) shows the forces and moments acting on the vehicle.

Vertical force equilibrium:

$$W - T\cos(\alpha - \theta_{FP})\cos\phi_s + D\sin\theta_{FP} - H\sin(\alpha - \theta_{FP}) + Y\sin\phi_s = 0 \qquad (9)$$

Longitudinal force equilibrium:

$$D\cos\theta_{FP} + H\cos(\alpha - \theta_{FP}) - T\sin(\alpha - \theta_{FP}) = 0 \qquad (10)$$

Lateral force equilibrium:

$$Y_f + Y\cos\phi_s + T\sin\phi_s = 0 \qquad (11)$$

Pitching moment:

$$M_y + M_{yf} - W(X_{cg} - h\sin\alpha) - D\cos(\alpha + \theta_{FP})h - D\sin(\alpha + \theta_{FP})\cdot X_{cg} = 0 \qquad (12)$$

Rolling moment:

$$M_x + M_{xf} + Y_f \cdot h\cos\phi_s + Y_f Y_{cg}\sin\phi_s + Wh\sin\phi_s - W Y_{cg}\cos\phi_s = 0 \qquad (13)$$

Where T is the rotor thrust and Y and H are the side and drag forces. These are five vehicle equilibrium equations. For trim solution one also needs rotor equilibrium equations in simplified form. These are

$$\frac{1}{2\pi}\int_0^{2\pi} (\text{Flapping equation})\, d\psi = 0 \qquad (14)$$

$$\frac{1}{2\pi}\int_0^{2\pi} (\text{Flapping equations})\cos\psi\, d\psi = 0 \qquad (15)$$

$$\frac{1}{2\pi}\int_0^{2\pi} (\text{Flapping equations})\sin\psi\, d\psi = 0 \qquad (16)$$

The induced inflow is related to the rotor thrust as

$$\lambda = \mu \tan \alpha + \frac{C_T}{2\sqrt{\mu^2+\lambda^2}} (1+k_x \cdot x \cos \psi + K_y \cdot x \sin \psi) \quad (17)$$

where K_x and K_y are obtained from Drees model[13] and is expressed as

$$K_x = 4/3[(1-1.8\mu^2)\sqrt{1 - (\lambda/\mu)^2} - \lambda/\mu]$$

$$K_y = -2\mu$$

For hover $K_x = K_y = 0$

These are nine equations with nine unknowns (β_0, β_{1c}, β_{1s}, θ_0, θ_{1c}, θ_{1s}, λ, α, ϕ_s) and these are solved numerically by iterative method.

BLADE RESPONSE SOLUTION

The blade response solution involves the determination of time dependent blade position and is calculated from the blade equations (6). For the calculation of response solution one needs vehicle trim solution. The nonlinear response solution is obtained from nonlinear periodic equations (6) using Floquet theory[11]. These equations are expressed in the state vector form

$$\dot{\underset{\sim}{Y}}_r - \underset{\sim}{A}(\psi)\underset{\sim}{Y}_r = \underset{\sim}{G}_r(\psi, \underset{\sim}{Y}_r, \dot{\underset{\sim}{Y}}_r) \quad (18)$$

where $\underset{\sim}{Y}_r$ is the state variable vector involving six states.

First a linear solution is calculated after dropping all nonlinear terms. For this the initial conditions are calculated from Floquet theory as

$$\underset{\sim}{Y}(0) = (\underset{\sim}{I} - \underset{\sim}{Q}(2\pi))^{-1} \underset{\sim}{Y}_e(2\pi) \quad (19)$$

where $\underset{\sim}{Y}_e(2\pi)$ is the complete solution after one revolution with rest initial conditions and $\underset{\sim}{Q}(2\pi)$ is the Floquet transition matrix. For numerical integration of the equations, a fourth order Runge-Kutta algorithm is used. The next step is to obtain the initial conditions for the complete nonlinear problem. This is done in an iterative manner. As a first guess, the above linear solution is used as an initial vector $\underset{\sim}{Y}_e(0)$ for the nonlinear solution and the complete response $\underset{\sim}{Y}_e(2\pi)$ after one revolution is calculated. The updated Floquet transition matrix $\underset{\sim}{Q}$ is function of response amplitude and is calculated by perturbing the estimated initial conditions $\underset{\sim}{Y}_e(0)$ by a small perturbation vector $\underset{\sim}{\varepsilon}$.

$$\underset{\sim}{Q}(2\pi) = [\frac{1}{\varepsilon_1}(\underset{\sim}{Y}^{(1)}(2\pi) - \underset{\sim}{Y}_e(2\pi)), \frac{1}{\varepsilon_2}(\underset{\sim}{Y}^{(2)}(2\pi) - \underset{\sim}{Y}_e(2\pi)), \ldots, \frac{1}{\varepsilon_6}(\underset{\sim}{Y}^{(6)}(2\pi) - \underset{\sim}{Y}_e(2\pi))] \quad (20)$$

Where $\underset{\sim}{Y}^{(i)}(2\pi)$ is the response with initial conditions of

$$\underset{\sim}{Y}_e(\iota) = \begin{Bmatrix} 0 \\ 0 \\ \varepsilon_i \\ 0 \end{Bmatrix} + \underset{\sim}{Y}_e(0)$$

So a new set of initial conditions for the nonlinear analysis are obtained

$$\underset{\sim}{Y}(0) = \underset{\sim}{Y}_e(0) + [\underset{\sim}{I} - \underset{\sim}{Q}]^{-1} (\underset{\sim}{Y}_e(2\pi) - \underset{\sim}{Y}_e(0)) \quad (21)$$

This procedure is repeated till a converged set of initial conditions is obtained. Typically it takes about 2 to 3 iterations to obtain converged solution. Once the initial conditions $\underset{\sim}{Y}(0)$ are obtained, then the total response $\underset{\sim}{Y}(\psi)$ for any time in a revolution is calculated numerically using time integration (Runge Kutta). This gives us the nonlinear equilibrium deflection of the blade along the azimuth.

FLUTTER SOLUTION

The linearized perturbed equations of motion (8) is written in the state vector form as

$$\dot{\delta\underset{\sim}{Y}}_r = A(\underset{\sim}{Y}_r, \dot{\underset{\sim}{Y}}_r, \psi)\delta\underset{\sim}{Y}_r \quad (22)$$

where $\underset{\sim}{Y}_r$, $\dot{\underset{\sim}{Y}}_r$ are the blade equillibrium position in the rotating reference frame and $\delta\underset{\sim}{Y}_r$ and $\dot{\delta\underset{\sim}{Y}}_r$ are perturbation states. These linearized equations are solved for stability using Floquet transition matrix theory[13]. Here the eigenvalues of transition matrix of A can be written in characteristic exponents form

$$\lambda_k = \alpha_k + i\omega_k \quad (23)$$

and the mode in stable when $\alpha_k < 0$.

For the perturbation solution the unsteady aerodynamics effect can be important and these are introduced in an approximate manner, through a dynamic inflow modelling. The wake inflow is perturbed about the steady inflow λ

$$\lambda = \lambda + \delta\lambda \quad (24)$$

where $\delta\lambda$ is the perturbed inflow component.

A linear variation of perturbed inflow is used

$$\delta\lambda = \delta\lambda_0 + \delta\lambda_{1C} \times \cos\psi + \delta\lambda_{1s} \times \sin\psi \quad (25)$$

The dynamic inflow components $\delta\lambda_0$, $\delta\lambda_{1C}$, $\delta\lambda_{1s}$ are related to rotor unsteady aerodynamic forces and moments

$$m\dot{\delta\lambda}^{*} + \ell^{-1}\,\delta\lambda = \delta F \qquad (26)$$

where $\delta F = \sum_{i=1}^{N_b} \begin{Bmatrix} \delta C_T \\ \delta C_{m_x} \\ \delta C_{m_y} \end{Bmatrix}_i \qquad \delta\lambda = \begin{Bmatrix} \delta\lambda_0 \\ \delta\lambda_{1s} \\ \delta\lambda_{1c} \end{Bmatrix}$

The δC_T, δC_{m_x}, δC_{m_y} are the perturbed thrust, roll moment and pitch moment and these are obtained for the ith blade. The $\underset{\sim}{m}$ and $\underset{\sim}{\ell}^{-1}$ matrices used here are evaluated analytically based on the actuator disk theory in Ref. 16. The nonzero elements of $\underset{\sim}{m}$ and $\underset{\sim}{\ell}$ are

$$m_{11} = \frac{128}{75\pi} \qquad m_{22} = m_{33} = -\frac{16}{45\pi}$$

$$\ell_{11} = \frac{1}{2v} \qquad \ell_{22} = \frac{\ell_{33}}{\sin\alpha} = -\frac{4}{1+\sin\alpha}\cdot\frac{1}{v}$$

$$\ell_{13} = \ell_{31} = \frac{15\pi}{64}\,\frac{1-\sin\alpha}{1+\sin\alpha}\cdot\frac{1}{v}$$

where $v = \dfrac{\mu^2+\lambda(\lambda+\lambda_1)}{\sqrt{\mu^2+\lambda^2}}$ and $\alpha = \tan^{-1}\left(\frac{\lambda}{\mu}\right)$

λ_1 is the induced inflow due to steady rotor thrust. This model gives a quite accurate description of dynamic inflow as concluded in reference 9.

The disk loading is approximated in terms of the blade loading, δF_z as

$$\delta C_T = \frac{\sigma a}{\gamma N_b} \sum_{k=1}^{N_b} \int_e^1 (\delta\bar{F}_z)_k \, dx$$

$$\delta C_{M_x} = -\frac{\sigma a}{\gamma N_b} \sum_{k=1}^{N_b} \int_e^1 (\delta\bar{F}_z)_k \, x\,dx \sin\psi_k \qquad (27)$$

$$\delta C_{M_y} = -\frac{\sigma a}{\gamma N_b} \sum_{k=1}^{N_b} \int_e^1 (\delta\bar{F}_z)_k \, x\,dx \cos\psi_k$$

With the inclusion of dynamic inflow, it is convenient to analyze blade stability in the fixed reference frame. The coupled blade equations are transformed to the fixed reference frame from rotating frame using Fourier co-ordinate transformation[13]. For four bladed rotor (N_b=4)

$$\frac{1}{N_b}\sum_{m=1}^{N_b} (\text{Differential equation}) \begin{Bmatrix} 1 \\ 2\cos\psi_m \\ 2\sin\psi_m \\ (-1)^m \end{Bmatrix} = 0 \qquad (28)$$

These transformations are carried out numerically. The final equations of motion in fixed co-ordinate frame can be written as

$$\dot{\delta\gamma}_F^{*} = \underset{\sim}{A}_f(\psi)\;\delta\gamma_F + \underset{\sim}{N}_f(\psi)\,\delta\lambda \qquad (29)$$

The unsteady force δF in dynamic inflow equations is given as

$$\delta F = \underset{\sim}{B}_1(\psi)\,\delta\gamma_F + \underset{\sim}{B}_2(\psi)\,\delta\lambda \qquad (30)$$

Putting together the rotor equations with the inflow equation, one gets

$$\begin{Bmatrix} \dot{\delta\gamma}_f^{*} \\ \dot{\delta\lambda}^{*} \end{Bmatrix} = \begin{bmatrix} \underset{\sim}{A}_f(\psi) & \underset{\sim}{N}_f(\psi) \\ \underset{\sim}{M}^{-1}\underset{\sim}{B}_1 & \underset{\sim}{M}^{-1}\underset{\sim}{B}_2 - \underset{\sim}{M}^{-1}\underset{\sim}{\ell}^{-1} \end{bmatrix} \begin{Bmatrix} \delta\gamma \\ \delta\lambda \end{Bmatrix} \qquad (31)$$

The above equations in the fixed frame contain only selected harmonics, for example third harmonic for 3 bladed rotor, second and fourth for 4 bladed rotor. These linearized periodic equations are solved using Floquet transition matrix theory and constant coefficient approximation approach. In the constant coefficient approximation approach the periodic terms are averaged out by applying the operator

$$\frac{1}{2\pi}\int_0^{2\pi} (\text{------})\, d\psi \qquad (32)$$

and then solved as an eigenvalue problem.

RESULTS AND DISCUSSION

The aeroelastic stability is examined for a four-bladed rotor with Lock number γ = 5.0, solidity ratio σ = 0.05, feather inertia to flap ratio I_f^{*}=0.0003 and with zero precone. The blade offsets such as the X_I, the chordwise center of gravity offset from pitch axis in terms of radius and X_A aerodynamic centre offset from elastic axis are set to zero. The

fuselage centre of gravity lies on the shaft axis and is assumed to be at a distance 0.2R below the rotor center. The aerofoil characteristics used are

$$C_\ell = 5.7\alpha$$

$$C_d = 0.01$$

$$C_m = -0.02$$

The helicopter drag coefficient in terms of flat plate area ratio ($f/\pi R^2$) of .01 is used. The blade flap and torsion frequencies (rotating) are 1.15/rev and 5.0/rev respectively. Two different lag frequencies are used; 0.57/rev for soft inplane rotor and 1.4/rev for stiff inplane rotor. The soft inplane rotor configuration was taken as a matched stiffness case ($\omega_\beta = \omega_\zeta$).

First, results were calculated for some selected cases to make comparison with those of other authors for identical conditions. The vehicle trim was calculated for uniform inflow conditon with the center of gravity lying at the rotor hub (h=0) and the results obtained were identical to those of Ref. 18. The blade stability of two-degree flap-lag blade was calculated using simple response solution (single flap harmonic) and for uniform steady inflow condition. The lag damping values calculated for various flight conditions were quite identical to those of Ref. 4. The inclusion of dynamic inflow on the stability of this two-degree motion blade was checked with the results of Ref. 9, and again, the comparison was quite satisfactory. Then, the flap-lag-torsion stability results were calculated for soft and stiff inplane configurations for steady inflow conditions. For perturbation solution, a nonlinear equilibrium position was used. The stability results showed some comparable trends with those of Ref. 6, in which results are obtained with improved structural modelling for the blade (elastic beam).

Figs. 2(a) and 2(b) show the vehicle trim solutions for $\frac{C_W}{\sigma}$ of .2 and .1 respectively. The propulsive trim parameters θ_0, θ_{1C}, θ_{1S}, α_{HP}, ϕ_s, λ, β_0, β_{1C}, β_{1S} are plotted for different forward speeds (in terms of advance ratio $\mu=\bar{V}/\Omega R$). The solution is calculated iteratively from nonlinear equilibrium equations (large angles). The flight path angle θ_{FP} is assumed to be zero. For steady inflow, a linear distribution model (Drees) is used. These trim parameters are defined in the hub plane axes system and so the cyclic flap angle β_{1C} is small for even large μ. For larger μ, the shaft has to tilt more to compensate the increase in parasite drag and hence α_{HP} increases with μ and thereby cause inflow λ to increase. For large thrust levels C_W/σ, control requirements are large but the angle α_{HP} is small. The reason for lower shaft angle at high C_W/σ is due to the fact that, for same parasite drag (for a given forward speed) the shaft has to tilt less to balance the parasite drag as the thrust magnitude is more. It is also observed that trim calculated from linearized equilibrium equations (small angles assumption) is quite close to the above nonlinear solution except for large advance ratios. The influence of inflow distribution is primarily on longitudinal and lateral cyclic pitch θ_{1S}, θ_{1C}. The effect of uniform inflow for $\frac{C_W}{\sigma} = 0.1$ is shown by dotted line in Fig. 2(b). The effect of inflow distribution on other trim parameters is quite small.

Figs. 3(a)-(c) present time dependent equilibrium position of blade for one complete revolution. The response solution in terms of flap, lag and torsion deflections (angles) is calculated iteratively from nonlinear blade equations (rotating frame) using the floquet theory described earlier. These results correspond to a $\frac{C_W}{\sigma} = 0.1$ and advance ratio $\mu = 0.2$. For comparison, the linear response solution (dotted) is also presented. The geometric nonlinearities are important for lag response and play less important role in flap and torsion response calculations.

For numerical results, a convergence study was conducted to determine time steps needed in one revolution for time integration (Runge-Kutta) for both response as well as stability calculations using Floquet Theory. It was concluded that 120 time steps are quite adequate for well converged (four significant-digit) response and stability solutions. For stability results, only the lowest damped lag mode is presented. The flap and torsion modes are comparitively high damped modes and are not presented here. The damping in terms of real part of complex eigenvalue, α_ζ is shown. Note $\alpha_\zeta = \zeta_L\omega_\zeta$, where ζ_L damping ratio of lag mode and ω_ζ/Ω is frequency of lag mode nondimensionalized with respect to rotational speed.

In Fig. 4, the effect of torsion flexibility on the blade stability is shown. For these solutions, the simple blade response is used and the stability roots are obtained in the rotating frame with steady uniform inflow conditions. There is a disparity between two results, clearly showing the importance of inclusion of torsion flexibility for blade stability analysis. This has been pointed out by other authors[6].

Fig. 5 shows the effect of blade response solutions on stability. The lag mode damping is calculated using three types of blade equilibrium solutions; these are complete nonlinear solution, linear solution and simple solution. The linear

and nonlinear solutions contain all harmonics for flap, lag and torsion modes whereas the simple solution consists of single flap harmonic only. These solutions are obtained in the rotating frame with steady uniform inflow conditions. Though it is computationally less involved to use simple response solution, the results are poor in accuracy. For accurate results it is needed to use a complete nonlinear blade response solution.

Fig. 6 presents the influence of steady inflow distribution on the blade stability. These solutions are obtained in the fixed frame with dynamic inflow included. In the figure the damping of the lowest damped, low frequency cyclic lag mode (regressive mode) is presented. Two types of steady inflow model are used; uniform distribution and linear distribution (Drees). The uniform distribution underpredicts lag damping. For subsequent results, the linear inflow model (Drees) is used.

Figs. 7 and 8 present the damping of low frequency cyclic lag mode for different advance ratio μ. Three sets of results are shown and these respectively represent dynamic inflow Floquet results (full line), dynamic inflow constant coefficient approximation results (big dots) and steady inflow results (small dots). In Figures 7(a) and 7(b), the stability results are shown for stiff inplane rotor for C_W/σ = .1 and .2 respectively. For this case the low frequency mode is a regressive mode. The constant coefficient approximation is quite satisfactory for small advance ratios μ. The inclusion of dynamic inflow is important for low forward speeds. This shows that for large forward speeds unsteady aerodynamic effects are not important and quasisteady approximation is quite adequate for blade stability analysis. At large thrust levels the influence of dynamic inflow and constant coefficient approximation is large because of larger aerodynamic forces involved. Figs. 8(a) and 8(b) show the blade stability results for soft inplane rotor for C_W/σ of .1 and .2 respectively. For this case the low frequency mode is a progressive mode. Again for the matched stiffness configuration, the results are quite identical to the stiff configuration. Constant coefficient approximation less satisfactory for high advance ratios, the dynamic inflow inclusion is more important for low advance ratios.

In Figs. 9 and 10 the effect of structural coupling on lag mode stability is presented for stiff inplane and soft inplane rotors respectively for C_W/σ of 0.1. The earlier results were calculated for blades with no structural coupling (R_S=0). This idealizes the configurations with blade part as rigid and all the flexibility concentrated at the hub. The structurally fully coupled is represented by R_S=1 and this idealizes flexible blade with rigid hub. The value of R_S less than 1 represents intermediate cases where both blade as well as hub are flexible. The stability results are obtained using Floquet theory with dynamic inflow effects included. The structural coupling has an important effect on blade stability for stiff inplane rotor. In fact with large structural coupling the blade becomes more stable. This is because with a large structural coupling R_S, the weakly damped lag mode gets coupled with well damped flap mode and thereby stabilizes the lag mode. The effect of structural coupling is negligible on the soft lag configuration and this is because the configuration considered is matched stiffness case. On these figures the results are also plotted with steady linear inflow aerodynamics. For stiff lag rotors, the effect of inclusion of dynamic inflow is large for configurations with zero structural coupling, and the influence is quite stabilizing. With large structural coupling R_S, the effect of dynamic inflow is less and it is destabilizing.

Figs. 11 and 12 show the effect of torsional stiffness on lag mode stability for stiff inplane and soft inplane rotors for C_W/σ of .1. Results are obtained for three different torsional frequencies and these are 2.5, 5 and 10 per revolution. For both soft inplane and stiff inplane rotors, increasing torional stiffness increases lag damping (more stable) for lower forward speeds (low μ) and decrease lag damping (less stable) at higher forward speeds.

The effect of pitch-flap and pitch-lag coupling terms on blade stability is studied by modifying the feather angle in the flap-lag equations (two-degree-of-freedom)

$$\theta_{eff} = \theta - K_{p_\beta}\,\beta - K_{p_\zeta}\,\zeta$$

The pitch-flap coupling K_{p_β} is positive flap up/pitch down, and the pitch-lag coupling is positive lag back/pitch down. These couplings are caused due to torsion dynamics or kinematic couplings. Figs. 13(a) and 13(b) show the influence of pitch-lag coupling on lag mode stability for stiff inplane and soft inplane rotors respectively for C_W/σ of 0.1. The positive pitch-lag coupling stabilizes the low freguency cyclic lag mode for stiff inplane rotors, and destablizes this lag mode for soft inplane rotors. The opposite effect is seen with the negative pitch-lag coupling. A similar type of observation is made for hovering blade stability in Ref. 17. Figs. 14(a) and 14(b) show the effect of pitch-flap coupling on lag mode stability for stiff inplane and soft inplane rotors respectively for C_W/σ of 0.1. A negative pitch-flap coupling reduces the flap frequency, and it produces a

stabilizing effect on lag mode for low forward speeds and a destabilizing effect at higher forward speeds. A positive pitch-flap coupling raises the flap frequency, and it has a comparatively small effect on lag mode stability. Also, it can be seen the effect of pitch-flap coupling on blade stability is much smaller as compared to that of pitch-lag coupling.

CONCLUSIONS

An aeroelastic stability of a simple three-degree-of-freedom blade model in forward flight is examined. The nonlinear time dependent blade equilibrium position is calculated using a quasilinearization procedure based on Floquet theory. The perturbation solution is obtained using Floquet transition matrix theory as well as constant coefficient approximation in the fixed reference frame. The stability results are calculated for both stiff-inplane and soft-inplane blade configurations. The inclusion of torsion degree of motion is important for blade stability. The nonlinear time dependent periodic blade response has a significant influence on blade stability. For steady inflow distribution, the linear variation (Drees) is somewhat stabilizing for lag mode damping as compared to uniform distribution. The effect of dynamic inflow on lag mode stability is small at high forward speeds ($\mu > .3$). The constant coefficient approximation appears satisfactory for low forward speeds ($\mu < .2$). The structural coupling produces stabilizing effect on blade stability for stiff lag rotors. For matched-stiffness configurations, there is no effect of structural coupling on blade stability. Raising of torsional stiffness increases lag mode damping (more stable) at lower forward speeds ($\mu < .15$) and decreases lag damping (less stable) at higher forward speeds ($\mu > .15$). A positive pitch-lag coupling stabilizes the low frequency cyclic lag mode for stiff lag rotors and destabilizes this mode for soft-lag rotors. An opposite effect is seen with negative pitch-lag coupling. The effect of pitch-flap coupling on lag mode damping is small as compared to pitch-lag coupling effect. The negative pitch-flap coupling stabilizes lag mode at low forward speeds and destabilizes it at higher forward speeds. The positive pitch-flap coupling has a little influence on lag mode stability.

REFERENCES

1. Ormiston, R.A., "Investigation of Hingeless Rotor Stability," Vertica, Vol. 7, No. 2, 1983, pp. 143-181.

2. Friedmann, P.P., "Recent Development in Rotoray-Wing Aeroelasticity," Journal of Aircraft, Vol. 14, No. 11, Nov. 1977, pp. 1027-1041.

3. Friedmann, P.P., "Formulation and Solution of Rotary-Wings Aeroelastic Stability and Response Problems," Vertica, Vol. 7, No. 2, 1983, pp. 101-141.

4. Peters, D.A., "Flap-Lag Stability of Helicopter Rotor Blades in Forward Flight," Journal of the American Helicopter Society, Vol. 20, No. 4, Oct. 1975, pp. 2-13.

5. Kaza, K.R.V. and Kvaternik, R.G., "Examination of Flap-Lag Stability of Rigid Articulated Rotor Blades," Journal of Aircraft, Vol. 16, No. 12, December 1979, pp. 876-884.

6. Friedmann, P.P. and Kottapalli, S.B.R., "Coupled Flap-Lag-Torsional Dynamics of Hingeless Rotor Blades in Forward Flight," Journal of the American Helicopter Society, Vol. 27, No. 4, Oct. 1982, pp. 28-36.

7. Johnson, W., "A Comprehensive Analytical Model of Rotorcraft Aerodynamics and Dynamics:Part I," NASATM81182, USAAVRADCOM TR80-A-5, June 1980.

8. Friedmann, P.P. and Shamie, J., "Aeroelastic Stability of Trimmed Helicopter Blades in Forward Flight," Vertica, Vol. 1, No. 3, 1977, pp. 189-211.

9. Gaonkar, G.H., Sastry, V.V.S.S., Reddy, T.S.R., Nagabhushanam, J., Peters, D.A., "The Use of Actuator Disc Dynamic Inflow for Helicopter Flap-Lag Stability," Journal of the American Helicopter Society, Vol. 28, No. 3, July 1983, pp. 79-88.

10. Peters, D.A. and Gaonkar, G.H., "Thoretical Flap-Lag Damping with Various Dynamic Inflow Models," Journal of the American Helicopter Society, Vol. 25, No. 3, July 1980, pp. 29-36.

11. Dugundji, J. and Wendell, H., "Some Analysis Methods for Rotating Systems with Periodic Coefficients," AIAA Journal, Vol. 21, No. 6, June 1983, pp. 890-897.

12. Peters, D.A. and Ormiston, R.A., "Flapping Response Characteristics of Hingeless Rotor Blades by a Generalized Harmonic Balance Method," NASA TN D-7856, Feb. 1975.

13. Johnson, W., "Helicopter Theory," Princeton University Press, Princeton, New Jersey, 1980.

14. Biggers, J.C., "Some Approximation to the Flapping Stability of Helicopter Rotors," Journal of the American Helicopter Society, Vol. 9, No. 4, Oct. 1974, pp. 24-33.

15. Chopra, I., "Dynamic Analysis of Constant-Lift and Free-Tip Rotors," Journal of the American Helicopter Society, Vol. 28, No. 1, Jan. 1983, pp. 24-33.

16. Pitt, D.M. and Peters, D.A., "Theoretical Prediction of Dynamic Inflow Derivatives," Vertica, Vol. 5, No. 1, 1981, pp. 21-34.

17. Ormiston, R.A. and Hodges, D.H., "Linear Flap-Lag Dynamics of Hingeless Helicopter Rotor Blades in Hover," Journal of the American Helicopter Society, Vol. 17, No. 2, April 1972, pp. 1-14.

18. Straub, F.K. and Friedmann, P.P., "A Galerkin type Finite Element method for rotary-wing aeroelasticity," Vertica, Vol. 5, No. 1, 1981, pp. 75-98.

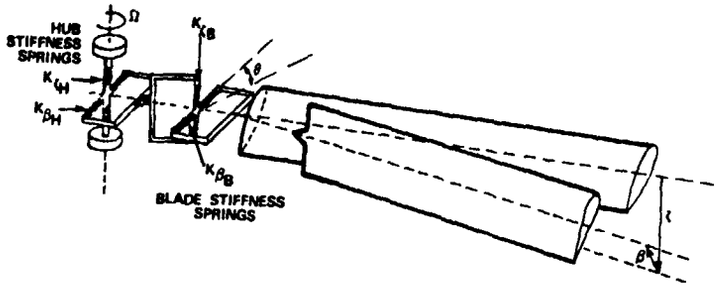

Fig. 1(a) Spring model for elastic blade and hub

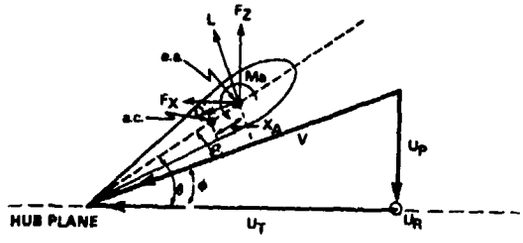

Fig. 1(b) Blade section Aerodynamics

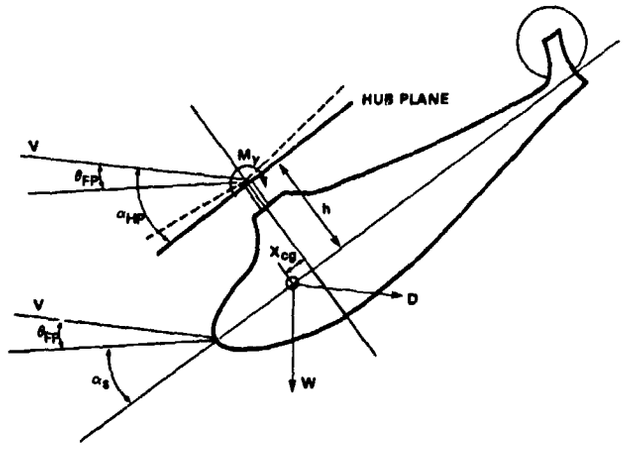

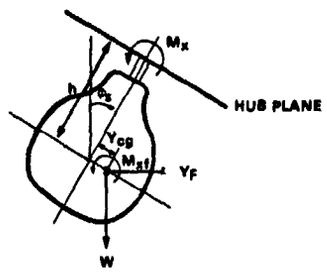

Fig. 1(c) Helicopter in forward flight showing vehicle trim configuration

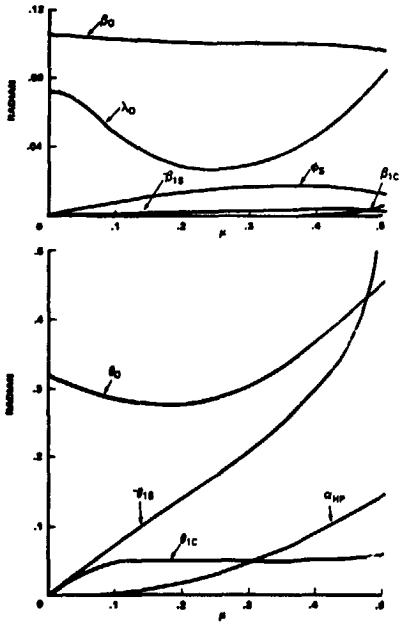

Fig. 2(a) C_W/σ = 0.2

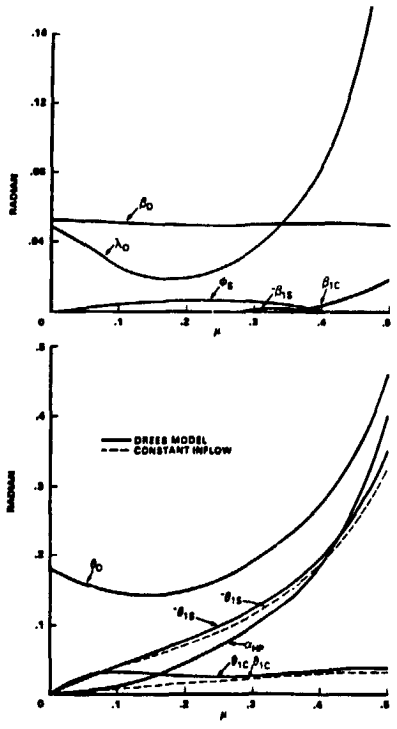

Fig. 2(b) C_W/σ = 0.1

Fig. 2 Vehicle propulsive trim (γ=5.0, σ=0.05, N_b=4, ν_β=1.15)

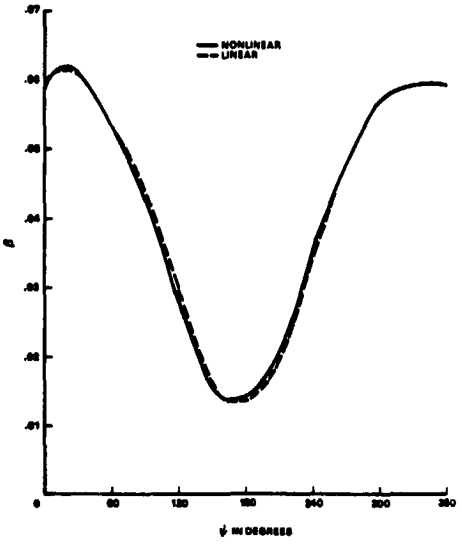

Fig. 3(a) Flap equilibrium angle

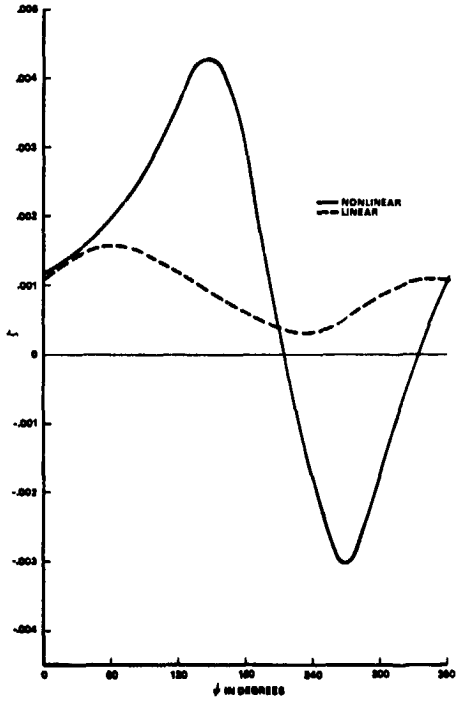

Fig. 3(b) Lag equilibrium angle

Fig. 3 Blade equilibrium position for C_W/σ=0.1 and μ=0.2

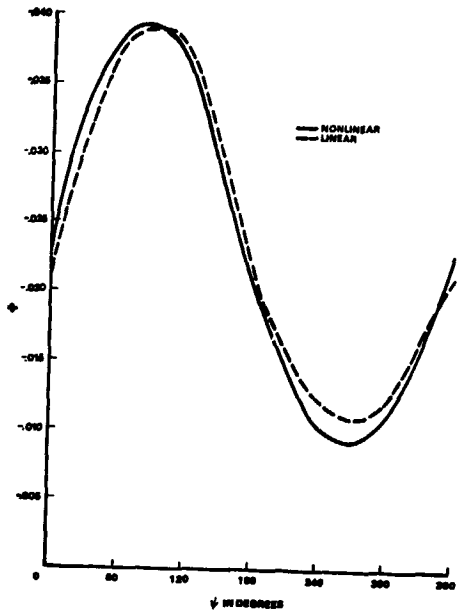

Fig. 3(c) Torsion equilibrium angle

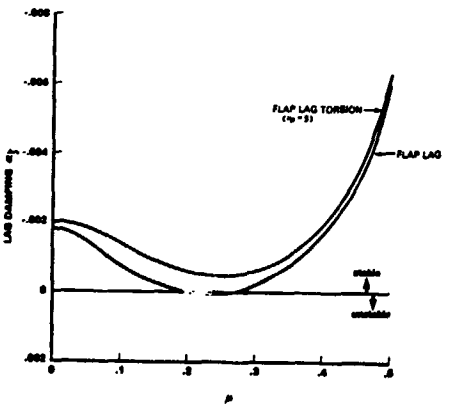

Fig. 4 Effect of torsion degree of freedom on lag mode stability for $C_W/\sigma=0.2$ ($\nu_\beta=1.15$, $\nu_\zeta=1.4$, $R_S=0$, steady uniform inflow)

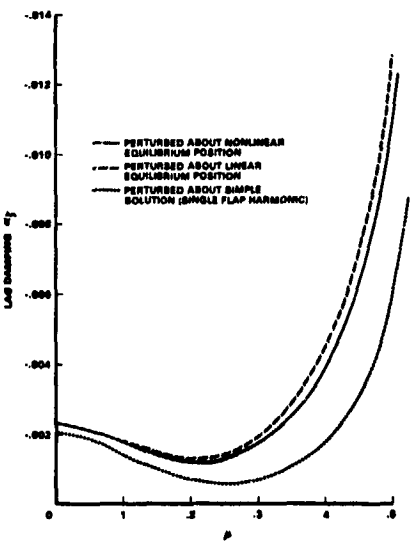

Fig. 5 Effect of blade response solutions on lag mode stability for $C_W/\sigma=0.2$ ($\nu_\beta=1.15$, $\nu_\zeta=1.4$, $\nu_\theta=5$, $R_S=0$, steady uniform inflow)

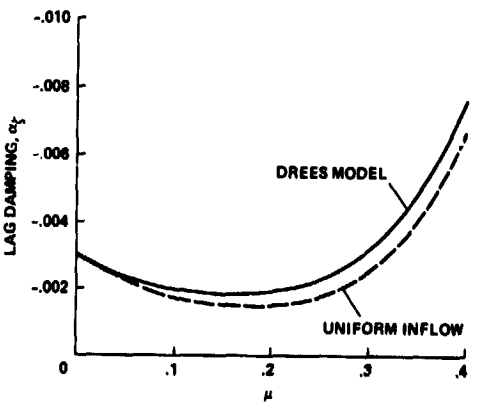

Fig. 6 Effect of steady inflow on low frequency cyclic lag mode (Regressive) stability for $C_W/\sigma=0.1$ ($\nu_\beta=1.15$, $\nu_\zeta=1.4$, $\nu_\theta=5$, $R_S=0$, Dynamic Inflow)

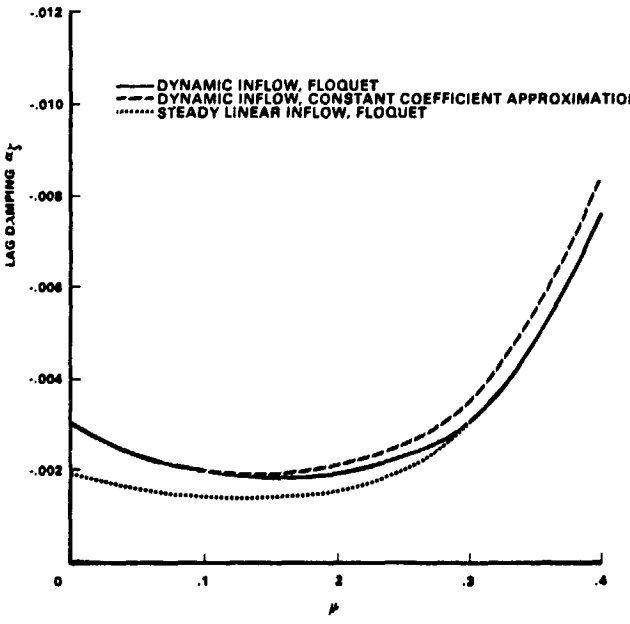

Fig. 7(a) Stiff-lag rotor, $C_w/\sigma=0.1$

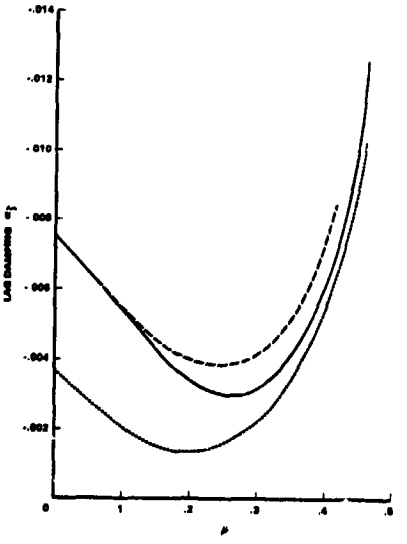

Fig. 7(b) Stiff-lag rotor, $C_w/\sigma=0.2$

Fig. 7 Damping of low frequency cyclic lag mode for different advance ratio μ for a stiff lag rotor (ν =1.15, ν_ζ=1.4, ν_θ=5, R_s=0)

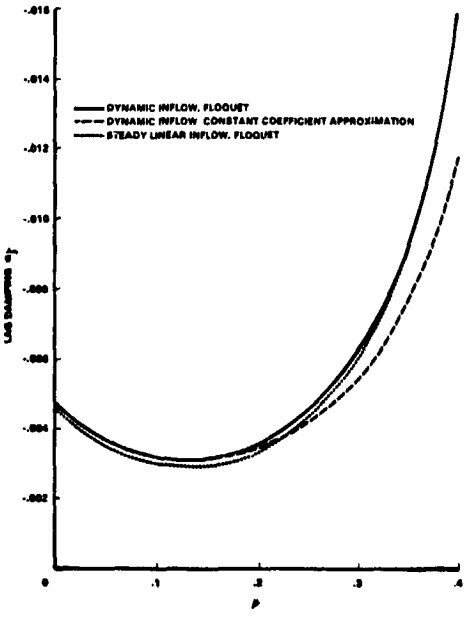

Fig. 8(a) Soft lag rotor, $C_w/\sigma=0.1$

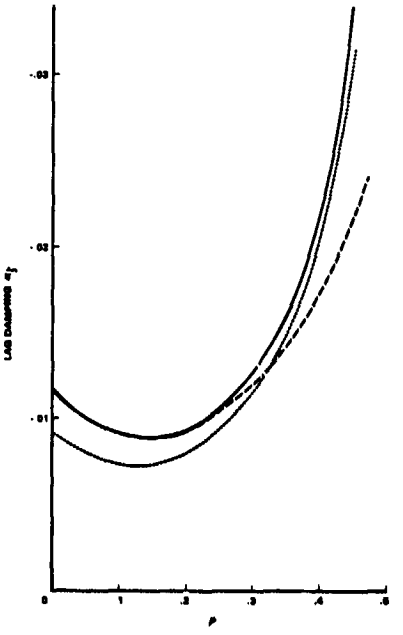

Fig. 8(b) Soft lag rotor, $C_w/\sigma=0.2$

Fig. 8 Damping of low frequency cyclic lag mode for different advance ratios of soft-lag rotor (ν_β=1.5, ν_ζ=0.57, ν_θ=5, R_s=0)

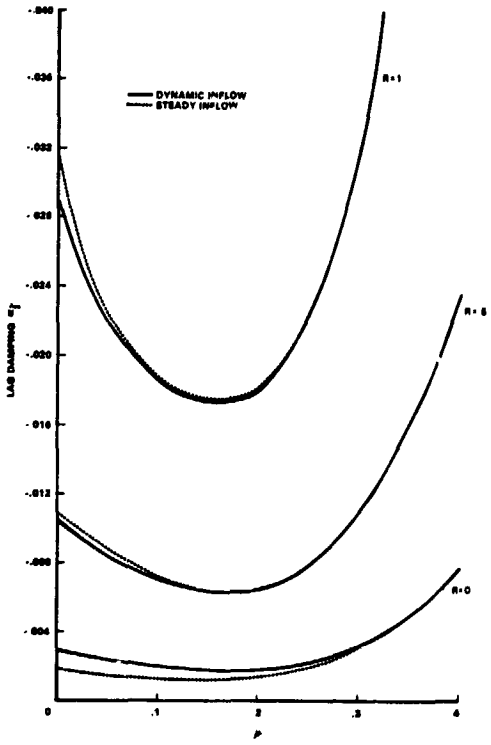

Fig. 9 Effect of structural coupling on low frequency cyclic mode (regressive) for stiff inplane rotor for $C_W/\sigma=.1$ ($\nu_\beta=1.5$, $\nu_\zeta=1.4$, $\nu_\theta=5$)

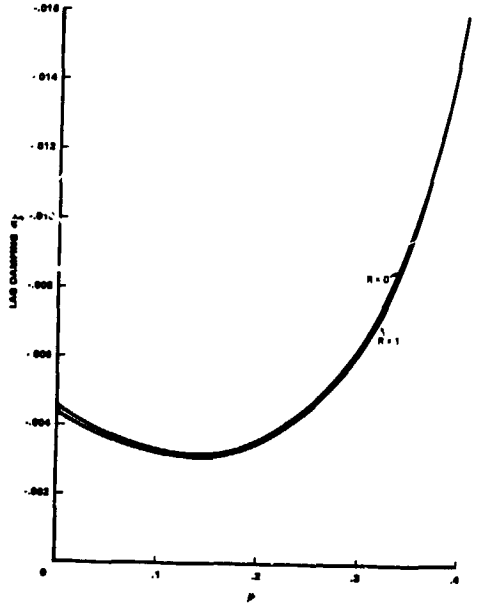

Fig. 10 Effect of structural coupling on low frequency cyclic mode for soft lag rotor ($C_W/\sigma=.1$, $\nu_\beta=1.15$, $\nu_\zeta=0.57$, $\nu_\theta=5$)

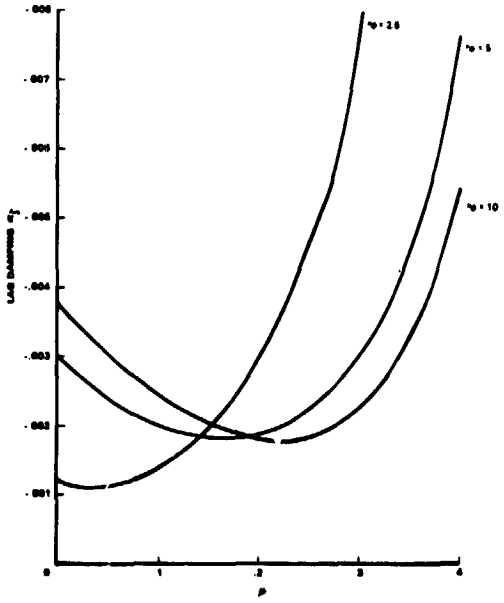

Fig. 11 Effect of torsional stiffness on low frequency cyclic mode for stiff lag rotor ($C_W/\sigma=.1$, $\nu_\beta=1.15$, $\nu_\zeta=1.4$, $R_S=0$, Dynamic Inflow)

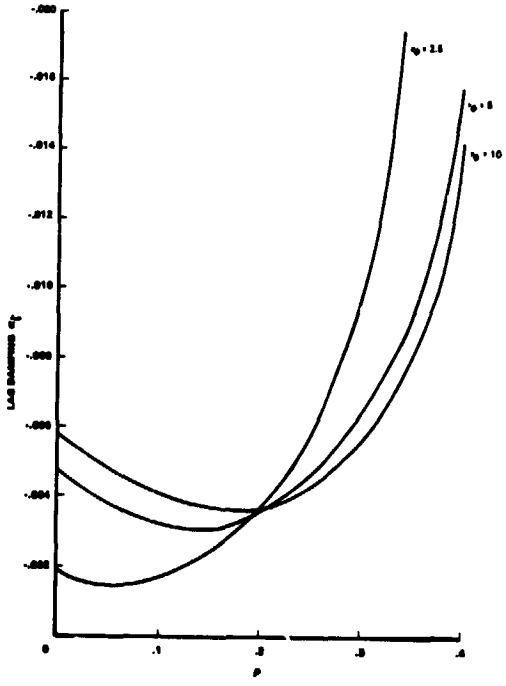

Fig. 12 Effect of torsional stiffness on low frequency cyclic mode for soft lag rotor ($C_W/\sigma=.1$, $\nu_\beta=1.15$, $\nu_\zeta=.57$, $R_S=0$, Dynamic Inflow)

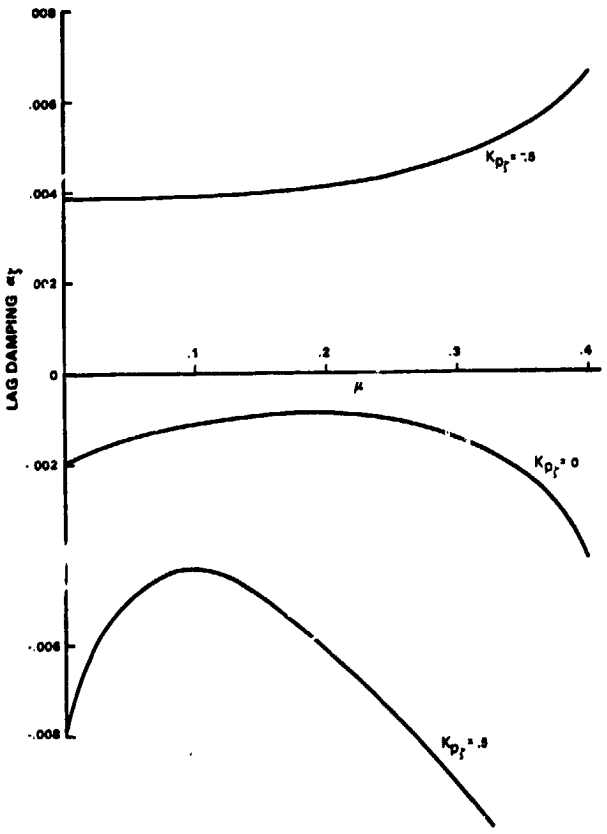

Fig. 13(a) Stiff lag rotor, ν_ζ=1.4

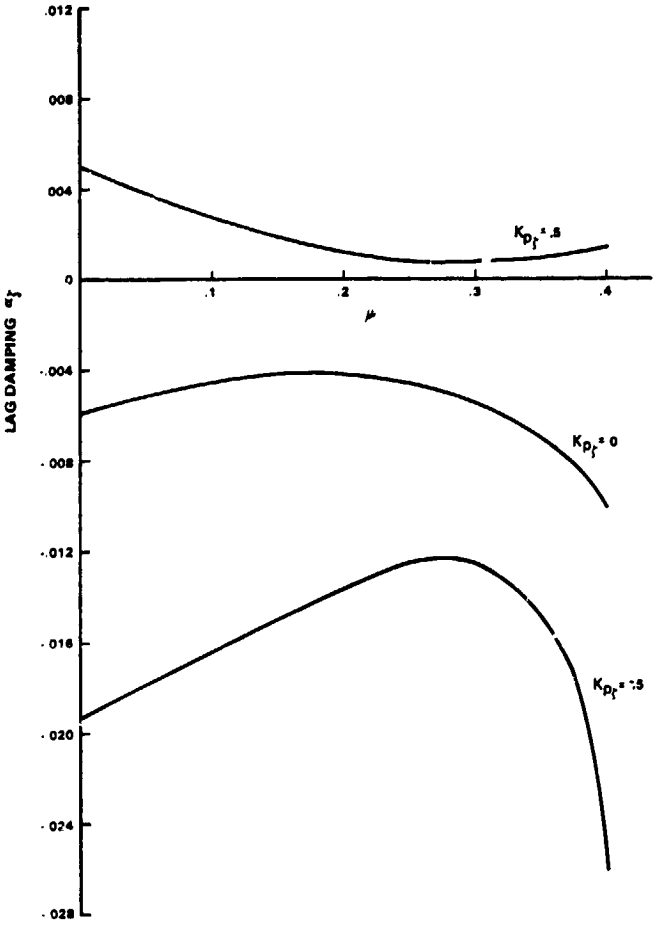

Fig. 13(b) Soft lag rotor, ν_ζ=.57

Fig. 13 Effect of pitch-lag coupling on low frequency cyclic lag mode (C_W/σ=.1, ν_β=1.15, R_S=0, Dynamic Inflow)

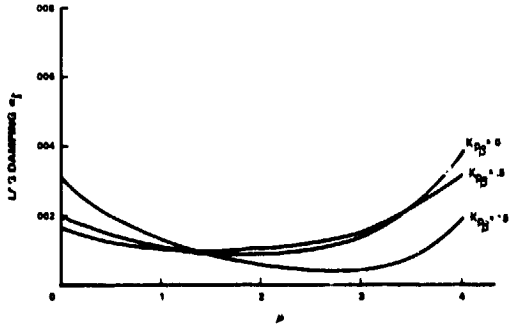

Fig. 14(a) Stiff lag rotor, ν_ζ=1.4

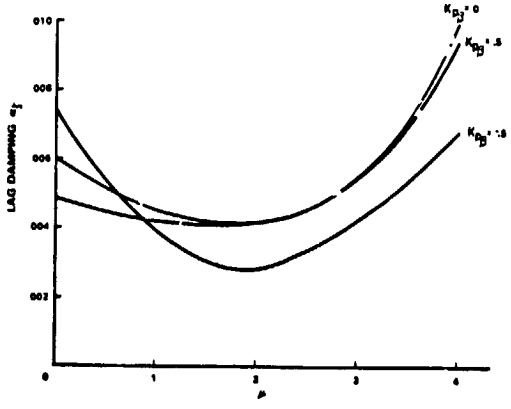

Fig. 14(b) Soft lag rotor, ν_ζ=.57

Fig. 14 Effect of pitch-flap coupling on low frequency cyclic lag mode (C_W/σ=.1, ν_β=1.15, R_S=0, Dynamic Inflow)

DISCUSSION
Paper No. 16

FLAP-LAG-TORSION STABILITY IN FORWARD FLIGHT
Brahmananda Panda
and
Inderjit Chopra

Wayne Johnson, NASA Ames Research Center: Could you describe again the manner in which you trimmed the rotor in forward flight? I noticed in your plot of flapping motion that you had about one degree of 1 per rev flapping motion, so could you tell us how the rotor was trimmed for these results?

Panda: First, we obtained the vehicle trim equations and calculate the control θ_o, θ_{1c}, and θ_{1s}. And using that with the coupled flap-lag-torsion blade equations for solving the trim.

Johnson: Did you trim to zero moment about some center of gravity of a helicopter below the rotor hub, is that what you did?

Panda: Yes.

Peretz Friedmann, University of California, Los Angeles: I wanted to be sure that I understand what kind of model you are using. You have an offset-hinged, spring-restrained blade model with flap, lag, and torsion degrees of freedom, is that correct?

Panda: Yes.

Friedmann: Then I just wanted to comment that at the European Rotorcraft Forum this August a gentleman by the name of Neelakanthan did exactly the same problem. He also did the elastic blade with two flap, two lag, and two torsional degrees of freedom and his results indicated that the model you are using is not safe at all times, so I am just suggesting that maybe you should qualify your conclusions.

Bill Bousman, U.S. Army Aeromechanics Laboratory: I haven't had time to look at these last two papers, but I think that most of the stuff Peretz has done over the years and other people--Dave Peters--has not shown an instability at high speed and there is none shown here in the lag mode. It's just the continuing stabilizing effect as the inflow increases. Dr. Reddy showed Floquet splitting roots and a destabilizing effect and I guess it's an open question [whether] this is something new. Was it just that his torsion [frequency] was 3 per rev or what?

Friedmann: I just wanted to say, Bill, that the instability that Reddy has shown is one which appeared for a stiff inplane case in the paper which Kottapalli and I have written and he just checked it out and he got the same instability.

DYNAMIC STABILITY OF A BEARINGLESS CIRCULATION CONTROL ROTOR BLADE IN HOVER

Inderjit Chopra
Center for Rotorcraft Education and Research
Department of Aerospace Engineering
University of Maryland
College Park, MD 20742

Abstract

The aeroelastic stability of flap bending, lead-lag bending and torsion of a bearingless circulation control rotor blade in hover is investigated using a finite element formulation based on Hamilton's principle. The flexbeam, the torque tube and the outboard blade are discretized into beam elements, each with fifteen nodal degrees of freedom. Quasisteady strip theory is used to evaluate the aerodynamic forces and the airfoil characteristics are represented either in the form of simple analytical expressions or in the form of data tables. The unsteady aerodynamic effects are introduced approximately through dynamic wake induced inflow modeling. The nonlinear equations of motion are solved for steady blade deflections using an iterative procedure. The flutter solution is calculated assuming blade motion to be a small perturbation about the steady solution, and the normal mode equations are used to reduce the number of equations. A correlation study of analytical results with the experimental data is attempted for selected bearingless blade configurations with conventional airfoil characteristics. Then stability results are obtained for circulation control bearingless configurations consisting of a single flexbeam with a wrap-around type torque tube and the pitch links located at both the leading edge and the trailing edge of the torque tube. The stability is examined at various thrust levels and collective pitch settings.

NOMENCLATURE

a_r	reference lift curve slope (5.7/rad)
c	blade chord, m
c_d	blade section drag coefficient
c_ℓ	blade section lift coefficient
$c_{m_{.5}}$	blade section moment coefficient about midchord
C_T	rotor thrust coefficient $\frac{T}{\rho(\Omega R)^2 \pi R^2}$
C_μ	blowing momentum coefficient $\frac{\dot{m}V_j}{1/2\rho V^2 c}$
d	pitch link location from torque tube center, m
D	blade section drag force, N
e_d	aerodynamic center offset from elastic axis, positive aft, m
e_g	center of mass offset from elastic axis, positive forward, m
I_b	blade mass moment of inertia about flap axis, N-m-sec^2
L	blade section lift force, N
L_u, L_v, L_w	aerodynamic force per unit length in u,v,w, directions, N/m
m	mass per unit length of blade, N-sec^2/m^2
m_o	reference mass per unit length, N-sec^2/m^2
$M_{.5}$	blade section aerodynamic moment about midchord, N-m
M_ϕ	aerodynamic moment per unit length about elastic axis, N
n	number of elements
s	constant defining blowing distribution
R	rotor radius, m
t	time, sec
$u,v,w,$	elastic displacements in the x,y,z directions respectively, m
u_p	blade section normal velocity, m/sec
u_T	blade section inplane velocity, m/sec
V	blade section resultant air velocity, m/sec
v_i	induced inflow, m/sec
V_j	jet velocity (blowing), m/sec
w_p	pitch link displacement, m
$x,y,z,$	undeformed blade coordinates, m

Presented at the Second Decennial Specialists' Meeting on Rotorcraft Dynamics at Ames Research Center, Moffett Field, CA, November 7-9, 1984.

a	blade section angle of attack, rad
β_p	blade precone angle, rad
γ	Lock number $\rho a_r c R^4/I_b$
ρ	air density, N-sec^2/m^4
$\delta T, \delta V$	variation of kinetic and strain energies respectively
δW	virtual work done due to aerodynamic loads
θ	blade pretwist, rad
λ	rotor induced inflow ratio, $v_i/\Omega R$
ξ, η, ζ	deformed blade coordinates nondimensionalized wrt R
σ	solidity ratio, blade area/disk area
ϕ	elastic twist about elastic axis, rad
$\$$	geometric apparent twist about deflected elastic axis, due to coordinate transformations, rad
ψ	dimensionless time, Ωt
$\omega_v, \omega_w, \omega_\phi$	fundamental coupled rotating lead-lag, flap and torsion natural frequencies respectively
Ω	rotor blade angular speed, rad/sec
ζ	ratio of modal damping to critical damping
η_t	torque tube center offset from elastic axis, positive forward, m
η_f	flexbeam center offset from elastic axis, positive forward, m

Introduction

A circulation control rotor (CCR) utilizes circulation control (CC) aerodynamics for main rotor blade design. A CC airfoil is typically of quasi-elliptic profile with rounded trailing edge, and a thin jet of air is blown from a spanwise slot (Fig. 1). The air jet remains attached over the curved profile because of Coanda effect (balance of centrifugal force and suction pressure). In a CCR, the thrust vector can be controlled by modulation of blowing as well as geometric pitch. With a CCR, a high thrust is possible at reduced tip speeds and also the hub design can be simplified because of elimination of cyclic pitch. The application of CC technology is currently being evaluated in the design development of a full-scale rotor. One concern is the influence of blowing on the dynamics of the rotor blade.

With the availability of improved materials, recent rotor design trends are leaning towards hingeless blade configurations. A bearingless rotor is one such example where flap and lag hinges as well as pitch bearing are eliminated, and these are replaced by a root flexure consisting of flexbeam(s) and a torque tube (Fig. 2). The torsionally soft flexbeam(s) extends from the hub to about 15-40% of blade radius where it is connected to the main blade. The pitch control to the blade is applied through the torsionally stiff torque tube by rotating it with the pitch link which elastically twists the flexbeam(s). This results in a multiple-load-path structure because of the redundancy of load paths at the flexure. This causes however a more involved dynamic analysis.

The objective of the present paper is to examine aeroelastic stability of flap bending, lead-lag bending and torsion of a circulation control bearingless blade in hover.

A general review on aeroelastic stability of a rotating blade with conventional aerodynamics is given in References 1-2. Chopra and Johnson[3] formulated and analyzed the flap-lag-torsion aeroelastic stability of a CCR blade in hovering flight. Three degrees of motion were considered: rigid flap, lag and feather rotations about hinges at the blade root. The CC airfoil characteristics were represented in the form of simple analytical expressions. It was shown that the trailing edge blowing can have a major influence on blade aeroelastic stability. Recently Chopra[4] analyzed the aeroelastic stability of flap bending, lead-lag bending, and torsion of a CCR blade in hover using a finite element formulation. The CC airfoil characteristics in the form of data tables were used. Results were presented for several hingeless blade configurations. Again, it was shown that the blowing has an important influence on blade dynamics which must be considered in rotor design.

Sivaneri and Chopra[5] applied a finite element formulation to analyze the dynamics of a bearingless rotor blade in hover with conventional aerodynamic characteristics. Each of the flexbeams and the torque tube were modelled as individual elastic beams. The displacement compatibility conditions at the clevis, between the inboard flexure beams and the outboard blade, were satisfied. Results were also calculated using a simple equivalent-beam modelling wherein a bearingless blade is represented as a single beam with equivalent properties. Comparison of the two sets of results showed that the equivalent-beam modelling can be quite erroneous for some cases.

In the present paper, the above finite element formulation is modified to study the aeroelastic stability of a bearingless CCR blade in hover. The multibeams of the flexure, and the outboard blade idealized as an elastic beam, are all discretized into beam elements, each element with fifteen nodal degrees of freedom. There is a continuity of axial displacement u, flap bending w and w', lead-lag bending v and v' and geometric twist $\$$ between elements. Quasisteady strip theory is used to evaluate aerodynamic forces. The airfoil

characteristics are represented in the form of data tables. The influence of unsteady aerodynamics is introduced by using dynamic inflow modelling. The formulation is made quite general for nonuniform blades keeping in view the application to different types of bearingless configurations. First, a correlation study of analytical results with the experimental data is attempted for selected bearingless configurations with conventional airfoil characteristics. Then, stability resulty are obtained for circulation control bearingless configurations.

Formulation

The formulation details can be seen in References 4-5. The blade is treated as an elastic beam and undergoes axial displacement u, lead-lag bending displacement v, flap bending displacement w and elastic twist ϕ about a deformed elastic axis. Fig. 3 shows the deformed as well as undeformed blade positions. The rectangular coordinate system x,y,z is attached to the undeformed blade, wherein the x-axis coincides with the elastic axis. A point P on the undeformed elastic axis undergoes displacements u, v, w in the x,y,z directions respectively and occupies the position P' on the deformed elastic axis. Then the blade section containing point P' undergoes a rotation θ_1 about deformed elastic axis.

$$\theta_1 = \theta + \phi \qquad (1a)$$

and

$$\phi = \phi - \int_0^x v''w'dx \qquad (1b)$$

where θ is pretwist, ϕ is the geometric twist with respect to the undeformed axis (compatible with u,v,w) and ϕ is the elastic twist about the deformed elastic axis ξ. The formulation is based on Hamilton's principle

$$\int_{t_1}^{t_2}(\delta U - \delta T - \delta W)\, dt = 0 \qquad (2)$$

where δU, δT and δW are respectively the variation of strain energy, the variation of kinetic energy and the virtual work done. These energy expressions are made independent of the time derivatives of virtual displacements, δu, δv, δw and $\delta\phi$ and hence Eq. (2) can be written as

$$\delta U - \delta T - \delta W = 0 \qquad (3)$$

The aerodynamic forces are obtained using quasisteady strip-theory approximation. Forces of non-circulatory origin are also included. The section lift, drag and moment about the mid-chord (per unit span) are

$$L = \frac{1}{2}\rho V^2 c\, C_\ell(\alpha, C_\mu)$$

$$D = \frac{1}{20}\rho V^2 c\, C_d(\alpha, C_\mu) \qquad (4)$$

$$M_{.5} = \frac{1}{2}\rho V^2 c^2 C_{m_{.5}}(\alpha, C_\mu)$$

The aerodynamic coefficients C_ℓ, C_d and $C_{m_{.5}}$ are taken from data tables, and the numerical values for these coefficients are given at small steps: $\Delta\alpha$ of $1/2°$ and ΔC_μ of 1/200. The C_μ is blowing momentum coefficient defined as

$$C_\mu = \frac{\dot{m}V_j}{1/2\rho V^2 c} \qquad (5)$$

where $\dot{m}V_j$ is the jet momentum, $1/2\rho V^2$ is the dynamic pressure, and c is the blade chord.

The wake induced inflow is assumed uniform along the length of the blade and the steady component is calculated from the momentum theory

$$\lambda_0 = K_h(C_T/2)^{1/2} \qquad (6)$$

where K_h is an empirical factor and is assumed to be 1.15 and C_T is the steady thrust coefficient. With blade vibratory motion, unsteady flow environments are created and which will naturally result in dynamic induced inflow condition. For hover, a simple dynamic inflow model is used

$$\tau\dot{\lambda} + \lambda = \frac{K_h^2}{4\lambda_0} \qquad (7)$$

where τ is the time lag in arc radian and can be approximately taken as $.85/\lambda_0$. The λ is a time induced inflow component, a perturbation about the steady component λ_0. The ΔC_T is the perturbation thrust component caused by blade motions. The blowing momentum coefficient C_μ is not uniform along the length of the blade, and a general distribution is used for the formulation

$$C_\mu = C_{\mu_T}/\xi^s \qquad (8)$$

where s is a constant, $\xi = r/R$ and C_{μ_T} is blowing coefficient at blade tip. For simplicity of analysis, it is assumed that the blowing coefficient is constant within each element (based on midpoint of element).

Finite Element Discretization

The finite element formulation is based on energy principles (Hamilton). The flexbeam(s), the torque tube and the main outboard blade are all discretized into a number of beam elements. Each element (Fig. 4) consists of fifteen degrees of freedom. There is a continuity of u, v, v', w, w' and ϕ between elements, and there are three internal nodes, two for u and one for ϕ. The distribution for deflections over an element are represented in terms of element degrees of freedom and shape functions; a second order polynomial for ϕ and cubic polynomials for u, v and w.

Hamilton's principle in discretized form for n elements is expressed as

$$\sum_{i=1}^{n}(\delta U_i - \delta T_i - \delta W_i) = 0 \qquad (9)$$

where δU_i, δT_i and δW_i are virtual energy contributions from i^{th} element. During the assembly of element matrices, one has to use the displacement compatibility conditions at interelement boundaries to form global matrices. A simple analytical model of bearingless blade is shown in Fig. 5. The displacement compatability at the clevis is

$$\begin{aligned} u_t &= u_f = u_b \\ v_t &= v_f = v_b \\ v_t' &= v_f' = v_b' \\ w_t - \eta_t \phi_t &= w_f - \eta_f \phi_f = w_b \\ w_t' &= w_f' = w_b' \\ \phi_t &= \phi_f = \phi_b \end{aligned} \qquad (10)$$

where subscripts t, f and b respectively represent torque tube, flexbeam and b'ade.

Fig. 6 shows the root end of the torque tube with the control actuator located at the leading edge. The blade pitch is changed through the up and down movement of pitch link. The torque tube typically is very stiff torsionally as compared to the flexbeam. Therefore any vertical movement of the pitch link results in nearly rigid body pitch for the torque tube and an elastic twist distribution for the flexbeam. To obtain different blade pitch angles, one has to adjust the vertical position of pitch link, W_p. The pitch link flexibility is represented by spring stiffness K_p. Because of the pitch link flexibility, there will be an extra strain energy contribution for the last element of the torque tube, say V_p.

$$V_p = \frac{1}{2} K_p [w_1 + \phi_1 (d + \eta_t) - w_p]^2 \qquad (11)$$

This will modify the element stiffness matrix and the load vector. The relationship between blade pitch and pitch link displacement w_p is calculated iteratively.

The assembly of n elements yields the equation of motion in terms of nodal displacements $\{q\}$ as

$$[M(q)]\{\ddot{q}\} + [C(q)]\{\dot{q}\} + [K(q)]\{q\} = \{Q\} \qquad (12)$$

These are nonlinear equations in q. The next step is to apply geometric boundary conditions. For the torque tube end, the axial and lead-lag displacements are freely permitted and the pitch link joint is pin-ended. Therefore, there is no geometric constraints for the torque tube. On the other hand, the flexbeam is cantilevered at the hub and therefore the displacements u, v, v', w, w', and ϕ are all zero at the root of the flexbeam. The boundary conditions are applied to the global equations (12) by canceling out the rows and columns corresponding to these constraint displacements.

Solution Procedure

The first step is to determine blade steady equilibrium position. For a known thrust level, the collective pitch is calculated. For this collective pitch, an approximate value of pitch link position w_p is determined. Now with a known w_p as a boundary condition, the blade steady deflected position is calculated from the nonlinear equations (12), after dropping time dependent terms.

The second step is to obtain the coupled natural vibration (rotating) characteristics of the blade about its steady equilibrium position. Then, the flutter solution is obtained by assuming vibratory motion to be small perturbation about equilibrium position. For this, the normal mode equations are obtained and an eigen analysis is made. The nature of the complex eigenvalues explains whether blade is stable or not.

Results and Discussion

Numerical results are calculated for bearingless blade configurations, consisting of single flexbeam with wrap-around type torque tube (as shown in Fig. 2). For calculations, the blade is discretized into seven elements; three elements for main blade, two elements for flexbeam and two elements for torque tube. The normal mode stability solution is calculated using six coupled rotating modes. For analysis, the flexbeam and the torque tube are modelled as individual beams. At the root end, the flexbeam is rigidly fixed, whereas for the torque tube there are no constraints on displacements except for a spring restraint in the pitch link direction. A limiting case of rigid pitch link will result in complete displacement constraint at the pitch link location.

First, a correlation study of analytical results with the experimental data is attempted for selected bearingless blade configurations with conventional airfoil characteristics. The experimental stability data for a model rotor is taken from Ref. 6. The model rotor characteristics are Lock number $\gamma = 5.9$, solidity ratio $\sigma = 0.03$, three-bladed, and zero precone. The airfoil characteristics used are:

$$C_\ell = 0.15 + 5.73\alpha$$

$$C_d = 0.0079 + 1.79\alpha^2$$

$$C_m = -0.012$$

The idealized nondimensional structural properties used for elements are given in Table 1. Three different bearingless rotor configurations are considered depending on the pitch link location. The pitch links are located at a distance of 0.085R in the radial direction from the rotation axis. Fig. 7 presents the lag mode stability results for case I, where the pitch link is located at the leading edge of the torque tube. This positioning of pitch link will cause a positive pitch-flap coupling (flap up causing nose down pitch). In the figure, the damping of the fundamental lag mode in the form of

real part of the eigenvalue is plotted for different collective pitch angles. For this lag mode, a structural damping idealized by an equivalent viscous damping ratio of 1% is used. Based on the experience of stability correlations of other authors, it appears that the present analytical results are in good agreement with the experimental results. Fig. 8 shows the lag mode stability results for case II, where the pitch link is located at the trailing edge of the torque tube. This will cause a negative pitch-flap coupling. In Fig. 9, the results are presented for case III, where one pitch link is located at the leading edge and the other at the trailing edge of the torque tube. This will not cause any pitch-flap coupling, but it will raise the torsional frequency of the blade. Again, the agreement of analytical results with the experimental data appears quite satisfactory. It is also noted here that the inclusion of dynamic inflow has only a slight influence on lag mode stability.

The subsequent results are obtained for bearingless CCR blade configurations. These results are calculated for a CCR blade with Lock number $\gamma = 7.2$, solidity ratio $\sigma = 0.13$, four bladed, and zero precone. For simple airfoil characteristics, the following analytical expressions are used:

$$C_\ell = 0.3 + 6.7\alpha + 16.1C_\mu^{.67}$$

$$C_d = 0.026 - 0.3C_\mu^{.67}$$

$$C_{m_{.5}} = 0.06 + 1.34\alpha - 0.644C_\mu^{.67}$$

and these are gross representations of the data in Ref. 7. For table aerodynamics, the airfoil characteristics of a typical CC airfoil with single trailing edge slot are used. The slot height to chord ratio is taken as 0.002 and the airfoil thickness to chord ratio is taken as 0.15. The chordwise offsets of the center of mass, the aerodynamic center, and the tension center from the elastic axis are considered to be zero, and the elastic axis is assumed to be at mid-chord position. The non-dimensional structural blade properties for different elements are given in Table 2. For stability results, the inherent structural damping is assumed to be zero for all modes. Results are calculated for the CCR bearingless configurations, case III only, for which the pitch links are located at the leading edge and the trailing edge of the torque tube.

Fig. 10 shows for trim solutions in hover, the blowing momentum coefficient at the blade tip plotted as a function of rotor thrust for several collective pitch angles. It is assumed that the blowing coefficient varies inverse to the square of the radial position ($C_\mu = C_{\mu_T}/\xi^2$). Results are calculated using simple expressions as well as airfoil tables. With airfoil tables, an iterative procedure based on Newton-Raphson method is used to calculate the trim solution. There is a considerable disparity between the two results. This is understandable since simple expressions are only gross representation of the airfoil characteristics below stall, whereas the table data covers the complete range of angle of attack and blowing coefficient.

Fig. 11 shows the damping ratio ζ for three modes with less damping as a function of thrust level for a case with zero collective pitch ($\theta_0 = 0$). These less damped modes happen to be fundamental lead-lag, fundamental torsion and second lead-lag modes. The other modes are more damped for this as well as for subsequent cases and hence are not plotted. These results are calculated using the airfoil tables. The negative value of damping represents the instability condition of a mode. The lag mode is stable at low thrust levels and becomes unstable at high thrust levels. The torsion mode and the second lag mode are moderately unstable. All three modes can be easily stabilized with the inclusion of small amount of structural damping in these modes. Most rotor designs inherently have enough structural damping to stabilize these levels of instability. A similar type of stability characteristics were observed in Ref. 4 for hingeless CCR blades with zero collective pitch. In Fig. 12, the stability results are shown for the same blade configurations using the simple analytical expressions presented previously for the airfoil characteristics. Though this approximation is quite gross as seen in the trim solution (Fig. 8), the stability results are quite reasonably predicted. The inclusion of dynamic inflow has a slight influence on lag mode stability, in fact, a destabilizing effect at high thrust levels.

Fig. 13 shows the stability results for a negative collective pitch of -10^0 using the table aerodynamics. For this pitch setting, one needs a larger amount of blowing to acheive certain thrust level. The fundamental lag mode becomes unstable at low thrust levels, and becomes quite stable at high thrust levels. In fact, at low thrust levels one needs a larger amount of damping to stabilize this mode. The effect of negative pitch on torsion and second lag mode is comparatively less, it stabilizes the torsion mode somewhat. The effect of positive collective setting on blade stability is shown in Fig. 14. For this pitch, one needs a small amount of blowing to achieve certain thrust level. Here, the fundamental lag mode gets very stabilized. The influence on the other two modes is again small.

Conclusions

The aeroelastic stability of a bearingless circulation control rotor blade in hover is examined using a finite element formulation. Airfoil characteristics are represented in the form of simple expressions as well as in the form of data tables. The flexbeam, the torque tube and the main blade are modeled individually as elastic beams. Numerical results are calculated for a circulation control bearingless rotor configuration consisting of a single flexbeam with a wrap-around type torque tube and the pitch links located at both the leading edge and the trailing edge of the torque tube.

Based on this effort the following conclusions can be drawn:

(1) A reasonable correlation of analytical results with the experimental data for selected bearingless configurations with conventional airfoils has introduced confidence to the methodology and the algorithms.

(2) For flutter solution, one needs to include at least four modes; these are fundamental flap, lag, and torsion modes and the second lag mode.

(3) Stability results have shown that the trailing edge blowing plays an important role in the determination of the aeroelastic stability of a rotor blade.

(4) The inclusion of dynamic inflow has a slight influence on lag mode stability.

(5) The negative pitch setting destabilizes lag mode, in particular, at low thrust levels.

(6) The positive pitch setting stabilizes lag mode.

(7) For a fixed thrust level, it appears that going to higher blowing is more destabilizing.

(8) The fundamental torsion and the second lag modes are weakly unstable for some thrust levels. The expected levels of internal structural damping appear adequate to stabilize these modes.

ACKNOWLEDGEMENTS

The author wishes to acknowledge helpful discussions with Kenneth Reader, James Biggers, and Al Schwartz of David W. Taylor Naval Ship Research and Development Center. The work was supported by DTNSRDC under contract no. N-00167-84-M-1548. Acknowledgements are also due t U.S. Army Aeromechanics Laboratory, Ames Research Center for providing the rotor model data.

References

1. Ormiston, R.A., "Investigation of Hingeless Rotor Stability", Vertica, Vol. 7, No. 2, 1983, pp. 143-181.

2. Friedmann, P., "Formulation and Solution of Rotary-Wing Aeroelastic Stability and Response Problems", Vertica, Vol. 7, No. 2, 1983, pp. 101-141.

3. Chopra, I. and Johnson, W., "Flap-lag-torsion Aeroelastic Stability of Circulation-controlled Rotors in Hover", Journal of the American Helicopter Society, Vol. 24, No. 2, April 1979, pp. 37-46.

4. Chopra, I., "Aeroleastic Stability of an Elastic Circulation Control Rotor Blade in Hover", Appearing in Vertica, 1984.

5. Sivaneri, N.T. and Chopra, I., "Finite Element Analysis for Bearingless Rotor Blade Aeroelasticity", Journal of the American Helicopter Society, Vol. 29, No. 2, April 1984, pp. 42-51.

6. Dawson, S., "An Experimental Investigation on the Stability of a Bearingless Model Rotor in Hover," Journal of the American Helicopter Society, Vol. 28, No. 4, Oct. 1983, pp. 29-34.

7. William, R.M., Rogers, E.O. and Leitner, R.T., "X-Wing Technology Summary, Vol. II," DTNSRDC Report TM-16-76-72, June 1976.

Table 1. Structural properties of elements for rotation speed of 1100 RPM.

Element	Length ℓ/R	Flapwise $EI_y/m_o\omega^2R^4$	Chordwise $EI_z/m_o\Omega^2R^4$	Torsion $GJ/m_o\Omega^2R^4$	Mass m/m_o	Torsion inertia K_m^2/R^2	
1	0.367	0.0055	0.1501	0.0029	1.0	0.00091	Blade
2	0.367	0.0055	0.1501	0.0029	1.0	0.00091	Blade
3	0.069	0.1216	0.1216	0.2433	39.6	0.0105	Blade
4	0.113	0.00158	0.0052	0.00021	0.299	0.000029	Flex beam
5	0.085	2.099	2.099	9.150	72.6	0.0346	Flex beam
6	0.0564	4.257	4.257	1.815	7.63	0.0020	Torque tube
7	0.0564	4.257	4.257	1.815	7.63	0.0020	Torque tube

Chord/radius = .0465

Pitch link spring $\frac{K_p}{m_o\Omega^2R}$ = 171.06

Pitch link offset from torque tube center $\frac{d}{R}$ = .0409

$\eta_t = \eta_f = 0$

Table 2. Structural properties of elements for the circulation control bearingless blade.

Element	Length ℓ/R	Flapwise $EI_y/m_o\omega^2R^4$	Chordwise $EI_z/m_o\Omega^2R^4$	Torsion $GJ/m_o\Omega^2R^4$	Mass m/m_o	Torsion inertia K_m^2/R^2	
1	0.2	0.0186	0.2303	0.0297	0.7067	0.000739	Blade
2	0.2	0.0372	0.3938	0.0557	1.0	0.000832	Blade
3	0.2	0.0929	0.7133	0.0929	1.624	0.001068	Blade
4	0.2	0.1858	0.2303	0.00297	1.383	0.000099	Flexbeam
5	0.2	0.5573	0.6687	0.00297	1.556	0.000279	Flexbeam
6	0.13	0.0817	0.5201	0.1560	1.398	0.001397	Torque tube
7	0.13	0.1486	0.3901	0.2823	1.549	0.001366	Torque tube

Chord/radius = .1034

Pitch link spring $\frac{K_p}{m_o\Omega^2R}$ = 10000

Pitch link offset from torque tube center $\frac{d}{R}$ = .033

$\eta_t = \eta_f = 0$

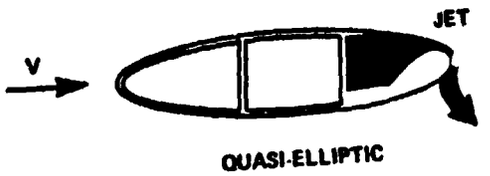

Fig. 1 Circulation control airfoil.

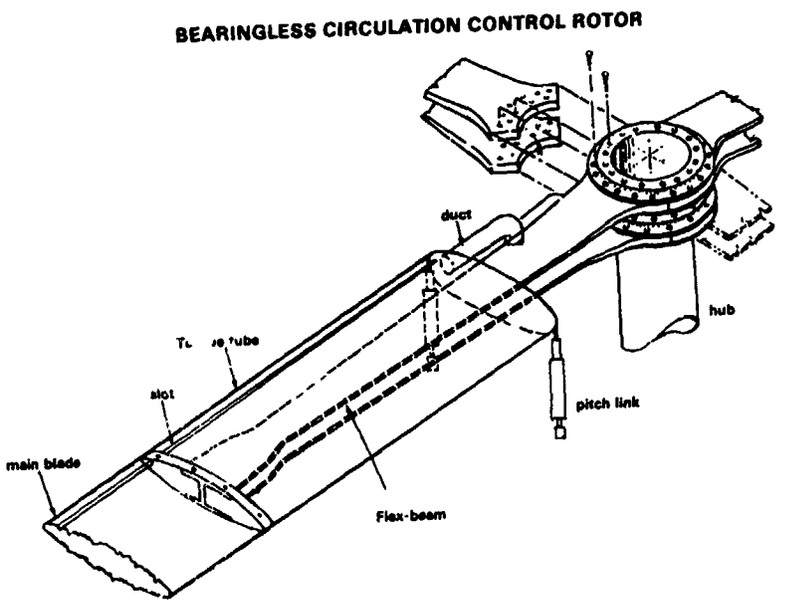

Fig. 2

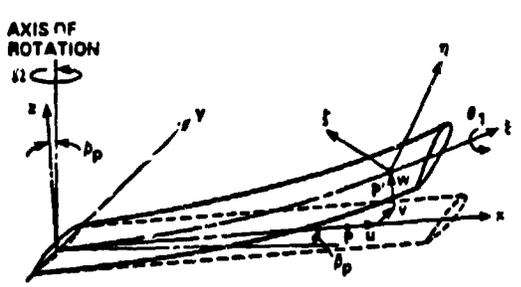

Fig. 3 Blade coordinate systems and deflections.

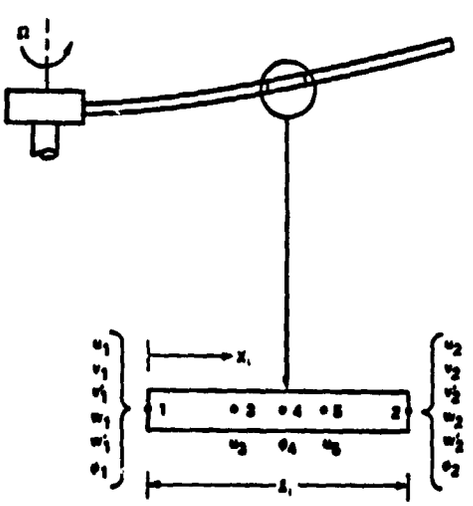

Fig. 4 A finite element showing nodal degrees of freedom.

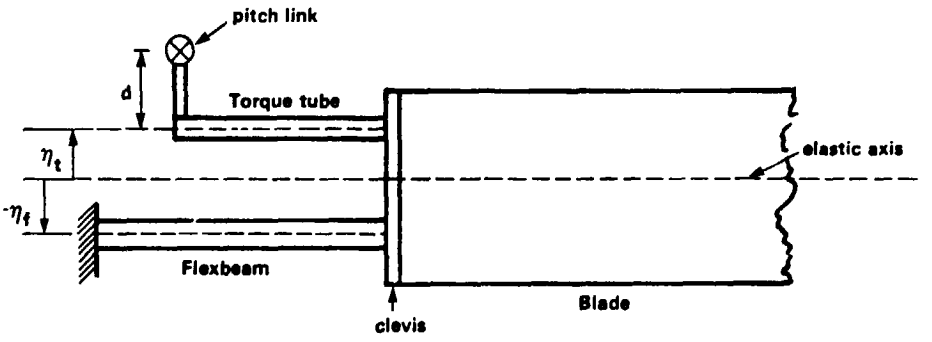

Fig. 5 Analytical model of a bearingless blade.

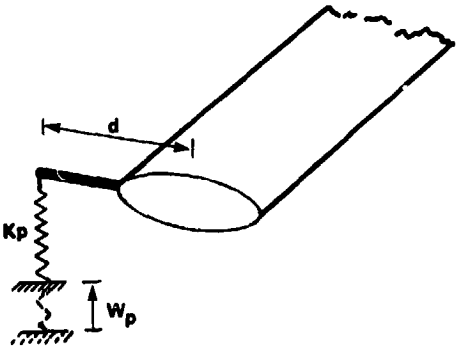

Fig. 6 Torque tube and pitch link.

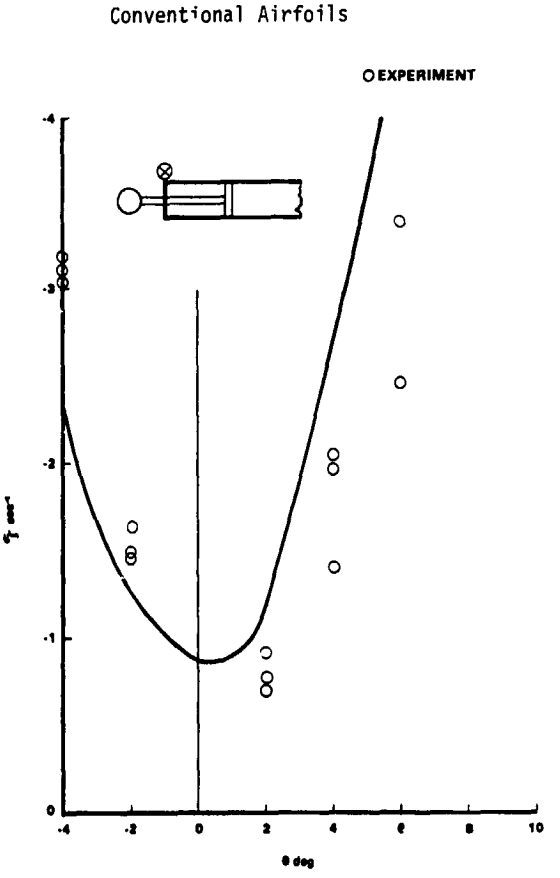

Fig. 7 Lag damping as a function of blade collective pitch, case I (pitch link at leading edge of torque tube).

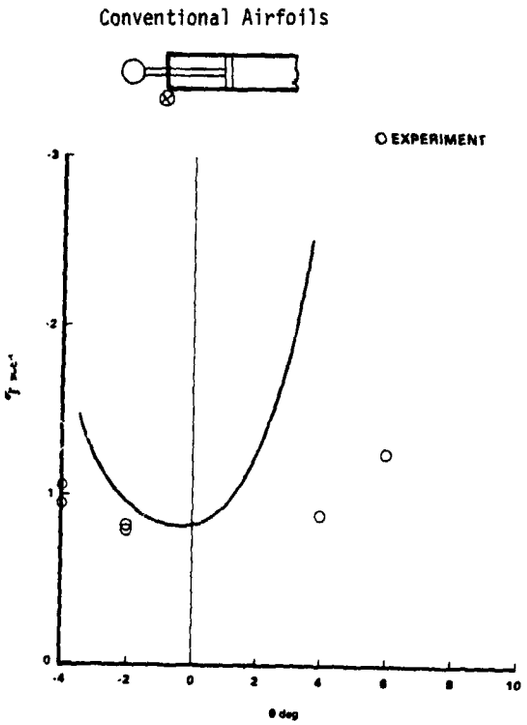

Fig. 8 Lag damping as a function of blade collective pitch, case II (pitch link at trailing edge of torque tube)

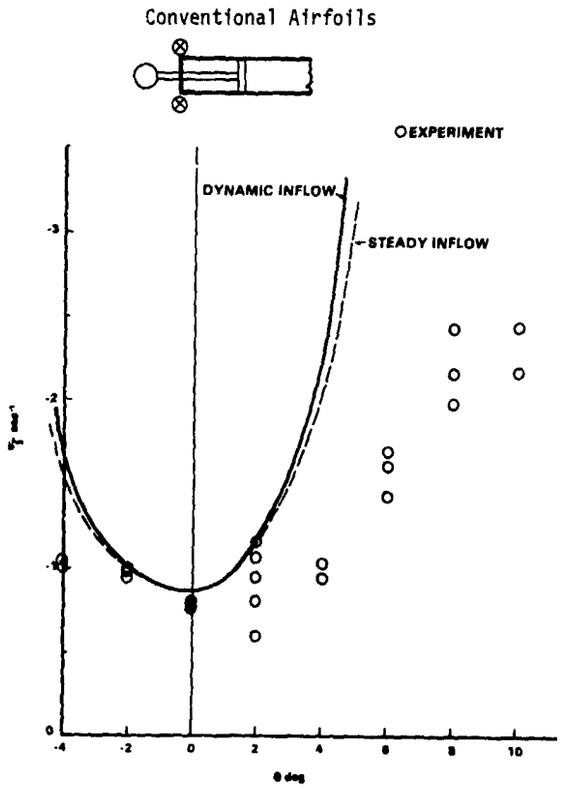

Fig. 9 Lag damping as a function of blade collective pitch, case III (pitch links at leading edge and trailing edge of torque tube).

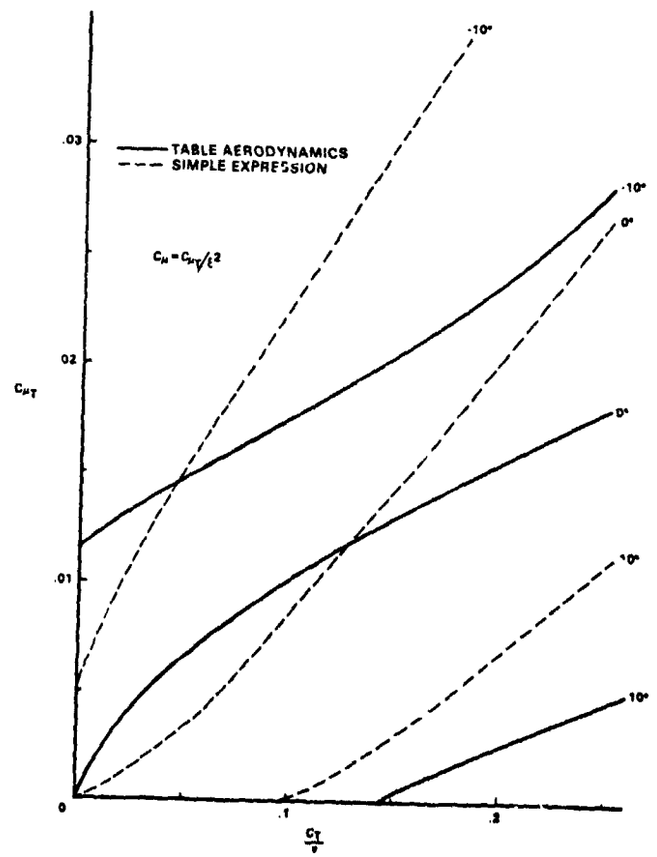

Fig. 10 Blade blowing coefficient as a function of rotor thrust and collective pitch.

CC Airfoils, $C_\mu = C_{\mu_T}/\xi^2$, Table Aerodynamics $\theta_o = 0$

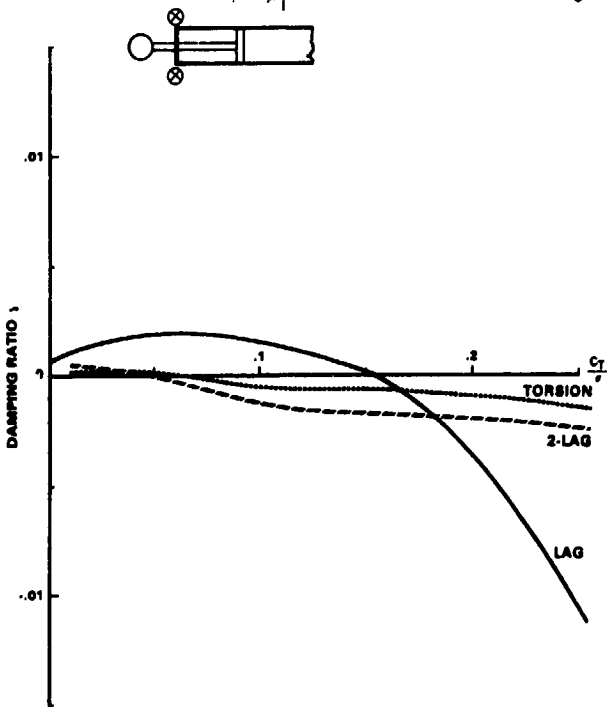

Fig. 11 Damping ratio for zero collective pitch (zero structural dampings, ω_v=2.5, ω_w=2.3, ω_ϕ=17.4)

CC Airfoils, $C_\mu = C_{\mu_T}/\xi^2$, Table Aerodynamics θ_o=-10°

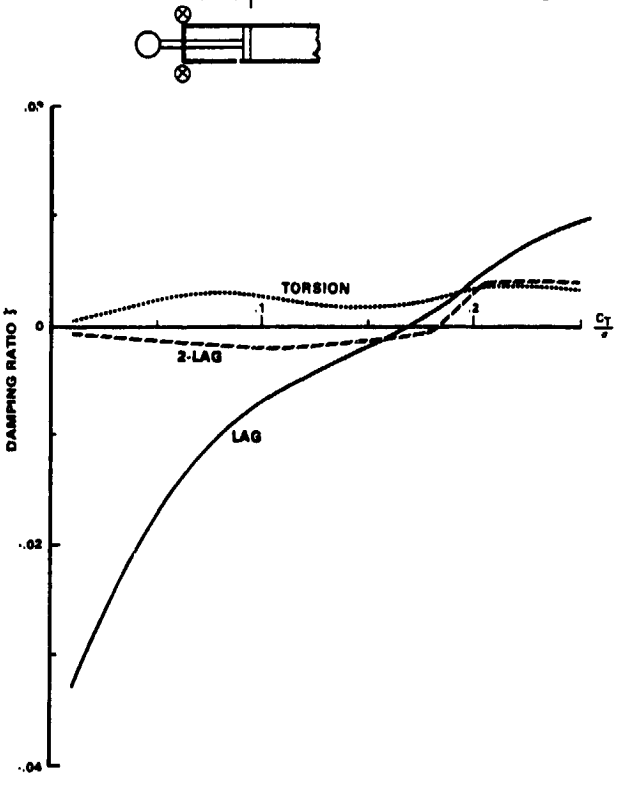

Fig. 13 Damping ratio for negative collective pitch (zero structural dampings, ω_v=2.5, ω_w=2.3, ω_ϕ=17.0)

CC Airfoils, $C_\mu = C_{\mu_T}/\xi^2$, Analytical Aerodynamics, θ_o=0

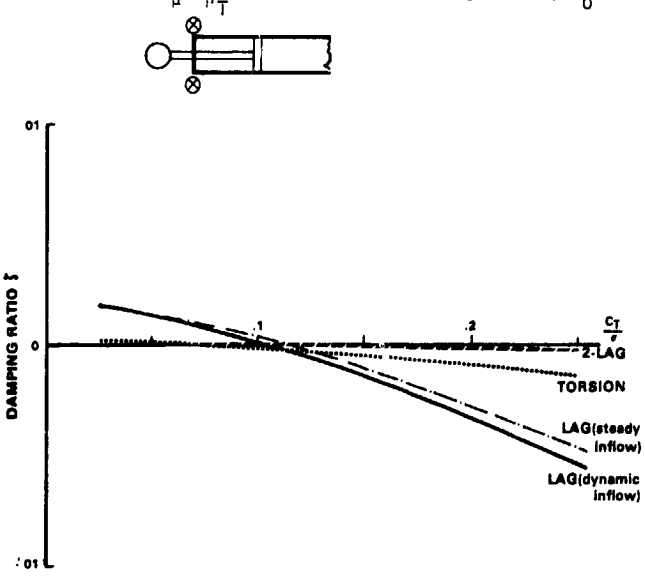

Fig. 12 Damping ratio for zero collective pitch (zero structural dampings, ω_v=2.5, ω_w=2.3, ω_ϕ=17.4)

CC Airfoils, $C_\mu = C_{\mu_T}/\xi^2$, Table Aerodynamics θ_o=10°

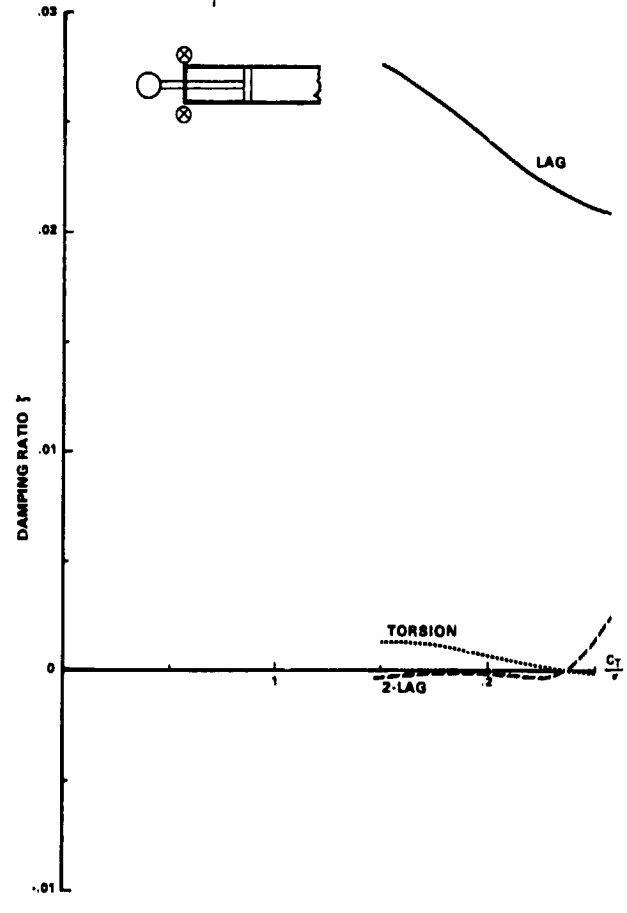

Fig. 14 Damping ratio for positive collective pitch (zero structural dampings, ω_v=2.5, ω_w=2.3, ω_ϕ=17.4)

DISCUSSION
Paper No. 17

DYNAMIC STABILITY OF A BEARINGLESS CIRCULATION CONTROL ROTOR BLADE IN HOVER
Inderjit Chopra

Jack Nielsen, NASA Ames Research Center: I have a serious question with regard to the fundamental aerodynamics of the problem. You have assumed you can calculate the flutter using steady aerodynamic results. Now we have a boundary layer on the Coanda plate and it isn't clear at all that at the frequencies of flutter that the boundary layer isn't going to have very important unsteady effects; we really don't know. But I don't think we can assume the quasisteady assumption offhand. Letting the amplitudes get small doesn't get around this problem if the unsteady effects are coupled into the flutter. So I would be interested to know since we don't have any data how you can be sure that you have really solved the real flutter problem for the CC airfoil.

Chopra: Are you posing the question [to me]? I do recognize that the unsteady aerodynamics for CCR is very important and it's not there. This is something that has to be looked at in the future. I am very much interested [and would] like to work on that problem if you give us the money.

Bill Warmbrodt, NASA Ames Research Center: The results that you showed for the circulation controlled airfoil showed damping ratios that were an order of magnitude lower than the hingeless configuration that you first showed the results for. You made mention that structural damping, had it been included, would have stabilized some of those modes. I think everybody in the audience here has a pretty good feel for what the influence of structural damping is for a hingeless rotor configuration. Would you say that you saw that same degree of sensitivity for the bearingless configurations that you analyzed?

Chopra: I think your first question is . . . let's look at it this way. You get lower damping here than you see in the hingeless [rotor]. I think that [you] have to go back and look first at the perturbation aerodynamics. Keep in mind that you are keeping your elastic axis at the half chord. Your perturbation aerodynamics has two components--[one] due to blowing, [one] due to conventional. The conventional part of the aerodynamics still has the quarter chord as the aerodynamic center and that will be destabilizing particularly for the torsion mode. So you expect to see lower damping. [This] means the people who have to design the X-Wing/CCR Rotor, they do need to--what should I say--add more structural damping or some sort of damping to stabilize these modes. I hope you may be agreeable to this point.

Jing Yen, Bell Helicopter: I understand that you used the normal modes approach to solve the problem. Would you like to tell us where and how you obtained the normal modes for the redundant or multiple load path hub? Also how much confidence [do] you have in [the modes]?

Chopra: The confidence is 100%. This is something [that is] a routine classroom problem. What we do is we look at first to the steady deflected shape and at that stage we solve the global equations. Solving the global [algebraic, eigenvalue] equation is very routine these days. It doesn't take any extra time. But when you are trying to solve the complex eigenvalue problem it is no good to use, say, a 100 by 100 equation, but it is good to use a 6 by 6 equation. There are two reasons for that--one is the computer and the second is the physical. You don't want to look at a hundred eigenvalues, you want to look at just five or six and see what is happening to [the major] mode shapes. Reducing to normal modes is the same [as] if you had got the mode shapes using the Myklestad method and reduce them to normal modes. I don't see any difference from the . . . if you were to [model] a beam [using], say, the Myklestad approach and 20 elements, you may be using only four or five modes. So the procedure is just the same. Did I satisfy?

Yen: This was a finite element model?

Chopra: It's a finite element model, yes. To start with it's a finite element model. We get the natural mode shape of [the blade] using finite elements. Redundancy doesn't come into the picture anywhere. This is only the way you are arranging the equations.

Peretz Friedmann: I think I misunderstood his question because I had the same concern about the redundancy. I think that when you have a redundant structure which is what [Jing] Yen alluded to you don't know exactly what the boundary conditions are and you might get incorrect mode shapes if you are not careful about the boundary conditions. I am not sure what those boundary conditions are because you have the cuff and you have the redundant load path and you really don't know what exactly the boundary condition is at the root. I think that's what he meant.

Chopra: I think that [is true with] any problem. If we don't know the boundary conditions we can make an error in any analysis. Some of the configurations I've seen, the pitch links seem to be . . . you can easily [get] the moment there and the only really important displacement is

the vertical displacement. But we did make a parametric study where we tried to constrain the pitch link. We tried to put various types of constraints on the pitch link. It is not very sensitive on stability.

Wayne Johnson: Aren't your normal modes, though, calculated after you find the deflected solution using the full finite element.

Chopra: That's right.

Johnson: So the normal modes are found after you have identified the boundary conditions.

Chopra: That's right, after identifying the boundary conditions, that's right.

Johnson: I think modes in this case is simply a way to reduce the dimension of the state vector. I don't think it really does anything more than that.

DYNAMIC RESPONSE CHARACTERISTICS OF A CIRCULATION CONTROL ROTOR MODEL PNEUMATIC SYSTEM

Charles B. Watkins
Professor
Howard University
Washington, D.C.

Kenneth R. Reader
Senior Aerospace Engineer
David W. Taylor Naval Ship Research
and Development Center
Bethesda, MD

and

Subash K. Dutta
Graduate Assistant
Howard University
Washington, D.C.

Abstract

Numerical and experimental simulation of unsteady airflow through the control valve and slotted air duct of a circulation control rotor is described. The numerical analysis involves the solution of the quasi-one-dimensional compressible fluid-dynamic equations in the blade air duct together with the coupled isentropic flow equations for flow into the blade through the valve and out of the blade through the Coanda slot. Numerical solutions are compared with basic experimental results obtained for a mockup of a circulation control rotor and its pneumatic valving system. The pneumodynamic phenomena that were observed are discussed with particular emphasis on the characteristic system time lags associated with the response of the flow variables to transient and periodic control valve inputs.

Notation

A	Cross-sectional area of duct
A_e	Effective expansion area at valve exit
A_v	Valve area
f	Duct friction factor
C_s	Slot discharge coefficient
C_v	Valve discharge coefficient
c_v	Specific heat at constant volume
D_h	Hydraulic diameter of duct
e	Total energy per unit volume
F	Flux times area vector
G	Vector of nonhomogeneous terms in flow equations
h	Heat transfer coefficient
H_D	Average duct height
k	Thermal conductivity
L	Length of duct
$\dot{m}$	Mass flow rate
m	Mass flow rate per unit area in duct
m_I	Mass flow rate per unit area computed from isentropic flow theory
m_s	Mass flow rate per unit area through slot
m_v	Mass flow rate per unit area through valve
p	Static pressure in duct
p_{ext}	External pressure at slot exit
p_0	Total pressure in duct
T	Duct static temperature
T_0	Duct total temperature
T_w	Duct wall temperature
t	Time
U	Vector of dependent variables
V	Vector of diffusion terms
v_x	Average duct velocity in spanwise or x direction
v_y	Approximate average duct velocity in chordwise or y direction
w_s	Slot width
x	Spanwise coordinate
x_e	Coordinate at duct entrance

x_{end}	Coordinate at duct end
y	Chordwise coordinate
γ	Ratio of specific heats
ρ	Density
ω	Angular frequency

Subscripts

I	Variable computed from isentropic flow at valve exit
pl	Variable in pressure supply plenum or rotor hub

Prefix

Peak-to-peak value of variable

Introduction

Circulation control rotor (CC) technology applied to rotary-wing aircraft or stopped-rotor vertical takeoff and landing (VTOL) aircraft, such as the X-Wing, offers several distinct advantages over conventional rotor technology. For rotary-wing aircraft, CC technology provides a solution to such problems as high vibration levels, retreating blade stall, hub/pylon drag, and implementing higher harmonic control. For stopped-rotor aircraft, the historical limitations of aeroelastic divergence, flutter, blade dynamic instability, and critical resonance conditions during rpm reduction are eliminated. Both types of aircraft use a shaft-driven rotor with blades having circulation control airfoils which generate lift through the Coanda principle. The CC airfoils employ a rounded trailing edge with a thin jet of air tangentially ejected from a spanwise slot adjacent to the rounded (Coanda) surface. The jet of air suppresses boundary layer separation and moves the rear stagnation streamline toward the lower surface, thereby increasing lift. Lift is increased in proportion to the mass flow rate of compressed air in the jet. Pitch and roll control requirements are obtained by cyclic modulation of the mass flow rate with valves in the nonrotating system. Higher harmonic cyclic control can be similarly applied for reducing blade stresses, transmitted shears, vibration, and power requirements.

The design of CC rotors and their pneumatic control systems requires an understanding and appreciation of the phenomenology involved in the control and distribution of airflow to the Coanda slots in these rotors. A capability for analytical prediction of rotor Coanda airflow is also essential. The term "pneumodynamics" has been coined to refer to the aerodynamic response characteristics of CC rotor system internal airflow.

In a recent paper, Watkins et al.[1] describe the modeling techniques employed in the HFPA (high frequency pneumodynamic analysis) computer code developed for CC rotor pneumodynamic analysis. The present paper reviews the modeling techniques described in Reference 1 and presents results obtained by applying the code to a simple experimental mockup of a model rotor blade and its pneumatic valving system. The discussion of the results, from both the HFPA predictions and the experiment, focuses on the dynamic response of the flow variables to periodic and transient control valve inputs. These response characteristics, particularly with reference to the characteristic system time lags, have implications for the performance of actual rotor systems.

Theory

The modeling techniques employed in the present research are described in Reference 1 where emphasis is on the details of the theoretical formulation and numerical technique. The theory is presented here in abbreviated form; a more complete discussion is contained in Reference 1.

Basic Equations

The HFPA code solves the quasi-one dimensional, compressible fluid dynamic equations for unsteady flow in a spanwise blowing air supply duct internal to a rotating CC rotor blade, together with the coupled isentropic flow equations for flow into the blade through the control valve and out of the blade through the Coanda slot. The duct flow equations have the conservative form representation

$$U_{,t} + \frac{1}{A} F_{,x} + G + V = 0 \qquad (1)$$

where the vector of dependent variables is

$$U = \begin{bmatrix} \rho \\ m \\ e \end{bmatrix}$$

and the flux is given by

$$F = \begin{bmatrix} mA \\ \left(\frac{m^2}{\rho} + p\right) A \\ (e + p) \frac{m}{\rho} A \end{bmatrix}$$

The vector of nonhomogeneous terms, which includes the effects of blade rotation at angular velocity ω, wall skin friction factor $c_f(x)$, wall heat transfer coefficient $h(x)$, and mass flux through the slot $m_s(x,t)$ is

$$G = \begin{bmatrix} \frac{m_s w_s}{A} \\ -\frac{p}{A}\frac{dA}{dx} + \frac{m_s w_s m}{\rho A} + \frac{2c_f m^2}{D_H \rho} - \rho\omega^2 x \\ \frac{m_s w_s (e+p)}{A\rho} - m\omega^2 x + \frac{4h}{D_H}(T - T_w) \end{bmatrix}$$

For completeness, the vector of axial diffusion terms is included, although it is insignificant in the present problem. It is

$$V = \begin{bmatrix} 0 \\ \frac{4}{3}\left(\frac{m}{\rho}\right)_{,xx} \\ -\frac{4}{3}\left[\frac{m}{\rho}\left(\frac{m}{\rho}\right)_{,x}\right]_{,x} - kT_{,xx} \end{bmatrix}$$

The equation of state is

$$p = (\gamma-1)\left(e - \frac{m^2}{2\rho} - \rho\,\frac{v_y^2}{2}\right) \qquad (2)$$

In the above relations, the conservative variables m and e are defined as

$$m = \rho v_x$$

$$e = \rho\left(c_v T + \frac{v_x^2}{2} + \frac{v_y^2}{2}\right)$$

and $w_s(x,t)$ and $m_s(x,t)$ are the local (with respect to spanwise x location) slot width and blowing mass flux, respectively.

The small average chordwise velocity component inside the duct can be crudely approximated as

$$v_y \simeq \frac{w_s m_s}{2\rho H_D} \qquad (3)$$

in which $H_D(x)$ is the local effective height of the duct.

The mass flux distribution through the Coanda slot is assumed to be well represented by one-dimensional isentropic flow theory with a discharge coefficient $C_s(x)$;

$$m_s(x,t) = C_s m_I(p_0, T_0, p_{ext}) \qquad (4)$$

The above functional relationship is the usual expression for isentropic flow expanding through a nozzle from a plenum (in this case the duct interior) to ambient conditions (in this case the exterior of the rotor blade). $p_0(x,t)$ and $T_0(x,t)$ are the local (internal) total pressure and temperature, respectively, and $p_{ext}(x,t)$ is the external pressure at the exit of the Coanda slot. Dependency upon external pressure is eliminated when the flow is choked.

Boundary Conditions

At the upstream boundary $x = x_e$, a plenum supplies blowing air to the duct through a valving system. The valve opening area has constant and rotor-azimuth-dependent components regulated by the collective and cyclic components, respectively, of the aircraft control system. The mass flow and duct pressures are thus determined by these valve settings in concert with the duct/slot configuration.

Figure 1 shows the idealized representation adopted for the cam type valve of interest in the present study. The controlled value of the valve opening is designated as $A_v(t)$, and A_e is the fixed effective opening at the duct entrance. Like the slot flow, one-dimensional isentropic flow theory with a discharge coefficient is used to represent flow through the valve. The valve mass flux is

$$m_v(t) = C_v m_I(p_{0_{pl}}, T_{0_{pl}}, p(x_e,t)) \qquad (5)$$

where p_0 and T_0 are the total pressure and temperature, respectively, in the air supply plenum in the rotor hub and $p(x_e,t)$ is the back pressure in the duct entrance downstream of the valve. When the flow is choked, the dependency on $p(x_e,t)$ is eliminated.

The other boundary condition, at $x=x_{end}$, is the stagnation of the flow at the end of the duct.

The discharge coefficients C_v and C_s, used as correlation parameters for a given system relate the geometric area of a system to the effective area. For simple configurations such as orifice plates or venturi tubes in a well conditioned system where the airflow is well behaved, the discharge coefficient value can be obtained from a standard engineering handbook.

Finite Difference Method

In applying the theory of the previous section to the analysis of a rotor blade, the entire blade, including the transition duct (ducting from hub valve exit to airfoil portion of rotor blade), is discretized by dividing it into spanwise (radial) segments. The governing differential equations, Eq. (1), are solved by the implicit, "delta form," finite-difference procedure of Beam and Warming[2] at the grid points located at segment boundaries, including the valve exit as shown in Fig. 1 and the duct end. The solution of the duct flow is actively coupled to the flow through the valve and through the upstream boundary condition. With the exception of the upstream boundary condition for flow into the duct from the valve, the numerical analysis is rather standard and is described fully in Reference 1.

In Reference 1, expressions are presented for an approximate numerical upstream boundary condition based on deriving for various valve types an auxiliary relationship by ignoring the time dependent term in the momentum equation between the first two grid points (grid point 1 and 2 in Fig. 1). The approximation for the idealized valve of Fig. 1 is

$$p_1 A_e + \frac{(p_1+p_2)}{2}(A_2-A_e) = \frac{m_2^2}{\rho_2} A_2 + p_2 A_2 + \frac{(A_e-A_2)\rho_2\omega^2}{4}(x_1^2-x_2^2) - 2\frac{C_f m_2^2}{\rho_2 D_H}(x_1-x_2) \qquad (6)$$

Approximations such as in Eq. (6) were applied because the investigators were unsuccessful in applying the more standard, and less approximate, procedures for inlet boundary conditions of applying

one-sided differencing or the method of characteristics. The presence of the valve poses special difficulties in the application of these standard techniques. In a recent communication, Anderson of United Technologies Research Center indicated that he was successful in applying the method of characteristics to derive inlet boundary conditions for the HFPA code for a sudden expansion or gate-type valve. The extension of his procedure to the cam valve type shown in Fig. 1, is not straightforward due to the 90 deg change in flow direction. Since this valve is the type considered in the present investigation, Eq. (6) was retained.

Numerical Solution Procedure

The basic approach followed in obtaining numerical solutions to control inputs, consisting of constant (collective) settings or constant collective settings with superimposed constant amplitude cyclic inputs, is to obtain the steady state or time periodic solutions by allowing them to evolve from a transient.

The solution starts with the system essentially at supply pressure conditions. The initial valve position is assumed to be fully open as specified by the sum of its Fourier components supplied as input. The solution is then advanced with time as the flow in the blade adjusts itself to reach steady state flow conditions for the fully open valve. If cyclic components are to be considered, the cyclic input is imposed after fully open steady state flow conditions are achieved. The solution is thereafter advanced further with time until periodic conditions are attained. A harmonic analysis of pressures, temperatures, and mass flow rates is performed on the results from the final cycle.

Experiment

The analytical formulation and the numerical methods described in the previous sections were validated by applying them to a basic experiment and comparing the results with the experimental data[3]. The experiment was performed using a mock-up of a rotor blade pneumodynamic system incorporating a valve similar to the idealized valve of Fig. 1. The model consisted of a supply plenum and two rotating cams with different profiles mounted on the same shaft allowing either a one-per-rev or two-per-rev profile to be selected by axially positioning the cams on the shaft. The flow was modulated by means of the cams from the plenum through a single nozzle into a stationary plugged pipe with a slot.

The pipe with a full-length slot represented a subscale circulation control rotor blade. The experiment was originally performed[3] to establish the feasibility of modulating the weight flow in a one-per-rev and two-per-rev manner and to show that the three components of the airflow were additive. For simplicity, the correct relative motion was established by interchanging the rotating and non-rotating components. The plenum and pipe (hub and rotor blade) were stationary, and the cams (the valving system) rotated. The pipe incorporated several pressure taps distributed along its length. The model is shown in Fig. 2, which is reproduced from Reference 1.

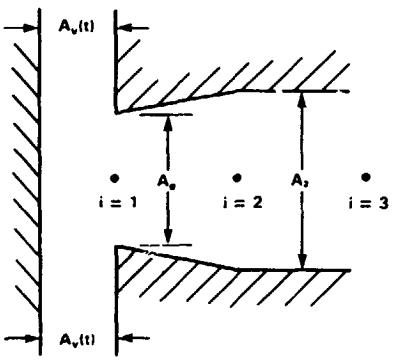

Fig. 1 Idealized valve

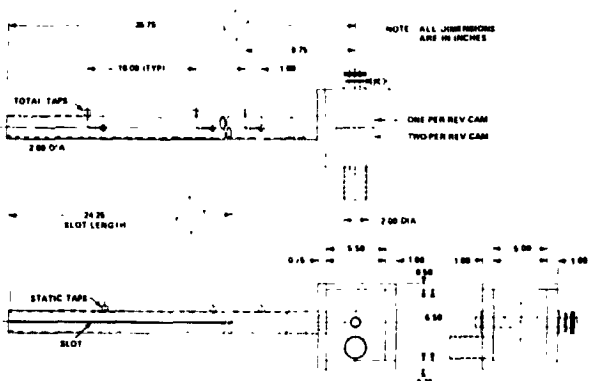

Fig. 2 Experimental model

Dynamic measurements of pipe pressure were obtained for a range of cam rotational speeds. In addition, quasi-dynamic results were obtained by positioning the cam at discrete increments of 30 deg. Average mass flow data were collected from a venturi tube located upstream of the plenum.

Figure 3, also from Reference 1, shows the measured valve area formed by the one-per-rev and two-per-rev cams spaced at a minimum distance of 0.01 in from the nozzle inlet. The points shown were calculated from the measured gap between the cam profile and the nozzle; the area variations are intended to approximate sinusoids as shown. The two-per-rev cam profile is a rather crude approximation and contains a significant higher harmonic content. The measured values were used in the numerical predictions.

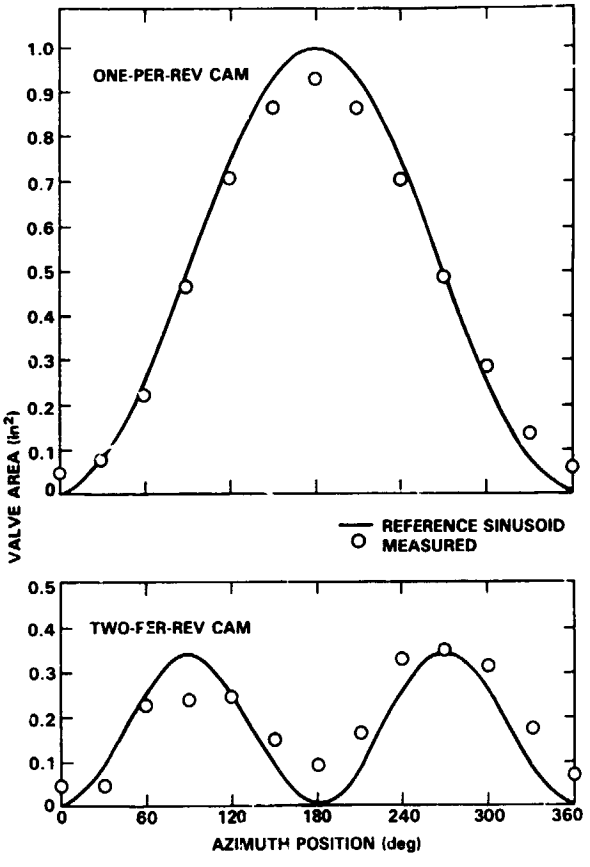

Fig. 3 Valve control area

Results and Discussion

Numerical results were obtained for the experimental configuration of Fig. 2 by discretizing the pipe into 16 segments of approximately equal length. The pipe was assumed to be adiabatic, and the friction coefficient was represented by the formulas for fully developed flow. The integration time-step for the calculations simulating the quasi-dynamic experiments was 5×10^{-4} sec. For the dynamic calculations, valve cycling was imposed after an elapsed time of 0.25 sec. and the time-step was reduced to 1200 steps per revolution thereafter. In general, the results were qualitatively similar for the one- and two-per-rev cams. Therefore, the results presented here are, with one exception, for the one-per-rev cam.

Typical quasi-dynamic numerical and experimental results, indicating the dependency of mass flow rates on nozzle control area at a constant slot height of 0.042 in., are displayed for the one-per-rev cam in Fig. 4. In this figure, the mass flow rate is presented as a function of total valve area at a set plenum pressure. As the valve area increases, the data show that mass flow rate tends toward a constant value, indicating that the flow has become controlled by the slot opening.

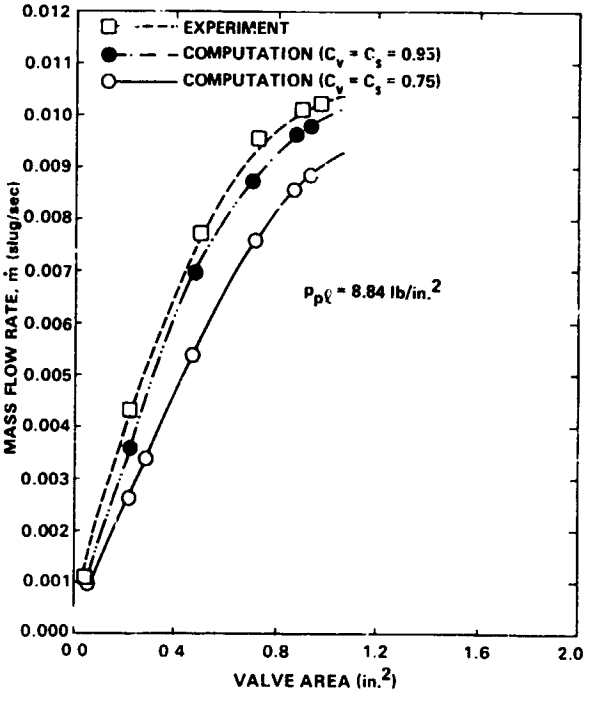

Fig. 4 Mass flow variation

Mass Flow and Pressure Comparison

Figure 4 shows the sensitivity of the discharge coefficients C_v and C_s for a wide range of valve areas. Also shown is the effect of assuming constant values of 0.95 and 0.75 for both the valve and slot discharge coefficients in the numerical solution. The results obtained for the higher value $C_v = C_s = 0.95$ agree more favorably with the experimental results, although the lower discharge coefficient is likely to be realistic physically. That a concept as simple as a discharge coefficient can be used to correlate the mass flow and pressure losses is very encouraging; this is discussed in depth in Reference 4. For the remainder of the theoretical results $C_v = C_s = 0.95$ were used without trying for a better correlation. As indicated in Reference 1, strict interpretation of C_v and C_s is probably not desirable since the various deficiencies and approximations in the computer model can, to some degree, be absorbed by adjusting them. Moreover, the concept of a constant nozzle discharge coefficient is only a first approximation for the actual flow losses which occur over a range of mass flow rates in the analysis. Recent experience with the HFPA code indicates that more physically realistic discharge coefficients can be obtained at the expense of decreased resolution of wave reflection phenomena by including second-order numerical damping in the HFPA algorithm.

Figure 5 illustrates the numerical and experimental cyclic variation of total pressure for a typical dynamic case. The numerical results of Fig. 5 were obtained with $C_v = C_s = 0.95$. The numerically computed pressure profiles have an

azimuthal phase lag from the valve area profiles of Fig. 3 of an approximately 35 deg phase shift. For this configuration, the phase shift is principally due to the finite speed of wave propogation, and is referred to as "sonic lag." A smaller portion of the delay is due to the "capacitance lag" effect caused by the finite pipe volume. The phase difference between the valve area setting and the pressure response to it has been eliminated from Fig. 5 because the experimental phase angle results were not accurate.

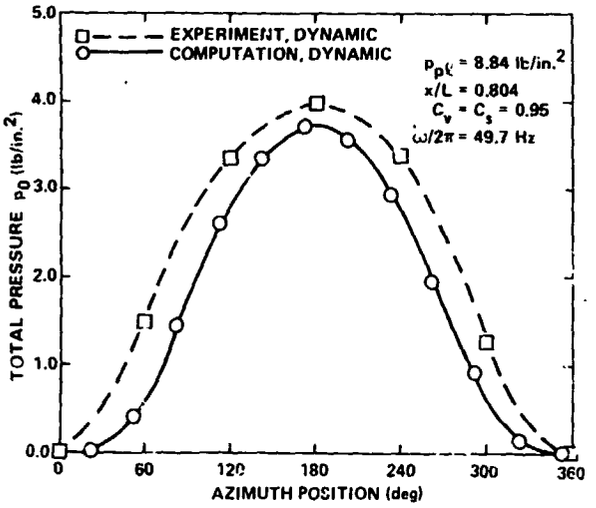

Fig. 5 Total pressure variation

Table 1 contains data obtained from a harmonic analysis of the dynamic numerical results of the case for which the pressures are plotted in Fig. 5. The numerical phase lag has been retained. A harmonic analysis of the experimental pressure data obtained from the experimental curve presented in Fig. 5 is also shown for comparison. Magnitude and phase for the valve opening area, total mass flow rate, and total pressures at two locations are given from the numerical results where the phases are referred to the maximum valve opening at zero deg. (The experimental pressure phase shifts given in the table have an arbitrary reference). The magnitudes are all normalized with respect to the peak-to-peak values.

Table 1 shows that the summation of the higher harmonic content of the mass flow rate output is a rather significant 20 percent while the one-per-rev valve control input contains only approximately 10 percent. Therefore, the mass flow exhibits some nonlinear amplification. The higher harmonic content of the pressure response does not exhibit similar amplification.

The phase shift phenomenon is clearly illustrated by the data in the table. The first harmonic of the mass flow rate lags the valve opening by 39 deg. The first harmonic pressure at, x/L = 0.524, lags the valve opening by 36 deg. At x/L = 0.804, this lag increases to 42 deg. due to the finite wave propogation speed or sonic lag. Because of the specification of a zero numerical integration dissipation parameter in the numerical algorithm used for the cyclic calculations, computed results contain slight, stable spatial numerical oscillations which make it difficult to place confidence in the exact amount of the lag in pressure predicted between locations. Based on the speed of sound, the pure sonic lag between the two points shown should amount to only about one-half the lag shown. The remaining lag may be due to a physical phenomenon or to numerical uncertainty. Although, as discussed previously, the problem of spatial oscillations can be reduced by employing numerical damping, this damping suppresses multiple wave reflections and renders the code less able to predict resonance phenomena. Fortunately, the computed mass flow rate is the result of a spatial integration which has the effect of smoothing the spatial oscillations and should be fairly accurate.

Peak-to-Peak Pressure Comparison

Figure 6 summarizes the results from the dynamic calculations in the form of peak-to-peak total pressures versus frequency for the one-per-rev cam.

Table 1. Harmonic analysis of typical results

HARMONIC n	$A_n/\delta A$ (δA=0.8904 IN^2) MAG(PHASE,DEG)	$\dot{m}_n/\delta\dot{m}$ ($\delta\dot{m}$=0.00331 SLUG/SEC) MAG(PHASE,DEG)	$p_{0n}/\delta p_0$ At x/L = 0.804 COMPUTATION δp_0=3.71 LB/IN^2 MAG(PHASE,DEG)	$p_{0n}/\delta p_0$ At x/L = 0.804 EXPERIMENT δp_0=3.99 LB/IN^2 (APPROXIMATE) MAG(PHASE,DEG)	$p_{0n}/\delta p_0$ At x/L = 0.524 COMPUTATION δp_0=3.77 LB/IN^2 MAG(PHASE,DEG)	$p_{0n}/\delta p_0$ At x/L = 0.524 EXPERIMENT δp_0=3.75 LB/IN^2 (APPROXIMATE) MAG(PHASE,DEG)
0	0.514	0.686	0.425	0.519	0.432	0.537
1	0.509 (353)	0.488 (32)	0.529 (35)	0.494 (350)	0.523 (29)	0.500 (350)
2	0.027 (197)	0.086 (241)	0.016 (55)	0.034 (176)	0.017 (131)	0.043 (171)
3	0.015 (128)	0.014 (100)	0.031 (262)	0.019 (205)	0.007 (275)	0.021 (203)
4	0.006 (26)	0.005 (21)	0 002 (179)	0.007 15)	0.003 (78)	0.005 (45)
5	0.004 (322)	0.002 (63)	0.002 (179)	0.011 (347)	0.003 (346)	0.007 (30)

NOTE: $\omega/2\pi$ = 49.7 Hz AND p_{pl} = 8.89 LB/IN^2.

In Fig. 6 the numerical solution is able to predict fairly well the trends and magnitudes of the pressure response. One possible source of error in the numerical calculations is the assumption of constant discharge coefficient for the wide range of area variation. Somewhat more remote are the possibilities for experimental error.

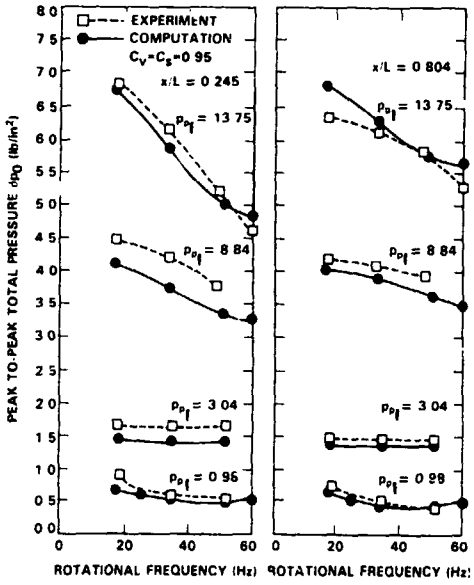

Fig. 6 Peak-to-peak total pressure

Figure 7 plots the dynamic results of the peak-to-peak total pressure near the beginning of the slotted portion of the pipe against plenum pressure for the one-per-rev cam at two different frequencies. The agreement between the measured and numerical results in this figure, in general, is seen to be fair. As shown, the peak-to-peak total pressure at the entrance of the pipe is dependent on the frequency of rotation of the cam. The data shows a droop in the peak-to-peak value of pressure at high plenum pressure and high frequencies; these trends with plenum pressure and frequency are predicted by the computer code. The peak-to-peak total pressure at the entrance of the pipe is shown to be dependent upon the frequency of rotation of the cam.

Figure 8 displays the peak-to-peak static presures versus rotational frequency for various plenum pressures for the one-per-rev cam. The experimental and numerical curves generally show good agreement and the computer code predicts the trends.

Figures 9 and 10 are plots of the ratio of pipe end-to-entrance pressure versus cam rotational frequency for both cams. The two-per-rev cam results are included since the two-per-rev cam extends the frequency range two-fold. Results are

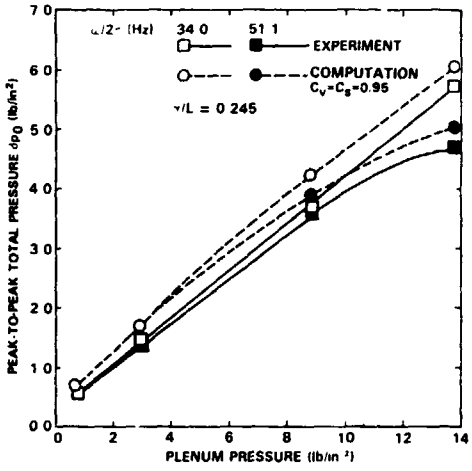

Fig. 7 Effect of plenum pressure

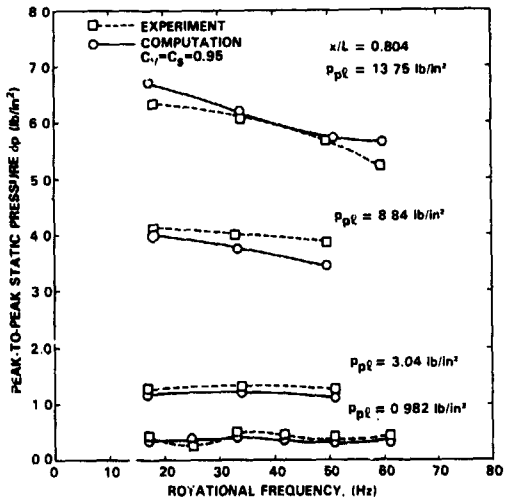

Fig. 8 Peak-to-peak static pressure

presented for two different plenum pressures for both one- and two-per-rev cams. These curves demonstrate the presence of a quarter-wavelength resonance phenomenon in the pipe. This phenomenon is better illustrated in Fig. 9 for the two-per-rev cam where a resonance peak occurs at a frequency of approximately 44 Hz for the numerical solution at the higher pressure and around 55 Hz for the corresponding experimental data. The differences in the resonant frequencies between the numerical and experimental results are likely due to the experiment having a shorter characteristic pipe length because of wave reflection from the end of the nozzle expansion section in the pipe entrance. The quasi-one-dimensional model is unable to simulate this reflection and instead reflects from the pipe entrance itself. It is interesting to note that

the resonance effect is much more pronounced at the higher pressure. For the one-per-rev cam plot shown in Fig. 10, no experimental data were obtained at the expected resonant frequencies of twice the resonant two-per-rev cam frequencies. However, the numerical results again show a resonance at around 75 Hz for the higher pressure and 80 Hz for the lower pressure. These resonant frequencies are somewhat less than twice the two-per-rev cam frequencies. The more pronounced resonant peak for the higher pressure in Fig. 10 is consistent with the two-per-rev cam results.

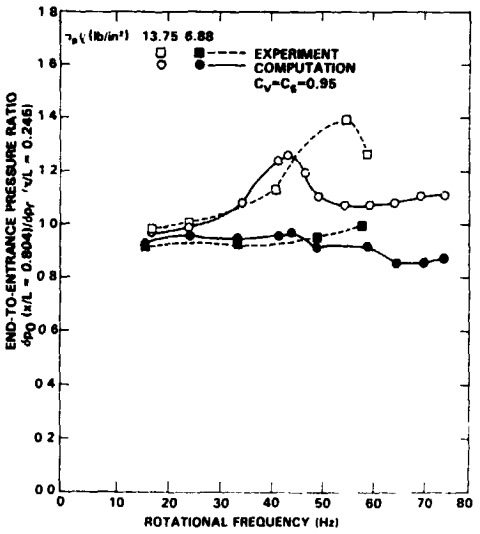

Fig. 9 Resonance phenomenon in pipe; two-per-rev

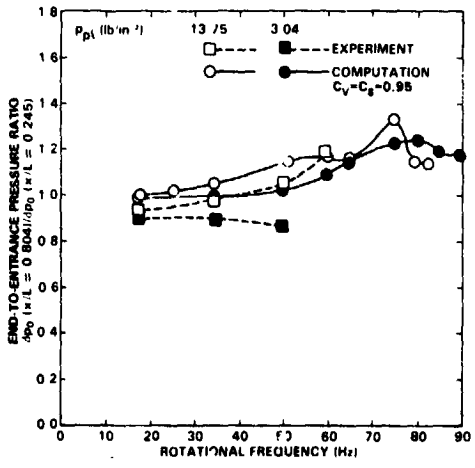

Fig. 10 Resonance phenomenon in pipe; one-per-rev

Effects of Rotational Frequency on Mass Flow Rate

Figures 11 and 12 show the effect of rotational frequency on the computed mean and peak-to-peak mass flow rates, respectively, for the one-per-rev cam at several different plenum pressures. No experimental data are available for comparison with the peak-to-peak data. The experimental lines shown for the mean mass flow rate represent an experimental average since no significant changes in average mass flow rate with frequency were obtained in the experimental data. Likewise very little change was observed in the numerical results.

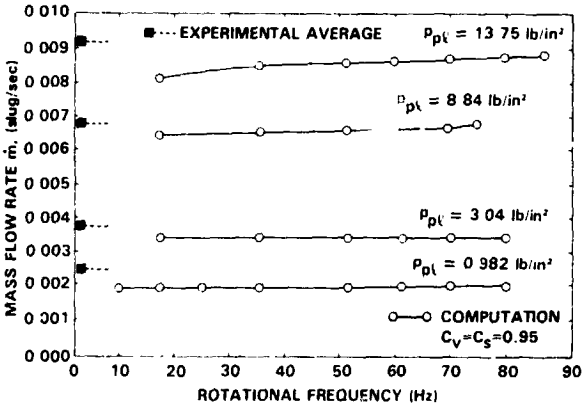

Fig. 11 Mean mass flow rate

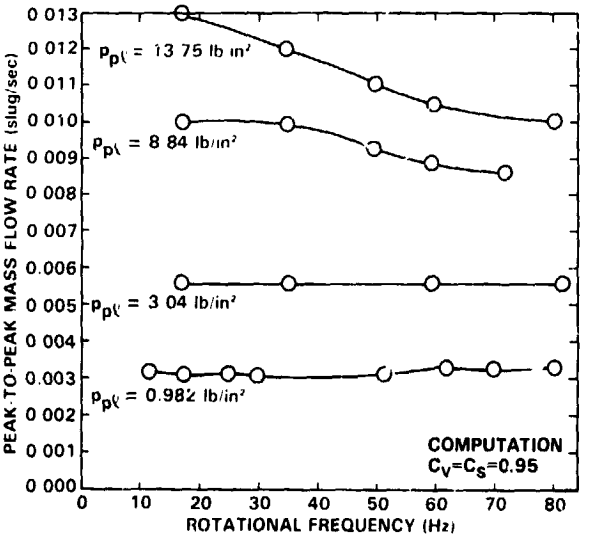

Fig. 12 Peak-to-peak mass flow rate

Figure 13 shows the effect of rotational frequency on the phase of the first harmonic of the mass flow results shown in Figs. 11 and 12. The phase shift increases with increasing plenum pressure (and increasing mass flow rate) and increases almost linearly with frequency over most of the range examined. The linear trend indicates that within this range there is a fixed time delay, almost independent of frequency, associated with a given set of system parameters such as plenum pressure and blade internal geometry. At the higher pressure, capacitance lag is controlling, while at the lower pressure, the lag should be principally sonic lag.

No experimental phase shift data are available for comparison because it is very difficult, if not impossible, to measure dynamic mass flow containing higher harmonics and obtain phase information.

In summary, the comparison of the numerical calculations with experiment, indicate that, even with a simple constant discharge coefficient model, the computer code satisfactorily predicts the system performance over a wide operating range. It is able to predict the trends and magnitudes of the total and static pressures as well as the mass flow rate for plenum pressures from 0.98 to 13.75 psig, for rotational frequencies from 15 to 120 Hz, and for valve area variations from 0 to approximately 1 in.

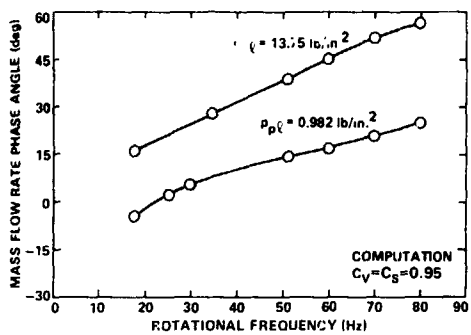

Fig. 13 Mass flow rate phase angle

Theoretical Transient Response

For pneumatic control system design, in addition to a knowledge of the periodic response of the system to periodic control inputs, the transient dynamics are also of interest. In the present study an independent numerical investigation of transient dynamics was conducted. This investigation simulated the pneumodynamic response of the model system to step inputs in control valve settings. This was accomplished by suddenly opening the control valve and allowing air to flow into a blade at atmospheric pressure, allowing steady flow to be established, and then suddenly shutting off the flow, allowing the pressure inside the pipe to return to atmospheric pressure.

The results of this investigation into the system's transient dynamics are shown in Figs. 14 to 17. Figure 14 shows the behavior of the mass flow rate in response to the two control actions for two plenum pressures. The rise or decay time for the mass flow is approximately 0.003 seconds and does not change significantly for the two plenum pressures. This suggests that in these cases the characteristic time phenomena are principally related to the time it takes for a pressure disturbance to propogate the length of the tube, since this is also about 0.003 seconds. This explanation is reinforced by examining Figs. 15 and 16 which are plots of the pressure distribution at various elapsed times after the sudden valve opening. Fig. 15 shows the propagation of the incident pressure wave created by the valve opening and Fig. 16 shows the propagation of the wave after its reflection from the end of the tube. The sonic lag is apparently controlling the transient response to the step input. However, for a system where the capacitance lag is much higher or lower than the sonic lag, the capacitance lag would tend to control the rise or decay. Figure 17 shows the propagation of the incident pressure wave created by sudden valve closing. To smooth these transient results, second-order spatial numerical damping has been added to the numerical algorithm[1] for computing the incremental or "delta" solution for a given time level from the solution for the preceding one. This was done by computing the increment from the weighted average of the second-order (in time) Beam and Warming algorithm and the first-order (in time) algorithm of Lax[5]. The weighting factors applied to the Beam and Warming method and the Lax method were 0.98 and 0.02, respectively.

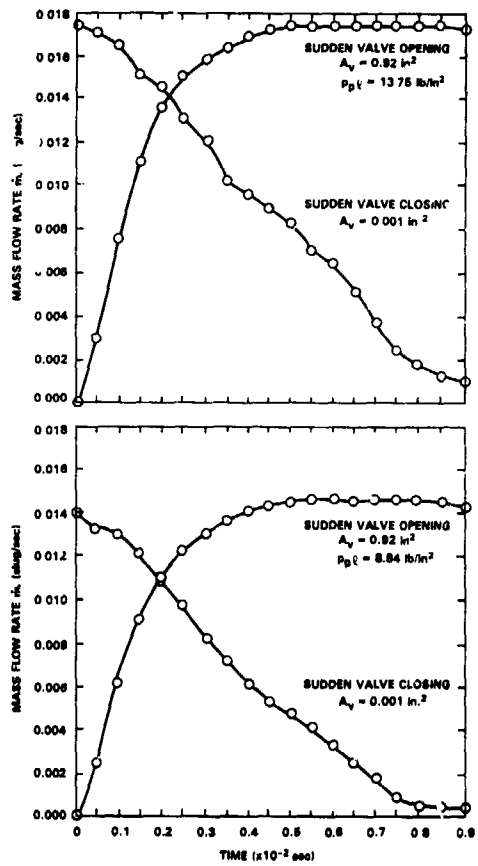

Fig. 14 Theoretical transient mass flow rate

Conclusions

The results presented indicate that quasi-one-dimensional unsteady flow theory can be applied to predict, with reasonable accuracy, the pneumodynamic response of an idealized circulation control rotor model to cyclic control valve inputs.

The results also show that, for a given set of system parameters, the phase lag in the response of the system to cyclic control input is a fixed time delay almost independent of frequency. Higher harmonic content of the mass flow rate output exhibits some amplication due to nonlinear effects, but the higher harmonic content of the pressure response

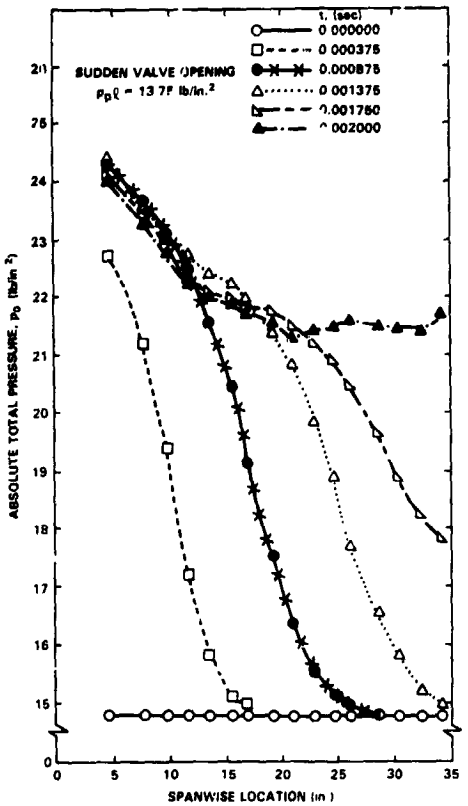

Fig. 15 Theoretical incident transient pressure wave

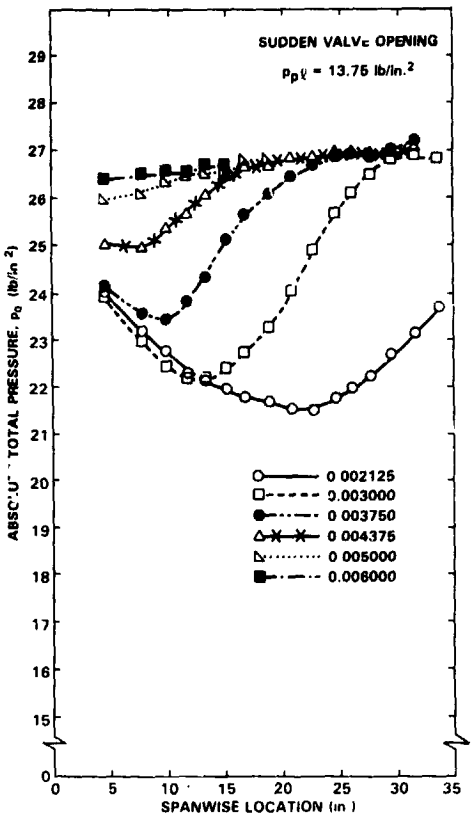

Fig. 16 Theoretical reflected transient pressure wave

does not.

A resonance phenomenon is predicted by the numerical results at approximately the frequency for quarter-wave acoustic resonance in a pipe. The predicted resonant frequencies are slightly different than the experimentally observed resonant frequencies. A possible explanation for this is the inability of the quasi-one-dimensional theory to predict wave reflection from the expansion in the entrance section of the experimental model.

Numerical investigation of the response of the flow variables to step inputs in the control valve area indicate that, for the cases examined, the response time is controlled by the characteristic time for wave propagation (sonic lag).

References

Watkins, C.B., Reader, K.R. and Dutta, S.K., "Numerical and Experimental Simulation of Circulation Control Rotor Pneumodynamics," AIAA Paper No. 83-2551, AIAA/AHS Aircraft Design, Systems and Operations Meeting, Fort Worth, Texas, Oct. 17-19, 1983.

Beam, R.M. and Warming, R.E., "An Implicit Factored Scheme for the Compressible Navier-Stokes Equations," AIAA Journal, Vol. 16, No. 4, pp. 393-402, May 1978.

Reader, K.R., "Evaluation of a Pneumatic Valving System for Application to a Circulation Control Rotor," Naval Ship Research and Development Center Report 4070, May 1973.

Reader, K.R., "The Effects of Cam and Nozzle Configurations on the Performance of a Circulation Control Rotor Pneumatic Valving System," David Taylor Naval Ship Research and Development Center Report ASED-393, Nov. 1977.

Lax, P.D., "Solutions of Nonlinear Hyperbolic Equations and Their Numerical Computation," Communications on Pure and Applied Mathematics, Vol. 7, 1954, pp. 159-193.

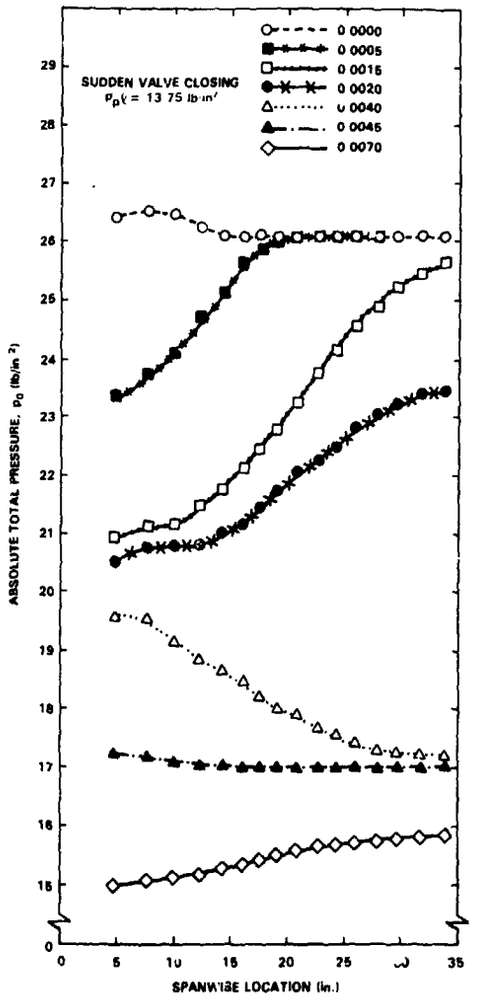

Fig. 17 Theoretical transient pressure wave

DISCUSSION
Paper No. 18

DYNAMIC RESPONSE CHARACTERISTICS OF A CIRCULATION CONTROL ROTOR MODEL PNEUMATIC SYSTEM
Charles B. Watkins
and
Kenneth R. Reader
and
Subash K. Dutta

Andy Lemnios, Kaman Aerospace: First, an observation. On the bench test that we did on the half scale model of the CCR several years ago I believe we observed about a 20 to 30 degree phase lag between the control input to the control valve to the actual buildup of pressure in the plenum chamber. We also observed that the duct of the blade itself charged and discharged as a plenum. Basically there was very little phase lag relationship between the root end of the blade and the tip end of the blade as far as pressure buildups were concerned. Those pressure variations have been documented. I was very pleased to see that in your high freqeuency pneumodynamic analysis you have included flexibility in there. I was wondering if you have any plans to validate the analysis?

Reader: Yes, Andy, over the years we have done that. We've used the H2 data [that] I had to a limited extent. The problem there is that all the tests that we've run so far we've always found we didn't have all the information we needed. In that rotor system we had total pressure at the inboard, [but] the outboard was very questionable. I've had very good results with this code with the H-2 experience, that is, if I look at the components I was able to look at the weight flow, the one per rev and two per rev component at the inboard station and get good correlation if I did a parametric study to identify it. We've looked at the Boeing Vertol data which was tested in Boeing's tunnel about two years ago. We've looked at fixed system results similar to these; half-scale [tests] that were done at UTRC about 3 or 4 years ago. We have not been fortunate enough to get this type of correlation across a large range of parameters, but we can always trace it to some unknown that we haven't been able to measure. One of the big problems we end up with the flexible slots is identifying what that slot area really is. The 25-foot rotor system, we ran correlation with that and we came back to the same position. Most of the time you end up measuring weight flow which goes into all the blades and you have to assume what it is for one blade and then the area variation. I think looking in the box we've worked with most of the data that exists and were fairly reasonable based on engineering level.

Lemnios: Getting back to your comment on the H-2, Ken, the half-scale data I was referring to was the one that was done at Honeywell under a subcontract.

Reader: Yes, I'm aware of that.

Wayne Johnson: I would like to put Andy's question a little bit differently. You describe what you have done in the past and described the capabilities of the analysis that you have. If you were making a list of the things that you didn't know about the duct aerodynamics and that you would really like to know next, where would you start?

Reader: First of all I think the code gives us a good representation analogy. It is a fairly good design tool. The [major] problem is we need more instrumentation on the blades; we need to know more specifics at different radial stations and that is being done.

Johnson: So until you do another round of experiments you really don't know . . .

Reader: That's right. We are using it as a design tool now based on our experiments up to now. The next thing we need is more data. I think we will be getting that, probably in the next year.

Johnson: Since I have the microphone I'm going to ask another question. To make a connection with some of the things we have heard earlier--the dynamic inflow [models] for all their simplicity are extraordinarily useful because they are a discrete state model of the dynamics. I know, at least I think I've seen in some of the earlier work on circulation control rotors that people have developed rather heuristic models of duct aerodynamics, mass-spring type models, which I think they just sort of guessed at Do you think there is a chance that one might start with the kind of model you are using and then use that as a basis for a more solid foundation for a discrete state model for the aerodynamics that then could be a little bit more useful? I think that with a two-dimensional Beam-Warming type solution that you are dealing with fairly significant computation time. I was just wondering if there are ways of that sort that you might go to make a better, but faster model.

Reader: There's one way and it was addressed earlier with Bob Jones' work. If you believe the code then you can regress a model that you need to operate with. But the thing of it is you need to identify all of your parameters up front. There's been some work done on that.

That is, you take the code, you can design a system, get it set up, and then you can linearly regress out of it a faster working model. One of the problems that we have had historically and what has led us to this code is that if you use your analogies to develop [the code] you end up with a lot of constraints on it. Now we had that with the SUPERFLOW code, that is, where we tailored it for specific configurations so that it's good for that specific configuration and it may run a little bit faster--not a whole lot--a little bit, but you ended up without a good design tool. If you go to a real simple model like we had done in the past for stability and control then you end up without the higher harmonic capability. So you end up with two codes and now you have to start keeping track of two codes. I think you are probably better off using a code like this and come up with a regressed model out of it for your actual application.

Bob Wood, Hughes Helicopters: I was interested in your model--the traveling wave [going] down the blade and then reflected back. I didn't really see the thing coming to equilibrium. In other words, is that wave--my question is in several parts, does that wave then come down and then travel back? Essentially, what is the amount of time that's required for a step input before the flow comes to equilibrium?

Watkins: In actuality it's going to reflect back and forth any number of times, but the phenomena tends to be obscured by the flow itself. But essentially it only takes one complete reflection for the flow in the duct to pretty much distribute itself evenly over the length.

Reader: I'd just like to make a comment on Wayne's question just a minute ago. I just had another thought. One thing that we found, for instance right now, to do this work we've run 16 elements in it and it has taken the cost up for running the code. However, if you back off the number of elements, depending upon what you are using it for, you may not need the fidelity, so if you back off the elements your time goes way down--probably a factor of 4 to maybe 5 depending upon the number of elements. Kaman did some of that work earlier with their codes and they found that, for instance, for some cases they needed 4 to 6 elements, but for general handling quality-type stuff they only needed one. I think that is what Andy was alluding to earlier. Depending upon what you are doing with the pneumodynamics and what you need out of it--if you only need one per rev cyclic in order to do stability and control you can come up with a fairly simple model for that.

AN EXAMINATION OF THE RELATIONS BETWEEN ROTOR VIBRATORY LOADS AND AIRFRAME VIBRATIONS

Charles F. Niebanck
Senior Dynamics Engineer

Sikorsky Aircraft Division
United Technologies Corporation
Stratford, Connecticut

Abstract

Harmonic rotor hub loads and airframe interactions in steady flight are reviewed, with regard to the objective of achieving lower airframe vibration by modifying blade root loads.

Flight test and wind tunnel data are reviewed, along with sample fuselage response data. Trends which could provide a generalized approach to the above objective are found to be very limited.

Recent analytical and corresponding experimental blade tuning modifications are reviewed and compared. Rotor vibratory load modification and substantial vibration changes were achieved over a wide range of rotor operating conditions.

It is still concluded that improvement of blade tuning has the potential for reduction in airframe vibration. Current analytical methods are found not accurate enough to confidently predict effects of blade tuning on vibration.

Test-based development of favorable blade configurations is shown to be feasible, and will also generate data to guide further development of analytical methods.

Introduction

Reduction in helicopter airframe vibration enhances crew and passenger effectiveness and comfort, and reduces vibration-related problems with the airframe structure and installed equipment. Higher speed operating regimes are planned for future helicopters, which will create a strong tendency for increased vibration. Furthermore, vibration levels even lower than those of presently operational helicopters are desired in these higher speed regimes. Therefore, the development of improved vibration control measures is receiving continued attention.

Analytical investigations such as those presented in Reference 1 have predicted that substantial reductions in helicopter rotor vibratory hub loads may be obtained by modifying the distributions of structural properties such as blade bending stiffness and mass, with little or no penalty in blade weight or structural complexity. The implied corresponding reduction in airframe vibration was verified by coupled rotor-airframe aeroelastic analysis.

This method of reducing vibration is quite attractive, since it can reduce or eliminate the need for other vibration control measures such as vibration absorbers or higher harmonic control. These other measures are effective, but entail additional cost, added parts, weight, and maintenance.

This paper examines the trending of rotor hub loads as indicated by various flight and wind tunnel test programs, and the typical airframe vibratory response to these loads, to assess the possibility of creating a generalized recommendation for modification of hub loads. Some recent analytical and corresponding experimental efforts to exploit the blade tuning concept are reviewed. These results of these attempts are diagnosed, and an assessment made of the feasibility of applying the concept analytically, through complete system experimentation, or from separate dynamic model and airframe testing.

Background

The reduction of helicopter blade vibratory elastic response in forward flight has long been intuitively recognized as a potential means of reducing vibratory hub loads and their consequent airframe vibration. Historically, this objective has been addressed during the design stage simply by providing blade designs whose elastic natural frequencies were well-separated from resonances with the harmonics of the rotational frequency.

Presented at the American Helicopter Society 2nd Decennial Specialist's Meeting on Rotorcraft Dynamics, Ames Research Center, Moffett Field CA, November 8, 1984.

The development of sophisticated analytical models and the computer programs to implement them provided a means for further understanding of the complex phenomena involved in the motions of a helicopter blade and the resulting forces transferred to the fuselage. The helicopter rotor math model described in Reference 2 is an example of a number of such tools available.

Analytical and experimental work described in References 3 and 4 indicated that passive tuning of the normal blade structural parameters was worthwhile pursuing. Reference 5 is a concise analysis of blade bending mode response to harmonic loadings. The traditional resonant amplification factor was considered; in addition, a Modal Shaping Parameter was developed which considered the modal generalized mass, the modal inertial shear integral, and the modal aerodynamic generalized force. The product of the resonant amplification and the Modal Shaping Parameter provided a quantity which reflected the response of a given blade mode root shear to a given harmonic. It was shown that the modal shaping parameter is at least as important as the natural frequency in determining the root shear for a given mode and harmonic forcing frequency.

The work of Reference 1 exploited the availability of advanced rotor and airframe mathematical modeling to pursue further refinements in rotor blade dynamic tuning. A detailed consideration of the various factors involved in the harmonic forcing of the individual blade modes was conducted, along with the influence of these factors on blade root shears for each harmonic. This analysis led to recommended design improvements aimed at reduction in the amplitude of modal root shears. These design improvements were the removal of blade mass from blade inboard span, an increase in blade mass at the tip, moving the mass center of gravity forward at the blade tip, and increasing the blade edgewise stiffness. Rotor-airframe coupled response calculations with the method of Reference 2 verified a substantial decrease in airframe vibration, amounting to better than 50% reduction for the higher amplitude vibration components.

Scope of Present Considerations

This paper considers the hub loads and airframe interactions of an articulated four-bladed rotor. The rotor is in steady flight, and has identical blades. The blade hinge and rotor shaft hub loads considered are shown in Figure 1. Explicit consideration of blade pitch control loads and lag damper loads are ignored, as is the effect of hub motion on the rotor loads. These restrictions do not result in the exclusion of any fundamental concept, and permit a simplification of the discussions to follow. The discussions herein are centered on the blade tuning concept, they do, however, have more general application to other means of altering blade vibratory responses or hub loadings.

Basic Relationships

The fundamental relationships that exist between the blade hinge loads and the vibratory response at an airframe point are reviewed in this section.

Transfer of Loads Between Rotor and Fuselage

The resolution of vibratory loadings between the turning rotor and the airframe has the well-known result presented in Table 1. The rotor applies vibratory loadings to the airframe at the blade passage frequency only (the rotational frequency times the number of blades). These airframe loadings are caused by vibratory loadings in the rotor system at frequencies equal to the blade passage frequency, the blade passage frequency minus the rotational frequency, and the blade passage frequency plus the rotational frequency. In the case of the four-bladed rotor, the four per revolution airframe loadings are caused by three, four, and five per revolution loadings in the rotor.

Generalizations related to the reduction in airframe loads and vibration that can be drawn from the relationships in Table 1 are limited. The vertical force FZ4 has a straightforward relationship with the A4 vibratory hinge force, so that a reduction in A4 has a corresponding reduction in FZ4. All the other airframe load components have the possibility of beneficial cancellation among the constituent components. Therefore, a reduction in the load component H3C, for example, may result in an increase in the in-plane loads FX4 and FY4. A generalized decrease in in-plane hub loads will result if all the radial and tangential 3 and 5 per revolution hinge load components are reduced in the same proportion. Another obvious generalization is that the hinge offset distance e controls the magnitude of the in-plane and torsional vibratory moments, and the relative importance of the vertical 3 and 5 per revolution hinge forces which give rise to them.

Airframe Vibratory Response to Loads

A presentation of representive vibratory responses of an airframe point to the rotor load components is provided in Figure 2. This figure shows the cosine and sine response of the cockpit floor at the pilot location in the vertical direction for a set of rotor load components. A graphical vector addition of the components is shown, along with the resultant pilot vertical vibration. These data are purely analytical, but do illustrate the manner in which the various component responses combine. The vibratory response at a point is generally dependent to some degree on beneficial cancellation between various components. In the example of Figure 2, a reduction in vertical vibratory force would cause very little change in the vibration level at the pilot floor. Furthermore, a reduction in in-plane moments (dependent on vertical hinge forces) would cause an increase in vibration at that point. Note that this example is purely illustrative; other points in the same aircraft, different aircraft, and actual test data would show different response results. One general modification that can be applied to the vibratory rotor load components that will result in a reduction in vibratory response is to reduce all of them in the same proportion. An increase in the number of blades provides a generalized decrease in the amplitudes of the loads and this decreases airframe vibration.

Review of Hub Load and Fuselage Response Data

Survey of Vibratory Hinge Load Test Data

In this section, a collection of measured hinge load data will be presented and examined, with the objective of searching out any evident general tendencies which could be useful in the development of guides or judgement for the application of beneficial blade tuning.

A total of six sources were used in preparation of this collection of data, which is presented in Figures 3 and 4. These are briefly described as follows:

(1) Unpublished data from the 1977 test of a prototype 4-bladed S-76 rotor in the Ames Research Center 40x80 foot Wind Tunnel. Hinge load data were obtained from calibrated strain gage readings of hub and shaft bending.

(2) Data from the Reference 6 report of a 5-bladed S-61F rotor flight test. Hinge load data were obtained from differences between strain gage readings of blade bending moments at two stations near the blade root. Corrections were applied in accordance with hinge motions, cyclic pitch, and blade mass distribution in the root area.

(3) Data from the Reference 7 report of a 6-bladed CH-53A rotor flight test. Data were obtained essentially in the same manner as for Reference 6.

(4) Unpublished data from a 1983 test of a specialized 4-bladed set of model blades with adjustable mass distribution. Hinge load data were obtained from a superposition of blade modal hub shears. Blade bending mode amplitudes were obtained from a least squares fit of the blade mode shapes to the measured blade harmonic vibratory bending moment distribution.

(5) Unpublished data from 1983 flight testing of an S-76 aircraft with modified main rotor blades. These modifications were increased edgewise stiffness and the addition of a 10-lb tip weight. Data obtained by the same method as for item (4) above.

(6) Data from Reference 8. A 4-bladed model rotor was provided with a specially instrumented hub for the measurement of blade hinge loads.

In Figure 3, the 3, 4, and 5 per revolution hinge loadings per blade are presented in non-dimensional form by dividing by rotor lift and plotting against advance ratio. Hinge loading phase angles are also presented for the more important of the hub loadings. Perhaps the most prominent trend visible is the relatively large magnitude of the 3 per revolution vertical load response A3. Most of the model and full-scale data for this parameter are reasonably consistant. Exceptions are the data from the flight testing with the edgewise stiffened S-76 blades, and the adjustable mass model blades. Adding tip mass to the stiffened S-76 created large A3, while the stiffened blades without tip mass had small A3. These changes in A3 itself, however, are believed to have had little effect on airframe vibration because of the relatively small hinge offset and consequent small in-plane moment. Note that the behavior of the A3 load will be of greater importance with 4-bladed hingeless rotors with larger virtual hinge offset.

Generalized trends which apply to the other loading components are not immediately evident, beyond the tendency of all load amplitudes to rise steeply after an advance ratio of .3. Some of the edgewise load data display a tendency toward lower amplitudes at moderate advance ratio, similar to rotor power required loadings. Data from the individual rotors does show individual trending as a result of increasing advance ratio. Except for the A3 amplitudes, however, the data vary widely between the various rotors.

Figure 4 presents a crossplot of the same hinge load data against the ratios of the natural frequencies of the various blades to various harmonics. The objective of this figure is to exhibit the extent to which the hinge loadings depend on resonance with harmonic frequencies.

In general, it appears that blade resonance with harmonics is a significant factor in the hinge load component magnitudes. It can also be seen that other influences are significant. The A3 loadings for the S-76 wind tunnel and flight test configurations appear to be responding to classical resonance with 3 per revolution airloadings. The earlier S-61F, CH-53A, and Reference 8 model data have, however, have relatively high A3 load response for their conventional flatwise frequency placement, suggesting that the aerodynamic spring effect discussed in Reference 1 may be active in moving the aeroelastic flatwise modal frequency closer to 3 per revolution for these rotors. As mentioned previously, the A3 load in itself does not strongly influence airframe vibration for 4-bladed articulated rotors with conventional hinge offsets. Further examination of Figure 4 shows that other influences such as the modal shaping effects discussed in Reference 1 are apparantly influencing the response of the individual hinge loads to a greater extent than the resonance effect. The H5 loadings, for example, become smaller for the adjustable mass and the S-76 flight blades even though the tuning attempts resulted in edgewise mode natural frequencies closer to 5 per revolution.

General tendencies which appear in Figures 3 and 4 may be summarized by stating that the 3 per revolution flatwise load is by far the largest, and this may dominate for larger virtual hinge offset rotors and airframes sensitive to in-plane moment forced vibration. The other load components range from very small up to about one-half of the 3 per revolution flatwise loading. Trends of amplitude with forward speed are upward beyond an advance ratio of .3, but other details such as phase angle are peculiar to the individual blade configurations. Some evidence of resonance with harmonic loadings is present, but it is also clear that other phenomena have an important contribution.

Variability in Airframe Dynamic Response

In this section, a limited sample of calculated and test airframe dynamic response data will be reviewed, in order to present the extent to which variability occurs in the airframe response to dynamic loading components, and show a sample of the predictive capability of current finite element methods.

Figure 7 presents the cosine and sine parts of the pilot vertical response due to a 1000 lb vibratory hub force at the 4 per revolution frequency in the longitudinal direction. The contours are formed as the frequency is varied to reflect rotor rotational speed variations between 90 and 110% of normal. Calculated data are shown for three aircraft. Also shown is a data point available from an S-76 shake test for a normal 4 per revolution frequency. From data of this nature, one can conclude that the phase response of an airframe point can be anywhere in the sine/cosine plane. The corresponding calculated data from finite element methods has at best a rough order of magnitude correspondence with the shake test data.

Review of Experimental Blade Tuning Results

The foregoing generalized considerations show that the application of blade tuning involves some uncertainty. Various loading components, as well as various blade aeroelastic effects have opposing effects on vibration. Therefore, reduction in a load component or components is not a sufficient condition for the reduction of airframe vibration level. Nevertheless, analytical results showed that reduction in blade mode harmonic response or a generalized reduction in the hub shears would usually lead to a reasonable reduction in the airframe vibration. Therefore, it was worthwhile to attempt experimental verification of the blade tuning concept.

Mass-Tuned Model Blade Wind Tunnel Test

A dynamically scaled model blade set was provided to NASA/Langley by Sikorsky Aircraft under Contract NAS1-12671 in 1976. The blade set was specially designed with removable and replaceable counterweight segments, such that a variety of blade mass and chordwise center of gravity distributions could be provided

for testing of their effect in the wind tunnel. The blade set is a traditional 4-bladed, untwisted, articulated design of 4.58 ft. radius. The blades were constructed with forward and aft counterweight tubes along the blade span. Up to 80 counterweight segments, each 1/2 inch long, may be inserted in the tubes and removed or replaced as desired by disassembling the blades from their cuffs. Alternate tungsten and aluminum segments are available to provide a variety of spanwise and chordwise distributions. The detailed physical properties of the blade set are described in Reference 9.

The design analysis used to provide favorable mass distributions for the model blade utilized the Reference 2 mathematical model as its major element. It was applied to the dynamical system comprised of the adjustable mass model rotor system coupled to a modal representation of the model rig and its support system. An objective function to be minimized was defined as the sum of the squares of the individual hub load components (i.e., the three forces and three moments - the moments were divided by twice the hinge offset distance). It was noted that the moment components had a relatively small contribution to the objective function. It was felt that this was a reasonable situation for the articulated model rotor.

A baseline configuration was defined with essentially constant mass distribution and quarter-chord center of gravity over the mass-adjustable portion of the blade. The mass-adjustable portion of the blade was divided up into eight spanwise zones, each including a forward and an aft counterweight increment, for a total of sixteen design variables.

At a defined rotor operating condition, uniform mass increments were added in turn to each of the sixteen counterweight zones. The change in the objective function was noted and a finite difference partial derivative formed with respect to each of the design variables. The favorable mass distributions were formed by adding or subtracting mass to the counterweight zones in proportion to the negatives of the objective function partial derivatives. The amount of mass that could be added or subtracted was constrained by the physically available counterweights. Favorable mass distributions were derived in this manner for a total of three operating conditions. The first of these dictated the removal of mass from the midspan region to the blade tip, with the blade center of gravity forward at the tip. The second was essentially the addition of tip mass. These distributions were constrained when a physical limit was reached at any one counterweight zone. The third distribution was practically the same as the first, so this was modified by adding or subtracting mass in the favorable direction in each zone until the physical limit was reached. Figures 8 and 9 show the spanwise mass and center of gravity distributions resulting for the baseline and the number 3 mass distribution. It was noted that this mass distribution was qualitatively similar to the favorable mass distribution resulting from the Reference 1 study, with mass removed from blade midspan and placed at the tip, and with the center of gravity moved forward at the tip.

When the tuning mass distributions were defined by the above analytical procedure, they were input to the coupled rotor-airframe analysis to confirm that an improvement had actually been obtained. Samples of the analytical results are provided in Figures 10 and 11. The large in-plane loadings are reduced by about 25%, and the vibratory response at the hub is reduced by a much larger percentage. In a purely analytical framework, the blade tuning optimization was shown to be successful.

The model blade set was mounted on the Sikorsky Aircraft Basic Model Test Rig, and tested in the United Technologies Corporation Main Wind Tunnel. A number of duplicate flight conditions were tested for the baseline and each of the three "optimized" mass distributions. Sample test results are shown in Figures 12 through 14. Figure 12 shows the response of a certain accelerometer on the model rig, indicating the blade passage frequency lateral vibration component amplitude as a function of advance ratio and nondimensional rotor lift. The blade tuning had a fairly substantial effect which extended over a wide range of flight conditions. The effect of the blade tuning, however, was to worsen vibration instead of improving it. Figure 13 shows the vibration level from the same accelerometer as a function of mass distribution and advance ratio. The baseline distribution had essentially constant mass versus span and a quarter-chord center of gravity over the mass-adjustable portion of the blade. The number 1 distribution removed mass from the blade midspan, increased mass at the blade tip, and moved the center of gravity forward at the tip. The number 2 distribution added mass to the tip area. The number 3 distribution was based on number 1, with further mass increments added or subtracted in each of the local zones where this was possible. Figure 13 shows an orderly relationship between the different mass distributions,

which extended over a reasonable range of flight conditions. Figure 14 shows the effects of blade tuning on harmonic hinge load amplitudes, as estimated from a summation of bending modal shears. The various bending mode amplitudes were estimated from a least-squares fit of the experimental blade bending moment distributions. The vertical 3 and 5 per revolution loads were raised, but this is not considered to have had a large effect on the rig vibration. The in-plane 3 per revolution hinge load was raised, while the 5 per revolution load was lowered. The loss of phase information during data processing is presently precluding a full diagnosis of the manner in which experimental hinge load components changed to create higher vibration. It is reasonable to expect the completion of data processing will show that the 3 and 5 per revolution in-plane loading are the source of increased vibration.

Figure 15 presents a comparison of test and analytical blade bending moment coefficients for pertinent harmonics and as a function of mass distribution, with the objective of evaluating the rotor aeroelastic analysis as a tool for determining favorable blade tuning adjustments. In the flatwise sense, the qualitative trending of the vibratory bending moment is quite faithfully predicted by the analysis, but the amplitude level is underpredicted by a factor of about one-half. In the edgewise sense, the loadings are also generally underpredicted, and the trending of the 3 per revolution and the 5 per revolution amplitudes is reversed. A detailed quantitative analysis of the results of these differences on the predicted hinge loadings has not been conducted. It is sufficiently evident from consideration of the relationships shown in Table 1 and Figure 2 that much greater accuracy will be needed from the analysis before it can be considered a reliable design tool for use in blade tuning.

Tuned Blade Flight Test

The success of analytical blade tuning considerations such as those described in Reference 1 also provided rationale for a flight evaluation of the concept conducted in the same time frame as the model test described above.

The main rotor blades of an S-76 helicopter were modified by adding a 10 lb tip weight at approximately the 92% radius. The edgewise bending stiffness was also increased by approximately 77% by adding boron strips to the trailing edge. This stiffness change raised the first edgewise bending frequency of the blade from 4.73 to 5.24 cycles per revolution. These modifications represented practical modifications to the existing blades which approximated the findings of Reference 1 with regard to favorable mass and stiffness changes. These specific modifications were also investigated with the blade aeroelastic analysis with the results shown in Figure 16 for hub loadings.

A sample of the flight test results appears in Figure 17. The aircraft vibration was generally increased rather than decreased by the analytically favorable blade modifications.

Figure 18 presents the effect of the tip weight on the vibratory hub load amplitudes for the stiffened S-76 blades only. The addition of tip weight significantly increased the 3 per revolution loadings, the 4 per revolution edgewise loadings, and decreased the 4 per revolution vertical and 5 per revolution edgewise loadings. These hinge loads were obtained from the blade modal fit and shear superposition method described earlier. Baseline aircraft blade bending moment data were not available to develop comparative data. It appears that the tip mass modification did create a substantial change in the blade response, although in the unfavorable direction. Common trends of tip mass addition and mass-tuned model blade distribution number 3 include increases in the 3 per revolution flatwise and edgewise loadings and a decrease in the 5 per revolution edgewise loading.

Figure 19 presents a comparison of flight test and analytical bending moment coefficients for the stiffened blades. Agreement between full scale analysis and test is lacking, especially the large increase in 3 per revolution loadings caused by the addition of tip mass.

Figure 20 presents test data for fixed system hub loads from the stiffened S-76 blades with tip weight on and off. These data are supplied by a resolution into the airframe system of the rotating system hinge loads from the blade modal fit and shear superposition method. The addition of the tip weight creates a substantial increase in lateral shear load and in-plane moments, but decreases the vertical shear loads.

Figure 21 compares the analytical and flight test hub loads applied to the airframe. It can be seen that there is no agreement between analysis and test that would allow reasonable use of the analysis as a tool for blade tuning to decrease airframe vibration.

Figures 22 and 23 are vector addition diagrams which illustrate the manner in which hub load component responses combine to create the resultant vibration amplitude at a point in the airframe. The various vector contributions are labeled with their corresponding force components. The factors p, q, m, and n represent transmissibility factors. The data used to construct these diagrams was obtained from S-76 airframe shake test results at the pilot seat, for in-plane vibratory force inputs at the rotor head. The shake test results showed an insensitivity to the vertical force, so this was not included in the vector diagrams. These shake test data also do not include the effects of the main rotor bifilar absorbers and the nose absorber which were active during the tuned blade flight testing. Despite this, the flight test data shows qualitative agreement with these figures.

Inspection of Figures 22 and 23 and use of Table 1 show that even for the simplified case considered here, wherein the radial force amplitudes are small, both the H3 and H5 force components are involved in the development of the resultant vibration level. Furthermore, Figure 18 shows that the 3 per revolution and the 5 per revolution in-plane load components are of the same order of magnitude.

This highlights a potential difficulty of making a straightforward choice of blade tuning modifications for vibration reduction. A modification of blade mass distribution which, for example, reduces the 3 per revolution amplitude response, may create an unfavorable change in 3 per revolution response phase angle, or in the 5 per revolution response amplitude and phase.

It appears that an attempt to predict even the qualitative result of a proposed blade tuning modification must consider the airframe response to the hub load combinations, unless the modification creates a profound reduction in all the hub load components which have a significant effect on airf ame vibration.

Application of Blade Tuning Modifications

In common with other vibration control methods, the effects of blade tuning modifications have been found to be poorly predicted by analytical means. It is technically feasible, however, to arrive at a favorably tuned blade configuration by conducting an organized set of experiments. An improved mass distribution based on the mass-tuned model experiments is presented in this section. In terms of full-scale aircraft application, this would correspond to a series of flight tests with trial blade configurations. As an alternative to this flight development stage experimentation, it may be advantageous to develop a favorable configuration by combining dynamic scale model wind tunnel experimental data with airframe shake test data as described below. This latter method would also yield a more organized body of detailed data on rotor loads response to blade modifications and of airframe dynamic response. These data could be used for the improvement of the analytical methods, with the ultimate objective or improving them to the point where they could be used early in the design process.

Development of Favorable Mass Distribution from Model Test Results

The current series of model tests are the basis of an improved vibration-tuned mass distribution for the mass-tuned model discussed earlier. Note that these results are, strictly speaking, peculiar to the model and its support system itself, and the mass distribution derived may not be suitable for any particular full-scale aircraft.

The process of developing a favorable vibration configuration started with the selection of a performance index. In the case of the model, a single accelerometer reading was sufficient, namely the top lateral accelerometer response presented earlier herein. Application to a full-scale aircraft could use a performance index comprised of the weighted sum of the amplitudes of a number of accelerometers at various points in the aircraft.

Each of the three mass distribution modifications tested had been scaled by the constraint of the maximum counterweight change which physically could be accommodated. The change in the accelerometer response from baseline for each distribution at a certain flight condition was then considered as a partial derivative with respect to that distribution. A combined distribution was formed by subtracting the three test distributions times a multiplier in proportion to their partial derivatives but also such that the total removed met the physical constraints of possible counterweight removals. It was assumed that magnesium counterweights could be manufactured to facilitate this.

The distribution resulting from this method is presented in Figures 24 and 25, compared with the baseline distribution. As one might expect, the distribution change from the baseline is similar to the inverse of the analytically derived number 3 distribution shown in Figures 8 and 9. To date, this new distribution has been neither tested nor investigated with

analytical methods. It should be noted, however, that the Reference 3 analytical study of the effects of added mass reported some trends that agree with the findings of this model test, such as an increase in 3 per revolution flatwise response when tip weight was added.

Alternative to Complete System Experimentation

Application of the above method of blade tuning to the full scale aircraft development process would imply flight testing the aircraft with a number of experimental blade configurations. This is feasible technically, but a means of arriving at the favorable tuning configuration earlier in the development process would certainly be desirable. Dynamic model test data for the blade configuration selected and airframe shake test data could potentially supply this earlier, and guide the choice of a starting point for flight testing of blade tuning. When a completely new aircraft is in development, the rotor design has been essentially frozen when the airframe becomes available for shake testing, so any blade tuning modifications would be limited. Therefore, the procedure outlined below should be most acceptable when an improved rotor system is to be developed for an exisiting airframe.

(1) Through relationships such as those in Table 1, the hub forces {F} may be developed as a function of the hinge or blade root loads {H}:

$$\{F\} = [R]\{H\}$$

(2) The fuselage accelerations {X} due to the hub forces are assumed to be accurately known from a well-implemented airframe shake test; the matrix [A] may include corrections for the influence of the rotor itself on hub motions:

$$\{X\} = [A]\{F\}$$

(3) A suitable performance index {Q} is developed to reflect the response of the aircraft at all the critical locations:

$$Q = \lceil X \rfloor [W]\{X\}$$

(In the above, {}, [], and $\lceil \rfloor$ denote column, rectangular, and row matrices respectively.)

(4) Run a dynamically scaled wind tunnel test for a baseline blade. Obtain baseline blade hinge or root loads {H0}. Use the above relationship to develop a baseline performance index Q0.

(5) Define a set of n distinct modifications, such as mass distribution, stiffness distribution, trailing edge reflex tab distribution, tip sweep, and the like. Scale these changes to a common portion (say 50%) of the allowable change.

(6) Run wind tunnel tests for the n modified blade sets and obtain n corresponding sets of hinge or blade root loadings. {H1}, {H2}, - - - {Hn}. Use these data to get corresponding performance function values Q1, Q2, - - - Qn.

(7) Examine Q1-Q0, Q2-Q0, - - - Qn-Q0. Apply the various modifications to the model blade in proportion to their favorable effect. Apply to the model and retest to verify the combined effect.

Execution of the plan outlined above would, in addition to providing a benefit to the subject aircraft, supply a body of data to support future applications and the development of analyses, which could ultimately allow the introduction of blade tuning refinements at an early stage in the design process.

Concluding Remarks

1. Helicopter harmonic vibration at an arbitrary local point in the airframe is affected by a number of distinct blade root load components and distinct airframe shaft load to vibration transmissibility components. In general these create reinforcement and cancellation effects which make the vibration change outcome of a change in blade root loads uncertain. The reduction of the amplitude of one or a number of blade root load components is not a sufficient condition to cause a reduction in airframe vibration.

2. A survey of some existing experimental blade root 3, 4, and 5 per revolution articulated rotor loadings has been conducted and examined for trends which could be helpful in developing lower vibration levels for helicopters with four blades. The three per revolution vertical force was the largest and had similar trends among several conventional model and full scale rotor configurations. Specialized tuned configurations were notably different from the conventional rotor trending for this load component. Other force component amplitudes were similar in size, and had no common trend beyond an increase at the higher speeds. There appears to be no specific modification in blade root loads which would be of generalized benefit, beyond a reduction of all components by a common factor.

3. Simple resonance of blade natural frequencies with harmonic loadings appears to have an effect on the blade root loads.

Analytical considerations and blade tuning experiments indicate that other important effects are present. These include aeroelastic or modal shaping influences on the aerodynamic forcing of the blade.

4. The response of an airframe to harmonic hub forces is highly variable with respect to frequency, location, and airframe. There appears to be no analytical prediction or characterization of this response beyond a rough estimate of the order of magnitude.

5. Modification of blade structural properties to alter blade response, root loads, and airframe vibration has been accomplished successfully within an analytical framework.

6. Model and full-scale experiments were successful in demonstrating that practical changes in blade structural properties could create substantial blade root load and airframe vibration changes. These changes were consistent over a reasonable range of flight conditions and were typically 20% to 60% of a baseline level. Individual load component reductions of this magnitude were achieved by tuning attempts, and therefore, vibration reductions of corresponding size are considered potentially available.

7. Experimental attempts to modify vibration by blade structural changes resulted in increases rather than the analytically predicted decreases in vibration.

8. Rotor aeroelastic response analyses and airframe dynamic response analyses do not generally provide an accurate prediction of the effects of blade structural changes on vibration. Some trends of individual response components are predicted correctly. Opposing and reinforcing interactions between a number of response components magnify the effects of predictive errors.

9. It appears that a series of organized experiments could be utilized to define favorable blade structural property distributions for reduced vibration.

10. Experimental determination of blade structural properties favorable for reducing the vibration of a specific aircraft could be based on a series of flight tests with experimental rotor blade configurations.

11. Experimental determination of blade structural properties favorable for reducing vibration might also be based on rotor flight test or wind tunnel data, combined with airframe shake test data.

References

1. Taylor, R. B., "Helicopter Rotor Blade Design for Minimum Vibration", UTRC Report R83-915783-27, United Technologies Research Center, NASA Contractor Report, December, 1983.

2. Bielewa, R. L., "Aeroelastic Analysis for Helicopter Rotor Blades with Time-Variable Nonlinear Structural Twist and Multiple Structural Redundancy - Mathematical Derivation and Program User's Manual." NASA CR-2638, October, 1976.

3. Blackwell, R. H., "Blade Design for Reduced Helicopter Vibration", American Helicopter Society National Specialist's Meeting on Helicopter Vibration, Hartford, CT, November 1981.

4. Blackwell, R. H. and Frederickson, K. C., "Wind Tunnel Evaluation of Aeroelastically Conformable Rotors", USAAVRADCOM-TR-80-D-32, Applied Technology Laboratory, U.S. Army Research and Technology Laboratories, January 1981.

5. Taylor, R. B., "Helicopter Vibration Reduction by Modal Shaping", American Helicopter Society 38th Annual Forum, Anaheim CA., May 1982.

6. Fenaughty, R. R. and Beno, E. A., "NH-3A Vibratory Airloads and Vibratory Rotor Loads." Sikorsky Aircraft, Naval Air Systems Command SER 611493, Department of the Navy, January, 1970.

7. Beno, E. A., "CH-53A Main Rotor and Stabilizer Vibratory Airloads and Forces." Sikorsky Aircraft, Naval Air Systems Command SER 65593, Department of the Navy, June 1970.

8. Bain, L. A., "Comparison of Theoretical and Experimental Model Rotor Blade Vibratory Shear Forces", Sikorsky Aircraft, USAAVLABS Technical Report 66-77, U.S. Army Aviation Materiel Laboratories, Fort Eustis, VA, October, 1967.

9. Murrill, R. J., "Design and Fabrication of 9-Foot Diameter Research Model Rotor Systems", Sikorsky Engineering Report SER-50963 Rev A, NASA Langley Research Center, Hampton, VA, August, 1976.

Table 1.
CORRESPONDENCE OF AIRFRAME LOADS AND BLADE HINGE LOADS

Airframe Loads	Blade Hinge Loads
FX4C =	2(R3C+H3S+R5C-H5S)
FX4S =	2(R3S-H3C+R5S+H5C)
FY4C =	2(-R3S+H3C+R5S+H5C)
FY4S =	2(R3C+H3S-R5C+H5S)
FZ4C =	4(A4C)
FZ4S =	4(A4S)
MX4C =	2e(-A3S+A5S)
MX4S =	2e(A3C-A5C)
MY4C =	2e(A3C+A5C)
MY4S =	2e(A3S+A5S)
MZ4C =	4e(H4C)+4MD4C
MZ4S =	4e(H4S)+4MD4S

Nomenclature:

As shown in Figure 1.
3, 4, 5: 3d, 4th, 5th harmonics
C,S: cosine, sine parts
R: radial
H: horizontal
A: axial
e: hinge radial offset

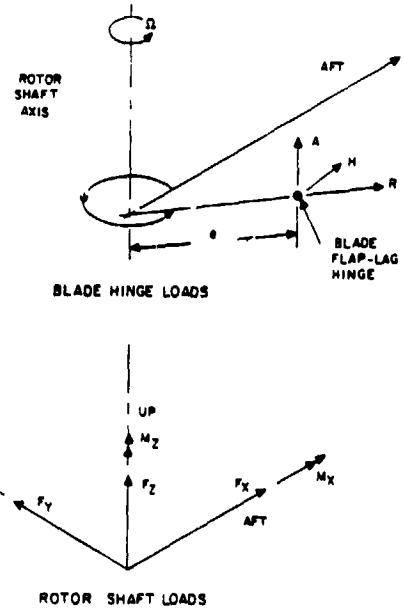

Fig. 1. Hinge and shaft loads.

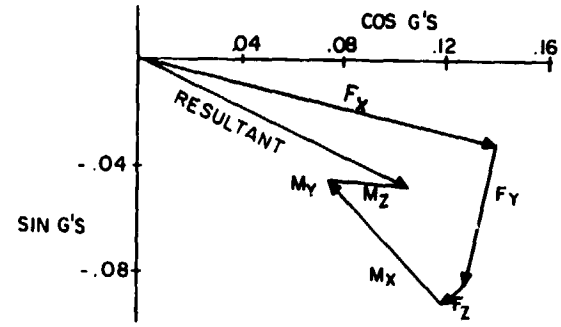

Fig. 2. Representative airframe response to rotor shaft loads.

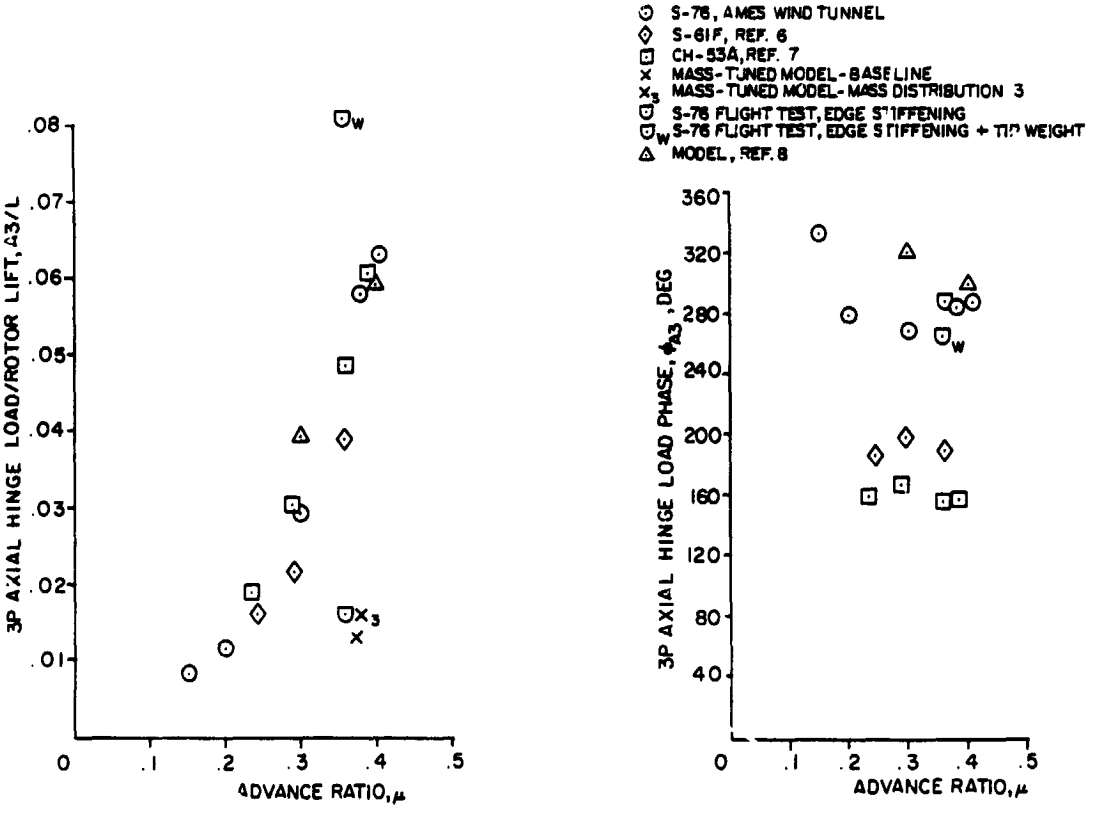

3(a) 3P Axial Amplitude and Phase

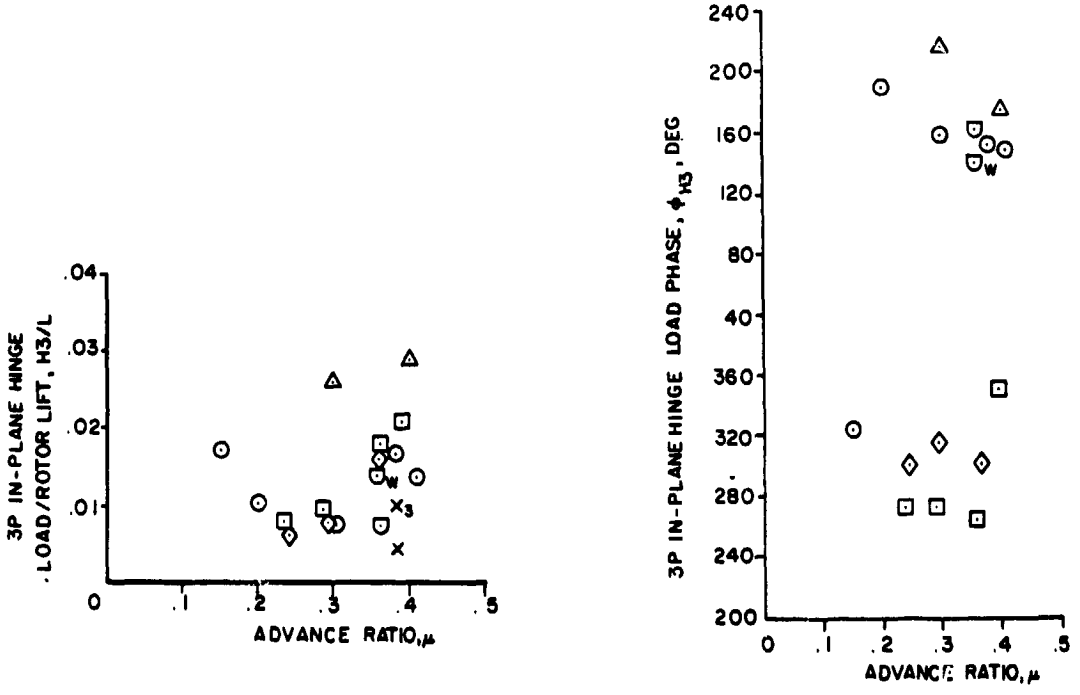

3(b) 3P In-Plane Amplitude and Phase

Fig. 3. Survey of harmonic hub load test data.

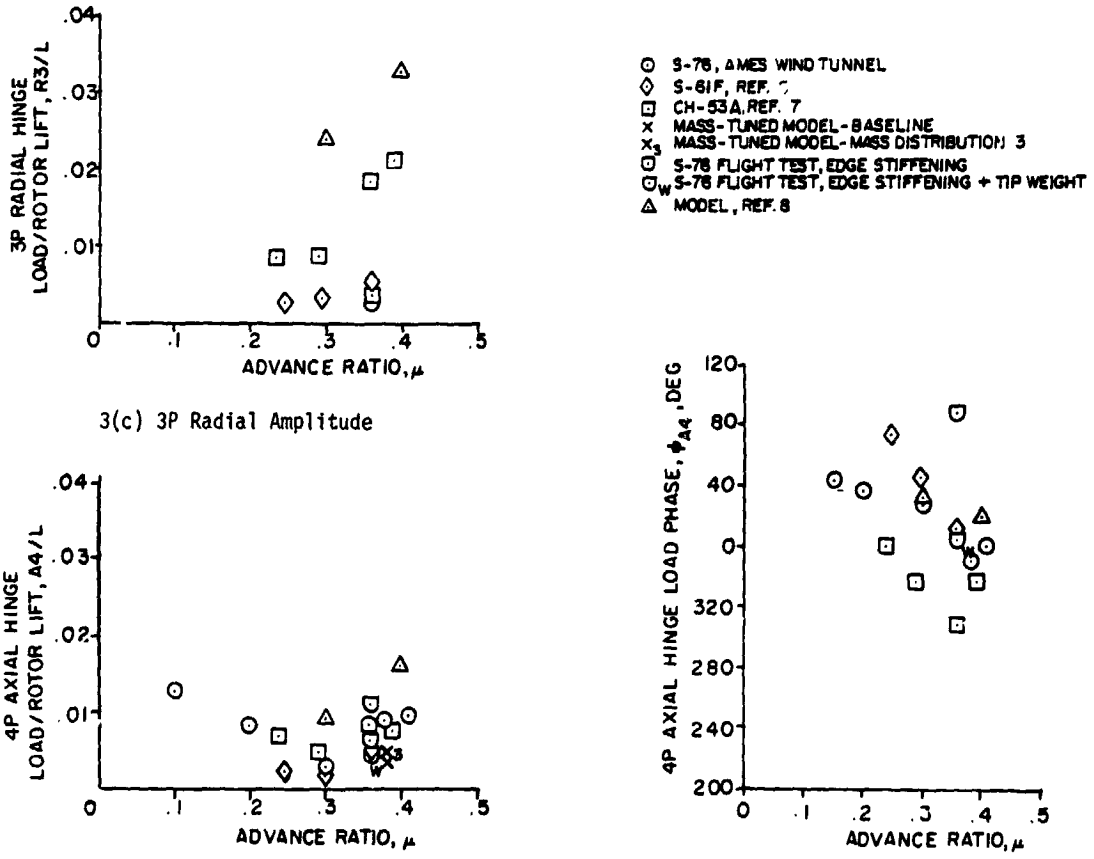

3(c) 3P Radial Amplitude

3(d) 4P Axial Amplitude and Phase

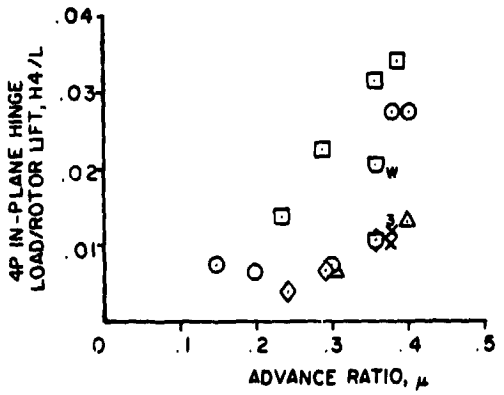

3(e) 4P In-Plane Amplitude

Fig. 3. Continued

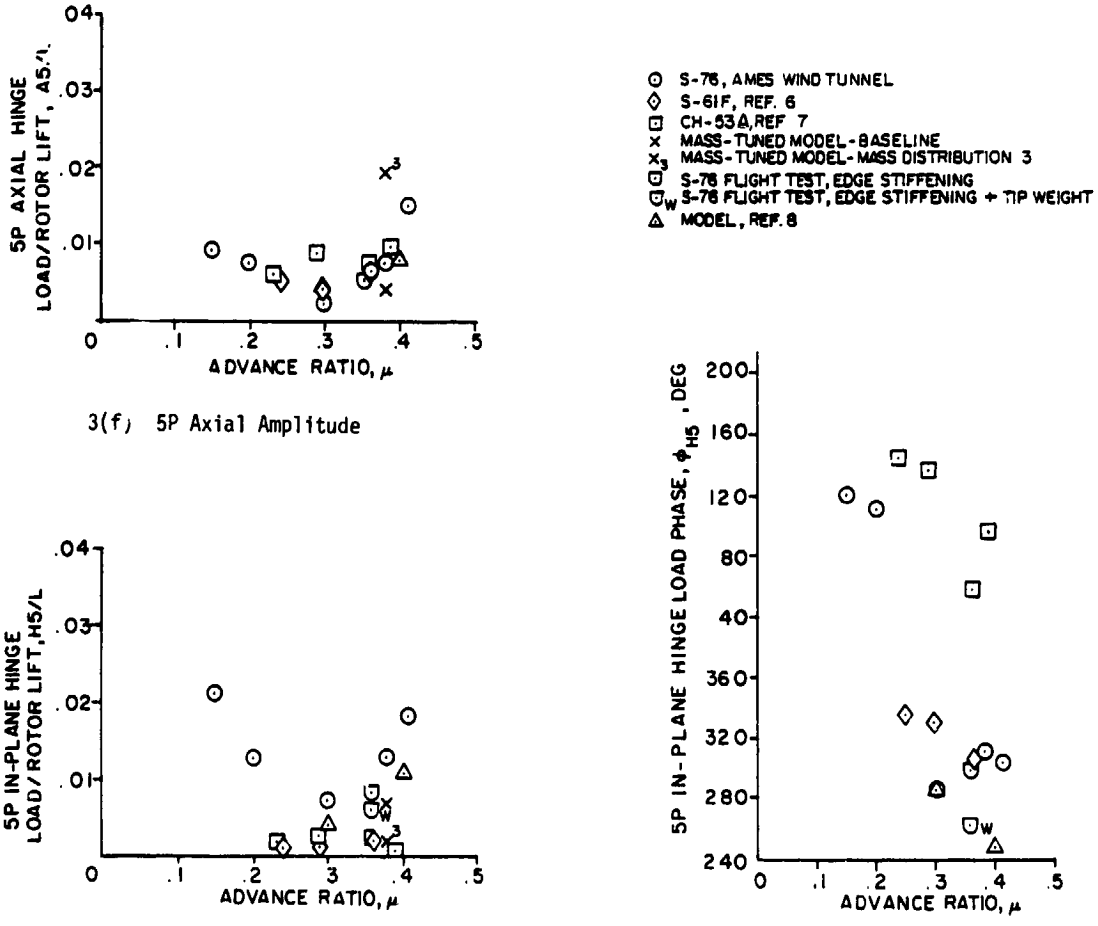

3(f) 5P Axial Amplitude

3(g) 5P In-Plane Amplitude and Phase

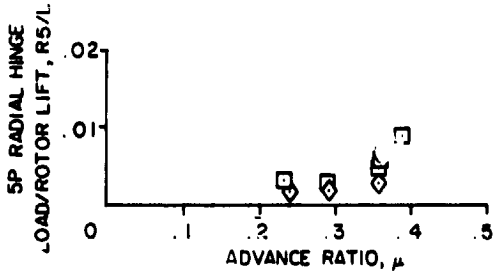

3(h) Radial 5/Rev Amplitude

Fig. 3 Concluded.

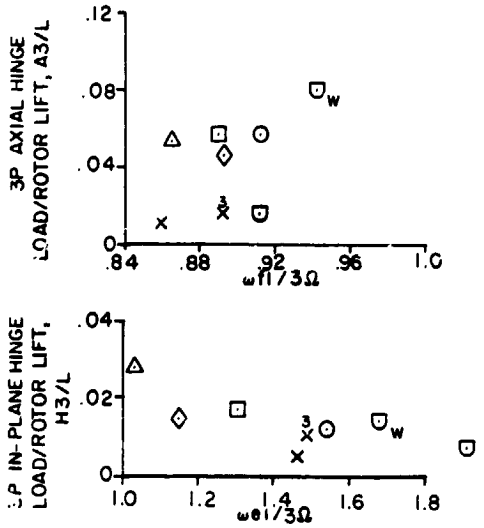

Fig. 4. Correlation of 3P Axial and In-Plane hinge loads with frequency ratio ($\mu \cong .375$)

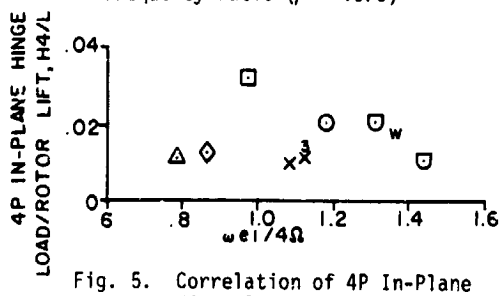

Fig. 5. Correlation of 4P In-Plane Hinge loads with frequency ratio ($\mu \cong .375$)

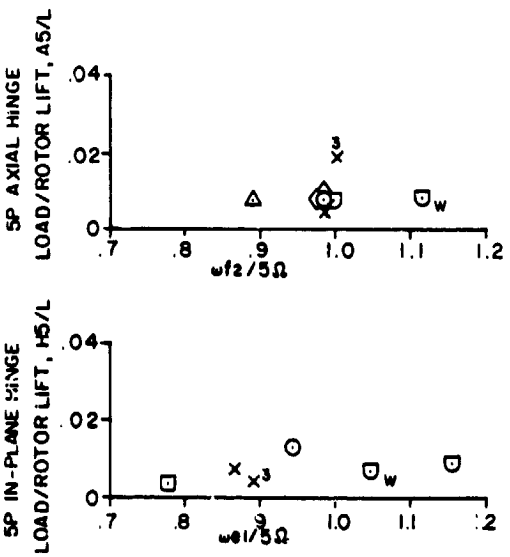

Fig. 5. Correlation of 5P Axial and In-Plane Hinge loads with frequency ratio ($\mu \cong .375$).

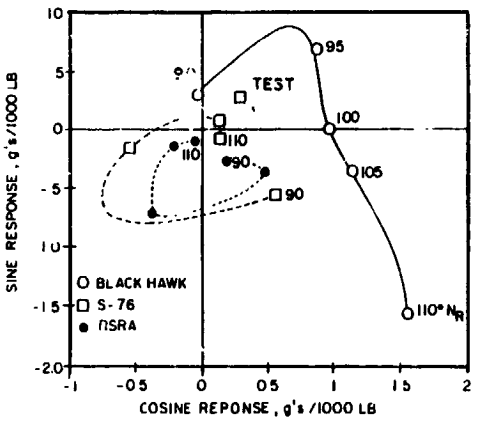

Fig. 7. Pilot station vertical vibration response.

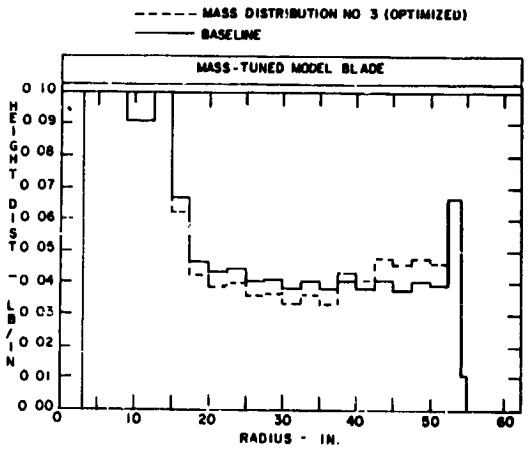

Fig. 8. Baseline and optimized mass distribution.

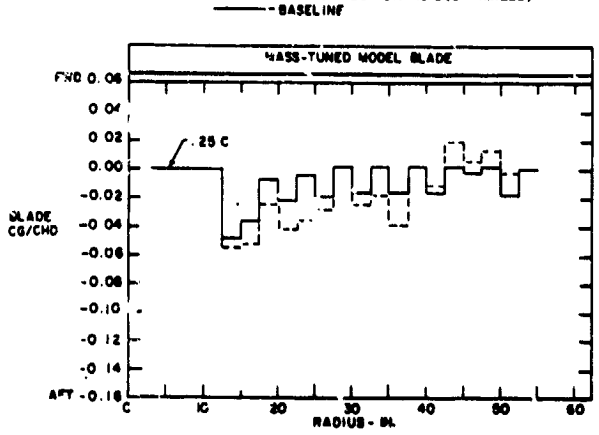

Fig. 9. Basel ne and optimized center of gravity distribution.

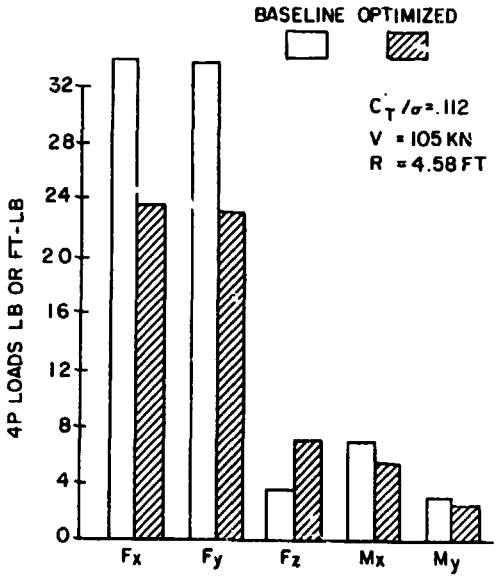

Fig. 10. Analytically predicted effects of spanwise mass distribution improvement on model hub loads.

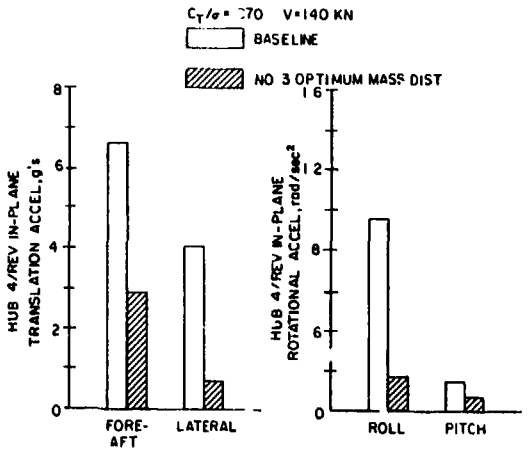

Fig. 11. Analytically predicted benefits in model rotor hub vibratory acceleration due to optimized mass distribution.

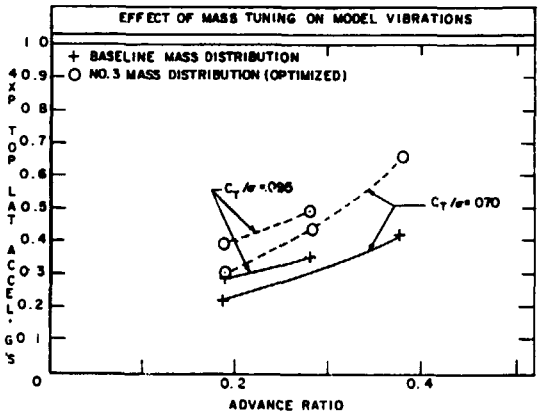

Fig. 12. Rotor support rig vibration levels as a function of flight condition.

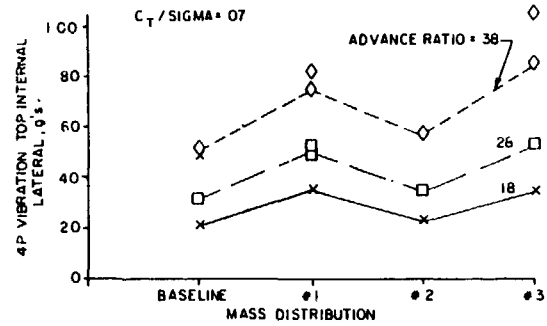

Fig 13. Rotor support rig vibration levels as a function of mass distribution.

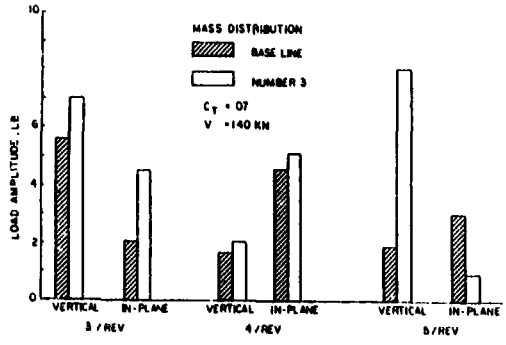

Fig. 14. Effect of mass tuning on model blade hinge load amplitudes.

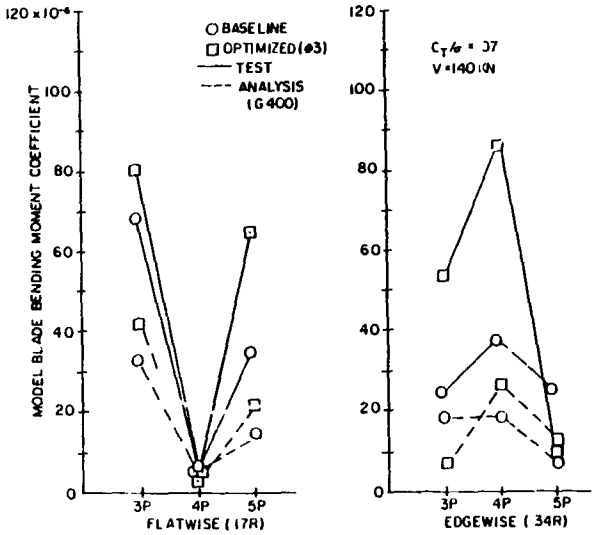

Fig. 15. Correlation of test and analysis blade bending response harmonics.

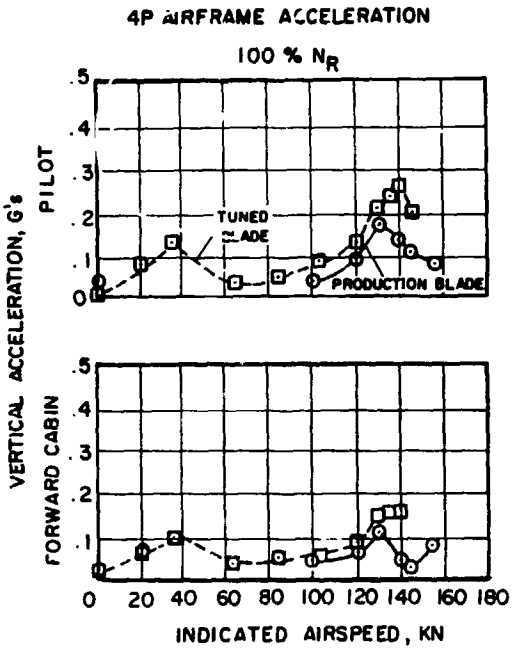

Fig. 17. Tuned blade flight test results.

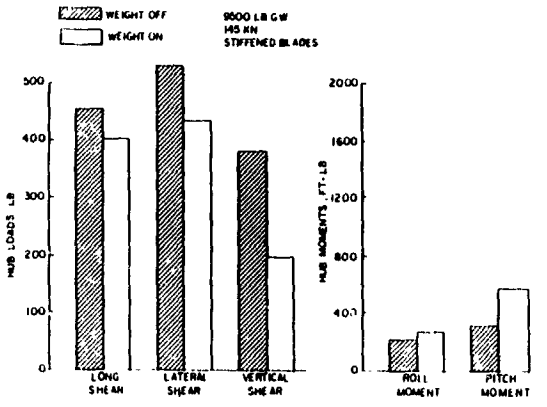

Fig 16. Effect of tip weight on analytical full scale 4P hub loads.

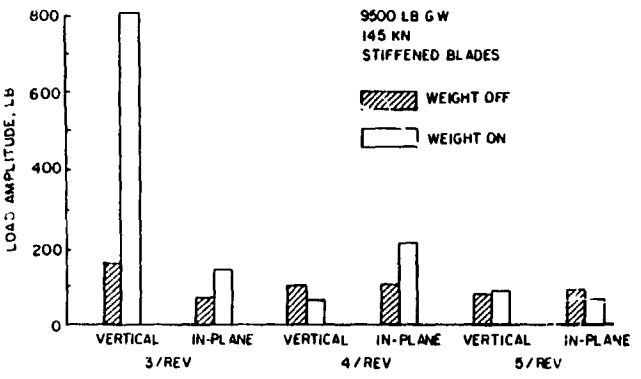

Fig. 18. Effect of tip weight on full-scale flight test hinge load amplitudes.

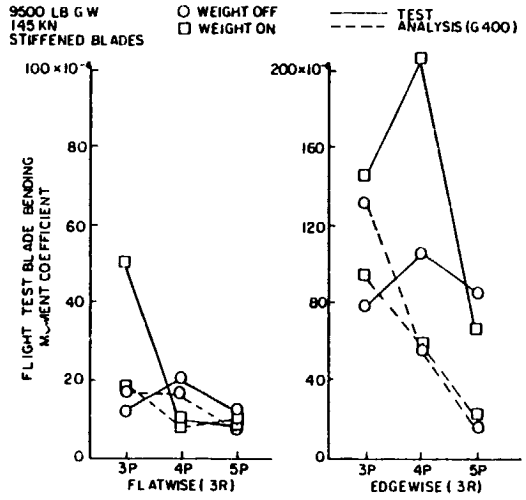

Fig. 19. Correlation of test and analysis blade bending response harmonics.

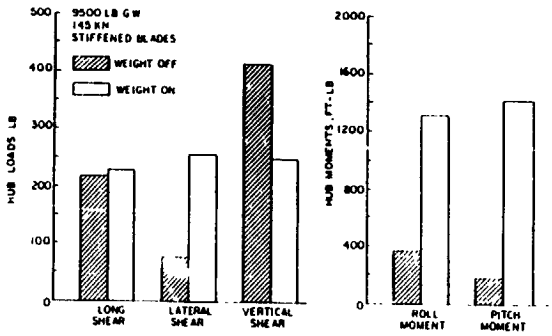

Fig. 20. Effect of tip weight on flight test 4P hub loads.

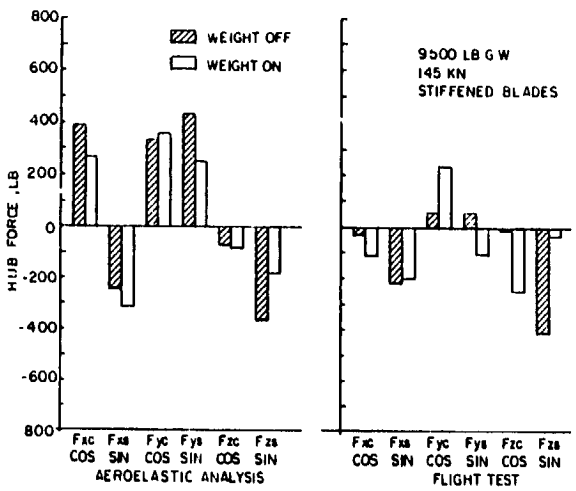

Fig. 21. Analytical and flight test in-plane hub load components.

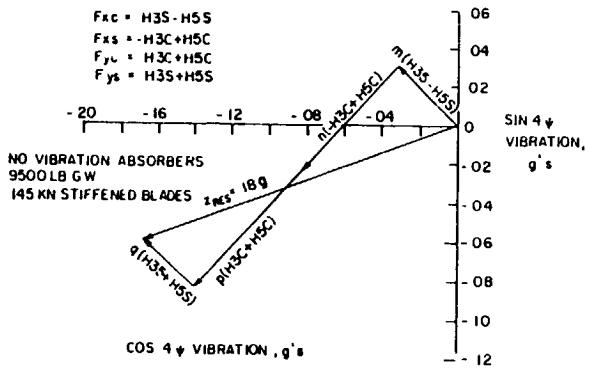

Fig. 22. Pilot vertical response to flight test in-plane shears-tip weight on.

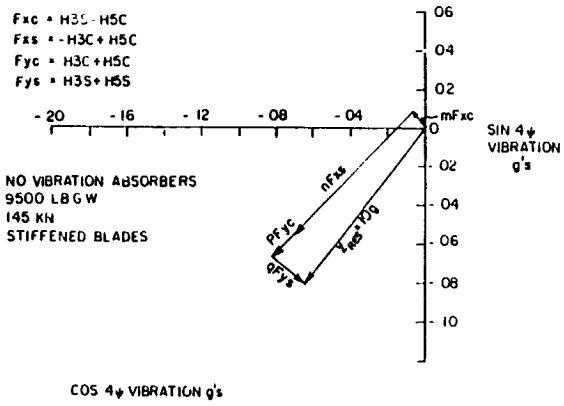

Fig. 23. Pilot vertical response to flight test in-plane shears-tip weight off.

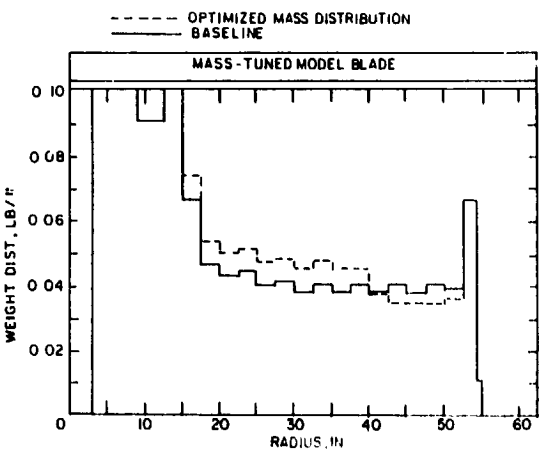

Fig. 24. Model blade mass distribution optimized from test data.

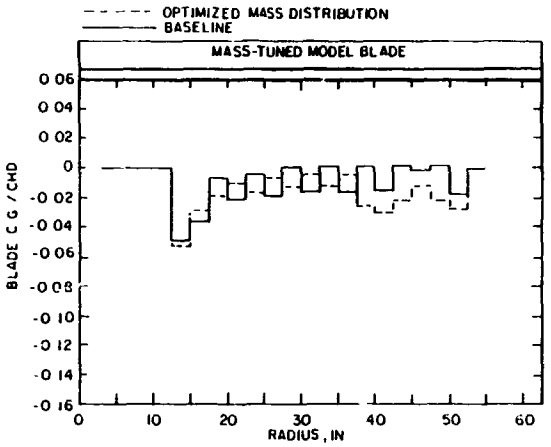

Fig. 25. Model blade mass center of gravity distribution optimized from test data.

DISCUSSION
Paper No. 19

AN EXAMINATION OF THE RELATIONS BETWEEN ROTOR VIBRATORY LOADS AND AIRFRAME VIBRATIONS

Charles F. Niebanck

Bill Weller, United Technologies Research Center: Did you verify the frequency placement on your analytical models [by] correlating with full scale or the model data prior to embarking on the optimization studies?

Niebanck: No, I didn't correlate the frequencies with model or full-scale [data].

Weller: I'd like to submit that we have problems with our analyses, but sometimes we have problems with our users. The structural data worked up may not have been the best representation. If your starting point is wrong your ending point may be as bad.

Niebanck: I can't dispute that.

Hooper: I assume it is a fair comment that the failure of the analysis was because of the failure of the aerodynamic modeling of the analysis?

Niebank: That could be part of it. I used uniform inflow and . . .

Hooper: You started off with an analysis--ours are no better than yours in this respect--which does not adequately represent the higher harmonic loading on the blades. If you draw conclusions about how to change the blades to improve the vibration it's as likely to be right as it is to be wrong.

Niebanck: Yes, I think that is a fair assessment. It seems like [from] the things that we have seen since we have been here that the unsteady aerodynamics makes a big change and [when] you look at the azimuth plot maybe that doesn't strike you as a big change, but when you do the harmonic analysis you may find a profound change in the harmonic distribution. I think that is part of the task of getting the analysis more accurate.

Dick Gabel, Boeing Vertol: I was interested in a mundane thing, Charlie, about how you measured the rotor loads. You did mention that you used modal fitting and we have tried it. We have done it routinely for the vertical, but never for the inplane. You report a lot of inplane loads that look just as good. I was curious as to how you did it.

Niebanck: It's the same way. We have a program that Bob Blackwell put together. It does this modal fit with respect to the flatwise and the edgewise loading. We think it is a fairly good assessment of what the loads are.

Gabel: Did you check it with shaft loads measurements or balance measurements?

Niebanck: They all seem to hang together fairly decently and some of them come from this modal fit method and some come from hub bending and shaft gauges and some come from strain gauges on the blade root. Especially the S-76 tunnel test; those were hub bending gauges. I see that I have relatively the same phase angle from the flight test and the wind tunnel data, so it gives me some confidence that this is working.

Bob Taylor, Boeing Vertol: I'd like to add one comment before we go on to the next paper. I'd like to second what Euan said. I think we are missing one of the most important ingredients in the problem and that is a definition of what the airloads are on the blade. We have been assuming for many years that at high speeds like 150 knots that the inflow is uniform and you can use that model for vibration predictions. I think that what Charlie has shown here indicates that is not true and we certainly need that information to go further. I might also add that I don't think the jury is in on this, it's still out and Bob Jones from Kaman will have more to say on this tomorrow in the panel sessions.

Planning, Creating and Documenting a NASTRAN Finite Element Model of a Modern Helicopter

R. Gabel, D. Reed, R. Ricks, W. Kesack

Boeing Vertol Company

Philadelphia, Pennsylvania

Abstract

Mathematical models based on the finite element method of structural analysis as embodied in the NASTRAN computer code are widely used by the helicopter industry to calculate static internal loads and vibration of airframe structure. The internal loads are routinely used for sizing structural members. The vibration predictions are not yet relied on during design. NASA's Langley Research Center sponsored a program to conduct an application of the finite element method with emphasis on predicting structural vibration. The Army/Boeing CH-47D helicopter was used as the modeling subject. The objective was to engender the needed trust in vibration predictions using these models and establish a body of modeling guides which would enable confident future prediction of airframe vibration as part of the regular design process.

Introduction

A better capability to calculate vibration of helicopters is a recognized industry goal. More reliable and accurate analysis methods and computer aids can lead to reduced developmental risk, improved ride comfort and fatigue life and even increased airspeeds. An important element in the overall vibration calculation is the finite element airframe model. Under a NASA Langley Contract, Boeing Vertol Company performed the program enunciated by the title of this paper, that is, the planning, creating and documenting of a NASTRAN finite element vibration model of a modern helicopter. Further, test requirements were established and a ground shake test performed to validate the model. An unusual requirement of the contract was that each major step of the program be presented to and critiqued by the Industry.

The contract consisted of two phases with multiple tasks in each phase:

- Phase I: Planning, Creating and Documenting A Helicopter NASTRAN Model

  Task 1 Planning
  Task 2 Modeling
  Task 3 Test Requirements
  Task 4 Industry Critique

- Phase II: Vibration Test to Verify a Helicopter NASTRAN Model

  Task 1 Aircraft Ground Shake Test
  Task 2 Industry Critique
  Task 3 Report

Presented at the Second Decennial Specialist's Meeting on Rotorcraft Dynamics, AHS/NASA Ames, Moffett Field, CA, Nov. 8, 1984.

Functions of the Finite Element Models (FEM's)

The forming of FEM's have become almost routine for new helicopter airframes. But to step back a moment, why are they being formed? ... what are the current uses after they are formed? ... and what are the future uses as the technology improves and the degree of correlation advances? "Today's" functions of the finite element model (FEM) static models are shown in Figure 1. They are commonly used to calculate fuselage internal loads. What formerly was an extensive job involving months of effort by many Stress engineers has been reduced to routine running of cases once the FEM is prepared. Then the same model can be the basis for a vibration model.

	FUNCTION	TECHNICAL DECISION IMPACT
TODAY	• USE STATIC FEM MODEL TO CALCULATE INTERNAL LOADS – THE CRITICAL LOADS ON EACH AIRFRAME ELEMENT TO PERMIT SIZING AND STRESS ANALYSIS	• MAJOR, FEM INTERNAL DESIGN LOADS USED – REDUCES STRESS MANLOADING FOR INTERNAL LOAD CALCULATIONS
TODAY	• STATIC MODEL USED AS BASIS FOR THE VIBRATION MODEL	• BASIS FOR MODEL LEADING TO VIBRATION CONFIGURATION DECISIONS – NOT COMMONLY DONE YET
FUTURE	• USE STATIC MODEL TO CALCULATE DEFLECTIONS	• OCCASIONAL USE
FUTURE	• CALCULATE AIRFRAME FATIGUE LOADS	• NONE YET – FUTURE CAPABILITY

Figure 1. Functions of Static Finite Element Models

"Future" functions of the FEM include calculation of airframe fatigue loads. Field problems with airframes often involve cracking of skin panels or stiffeners from vibratory loads. Early prediction and correction of such problems would be a useful improvement to the aircraft.

For vibration models, the categories of functions can be discerned for the engineering development of helicopters. These are (1) guiding structural design so as to avoid resonance with rotor exciting frequencies, (2) predicting flight forced vibration levels, and (3) supporting design of vibration control devices.

There are two "Today" functions in Figure 2 which are in routine use. The first row is the function to predict and control resonances in the basic design. Three forcing frequencies are addressed; 1/rev, b/rev and 2b/rev. By far the most severe and limiting vibration occurs at b/rev. However, even relatively low vibration levels at 1/rev can be annoying. 2b/rev levels are next in importance, and can be significant when seeking very low overall vibration. FEM's are employed at the detail design stages to check proximity of the lower natural modes to 1/rev. If analysis indicates a proximity which is judged to be a concern, the procedure would be to utilize the analysis to explore corrective structural changes and to implement these changes in the design before construction. The changes could affect both the structural arrangement and the structural gages.

FUNCTION	TECHNICAL DECISION IMPACT
• PREDICT NATURAL FREQUENCY PLACEMENT AND • MODIFY DESIGN BEFORE DRAWING RELEASE TO ASSURE REQUIRED NATURAL FREQUENCY PLACEMENT	• MINOR FOR b/REV AND 2b/REV CREDIBILITY FOR THESE HIGHER MODES POOR SO GENERALLY LITTLE IMPACT • MODERATE FOR 1/REV AND AEROELASTIC MODES SOME RECOGNITION IN AVOIDING THESE PROBLEMS BEFORE DRAWING RELEASE
• IDENTIFY STRUCTURAL MODEL MODIFICATIONS IN ANTICIPATION OF NEED FOR IMPROVED TUNING AFTER SHAKE TEST OR FLIGHT TEST	• MODERATE SOME USE FOR PREPARING HARDWARE READY FOR SHAKE TEST OR FLIGHT TEST FREQUENCY TUNING
• PREDICT FORCED VIBRATION UNDER INDIVIDUAL UNIT LOADS (I E INDIVIDUAL ROTOR LOAD DIRECTION CROWN PRESSURE) AND • MODIFY DESIGN BEFORE DRAWING RELEASE TO ACHIEVE MINIMUM FORCED G'S	• NONE FUTURE FUNCTION
• PREDICT UNTREATED FORCED VIBRATION AND • MODIFY DESIGN BEFORE DRAWING RELEASE TO ACHIEVE MINIMUM FORCED G'S	• NONE - FUTURE FUNCTION
• DETERMINE SIZE AND EFFECTIVENESS OF VIBRATION TREATMENT DEVICES	• NONE - OCCASIONAL AIRFRAME ABSORBER SIZING
• PREDICT TREATED FLIGHT VIBRATION AND • MODIFY TREATED DESIGN BEFORE DRAWING RELEASE TO MEET FLIGHT VIBRATION SPECS	• NONE - FUTURE FUNCTION

Figure 2. Functions of Vibration Finite Element Models

The FEM is almost certainly applied during detail design to check for proximity of any of the higher airframe modes with b/rev. But, based on today's perspective it is not so predictable what actions engineers would undertake preceding prototype fabrication if a proximity of concern should be indicated by the analysis. Two reasons for the uncertainty are present: (1) higher mode behavior of the airframe has been regarded as difficult to predict, and (2) due to weaknesses of the currently available tools to predict vibration levels of the coupled rotor/airframe system it could be difficult to reach a consensus on whether any predicted coincidence of a natural frequency with b/rev reflects a real problem. There has, however, been some use of FEM for estimation of the effectiveness of stiffening hardware in raising natural frequencies. This is perceived to be more dependable because only the delta frequency rather than the absolute frequency is used.

For the future, it is expected that forced vibration from individual rotor vibratory loads and from combined rotor loads will be predicted on a routine basis. Not only will they be predicted, but the airframe design will be iterated before drawing release to minimize forced vibration levels.

Modeling Plan

As a counterpoint to most modeling efforts, this program emphasized the planning of the modeling as the prime portion of the effort. All of us have modeled by spreading out the drawings and getting down to work, typically without a very clear idea of where we were headed. In contrast to this, the NASA Technical Monitor insisted on a well thought out plan of attack, accompanied by detailed preplanned instructions, labeled "guides". These guides defined the modeling approach for each type of structure-frames, stringers, rotor shafts, etc. Even the documentation of the modeling had to be preplanned. A very extensive modeling plan report, Ref.(1) was published. The plan was reviewed by other Industry representatives prior to undertaking the actual modeling. Another unique feature was that at the end of the modeling, deviations from the planned guides due to cause were reported.

The objectives of the modeling plan were as follows:

- Define guides for modeling, coding, documenting and demonstrating (1) stress (static) modeling, (2) mass modeling, and (3) vibration modeling (by modification of the stress model).
- Establish the organization, schedule and resources for performing detailed finite element modeling of a CH-47D helicopter.
- Identify and discuss the functions of finite element vibration models in the design process.
- Provide for plan critique by the industry.

Modeling Guides

Guides for static, mass and vibration modeling were developed. These included

- Node and element numbering
- Frame, stringer, skin treatment.
- Rotor shaft and transmission modeling.
- Concentrated and distributed masses.
- Changes from the static model to form a vibration model.

The aircraft was first divided into major areas for convenience in scheduling and tracking FEM activities. For the CH-47D, the breakdown was as shown in Figure 3.

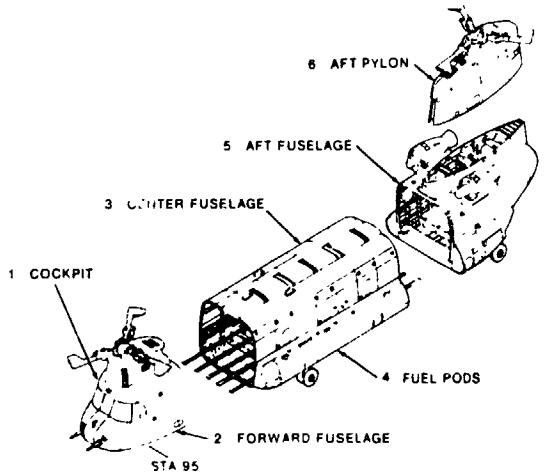

Figure 3. Breakdown into Major Areas for Static Modeling

A logical grid and element numbering scheme was selected to permit traceback of the elements. Blocks of numbers were assigned to major sections as indicated in Figure 4.

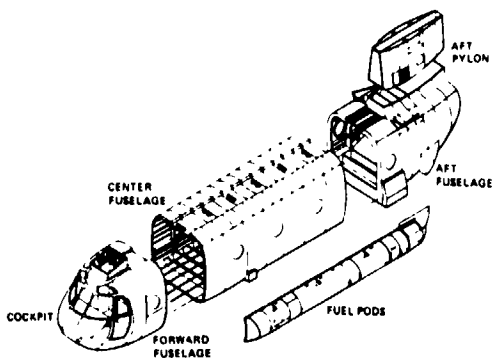

AIRCRAFT SECTION	COCKPIT	FORWARD FUSELAGE	CENTER FUSELAGE	FUEL PODS	AFT FUSELAGE	AFT PYLON
GRID NUMBERS	101 TO 300	301 TO 600	601 TO 1600	1601 TO 2000	2001 TO 2600	2601 TO 2900
ELEMENT NUMBERS	1 TO 1000	1001 TO 2000	2001 TO 6000	6001 TO 7000	7001 TO 9000	9001 TO 9999

Figure 4. Node and Element Numbering Scheme

Detail guides for modeling were described. Several typical guides are illustrated in Figures 5 and 6.

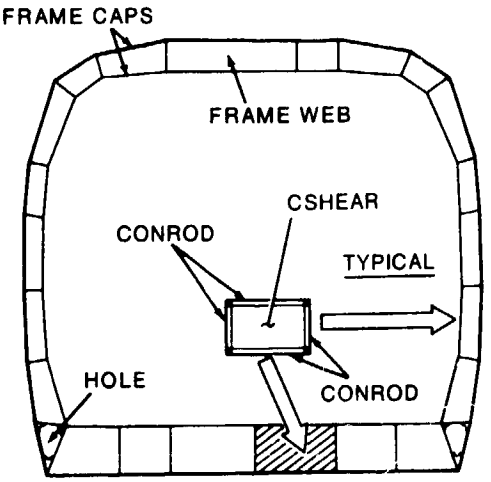

STRUCTURAL COMPONENT	TYPE OF LOADING	ELEMENT TYPE
CAP/STIFFENER	AXIAL	CONROD
WEBS	SHEAR	CSHEAR

Figure 5. Static Modeling Guides - Frames

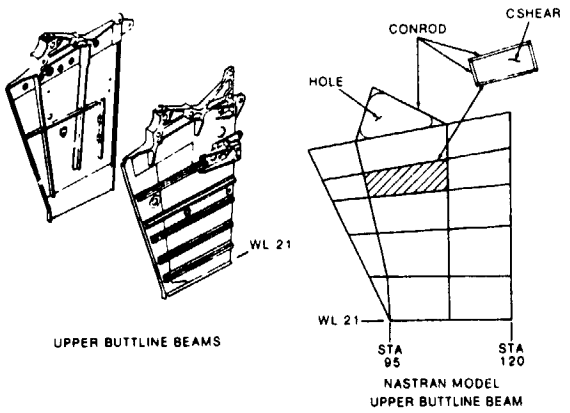

Figure 6. Static Modeling Guides - Bulkheads, Decks, and Butt-Line Beams

The mass modeling procedure is summarized in Figure 7. Mass data for the aircraft were first compiled on a standard weights tape per MIL-STD-451 or MIL-STD-1374. Masses were then divided into concentrated items and distributed items. Concentrated items such as transmissions and engines were allocated to individual NASTRAN nodes of the static model. Distributed items, structure, wiring etc., were allocated to frame stations by Boeing program W-17, and then manually distributed to nodes at that station.

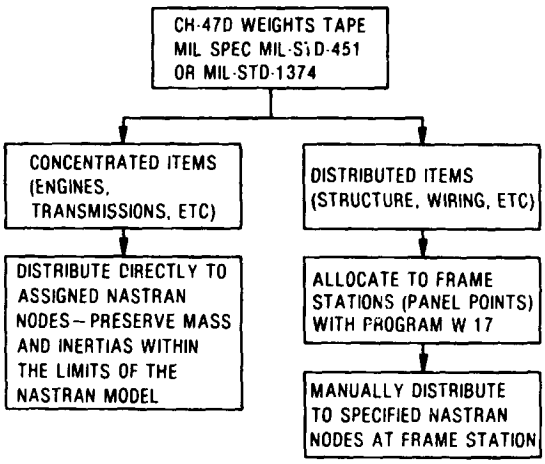

Figure 7. Mass Modeling Guides

The planning effort highlighted the fact that a good static model may serve as the vibration model with relatively small changes as shown in Figure 8.

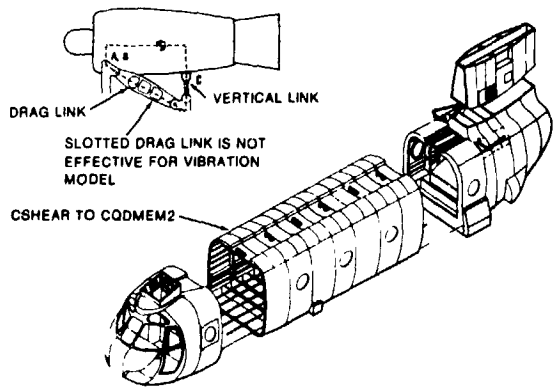

Figure 8. Vibration Modeling Guides - Changes from Static to Vibration FEM

The vibration model used CQDMEM2 elements to include the axial stiffening effectiveness of skin panels and webs, which were neglected in the static model by the use of CSHEAR elements. The logic was that under limit loads, the skins buckle and do not contribute much to axial stiffness. In the vibration case under 1g static loads, the skins are unbuckled and effective.

Documentation

An important aspect was the documentation plan, Figure 9. Quite often, modeling and documentation are done on an "as I get to it" basis. In this program, all of the steps were preplanned. The documentation was planned at four levels: overview, major sections, subsection breakdowns and modeling details. The documentation was to provide a clear illustration of each major area being modeled, a clear illustration of particular details

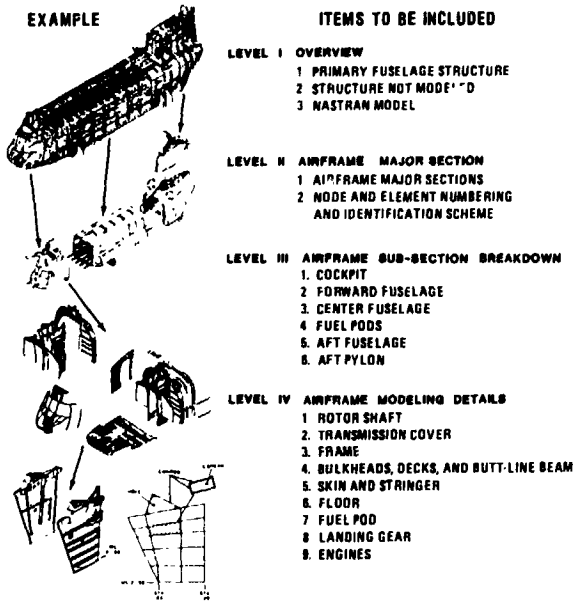

Figure 9. Formal Documentation Plan for Static Modeling

being modeled, its relationship to the major area and its corresponding NASTRAN model, and the rationale for modeling assumptions along with the details of section property computations.

Industry Critique of Modeling Plan

In an approach which is becoming more common in government supported research, other industry members participated in the program.

Boeing, the prime contractor, was required to subcontract to other major helicopter manufacturers, a series of review tasks. Bell, Hughes and Sikorsky were the participants. Upon completion of the modeling plan, Boeing briefed the subcontractors at their own sites, and reviewed verbal and written commentary on what the others thought of the plan from their own background of experience.

Examples of the comments were:

- the use of substructuring via superelements was suggested for cost and time saving.
- a more detailed mass model was recommended
- stringer lumping to save complexity and cost was questioned.
- the forward transmission cover model was too simplified
- procedures for checking the model should have been defined, such as SPC checks, rigid body checks etc.

This review procedure was repeated later for the test plan, and for the analytical correlation.

Actual Modeling Experience

The static model was prepared by a senior stress engineer and a technician working from the drawings of the CH-47D. Figure 10 shows the final NASTRAN model of the aircraft with the statistics indicated.

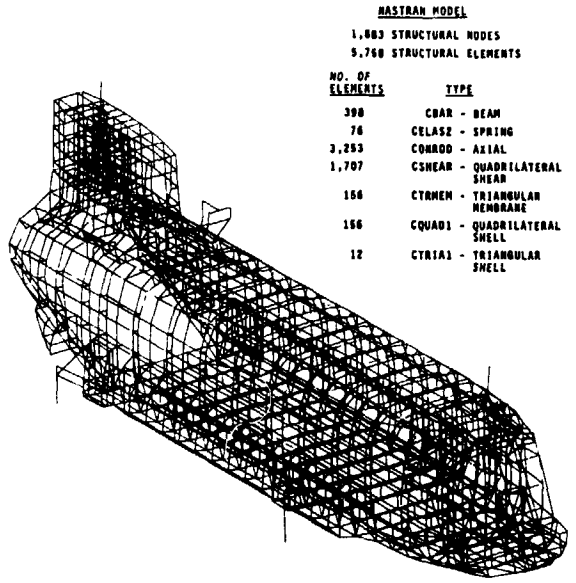

Figure 10. CH-47D NASTRAN Structural Model

The planned numbering system, previously presented in Figure 4, was straightforward, easily applied, and required a maximum of only four digits for grid points and five digits for elements. In the case of the grid points, sequential numbering was possible which facilitated checking for missing points in the listing. Capability was provided for independent modeling (except at interfaces) of the major airframe sections which is a necessary feature for rapid development of a model.

There were disadvantages turned up. The locations of nodes and elements were not obvious from the numbers. Only general location was implied by the block number. Any later revisions or additions tended to disrupt the numbering sequence and patterns. A principal difficulty was the estimation of the number block sizes. If sufficient space was not allocated, the numbering sequence was interrupted. Estimating an adequate number of grid points was relatively simple, but estimating sufficient space for the elements was difficult. This situation could have been partially alleviated by coding the element types which then would have made the full block of numbers available for each element type. The system of using station numbers in the code is probably the best, although it increases the size of the identification numbers.

Details of a typical subassembly static modeling task are illustrated by the model of the forward rotor shaft and transmission in Figure 11.

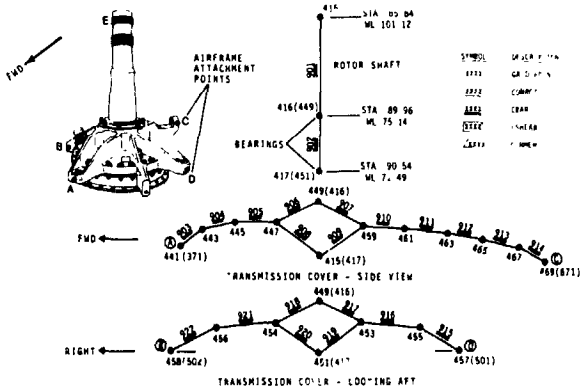

Figure 11. Static Modeling of Forward Rotor Shaft and Transmission Cover

The rotor shaft was represented by two CBAR elements with node points at the bearing locations. A cruciform structure comprised of CBAR elements was used to model the transmission cover. The cover model provided bearing node points to support the rotor shaft, and node points at the airframe attachments. Bending stiffness of the transmission cover legs was represented by the four legs of the cruciform model.

Modeling details of a typical center fuselage frame are shown in Figure 12.

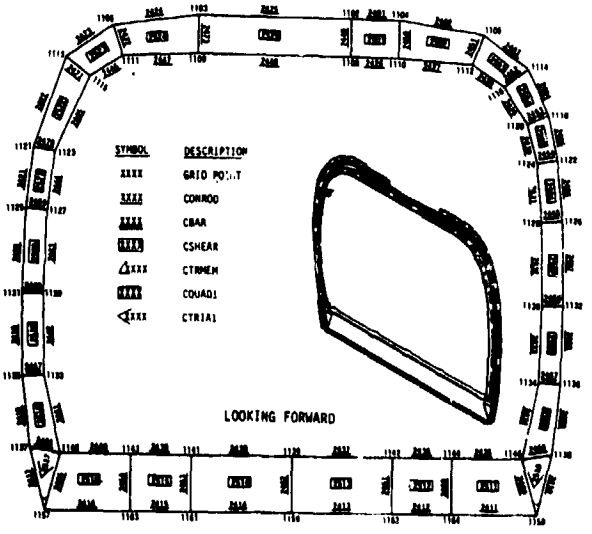

Figure 12. Static Modeling of Sta. 200 Frame

The caps carried axial load only and were represented by CONROD's. Average cap area was used between nodes where the cap was tapered. Cap areas were reduced for fastener holes, and local cap notches were ignored. No portions of adjacent skin or effective areas of webs were lumped with the caps. Webs carried only shear and were modeled with CSHEAR's. Web holes and stiffeners were ignored.

The model for the forward pylon upper buttline beams is shown in Figure 13.

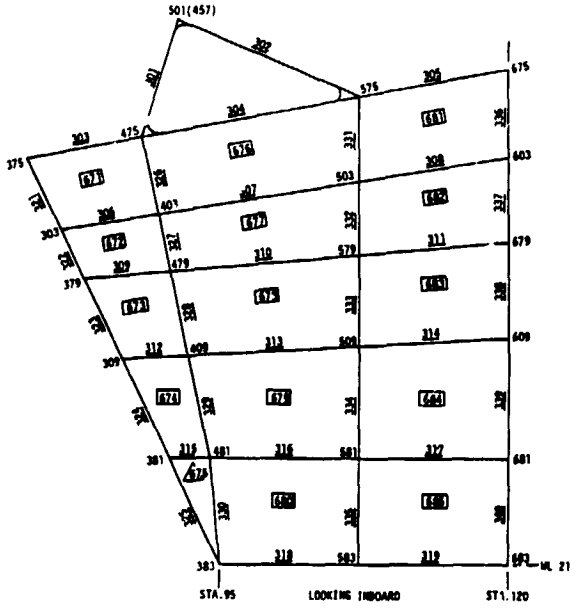

SYMBOL	DESCRIPTION
XXXX	GRID POINT
XXXX	CONROD
XXXX	CBAR
XXXX	CSHEAR
XXX	CTRMEM

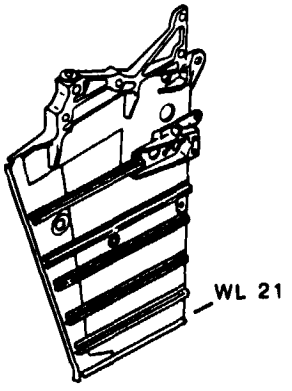

Figure 13. Static Modeling of Forward Pylon Upper Butt-Line Beam

The transmission support fitting at the top of the beam was designed to act as a truss and is modeled with axial CONROD's. Otherwise the model was like a frame in that caps were represented by CONROD's and webs by CSHEAR's. Stiffeners used only for web stability were not all modeled (some were to break up panel sizes).

Longerons, stringers and side skins were modeled as in Figure 14. Longerons were modeled as CONROD's using their actual areas. Stringers, because there are 36 of them on the cross-section, were lumped into 13 effective stringers (or lumped with longerons) to limit the size of the model. Skin panels were represented by CSHEAR's.

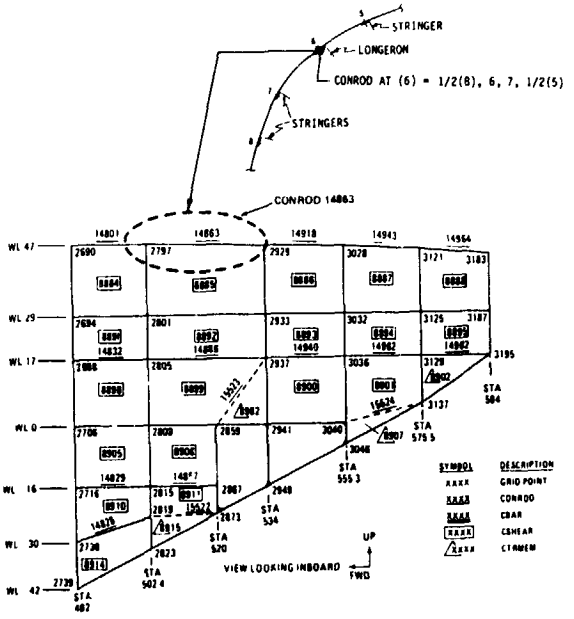

Figure 14. Static Modeling of Stringers, Longerons, and Side Skins

Modeling of effective skin near longerons and stringers as an addition to their area was one of a number of instances where the guides were violated for cause. The logic was originally that the static (stress) model would recognize buckled skins occurring under design maneuver loads. Then with this buckled skin model, internal load distributions would be obtained for detailed stressing of the elements. Locally effective areas of skin were to have been added to stringer areas for potentially improved accuracy.

For the vibration model, the airframe was to have been treated as in 1g level flight without maneuver induced buckling. The original guide was written to remove the locally effective skin area from the stringers for the vibration model where the skins were to be fully effective.

It was realized when the actual modeling was underway, that the labor of adding and then removing these small delta areas was not worthwhile. The static model internal load distributions would not really be affected by these small delta areas. This change was the most significant of the deviations made from the planned guides.

A demonstration run was made with the static model to determine whether the model generated reasonable (error free) results. Internal loads were calculated for a 3 g pull-up at a gross weight of 50000 pounds. Element forces, grid point displacements, and grid point force balances were examined. The static deflection plot for selected grid points illustrated in Figure 15 indicates apparently rational results.

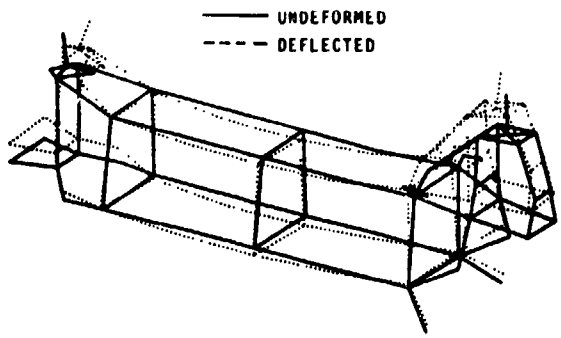

Figure 15. Static Demonstration Case, Deflections for 3.0 G Pull-Up

Next, the model had to undergo certain modifications from a static to a vibration model. One of these changes was the drag strut of the engine mount. The drag strut, Figure 16, is slotted and only acts under extreme maneuver and crash loads. It was included in the static model, but was removed from the vibration model. The inactive strut has a vibration purpose; it prevents the drag strut from adding a yaw stiffness increment which would have placed the engine yaw natural frequency on 3/rev. Further, since the forward yoke support fitting is significant in forming the stiffness of the engine mounting, this yoke was remodeled to provide better detail. Cap areas of the forging were modeled with CBAR's and the webs with CQUAD2 shell elements.

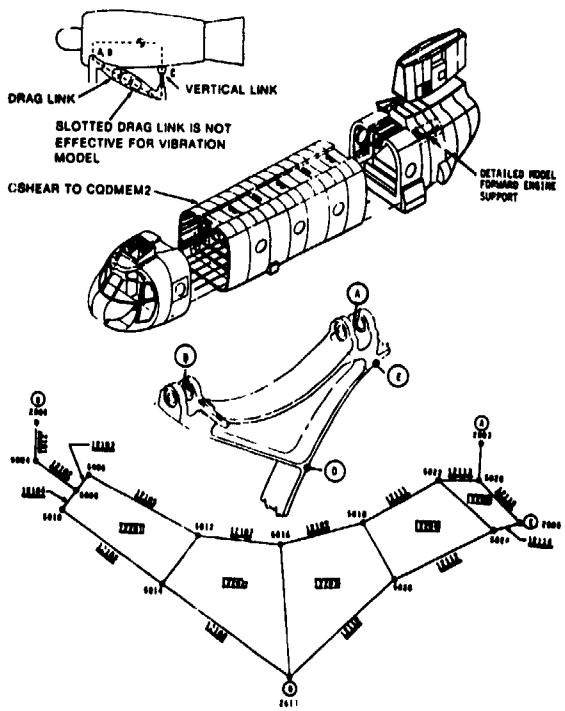

Figure 16. Vibration Modeling Structural Changes

The most important change to form the vibration model was the change of airframe skin from CSHEAR's to CQDMEM2 elements. The latter are membranes which provide both the skin shear capability and are effective in adding bending area. The change is associated with the buckled versus unbuckled skin configurations of the static and vibration models discussed previously.

Concentrated weights of the engines, transmissions, and APU were initially distributed to the attachment points in the static model while preserving the mass and inertia of the overall aircraft. For the vibration model, center of gravity grid points were introduced at the engines and transmissions and appropriate inertias used.

A demonstration run was performed with the vibration model. It was done in the free-free condition to represent an inflight situation. Emphasis was placed on the basic airframe structure by modeling an empty aircraft without fuel. This avoided the need for dealing with the nonlinear cargo and fuel isolation systems. The demonstration run included the calculation of natural frequencies and modes and forced response. Results of the natural frequency calculation are summarized in Table 1. Based on previous CH-47 modeling and test experience, these results were judged to be reasonable. The modeling process was reported in Ref. 3.

Table 1. Vibration Demonstration Case, Airframe Natural Modes

MODE NO.	FREQUENCY (HZ)	DESCRIPTION
1	6.36	1ST LATERAL - AFT PYLON LATERAL
2	7.24	ENGINE LATERAL YAW - OUT OF PHASE
3	7.52	1ST VERTICAL - AFT PYLON LONGITUDINAL
4	8.24	ENGINE LATERAL YAW - IN PHASE
5	11.89	2ND VERTICAL - PYLON LONGITUDINAL IN PHASE
6	12.89	2ND LATERAL - FWD PYLON LATERAL
7	13.81	3RD LATERAL - PYLON LATERAL IN PHASE
8	16.01	AFT LANDING GEAR LATERAL - OUT OF PHASE
9	16.22	UNDEFINED VERTICAL
10	17.41	UNDEFINED LATERAL
11	19.20	UNDEFINED LATERAL
12	20.71	UNDEFINED VERTICAL
13	21.61	UNDEFINED VERTICAL
14	22.92	UNDEFINED COUPLED VERTICAL-LATERAL
15	24.79	UNDEFINED COUPLED VERTICAL-LATERAL

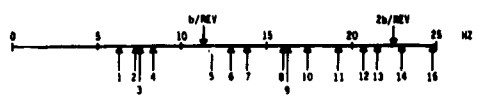

Time and Cost

A key question has long been, can an FEM be assembled and used in time to influence the design of a new helicopter airframe?

This was estimated in great detail, as illustrated in Figure 17, and it appears that an initial vibration result can be obtained in 6 months from Contract Award. This is certainly timely, because primary structure releases are not completed until the 15th month.

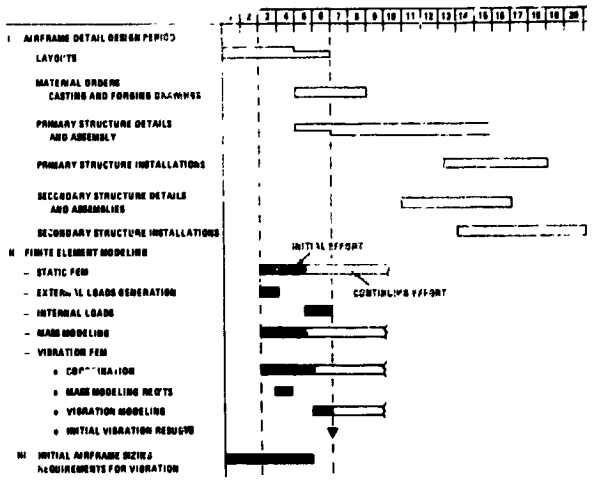

Figure 17. Vibration Modeling Schedule for a New Helicopter Program

The cost of the modeling is 4430 manhours or 5% of a typical 85000 manhour airframe design effort. Of this 5%, 4% is for the static model - an activity that is becoming routine by Stress, and only 1% more to obtain the first vibration model results. Beyond this point vibration iterations of the design will add to the cost, but will certainly be cost effective if it provides a well tuned fuselage prior to manufacture.

Test Plan

In addition to flight vibration measurements, two categories of ground tests can be identified as a means of evaluating a finite element model of a helicopter airframe for vibration analysis; namely, static deflection tests and shake tests. The ground test approaches have two significant advantages: (1) the rotor is removed which is a great simplification, and (2) all applied forces can be measured and controlled.

Static deflection tests seem attractive because: (1) Inertia effects are eliminated allowing independent evaluation of stiffness. (2) To some extent, selected parts of the airframe can be loaded facilitating identification of model deficiencies. On the negative side, industry experience with complete airframe deflection tests is extremely limited. Finally, it is noted that correlation with a shake test directly addresses the proposed application.

Deflection Test

The objective of the deflection test was to verify the stiffness modeling performed analytically. The approach was to obtain detailed deflection data under loading conditions which exercised all major structural elements of the airframe. These included bending, torsion and frame racking of the constant section, pylon bending, and pylon to constant section load path.

The proposed deflection test loadings of Figure 18 were designed accordingly.

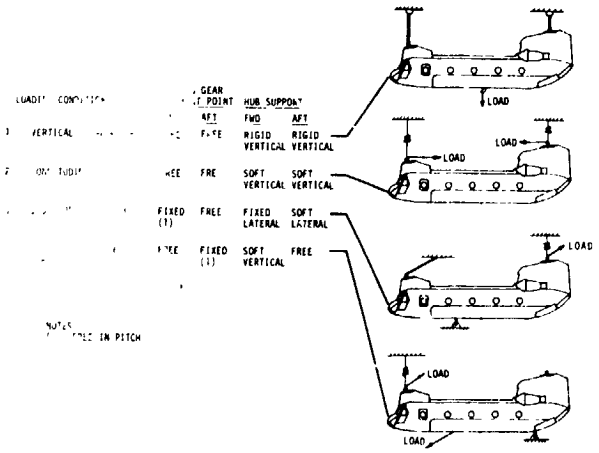

Figure 18. Summary of Deflection Test Load Conditions

While the deflection test was deemed to be very desirable, it was not performed because of cost limitations.

Shake Test

The objective of the shake test was to verify the NASTRAN finite element vibration model. The approach was to obtain detailed frequency response and mode shapes under conditions which exercised all elements of the model. These included excitation at both forward and aft hubs using all flight hub forces and moments except torque and covering the frequency range from 5 to 35 Hz (9/rev is 33 Hz).

The planned method of excitation was to suspend electrodynamic shakers and the aircraft from a shake test gantry, Figure 19.

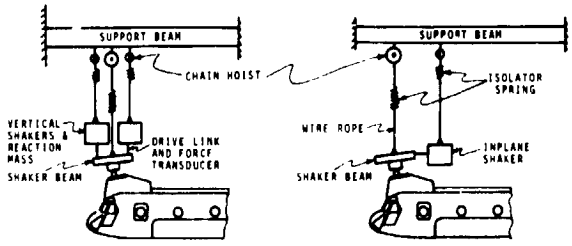

Figure 19. Shake Test Method of Excitation

Dual vertical shakers operating in a master/slave mode are driven in or out of phase to provide either vertical, pitch or roll excitation. In the vertical direction, the soft suspension of both the aircraft and shaker isolates the shaker from the aircraft except through the drive link. In the horizontal plane, isolation of the shaker is provided by the low frequency pendulum modes of the aircraft and shaker on the suspension cables.

Airframe accelerometer locations are shown in Figure 20.

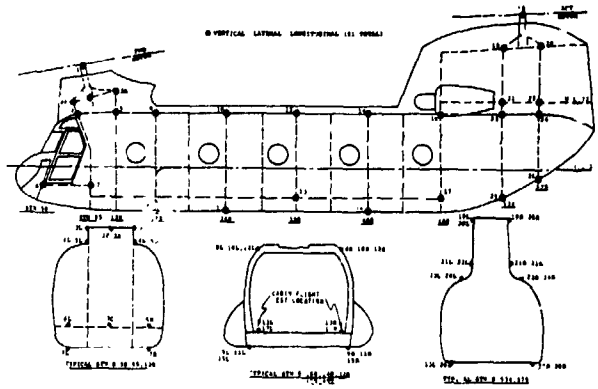

Figure 20. Shake Test Airframe Measurement Locations

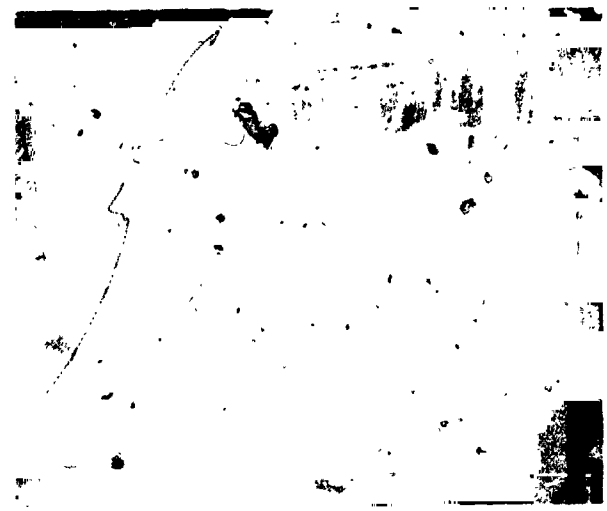

Figure 21. CH-47D Test Specimen in Shake Test Support Fixture

Response measurements were to be obtained at 51 locations in three axes. Locations correspond to node points of the NASTRAN vibration model.

Pretest NASTRAN forced analysis results were to be compared with the shake test results. The primary criteria for correlation was intended to be the forced response plots. Secondary criteria would be the mode shapes at the natural frequencies.

Industry Critique of Test Plan

As with the modeling plan, an industry review of the Ref. 2 test plan took place. With regard to the desirability of the deflection test, one considered the cost to outweigh the benefit. Two pointed out that modal parameters including damping should not be neglected. Two noted that the selection of hub mass effect is an important aspect of the test. And two reminded us that rotor shaft and drive system free play may have a significant impact on results.

Ground Shake Test and Correlation

The test specimen was the second prototype of the YCH-47D helicopter, Figure 21.

As per the test plan, the aircraft was suspended at the rotor heads in a large structural steel fixture which also supported the rotor head shakers. A low frequency suspension, all less than 2. Hz, was employed for both the aircraft and shakers. Three linear vibratory forces and two moments were applied at each rotor head. Selection of force levels was based on practical considerations including sufficient magnitude of response, shaker stroke limits and stable behavior of the suspended shakers. Results were obtained in the form of transfer function plots and mode shapes for each excitation, Figure 22.

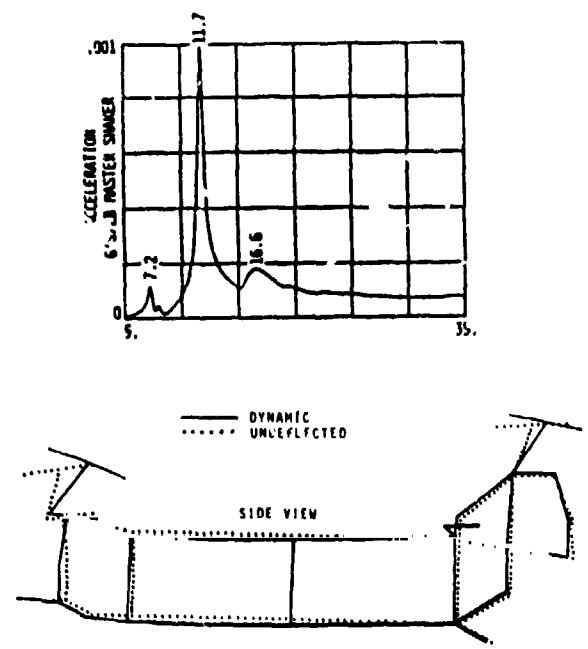

Figure 22. Format of Typical Shake Test Results

For each excitation an extensive matrix of forced response plots was obtained. Figure 23 is an example.

A summary of the test natural frequencies developed from the matrix of response peaks is presented in the Figure 24 bar chart. The shaker excitation which provided the best excitation is noted.

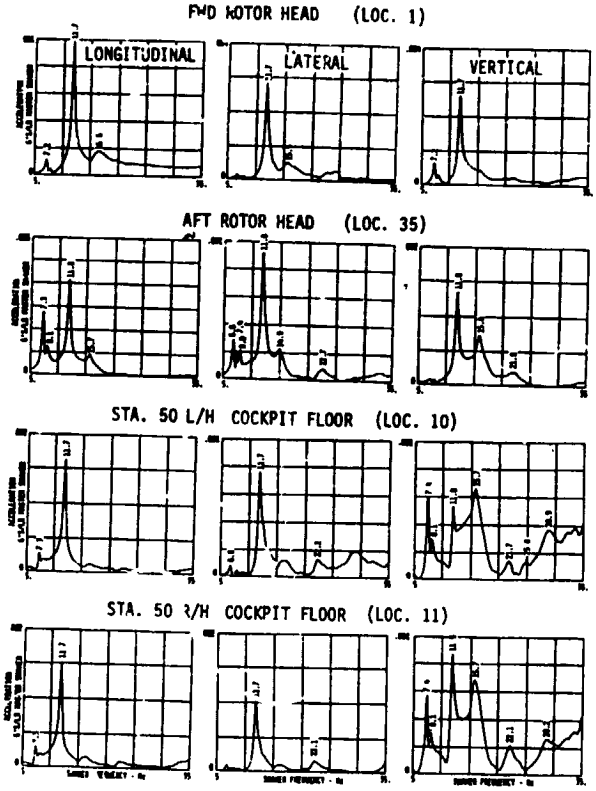

Figure 23. Frequency Response Summary for Forward Longitudinal Excitation

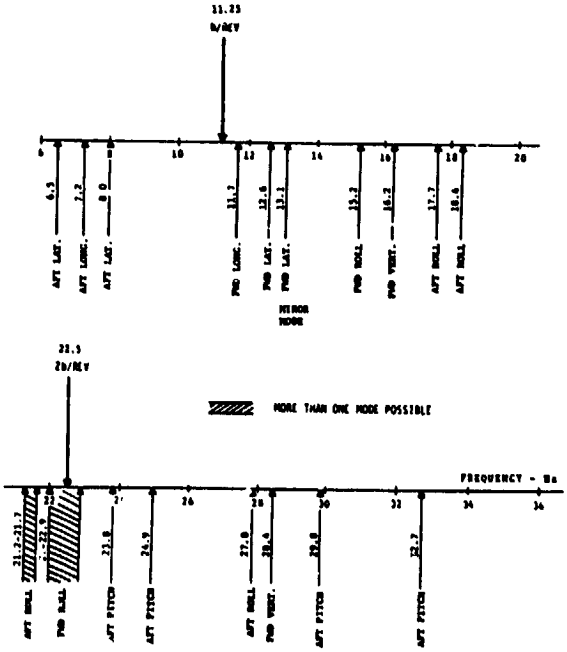

Figure 24. Summary of Test Natural Frequencies

From location to location, considerable scatter was sometimes evident in the frequency at which a given mode appeared. This made it difficult to precisely define the natural frequencies. Observed nonlinear behavior with force level is believed to be at least partially responsible for the scatter in the peak frequencies. In the bar chart of Figure 24, the frequency with the largest response was favored.

Forced mode shapes for the two vertical and two lateral modes closest to 3/rev are displayed in Figures 25 through 28. All of the shapes represent the total forced response normalized by the maximum deflection. The first response shape at 11.7 Hz (Figure 25) is dominated by the longitudinal pitch motion of the forward pylon with a smaller in-phase motion of the aft hub. Motions of the two hubs are balanced by an essentially rigid body motion of the remainder of the aircraft.

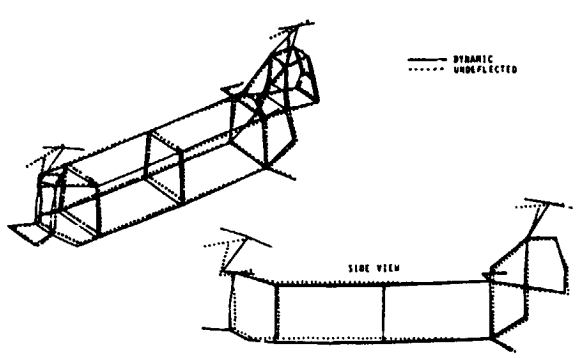

Figure 25. Forced Mode Shape at 11.7 Hz with Forward Hub Longitudinal Excitation

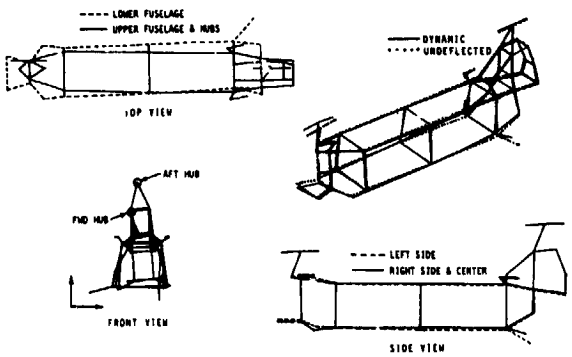

Figure 26. Forced Mode Shape at 12.6 Hz with Forward Hub Lateral Excitation

The characteristic of the 12.6 Hz mode, Figure 26, is essentially that of a classical second torsion mode. A relatively large lateral/roll motion of the forward pylon is accompanied by a small in-phase motion of the aft pylon. The pylon motions are opposed by a differential lateral motion of the upper and lower cabin structure. A large lateral motion of the aft landing gear also contributes to the inertial balance.

Like the previous mode at 12.6 Hz, the response at 15.2 Hz, Figure 27, is also basically a second torsion mode. In this case, however, the in-phase hub motions are opposed by what more nearly resembles a twisting motion of the cabin, as indicated by differential motion from left to right as well as top to bottom. Note also that the phase of the aft landing gear is reversed in the mode.

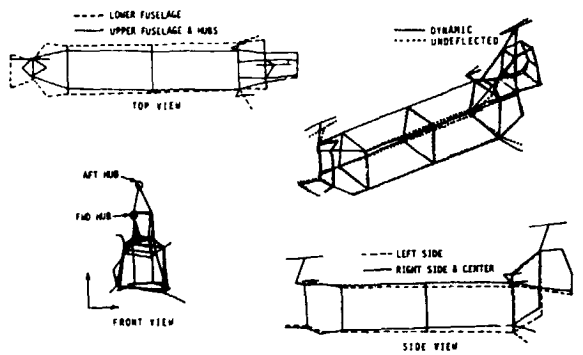

Figure 27. Forced Mode Shape at 15.2 Hz with Forward Hub Lateral Excitation

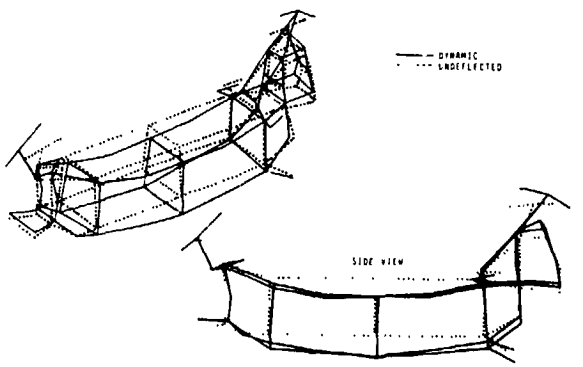

Figure 28. Forced Mode Shape at 16.2 Hz with Forward Hub Vertical Excitation

At 16.2 Hz, Figure 28, the response shape displayed is the fundamental vertical bending mode of the cabin section. Bending motion of the cabin is opposed by large out-of-phase pitch motions of the pylons.

NASTRAN Analysis of Test Configuration

The basic airframe vibration FEM initially demonstrated in the free-free condition was modified to the test configuration. Changes to the basic airframe model included incorporation of the test hub fixtures (hub weight and shaker beam assembly) and adjustments to the mass distribution to account for equipment not installed.

The total NASTRAN model incorporated several unique features. A persistent issue with regard to analytical correlation of test and analysis has been the question of the suspension system and shaker effects. Consequently, the total model was fully representative of the test configuration including the support fixture, the shakers and the aircraft and shaker suspension systems in addition to the basic airframe model. A differential stiffness correction was also developed and applied to the stiffness matrix to include gravitational effects (pendulum modes) on the suspended aircraft.

Shaker and Support System Modeling

Modeling of a typical shaker configuration is illustrated in the schematic of Figure 29. The shaker stator mass and a portion of the cradle assembly mass are located at the shaker pivot point (grid 7011). The remaining cradle assembly weight is located at the cradle suspension point (grid 7012). The armature flexures (armature spring) connect the stator and the coincident armature mass. Motion of the armature mass is constrained to act along the axis of the drive rod. The drive rod, represented by a CONROD, is assumed to carry only axial loads due to the flexures oriented at 90°.

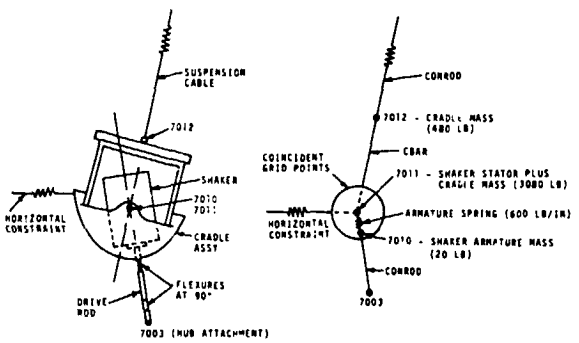

Figure 29. Typical Shaker and Suspension Modeling

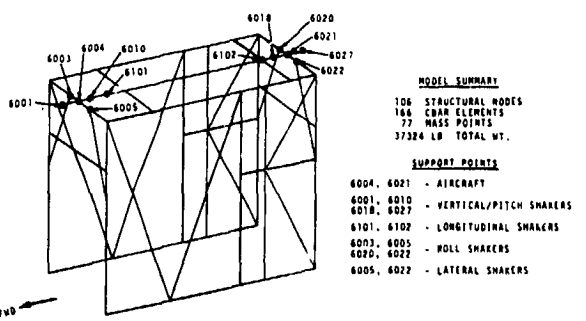

Figure 30. Support Fixture NASTRAN Model

The NASTRAN model of the shake test support fixture which weighs approximately 37,324 pounds is shown in Figure 30. Grid points corresponding to the aircraft and shaker support points are identified. Typical modeling of the hub and shaker suspension which is the interface between the support fixture and the basic airframe is illustrated in Figure 31.

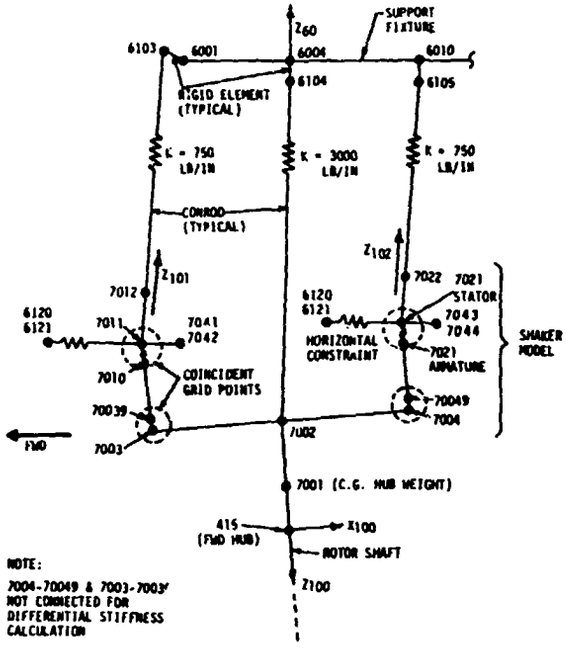

Figure 31. Forward Hub Suspension Modeling for Vertical/Pitch Excitation

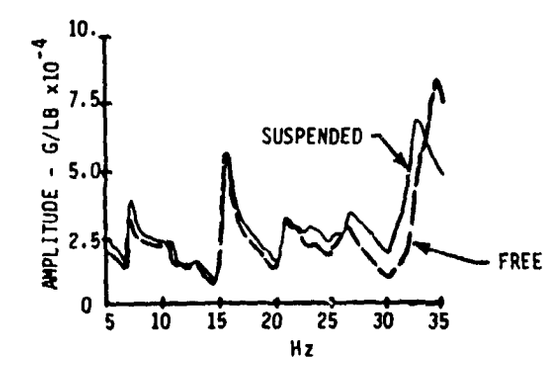

Figure 32. Typical Analytical Response for Free and Suspended Conditions

With regard to the question of the suspension system and shaker effects, the support fixture is always likely to have modes in the test range. The question, therefore, can only be resolved by a comparison of analytical aircraft responses for the free and suspended conditions. Typical results illustrated in Figure 32 show only minor effects with the most significant changes in the 30 to 35 Hz range. While these results are applicable only to the test equipment used in this program, they generally support the accepted suspension concept. Physically, frequency shifts and amplitude variations may result from any of the following or combination of the following:

- Coupling with shaker system
- Minor coupling with the support fixture
- Prestiffening of the airframe due to gravity preload.
- Other coupling mechanisms in the airframe due to gravity preload.

Also, it should be remarked that the theoretical appropriateness of representing pendulum modes by a differential stiffness correction, while plausible, has not been thoroughly explored.

Correlation of Test and Analysis

Conventional correlation of test and analysis for airframe vibration is a comparison of natural frequencies and modes first, and forced vibration second. In this program the criteria order was reversed; more emphasis was placed on the ability of the analysis to predict reasonable forced amplitudes throughout the airframe. Natural modes were in second place, although it is recognized that specific forced peaks and valleys follow natural frequency placement. If able to predict reasonable forced amplitudes from individual rotor forces, then the analysis would be a reasonable tool for predicting vibration arising from actual mixed forces and directions.

To keep the correlation process within reasonable bounds, forced vibration results were presented at only four representative and widely separated locations, Figure 33, each in the vertical, lateral and longitudinal directions. The forces for illustration were the forward rotor vertical, pitch and lateral excitations. A single structural damping value of 2.5% critical was assumed.

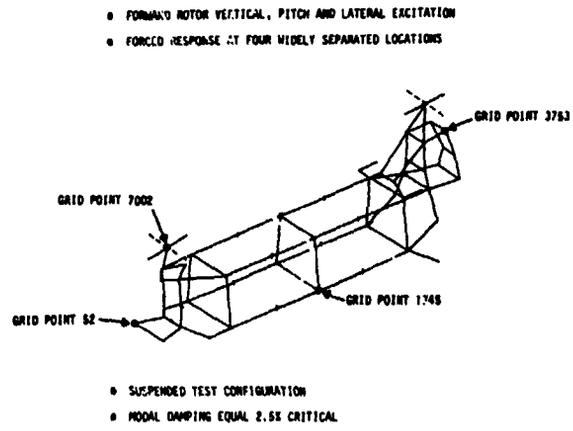

Figure 33. Airframe Locations and Conditions for Forced Response Correlation

Forced response comparisons with forward vertical excitation are presented in Figure 34; with forward pitch excitation in Figure 35; and with forward lateral excitation in Figure 36. The response scale is in ±g per pound of force.

Vertical vibration prediction from forward rotor vertical excitation in Figure 34 shows fairly good absolute magnitude correlation with test at the important 3/rev and 6/rev forcing frequencies There is generally an analytical response which can be associated with the major test peaks and usually the minor ones as well. In the coupled direction, i.e. longitudinal motion under vertical excitation, the absolute magnitudes, which are usually smaller than in the prime directions, are reasonably well produced.

On the negative side, the very prominent cockpit Sta 52 test response at 28 Hz in the vertical direction has no strong analytical counterpart.

Results of the forward rotor pitch excitation are in Figure 35. Comparison of test and analysis here gives generally good agreement. Again absolute magnitude predictions are good, especially at 3/rev and 6/rev. Longitudinal motion at the forward hub shows the strong peak near 10 Hz that is close to the test peak. Even the secondary peak near 17 Hz is reproduced. Vertical motion from pitch excitation is acceptable on an absolute basis at 3/rev and 6/rev, but the magnitudes of the peaks disagree.

The analytical peak at 32.7 Hz is generally over-predicted in amplitude. This implies that the proper choice of damping, rather than the constant 2.5% structural critical damping assumed, would improve the correlations.

Results of the forward rotor lateral excitation are in Figure 36. Again, the absolute magnitudes are reasonable. On the negative side, the lateral peak near 21 Hz is over predicted. Again the use of non-constant structural damping would improve this situation.

Figure 37 is a bar chart comparing analytical and test frequencies. In the cluster of modes from 6 to 8 Hz, there is one more analytical than test mode. Since this analytical mode is an out-of-phase engine to engine yaw motion, it may exist but be masked within the adjacent aircraft longitudinal mode at 7.2 Hz. In the cluster of modes from 10 to 20 Hz, there is an analytical mode corresponding to every test mode. The frequency error ranges from near zero to 0.8 Hz for the test mode at 11.7 Hz. Above 20 Hz there are more analytical than test modes.

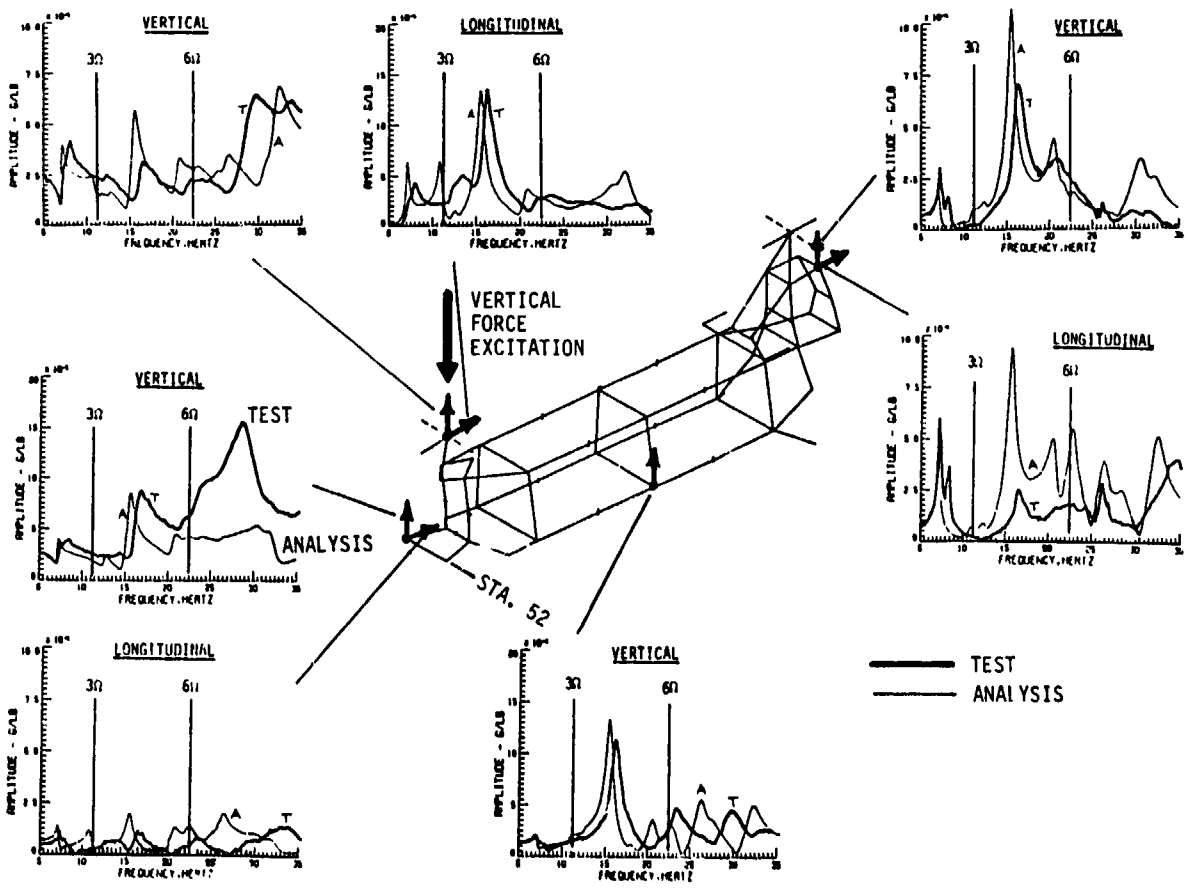

Figure 34. Comparison of Test and Analytical Forced Response with Forward Vertical Excitation

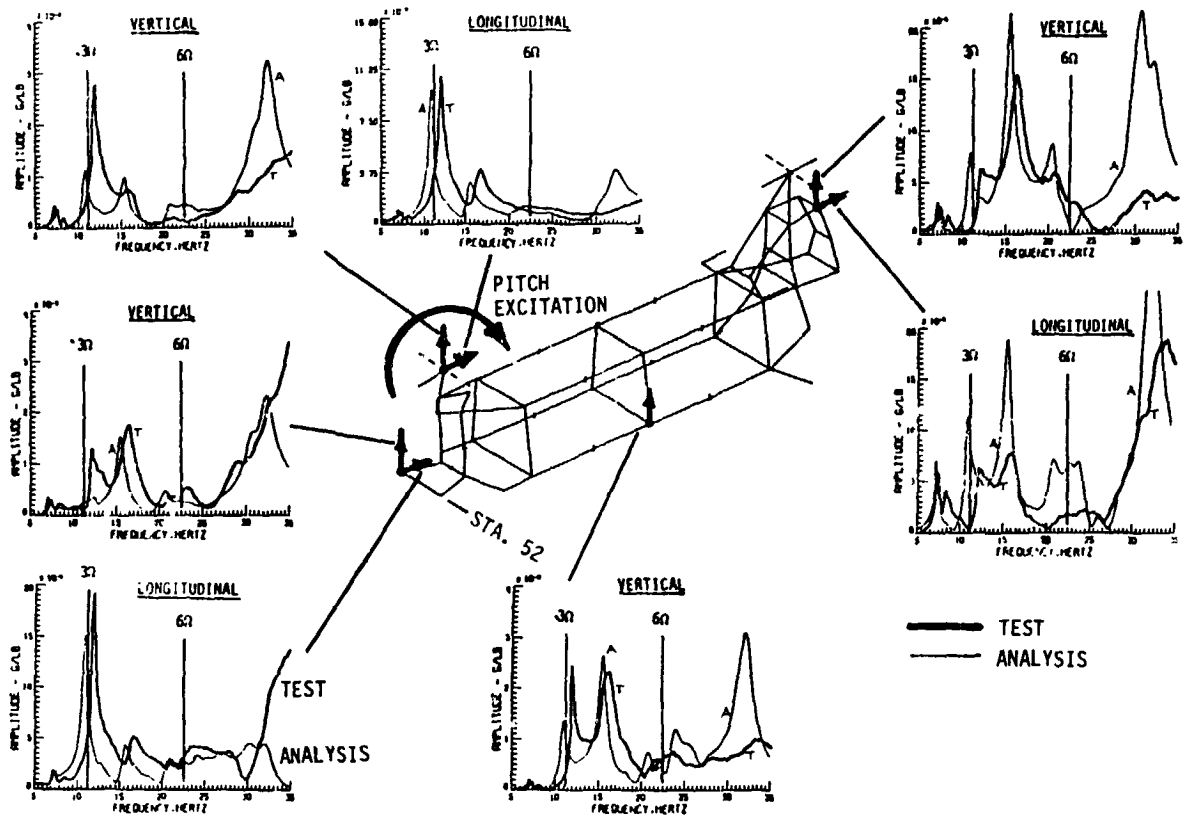

Figure 35. Comparison of Test and Analytical Forced Response with Forward Pitch Excitation

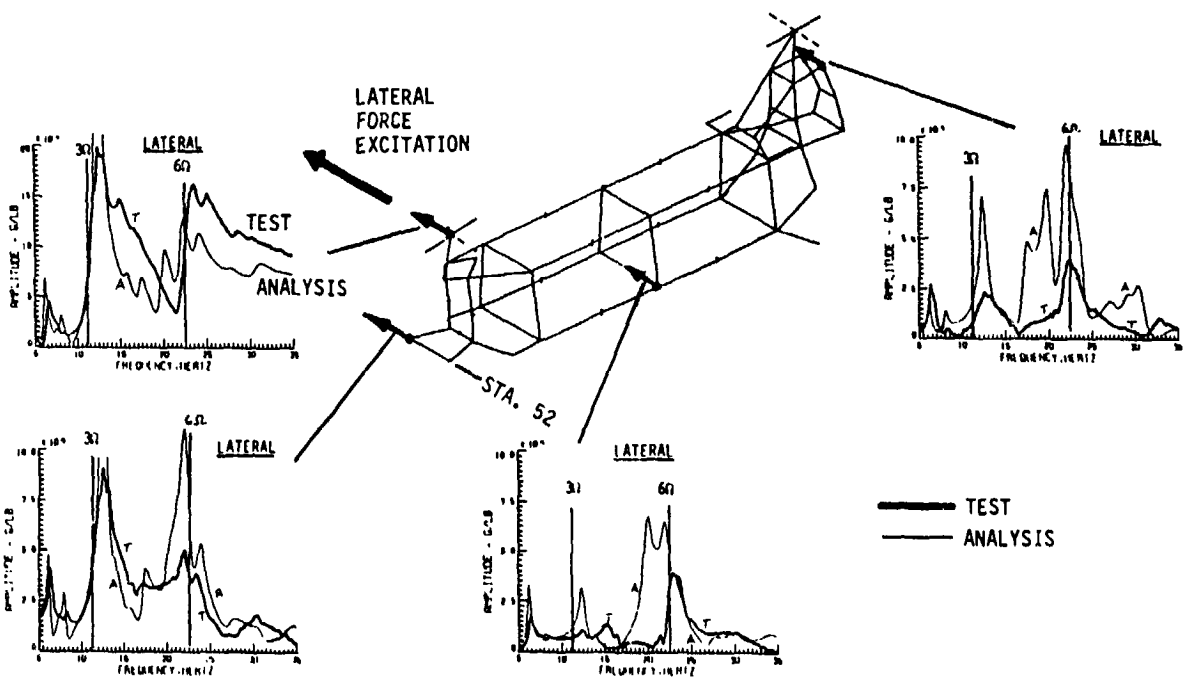

Figure 36. Comparison of Test and Analytical Forced Response with Forward Lateral Excitation

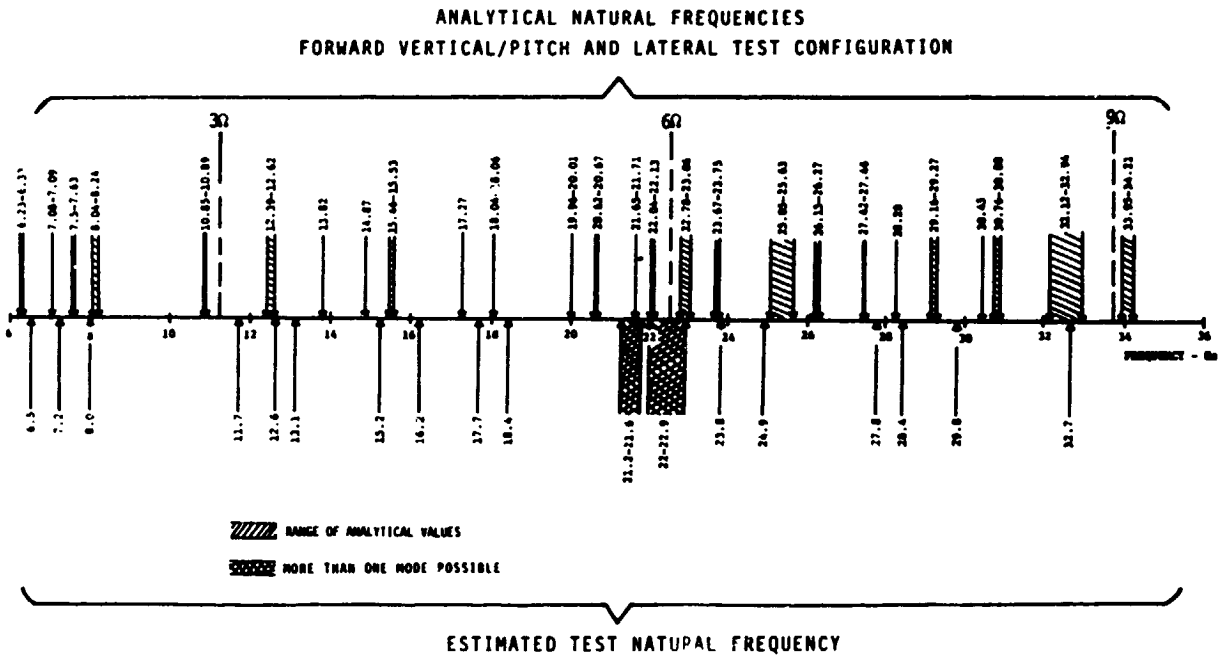

Figure 37. Comparison of Test and Analytical Natural Frequencies

Correlation Improvements

A number of items arose from the modeling and correlation experience which have the potential for further improvement of correlation.

1. Correct modeling of damping is a major need. The current use of a constant assumed value of structural damping is not adequate. Some form of nonuniformly distributed damping is required.

2. Stringer area is not included in shear area of the cross-section, since the usual assumption of skin areas carrying all shears is made. When summed the shear area of stringers is as much as 50% of the skin area.

3. The upper portion of the splice joints is in compression under 1g loading and unconnected stringers may be axially effective.

4. More thorough modeling of the forward transmission cover, shaft, bearings and bearing clearances may be necessary to obtain a still closer match of the mode near 3/rev.

5. The hub test fixture should be remodeled to better reflect elastic effects at the interface with the rotor shaft

6. Masses are distributed to approximately 10% of the structural grid points. A finer mesh may be necessary to improve higher mode predictions.

A preliminary effort to evaluate some of these improvements has been conducted. In Figure 38, damping has been adjusted in an attempt to improve the forced response correlation. Instead of using a constant 2.5% structural damping, the damping has been varied by mode as indicated in the tabulation.

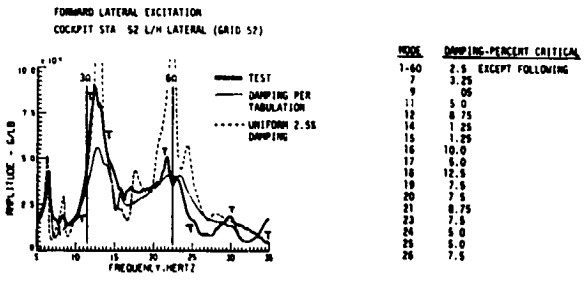

Figure 38. Effect of Modal Damping on Forced Response Correlation

The damping was varied here to obtain the best match at the bottom of the response, away from the resonance points.

A second improvement item has been explored. Table 2 summarizes the results of a number of exploratory runs to investigate the effect of splice joint continuity and stringer shear area. For

Table 2. Effect of Splice Joint Continuity and Stringer Shear Area on Natural Frequency

ANALYTICAL FREQUENCIES - Hz

SPLICE JOINT CONFIGURATION →	BASELINE MODEL	STA. 160 AND 440 ALL STRINGERS CONTINUOUS				STA. 160 CONTINUOUS
SHEAR MODULUS →	BASELINE	BASELINE	X1.13	X1.5	X2.0	X1.13
	6.25	6.26	6.40	6.73	7.08	6.40
	7.00	7.11	7.18	7.40	7.64	7.18
	7.91	7.92	8.00	8.19	8.37	8.00
	8.48	8.49	8.59	8.82	9.07	8.59
TEST VALUE = 11.7 Hz →	10.85	11.31	11.42	11.68	11.97	11.42
	12.62	12.63	13.00	13.84	14.68	13.00
	13.81	13.89	14.28	15.15	16.07	14.28
	14.87	14.88	15.69	16.42	17.06	15.69
	15.47	15.59	15.84	17.74	19.16	15.84
	17.30	17.34	17.70	18.60	19.81	17.70
	18.09	18.11	18.44	19.25	20.72	18.44
	20.01	20.02	20.36	21.12	21.43	20.36
	20.64	20.78	21.00	21.29	22.00	21.00
	21.69	21.74	22.00	22.96	24.23	22.00
	22.10	22.17	22.81	24.32	25.92	22.81
	23.41	23.52	23.91	24.98	26.30	23.91
	23.99	24.09	24.61	26.03	27.35	24.61
	25.30	25.38	25.93	27.35	28.83	25.94
	26.12	26.29	26.81	27.81	28.96	26.81
	27.42	27.46	27.78	28.85	30.47	27.77
	28.41	28.46	29.16	31.07	33.27	29.16
	29.36	29.33	30.02	31.72	33.61	30.02

expediency, the stringer shear area was simulated by modifying the shear modulus so as to effectively increase the shear area. The thrust of the effort was to raise the baseline analytical frequency at 10.85 Hz to the test value at 11.7 Hz. The chart shows that with all the stringers continuous at Stations 160 and 440, the frequency did increase from 10.85 to 11.31 Hz. This change in splice joint continuity has remarkably little effect on the frequency of the remaining modes.

Next, to represent the actual stringer shear area, the shear modulus is increased by a factor of 1.5, the frequency of this mode increased to 11.68 Hz, almost exactly the 11.7 Hz test value.

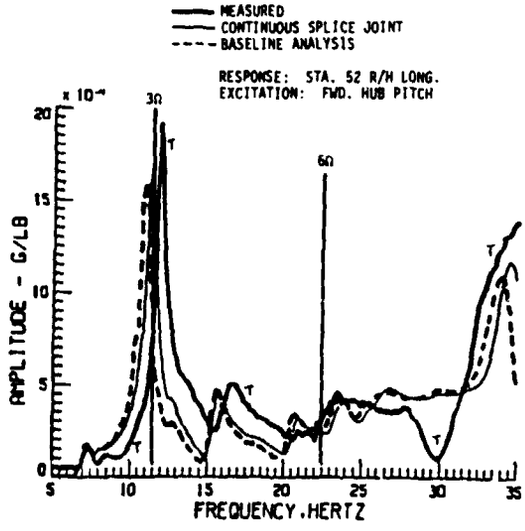

Figure 39. Effect of Splice Joint Continuity on Forced Response Correlation

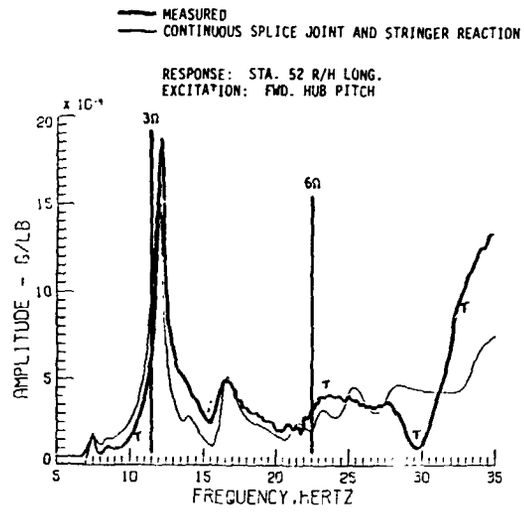

Figure 40. Combined Effect of Splice Joint Continuity and Stringer Shear Reaction

Forced response runs were then made with these two improvements. As representative, look at cockpit longitudinal response under forward rotor pitching moment excitation shown in Figures 39 and 40.

The inclusion of these two, somewhat secondary effects, thus have an impressive effect on improvement of the correlation.

Industry Critique of Test and Correlation

Rather than a series of on site briefings, the presentation and critique of the test and correlation activity was made at a joint meeting of industry representatives. The analytical approach of modeling the shakers and support systems in addition to the basic airframe received favorable comments from all attendees. Reasons cited included: (1) verification of normally accepted suspension concept, (2) insured one-to-one comparison, and (3) directly addressed interaction issue. Overall, the correlation below 20 Hz was deemed good. However, the consensus of opinion was that the higher frequency range needed more work. A finer mass breakdown was considered to be a key aspect in improving high frequency correlation.

Several comments unrelated to specific test results are also worthy of mention. One observer suggested that study of the available results might provide guidelines for a realistic validation criteria. A second noted that a stronger management commitment to adequate shake testing and correlation was needed.

Ref. 4 reported the details of the ground shake test and the correlation effort. Ref. 5 is an overall program summary.

Conclusions

- Guides prepared during the planning phase enabled proper planning, scheduling and control of the present modeling effort.
- Error free demonstration runs for the resulting static and vibrations models displayed rational internal loads and reasonable natural frequencies and mode shapes.
- Management enforced cooperation of Design-Stress-Weights-Dynamics is key to achieving an FEM suitable for internal loads, structural member sizing and vibration analysis.
- Cost of the total effort is 4,430 man-hours or 5%, 4% is already usual for internal loads; the vibration model is another 1%.
- Satisfactory procedures were developed for analysis of the suspended aircraft. Comparison of free and suspended configuration indicates only minor differences.
- Reasonable correlation was obtained between test and analytical results. Adequate modeling of damping appears as a major stumbling block to improved correlation.
- Nonlinear effects result in test scatter of peak responses about the natural frequencies. Force level was identified as one source of nonlinearity.
- Significantly improved correlation appears possible by including secondary effects such as stringer shear area and effective splice joint stringer continuity due to lg loading.

Acknowledgment

This work was sponsored by NASA Langley under Contract NAS1-16460. The authors wish to acknowledge the contributions of NASA Langley participants in this program. Technical guidance was provided by Messrs. Eugene C. Naumann and Raymond G. Kvaternik. The program was conceived and supervised by Mr. William C. Walton, Jr. The YCH-47D prototype aircraft was provided to NASA for the test period by the U.S. Army AVSCOM, St. Louis.

References

1. Gabel, R., Ricks, R. G., and Magiso, H., "Planning, Creating and Documenting a NASTRAN Finite Element Vibrations Model of a Modern Helicopter, Planning Report," NASA CR165722, April 1981.
2. Gabel, R., Reed, D. A. "Planning, Creating, and Documenting a NASTRAN Finite Element Vibrations Model of a Modern Helicopter, Test Requirements Report," NASA CR165855, April 1982.
3. Gabel, R., Kesack, W.J. and Reed, D. A., "Planning, Creating and Documenting a NASTRAN Finite Element Vibrations Model of a Modern Helicopter, Modeling Documentation Report," NASA CR166077, March 1983.
4. Gabel, R., Reed, D. A., Ricks, R.G., "Planning, Creating and Documenting a NASTRAN Finite Element Vibrations Model of a Modern Helicopter, Ground Shake Results and Correlation Report," NASA CR166107, May 1983.
5. Gabel, R., Kesack, W. J., Reed, D. A., Ricks, R. G., "Planning, Creating and Documenting a NASTRAN Finite Element Model of a Modern Helicopter, Summary Report," NASA CR17229, October 1983.

DISCUSSION
Paper No. 20

PLANNING, CREATING AND DOCUMENTATING A NASTRAN FINITE ELEMENT MODEL OF A MODERN HELICOPTER
R. Gabel
D. Reed
R. Ricks
and
W. Kesack

Charlie Fredrickson, Sikorsky Aircraft: Dick, I think that was a really neat paper, well thought out, and very nicely presented and so on. I'd like to ask you three questions. Did you previously do a NASTRAN model on the Chinook, in other words had you previously taken an earlier FEM model on the Chinook and upgraded it to the D before it actually flew and if you did, how did that compare with this well-planned FEM model that you did later on?

Gabel: Well, we did do that, Charlie, many, many years ago for the A model of the Chinook. There was a model built and there was even hardware made to try to tune it and the fact that the Chinooks had vibration troubles through their whole life means that it didn't work very well.

Fredrickson: I was trying to find out if you had upgraded that model for the D.

Gabel: No, we were too stupid to do that. We actually started from scratch and used the design drawings for the D. Since many of the people who did the early model were long gone anyway, it didn't really matter.

Fredrickson: In the actual shake test, how did you actually identify what you considered to be natural modes of the aircraft?

Gabel: Combinations of things: we used the peak, the forced amplitude, we used the 90° phase between the amplitudes and the shaker force, we used the frequency circle diagrams--about 3 or 4 different ways.

Fredrickson: Okay. I know in my own experience, if you use one or another method and don't use kind of a combination, you're liable to miss a few modes along the way.

Gabel: But then they're not pure because we were shaking with one shaker at a time at one rotor head and to get a pure mode you have to have distributed shakers which nobody does any more.

Fredrickson: Another question about how the shake test was done. Was that a swept sine or random input or just exactly what was the methodology behind the shake test itself?

Gabel: It was a slow sweeping sine.

Wayne Johnson, NASA Ames Research Center: With the coming switch to composite airframes, do you think that's going to make this job harder or easier?

Gabel: Different. So far the elements being used are really the same as the stress people have been using for the metal elements. They are not going into it layer by layer because of the magnitude of the structure.

Johnson: Do you think the composite structures will have more or less small scale variations? It seemed that one of the things you were saying is that small scale variations which are not modeled are almost certainly a cause of some of the discrepancies. Do you think composites will have more or less of that?

Gabel: It's hard to say. I would think they might have more because the way they're laid up--it's not quite the same as a rolled out metal sheet. There may be variations in thickness and such things that may be more complex. I might comment that Langley is underway on a continuation of this program, where Sikorsky, Hughes, and Bell are analyzing their production metal aircraft. Since we have already done the first metal one, we're underway on the first composite aircraft. We are modeling it and we're going through the same process that's shown here.

Bob Wood, Hughes Helicopters: Dick, I'd like to compliment you on a fine presentation. As Hughes is one of the participants in it, I just wanted to bring out one of the values among many of the values I think we're finding from this NASTRAN analysis. In the case of the Apache, the second vertical bending mode came out to be practically right on our N per rev and we thought that was really the problem. But using our NASTRAN [model] and taking the percentage of modal contributions, it turned out that for the forced response, the primary contributor to the pilot and cockpit vibration was a wing-symmetric mode down at 14 Hertz. I think this is one of the values we can get out of NASTRAN.

COUPLED ROTOR-BODY VIBRATIONS WITH INPLANE DEGREES OF FREEDOM

Huang Ming-Sheng
Research Assistant
and
David A. Peters
Professor and Chairman
Department of Mechanical Engineering
Washington University, Campus Box 1185
St. Louis, Missouri 63130

Abstract

In an effort to understand the vibration mechanisms of helicopters, the following basic studies are considered. A coupled rotor-fuselage vibration analysis including inplane degrees of freedom of both rotor and airframe is performed by matching of rotor and fuselage impedances at the hub. A rigid blade model including hub motion is used to set up the rotor flaplag equations. For the airframe, 9 degrees of freedom and hub offsets are used. The equations are solved by harmonic balance. For a 4-bladed rotor, the coupled responses and hub loads are calculated for various parameters in forward flight. The results show that the addition of inplane degrees of freedom does not significantly affect the vertical vibrations for the cases considered, and that inplane vibrations have similar resonance trends as do flapping vibrations.

Notation

a	= slope of lift curve, rad^{-1}
A	= ratio of rotor mass to moment of inertia, $M\bar{x}R/I_y$
$\begin{Bmatrix} a \\ b \end{Bmatrix}_F$	= cosine and sine harmonics of F
b	= number of blades
$\hat{C}_z$	= conventional thrust coefficient, thrust/$\rho\pi\Omega^2R^4$
C_x, C_y, C_z, C_M, C_L	= vibratory portion of nondimensional longitudinal force, lateral force, thrust, pitch and roll moment over σa
$\bar{C}_x, \bar{C}_y, \bar{C}_z, \bar{C}_M, \bar{C}_L$	= steady portion
$\bar{d}_F$	= offset between focus and center of fuselage, divided by R
$\bar{d}_p$	= offset between focus and center of pylon, divided by R
$\bar{d}_r$	= offset between hub and center of pylon, divided by R
EI	= beam cross-section bending stiffness
$\{F\}$	= vector of harmonics of C_M, C_L, C_x, C_y, C_z
$\bar{g}$	= nondimensional acceleration of gravity, g/Ω^2R
g_z, g_y, g_m, g_L	= plunge, lateral, pitch and roll structural damping, $= 2\zeta$
$\bar{h}$	= offset between hub and focus, divided by R
$[H]$	= fuselage receptance
$[I]$	= identity matrix
$\bar{I}_{y1}$	= pitch inertia moment of pylon, divided by M_pR^2
I_{x1}	= roll inertia moment of pylon, divided by M_pR^2
$\bar{I}_{y2}$	= pitch inertia moment of fuselage, divided by M_FR^2
$\bar{I}_{x2}$	= roll inertia moment of fuselage, divided by M_FR^2
$K_{\alpha c}$	= fuselage pitch-spring-restraint stiffness, N-m/rad
$K_{\alpha s}$	= fuselage roll-spring-restraint stiffness, N-m/rad
ℓ	= length of the beam, m
m	= mass per unit beam length, kg/m
M_C	= lumped mass on the center of the fuselage, kg
M_p	= mass of pylon, kg
M_F	= mass of fuselage, $M_C + m\ell$, kg
M_f	= mass of whole fuselage, $M_C + m\ell + M_p$, kg
p	= first flap frequency divided by R
P	= p^2

$\bar{r}_{pm}$, $\bar{r}_{pL}$ = radius of gyration of pylon in pitch, roll, divided by R

$\bar{r}_{Fm}$, $\bar{r}_{FL}$ = radius of gyration of fuselage in pitch, roll, divided by R

R = rotor radius, m

R_V = beam mass divided by whole airframe mass, $m\ell/(m\ell + M_C + M_P)$

$[S_i]$ = general matrices

[T] = transformation matrix

W = rotor stiffness parameter[11]

$\bar{x}$ = distance along fuselage, tail to nose, or distance along radius of rotor, root to tip, divided by R

x,y,z = rotating coordinates fixed on the blade

x',y',z' = rotating coordinates if flapping and lead-lag are zero

X,Y,Z = fixed fuselage coordinates

$\bar{X},\bar{Y},Z$ = dimensionless displacements, X/R, Y/R, Z/R

$\bar{Y}_F$, $\bar{Z}_F$ = dimensionless fuselage elastic degree of freedom in vertical and lateral directions

Z = rotor stiffness parameter[11]

[Z] = rotor impedance

α_c, α_{CF} = pitch angle of hub, fuselage, positive nose up, rad

$\bar{\alpha}_c$ = steady hub pitch angle, rad

α_s, α_{SF} = roll angle of hub, fuselage, positive advancing side down, rad

$\bar{\beta}$ = equilibrium flapping angle, $\beta_o + \beta_s\sin\psi + \beta_c\cos\psi$, rad

β_o = coning angle, rad

β_s = lateral cyclic flap angle, rad

β_c = longitudinal cyclic flap angle, rad

β_{pc} = pre-cone angle

γ = Lock number

λ = inflow ratio

μ = advance ratio

μ_p = ratio of mass of pylon to mass of fuselage, $M_p/(M\ell + M_C)$

μ_{mc} = ratio of lumped mass to the uniformly distributed mass, $M_C/m\ell$

μ_{mp} = ratio of mass of pylon to the uniformly distributed mass, M_p/m_ℓ

σ = rotor solidity

$\{\upsilon\}$ = vector of control variables

$\bar{\theta}$ = equilibrium pitch angle, $\theta_o + \theta_s\sin\psi + \theta_c\cos\psi + \theta_\beta(\bar{\beta}-\beta_{pc}) + \theta_\zeta\bar{\zeta}$

θ_o, θ_s, θ_c = collective and cyclic pitch, rad

θ_β, θ_ζ = pitch-flap and pitch-lag coupling ratios

ψ = azimuth angle, nondimensional time,

$\bar{\omega}$ = natural frequency of fuselage, divided by Ω

$\bar{\omega}_{xy}$ = frequency of "y" motion with "x" boundary condition, divided by Ω; y = z,y,m,L plunge, lateral, pitch, roll, x = c,f cantilevered, free

Ω = rotor speed, rad/sec

$(^*)$ = $d(\ )/d\psi$

$(\cdot)$ = $d(\ )/dt$

C_{do} = blade profile drag coefficient

ζ = lag angle, positive forward, rad

$\bar{\zeta}$ = equilibrium lag angle, rad

$\tilde{\zeta}$ = small perturbation of lag angle

$\tilde{\beta}$ = small perturbation of flapping angle

Introduction

Helicopter vibration reduction has become more and more important in recent years because of human factors and expanded operational capabilities. Unlike the

conventional fixed-wing aircraft, the helicopter suffers an intrinsic, severe vibration source - the main rotor. The main rotor is connected flexibly to the fuselage by a hub-pylon system which makes the problem sophisticated. The fuselage motions due to rotor vibrations can cause the hub to move in all degrees of freedom which, in turn, can alter the hub loads obtained for a fixed-hub condition. This alteration can often be an order-of-magnitude change. Therefore, what we are studying is a feedback or coupled system.

The concept of performing a coupled rotor/airframe vibration analysis by impedance matching goes back about 20 years, Reference 1. That reference points out two important facts. First, a coupled rotor/airframe analysis can be performed in a rigorous manner by separate calculation of rotor and fuselage impedances followed by a matching of forces and displacements at the hub. Second, the rotor impedance need only be calculated for a single blade and then appropriately transformed to apply to any number of blades. In 1974, Staley and Sciarra treated the vertical vibrations of a coupled rotor and fuselage, including the effect of vertical hub motions.[2] They used a rigid-body mass as a model for rotor impedance and showed that hub motions could create order-of-magnitude changes in hub loads. In Reference 3, Hohenemser and Yin further investigate the effects of rotor-body coupling. Their model for rotor impedance is based on a rotor representation that includes two masses (each equal to one-half of the total rotor mass) connected by a spring to represent the first flapping frequency. Thus, Reference 3 contains a more sophisticated rotor impedance than does Reference 2. Reference 3 presents some very interesting conclusions that pertain to fuselage design. Particularly, it notes that under certain conditions it may be desirable to tune a fuselage frequency to the blade passage frequency in order to eliminate hub loads. Also, it outlines a method of computing the complete rotor impedance by finite elements and transfer matrices. Other work on the importance of hub impedance may be found in References 4-6.

When one considers the rather crude models that have been used for hub impedance (rigid mass, no aerodynamics, etc.) one might wonder why more sophisticated models were not used. The answer is straightforward. These were only the initial investigations into this effect. Furthermore, although most analysts realized the importance of detailed blade modeling (blade modes, unsteady aerodynamics, periodic coefficients, etc.) for fixed hub loads, it was not clear in the beginning which of these effects would be important for finding the role of hub motion on loads. Because of the high frequencies involved (4/rev, 8/rev), many felt that inertial terms would dominate.

Reference 7 offers a sophisticated (but linear) rotor flapping model that allows for a detailed investigation of both rotor loads and impedance (even in the presence of periodic coefficients). The method, generalized harmonic balance, involves a computer-based manipulation of equations that allows many degrees of freedom, many modes, and many harmonics. In Reference 8, Hsu and Peters apply this method to a flexible rotor and then use impedance matching to include plunge, pitch, and roll of the hub. This combined solution technique proves to be very efficient on two counts. First, the calculation for only one blade can be used for n-blades (as in Reference 1). Second, wholesale changes in fuselage properties can be made without a requirement to recalculate rotor properties. It is interesting that other investigators who began with a full-blown, coupled analyses later changed to the impedance matching technique, References 9-10.

The next step, outlined in this paper, is to add inplane loads and inplane motions to the work of Reference 8. To do this, we need to consider a model for the inplane blade dynamics. Our plan is to begin with a rigid-blade rotor analysis, as outlined in Reference 11, and then to add hub motions to it. Later, we plan to do the same for the elastic flap-lag model of Reference 12. The work reported here is the former of these and is based on a Master of Science Thesis by the first author, Reference 13.

Rotor Model

The rotor model used here is that of Reference 9 but with the addition of hub motions. Fig. 1 shows the rotor model used in this paper.

The equations of motion of this system can be obtained from LaGrange's method with appropriate linearization about an equilibrium condition, $\bar{\beta}$. The aerodynamic terms are obtained from inviscid, linear, quasi-steady strip theory with the small-angle assumptions. Details of the derivation are given in Reference 11, upon which this paper is based. They can be expressed in matrix form as follows.

$$\begin{Bmatrix} \ddot{\bar{\beta}} \\ \ddot{\zeta} \end{Bmatrix} + \left[C(\Psi)\right]\begin{Bmatrix} \dot{\bar{\beta}} \\ \dot{\zeta} \end{Bmatrix} + \left[K(\Psi)\right]\begin{Bmatrix} \bar{\beta} \\ \zeta \end{Bmatrix}$$

$$= \left[Q(\Psi)\right]\begin{Bmatrix} \theta_0 \\ \theta_s \\ \theta_c \\ \lambda \\ \bar{\beta} \\ \beta_{pc} \\ \frac{c_{lo}}{a} \\ \bar{\alpha}_c \end{Bmatrix} + \left[\bar{A}(\Psi)\right]\begin{Bmatrix} \alpha_c \\ \alpha_s \\ \bar{X} \\ \bar{Y} \\ \bar{Z} \end{Bmatrix} + \left[\bar{B}(\Psi)\right]\begin{Bmatrix} \dot{\alpha}_c \\ \dot{\alpha}_s \\ \dot{\bar{X}} \\ \dot{\bar{Y}} \\ \dot{\bar{Z}} \end{Bmatrix} + \left[\bar{D}(\Psi)\right]\begin{Bmatrix} \ddot{\alpha}_c \\ \ddot{\alpha}_s \\ \ddot{\bar{X}} \\ \ddot{\bar{Y}} \\ \ddot{\bar{Z}} \end{Bmatrix} \qquad (1a)$$

Where,

$$[C(\Psi)] = \begin{bmatrix} \frac{\gamma}{8} + \frac{\gamma}{6}\cdot\mu s\Psi & \frac{\gamma}{6}\lambda + \frac{\gamma}{6}\bar{\beta}\mu c\Psi \\ & -\frac{\gamma}{8}\bar{\theta} - \frac{\gamma}{8}\bar{\theta}\mu s\Psi \\ & +2\bar{\beta} \\ \hline \frac{\gamma}{8}\bar{\theta} + \frac{\gamma}{6}\mu\bar{\theta}s\Psi & \frac{\gamma}{6}\lambda\bar{\theta} + \frac{\gamma}{6}\mu\bar{\theta}\bar{\beta}c\Psi \\ -\frac{\gamma}{3}\lambda - \frac{\gamma}{3}\mu\bar{\beta}c\Psi & +\frac{\gamma}{3}\frac{C_{d_\beta}}{a}\mu s\Psi + \frac{\gamma}{4}\frac{C_{d_0}}{a} \\ -2\bar{\beta} & \end{bmatrix}$$

$$[\bar{D}(\Psi)] \begin{bmatrix} c\Psi & s\Psi & -A\bar{\beta}c\Psi & A\bar{\beta}s\Psi & A \\ \hline \bar{\beta}s\Psi & -\bar{\beta}c\Psi & -As\Psi & -Ac\Psi & 0 \end{bmatrix}$$

$$[K(\Psi)] = \begin{bmatrix} P & Z \\ +\frac{\gamma}{6}\mu c\Psi & +\frac{\gamma}{4}\mu\lambda c\Psi \\ +\frac{\gamma}{4}\mu^2 s\Psi c\Psi & +\frac{\gamma}{4}\mu^2\bar{\beta}(c^2\Psi - s^2\Psi) \\ -\frac{\gamma}{8}\theta_\beta & -\frac{\gamma}{4}\mu^2\theta_\zeta s^2\Psi \\ -\frac{\gamma}{4}\mu^2\theta_\beta s^2\Psi & -\frac{\gamma}{2}\mu^2\bar{\theta}s\Psi c\Psi \\ -\frac{\gamma}{3}\mu\theta_\beta s\Psi & -\frac{\gamma}{3}\bar{\theta}\mu c\Psi \\ & -\frac{\gamma}{3}\mu\theta_\zeta s\Psi \\ & -\frac{\gamma}{6}\mu\bar{\beta}s\Psi \\ & -\frac{\gamma}{8}\theta_\zeta \\ \hline Z & W \\ +\frac{\gamma}{6}\lambda\theta_\beta & +\frac{\gamma}{4}\mu^2\bar{\beta}^2 c\Psi s\Psi \\ +\frac{\gamma}{4}\mu\bar{\theta}c\Psi & +\frac{\gamma}{3}\lambda\mu\bar{\beta}s\Psi \\ +\frac{\gamma}{6}\mu\bar{\beta}\theta_\beta c\Psi & +\frac{\gamma}{6}\lambda\theta_\zeta \\ +\frac{\gamma}{4}\mu\lambda\theta_\beta s\Psi & +\frac{\gamma}{6}\mu\bar{\beta}\theta_\zeta c\Psi \\ +\frac{\gamma}{4}\mu^2\bar{\beta}s\Psi c\Psi & +\frac{\gamma}{4}\mu\lambda\theta_\zeta s\Psi \\ +\frac{\gamma}{4}\mu^2\theta_\beta\bar{\beta}s\Psi c\Psi & +\frac{\gamma}{4}\mu\lambda\bar{\theta}c\Psi \\ -\frac{\gamma}{2}\bar{\beta}\mu^2 c^2\Psi & +\frac{\gamma}{4}\mu^2\bar{\theta}\bar{\beta}(c^2\Psi - s^2\Psi) \\ -\frac{\gamma}{3}\lambda\mu c\Psi & +\frac{\gamma}{2}\frac{C_{d_\beta}}{a}\mu^2 s\Psi c\Psi \\ & -\frac{\gamma}{6}\mu\bar{\theta}\bar{\beta}s\Psi \\ & +\frac{\gamma}{4}\mu^2\theta_\zeta\bar{\beta}s\Psi c\Psi \\ & +\frac{\gamma}{3}\frac{C_{d_\beta}}{a}\mu c\Psi \end{bmatrix}$$

$$[Q(\Psi)] = \begin{bmatrix} \frac{\gamma}{8} & \frac{\gamma}{8}s\Psi & \frac{\gamma}{8}c\Psi & -\frac{\gamma}{6} & -\frac{\gamma}{6}\mu c\Psi & P-1 & 0 & \frac{\gamma}{6} \\ +\frac{\gamma}{4}\mu^2 s^2\Psi & +\frac{\gamma}{4}\mu^2 s\Psi c\Psi & +\frac{\gamma}{4}\mu^2 c^2\Psi & -\frac{\gamma}{4}\mu s\Psi & -\frac{\gamma}{4}\mu^2 s\Psi c\Psi & & & +\frac{\gamma}{4}\mu^2 s^2\Psi \\ +\frac{\gamma}{6}\mu s\Psi c\Psi & +\frac{\gamma}{6}\mu s^2\Psi & +\frac{\gamma}{6}\mu c^2\Psi & & -P & & & \\ \hline -\frac{\gamma}{8}\lambda & -\frac{\gamma}{6}\lambda s\Psi & -\frac{\gamma}{6}\lambda c\Psi & \frac{\gamma}{6}\lambda & -Z & Z & -\frac{\gamma}{6}\mu s\Psi & -\frac{\gamma}{6}\mu\bar{\beta}c\Psi \\ -\frac{\gamma}{6}\mu\bar{\beta}c\Psi & -\frac{\gamma}{6}\mu\bar{\beta}s\Psi c\Psi & -\frac{\gamma}{6}\mu\bar{\beta}c^2\Psi & -\frac{\gamma}{6}\mu\bar{\beta}c\Psi & -\frac{\gamma}{4}\mu^2\bar{\beta}\bar{\zeta}c\Psi & & -\frac{\gamma}{8} & -\frac{\gamma}{6}\mu\lambda \\ -\frac{\gamma}{6}\mu\lambda s\Psi & -\frac{\gamma}{6}\mu\lambda s^2\Psi & -\frac{\gamma}{6}\mu\lambda s\Psi c\Psi & & & & -\frac{\gamma}{4}\mu^2 s^2\Psi & \\ -\frac{\gamma}{4}\mu^2\bar{\beta}s\Psi c\Psi & -\frac{\gamma}{4}\mu^2\bar{\beta}s^2\Psi c\Psi & -\frac{\gamma}{4}\mu^2\bar{\beta}s\Psi c^2\Psi & & & & & \\ +\frac{\gamma}{6}\mu\bar{\alpha}_c & +\frac{\gamma}{6}\mu\bar{\alpha}_c s\Psi & +\frac{\gamma}{6}\mu\bar{\alpha}_c c\Psi & & & & & \\ +\frac{\gamma}{4}\mu^2\bar{\alpha}_c s\Psi & +\frac{\gamma}{4}\mu^2\bar{\alpha}_c s^2\Psi & +\frac{\gamma}{4}\mu^2\bar{\alpha}_c s\Psi c\Psi & & & & & \end{bmatrix}$$

$$[\bar{A}(\Psi)] = \begin{bmatrix} \frac{\gamma}{6}\mu & 0 & 0 & 0 & 0 \\ +\frac{\gamma}{4}\mu^2 s\Psi & & & & \\ \hline -\frac{\gamma}{2}\mu^2\bar{\beta}c\Psi & 0 & 0 & 0 & 0 \\ -\frac{\gamma}{2}\mu\lambda & & & & \\ +\frac{\gamma}{6}\mu\theta_0 & & & & \\ +\frac{\gamma}{6}\mu\theta_s s\Psi & & & & \\ +\frac{\gamma}{6}\mu\theta_c c\Psi & & & & \\ +\frac{\gamma}{4}\mu^2\theta_0 s\Psi & & & & \\ +\frac{\gamma}{4}\mu^2\theta_s s^2\Psi & & & & \\ +\frac{\gamma}{4}\mu^2\theta_c s\Psi c\Psi & & & & \end{bmatrix}$$

$$[\bar{B}(\Psi)] = \begin{bmatrix} \frac{\gamma}{8}c\Psi & \frac{\gamma}{8}s\Psi & \frac{\gamma}{3}\theta_0 s\Psi & \frac{\gamma}{3}\theta_0 c\Psi & \frac{\gamma}{6} \\ +\frac{\gamma}{6}\mu s\Psi c\Psi & +\frac{\gamma}{6}\mu s^2\Psi & +\frac{\gamma}{3}\theta_s s^2\Psi & +\frac{\gamma}{3}\theta_s c\Psi s\Psi & +\frac{\gamma}{4}\mu s\Psi \\ -2s\Psi & +2c\Psi & +\frac{\gamma}{3}\theta_c s\Psi c\Psi & +\frac{\gamma}{3}\theta_c c^2\Psi & \\ & & +\frac{\gamma}{4}\mu\theta_0 s^2\Psi & +\frac{\gamma}{4}\mu\theta_0 c\Psi s\Psi & \\ & & +\frac{\gamma}{4}\mu\theta_s s^2\Psi & +\frac{\gamma}{4}\mu\theta_s c\Psi s^2\Psi & \\ & & +\frac{\gamma}{4}\mu\theta_c s^2\Psi c\Psi & +\frac{\gamma}{4}\mu\theta_c c^2\Psi s\Psi & \\ & & -\frac{\gamma}{4}\lambda s\Psi & -\frac{\gamma}{4}\lambda c\Psi & \\ & & -\frac{\gamma}{4}\mu\bar{\beta}s\Psi c\Psi & -\frac{\gamma}{4}\mu\bar{\beta}c^2\Psi & \\ & & -\frac{\gamma}{6}\bar{\beta}c\Psi & +\frac{\gamma}{6}\bar{\beta}s\Psi & \\ & & & +\frac{\gamma}{4}\mu\bar{\beta}s^2\Psi & \\ \hline -\frac{\gamma}{3}\lambda c\Psi & -\frac{\gamma}{3}\lambda s\Psi & -\frac{\gamma}{3}\frac{C_{d_\beta}}{a}s\Psi & -\frac{\gamma}{3}\frac{C_{d_\beta}}{a}c\Psi & -\frac{\gamma}{2}\lambda \\ -\frac{\gamma}{6}\mu\bar{\beta}c^2\Psi & -\frac{\gamma}{6}\bar{\beta}\mu s\Psi c\Psi & -\frac{\gamma}{2}\frac{C_{d_\beta}}{a}\mu s^2\Psi & -\frac{\gamma}{2}\frac{C_{d_\beta}}{a}\mu s\Psi c\Psi & +\frac{\gamma}{6}\theta_0 \\ +\frac{\gamma}{8}\theta_0 c\Psi & +\frac{\gamma}{8}\theta_0 s\Psi & & & +\frac{\gamma}{6}\theta_s s\Psi \\ +\frac{\gamma}{8}\theta_s s\Psi c\Psi & +\frac{\gamma}{8}\theta_s s^2\Psi & & & +\frac{\gamma}{6}\theta_c c\Psi \\ +\frac{\gamma}{8}\theta_c c^2\Psi & +\frac{\gamma}{8}\theta_c s\Psi c\Psi & & & +\frac{\gamma}{4}\mu\theta_0 s\Psi \\ +\frac{\gamma}{6}\mu\theta_0 s\Psi c\Psi & +\frac{\gamma}{6}\mu\theta_0 s^2\Psi & & & +\frac{\gamma}{4}\mu\theta_s s^2\Psi \\ +\frac{\gamma}{6}\mu\theta_s s^2\Psi c\Psi & +\frac{\gamma}{6}\mu\theta_s s\Psi c^2\Psi & & & +\frac{\gamma}{4}\mu\theta_c s\Psi c\Psi \\ +\frac{\gamma}{6}\mu\theta_c s\Psi c^2\Psi & +\frac{\gamma}{6}\mu\theta_c s^2\Psi c\Psi & & & -\frac{\gamma}{4}u\bar{\beta}c\Psi \end{bmatrix}$$

and $\quad s\Psi = \sin\Psi \qquad c\Psi = \cos\Psi \qquad (1b\text{-}g)$

One can also derive a detailed set of equations for hub loads (pitch moment, roll moment, propulsive force, side force, thrust) in terms of known parameters, unspecified hub motions ($\alpha_c, \alpha_s, \bar{X}, \bar{Y}, \bar{Z}$), and blade motions ($\beta, \zeta$).

$$\begin{Bmatrix} C_M \\ C_L \\ C_H \\ C_Y \\ C_S \end{Bmatrix} = [O(\Psi)] \begin{Bmatrix} \theta_0 \\ \theta_s \\ \theta_c \\ \lambda \\ \bar{\beta} \\ \beta_{FC} \\ \frac{C_{d_\beta}}{a} \\ \bar{\alpha}_c \end{Bmatrix} + [A(\Psi)] \begin{Bmatrix} \alpha_c \\ \alpha_s \\ \bar{X} \\ \bar{Y} \\ \bar{Z} \end{Bmatrix} + [B(\Psi)] \begin{Bmatrix} \dot{\alpha}_c \\ \dot{\alpha}_s \\ \dot{\bar{X}} \\ \dot{\bar{Y}} \\ \dot{\bar{Z}} \end{Bmatrix}$$

$$+\left[D(\psi)\right]\left\{\begin{matrix}\ddot{\alpha}_c\\ \ddot{\alpha}_s\\ \ddot{X}\\ \ddot{Y}\\ \ddot{Z}\end{matrix}\right\}+\left[E(\psi)\right]\left\{\begin{matrix}\tilde{\beta}\\ \tilde{\zeta}\end{matrix}\right\}+\left[F(\psi)\right]\left\{\begin{matrix}\dot{\tilde{\beta}}\\ \dot{\tilde{\zeta}}\end{matrix}\right\}+\left[G(\psi)\right]\left\{\begin{matrix}\ddot{\tilde{\beta}}\\ \ddot{\tilde{\zeta}}\end{matrix}\right\}$$

The equations expressed by Eqs. (1) and (2) are systems of ordinary differential equations with periodic coefficients. These can be solved for the periodic response by the harmonic balance method, Reference 3. This method involves operator matrices $[\pi]$ and $[\Box]$ which can be used to transform a system of periodic-coefficient differential equations into a set of linear, algebraic equations. For example, the single equation

$$M(\psi)\ddot{X} + C(\psi)\dot{X} + K(\psi)X = F(\psi) \qquad (3)$$

(where M, C, and F are periodic), can be transformed into algebraic equations for the unknown Fourier coefficients of x

$$x = a_o + \sum_{n=1}^{N} a_n\cos(n\psi) + b_n\sin(n\psi) \qquad (4)$$

$$[\pi(M)][\Box]^2\left\{\begin{matrix}a_n\\ b_n\end{matrix}\right\}_x + [\pi(C)][\Box]\left\{\begin{matrix}a_n\\ b_n\end{matrix}\right\}_x + [\pi(K)]\left\{\begin{matrix}a_n\\ b_n\end{matrix}\right\}_x = \left\{\begin{matrix}a_n\\ b_n\end{matrix}\right\}_F \qquad (5)$$

$$\left\{\begin{matrix}a_n\\ b_n\end{matrix}\right\}_x = [\pi(M)\Box^2+\pi(C)\Box+\pi(K)]^{-1}\left\{\begin{matrix}a_n\\ b_n\end{matrix}\right\}_F \qquad (6)$$

where $[\pi]$ is a function of the Fourier coefficients of its argument. The same operations can be applied to Eqs. (1) and (2) to give equations for the unknown harmonics of blade motions and loads,

$$\{\delta\} = [S_1]\{\theta\} + [S_2]\{z\} \qquad (7)$$

$$\{F\} = [S_3]\{\theta\} + [S_4]\{z\} + [S_5]\{\delta\} \qquad (8)$$

where $\{\delta\}$ are the harmonics of $\tilde{\beta}$ and $\tilde{\zeta}$, $\{F\}$ are the harmonics of hub loads, $\{z\}$ are harmonics of hub motions, and $\{\theta\}$ are specified rotor parameters.

$$\{\delta\} = \left\{\begin{matrix}\left\{\begin{matrix}a_n\\ b_n\end{matrix}\right\}_{\tilde{\beta}}\\ \left\{\begin{matrix}a_n\\ b_n\end{matrix}\right\}_{\tilde{\zeta}}\end{matrix}\right\} \qquad \{\theta\} = \left\{\begin{matrix}\theta_o\\ \theta_s\\ \theta_c\\ \lambda\\ \tilde{\beta}_o\\ \tilde{\zeta}_o\\ \alpha_c\end{matrix}\right\} \qquad (9a\text{-}b)$$

$$\{F\} = \left\{\begin{matrix}\left\{\begin{matrix}a_n\\ b_n\end{matrix}\right\}_{C_M}\\ \left\{\begin{matrix}a_n\\ b_n\end{matrix}\right\}_{C_L}\\ \left\{\begin{matrix}a_n\\ b_n\end{matrix}\right\}_{C_X}\\ \left\{\begin{matrix}a_n\\ b_n\end{matrix}\right\}_{C_Y}\\ \left\{\begin{matrix}a_n\\ b_n\end{matrix}\right\}_{C_Z}\end{matrix}\right\} \qquad \{z\} = \left\{\begin{matrix}\left\{\begin{matrix}a_n\\ b_n\end{matrix}\right\}_{\alpha_C}\\ \left\{\begin{matrix}a_n\\ b_n\end{matrix}\right\}_{\alpha_S}\\ \left\{\begin{matrix}a_n\\ b_n\end{matrix}\right\}_{\bar{X}}\\ \left\{\begin{matrix}a_n\\ b_n\end{matrix}\right\}_{\bar{Y}}\\ \left\{\begin{matrix}a_n\\ b_n\end{matrix}\right\}_{\bar{Z}}\end{matrix}\right\} \qquad (9c\text{-}d)$$

Equation (7) can be substituted into Eq. (8) to remove the blade motions. This gives rotor loads in the form

$$\{F\} = [\theta] + [Z]\{z\} \qquad (10)$$

where

$$[\theta] = [S_3] + [S_5][S_1] \qquad (11a)$$

$$[Z] = [S_4] + [S_5][S_2] \qquad (11b)$$

The matrix $[\theta]\{\theta\}$ represents the rotor loads with a fixed hub (e.g., without feedback due to hub motion), and the impedance matrix $[Z]$ represents the effect of hub motion on rotor loads. The calculation of $[\theta]$ and $[Z]$ in Eq. (10) need be performed for a single blade only. Subsequently, the corresponding matrices for a b-bladed rotor can be found by simply eliminating all harmonics that are not integer multiples of b. (Complete details are in Reference 3.)

It should be noted here that the present method of calculation of rotor impedance has experimental verification which can be found in Reference 8.

Fuselage Model

The mathematical description of the flexible fuselage includes 9 degrees of freedom. These are: 1) vertical rigid-body, 2) rigid-body pitch, 3) rigid-body roll, 4) rigid-body lateral, 5) rigid-body longitudinal, 6) elastic vertical, 7) elastic lateral, 8) elastic pylon in pitch, and 9) elastic pylon in roll. The model also includes vertical offsets between the fuselage center of mass, the pylon focus, the pylon center of mass, and the rotor center. Fig. 2 illustrates the vertical, longitudinal, and pitch degrees of freedom. The plunge and lateral model is the same as that of the plunge model in Reference 8, which is a uniform beam with a lumped mass M_C added at the center. The mass and inertial moment of the pylon are separated from the fuselage. The offsets are shown in Fig. 2. One can imagine that the lateral and roll directions have a similar schematic as that in Fig. 2 if X, α_c and α_{CF} are replaced by Y, α_s and α_{SF}.

The fuselage equations of motion are obtained from Lagrange's Method and the Rayleigh-Ritz Method. They are given in nondimensional form below (where blank elements are taken to be zero).

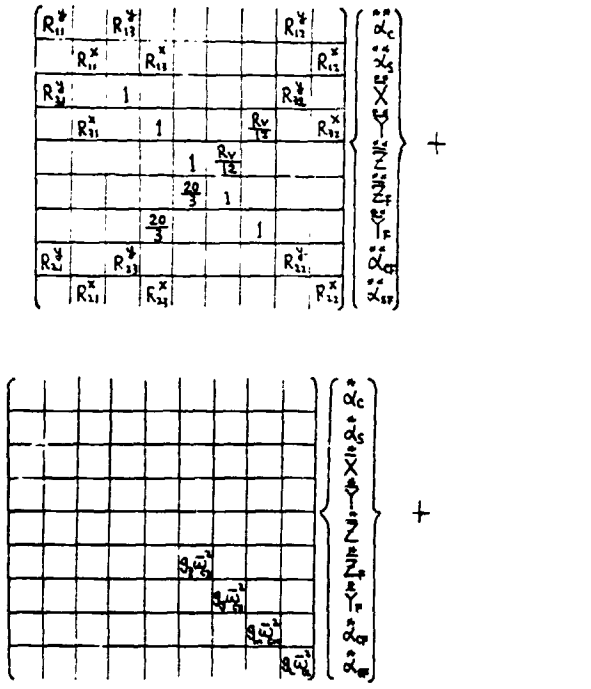

. . . (12)

Using the harmonic-balance method, Eq. (12) can be easily solved as the form below.

$$\begin{Bmatrix} \{z\} \\ \{z_F\} \end{Bmatrix} = [H][T]\{F\} \qquad (13a)$$

Where:

$$\{z_F\} = \begin{Bmatrix} \begin{Bmatrix} a_n \\ b_n \end{Bmatrix}_{\bar{Z}_F} \\ \begin{Bmatrix} a_n \\ b_n \end{Bmatrix}_{\bar{Y}_F} \\ \begin{Bmatrix} a_n \\ b_n \end{Bmatrix}_{\alpha_{CF}} \\ \begin{Bmatrix} a_n \\ b_n \end{Bmatrix}_{\alpha_{SF}} \end{Bmatrix} \qquad (13b)$$

$\bar{Z}_F$, $\bar{Y}_F$, α_{CF}, α_{SF} are elastic deflections in plunge, lateral, pitch, roll directions respectively.

[H] is receptance (inverse of impedance) of the fuselage.

[T] is a transformation matrix which is defined as

$$[T] = \begin{pmatrix} \frac{1}{\bar{r}_{gm}^2} & & -\frac{\bar{h}}{\bar{r}_{gm}^2} & & \\ & \frac{1}{\bar{r}_{gn}^2} & & \frac{\bar{h}}{\bar{r}_{gn}^2} & \\ & & 1 & & \\ & & & 1 & \\ & & & & 1 \\ & & & & \\ & & & & \\ & & & & \\ & & & & \end{pmatrix} \qquad (14)$$

As before, only integer-multiple harmonics of the blade number (b,2b,...) are retained. Furthermore, higher harmonics may be truncated as deemed appropriate.

The combined rotor/airframe vibrations may be performed by the matching of the impedances from Eq. (10) with those of Eq. (13). This implies the matching of harmonics of both loads {F} and displacements {z} at the hub. Therefore, we have

$$\{F\} = [\theta]\{\theta\} + [Z|0][H][T]\{F\} \qquad (15)$$

$$\{F\} = [I-[Z|0][H][T]]^{-1}[\theta]\{\theta\} \qquad (16)$$

It is noted that these loads include vertical, inplane, and radial loads.

Coupled Response

We now calculate vibrations. To begin, we look at the coupled rotor-fuselage response of a system with the following baseline parameters.

Rotor: 4 blades, $p = 1.09$, $\omega_\zeta = 0.7$ (soft inplane) and $\omega_\zeta = 1.4$ (stiff inplane)

$\gamma = 6.0$, $\bar{C}_z = 0.0144$,
$\bar{C}_L = \bar{C}_M = \bar{C}_X = \bar{C}_Y = 0$,
$\mu = 0.3$, $\bar{\alpha}_c = 0.7$, $\sigma = 0.07$,
$a = 5.73$

$\lambda = 0.0306$, $\hat{C}_z = 0.0058$

Fuselage: $\bar{\gamma}_{Fm} = .379$, $\bar{\gamma}_{FL} = .143$

$\bar{\gamma}_{pm} = .171$, $\bar{\gamma}_{pL} = .148$

$\bar{\omega}_{fz} = 1.45\ \bar{\omega}_{cz}$, $\bar{\omega}_{fL} = 1.18\ \bar{\omega}_{fm}$

$\bar{\omega}_{fm} = 10.0\ \bar{\omega}_{cm}$, $\bar{\omega}_{fL} = 4.47\ \bar{\omega}_{CL}$

$\bar{\omega}_{cz} = 1.06$, $\bar{\omega}_{cm} = 0.26$

$g_z = g_y = g_m = g_L = 0.02,\ 0.002$

Frequencies with subscript "c" denote cantilevered modes in which the hub degree of freedom is constrained but the remainder of the fuselage is free to move elastically. Frequencies with subscript "f" denote free modes for which neither the hub nor the fuselage is fixed. The parameters above are very close to those in Reference 8 (for comparison purposes) except for the parameters of inplane characters and offsets.

Results are presented for $g_y = g_z = 0.02,\ 0.002$, and $g_m = g_L = 0.02,\ 0.002$. Also shown are curves labeled "without feedback", which give the fixed-hub loads. As mentioned in Reference 8, for the coupled response, the natural frequency with the rotor is different from the frequency without the rotor.

The C_z curve ($g_z = 0.02$) in Fig. 3 is nearly identical to the corresponding curve in Reference 8. Therefore, the rigid, inplane degree of freedom does not affect vertical vibrations very much in the case considered. Figs. 4 and 5 show the lateral and longitudinal forces versus the fuselage bending frequency, which is assumed to be equal for vertical and lateral modes, $\omega_{cz} = \omega_{cy}$. It is seen that the lateral response is significant. The lateral response, therefore, can be an important consideration in helicopter dynamic design. Figs. 6 and 7 show that pitch and roll loads are not affected by the vertical vibration. Figs. 8-12 show the hub loads as a function of fuselage vertical frequency with a stiff inplane rotor and without offsets. The response is a little bit larger than that of soft inplane mentioned above, but the same conclusions hold.

Figs. 13-17 and Figs. 18-22 present the hub loads versus $\omega_{cm} = \omega_{cL}/1.18$, the pylon pitch and roll frequencies. Both the soft inplane and stiff inplane cases are shown. Because of aerodynamic coupling, all loads are affected by $\bar{\omega}_{cm}$ and ω_{cL}. For the smaller damping, $g_m = g_L = 0.002$, most of couplings are apparent (two resonant peaks), while at large damping they are less noticeable (one resonant peak).

Fig. 23 shows the effect of hub offsets on the vertical vibration. Comparison with Fig. 3 shows that there is little effect of hub offsets for plunge. For the pitch and roll modes, however, the effect of offsets is very significant, as shown in Figs. 24-28. (Compare with Figs. 18-22). In addition to the large change in magnitude due to the offsets, one notices that the resonance point is moved to approximately $\bar{\omega}_{cm} = 0.95$. The reason for this is that the rotor-fuselage coupling due to offsets ($\bar{h}$, $\bar{d}F$) shifts the fuselage natural frequency, so that the resonance with 4/rev is moved.

This phenomenon is illustrated in Fig. 29, which presents the fuselage natural frequency (without the rotor) vs. offsets $\bar{h}$ and $\bar{d}F$. Similarly, Figs. 30-31 show fuselage natural frequencies without the rotor vs. fuselage constrained vertical and pitch frequencies, respectively.

One can further appreciate that the rotor itself has an effect on the system frequencies, therefore, the 4/rev resonances in Figs. 29-31 do not exactly match the 4/rev resonances of the coupled rotor/body system. (See Reference 13 for details.) More calculations have been made, and one can find more figures in Reference 13. A few of the more interesting curves have been presented here.

Conclusions

The conclusions based on the assumptions and results of this study are:

1) Helicopter coupled rotor/fuselage vibrations with inplane degrees of freedom of both rotor and fuselage can be easily solved by harmonic balance and impedance matching and a single-blade analysis.

2) The addition of inplane degrees of freedom does not significantly affect the plunge vibrations for the cases considered, and these cases are for reasonable configurations.

3) The lateral response is significant, it should not be neglected in helicopter vibration analysis.

4) The hub offsets will significantly affect the coupled response.

Acknowledgment

The work was sponsored by the United States Army Research Office, Grant No. ARO-DAAG-29-80-C-0092. The view, opinions, and/or findings contained in this report are those of the author and should not be construed as an official Department of the Army position, policy, or decision, unless so designated by other documentation.

References

(1) Gestenberger, Walter and Wood, Edward R., "Analysis of Helicopter Aeroelastic Characteristics in High-Speed Flight," AIAA Journal, Vol. 1, No. 10, October 1964.

(2) Staley, J.A. and Sciarra, J.J., "Coupled Rotor/Airframe Vibration Prediction Methods," Rotorcraft Dynamics, NASA SP-352, 1974.

(3) Hohenemser, Kurt H. and Yin, Sheng-Kuang, "The Role of Rotor Impedance in the Vibration Analysis of Rotorcraft," Fourth European Powered Lift Aircraft Forum, Stressa, Italy, September 1978.

(4) Kato, Kanichiro and Yamane, Takaski, "Calculation of Rotor Impedance for Hovering Articulated-Rotor Helicopters," AIAA Journal, Vol. 16, No. 1.

(5) Kuczynski, W.A. and Sissingh, G.J., "Characteristics of Hingeless Rotors with Hub Moment Feedback Controls Including Experimental Rotor Frequency Response," NASA CR 114427, January 1972.

(6) Viswanthan, S.P. and Meyers, A.W., "Reduction of Helicopter Vibration through Control of Hub Impedance," Journal of the American Helicopter Society, Vol. 25, No. 4, October 1980, pp. 5-12.

(7) Peters, David A. and Ormiston, Robert A., "Flapping Response Characteristics of Hingeless Rotor Blades by a Generalized Harmonic Balance Method," NASA TN D-7856, February 1975.

(8) Hsu, T-K and Peters, David A., "Coupled Rotor/Airframe Vibration Analysis by a Combined Harmonic-Balance, Impedance-Matching Method," Journal of the American Helicopter Society, Vol. 27, No. 1, January 1982, pp. 25-34.

(9) Kunz, D., "Effects of Rotor-Body Coupling in a Linear Rotorcraft Vibration Model," Proceedings of the 36th Annual Forum of the American Helicopter Society, Washington, DC, May 1980.

(10) Kunz, D., "A Nonlinear Response Analysis and Solution Method for Rotorcraft Vibration," Journal of the American Helicopter Society, Vol. 28, No. 1, January 1983.

(11) Schrage, Daniel P., Effect of Structural Parameters on Elastic Flap-Lag Forced Response of a Rotor Blade in Forward Flight, Doctor of Science Thesis, Washington University in St. Louis, May, 1978.

(12) Eipe, Abraham, Effect of Some Structural Parameters on Elastic Rotor Loads by an Iterative Harmonic Balance, Doctor of Science Thesis, Washington University in St. Louis, December, 1979.

(13) Huang, Ming-Sheng, Coupled Rotor-Airframe Vibrations with Elastic Fuselage and Inplane Degrees of Freedom, Master of Science Thesis, Washington University, June, 1983.

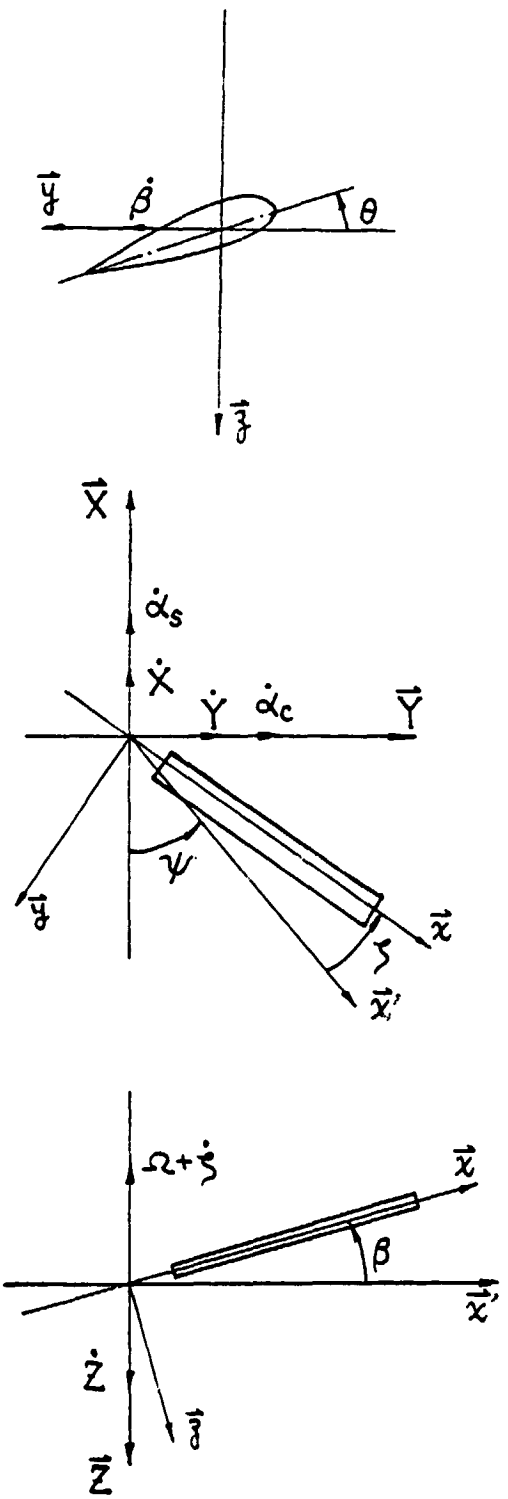

Figure 1. Rotor Model

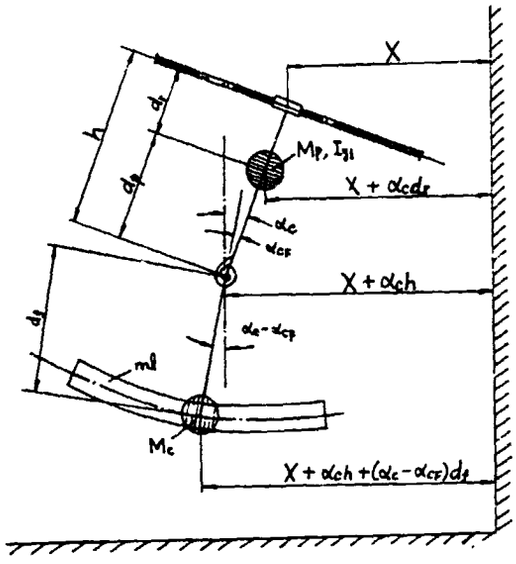

Figure 2. Fuselage Model in Longitudinal and Pitch Direction.

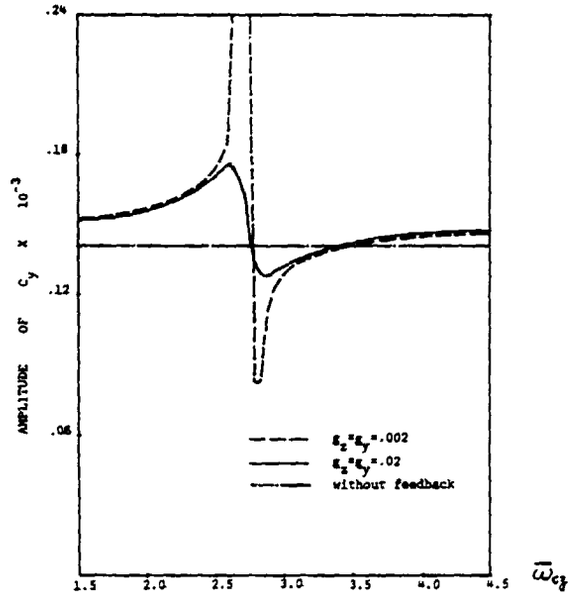

Fig. 4 4/rev lateral loads as a function of fuselage vertical constrained frequency $\omega_y = .7$, $\bar{h} = \bar{d}_p = \bar{d}_f = 0$

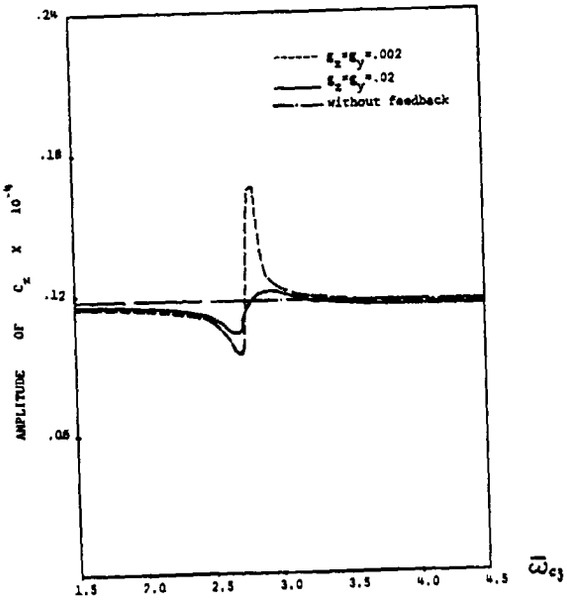

Fig. 3 4/rev vertical loads as a function of fuselage vertical constrained frequency $\omega_y = .7$, $\bar{h} = \bar{d}_p = \bar{d}_f = 0$

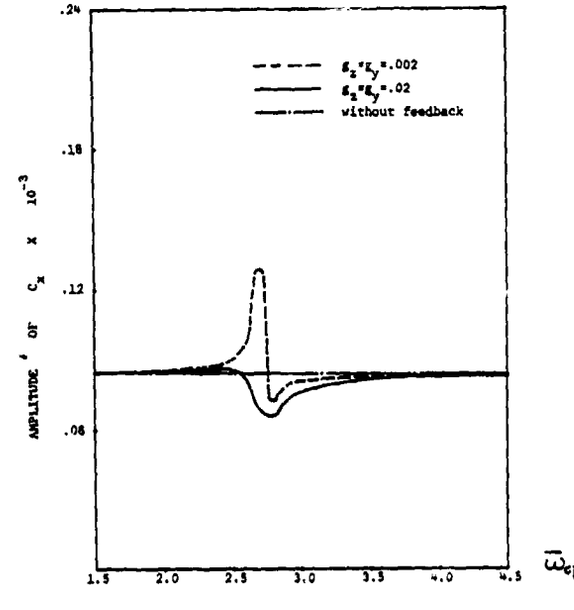

Fig. 5 4/rev longitudinal loads as a function of fuselage vertical constrained frequency $\omega_y = .7$, $\bar{h} = \bar{d}_p = \bar{d}_f = 0$

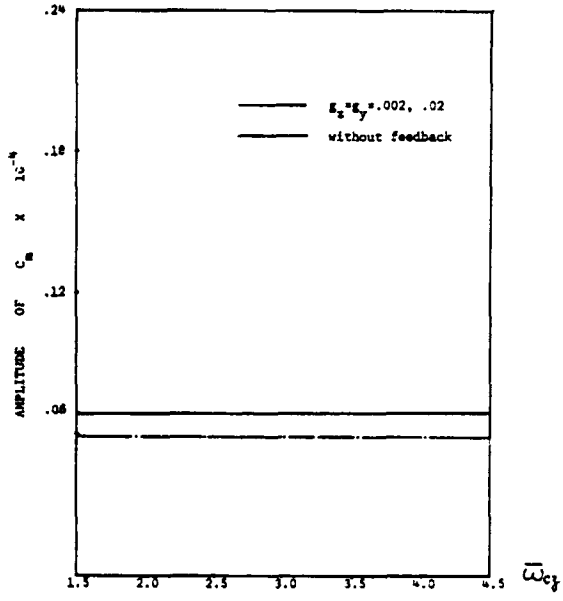

Fig. 6 4/rev pitch loads as a function of fuselage vertical constrained frequency
$\omega_\zeta=.7$, $\bar{d}_p=\bar{d}_r=\bar{h}=0$

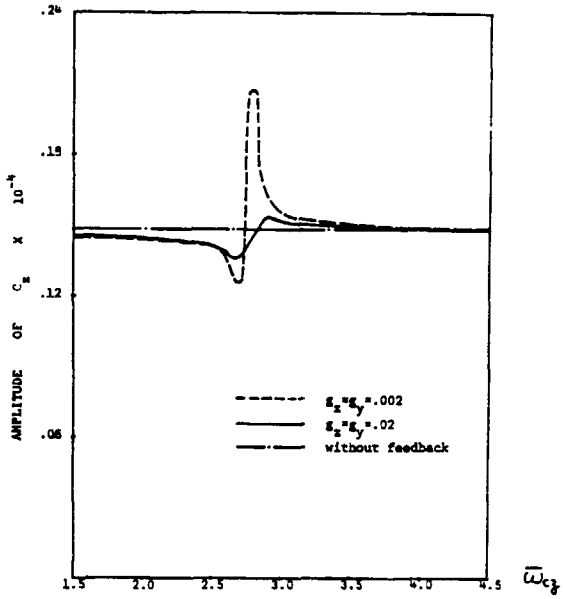

Fig. 8 4/rev vertical loads as a function of fuselage vertical constrained frequency
$\omega_\zeta=1.4, \bar{h}=\bar{d}_p=\bar{d}_r=0$

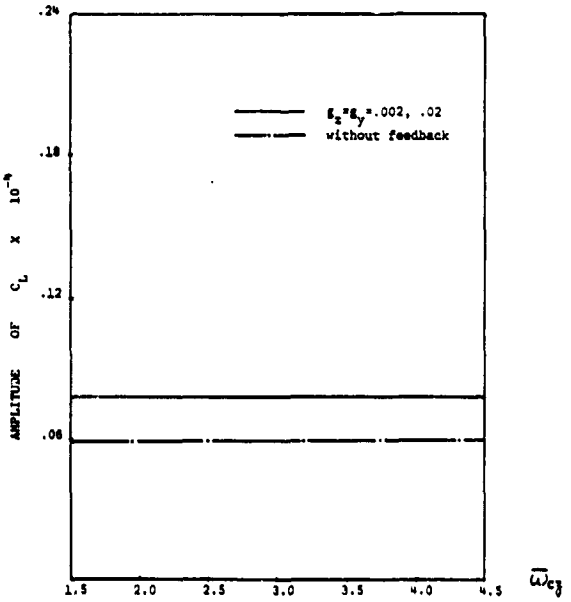

Fig. 7 4/rev roll loads as a function of fuselage vertical constrained frequency
$\omega_\zeta=.7$, $\bar{h}=\bar{d}_p=\bar{d}_r=0$

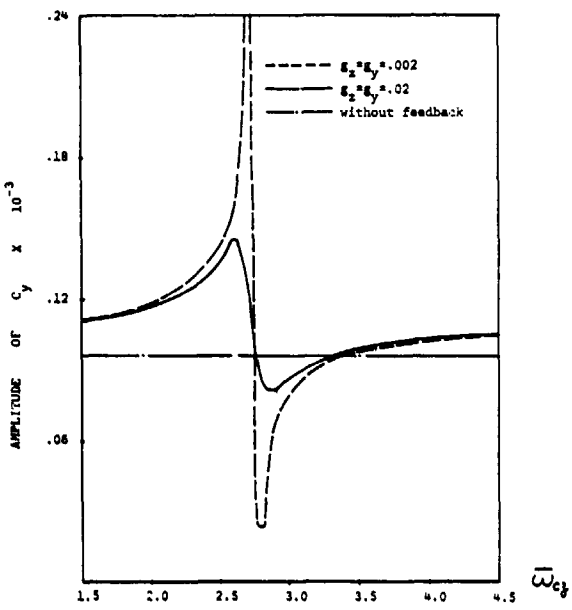

Fig. 9 4/rev lateral loads as a function of fuselage vertical constrained frequency
$\omega_\zeta=1.4$, $\bar{h}=\bar{d}_p=\bar{d}_r=0$

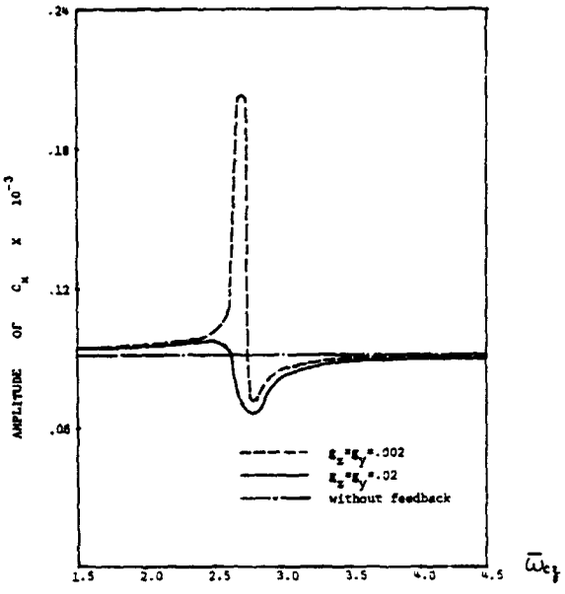

Fig. 10 4/rev longitudinal loads as a function of fuselage vertical constrained frequency
$\omega_f = 1.4, h = d_p = d_z = 0$

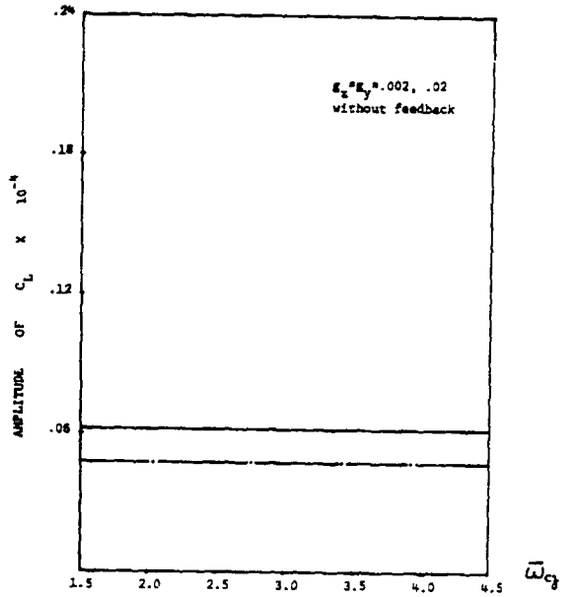

Fig. 12 4/rev roll loads as a function of fuselage vertical constrained frequency
$\omega_f = 1.4, h = d_p = d_z = 0$

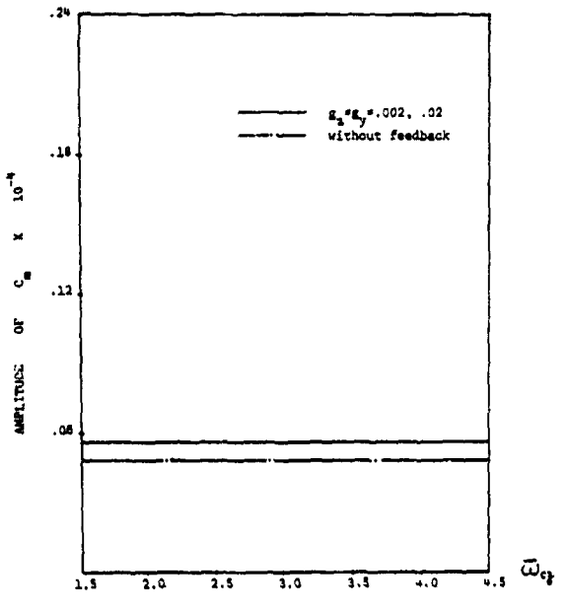

Fig. 11 4/rev pitch loads as a function of fuselage vertical constrained frequency
$\omega_f = 1.4, h = d_p = d_z = 0$

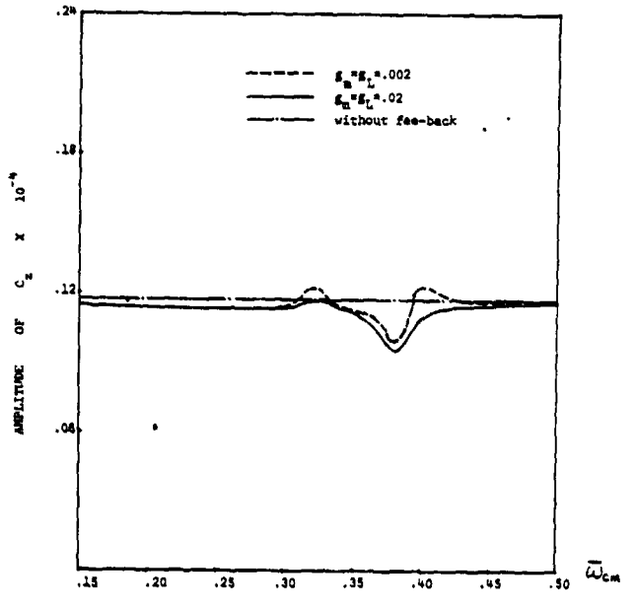

Fig. 13 4/rev vertical loads as a function of fuselage pitch constrained frequency
$\omega_f = .7, h = d_p = d_z = 0$

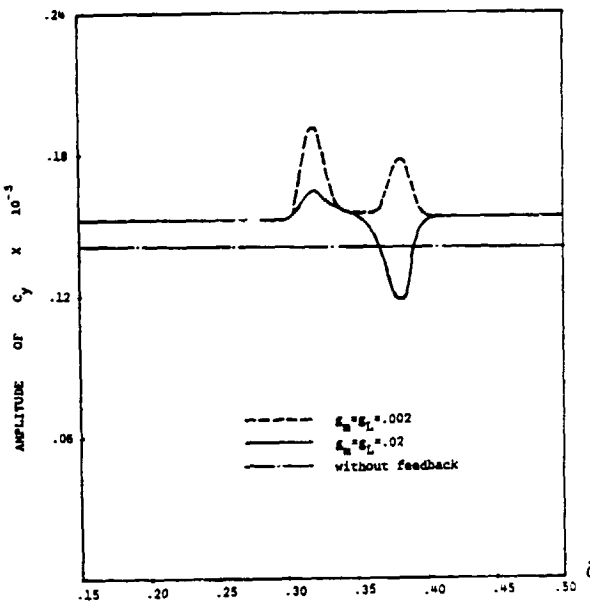

Fig. 14 4/rev lateral loads as a function of fuselage pitch constrained frequency
$\omega_\beta = .7$, $\bar{h} = \bar{d}_p = \bar{d}_\beta = 0$

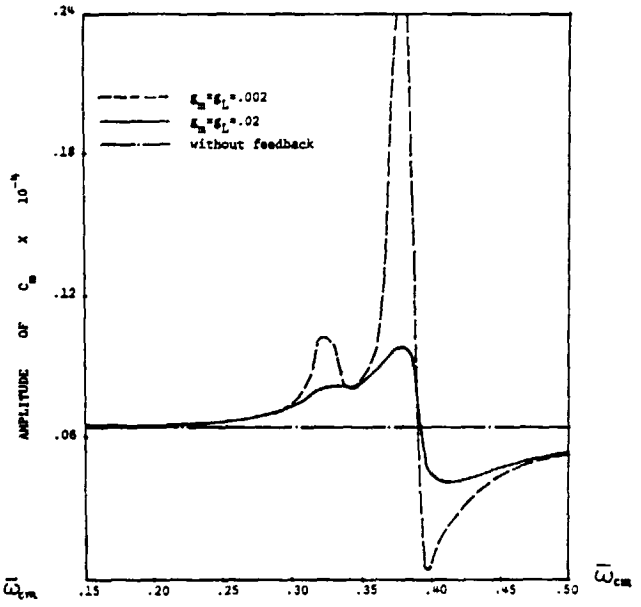

Fig. 16 4/rev pitch loads as a function of fuselage pitch constrained frequency
$\omega_\beta = .7$, $\bar{h} = \bar{d}_p = \bar{d}_\beta = 0$

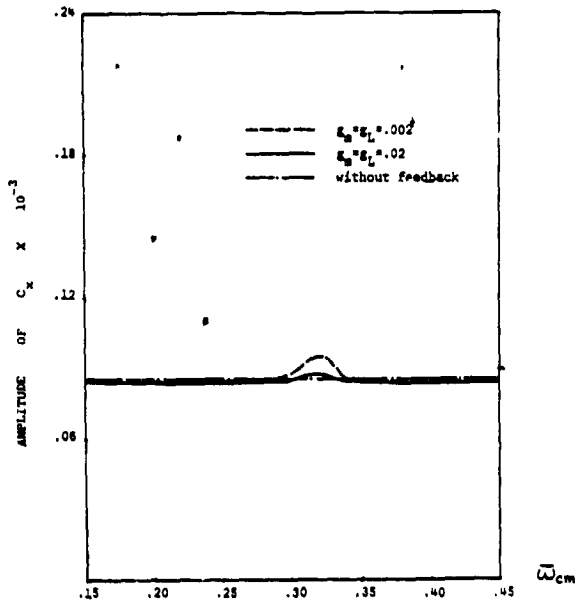

Fig. 15 4/rev longitudinal loads as a function of fuselage pitch constrained frequency
$\omega_\beta = .7$, $\bar{h} = \bar{d}_p = \bar{d}_\beta = 0$

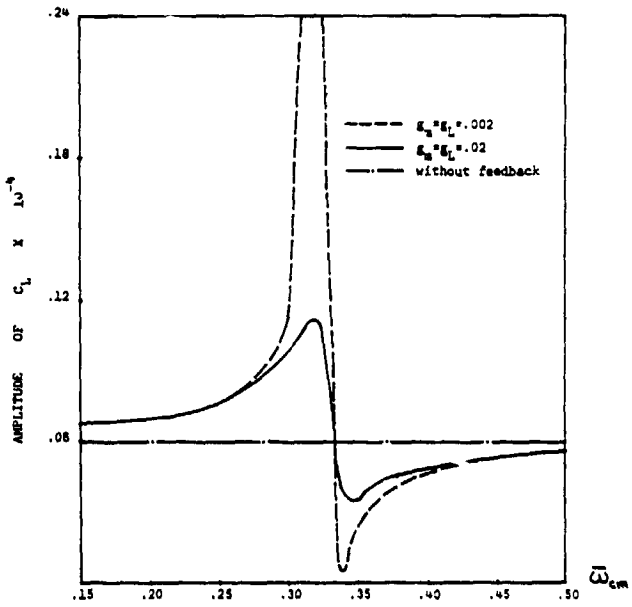

Fig. 17 4/rev roll loads as a function of fuselage pitch constrained frequency
$\omega_\beta = .7$, $\bar{h} = \bar{d}_p = \bar{d}_\beta = 0$

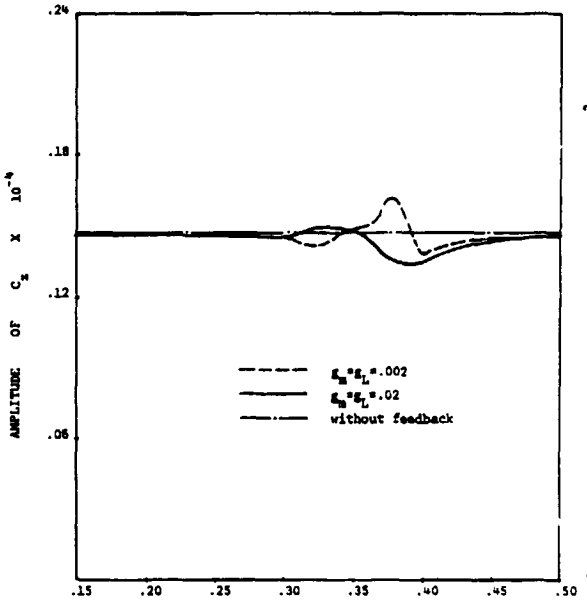

Fig. 18 4/rev vertical loads as a function of fuselage pitch constrained frequency
$\omega_f=1.4$, $\bar{h}=\bar{d}_p=\bar{d}_f=0$

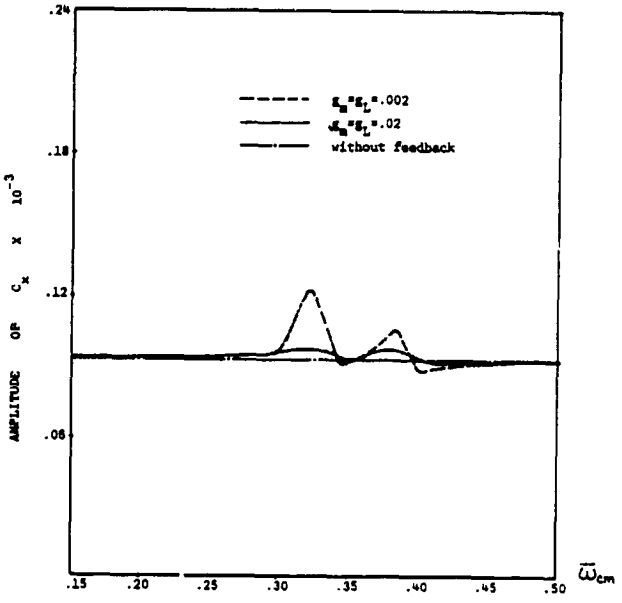

Fig. 20 4/rev longitudinal loads as a function of fuselage pitch constrained frequency
$\omega_f=1.4$, $\bar{h}=\bar{d}_p=\bar{d}_f=0$

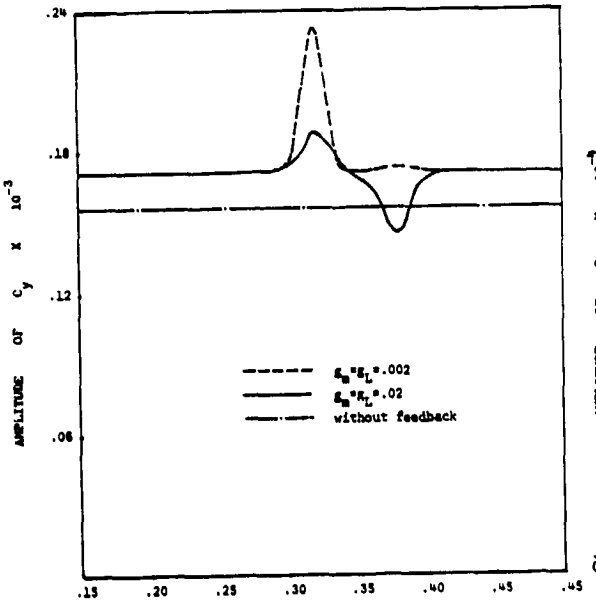

Fig. 19 4/rev lateral loads as a function of fuselage pitch constrained frequency
$\omega_f=1.4$, $\bar{h}=\bar{d}_p=\bar{d}_f=0$

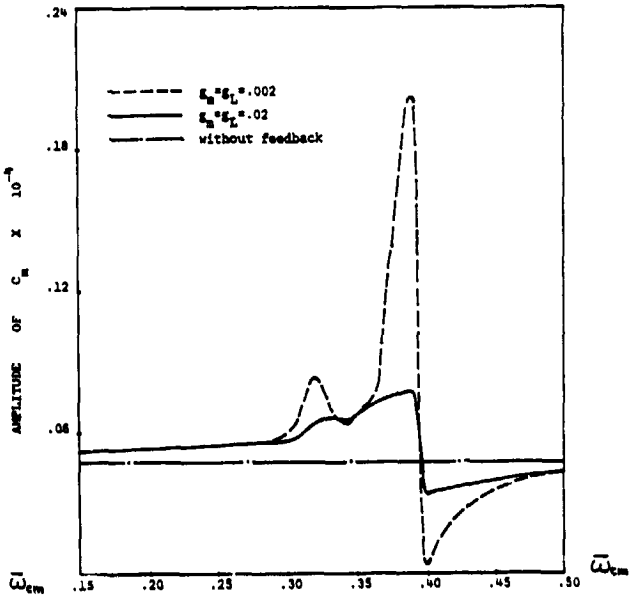

Fig. 21 4/rev pitch loads as a function of fuselage pitch constrained frequency
$\omega_f=1.4$, $\bar{h}=\bar{d}_p=\bar{d}_f=0$

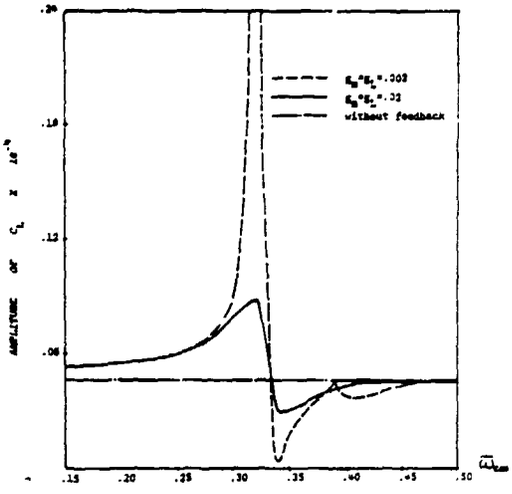

Fig. 23 4/rev roll loads as a function of fuselage pitch constrained frequency
$\omega_{pl.s}$, $\bar{h}_{cg}$=.2, $\bar{z}_p$=0

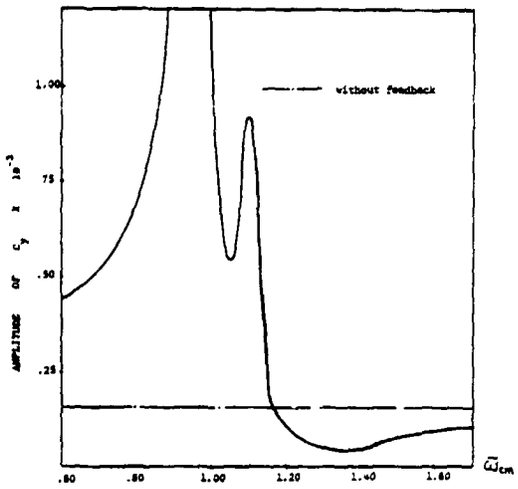

Fig. 25 4/rev lateral loads as a function of fuselage pitch constrained frequency
$\omega_{pl.s}$, $\bar{h}$=.4, $\bar{z}_p$=0, $\bar{z}_c$=.2, ζ_α=ζ_{z_c}=.302

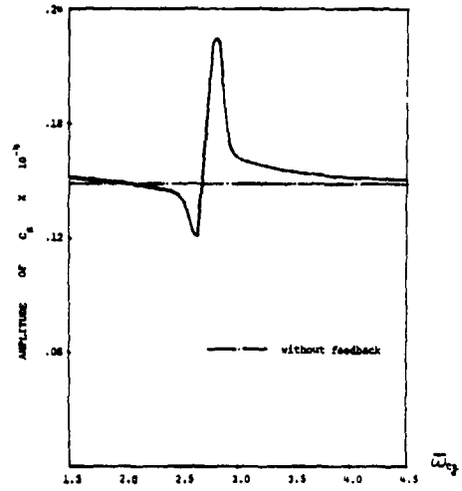

Fig. 23 4/rev vertical loads as a function of fuselage vertical constrained frequency
$\omega_{pl.s}$, $\bar{h}$=.4, $\bar{z}_p$=0, $\bar{z}_c$=.2, ζ_α=ζ_{z_c}=.002

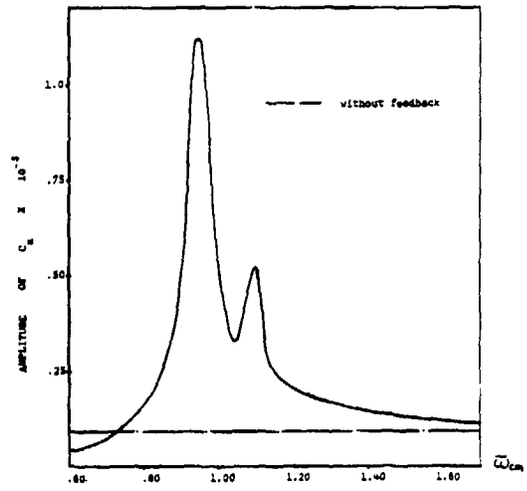

Fig. 26 4/rev longitudinal loads as a function of fuselage pitch constrained frequency
$\omega_{pl.s}$, $\bar{h}$=.4, $\bar{z}_p$=0, $\bar{z}_c$=.2, ζ_α=ζ_{z_c}=.302

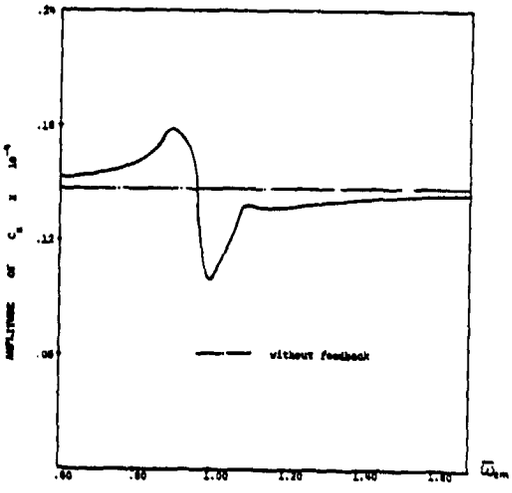

Fig. 24 4/rev vertical loads as a function of fuselage pitch constrained frequency
$\omega_{pl.s}$, $\bar{h}$=.4, $\bar{z}_p$=0, $\bar{z}_c$=.2, ζ_α=ζ_{z_c}=.002

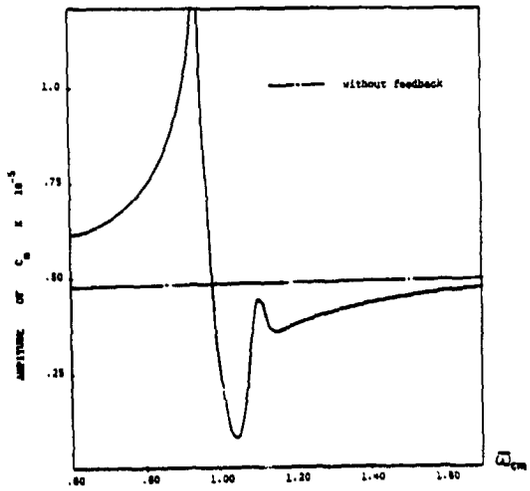

Fig. 27 4/rev pitch loads as a function of fuselage pitch constrained frequency
$\omega_{pl.s}$, $\bar{h}$=.4, $\bar{z}_p$=0, $\bar{z}_c$=.2, ζ_α=ζ_{z_c}=.302

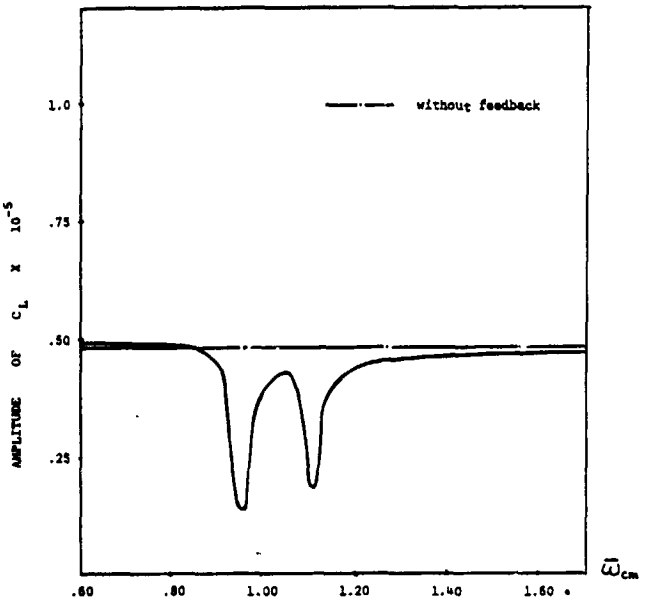

Fig. 28 4/rev roll loads as a function of fuselage pitch constrained frequency
$\bar{\omega}_y$=1.4, $\bar{h}$=.4, $\bar{d}_p$=0, $\bar{d}_f$=.2, ζ_m=ζ_L=.002

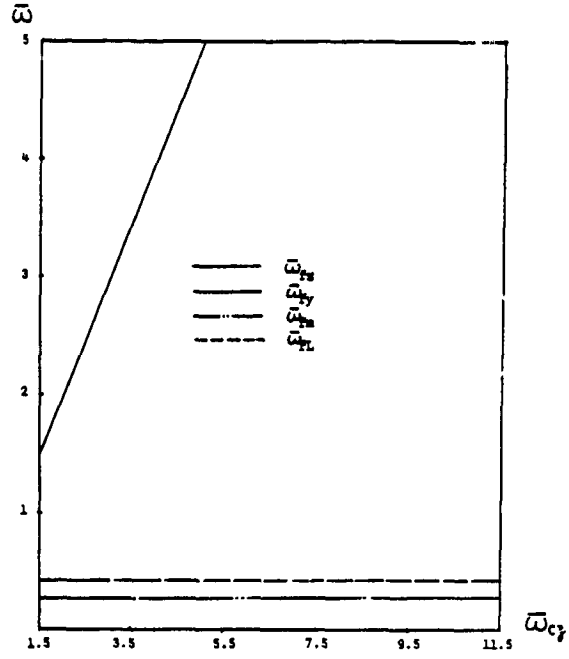

Fig. 30 fuselage natural frequency without rotor vs fuselage constrained vertical frequency

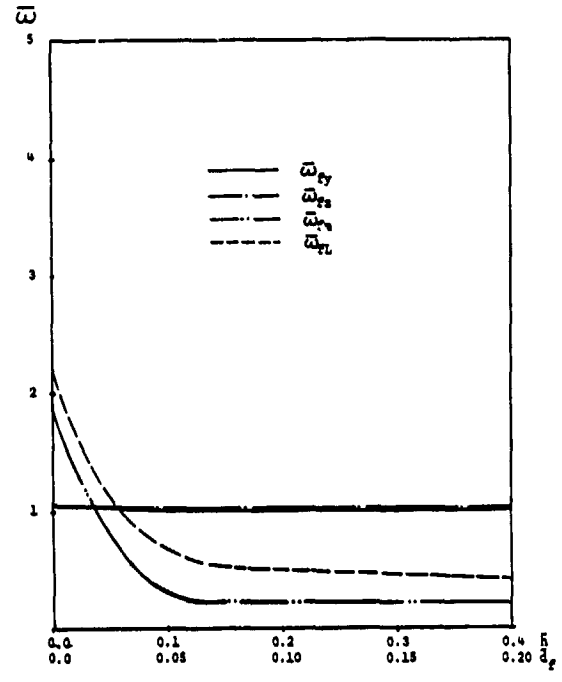

Fig. 29 fuselage natural frequency without rotor vs offsets $\bar{h}$, $\bar{d}_f$

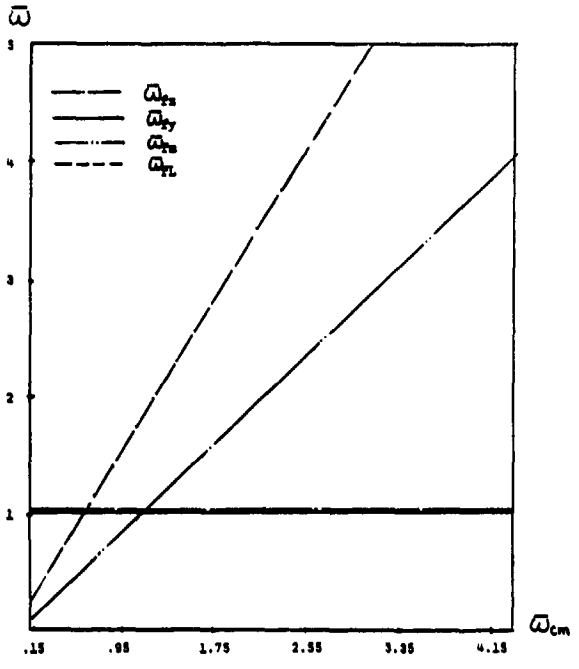

Fig. 31 fuselage natural frequency without rotor vs fuselage constrained pitch frequency

DISCUSSION
Paper No. 21

COUPLED ROTOR-BODY VIBRATIONS WITH INPLANE DEGREES OF FREEDOM
Huang Ming-Sheng
and
David A. Peters

Dev Banerjee, Hughes Helicopters: Dave, I'm glad to see a concerted effort at doing impedance matching at the hub and coupling the rotor with the fuselage. I think that's an important contribution to determining hub loads and hence fuselage vibrations. I'd like to go back to the 1964 paper of Gerstenberger and Wood. I think the displacement formulation approach that you've taken would require adding additional hub motion as degrees of freedom. However, if you take the mixed formulation approach as taken by Gerstenberger and Wood, that'll all come out as part of the solution. In other words your 6X6 complex hub-impedance matrix which is the exact hub coupling of the rotor with the fuselage would be included in the solution of the problem.

Peters: It would solve the whole problem at once.

Banerjee: Exactly.

Peters: There's nothing wrong with that, except you lose the advantage of making small changes to the fuselage at a very cheap computational cost [since] you have to do the whole problem. Another thing, remember the rotor impedance now is more complicated than normal rotor impedance because of the periodic coefficients. Now you have four per rev due to 4 per rev, and four per rev due to 8 per rev. If you had read Tom Hshu's original paper, he's got a whole section dedicated to figuring out how all these sines and cosines and phases come together. It's a big job.

Bob Loewy, Rensselaer Polytechnic Institute: Dave, I want to add my voice raised in praise for your work here. I think it's excellent and you're making a major contribution to helicopter vibrations in this. Maybe I should stop there, but I can't resist the urge to play "Trivial Pursuit." Just sort of really as a historical curiosity: the first time I ever saw a rotor impedance derivation, it was in the work of Alexander Flax--some of you may remember--and this was dated in the late 40s.

Peters: Oh, I'd love to have a copy of that or get the reference.

Loewy: It was never published as far as I know, and I wouldn't want you to think I was there, but I found it in some of the old Piasecki Helicopter Company literature. What he did was, he was solving a drive system vibration problem, and he derived the polar moment of inertia impedance of a rotor. It's interesting that John Burkam, as far as I know, was the first one to do an inplane impedance with a rigid hinged blade, and if you took his impedance expression and put it on a mass on a spring and then ran the equations out, you found that you got the ground resonance equations. As a third point of this kind, Bob Yntema then took blades which were flexible and derived impedances in all directions, for twisted blades as well as untwisted blades. And I remember being amazed to see that in those expressions, even though you shook inplane, you got flapping deflections of the blades, of course, because they were twisted. None of those included aerodynamics, but they were very early efforts in rotor impedance calculation.

Peters: Oh, I'd love to have those. Why don't you write them down on a piece of paper for me and let me go run them down?

Loewy: Sure will.

Don Kunz, U.S. Army Aeromechanics Laboratory: Dave, when you were doing your presentation, I was wondering if you were linearizing your equations. At the end you said you did--would you explain what you did?

Peters: Yes, on the very first slide where I showed the blade equations, those were already linearized. Since we're running a trimmed condition, that means there's no β_s and no β_c, we linearized about a steady coning angle. So the very first flapping equations up there are linearized, and that's why β, that steady coning angle appears as a forcing function. Now, if we weren't trimmed, then we'd have to linearize about a periodic equilibrium including the β_s and β_c.

Bob Wood, Hughes Helicopters: Dave, I just wanted to comment--I thought it was particularly interesting, your fuselage model and the fact that you could study the parameters and move that on. I wanted to add just one point to it, and that is what a number of us are looking at right now, which ties your paper really together somewhat with Dick Gabel's [paper]. If you think about it, if you're interested purely in getting the forced response in detail for a [production] helicopter, with dynamic NASTRAN now it's extremely simple to calculate that hub impedance matrix, just by putting in the three-unit loads and the three-unit moments. [You can

then] solve the combined problem and then [combine] by superposition the appropriate NASTRAN responses.

Peters: And just match that to your rotor impedance and see what happens.

Wood: So in other words, a full dynamic NASTRAN model, such as Dick has, can be treated relatively easily.

Bob Taylor, Boeing Vertol: I'd just like to comment that I wouldn't want to use that in a preliminary design study. I'd much rather depend upon something like Dave has here; but your point is well taken, Bob.

ANALYSIS OF POTENTIAL HELICOPTER VIBRATION REDUCTION CONCEPTS

Anton J. Landgrebe
Manager, Aeromechanics Research

and

Mark W. Davis
Associate Research Engineer, Aeromechanics Research

United Technologies Research Center
East Hartford, Connecticut

Abstract

Several recent helicopter vibration reduction research programs of the United Technologies Research Center (UTRC) are described. Results of analytical investigations to develop, understand, and evaluate potential helicopter vibration reduction concepts are presented in the following areas: identification of the fundamental sources of vibratory loads, blade design for low vibration, application of design optimization techniques, active higher harmonic control, blade appended aeromechanical devices, and the prediction of vibratory airloads. Primary sources of vibration are identified for a selected four-bladed articulated rotor operating in high speed level flight. The application of analytical design procedures and optimization techniques are shown to have the potential for establishing reduced vibration blade designs through variations in blade mass and stiffness distributions, and chordwise center-of-gravity location. Analytical evaluation of a computerized generic active controller for implementing higher harmonic control indicates the potential for good controller performance and extensive fuselage vibration reduction with low pitch amplitudes for three controller approaches investigated. Exploratory evaluation of a passive tuned blade tab concept indicates considerable sensitivity of vibratory load alleviation to design parameters with an improvement in inplane hub excitation but an increase in vertical excitation. The prediction of vibratory airloads, attributable to rotor/wake, rotor/fuselage, and rotor/empennage interactional aerodynamics, is also described.

Introduction

For future helicopters to reach their full potential, significant reduction in vibration must be accomplished. Helicopter vibration is becoming an increasingly important consideration because of requirements for crew and passenger comfort as well as increased reliability of structural components and on-board electronic equipment. A vibration-free weapons platform is also a requirement for some military helicopters. As helicopters are required to fly more at both faster cruise speeds and slow "transition" speeds for nap-of-the-earth flying, the need to minimize vibration becomes more important, and it becomes necessary to consider alternative and complementary approaches for vibration reduction.

Helicopter vibration research has been a primary activity at the United Technologies Research Center (UTRC) for the past six years. Various helicopter vibration related programs involving analytical investigation have been conducted in the following areas:

- Blade design for low vibration
- Design optimization techniques applicable to vibration reduction
- Active higher harmonic control for vibration alleviation
- Blade appended devices for vibration alleviation
- Prediction of vibratory airloads (rotor, fuselage, empennage).

In the Ref. 1 analytical investigation, rotor vibratory response and loads transmitted to the fuselage were predicted and analyzed to determine the relative contributions and sources of the various components of blade force excitation. Primary sources of vibration were identified for a selected four-bladed articulated rotor operating in high speed level flight. Subsequently, blade modal shaping (Ref. 2), frequency placement, structural and aerodynamic coupling, and intermodal cancellation were investigated to systematically identify and evaluate blade design parameters that influence vibratory airloads, blade modal response, hub loads, and fuselage vibration. Through variations in blade mass distribution, stiffness distribution and chordwise center-of-gravity location, blade designs were developed with predicted reductions in vibration. These designs remain to be validated by test.

An automated optimization procedure is being developed at UTRC for the rotor blade design

Presented at the American Helicopter Society and NASA Ames Research Center 2nd Decennial Specialists' Meeting on Rotorcraft Dynamics, November 7-9, 1984.

process. A simplified approach for minimizing vibration (Refs. 1, 2) has been developed and applied (Ref. 3). A modal analysis was used to calculate key vibration parameters. Through frequency placement and modal shaping with a constrained optimization program, COPES/CONMIN, (Refs. 4, 5) a blade design was determined for reduced fuselage vibration. A forced response aeroelastic analysis (Ref. 6) was used in the process to identify key modes, the desired frequency placement and modal shaping criteria, and to perform a final calculation of the vibration characteristics of the new blade designs.

A computerized generic active controller was developed for alleviating helicopter vibration by closed-loop implementation of higher harmonic control (HCC) (Refs. 7, 8). This controller provides the unique capability to readily define and evaluate many different algorithms by selecting from three controller approaches (deterministic, cautious, and dual), two linear system models (local and global), and several methods of limiting control. A non-linear aeroelastic rotor analysis (Ref. 6) was used to evaluate alternative controller configurations as applied to a four-bladed H-34 rotor mounted on the NASA-Ames Rotor Test Apparatus used to represent the fuselage. It will be shown that excellent controller performance was predicted for all three controller approaches for steady flight conditions having moderate to high values of forward velocity and rotor thrust. Reductions in vibration from 75 to 95 percent were predicted with HHC pitch amplitudes of less than one degree. Good transient vibration alleviation was also predicted for short duration maneuvers involving a sudden change in collective pitch.

Analytical evaluations of aeroelastic devices appended to helicopter rotor blades have been conducted to determine their potential for reducing hub shears and vibratory control loads (Ref. 9). The results for a passive tuned tab shall be discussed.

The development of methodology to predict vibratory blade airloads has proceeded at UTRC along with the determination of primary airload sources. Wake, airflow, and airload methodology have advanced for both low and high speed flight (Refs. 10-19). For example, a first level generalization of the forward flight rotor wake has recently been formulated for use in unsteady airload calculations (Refs. 10, 11, 12). Synthesization procedures for incorporating unsteady airfoil test data in rotor aeroelastic response methods have been developed (Ref. 18). Also, methodology for predicting vibratory airload excitation at tail surfaces due to the rotor wake has been developed and initial validation has been performed (Ref. 19). The aerodynamic interaction of the fuselage on the rotor vibratory airloads has been analytically demonstrated (Ref. 17). Development of a computer method for predicting the induced unsteady vibratory excitation of the rotor wake on the fuselage is in progress.

The aforementioned investigations are described in the following sections.

Blade Design for Vibration Reduction

An analytical investigation was conducted to develop an understanding of the importance and role played by blade design parameters in rotor vibratory response and to design an advanced blade for reduced vibration based upon this understanding. This investigation was conducted at UTRC by Taylor (Ref. 1). Various design approaches were examined for a four-bladed articulated rotor operating at a high-speed, level flight condition. Blade modal shaping, frequency placement, structural and aerodynamic coupling, and intermodal cancellation were investigated to systematically identify and evaluate blade design parameters that influence blade vibratory airloads, blade modal responses, hub loads, and fuselage vibration.

The baseline rotor system selected for the investigation was a four-bladed articulated rotor system, similar in design to the Sikorsky S-76 rotor system, but without vibration alleviation devices and tip sweep. Tip sweep can provide vibration alleviation through aeroelastic coupling between the blade flatwise and blade torsion modes. However, it was decided to omit tip sweep from the baseline blade design to study the potential of improving the vibration characteristics of a basic rectangular planform blade. A complete set of baseline blade properties is presented in Ref. 1. The blade spanwise mass distribution for the baseline and modified blade designs will be presented in the following section on blade design optimization. Some of the relevant properties of the baseline blade are the blade twist (-10 deg, nonlinear), blade weight (100 lb) and non-dimensionalized natural frequencies (flatwise modes: rigid body = 1.03 per rev, first elastic = 2.75 per rev, second elastic = 4.9 per rev; edgewise modes: rigid body = 0.26 per rev, first flexible = 4.7 per rev; torsion mode: first elastic = 5.30 per rev). The baseline blade pitch axis, elastic axis, aerodynamic center, and center-of-gravity (CG) were nominally located at the 25 percent chord (outboard, CG was at 26%). The flight condition selected was a high speed cruise condition of 160 kt. A 10,800 lb rotor lift and an 1190 lb propulsive force were selected to be representative for a helicopter the size of the S-76.

The analytical simulation used for this study was the G400 analysis documented in Ref. 6. This computer analysis is based on the Galerkin method and uses precalculated uncoupled normal blade modes. A time history solution of airloads, blade responses, and vibratory blade hub forces and moments due to the rotor are calculated based on modal coupling within the analysis. For this study, the fuselage vibrations were determined by means of a measured S-76 mobility transfer matrix

between the hub loads and vibrations at several locations in the airframe. This approach was used to separate rotor design effects from hub impedance and airframe dynamic effects in the analysis. Uniform inflow was used in this initial exploratory study to model the rotor downwash for the high speed flight condition. The influence of variable inflow on vibratory airloads will be included in subsequent blade design studies.

In order to design blades for reduced helicopter vibration, it is necessary to first acquire a fundamental understanding of the interrelationship of the fuselage vibrations, the hub loads in the fixed system, the blade root loads in the rotating system, the blade vibratory response, and the blade airloads. It is then necessary to identify the primary contributors of the various harmonic modal components to vibratory excitation. As indicated in Fig. 1, for a helicopter with a four-bladed articulated rotor, the predominant 4P (4 per rev) cockpit and cabin vibrations are mainly produced by the 4P vertical and inplane (lateral and longitudinal) hub forces, since for a low-offset articulated rotor the 4P moment contribution is of secondary importance. For a four-bladed rotor in a steady-state condition, the 4P hub fixed system vertical shear results directly from the azimuthal summation of the 4P blade root rotating vertical shear from all blades. When the contributions of all four blades are summed in the fixed system, the 4P hub fixed system inplane shears result from the summation of 3P and 5P blade root rotating inplane shears. As indicated in Fig. 1, the contribution of the 5P inplane shears were found early in this investigation to be small relative to the 3P contribution.

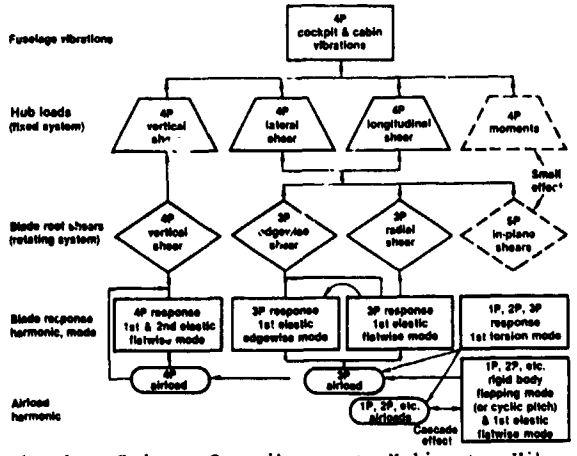

Fig. 1. Primary Contributors to Helicopter Vibrations (4-Bladed Articulated Rotor, High Speed Flight)

With the awareness of the above information at the beginning of the investigation, the analytical study was directed toward identifying the primary blade response contributors and related airload harmonics, as will be discussed. With this information and an understanding acquired from sensitivity studies, several blades were designed and reported in Ref. 1 which resulted in lower predicted vibration levels. Results for the baseline and the two final modified blade designs (Designs A and B) are summarized herein. It should be noted that these blade designs were achieved via closed-loop optimization techniques as discussed in the next section.

The predicted 4P hub loads and fuselage vibrations for the baseline and two modified blade designs are presented in Figs. 2 and 3, respectively. For the baseline articulated rotor, the vibratory hub load components with the most influence on fuselage vibration are, in order of importance, the longitudinal, lateral, and vertical shears. On other helicopters having a different mobility matrix, the vertical shear may be more

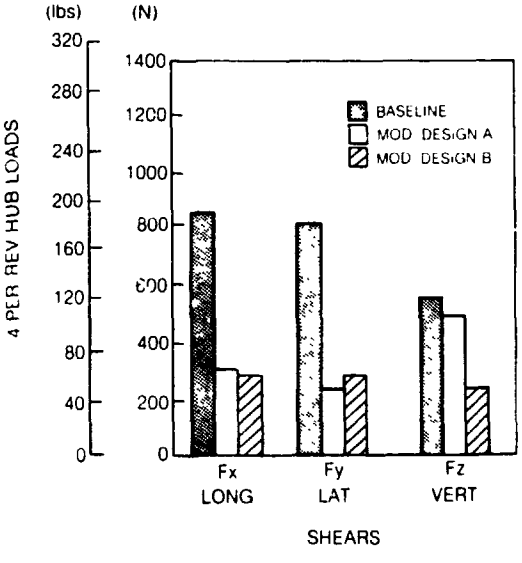

Fig. 2. Predicted Vibratory Fixed-System Hub Loads for the Baseline and Modified Blade Designs (V = 160 kt)

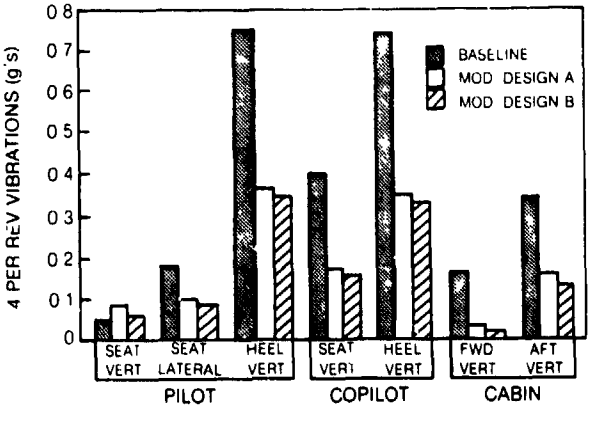

Fig. 3. Predicted 4 Per Rev Fuselage Vibrations for the Baseline and Modified Blade Designs (V = 160 kt)

important than the inplane shears. For hingeless or bearingless rotors, the hub moments can become important. Of the fuselage vibrations shown in Fig. 3, the dominant vibrations for the aircraft studied are the heel-slide vibrations for the pilot and copilot. Important vibrations are those affecting crew and passenger comfort. Thus, it was considered a good objective to reduce the cockpit seats and cabin vibrations to approximately 0.1 g while reducing the heel-slide vibrations to the extent possible. As shown in Fig. 3, the predicted fuselage vibrations for modified Designs A and B are lower by about 50 percent (except the small pilot seat vertical vibration) compared to the baseline vibrations. Of particular importance are the seat and cabin vibrations which are approaching the 0.1 g level. These results indicate that acceptable seat and cabin vibration levels can be attained, at least theoretically, by improved blade design and without the use of vibration treatment equipment (bifilars, absorbers, etc.). The vibratory hub loads that produced these vibrations are shown in Fig. 2 to also have been reduced significantly.

To achieve the vibration levels predicted for Designs A and B, the following modifications were made to the baseline blade. For Design A, a combination of blade spanwise mass redistribution and increased edgewise blade stiffness was used to change the blade mode shapes and increase the uncoupled frequencies of the first elastic flatwise and edgewise modes from 2.75 to 3.4 per rev and 4.8 to 5.8 per rev, respectively. Modal shaping techniques described in Refs. 1 and 2 and summarized in the next section on optimization were applied in addition to frequency placement techniques. A small change in blade weight (100 to 104 lb) resulted. Increasing the flatwise frequency to 3.4 per rev improved the inplane shear, but did not significantly reduce the vertical shear, as shown in Fig. 2. For Design B, the generalized airload producing a large response of the first flatwise mode was decreased by moving forward the CG location of the outer 20 percent of the blade from 26 to 24 percent of the chord. The basis for these design changes are discussed below.

In order to understand the source of the rotating blade root shears, the G400 analysis was used to decompose the vertical and inplane shear components (edgewise and radial) into the individual contributing components. This is exemplified in Fig. 4 for the 3P rotating edgewise shear transmitted to the hub by the baseline blade. The force vectors are presented in polar format showing the amplitude and phase of the total shear and contributing components. It is important to note that the two principal components due to rigid body motion (rigid flapping coriolis and lag inertia) vectorially combine with the drag component to form a small contribution to the total.

As a result of this cancellation effect, the elastic blade components of shear acquire a primary role. In particular, the elastic flatwise inertia component is the predominant contributor to the 3P edgewise shear. This component arises from the flatwise mode coupling with the edgewise mode associated with blade twist and collective pitch. In Fig. 5, it is shown that the elastic flatwise contribution is also important to the radial shear

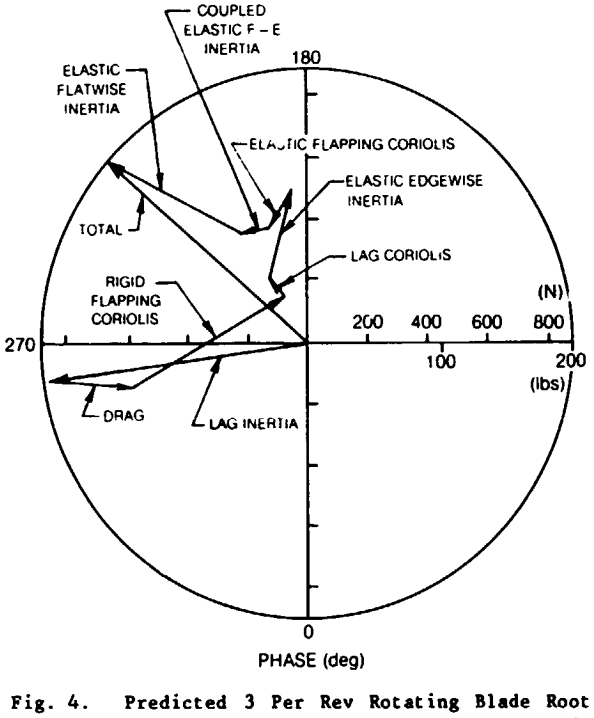

Fig. 4. Predicted 3 Per Rev Rotating Blade Root Edgewise Shear for the Baseline Blade (V = 160 kt)

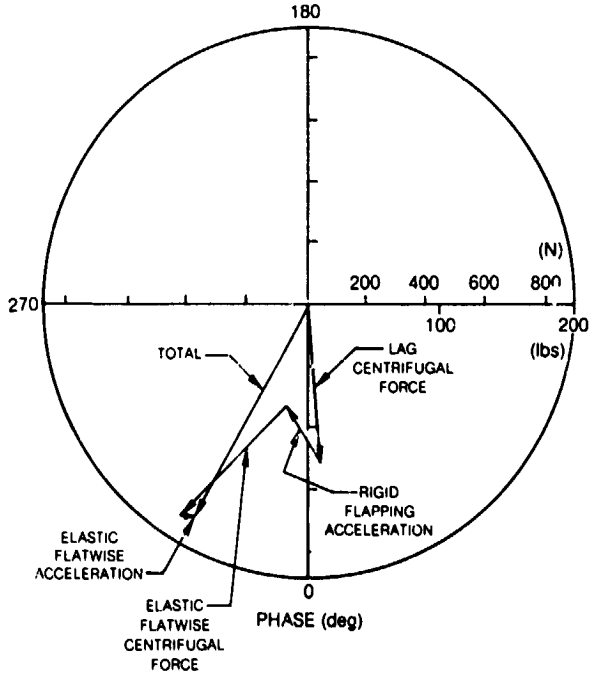

Fig. 5. Predicted 3 Per Rev Rotating Blade Root Radial Shear for the Baseline Blade (V = 160 kt)

component. It thus became evident that significant intermodal coupling occurs, and reduction of the vibratory inplane hub loads is heavily dependent upon reduction in the response of the first elastic flatwise mode in addition to the first elastic edgewise mode as summarized in Fig. 1. It was also noted that significant vectorial cancellation of components of shear due to phase as well as amplitude differences occurred. Thus, the predicted total shears are very sensitive to the accuracy of the simulation analysis.

Also, it is described in Ref. 1 that significant interharmonic and intermodal coupling occurs between the blade flatwise response and the airloads. This is indicated in Fig. 1 as a "cascade effect" in which modal motions at one harmonic induce modal motions at other harmonics through the coupling with the harmonics of airloads. For forward flight, the one per rev airloads created by flapping (or cyclic pitch), required for aircraft trim, result in one per rev response of all blade modes. The resulting one per rev motions create 2, 3, 4, and 5 per rev response of the blade modes and so on. The end result for the rotor investigated was that significant 3P and 4P airloads were generated which excited the important 3P and 4P responses shown in Fig. 1. The rotor thus largely excites itself through the blade motion-airload cascade effect. Also, as will be described, harmonic inflow and airloads due to rotor wake effects provide vibratory excitation which, for steady level flight, is large at low speeds and less at high speeds.

For modified Design A, the reduction of the 3P root edgewise shear and its components is shown in Fig. 6 (note the scale change relative to Fig. 4). The important elastic inertia components were substantially reduced. The reduction in the predicted 3P and 4P modal responses are shown in Fig. 7. Although the inplane hub shear was largely reduced for Design A, the vertical hub shear was not, as shown in Fig. 2. This was attributed to an over reduction of the second elastic flatwise mode contribution and the fact that the second mode provided phase cancellation with the first mode. Although cancellation between the two modal contributions to vertical shear could have been pursued by blade design retuning with mass and stiffness variations, it was decided not to depend upon this cancellation due to intermodal phasing which could change with rotor configuration or flight condition. Instead, the 4P vertical shear was reduced, as reported in Ref. 1, by changing the blade outboard center-of-gravity location to reduce the generalized airload.

Changing the center-of-gravity (CG) location, over the outer blade region, from 26 to 24 percent of the chord moved the CG forward of the elastic axis (EA) and influenced the blade airloads through inertial coupling between the blade flatwise and torsion responses. The predicted change in the torsion response time history around the azimuth for this modified blade Design B is shown in Fig.

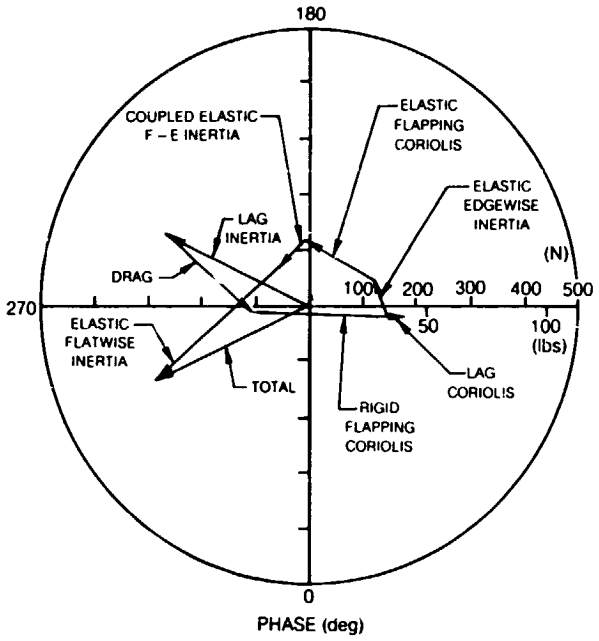

Fig. 6. Predicted 3 Per Rev Rotating Blade Root Edgewise Shear for Modified Blade Design A (V = 160 kt)

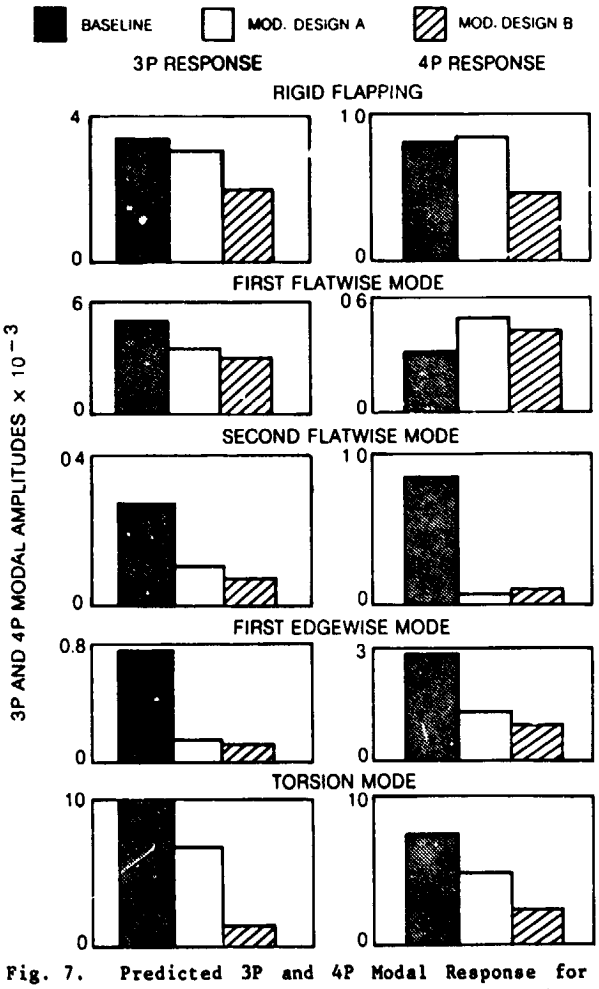

Fig. 7. Predicted 3P and 4P Modal Response for the Baseline and Modified Blade Designs (V = 160 kt)

8. For the baseline design, the torsion response is characterized by a strong nose-down deflection on the rotor advancing side. For blade Design B, the nose-down response on the advancing side was eliminated leaving a waveform that consists of a 1P response, maximum nose down at 180 degrees azimuth, plus smaller contributions of higher harmonics. The mechanism involved in this phenomenon is the CG-EA offset. When the blade tip bends downward on the advancing side, a forward CG induces a nose-up torsion increase on the blade near the blade tip. This moment counteracts the nose-down aerodynamic pitching moment due to high Mach number on the advancing side. It was found that, when the CG is moved further forward, the increased advancing side nose-up response can produce increased vibration. Blade tip sweep is an alternate approach that has been used to reduce the advancing side vibratory airloads through blade aeroelastic torsional deformation.

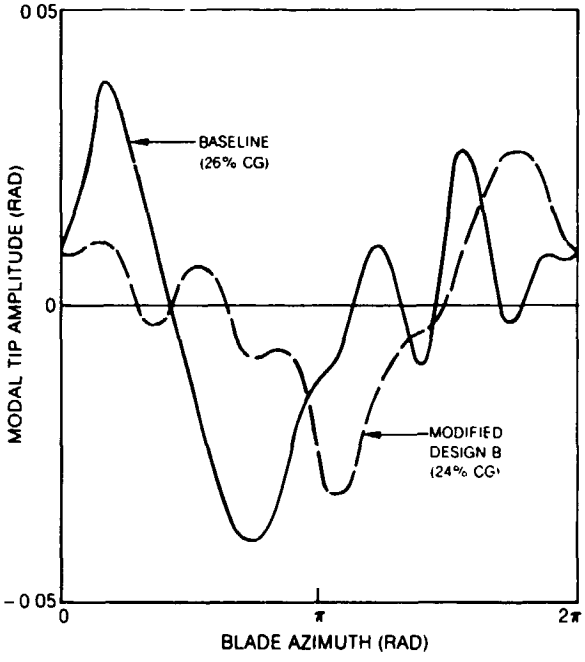

Fig. 8. Predicted Effect of Outboard CG Location on Blade Torsion Mode Response (V = 160 kt)

The reduction of the torsion mode response of modified Design B is shown in Figs. 7 and 8. The reduction of the 4P vertical shear relative to the baseline and Design A blade levels is shown in Fig. 2. Relative to Design A levels, a small further reduction in 4P fuselage vibration is indicated at all fuselage locations in Fig. 3. The resulting fuselage vibration are generally about half the baseline blade levels.

In summary, the predicted results for the modified blade designs in Ref. 1 indicate the potential for substantially reducing helicopter vibration by viable changes in blade design. Further study in the area of blade design for vibration could possibly result in rotors with vibration levels that are acceptable without the use of vibration alleviation devices or higher harmonic control. However, it is recognized that the predicted results have not yet been substantiated with test. Due to the absence of a systematic, consistent set of experimental data for vibratory blade, hub, and fuselage loads, the G400 analysis, like other rotor aeroelastic analyses, has not been validated for vibration prediction. The high degree of interharmonic and intermodal coupling and the predicted cancellation effects of large components of hub loads make the results sensitive to the prediction accuracy of the analysis for the individual components. In fact, differences of the predictions with the vibration results of preliminary exploratory tests at Sikorsky have been noted. The provision of a model test rig to systematically and accurately measure vibratory hub loads is currently being pursued at UTRC to validate computer codes and evaluate new blade designs for vibration. Also, application of blade design techniques for vibration to other rotor types (hingeless, bearingless) is underway and application to other flight conditions (particularly low speed) with variable inflow is planned. The inclusion of design optimization techniques has been initiated as described below.

Rotor Blade Design Optimization for Vibration

The optimization approach discussed below is part of an ongoing effort at UTRC to develop a general automated procedure for rotor blade design. This procedure can be used to determine the necessary geometric, structural, and material properties of a rotor system to achieve desired design objectives relating to vibration, stress, and aerodynamic performance. This section concentrates on the approach used for helicopter vibration summarized in Ref. 3. Based on the analytical studies discussed above, a simplified vibration analysis has been developed for use in conjunction with a forced response analysis in the optimization process. This simplified analysis significantly improves the efficiency of the design process.

Optimization Approach

As shown in Fig. 9, the approach for rotor blade design has been formulated as three separate component optimization problems concerned with areas such as vibration, stress, and aerodynamic performance. Appropriate constraint functions are formulated to account for the influence of design changes in areas other than those of primary concern for a given problem. After gaining experience with each component problem, the goal is to develop a completely integrated approach to optimize on several design considerations simultaneously. Based on experience with the individual optimization problems, it will be possible to better formulate an integrated and efficient overall approach. Furthermore, experience will be gained as to the design variables having the largest impact on each individual problem, the

tradeoffs to be expected between various design considerations, and the capability to meet specified design criteria for a given problem.

Figure 9 also shows a few potential design parameters that might be used for the optimization problems. These include: blade geometrical properties, primarily associated with aerodynamic performance; material properties, generally associated with blade stress; and structural properties, associated with vibration and stress. In this section, only the vibration problem is considered. The design parameters used are mass and bending stiffness distributions along the blade.

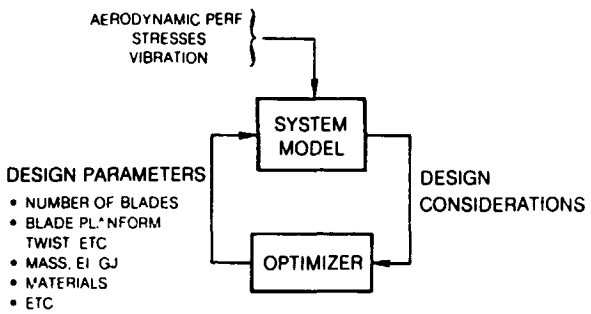

Fig. 9. Overall Approach for Rotor Blade Design Optimization

Figure 10 outlines the approach to be used for helicopter vibration. In order to achieve the computer efficiency required of any useful design optimization tool, a simplified vibration analysis is used in the primary or inner loop to develop the vibration parameters and other criteria to be optimized. Since this simplified analysis may be performed many times faster than the forced response analysis, the potential savings in time is significant for the many iterations that may be required by any constrained optimization program. The forced response analysis G400 is then used to verify the vibration characteristics of the new blade design in the outer optimization loop, where closed-loop optimization can also be performed.

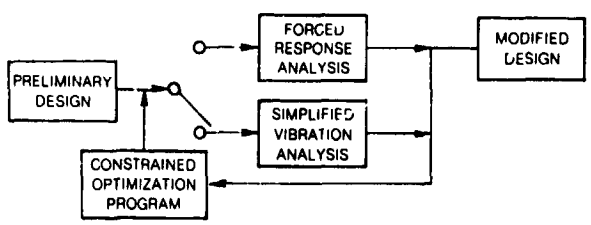

Fig. 10. Optimization Approach for Vibration

The simplified vibration analysis is based on the assumption that appropriate modal parameters can be defined that indirectly relate changes in vibration characteristics to changes in blade design. Traditionally, frequency placement has been used to minimize vibration response. As discussed above, modal shaping has also been shown to be important, and associated parameters have been identified as indicators of rotor blade vibration characteristics. In particular, it has been predicted that vibration can be reduced by minimizing certain weighted modal integrals. In studies performed to date, polynomial approximations to the airload distribution have been used as weightings in the modal integrals. As shown conceptually in Fig. 11, mode shaping is accomplished by driving these generalized airloads to zero to desensitize the blade to vibratory airloading.

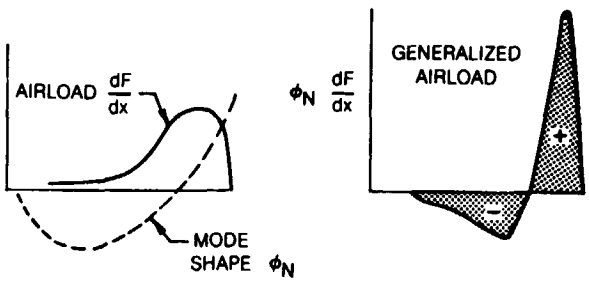

• DESENSITIZE BLADE TO VIBRATORY AIRLOADS BY SHAPING OF CRITICAL MODES:

$$\text{GENERALIZED AIRLOAD} = \int \phi_N \frac{dF}{dx}\, dx - 0$$

Fig. 11. Modal Shaping Design Concept

Figure 12 shows a more detailed schematic of the inner optimization loop presented in Fig. 10. A blade eigensolution analysis (E159) is used to calculate blade natural frequencies and mode shapes for a given set of design variables. This information and the assumed airload distributions are used to calculate the appropriate modal integrals and the difference between the actual and optimum modal frequencies. Frequency placement and modal shaping are accomplished by simultaneously driving these parameters to zero via minimization of a quadratic performance index that consists of the weighted sum of the squares of each vibration parameter. The weighting matrix, W_Z, is used to reflect the relative importance of each vibration parameter.

The constrained optimization program used for the results presented in this paper is COPES/CONMIN (Refs. 4 and 5), which is based on the Method of Feasible Directions. This program minimizes the performance index in an iterative manner. At each step, it attempts to satisfy all specified constraints, which may be either explicit or implicit functions of the design variables. As shown by the dashed line in Fig. 12, blade frequencies and modal integrals can also be included as constraints rather than added to the performance index. Based on gradient and functional information for the objective and constraint functions, COPES/CONMIN

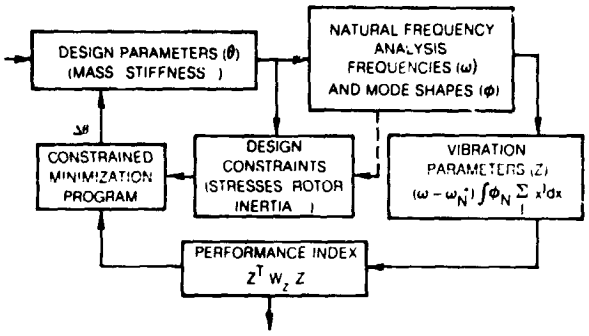

Fig. 12. Automated Design Procedure for Vibration Based on Simplified Approach

calculates necessary changes in the design variables to further reduce the performance index at the current iteration. The necessary gradients are calculated by finite differences.

Analytical Results

The simplified approach outlined in Figs. 10 through 12 was used to optimize the previously described baseline articulated rotor operating at a steady 160 kt flight condition. Thirty (30) design variables were used to tailor three selected modes. The design variables consisted of the flatwise and edgewise bending stiffnesses and the mass at each of ten (10) spanwise blade stations. Optimum frequency and modal integral values were specified for three selected modes to give a total of six (6) vibration parameters to be reduced. As discussed in the last section on blade design for reduced vibration, G400 was used to identify the key modes and the associated frequency placement and modal shaping criteria for the articulated rotor investigated. The three modes selected were the first and second elastic flatwise modes and the first elastic edgewise mode. These modes were selected to reduce the response of the two inplane hub shears, which were identified as primary contributors to fuselage vibration in this rotorcraft. The modal integral used for each mode included a cubic weighting function of the blade spanwise location (x) to approximate the airloading for this high speed flight condition.

Analytical studies with G400 indicated the potential for reduced vibration response in this articulated rotor if the first elastic flatwise and edgewise frequencies could be tuned to the range of 3.2 to 3.5/rev and 5.5 to 5.7/rev, respectively. These studies also showed shaping of the first and second elastic flatwise modes to be of prime importance. Thus, the overall objectives of the design problem were to meet the specified frequency criteria, to drive the first two flatwise modal integrals with cubic weighting to zero, and to maintain about the same blade weight if possible. The second flatwise frequency and the first edgewise modal integral were monitored but not included in the performance index.

The automated design procedure was used to achieve an optimized design (modified Design A) having the desired dynamic characteristics shown in Fig. 13. As shown in this figure, the automated design procedure met all the criteria specified for the primary vibration parameters. Furthermore, these significant changes in dynamic characteristics were achieved while allowing only a 4 percent increase in blade weight. In order to obtain this design, blade weight was added to the performance index to be minimized along with the frequency and modal shaping criteria. In addition to practical upper and lower bounds placed on each design variable, constraints were applied to the first two flatwise modal integrals to emphasize their importance and to ensure satisfaction of a threshold value of ±0.005. Note that this value corresponds to the dashed line shown in Fig. 13 and represents reductions of eighty and ninety percent in the first two flatwise modal integrals, respectively. As added benefits, the second flatwise frequency was driven away from 5/rev and the first edgewise modal integral was reduced by over 95 percent.

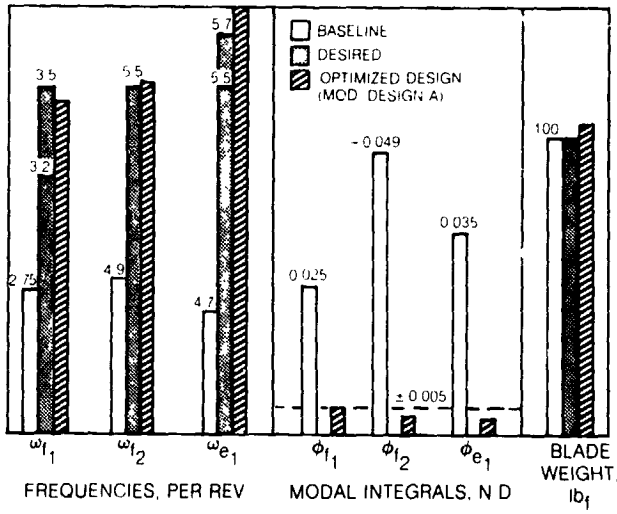

Fig. 13. Dynamic Characteristics of the Baseline and Optimized Blade Designs

Figure 14 compares the final mass distribution for the optimized blade design (modified Design A) to the distribution for the baseline production blade. The cross-hatched region represents blade root-end hardware which was not modified. While the blade weight for both the production blade and the optimized design were about the same, the mass distributions were significantly different. The automated design procedure shifted almost 15 lbs from mid-span to the outer 25 percent of the blade. This was required to achieve the substantial increase specified in the first flatwise natural frequency. As an added benefit, the increased mass outboard also improves rotor auto-rotation characteristics. About a 40 percent increase in edgewise stiffness across most of the blade span was required to achieve the high frequency specified for the first elastic edgewise mode. Changes made by the analysis in flatwise structural stiffness

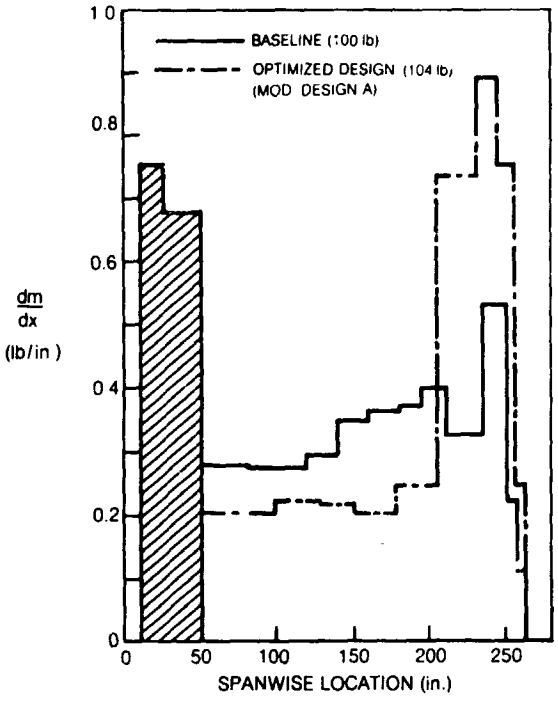

Fig. 14. Comparison of Mass Distributions for Baseline and Optimized Blade Designs

along the blade span were insignificant, since flatwise frequency and mode shape requirements were accomplished through changes in the spanwise mass distribution.

The vibration characteristics for the optimized blade design determined by the simplified automated design procedure were verified in G400. These characteristics were presented in Figs. 2 and 3 and were discussed in the section on blade design for reduced vibration. In summary, the two inplane hub shear components were reduced by over 65 percent and the vertical shear by 20 percent. As a result, predicted reductions in vibration on the order of 50 percent were achieved in cockpit and cabin vibration.

Furthermore, significant reductions in flatwise and edgewise bending stresses and in torsional stress all along the blade span were predicted. Reductions of nearly 50 percent were achieved at all the critical stress areas (outboard flatwise, midspan edgewise, and inboard torsional) despite the lack of stress constraints and stress terms in the performance index.

Closed-Loop Higher Harmonic Control

The use of a self-adaptive controller to implement higher harmonic control (HHC) in closed-loop fashion potentially allows significant vibration reduction to be achieved throughout the flight envelope. In this approach, higher harmonic blade root pitch, which can be input through the standard swashplate configuration, is used to modify blade airloads and reduce harmonic blade forcing of the fuselage. Reference 20 presents an excellent review of past analytical and experimental work in helicopter higher harmonic control. More recently, the concept of closed-loop HHC has been successfully demonstrated in flight tests (Ref. 21).

In recent years, UTRC has focused on the analytical development, evaluation, and refinement of closed-loop self-adaptive higher harmonic control algorithms. References 22 and 23 present the results for a numerical simulation of a closed-loop deterministic control algorithm. The simulation was based upon a Black Hawk (UH-60) aircraft flying at various steady flight conditions. References 7 and 8 present the results of a more recent analytical study involving a simulation of the H-34 rotor mounted on the NASA Ames Rotor Test Apparatus (RTA) of the 40 x 80 ft wind tunnel. This investigation involved the refinement and evaluation of alternative controller configurations in order to compare their performance and to more fully understand the effects of tuning parameters within the algorithms. A generic controller computer code was developed to give the capability to readily define many different algorithms by selecting from three control approaches (deterministic, cautious, and dual), two linear system models (local and global), and several methods of limiting control. The generic controller is currently being used in analytical studies in preparation for open- and closed-loop flight tests of the Sikorsky S-76 (Ref. 24). An overview of the generic controller, analytical simulation of closed-loop control, and results presented in detail in Ref. 7 is given below.

Generic Active Controller

Figure 15 shows the computer simulation used to evaluate and compare the performance of the alternative algorithms included in the generic active controller. This simulation of closed-loop control is achieved by linking the generic controller to a nonlinear aeroelastic analysis (G400), which simulates the rotorcraft by calculating the

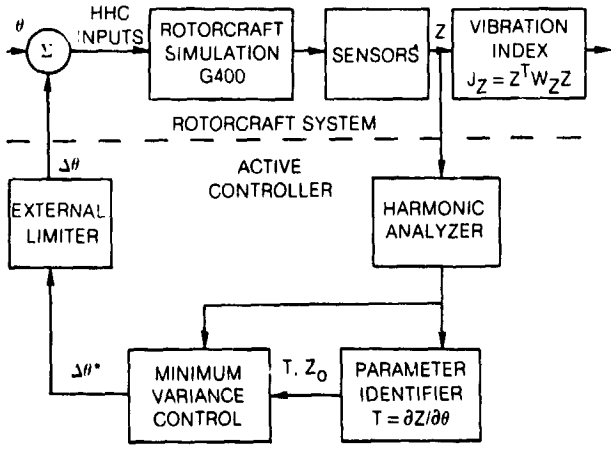

Fig. 15 Simulation of Active Vibration Control System

vibration response at a set of fixed-system sensor locations. Based on this response and on-line identification of system parameters, the active controller calculates and commands the HHC inputs required to further reduce vibration in the fuselage. These commanded inputs are imposed on the rotor by the G400 analysis with the inputs prescribed by the rotating system components (i.e., 3, 4 and 5 per rev). For computational efficiency, a constant inflow model has been used in G400. No measurement noise was simulated in this initial investigation.

Regardless of the control approach or system model implemented by the generic controller, there are two fundamental characteristics of the active controller: (1) a quasi-static linear transfer matrix (T-matrix) relationship between the vibration response and the HHC inputs is assumed and (2) the T-matrix is identified on-line to account for changes due to system nonlinearities or variations in flight condition. Each control approach can be based on one of two system models. The local model linearizes the system T-matrix about the current vibration response, Z, while the global model linearizes about the uncontrolled vibration level, Z_o (zero HHC), which must also be identified.

As shown in Fig. 15, accurate identification of the T-matrix, as well as Z_o for the global model, is important for good vibration reduction, since the minimum variance control algorithms all depend explicitly on the estimates of these parameters. The method used for estimating and tracking these system parameters is discussed in detail in Ref. 7. In short, each row of the T-matrix is considered to be a time-varying state vector, which is tracked by a Kalman filter identification algorithm.

Once system identification is completed, the required change in control for minimum vibration in the ith control update is calculated by a minimum variance control algorithm (Ref. 7). This algorithm is based on minimization of a quadratic performance index that consists of a weighted sum of the squares of the input and output variables. The performance index can be written in matrix notation as follows:

$$J=Z_i^T W_Z Z_i+\gamma_i^T(\beta\cdot\lambda\cdot P_i\sum_j W_{Z_{jj}})\gamma_i+\theta_i^T W_\theta \theta_i+\Delta\theta_i^T W_{\Delta\theta}\Delta\theta_i \quad (1)$$

where $\gamma_i=\Delta\theta_i$ for the local model and $\gamma_i=(\theta_i^T\ 1)^T$ for the global model. The index β acts as a switching function dependent on the control approach used. The performance index J is a function of not only the vector of computed harmonics of vibration (Z), but also the vector of pitch control inputs (θ) and incremental change in control ($\Delta\theta$). In the first term, W_Z is a diagonal weighting matrix used to reflect the relative importance of each vibration component. This term, referred to later as the vibration index, is indicative of overall effectiveness in reducing vibration. The second term is used to modify the controller algorithms to account for uncertainties in identified system parameters according to the underlying assumptions of the control approach being used. These uncertainties are reflected in P_i, the covariance matrix calculated by the Kalman filter identification algorithm. The effect of this stochastic control term is determined by β, and the arbitrary stochastic control constant λ. Finally, the last two terms use diagonal weighting matrices W_θ and $W_{\Delta\theta}$ to inhibit excessive control amplitudes and rates of change in control, respectively. This "internal limiting" is used not only to satisfy hardware requirements, but also to enhance controller performance.

For the deterministic control approach, β is set to zero, since all system parameters are assumed to be explicitly known despite the fact that only estimates for the T-matrix are available. In the cautious approach, it is recognized that some of the system parameters are only estimates, and control inputs are implemented more cautiously than for the deterministic approach. This is accomplished by setting β equal to one. The resulting positive stochastic control term has a similar effect to that of $W_{\Delta\theta}$ or W_θ, depending on the system model, but is dependent on the uncertainty in the identified T-matrix, as reflected by P_i. In the dual control approach, an attempt is made to improve long term system identification by actively probing the system, while maintaining good control. In the generic controller, this is achieved with a negative value for β. The effect, analagous to reductions in weighting placed on control inputs, causes the system probing inherent to the dual controller. Whereas the cautious controller penalizes control when identification is poor, the dual controller increases control.

Finally, Fig. 15 shows that the active controller externally limits the optimum control inputs calculated by the minimum variance control algorithm before implementing new inputs in the rotorcraft simulation. This is referred to as external limiting since it is done outside the minimum variance control algorithm and without regard to optimality of the resulting solution. With external limiting, satisfaction of absolute control limits can be ensured. In contrast, internal limiting, which is accomplished by appropriate tuning of the weighting matrices, W_θ and $W_{\Delta\theta}$, takes into account the desire to inhibit magnitudes and rates of change of control while calculating the optimum solution.

Analytical Results

The aeroelastic simulation of the rotorcraft in Refs. 7 and 8 was based on a fully articulated, four-bladed H-34 rotor mounted on the Rotor Test Apparatus (RTA), which is used to represent the fuselage in full scale rotor tests in the NASA Ames 40 x 80 ft wind tunnel. Vibration response information was calculated at six locations in the RTA. These components included three orthogonal directions (vertical, longitudinal, and lateral) and

were spread throughout the RTA (nose, main crossbeam, and tail).

A steady level-flight condition was selected for the initial tuning and evaluation of all primary controller configurations. This baseline condition had a forward velocity of 150 kt and a nominal value of 0.058 for C_T/σ (8250 lb thrust). Based on these results, a representative controller configuration was selected and tuned for each of the three control approaches. All three controllers were based on the global system model. The deterministic controlier used internal weighting on $\Delta\theta$ with $W_{\Delta\theta}$ to maintain an acceptable rate of change of control. The cautious controller used neither external nor internal $\Delta\theta$ limiting, but inherently slowed down the implementation of control via the stochastic control term. The dual controller used external rate limiting to allow the i herent perturbations in control inputs to occur without excessively compromising short term control. The performance of these controllers were subsequently evaluated at several steady flight conditions and during several short duration maneuvers as discussed below.

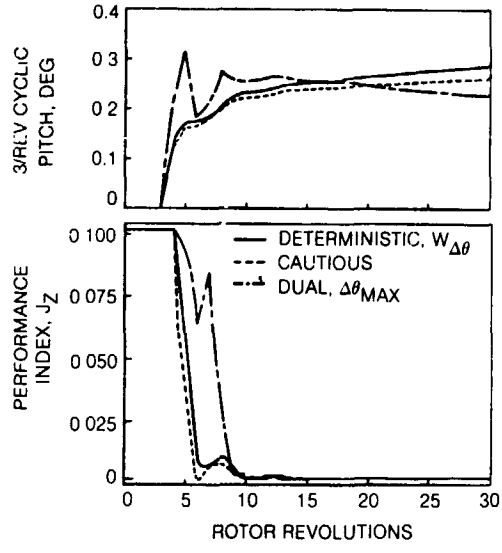

Fig. 16. Time History of Vibration Index and 3 Per Rev Control at Baseline Flight Condition ($V = 150$ kt, $C_T/\sigma = 0.058$)

Steady Level Flight Conditions - Figure 16 presents the G400 predicted results for each of the three controllers operating closed-loop at the baseline flight condition. The simulation included three revs of uncontrolled flight to allow initial numerical transients to die out before activating each controller at rev 4. Figure 16 shows predicted time histories of the vibration index J_Z and the amplitude of the 3 per rev HHC input commanded by each control approach. While not shown, 4 and 5 per rev inputs commanded by each controller had similar time histories. Since the vibration index is a weighted sum of the squares of all the vibration components being actively controlled, it is a good indicator of overall controller performance in reducing vibration. Note that the vibration index plotted involves only the first term shown in Eq. (1). While the other terms are important to overall controller performance and stability, they are not indicative of vibration reduction achieved by the controller.

Figure 16 shows that all three controllers did an excellent job of reaching a new steady vibration level that is greatly reduced from the uncontrolled vibration level at rev 4. After only two revs of active control, both the deterministic and cautious controllers achieved and maintained at least a 90 percent reduction in the vibration index. The dual controller required about 5 revs of active control to achieve the same level. By rev 10, all three controllers had essentially converged to a value of the vibration index that was only 3 percent of the uncontrolled value.

This figure also shows the time history of 3 per rev HHC amplitude commanded by the three controllers. The deterministic and cautious controllers smoothly increased the amplitude of all three control inputs, while continually reducing the vibration index. In contrast, the dual controller exhibited a tendency to probe the system by perturbating the higher harmonic cyclic inputs. This probing initially resulted in a slight degradation in short term control as can be seen in the vibration index. After identification improved, system probing diminished and the final controller solution was as good as that of the deterministic and cautious controllers. The dual controller's tendency to probe the system was somewhat inhibited by an application of external rate limits. Without these limits, the perturbation in control inputs used to probe the system were much larger and resulted in much worse short term control before converging to a final solution.

Figure 17 compares the uncontrolled 4 per rev vibration levels at rev 4 to those at rev 30 with active control. All three controllers substantially reduced vibration at all locations except the two lateral components that had very low initial levels of vibration, which were maintained. Reductions in vibration for the four primary components were between 75 and 95 percent.

Also shown in Fig. 17 are the fixed system hub vibrations. Note that angular accelerations have been multiplied by 1 ft to be plotted in g's in this figure. The two largest contributors (vertical and longitudinal) were reduced by all three controllers. A substantial 75 percent decrease in the longitudinal component was achieved, while a more modest 20 percent reduction was achieved in the vertical component. The other four components, which were smaller initially, remained at about the same levels. The reductions in vibration in the RTA were achieved by a combination of reduced forcing at the rotor hub and vectorial cancellations of hub component contributions.

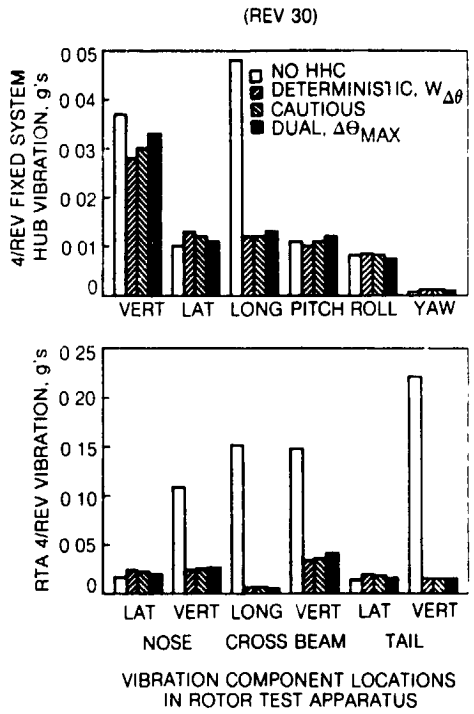

Fig. 17. Effect of Active Control on 4 Per Rev Vibration at Baseline Flight Condition (V = 150 kt, C_T/σ = 0.058)

In addition to the baseline flight condition, each of the three controllers was also evaluated over a range of forward velocities from 112 to 150 kt at a nominal value of 0.058 for C_T/σ and over a range of rotor thrusts having values of 0.058 to 0.085 for C_T/σ at a velocity of 150 kt. Between 75 to 95 percent reductions in vibration were achieved by all three controllers at all steady flight conditions. These reductions in the individual components in vibration correspond to at least a 97 percent reduction in the vibration index at all steady flight conditions. Convergence to an acceptable control solution occurred quickly and smoothly. After 5 control updates, at least an eighty percent reduction in the vibration index was achieved and maintained. These results were obtained at all steady flight conditions with no retuning of the controller and with the same initial T-matrix developed and used at the baseline (V=150 kt, C_T/σ=0.058) flight condition. The required amplitudes of 3, 4, and 5 per rev control increased with both velocity and rotor thrust, but were each less than 1.0 degree for all steady flight conditions.

All the steady flight results presented above for the global system model are generally applicable to the local model as well. It was not until controller performance was evaluated during the short duration maneuvers discussed below that any significant difference in controller behavior due to system model was noticed. From the steady flight conditions studied to date, no distinct advantage in terms of controller performance has been identified for either the deterministic or cautious control approaches. The dual controller, while equally effective in reducing vibration, tended to have worse short term control and somewhat more oscillatory behavior due to system probing. The baseline deterministic and cautious controllers were relatively insensitive to less than optimum tuning of internal parameters. However, it should be noted that the use of internal limiting in the deterministic approach dramatically improved controller stability and performance compared to that achieved with external limiting. The use of properly tuned internal weightings on control inputs significantly improved the deterministic controller performance according to all criteria: much greater vibration reduction in the first step of active control; faster convergence; significantly greater reduction in vibration at convergence; and smaller final control inputs. The dual controller was very sensitive to the tuning of λ. It remains to evaluate the effect of measurement noise on the performance of each control approach.

Short Duration Maneuvers - Each of the three controllers was also evaluated during several short duration maneuvers, while using the same initial T-matrix and tuning developed at the steady baseline condition. Each of the maneuvers involved an increase in rotor thrust from the initial steady baseline condition, C_T/σ = 0.058, via step and ramp changes in collective pitch during an otherwise steady flight condition at 150 kt. These changes in collective pitch resulted in 40 to 50 percent increases in rotor thrust relative to the baseline condition. After all transients subsided, the final flight condition corresponded to one of the steady flight conditions investigated (i.e., C_T/σ = 0.08 or 0.085). For each of these maneuvers, the active controllers remained stable, maintained peak vibration response well below uncontrolled levels, and reduced vibration to the same levels achieved at equivalent steady conditions. Retuning of the controllers was necessary to achieve satisfactory performance during some maneuvers. Without retuning, the local model was much more oscillatory and required more time to converge than the global model during maneuvers. This may indicate that the local model is more sensitive to tuning at different flight conditions or perhaps more sensitive to inaccurate vibration response information due to transient effects. Detailed results for the various steady flight conditions and short duration maneuvers are presented in Ref. 7. The results for the maneuvers investigated indicate the need for further evaluation during extended continuous maneuvers.

Blade Stresses and Rotor Performance - Increases in rotor blade stresses were noted at most flight conditions investigated. However, results also suggest that the penalty of increased vibratory blade loads may be reduced by tailoring of HHC inputs with unequal W_θ weighting. It may

also be possible to alleviate the increases in stress, without compromising vibration reduction, by including appropriately weighted terms representative of blade stresses in the performance index shown in Eq. (1). While these approaches were not pursued, certain results did indicate that they might be feasible. For example, multiple control solutions resulting in similar vibration reductions, but having different effects on rotor blade stresses, were obtained. One such solution involved an arbitrary elimination of 5 per rev control at the highest thrust condition investigated. The result was relatively small increases in blade stresses and excellent reductions in vibration. The increase in blade stresses were much smaller than those where 5 per rev control was implemented, even though vibration reductions for both cases were comparable.

A degradation in rotor performance was also noted at many flight conditions. At the baseline condition, the application of HHC caused an increase in required torque on the order of 5 percent. An analytical study of the effect of closed-loop HHC on rotor performance should be performed when using a variable inflow model that includes unsteady aerodynamic effects. Again, it may be possible, if necessary, to guide the controller to better control solutions in terms of rotor performance, as well as vibration, by including a term indicative of rotor torque in the performance index.

Blade Appended Aeroelastic Device

In addition to alleviating vibration through blade design and active pitch control, the use of blade appended aeroelastic devices has been analytically explored at UTRC. One such device, as reported in Ref. 9, is a passive tuned tab shown in Fig. 18. The objective of this tab is to create harmonic airloading of favorable amplitude and phase to cancel the inherent harmonic airloading which acts as a source of main rotor vibration. Physically, the passive blade tab is appended near the trailing edge of a standard rotor blade by some hinge configuration so that the tab can deflect freely about the hinge. The hinge could be mechanical in nature with bearings or it could be made of a composite material that has a large allowable strain such that the tab is actually "taped" to the blade by the composite hinge. The latitude in selecting the spring rate of the tab would provide a dynamic tuning capability; the spring rate could be provided either mechanically or by the elasticity of the material for a composite hinge.

The basis of the concept, as described in Ref. 9, is as follows: when a rotor blade tab deflects, it creates an incremental airload and pitching moment on the rotor blade as a result of the increased camber. The pitching moment also creates an additional airloading on the rotor blade by elastic twisting to create an incremental angle-of-attack. The importance of this source of airloading is closely tied to the blade torsional stiffness and natural frequency, and is secondary to that obtained from the effective camber change for this concept. When the tab deflects harmonically, the airloads and pitching moment created by the tab deflection are also harmonic. Therefore, to derive benefit from the tab, the tab motion must be correctly phased to cancel the inherent harmonic airloading that excites the blade flatwise modes and produces vibration.

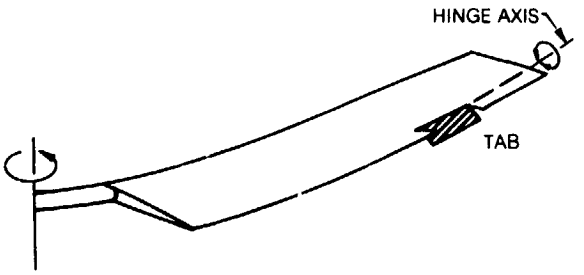

Fig. 18. Blade Vibration Control Device -- Passive Tuned Tab

The driving forces on the tab are its own inertial loading as the blade flaps and pitches (rigid body and flexible motions) and the aerodynamic forces arising from blade and tab motion. By increasing the offset of the tab center of gravity from the hinge, the inertial forcing can be increased. For a tab located at the blade tip, most of the vertical harmonic motion would come from the response of the flexible flatwise modes and nearly all of the torsion motion would be due to the response of the blade first torsion mode. Hence, there is a direct relationship between the motion that is inertially forcing the tab to deflect and the vibration that is a result of that same motion. Therefore, the success of this concept depends on correctly sizing and placing the tab along the rotor blade span and choosing its mass and natural frequency to achieve the maximum vectorial cancellation of inherent harmonic airloading.

An initial analytical evaluation of this concept has been conducted (Ref. 9) using the G400 rotor aeroelastic analysis (Ref. 6), together with data for a realistic helicopter rotor blade (UH-60A, Blawk Hawk) in high speed flight (175 kts). Variations in tab mass, frequency, and center-of-gravity location were investigated for two tab spanwise locations. While some modest reductions in the inplane components (longitudinal and lateral) of vibratory hub shear were predicted, unacceptable increases in the vertical component have been predicted for the blade/tab as configured in the study. The reason for the vertical shear increase remains to be determined before any further investigation to determine if other configurations have potential for overall vibration reduction.

Vibratory Airloads

An ongoing activity at UTRC has been directed toward the development of helicopter airload meth-

odology and the advancement of the understanding of vibratory airloads of the rotor and fuselage. A representative sampling of results of this activity are presented in Refs. 10 to 19. This activity has included investigations of rotor wake and airflow, unsteady airloads related to dynamic stall, blade airload coupling with blade response and aeroelastic flexibility, and both rotor/fuselage and rotor/empennage interactional aerodynamics.

Wake Induced Blade Airloads

A recent investigation of helicopter rotor wake geometry and its influence in forward flight is reported in Refs. 10 and 11 and summarized in Ref. 12. This analytical investigation was conducted to generalize the wake geometry of a helicopter rotor in forward flight and to demonstrate the influence of including wake deformation in the prediction of rotor airloads and performance. Predicted distortions of the tip vortex of each blade relative to the classical undistorted geometry were generalized for vortex age, blade azimuth, advance ratio, thrust coefficient, rotor disc attitude, and number of blades based on a representative blade design. A computer module and charts (Ref. 11) were developed for approximating wake geometry and identifying wake boundaries and locations of blade-vortex passage. Predicted H-34 rotor airloads for several rotor inflow/wake models were compared with test data for several flight conditions.

An example of the tip vortex geometry in forward flight (30 kts), as predicted by the UTRC Wake Geometry Analysis (Ref. 13), is shown in Fig. 19. A sample isometric view of distorted tip vortices from the generalized wake model is shown in Fig. 20. The characteristic wake distortion features observed from experimental results are presented in the predicted tip vortex geometries. The forward and lateral sides of the wake are distorted toward the rotor relative to the undistorted wake model. This results in close blade-vortex passages which can introduce severe local azimuthal and spanwise gradients in blade airloads which are not predicted with uniform inflow and undistorted wake (rigid wake) analytical models. This is shown in Fig. 21 where the predicted airloads (blade lift distributions) based on the different inflow/wake models are presented in the form of surface contour plots. As indicated, inclusion of tip vortex deformation in the wake model results in increased higher harmonic content in the airload prediction. The outboard advancing side of the rotor typically exhibits the most severe vibratory airload gradients with significant but lesser variations on the outboard retreating side. This is exemplified in the H-34 airload test data shown in Fig. 22, taken from Ref. 10, as acquired at 48 kts (0.129 advance ratio) in flight test (Ref. 25).

Typical of low speed transition conditions, a sharp "down-up" impulse is applied to the tip region of the advancing blade and an "up-down" impulse is applied to the tip region of the

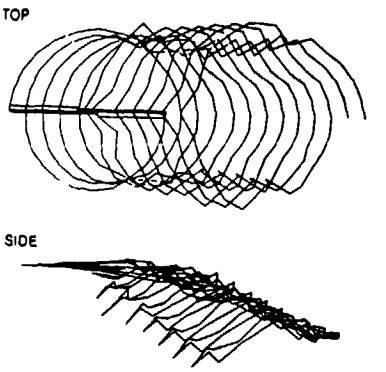

Fig. 19. Predicted Distorted Tip Vortex Geometry

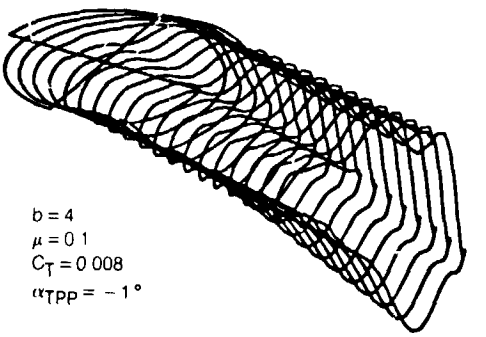

Fig. 20. Isometric View of Generalized Distorted Tip Vortices

retreating blade (Fig. 22). For higher speed flight the vibratory airloads are concentrated at the outboard region of the advancing side where a characteristic "up-down" impulse occurs. This is exemplified in Fig. 23 where the airloads are shown for the H-34 rotor operating at 110 kts (0.29 advance ratio), as measured in a wind tunnel (Ref. 26). These airload characteristics have been shown by Hooper (Boeing-Vertol) in Ref. 27 to be surprisingly consistent for different helicopters with substantial differences in size, trim, and number of blades per rotor. In this reference, the combined higher harmonic components of airloading (harmonics 3-10) are plotted for several aircraft and, with some exceptions at high speed, these vibratory components are shown to be characteristically consistent.

The ability to predict the vibratory airloading characteristics is depicted in Fig. 22 from Refs. 10 and 12, where the results of combining the Sikorsky Generalized Performance Analysis (airloads), the UTRC Rotorcraft Wake Analysis (induced airflow), and the UTRC Wake Geometry Analysis (distorted wake) are presented for the H-34, 48 kt condition. The general ability to predict the induced airflow of the rotor wake in the vicinity of the blades is shown through comparisons with laser velocimeter and other test data in Refs. 15 and 16. The influence of wake distortions on blade

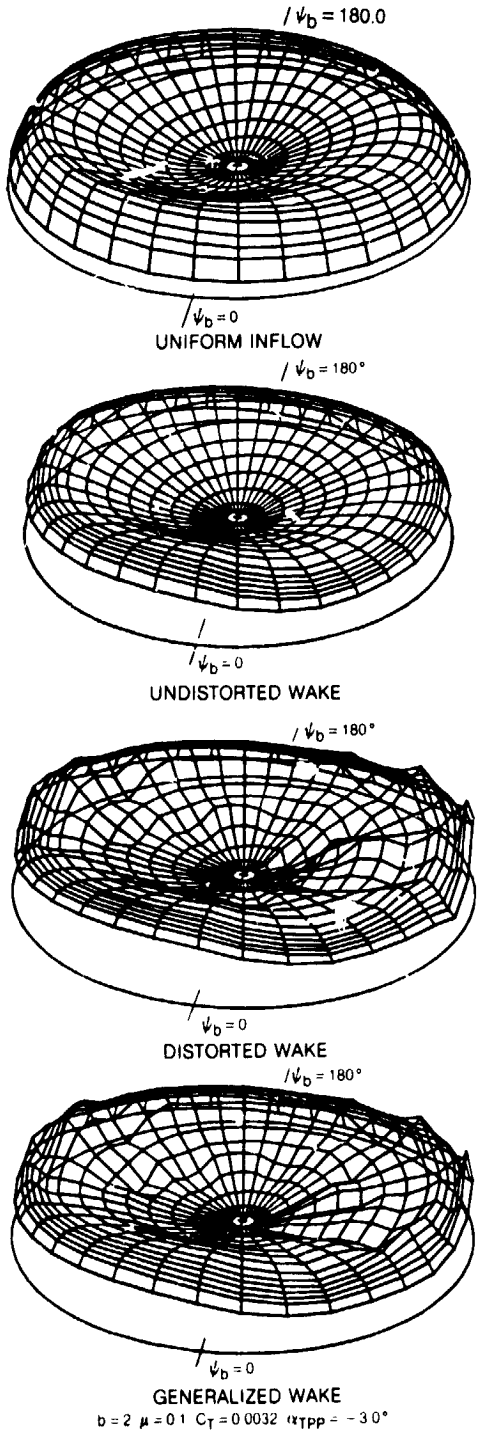

Fig. 21. Blade Lift Distributions Predicted with Various Wake/Inflow Models

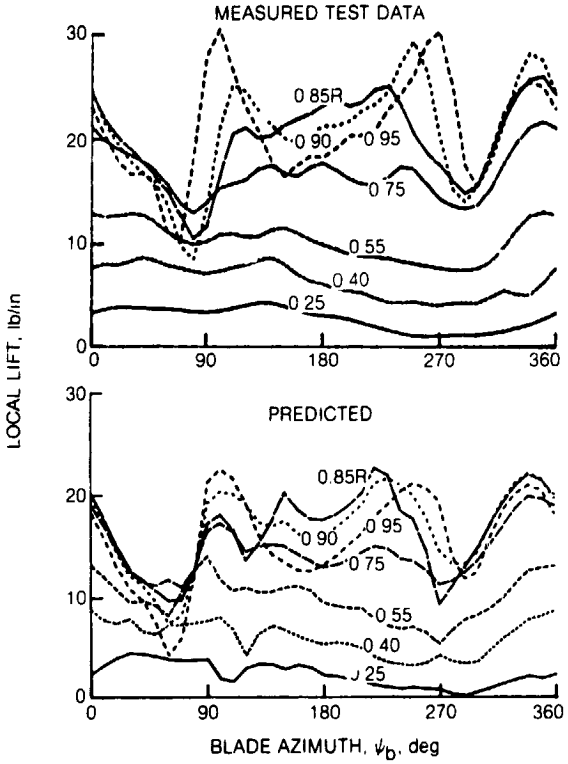

Fig. 22. Measured and Predicted Blade Airloads. (H-34, 48 kts)

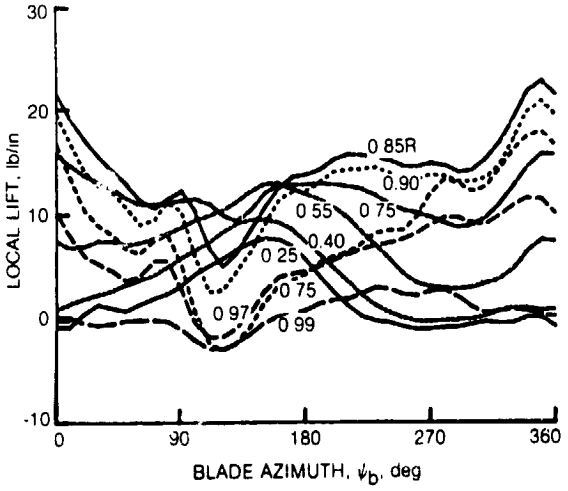

Fig. 23. Measured Blade Airloads. (H-34, 110 kts).

airloads is described in these references to be related to the degree of proximity of the tip vortices to the rotor blades and the number of locations of close blade-vortex passages. For steady level flight, the wake influence generally increases with decreasing advance ratios, decreasing disc attitude and increasing number of blades. The wake distortions and related airload influence are most complex at low advance ratios, where the difficulty of accurate wake geometry and airloads prediction is compounded by the larger number of close blade-vortex passages and by blade-vortex impingement due to the movement of the tip vortices above and then down through the rotor disk.

The prediction of tip vortex distortions, which are in close proximity to the blades at localized regions of the rotor, results in a high sensitivity of predicted airloads to small differences in tip vortex geometry and the theoretical blade-vortex aerodynamic interaction model used. This sensitivity is demonstrated in Refs. 10 and 12. For example, the airload predictions in Fig. 22 resulted from the use of an expanded vortex core model to simulate vortex bursting near close blade passages. Both higher and lower amplitudes of vibratory airloading on the advancing and retreating sides were predicted with other vortex core models and small variations in wake geometry (blade-vortex spacing). Although the need for further analytical refinement is evident, the degree to which the analysis, with a distorted wake model, was able to reproduce the measured airload distributions is encouraging and indicative that, with future emphasis on blade-vortex interaction modeling, wake methodolgy has the potential to provide a useful predictive tool for vibratory airloads.

Wake geometry and blade-vortex intersection plots in Refs. 10 and 27 indicate the source of the impulsive type airloads on the advancing and retreating sides to be at least partially attributable to close blade-vortex interaction. It is shown that the blade passes close to a nearly parallel tip vortex from a preceding blade in the first quadrant and the fourth quadrant of the rotor. At higher flight speeds, where the vibratory airloading is predominantly on the advancing side, the vibratory airloads are caused by a combination of blade-vortex interaction, blade motions, and the characteristic blade "Mach tuck" phenomenon. This phenomenon is known to result from the aft movement of the blade aerodynamic center, due to compressibility, which results in a nose down pitching moment for positive lift and a corresponding blade torsional deformation. This produces a negative azimuthal gradient in blade lift. Blade sweep has been used to counte this effect in the advancing side negative lift region. In Ref. 27, it is hypothesized that the "up-down" impulse on the advancing side at high speed conditions is opposite to the "down-up" impulse at lower speeds due to the opposite direction of vorticity produced by the negative lift region at the tip at high speed. In high speed flight, vibratory airloads on the retreating side can also be caused by dynamic stall as shown and predicted in Ref. 18.

Airloads From Blade Motions

The mechanism by which vibratory airloads couple with blade motions and modal response are described in Ref. 1. A primary source of vibratory airloads in forward flight is the interharmonic coupling of airloads and blade response that increases with forward speed. As mentioned earlier, the phenomenon can be viewed as a cascade effect (Fig. 1), starting with the basic characteristic of helicopter rotors in forward flight. One per rev airloads are created by either blade flapping or cyclic pitch. The one per rev airloads cause one per rev response of the blade modes. The resulting one per rev motions create 2 and 3 per rev airloads. These airloads in turn cause 2, 3, 4, and 5 per rev response of the blade modes and so on. Different blade modes respond more than others due to resonant type responses, and cause vibration from the combination of inertial, elastic, and direct airloading. Thus, significant vibratory airloads are created by blade motions and elastic response as well as wake induced, compressibility, and dynamic stall effects.

Interactional Rotor-Fuselage Airloads

In order to accurately predict coupled rotor-fuselage vibrations, it is necessary to consider the aerodynamic interaction of the individual components of the helicopter. In Ref. 17 it is shown that the presence of the fuselage distorts the rotor airflow and wake causing two-per-rev as well as other harmonic airload excitations at the rotor. Examples from Ref. 17 of the calculated effect of the airframe presence on the rotor inflow velocities and inner blade angle-of-attack distribution are shown in Fig. 24. Here, the influence of the fuselage on the rotor inflow velocities (ΔV_N) is shown as predicted using the Sikorsky fuselage panel method (WABAT) for a relatively low rotor

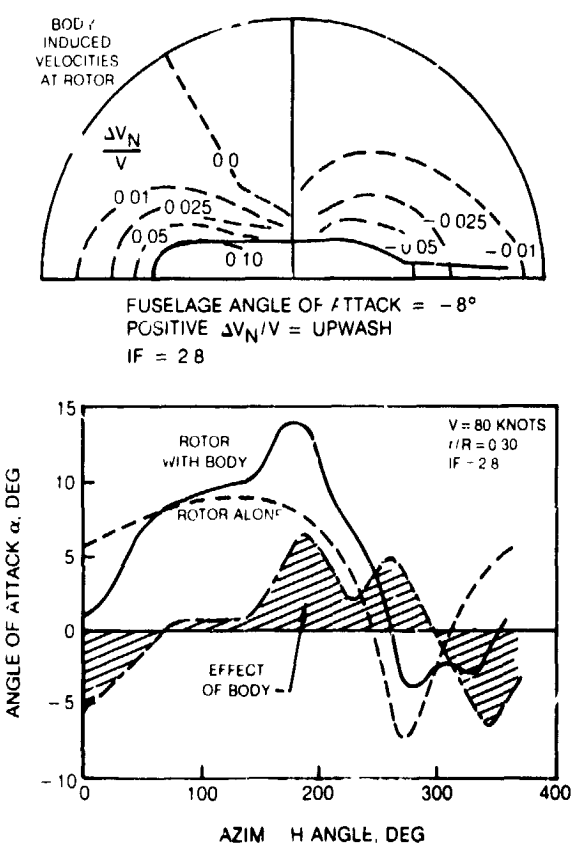

Fig. 24. Predicted Body Induced Velocities at Rotor Plane and Body Effect on Rotor Angle of Attack Distribution

configuration (IF=2.8). (The interference factor, IF, defined in Ref. 17, is representative of the ratio of the fuselage upper surface area to the rotor hub to fuselage distance.) The perturbation of the flow field at the rotor disc produces changes in the blade local angle-of-attack distributions which influence the blade response and airloads. Also in Fig. 24, the angle-of-attack distribution at one radial station is presented as predicted using the UTRC Rotorcraft Wake Analysis coupled with the Sikorsky Generalized Rotor Performance Analysis. In addition to two-per-rev, there is a significant third harmonic content in the increment representing the body induced effect. For low rotor configurations, this should be considered in computations of the vibration spectrum.

The influence of the rotor airflow on fuselage vibratory airloading must also be considered. Experimental results have indicated that the rotor blades and wake can produce significant oscillating fuselage pressures at principally the fundamental blade passage frequency. These pressure pulses have been recognized as a fuselage vibration mechanism, but this mechanism and its effect have not been fully investigated analytically. Methodology is currently being developed at UTRC to approximate the rotor wake deformation due to the fuselage and to calculate the unsteady fuselage pressures.

Interactional Rotor - Empennage Airloads

The Rotorcraft Wake Analysis and laser velocimeter measurements have been used at UTRC to demonstrate the significant influence of the rotor wake on fluctuating flow velocities in the vicinity of tail surfaces (Ref. 16). More recently, a computer program (RIEVA) has been developed that predicts the unsteady airloads that are imposed on the empennage surfaces due to its aerodynamic interaction with the main rotor wake (Ref. 19). A rotor wake program is used to determine the position and the strength of blade tip vortices that pass near the empennage surfaces. A nonlinear lifting surface analysis is utilized to predict the aerodynamic loads on the empennage surfaces in the presence of these concentrated vortices. The nonlinear analysis was formulated to include pertinent effects such as suction effects of the interacting vortices and the effects of time-variant shed vorticity behind the empennage surfaces. The problem is solved in a stepwise manner (time-domain); that is, a period corresponding to one blade passage is divided into a large number of time intervals and empennage unsteady airloads are computed at each time step. The output of the analysis consists of chordwise and spanwise airload distributions at each time step. These airload distributions are converted into harmonic airloads that can be applied to excite the tail boom in a vibration analysis. The results of a limited correlation study involving the application of the computer program to a full-scale helicopter stabilizer indicate an encouragingly good correlation between the analytical vibratory airload predictions and flight test data. Sample results are shown in Fig. 25 for the 6 per rev airloads of the CH-53A horizontal stabilizer that are induced by the wake of the six-bladed rotor at a high speed condition (159 kts).

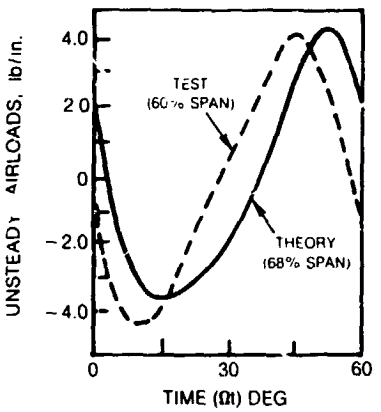

Fig. 25. Unsteady Airloads Induced by Rotor Wake on Empennage Lifting Surface

Concluding Remarks

Analytical studies have demonstrated the potential of various approaches to alleviate helicopter vibration. The approaches described herein should be considered to be complementary rather than entirely competitive. Blade design for vibration is the most desirable approach if vibration reduction can be achieved throughout the flight regime without penalties in performance, stresses, and weight. However, it may still be necessary to complement design optimization with other approaches such as active higher harmonic control to achieve the industry goal of 0.1 g vibration levels.

A blade design study has been conducted to identify important contributing components and establish appropriate vibration criteria. The availability of optimization techniques makes the design process more tractable and allows new designs that satisfy specified design criteria to be achieved in a much more efficient fashion than is possible in the traditional design process. As a result, it is possible to pursue more sophisticated design criteria and to achieve designs previously unobtainable. Since it is computationally inefficient to base a closed-loop design optimization procedure on a forced response analysis, vibration criteria based on blade modal properties have been developed. Results from the closed-loop analysis are then verified in a forced response analysis. Results of the blade design study for a high speed cruise condition indicate the potential for developing enhanced blade designs that can offer significant reductions in baseline vibration without resorting to special vibration alleviation devices, radical blade geometries, or weight penalties. Efforts to define further vibration criteria are underway.

Analytical studies have also demonstrated the potential for active higher harmonic control to reduce helicopter vibration. The results of the generic controller study indicate the potential for various control approaches to reduce vibration by 75 to 95 percent with small blade pitch amplitudes at a range of moderate to high speed and thrust conditions. Good controller performance was also demonstrated during short duration maneuvers. However, the potential for adverse effects on blade stresses and rotor performance was noted at many flight conditions. Analytical investigations are planned to determine the drivers of these effects and to develop methods for their alleviation.

The results for a passive tuned tab have been somewhat disappointing, with increases in some vibration components occurring at the same time that reductions in other components are achieved. Further investigation of blade appended devices, such as the passive tuned tab, is required.

Computerized analyses have been used as diagnostic tools to acquire a better understanding of the fundamentals of vibration by tracing the principal sources of vibration and loads and identifying the important contributing components. These analyses have also been used in simulating closed-loop higher harmonic control and in verifying the results of blade design changes or the effects of blade appended devices. Since the analyses remain to be validated, qualitative results regarding dynamic trends and characteristics of the rotor should be accepted more than quantitative results. The predicted absolute vibration and load levels are approximate as are the predictions of all other forced response helicopter analyses in use today. Significant progress has been made toward establishing a blade design procedure, and preparations for model tests to provide vibration data are underway.

Recent advancements of aerodynamic analytical tools are providing an understanding of the sources of vibratory airloads. Although further analytical refinment is continuing, the degree to which the distorted wake model is able to predict measured airloads is encouraging. Indications are that, with future emphasis on modeling blade-vortex interaction, the combination of distorted wake and aeroelastic response methodologies has the potential to provide a useful predictive tool for vibratory airloads.

Acknowledgements

The authors especially acknowledge the contribution of Robert B. Taylor who, as Supervisor, Advanced Rotorcraft Concepts and Dynamics, directed the vibration research activity within the Aeromechanics Research Section while he was at UTRC. He initiated the active higher harmonic control activity (Refs. 22 and 23), and conceived the passive tab vibration alleviation device. His work on blade design for vibration reduction (Ref. 1) provided the technical material for that section of this paper. The contributions of T. Alan Egolf, Aeromechanics Research, UTRC, to results reported in the vibratory airloads section is also acknowledged. Dr. Richard L. Bielawa analyzed the passive vibration alleviation devices reported herein from Ref. 9, and Santu T. Gangwani developed the empennage analysis (Ref. 19).

The work reported herein was supported by the NASA Ames and Langley Research Centers, the U.S. Army Research and Technology Laboratories, and the United Technologies Corporation.

References

1. Taylor, R. B.: Helicopter Rotor Blade Design for Minimum Vibration. NASA Contractor Report 3825, (USAAVSCOM Report No. 84-A-2), August 1984.

2. Taylor, R. B.: Helicopter Vibration Reduction by Rotor Blade Modal Shaping. Proceedings of the 38th Annual Forum of the American Helicopter Society, May 1982.

3. Davis, M. W.: Optimization of Helicopter Rotor Blade Design for Minimum Vibration. Proceedings of the Multidisciplinary Analysis and Optimization Symposium, NASA Langley Research Center, Hampton, VA, April 1984.

4. Madsen, L. E. and G. N. Vanderplaats: COPES--A Fortran Control Program for Engineering Synthesis. Naval Postgraduate School, NPS69-81-003, March 1982.

5. Vanderplaats, G. N.: CONMIN--A Fortran Program for Constrained Function Minimization; User's Manual. NASA TMX-62, 282, August 1982.

6. Bielawa, R. L.: Aeroelastic Analysis for Helicopter Rotors with Blade Appended Pendulum Absorbers - Program User's Manual. NASA CR-165896, June 1982.

7. Davis, M. W.: Refinement and Evaluation of Helicopter Real-Time Self-Adaptive Active Vibration Controller Algorithms. NASA Contractor Report 3821, September 1984.

8. Davis, M. W.: Development and Evaluation of a Generic Active Helicopter Vibration Controller. Proceedings of the 40th Annual Forum of the American Helicopter Society, May 16-18, 1984.

9. Bielawa, R. L.: Analytic Investigation of Helicopter Rotor Blade Appended Aeroelastic Devices. NASA Contractor Report 166525, February 1984.

10. Egolf, T. A., and A. J. Landgrebe: Helicopter Rotor Wake Geometry and Its Influence in Forward Flight, Volume I - Generalized Wake Geometry and Wake Effect on Rotor Airloads and Performance. NASA CR-3726, October 1983.

11. Egolf, T. A., and A. J. Landgrebe: Helicopter Rotor Wake Geometry and Its Influence in Forward Flight, Volume II - Wake Geometry Charts. NASA CR-3727, October 1983.

12. Egolf, T. A., and A. J. Landgrebe: Generalized Wake Geometry for a Helicopter Rotor in Forward Flight and Effect of Wake Deformation on Airloads. Proceedings of the 40th Annual Forum of the American Helicopter Society, May 1984.

13. Landgrebe, A. J.: An Analytical Method for Predicting Rotor Wake Geometry. Journal of the American Helicopter Society, Vol. 14, No. 4, October 1969.

14. Landgrebe, A. J., R. B. Taylor, T. A. Egolf, and J. C. Bennett: Helicopter Airflow and Wake Characteristics for Low Speed and Hovering Flight from Rocket Interference Investigations. Proceedings 37th Annual Forum, American Helicopter Society, May 1981, pp. 51-65; also, Journal of the American Helicopter Society, Vol. 27, No. 4, October 1982.

15. Landgrebe, A. J., and T. A. Egolf: Rotorcraft Wake Analysis for the Prediction of Induced Velocities. USAAMRDL TR-75-45, January 1976. (Available from DTIC as AD A021 202.)

16. Landgrebe, A. J., and T. A. Egolf: Prediction of Helicopter Induced Flow Velocities Using the Rotorcraft Wake Analysis. Proceedings of the 32nd Annual Forum of the American Helicopter Society, March 1975.

17. Landgrebe, A. J., R. C. Moffitt, and D. R. Clark: Aerodynamic Technology for Advanced Rotorcraft. Journal of the American Helicopter Society, Vol. 22, Nos. 2 and 3, April and July 1977--Parts I (pp. 21-27) and II. Also, Proceedings of Symposium on Rotor Technology, American Helicopter Society, August 1976.

18. Gangwani, S. T.: Prediction of Dynamic Stall and Unsteady Airloads for Rotor Blades. Journal of the American Helicopter Society, October 1982.

19. Gangwani, S. T.: Determination of Rotor Wake Induced Empennage Airloads. Proceedings of the American Helicopter Society National Specialists' Meeting on Helicopter Vibration, November 1981.

20. Johnson, W.: Self-Tuning Regulators for Multicyclic Control of Helicopter Vibration. NASA Technical Paper 1996, March 1982.

21. Wood, E. R., R. W. Powers, J. H. Cline, and C. E. Hammond: On Developing and Flight Testing a Higher Harmonic Control System. Proceedings of the 39th Annual Forum of the American Helicopter Society, May 1983.

22. Taylor, R. B., F. A. Ferrar, and W. Miao: An Active Control System for Helicopter Vibration Control by Higher Harmonic Pitch, presented at the AIAA/ASME/ASCE/AHS 21st Structures, Structural Dynamics Conference, AIAA Paper 80-0672, May 1980.

23. Taylor, R. B., P. E. Zwicke, P. Gold, and W. Miao: Analytical Design and Evaluation of an Active Control System for Helicopter Vibration Reduction and Gust Response Alleviation. NASA CR-152377, July 1980.

24. O'Leary, J. J., S. B. Kottapalli, and M. W. Davis: Adaptation of a Modern Medium Helicopter (Sikorsky S-76) to Higher Harmonic Control. Presented at the 2nd Decennial Specialists' Meeting on Rotorcraft Dynamics, Ames Research Center, November 7-9, 1984.

25. Scheiman, J.: A Tabulation of Helicopter Rotor-Blade Differential Pressures, Stresses, and Motions as Measured in Flight. NASA TM X-952, March 1964.

26. Rabbott, Jr., J. P., A. A. Lizak, and V. M. Paglino: A Presentation of Measured and Calculated Full Scale Rotor Blade Aerodynamic and Structural Loads, USAAVLABS TR 66-31, July 1966. (Available from DTIC as AD 639 981.)

27. Hooper, W. E.: The Vibratory Airloading of Helicopter Rotors. VERTICA, Vol. 8, No. 2, 1984. Also, Proceedings of the Ninth European Rotorcraft Forum, Stresa Italy, September 1983.

DISCUSSION
Paper No. 22

ANALYSIS OF POTENTIAL HELICOPTER VIBRATION REDUCTION CONCEPTS
Anton J. Landgrebe
and
Mark W. Davis

Ed Austin, U.S. Army Applied Technology Laboratory: Jack, I was wondering on your higher harmonic control work, first of all, what sort of a frame time were you using for updating your controller, and did you try investigations of various frame times to see what was necessary?

Landgrebe: As far as frame time, you're talking about azimuth?

Austin: Right, the computation time for the controller.

Landgrebe: That was basically going through a one rev-type update. There was not that much done in [determining] the sensitivity. It seemed to be adequate--if we had not gotten good results, we would have looked at other updates.

Andy Lemnios, Kaman Aerospace: Jack, I'm absolutely delighted to have you relook at the dynamics end of blade design in addition to the aerodynamics end, because I think this is a very fertile area for some very serious vibration reductions. As you know, we feel very strongly about the proper inertial coupling among the various modes, and by doing so you can very strongly influence what happens to the hub shears and hub moments. Also we feel that the first flapwise frequency being above 3 per rev as we talked about last night, is a very important parameter to design for. I did have a couple of questions for you. In your look at loads being transmitted to the fuselage from the rotor, did you also include the pitch link loads in that analysis?

Landgrebe: No, that was not included.

Lemnios: Typically, I know that in some helicopters, for example, those pitch link loads can account for 25 to 30% of the excitation forces. They're very significant and they cannot be ignored.

Landgrebe: Yes, we recognize that. They have been looked at in other studies as far as our unsteady aerodynamics studies, and you're right, they can be quite formidable.

Lemnios: The second question I had was, in this particular model did you have a lead-lag damper on this or not, or was it a bearingless rotor that you were looking at? Do you remember?

Landgrebe: In which study, in the vibrations study?

Lemnios: The vibrations study, yes.

Landgrebe: That was basically an S-76 type articulated blade.

Lemnios: The reason I ask is, did you put in the appropriate frequency characteristics of the lag damper? I know from our experience, lag dampers typically have a very uniform damping characteristic, and essentially zero spring rate, at the low frequencies; but that lag damper characteristic falls off, and the spring rate builds up to a liquid spring at the 4 and higher rev frequency and by ignoring the 5 per rev frequency, again you may be overlooking some very significant vibratory forces.

Landgrebe: Bob [Taylor] can probably answer that question better than I can, but the point is that in the G400 analysis, there is a representation for the lag damper, but it doesn't take into account all the features that you have mentioned.

Bob Taylor, Boeing Vertol: I personally haven't seen any Sikorsky data or any other data at high speed where the 5 per rev vibration responses are important.

Lemnios: Strictly from our own experience, again, our frequency inplane is on the order of I think it was 5.4 per rev with the lag damper characteristics thrown in there, and that could be a significant contributor.

Taylor: I do believe that the [G400] model just used a linear lag damper.

Lemnios: Last but not least, the conclusion on your passive tuned damper may be appropriate, but you ought to also think about our favorite, which is a controlled tab instead of a passive tuned tab.

Peretz Fiiedmann, University of California, Los Angeles: I like the way you do the optimization with that modal-shaping type of concept. One of the things I was wondering--when you change the mass and stiffness distribution of your blade in order to reduce your vibration levels, you probably affect also the aeroelastic stability of the blades. Yet among the various constraints which you have enforced and listed in your slide, you had no aeroelastic stability constraint.

Landgrebe: That is correct, Peretz, that was not included within the constraint itself. The tack was taken to run the analysis and look to see if the analysis indicated any stability problems, which it did not. So that was not within the [constraint], but it could very well be put in in the future.

Friedmann: You miss the point of what the constraint means. It means that if you have a certain given aeroelastic stability margin, as a result of going through your procedure, that margin is not diminished. You still have a stable blade, yet you wouldn't like to trade off aeroelastic stability for vibration reduction of if you want to do it you should put some penalty on it.

Landgrebe: Obviously the concentration here was on vibration. I showed in one of the slides that really what you want to do is include performance, stability, loads, put them all in at the same time and that is the direction to go in, but we are not to that point yet.

ADAPTATION OF A MODERN MEDIUM HELICOPTER (SIKORSKY S-76) TO HIGHER HARMONIC CONTROL

James J. O'Leary
Chief, Aeromechanics Risk Reduction
and
Dr. Sesi B. R. Kottapalli
Dynamics Engineer

Sikorsky Aircraft Division
United Technologies Corporation
Stratford, Connecticut

and

Mark Davis
Associate Research Engineer
United Technologies Research Center
E. Hartford, Connecticut

Abstract

Sikorsky Aircraft has performed analytical studies, design analyses, and risk reduction tests for Higher Harmonic Control (HHC) on the S-76. The S-76 is an 8-10,000 lb helicopter which cruises at 145 kts. Flight test hardware has been assembled, main servo frequency response tested and upgraded, aircraft control system shake tested and verified, open loop controllers designed and fabricated, closed loop controllers defined and evaluated, and rotors turning ground and flight tests planned for the near future. Open loop analysis shows that about 2° of higher harmonic feathering at the blade 75% radius will be required to eliminate 4P vibration in the cockpit. Analytical computer simulations of a closed loop controller have been evaluated, relative to the theses of reducing vibration to low levels while maintaining good ride quality and aircraft structural stress attributes. The analytical results, design concepts, program approach, and risk reduction tests are reviewed herein, providing a status report on HHC for the S-76.

Introduction

As we move toward the end of this century, where the design and fielding of many thousands of new helicopters is a major objective, it is mandatory to develop weight-effective, high technology airframe vibration control. This is true for both high speed level flight (advance ratio μ = 0.40) and low speed maneuvering flight The rotor speed may be varied by large percentages (10 to 30%) to optimize other aircraft characteristics such as acoustics, performance, load factor, and time on station. This could preclude the use of more conventional vibration treatment devices because of adverse frequency response characteristics and/or weight considerations. Over two decades of analytical studies, wind tunnel tests, and light aircraft flight tests (μ = 0.26) have demonstrated HHC to be a viable concept for vibration control. Application of HHC to larger aircraft with the design requirements discussed above has not occurred.

The concept underlying HHC is that reductions in airframe vibrations and blade loads can be achieved by oscillating the rotor blade in pitch at $(N-1)\Omega$, $N\Omega$, $(N+1)\Omega$ frequencies where N is the number of blades and Ω is the rotor speed.

Vibration reduction using HHC was successfully demonstrated in full scale testing on an OH-6A helicopter in the early part of 1984 (Reference 1) after an eight year effort which included wind tunnel testing. In this effort a closed loop controller was employed to reduce vibration from 0.45 g's to 0.03 g's at 100 kts (advance ratio of 0.26) in a 2500 lb aircraft. This fifteen fold reduction is impressive for a steady state flight condition. Much smaller (3 to 1) reductions in vibrations were obtained in maneuvers. The next logical question is whether such high magnitudes of vibration reductions are attainable in a larger and heavier aircraft (8,000 - 10,000 lbs) flying at speeds typical of modern helicopters without significant reductions in the life of control and rotor system parts

Presented at the 2nd Decennial Specialists Meeting on Rotorcraft Dynamics, NASA, Ames Research Center, Moffett Field, California, November, 1984.

(e.g. Sikorsky S-76 at 145 knots flying at an advance ratio of about 0.36). This is important since the vibratory hub loads increase at least as $(\mu)^2$. This means that the loads at 145 knots are 2 1/4 times those at 100 knots. Also, at higher advance ratios, the potential for greater interharmonic coupling exists.

Sikorsky Aircraft is currently engaged in a comprehensive program for the prototype development of an HHC system for the S-76 which is more in the LHX weight category and speed regime than the aircraft in Reference 1. This program will reach major milestones of open loop flight testing in the fourth quarter of 1984 and closed loop testing in 1985. The extensive design analysis and risk reduction tests Sikorsky Aircraft has employed in the S-76 program will be discussed in this paper.

Sikorsky Aircraft has extensive interest and experience in HHC technology. References 2 and 3 present analytical HHC design studies on vibration reductions in the BLACK HAWK UH-60A and the Sikorsky ABC™. These efforts are described next.

The BLACK HAWK study (by Sikorsky and the United Technologies Research Center (UTRC)) projected 80-90 percent reduction in fuselage vibrations. Implementation requirements for an HHC system were also explored in Reference 2. For example it was projected that an HHC system would weigh roughly 1 percent of the BLACK HAWK design gross weight, compared to the 2.2 percent weight of the rotorhead bifilar absorber and the three other conventional absorbers in the current BLACK HAWK.

The U.S. Army is funding a preliminary design investigation to define a production HHC system for Army inventory aircraft (such as the BLACK HAWK and APACHE). The HHC design and its impact on the aircraft systems will be defined and a production solution suggested. This will take HHC into the 16-20,000 lbs, 160 knot regime.

In Reference 3 Sikorsky Aircraft conducted a preliminary design study on the use of HHC for the ABC™. This included the definition of the higher harmonic control required to reduce vibrations as well as the method and hardware to input this control. It was projected that a 90 percent reduction in vibration was feasible with relatively small amplitudes of HHC input (½ to 2 degrees) at flight speeds up to 300 knots. The design study considered blade and pushrod loads, as well as the actuation and control system capabilities and its integration into the aircraft systems. A primary conclusion of this study was that blade and control loads could be accommodated in the detailed design phase and that no fatal flaw was obvious for system integration. This study provided information for applications of HHC to a counter-rotating aircraft at very high speed in the 12000 lb range of gross weight. The added mechanical challenge of the two coaxial rotors is perhaps a drawback, but the potential cancellation of upper and lower rotor forces in 3 of the 6 degrees of freedom is beneficial. In any event, the design experience and risk identification forthcoming from the HHC application to the ABC™ provided valuable training aspect to Sikorsky Aircraft in future HHC applications. A detailed program has been laid out for HHC on the ABC™.

Vibration Characteristics of the S-76

The S-76 is a modern medium size helicopter used mostly in the commercial market for VIP transport and offshore oil missions. For both these missions the ride quality in the cockpit and cabin is extremely good. This four bladed rotor system is designed to minimize the 4P (19.5 Hz at 100% NR) vibration in conjunction with rotating system 3P and 5P inplane bifilar absorbers with cycloidal tuning bushings. The ride quality in the forward cockpit is further enhanced by the use of a variable tuned fixed system vibration absorber. Reference 4 discusses the details of the dynamic design. The self tuning nature of the bifilars and the nose absorber allow for rotor speed operation over a 11 percent range to optimize mission performance. While this system works well, it requires 2.75% of the design gross weight. The goal of 1% weight factor with an active self adaptive controller - lumped into a existing fly by wire (FBW) computer - is thus attractive. Additionally, while the self tuning features of the current system allow for rotor speed variations to optimize performance, a much larger range of operating speed changes can be accommodated with HHC. This is especially important for military applications.

Analytical Study

The analytical study was conducted for basically three reasons: 1) to demonstrate the effectiveness of HHC on the S-76 in cruise at an airspeed of 145 knots; 2) to define the design requirements of HHC; and 3) to support subsequent ground and flight tests. Both open and closed loop cases were considered in this study with emphasis on the open loop analysis so as to identify design require-

ments and provide response sensivities to HHC inputs. While the closed loop study for the S-76 has been of a preliminary nature, analytical results in References 2 and 5 show that closed loop algorithms can be used to reduce vibration in an aircraft with gross weight in the 8000 - 16000 lbs range. All open and closed loop analytical results obtained to date indicate that HHC inputs of 2° or less are sufficient to reduce vibration in a helicopter at a cruise condition of 145 knots and 10000 lbs lift. Note that it is not necessary to completely eliminate 4P vibrations; what is required is excellent ride quality while maintaining acceptable blade loads. This implies that the vibrations need to be reduced only to a specified level. Open loop flight testing will establish this level and provide blade and control load derivatives coupled with performance and acoustic benefits (or detriments) to define the closed loop parameters.

The aeroelastic analysis used was G400 (Reference 6) a time history analysis. The S-76 fuselage was represented by modes derived from a NASTRAN analysis. The baseline absolute predicted values of the vibrations in the S-76 study are smaller than the flight results. Hence, the S-76 analytical results presented herein should be interpreted as representative of trends. The configuration studied was an S-76 operating at 145 knots and 10000 lbs lift. Vibration levels, pushrod loads, and blade bending moments were obtained from G400. It is possible that the analytical results can be improved by using fuselage modes derived from shake test results.

Open Loop

Open loop results were obtained from a parametric study involving 3P, 4P, and 5P blade pitch changes. The amplitude and phase of the HHC inputs were systematically varied to determine their effect on fuselage vibration, control loads, and blade vibratory moments.

Vibration The effect of the amplitude and phase of a pure 3P input on pilot vertical vibration is shown in Figure 1. The 3P input is expressed as a sine function $\theta_3 \sin(3\Psi + \Phi_3)$ where Φ_3 is the amplitude, Φ_3 is the phase, and Ψ the blade azimuth. Two contours are given in Figure 1, one for a 3P amplitude of 1° and the other for an amplitude of 2°. Note that the phase difference between adjacent data points in this figure is 30°. Because of the shape of the closed contour it is evident that the pilot vertical vibration varies nonlinearly with the 3P input. The results in this figure indicate that a 3P input with an amplitude of 2° and a phase of 115° will eliminate pilot vertical vibration.

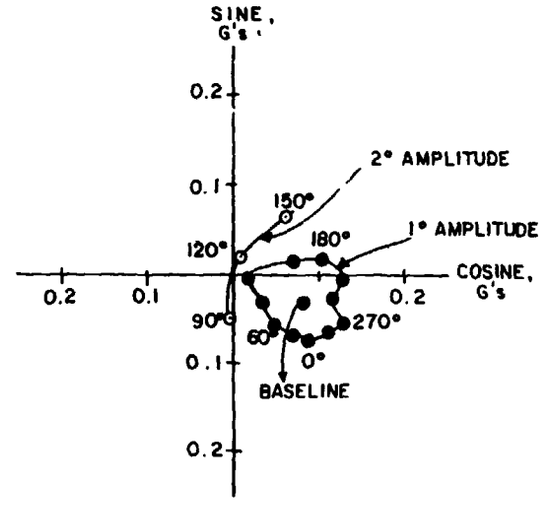

Figure 1. Pilot Vertical Vibration versus Phase and Amplitude of 3P Input

Figure 2 shows that a pure 4P open-loop input is less effective than the 3P input in reducing pilot vertical vibration. Even a properly phased 4P input would require more than 2° of amplitude to eliminate pilot vertical vibration. This suggests that the S-76 4P vibration is due more to 4P inplane loads that come from 3P and 5P rotating loads, and not the 4P vertical shear.

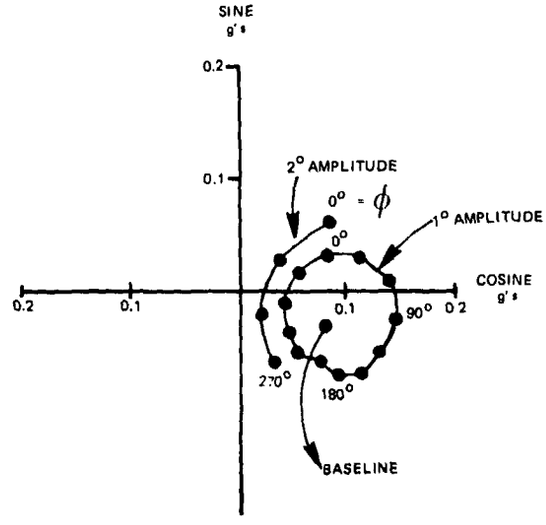

Figure 2. Pilot Vertical Vibration versus Phase and Amplitude of 4P Input

Note that the pilot vertical vibration variation with 4P HHC is less nonlinear than with 3P. Figure 3 shows the effect of a 4P input on cabin vertical vibration. A comparison of Figures 2 and 3 shows that a 4P input that reduces pilot vertical vibration increases cabin vertical vibration. This anomaly may be due to the phasing of rotor loads and fuselage modal cancellation and shows that pure 4P control would not be optimal. While these are open loop results with individual inputs, a closed loop controller would identify and implement the correct combinations of 3P, 4P, and 5P inputs and be able to accommodate such opposing trends by minimizing a specified performance index that includes vibration at several locations, if necessary.

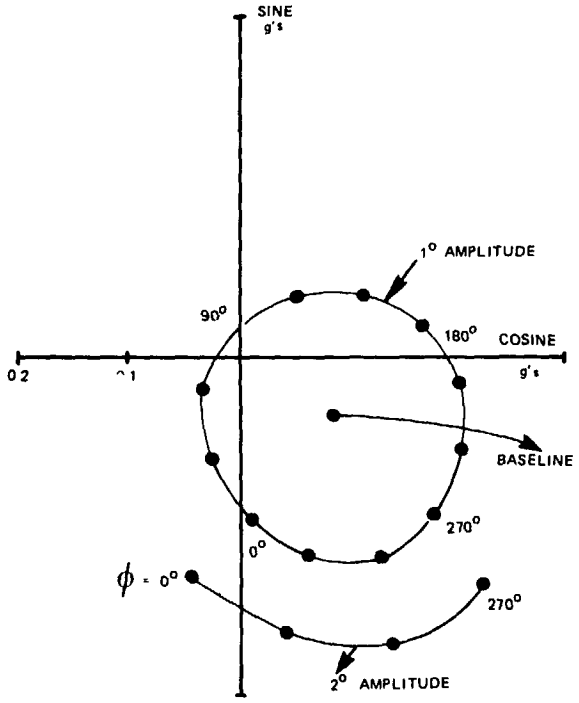

Figure 3. Cabin Vertical Vibration versus Phase and Amplitude of 4P Input

Figure 4 shows the effect of 5P control on pilot vertical vibration and indicates that the pilot vertical vibration variation with 5P control is not as nonlinear as with 3P. Further, a 5P input of 1.5° amplitude and 220° phase will virtually eliminate this vibration component.

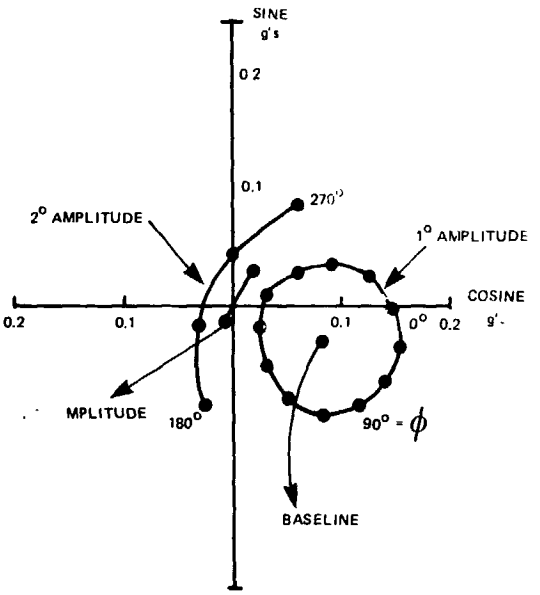

Figure 4. Pilot Vertical Vibration versus Phase and Amplitude of 5P Input

The above results indicate that an individual harmonic input can be used to reduce a particular component of vibration (e.g., pilot vertical) with various levels of effectiveness. The resultant vibration at other locations in the fuselage may or may not be lower due to the phasing of rotor loads and modal cancellation. In order to achieve overall vibration reduction throughout the fuselage, it may be necessary to prescribe multi-harmonic control inputs to reduce vibration at several sensor locations. Due to the interharmonic coupling effects between the three inputs and the intermodal cancellation effects in the airframe, the task of defining the amplitude and phase of each input to minimize overall vibration becomes complex. Therefore, this task will be accomplished by a self-adaptive controller algorithm used in a closed-loop system. However, open-loop flight testing will be used to verify trends as well as determine the sensitivity of vibration and loads to a matrix of inputs. Based upon the open-loop results presented herein it may be expected that for the S-76, 1.5° of 3P input will have a substantial effect on pilot vibration.

Pushrod Load and Bending Moments The maximum effect of a 1° open loop input on the pushrod load is shown in Figure 5. The figure shows that open loop higher harmonic control can increase the pushrod load. Though not shown here, a 2° 5P

input at a phase of 240° results in a half peak-to-peak pushrod load of 721 lbs which is close to the endurance limit of 755 lbs. Thus, the effect of control system fatigue damage due to HHC will have to be considered in the design stage.

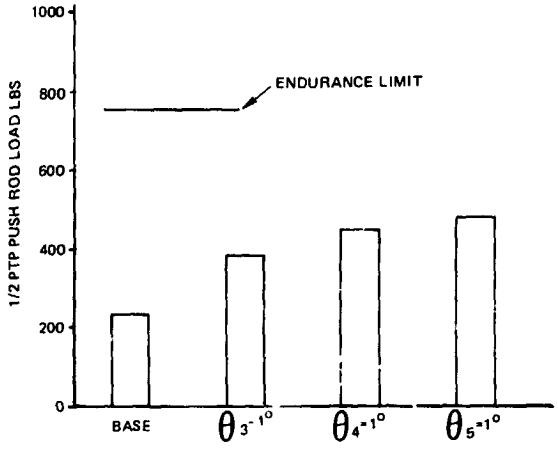

Figure 5. Increase in Pushrod Load due to 1° HHC Input

Figure 6 shows that the peak-to-peak flatwise and edgewise moments increase by about 20 percent due to 1° of higher harmonic input. A 2° 4P input causes approximately a 40% increase in the flatwise moment and a 2° 5P input results in a 55% increase in the edgewise moment (these increases were the maximum increases obtained for all the cases). Therefore, blade bending moment increases due to HHC are potentially signficant for higher amplitude control angles and will need to be considered. Open-loop testing combined with fatigue life calculations will determine the importance of these increases. A plan to incorporate blade and control loads into the closed loop controller so that vibration may be reduced with a minimum increase in blade loads is under consideration.

Closed Loop

Vibration The self-adaptive deterministic controller algorithm documented in Reference 5 was used in a preliminary analytical study of closed-loop control for the S-76. The flight condition investigated was a cruise condition at 145 knots and 10000 lbs of lift. The results of vibration reduction achieved by the closed-loop controller, when using equally weighted 3P, 4P, and 5P inputs to reduce vibration of six equally weighted components, is shown in Table 1. Reductions of at least 20 percent were achieved at all locations. Even larger reductions of 50

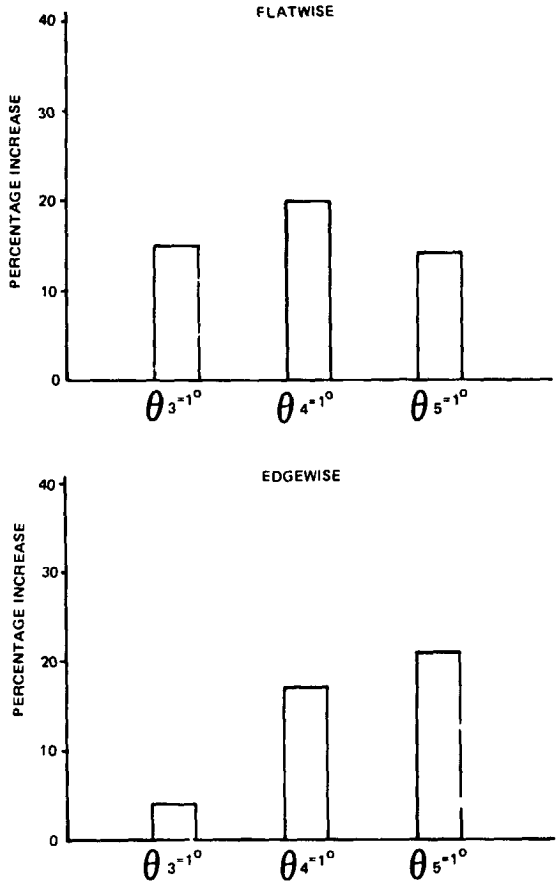

Figure 6. Percentage Increases in half Peak-to-Peak Blade Bending Moments due to 1° HHC Input

to 70 percent were achieved in the cabin vertical and pilot lateral components, respectively. These results can be improved by fine tuning the controller for the S-76. This involves weighting the importance of various vibration locations as well as the tailoring of the controller algorithm for identification and tracking.

Results from both References 2 and 5 suggest that very good controller performance can be achieved for the S-76 at forward flight speeds of 145 knots. In Reference 2, a similar deterministic control algorithm was evaluated in an analytical simulation of the BLACK HAWK at a speed of 150 knots and at gross weights of 13200 and 16500 lbs. Vibrations were calculated at components that directly correspond to those shown in Table 1 for the S-76. At both of these gross weights, reductions on the order of 90 percent were achieved in the pilot, copilot, and cabin

vertical components, while 50 percent reductions were obtained in the pilot lateral and longitudinal components The vibration reductions and the HHC inputs for the 16500 lbs case are shown in Figure 7. In Reference 5, the closed-loop controller algorithm was evaluated in an analytical simulation of the H-34 rotor mounted on the NASA/Ames rotor test apparatus (RTA) in the 40 x 80 wind tunnel. Forward flight conditions at 150 knots and rotor thrust levels of about 8000 and 12000 lbs were investigated. Reductions of the order of 75 to 95 percent were achieved, in vertical and longitudinal vibration components calculated at the nose, tail, and a main structural member corresponding to the cabin. The vibration reductions are shown in Figure 8. In both studies, the required amplitudes of 3P, 4P, and 5P control increased with rotor thrust, but were less than 1.0° for all rotor thrusts.

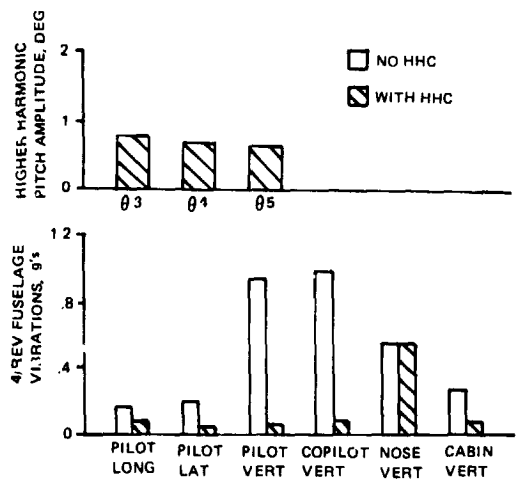

Figure 7. Effect of Closed Loop Control on Black Hawk Vibrations, 150 Kts, 16500 lbs.

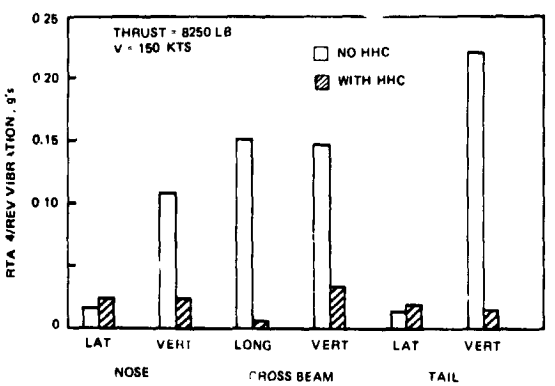

Figure 8. Effect of Active Control on Predicted 4P RTA Baseline Vibrations

The transient response of the deterministic controllers used in References 2 and 5 exhibited good behavior, since they were appropriately tuned for the particular aircraft investigated. For example, the time history of the performance index and higher harmonic control inputs for the H-34 study are shown in Figure 9, which is taken from Reference 5. The figure represents the transient behavior of the closed loop controller for an operating condition of 150 knots and 12000 lbs of thrust. Note that convergence to the final solution is smooth and the controller shows well-mannered behavior. The performance index is reduced by over 90 percent in only four rotor revolutions. This amounts to approximately one second in real time. Flight test results from Reference 1 indicate that such short time periods do not pose any problems to present state of the art controllers and computers which can operate within these time constraints.

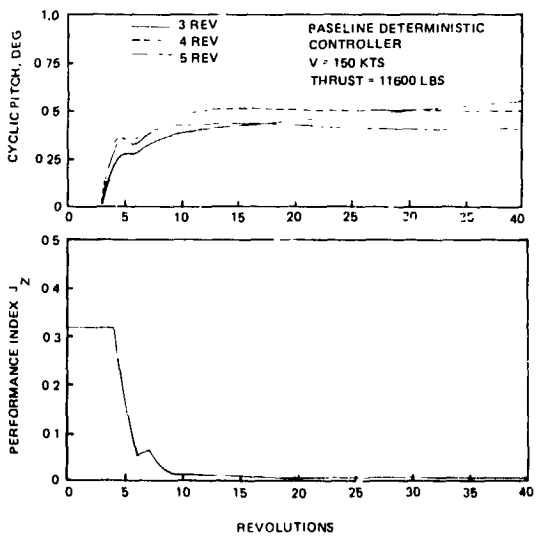

Figure 9. Time History of Vibration Controller

Pushrod Load and Bending Moments The half peak-to-peak S-76 pushrod loads for the closed loop cases are shown below:

Baseline	232 lbs
With HHC	486 lbs

Compared to the pushrod load, the bending moments were less sensitive to HHC inputs. The maximum change in the maximum bending moments, both flatwise and edgewise, were less than 5%.

If these increases are found to be significant with respect to the fatigue endurance limit, it may be possible to

TABLE 1
REDUCTION IN VIBRATION WITH HHC
Vibration g's (after 24 revolutions)

	Pilot Long.	Pilot Lat.	Pilot Vert.	Co-Pilot Vert	Nose Vert.	Cabin Vert.
Controller Off	0.078	0.053	0.082	0.029	0.033	0.116
Controller On	0.054	0.015	0.067	0.023	0.022	0.061
Percentage Reductions	30	70	20	20	30	50

achieve acceptable tradeoffs in vibration reduction and blade/control loads by incorporating parameters that are representative of these loads into the controller performance index. With appropriate weighting on vibration and load parameters, the controller would be guided to a better solution in terms of both considerations. Analytical results which indicate such an approach may be feasible are presented and discussed in Reference 5. For example, Figure 10 from Reference 5, shows the effect of arbitrarily eliminating 5P control, while reducing vibration at a 150 knot, 12000 lb thrust condition. When all three inputs are used, increases in blade moments result. When 5P control is eliminated, both flatwise and torsion moments are about the same as those with no HHC, while the increase in the edgewise moment is only 20 percent. Both sets of HHC control inputs resulted in about the same vibration reductions. If the change in control mix of amplitude and phase were less arbitrary, it may be possible to achieve acceptable vibration levels with minimal detrimental effects on other considerations.

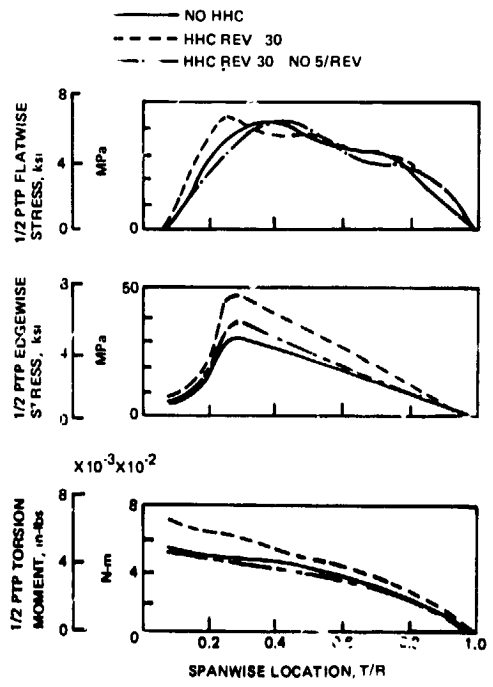

Figure 10. Effect of Active Vibration Control on Blade Vibratory Moments and Stresses, 150 Kts, 12000 lbs.

S-76 HHC Hardware Development Program

In 1981 an Independent Research and Development project was initiated to flight test an HHC system on the Sikorsky S-76. This effort is now in its final stages with open loop testing scheduled to take place in the last quarter of 1984 and closed loop testing planned for 1985. This project covers analytical studies, conceptual design, preliminary and detailed design, system risk reduction tests, system integration, and procurement and manufacture of HHC system components. Figure 11 shows an S-76 control system schematic with the HHC modifications added. Figure 12 shows the completed mechanical/electrical elements that are ready for flight.

Figure 11. Modified Control System of the S-76

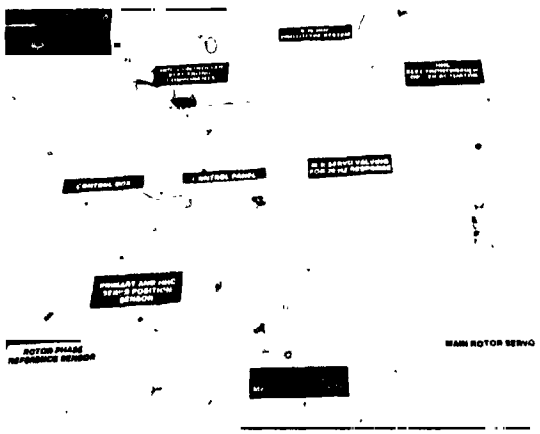

Figure 12. Mechanical and Electrical Elements of the HHC System

Philosophy

The principal design issues that have been identified include the frequency response of the main servos, frequency response of the HHC actuation system and controls, hydraulic power requirements, failure modes, rotor and control loads, and the hydraulic/mechanical implementation of the system on the S-76. The basic philosophy is to design and test a prototype system as "proof of concept" on an S-76 with minimum change to the aircraft. The program goal is to demonstrate HHC at 145 knots and 10000 lbs lift. The long term goal is to define design loads and issues for a production version of the HHC system. To accomplish these goals in a safe and logical manner, a risk reduction plan has been established (Table 2) to eliminate uncertainties in structural issues (blade loads, control loads) prior to flying open and closed loop. This risk reduction program, extending over a four year period, was based upon lessons learned at Sikorsky and Government/Industry published results.

Risk Reduction

The first risk reduction test was conducted in 1981 on the main servo to define its gain at 20 Hz which is approximately the 4P frequency at 100% NR. Modifications were made to the valving, shown in Figure 12, to improve this gain. Figure 13 shows the old and new gains where a significant increase in the gain at 20 Hz is attained, going from 0.50 to 0.75.

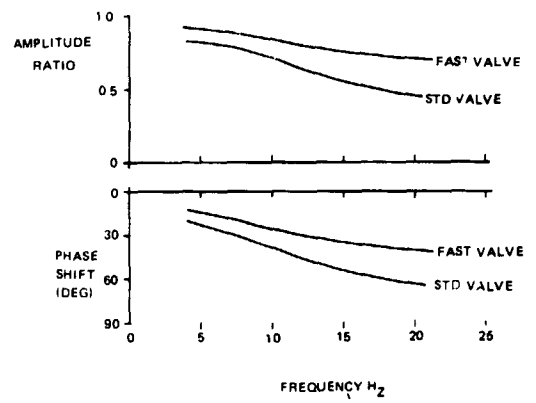

Figure 13. S-76 Primary Servo Frequency Response with higher Gain Valve

TABLE 2

RISK REDUCTION PLAN

	ISSUE	ACTION	DATE
1.	Adequate Servo Frequency Response	Change Valves and Test	1981
2.	Blade Pitch Response With Mechanical System	Conduct nonrotating Shake Test (Without Rotor Turning	1982
3.	Analytical Vibration Reduction	Analyze System (Need 1.5 Degrees)	1983
4.	Adverse Rotor Impedance	Conduct Rotating Ground Test	1994
5.	A/C Hydraulics Capable of Inputting Desired HHC	Conduct Rotating Ground Test	1984
6.	Open Loop HHC (Loads, Slop, Effectiveness)	Conduct Flight Test	1984
7.	Closed Loop Controller Functional Adequacy	Conduct Flight Test	1985

A second risk reduction 4P frequency response test was performed in 1982 on the entire S-76 HHC control system to define its dynamic response. In this test the rotor was stationary and the blades were lifted out of their drooped position to better represent their torsional dynamics. The result of this nonrotating test was that blade angles of 2° to 3° at 4P could be obtained with the present controls, hydraulics, and the modified higher gain servo. It is projected that on the S-76 about 2° of 4P input is required at high flight speed. Figure 14 shows the schematic of the test setup. Figure 15 shows the test results for various levels of 4P frequency input to the main rotor servo. As much as ±3° were output at the blade 75% radius station without exceeding pushrod endurance limit, and no problems were discovered in the rest of the system shown in Figure 14. This was very encouraging and implied that there is beneficial dynamic amplification taking place within the S-76 pitch control system. This testing reduced a big risk seen in OH-6A testing where high frequency control system deflections were excessive and blade response in pitch was inadequate.

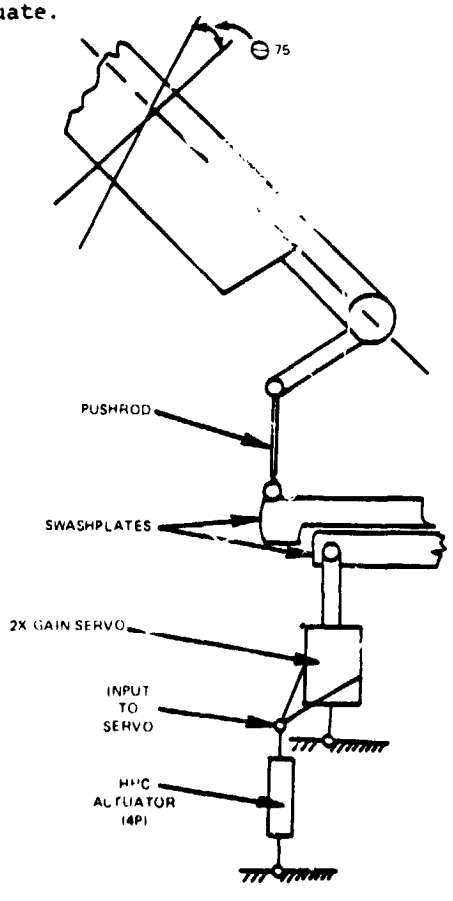

Figure 14. HHC Risk Reduction Test Setup

While this nonrotating frequency response test demonstrated that the S-76 control system bearing slop (free play) and flexibility do not attenuate the 4P input getting to the blade, the effect of rotation of the blades on rotor impedance is still a big question. The power and flow required to stroke the actuators, either collectively or cyclically, is obviously dependent on these "unknowns" which are difficult to calculate or simulate in a non-rotating test. Therefore as shown in Table 2 risk reduction tests will be performed prior to flight testing and include another ground test with the rotor turning so as to define pitch angles, flows, and hydraulic power required.

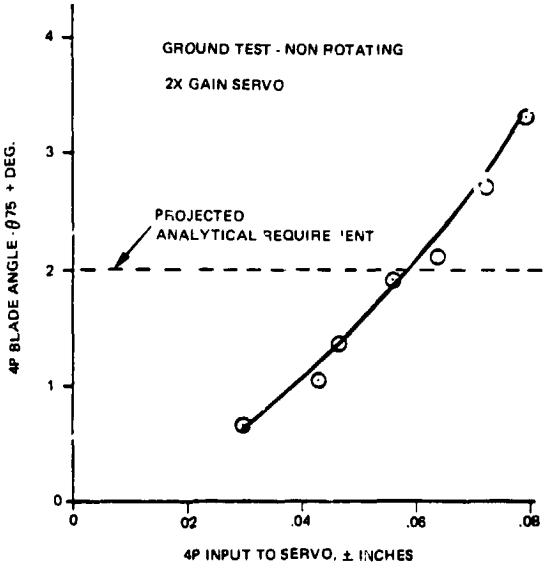

Figure 15. S-76 HHC Risk Reduction Test Results

Mechanical Design - Prototype

To perform this rotor turning ground test, inputs at 20 Hz would have to be made to the S-76 control system at an appropriate location. As shown in Figure 11 the HHC driver actuators are placed to excite the input side of the three main rotor servos. The HHC design is prototype in nature so that off the shelf driver actuators can be used. These are shown in Figure 12. Their stroke requirements are of the order of ±0.080" maximum at 20 Hz, and they are nominally limited in authority to ten percent of the main rotor servo stroke, which can be built-up incrementally to that value.

The placement of these driver actuators in the system as close as possible to the input of the main servo is to assure

that the high frequency vibratory inputs feed toward the rotor and not toward the pilot (the ratio of impedance is estimated to be 80 to 1). Since the S-76 has no pilot boost, the mechanical design relies on this principle. Figure 16 is a drawing of the prototype mechanical installation for the S-76. The design basically replaces the last control rod to each main rotor servo input with a shorter control rod, an idler bracket, and the driver actuator. This mechanical design is critical since it had to be completed in order to perform the next risk reduction test which is the crucial rotating rotor ground test to assure that there is no adverse rotor impedance, no hydraulic flow anomalies, and no problems of fit and function. Figure 17 shows the HHC mechanical parts.

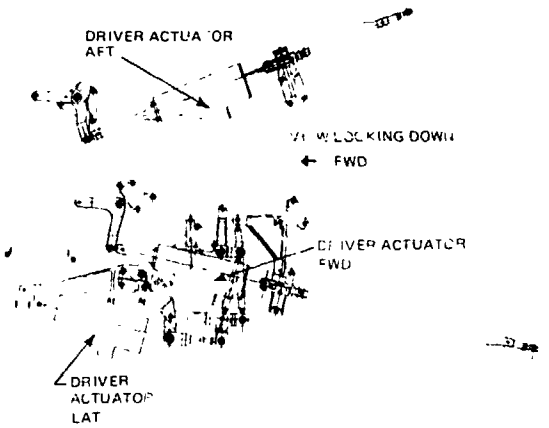

Figure 16. S-76 HHC Installation Drawing

Figure 17. S-76 Modified Mechanical Parts for HHC

Hydraulic Design - Prototype

In the S-76, hydraulic power is developed by the first and second stage hydraulic systems. These two hydraulically independent systems provide the power boost necessary to operate the flight controls. In addition, the second stage provides a utility system for operation of the landing gear and nose vibration absorber. The non-rotating test results in Figure 15 showed that flow requirements may be reduced by dynamic amplification within the pitch control system with the increased gain main rotor servo. With a maximum flow rate of 4 gpm for the S-76 and no dynamic amplification, vibratory amplitudes of ±0.030" are projected and this translates into about 1° of blade pitch at 4P. Since extensive modification would have been required to upgrade the hydraulic system in this "proof of concept HHC test" and because the non-rotating rotor ground test did show amplification through the system, it was decided to proceed to the next step in the risk reduction plan, i.e., a rotating rotor ground test with the existing S-76 hydraulics in order to get design information. The net weight increase due to the mechanical and hydraulic parts is approximately 35 lbs which is 0.35% of the design gross weight of the S-76. The total weight increase due to HHC is given in the subsection on open loop control in this paper.

Electronic Design - Prototype

The primary requirement of an HHC system is to improve ride quality by reducing vibration while maintaining acceptable loads during steady flight and maneuver conditions within the flight envelope. The HHC system is not flight critical and in case of failure, the system will be shut off.

The primary generic elements of a closed loop HHC system (Figure 18) can be identified as follows:

i) Sensors. These could be accelerometers for monitoring and reducing vibrations and strain gages for monitoring and optimizing blade, control, and hub loads.

ii) A flight-worthy microcomputer programmed with stable mathematical algorithms that provides optimal control inputs to reduce vibrations and loads based upon the state of the helicopter. This system must also be capable of performing adaptive computations, providing NP feathering signals in response to changes in the flight conditions, and limited self testing.

iii) An electronic control unit (ECU) may also be required, depending upon the HHC system design. The ECU may interface with other elements of the HHC system and perform functions such as extracting NP components from the accelerometer signals (Reference 1).

Note that the ECU may not be required in some designs if its functions are performed by other devices. An alternative design of the controller may contain all hardware necessary to communicate with the sensors and actuators as well as the self-adaptive control algorithms, self test, and failure mode protection functions. However, for purposes of understanding it may be better to identify an ECU and its functions. One important design issue is that it may be better to unload the computer to let it do pure processing. Functions such as signal generation and signal conditioning are best performed by an ECU.

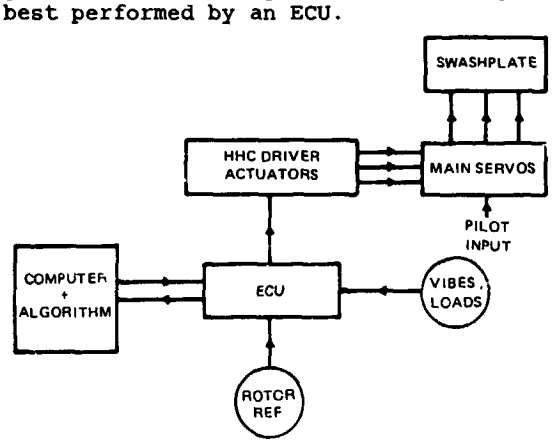

Figure 18. HHC Concept Diagram

Open Loop Control

Item 6 of Table 2 shows that open loop testing will follow the successful rotating ground test. This testing will allow an organized look at the effect of HHC amplitude and phase at several flight conditions to define the sensitivities of vibration, loads, performance, and acoustic changes. To this end a control and measuring system to define HHC inputs/outputs has been designed and fabricated and is shown in Figure 12. The net weight increase due to open loop electronic hardware is 40 lbs which is 0.40% of the S-76 design gross weight. This means that the total weight of the open loop HHC system is 75 lbs which is 0.75% of the design gross weight of the S-76 and is within the 1% target weight.

Production Issues

The present hydraulic and mechanical controls on the S-76 are designed and manufactured to MIL standards and FAA specifications. Any additional items due to HHC would be designed to the same standards with updated design loads derived from the prototype flight testing. Table 3 presents a list of the issues identified in past HHC designs and tests. Mechanical systems of future helicopters may be simplified by the use of FBW so that the potential of adverse vibratory effects in the control linkages may be minimized. The NP excitation to the blade pitch control system may be performed by one actuator with special provisions to preclude seal wear and leakage.

TABLE 3

HHC DESIGN ISSUES

1. Weight, Volume, and Overall Power
2. Hydraulic System Pressure and Flow Requirements
3. Modification of Existing Components
4. Actuator Placement and Frequency Response
5. Effects of Slop, Hysteresis and Control Flexibility
6. Mechanical Feedback to Pilot Stick
7. Structural Loads in Components
8. Fail Safety and Need for Redundancy
9. Available Travel in the Controls
10. Mission Effectiveness and Reliability
11. System Cost
12. Maintenance
13. Survivability
14. Development Risks

The electronic system reliability can be enhanced by embedding interface hardware and the microprocessor in a single line replaceable unit, interconnecting sensors with fiber optic links wherever possible, and incorporating self test features into the sensors.

Extensive self test capabilities will

ease maintenance of the HHC electronic system. Faults detected in flight could be allocated a specific code and could be stored in non-volatile memory for later recall by maintenance personnel via a built-in-test (BIT) code display and code advance switch. Preflight tests may be initiated by toggling a ground test switch. Detected faults will be stored and displayed in the same manner as flight BIT's. Maintenance can also be eased by breaking of electronic units into modules and bread boards.

Plans

At the time of writing this paper a major portion of the groundwork of analysis, testing and fabrication of system prototype parts, and bench testing has been accomplished. Detailed testing will be performed to address the following issues:

1. Reduction in cockpit and cabin NP vibrations for the following flight conditions:
   - steady state cruise
   - turns and maneuvers
   - low speed maneuvers
   - rotor speed changes
   - gusts
   - mission profiles for simulated LHX.
2. Effect of HHC on blade and control loads.
3. Trade off in loads/life and acceptable vibration reduction for good unintrusive ride quality for the crew and vibratory environment for weapons sensors, equipment, avionics, etc.
4. Hydraulic power, flow, fluid temperature.
5. Mechanical control function, wear, slop, and seal life.
6. Acoustics
7. Aerodynamic performance.
8. Reliability and maintainability of HHC parts and the aircraft system.
9. Electronic controller gains, time constants, update time, algorithm optimization, and potential preprogramming of the controller.

Concluding Remarks

Analytical evaluation of HHC for the S-76 aircraft (8-10,000 lb, 145 knots) indicates 1°-2° for HHC will be required.

It is expected that reasonable blade loads and control loads can be maintained by including them into the self adaptive controller algorithm.

Hardware test results to date demonstrate that the S-76 HHC system can provide the required one to two degrees input at the blades with a reasonable weight increase.

The S-76 will be ready for flight evaluation of HHC after successful risk reduction tests of the actuator and the control system. These tests are based on industry and government work and "lessons learned".

Production implementation efforts have been initiated at Sikorsky Aircraft on mechanical, hydraulic, electronic, and computer fronts to integrate HHC into designs from the beginning as mature systems. U.S. Army programs to install production HHC systems on its fleet of latest generation aircraft will make HHC successful in the long term when combined with prototype design/test programs such as those for the S-76 and OH-6A.

REFERENCES

1. Wood, E.R., Powers, R.W., Cline, J.H., and Hammond, C.E. "On Developing and Flight Testing A Higher Harmonic Control System," Presented at the 39th Annual Forum of the American Helicopter Society, St. Louis, Missouri, May 1983. Also, "HHC Program Review" by Hughes Helicopter, Inc., May 10, 1984, Mesa, Arizona.
2. Taylor, R.B., Zwicke, P.E., Gold, P. and Miao, W., "Analytical Design and Evaluation of an Active Control System for Helicopter Vibration Reduction and Gust Response Alleviation," NASA CR 152377, July 1980.
3. O'Leary, J. and Miao, W., "Design of Higher Harmonic Control for the ABC ," Presented at the American Helicopter Society National Specialists' Meeting on "Rotor System Design", October 1980, Philadelphia, Pennsylvania.
4. Niebanck, C. Girvan, W., "Sikorsky S-76 Analysis, Design and Development for Successful Dynamic Characteristics" Presented at 34th Annual Forum of the American Helicopter Society, Washington, D.C., May 1979.
5. Davis, M.W. "Refinement and Evalua-

tion of Helicopter Real-Time Self-Adaptive Active Vibration Controller Algorithms," NASA CR 3821, September 1984.

6. Bielawa, R.L., "Aeroelastic Analysis for Helicopter Rotor Blades with Time-Variable, Nonlinear Structural Redundancy - Mathematical Derivation and User's Manual", NASA CR-2638, October 1976.

7. Molusis, J.A., Hammond, C.E., Cline, J.H., "A Unified Approach to the Optimal Design of Adaptive and Grain Scheduled Controllers to Achieve Minimum Helicopter Vibrations," Proceedings of the 37th Annual Forum of the American Helicopter Society, New Orleans, LA., May 1981.

8. Davis, M.W., "Documentation for a Generic Active Controller," United Technologies Research Center Report R83-95614917, November 1983.

DISCUSSION
Paper No. 23

ADAPTION OF A MODERN MEDIUM HELICOPTER (SIKORSKY S-76) TO HIGHER HARMONIC CONTROL
James J. O'Leary
Dr. Sesi B. R. Kottapalli
and
Mark Davis

Walter Gerstenberger, Consultant: Could you introduce this added control in the regular autopilot servo?

Kottapalli: It's a parallel arrangement. We did not introduce [it] in the autopilot system.

Gerstenberger: Why not put it in series?

Kottapalli: We did not want to affect the safety of the control system.

Gerstenberger: The autopilot doesn't, it's limited authority.

Kottapalli: That's right, but we did not want to tamper with anything in the primary control system. The autopilot is limited authority, but it's a very low frequency type of system, and what we're talking about here is 20 Hertz.

Gerstenberger: Okay, it's what you say, I'll have to listen to it.

Jing Yen, Bell Helicopter: I have two questions for you. Number one, I understand the higher harmonic control [is] for the 4 per rev. The magnitudes we've been talking about are 1/2 degree and 1/4 degree. Here you show 1 and 2 degrees.

Kottapalli: Yes.

Yen: So you are very confident that these would be the magnitude you would need?

Kottapalli: That's right. Actually we are talking about something like 1-1/2 degrees, and we are hoping that we could do with one degree only. We don't want to perturb the system too much. One philosophy that we have is that we need not reduce the vibration to zero level. What we want is a comfortable ride quality. So that's our outlook. We could live with some residual vibration. Let's say you go from .45 g's to .03 g's--you may not even perceive anything at .03 g's. You may be able to live with something higher than that.

Yen: Does your higher harmonic control requirement vary with the air speed? I understand that you are aiming at the high speed end.

Kottapalli: That's right; that's the primary condition we're looking for, and it does vary somewhat. In any case, all of them would be less than 2 degrees or 1-1/2 degrees.

Yen: How about the low speed transition?

Kottapalli: Low speed transition? We did not conduct any studies on that. I guess we're most interested in the cruise condition. The primary program goal was to have something that works at the cruise speed of the S-76, but I would expect that it would vary at low speeds.

Bob Wood, Hughes Helicopters: I was interested in your talk, Sesi, and of course we were following it with great interest. I just wrote down some numbers and thought you might be interested in them. When you go to doing your open loop testing, of course, HHC can make the ship rougher as well as smoother.

Kottapalli: Yes, we are aware of that.

Wood: I scaled up with our OH-6--we were .7 g's with a third of a degree, so if you went to 3 degrees we would have been at 6.3 g's. If you allow for the fact that you're four times our gross weight you will be at 1.7 g's, so just be careful with that amplitude when you are flying open loop.

Kottapalli: Yes. You are absolutely right. What we intend to do is conduct a phase sweep, let's say, with the lateral tilt of the swash plate and go from zero to 360 degrees. Most likely, for some values of the phase, we are going to increase the vibration. We are looking for the other values of the phase where we reduce the vibration. Yes, that is a very important point and we have had to tell our flight test people about that so that they don't get nervous.

EVALUATION OF A LOAD CELL MODEL FOR DYNAMIC CALIBRATION OF THE ROTOR SYSTEMS RESEARCH AIRCRAFT

R. W. Du Val and M. Bahrami
Advanced Rotorcraft Technology, Inc.
Los Altos, California

B. Wellman
Aeromechanics Laboratory,
U.S. Army Research & Technology Laboratories (AVSCOM)
NASA Ames Research Center
Moffett Field, California

Abstract

The Rotor Systems Research Aircraft uses load cells to isolate the rotor/transmission system from the fuselage. An analytical model of the relationship between applied rotor loads and the resulting load cell measurements is derived by applying a force-and-moment balance to the isolated rotor/transmission system. The model is then used to estimate the applied loads from measured load cell data, as obtained from a ground-based shake test. Using nominal design values for the parameters, the estimation errors, for the case of lateral forcing, were shown to be on the order of the sensor measurement noise in all but the roll axis. An unmodeled external load appears to be the source of the error in this axis.

Introduction

The Rotor Systems Research Aircraft (RSRA) has a set of seven load cells connecting the main rotor transmission to the fuselage. Their purpose is to make high-accuracy measurements of the net rotor loads, as resolved at the rotor hub, from flight data (Ref. 1). The use of these load cells to estimate applied rotor forces and moments at the hub requires an accurate mathematical expression relating rotor loads, inertial loads, and load cell readings. Both the structure and parameters of this model must be specified. Previous approaches to processing ground-test data have not yielded an acceptably accurate relationship. This is particularly true for the case of applied high frequency dynamic loads. This paper describes a new approach to obtaining the relationship, and presents the results of a preliminary evaluation of the resulting model from experimental data.

Nomenclature

A,B,C,D,E,F,G	= individual load cell outputs (Fig. A1)
a	= linear acceleration at C.G.
b	= position of C.G. from shaft attach point
d	= longitudinal distance between vertical load cell attach points
$E\{\ \}$	= expected value operator
e	= lateral offset of forward lateral load cell from centerline
e_H	= error in estimate of applied hub loads
f	= lateral offset of aft lateral load cell from centerline
H	= vector of six applied hub loads
$\hat{H}$	= estimates of applied hub loads
h	= position of hub from C.G.
I	= moment of inertia about C.G.
J	= vector of six inertial loads
l	= position of C.G. from aft load cell attach points
M	= mass matrix
m	= effective mass of rotor/transmission/engine system
N_s	= number of samples

n	= index of measurement samples
p,q,r	= rotational rates about x,y,z axes
Q	= covariance of measurement noise
Q_t	= total applied engine and tail rotor drive torques
R	= transformation matrix for hub loads
S	= transformation matrix for load cells
T	= vector of seven load cell measurements
w	= lateral distance between vertical load cell attach points
X,Y,Z,L,M,N	= force and moment components (Fig. A2)
Γ	= gyroscopic coupling coefficients
Θ	= set of unknown parameters
$\bar{\Theta}$	= a priori estimate of parameters
$\hat{\Theta}$	= post-calibration estimate of parameters
ν	= measurement noise
ϕ,θ,ψ	= load cell deformation angles about x, y, and z axes, respectively
ω	= frequency

Subscripts

A	= accelerometer
a,b,c,d,e,f,g	= attach point of each load cell
C	= total load
H	= hub load
I	= inertial load
m	= measured data
T	= load cell
x,y,z	= component for x,y,z axis

Background

Previous Methods

The initial attempt to determine the load cell response to the applied rotor loads involved applying static loads at the hub and measuring the resulting load cell response. A least-squares regression approach was used to identify a coefficient matrix relating the seven load cells to the six hub loads. A six element bias vector was also estimated. It was found (Ref. 2) that the coefficient matrix varied as a function of the applied multiple axis load. This indicates a nonlinear dependence of the load cell response to the applied rotor loads, and would require a polynomial expansion of the multi-input multi-output relationship to characterize it in terms of constant parameters.

The next calibration was a ground-based shake test in which a pair of inertial shakers were mounted on the rotor hub to apply dynamic loads at specified amplitudes and frequencies. During this experiment, the RSRA was suspended from the hub so the static loading was the same for all tests. As a result, the nonlinear variation of the relationship with static loads observed in the static test should not be present in the shake test. The Force Determination Method (Ref. 3) was utilized to estimate applied rotor loads from a variety of sensors around the aircraft. This method first identifies the transfer functions between the applied rotor loads and sensors at various points on the aircraft, then identifies the applied rotor load from a least squares fit to the transfer functions and measured sensor responses. The results were unacceptable because the identified transfer functions varied with the magnitude of the applied load; hence, they could not be used to estimate the applied load without a more extensive calibration procedure. Since there was only one static load condition, it appears that this nonlinearity is due to a different mechanism than the nonlinearity observed in the static tests.

Proposed Metho

Since the sensors utilized in the Force Determination Method (FDM) included numerous accelerometers and strain gauges mounted on the fuselage, transfer functions of these sensors will be affected by any nonlinear dynamic behavior in the fuselage. This effect complicates the use of fuselage sensors to determine applied rotor loads. The RSRA was designed to use load cells to isolate applied loads from diffrerent sources, such as the main rotor, tail rotor, engine, and wings. The

proposed approach takes advantage of this concept by treating the rotor transmission as an isolated system with externally applied loads from the load cells and the rotor (Fig. 1). The applied rotor loads are then measured from a force-and-moment balance using measured load cell loads (T) and inertial loads (J) as derived from transmission acceleration measurements. In order to utilize this approach, a model is required that relates applied external loads on the rotor/transmission system to the resulting forces and moments at the center of mass of the system. This model is derived analytically from physical principles, using the known geometry of the rotor/transmission system. Parameters with potentially uncertain values in this model are explicitly represented to provide the capability to calibrate the model.

The advantages of this approach predominantly arise from the physical insight obtained in using an analytically derived model. With such a model, sensitivity analysis and physical judgment can be used to select the most appropriate set of available parameters for calibration. Consequently, fewer parameters need be calibrated than when no physical insight is used. In addition, the parameters to be calibrated now have a physical interpretation so that the validity of the calibration results may be assessed. The model should initially be derived to be as simple as possible. If it cannot adequately explain the observed experimental behavior with a physically reasonable set of parameter values, it may be expanded to include additional effects, as required. It is important that all major effects be identified and incorporated into the model before calibration of the parameters is attempted, or the parameter values will compensate for the unmodeled effects as best they can and achieve physically unrealistic values in the process.

Objective and Approach

The objective of this study is to derive a simple dynamic model of the isolated rotor transmission system and test its accuracy with experimental data.

The approach is first to derive a simple model of the rotor transmission system, treating it as a linear, rigid, isolated body. Known or assumed values are used for all parameters of the derived model. The model is then applied to test data to determine its accuracy. If it appears that calibration can further improve the accuracy, the appropriate parameter set will be selected and calibrated. If the accuracy appears limited by an unmodeled effect, the model will be expanded to evaluate potential sources of the unmodeled effect.

Rotor/Transmission Model

The arrangement of the load cells below the rotor/transmission system is shown in Fig. 2. A detailed description of this system, including all inertia contributions, is given in Ref. 2. There are seven load cells; four are mounted vertically at the corners of the transmission mounting plate, two are mounted laterally at the fore and aft edges of the mounting plate, and one is mounted longitudinally at the forward edge of the mounting plate. An inertial load vector, J, is located at the center of gravity of the rotor/transmission system, and the applied rotor load vector (H) is located at the rotor hub (Fig. 3). The rotor hub is located at the end of the rotor shaft which is tilted forward at an angle of 2°. The load cells are connected to the transmission and the fuselage by spherical bearings.

The proposed approach is to estimate the applied hub loads from a force-and-moment balance of the external loads and the inertial loads. In order to accomplish this, all externally applied loads must be transformed to the center of mass where the inertial loads act. By treating the rotor/transmission as an isolated system, the load cell forces are considered a measured, externally applied load on the system. A 6 x 7 matrix (S) is derived that transforms the seven load cell loads (T) at their attach points to a set of six load components at the center of mass. A 6 x 6 matrix (R) is derived that transforms the applied rotor load (H) at the hub to the center of mass. An inertial load (J) at the center of mass is derived from measured accelerations and assumed inertial parameters. Using the derived matrices, a force-and-moment balance at the center of mass results in a set of six simultaneous equations which may be written in matrix form as:

$$J + S \cdot T + R \cdot H = 0 \qquad (1)$$

A detailed description of these vectors and matrices are given in Appendix A.

The assumptions used in deriving the matrices and Eq. (1) are that the rotor/transmission system is a rigid body and that there is no friction in the load cell bearings. These assumptions were made to simplify the initial approach. Both nonrigid body effects and friction in the load cell bearings could be added to

the model in order to match the experimental data if that appears to be required.

The transformation matrices S and R and the inertial load vector J were all derived to explicitly contain all potentially uncertain parameters of the system, so that any subset of parameters can be selected for calibration. The parameters defined in the model are:

a) All distances and angles required to define the resultant moment arm from the center of mass to load application points.

b) All angles and magnitudes required to define load cell load components acting on the rotor/transmission system.

c) All mass properties required to determine inertial loads from measured rates and accelerations.

Test Conditions

Having derived a model, the next step is to evaluate it with experimental data. Both static and dynamic ground test data are available. The dynamic data generated by the shake test were chosen since they would provide a more rigorous test of the model structure than would the static test data. The dynamic data are not, however, suitable for testing the calibration procedure. This is because the same static load condition exists for all dynamic tests, and parameter variations are mostly dependent on variations in the static loading. Once the model structure has been validated with the dynamic data, the model can be applied to the static test data to evaluate the calibration procedure.

The test datum selected was a frequency sweep from 15 to 18.5 Hz in the y-axis applied rotor load (lateral force). This frequency range was chosen because it contains the N/rev frequency, and identification of applied rotor loads at this frequency is of special interest. The lateral forcing was chosen because previous tests have shown the poorest results with y-axis forcing, so it would provide the most rigorous test. Transfer function data were generated from the raw test data by a harmonic analyzer for four levels of applied load. Equation (1) was then used to generate the applied load estimate from the transfer function data. Equation (1) was processed with all of the model parameters set to assumed nominal values.

Error Analysis

Total Estimation Error

In a controlled ground test environment, the actual values of the applied rotor loads are known so the total error in the estimate can be readily obtained. Given the measured load cell readings, Tm, and inertial loads derived from accelerometer measurements, Jm, Eq. (1) may be used to estimate the applied rotor loads as:

$$H = -R^{-1} \cdot [Jm + S \cdot Tm] \qquad (2)$$

The total error in the estimate is obtained by subtracting the known values of applied rotor load from the estimate of Eq. (2) to get:

$$e_H = H - H = -R^{-1} \cdot [Jm + S \cdot Tm] - H \qquad (3)$$

$$e_H = -R^{-1} \cdot [Jm + S \cdot Tm + R \cdot H]$$

The available shake test data were in the form of transfer functions that had been generated from the raw data by a harmonic analyzer. In order to utilize these data with the proposed model, it was necessary to transform the model to the frequency domain and write it in terms of the transfer functions. Transforming Eq. (3) to the frequency domain gives:

$$e_H(\omega) = -R^{-1} \cdot [Jm[\omega) + S \cdot Tm(\omega) + R \cdot H(\omega)] \qquad (4)$$

If only a y-axis rotor load, Hy(ω), is applied, Eq. (4) may be written in terms of the transfer functions as:

$$e_H(\omega) = -R^{-1} \cdot [(Jm(\omega)/Hy(\omega)) + S \cdot (Tm(\omega)/Hy(\omega)) + R] \cdot Hy(\omega) \qquad (5)$$

where $Jm(\omega)/Hy(\omega)$ and $Tm(\omega)/Hy(\omega)$ are vectors of transfer functions of the inertial and load cell loads with respect to the y-axis rotor load. Equation (5) is used to evaluate the total error in the estimate using the available transfer function data.

Numerous potential sources of error are present in this system. The evaluation procedure is to examine the total error and attempt to categorize it into the potential sources. Once identified, the sources would be modeled and included in the system. Most of the error will probably be attributable to one of five sources:

A) Systematic errors in data collection.

B) Unmodeled static and dynamic effects.

C) Unmodeled external loads.

D) Random errors in sensors.

E) Incorrect parameter values.

Systematic Errors in Data Collection

One source of error is the use of transfer function data. Since this is treated as raw data in this study, any errors in the identification of the transfer functions would propagate through the proposed approach. The recorded time domain data should be reprocessed by the harmonic analyzer to provide only Fourier transformed data, not transfer functions.

Angular accelerometers and rate gyros were not available on the rotor transmission system for the shake test. Since there is no way to obtain all such data, the approach taken is to assume it is negligible and see how the estimates compare with this assumption. Some justification for this assumption comes from comparing the response of the two linear accelerometers mounted on the transmission with a 2-ft vertical displacement between them. The difference in the y-axis components divided by the vertical displacement should give the roll axis angular acceleration. The average value of this derived roll acceleration over the frequency range for an applied load of 800 lb was found to be 0.09 rad/sec/sec, supporting the low angular acceleration assumption. The derived angular acceleration data was not used with the model because the errors in the linear accelerometers are such that the accuracy of the derived angular acceleration is 0.6 rad/sec/sec. The derived values are therefore in the noise level. The angular acceleration affects the translational equations since the linear accelerometer is not mounted at the center of mass and will, therefore, be affected by angular accelerations. The moment equations are affected since the angular inertial loads are dependent on the angular accelerations. The errors associated with neglecting a 0.09 rad/sec/sec roll angular acceleration are 12 lb in the y-force and 27 ft-lb in the rolling moment so the assumption appears justified.

Unmodeled Static and Dynamic Effects

The model derived for this study was kept deliberately simple to facilitate the analysis. It can be expanded if necessary to account for the observed error. Unmodeled effects with potentially significant impact on the model include friction in the load cell bearings, flexibility in the rotor/transmission system and nonlinearity in the dynamic response to applied loads. The nature of the error signal should suggest which of these effects are present. Friction and deadbands will be characterized by hysteresis in the response. This effect is more readily observed in static data than in dynamic data. Flexibility will show up as a resonance at some frequency and will result in a phase and amplitude shift between the input and output signals. Nonlinear dynamics will be readily detected by a frequency shift between the input and output data. Static nonlinearities result in parameter variations and are corrected by calibration rather than by expanding the model.

Random Errors in Sensors

Both load cells and accelerometers have measurement noise that produces a lower bound on the accuracy of the applied load estimates. It is possible to obtain accuracies below this limit, but this requires the use of statistical processing techniques such as Kalman Filtering and Smoothing. This effect can certainly not be reduced by any modifications to the model. The effect of accelerometer and load cell noise on the applied rotor load estimate is derived in Appendix B and used to generate the errors given in Table I. These numbers were based on the assumption of independent random errors for each sensor with accuracies of 1% of full scale for the accelerometers and 0.1% of full scale for the load cells.

Unmodeled External Loads

The derived model will be in error if all externally applied loads are not included. If the levels are low, then this can be the most difficult source of error to identify. This is because it can take on virtually any characteristics and will blend in with other error sources. The only possibility for detecting this type of error is if it is sufficiently large that it cannot be logically explained by any of the other error

sources. Once the presence of an unmodeled load is suspected, the error data may assist in isolating its source, but a thorough examination of the test conditions is usually required to resolve this effect.

Incorrect Parameter Values

once the model structure has been validated to the fullest extent possible, the remaining errors should be due only to incorrect values for the parameters. At this point, calibration may be applied to reduce this error source. If calibration is attempted before the model structure is adequately determined, the parameters will take on whatever values are required to compensate for the model structure errors. This will result in physically unrealistic values for the parameters and could, in fact, be a test for whether the model structure is accurate.

The conventional approach to calibration has been to apply least-squares minimization of the error with respect to the parameters to be calibrated. Since the parameters are now imbedded in a model, the least-squares minimization of the error must be done subject to the constraint that the model equations are satisfied. This is refered to as a constrained least-squares approach (Ref. 4) and the algorithm is derived in Appendix C for the constraint of Eq. (1).

Since the available data are in the frequency domain, the calibration must be performed in the frequency domain. This is actually an advantage since the frequency domain transformation has concentrated information for the required frequency range into fewer data points than required for a time domain representation. Calibration may then be performed with fewer data in the frequency domain. The least-squares minimization may be applied to frequency domain data in the same way as it is applied to time domain data (Ref. 5). The only modification is that the data are organized with the real and imaginary parts stacked end to end rather than using the data in complex form. This insures that the identified parameter values will not be complex.

Results

Equation (3) was applied to transfer function data for the load cells and the main rotor gear box accelerometers to generate the estimation error of the derived model in the frequency domain. Assumed, nominal values, based on aircraft design specifications, were used for all parameters in the model. Figures 4 and 5 show the magnitude of the transfer function data for the seven load cells and two accelerometers for an 800 lb y-axis excitation. The location of the load cells may be seen by finding the correspondingly labeled load cell in Fig. 2. The accelerometer transfer functions have been multiplied by the system mass to produce inertial loads. The strong coupling in the system is apparent from the large vertical load cell values for a y-axis excitation. The strong correlation in the z-axis is particularly apparent from the sudden drop in z-axis acceleration at the same frequency (16.6 Hz) where two vertical load cells (A and B) suddenly assume equal and opposite values.

Figures 6 through 11 show the error in the model, as defined by Eq. (3), using nominal parameter values. Table I shows the average error over the frequency range as compared to the accuracy limit set by the instrumentation noise. With the exception of applied rolling moment, the average error shown in Table I and the frequency plots shown in Figs. 6-11 demonstrate that the rigid body model of the isolated rotor transmission system produces applied load estimates with error levels comparable to the instrumentation noise level.

The pronounced roll moment error (Fig. 9) is too great to be explained by parameter errors, sensor errors, or angular accelerations. The demonstrated lack of significant angular accelerations about the roll axis indicates that it is not due to a nonrigid body effect. It can also be seen that there is no frequency shift (the hump at 16.6 Hz in the error signal matches the hump in the load cell data at that frequency) so the error is not a nonlinear function of the modeled variables. The only remaining explanation is that the error is due to an unmodeled external load with predominant effect in the roll axis. A potential candidate for the source of this load is the drive train since it would affect only the roll moment. Measurements of the shaft torques from the engine and the tail rotor are required to verify this and could be used to compensate for this effect.

Nominal parameter values produce estimation errors on the order of the instrumentation noise level in all but the roll axis, and the roll axis error is too great to be explained by parameter uncertainties; therefore, calibration is not needed to improve the accuracy in five axes and would not help in the sixth. The source of unknown roll axis loading must be determined and modeled before the model can be used for roll moment estimation.

Conclusions

An analytically derived model with nominal parameter values has been used to estimate applied rotor loads from measured load cell and accelerometer data. This approach has also provided a check on the consistency of measured input/output data. The presence of an unmodeled external load was detected in the roll axis and its source is being investigated.

The following conclusions are drawn from this work:

For the y-axis case, an analytically derived linear, rigid body model of the isolated rotor/transmission system with nominal parameter values performs well in all but the roll axis.

Nonrigid body effects or nonlinear behavior cannot explain the roll moment error. The error must be due to an externally applied, unmodeled load.

Calibration is unnecessary for this case since improved parameter estimates will not improve the estimation error further. The estimation error in all but the roll axis is already in the noise level and the error in the roll axis is too great to be logically explained by different parameter values.

Recommendations for Further Research

The following recommendations are made:

Apply the model to data generated by excitation in other axes to validate it under a broader range of conditions and to further isolate the source of the unmodeled load. This analysis should be backed up by a follow-on physical error source analysis.

Apply the model to static test data to evaluate the calibration technique. Nominal parameter values have done surprisingly well in allowing accurate hub load estimation for the specific static load condition present in the dynamic data. Static test experience suggests that this will not be true under all static load conditions. Once the model structure is fully validated it should be applied to static test data to determine which parameters to calibrate and to determine the range of variation of the parameters through calibration.

Appendix A: Load Cell Model Derivation

A diagram of the undeformed load cell geometry is shown in Fig. A1. The load cells are mounted to the fuselage and to the transmission base by spherical bearings. It is assumed that the transmission base does not warp, so all changes in the load cell geometry are due to deformations in the load cells themselves or in the fuselage mounting points. With this assumption it is possible to completely model the load cell response using a general three-component representation of the reaction force at each attach point on the transmission base; no knowledge of the fuselage deformation is required.

Three plane views of the load cell geometry with the three-component reaction force representation are shown in Fig. A2. Inertial loads, including gravity and the drive shaft torque, are assumed to be concentrated at the transmission center of gravity. The rotor loads are concentrated at the hub. Taking the sum of the forces and moments about the center of gravity gives:

$$X_C = X_I + X_H + G_x + E_x + F_x + A_x + B_x + C_x + D_x = 0$$

$$Y_C = Y_I + Y_H + G_y + E_y + F_y + A_y + B_y + C_y + D_y = 0$$

$$Z_C = Z_I + Z_H + G_z + E_z + F_z + A_z + B_z + C_z + D_z = 0$$

$$L_C = L_I + L_H + Y_H \cdot h_z + (A_z + D_z) \cdot w/2 \; E_z \cdot e - (B_z + C_z) \cdot w/2 + F_z \cdot f - (B_y + C_y + F_y + G_y + E_y + A_y + D_y) \cdot b_z = 0$$

$$M_C = M_I + M_H - X_H \cdot h_z - Z_H \cdot h_x - (B_z + A_z + E_z + G_z) \cdot (d - 1) + (C_x + D_x + F_x + B_x + A_x + E_x + G_x) \cdot b_z + (C_z + D_z + F_z) \cdot 1 = 0$$

$$N_C = N_I + N_H + (A_y + E_y + G_y + B_y) \cdot (d - 1) - (C_y + F_y + D_y) \cdot 1 - (A_x + D_x) \cdot w/2 - E_x \cdot e + (C_x + B_x) \cdot w/2 - F_x \cdot f + Y_H \cdot h_x = 0 \quad (A1)$$

Using the transformations:

$$A_x = A \cos(\phi_a)\sin(\theta_a)$$
$$A_y = -A \sin(\phi_a)$$
$$A_z = A \cos(\phi_a)\cos(\theta_a)$$
$$B_x = B \cos(\phi_b)\sin(\theta_b)$$
$$B_y = -B \sin(\phi_b)$$
$$B_z = B \cos(\phi_b)\cos(\theta_b)$$
$$C_x = C \cos(\phi_c)\sin(\theta_c)$$
$$C_y = -C \sin(\phi_c)$$
$$C_z = C \cos(\phi_c)\cos(\theta_c)$$
$$D_x = D \cos(\phi_d)\sin(\theta_d)$$
$$D_y = -D \sin(\phi_d) \quad (A2)$$
$$D_z = D \cos(\phi_d)\cos(\theta_d)$$
$$E_x = -E \cos(\phi_e)\sin(\psi_e)$$
$$E_y = E \cos(\phi_e)\cos(\psi_e)$$
$$E_z = E \sin(\phi_e)$$
$$F_x = F \cos(\phi_f)\sin(\psi_f)$$
$$F_y = -F \cos(\phi_f)\cos(\psi_f)$$
$$F_z = -F \sin(\phi_f)$$
$$G_x = G \cos(\theta_g)\cos(\psi_g)$$
$$G_y = G \cos(\theta_g)\sin(\psi_g)$$
$$G_z = -G \sin(\theta_g)$$

the equations become

$$J + R \cdot H + S \cdot T = 0 \quad (A3)$$

where:

$$J' = [X_I, Y_I, Z_I, L_I, M_I, N_I] \quad (A4)$$

and

$$\begin{bmatrix} X_I \\ Y_I \\ Z_I \\ L_I \\ M_I \\ N_I \end{bmatrix} = \begin{bmatrix} -m_x \cdot a_x \\ -m_y \cdot a_y + \Gamma_y \cdot q \\ -m_z \cdot a_z \\ -Ix \cdot p + Qt + \Gamma_L \cdot q \\ -Iy \cdot q + \Gamma_M \cdot p \\ -Iz \cdot r \end{bmatrix} \quad (A5)$$

In Eq. (A5), a_x, a_y, and a_z are linear accelerations in each direction measured at the rotor/transmission system center of gravity, and p, q, and r are rotational accelerations. Because of the nonrigid engine mountings, the engine contributions to inertial forces are not equal in all directions when measured at the system center of gravity. This effect can be adequately modeled by assigning different values to the total effective mass of the combined rotor/transmission/engine system in each direction: m_x, m_y, and m_z. There are also a few minor error terms not given here that are discussed fully in Ref. 2. Ix, Iy, and Iz are moments of inertia; related terms in the cross-products of rotational rates are negligible. Qt is total applied engine and tail rotor shaft torque. Gyroscopic coupling forces due to engine and transmission rotational moments of momentum are represented by the coefficients Γ, with subscripts for the appropriate axis. The hub forces (H) and load cell readings (T) in Eq. (A3) are given by:

$$H' = [X_H, Y_H, Z_H, L_H, M_H, N_H] \quad (A6)$$

$$T' = [A, B, C, D, E, F, G] \quad (A7)$$

The geometric transformations from the applied loads to the center of mass (R and S) are given by:

$$R = \begin{bmatrix} 1 & 0 & 0 & 0 & 0 & 0 \\ 0 & 1 & 0 & 0 & 0 & 0 \\ 0 & 0 & 1 & 0 & 0 & 0 \\ 0 & h_z & 0 & 1 & 0 & 0 \\ -h_z & 0 & -h_x & & 1 & 0 \\ & h_x & 0 & 0 & 0 & 1 \end{bmatrix} \quad (A8)$$

and

$$S = \begin{bmatrix} C\phi aS\theta a & C\phi bS\theta b & C\phi cS\theta c & C\phi dS\theta d & -C\phi eS\psi e & -C\phi fS\psi f & C\phi gC\psi g \\ -S\phi a & -S\phi b & -S\phi c & -S\phi d & C\phi eC\psi e & C\phi fC\psi f & C\phi gS\psi g \\ C\phi aC\theta a & C\phi bC\theta b & C\phi cC\theta c & C\phi dC\theta d & S\phi e & S\phi f & -3\theta g \\ w/2C\phi aC\theta a & bzS\phi b & bzS\phi c & bzS\phi d & -eS\phi e & -fS\phi f & -bzC\phi gS\psi g \\ +bzS\phi a & -w/2C\phi bc\theta b & -w/2C\phi cC\theta c & +w/2C\phi dC\theta d & -bzC\phi eC\psi e & +bzC\phi fC\psi f & \\ bzC\phi aS\theta a & bzC\phi bS\theta b & bzC\phi cS\theta c & bzC\phi dS\theta d & -bzC\phi eS\psi e & +bzC\phi fS\psi f & bzC\theta gC\psi g \\ -(d-1)C\phi aC\theta a & -(d-1)C\phi bC\theta b & +1C\phi cC\theta c & +1C\phi dC\theta d & -(d-1)S\phi e & +1S\phi f & +(d-1)S\theta g \\ -w/2C\phi aC\theta a & w/2C\phi bS\theta b & 1S\phi c & 1S\phi d & -eC\phi eS\psi e & +1C\phi fC\psi f & (d-1)C\theta gS\psi g \\ -(d-1)S\phi a & -(d-1)S\phi b & +w/2C\phi cS\theta c & -w/2C\phi dS\theta d & +(d-1)C\phi eC\psi e & -fC\phi fS\psi & \end{bmatrix} \quad (A9)$$

where C and S denote cosine and sine functions, respectively

Appendix B: The Effect of Sensor Noise on Load Estimation

The analytical model of the rotor/transmission system derived in the text has the form:

$$J + S \cdot T + R \cdot H = 0 \quad (B1)$$

Given the measured load cell readings, Tm, and inertial loads derived from accelerometer measurements, Jm, the applied rotor loads, H, are estimated from Eq. (B1) as:

$$H = -R^{-1} \cdot [Jm + S \cdot Tm] \quad (B2)$$

The measured load cell and accelerometer values may be written in terms of their true values and a random measurement noise component as follows.

$$am = a + \nu_A , \qquad \nu_A = N(0,Q_A) \quad (B3)$$

$$Tm = T + \nu_T , \qquad \nu_T = N(0,Q_T) \quad (B4)$$

Writing the derived inertial load vector, Jm, as the product of an inertia matrix, M, and the accelerometer measurements, am, gives

$$Jm = M \cdot am = M \cdot a + M \cdot \nu_A = J + M \cdot \nu_A \quad (B5)$$

where J is the actual inertial load vector.

Substituting Eqs. (B4) and (B5) into Eq. (B2) gives:

$$H = -R^{-1} \cdot [J + S \cdot T] + \nu_H \quad (B6)$$

where

$$\nu_H = -R^{-1} \cdot [M \cdot \nu_A + S \cdot \nu_T] \quad (B7)$$

Substituting Eq. (B1) into Eq. (B6) then gives:

$$H = H + \nu_H , \qquad \nu_H = N(0,Q_H) \quad (B8)$$

From Eq. (B8) it is seen that ν_H, as given by Eq. (B7), is the combined effect of the instrumentation errors on the applied rotor load estimate, H. This error represents a lower bound on the accuracy of the estimation that is attainable without applying statistical processing, such as Kalman filtering or smoothing. The covariance of this error, Q_H, may be computed from Eq. (B7) using the known covariance of the instrumentation errors, Q_A and Q_T, as follows.

$$Q_H = E\{\nu_H \nu_H'\}$$

$$= E\{[-R^{-1} \cdot (M \cdot \nu_A + S \cdot \nu_T)] \cdot [-R^{-1} \cdot (M \cdot \nu_A + S \cdot \nu_T)]'\} \quad (B9)$$

$$Q_H = R^{-1} \cdot M \cdot E\{\nu_A \nu_A'\} \cdot M' \cdot (R^{-1})' + S \cdot E\{\nu_T \nu_A'\} \cdot M' \cdot (R^{-1})' + R^{-1} \cdot M \cdot E\{\nu_A \nu_A'\} \cdot M' \cdot (R^{-1})' + S \cdot E\{\nu_T \nu_A'\} \cdot M' \cdot (R^{-1})' + R^{-1} \cdot M \cdot E\{\nu_A \nu_T'\} \cdot S' \cdot (R^{-1})' + R^{-1} \cdot S \cdot E\{\nu_T \nu_T'\} \cdot S' \cdot (R^{-1})' \quad (B10)$$

The sensor noise components are assumed independent so the term $E[v_A v_T]$ is zero. Substituting the known covariance matrices of the sensors for the other expected value terms gives:

$$Q_H = R^{-1} \cdot [M \quad Q_A \cdot M' + S \cdot Q_T \cdot S'] \cdot (R^{-1})' \quad (B11)$$

Appendix C: Calibration Algorithm

The applied rotor load estimation error is given by Eq. (3) in the text as:

$$e_H = \cdot^{1} \cdot [Jm + S \cdot Tm + R \cdot H] \quad (C1)$$

The coefficient matrices, R and S contain geometric parameters of the model and the derived inertial loads vector, Jm, include inertial parameters of the model. A subset, θ, of the parameters is selected for calibration and the error is treated as a function of those parameters. A cost function is written in the form:

$$V(\theta) = 1/2 \cdot \sum_{n=1}^{N_s} e_H(\theta,n)' \cdot W^{-1} \cdot e_H(\theta,n) \quad (C2)$$

where W is a weighting matrix given by:

$$W = 1/N_s \cdot \sum_{n=1}^{N_s} e_H(\theta,n) \cdot e_H(\theta,n)' \quad (C3)$$

Expanding the first partial of V with respect to the parameter set θ about their nominal values of $\bar{\theta}$ gives:

$$\partial V(\hat{\theta})/\partial\theta = \partial V(\bar{\theta})/\partial\theta + (\hat{\theta} - \bar{\theta}) \cdot \partial^2 V(\bar{\theta})/\partial\theta^2 \quad (C4)$$

Setting the desired value at $\hat{\theta}$ to zero, corresponding to an extremum, gives:

$$\hat{\theta} = \bar{\theta} - (\partial^2 V(\bar{\theta})/\partial\theta^2)^{-1} \cdot (\partial V(\bar{\theta})/\partial\theta)' \quad (C5)$$

Taking the first partial of V with respect to θ gives:

$$\partial V(\bar{\theta})/\partial\theta = \sum_{n=1}^{N_s} e_H(\bar{\theta},n)' \cdot W^{-1} \cdot \partial e_H(\bar{\theta},n)/\partial\theta \quad (C6)$$

The second partial, to first order, is then:

$$\partial^2 V(\bar{\theta})/\partial\theta^2 = \sum_{n=1}^{N_s} (\partial e_H(\bar{\theta},n)/\partial\theta)' \cdot W^{-1} \cdot (\partial e_H(\bar{\theta},n)/\partial\theta) \quad (C7)$$

Once the parameter set has been chosen, the partial derivative of the errors, e_H, with respect to the parameters must be generated analytically from Eq. (C1). the parameter estimates are then obtained from Eqs. (C5) to (C7) using the measurement error sequence, e_H, generated by Eq. (C1).

References

1. Burks, J. S., "Rotor Systems Research Aircraft (RSRA) Rotor Force and Moment Measurement System," AIAA First Flight Test Conference, Las Vegas, Nev., Nov. 1981.

2. Acree, C. W., "Results of the First Complete Static Calibration of the RSRA Rotor Load Measurement System," NASA TP-2327, 1984.

3. Giansante, N., Berman, A., Flannely, W. G., and Nagy, E. J., "Structural System Identification Technology Verification," USAAVRADCOM Report No. TR-81-D-28, Nov. 1981.

4. Bryson, A. E., Jr., and Ho, Y. C., Applied Optimal Control, Blaisdell Publishing Co., Waltham, Mass., 1969.

5. Du Val, R. W., "The Use of Frequency Methods in Rotorcraft System Identification," AIAA Paper 81-2386, AIAA 1st Flight Testing Conference, Las Vegas, Nev., Nov. 1981.

C-5

Table I

Load	Estimation error				Instrumentation noise		
	200 lb	400 lb	600 lb	800 lb	Total	Load cells	Accelerometers
X	84	76	173	214	309	25	308
Y	10	25	35	96	312	35	308
Z	12	17	28	39	312	50	308
L	592	1648	1772	2477	446	179	408
M	27	17	24	47	436	143	412
N	84	76	173	214	81	61	54

Load cell full scale = 25,000 lb, error = 0.1%
Accelerometer full scale = 7 G's, error = 1%
Mass = 4400 lb

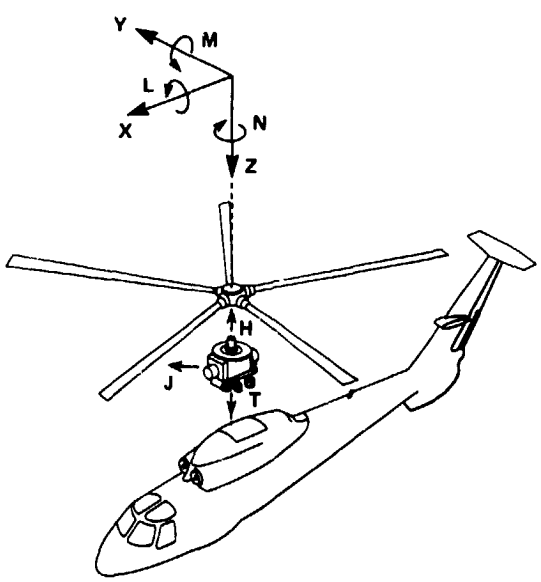

Fig. 1 Loads acting on isolated rotor/transmission system.

MAIN ROTOR LOAD MEASUREMENT SYSTEM

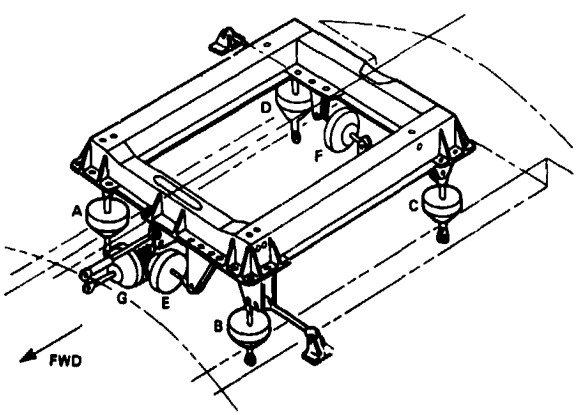

Fig. 2 Load cell arrangement for rotor/transmission system.

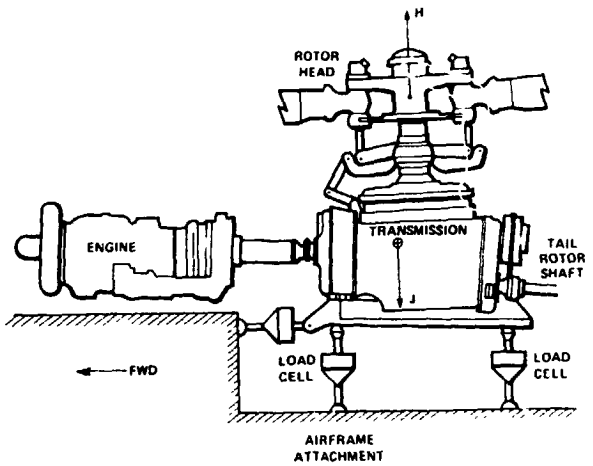

Fig. 3 Rotor/transmission system.

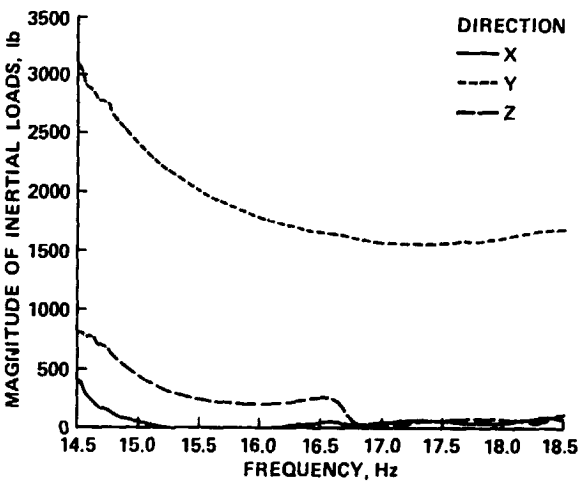

Fig. 5 Magnitude of inertial load transfer functions for 800 lb. applied lateral force.

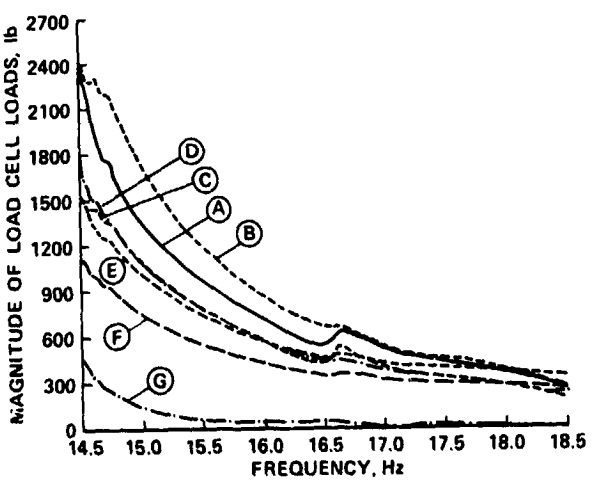

Fig. 4 Magnitude of load cell transfer functions for 800 lb. applied lateral force.

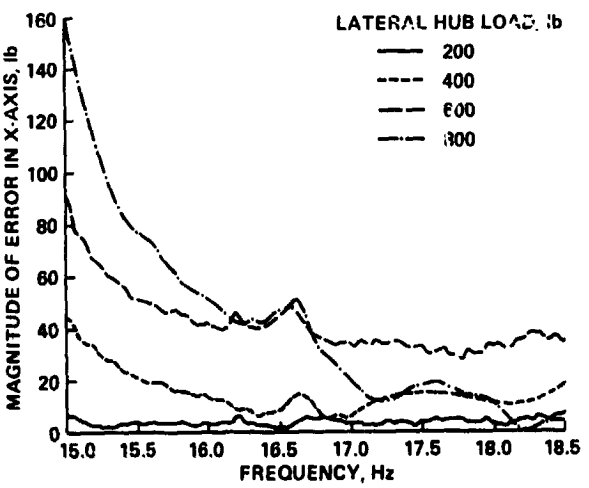

Fig. 6 Magnitude of x-axis applied force estimation error.

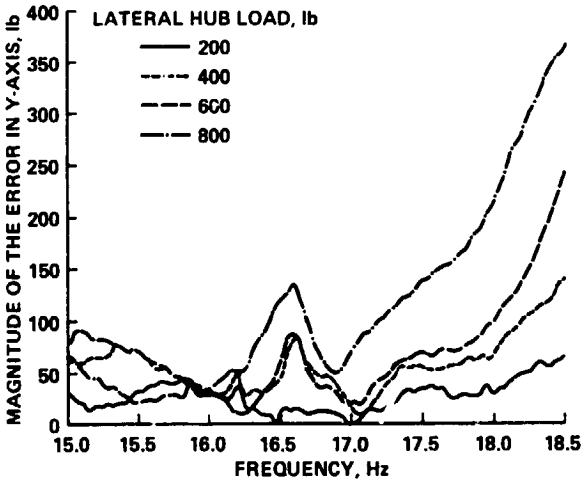

Fig. 7 Magnitude of y-axis applied force estimation error.

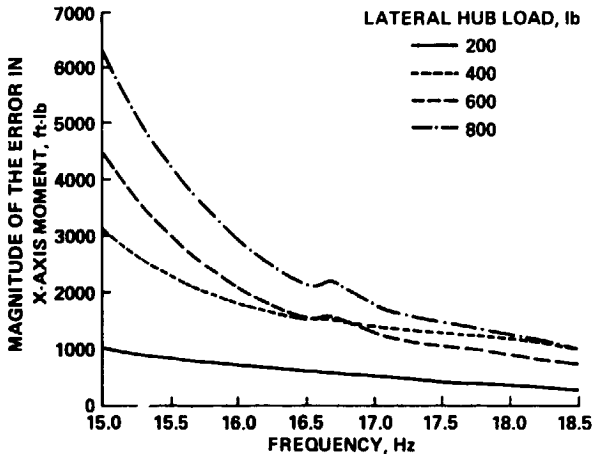

Fig. 9 Magnitude of x-axis applied moment estimation error.

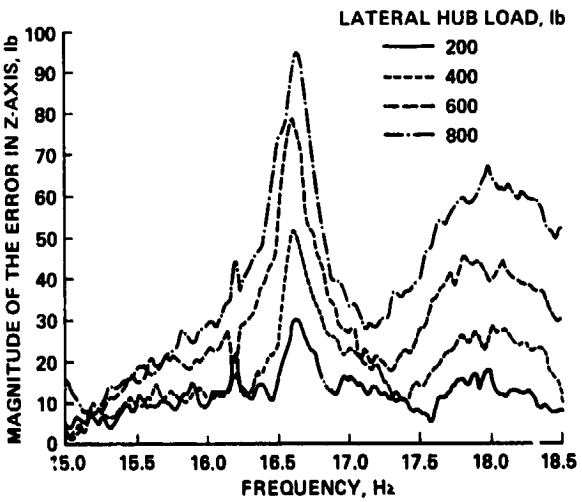

Fig. 8 Magnitude of z-axis applied force estimation error.

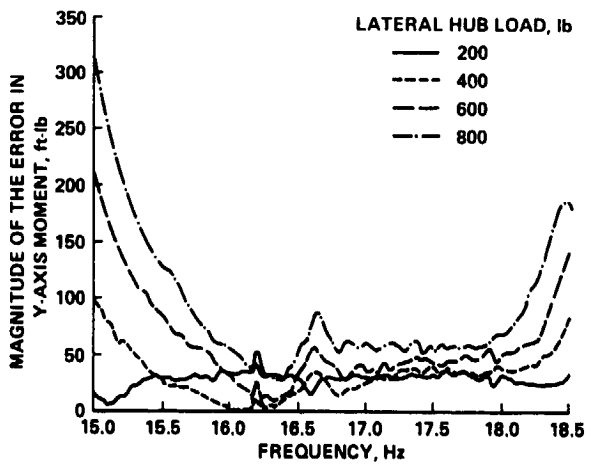

Fig. 10 Magnitude of y-axis applied moment estimation error.

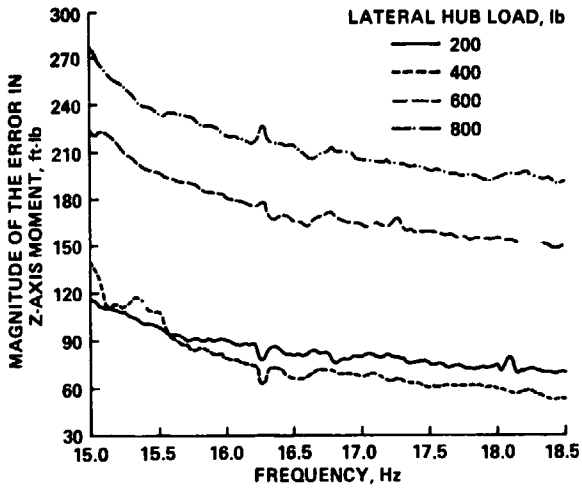

Fig. 11 Magnitude of z-axis applied moment estimation error.

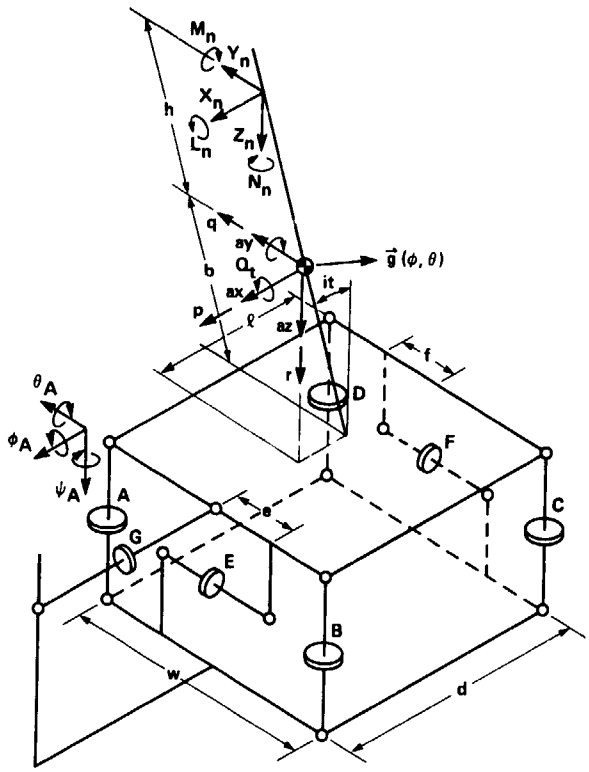

Fig. A1 Undeformed load cell geometry.

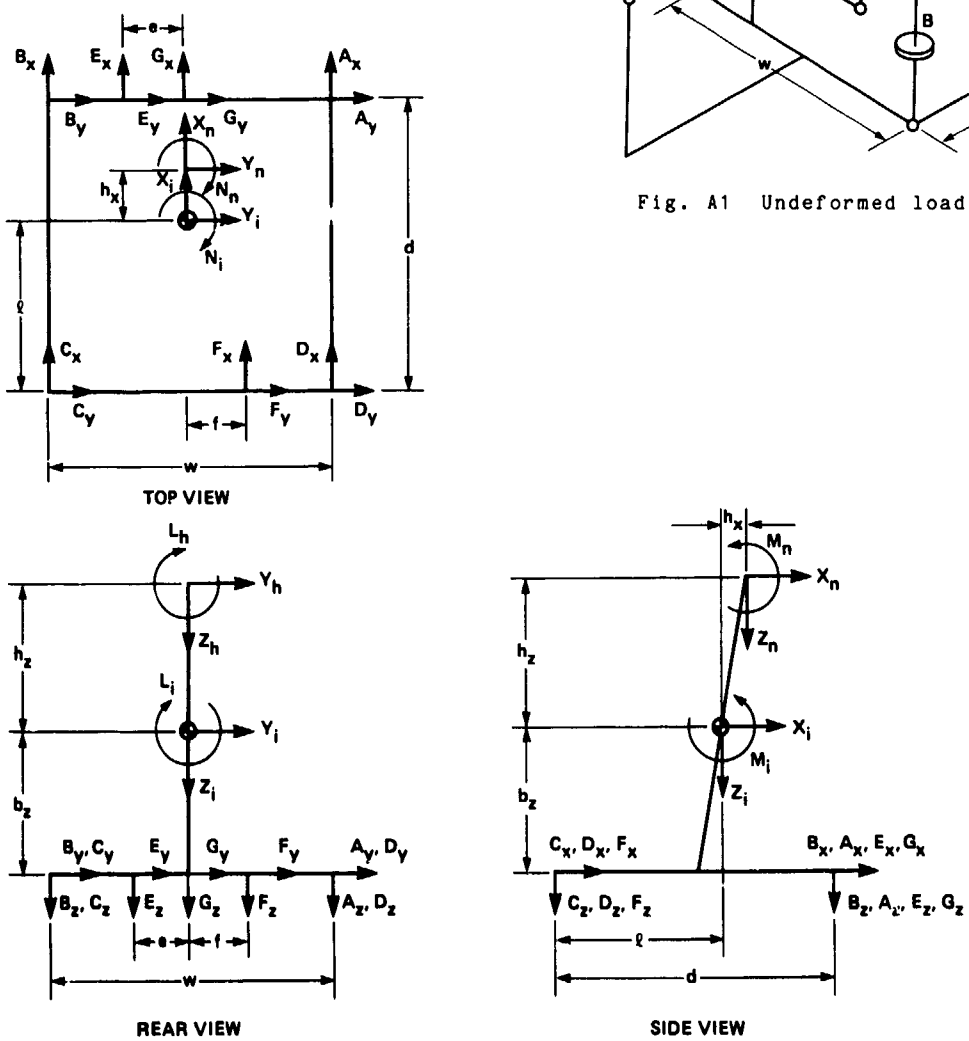

Fig. A2 Load cell geometry with generalized reaction force components.

DISCUSSION
Paper No. 24

EVALUATION OF A LOAD CELL MODEL FOR DYNAMIC CALIBRATION OF THE ROTOR SYSTEM RESEARCH AIRCRAFT
R. W. Du Val
M. Bahrami
and
B. Wellman

Charlie Fredrickson, Sikorsky Aircraft: I'd like to thank you for your paper and for mentioning the drive train and its possible impact on rotor loading, transmission loading, etc. One effect that you may not have modeled seems to be kind of glaring and looking at the analytical model in your paper was the engine. I see the engine kind of cantilevered off the transmission [or] the drive shaft and I am sure that is not the way it is supported. If it does have a longitudinal restraint to the airframe that may account for part of the modeling error that you may not have accounted for.

Du Val: Yes, in fact the way the engine is mounted is that there are swivel mounts in a universal joint that should prevent any longitudinal restraint on the engine. Now just how well those are working is another question.

Dev Banerjee, Hughes Helicopters: Ron, a very logical and systematic modeling approach to identifying the model of the transmission mount. When you get to correlating the test results with your analytical model, I presume you would include the noise characteristics into your error function. How do you intend putting in the covariance of the noise of the load cell? [How do you] intend to find it?

Du Val: That basically was done analytically. Since we have a covariance for the load cells and for the accelerometers we can use our analytical model to determine what the resulting covariance would be in the estimation of the hub loads, using those assumed covariances for the sensor data, and in fact that is the way we arrived at the noise level lines that we put on the charts.

PANEL ONE--PRACTICAL DYNAMICS PROBLEM SOLVING EXPERIENCES

PANEL MEMBERS

Richard Gabel, Chairman	Manager, Dynamics Technology Boeing Vertol Company
Wen-Liu Miao	Chief, Dynamics Sikorsky Aircraft
James Neff	Aeromechanics Staff Engineer Hughes Helicopters, Inc.
Rod W. Balke	Chief, Structural Dynamics Bell Helicopter Textron Incorporated
Robert Jones	Assistant Director for Aeromechanics Kaman Aerospace Corporation

OPENING COMMENTS

Richard Gabel
Manager, Dynamics Technology
Boeing Vertol Company

Thank you, for those who stayed on. I think the audience has dwindled a little bit this morning. But you're all going to be pleased that you did I'm sure. Nearly everyone who gave a paper in the past two days opened with some introduction--how the helicopter suffers from various instabilities, vibration, and high loads. It is a wonder if any of them are ever sold by all the negative news that comes out of you dynamicists. And yet they prosper and grow each year. The credit must go to a small, but valiant few who stand together and hold back the tide of management panic. Such as, "How do we fix No. 17? It's sitting on the ramp shaking and the pilot refuses to fly it. What do we do?" Or, "The gyro is vibrating and it's holding up delivery. Do something!" Or, "That yellow blade keeps going out of track and nobody can fix it!" To that group of stalwart souls we dedicate this panel.

Now you are privileged to be let in on a few of their problem solving secrets. First, two of us will give you some information about aircraft vibration experiences. And two of us will talk to you about engine vibration experiences. And one of us will tell you about rotor development experiences. Then each speaker will handle a few questions on his topic and after we're all finished, then we would like to hear from the audience about similar experiences you've had, or advice that you would like from this distinguished panel.

Rotor Mast Height

Richard Gabel
Manager, Dynamics Technology
Boeing Vertol Company

Army transportability requirements for recent helicopters have dictated that the aircraft overall height be minimized. This design constraint resulted in the YUH-60 and the YUH-61 prototype aircraft with unacceptable vibration levels due in part to the close proximity of the rotor to the fuselage. The problem was resolved on the Black Hawk by introducing a shaft extension which reduced vibration in flight, but permitted lowering of the rotor for transport. In recent years, Boeing supported an ATL Eustis in-house effort to develop a data base to quantify the relationship between rotor mast height and the resulting rotor loads and vibration levels. A YUH-61 prototype (Slide 1) was refurbished, instrumented, and flight tested at Ft. Eustis. So far the standard mast height and a 24" mast extension have been tested on this hingeless rotor helicopter.

Vibration pickups were located throughout the cockpit and cabin-occupied areas (Slide 2) and in addition there were pressure pickups along the crown. There were shaft gages on the rotor shaft and there was some instrumentation on the rotor blades. The aircraft was flown at a light gross weight of 14,000 lb. There were no vibration treatment devices in the aircraft.

You can see in Slide 3 the vibration for the copilot heelslide vertical, pilot heelslide vertical, pilot heelslide lateral, and Station 78 which is under the pilot's seat left and right. The baseline levels for the standard short shaft are shown here--over 1 g at 140 knots; nearly 1 g on the right side; laterals of about four tenths; and nine tenths under the seat. Now by raising that shaft 24" and absolutely nothing else in the airplane, we got a reduction to 0.2 g; the lateral down to 0.3 g; and 0.2 g under the seat--a tremendous reduction. Now that is very dramatic compared to everything I think we have talked about in this whole conference. No single change has ever done anything like that!

Now what did it? Well, we are not entirely sure, but we did measure several contributors. There was shaft instrumentation and a small amount of blade instrumentation. On Slide 4 we have main rotor shaft bending at 3 per rev and at 5 per rev, which of course created the 4 per rev vibratory moments in the shaft. The lower pair of charts are 7 per rev and 9 per rev. The slide shows air speed versus vibratory moments at these gages. There is about a 50% reduction with the extended shaft. The 5 per rev is also reduced in half, but the starting level is smaller. The 7 per rev which with 9 per rev produces the 8 per rev forces is reduced by various percentages and over 50% at high speed on the 9 per rev. We had no way of directly measuring the vertical load and the inplane load, but I would venture a guess that they all came down at least in similar percentages.

We measured pressures on the crown (Slide 5). These were pressure instrumentation locations both on the cabin and on the tail. I'm just showing a sample here. These three plots are Station 80 on the left side, Station 80 on the right, and Station 80 on the center. On the right-hand crown you see a reduction from 0.1 to .05 psi. Integrating those, roughly gives about 300 pounds of vibratory 4 per rev; another vibratory load.

For curiosity then, what would have happened if we put the normal vibration treatment back in the airplane which consisted of five fixed-tuned absorbers: two verticals under the seats, one in the nose and one on each side of the cabin. Slide 6 repeats the previous plot except adds the dots which are the airframe absorbers. On the copilot heelslide side the solid line is the reduction from the shaft extension alone, and the dotted line is the addition of the absorbers. On the right side there is a further reduction down to about 0.1 g. The heelslide lateral is reduced to nearly .05 g, and under the seats about 0.1 g on the right and about 0.05 g on the left, a further reduction.

Now I think that one comment about this is that the hingeless rotor has gotten a bad reputation because of the experience on the YUH-61. I think that the hinge offset and the vibratory moments are not really responsible for the vibration of this aircraft. As a matter of fact during the development program we had pendulums on the rotor which nulled the vibratory moments to zero, and there was not much change in the vibration levels. I believe that the vibratory forces in the shaft, the verticals, the inplanes and perhaps the pressures were really responsible for the difference. And woe to all you designers who would dare to put a rotor down near the fuselage again.

I'd like to give credit to ATL and Don Merkley who was the project engineer on this program. The aircraft is still at Eustis and there are plans by Eustis to fly some of the other intermediate shaft heights to understand the problem more fully. Perhaps Don will put out a very detailed paper sometime in the future with a good story about the source data.

Slide 1.

Vibration Pickup Locations

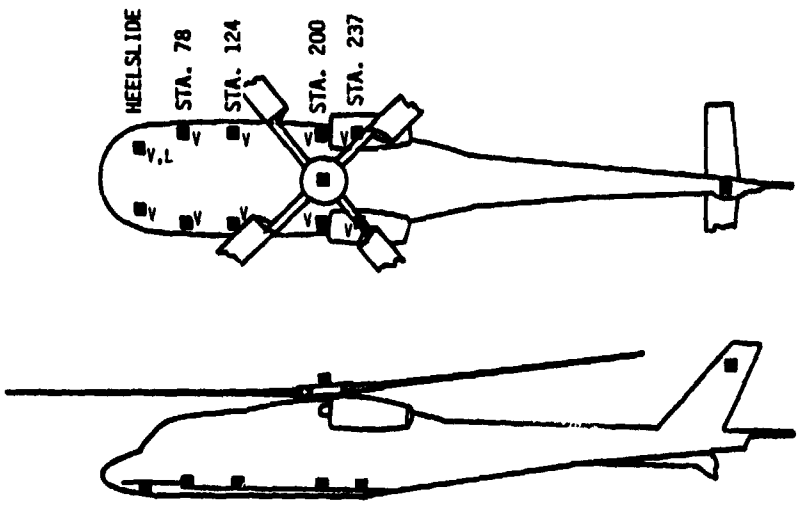

Slide 2.

4/Rev Cockpit Vibration - Extended Shaft

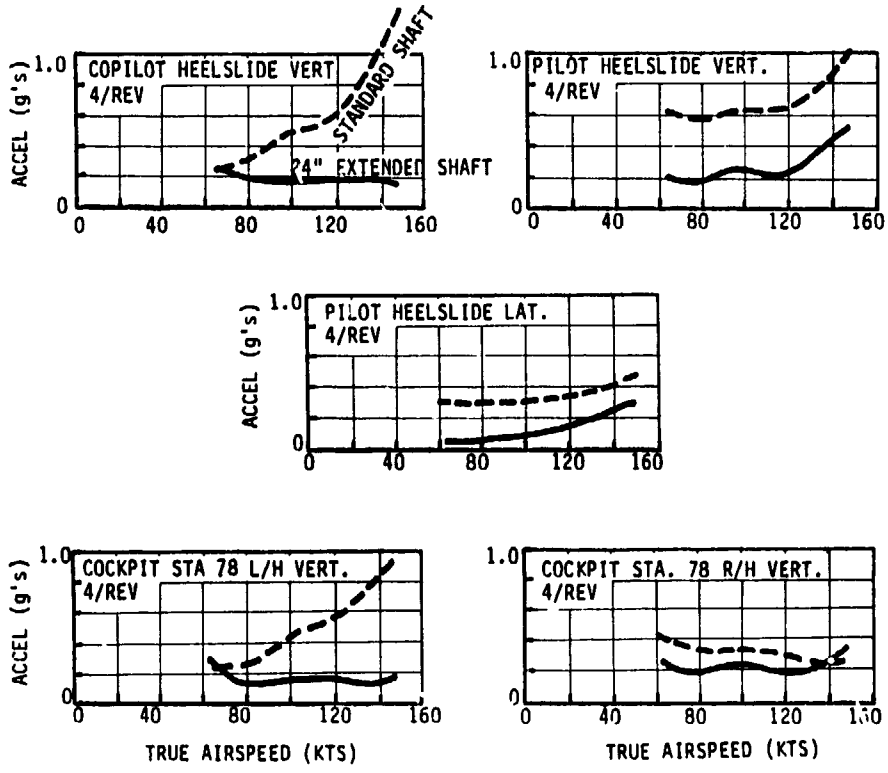

Slide 3.

Rotor Loads

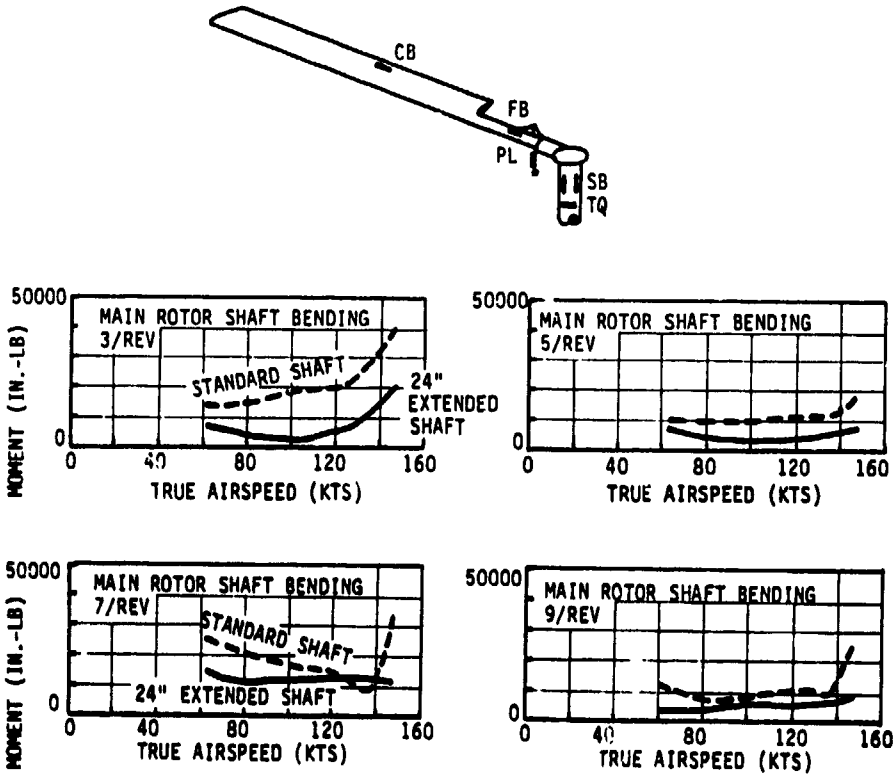

Slide 4.

4/Rev Airframe Crown Pressures

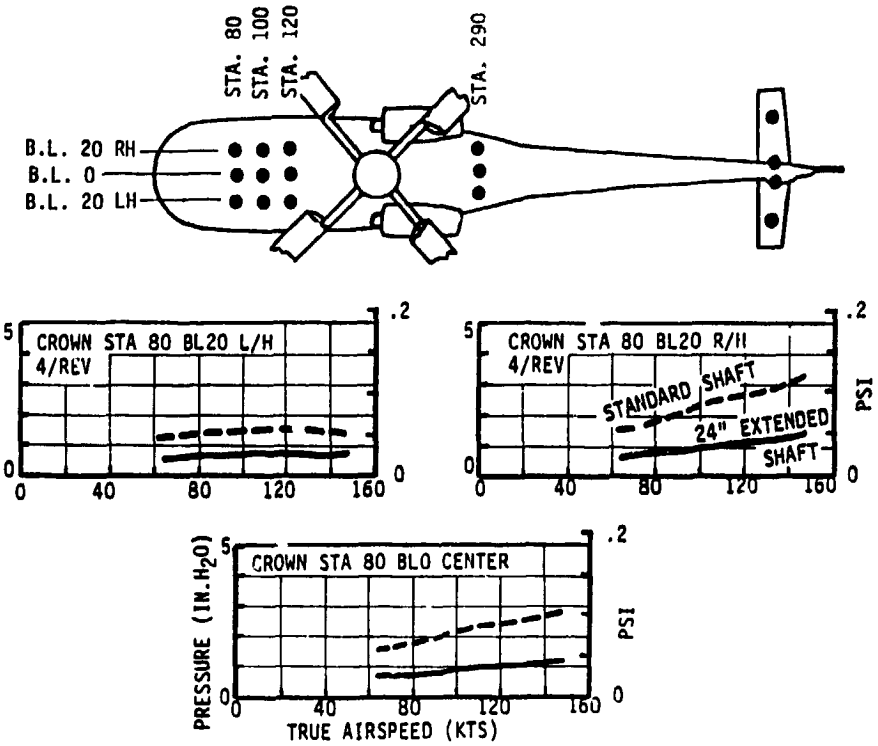

Slide 5.

4/Rev Cockpit Vibration - Extended Shaft and Cockpit Absorbers

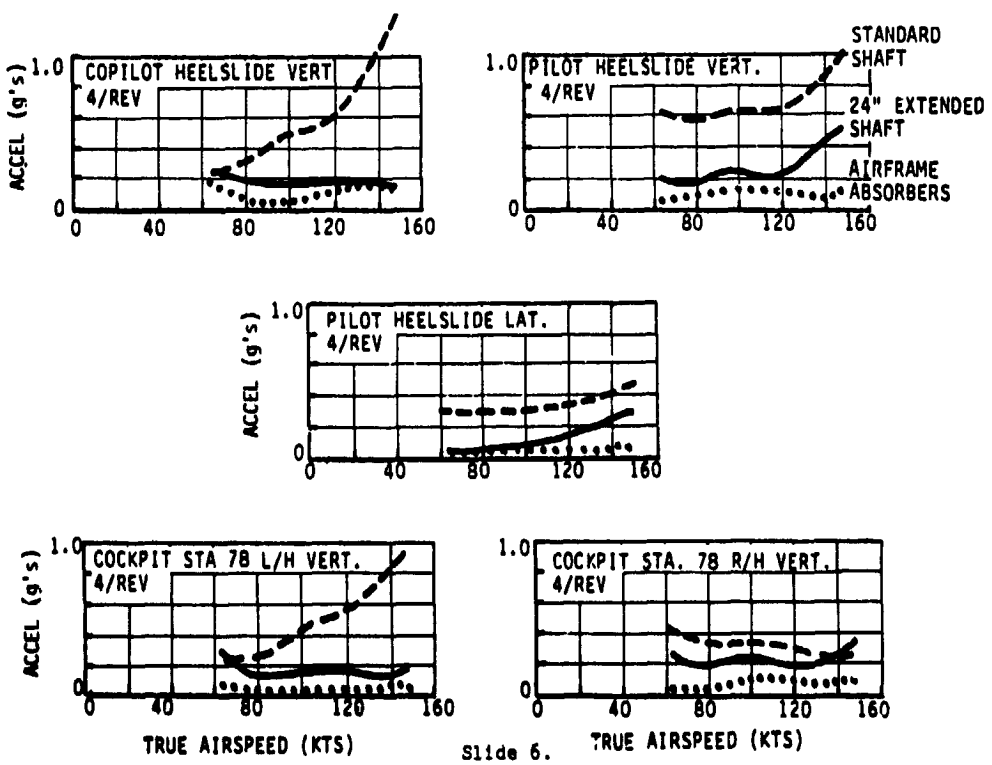

Slide 6.

DISCUSSION

Charlie Fredrickson, Sikorsky Aircraft: I want to commend Vertol for showing the results of your years of work in raising the rotor and just what has happened. I went through a lot of that experience ten years ago with you. What was the result of raising the rotor on vibration in maneuvers or in flare to hover and that type of thing? Was that as improved as level flight?

Gabel: Everything was reduced. I don't have any documentation here, but everything was reduced. The pilot comment was "spectacularly reduced."

Wally Acree, NASA Ames: I notice that the Italians, Agusta, on the 129 have a rotor extremely close to the fuselage, but their fuselage is a very different shape. Can you give us any insight as to how much the shape of the fuselage influences the vibration as opposed to just the proximity of the rotor?

Gabel: Yes. Well I think that is important, it's a good point. We had done some wind tunnel tests and some analysis of the flow over the fuselage, and I think Sikorsky had a paper on the same thing at an earlier conference, and there is an effect on the scoop shape on the front of the fuselage--how the airflow is directed up into the rotor. I think that if the flow is such that it gets into the working parts of the blade--the tip sections--it's very bad; if it comes into the center portion it may not be as serious. But I think a lot more work really needs to be done to understand the science of that.

Jack Landgrebe, United Technologies Research Center: Back in the early days of the Black Hawk, when we were first looking at the design and playing with the movement of the rotor, we did some analytical work which showed the effect of the body on the rotor and indicated the potential for the fuselage vibration. We did some preliminary work as far as the effect of the rotor back on the fuselage. The effect at the rotor was very dramatic, or at least predicted to be very dramatic and that helped to convince some people that raising the rotor was necessary, but going the other way as far as the effect of the rotor on the fuselage we found that to be quite speed-dependent. As you get up to high speed, the wake skew angle is much shallower and also because of the disk attitude it very much influences how close that wake comes to the fuselage and that was a very important factor in our calculations--just how close the wake comes to the fuselage. In the pressure measurements that were made on the fuselage, did you see activity up at those forward pressure locations, those forward of the rotor shaft for the high speed condition? I presume what you have shown here has been at that 140 knot condition?

Gabel: They were airspeed sweeps.

Landgrebe: Okay, but where it went up . . .

Gabel: . . . was the 140.

Landgrebe: Did you see a lot of activity at the forward pressure locations on the fuselage?

Gabel: Yes, in fact they have a sequence, if you look at the time histories, that I think were from left to right as a pressure peak that you can watch pass over the top of the fuselage.

Landgrebe: Did it move back with speed--did it move back on the fuselage considerably with speed?

Gabel: I'm not sure, we haven't really studied the data thoroughly.

Euan Hooper, Boeing Vertol: We did a wind tunnel test at the same time and we had a matrix of 9 pickups over the top of the cockpit canopy and we plotted the vibratory pressures from those pickups against speed and they just go steadily up with speed--I sense you are saying the other way, it might come down with speed, but they were almost zero in hover, and they went steadily up with speed and you could very clearly see a wave sweeping from right to left across the canopy as the blade passed. It wasn't a vortex coming back this way; it went from right to left. The magnitude was about .1 psi (it was a Mach-scale test) just as you have shown in flight test. As you raise the rotor shaft it came down by about a factor of two just like the flight test. It was very pronounced.

Landgrebe: So it was very noticeable even at the high speed?

Hooper: Very severe effect above the cockpit, in front of the rotor.

Landgrebe: Very interesting.

Peretz Friedmann, University of California, Los Angeles: I was wondering, how long was the shaft before you raised it? You might have mentioned it; how much is 24 inches of the original length of the shaft?

Gabel: It was close to the fuselage; it was just enough to provide clearance for the swashplate and had all the hardware under it. It was perhaps like 6 inches.

Friedmann: So it went from 6 to 6 plus 24?

Gabel: Something like that.

Friedmann: The question I really had, considering percentage-wise the tremendous increase in length; do you feel the flexibility of the shaft might have anything to do with the reduction in loads?

Gabel: No, I don't think so.

Bob Hansford, Westland Helicopters: I'd like to ask whether you measured any differences in control loads at high speed? The reason why I ask is that in the work that we have been doing in modeling flow over the fuselage and up into the rotor we found that at high speed conditions, you can induce a stall over the nose of the aircraft and from one of your graphs it doesn't seem to be a distinctive change in trend of the gradient of the 3 per rev shaft bending past about 120-140 knots.

Gabel: Well, we haven t gone into all the data that thoroughly yet and I think ATL is going to be doing more of that, so I can't answer you about the pitch links, except that they were instrumented.

Jing Yen, Bell Helicopter: How did the mast length increase affect the hub loads?

Gabel: Well, I showed some of that. The vibratory moments which we were able to measure came down 50% or more. The other loads were not measured directly.

Bob Sopher, Sikorsky Aircraft: One of the things of raising the shaft that could be considered is that the moment of inertia of the rotor about the CG has changed substantially. Have you made any kind of estimates of the impact of that change?

Gabel: No, but we did fly an isolation system on a different aircraft with the raised shaft and there the inertia was significant in the mounting of the isolation system. We got good vibration levels from that, but that really was for an entirely different reason.

Sopher: Well, that is a factor which may have nothing to do with the excitation sources, which could be responsible for changing the response of the system.

Gabel: You mean increasing the inertia of the airplane and therefore the roll response, for instance?

Sopher: Yes.

Gabel: Less vibration?

Sopher: Definitely.

Gabel: Yes. There could be some influence.

Hooper: While we've got a couple of Westland representatives here, would they care to say anything about the experience they had in raising the rotor on the Lynx?

Steve King, Westland Helicopters: We've raised the Lynx rotor head, I think it was about 15 inches, and the effect really was an increase in vibration.

Gabel: An increase?

King: An increase. I can't remember the details but the results were so disappointing that we abandoned the whole exercise. So we didn't go into details of what the rotor loads were.

Gabel: So you have no knowledge of why it did that?

King: That's right. There was no benefit at all, in fact it was worse so we just gave up.

Gabel: In this country, this aircraft was one of the four contenders at that time, all of which raised their rotor shafts and it did good things for all of them.

Walter Gerstenberger, Consultant: It's quite a shock coming to this meeting, I thought we were going to get a run down on how a Boeing engineer reduces vibration on a Boeing aircraft.

Gabel: We did!

Gerstenberger: I know you keep trying, you mention something, you keep trying. How did you get it so rough in the beginning? So you got that big baseline to make these wonderful reductions. That isn't a standard Black Hawk way up there, is it?

Gabel: No, that's the standard of the YUH-61, but I am sure that the standards of any of these airplanes if they were to be displayed would not be much different than that.

Gerstenberger: Well, didn't you have something around 1 g?

Gabel: Yes. Take any of these airplanes and take everything off and see where the baseline is. People don't publish them but they are there.

Gerstenberger: That's a good baseline for making improvements because anything you do will make it better. Getting back to serious things as far as ground resonance is concerned, I think you can show analytically that the higher your mass the more coupling you get. See, you are bringing your rotor head up and it works out that your worst case is when you have a large arm for your ground resonance coupling and with your rotation about the CG you have minimum inertia and I'm almost sure that if you increase the mast that much you would have greater damping requirements in your landing gear.

Gabel: Well, that wasn't the issue. First of all, we didn't have any damping in the landing gear. The stability was provided entirely by the rotor--roll aerodynamic damping. It made no difference with the extended shaft.

ACAP: A Case Study of Airframe Dynamics Problems and Their Solutions

Wen-Liu Miao
Chief, Dynamics
Sikorsky Aircraft

I will be speaking about how the dynamicist solved practical problems on the ACAP program. Before we get into that, however, I would like to set the stage by discussing the problems that the dynamicists face. You have heard during the past few days about the kind of specific dynamics problems there are. I think most significantly the dynamicist has to face not one, but three Mr. T's (Slide 1). The first T, of course, is the technical complexity. In the past few days, we have heard a lot about the technical complexity. For instance Pam Phelan showed that when redoing the C-60 analysis, they found a coding error which changed the downwash calculation. The change in downwash is in the proper direction which Euan Hooper showed last year is very important in predicting the vibratory blade loads. Peters showed that hub motion is also very important and could have significant effects on vibratory loads. Gabel showed their efforts on the CH-47D. They did a super job using the NASTRAN and conducting the shake test under NASA Langley FEM contract, but still have discrepancies in the mode shape and frequencies. With all the uncertainties in the vibratory loads and the difficulties in getting the airframe dynamic characteristics, how are you going to get an accurate bottom line vibration? Niebanck showed that the bottom line vibration really is a vector sum of the vibration due to three forces and three moments. You have to get the amplitude correctly as well as the phase correctly. So the problem is very complex. The next T is the trustworthiness of our tools. We said earlier that we have a lot of questions about whether we can generate proper rotor loads and the proper airframe dynamics characteristics. Now, the last, but not the least is the so called timeliness of the solution. We face that a lot. In fact, that T makes our life difficult.

Slide 2 succinctly summarizes our problem. At the beginning of a project, everybody comes to the dynamicists asking for solutions. But the dynamicists can't generate anything because there is scarcely any data to do any calculations with. The best thing we can do probably is based on past experience, to set some criteria and goals. As time goes by the design gradually firms up and we can do better calculation as evident by the increase in the data available. But, by that time, the project generally loses interest in the data. They have the system designed already, why should they change the design based on the dynamicists's findings? Now that is really a key difficulty we have. But it is not incurable. I believe we can move the solid curve to the right, that is, the need for data and the data available will meet. When that happens, the dynamicist can input more into the program and interact with the design better. That takes commitment. The commitment from the program to iterate the design and that is not a small matter.

The next topic is how we typically approach a program solution. Starting from the left of Slide 3, we define the problem--what are we dealing with--and we select tools. The tools are basically of three kinds: data base, namely past experience or whatever is available that we can use to project to a new design, and analysis, and model test. Once we go through some or all of these, we reach a solution. We also conduct risk reduction tests. And if necessary we may iterate on the solution. Then we'll proceed to full scale evaluations. Of course, knowing that there are uncertainties and being practical about it we always have a backup approach. That actually makes our life a little bit messier because we have to deal with not one, but a number of solutions. If the full scale evaluation is not successful, we go to the backup solution. And we may even iterate between the full scale evaluation and backup solution if time allows and if the problem is not readily resolved. An example of the backup solution is one that was developed during the S-76 development period. The transmission pitching and rolling degrees of freedom are known to cause vibration. What should we do if the vibration treatment on the S-76 does not provide the desired results? So we developed a flexible transmission mount and tested in full-scale hardware. Fortunately, this backup solution was never needed. Now that the full scale solution is a success do we see the end of it? On the lower right of the slide, it says E-C-P. That's not a misspelling. It's not e-n-d. We normally will submit an Engineering Change Proposal to improve the product. So the entire solution approach starts over again. It's a never-ending process.

After having said all this, how have we approached the ACAP? I choose ACAP (Slide 4) because ACAP presents a simpler dynamics problem which can serve as a good example. ACAP uses the S-76 main rotor system, the transmission, engine, drive train, and tail rotor. We don't have to develop all these dynamic components. ACAP basically is an airframe dynamics problem from a dynamicist's point of view. Shown on Slide 5 are the ACAP major milestones. You would note that from contract award to the first airframe completion, it takes about 2-1/2 years and this schedule is not any different from, say, the YUH-60, YUH-61, or the YAH-64. The time span is about the same. The reason I am bringing this point up is: during the development of a brand new airframe, why doesn't the dynamicist have enough say during the design process about how to design the airframe? That is because of no commitment. The ACAP program, on the other

ACAP - SUPERELEMENT FEM

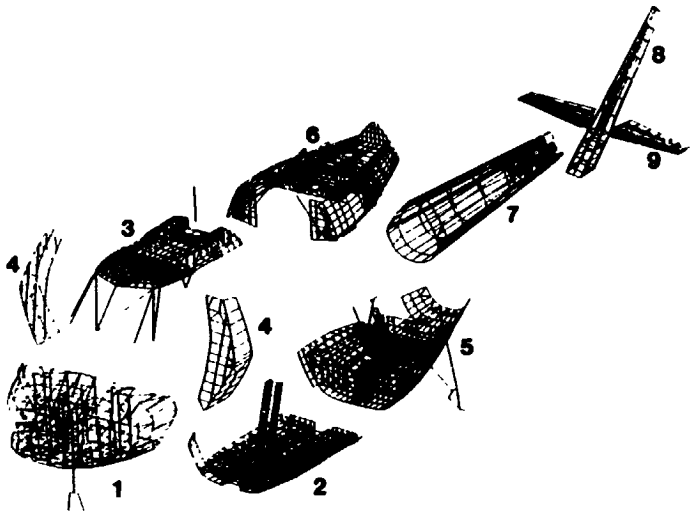

Slide 8.

ACAP NASTRAN MODE TUNING SUMMARY

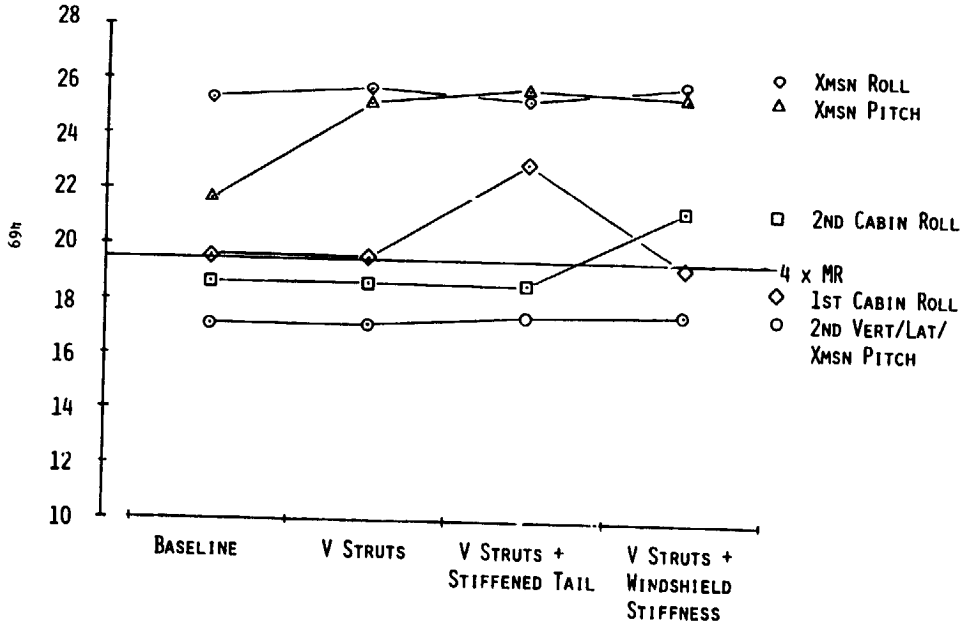

Slide 9.

hand, has made the commitment right at the beginning. The program decided that they would take the dynamics input and incorporate it into the design.

At the start of the ACAP program we set down three goals for the airframe as shown on Slide 6. The first one is obvious. We would like to have a non-resonant airframe. The third one is to use the existing S-76 vibration control devices or less. The second one may be a little bit obscure. This is based on the S-76 experience. There is a transmission mode above 4 per rev and a transmission mode below 4 per rev on the S-76 and the resultant hub impedance will create certain difficulties for vibration treatment using the bifilar absorbers. The ordinate shown in Slide 7 is the ratio of bifilar dynamic mass with respect to hub longitudinal 4P impedance and the abscissa is the lateral impedance ratio. The family of curves shows the transmissibility or the bifilar effectivity. The curve labeled one means all the hub forces are transmitted. For the curve labeled .2, only 20% of the forces are transmitted. From this chart it becomes obvious that for bifilars working effectively, it is best to have the hub impedance of the same sign, that is to have modes both above 4P or both below 4P and also of the same magnitude. This point is where ACAP finally winds up.

The ACAP superelement model is shown in Slide 8. The fact that we got this model in a timely fashion is an indication of the program's commitment of getting good dynamics input. With the baseline design we found the five modes of interest as shown in Slide 9. There is a transmission pitch mode at 21 Hz, and transmission roll mode at 25.5 Hz. Our goal is to make the two modes about the same frequency. And we also have two modes very close to 4P which we don't like. What do we do? Let me show you on the next chart (Slide 10) what we did. This is what is called the V struts. There are two V struts at the transmission and tied onto the floor to stiffen up the transmission pitch mode. We put two struts at the windshield to find out the windshield stiffness effect. The tail has also been stiffened to see what kind of effect that has. The sensitivities are shown in Slide 9. With two V struts, the transmission pitch mode has been moved close to the roll mode. That satisfies one of our goals. Next, we stiffen up the tail to see if we can move any cabin roll mode at all. We find that the first cabin roll mode frequency has been increased to 23 Hz. Also, by putting in some windshield stiffness we can increase the frequency of the second cabin roll mode. Now is the time for engineering judgment. Decisions have to be made. Should we propose to incorporate the V struts? Should we propose to stiffen the tail and the windshield? The sensitivity of the V struts makes sense. The V struts move the transmission pitch mode up and you can see that the transmission support mode will definitely be affected by anchoring the transmission support beams to the rest of the fuselage with these V struts. Stiffening the tail drastically increases the first cabin roll mode frequency. Examination of the mode shape reveals that the lateral tail wagging motion is predominant in this mode. Accordingly, we should have some design modifications ready in case the shake test shows that this mode is at 4/rev as calculated. As for the second cabin roll mode, the mode shape suggests that there is relative motion at the windshield. Stiffening the windshield moves this mode very readily. Now this makes us very suspicious. Do we have all of the skin's stiffness of the airframe in there properly? Will the modal frequency truly be where the calculation shows? We decided to wait for the shake test to answer this question.

We went ahead with an airframe with the V struts. A trade study on the V strut was conducted. Plotted on Slide 11 are the weight penalty and the transmission pitch mode frequency as the size of the V struts varied. What's the weight penalty and how much frequency separation do we get? We selected a V strut area which weighs about 20 pounds and raises the pitch mode to 25 Hz, the goal. With this airframe configuration, the untreated aircraft vibration versus airspeed was calculated and shown on Slide 12. With the S-76 nose absorber functioning, the vibration level reduces to about one third. The S-76 also has 3P and 5P bifilar absorbers on the rotor head. With the 3P bifilar, the cockpit vertical vibration is well within the target level. The 5P bifilar provides practically no further reduction. This is attributed to the proper tuning of the transmission modes. So the decision was made to remove the 5P bifilar, retain the 3P and the nose absorber.

Finally we come down to the shake test. Shown on Slide 13 are the test frequencies of the five modes of interest as compared to the calculated values. The transmission roll mode and pitch mode are close to the calculated values. The worrisome mode, the first cabin roll mode calculated to be very close to 4P, is actually here, about 15.5 Hz. Being a practical dynamicist I am not going to argue about why my analysis is wrong--I'll take it. The second cabin roll mode that is sensitive to the windshield stiffness cannot be found. This is an indication that our original NASTRAN model may not have taken all the proper stiffness into account to predict this mode properly. My suspicion is that this mode depends a lot on the shear stiffness and in reality is of a much higher frequency. Of course, ACAP has been flown and its vibration level with the nose absorber and the 3P bifilar is about .05 to .1 g, depending on the airspeed.

After going through this practical example, my conclusions are shown on Slide 14. Dynamicists can make meaningful input into the program, but it requires quite a bit of judgment based on experience, or data base. We also need the commitment from the program to iterate the design based on dynamics findings. Of course, we must set up proper design criteria at the beginning of the program. These criteria should be well understood so that every effort will be devoted to achieving these goals.

With all that, I have some recommendations as shown on Slide 15. Number one, we should have a very comprehensive data base. By data base I am thinking of something of the nature of a DATAMAP-type of system. For every aircraft tested, the data should be stored in the manner that can be retrieved readily and cross-plotted to aid in design decisions. We all know our analysis is woefully inadequate. Now that 2GCHAS is coming on line I hope it will come on line quickly. NASA Langley's FEM contract activity is a very useful one because it will give us a good handle on airframe dynamics. And we should do a lot more model testing and generate enough parametric sensitivity so that we can make smart design decisions.

DYNAMICIST MUST FACE THREE MR. T'S

- TECHNICAL COMPLEXITIES
- TRUSTWORTHINESS OF TOOLS
- TIMELINESS OF SOLUTIONS

Slide 1.

A SITUATION THAT DYNAMICIST FREQUENTLY FINDS HIMSELF DURING A PROJECT

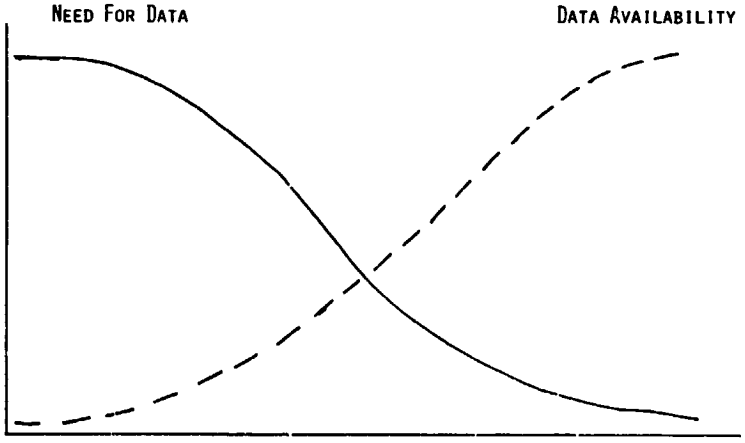

Slide 2.

TYPICAL SOLUTION APPROACH

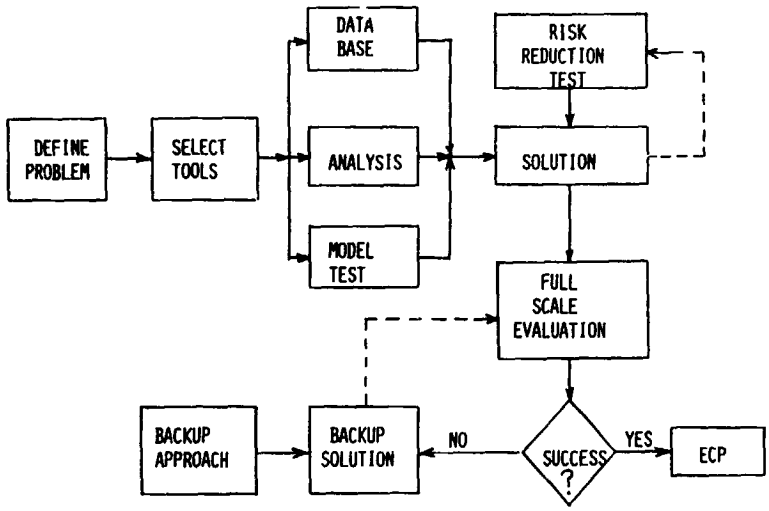

Slide 3.

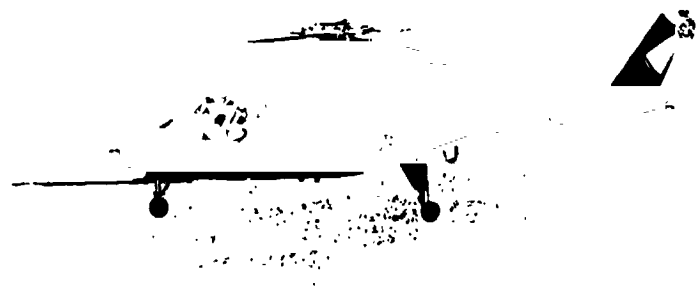

SIKORSKY/ARMY ADVANCED COMPOSITE AIRFRAME PROGRAM DEMONSTRATOR IN FLIGHT

Slide 4.

ACAP MAJOR MILESTONES

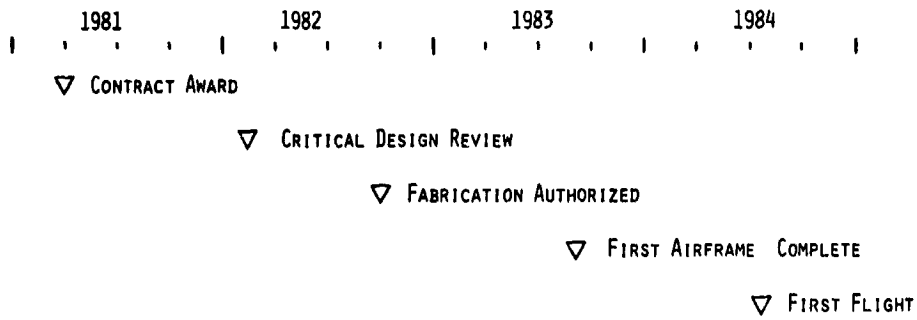

Slide 5.

VIBRATION DESIGN GOALS FOR ACAP
AIRFRAME DESIGN

1. Avoid Having Airframe Modes At 4P
2. Make Transmission Pitch Mode As Close To Roll As Possible Or At Least 25% Above 4P
3. Use Existing S-76 Absorbers Or Less

Slide 6.

HAVING HUB INPEDANCES IN THE LONGITUDINAL AND LATERAL DIRECTION OF THE SAME SIGN AND MAGNITUDE IMPROVES BIFILAR EFFECTIVITY

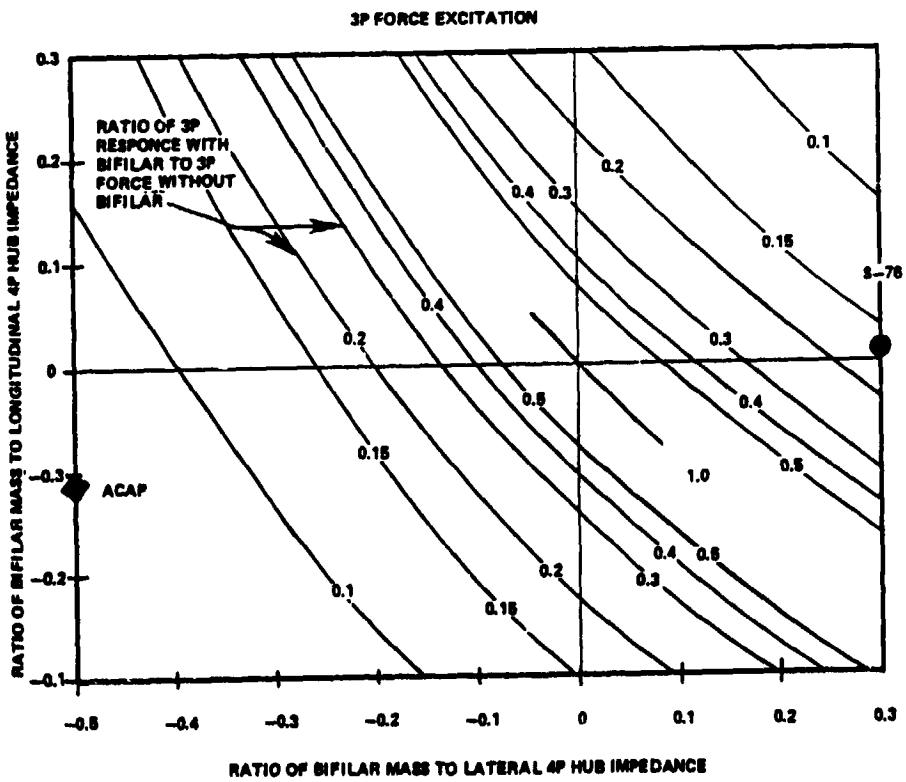

Slide 7.

STIFFENED AREAS OF ACAP NASTRAN MODEL

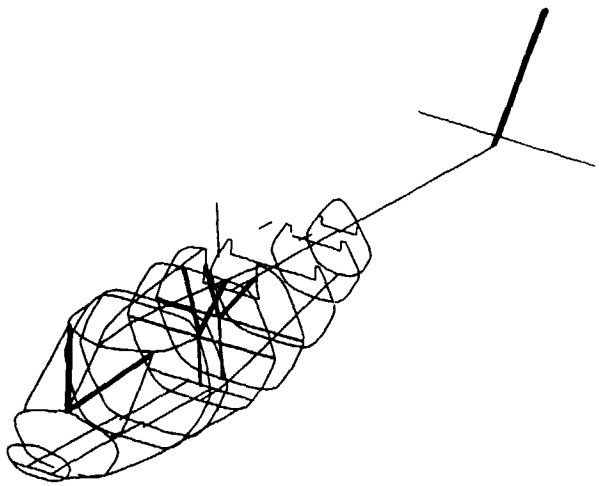

Slide 10.

WEIGHT TRADEOFF FOR MOVING THE TRANSMISSION PITCH MODE

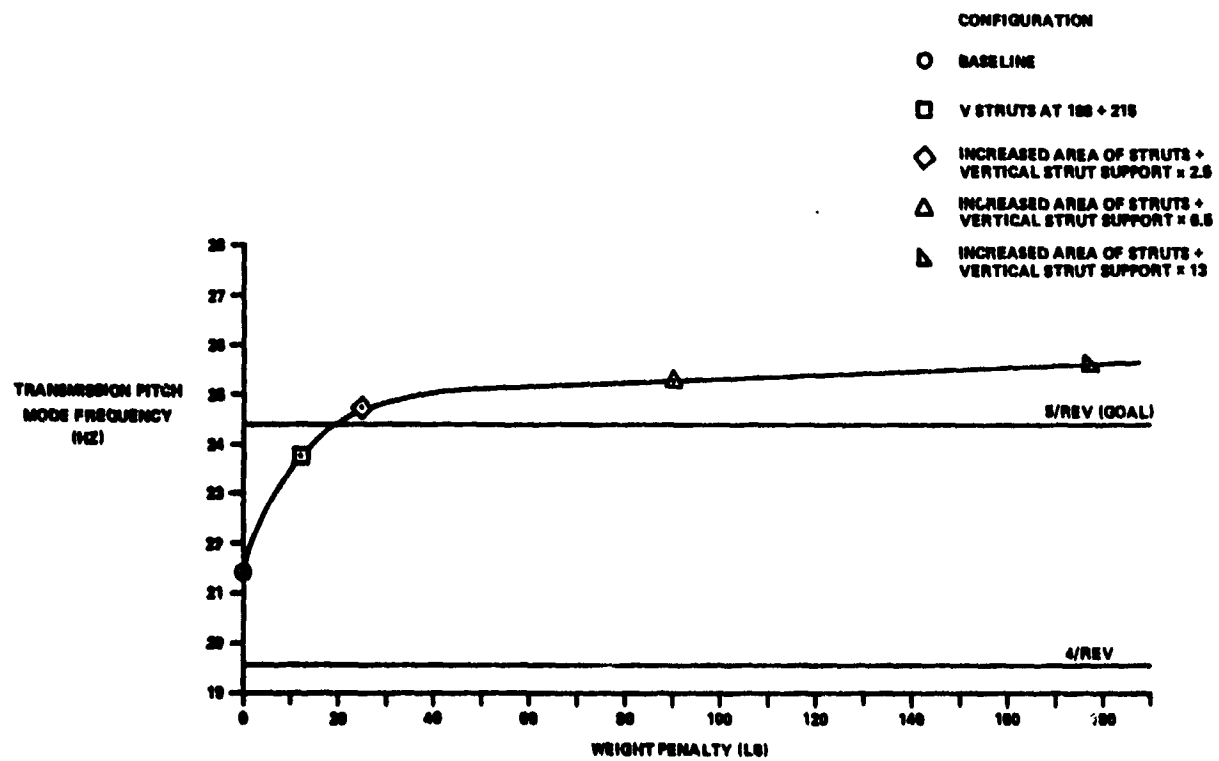

Slide 11.

COUPLED ROTOR/FUSELAGE VIBRATION ANALYSIS (SIMVIB) SHOWS THAT 5P BIFILAR CAN BE ELIMINATED

COCKPIT VERTICAL

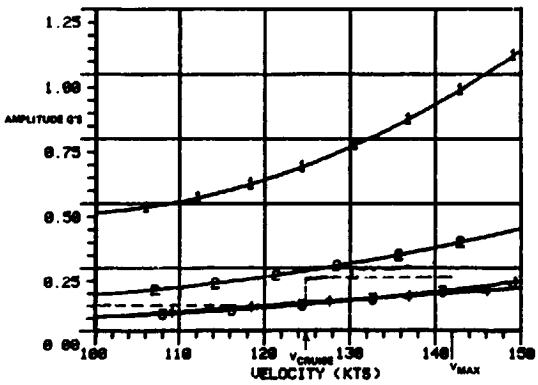

CASE DEFINITIONS

1. UNTREATED
2. NOSE ABSORBER
3. NOSE ABS + 3P BIFILAR
4. NOSE ABS + 3P + 5P BIFILARS

Slide 12.

COMPARISON OF PREDICTED AND EXPERIMENTAL MODAL FREQUENCIES

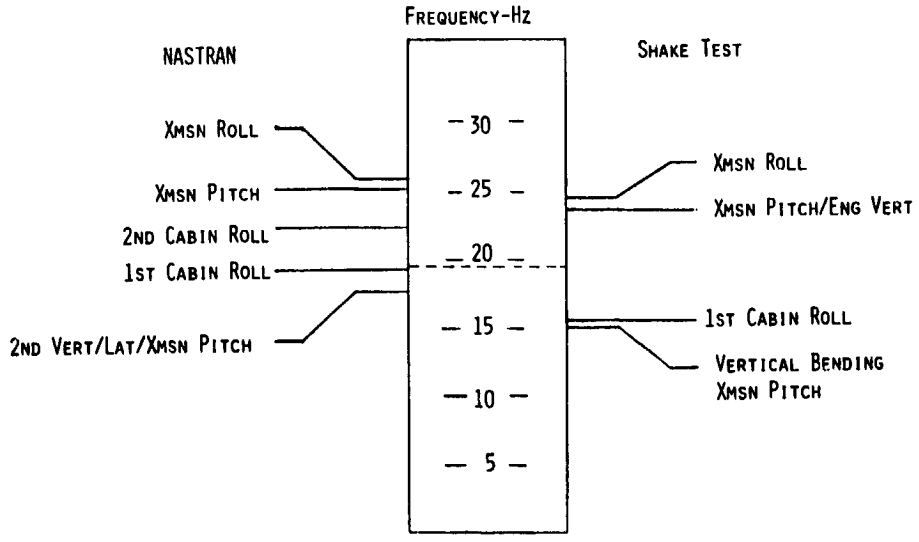

Slide 13.

CONCLUSIONS

- Dynamics Can Make Meaningful Inputs To Design But Considerable Judgment Is Required
- To Maximize Chances For Success, Industry and Government Must:
  1. Improve Analytical Capability
  2. Allow For Feedback From Test To Design
- Dynamics Design Criteria Should Be Well Defined And Understood At The Beginning Of A Program

Slide 14.

RECOMMENDATIONS

- Support Formulation Of Comprehensive Data Base
- Expedite 2GCHAS Development
- Continue Studies Of NASTRAN Modeling Techniques
- Support Model Tests And Dissemination Of Results

Slide 15.

DISCUSSION

Ray Piziali, U.S. Army Aeromechanics Laboratory: As one who has worked primarily in aerodynamics you make me feel a little bit better. I have had long discussions with some of my colleagues that dynamics is well in hand and we can handle all the dynamics problems, but I make the observation that the capability with the NASTRAN model reminds me of our capability with the free wake models. We do well at 1P at steady airloads maybe, sometimes they provide guidelines, but we have got a long ways to go and I see the same kind of general observation with the NASTRAN application. I think we've got a long ways to go in applying them.

Wayne Johnson, NASA Ames Research Center: I would like to address the comment we heard from Bob Sopher about RDYNE developments. I think it would be nice to have more than just a general statement that you made, but can you be more specific in terms of what you expect from the future that you don't think you're getting now?

Miao: As far as data management is concerned maybe I can give a practical illustration. For instance, if I want to find out how does the S-76 vibration levels vary from aircraft to aircraft, I would like to be able to go to a terminal and sit down and recall the data and obtain a statistical distribution of the vibration. For certain flight regimes and certain kinds of maneuvers I would like to examine data in ways that are convenient. Right now there are a lot of data scattered in various reports. You have to dig into various pieces, put them together, replot it to suit your need--it's not very convenient. And that's just a starter. The data base I am thinking about is a comprehensive one. We test different models, for instance. You heard Charlie Niebanck talking about our optimization work on the blades. We have done some testing of that. Why can't we test the optimization parameters in a more systematic way and have all the data stored so that they are readily retrievable and displayed any way I want? That is the type of data base I am looking for. As far as 2GCHAS is concerned, my statement has been very general. I just said "2GCHAS come on line quickly, please." What I am really looking for is a tool that I can really rely on. When it provides an answer for me, I say, ah ha, I can trust it 100%, 90% maybe. I'm not saying that we don't have any tools now. Yes, we have tools now, but I have to apply judgment to it. I would like to be able to rely on a tool which can provide, say, 80% of my answer here and now.

Gabel, Boeing Vertol: I think our next panel will go into the subject of data bases very thoroughly. I have one comment for Mr. Gerstenberger. You may have noticed that Jerry has displayed the baseline level (although his was calculated) of .9 g's at 140 knots.

AH-64 Engine Mount

James Neff
Aeromechanics Staff Engineer
Hughes Helicopters, Inc.

I am going to tell you about the fun I had playing tag with the rigid body engine pitch mode on the AH-64 attack helicopter. It was a rigid body pitch mode, and didn't involve any engine bending so I can't blame any of the problems we had on my good friends at GE which I would normally do if I possibly could. Slide 1 shows the mounting system, which is a statically determinate system, always required for engines to keep from inducing loads into the engine from the airframe deflection. It has a front engine mount which takes loads in three directions, longitudinal, vertical, and lateral; an aft engine mount which takes vertical and lateral loads, but not fore and aft loads; and it has a roll bar at the bottom to take out rolling moments. So it is statically determinate, a fact that is an important factor in what I am going to discuss later on. Now, in addition to that, there is also a requirement to be fail-safe if there is ballistic damage or failures. We get around that by having a secondary mounting system which does not pick up loads until the other system has failed. That is also a significant point in what will follow.

This program started back in the early 70's and we had indications at that time that the engine pitch mode was going to be near 4 per rev. We had some first indication of 4 per rev resonance in the initial shake test on a very incomplete airframe on which the engines were simulated with rigid masses, and also several other things were simulated. We were not really sure how close we were; therefore we didn't try to correct the resonance. We flew the airplane and everything was all right. We finally got a NASTRAN model going along about that time and it also indicated that we had engine natural frequencies near 4 per rev; both a symmetric engine pitch mode and antisymmetric engine pitch modes. But we were not sure whether it would cause a problem; it depends on how much response you get in that pitch mode to the airframe excitation. We decided, well, maybe the thing to do is not to do anything about it and see if it works out. We went through the flight loads survey in the initial aircraft and all the loads were acceptable, the vibration levels were acceptable, and the engine mounting system fatigue lives came out acceptable. We did that survey on the second air vehicle and then we did it again on the fourth air vehicle. On the fifth air vehicle we did a flight loads survey with the -700 engine and then we did it again with the -701 engine. In all four cases we came out with acceptable loads on the engine mounts. It looked like we had made a very shrewd decision in not doing anything about the engine mount stiffness to try to get away from the 4 per rev problems. So with back-up data from that many sources you certainly don't expect that when you go to a production vehicle that duplicates the prototype you are gong to have a problem.

When we flew the first production vehicle, there (on Slide 2) is where the loads went. Slide 2 shows load versus airspeed compared to the endurance limit and we see loads above endurance limit well before reaching V_H (164 knots). The prototype was below endurance limit over the entire speed range. There had been no change made to the production vehicle. We had gone through all of the development programs with the prototype and made no changes. Why did we suddenly get loads that high? It could be a change in the frequency or it could be a change in the excitation. No other loads were higher on the ship. Blade loads were the same, the cockpit vibration levels were lower, and the ship was very good in every other respect, so evidently there was a change in the engine natural frequency. So we had to look to see whether indeed that was the case and that we were getting close to the 4 per rev.

I will show Slide 3 to indicate what a 4 per rev response engine vibration is. We are looking at the accelerometer output on the exhaust frame near the aft end of the engine and we have velocity in inches per second plotted against time. The frequency is 19.3 Hz which is 4 per rev of the main rotor. When you see a response that clean, no other frequencies showing up except some of the very high frequency noise, it is clear that something is amplifying the 4 per rev input very sharply to mask anything else that might be in it.

Looking at the engine mount load in Slide 4 shows the same thing very clearly, a pure, clean 4 per rev response. Looking at a spectrum analysis of that in the lower part of the chart we see a very sharp spike at main rotor 4 per rev, right on the button. Clearly, we have 4 per rev resonance. We started looking for reasons why we would have that resonance on the production ship and did some ground shake tests. We found the engine pitch mode frequency on the first production ship (that had the high loads) was at 22.2 Hz compared to the main rotor 4 per rev of 19.3 Hz as shown in Slide 5. There is no good reason with the frequency at 22.2 Hz that there should be a large 19.3 Hz response.

We went back and looked at the prototype which had had acceptable loads, and it had a natural frequency of 20.8 Hz. If anything, the prototype should have been worse than the production ship based on the frequency placement relative to 4 per rev. Flight data on the prototype indicated we might have a 19.7 Hz frequency, which would be even worse.

We had done a lot of improvements to the NASTRAN model over the period of time--this was nearly 10 years ago that we first started on the model. We were still getting essentially the same frequencies originally predicted in NASTRAN, somewhere in that ballpark. We had an error in the initial formulation, but after chasing down all the errors and refining the mass distributions a little bit we came up with a frequency prediction of 19.83 Hz. We have many modes in the NASTRAN model that have frequencies in this range, none of which really correspond to what we see from the flight test that that frequency is really almost right on 19.3 Hz.

So I started looking for some sneaky way of finding out what the frequency really was. I knew there had to be some more subtle way of approaching the problem. Sifting through the flight test data I found a point here at 80 knots which showed some very interesting traits (Slide 6). I know you think that I copied that out of a dynamics textbook, but I didn't. It's the response of the aft engine mount load--a strain gage on the aft engine mount. It shows about the cleanest 0.6 Hz beat that you can imagine. I did a spectral analysis of that response and you see that it has the main rotor 4 per rev frequency of 19.5 Hz. In that case the rotor was turning a little bit above the normal RPM, so the frequency was 19.5 Hz. The other frequency that's combining with that to cause the beat is 18.9 Hz. The only way that I know to explain that is that 18.9 Hz is the natural frequency and in this very mild flight condition the random excitation is causing the natural frequency to respond at a level that is significant compared to the relatively low level of main rotor 4 per rev. So, it looks like the frequency is 18.9 Hz and even though I would not have expected that to cause a significant response problem, nonetheless, it indicated that we did have a resonance and we should do something about it.

We immediately went to look at various types of fixes (Slide 7). The first thing we figured was that we needed to either stiffen or soften the mounting to change the natural frequency. It appeared to be right on 4 per rev so we could go either way. This kind of change to the hardware takes some time so we looked at a lot of other things in the meantime while we were designing and building both a stiffened and softened aft mount. People in flight test had noticed that the barrel nuts that attached the engine to the airframe had loosened a little bit. They tried tightening those, but it didn't help any. During the shake test we had noticed that the IR suppressor (which we call the "black hole") had a resonance right at 4 per rev. We tried stiffening that up with both internal and external braces and it didn't help. We tried a few other things, none of which did much good and finally we had our stiffened mount available. It looked something like what we show in Slide 8. We see a cross section through the right hand engine nacelle here. If you were looking forward, say, the engine is on the right, we have a V brace on the engine, a V brace that attaches to a buttress on the fuselage, the fuselage is below the buttress, and the nacelle structure is below the engine. What we did was to add a brace from the apex of the V braces down to the engine nacelle in order to stiffen the engine enough to get away from the 4 per rev resonance.

The flight test results looked as shown in Slide 9. This was a case in hover. We get a nice beat again; that's another classical beat, but this time its's a 4.1 Hz beat and it's between the tail rotor 1 per rev and the main rotor 4 per rev. You might conclude from that, that with the stiffened aft mount, we were above 4 per rev and nearer the tail rotor frequency. So what happened to the loads? They indicated the same thing; (an adequate separation from 4 per rev resonance) they were way down as shown in Slide 10. The loads on the stiffened mount were well below endurance limit and certainly well below the baseline. So that looks like a good solution but this is where some of the practical aspects of dynamics engineering come in. It was great from my standpoint (dynamics), but from a lot of other people's standpoint, it wasn't good. There were a lot of practical problems involved with that stiff mount as described in Slide 11. Fabrication aspects of it--it is a very complex joint--two V braces and the added brace all coming together at a point it is very hard to fit that together. It also is redundant with all three of them coming together there so there is a fit problem--the added brace would have to be adjustable in order to be able to fit the three of them together on a production basis. Also it would have required a lot of additional fatigue testing of components associated with the additional load path. Another serious problem that happens when you stiffen something up and get the natural frequency above resonance is that in service, that frequency is going to tend to come down either due to damage, failure, or just due to wear; the frequency is going to come down as service time accumulates. As it comes down it's going to be approaching 4 per rev resonance again. Stiffening it is therefore not really a good solution.

We therefore tried a soft mount as shown on Slide 12. In this design the V brace was replaced by a mount with curved members that bend instead of taking a pure axial load. The results are shown in Slide 13. Again we have our 0.6 hz beat, but now we are talking about 18.6 Hz versus 19.2 Hz. All right, that's not much lower than what we had. We had 18.9 Hz and we have 18.6 Hz here, so why was it effective? This is shown in Slide 14; the loads were not as low as the stiff mount, but they were below endurance limit and they were acceptable.

Just a little explanation of why such a small reduction in stiffness solves the problem when it wouldn't be expected to. Mainly it's related to the fact that the engine had a statically determinate mount; therefore, any free play in the system, clearances in the bolted joints, and so forth cause a decrease in the effective stiffness. Normally with a statically indeterminate system those joint clearances are not very important. In this case they did appear to be important and the effect of that free play, then, is a nonlinear function of the

amplitude of motion. The higher the motion the less the effect of the free play is. At low amplitudes of motion you have quite a large effect. What we were seeing at 18.6 Hz at the 60 knot condition was a very low amplitude, but when we went up to high speed we went up to larger amplitudes and the effect of the free play tended to disappear. If we plot the theoretical calculation of frequency versus excitation amplitude, Slide 15 shows that it increases considerably more for the baseline mount than it does for the soft mount. Therefore, although the baseline mount and the soft mount were only slightly different at low amplitude, theory shows that the baseline natural frequency increased to become resonant with 4 per rev, whereas the soft mount natural frequency stayed significantly below 4 per rev.

So, if the soft mount is so good why not make it softer? We had at least two good reasons not to, as given in Slide 16. The deflection due to steady load causes secondary mount clearance to go away and the engine people are very concerned about having any loads going through the secondary mount. They don't like that at all. Another thing is that shaft coupling fatigue would increase due to steady load deflection.

AH-64 ENGINE MOUNTING SYSTEM

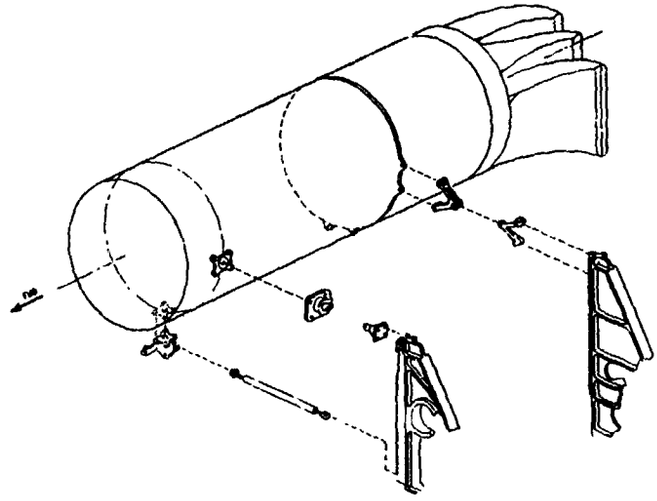

Slide 1.

AFT ENGINE MOUNT LOAD

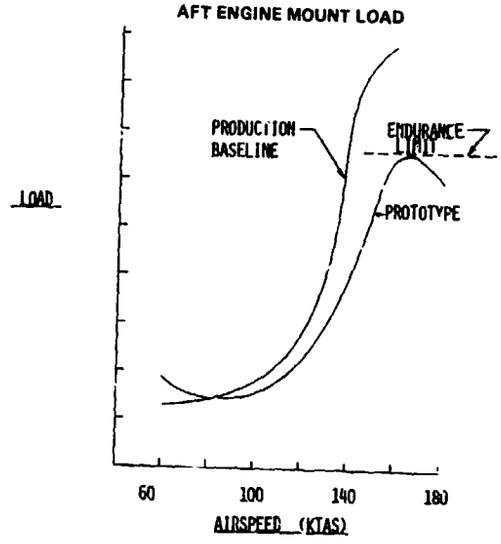

Slide 2.

EXHAUST FRAME VERTICAL ACCELERATION BASELINE PRODUCTION CONFIGURATION

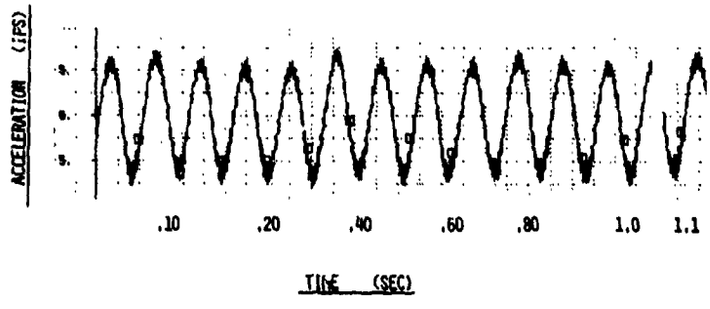

Slide 3.

AFT ENGINE MOUNT LOAD AT V_H

BASELINE PRODUCTION CONFIGURATION

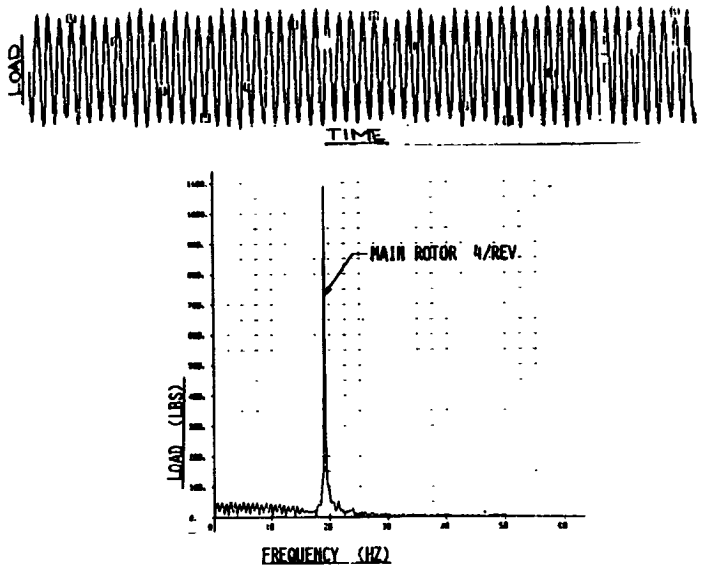

Slide 4.

ENGINE PITCH FREQUENCY

ANTI-SYMMETRIC MODE

SOURCE	FREQUENCY (HZ)	
	PROTOTYPE	PRODUCTION
GROUND SHAKE TESTS	20.8	22.2
FLIGHT DATA	19.7	18.6 -19.3
NASTRAN		1st CUT 17.69* FINAL 19.83
M/R 4/REV	19.3	19.3

* BALL JOINT INCORRECT

Slide 5.

AFT ENGINE MOUNT LOAD AT 80 KTS.

BASELINE PRODUCTION CONFIGURATION

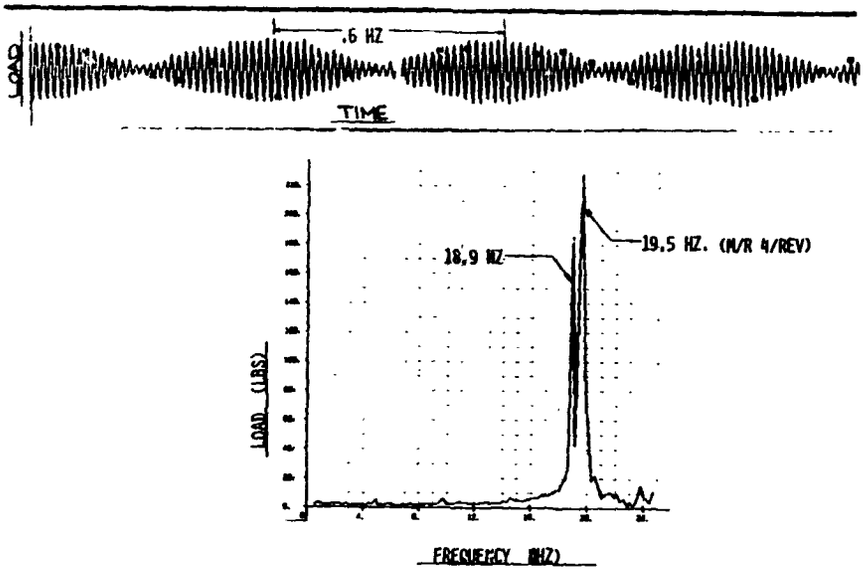

Slide 6.

FIXES INVESTIGATED

- TIGHTEN BOLTED JOINT
- BHO BRACES
  - INTERNAL
  - EXTERNAL
- STIFFENED AFT MOUNT
- SOFTENED AFT MOUNT

Slide 7.

STIFFENED AFT ENGINE MOUNT

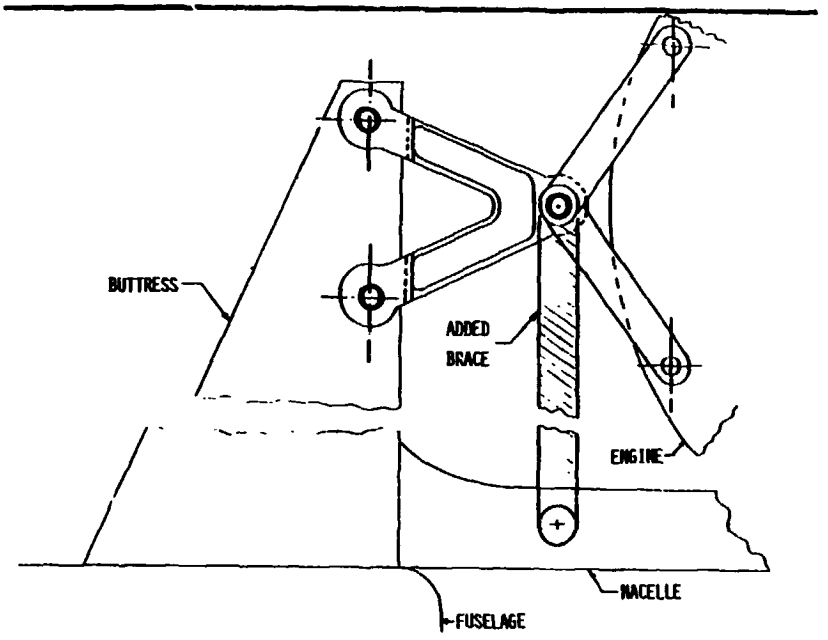

Slide 8.

AFT ENGINE MOUNT LOAD IN HOVER
STIFFENED CONFIGURATION

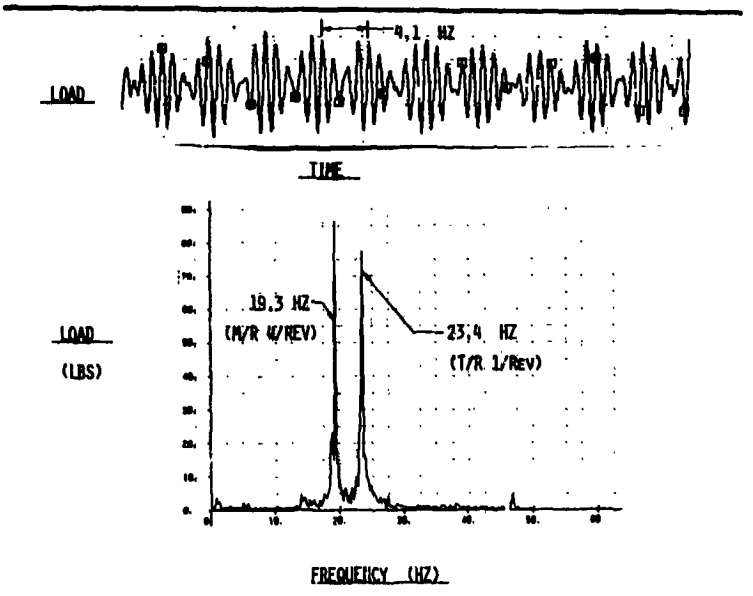

Slide 9.

AFT ENGINE MOUNT LOAD

STIFFENED CONFIGURATION

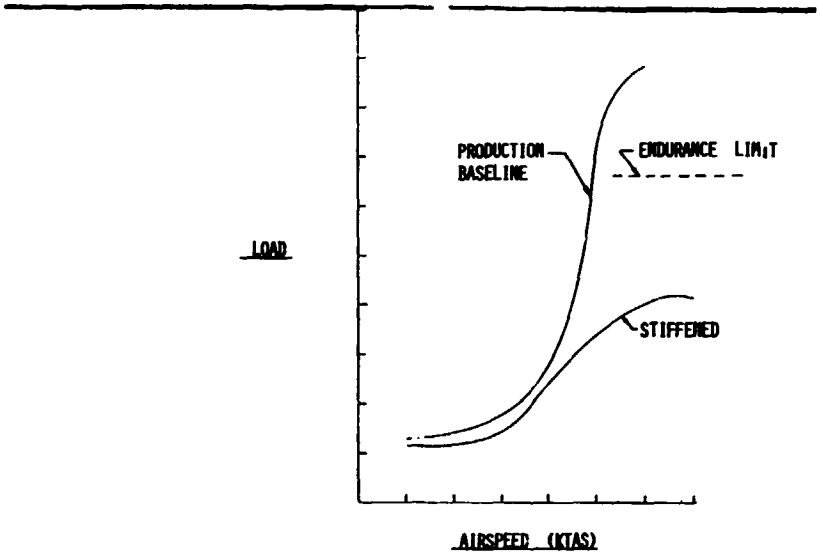

Slide 10.

STIFF MOUNT - PRACTICAL PROBLEMS

- FABRICATION
  - COMPLEX JOINT
  - REDUNDANT (FIT PROBLEM)
- ADDITIONAL FATIGUE TESTING OF MUCH STRUCTURE REQUIRED
- DAMAGE OR FAILURE TENDS TOWARD RESONANCE

Slide 11.

SOFTENED AFT ENGINE MOUNT

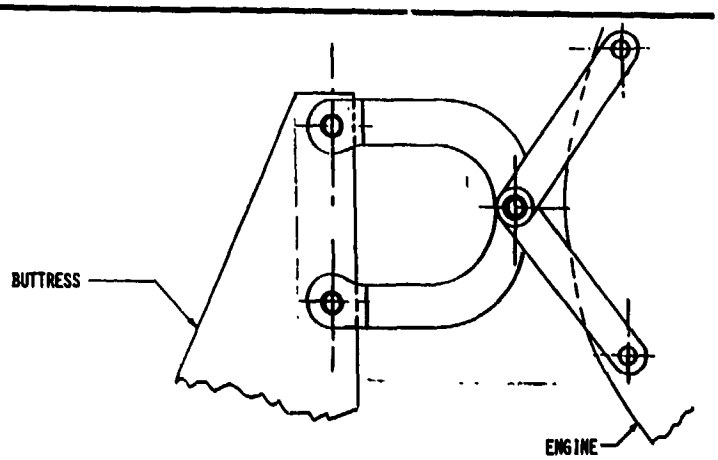

Slide 12.

AFT ENGINE MOUNT LOAD AT 60 KTAS
SOFTENED CONFIGURATION

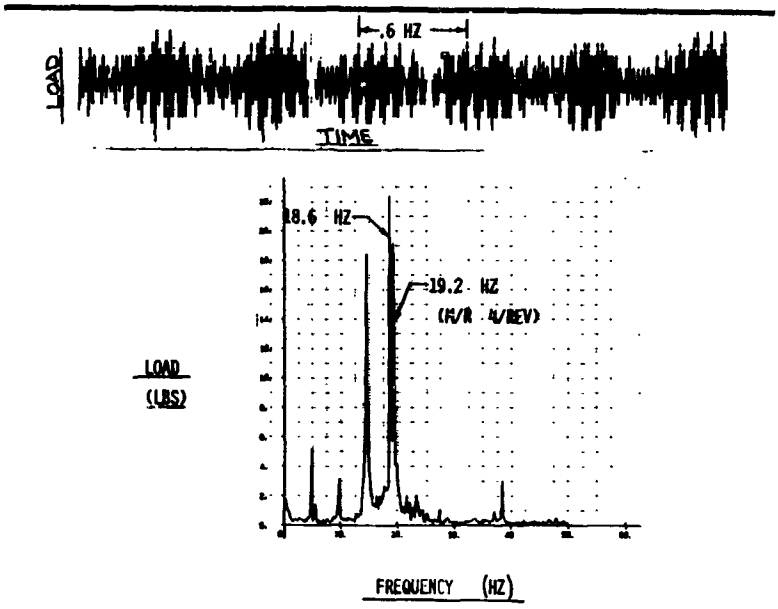

Slide 13.

AFT ENGINE MOUNT LOAD
SOFTENED CONFIGURATION

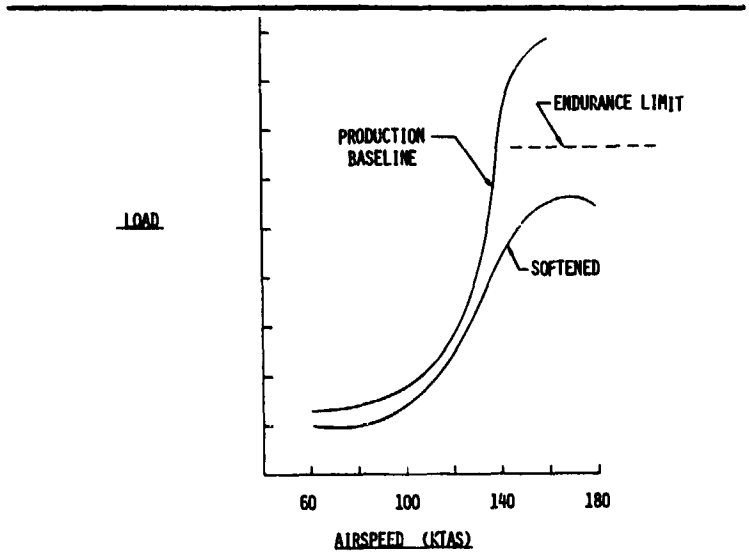

Slide 14.

EFFECT OF AMPLITUDE ON FREQUENCY

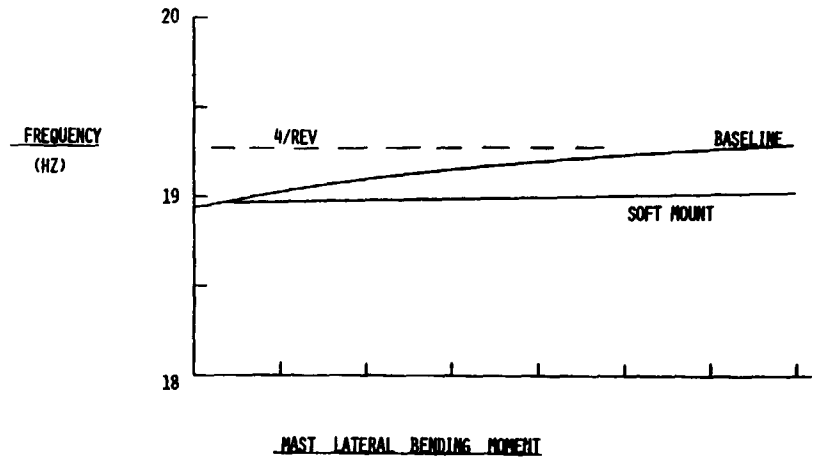

Slide 15.

SOFT MOUNT - WHY NOT SOFTER ?

- DEFLECTION DUE TO STEADY LOAD
- SECONDARY MOUNT CLEARANCE
- SHAFT COUPLING FATIGUE

Slide 16.

Integration of the General Electric T700 Engine in the AH-1T Helicopter

Rodney W. Balke
Chief, Structural Dynamics
Bell Helicopter Textron Inc.

I have chosen as my practical dynamics problem solving experience the installation/integration of the GE T700 engine into the AH-1T aircraft. Now I am sure that most of you have a file drawer full of very similar experiences so I think you will find a lot of things in common. As Jim Neff has indicated a number of you out there have experience with the T700 engine itself.

How many of you have experienced a program which had a very simply stated objective, but had a number of criteria tied to it that says "fix the problem but don't change anything?" Then on top of that things got rather complex. The objective as shown in Slide 1 was to increase power for critical tactical situations, not so much for a higher performance airspeed or those sorts of things. The constraints, which were basically in-house constraints, for cost and schedule reasons and commonality was to use the Model 214ST combining gearbox design and to use the Model 214ST engine mount configuration. I should point out to you that this was our third experience of installing a T700 engine in one of our designs so we did have some background which gave us a better handle on what to expect. Slide 2 shows the AH-1T as configured with the T700. The cowling has been changed some and the forward contour has been changed; there has been some weight moved forward because the engine c.g. is further aft. The engine packages are shown in Slide 3. the T400 engine package, which was the previous package, has the combining gearbox at the aft end. There was for the T400 engine a long drive shaft driving forward between the engines to the main transmission. The T700 engine package mounts onto a Bell-designed combining gearbox on the forward end, the drive shaft to the main transmission comes from the forward side of the combining gearbox. We incurred a 73% reduction in drive shaft length, which for our soft-mounted transmissions becomes somewhat significant. The 214ST-type mounting is shown in Slide 4. Both a tripod and a bipod attach to the combining gearbox at the front end, and at the back end there is a vertical monopod under each engine on centerline. There is a lateral tie--with pin ended links--across to a bipod to rigidize the center point. We did change the tripod and bipod configuration some in order to accommodate the structure of the AH-1T and to give better dynamic load paths.

The by-products of the engine change are shown in Slide 5 and this is where things begin to cascade into problems. We installed the engine package, and we got the increased power that we were looking for, of course. But along with it we got other things such as added weight which gives us a c.g. shift. The combination of these resulted in a change in frequencies and mode shapes. The increased power gives us increased pylon windup. This results in increased shaft misalignment. Increased power gives us increased performance, increased aerodynamic loading, and increased pylon pitch due to the steady loads. These all result in problem areas. The engine package installation design had to address different crash load requirements and deck warpage due to the aft end of the aircraft torqueing under the combination of main rotor and tail rotor thrust loads. These problems then, including a pylon rock that we encountered at high g levels, were the problems we had to deal with. The primary one that we forecast was the high engine vibration and this was one of the prime problems; the second one was the crew vibrations. The others were not anticipated as much.

A significant problem that we were aware of or anticipated was the effect of the mode shape--2 per rev mode shape--from the AH-1T previous flight test. When we looked at these mode shapes in the location of the engine mounts we found that the aft-monopod incurred about 50% more input than the forward end. Slide 6 shows the planform deck attachments of the tripod and bipod. This meant that we were going to be driving the engine in bending at 2 per rev. So we began doing some studies of this. We put together a structured program which included analyses, support tests, and flight tests as shown in Slide 7 to try to provide an early identification of the problem; to provide an alternate design; and to provide enhanced capability to understand and resolve problems encountered in flight. After quite a few overtures we were finally successful in getting the program commitment from the project to pursue this. The tasks that we conducted to ensure acceptable engine vibrations are outlined in Slide 8. We did develop an alternate mount configuration for two purposes: to counter the static deck warpage, and to provide some isolation. We measured the engine deck dynamic compliance, and we did static load deflection tests on the engine package to get parameters for our NASTRAN model. We did not model the gearbox in detail; we had some springs and masses to simulate it. We got the data from the static and dynamic tests. We determined the engine package frequencies and mode shapes in several different ways. We did it free-free because this gave us the best check on the NASTRAN model of the engine package and gearbox. We tested it on a rigid deck, just mounted to the floor, then we looked at it on a flexible plate. There we were primarily looking at the alternate mount and deck warpage. And then we tested in the aircraft. We did NASTRAN analyses, correlation of each test; we predicted the crew vibrations and engine vibrations at the new V_{LIMIT} with the increased power; and we did a simulated gun recoil test of the alternate engine

mount installed in the aircraft. We were concerned that the lateral gunfire might trigger a particular engine mode.

The solutions to the problems are shown in Slide 9. I won't go over these problems again--these are the same problems we ended up with before. For the pylon rock we added additional damping. For the increased shaft misalignment we relocated the engine and added stiffer axial and radial pylon mounts. For the crash load requirement we added a constraint that was effective only during crash. The alternate engine mount took care of the deck warpage and the increased vibrations. Along the way though, with the alternate engine mount we ran into another flag and that was that the engine manufacturer said, "Okay, now that you are redundant or semi-redundant you have to meet some additional criteria to prevent compressor rub." These were really complex criteria, but we were able to implement them on the computer and monitor them on-line. For the increased crew vibration, we added an active vibration suppression system in the nose of the aircraft. This was one we had offered the Navy in the original T and they had chosen at that point not to take it. For the increased empennage vibrations, we beefed up the fin spar. Now when we added the active suppression system we incurred a delta in increased engine vibrations which was predictable. We also got some increase in the fin spar stresses, which was also predictable. So we ended up with a mounting system where we could meet both the standard and the new criteria. The fin spar ended up with acceptable stresses with no damage. For the rotor and control components we modified components or revised the service lives to accommodate the higher airspeeds. There were two other things that we did that are not shown here to counter the deck warpage. Torsional stiffness was added to the fuselage underneath the engine deck where there were some large cutouts for cooling systems. Additionally, stiffness was added to the neck of the combining gearbox.

The alternate engine mount is shown in Slide 10. This is one of those "fix it but don't change it" responses. We didn't change the tripod or the bipod location nor the lateral restraint systems. The only change was underneath the aft monopods where we installed an isolator which is essentially a pivot to the deck with a rigid arm and mass and a torsional spring. The two isolators, one on the left and one on the right, act independently of each other and therefore can accommodate static deck warpage and they can isolate both symmetric and asymmetric engine motions or deck motions. The torsion spring is two tubes, one within the other, with a flange at the end. The measured results for three locations on the engine are shown in Slide 11: the mainframe, the aft mount, and the exhaust frame. This shows the left engine vibration with the baseline mount and the reduction with the alternate mounting configuration. These data were with a prototype isolator of 15 pounds; the production isolator is reconfigured and the tuning weight is down to 3 pounds.

The vibration suppressor mounts up in the nose as shown in Slide 12. It's an enclosed hydraulic actuator with an internal inertial mass driven internally, synchronous with the rotor. It has an accelerometer mounted just above it and an electronic feedback circuit. The results measured on the prototype reduced the 2 per rev significantly as shown on Slide 13. Data are shown without the VSS on and with the VSS on. We were able to achieve this without incurring a significant increase in other frequencies, although on the prototype we did incur some 6 per rev which we have since worked out.

A conclusion that I have drawn from this (Slide 14) is that helicopter dynamic response is highly sensitive to configuration changes. Modifications such as an engine change can significantly impact the crew and component vibration service lives. As I say, most of you I think have been through that. Changes made to resolve one problem may actually increase vibration in other areas. This is what we experienced with the installation of the VSS. Major modifications should be approached with the expectation that vibration problems will require resolution. There are a couple of other conclusions I might make. I think one would be that the dynamicist needs a veritable arsenal of tools, reliable tools, if you will. Where there is a high risk in either cost or schedule, or there is a high probability of encountering such a problem, I think a structured program is recommended. I believe we need improved and faster test algorithms; shake test algorithms such as structural modification and that sort of thing, and we need improved NASTRAN correlation at higher frequencies.

PROGRAM OBJECTIVE AND CONSTRAINTS

OBJECTIVE

INCREASED POWER FOR CRITICAL TACTICAL SITUATIONS

CONSTRAINTS

- o USE MODEL 214ST COMBINING GEARBOX DESIGN
- o USE MODEL 214ST ENGINE MOUNT CONFIGURATION

Slide 1.

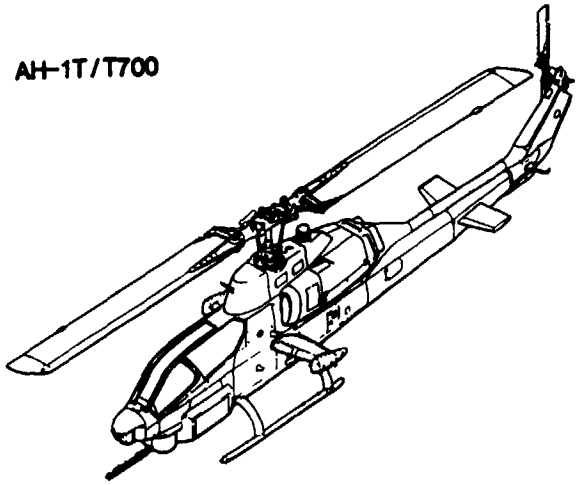

Slide 2.

PREVIOUS AND NEW ENGINES

T400-PW ENGINE PACKAGE

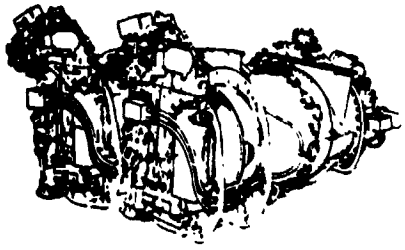

T700-GE ENGINE PACKAGE

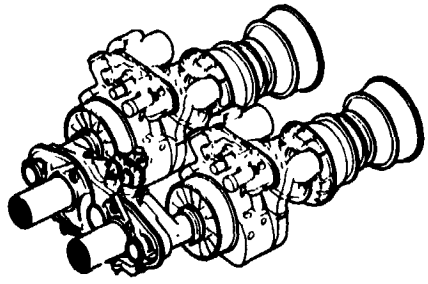

Slide 3.

214 ST TYPE MOUNTING

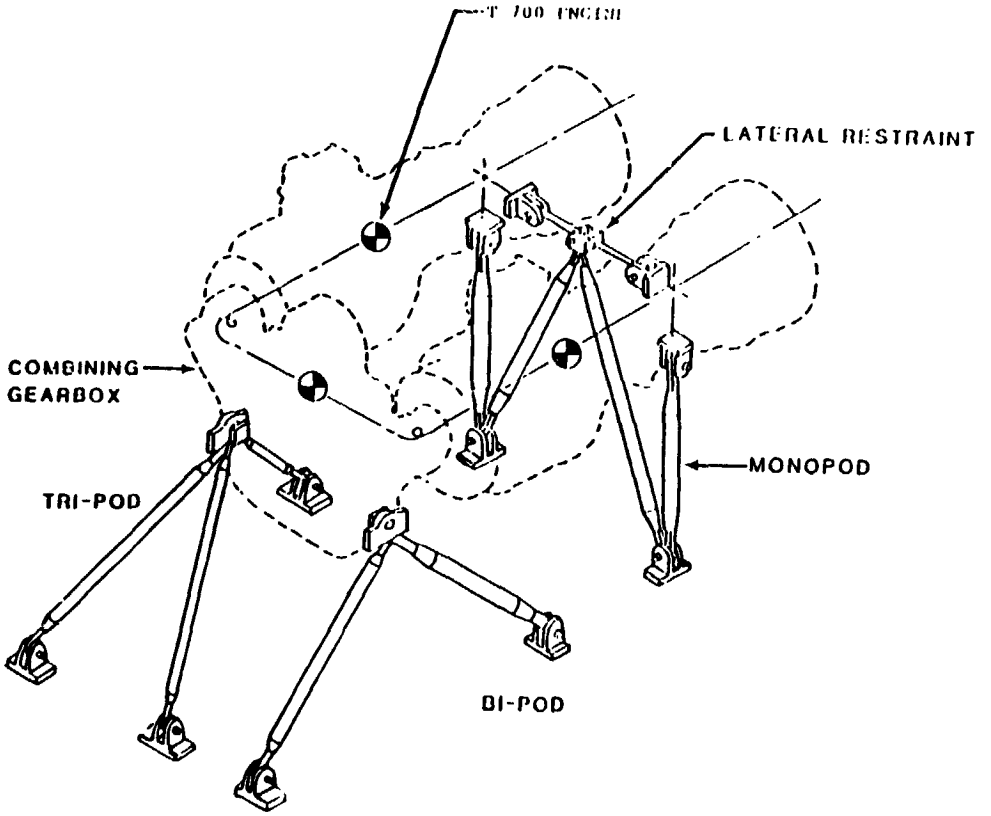

Slide 4.

BY-PRODUCTS OF ENGINE CHANGE

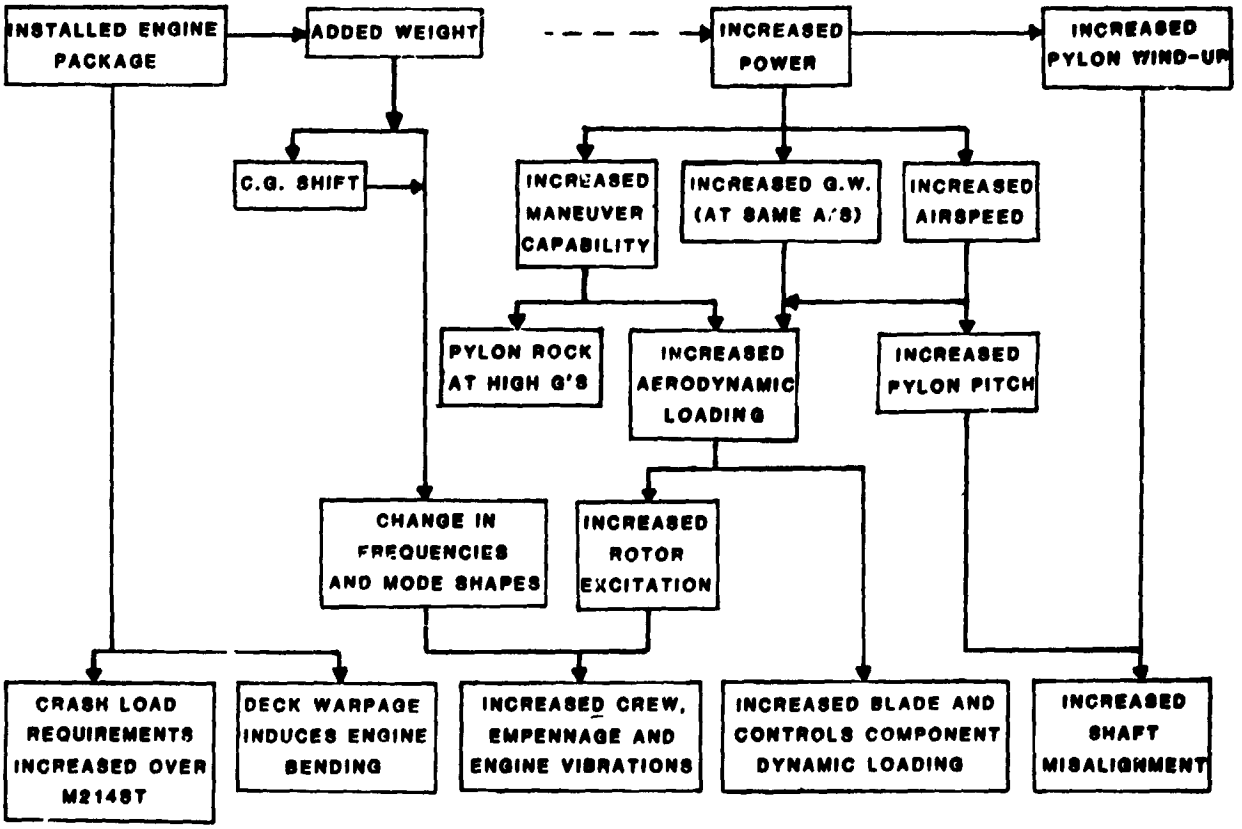

Slide 5.

AH-1T 2/REV FORCED RESPONSE MODE SHAPE

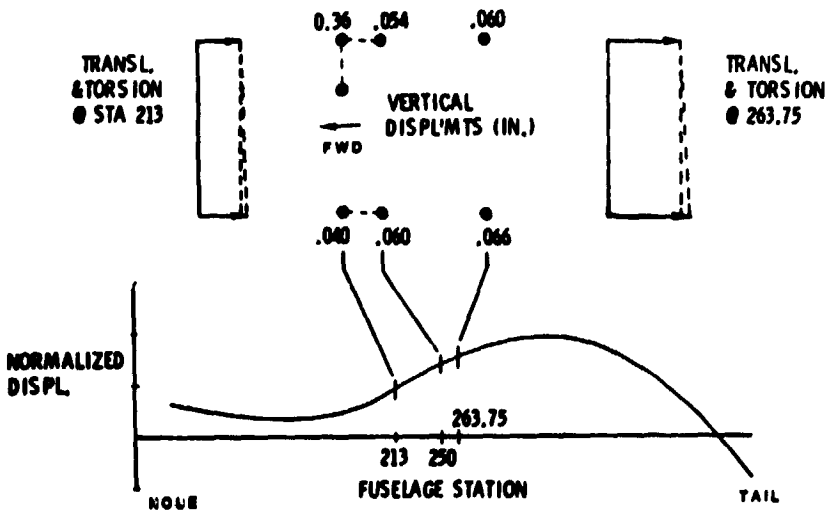

Slide 6.

BHTI DYNAMICS APPROACH TO AH-1T / T700 ENGINE MOUNTING

- STRUCTURED PROGRAM
- BALANCED BETWEEN ANALYSES, SUPPORT TESTS, FLIGHT TESTS
- PROVIDE EARLY IDENTIFICATION OF POTENTIAL PROBLEMS
- PROVIDE ALTERNATE DESIGN & HARDWARE
- PROVIDE ENHANCED CAPABILITY TO UNDERSTAND AND RESOLVE PROBLEMS ENCOUNTERED IN FLIGHT TEST

Slide 7.

TASKS CONDUCTED TO ENSURE ACCEPTABLE ENGINE VIBRATIONS

- o DEVELOPMENT OF ALTERNATE MOUNT CONFIGURATION TO ACCOMMODATE STATIC DECK WARPAGE AND ATTENUATE 2/REV DECK MOTIONS.
- o MEASUREMENT OF ENGINE DECK DYNAMIC COMPLIANCE.
- o STATIC LOAD - DEFLECTION TEST OF ENGINE PACKAGE
- o DETERMINATION OF ENGINE PACKAGE FREQUENCIES AND MODE SHAPES WITH BOTH PRIMARY AND ALTERNATE MOUNTS:
  - o FREE-FREE
  - o ON RIGID DECK
  - o ON FLEXIBLE PLATE
  - o IN AIRCRAFT
- o NASTRAN ANALYSIS AND CORRELATION WITH EACH TEST.
- o NASTRAN PREDICTION OF CREW AND ENGINE VIBRATIONS AT NEW V_{LIMIT}.
- o SIMULATED GUN RECOIL TEST OF ALTERNATE ENGINE MOUNTING INSTALLED IN AIRCRAFT.

Slide 8.

SOLUTIONS TO PROBLEMS

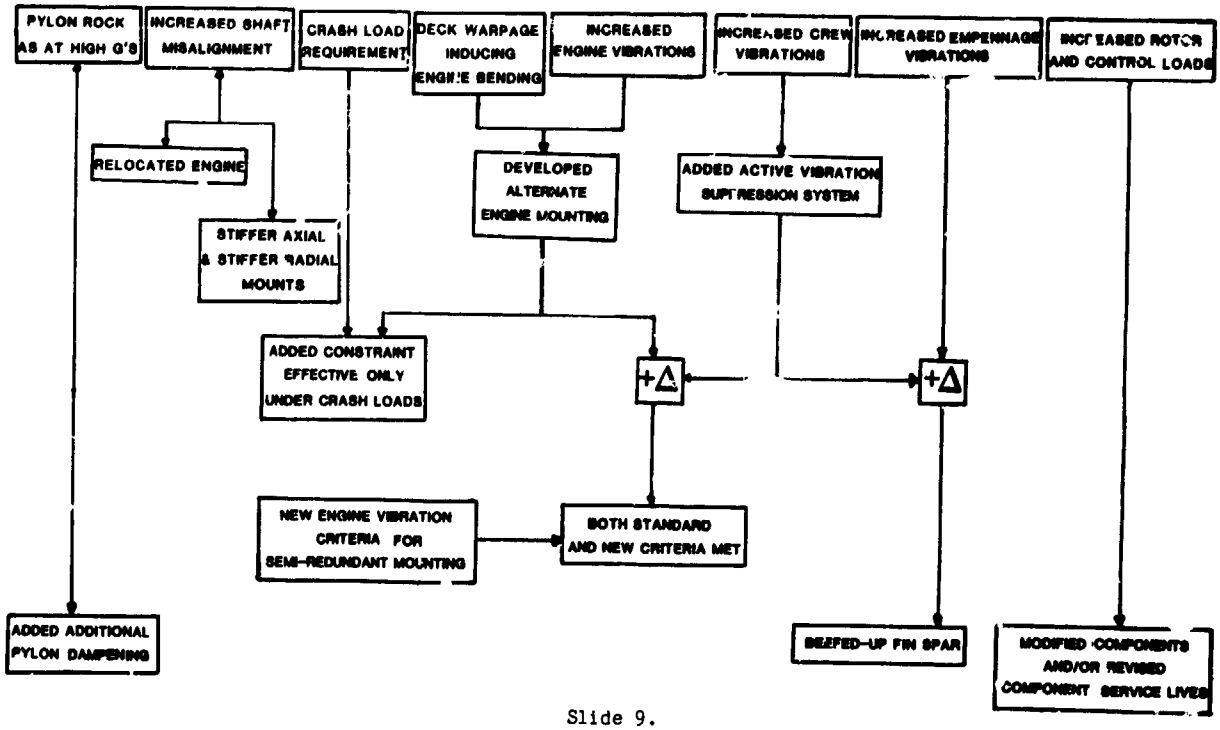

Slide 9.

AH-1T/T700 ALTERNATE MOUNTING

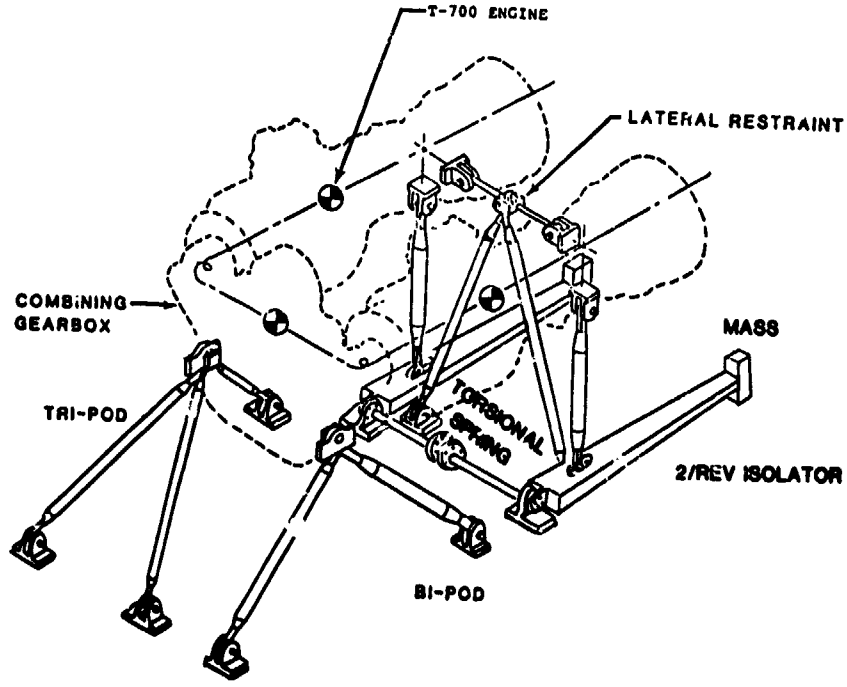

Slide 10.

AH-1T/T700 DISPLACEMENT ISOLATOR EFFECT

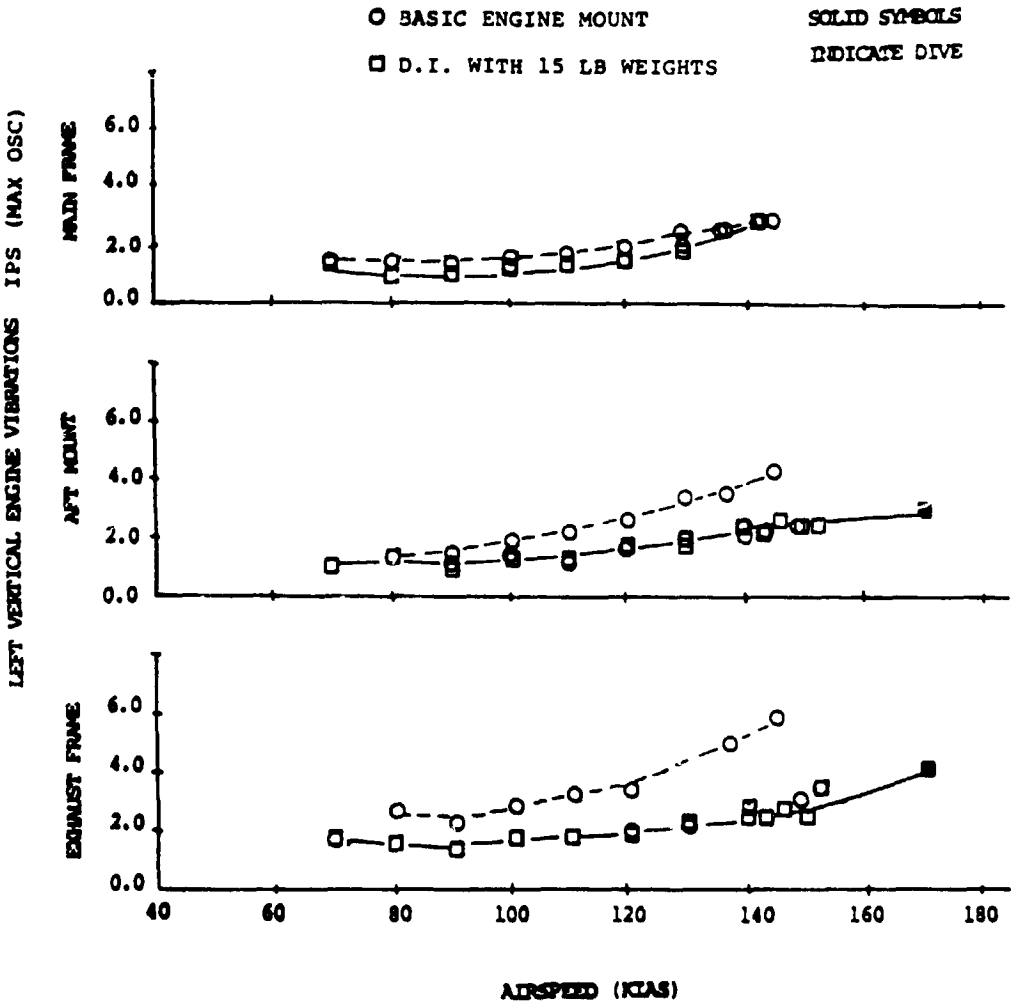

Slide 11.

AH-1T/T700

SuperCobra

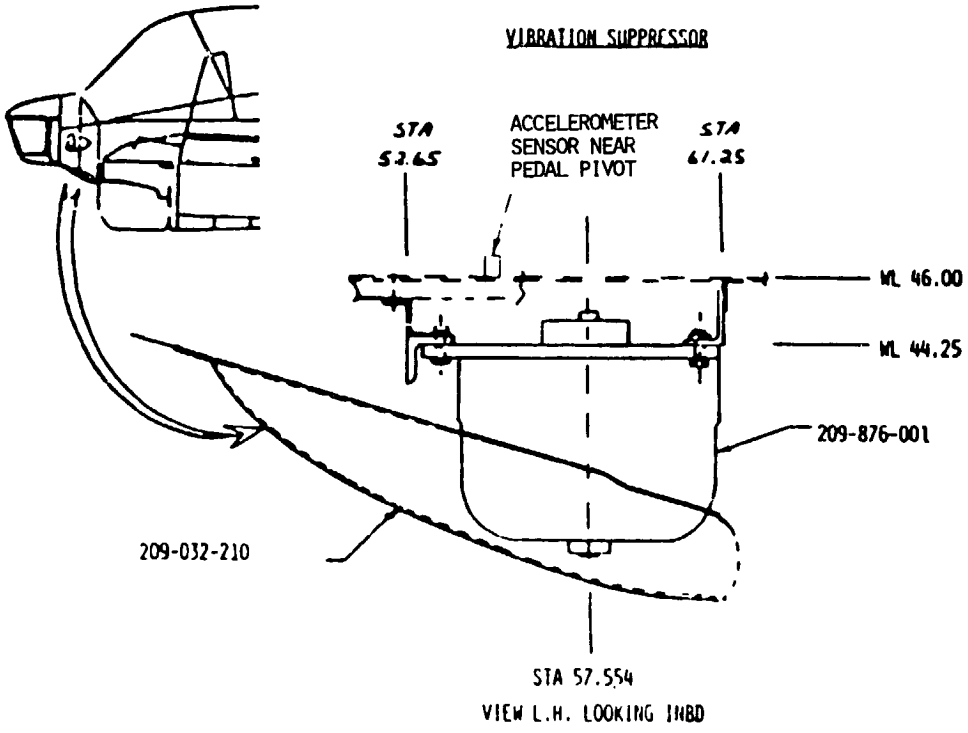

Slide 12.

AH-1T/T700 VIBRATIONS, VSS EFFECT

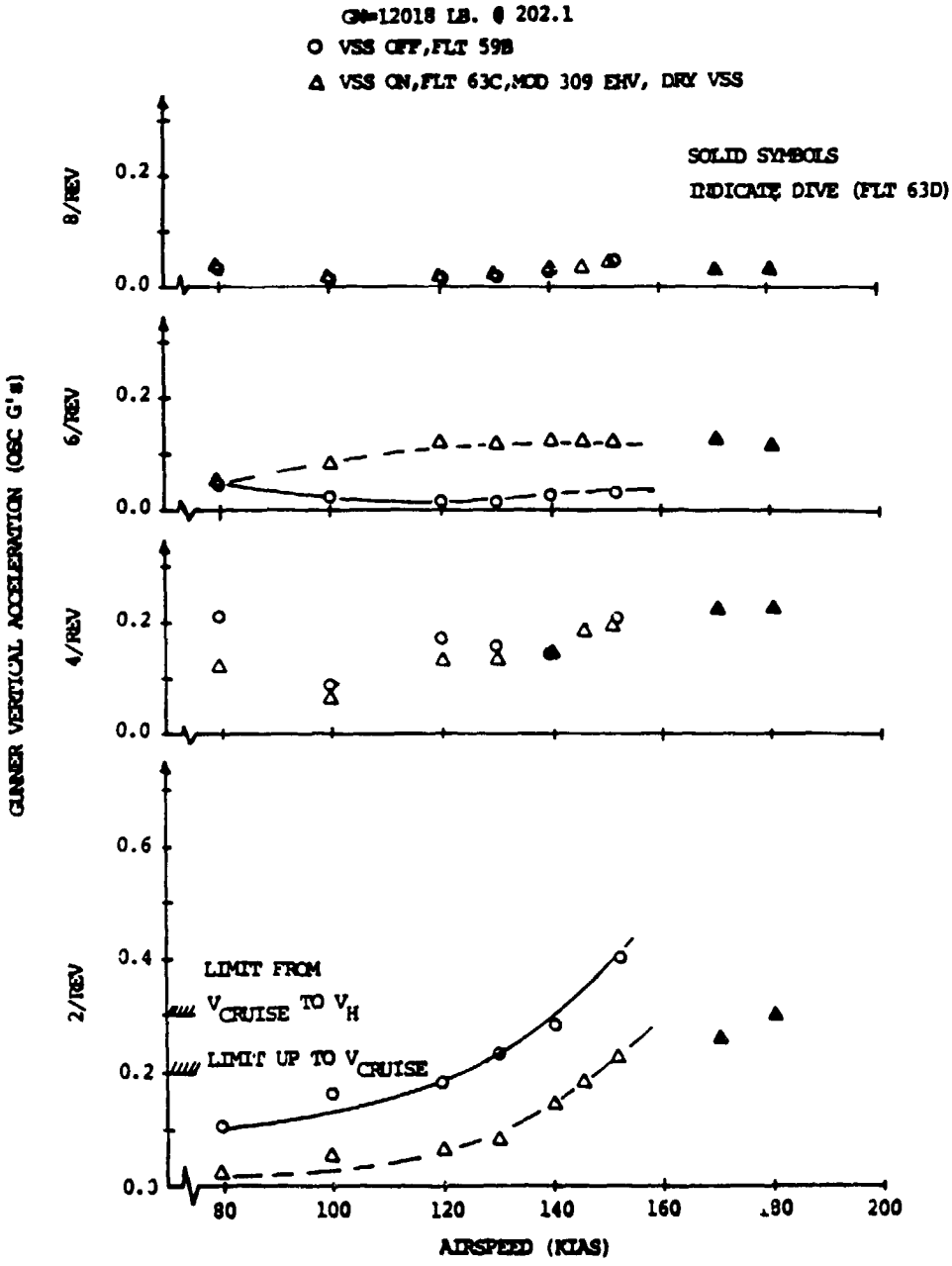

Slide 13.

CONCLUSION

- HELICOPTER DYNAMIC RESPONSE IS SENSITIVE TO CONFIGURATION CHANGES.
- MODIFICATIONS, SUCH AS AN ENGINE CHANGE WITH INCREASED POWER, CAN SIGNIFICANTLY IMPACT ON CREW AND COMPONENT VIBRATIONS AND SERVICE LIVES.
- CHANGES MADE TO RESOLVE ONE PROBLEM MAY ACTUALLY INCREASE VIBRATIONS IN OTHER AREAS.
- MAJOR MODIFICATIONS SHOULD BE APPROACHED WITH THE EXPECTATION THAT VIBRATION PROBLEMS WILL REQUIRE RESOLUTION.

Slide 14.

Use of Approximation Methods in the Development of the SH-2 Rotor

Robert Jones
Assistant Director for Aeromechanics
Kaman Aerospace Corporation

Approximation methods were used to assist in the development of the SH-2 rotor. The reason for using approximation techniques is that once you are in flight test and you have a rotor problem you don't have time to run back to your desk and use your complex analyzers. So you look for a simple tool to solve problems and approximation methods are this tool.

The problem I'm going to talk about is in the development of our SH-2 101 rotor. But first I'd like to give you just a brief history of the SH-2 (Slide 1). First of all, it went into the fleet in 1961. It was a single engine helicopter, 8500 lb gross weight. It had a flat plate area of about 16 ft^2. In 1971, it was a twin engine helicopter. It was then 12,800 lb, and 25 ft^2, and this is when we developed our present 101 rotor. Right at the given moment, it's still a twin engine, flying at 13,500 lb and has 35 ft^2. Why I would like to talk about the SH-2 101 rotor is for two reasons. First of all, it was a very interesting problem which I think all of you will also find interesting. And secondly, if you have any questions I can always use the excuse "I don't remember." I also want to point out that this is not the last problem Kaman has solved; we have solved a few since then.

Shown in Slide 2 is the objective: first of all we wanted to improve the rotor system to retain similar flying qualities, vibration levels, and stall characteristics of the 8500 lb vehicle at this new 12,800 lb. The constraints were we must retain the rotor diameter, retain the rotor blade spar, retain the rotor retention hardware and retain the hub, in other words, the same size rotor. I think this is quite a significant achievement when flying the present helicopter configuration having doubled the flat plate area and it still has essentially the same size rotor on it. It's a very good improvement.

I'll try to go through this quickly because I know that we have a time problem. Our solution is shown in Slide 3. From a stall standpoint we wanted to unload the tip. We can do this by changing the retention strap windup and decreasing the C_T over sigma. The half inch chord didn't really do much, that was put on for another reason. We did change the tip speed by 4%. We got vibration and bending moment reduction by retuning the blade and of course our R&M was done by simplifying the control system--we made 60% fewer parts. The proposed solution was verified by both analysis and testing (Slide 4). In the analysis we used our Kaman 6F program and we looked at indexing effects and tuning effects on the blade (Slide 5).

Just to give you a little bit about our servoflap rotor, as I say, the SH-2 is a servoflap-controlled rotor system as shown in Slide 6. We have a very soft root retention spring achieved by retention straps that have a spring rate of about 116 in-lb/deg which gives a torsional natural frequency of that blade of 1.3 per rev. We do have aerodynamic feedback which gives an additional aerodynamic spring rate in flight of about 2.5 per rev in feathering. The original rotor had a straignt strap and we in essence needed a download from the servoflap to produce a nose-up pitching moment to achieve our control. In the analysis we put in 60 degrees of pre-twist, this then required an upload from the servoflap to get a nose-down pitching moment for control. We did some analyses using our 6F program and as you can see in Slide 7 this indexing affects the air load distribution tremendously. In fact you can see we did unload the tip in certain areas over the present rotor and this allowed us to control the angle of attack at the tip. The analysis also showed (Slide 8) that we reduced the angle of attack with the retuning of the blade.

We did two series of flight tests (Slide 9). The first was to determine the best indexing position of the root spring using the existing blade and the second flight test was ballasting the new rotor blade. We first indexed the blades 45 degrees and the pilot attempted to find a stall boundary. He couldn't find stall, but unfortunately he found a lot of 4 per rev. So we did vary the indexing of the rotor, ending up with 27-1/2 degrees of root indexing and got a 24 knot increase in stall speed as shown in Slide 10. This was with the same rotor blade and the results were obtained with only a change in indexing of the root spring.

Now at Kaman, since we have a very soft torsional rotor, we do run into stability problems that most of you have been talking about the first two days of this meeting. And what we do is shown in Slide 11. We do analysis, but only depend upon it for trending purposes. For previous rotors we have normally worried about the flap-feathering mode from a flutter standpoint which gives us a weave and/or divergence problems. We determine our stability boundary experimentally by whirling on the rig. And we do this by destabilizing the blade. The blade is destabilized by putting lead tape on the trailing edge of the blade and this produces an adverse coupling of flapping-feathering which we call an I_R. We do determine the stability boundary from the rig.

So having determined the experimental stability boundary of this particular rotor designated R-10 (the ballast configuration having been determined analytically) the rotor was ready

for flight test (Slide 12). It had 30 inches of tungsten ballast of about 30 pounds and 21 inches of aluminum spacer to bring the ballast weight inboard. Our analysis indicated we saved two degrees of angle of attack at the tip and a major reduction in bending moment.

We initially flew 3 blades as shown on Slide 13. One thing I do want to point out is that we're very good at changing ballast at Kaman. We do it quite readily. We designed in our blades the capability of changing this ballast so that it is an overnight change. We will fly the blade, if it's not good, we will go in and change the ballast and fly the next day. Slide 13 also shows the results of flight testing. The R-10 was not an acceptable blade from the pilot's standpoint--the vibration was too high. But it was stable. We flew what we then called an R-16 blade which had three ballast weights at the tip, about 42 inches of aluminum spacers, and 9 inboard ballast weights. You can see the stability criteria was quite good; however, we had high bending moments. So we went to the R-17 blade. In fact, we whirled this blade on the whirl stand--it was stable by the I_R criteria (flapping-feathering mode). The bending moments are shown at 40 knots; it was a very good blade, we had low bending moments, the pilot liked it, but at 106 knots we literally had a flutter--in flight. The pilot didn't like that very well; in fact, I think he cussed a little bit when he came down. He was able to control it--he dropped collective and lowered speed. Now our problem was we couldn't fly anymore. We did have to go back to the desk and do a little work. But we did not have time to use complex analyses, such as our 6F. Our 6F does have a stability prediction capability. So we did run three blades as shown on Slide 14--the one that went unstable (R-17), which you notice our program predicted to be much less stable, our standard blade, and the R-10. However, the R-17 was predicted to be much less stable than the other two blades. Since our stability calculations could only be used for trending, we used the stability of the standard blade as a criterion in that a new blade could not deteriorate from the stability of the standard blade.

To determine a good flight blade, we looked at 48 different ballast configurations (Slide 15). We calculated natural frequency, stability parameters, that is, the flapping-feathering product of inertia, and the bending-feathering product of inertia. I should have pointed out that the stability problem encountered appeared to be a bending-feathering coupling problem. It was not the flap-feathering coupling that we have run into normally before. And of course we got our modal parameters. We could look at quite a few blades because running our digital frequency program requires little time. We selected from these 48 blades, 8 possible candidates for the flight blades as shown on Slide 16. And we did run stability on these blades, in our 6F program, and we did fit an approximation curve to the results that were obtained. Slide 17 shows the fit, and it is seen that a good fit was obtained. We used this equation to quickly determine the stability of the various blades we were going to consider. We had several criteria. Slide 18 shows the frequency criterion. Of these blades, the R-16 was flown and had high bending moments and was assumed to be the worst blade. We had blades above 3 per rev and blades below 3 per rev. At Kaman, because of the location of the servoflap and ballast requirements to achieve stability, the blade's above 3 per rev. We have found that blades about 3 per rev are very good from a vibration standpoint. We also have a flapping-feathering coupling criterion. We had a preferred and an acceptable margin for this coupling for the various candidates as shown in Slide 19. All of them from this standpoint were an acceptable blade including the R-17 we had flown. We found the blade bending-feathering coupling term to be the most important criterion. (Slide 20). The R-17 that went unstable had mass balance at the leading edge at the tip. That's a point I don't think I made clear. Our mass balance is always going in the leading edge of the blade so it is a forward c.g. This means that in the R-17 we had a weight at the tip that gave the best type of c.g.-a.c. offset from the standpoint of the flapping-feathering mode. However, it was the blade that was unstable. The blades that were acceptable, we had to put ballast inboard of the tip. We always had to have a spacer. That is, we had aluminum and then our tungsten weights. And we found that bending-feathering is a very critical mode. So not only flapping-feathering is a problem, but bending-feathering. I think once you get into torsionally very soft rotors you are going to find this to be a major problem.

Slide 21 shows all of the blades, including the R-17, that were flown. The estimate of stability using the regression equations compares well with the 6F calculated stability where applicable. Even our regression equations, after the fact, did predict the R-17 to be unstable. We did also use an estimate of bending moment by the approximation method. It was done at 40 knots and compared to the flight results. As you can see we did get a big variation of 3 per rev bending moment, but our prediction capability using the approximation was not bad. We selected the R-28 as the production blade. It had fairly low bending moments, it had good stability characteristics, and, of course, we relied on our flight test results and pilot opinion to determine that the blade was very acceptable from a vibration standpoint. On the NPE #1 blades we did not do any analysis except via the approximation method. The blade was stable and had low bending moments and this became our production blade. Incidentally, this approximation analysis required about two weeks and we got back into flight testing in a two week period of time.

Shown on Slide 22 was the final result of increase in stall. We got a 45 knot increase in stall for the final 101 rotor blade over the standard rotor. Twenty-four knots of it was due to indexing, only three knots was due to the solidity change, mainly because the increased chord was not done for this purpose, and we got 18 knots due to the increased tip speed for a total of

45 knots. This is the present rotor that is on our SH-2 helicopter, which is now flying at 13,500 lb, 35 ft^2 and has very low vibration. It's very competitive from that standpoint. It has good flying qualities and the fleet pilots like the rotor very much.

SH-2 GROWTH

1961 ENTERED FLEET
SINGLE ENGINE
8500 LB. GROSS WEIGHT
16 FT^2 DRAG AREA

1971 DEVELOPED PRESENT 101 ROTOR
TWIN ENGINE
12,800 LB. GROSS WEIGHT
25 FT^2 DRAG AREA

1984 TWIN ENGINE
13,500 LB. GROSS WEIGHT
35 FT^2 DRAG AREA

Slide 1.

101 ROTOR DEVELOPMENT

OBJECTIVE

IMPROVE ROTOR SYSTEM TO RETAIN SIMILAR FLYING QUALITIES, VIBRATION CHARACTERISTICS, AND STALL MARGINS OF THE 8500 LB. VEHICLE AT 12,800 LB. WITH INCREASED BLADE LIFE AND BETTER R&M CHARACTERISTICS.

CONSTRAINTS

RETAIN ROTOR DIAMETER

RETAIN ROTOR BLADE SPAR

RETAIN ROTOR RETENTION HARDWARE

RETAIN HUB.

Slide 2.

SOLUTION

- STALL
  - UNLOAD TIP AERODYNAMICALLY
    CHANGE RETENTION STRAP WINDUP
  - DECREASE C_T/σ
    1/2 IN. CHORD INCREASE
    4% INCREASE IN TIP SPEED
- VIBRATION AND BENDING MOMENT REDUCTION
  - RETUNE BLADE
- R&M
  - SIMPLIFIED CONTROL SYSTEM
    60% FEWER PARTS

Slide 3.

VERIFICATION

- ANALYSIS
- TEST
  - INTERIM 101 ROTOR (INDEXING ONLY)
  - 101 ROTOR (NEW BALLASTED BLADE)

Slide 4.

ANALYSIS

- KAMAN 6F AEROELASTIC DIGITAL PROGRAM
  - INDEXING EFFECTS
  - TUNING EFFECTS

Slide 5.

EFFECT OF RETENTION STRAP WINDUP ON SERVOFLAP LIFT

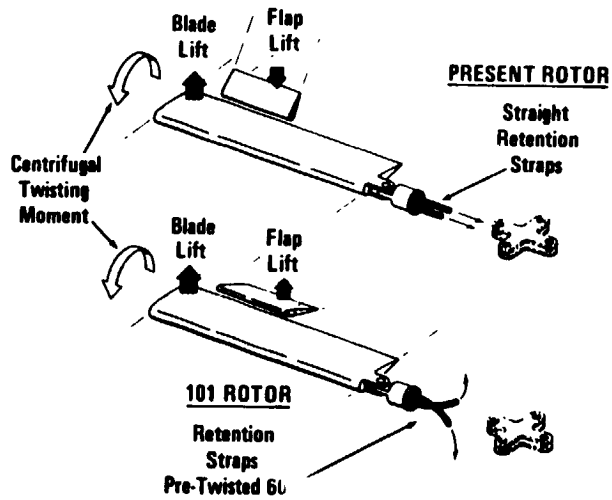

Slide 6.

BLADE LIFT DISTRIBUTION

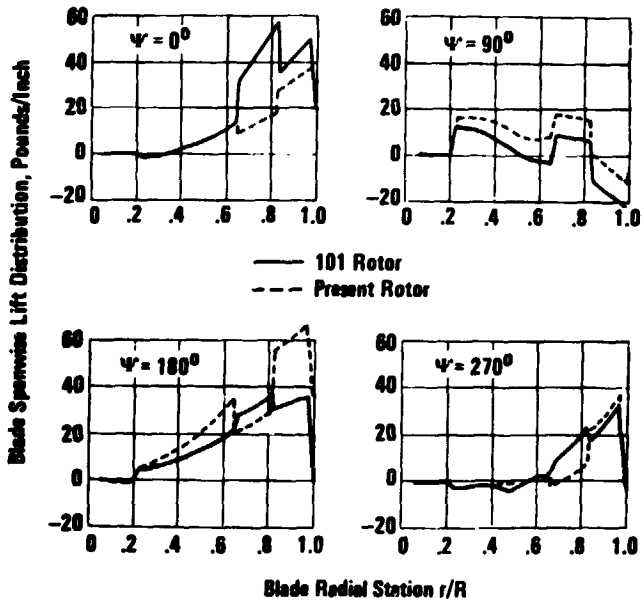

Slide 7.

MAIN ROTOR CHARACTERISTICS AT 11500 LBS

⊙ PRESENT ROTOR △ 101 ROTOR (STD. BLADES) ⊡ 101 ROTOR (BAL. BLADES)

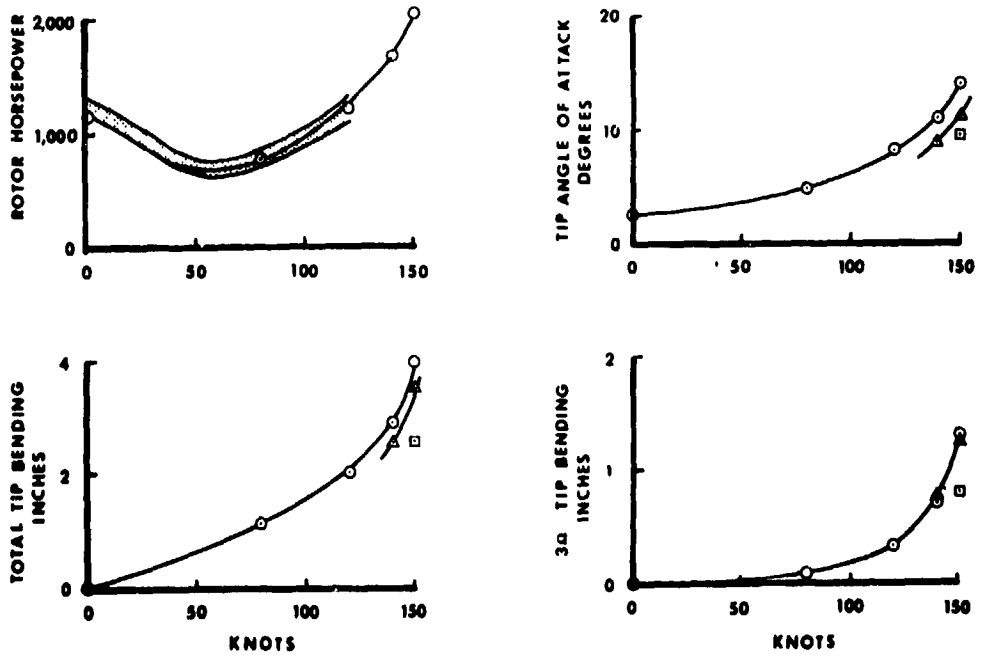

Slide 8.

TEST

- INTERIM 101 ROTOR (INDEXING ONLY)
- 101 ROTOR (NEW BALLASTED BLADE)

Slide 9.

H-2 RETREATING BLADE STALL BOUNDARY

GW = 12800# N_R = 102%

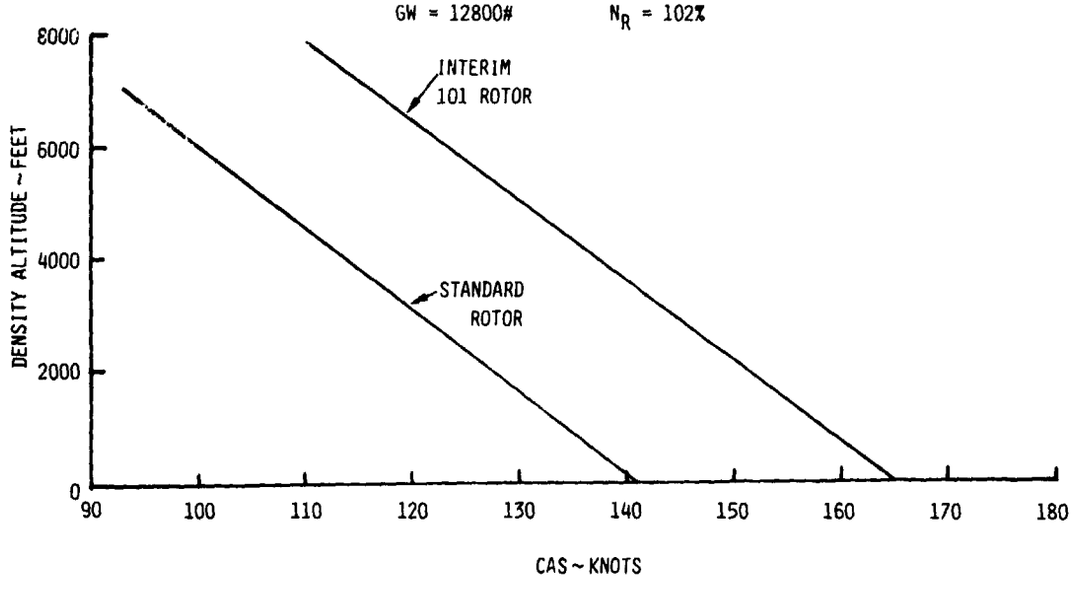

Slide 10.

KAMAN PROCEDURE FOR DETERMINING STABILITY OF NEW ROTOR BLADE

- IN PREVIOUS ROTOR DEVELOPMENTS, STABILITY WAS CONCERNED WITH FEATHERING/FLAPPING MODE.
  - WEAVE
  - DIVERGENCE
- STABILITY BOUNDARY EXPERIMENTALLY DETERMINED.
  - WHIRL THE ROTOR ON KAMAN'S WHIRL RIG.
  - DESTABILIZE BLADE UNTIL INSTABILITY OCCURS.
    - LEAD TAPE ON TRAILING EDGE OF BLADE.
    - PRODUCT OF INERTIA OF FLAPPING/FEATHERING (I_R).

Slide 11.

ANALYTICALLY DETERMINED BLADE

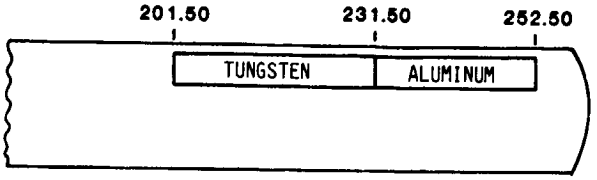

R-10 BLADE

TUNGSTEN BALLAST	30" ~ 30;564#
ALUMINUM SPACER	21" ~ 2,591#

COMPARISON

	STANDARD ROTOR	R-10 ROTOR
α_{MAX}	13.77°	11.73°
P-F BENDING MOMENT	17.9 KIP-IN	11.10 KIP-IN

Slide 12.

BLADE CONFIGURATIONS FLOWN

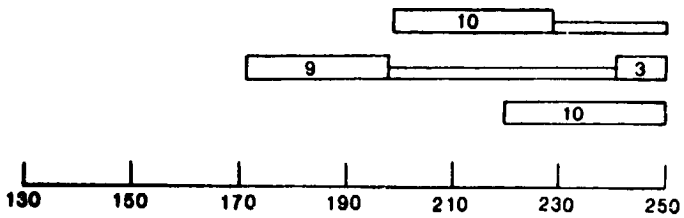

R-10	33.155#
R-16	44.449#
R-17	30.564#

RESULTS AT 40 KNOTS

BLADE	MEASURED VIB PENDING MOMENT	I_R $\times 10^{-3}$	STABLE
R-10	4500	-26.42	YES
R-16	7384	-21.75	YES
R-17	3400	-26.31	NO @ 106 KTS

Slide 13.

DAMPING OF FEATHERING/BENDING VS. SPEED

$Y = Ae^{\alpha t}$

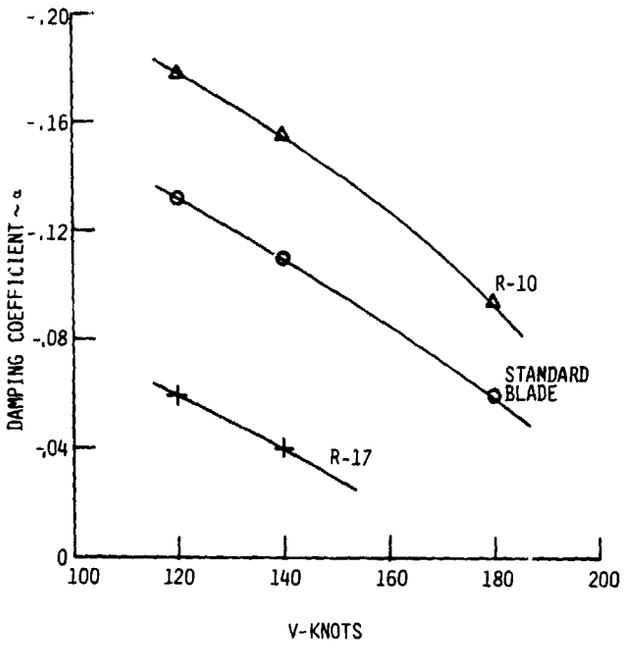

Slide 14.

FORTY-EIGHT DIFFERENT BALLAST BLADES

- NATURAL FREQUENCY
- STABILITY PARAMETERS
  - FLAPPING/FEATHERING PRODUCT OF INERTIA (I_R)
- MODAL PARAMETERS
  - SHAPE
  - GENERALIZED MASS

Slide 15.

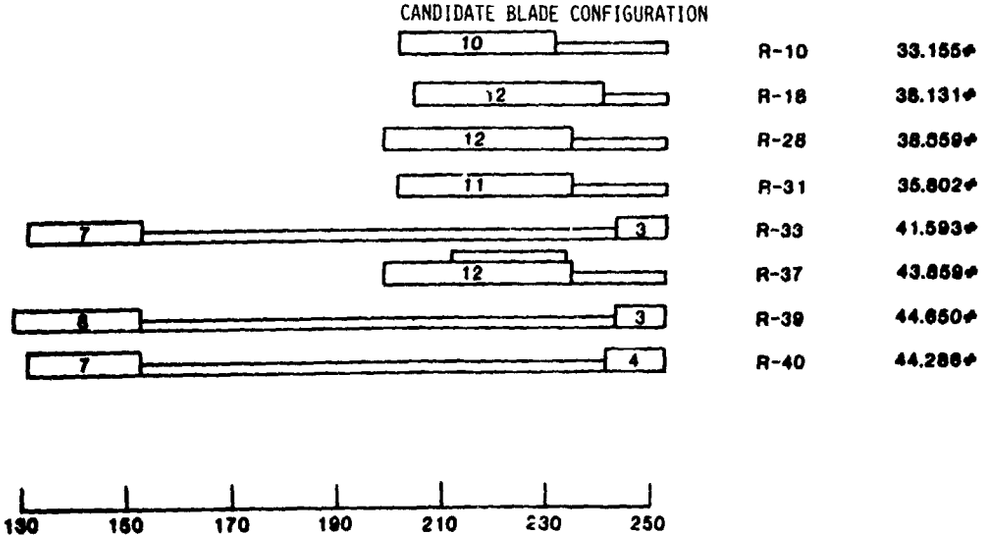

Slide 16.

RESPONSE SURFACE CORRELATION FEATHERING/BENDING
DAMPING COEFFICIENT

$$A_2 = -1.578 + .37\,\eta + 1.785\, I_{R_2} \times 10^{-2} - 2.097\, I_{R_2} \times 10^{-4} + .713\, I_{R_2} \times 10^{-6}$$

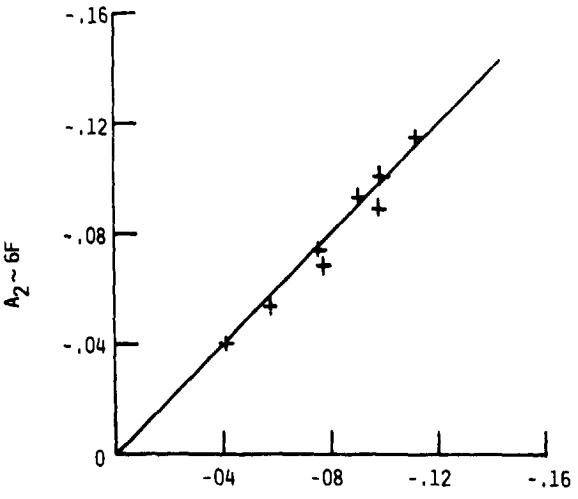

A_2 ~ RESPONSE SURFACE

Slide 17.

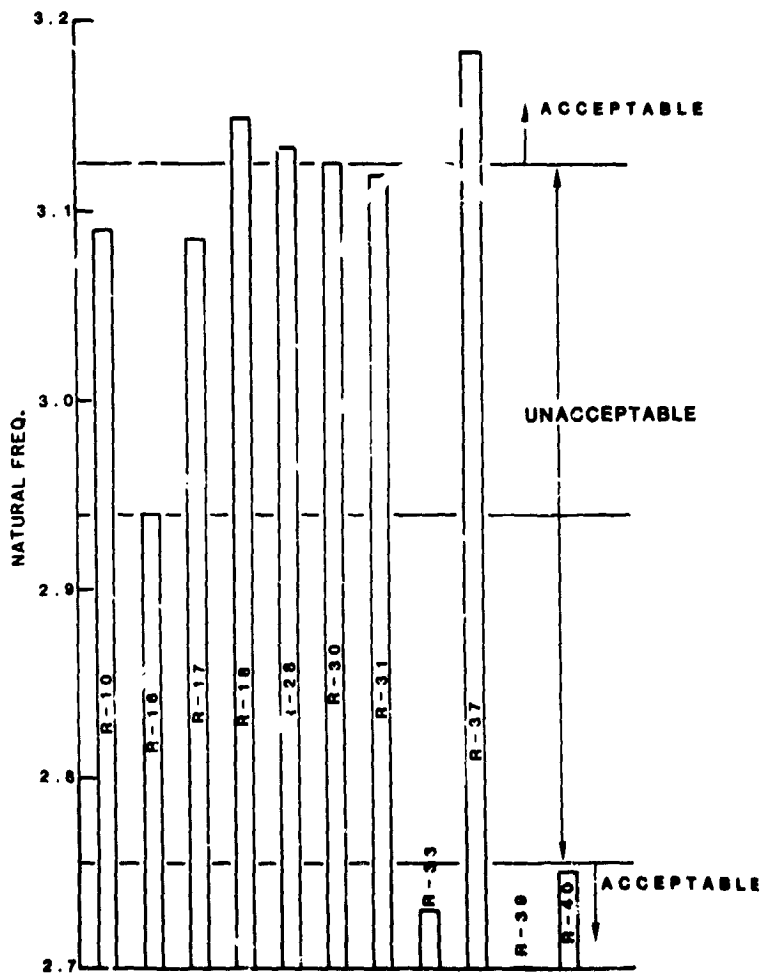
3.2
3.1
3.0
2.9
2.8
2.7
NATURAL FREQ.
ACCEPTABLE
UNACCEPTABLE
ACCEPTABLE
R-10
R-16
R-17
R-18
I-28
R-30
R-31
R-33
R-37
R-38
R-40

Slide 18.

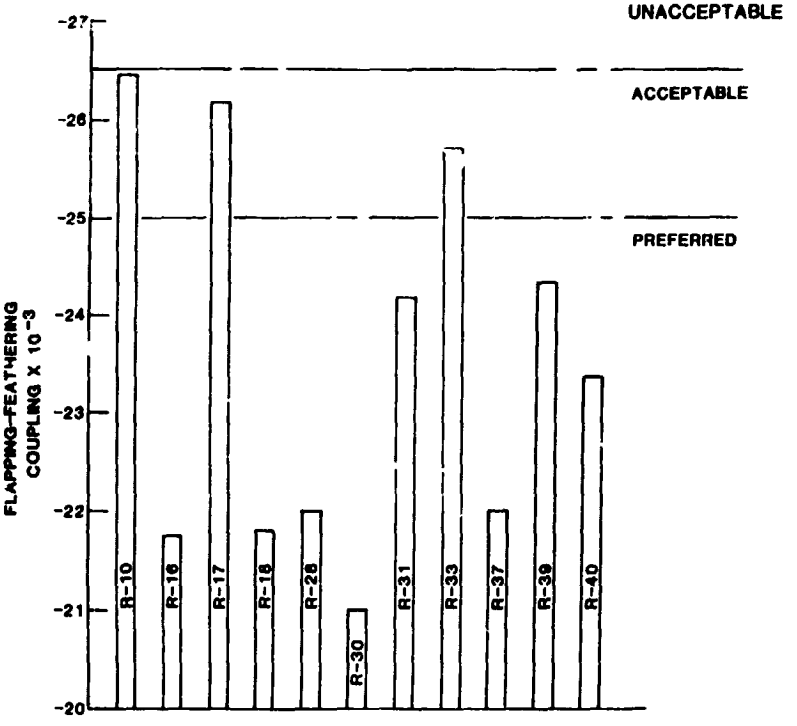

Slide 19.

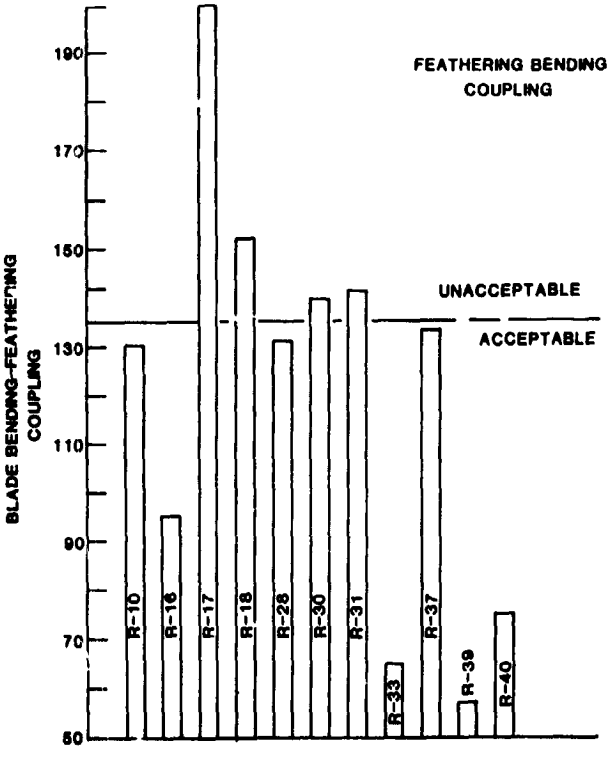

Slide 20.

-101 BLADE CHARACTERISTICS

BLADE	IR_1 x 10^{-3}	I_{R_2}	M_{B_2}	ω_n/Ω	3ΩBM - 40K FST.	3ΩBM - 40K FLIGHT	DAMP. COEFF. -180K A2 EST.	DAMP. COEFF. -180K A2 6F
ST BL	NA	NA	NA	3.054	NA	4500	NA	-.0596
R-10	-26.42	129.5	46.6	3.090	4154	4170	-.0914	-.0930
R-16	-21.76	94.7	44.7	2.932	7384	7350	-.0778	NC
R-17	-26.30	200.0	72.1	3.085	3344	3400	+.4494	NC
R-18	-21.81	152.0	53.9	3.148	3157	3000	-.0410	-.0401
R-28	-22.00	131.3	47.3	3.135	3494	3600	-.0756	-.0744
NPE#1	-22.65	141.1	48.4	3.155	3229	NA	-.064	---

$$M_0 = 686.4 - 3.5M_{B_2} - .216\, I_{R_2}$$

$$M_{EST} = M_0 \times R_M$$

$$R_M = \frac{1}{\sqrt{\left|1 - \left(\frac{2.932}{\omega_n}\right)^2\right| + .138\left(\frac{2.932}{\omega_n}\right)^2}}$$

NA - NOT APPLICABLE
NC - NOT CALCULATED

Slide 21.

SH-2 RETREATING BLADE STALL BOUNDARY

G.W. 12800#

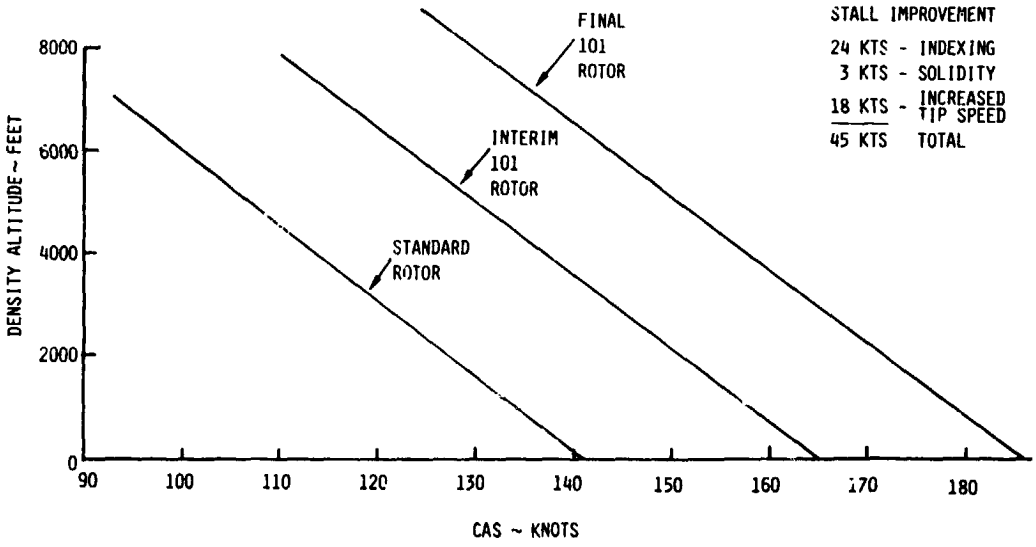

Slide 22.

PANEL TWO: DATA BASES--THE USER'S VIEWPOINT

PANEL MEMBERS

W. Euan Hooper, Chairman	Director, Vehicle Technology Boeing Vertol Company
Robert H. Blackwell	Senior Dynamicist Sikorsky Aircraft
Michael J. Bondi	Data Systems Manager NASA Ames Research Center
Donald A. Boxwell	Research Scientist U.S. Army Aeromechanics Laboratory
E. Roberts Wood	Manager, Aeromechanics Hughes Helicopters, Inc.
Jing G. Yen	Manager, Flight Technology Bell Helicopter Textron, Inc.
Colin Young	Royal Aircraft Establishment, Farnborough

PREPARED COMMENTS

W. Euan Hooper
Director, Vehicle Technology
Boeing Vertol Company

I really welcome this opportunity to discuss data bases because it's a process in which we're seeing enormous changes. Some of you may have seen the paper on vibratory airloading that I gave a year ago at the European Forum. That's what really got me into the data base thing. I had a lot of diagrams made up like shown in Slide 1 where I researched all the existing data on a wide variety of aircraft, which are all documented in the public domain, and put them into a common basis like this. We were getting interested in modes of forcing so we wanted to look and compare one configuration with another and in total there were something like 10 major pressure tests that had been conducted over the last 30 years. Collecting all these data from the various reports, working on them to be able to reduce them to a common format; this was the challenge of what I set out to do. Extremely interesting, very educational, and I found many more test programs available than I had previously been aware of. As soon as I came across a new one I was able to go down to the library and within a matter of minutes I could lay my hands on the file, be looking at some data. That was the good news. The bad news is when you come to try to compare between data sources. Then it's a headache. What I ended up doing was writing a little program in BASIC, got it working on an HP minicomputer, and then I soon ran out of space on that and had to put it into FORTRAN, use the mainframe with a certain plotter and then the equipment changed, and I had to change something else again, and, you know, that's when it's a headache. But the retrieval of all this old data was super easy. You can go to the library and within minutes you've got it. Out of all the reports there were only two that weren't in the library and those I got within a week or so. So the retrieval was easy, the manipulation was hard. But this is a process that most of us are familiar with; we've all been involved in these data-gathering exercises. So this is the one we all know. But it's changed, totally. It's never going to happen again. We are never going to get data as easy to get hold of as we have been able to in the past. It's a completely new situation now, and I don't think we've yet stabilized in a new way of being able to handle large data bases of the type of data we need to look at. I think we are emerging from the golden days of data retrieval--it's been so easy up to now to actually find it. Now it's difficult. I expect some of these statements to be controversial.

Slide 2 shows how it used to be. I think everybody in this room at some time has referred to this report on the H-34 testing. This was a flight test program conducted at NASA Langley in the summer of '61 to provide a data base. I did an approximate count--there were about 75 transducers, mainly rotor blade pressures and a few other useful gauges as well. But just look at the statistics here: 691 pages, 1-1/2 inches thick report with 8 pages of introductory text, 683 pages of tabulated data. That is what a data base used to be. In no time flat you can be hand-plotting some data. But then when you come to compare it with something else, that's when it gets difficult. But notice it was put out by Scheiman in March 1964. That was less than

3 years after the test was completed and I have spoken to both Scheiman and Ted Carter from the Sikorsky end and I understand that was at least a year longer than it should have been by both those guy's accounts because there was a great deal of delay. In fact, it's probably been forgotten by most of the participants, (and I wasn't one), but there were a lot of short tempers over that program because of the delay in getting out the data. The whole study and documentation was completed by Jim Scheiman and two female technicians who helped him. They had oscillograph data and they spread the data out and they made hand measurements. I'm sure they had some mechanical automation in reducing the data, but the whole lot was done by three people. I think we all agree that this program was monumentally useful--practically everybody has used the data. It's not just restricted to industry, the universities have used it, numerous references in the literature--it's a fine example of a data base.

Now we come to today. We've got computers to help us. Everything should be easier, but paradoxically it is not. With all this help that we've got there are numerous problems as shown on Slide 3. We've got increased numbers of data channels, increased frequency response with the acoustics people getting into it. Where Scheiman's data were tabulated every 15 degrees, that's not good enough for the acoustics people, they want every one degree. More flight conditions. And another factor: you can't see the data when it's on magnetic tape. With oscillographs, you can go to a stack and roll it out and see it in no time. Increased numbers of instrumentation and data problems. The guy who is responsible for the data, for documenting it, because there are so many channels, with more instrumentation and data handling problems that have to be resolved, doesn't want to release any data until he has validated all the data. I've experienced this--it causes major delays. Formatting is a challenge and incompatibility of user systems--we've all been experiencing this. The present Tip Aero Acoustics Test Program has been compiled on a VAX data system. We have an IBM mainframe. Getting those two to work together is a major problem.

So how is it handled now? Slide 4 shows a recent example. This is probably the major recent example. The OLS-DME test conducted at Langley in about 1974-1975 produced a vast amount of data, 314 transducers, and here's the report. Compare this to the previous one. This is the way it's going to be done in the future: 370 pages, 3/4" thick, 281 pages of text all describing the test. No data at all. Just describing the instrumentation, the data processing system, everything, all the flight conditions in great detail. That compares with 8 pages in Scheiman's report. Ninety pages of sample plots; no tabulated data at all. I couldn't use that report to look at the type of stuff I was showing you earlier. No way I could get that information out of this report and it was never intended to put the data in that format. Now Slide 5 shows a couple of excerpts straight out of that report. The intention was "the primary product of this is a documented data-tape library, consisting of analog and digital magnetic tapes . . . Because of the volume of data obtained, the presentation of the results is limited to: samples of . . . data." There were just data samples plotted in the report, nothing tabulated that you could take off and use. "Data from the magnetic tape library can be readily retrieved and displayed in various formats." That's the intention and to some extent it has been accomplished and to be fair for the OLS test it is mainly accomplished. But that is the type of documentation that we are living with now.

Knowing that I was going to be on this panel, I wanted to get familiar with DATAMAP and the OLS data so I started a little activity in March to get some data from the OLS test and we contacted Don Merkley at Ft. Eustis and he was very helpful. Here's a chronology (Slide 6). We started in March and we reviewed the report, requested a lot of data, and about two weeks later it came in, and then we spent some time getting familiar with DATAMAP, and by July we got useful plots out. Now, we didn't work this continuously--it was done off and on--it wasn't a high priority operation. If it was a high priority operation I am assuming that process would have taken about a month. And that's the thing that we've all got to realize in these data base access situations that it takes a while. It's not like walking down to the library and within minutes having the report in your hands--it takes a long time to get hold of it. Once you've got it, then the world is quite different. You can play around with it, you can replot it, you can do all sorts of things with it, but it's a big, initial access transient. Now, we had another exercise going which we started in January. This one didn't turn out so well. This was a real exercise where we needed data for the NASA-AHS Noise Reduction Program. We needed data from the Tip Aero Acoustic Test Program and we needed it for our acoustics group. There is no report out on this program so we reviewed the informal list of data. We requested two airspeeds, and a month later we got the tapes, and now in October we still have no useful plots. It has been a long, complicated story. We spent a lot of effort, we had one of our top programmers working this problem and the bottom line is as yet we've still got no useful data. We will, I am sure. We are going to have to change over to another computer because we found our IBM is incompatible with the VAX because of the way the data is formatted on the VAX. We are going to put it on our Wind Tunnel computer which is a VAX and I am sure we will be able to make it work eventually. I'm only showing you this example to show that it can be an uphill process and I think we are in a transition period. In a few years' time we will have all this set up, and the wheels greased, and we will be able to communicate better. But at the moment communication is poor.

What it boils down to is that we've all got to answer the question: Are we ready, are we prepared, to give up on data reports which are becoming a thing of the past and go over to these

terminal access data bases for studies that we all want to do? It isn't just industry--it is academia and any other user who has got a right to know and I think the answer to that is: No, we are not ready. But at the same time we've got to make it work because the type of system which DATAMAP represents is here to stay and the potential is very great, but I think it's nowhere near the useful system that it's intended to be, yet. Slide 7 shows how the questions boil down, really. We have to speed the establishment of data bases. We are very slow in this process at the moment. We have to facilitate the accessing and interfacing process, improve the readability. The data base can be very powerful in presenting the results, but not quite in the format you want so you must have the flexibility to change format. And ensure accessibility over the long term. I was able to go to the library and pull out 20 year old reports in minutes and look at them. Now is NASA really going to provide that these data are available after 20 years for rapid access by anybody? It's a challenging problem. So these are the questions that are facing the panel.

H-34 AIRLOADING — LINEAR PLOT

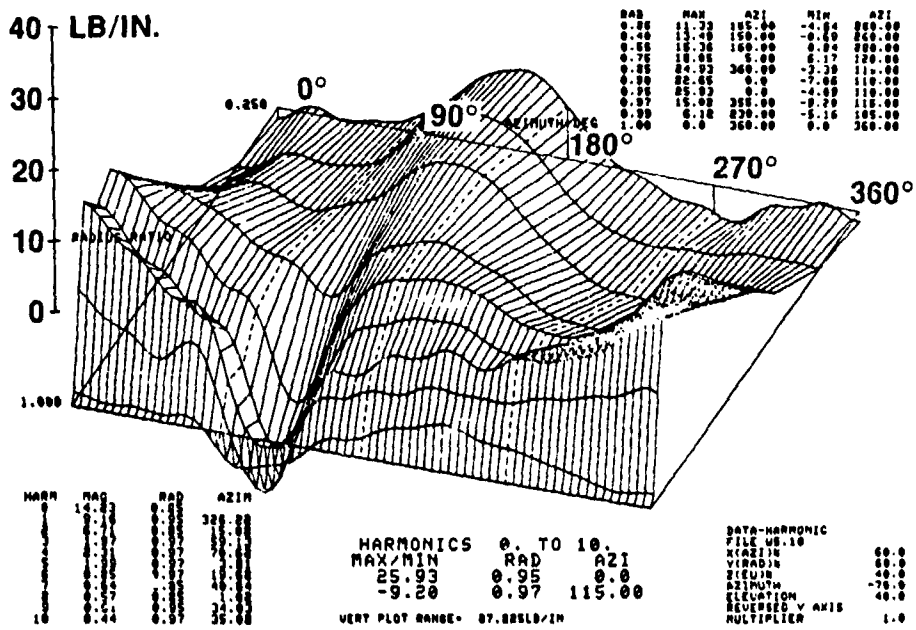

Slide 1.

DATA BASES - HOW IT USED TO BE

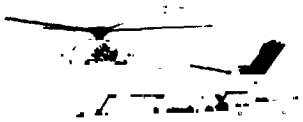

H-34

FLIGHT TEST PROGRAM CONDUCTED AT NASA LANGLEY IN THE SUMMER OF 1961 TO PROVIDE A DATA BASE FROM 75 TRANSDUCERS INCLUDING ROTOR BLADE PRESSURES, BLADE STRESSES, ETC.

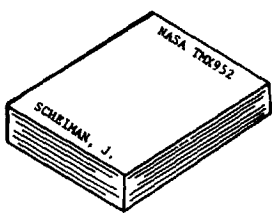

691 PAGES, 1¾ INCHES THICK
- 8 PAGES OF INTRODUCTORY TEXT
- 683 PAGES OF TABULATED DATA

SCHEIMAN, J. A., A TABULATION OF HELICOPTER ROTOR BLADE DIFFERENTIAL PRESSURES, STRESSES AND MOTIONS AS MEASURED IN FLIGHT," NASA TM X-952, MARCH 1964

Slide 2.

DATA BASES - THE PARADOX

EVEN WITH COMPUTERS TO 'HELP', IT NOW TAKES LONGER TO COMMUNICATE TEST RESULTS TO THE USER COMMUNITY

- INCREASED NUMBER OF DATA CHANNELS
- INCREASED FREQUENCY RESPONSE REQUIREMENTS
- MORE FLIGHT CONDITIONS
- 'INVISIBILITY' OF DATA OR MAGNETIC TAPES VS. OSCILLOGRAPHS
- INCREASED NUMBER OF INSTRUMENTATION AND DATA PROBLEMS TO BE RESOLVED BEFORE THE ORIGINATOR FEELS COMFORTABLE IN RELEASING ANY DATA
- FORMATTING A DATA BASE SO THAT IT IS AS READABLE ON A TERMINAL AS TABLES IN A REPORT
- INCOMPATIBILITY OF USER COMPUTER SYSTEMS

Slide 3.

DATA BASES - A RECENT EXAMPLE

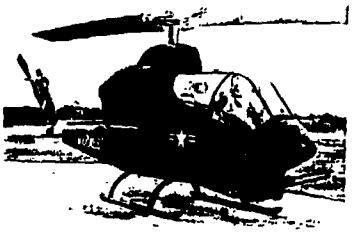

AH-1G

FLIGHT TEST PROGRAM CONDUCTED BY ARMY, FT. EUSTIS, 1974-75, TO PROVIDE A DATA BASE FROM 314 TRANSDUCERS, INCLUDING BLADE SURFACE PRESSURES AND VELOCITIES.

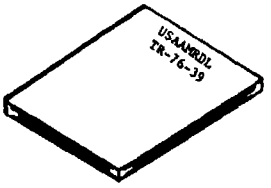

371 PAGES, 3/4 INCH THICK
- 281 PAGES DESCRIBING THE TEST
- 90 PAGES OF SAMPLE PLOTS
- NO TABULATED DATA

SHOCKEY, G. A., COX, C. R. AND WILLIAMSON, J. W., AH-1G HELICOPTER AERODYNAMIC AND STRUCTURAL LOADS SURVEY, USAAMRDL-TR-76-39, FEBRUARY 1977

Slide 4.

OLS REPORT EXCERPTS

Page 66

3.4 DIGITAL TAPES

Digital data tapes that were delivered under this test program were produced on a Xerox Model 530 Digital Data System by processing the analog tape prime data records into a digital format. Reference 8 describes the digital data tape format generated by the Bell Helicopter Textron XDS530 computer system at the Ground Data Center. This format was developed to provide a standardized tape format for interfacing digital data tapes with flight test analysis software programs residing on both BHT XDS530 and IBM 370 computer systems.

Page 95

5. TEST RESULTS AND CORRELATION

The primary product of this program is a documented data-tape library, consisting of analog and digital magnetic tapes. Continuously and simultaneously recorded time histories of rotor blade airloads, blade bending and accelerations and the resulting control loads, and fuselage vibration responses produced a great volume and large variety of data. Because of the volume of data obtained, the presentation of the results is limited to:

- Samples of each type of data and a brief comparison of the results with theoretical predictions
- A correlation of five representative flight conditions with a theoretical flight simulation program (C81)
- A fatigue evaluation of NOE operations
- A summary of ground vibration testing
- An analysis of airloads and resulting rotor acoustics for selected flight conditions

Data from the magnetic tape library can be readily retrieved and displayed in various formats. These formats can be tailored to meet the specific requirements of the individual areas. The digital tapes have standard labels and are compatible with current-model IBM 370 computers. Access to the data tapes is made available for government and industry users from the Eustis Directorate, USAAMRDL.

Slide 5.

DATA BASES - HOW ACCESSIBLE?

OLS PRESSURE DATA FROM 1975 TEST

MAR, '84	REVIEWED REPORT AND REQUESTED PRESSURES AT 13 AIRSPEEDS AND 10 DESCENT RATES
APR	TAPES RECEIVED; FAMILIARIZATION WITH DATAMAP
JUL	USEFUL PLOTS OBTAINED AFTER 4 MONTHS (MONTH IF COMPRESSED)

TAAT PRESSURE DATA FROM 1981 TEST

JAN, '84	REVIEWED INFORMAL LIST OF DATA AVAILABLE
FEB	REQUESTED 2 AIRSPEEDS
MAR	TAPES RECEIVED
OCT	NO USEFUL PLOTS AFTER 9 MONTHS (34 MONTHS IF COMPRESSED)

Slide 6.

DATA BASES - WHAT IS NEEDED?

HOW CAN WE

- SPEED THE ESTABLISHMENT OF DATA BASES
- FACILITATE THE ACCESSING AND INTERFACING PROCESS
- IMPROVE THE READABILITY
- ENSURE ACCESSIBILITY OVER THE LONG TERM (COMPUTER CHANGES, PERSONNEL CHANGES, TAPE MAINTENANCE, ETC.)

Slide 7.

PREPARED COMMENTS

Robert H. Blackwell
Senior Dynamicist
Sikorsky Aircraft

I'm not sure that I have particularly profound comments to make on the subject. I have plenty of experience trying to use different data bases. I'm sure it's similar to some that you all may have. Euan asked us to speak on experience and particularly to cite examples of data bases we've used successfully and unsuccessfully, to try to talk about the reasons it had come out that way, and then to offer suggestions, observations and recommendations with regard to a data base-type program.

So the way I thought I would start would be first of all to cite briefly some examples of data bases that I'm intimately familiar with and talk about how that has worked out in each case (Slide 1). The first two are pretty commonly known--those are the so-called S-61F and CH-53A rotor loads programs. It is work that was sponsored by the Navy in the late '60s and the reports came out in 1970. Those reports consist of Vol. I which is 3/4 of an inch thick or so and which has a good description of instrumentation, test procedures, photographs of where the gauges were and so forth and so on, fairly substantial data analysis, and even some correlation with theory. And then Vol. II which is 2 to 2-1/2 inches thick has just tabulated data. The number of measurements are typically 100 and the number of flight conditions about 70. My experience with that is back in the early 1970s. We didn't have much in terms of automated plotting capability. There was a lot of labor-intensive work in terms of plotting which of course is to be avoided, but in terms of the accessibility and usefulness of the data I found that format to be quite acceptable at the time. As I say, there are certainly improvements to be made in efficiency, but the data I still keep within arm's length at my desk. I find that to be a very useful source.

The second group I have listed is the experience with looking at ABC, UH-60, and S-76 data bases. Now I want to put that up for two reasons. First of all, to distinguish between what would be called research data bases where specific objectives were to go out to gather data and then secondly, the data bases that are generated in the process of a development program. And the two aren't very similar frankly. As many of you probably know, the process of developing an aircraft leads to continuous changes in configurations, dropping off of instrumentation that isn't reading a high stress at that particular time and frankly, despite the fact that there is a lot of good data there, it would be a frustrating process to try to go back and make consistent comparisons where only one parameter at a time was changed. So I think the type of data base that we are really aiming toward, unless of course we are ready to put in a monumental effort, is that which relates to aeromechanics-type research. The second thing that is pointed out by those large data bases (the UH-60A and S-76 probably have numbers of tapes in the thousands each) is that even though we have a good capability in house to access that data--a RAPID system at the flight test development center allows us to look at data pretty conveniently and so forth--it still doesn't do some of the things you might like to do such as to make cross comparisons between flights in a convenient manner. It's still a cumbersome job to manage multiple parameters and multiple test points and various tapes spread out over years. So I could conclude from that line frankly that those kind of data bases are not really exportable and probably best used, most efficiently used by the people who generated them and for the immediate purposes they were generated for.

The next line item is the S-76 rotor tested in the 40 × 80 tunnel. Here is an example where there is good research potential; several tips were tested in a consistent fashion in the 40 × 80 system, but when it comes time to reducing that data now we begin to be inundated by data as Euan mentioned. Now the tapes and the information wouldn't fit into a 2 inch report, it would probably be a 2 foot report or something. The data as I have it is on microfiche which takes up a drawer and I could only guess that a drawer of microfiche would expand to a lot of paper or a very thick report. So we at Sikorsky put together an ad hoc data access and processing program; nothing fancy. I think it was done extracurricularly, frankly, but something that allows you to go into a given tape, pull out the appropriate information, harmonically analyze or cross plot data and so forth. It was good, but it left something to be desired certainly, and it likewise didn't allow us to cross plot across different tapes. So the conclusion I draw from that is that that data is probably under-used for the lack of access.

The next to last one, the Lockheed test of the X-Wing model in the 40 × 80 tunnel is an example where there is a good data report, a lot of text, data analysis, and data presented in summarized form. I found that this was convenient and satisfied most of our needs. Again, however, there is no question that there is more goodness in the data which probably could be gleaned if people had convenient access to the raw data themselves.

The last entry here is the Boeing Vertol X-Wing model test data which Ken Reader and Bill Dixon from Vertol talked about at the last AHS Forum. In that case again we are up into the 2000 test point 70 measurement range, a volume of data that is prohibitive, I suppose, to put

into a report unless they reserve a new shelf in the library. In that case it was a unique problem, further, in that when we, Sikorsky, got involved in this program there was no report yet. We had some handouts describing the test and had no real first hand familiarity with the test or various things that you would have if you had done it yourself from the beginning. We received the tapes and as might be anticipated, we were not able to read them. So that took another go around through the cycle to get tapes that we could read. When we got the tapes, we realized we could read them, but all we could do with them was to print them out on paper. And the paper was over my head. It was a tall stack of paper and as a result it just gathered dust and nobody looked at it for quite a while. Once again our computer people came to the fore and in fact just using capability that already existed on our IBM computer, put together an ad hoc data access and analysis capability which is actually very good. And I'll talk about it for a few minutes later on, but once again that is a wasteful process, to repeat the development of a program. This case is certainly one where a unified data access and data analysis capability would have permitted the transfer of information between two groups to happen much more efficiently.

Well, getting on to DATAMAP and my observations against that background. First of all, I have no direct experience with using DATAMAP myself. We at Sikorsky have DATAMAP, several of the individuals have used it, and apparently with success as indicated in Slide 2. Their suggested improvements were relatively minor and I think they have already been communicated to Don Merkley. I looked over the User's Manual and it appears to be well written, and so forth.

But in order to speak to the larger questions of a data access program and the problems associated with that, I tried to take a survey among various users. I talked to our handling qualities people, aerodynamicists, dynamicists and acoustics people. There was general agreement that systematic, standardized data access programs would certainly provide a valuable capability. I think that is probably like asking the fox if he'd like some more chickens--of course people would like access to more information. The question that is more important, however, is how that can be made to happen and what issues must be considered along the way. Some of the comments that I collected from the people I talked to are Number 3 through 5. For instance, the feeling that the availability of such a data tape should not be considered to relieve report-writing requirements. Certainly the data analysis that you would typically expect to find in a report should go on in at least the current depth. Ninety-five percent of the people, perhaps, aren't going to need or want to go into the details of going through a tape system and it would be, I think, a miscarriage of justice to prevent the flow of information to those people. Number 4, a significant concern was expressed that to pick up someone else's test data would require that the detail and level of documentation that goes into describing how the test was done, the run logs, the calibration procedures, and so forth, would probably have to be greater than is presently the case or else the opportunities to get befuddled would be greatly increased. Number 5 . . . as it says "most effective use of data may require more detailed description of tested systems than companies are willing to share." I would suggest that when I have worked with data, various parts of the ability I had to look at that data came from company airfoil data and company information about how their instrumentation works and so forth, and if the process really is intended to allow information from Group A to transfer to Group B, I'm sure a lot of backup information that would be valuable to the receivers may or may not be readily available from the originators.

My recommendations, very quickly, would be what I would see as the process that would best move this job along (Slide 3): Number 1, publicize data that are currently available in DATAMAP form or available to be converted so that people would begin to make more use of it. Number 2, as I think probably goes on anyway, to solicit feedback from users to enhance program capabilities--it would be a unique program if it didn't need enhancement with increased use. Number 3, impress upon originators of this potential data the need for such things as user-oriented run logs, good instrumentation documentation, appropriate data quality checks, calibration, and various supporting data that would be useful to an end user, namely such things as natural frequencies of the system, verified structural descriptions of the blades and wind tunnel model stands and airfoil data if possible. Number 4 refers to an item that I have found to be a very useful capability in the data analysis program we have put together for the Boeing X-Wing data. It is the ability to make a quick and easy access to the data for the purposes of sorting, displaying data trends and identifying bad data. A simple command allows plotting or tabulating any parameter versus any other parameter for selected ranges of other parameters. For example we can plot 4P control load vs rotor thrust for all conditions having positive shaft angles and advance ratios between .5 and 1. An example is shown in Slide 4 where tunnel speed is plotted versus rotor speed for all test points. The letters refer to the number of data points superimposed at a given position (A denotes 1 point; D, 4 points, etc.). This has been a valuable capability for us and, if it isn't already, should be considered as an ingredient to DATAMAP or any other future data analysis system.

DATA BASES USED

S-61F ROTOR LOADS

CH-53A ROTOR LOADS

ABC, UH-60A, S-76 FLIGHT DATA

S-76 ROTOR IN 40 X 80 TUNNEL

LOCKHEED X-WING MODEL TEST

BOEING-VERTOL X-WING MODEL

Slide 1.

OBSERVATIONS ON DEVELOPING A STANDARDIZED
DATA ACCESS/ANALYSIS CAPABILITY

1. DATAMAP IN USE BY A LIMITED SET OF USERS AT SIKORSKY. COMMENTS MOSTLY FAVORABLE.
2. GENERAL AGREEMENT THAT THIS WOULD BE A VALUABLE CAPABILITY.
3. AVAILABILITY OF TAPE DATA SHOULD NOT ALTER REPORT WRITING REQUIREMENTS. MAJORITY OF PEOPLE WILL STILL RELY ON REPORT.
4. CONCERN EXPRESSED THAT TEST DOCUMENTATION WILL REQUIRE SIGNIFICANT EXPANSION FOR USER TO EFFECTIVELY ANALYZE DATA.
5. MOST EFFECTIVE USE OF DATA MAY REQUIRE MORE DETAILED DESCRIPTION OF TESTED SYSTEMS THAN COMPANIES ARE WILLING TO SHARE.

Slide 2.

RECOMMENDATION FOR DEVELOPING DATA
ACCESS/ANALYSIS CAPABILITY

1. PUBLICIZE DATA WHICH ARE AVAILABLE IN DATAMAP FORM OR AVAILABLE TO BE CONVERTED.

2. SOLICIT FEEDBACK FROM USERS AND ENHANCE PROGRAM CAPABILITIES.

3. IMPRESS ON ORIGINATORS THE NEED FOR:

   . USER-ORIENTED RUN LOGS, INSTRUMENTATION DOCUMENTATION

   . DATA QUALITY CHECKS

   . FREQUENT CALIBRATIONS AND REPEAT POINTS

   . SUPPORTING DATA SUCH AS NATURAL FREQUENCIES, VERIFIED STRUCTURAL DESCRIPTION, AIRFOIL DATA

4. ADD FEATURES TO PROGRAM WHICH PERMIT EASY DATA SORTING PLOTTING AND QUALITY CHECKING.

Slide 3.

USE OF DATA ANALYSIS PROGRAM TO DISPLAY TEST CONDITIONS

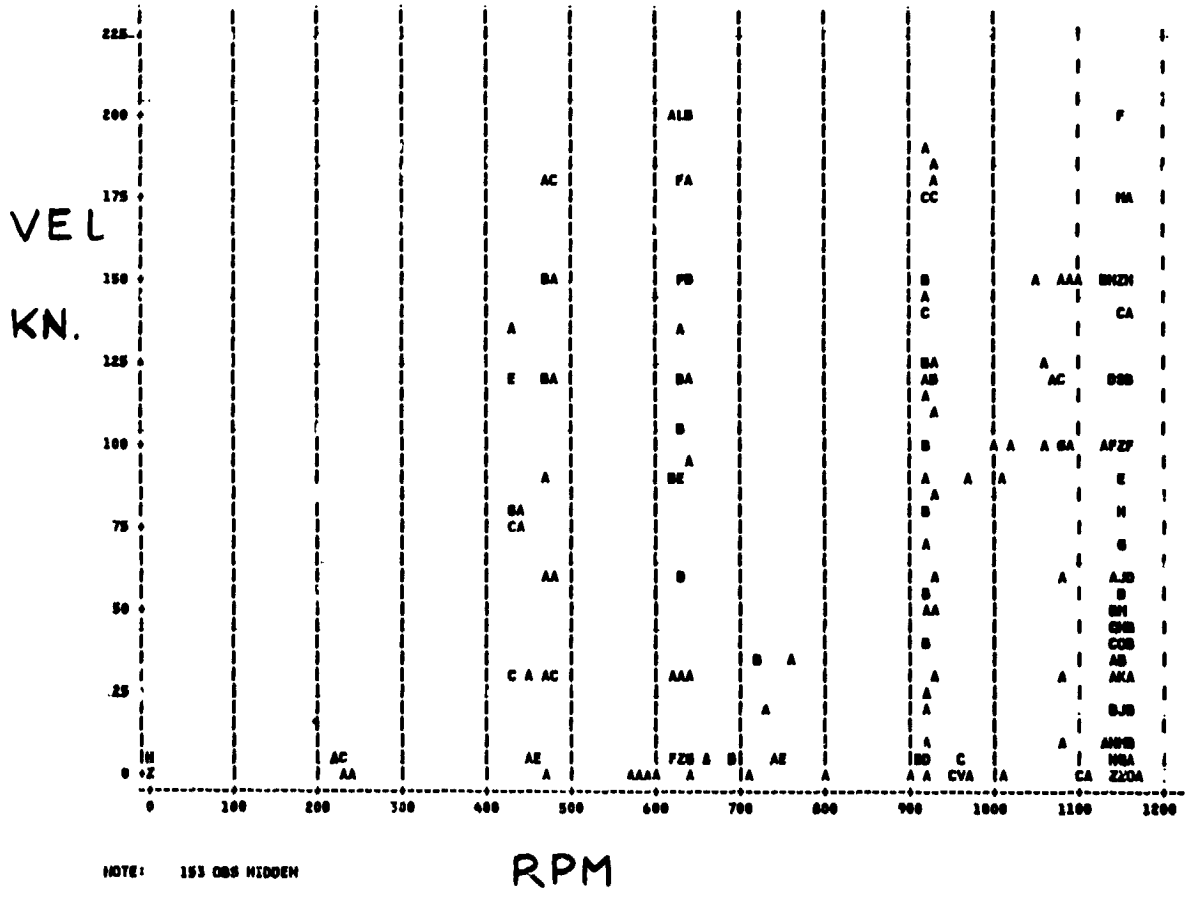

Slide 4.

Peretz Friedmann, UCLA: I don't really have a question, I have an observation and maybe I should make a small comment before I make my observation. I've been married for 20 years to a person who is a professional data base management person and I have acquired a lot of information on data base management systems by osmosis. I have two comments, one on what Euan Hooper said and the second one on what Bob Blackwell said. I think that it is important that you realize that you don't have a data base, you have data. And your data is not well organized and what you would like to have is a data base. And as you probably are aware there are about 500 different data base management systems around and depending upon your obligation you have to get expert help to organize data to develop a data dictionary which enables you to access the data and then develop user-friendly graphics features which you wou'd like to have. I am somewhat amazed that you call the report a data base. The report is raw data and then unless you put it in a data base, you don't have it on the data base.

Hooper: I think that is semantics. But I take your point that we are lacking an organized approach to this and I think we are in a transition situation. Where DATAMAP is being . . . the government has taken the initiative in getting this program underway. I think we all have to work very hard with it and gradually tailor our test programs so they fit into the data base straight away and then we will call them data bases.

Jim Biggers, Naval Ship R&D Center: It seems to me we are caught in a trap. The papers and things that we have heard the past couple of days indicate a need for increasingly detailed test information with which to compare our increasingly capable theories. And yet we are not terribly well equipped to handle the test information that we can go out and acquire. We also have the ability to go out and acquire a great deal of detailed test data with many surface presures and things of the nature you have just described. But yet the need is obviously there or we wouldn't have this panel. So we have a problem of data volume versus accessibility. We have problems in tape formatting and in data formatting. At our place, one of the worst things you can do to our computer people is to bring in what they call a stranger tape. I think we need to cast that problem at the feet of the computer people and push on them hard enough to get it solved. It's incredible. I recently went through an experience on some of the data that you have described and it turns out the computer industry has not even defined the terms in enough detail to define the tape formats adequately. Each computer company wants to retain its own proprietary format. That's an outrage--we shouldn't tolerate it any longer. You mentioned microfiche. We have an automatic microfiche capability at our place and they have them in the 40 x 80 and other places. Microfiche is a help, but it is certainly not a total answer. We need to start using our desk top computers as a place to temporarily work with smaller portions of the data and as more and more of us get desk top computers we need to again use those. In summary, it looks to me like there is a need for a broadly-based, industry-wide coordinating effort to make this thing happen. We have a very strong need for a broadly coordinated data base system similar to, perhaps, DATAMAP or some enhanced version thereof. But it seems to me we better get on with it because as many of you here are aware, there are a number of similar data-gathering experiments on the horizon where we are going to be again inundated with large quantities of data. I think we need the data, but we also need to access, sort, plot, cross-plot, and do all the other things.

PREPARED COMMENTS

Michael J. Bondi
Data Systems Manager
NASA Ames Research Center

Listening to all these comments, I'm not sure if I really want to go through this entire production. Basically, two years ago the Tilt Rotor Office decided to build a computer-oriented, data base system (Slide 1). And this work was done under contract by the AMA Corporation, Mountain View, California. My involvement was as a user and a developer of the system. So as I listened to all these comments, I sympathized with the users and then I think, "Ah, but our data base, our tilt rotor engineering data base, may have solved some of these problems." We call it TRENDS, hoping that maybe this acronym is significant (Slide 2). We believe it is a true data base in response to a question posed by an earlier speaker. Basically the data base is only 70% complete now (Slide 3), but it's fairly operational. It consists of nine major areas, the first four being information-oriented, the last five being function-oriented as follows (refer to Slide 3): management and narrative information, time history information for multi-discipline users, and the min/max loads information. The remaining five function-oriented items are: the pseudoflight generation functions, search function on data sets, algorithm generation for the manipulation of data, plotting functions, analysis functions, which in our case we are using DATAMAP.

Just to give a little sample of detail (Slide 4), when I say management, what I mean is: flight logs, flight descriptions, problem areas of flight. This information is in the data base. Narrative search functions would be broken down into pilot comments for each test point, parameter definition, summarize flight logs, and data base definitions.

Now as a user of the system, I found the function shown on Slide 5 very useful. Pilot comments are entered into the system, for the most part, for both aircraft. These comments are on the right side, and they are fairly brief. But these comments can be searched with the data base; in other words, the user can search for all the turn information or 1-1/2 g information the user then qualifies which flight he is interested in. If, however, he does not know which flight then he may want to look at more narrative to really zero in on what he is after. But he is able with the computer on his terminal to search for any single flight or multiple flights. There's approximately 200 flights on one aircraft and probably 20 or 30 flights on the other aircraft. The one thing that Bob Blackwell mentioned that we don't have in the system right now, but are close to getting there, is that we are going to designate on the far right of these pilot comments which test points have time history data for performance, aeroelastics, etc. For the most part they all have loads data otherwise they wouldn't be in the base. So I agree with him, wholeheartedly, that this is a very important feature--when you're trying to use the system.

Now my experience as a user (Slide 6) has been that the narrative information is extremely important, something that I don't think any of us in the tilt rotor office really appreciated when we started, i.e., search functions on narrative and numerics. In other words, you usually start in looking at the narrative data and once you have zeroed in on the areas of interest then you start looking at the numerical data, usually a loads type of thing. As a result of that search you usually generate test points, maybe within one flight or within multiple flights. This is called pseudo flight generation. Obviously, the necessary rapid system response that was mentioned earlier is extremely important and since the system is on a disk we found it quite good. The only problem there is that all the data has to be put on the disk and it takes a fair amount of effort. But as far as the user goes, he doesn't have to suffer through that time delay. Next item, multiple flight access is very useful in this system. Next item, the system is available via telephone access. Next item, the data in the base is both filtered and unfiltered For performance data usually the individual users do not want the full spectrum of frequencies available so it's been filtered. But in the case of frequency analysis, aeroelastics, and other types of data, it's raw data. [Hooper: Excuse me, Mike you are talking about a system that has been interposed before DATAMAP gets access, aren't you?] That's correct. [Hooper: Not to tell tales out of school, but I was asking Mike just before, "Why did you have to do that? Why couldn't you have worked directly? Why weren't your files in DATAMAP format?" And Mike's answer was, "Well, we don't like DATAMAP data format very much." This has been a problem that everyone's going to encounter because everyone likes their own flight test data formats. We have data formats, NASA has them.] Obviously, I think we do have a rationale for the way we went. Basically, multiple flight, multiple aircraft dictated to a great extent the file selection.

As a developer, fast response, multi-user capability and the user-friendliness is very important (Slide 7) and one figure of merit that I have used as a developer: Does another user sitting in another office in our tilt rotor group go to the file cabinet or does he go to the terminal. I must say that I think we have had a breakthrough here the last two or three months. Our users are tending to go to the terminal now as opposed to the filing cabinet. The dial-up system we feel is important, 1200 baud is really minimal, but it does work. The multi-terminal work station is something I'll go into just a little later; I think it's an area we are

neglecting. You need more than one terminal. Single Parameter, Multiflight File Structure: I mentioned that in order to get multiflight access the file structure is very important. Redundant Narrative Data: as a user uses the system he'd like "Help," and he would like to be able to put a question mark in and immediately find out what the pilot comments were. So I think this area is very important and it is a part of this system. Multidisciplined: what I mean by that is aeroelastics, performance, loads, etc. It's not adequate to build a data base for one type of user. Whether he's a performance, aeroelastics, or loads user, inevitably the system will not be used unless it meets the needs of all types of users, and that is very difficult to achieve without the help of the user community. A system should be tailored to the aircraft type; here I have broken it down in three general categories: Helicopter, Tilt Rotor and Conventional. And the system must have immediate user acceptance. If the system is not immediately accepted, usually the user will resort back to the file cabinet or not use it at all.

Slide 8 shows the conclusions. It is felt that the system must be operational before the flight test if it's going to be accepted, preferably during wind tunnel test. That way all the bugs can be worked out of it. The system should be disk-oriented in order to get the response and here we are talking of a dedicated drive. In our case, one for each airplane and we're talking 300 megabytes. I feel like that is probaoly a reasonable amount. Possibly the system could go to 2 disk drives with 600 megabytes, even this is not so unreasonable anymore, because in a very short time there will be one gigabyte platters so I don't think the availability of a large disk is a real consideration now. I feel DATAMAP or some other analysis program should be a part of the system. Probably you would like more than one data analysis program. The narrative data is extremely important, especially the pilot comments and flight descriptions. This is especially true for people that aren't locally at the facility. Search capability, like I say, is an absolute must and also the specialized multiterminal hard copy work station. This is an area we've got to really address because if we are going to expect a person to be doing serious analysis he needs at least, I would say, three terminals: one graphics, one text, and one hard copy and preferably two text. These should all be addressable through one keyboard. So I think we need a specialized work station. Not a grandiose one, but one that on a single telephone line a user without losing the information on his screen that he's trying to view, is able to go from one to another screen easily. I think this is very doable by the way. Possibly TRENDS has in some respects answered a lot of the problems brought up earlier and maybe even Jerry Miao, the second speaker in the first panel, might even be satisfied.

TRENDS

NASA'S

Tilt Rotor Engineering Database System

For The

XV-15

N702 ——— N703

Slide 1.

TRENDS

MULTIUSER ——— USER FRIENDLY

XV-15 Database

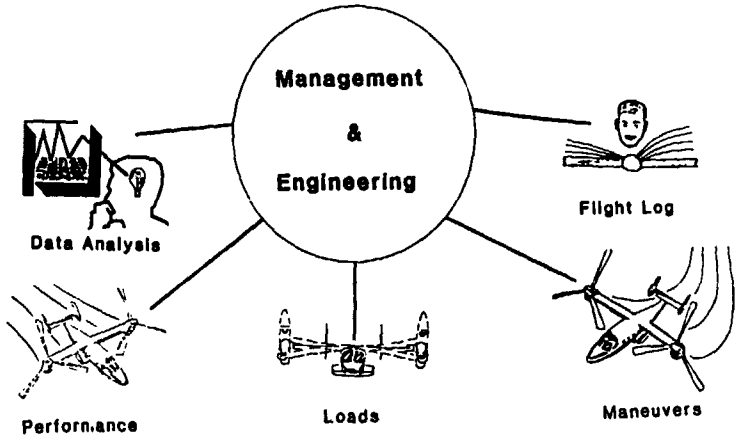

Slide 2.

TRENDS

The Tilt Rotor Engineering Database System (TRENDS) is a MULTI–USER, MULTI–DISCIPLINED, MULTI–AIRCRAFT, User–Friendly system which is 70% complete.

I. TRENDS currently provides the following functions and information for two TILT ROTOR AIRCRAFT, N702 & N703

1. Management Information
2. Narrative Information
3. Times History Information (Multi–Disciplined)
4. Min/Max Loads Information
5. Pseudo Flight Generation Function
6. Search Function on Data Sets
7. Algorithm Generation Function
8. Plotting Function
9. Analysis Function of Data via (DATAMAP)

Slide 3.

TRENDS

The Tilt Rotor Engineering Database System (TRENDS)
is a Multi–Disciplined, Multi–User, Multi–Aircraft, User–Friendly
system which is 70% complete.

I. TRENDS currently provides the following data manipulations
& informations for two TILT ROTOR AIRCRAFT, N702 & N703

1. Management Information
   a. Flight Logs
   c. Flight Descriptions
   d. Problem Areas of flight

2. Narrative/Search
   a. Pilot comments for each test point
   b. Parameter definitions
   c. Summarized flight logs
   d. Database definition

Slide 4.

WORDSCAN OUTPUT

FLT	165	CTR	2970	HOVER
FLT	165	CTR	2987	2.1 G PULLUP/PUSHOVER
FLT	165	CTR	2988	2.28G RT TURN A/S 210 MQ 105
FLT	165	CTR	2989	2.3 G LT TURN A/S 210 MQ 105
FLT	165	CTR	2990	2.22 G PULLUP/PUSHOVER
FLT	165	CTR	2992	1.5 G LT TURN A/S 230 MQ 130
FLT	165	CTR	2993	1.5 G RT TURN A/S 230 MQ 130
FLT	165	CTR	2994	1.5 G PULLUP/PUSHOVER
FLT	165	CTR	2995	2.0 G RT TURN A/S 230 MQ 130
FLT	165	CTR	2996	2.0 G LT TURN A/S 230 MQ 130
FLT	192	CTR	4875	LIFT TO HOVER
FLT	192	CTR	4878	LEVEL CRUISE 75 DEG IN
FLT	192	CTR	4879	NOR LT TURN 1.5 G'S
FLT	192	CTR	4880	NORMAL RT TURN 1.5 G'S
FLT	192	CTR	4881	FAST LT TURN 1.5 G'S
FLT	192	CTR	4882	FAST RT TURN 1.5 G'S
FLT	192	CTR	4927	ACCELEROMETER 86 RPM 0 FLPS
EOF				

Slide 5.

EXPERIENCE ---- DEVELOPMENT OF TRENDS DATABASE

IMPORTANT CONSIDERATIONS WITHIN TRENDS

1. NARRATIVE INFORMATION IN DATABASE

2. SEARCH FUNCTION ON NARRATIVE and/or NUMERICS

3. PSEUDO FLIGHT GENERATION
   e.g. as a result of a search function
4. RAPID RESPONSE & USER–FRIENDLY
   entire database on disk
5. MULTIPLE FLIGHT ACCESS CAPABILTY

6. MULTIUSER TELEPHONE ACCESS

7. DATA COMPRESSION ALGORITHMS
   e.g. convolution filter,Butterworth etc
8. FLIGHT DATA SELECTION

Slide 6.

OBSERVATIONS -- SYSTEM SHOULD HAVE THE FOLLOWING:

1. FAST RESPONSE, MULTIUSER & USER-FRIENDLY
   e.g. easier to use than the file cabinet
2. REMOTE ACCESS Tel-dialup -- 1200 baud min. rate

3. MULTI-TERMINAL WORKSTATION
   e.g. graphics, texts & hardcopy terminals
4. SINGLE PARAMETER MULTI-FLIGHT FILE STRUCTURE

5. REDUNDANT NARRATIVE DATA
   e.g. used as a Help function
6. MULTI-DISCIPLINED DATA SELECTION FOR DATABASE
   e.g. aeroeleastics, performance, loads, etc
7. SYSTEM SHOULD BE TAILORED TO A/C TYPE
   e.g. Helicopter, Tilt-Rotor, Conventional
8. SYSTEM MUST HAVE IMMEDIATE USER ACCEPTANCE
   or else you may lose user permanently

Slide 7.

CONCLUSIONS & RECOMMENDATIONS

1. DATA SYSTEM MUST BE OPERATIONAL BEFORE FLIGHT TEST
   e.g. during wind tunnel test

2. DATA SYSTEM SHOULD BE DISK ORIENTED
   300 mb. min.-- digital tape backup only

3. DATAMAP SHOULD BE PART OF SYSTEM

4. NARRATIVE DATA EXTREMELY IMPORTANT TO SYSTEM
   e.g. pilot comments, flight descriptions, log

5. SEARCH CAPABILITY EXTREMELY IMPORTANT TO S[illegible]M
   e.g. search on flight conditions -hover-trim-[illegible]

6. SPECIALIZED MULTI-TERMINAL/HARDCOPY WORKSTA[illegible]N
   accessible by single keyboard & telephone line

Slide 8.

Wayne Johnson, NASA Ames Research Center: I think that the remarks that were made about the sense of building a preprocessor before you go to DATAMAP highlight an observation of mine and that is that what you do with the data really is the end product, but first you have to face the fact that the type of data often shapes the data base and the way it's acquired has a lot to do with that. The example that I was thinking of after hearing the first couple of speakers is that we have been talking about flight test data bases. A wind tunnel data base is really quite a different structure. The kind of things that have been done for DATAMAP and with the tilt rotor preprocessor if you like, really don't encompass what you have to do for wind tunnel data and again it has to do with the fact that a flight in a wind tunnel can produce different types of data and therefore the organization and the manipulation that follows must be different. As an example, flight data will have very limited gross weight and drag ranges, whereas wind tunnel data will ordinarily have a wide map of thrusts and shaft tilts. That means that you are going to have different sorts of organization of your data; it means you are going to make different kinds of plots, make different kinds of comparison of data. To date what that has meant is that for every facility you are developing your own data base manipulation system. I think that for the near future that is probably going to continue. I don't think it is really realistic to have a single, all-encompassing data management system that will satisfy everybody. Maybe some day we will all be driven there by costs, or maybe the systems will just catch up with us. So I think the real problem that we want to address is not so much that the software manipulates the data, but the communication--knowing enough about each other's data bases so that taking a disk or tape from one system to another does not become a four month job, but can become a relatively minor task. So I think it is the transfer of data--the "data" in Peretz's words--from one data base to another is the thing that will be the most useful in the near future.

Bondi: Wayne, if I could comment on that, I think that you are absolutely right as far as having it tailored to the aircraft or the wind tunnel. However, I think transferring the data possibly is a mistake because it does always involve a tremendous amount of effort and I think having terminal access to the user who generated it, using their computer, using their support, is maybe a more realistic way to meet that.

Jim McCroskey, U.S. Army Aeromechanics Laboratory: Well, that's one way of insuring that the data stays in some semblance of control, but what about the permanence of that? Do you anticipate that ten years from now someone will be able to dial in to the computer at Ames Research Center and access the data you were just talking about?

Bondi: Euan mentioned that, and I have thought about it. I think maybe what has to be done is industry should request NASA--certainly not me in particular--to support that function. Because you are right, computers change and it's very difficult to keep a system going for more than three or four years. But possibly if industry is really serious about this, they should task NASA with that job, like they have done with reports.

McCroskey: But if you had asked industry to do something to preserve Scheiman's data I will guarantee it wouldn't be around today. It's because NASA has a library system and there is something called a Dewey Decimal System that it is built on, that it took not just decades, not just generations, but many, many years to develop and that permanence is something that didn't come overnight. I think if you ask industry to set up Congress to get NASA funded to preserve this stuff for 20 years, I don't think it will happen.

Bondi: I don't know. I think it's worth a try from the seriousness of the . . .

Ed Austin, U.S. Army Applied Technology Laboratory: I just wanted to comment that we have been deeply involved in the DATAMAP program, which was developed by Bell Helicopter, and we have had a considerable amount of experience in converting various sets of data on to the DATAMAP data base. And we have not found it to be a major problem. You others may have had a different experience, and we may have had a particularly adept programmer, but we stand willing to consult with anyone who is interested in converting data sets into the DATAMAP data base. All you have to do is give us a call and we would be happy to talk with you about it.

Hooper: Ed, one of the big difficulties that we have experienced was because we are putting it on an IBM system and we are taking the data from a VAX system. The compatibilities simply haven't been formalized, and you are working IBM system to IBM system. We have had many, many conversations with your people and with Bell's people also, and with NASA Ames and there is a lot of work that needs to be done to make it a hardened system.

Bondi: Ed, one comment that I have is that a person who is very familiar with their data base is only up against the problem of getting the tapes mounted and getting it on there. A person who is a non-familiar user has the problem of knowing what the item codes or what the parameter names are. We have tried to get around that problem by grouping them as either aeroelastics, performance, maneuvers, etc. so that the user only qualifies his grouping in a manner that is usually fairly straightforward and the computer picks up the associated parameters. So I think it depends on whether or how knowledgeable you are about your own system.

Austin: Well, that is why I volunteered to consult with anyone who is interested in doing that, and we do have experience now in both VAX and IBM systems.

PREPARED COMMENTS*

Donald A. Boxwell
Research Scientist
U.S.Army Aeromechanics Laboratory

As Euan Hooper said, the Aeromechanics Laboratory is approaching the data base issue from a different perspective and that is from the standpoint of rotor acoustics and blade pressures as they relate specifically in aiding the prediction of the acoustic signature. What I would like to do today is show you some of our experiences in the areas of gathering data for acoustics and blade pressures. I'll just run through these experiences quickly, in the interest of time, showing you some photographs of the various tests that we have conducted in order to acquire this data. The tests are well documented in the literature, and I just wanted to outline for you where we have been. Then we will go through some of our major observations, some of the things I feel are important in the data collection process. Again, I think you will see a difference from some of the other data base presentations. We are not so concerned with the mechanics of the data base: is it on disk or mag tape, etc., but more the principle of how one goes about defining what one wants to accomplish and how this maybe is reflected in the outcome. Then I have some recommendations that reflect directly from these observations.

Experimentally, we have done both full-scale and model-scale testing. In full-scale (Slide 1, Item 1) we have conducted a number of in-flight programs using six different helicopters and eight actual programs. All the in-flight testing was based on a technique shown in Slide 2 in which the subject helicopter was flown in formation with a quiet fixed-wing aircraft. The data that was collected was acoustic data from microphones on the tail and each wing tip. We started with a UH-1H and an OV-1C aircraft and then progressed to the Cobra (and YO-3A) on which we tested three different rotor systems. From there, we conducted similar tests on both of the UTTAS aircraft and both attack helicopters during the SSEB competitions. From these flight tests we were able to identify a basic acoustic signature coming from the rotor as shown in Slide 3 and identify the major noise components as shown in the slide. The data were stored on analog mag tape and digitized in accordance with our specific program requirements. What we were able to achieve then was some data documentation in terms of important non-dimensional parameters as shown for example in Slide 4: here at a given value of advance ratio, hover tip Mach number and thrust coefficient we documented the effect of tip path plane angle or rate of descent on the BVI acoustic signature.

We also have experimented in model-scale as indicated in Slide 1, Item 2 in which we have had three major programs in the last ten years. The first program was in our 7 × 10 tunnel with an acoustically treated test section and tested a UH-1H model rotor. From there we went to France into the CEPRA-19 anechoic wind tunnel and from there to the Netherlands for some 1/7th scale Cobra model testing in the DNW anechoic wind tunnel. This photo (Slide 5) shows an aerial view of the DNW. Slide 6 is a picture of our rotor installation in this tunnel. Here the acoustic data collected were from 19 microphones and also the rotor, shown better in Slide 7, was instrumented with blade pressures. There were 32 absolute blade pressures on 1 blade and 18 differentials on the other. This test generated a data set of simultaneous blade pressures and acoustic data. Here we were specifically looking at areas of high-speed impulsive noise and blade-vortex interaction noise as non-dimensionally scaled flight conditions of the previous full-scale efforts. Our goal was not to map out a large data base; not to gather everything that was possible, but to look for and gather data for the problems at hand. The model-scale results are similar to full-scale as shown on Slide 8 and can be displayed in terms of the same important parameters. As Wayne Johnson indicated, in the tunnel you have the much broader ability to look at the major parameters that are involved and the data set was collected in this fashion by varying tip path plane angle, thrust coefficient, Mach number, advance ratio around the comparable full-scale flight conditions.

Up to this point we have described our own data sets. We have also tried to use data sets generated by other people (Slide 1, Item 3) with some successes and some failures. We have looked at the DATAMAP OLS data base (Slide 9) in which simultaneous microphone data and blade pressures were acquired. We have looked at these data from the standpoint of trying to use them as input to an acoustic prediction program. Slide 10 is a chart that shows some of the typical blade pressures from the OLS test. Yoshi Nakamura, while at the Aeromechanics Laboratory a few years back, tried to use this OLS data from DATAMAP as input to an acoustic prediction code. He was not very successful as you can see from Slide 11. The upper trace is the actual acoustic measurement from the OLS. The bottom is the acoustic prediction using non-compact theories and the blade pressure data from DATAMAP. As you can see we were not very successful using the DATAMAP data. The amplitude is underpredicted and the waveform width is overpredicted (Slide 12). [Hooper: I don't think you are blaming DATAMAP for that are you?] Not DATAMAP

*The material was prepared by Fredric H. Schmitz, U.S. Army Aeromechanics Laboratory.

per se, but the data in DATAMAP are suspect for this application. There are obviously two areas where something could be wrong; one is the theory and one is the OLS data base. Since we are talking about data bases here, we are definitely looking into the possibility that the frequency response is not sufficient in the DATAMAP OLS data. The data were acquired using a multiplexed type of arrangement and we suspect very highly that there could be some frequency response degradation in that data due to the way it was collected.

When we compare our own data bases (Slide 1, Item 4) as acquired in full-scale, as shown at the top of Slide 13 and model-scale at the bottom, you can see that we tried to set these programs up so that the data collected were for a specific purpose, and so that there would be a one-to-one relationship between full-scale data and the model-scale testing techniques. We paid particular attention to this kind of detail and found that when you do that you can achieve some of your desired goals such as assessing the acoustic data scaleability between full-scale and model-scale. Slide 14 shows side-by-side, model-scale and full-scale BVI acoustic signatures and we see a good similarity in acoustic waveform. My point is that data bases can become large and of limited usefulness by trying to collect too much without a specific purpose.

Let me go to my formal observations (Slide 15). I'd like to say that a carefully planned test with clearly defined objectives that are relevant to the sponsoring organization's goals has the highest chance of success. If an organization is tasked with a job collecting data and if they are not the end users of it, I think the chances of success are much more limited. Obviously the individuals who are responsible for the test direction have to be motivated. They have to be the ones who are technically cognizant of the data that they are trying to collect. They should not be simply a service organization. The individuals must care about what the data means and they must be willing and able to sometimes stop before the test is completed and verify that results are meaningful or usable before the whole data base is collected. Obviously, this has to be a team effort; everybody has to know a little bit about different aspects of the test. The release of the data should be specific and deliberate. Generating large data bases and publishing them as simply that can often lead to little or incorrect use. One should have a definite goal that they are looking at and publish, deliberately, reports using that data base.

Finally, my recommendations are shown on Slide 16. They follow pretty closely the observations that were made. One needs to choose test programs with clearly defined objectives in order to assure that you are going to end up with a usable data base. One must have capable engineers, again, who are motivated. Also one must involve the key test engineers in the entire process of reaching scientific research objectives. There is the need to maintain high technical standards. The reward then is that you have achieved your objective. It is achieving an objective, not the completion of the test and the publication of a lot of reports, that gives rise to useful data bases.

EXPERIENCE

- FULL SCALE IN-FLIGHT ACOUSTIC DATA
  - 6 HELICOPTERS, 8 PROGRAMS IN 10 YEARS
  - DESIGNED THE TEST PROGRAM, GATHERED THE DATA, HELPED REDUCE THE DATA, PUBLISHED NUMEROUS REPORTS AND PAPERS
- MODEL SCALE BLADE SURFACE PRESSURE AND ACOUSTIC DATA
  - 3 PROGRAMS IN THE PAST 10 YEARS
  - DESIGNED THE TEST PROGRAM, GATHERED THE DATA, HELPED GUIDE THE REDUCTION, PUBLISHED NUMEROUS REPORTS AND PAPERS
- USE OF "DATA-MAP" AS INPUT TO FAR-FIELD ACOUSTIC PREDICTION OF BLADE-VORTEX-INTERACTION NOISE
  - HELPED Y. NAKAMURA USE "DATA-MAP" TO RETRIEVE THE AERODYNAMIC INPUTS FROM THE O.L.S. TEST FOR ACOUSTIC PREDICTIONS
- ATTEMPTED TO COORDINATE MODEL SCALE/FULL SCALE TESTING
  - SUCCESSFUL WHEN USING ARMY FLIGHT DATA
  - NOT SUCCESSFUL WHEN USING OLS-TAAT DATA

Slide 1.

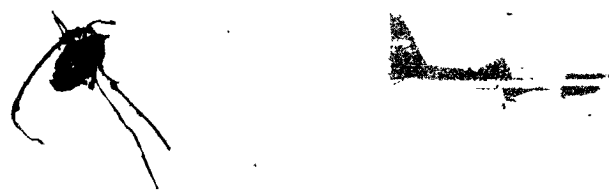

Slide 2.

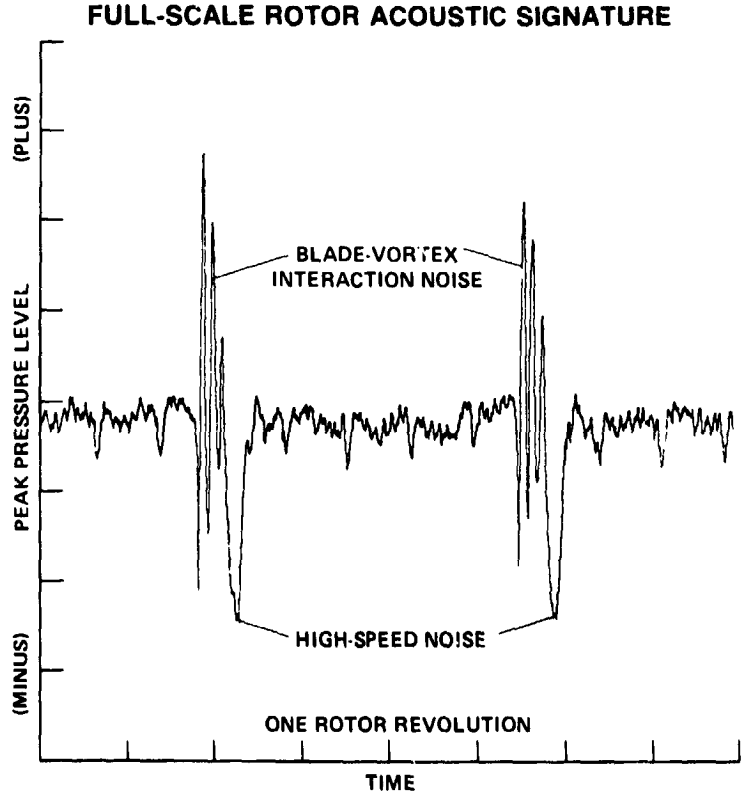

Slide 3.

FULL-SCALE (540) ROTOR BVI ACOUSTIC DATA

μ = 0.164

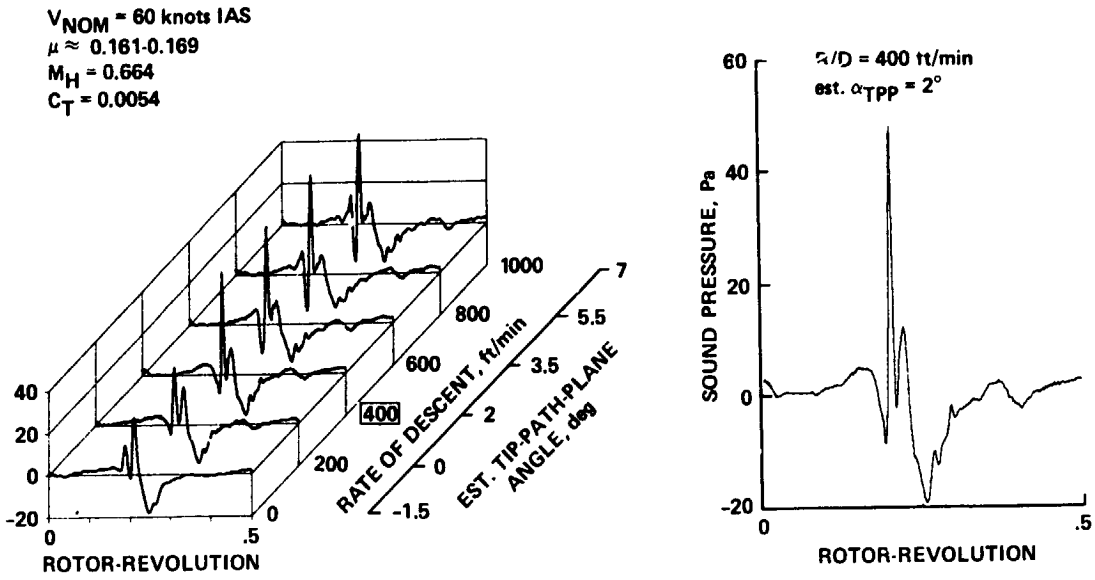

Slide 4.

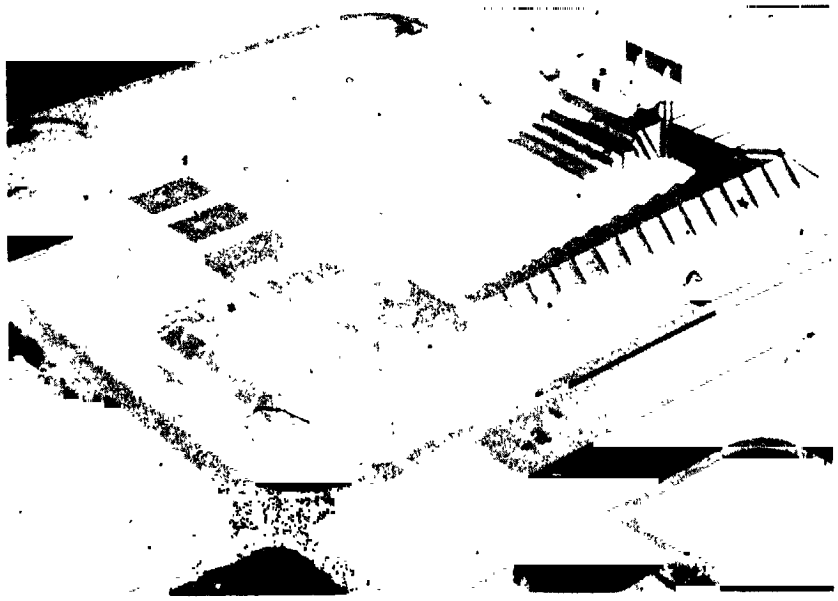

Slide 5.

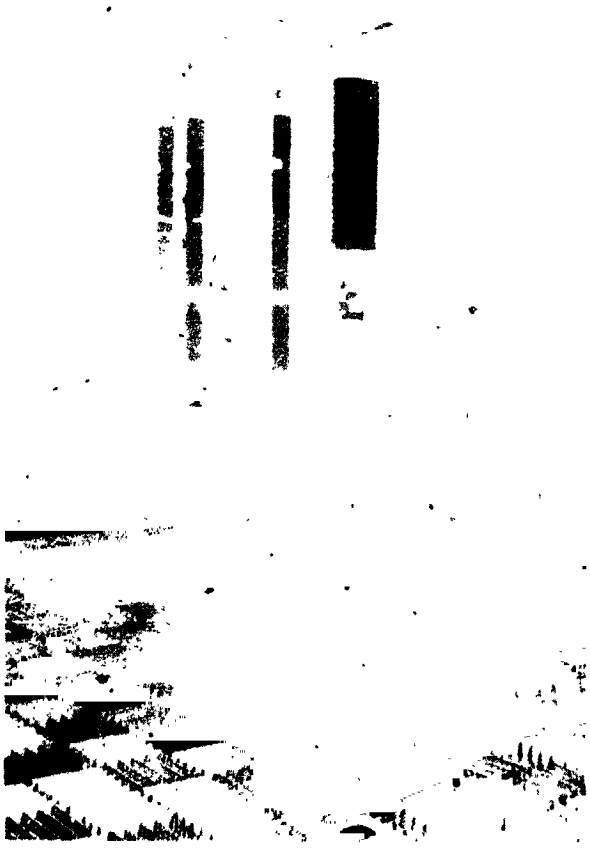

Slide 6.

Slide 7.

MODEL ROTOR (OLS) BVI ACOUSTIC DATA

μ = 0.164

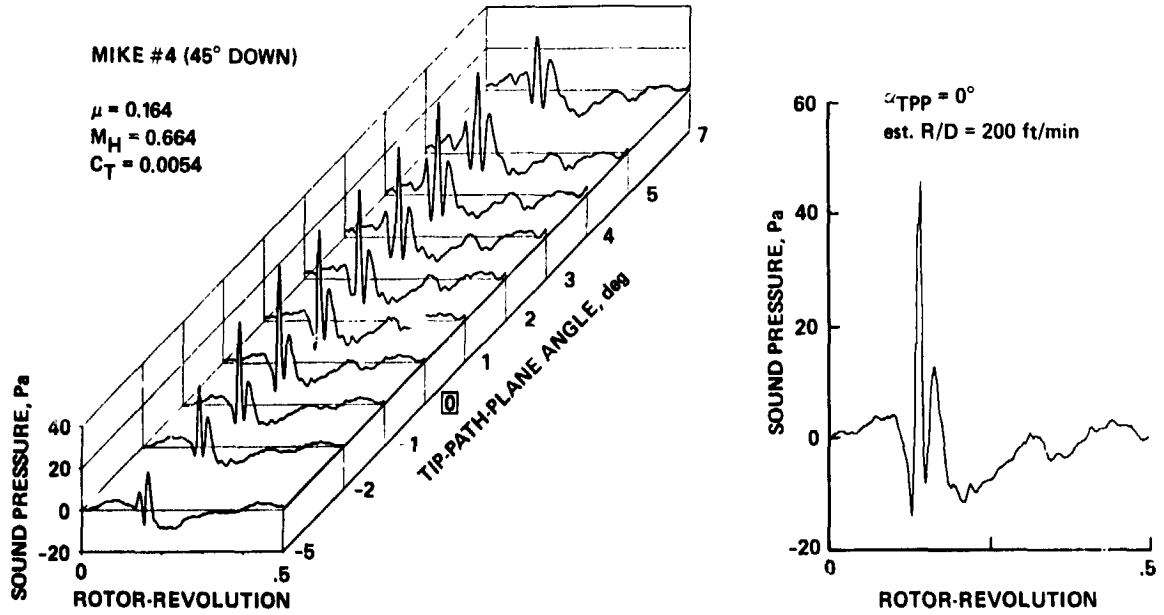

Slide 8.

SIMULTANEOUS MEASUREMENT OF BLADE SURFACE PRESSURE AND NOISE

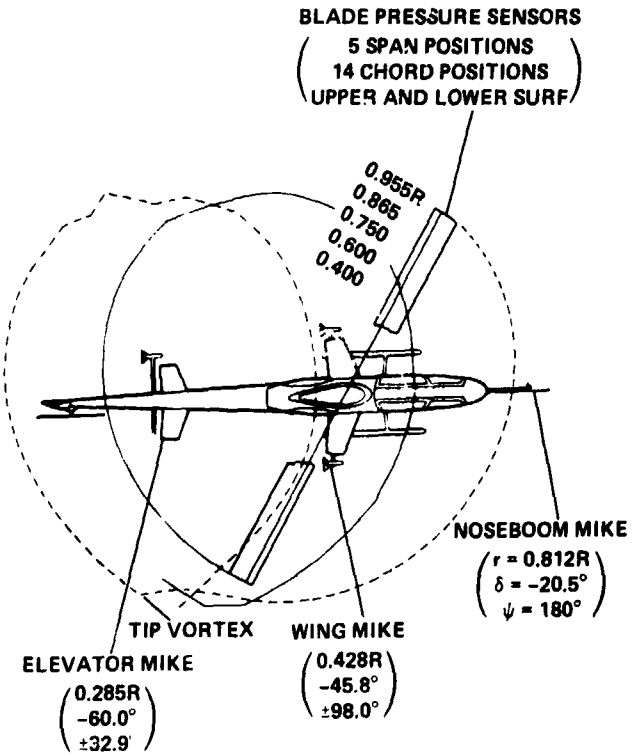

Slide 9.

EXAMPLE OF BLADE SURFACE PRESSURE HISTORY AT DIFFERENT SPAN POSITIONS

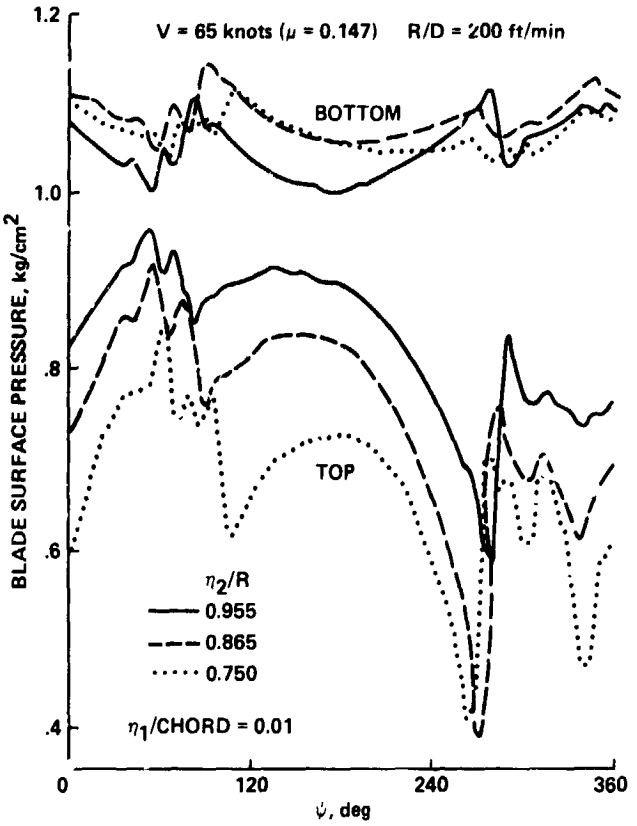

Slide 10.

COMPARISON OF ACOUSTIC WAVEFORM BETWEEN MEASUREMENT AND COMPUTATION

(NOSE BOOM MICROPHONE)

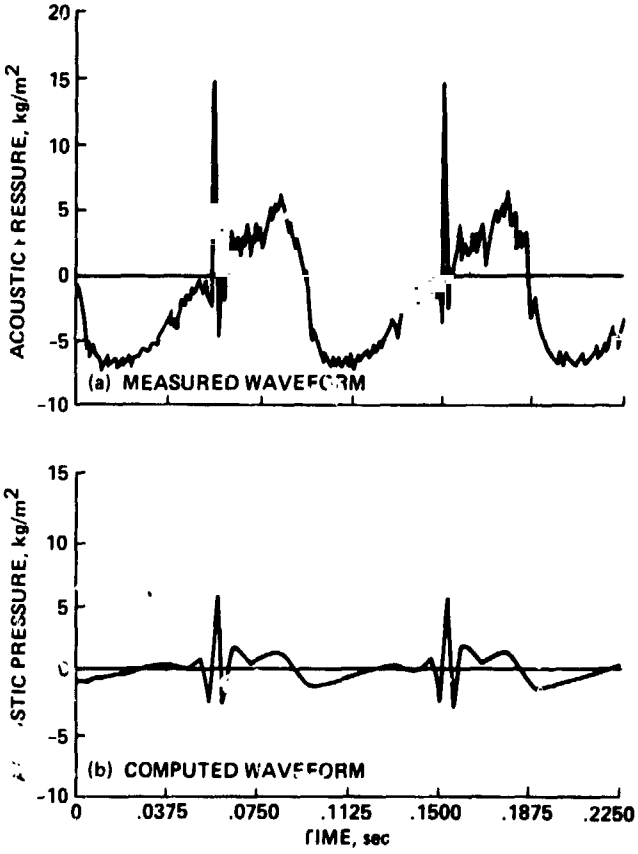

Slide 11.

COMPARISON OF EXPANDED ACOUSTIC IMPULSE BETWEEN MEASUREMENT AND COMPUTATION

(NOSE BOOM MICROPHONE)

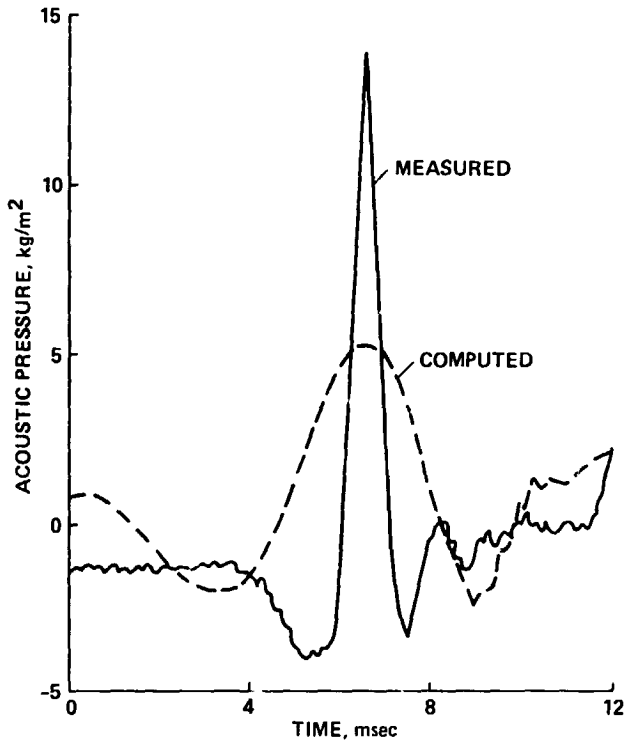

Slide 12.

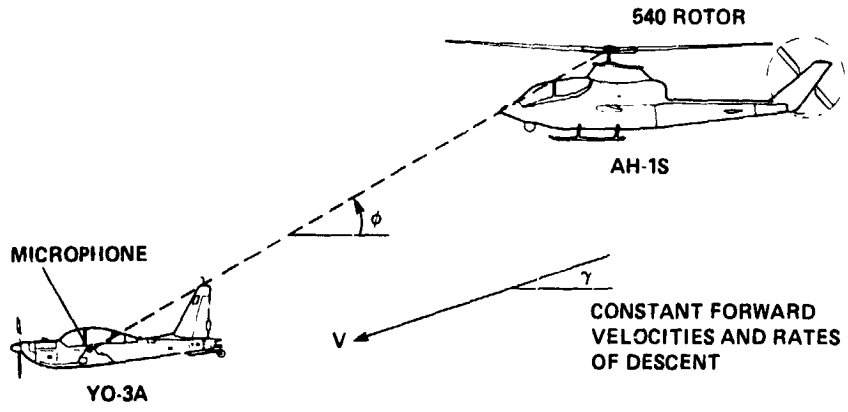

EQUIVALENCE OF MODEL-/FULL-SCALE ACOUSTIC TESTING

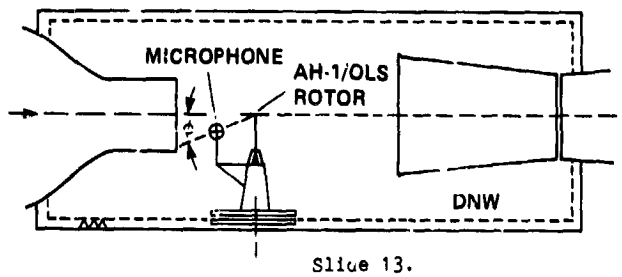

Slide 13.

MODEL AND FULL-SCALE ROTOR BVI ACOUSTIC DATA

μ = 0.164

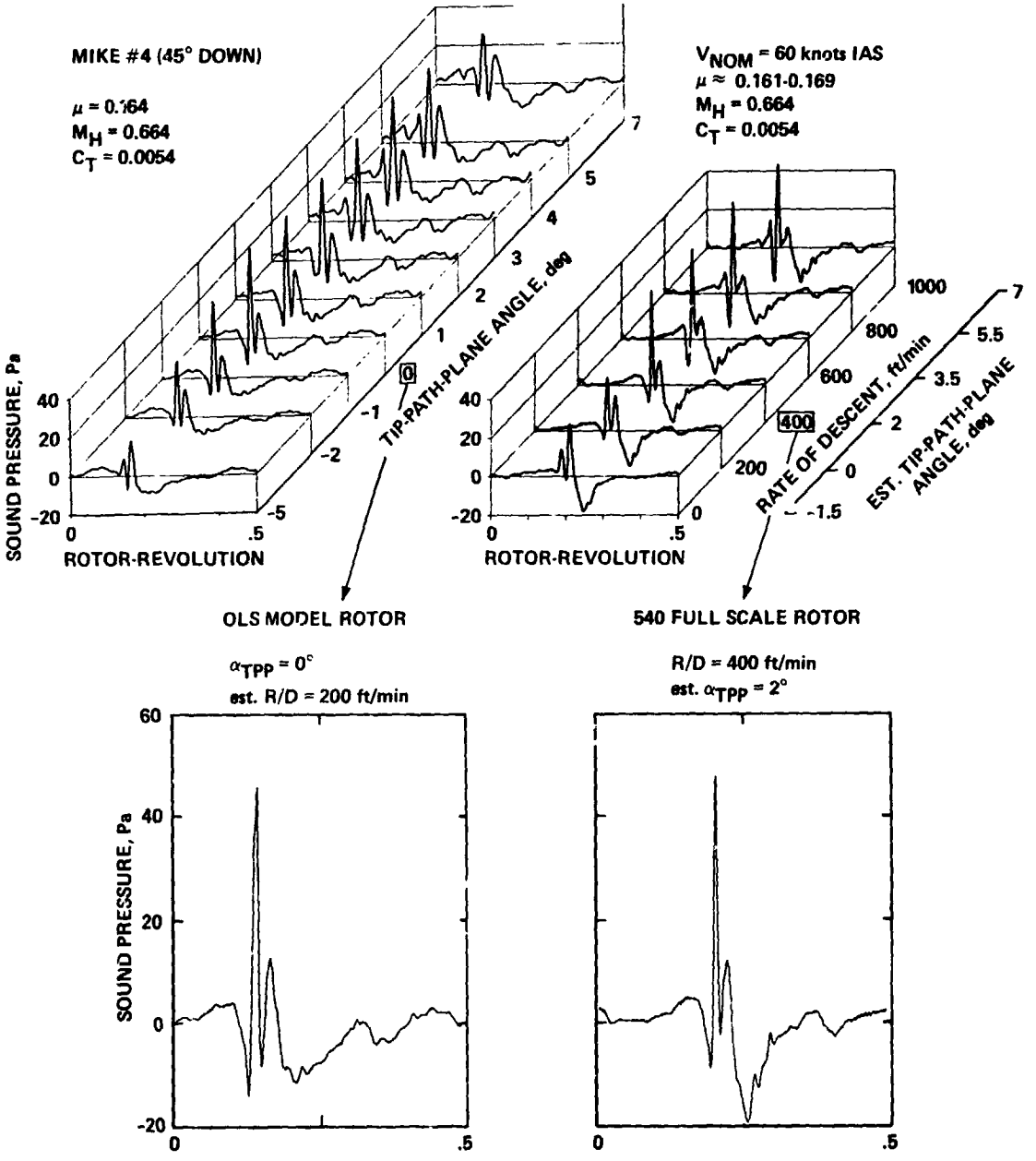

Slide 14.

OBSERVATIONS

- THE CAREFULLY PLANNED TEST (OR EXPERIMENT) WITH CLEARLY DEFINED SCIENTIFIC/ENGINEERING OBJECTIVES THAT ARE RELEVANT TO THE SPONSORING ORGANIZATION'S GOALS HAS THE HIGHEST CHANCE OF SUCCESS
- IF THE INDIVIDUALS WHO ARE RESPONSIBLE FOR TEST DIRECTION ARE TRULY MOTIVATED TO ACCOMPLISH THE SCIENTIFIC/ENGINEERING OBJECTIVES, THE TEST WILL HAVE A HIGH PROBABILITY OF SUCCESS
- IN ALL TESTS, INITIAL RESULTS MUST BE VERIFIED (AND CRITICAL PROBLEMS SOLVED) BEFORE THE ENTIRE DATA BASE IS COLLECTED
- IN TESTS THAT ARE NECESSARILY COMPLEX, IF THE TEAM OF TEST ENGINEERS ARE INVOLVED IN MOST ASPECTS OF THE TEST PLANNING, TEST IMPLEMENTATION, DATA REDUCTION, AND REPORT PREPARATION EFFORTS, THE CHANCES OF ATTAINING THE SCIENTIFIC/ENGINEERING OBJECTIVES ARE SIGNIFICANTLY ENHANCED
- ONE GOOD TEST IS WORTH A HUNDRED MEDIOCRE TESTS WITH THE SAME OBJECTIVES
- DELIBERATE RELEASE OF CORRECT TEST RESULTS IS BETTER THAN A HURRIED RELEASE OF PRELIMINARY DATA

Slide 15.

RECOMMENDATIONS

- CHOOSE TEST PROGRAMS THAT ARE DIRECTED TOWARD CLEARLY DEFINED SCIENTIFIC/ENGINEERING OBJECTIVES THAT ARE CONSISTENT WITH THE SPONSORING AGENCY'S PROGRAMMATIC GOALS

  [ACQUIRING DATA BASES IS NOT A SCIENTIFIC/ENGINEERING OBJECTIVE BY ITSELF]

- FIND CAPABLE ENGINEERS WHO ARE TRULY MOTIVATED TO REACH THE SCIENTIFIC/RESEARCH OBJECTIVES AND CLEARLY SUPPORT THEM IN THEIR EFFORTS
- INVOLVE THE KEY TEST ENGINEERS IN THE ENTIRE PROCESS OF REACHING THE SCIENTIFIC/RESEARCH OBJECTIVES

  [i.e., INCLUSION IN PLANNING, TESTING, DATA REDUCTION, AND REPORT WRITING EFFORTS]

- MAINTAIN HIGH TECHNICAL STANDARDS THROUGH ALL PHASES OF THE PROGRAM
- REWARD ACCOMPLISHMENT OF SCIENTIFIC/ENGINEERING OBJECTIVES RATHER THAN PROLIFIC PUBLICATION OF PAPERS AND REPORTS

Slide 16.

PREPARED COMMENTS

E. Roberts Wood
Manager, Aeromechanics
Hughes Helicopters, Inc.

When Euan asked us to serve on this panel he hit on four key areas. One was the need, the second was the source, the third was to reflect on experience, and the fourth was the individual panelists' recommendations. I am going to go through these perhaps a little differently than some of the other speakers have and since we are running a little late, I will move along quickly.

With respect to the need--the need is pretty obvious to all of us as shown in Slide 1, but I think we all have different interests. It's to substantiate existing analyses, increase knowledge of helicopter structural dynamics, aerodynamics, aeroelastic behavior, or acoustics, say, and to serve as a yardstick for future helicopter designs. And I think the last statement on Slide 1 cites an especially important need for a data base--that is to provide information that will help us to understand previously unexplained phenomena.

On the subject of sources--sources have been very adequately covered by the panel, so I'll be very brief (Slide 2). I simply listed the OLS data which we have used at Hughes. I've also listed Scheiman's data which we make extensive use of because it is tabulated in such easily accessible form. Further, we make limited use of DATAMAP. A major source for us is our own company's data. At Hughes, in particular, we have extensive data on the Apache (AH-64), the Model 500 Series helicopters, and the higher harmonic control program with the modified OH-6A.

Just going back over the years and thinking of my own experiences (Slide 3), I recall that when I first entered the helicopter field there was a lack of understanding in identifying the primary source of high vibrations in the 40-knot regime. And that was not adequately explained until Scheiman's data was published. Also the low vibrations in the 60, 80 to 100 knot regimes were well explained by Scheiman's data. I think we don't have an adequate explanation of the high vibrations we see at high airspeed, and I will show you why I make that statement. And finally, the importance of better understanding of 3-dimensional flow around the blade tip can be highlighted from Scheiman's and other people's data.

Slide 4 is a typical plot of helicopter vibrations versus forward speed. Twenty years ago a major problem, and of course we still have it today, was in the transition or 40-knot regime and its cause. And it was very nice the way Scheiman's data showed the source so clearly. Basically as you see in Slide 5, in the 40-knot regime we have the wake very near the rotor. There is a low component of forward velocity going through the rotor disk, and one would postulate that the path of the tip vortex would follow a helical trend. At the higher speeds, say 70 or 80 knots, we have the normal component of forward velocity driving the tip vortex further away from the main rotor. This is similar to extending the tip vortex as a helical spring, if you want to envision it as that.

Shown in Slide 6 is Scheiman's data which began to conclusively answer the 40-knot question. Here you have the airload at 95% blade radius plotted versus azimuth. You see clearly the sharp blade-vortex interactions occurring at 90 degrees and at 270 degrees. If one looks at the corresponding data for the 70-knot region in Slide 7, at the same radial position on the blade, it is not surprising that vibration levels are down because this blade-vortex interaction is substantially decreased. If one looks at the data plotted versus azimuth for 4 radial locations at 42 knots (Slide 8), the cycloidal-path of the trailing tip vortex is apparent. Since it is the succeeding blade going through the vortex shed by the preceding blade, then we would expect as we move inboard radially that these peaks should move closer together and indeed they do as you see here going from 95% to 90% blade radius, then 85% to 75% blade radius.

One reason it's difficult to explain from airloads, the high vibrations we have at high speeds is the type of data he shows at 122 knots (Slide 9). We see outboard at 95% blade radius, some higher harmonic content, but as we move in at 90%, 85%, 75% this is practically purely 2 per rev. As you go inboard the data continues to follow this trend, and one wonders why the helicopter at this speed is vibrating as much or more than when it was encountering the 42-knot airloads.

Recently, a reason that has been postulated as a potential cause for increased vibrations at higher airspeeds is the impingement of the wake on the tail cone and on the empennage. What I show in Slide 10 is higher harmonic control open-loop data that I think is interesting in this regard. What I have plotted here is basically the vibration levels versus g's with lateral control input only from the HHC manual controller. A third-of-a-degree blade angle at all airspeeds is used. Rather than look at the valley or reduction that HHC is achieving, I'd rather concentrate here at looking at maximum vibration levels to which HHC is driving the

helicopter for the same input at different airspeeds. We notice here at 60 knots, that the maximum level that is generated is .4 g's. We move to 70 knots and we see the maximum level is .4 g's. We move to 80 knots and we see that maximum level remains .4 g's. It seems to imply that the third-of-a-degree oscillation can generate no more than .4 g's. However, when we move from these plots to those for the 90-knot and 100-knot conditions shown on Slide 11, the trend suddenly changes. We find here the HHC at a third-of-a-degree is generating .52 g's, and at 100 knots .68 g's. Understandably, the crew declined to test any further for these vibration peaks, but the point is, why the increase in maximum levels at 90 and 100 knots when they had remained constant at 60, 70, and 80 knots? Could airframe vibrations be solely rotor induced at 60, 70, and 80 knots, and the increase in vibrations at 90 and 100 knots be attributed to wake impingement on the empennage?

Also, I'll just show this briefly (Slide 12) because I think it's an interesting subject, and that is the importance of tip loss on blade bending moments. This also comes out of Scheiman's data. Slide 12 compares blade outboard moments (r/R = 0.8) as measured by Scheiman with an analysis where we: (a) assumed a constant tip loss; and (b) assumed tip loss area varying as $(1 - \cos 2\psi)B$. Note the significant change in the time histories. We continue to look for a better understanding of tip airloads. It looks like it's a much more complex problem than that of a simple constant tip loss factor.

Finally, for this panel, I really wanted to get the consensus, not only of my own opinion, but perhaps that of a number of others at Hughes and so I did as one or two other panel members did, and that is I asked for recommendations, compiled them and put them together. And with that I will discuss the recommendations shown on Slides 13 and 14 and then close. For many of these recommendations, a number of people repeated the same suggestion.

The recommendations were as follows: 1) Data bases should be the responsibility of a Central Data Base Management Group and several people thought that that was preferably NASA. 2) In addition to flight test data what one would like to be able to access would be both full scale wind tunnel and model wind tunnel as well. 3) Preferred standard data acquisition formats be established between the government and manufacturers. 4) Assign a supporting budget. I guess what this really means is set aside a definite line item by which NASA and the manufacturers would maintain, update, and add to the data base. 5) And this was emphasized by several people, that is the data base rotor systems measured parameters should also include--and I think we have all run into this--detailed information on aircraft configuration and physical properties. 6) By that I mean detailed information on the aircraft c.g.; roll, pitch, and yaw inertias; hub impedance, etc.; if it's available, because frequently it is frustrating to have the detailed data and yet lack the overall or rather broad information on the aircraft. 7) This has been brought out by other panelists and, that is, hopefully, as the data base is put together it would be reviewed, I should say, perhaps, the best word to use with data is as the data is reduced, it should be reviewed and debugged to the best of our ability of faulty data where it can be seen. 8) Finally, it would be hoped that a representative amount of data from each sampling would be in hard form so that data could be accessed and used immediately without the need for going to, say, something like DATAMAP.

DATA BASES — THE USER'S VIEWPOINT
THE NEED

DATA BASES ARE NEEDED

- **TO SUBSTANTIATE EXISTING ANALYSES**
- **TO INCREASE KNOWLEDGE OF HELICOPTER STRUCTURAL DYNAMICS, AERODYNAMICS, AEROELASTIC BEHAVIOR, AND ACOUSTICS**
- **TO SERVE AS A YARDSTICK FOR FUTURE HELICOPTER DESIGNS**
- **TO PROVIDE INFORMATION THAT WILL HELP UNDERSTAND PREVIOUSLY UNEXPLAINED PHENOMENA**

Slide 1.

DATA BASES — THE USER'S VIEWPOINT

PRESENT SOURCES

SOURCES OF DATA BASE INFORMATION ARE FEW:

- SCHEIMAN, J.A., NASA TM X-952, MARCH 1963. (THIS CONTAINS EXTENSIVE H-34 DATA IN EASILY ACCESSIBLE AND REDUCED FORM)
- SHOCKEY, G.A., COX, C.R., AND WILLIAMSON, J.W., USAAMRDL-TR-76-39, FEBRUARY 1977. (PLOTS SHOWING SELECTED SAMPLES OF DATA FROM AH-1G OPERATIONAL LOADS SURVEY (OLS)
- PHILBRICK, R.B., USAAVRADCOM-TR-80-D-30A, (DATAMAP VOLS 1 & 2), DECEMBER 1980. (DEVELOPED BY NASA AND U.S. ARMY FOR ACCESSING DATA BASES SUCH AS OLS)
- INDIVIDUAL COMPANY'S DATA (FOR HHI, WE HAVE EXTENSIVE DATA ON AH-64, MODEL 500, AND HHC)

Slide 2.

DATA BASES — THE USER'S VIEWPOINT

SOME EXPERIENCE OF THIS PANEL MEMBER

STUDY OF SCHEIMAN'S H-34 DATA INDICATES:

- PRIMARY SOURCE OF HIGH VIBRATIONS IN 40-KNOT REGIME IS BLADE VORTEX INTERACTION
- IN 40-KNOT REGIME PLOTS OF TIP VORTEX INTERACTIONS TAKE FORM OF CLASSICAL CYCLOIDS, AS EXPECTED
- LOW VIBRATIONS IN 60-80 KNOT REGIME CAN BE ATTRIBUTED TO SUBSTANTIALLY REDUCED BLADE VORTEX INTERACTION
- SCHEIMAN'S DATA PLUS RECENT HHC DATA INDICATE THAT FOR HIGH-SPEED VIBRATIONS, WAKE IMPINGEMENT ON FUSELAGE AND EMPENNAGE MAY BE PRIMARY SOURCE OF EXCITATION, NOT LOADS THRU MAST
- TIP LOSS VARIES WITH AZIMUTH AND CANNOT BE TREATED AS CONSTANT FOR DYNAMIC LOADS

Slide 3.

VARIATION OF HELICOPTER VIBRATION WITH AIRSPEED

HELICOPTER VIBRATIONS —
TYPICAL VARIATION WITH AIRSPEED

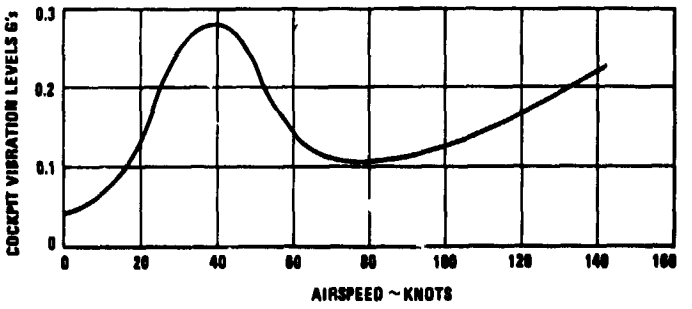

Slide 4.

ROTOR WAKE GEOMETRY FOR LOW AND HIGH-SPEED FLIGHT

NON-DISTORTED ROTOR WAKE GEOMETRY

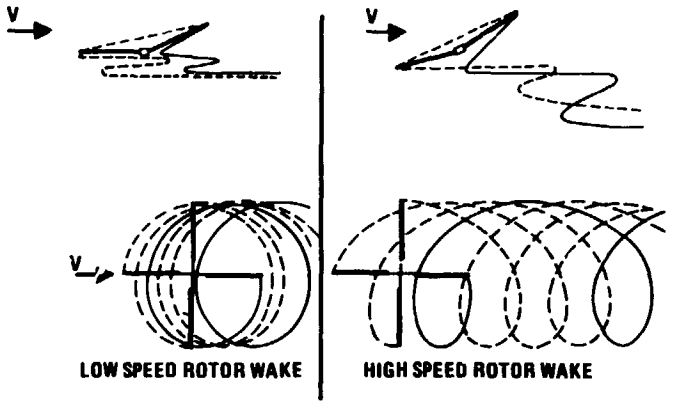

Slide 5.

BLADE-VORTEX INTERACTION IN LOW SPEED FLIGHT

AIRLOADS vs AZIMUTH (NASA TMX-952)
H-34 HELICOPTER; V = 42 KNOTS

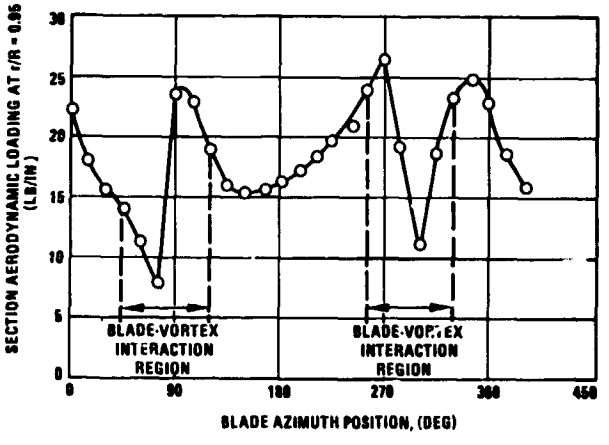

Slide 6.

BLADE-VORTEX INTERACTION IN MODERATE SPEED FLIGHT

AIRLOADS VS AZIMUTH (NASA TMX-952)
H-34 HELICOPTER; V = 68 KNOTS

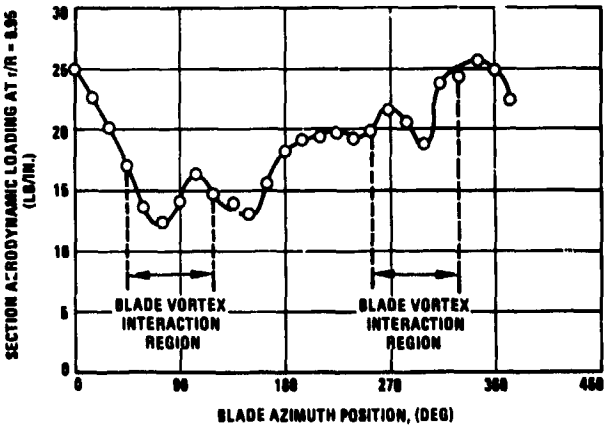

Slide 7.

INTERACTION DATA SHOWS PEAK LOADS FOLLOW CYCLOIDAL TREND

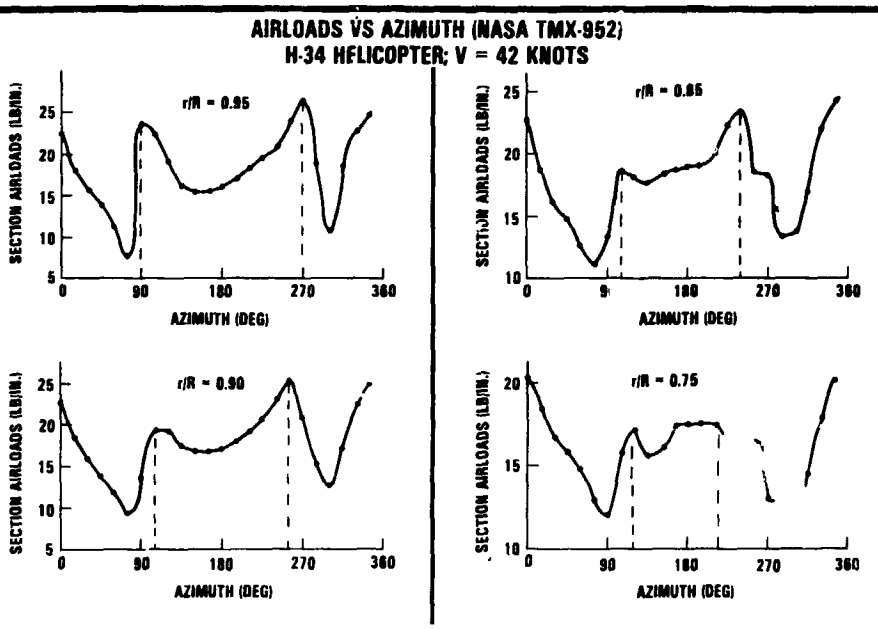

Slide 8.

HIGH SPEED DATA SHOWS ABSENCE OF BLADE-VORTEX INTERACTION

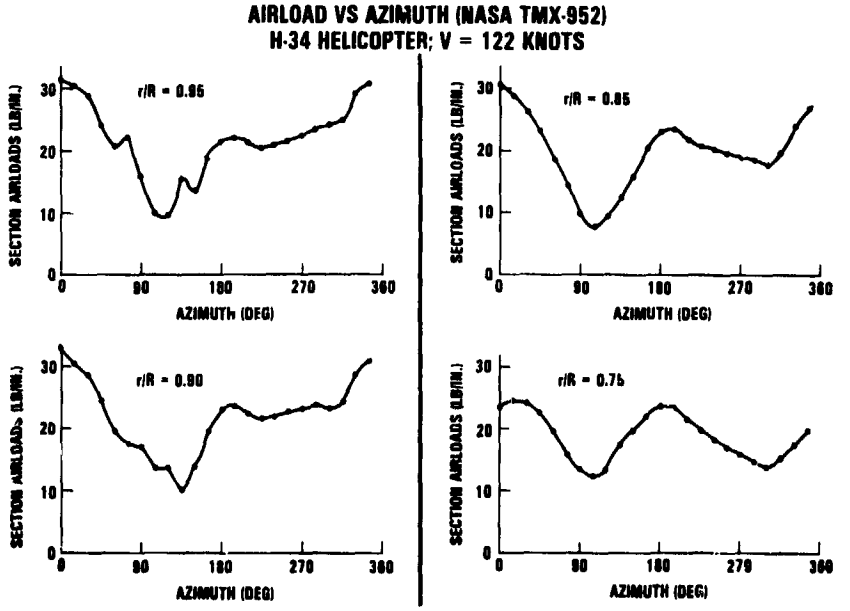

Slide 9.

THROUGH MODERATE AIRSPEEDS HHC MAXIMUM VIBRATION IS CONSTANT

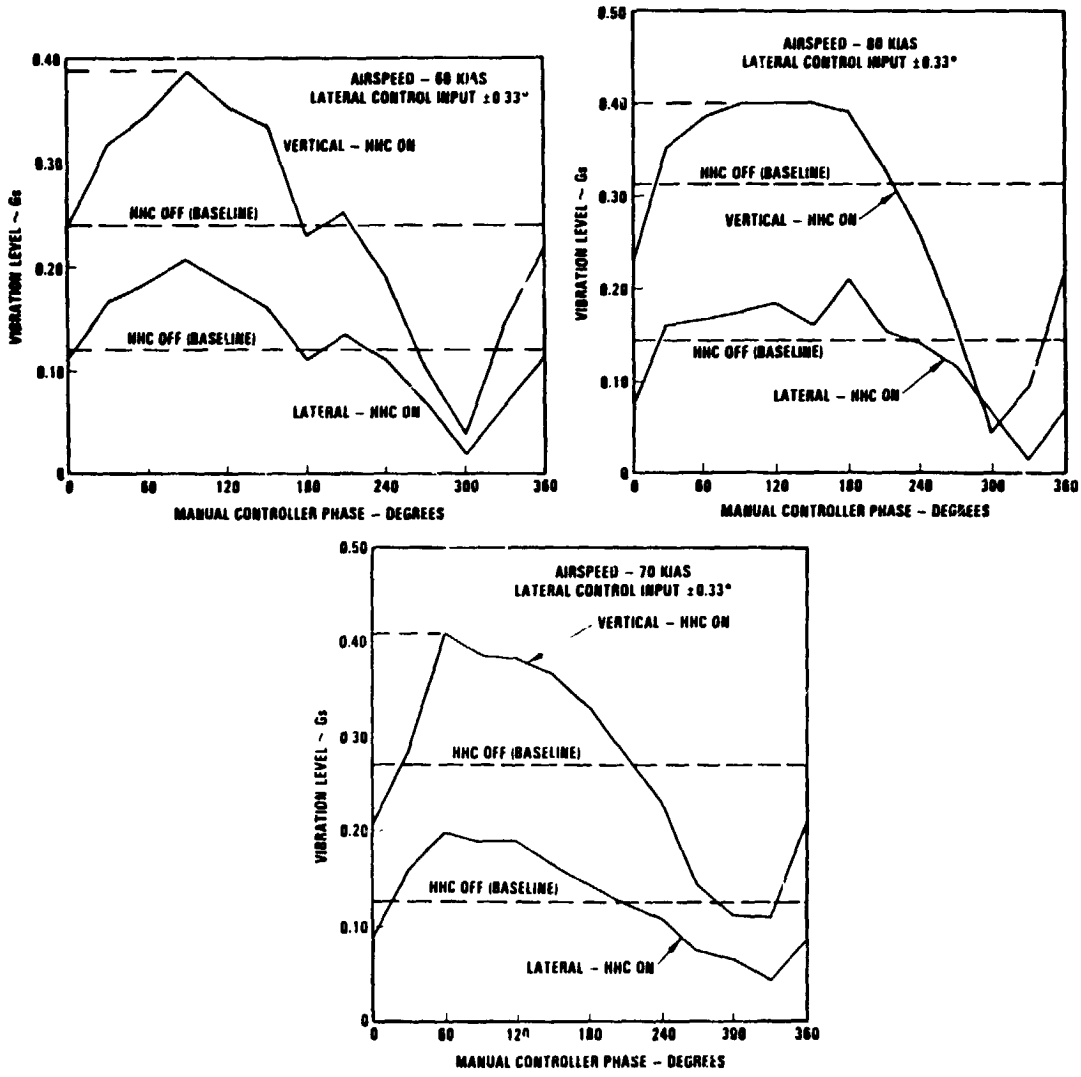

Slide 10.

AT HIGHER AIRSPEEDS HHC MAXIMUM VIBRATION INCREASES

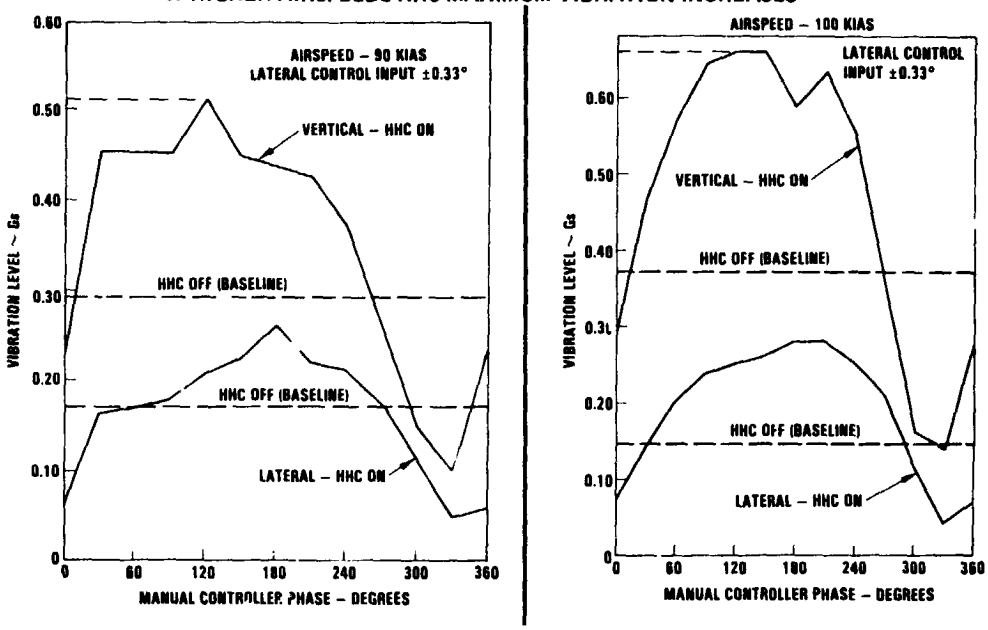

Slide 11.

H-34 BLADE LOADS WITH AND WITHOUT AZIMUTHALLY VARYING TIP LOSS

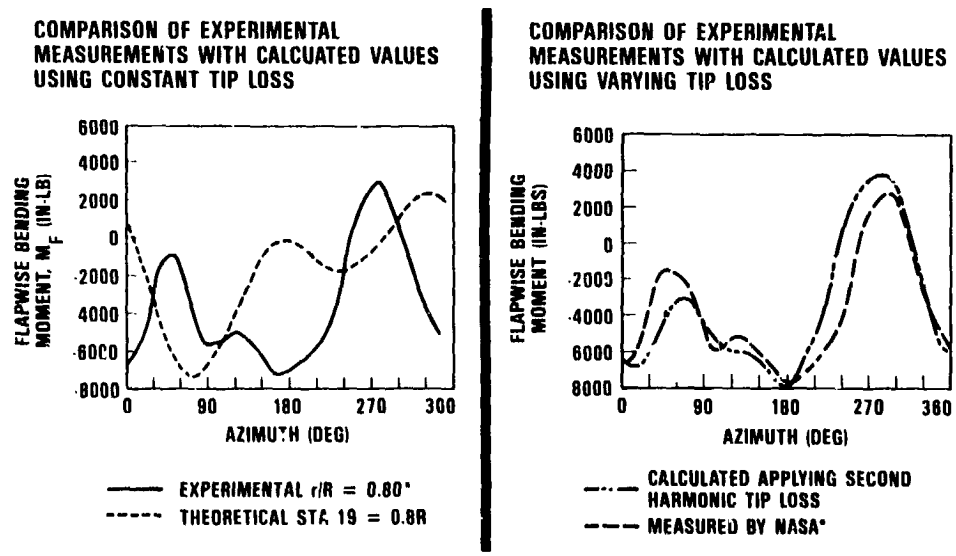

CONCLUSION: TO PROPERLY PREDICT BLADE LOADS AND CORRESPONDING BENDING MOMENTS, THE TIP AERODYNAMIC LOADING MUST BE BETTER DEFINED

*NASA TM X-952, SCHEIMAN, J., MARCH 1964.

Slide 12.

DATA BASES — THE USER'S VIEWPOINT

RECOMMENDATIONS

- DATA BASES SHOULD BE THE RESPONSIBILITY OF A CENTRAL "DATA BASE MANAGEMENT" GROUP, PREFERABLY BY NASA
- IN ADDITION TO FLIGHT TEST DATA, BOTH FULL SCALE WIND TUNNEL AND MODEL WIND TUNNEL DATA SHOULD BE COMPILED
- ESTABLISH PREFERED STANDARD DATA ACQUISITION FORMAT COMMON TO NASA AND MAJOR MANUFACTURERS
- ASSIGN A SUPPORTING BUDGET TO NASA AND TO THE MANUFACTURERS TO MAINTAIN, UPDATE AND ADD TO THE DATA BASE
- DATA BASE ON ROTOR SYSTEM MEASURED PARAMETERS SHOULD ALSO INCLUDE DETAILED INFORMATION ON AIRCRAFT CONFIGURATION AND PHYSICAL PROPERTIES

Slide 13.

DATA BASES — THE USER'S VIEWPOINT

RECOMMENDATIONS (CONT)

- DETAILED INFORMATION ON AIRCRAFT SHOULD INCLUDE A/C WEIGHT; C.G.; ROLL, PITCH AND YAW INERTIAS; HUB IMPEDANCE ETC.
- DATA BASES SHOULD BE "DEBUGGED" OF FAULTY DATA
- A REPRESENTATIVE AMOUNT OF DATA ON EACH AIRCRAFT SHOULD BE IN "HARD" FORM SO THAT SOME OF THE DATA CAN BE ACCESSED AND USED WITHOUT THE NEED FOR DATAMAP

Slide 14.

Hooper: An outstanding series of recommendations, I fully support them.

Wayne Johnson, NASA Ames Research Center: I have a couple of remarks based on your conclusions. I think the need for getting the data base debugged highlights the need for keeping the people running the experiments in the act, the engineers in the act. Two major milestones of releasing the data for general use. This is complicated by the multi-access capability that computer systems give us. Since you can have many people getting into the data before it has been certified as valid by the engineer, you have a problem that the data may find itself being propagated before it has really been validated. Again the old way of having a data report, at least, that was a milestone. Presumably the person published what he thougnt was valid. I think the engineers also have to stay in the loop to handle the compression of the data. We recognize that as we do more complex investigations we acquire more data, but people can only use a finite amount of data and as you increase the data in one dimension you have to decrease it in another and I think that's the job of the engineer. An example is provided by the H-34 data. In the wind tunnel, for example, I think they probably collected maybe 1,000 data points on performance. I don't know how much they collected on pressure, but they only published a dozen and that's just fine. Regarding the proposal that has been made a couple of times for a central organization for coordinating and maintaining data bases, I think it is unrealistic for us to push too hard for NASA to do that simply because the resources would not be inconsiderable. And I'm talking more about people than money. That sort of thing is very, very difficult to get going and to maintain in an environment where people want to collect the data and where people want to build airplanes and things like that. I don't really see that there is much hope there at all.

Wood: Well, if I could respond to that, Wayne. Perhaps maybe that should be changed to NASA establishing a center where only hard form data is kept in a limited amount . . .

Jonnson: They are called libraries.

Wood: . . . from each program which would be like a library.

Johnson: But the problem is getting the data into that form. Any kind of a central organization implies people, though. That's what I'm getting at. When you start counting how many people it would take I don't think you are going to find it. What I think would be more practical would, however, be some standards for format both on paper and on tapes that NASA or the Army or the government could take a lead role in promulgating the format. And one comment to end really goes back to Euan's . . . I was rather disappointed that he seemed to acquiesce to the new age, the new way of doing things. We have had paper for a couple of thousand years, printing presses for a couple of hundred, computers have been with us for maybe a couple of decades and I am certainly as fond of the computer as anybody in the room, but I'm not quite ready to say it's right up there with the creation of writing. I think actually putting things down on paper and saving them has a lot to be recommended.

Wood: Well, that is very true. I think just one comment that I gathered just during the meeting up to this point regarding data bases and that is if we look at the literature today, we have already pointed out what few sources there are for data and then if we look at the papers published we begin to reflect on really how relatively few papers we see published today that compare theory with test. It's a very limited amount.

Hooper: That's very true. I'd like to assert the Wayne Jonnson privilege and make another point as chairman. NASA and the Army really have to put up or shut up about documentation. They have either got to do a good job of paper documentation or if they don't they have got to do a very thorough job of using DATAMAP-type recording of data and increasingly we in the industry are being asked to put the output of our actual reports into DATAMAP format so that it can be accessed by the government and other users. And that's fine, but if you are going to do that, if you are going to go that way there's got to be a system set up for retrieval over the long term and I think that it's got to be staffed on the side of the government.

Don Merkley, U.S. Army Applied Technology Laboratory: I'd like to make a few comments. One, we're talking about a central organization and so forth to support dissemination and gathering and standardization of such things and we are in the process of trying to organize a DATAMAP user's group. We have sent out a set of questionnaires to 18 different facilities that have DATAMAP in use. Admittedly, some are not using it very much and some are using it very much but in an effort to try to . . . we recognize this problem of transferring data and the government's requirement of having DATAMAP delivered under contract--DATAMAP-format data. In an effort to promote this use of the system we are trying to get an organization of users and [implement] some of the ideas of having sort of an infrequent newsletter of contributions from different users of how they are using the system that others aren't--because they are using it with different diverse data bases, and also workshops, possibly, getting together and talking about and working out data transfer file problems in going from one computer to another and possibly in making modifications to the system and also the whole problem of configuration management.

Wood: Don, I think that sounds like an excellent idea. I think it is through such a group, if you got a group going like that, and I think perhaps the activity of that group would determine whether or not eventually there would be sufficient interest to justify this question that I did make as a recommendation, which did come from a number of people, of having NASA or the government [become] the central point. It might be that the user's group itself would be sufficient.

Merkley: Well, that's another whole question if I interpret what you are saying there. The distribution of the pieces of these data bases to the various users, you know we are talking like a clearinghouse of data and it can be a big problem and a full time job and that's another topic that I think the user's group should try to handle.

PREPARED COMMENTS

Jing G. Yen
Manager, Flight Technology
Bell Helicopter Textron

Before I came here, Mr. Euan Hooper told me that he would not allow me to exceed the ten minutes and warned me he was going to monitor this panel as carefully as Barbara Walters monitored the first presidential debate. I'm not sure though whether he is going to treat me as Mr. Reagan or Mr. Mondale.

The topic I selected is the XV-15 data base. You have heard Mike Bondi, another panel member, discuss this earlier. You can take his view from the project management point of view, you can take mine from the user's viewpoint. In speaking of the XV-15 data base, we cannot but talk about TRENDS (Slide 1). As you already know TRENDS stands for Tilt Rotor ENgineering Database System. This is a software system that organizes the XV-15 data and provides the software to permit a local or remote access to the XV-15 data base. The data base was developed by Analytical Mechanics Associates under a NASA contract. The current data base includes numerical test data as well as narrative and descriptive data. The software and the data right now reside on a NASA Ames VAX computer.

The current XV-15 data base is based on the two aircraft: Ship No. 2 and Ship No. 3 (Slide 2). Both aircraft have made several hundred flights and have completed several hundred ground runs. Some of the test data for some of the flights and some of the ground runs are included in the data base. A particular data set can be identified by first specifying which aircraft--Ship No. 2 or Ship No. 3, then by specifying the flight and counter numbers and item code.

The types of data include the following functions as shown on Slide 3: performance, handling qualities, loads and vibration, and aeroelastic stability. The output of performance includes time history, min/max, or average mean. Some of the data are also in harmonic form. The output display includes either tables or plots. The plots include x-y plots, 3-dimensional contour plots, or 3-dimensional surface plots (I know Euan Hooper loves this).

Slide 4 illustrates the XV-15 data base system. The source of the data was based on airborne magnetic tapes recorded in the test aircraft. After processing by a Xerox 530 computer or an equivalent computer, digital tapes are produced. The users now can either send these tapes by mail or by other means of transportation to NASA Ames to put these data on TRENDS. NASA then establishes accounts on this computer for those interested parties to access this data base via the TRENDS software. Right now the data can be plotted on a Tektronix terminal or can be obtained in tabular forms. Should the user choose not to interface with the TRENDS data base he could also obtain report quality hard copies or plots using DATAMAP from the digital tapes. I should point out that the DATAMAP is not a part of the current TRENDS software. Yet the TRENDS could interface with DATAMAP to provide time history plots.

From a user's viewpoint, the advantages of the current XV-15 data base system include the following (Slide 5): it can search the flight log for word strings, it can search counter descriptions for word strings. It can also place conditions on certain item codes and then search for all flights that satisfy these conditions. It also can tabulate the results in a desired format which could include the min/max, mean, harmonics, average oscillatory, and maximum oscillatory. And the last, but not the least, it also has adequate plotting capabilities.

Slide 6 lists a few shortcomings of the current XV-15 data base from a user's viewpoint. I would like to emphasize that TRENDS should not be blamed for most of the shortcomings shown here, the reasons should be very obvious. As a matter of fact, the software on TRENDS provides one of the best, if not the best, software capability for an engineering data base up to date. Therefore, from a user's viewpoint, the user community should be mostly responsible for minimizing these shortcomings.

From a user's viewpoint, a desired engineering data base system in general should possess these features (Slide 7): the on-line access to all flight logs and not depending on pilot cards, a data search and request right at the user's computer terminal; providing the software capability to perform a quality check to get rid of these examples of poor quality data; also to perform a complete data compression; and the ability to interface with modern plotting software and hardware so that we can produce report-quality output.

All these features can be summarized in Slide 8. As you can see, then, these features should be available for such important engineering development programs as UTTAS, AAH, ACR, ITR, and the forthcoming JVS, LHX and so on and so forth. After hearing Bob Wood talk on higher harmonic control, we should also include the higher harmonic control here. If you want to validate any particular codes, the measurements do not do much good for you if you do not know where and how to input to the computer program. ITR was a good example. We were provided with the input and also with the measurements. At this point I would like to emphasize that a

TYPES OF XV-15 DATA

FUNCTIONS

- PERFORMANCE
- HANDLING QUALITIES
- LOADS AND VIBRATION
- AEROELASTIC STABILITY

OUTPUT FORMAT

- TIME HISTORY
- MIN/MAX
- AVERAGE MEAN
- HARMONICS (LIMITED)

OUTPUT DISPLAY

- DATA TABLES
- X-Y PLOTS
- 3-D CONTOUR PLOTS
- 3-D SURFACE PLOTS

Slide 3.

THE XV-15 DATA BASE SYSTEM

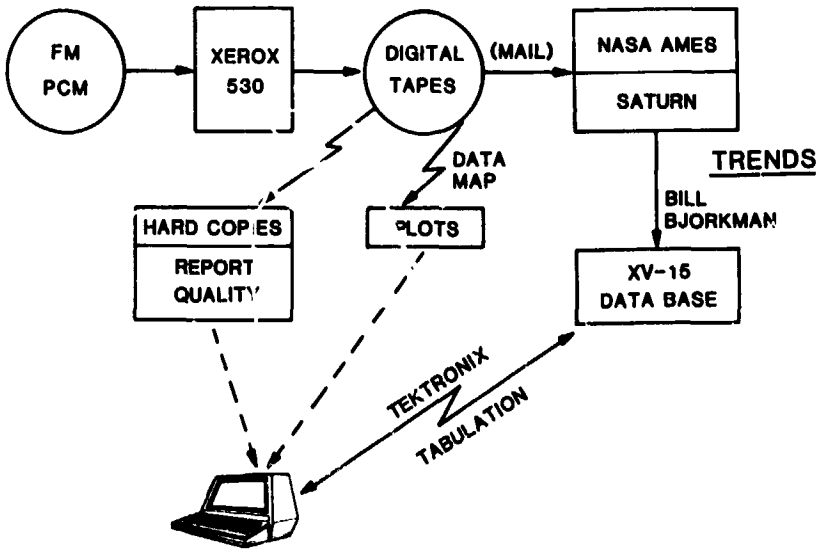

Slide 4.

C-6

ADVANTAGES OF THE XV-15 DATA BASE SYSTEM

A USER'S VIEWPOINT

- CAN SEARCH FLIGHT LOG FOR WORDS OR WORD STRINGS
- CAN SEARCH COUNTER DESCRIPTIONS FOR WORDS OR WORD STRINGS
- CAN PLACE CONDITIONS ON CERTAIN ITEM CODES AND THEN SEARCH FOR ALL FLIGHTS THAT SATISFY THOSE CONDITIONS
- CAN TABULATE MIN/MAX, MEAN, HARMONICS, AVERAGE OSCILLATORY, AND MAXIMUM OSCILLATORY
- HAS ADEQUATE PLOTTING CAPABILITIES

Slide 5.

SHORTCOMINGS OF THE XV-15 DATA BASE SYSTEM

A USER'S VIEWPOINT

- DATA BASE DOES NOT INCLUDE ALL FLIGHTS
- ONLY THOSE PEOPLE WHO ARE FAMILIAR WITH FLIGHT TEST PROGRAMS CAN DETERMINE FLIGHTS FOR QUALITY DATA
- DEPENDS HEAVILY ON PILOT CARDS
- PLOTS ARE NOT REPORT QUALITY - ONLY TEKTRONIX

Slide 6.

FEATURES OF A DESIRED ENGINEERING DATA BASE SYSTEM

A USER'S VIEWPOINT

- ON-LINE ACCESS TO DETAIL FLIGHT LOG IN LIEU OF PILOT CARDS
- DATA SEARCH AND REQUEST AT USER'S COMPUTER TERMINAL
- QUALITY CHECK TO ELIMINATE BAND EDGE, SPIKES, AND LOSS OF LOCK
- DATA COMPRESSION
- INTERFACE WITH MODERN PLOTTING SOFTWARE AND HARDWARE, SUCH AS TELEGRAF AND COLOR GRAPHIC TERMINALS TO PRODUCE REPORT QUALITY OUTPUT

Slide 7.

DESIRED FEATURES OF AN ENGINEERING DATA BASE SYSTEM

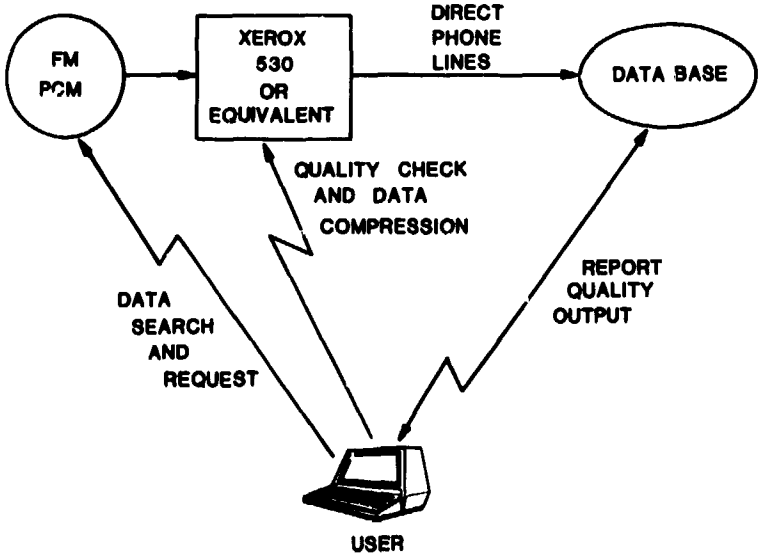

Slide 8.

successful implementation of an engineering data base system requires a very firm commitment from upper management because of the system's organization and cost. When I mean upper management I really don't mean the helicopter industry's, but I also include the government. As we have heard, the industries have been very reluctant and are reluctant and will be reluctant to exchange data among themselves. It's very ideal to ask the government to take a leadership role here. Bob Wood recommended NASA; Dr. Johnson said, no, no, no. I'm going to say the Army would be ideal, especially ATL. ATL has been doing a good job on DATAMAP. Also in view of the validation importance of 2GCHAS which will come up not before too long and that will require a very broad engineering data base. Here again, I mean not just the test data, but also the input. So I would, if I may, recommend that the government, especially the Army take leadership here.

TRENDS

TILT ROTOR ENGINEERING DATABASE SYSTEM

- SOFTWARE WAS DEVELOPED BY ANALYTICAL MECHANICS ASSOCIATES (AMA) UNDER CONTRACT NAS2-11515
- XV-15 DATABASE INCLUDES NUMERICAL TEST DATA AND NARRATIVE/DESCRIPTIVE DATA
- SOFTWARE AND DATA RESIDE ON NASA-AMES' SATURN VAX COMPUTER

Slide 1.

XV-15 TILT ROTOR DATA BASE

- THERE ARE TWO AIRCRAFT, N702 AND N703
- EACH AIRCRAFT IS INSTRUMENTED 300-400 SENSORS
- SOME OF THE DATA FOR SOME OF THE 430 FLIGHTS ARE ON TRENDS
- LITTLE DATA OF THE SEVERAL HUNDRED GROUND RUNS ARE INCLUDED IN THE DATA BASE
- PARTICULAR DATA ARE IDENTIFIED BY SPECIFYING FOUR PARAMETERS: AIRCRAFT, FLIGHT, COUNTER, AND ITEM CODE

Slide 2.

DISCUSSION

Jim Biggers, Naval Ship R&D Center: Granting that I am not totally familiar with DATAMAP, nor am I totally familiar with TRENDS, but based on my understanding of DATAMAP's capability, it sounds like you folks have gone and reinvented DATAMAP or at least some portion thereof for reasons that aren't totally clear to me. Maybe this is a question for you as well as Don Merkley, what is the degree of reinvention going on here and how come. As a devout taxpayer it sounds to me like it's not too terribly good an idea.

Yen: Well, I can answer part of the question. The way I understand it, DATAMAP has the capability for time history data only, number one. And number two, DATAMAP is a kind of tool. I'm not quite sure whether you can name that as a general engineering data base software. Don Merkley, would you comment on that if I am wrong.

Don Merkley, U.S. Army Applied Technology Laboratory: Well, I think you can call it a general engineering data base software tool. I don't think I would have any trouble calling it that. But again I am not really familiar with TRENDS. But I don't think they have reinvented the wheel. Mike Bondi can make some comments on that.

Mike Bondi, NASA Ames Research Center: I'd like to comment to Jim. We did not reinvent the wheel at all. All we did is use one specific area of DATAMAP. The disk-oriented I/O part of it, we picked up from DATAMAP intact; it has not been changed in any way except for the interface to it. So nothing was done except to interface with it.

Ron Du Val, Advanced Rotorcraft Technology: I've noticed that there is a lot of . . . everyone seems to have their own data base management approach. There is TRENDS, there is DATAMAP. In this modern computer age we have now got general purpose data base management systems which are not specific to any special type of data base, but are generic pieces of software that you can go into and structure a data base, restructure it conveniently, under control of the software, and have basically a generic form of data base that is completely independent of the nature of the software that you are dealing with. It seems that what really would be useful would be to specify a format for the structure of the data that you want to catalog and allow the users to use generic data base management systems to implement that structure rather than have everybody go off and write their own special purpose data base management systems to implement that structure.

Bondi: I'd like to make a comment on that. The reason that I think it is not possible at this time to really do what you are saying is because the state of the art of all these technologies and software is not there yet. It's like you tend to solidify on a 3 or 5 inch or 3-1/4 floppy. It isn't here. Maybe in 5 years it will be here. I don't think we know. The other aspect of your point is that we found the efficiency of some of these systems is not adequate to satisfy a user.

Dick Gabel, Boeing Vertol: If it's becoming a little negative I would like to put in a plug for Mike Bondi and how we have used his system. He came in a few months ago and gave us a demonstration of it and we were quite impressed with it. In just a few hours he walked away after teaching us how to use it. And subsequent to that we had some discussions with the Navy about loads on the XV-15 tail. Rather than look into reports we turned on the machine, went to this data base on the telephone, and we asked for the loads above a certain inch-pounds. And he searched through something like 75 flights and it gave us all the loads that were above that threshold level, in minutes. And then we saw some very high loads that were even higher than the threshold and so we said what are they You ask the machine to identify those particular ones. It went to the log and told us that those were a different rpm. Then we went to the log for the flight and it told us the governor was not operating because that was what the pilot said. Through these means we could actually find out something that we knew absolutely nothing about from that flight program. And starting at a point like that we got ourselves into the whole detail and understood all the details of that source of high loads.

PREPARED COMMENTS

Colin Young
Royal Aircraft Establishment, Farnborough

I would like to give a brief account of RAE experience with data bases, and will start with a little bit of history, Slide 1. A system developed at RAE Bedford was used prior to 1981 mainly for the Wessex flight test data. It had limited capabilities, was not easy to use, was inflexible, and had relatively crude graphics. The system did show, however, the benefits of computer generated displays. In 1981 DATAMAP was provided at RAE Farnborough under the auspices of TTCP, and in 1982 DATAMAP became operational at RAE Bedford.

I am supposed to be one of the biggest users of DATAMAP and I would like to show the type of data accessed, Slide 2. The flight test data has come from the Operational Loads Survey (OLS), the Tip Aero Acoustics Test (TAAT), the extensive series of measurements on the Puma (stresses and pressures), the split load path model rotor, the Scheiman data, and Lynx flight test data. Incidentally, the TAAT data was being looked at in 1981 and I am surprised that others have had difficulty in using this valuable source of measurements. Other experimental data used with DATAMAP has come from the unsteady aerofoil tests made at ARA Bedford. The predictions from our analyses are also added to the data base. We use the C81 analysis, RAE developed analyses, and the results from transonic flow calculations. The data base is therefore quite large and is accessed by 10 to 12 people on a regular basis.

I asked the users what they liked and disliked about DATAMAP and the results are shown in Slide 3. The good features were the ease of adding data to the data base and the way the data from various sources can be combined. This is something that was not possible with the Bedford system. Most users found DATAMAP easy to operate and this was aided by internal RAE documentation as they found the U.S. reports lacking in some detail. The variety of displays was liked as was the excellent "help" facility. The command sequences found favor for taking the drudgery out of repetitive tasks. The features not liked were the difficulty of adding new derivations. Some means of aborting command sequences was also thought desirable. Some users preferred the azimuth plots to go to 360 rather than 400 degrees but this was a minor quibble. Some labeling should also be changed, perhaps made more flexible to suit different purposes.

Finally, I would like to make some recommendations as far as DATAMAP is concerned (Slide 4). We have already made some modifications. The derivations of p/H and local Mach number have been added. The trapezium rule for the integration of force and moment coefficients has also been replaced by a spline procedure which uses $C_p\sqrt{x/c}$ against $\sqrt{x/c}$. This gives more accurate integrals when there are few pressures near the leading edge on the lower surface of the blade. We would like to see however an even more refined curve fitting technique used especially when the pressure distribution contains shocks. (You have to be careful when looking at the force and moment coefficients generated with DATAMAP because sudden changes can be introduced as a shock sweeps over one of the sensors). More flexible annotation of the plots is desirable and some additional derivations, such as dimensional blade load, would be useful. Arithmetic manipulation of complete scratch files would be helpful on occasions. In general, and Don Merkley has already mentioned this, there should be better communication between users to advise of updates and to identify data that can be freely exchanged. A DATAMAP users group is therefore recommended.

RAE EXPERIENCE OF DATABASES

PRE 1981

SYSTEM DEVELOPED AT RAE BEDFORD FOR ANALYSING WESSEX DATA

- LIMITED CAPABILITIES
- NOT EASY TO USE
- INFLEXIBLE
- FAIRLY CRUDE GRAPHICS

BUT BENEFITS OF COMPUTER GENERATED DISPLAYS DEMONSTRATED

MID 1981

DATAMAP GIVEN TO RAE FARNBOROUGH UNDER AUSPICES OF TTCP

1982

DATAMAP OPERATIONAL AT RAE BEDFORD

Slide 1.

DATA ON THE DATABASE

DATA	SOURCE
OPERATIONAL LOADS SURVEY DATA	US ARMY - TTCP COLLABORATION
TIP AEROFOIL ACOUSTIC TEST DATA	NASA - TTCP COLLABORATION
PUMA FLIGHT TEST DATA	RAE BEDFORD
RAE MODEL TEST DATA	RAE FARNBOROUGH
SCHEIMAN DATA	NASA LANGLEY
LYNX TEST DATA	WESTLAND HELICOPTERS
UNSTEADY AEROFOIL TEST DATA	ARA BEDFORD
C81 ANALYSIS	US ARMY - TTCP COLLABORATION
RAE ANALYSES	RAE FARNBOROUGH
TRANSONIC FLOW CALCULATIONS	RAE FARNBOROUGH

Slide 2.

EXPERIENCE WITH DATAMAP

GOOD FEATURES

EASE OF ADDING DATA TO THE MASTER FILE VIA DATA TRANSFER FILES

DATA FROM VARIOUS SOURCES CAN BE COMBINED

EASE OF USE - AIDED BY INTERNAL RAE DOCUMENTATION

VARIETY OF DISPLAYS

EXCELLENT HELP FACILITY

COMMAND SEQUENCES

MINOR DISLIKES

NOT EASY TO ADD NEW DERIVATIONS

SOME MEANS OF ABORTING COMMAND SEQUENCES REQUIRED

AZIMUTHAL PLOTS SHOULD GO TO 360 RATHER THAN 400 DEGREES

SOME LABELLING COULD BE ANGLICISED AND MADE MORE FLEXIBLE

Slide 3.

IMPROVEMENTS TO DATAMAP

MODIFICATIONS ALREADY MADE

DERIVATION OF P/HO ADDED

DERIVATION OF LOCAL MACH NUMBER ADDED

TRAPEZIUM RULE INTEGRATION FOR FORCE AND MOMENT COEFFICIENTS REPLACED WITH 'SPLINE' INTEGRALS AGAINST SQRT(X/C)

MODIFICATIONS DESIRED

REFINEMENT OF CURVE FITTING METHODS FOR INTEGRATING PRESSURE DISTRIBUTIONS WITH SHOCKS - MAY BE DIFFICULT BUT PROBLEM SHOULD BE RECOGNISED

MORE FLEXIBLE ANNOTATION OF PLOTS - USER DEFINED FILE ?

DERIVATION OF SOME DIMENSIONAL QUANTITIES SUCH AS BLADE LOAD

ARITHMETIC MANIPULATION OF SCRATCH FILES, EG SCF1 + SCF2

GENERAL

BETTER COMMUNICATION BETWEEN USERS TO ADVISE OF UPDATES AND DATA THAT CAN BE FREELY EXCHANGED

Slide 4.

Bill Snyder, NASA Ames Research Center: I thought I'd wait to the last, Euan, to get in the last word. We are right in the thick of this data base business both from the [Tip Aero Acoustics Test] which I graciously accept all criticism from Euan over the past year and from the standpoint of the RSRA where we are taking a somewhat different tack than the XV-15. I'd like to back up what Ron Du Val has mentioned, we feel that the available software is there for the type of data base we want to create for the RSRA. In the XV-15 case it's a specific aircraft whereas we are in the process of developing a system that can apply to a great many aircraft or rotor systems or what have you. So we do feel that the software is coming along well as Ron mentioned. To go back to the Scheiman data I am one that dreams of going back to the oscillograph records and being able to write them off like we have in the past. And I haven't been comfortable with data since then. But unfortunately those now not so young ladies that aided Jim Scheiman are no longer around, I don't think we have that kind of capability because we have upward mobilized them in many cases right out of that business. We refuse to compensate those people adequately for the job and contributions they are making. So I don't think we have that luxury anymore. I know that in Wayne Johnson's case, in the tunnel, they probably have continued that capability because of an existing organization, whereas being a fairly new organization in our case we don't have that capability and you can't just go out and pick it up. Anyway, I think we have to then turn to these newer, computer-based systems to handle the data. I think that we have to grow into them. Mike Bondi has certainly done an excellent job in the case of the XV-15, but in all cases, as all of the speakers have mentioned, we do have to continue to try to make use of the tools that are there and improve them and that is certainly our intent and we will work with you in any way we can.

Ray Piziali, U.S. Army Aeromechanics Laboratory: The panel is supposed to be on data management systems or data base systems in general and somebody earlier in the session said something about (I guess it was Jim Biggers) what about these test programs that are coming down the pike--how are we going to be able to dovetail the data that is acquired in the future into the existing programs, existing data analyses, data management systems? It looks like there are two aspects to the problem. There is data management and manipulation--getting it off the raw data, and then there is data analysis. DATAMAP does both and it sounds like TRENDS does both and maybe what we need is every time there is a data base generated, as part of the generation of that data base there is a program that does nothing more than access it in its own format and all you type into it is what format do I want it to come out in. And then I take that and I feed it into my data analysis programs so that every data base that is generated should just have a translator attached to it, then the user has his own data analysis program such as there exists in TRENDS and everyone has their own.

Bondi: I think it's a good point and actually we ran into that with TRENDS. One of the users wanted to use his own home computer so we made it so you could generate an ASCII file. This is a much more limited type of capability, but if a person had his own microcomputer system, I think you are right, we never get enough analysis programs on any system so probably it's an area that needs to be really looked at even further than what we have looked at.

LIST OF ATTENDEES

C. W. Acree
NASA Ames Research Center

Thomas N. Almojuela
U.S. Army Research & Technology Laboratory

Edward E. Austin
U.S. Army Applied Technology Laboratory

Mohsen Bahrami
Advanced Rotorcraft Technology

Fred Baker
NASA Ames Research Center

Rodney W. Balke
Bell Helicopter Textron Inc.

William F. Ballhaus, Jr.
NASA Ames Research Center

Claudio Baserga
U.S. Army Research & Technology Laboratory

Debashis Banerjee
Hughes Helicopters, Inc.

Alex Berman
Kaman Aerospace Corporation

Richard L. Bielawa
Rensselaer Polytechnic Institute

James C. Biggers
David Taylor Naval Ship R&D Center

Robert H. Blackwell
Sikorsky Aircraft

Chris Blanken
U.S. Army Aeromechanics Laboratory

Michael J. Bondi
NASA Ames Research Center

William G. Bousman
U.S. Army Aeromechanics Laboratory

Lynn Bowman
U.S. Army Structures Laboratory

Donald A. Boxwell
U.S. Army Aeromechanics Laboratory

Mauricio P. Brandao
Stanford University

John Brilla
NASA Ames Research Center

Francis X. Caradonna
U.S. Army Aeromechanics Laboratory

Charles Cassill
U.S. Army Aviation Engineering Flight Activity

David P. Chappell
U.S. Army Research & Technology Laboratory

Robert Chen
NASA Ames Research Center

S.-Y. Chen
Kaman Aerospace Corporation

Ray M. Chi
United Technologies Research Center

Inderjit Chopra
University of Maryland

Sam T. Crews
U.S. Army Aviation Systems Command

George Cunliffe
DAF Indal Ltd., Canada

Seth Dawson
U.S. Army Aeromechanics Laboratory

William Decker
NASA Ames Research Center

Ronald Du Val
Advanced Rotorcraft Technology

H. Kipling Edenborough
NASA Ames Research Center

Reuben E. Erickson
NASA Ames Research Center

John Foster
NASA Ames Research Center

Charles Fredrickson
Sikorsky Aircraft

Celeste Freeman
U.S. Army Aviation Systems Command

Fort Felker
NASA Ames Research Center

Peretz P. Friedmann
University of California, Los Angeles

Richard Gabel
Boeing Vertol Company

Santu T. Gangwani
Hughes Helicopters

Gopal H. Gaonkar
Florida Atlantic University

Paul Gelhausen
NASA Ames Research Center

Walter Gerstenberger
Structural Dynamics Consultant

Robert K. Goodman
Sikorsky Aircraft

Greg Gordon
U.S. Army Foreign Science & Technology Center

Stephen L. Haff
NASA Ames Research Center

M-Nabil Hamouda
Kentron International Incorporated

Raymond Hansen
NASA Ames Research Center

Robert Hansford
Westland Helicopters, Great Britain

Leonard Haslim
NASA Ames Research Center

James S. Hayden
U.S. Army Aviation Engineering Flight Activity

Howard Hinnant
U.S. Army Aeromechanics Laboratory

W. Euan Hooper
Boeing Vertol Company

Stuart Hopkins
U.S. Army Aeromechanics Laboratory

Steve Jacklin
NASA Ames Research Center

Wayne Johnson
NASA Ames Research Center

Henry Jones
U.S. Army Aeromechanics Laboratory

Robert Jones
Kaman Aerospace Corporation

Andrew Kerr
U.S. Army Research & Technology Laboratory

Stephen King
Westland Helicopters, Great Britain

Dick Kirkowski
NASA Ames Research Center

Sesi Kottipalli
Sikorsky Aircraft

Robert M. Kufeld
NASA Ames Research Center

Donald L. Kunz
U.S. Army Aeromechanics Laboratory

Anton J. Landgrebe
United Technologies Research Center

Henry C. Lee
U.S. Army Research & Technology Laboratory

A. Z. Lemnios
Kaman Aerospace Corporation

Michael Lewis
U.S. Army Aeromechanics Laboratory

Jane Leyland
NASA Ames Research Center

Robert G. Loewy
Rensselaer Polytechnic Institute

John F. Madden, III
NASA Ames Research Center

Martin D. Maisel
U.S. Army Aeromechanics Laboratory

Wayne R. Mantay
U.S. Army Structures Laboratory

William J. McCroskey
U.S. Army Aeromechanics Laboratory

Jim McAvoy
Lockheed-Georgia Company

Michael J. McNulty
U.S. Army Aeromechanics Laboratory

Dave Malcolm
DAF Indal, Ltd., Canada

Don Merkley
U.S. Army Applied Technology Laboratory

Robert Meyer
Lockheed-Georgia Company

Wen-Liu Miao
Sikorsky Aircraft

Hirokazu Miura
NASA Ames Research Center

Andrew Morse
U.S. Army Aeromechanics Laboratory

Ken-Ichi Nasu
NASA Ames Research Center

James Neff
Hughes Helicopters, Inc.

Charles F. Niebanck
Sikorsky Aircraft

David Nguyen
NASA Ames Research Center

John B. Nichols
United Technologies

Robert A. Ormiston
U.S. Army Aeromechanics Laboratory

B. H. Panda
University of Maryland

David A. Peters
Washington University

Randall Peterson
NASA Ames Research Center

Richard J. Peyran
U.S. Army Research & Technology Laboratory

Pamela G. Phelan
Boeing Vertol

Raymond A. Piziali
U.S. Army Aeromechanics Laboratory

Robert D. Powell
Kaman Aerospace Corporation

Kenneth R. Reader
David Taylor Naval Ship R&D Center

T. S. R. Reddy
University of Toledo

M. J. Riley
Royal Aircraft Establishment, Great Britain

Harry L. Runyan
College of William and Mary

Anselmo Russo
Agusta, Italy

Michael J. Rutkowski
U.S. Army Aeromechanics Laboratory

Fredric Schmitz
U.S. Army Aeromechanics Laboratory

Martin Schroeder
Solar Energy Institute

Michael P. Scully
U.S. Army Research & Technology Laboratory

Edward I. Seto
NASA Ames Research Center

David L. Sharpe
U.S. Army Aeromechanics Laboratory

C. Thomas Snyder
NASA Ames Research Center

William J. Snyder
NASA Ames Research Center

Robert Sopher
Sikorsky Aircraft

A. V. Srinivasan
United Technologies Research Center

Wendell Stephens
U.S. Army Aeromechanics Laboratory

Friedrich K. Straub
Hughes Helicopters, Inc.

Robert Stroub
NASA Ames Research Center

Peter D. Talbot
NASA Ames Research Center

De Man Tang
Duke University

Frank J. Terzanin, Jr.
Boeing Vertol Company

Robert B. Taylor
Boeing Vertol Company

Robert Thresher
Solar Energy Institute

Benson H. Tongue
Georgia Institute of Technology

Chee Tung
U.S. Army Aeromechanics Laboratory

George Unger
NASA Headquarters

C. Venkatesan
University of California, Los Angeles

Henry Voelkoff
Ohio State University

William Warmbrodt
NASA Ames Research Center

Charles B. Watkins, Jr.
Howard University

Robert T. Weaver
Federal Aviation Administration

F.-S. Wei
Kaman Aerospace Corporation

William H. Weller
United Technologies Research Center

Brent Wellman
NASA Ames Research Center

Matthew Wilbur
NASA Langley Research Center

Ellick Wilson
Department of the Navy

E. Roberts Wood
Hughes Helicopters, Inc.

Allen Wright
Solar Energy Institute

Gloria Yamauchi
NASA Ames Research Center

William T. Yeager, Jr.
NASA Langley Research Center

Jing G. Yen
Bell Helicopter Textron Inc.

Colin Young
Ministry of Defence, Great Britain

Larry Young
NASA Ames Research Center

Yung Yu
U.S. Army Aeromechanics Laboratory

John [illegible]
NASA Ames Research Center

1. Report No.	2. Government Accession No.	3. Recipient's Catalog No.
NASA CP-2400		

4. Title and Subtitle	5. Report Date
ROTORCRAFT DYNAMICS 1984	November 1985
	6. Performing Organization Code

7. Author(s)	8. Performing Organization Report No.
The authors and their affiliations are shown in the list of attendees.	85122
	10. Work Unit No.

9. Performing Organization Name and Address	11. Contract or Grant No.
Ames Research Center, Moffett Field, CA 94035 and San Francisco Bay Area Chapter of the American Helicopter Society, Washington, DC 20036	
	13. Type of Report and Period Covered
12. Sponsoring Agency Name and Address	Conference Publication November 7-9, 1984
National Aeronautics and Space Administration Washington, DC 20546 and the American Helicopter Society, Washington, DC 20036	14. Sponsoring Agency Code 505-42-11

15 Supplementary Notes

Technical Chairman: William G. Bousman, Aeroflightdynamics Directorate, U.S. Army Aviation Research and Technology Activity-AVSCOM, Ames Research Center, MS 215-1, Moffett Field, CA 94035 (415) 694-5890, FTS 464-5890

16 Abstract

This conference publication contains the formal papers of the Second Decennial Specialists' Meeting on Rotorcraft Dynamics. The conference was cosponsored by Ames Research Center and the American Helicopter Society, and was held at Ames Research Center, Moffett Field, California, on November 7-9, 1984.

In the conference proceedings are 24 presented papers, their discussions, and material given in two panels. The presented papers address the general areas of the dynamics of rotorcraft or helicopters. Specific topics include the stability of rotors in hover and forward flight, the stability of coupled rotor-fuselage systems in hover, the loads on a rotor in forward flight including new developments in rotor loads calculations, and the calculation of rotorcraft vibration and means for its control or suppression. Material in the first panel deals with the successful application of dynamics technology to engineering development of flight vehicles. Material in the second panel is concerned with large data bases in the area of rotorcraft dynamics and how they are developed, managed, and used.

17. Key Words (Suggested by Author(s))	18. Distribution Statement
Helicopter Rotorcraft Stability Rotor loads Vibration	Unlimited Subject category-05

19. Security Classif. (of this report)	20 Security Classif. (of this page)	21. No. of Pages	22. Price*
Unclassified	Unclassified	512	A22

*For sale by the National Technical Information Service, Springfield, Virginia 22161